Journal of Chemistry

Mathematical Tools for Solving Problems of Chemical Structure Generation

Lead Guest Editor: Jia-Bao Liu
Guest Editors: Juan L. G. Guirao and Shaohui Wang

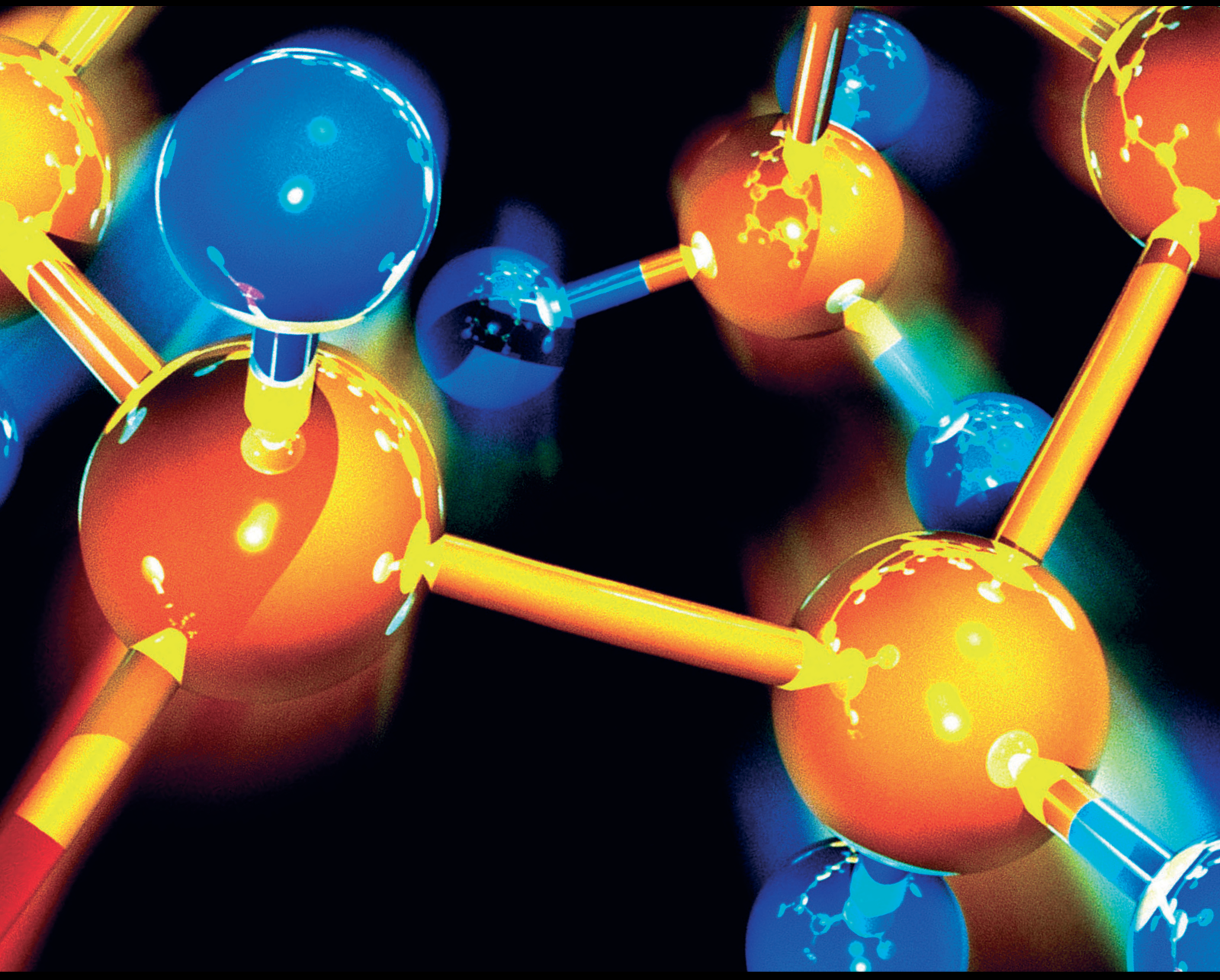

Mathematical Tools for Solving Problems of Chemical Structure Generation

Journal of Chemistry

Mathematical Tools for Solving Problems of Chemical Structure Generation

Lead Guest Editor: Jia-Bao Liu
Guest Editors: Juan L. G. Guirao and Shaohui Wang

Contents

Contents

Hindawi
Journal of Chemistry
Volume 2020, Article ID 8791741, 2 pages
https://doi.org/10.1155/2020/8791741

Erratum

Erratum to "Reverse Zagreb and Reverse Hyper-Zagreb Indices for Crystallographic Structure of Molecules"

Zhen Wang,[1] Faryal Chaudhry,[2] Maria Naseem,[3] and Adnan Asghar[2]

[1]*School of Computer Engineering, Anhui Wonder University of Information Engineering, Hefei 231201, China*
[2]*The University of Lahore, Lahore, Pakistan*
[3]*University of Central Punjab, Lahore, Pakistan*

Correspondence should be addressed to Adnan Asghar; adnan.asghar@math.uol.edu.pk

Received 13 May 2020; Accepted 14 May 2020; Published 27 June 2020

In the article titled "Reverse Zagreb and Reverse Hyper-Zagreb Indices for Crystallographic Structure of Molecules" [1], 21 references were added by the authors to the reference list following editorial acceptance. A reassessment of the article by the editor confirmed that the following references should be removed from the article:

[18] W. Gao, M. Asif, and W. Nazeer, "The study of honey comb derived network via topological indices," Open Journal of Mathematical Analysis, vol. 2018, no. 2, pp. 10–26, 2018.

[21] M. Munir, W. Nazeer, S. Rafique, and S. Kang, "M-polynomial and degree-based topological indices of polyhex nanotubes," Symmetry, vol. 8, no. 12, p. 149, 2016.

[22] M. Munir, W. Nazeer, A. Nizami, S. Rafique, and S. Kang, "M-polynomials and topological indices of titania nanotubes," Symmetry, vol. 8, no. 11, p. 117, 2016.

[23] Y. C. Kwun, M. Munir, W. Nazeer, S. Rafique, and S. M. Kang, "M-polynomials and topological indices of V-phenylenic nanotubes and nanotori," Scientific Reports, vol. 7, no. 1, pp. 1–9, 2017.

[27] W. Gao, A. Asghar, and W. Nazeer, "Computing degree-based topological indices of Jahangir graph," Engineering and Applied Science Letters, vol. 2018, no. 1, pp. 16–22, 2018.

[29] W. Gao, M. Younas, A. Farooq, A. Virk, and W. Nazeer, "Some reverse degree-based topological indices and polynomials of dendrimers," Mathematics, vol. 6, no. 10, p. 214, 2018.

[30] A. Ali, W. Nazeer, M. Munir, and S. Min Kang, "M-polynomials and topological indices of zigzag and rhombic benzenoid systems," Open Chemistry, vol. 16, no. 1, pp. 73–78, 2018.

[31] Y. C. Kwun, A. Ali, W. Nazeer, M. Ahmad Chaudhary, and S. M. Kang, "M-polynomials and degree-based topological indices of triangular, hourglass, and jagged-rectangle benzenoid systems," Journal of Chemistry, vol. 2018, 2018.

[32] W. Gao, M. Younas, A. Farooq, A. Mahboob, and W. Nazeer, "M-polynomials and degree-based topological indices of the crystallographic structure of molecules," Biomolecules, vol. 8, no. 4, p. 107, 2018.

[33] J.-B. Liu, M. Younas, M. Habib, M. Yousaf, and W. Nazeer, "M-polynomials and degree-based topological indices of VC5C7[p,q] and HC5C7[p,q] nanotubes," IEEE Access, vol. 7, pp. 41125–41132, 2019.

[34] Y. C. Kwun, A. Farooq, W. Nazeer, Z. Zahid, S. Noreen, and S. M. Kang, "Computations of the M-polynomials and degree-based topological indices for dendrimers and polyomino chains," International Journal of Analytical Chemistry, vol. 2018, 2018.

[35] S. M. Kang, M. A. Zahid, A. u. R. Virk, W. Nazeer, and W. Gao, "Calculating the degree-based topological indices of dendrimers," Open Chemistry, vol. 16, no. 1, pp. 681–688, 2018.

[36] W. Nazeer, A. Farooq, M. Younas, M. Munir, and S. Kang, "On molecular descriptors of carbon nanocones," Biomolecules, vol. 8, no. 3, p. 92, 2018.

[38] M. A. Rehman, C. Shi, and W. Nazeer, "Useful irregularity indices in QSPR study for bismuth tri-iodide," Journal of Chemistry, vol. 2019, 2019.

[40] A. Farooq, M. Habib, A. Mahboob, W. Nazeer, and S. M. Kang, "Zagreb polynomials and redefined zagreb indices of dendrimers and polyomino chains," Open Chemistry, vol. 17, no. 1, pp. 1374–1381, 2009.

[42] M. K. Jamil, A. Javed, W. Nazeer, M. R. Farahani, and Y. Gao, "Four vertex-degree-based topological indices of VC 5 C 7[p; q] nanotubes," Communications in Mathematics and Applications, vol. 8, no. 1, pp. 99–105, 2017.

[45] Y. C. Kwun, M. A. Zahid, W. Nazeer, A. Ali, M. Ahmad, and S. M. Kang, "On the zagreb polynomials of benzenoid systems," Open Physics, vol. 16, no. 1, pp. 734–740, 2018.

[46] S. M. Kang, M. Yousaf, M. A. Zahid, M. Younas, and W. Nazeer, "Zagreb Polynomials and redefined Zagreb indices of nanostar dendrimers," Open Physics, vol. 17, no. 1, pp. 31–40, 2019.

[48] Z. Hussain, M. Munir, W. Nazeer, M. S. Saleem, S. M. Kang, and Y. C. Kwun, "Computational aspects of line graph of carbon nanocones," Journal of the National Science Foundation of Sri Lanka, vol. 47, no. 4, 2019.

[50] Y. J. Ge, J. B. Liu, M. Younas, M. Yousaf, and W. Nazeer, "Analysis of and nanotubes via topological indices," Journal of Nanomaterials, vol. 2019, 2019.

[52] W. Gao, B. Muzaffar, and W. Nazeer, "K-Banhatti and K-hyper Banhatti indices of dominating David Derived network," Open Journal of Mathematical Analysis, vol. 2017, no. 1, pp. 13–24, 2017.

References

[1] Z. Wang, F. Chaudhry, M. Naseem, and A. Asghar, "Reverse zagreb and reverse hyper-zagreb indices for crystallographic structure of molecules," *Journal of Chemistry*, vol. 2020, Article ID 9805829, 13 pages, 2020.

Hindawi
Journal of Chemistry
Volume 2020, Article ID 3794592, 7 pages
https://doi.org/10.1155/2020/3794592

Research Article

Computing Eccentricity-Based Topological Indices of 2-Power Interconnection Networks

Muhammad Imran,[1] Muhammad Azhar Iqbal,[2] Yun Liu,[3] Abdul Qudair Baig,[4] Waqas Khalid,[5] and Muhammad Asad Zaighum[2]

[1]*Department of Mathematical Sciences, College of Science, United Arab Emirates University, P. O. Box 15551, Al Ain, UAE*
[2]*Department of Mathematics and Statistics, Riphah International University, Islamabad, Pakistan*
[3]*School of Electronic Engineering, Huainan Normal University, Huainan 232038, China*
[4]*Department of Mathematics and Statistics, Institute of Southern Punjab, Multan, Pakistan*
[5]*Punjab College of Science and Commerce, Attock Campus, Pakistan*

Correspondence should be addressed to Muhammad Imran; imrandhab@gmail.com

Received 11 October 2019; Accepted 11 May 2020; Published 13 June 2020

Academic Editor: Juan L. G. Guirao

In a connected graph G with a vertex v, the eccentricity $\varepsilon(v)$ of v is the distance between v and a vertex farthest from v in the graph G. Among eccentricity-based topological indices, the eccentric connectivity index, the total eccentricity index, and the Zagreb index are of vital importance. The eccentric connectivity index of G is defined by $\xi(G) = \sum_{v \in V(G)} d(v)\varepsilon(v)$, where $d(v)$ is the degree of the vertex v and $\varepsilon(v)$ is the eccentricity of v in G. The topological structure of an interconnected network can be modeled by using graph explanation as a tool. This fact has been universally accepted and used by computer scientists and engineers. More than that, practically, it has been shown that graph theory is a very powerful tool for designing and analyzing the topological structure of interconnection networks. The topological properties of the interconnection network have been computed by Hayat and Imran (2014), Haynes et al. (2002), and Imran et al. (2015). In this paper, we compute the close results for eccentricity-based topological indices such as the eccentric connectivity index, the total eccentricity index, and the first, second, and third Zagreb eccentricity index of a hypertree, sibling tree, and X-tree for k-level by using the edge partition method.

1. Introduction

The advancement of large-scale integrated circuit technology has enabled the construction of complex interconnection networks. Graph theory provides a fundamental tool for designing and analyzing such networks. Graph theory and interconnection networks provide a thorough understanding of these interrelated topics [1–3] The architecture of an interconnected network is represented by a graph, where nodes represent the processors and edges represent the links between processors. Electric power companies need to continually monitor the state of their systems as in the case of the voltage magnitude at loads and the machine phase angle at generators. In the electric power system, a vertex represents an electric node and an edge represents a transmission line joining two electrical nodes [4, 5]. *Chemical graph theory* is a branch of mathematical chemistry in which we apply tools of graph theory to model the chemical phenomenon mathematically. This theory contributes a prominent role in the fields of chemical sciences. A molecular or chemical graph is a simple finite graph in which vertices denote the atoms and edges denote the chemical bonds in the underlying chemical structure. A *topological index* is actually a numeric quantity associated with chemical constitution purporting for correlation of the chemical structure with many physiochemical properties, chemical reactivity, and biological activities. Let G be a graph with u and v being the vertices of G, then the distance $d(u, v)$ is

defined as the shortest length between u and v. The *eccentricity* $\varepsilon(v)$ of a vertex $v \in V(G)$ is defined as

$$\varepsilon(v) = \max\{d(v,w) | w \in V(G)\}. \tag{1}$$

The minimum eccentricity in a graph G is known as the *radius* G $\mathrm{rad}(G)$, while the maximum eccentricity in a graph G is known as the *diameter* $2p-2$. Topological descriptors play an important role in the quantitative structure-activity (QSAR) and structure-property (QSPR) study. Topological indices, which are based on eccentricity of the vertices in a graph G, are known as eccentricity-based topological indices. The *eccentric connectivity index* [6] of G is defined by

$$\xi(G) = \sum_{v \epsilon V(G)} d(v)\varepsilon(u), \tag{2}$$

where $d(v)$ is the degree of the vertex v and $\varepsilon(v)$ is the eccentricity of v in G.

The *total eccentricity index* [7] is defined as the summation of eccentricity of each vertex in graph G. In other words, when the vertex degrees are not considered in the eccentric connectivity index, then we obtain the total eccentricity index:

$$\zeta(G) = \sum_{u \epsilon V(G)} \varepsilon(u), \tag{3}$$

where $\varepsilon(v)$ is the eccentricity of u in G.

Zagreb indices [8] have been introduced more than thirty years ago. Let G be a graph with u and v being the vertices of G; then the Zagreb indices are defined as follows:

$$\begin{aligned} M_1(G) &= \sum_{v \epsilon V(G)} (d(v))^2, \\ M_2(G) &= \sum_{uv \epsilon E(G)} (d(u)d(v)). \end{aligned} \tag{4}$$

Some new modified versions of Zagreb indices [9] are expressed in terms of eccentricity as follows:

$$\begin{aligned} M_1^{\star}(G) &= \sum_{uv \epsilon E(G)} (\varepsilon(u) + \varepsilon(v)), \\ M_1^{\star\star}(G) &= \sum_{v \epsilon V(G)} (\varepsilon(v))^2, \\ M_2^{\star}(G) &= \sum_{uv \epsilon E(G)} (\varepsilon(u)\varepsilon(v)). \end{aligned} \tag{5}$$

On further results for certain degree-based topological indices of networks and nanostructures, consult [1, 10–13]. A *tree* is a connected acyclic graph, and the common type of a tree is a binary tree. A *binary tree* is made of nodes, where each node contains a left reference, a right reference, and a data element. The top most node is called the root. The vertex of the binary tree has three fields. The first field represents data, while the second and third contain information of the left and right sons of the vertex. If each internal vertex/node has exactly two descendents, then the binary tree is said to be a complete binary tree as shown in Figure 1. The basic skeleton of the *hypertreek*-level is a complete binary tree $\mathrm{HT}(k)$. The nodes of the trees are labeled in such a way that root node has label 1. The root is at level 0. Labels

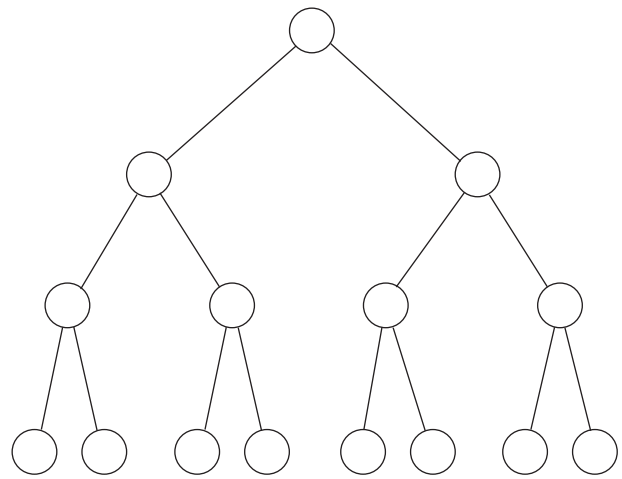

Figure 1: Binary tree.

of the left and right children are formed by appending 0 and 1, respectively, to the labels of the parent node. Here, the children of the nodes x are labeled as $2x$ and $2x+1$. Additional links in a hypertree are horizontal, and two nodes in the same level of the tree are joined if their label difference is 2^{i-2} [14]. The hypertree k-level $\mathrm{HT}(k)$ shown in Figure 2 has vertices $2^{k+1}-1$ and edges $3(2^k-1)$.

2. Main Results

In this section, we compute the close results for eccentricity-based topological indices such as the eccentric connectivity index, the total eccentricity index, and the first, second, and third Zagreb eccentricity index of a hypertree, sibling tree, and X-tree for k-level by using the edge partition method. The molecular topological descriptors of fullerenes and several interconnection networks have been already computed in the literature [1–3, 15].

In the next theorem, an exact expression for the eccentric connectivity index for a binary tree is computed.

Theorem 1. *Consider the graph $G \cong HT(k)$, then the eccentric connectivity index is equal to*

$$\xi(G) = 2k + 4\sum_{i=1}^{k-1}\sum_{p=k}^{2k-2} 2^i p + 2^{k+1}(2k-1). \tag{6}$$

Proof. In order to prove the above result, we use the formula of the eccentric connectivity index:

$$\xi(G) = \sum_{v \epsilon V(G)} d(v)\varepsilon(v). \tag{7}$$

By using Table 1, we have

$$\xi(G) = 2\sum_{p=k}\sum_{i=0} 2^i p + 4\sum_{i=1}^{k-1}\sum_{p=k}^{2k-2} 2^i p + 2\sum_{i=k}\sum_{p=k}(2p-1)2^i. \tag{8}$$

After an easy calculation, we get

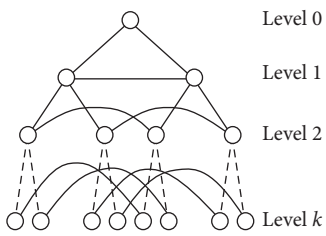

Figure 2: k-level hypertree HT(k).

Table 1: Vertices partition of a hypertree (k-level) based on degree and eccentricity of each vertex with the existence of its frequencies.

$d(v)$	$\varepsilon(v)$	Frequency	Range of i	Range of p
2	p	2^i	$i=0$	$p=k$
4	p	2^i	$1\le i\le k-1$	$k\le p\le 2k-2$
2	$2p-1$	2^i	$i=k$	$p=k$

$$\xi(G)=2k+4\sum_{i=1}^{k-1}\sum_{p=k}^{2k-2}2^i p+2^{k+1}(2k-1). \tag{9}$$

The total eccentricity index of a binary tree is computed in the following theorem. □

Theorem 2. *Consider the graph $G\cong HT(k)$, then the total eccentricity index is equal to*

$$\zeta(G)=k+\sum_{i=1}^{k-1}\sum_{p=k}^{2k-2}2^i p+(2k-1)2^k. \tag{10}$$

Proof. Let G be a graph of a hypertree (k-level). To prove (10), we use the total eccentricity index formula:

$$\zeta(G)=\sum_{u\varepsilon V(G)}\varepsilon(u). \tag{11}$$

By using Table 1, we get

$$\zeta(G)=\sum_{p=k}\sum_{i=0}2^i p+\sum_{i=1}^{k-1}\sum_{p=k}^{2k-2}p\times 2^i+\sum_{i=k}\sum_{p=k}2^i(2p-1). \tag{12}$$

After an easy calculation, we get

$$\zeta(G)=k+\sum_{i=1}^{k-1}\sum_{p=k}^{2k-2}2^i p+(2k-1)2^k. \tag{13}$$

The first Zagreb eccentricity index of a binary tree is computed in the following theorem. □

Theorem 3. *Consider the graph $G\cong HT(k)$, then the first Zagreb eccentricity index is equal to*

$$M_1^\star(G)=6k+\sum_{i=1}^{k-1}\sum_{p=k}^{2k-2}(2p+1)2^{i+1}+\sum_{i=1}^{k-1}\sum_{p=k}^{2k-2}(2p+2)2^i. \tag{14}$$

Proof. In order to proof (14), we use the first Zagreb eccentricity index formula:

$$M_1^\star(G)=\sum_{uv\epsilon E(G)}\{\varepsilon(u)+\varepsilon(v)\}. \tag{15}$$

By using Table 2, we get

$$M_1^\star(G)=3\sum_{p=k}\sum_{i=0}2p2^i+\sum_{i=1}^{k-1}\sum_{p=k}^{2k-2}(2p+1)2^{i+1}+\sum_{i=1}^{k-1}\sum_{p=k}^{2k-2}(2p+2)2^i. \tag{16}$$

After an easy calculation, we get

$$M_1^\star(G)=6k+\sum_{i=1}^{k-1}\sum_{p=k}^{2k-2}(2p+1)2^{i+1}+\sum_{i=1}^{k-1}\sum_{p=k}^{2k-2}(2p+2)2^i. \tag{17}$$

□

Theorem 4. *Consider the graph $G\cong HT(k)$, then the second Zagreb eccentricity index is equal to*

$$M_1^{\star\star}(G)=k^2+\sum_{i=1}^{k-1}\sum_{p=k}^{2k-2}p^2 2^i+(2k-1)^2 2^k. \tag{18}$$

Proof. Let G be a graph of a hypertree (k-level). The formula of the second Zagreb eccentricity index is given by

$$M_1^{\star\star}(G)=\sum_{v\epsilon V(G)}[\varepsilon(v)]^2. \tag{19}$$

By using Table 1, we get

$$M_1^{\star\star}(G)=\sum_{p=k}\sum_{i=0}p^2 2^i+\sum_{i=1}^{k-1}\sum_{p=k}^{2k-2}p^2 2^i+\sum_{i=k}\sum_{p=k}(2p-1)^2 2^i. \tag{20}$$

After an easy calculation, we get

$$M_1^{\star\star}(G)=k^2+\sum_{i=1}^{k-1}\sum_{p=k}^{2k-2}p^2 2^i+(2k-1)^2 2^k. \tag{21}$$

□

Theorem 5. *Consider the graph $G\cong HT(k)$, then the third Zagreb eccentricity index is equal to*

$$M_2^\star(G)=3k^2+\sum_{i=1}^{k-1}\sum_{p=k}^{2k-2}p(p+1)2^{i+1}+\sum_{i=k}\sum_{p=k}(p+1)^2 2^i. \tag{22}$$

Proof. In order to prove (22), we use the formula of the third Zagreb eccentricity index:

$$M_2^\star(G)=\sum_{uv\epsilon E(G)}\varepsilon(u)\times\varepsilon(v). \tag{23}$$

By using Table 2, we get

Table 2: Edge partition of a hypertree (k-level) based on eccentricity of end vertices of each edge with existence of its frequencies.

$(\varepsilon(u), \varepsilon(v))$	Frequency	Range of i	Range of p
(p, p)	3.2^i	$i = 0$	$p = k$
$(p, p+1)$	2^{i+1}	$1 \le i \le k-1$	$k \le p \le 2k-2$
$(p+1, p+1)$	2^i	$1 \le i \le k-1$	$k \le p \le 2k-2$

$$M_2^\star(G) = 3\sum_{p=k}\sum_{i=0} p^2 2^i + \sum_{i=1}^{k-1}\sum_{p=k}^{2k-2} p(p+1)2^{i+1} + \sum_{i=k}\sum_{p=k} (p+1)^2 2^i. \tag{24}$$

After an easy calculation, we get

$$M_2^\star(G) = 3k^2 + \sum_{i=1}^{k-1}\sum_{p=k}^{2k-2} p(p+1)2^{i+1} + \sum_{i=1}^{k-1}\sum_{p=k}^{2k-2} (p+1)^2 2^i. \tag{25}$$

The 1-rooted *sibling tree* ST_k^1 shown in Figure 3 is obtained from the 1-rooted complete binary tree T_k^1 by adding edges (sibling edges) between the left and right children of the same parent node [16].

An *X-tree* $\mathrm{XT}(k)$ shown in Figure 4 is obtained from a complete binary tree on $2^{k+1}-1$ vertices of height $2^i - 1$ and adding paths P_i left to right through all the vertices at level i, $1 \le i \le k$.

A graph $G_1 = (V_1, E_1)$ is said to be isomorphic to the graph $G_2 = (V_2, E_2)$, if there is a one-to-one correspondence between the vertex sets V_1 and V_2 and a one-to-one correspondence between the edge sets E_1 and E_2 in such a way that if e_1 is an edge with end vertices u_1 and v_1 in G_1, then the corresponding edge e_2 in G_2 has its end points in the vertices u_2 and v_2 in G_2 which correspond to u_1 and v_1, respectively. Such a pair of correspondences is called the *graph isomorphism*. □

Remark 1. $\mathrm{HT}(k) \ncong \mathrm{ST}_k^1$, but their topological eccentricity-based indices are equal:

$$\begin{aligned} &\xi(\mathrm{HT}(k)) = \xi\left(\mathrm{ST}_k^1\right),\ \zeta(\mathrm{HT}(k)) = \zeta\left(\mathrm{ST}_k^1\right),\ M_1^\star(\mathrm{HT}(k)) \\ &\quad = M_1^\star\left(\mathrm{ST}_k^1\right), \\ &M_1^{\star\star}(\mathrm{HT}(k)) = M_1^{\star\star}\left(\mathrm{ST}_k^1\right),\ M_2^\star(\mathrm{HT}(k)) = M_2^\star\left(\mathrm{ST}_k^1\right). \end{aligned} \tag{26}$$

Theorem 6. *Consider the graph $G \cong XT(k)$ and $k \ge 3$, then the eccentric connectivity index is equal to*

$$\begin{aligned} \xi(G) = {} & 2k + 8\sum_{p=k}^{2k-2} p + 4(2k-1) + 5\sum_{p=k}^{2k-3}\sum_{i=1}^{k-2} 2^i p + 3(2k-2)2^{k-1} \\ & \cdot 5\sum_{p=k+2,k>3}^{2k-2}\sum_{i=1,k>3}^{k-3}\left(2\left(2^i-1\right)p\right) + 3(2k-1)\left(2\left(2^{k-2}-1\right)\right). \end{aligned} \tag{27}$$

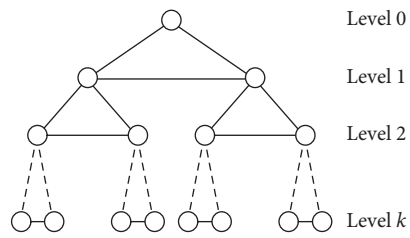

Figure 3: 1-rooted sibling tree ST_k^1.

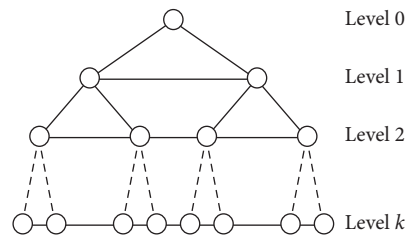

Figure 4: k-level X-tree $\mathrm{XT}(k)$.

Proof. In order to prove the above result, we use the formula of the eccentric connectivity index:

$$\xi(G) = \sum_{v \in V(G)} d(v)\varepsilon(v). \tag{28}$$

By using Table 3, we have

$$\begin{aligned} \xi(G) = {} & 2\sum_{p=k,k\ge3} p\sum_{i=0} 2^i + 4\sum_{i=1} 2^i \sum_{p=k,k\ge3}^{2k-2} p \\ & + 2\sum_{i=1} 2^i \sum_{p=k,k\ge3}(2p-1) + 5\sum_{p=k,k\ge3}^{2k-3} p \sum_{i=1,k\ge3}^{k-2} 2^i \\ & + 5\sum_{p=k+2,k>3}^{2k-2} p \sum_{i=1,k>3}^{k-3} 2\left(2^i-1\right) \\ & + 3\sum_{p=k,k\ge3}(2p-2)\sum_{i=k-1,k\ge3} 2^i. \end{aligned} \tag{29}$$

After an easy calculation, we get

$$\begin{aligned} \xi(G) = {} & 2k + 8\sum_{p=k}^{2k-2} p + 4\sum_{p=k}(2p-1) + 5\sum_{p=k}^{2k-3}\sum_{i=1}^{k-2} 2^i p + 3(2k-2)2^{k-1} \\ & 5\sum_{p=k+2,k>3}^{2k-2}\sum_{i=1,k>3}^{k-3}\left(2\left(2^i-1\right)p\right) + 3(2k-1)\left(2\left(2^{k-2}-1\right)\right). \end{aligned} \tag{30}$$

□

Theorem 7. *Consider the graph $G \cong XT(k)$ and $k \ge 3$, then the total eccentricity index is equal to*

$$\begin{aligned} \zeta(G) = {} & k + 2\sum_{p=k}^{2k-2} p + 2(2k-1) + \sum_{p=k}^{2k-3}\sum_{i=1}^{k-2} 2^i p \\ & + \sum_{p=k+2,k>3}^{2k-2}\sum_{i=1,k>3}^{k-3}\left(2\left(2^i-1\right)p\right) \\ & + (2k-1)\left(2\left(2^{k-2}-1\right)\right) + (2k-2)2^{k-1}. \end{aligned} \tag{31}$$

Table 3: Vertices partition of an X-tree (k-level) based on degree and eccentricity of each vertex with the existence of its frequencies.

$d(v)$	$\varepsilon(v)$	Frequency	Range of i	Range of p
2	p	2^i	$i=0$	$p=k$
4	p	2^i	$i=1$	$k\le p\le 2k-2$
2	$2p-1$	2^i	$i=1$	$p=k$
5	p	2^i	$1\ge i\ge k-2$	$k\ge p\ge 2k-3$
5	p	$2(2^i-1)$	$1\ge i\ge k-3$, $k>3$	$k+2\ge p\ge 2k-2$, $k>3$
3	$2p-1$	$2(2^i-1)$	$i=k-2$	$p=k$
3	$2p-2$	2^i	$i=k-1$	$p=k$

Proof. Let G be a graph of an X-tree (k-level). In order to prove, we use the total eccentricity index formula:

$$\zeta(G)=\sum_{u\epsilon V(G)}\varepsilon(u). \tag{32}$$

By using Table 3, we get

$$\begin{aligned}\zeta(G)=&\sum_{p=k}p\sum_{i=0}2^i+\sum_{i=1}2^i\sum_{p=k}^{2k-2}p+\sum_{i=1}2^i\sum_{p=k}(2p-1)\\&+\sum_{p=k}^{2k-3}p\sum_{i=1}^{k-2}2^i+\sum_{p=k+2,k>3}^{2k-2}p\sum_{i=1,k>3}^{k-3}\left(2\left(2^i-1\right)\right)\\&+\sum_{p=k}(2p-1)\sum_{i=k-2}\left(2\left(2^i-1\right)\right)\\&+\sum_{p=k}(2p-2)\sum_{i=k-1}2^i.\end{aligned} \tag{33}$$

After an easy calculation, we get

$$\begin{aligned}\zeta(G)=&k+2\sum_{p=k}^{2k-2}p+2(2k-1)+\sum_{p=k}^{2k-3}\sum_{i=1}^{k-2}2^ip\\&+\sum_{p=k+2,k>3}^{2k-2}\sum_{i=1,k>3}^{k-3}\left(2\left(2^i-1\right)p\right)\\&+(2k-1)\left(2\left(2^{k-2}-1\right)\right)+(2k-2)2^{k-1}.\end{aligned} \tag{34}$$

□

Theorem 8. *Consider the graph $G\cong XT(k)$ and $k\ge 3$, then the first Zagreb eccentricity index is equal to*

$$\begin{aligned}M_1^{\star}(G)=&12k+\sum_{i=1}^{k-2}\sum_{p=k+1}^{2k-2}(2p)\left(3\left(2^i-1\right)\right)\\&+(4k-3)\left(2^{k-1}+2\right)\\&+\sum_{i=1}^{k-2}\sum_{p=k}^{2k-3}(2p+1)\left(2\left(3\left(2^{i-1}\right)+1\right)\right)\\&+(4k-2)\left(2\left(2^{k-2}-1\right)\right).\end{aligned} \tag{35}$$

Proof. In order to prove the above result, we use the first Zagreb eccentricity index formula:

$$M_1^{\star}(G)=\sum_{uv\epsilon E(G)}\{\varepsilon(u)+\varepsilon(v)\}. \tag{36}$$

By using Table 4, we get

$$\begin{aligned}M_1^{\star}(G)=&\sum_{p=k}(p+p)\sum_{i=0}6\left(2^i\right)+\sum_{i=1}^{k-2}3\left(2^i-1\right)\sum_{p=k+1}^{2k-2}(p+p)\\&+\sum_{i=1}^{k-2}\left(2\left(3\left(2^{i-1}\right)+1\right)\right)\sum_{p=k}^{2k-3}(p+p+1)\\&+\sum_{p=k}(2p-2+2p-1)\sum_{i=k-2}\left(2^{i+1}+2\right)\\&+\sum_{p=k}(2p-1+2p-1)\sum_{i=k-2}\left(2\left(2^i-1\right)\right).\end{aligned} \tag{37}$$

After an easy calculation, we get

$$\begin{aligned}M_1^{\star}(G)=&12k+\sum_{i=1}^{k-2}\sum_{p=k+1}^{2k-2}(2p)\left(3\left(2^i-1\right)\right)\\&+(4k-3)\left(2^{k-1}+2\right)\\&+\sum_{i=1}^{k-2}\sum_{p=k}^{2k-3}(2p+1)\left(2\left(3\left(2^{i-1}\right)+1\right)\right.\\&\left.+(4k-2)\left(2\left(2^{k-2}-1\right)\right)\right).\end{aligned} \tag{38}$$

□

Theorem 9. *Consider the graph $G\cong XT(k)$ and $k\ge 3$, then the second Zagreb eccentricity index is equal to*

$$\begin{aligned}M_1^{\star\star}(G)=&k^2+2\sum_{p=k}^{2k-2}p^2+2(2k-1)^2+\sum_{p=k}^{2k-3}\sum_{i=1}^{k-2}2^ip^2\\&+\sum_{p=k+2,k>3}^{2k-2}\sum_{i=1}^{k-3}\left(2\left(2^i-1\right)p^2\right)\\&+(2k-1)^2\left(2\left(2^{k-2}-1\right)\right)+(2k-2)^2 2^{k-1}.\end{aligned} \tag{39}$$

Proof. Let G be a graph of an X-tree (k-level) and $k\ge 3$. The formula of the second Zagreb eccentricity index is given by

$$M_1^{\star\star}(G)=\sum_{v\epsilon V(G)}[\varepsilon(v)]^2. \tag{40}$$

By using Table 3, we get the following expression:

$$\begin{aligned}M_1^{\star\star}(G)=&\sum_{p=k}p^2\sum_{i=0}2^i+\sum_{i=1}2^i\sum_{p=k}^{2k-2}p^2+\sum_{i=1}2^i\sum_{p=k}(2p-1)^2\\&+\sum_{i=1}^{k-2}2^i\sum_{p=k}^{2k-3}p^2+\sum_{i=1,k>3}^{k-3}\left(2\left(2^i-1\right)\right)\sum_{p=k+2,k>3}^{2k-2}p^2\\&+\sum_{i=k-2}\left(2\left(2^i-1\right)\right)\sum_{p=k}(2p-1)^2\\&+\sum_{i=k-1}2^i\sum_{p=k}(2p-2)^2.\end{aligned} \tag{41}$$

Table 4: Edge partition of an X-tree (k-level) based on eccentricity of end vertices of each edge with existence of its frequencies.

$(\varepsilon(u), \varepsilon(v))$	Frequency	Range of i	Range of p
(p, p)	$6(2^i)$	$i = 0$	$p = k$
(p, p)	$3(2^i - 1)$	$1 \le i \le k-2$	$k+1 \le p \le 2k-2$
$(p, p+1)$	$2(3(2^{i-1}) + 1)$	$1 \le i \le k-2$	$k \le p \le 2k-3$
$(2p-2, 2p-1)$	$2^{i+1} + 2$	$i = k-2$	$p = k$
$(2p-1, 2p-1)$	$2(2^i - 1)$	$i = k-2$	$p = k$

After an easy calculation, we get

$$\begin{aligned} M_1^{\star\star}(G) = {} & k^2 + 2\sum_{p=k}^{2k-2} p^2 + 2(2k-1)^2 + \sum_{p=k}^{2k-3}\sum_{i=1}^{k-2} 2^i p^2 \\ & + \sum_{p=k+2,k>3}^{2k-2}\sum_{i=1}^{k-3}\left(2\left(2^i - 1\right)p^2\right) \\ & + (2k-1)^2\left(2\left(2^{k-2} - 1\right)\right) + (2k-2)^2 2^{k-1}. \end{aligned} \tag{42}$$

□

Theorem 10. *Consider the graph $G \cong XT(k)$ and $k \ge 3$, then the third Zagreb eccentricity index is equal to*

$$\begin{aligned} M_2^{\star}(G) = {} & 6k^2 + \sum_{p=k+1}^{2k-2}\sum_{i=1}^{k-2} 3\left(2^i - 1\right)p^2 \\ & + \sum_{p=k}^{2k-3}\sum_{i=1}^{k-2} p(p+1)\left(2\left(3\left(2^{i-1}\right) + 1\right)\right) \\ & + (2k-1)(2k-2)\left(2^{k-1} + 2\right) \\ & + (2k-1)^2\left(2\left(2^{k-2} - 1\right)\right). \end{aligned} \tag{43}$$

Proof. In order to prove the above result, we use the formula of the third Zagreb eccentricity index:

$$M_2^{\star}(G) = \sum_{uv \in E(G)} \varepsilon(u) \times \varepsilon(v). \tag{44}$$

By using Table 4, we get

$$\begin{aligned} M_2^{\star}(G) = {} & \sum_{p=k} (p)^2 \sum_{i=0} 6\left(2^i\right) + \sum_{i=1}^{k-2}\left(3\left(2^i - 1\right)\right) \sum_{p=k+1}^{2k-2} (p)^2 \\ & + \sum_{i=1}^{k-2}\left(2\left(3\left(2^{i-1}\right) + 1\right)\right) \sum_{p=k}^{2k-3} p(p+1) \\ & + \sum_{i=k-2}\left(2^{i+1} + 2\right) \sum_{p=k} (2p-2)(2p-1) \\ & + \sum_{i=k-2}\left(2\left(2^i - 1\right)\right) \sum_{p=k} (2p-1)(2p-1). \end{aligned} \tag{45}$$

After an easy calculation, we get

$$\begin{aligned} M_2^{\star}(G) = {} & 6k^2 + \sum_{p=k+1}^{2k-2}\sum_{i=1}^{k-2} 3\left(2^i - 1\right)p^2 \\ & + \sum_{p=k}^{2k-3}\sum_{i=1}^{k-2} p(p+1)\left(2\left(3\left(2^{i-1}\right) + 1\right)\right) \\ & + (2k-1)(2k-2)\left(2^{k-1} + 2\right) \\ & + (2k-1)^2\left(2\left(2^{k-2} - 1\right)\right). \end{aligned} \tag{46}$$

□

3. Conclusion

In this paper, we have computed the eccentricity-based topological indices such as the eccentric connectivity index, the total eccentricity index, and the first, second, and third Zagreb eccentricity index for certain interconnection networks such as a hypertree, sibling tree, and X-tree k-level. These results are useful in topological characterization of these important chemical networks.

Data Availability

The data used to support the findings of this study are included within the article.

Conflicts of Interest

The authors declare that there are no conflicts of interest regarding the publication of this paper.

Acknowledgments

This work was supported by the research foundation of Huainan Normal University (Grant no. 2019XJZD05) and UPAR grants of United Arab Emirates University (Grant nos. G00002590 and G00003271).

References

[1] S. Hayat and M. Imran, "Computation of topological indices of certain networks," *Applied Mathematics and Computation*, vol. 240, pp. 213–228, 2014.

[2] M. Imran, A. Q. Baig, and H. Ali, "On topological properties of dominating David derived networks," *Canadian Journal of Chemistry*, vol. 93, pp. 730–739, 2015.

[3] M. Imran, S. Hayat, and M. Y. H. Malik, "On topological indices of certain interconnection networks," *Applied Mathematics and Computation*, vol. 244, pp. 936–951, 2014.

[4] T. W. Haynes, S. M. Hedetniemi, S. T. Hedetniemi, and M. A. Henning, "Power domination in graphs applied to electrical power networks," *SIAM Journal on Discrete Mathematics*, vol. 15, no. 4, pp. 519–529, 2002.

[5] R. S. Rajana, J. Anithaa, and I. Rajasingha, "2-power domination in certain interconnection networks," *Procedia Computer Science*, vol. 57, pp. 738–744, 2015.

[6] V. Sharma, R. Goswami, and A. K. Madan, "Eccentric connectivity index: a novel highly discriminating topological descriptor for structure property and structure activity studies," *Journal of Chemical Information and Computer Sciences*, vol. 37, pp. 273–282, 1997.

[7] R. Farooq and M. Ali Malik, "On some eccentricity based topological indices of nanostar dendrimers," *Optoelectronics and advanced materials-rapid communications*, vol. 9, pp. 842–849, 2015.
[8] I. Gutman and N. Trinajstić, "Graph theory and molecular orbitals total φ-electron energy of alternant hydrocarbons," *Chemical Physics Letters*, vol. 17, no. 4, pp. 535–538, 1972.
[9] M. Ghorbani and M. A. Hosseinzadeh, "A new version of Zagreb indices," *Filomat*, vol. 26, no. 1, pp. 93–100, 2012.
[10] S. Hayat and M. Imran, "Computation of certain topological indices of nanotubes," *Journal of Computational and Theoretical Nanoscience*, vol. 12, no. 1, pp. 70–76, 2015.
[11] S. Hayat, M. A. Malik, and M. Imran, "Computing topological indices of honey-comb derived networks," *Romjist*, vol. 18, pp. 144–165, 2015.
[12] S. Hayat and M. Imran, "Computation of certain topological indices of nanotubes covered by $C_5$and C_7," *Journal of Computational and Theoretical Nanoscience*, vol. 12, pp. 533–541, 2015.
[13] S. Hayat and M. Imran, "On degree based topological indices of certain nanotubes," *Journal of Computational and Theoretical Nanoscience*, vol. 12, no. 8, pp. 1599–1605, 2015.
[14] F. F. Dragan and A. Brandstadt, "r-dominating cliques in graphs with hypertree structure," *Discrete Mathematics*, vol. 162, pp. 93–108, 1996.
[15] M. Baca, J. Horvathova, M. Mokrisova, and A. Suhanyiova, "On topological indices of fullerenes," *Applied Mathematics and Computation*, vol. 251, pp. 154–161, 2015.
[16] R. S. Rajan, I. Rajasingh, T. M. Rajalaxmi, and N. Parthiban, "Embedding of circulant networks into k-rooted sibiling trees," *International Journal of Pure and Applied Mathematics*, vol. 86, no. 6, pp. 1005–1012, 2013.

Hindawi
Journal of Chemistry
Volume 2020, Article ID 3838710, 10 pages
https://doi.org/10.1155/2020/3838710

Research Article

Multiplicative Valency-Based Descriptors for Silicon Carbides $Si_2C_3 - I[p, q]$, $Si_2C_3 - II[p, q]$, $Si_2C_3 - III[p, q]$, and $SiC_3 - III[p, q]$ in Drug Applications

Jin Xu,[1] **Nasir Javaid**,[2] **Shamas Bilal**,[2] **Muhammad Rafaqat**,[3] **and Iskander Tlili**[4,5]

[1]*Department of Applied Mathematics, Huainan Normal University, Huainan 232038, China*
[2]*Department of Mathematics, University of Sialkot, Lahore, Pakistan*
[3]*Department of Mathematics and Statistics, The University of Lahore, Lahore 54000, Pakistan*
[4]*Department for Management of Science and Technology Development, Ton Duc Thang University, Ho Chi Minh City, Vietnam*
[5]*Faculty of Applied Sciences, Ton Duc Thang University, Ho Chi Minh City, Vietnam*

Correspondence should be addressed to Iskander Tlili; iskander.tlili@tdtu.edu.vn

Received 20 October 2019; Revised 17 December 2019; Accepted 20 December 2019; Published 8 June 2020

Academic Editor: Jia-Bao Liu

Topological indices help us to collect information about algebraic graphs and give us a mathematical approach to understand the properties of algebraic structures. In literature, there are more than 148 topological indices, but none of them can completely describe all properties of chemical compounds. Together, they do it to some extent, so there is always room to define new topological indices. In this paper, we introduced the multiplicative version of Shingali and Kanabour indices and computed these indices for Silicon Carbides $Si_2C_3 - I[p, q]$, $Si_2C_3 - II[p, q]$, $Si_2C_3 - III[p, q]$, and $SiC_3 - III[p, q]$.

1. Introduction

In discrete mathematics, graph theory is not only the study of different properties of objects, but it also tells us about objects having the same properties as investigating objects [1]. These properties of different objects are of main interest. In particular, graph polynomials related to graph are rich in information. Mathematical tools like polynomials and topological based numbers have significant importance in collecting information about the properties of chemical compounds. We can find out much hidden information about compounds through these tools [2].

Actually, topological indices are numeric quantities that tell us about the whole structure of graph. There are many topological indices that help us to study physical, chemical reactivities, and biological properties [3–5]. Wiener, in 1947, firstly introduced the concept of the topological index while working on a boiling point [6]. In particular, Hosoya polynomial [7] plays an important role in the area of distance-based topological indices; we can find out Wiener index, hyper-Wiener index, and Tratch-stankevich-zefirove index by Hosoya polynomial [8]. In the whole paper, we take d_u a degree of vertex u which is equal to the number of vertices that are at a distance one from u.

Gutman and Trinajstić introduced the first and second Zagreb indices, which are defined as follows:

$$M_1(G) = \sum_{uv \in E(G)} (d_u + d_v),$$
$$M_2(G) = \sum_{uv \in E(G)} (d_u \times d_v), \tag{1}$$

respectively. Further details about these indices can be found in reference [9].

The modified Randić index is defined as follows:

$$R'(G) = \frac{1}{\max\{d_u, d_v\}}. \tag{2}$$

Shigehalli and Kanabur [9] introduced the following new degree-based topological indices. Arithmetic-Geometric index is defined as follows:

$$\mathrm{AG}_1 = \sum_{uv\in E(G)} \frac{d_u + d_v}{2\sqrt{d_u \times d_v}}. \tag{3}$$

Shigehalli and Kanabur indices are defined as follows:

$$\begin{aligned} \mathrm{SK}(G) &= \frac{d_u + d_v}{2}, \\ \mathrm{SK}_1(G) &= \frac{d_u \times d_v}{2}, \\ \mathrm{SK}_2(G) &= \left(\frac{d_u + d_v}{2}\right)^2. \end{aligned} \tag{4}$$

Our aim is to introduce the multiplicative version of Shigehalli and Kanabur indices and modify the Randić index. The multiplicative modified Randić index is defined as follows:

$$\mathrm{MR}'(G) = \prod_{uv\in E(G)} \frac{1}{\max\{d_u, d_v\}}. \tag{5}$$

The multiplicative version of Shigehalli and Kanabur indices and multiplicative Arithmetic-Geometric index are defined as follows:

$$\begin{aligned} \mathrm{MAG}_1 &= \prod_{uv\in E(G)} \frac{d_u + d_v}{2\sqrt{d_u \times d_v}}, \\ \mathrm{MSK}(G) &= \prod_{uv\in E(G)} \frac{d_u + d_v}{2}, \\ \mathrm{MSK}_1(G) &= \prod_{uv\in E(G)} \frac{d_u \times d_v}{2}, \\ \mathrm{MSK}_2(G) &= \prod_{uv\in E(G)} \left(\frac{d_u + d_v}{2}\right)^2. \end{aligned} \tag{6}$$

For detailed study about topological indices and their applications, we refer [10, 11] and references therein. It is a proven fact that topological indices help to predict many properties without going to the wet lab [12–17]. For example, the first and second Zagreb indices were found to happen for the calculation of the π-electron energy of dendrimers, the Randić index corresponds with boiling point, the atomic bond connectivity (ABC) index gives an exceptionally decent relationship to figuring the strain energy of dendrimers and augmented Zagreb index is a good tool to guess the heat of formation of dendrimers, etc. There are more than around about 148 topological indices, but none of them can completely describe all properties of a chemical compound. Therefore there is always room to define and study new topological indices. Redefined Zagreb indices are one step in this direction and are very close to Zagreb indices. Zagreb indices are very well studied by chemists and mathematicians due to their huge applications in chemistry [18–22].

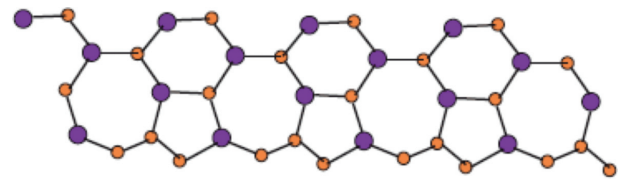

Figure 1: $\mathrm{Si_2C_3} - \mathrm{I}[4, 1]$.

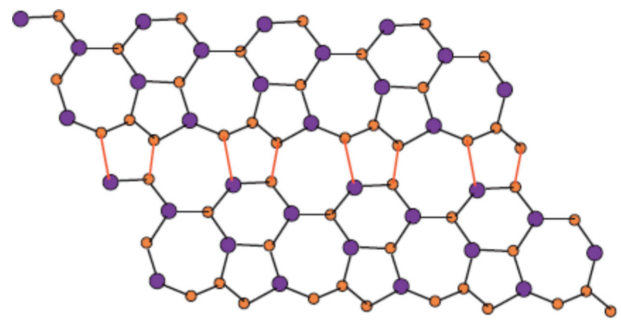

Figure 2: $\mathrm{Si_2C_3} - \mathrm{I}[4, 3]$.

In this paper, we aim to compute the above newly defined topological indices of Silicone Carbides $\mathrm{Si_2C_3} - \mathrm{I}[p, q]$, $\mathrm{Si_2C_3} - \mathrm{II}[p, q]$, $\mathrm{Si_2C_3} - \mathrm{III}[p, q]$, and $\mathrm{SiC_3} - \mathrm{III}[p, q]$.

2. Computational Results

In this section, we give our main results.

2.1. Multiplicative Shingali and Kanabour Indices for $Si_2C_3 - I[p, q]$. In order to describe the molecular graph of $\mathrm{Si_2C_3} - \mathrm{I}$, we have set this way. We define p as the number of connected units in a row (chain) and p as the number of connected rows, the number of p cells per connection. In Figures 1 and 2, we demonstrate how cells are connected in one row (chain) and how one row is connected to another row. For $\mathrm{Si_2C_3} - \mathrm{I}[p, q]$, $V(\mathrm{Si_2C_3} - \mathrm{I}[p, q]) = 10pq$ and $E(\mathrm{Si_2C_3} - \mathrm{I}[p, q]) = 15pq - 2p - 3q$.

The degree-based edge partition of $\mathrm{Si_2C_3} - \mathrm{I}$ is given in Table 1, which can be obtained easily by counting methods form Figures 1 and 2.

Theorem 1. *Let $Si_2C_3 - I[p, q]$ be Silicon Carbide. Then, we have the following:*

(1) $M\chi(Si_2C_3 - I[p, q]) = (1/20)\sqrt{10}(p + 2q)3((2p - 3) + 8q)(3p(5q - 3) - 13q + 7)$

(2) $MR'(Si_2C_3 - I[p, q]) = (1/108)(p + 2q)(3(2p - 3) + 8q)(3p(5q - 3) - 13q + 7)$

(3) $MAG_1(Si_2C_3 - I[p, q]) = (5/4)(p + 2q)(3(2p - 3) + 8q)(3p(5q - 3) - 13q + 7)$

(4) $MSK(Si_2C_3 - I[p, q]) = 45(p + 2q)(3(2p - 3) + 8q)(3p(5q - 3) - 13q + 7)$

(5) $MSK_1(Si_2C_3 - I[p, q]) = (81/2)(p + 2q)(3(2p - 3) + 8q)(3p(5q - 3) - 13q + 7)$

(6) $MSK_2(Si_2C_3 - I[p, q]) = 2025(p + 2q)(3(2p - 3) + 8q)(3p(5q - 3) - 13q + 7)$

Proof.

$$
\begin{aligned}
M\chi(\mathrm{Si_2C_3-I}[p,q]) &= \left(\frac{1}{\sqrt{1+2}}\right)(1)\times\left(\frac{1}{\sqrt{1+3}}\right)(1)\times\left(\frac{1}{\sqrt{2+2}}\right)(p+2q)\\
&\quad\times\left(\frac{1}{\sqrt{2+3}}\right)(p+2q)\times\left(\frac{1}{\sqrt{3+3}}\right)(3p(5q-3)-13q+7)\\
&= \frac{1}{20}\sqrt{10}(p+2q)(3(2p-3)+8q)(3p(5q-3)-13q+7),\\
\mathrm{MR}'(\mathrm{Si_2C_3-I}[p,q]) &= \prod_{uv\in E(\mathrm{Si_2C_3-I}[p,q])}\frac{1}{\max\{d_u,d_v\}}\\
&= \left(\frac{1}{2}\right)(1)\times\left(\frac{1}{3}\right)(1)\times\left(\frac{1}{1}\right)(p+2q)\\
&\quad\times\left(\frac{1}{3}\right)(3(2p-3)+8q)\times\left(\frac{1}{3}\right)(3p(5q-3)-13q+7)\\
&= \frac{1}{108}(p+2q)(3(2p-3)+8q)(3p(5q-3)-13q+7),\\
\mathrm{MAG_1}(\mathrm{Si_2C_3-I}[p,q]) &= \prod_{uv\in E(\mathrm{Si_2C_3-I}[p,q])}\frac{d_u+d_v}{2\sqrt{d_u\times d_v}}\\
&= \left(\frac{1+2}{2\sqrt{1\times 2}}\right)(1)\times\left(\frac{1+3}{2\sqrt{1\times 3}}\right)(1)\times\left(\frac{2+2}{2\sqrt{2\times 2}}\right)(p+2q)\\
&\quad\times\left(\frac{2+3}{2\sqrt{2\times 3}}\right)(3(2p-3)+8q)\times\left(\frac{3+3}{2\sqrt{3\times 3}}\right)(3p(5q-3)-13q+7)\\
&= \frac{5}{4}(p+2q)(3(2p-3)+8q)(3p(5q-3)-13q+7),\\
\mathrm{MSK}(\mathrm{Si_2C_3-I}[p,q]) &= \prod_{uv\in E(\mathrm{Si_2C_3-I}[p,q])}\frac{d_u+d_v}{2}\\
&= \left(\frac{1+2}{2}\right)(1)\times\left(\frac{1+3}{2}\right)(1)\times\left(\frac{2+2}{2}\right)(p+2q)\\
&\quad\times\left(\frac{2+3}{2}\right)(3(2p-3)+8q)\times\left(\frac{3+3}{2}\right)(3p(5q-3)-13q+7)\\
&= 45(p+2q)(3(2p-3)+8q)(3p(5q-3)-13q+7),\\
\mathrm{MSK_1}(\mathrm{Si_2C_3-I}[p,q]) &= \prod_{uv\in E(\mathrm{Si_2C_3-I}[p,q])}\frac{d_u\times d_v}{2}\\
&= \left(\frac{1\times 2}{2}\right)(1)\times\left(\frac{1\times 3}{2}\right)(1)\times\left(\frac{2\times 2}{2}\right)(p+2q)\\
&\quad\times\left(\frac{2\times 3}{2}\right)(3(2p-3)+8q)\times\left(\frac{3\times 3}{2}\right)(3p(5q-3)-13q+7)\\
&= \frac{81}{2}(p+2q)(3(2p-3)+8q)(3p(5q-3)-13q+7),\\
\mathrm{MSK_2}(\mathrm{Si_2C_3-I}[p,q]) &= \prod_{uv\in E(\mathrm{Si_2C_3-I}[p,q])}\left(\frac{d_u+d_v}{2}\right)^2\\
&= \left(\frac{1+2}{2}\right)^2(1)\times\left(\frac{1+3}{2}\right)^2(1)\times\left(\frac{2+2}{2}\right)^2(p+2q)\\
&\quad\times\left(\frac{2+3}{2}\right)^2(3(2p-3)+8q)\times\left(\frac{3+3}{2}\right)^2(3p(5q-3)-13q+7)\\
&= 2025(p+2q)(3(2p-3)+8q)(3p(5q-3)-13q+7).
\end{aligned}
\tag{7}
$$

□

Table 1: Partition of $E(\mathrm{Si_2C_3}-\mathrm{I}[p,q])$.

(d_u, d_v)	Frequency
(1, 2)	1
(1, 3)	1
(2, 2)	$p+2q$
(2, 3)	$6p-1+8\ (q-1)$
(3, 3)	$3p\ (5q-3)-13q+7$

2.2. Multiplicative Shingali and Kanabour Indices for $Si_2C_3-II[p,q]$. In order to describe the molecular graph of $\mathrm{Si_2C_3}-\mathrm{II}[p,q]$, we denote p as the number of unit cells connected in a row (chain) and q denotes the number of connected rows, the number of rows per connection. In Figures 3 and 4, we demonstrate how cells are connected in a row (chain) and how a row is connected to another row. For $\mathrm{Si_2C_3}-\mathrm{II}[p,q]$, $V(\mathrm{Si_2C_3}-\mathrm{II}[p,q]) = 8pq$ and $E(\mathrm{Si_2C_3}-\mathrm{II}[p,q]) = 15pq-3p-3q$.

The degree-based edge partition of $\mathrm{Si_2C_3}-\mathrm{II}$, is given in Table 2.

Theorem 2. *Let $Si_2C_3-II[p,q]$ be Silicon Carbides. Then, we have the following:*

(1) $M\chi(Si_2C_3-II[p,q]) = (1/15)\sqrt{10}(p+q)(4p+4q-7)(15pq-13(p+q)+11)$

(2) $MR'(Si_2C_3-II[p,q]) = (2/27)\sqrt{10}(p+q)(4p+4q-7)(15pq-13(p+q)+11)$

(3) $MAG_1(Si_2C_3-II[p,q]) = 10(p+q)(4p+4q-7)(15pq-13(p+q)+11)$

(4) $MSK(Si_2C_3-II[p,q]) = 360(p+q)(4p+4q-7)(15pq-13(p+q)+11)$

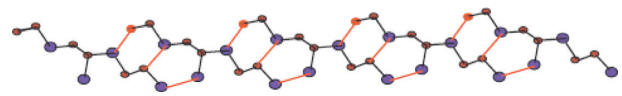

Figure 3: $\mathrm{Si_2C_3}-\mathrm{II}[5,1]$.

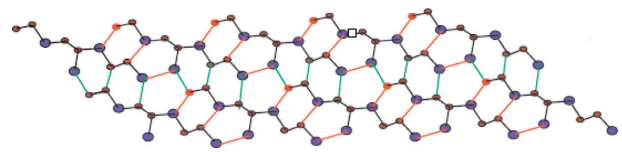

Figure 4: $\mathrm{Si_2C_3}-\mathrm{II}[5,2]$.

Table 2: Partition of $E(\mathrm{Si_2C_3}-\mathrm{II}[p,q])$.

(d_u, d_v)	Frequency
(1, 2)	2
(1, 3)	1
(2, 2)	$2\ (p+q)$
(2, 3)	$2\ (4p+4q-7)$
(3, 3)	$15pq-13\ (p+q)+11$

(5) $MSK_1(Si_2C_3-II[p,q]) = 324(p+q)(4p+4q-7)(15pq-13(p+q)+11)$

(6) $MSK_2(Si_2C_3-II[p,q]) = 7200(p+q)(4p+4q-7)(15pq-13(p+q)+11)$

Proof

$$M\chi(\mathrm{Si_2C_3}-\mathrm{II}[p,q]) = \prod_{uv\in E(\mathrm{Si_2C_3}-\mathrm{II}[p,q])} \frac{1}{\sqrt{d_u+d_v}}$$

$$= \left(\frac{1}{\sqrt{1+2}}\right)(2)\times\left(\frac{1}{\sqrt{1+3}}\right)(1)\times\left(\frac{1}{\sqrt{2+2}}\right)(2(p+q))$$

$$\times\left(\frac{1}{\sqrt{2+3}}\right)(2(4p+4q-7))\times\left(\frac{1}{\sqrt{3+3}}\right)(15pq-13(p+q)+11)$$

$$= \frac{1}{15}\sqrt{10}(p+q)(4p+4q-7)(15pq-13(p+q)+11),$$

$$\mathrm{MR}'(\mathrm{Si_2C_3}-\mathrm{II}[p,q]) = \prod_{uv\in E(\mathrm{Si_2C_3}-\mathrm{II}[p,q])} \frac{1}{\max\{d_u,d_v\}}$$

$$= \left(\frac{1}{2}\right)(2)\times\left(\frac{1}{3}\right)(1)\times\left(\frac{1}{1}\right)(2(p+q))$$

$$\times\left(\frac{1}{3}\right)(2(4p+4q-7))\times\left(\frac{1}{3}\right)(15pq-13(p+q)+11)$$

$$= \frac{2}{27}\sqrt{10}(p+q)(4p+4q-7)(15pq-13(p+q)+11),$$

$$\begin{aligned}
\mathrm{MAG}_1(\mathrm{Si}_2\mathrm{C}_3-\mathrm{II}[p,q]) &= \sum_{uv\in E(\mathrm{Si}_2\mathrm{C}_3-\mathrm{II}[p,q])} \frac{d_u+d_v}{2\sqrt{d_u\times d_v}} \\
&= \left(\frac{1+2}{2\sqrt{1\times 2}}\right)(2)\times\left(\frac{1+3}{2\sqrt{1\times 3}}\right)(1)\times\left(\frac{2+2}{2\sqrt{2\times 2}}\right)(2(p+q)) \\
&\quad\times\left(\frac{2+3}{2\sqrt{2\times 3}}\right)(2(4p+4q-7))\times\left(\frac{3+3}{2\sqrt{3\times 3}}\right)(15pq-13(p+q)+11) \\
&= 10(p+q)(4p+4q-7)(15pq-13(p+q)+11), \\
\mathrm{MSK}(\mathrm{Si}_2\mathrm{C}_3-\mathrm{II}[p,q]) &= \sum_{uv\in E(\mathrm{Si}_2\mathrm{C}_3-\mathrm{II}[p,q])} \frac{d_u+d_v}{2} \\
&= \left(\frac{1+2}{2}\right)(2)\times\left(\frac{1+3}{2}\right)(1)\times\left(\frac{2+2}{2}\right)(2(p+q)) \\
&\quad\times\left(\frac{2+3}{2}\right)(2(4p+4q-7))\times\left(\frac{3+3}{2}\right)(15pq-13(p+q)+11) \\
&= 360(p+q)(4p+4q-7)(15pq-13(p+q)+11), \\
\mathrm{MSK}_1(\mathrm{Si}_2\mathrm{C}_3-\mathrm{II}[p,q]) &= \sum_{uv\in E(\mathrm{Si}_2\mathrm{C}_3-\mathrm{II}[p,q])} \frac{d_u\times d_v}{2} \\
&= \left(\frac{1\times 2}{2}\right)(2)\times\left(\frac{1\times 3}{2}\right)(1)\times\left(\frac{2\times 2}{2}\right)(2(p+q)) \\
&\quad\times\left(\frac{2.\times 3}{2}\right)(2(4p+4q-7))\times\left(\frac{3\times 3}{2}\right)(15pq-13(p+q)+11) \\
&= 324(p+q)(4p+4q-7)(15pq-13(p+q)+11), \\
\mathrm{MSK}_2(\mathrm{Si}_2\mathrm{C}_3-\mathrm{II}[p,q]) &= \sum_{uv\in E(\mathrm{Si}_2\mathrm{C}_3-\mathrm{II}[p,q])} \left(\frac{d_u+d_v}{2}\right)^2 \\
&= \left(\frac{1+2}{2}\right)^2(2)\times\left(\frac{1+3}{2}\right)^2(1)\times\left(\frac{2+2}{2}\right)^2(2(p+q)) \\
&\quad\times\left(\frac{2+3}{2}\right)^2(2(4p+4q-7))\times\left(\frac{3+3}{2}\right)^2(15pq-13(p+q)+11) \\
&= 7200(p+q)(4p+4q-7)(15pq-13(p+q)+11).
\end{aligned} \tag{8}$$

□

2.3. Multiplicative Shingali and Kanabour Indices for $Si_2C_3-III[p,q]$. The 2D molecular graph of Silicon Carbide $\mathrm{Si}_2\mathrm{C}_3-\mathrm{III}$ is given in Figures 5 and 6. We can define the molecular graph in this way, where p represents the unit cell in a row and q represented the number of connected rows. For $\mathrm{Si}_2\mathrm{C}_3-\mathrm{III}[p,q]$, $V(\mathrm{Si}_2\mathrm{C}_3-\mathrm{III}[p,q])=10pq$ and $E(\mathrm{Si}_2\mathrm{C}_3-\mathrm{III}[p,q])=15pq-2p-3q$.

The degree-based edge partition of $\mathrm{Si}_2\mathrm{C}_3-\mathrm{III}$ is given in Table 3.

Theorem 3. *Let $Si_2C_3-III[p,q]$ be Silicon Carbides. Then, we have the following:*

(1) $M\chi(Si_2C_3-III[p,q]) = (2/15)\sqrt{30}(p+1)(2(p+q)-3)(5p(3q-2)-13q+8)$

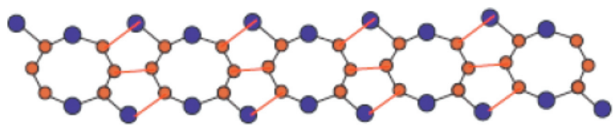

Figure 5: $Si_2C_3 - III[5,1]$.

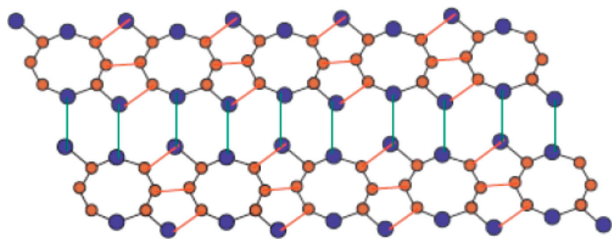

Figure 6: $Si_2C_3 - III[5,2]$.

Table 3: Partition of $E(Si_2C_3 - III[p,q])$.

(d_u, d_v)	Frequency
(1, 3)	2
(2, 2)	$2p+2$
(2, 3)	$4\ (2p+2q-3)$
(3, 3)	$5p\ (3q-2)-13q+8$

(2) $MR'(Si_2C_3 - III[p,q]) = (8/27)(p+1)(2(p+q)-3)(5p(3q-2)-13q+8)$

(3) $MAG_1(Si_2C_3 - III[p,q]) = (40/3)\sqrt{2}(p+1)(2(p+q)-3)(5p(3q-2)-13q+8)$

(4) $MSK(Si_2C_3 - III[p,q]) = 480(p+1)(2(p+q)-3)(5p(3q-2)-13q+8)$

(5) $MSK_1(Si_2C_3 - III[p,q]) = 648(p+1)(2(p+q)-3)(5p(3q-2)-13q+8)$

(6) $MSK_2(Si_2C_3 - III[p,q]) = 14400(p+1)(2(p+q)-3)(5p(3q-2)-13q+8)$

Proof.

$$
\begin{aligned}
M\chi(\mathrm{Si_2C_3} - \mathrm{III}[p,q]) &= \prod_{uv\in E(\mathrm{Si_2C_3}-\mathrm{III}[p,q])} \frac{1}{\sqrt{d_u + d_v}} \\
&= \left(\frac{1}{\sqrt{1+3}}\right)(2) \times \left(\frac{1}{\sqrt{2+2}}\right)(2p+2) \\
&\quad \times \left(\frac{1}{\sqrt{2+3}}\right)(4(2p+2q-3)) \times \left(\frac{1}{\sqrt{3+3}}\right)(5p(3q-2)-13q+8) \\
&= \frac{2}{15}\sqrt{30}(p+1)(2(p+q)-3)(5p(3q-2)-13q+8),
\end{aligned}
$$

$$
\begin{aligned}
\mathrm{MR}'(\mathrm{Si_2C_3} - \mathrm{III}[p,q]) &= \prod_{uv\in E(\mathrm{Si_2C_3}-\mathrm{III}[p,q])} \frac{1}{\max\{d_u, d_v\}} \\
&= \left(\frac{1}{3}\right)(2) \times \left(\frac{1}{1}\right)(2p+2) \\
&\quad \times \left(\frac{1}{3}\right)(4(2p+2q-3)) \times \left(\frac{1}{3}\right)(5p(3q-2)-13q+8) \\
&= \frac{8}{27}(p+1)(2(p+q)-3)(5p(3q-2)-13q+8),
\end{aligned}
$$

$$\begin{aligned}
\mathrm{MAG}_1(\mathrm{Si}_2\mathrm{C}_3-\mathrm{III}[p,q]) &= \prod_{uv\in E(\mathrm{Si}_2\mathrm{C}_3-\mathrm{III}[p,q])} \frac{d_u+d_v}{2\sqrt{d_u\times d_v}} \\
&= \left(\frac{1+3}{2\sqrt{1\times 3}}\right)(2)\times\left(\frac{2+2}{2\sqrt{2\times 2}}\right)(2p+2) \\
&\quad\times\left(\frac{2+3}{2\sqrt{2\times 3}}\right)(4(2p+2q-3))\times\left(\frac{3+3}{2\sqrt{3\times 3}}\right)(5p(3q-2)-13q+8) \\
&= \frac{40}{3}\sqrt{2}(p+1)(2(p+q)-3)(5p(3q-2)-13q+8), \\
\mathrm{MSK}(\mathrm{Si}_2\mathrm{C}_3-\mathrm{III}[p,q]) &= \prod_{uv\in E(\mathrm{Si}_2\mathrm{C}_3-\mathrm{III}[p,q])} \frac{d_u+d_v}{2} \\
&= \left(\frac{1+3}{2}\right)(2)\times\left(\frac{2+2}{2}\right)(2p+2)\times\left(\frac{2+3}{2}\right)(4(2p+2q-3))\times\left(\frac{3+3}{2}\right)(5p(3q-2)-13q+8) \\
&= 480(p+1)(2(p+q)-3)(5p(3q-2)-13q+8), \\
\mathrm{MSK}_1(\mathrm{Si}_2\mathrm{C}_3-\mathrm{III}[p,q]) &= \prod_{uv\in E(\mathrm{Si}_2\mathrm{C}_3-\mathrm{III}[p,q])} \frac{d_u\times d_v}{2} \\
&= \left(\frac{1.3}{2}\right)(2)\times\left(\frac{2.2}{2}\right)(2p+2) \\
&\quad\times\left(\frac{2.3}{2}\right)(4(2p+2q-3))\times\left(\frac{3.3}{2}\right)(5p(3q-2)-13q+8) \\
&= 648(p+1)(2(p+q)-3)(5p(3q-2)-13q+8), \\
\mathrm{MSK}_2(\mathrm{Si}_2\mathrm{C}_3-\mathrm{III}[p,q]) &= \prod_{uv\in E(\mathrm{Si}_2\mathrm{C}_3-\mathrm{III}[p,q])} \left(\frac{d_u+d_v}{2}\right)^2 \\
&= \left(\frac{1+3}{2}\right)^2(2)\times\left(\frac{2+2}{2}\right)^2(2p+2) \\
&\quad\times\left(\frac{2+3}{2}\right)^2(4(2p+2q-3))\times\left(\frac{3+3}{2}\right)^2(5p(3q-2)-13q+8) \\
&= 14400(p+1)(2(p+q)-3)(5p(3q-2)-13q+8).
\end{aligned} \tag{9}$$

□

2.4. Multiplicative Shingali and Kanabour Indices for $SiC_3-III[p,q]$. Figures 7 and 8 represented the algebraic graphs of Silicon Carbide $\mathrm{SiC}_3-\mathrm{III}[p,q]$ for different values of p and q, and with the help of these structures, we gave a demonstration of how the cells connect in a row (chain) and how one row connects to another row. For $\mathrm{SiC}_3-\mathrm{III}[p,q]$, $V(\mathrm{SiC}_3-\mathrm{III}[p,q])=8pq$ and $E(\mathrm{SiC}_3-\mathrm{III}[p,q])=12pq-3p-2q$.

The degree-based edge partition of $\mathrm{SiC}_3-\mathrm{III}$ is given in Table 4.

Theorem 4. *Let $SiC_3-III[p,q]$ be Silicon Carbides. Then, we have the following:*

(1) $M\chi(SiC_3-III[p,q]) = (2/15)\sqrt{10}(3p+2q-3)(3p+2q-4)(3pq-3p-2q+2)$

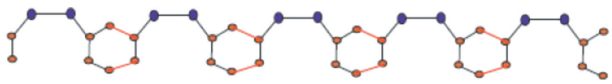

Figure 7: $SiC_3 - III[5,1]$.

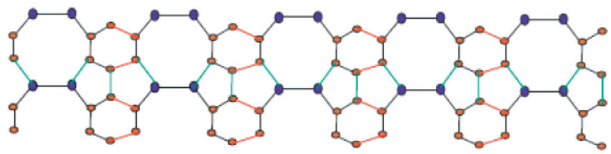

Figure 8: $SiC_3 - III[5,1]$.

Table 4: Partition of $E(SiC_3 - III[p,q])$.

(d_u, d_v)	Frequency
(1, 2)	2
(1, 3)	1
(2, 2)	$3p+2q-3$
(2, 3)	$2\ (3p+2q-4)$
(3, 3)	$4\ (3pq-3p-2q+2)$

(2) $MR'(SiC_3 - III[p,q]) = (4/27)(3p+2q-3)(3p+2q-4)(3pq-3p-2q+2)$

(3) $MAG_1(SiC_3 - III[p,q]) = 20(3p+2q-3)(3p+2q-4)(3pq-3p-2q+2)$

(4) $MSK(SiC_3 - III[p,q]) = 720(3p+2q-3)(3p+2q-4)(3pq-3p-2q+2)$

(5) $MSK_1(SiC_3 - III[p,q]) = 14400(3p+2q-3)(3p+2q-4)(3pq-3p-2q+2)$

(6) $MSK_2(SiC_3 - III[p,q]) = 32400(3p+2q-3)(3p+2q-4)(3pq-3p-2q+2)$

Proof.

$$M\chi(\mathrm{SiC}_3 - \mathrm{III}[p,q]) = \prod_{uv\in E(\mathrm{SiC}_3-\mathrm{III}[p,q])} \frac{1}{\sqrt{d_u+d_v}}$$

$$= \left(\frac{1}{\sqrt{1+2}}\right)(2)\times\left(\frac{1}{\sqrt{1+3}}\right)(1)\times\left(\frac{1}{\sqrt{2+2}}(3p+2q-3)\right)$$

$$\times\left(\frac{1}{\sqrt{2+3}}\right)(2(3p+2q-4))\times\left(\frac{1}{\sqrt{3+3}}\right)(4(3pq-3p-2q+2))$$

$$= \frac{2}{15}\sqrt{10}(3p+2q-3)(3p+2q-4)(3pq-3p-2q+2),$$

$$\mathrm{MR}'(\mathrm{SiC}_3 - \mathrm{III}[p,q]) = \prod_{uv\in E(\mathrm{SiC}_3-\mathrm{III}[p,q])} \frac{1}{\max\{d_u,d_v\}}$$

$$= \left(\frac{1}{2}\right)(2)\times\left(\frac{1}{3}\right)(1)\times\left(\frac{1}{1}\right)(3p+2q-3)$$

$$\times\left(\frac{1}{3}\right)(2(3p+2q-4))\times\left(\frac{1}{3}\right)(4(3pq-3p-2q+2))$$

$$= \frac{4}{27}(3p+2q-3)(3p+2q-4)(3pq-3p-2q+2),$$

$$\mathrm{MAG}_1(\mathrm{SiC}_3 - \mathrm{III}[p,q]) = \prod_{uv\in E(\mathrm{SiC}_3-\mathrm{III}[p,q])} \frac{d_u+d_v}{2\sqrt{d_u\times d_v}}$$

$$= \left(\frac{1+2}{2\sqrt{1\times 2}}\right)(2)\times\left(\frac{1+3}{2\sqrt{1\times 3}}\right)(1)\times\left(\frac{2+2}{2\sqrt{2\times 2}}\right)(3p+2q-3)$$

$$\times\left(\frac{2+3}{2\sqrt{2.\times 3}}\right)(2(3p+2q-4))\times\left(\frac{3+3}{2\sqrt{3\times 3}}\right)(4(3pq-3p-2q+2))$$

$$=20(3p+2q-3)(3p+2q-4)(3pq-3p-2q+2),$$

$$\begin{aligned}
\mathrm{MSK}(\mathrm{SiC}_3-\mathrm{III}[p,q]) &= \prod_{uv\in E(\mathrm{SiC}_3-\mathrm{III}[p,q])}\frac{d_u+d_v}{2}\\
&=\left(\frac{1+2}{2}\right)(2)\times\left(\frac{1+3}{2}\right)(1)\times\left(\frac{2+2}{2}\right)(3p+2q-3)\\
&\quad\times\left(\frac{2+3}{2}\right)(2(3p+2q-4))\times\left(\frac{3+3}{2}\right)(4(3pq-3p-2q+2))\\
&=720(3p+2q-3)(3p+2q-4)(3pq-3p-2q+2),\\
\mathrm{MSK}_1(\mathrm{SiC}_3-\mathrm{III}[p,q]) &= \prod_{uv\in E(\mathrm{SiC}_3-\mathrm{III}[p,q])}\frac{d_u\times d_v}{2}\\
&=\left(\frac{1\times 2}{2}\right))(2)\times\left(\frac{1\times 3}{2}\right)(1)\times\left(\frac{2\times 2}{2}\right)(3p+2q-3)\\
&\quad\times\left(\frac{2\times 3}{2}\right)(2(3p+2q-4))\times\left(\frac{3\times 3}{2}\right)(4(3pq-3p-2q+2))\\
&=14400(3p+2q-3)(3p+2q-4)(3pq-3p-2q+2),\\
\mathrm{MSK}_2(\mathrm{SiC}_3-\mathrm{III}[p,q]) &= \sum_{uv\in E(\mathrm{SiC}_3-\mathrm{III}[p,q])}\left(\frac{d_u+d_v}{2}\right)^2\\
&=\left(\frac{1+2}{2}\right)^2(2)\times\left(\frac{1+3}{2}\right)^2(1)\times\left(\frac{2+2}{2}\right)^2(3p+2q-3)\\
&\quad\times\left(\frac{2+3}{2}\right)^2(2(3p+2q-4))\times\left(\frac{3+3}{2}\right)^2(4(3pq-3p-2q+2)\\
&=32400(3p+2q-3)(3p+2q-4)(3pq-3p-2q+2).
\end{aligned}\tag{10}$$

□

3. Conclusion

In this paper, we have introduced some new multiplicative degree-based indices. We also computed the newly introduced indices for Silicone Carbides $\mathrm{Si}_2\mathrm{C}_3-\mathrm{I}[p,q]$, $\mathrm{Si}_2\mathrm{C}_3-\mathrm{II}[p,q]$, $\mathrm{Si}_2\mathrm{C}_3-\mathrm{III}[p,q]$, and $\mathrm{SiC}_3-\mathrm{III}[p,q]$. Our results are applicable in chemistry, physics, and other applied sciences.

4. Future Directions

To compute distance-based indices and polynomials of understudy Silicone Carbides is an interesting problem for the researchers.

Data Availability

The data used to support the findings of this study are included within the article.

Conflicts of Interest

The authors declare that they have no conflicts of interest.

Authors' Contributions

All authors have an equal contribution.

Acknowledgments

This work was jointly supported by the Key Natural Science Research Projects in Anhui Universities (KJ2019A0696).

References

[1] N. Ali, M. A. Umar, M. A. Umar, A. Tabassum, and A. Raheem, "Super (a, d)-C3-antimagicness of a corona graph," *Open Journal of Mathematical Sciences*, vol. 2, no. 1, pp. 371–378, 2018.

[2] M. K. Jamil, M. R. Farahani, M. Imran, and M. Ali Malik, "Computing eccentric version of second zagreb index of polycyclic aromatic hydrocarbons (PAHk)," *Applied Mathematics and Nonlinear Sciences*, vol. 1, no. 1, pp. 247–252, 2016.

[3] D. Amić and D. Bes, lo, B. Lucic, S. Nikolic, and N. Trinajstic, The vertex-connectivity index revisited," *Journal of Chemical Information and Computer Sciences*, vol. 38, no. 5, pp. 819–822, 1998.

[4] B. Bollobás and P. Erd, os, Graphs of extremal weights," *Ars Combinatoria*, vol. 50, pp. 225–233, 1998.

[5] F. M. Brückler, T. Došlić, A. Graovac, and I. Gutman, "On a class of distance-based molecular structure descriptors," *Chemical Physics Letters*, vol. 503, no. 4–6, pp. 336–338, 2011.

[6] H. Wiener, "Structural determination of paraffin boiling points," *Journal of the American Chemical Society*, vol. 69, no. 1, pp. 17–20, 1947.

[7] H. Hosoya, "On some counting polynomials in chemistry," *Discrete Applied Mathematics*, vol. 19, pp. 239–257, 1998.

[8] L. Kier, *Molecular Connectivity in Chemistry and Drug Research*, Vol. 10, Elsevier, Amsterdam, Netherlands, 1999.

[9] V. S. Shigehalli and R. Kanabur, "Computation of new degree-based topological indices of graphene," *Journal of Nanomaterials*, vol. 2016, Article ID 4341919, 6 pages, 2016.

[10] G. Caporossi, I. Gutman, P. Hansen, and L. Pavlović, "Graphs with maximum connectivity index," *Computational Biology and Chemistry*, vol. 27, no. 1, pp. 85–90, 2003.

[11] H. Deng, J. Yang, and F. Xia, "A general modeling of some vertex-degree based topological indices in benzenoid systems and phenylenes," *Computers & Mathematics with Applications*, vol. 61, no. 10, pp. 3017–3023, 2011.

[12] B. Basavanagoud, W. Gao, S. Patil, V. R. Desai, K. G. Mirajkar, and B. Pooja, "Computing first zagreb index and F-index of new C-products of graphs," *Applied Mathematics and Nonlinear Sciences*, vol. 2, no. 1, pp. 285–298, 2017.

[13] V. Lokesha, T. Deepika, P. S. Ranjini, and I. N. Cangul, "Operations of nanostructures via sdd, ABC4 and GA5 indices," *Applied Mathematics and Nonlinear Sciences*, vol. 2, no. 1, pp. 173–180, 2017.

[14] S. M. Hosamani, B. B. Kulkarni, R. G. Boli, and V. M. Gadag, "QSPR analysis of certain graph theocratical matrices and their corresponding energy," *Applied Mathematics and Nonlinear Sciences*, vol. 2, no. 1, pp. 131–150, 2017.

[15] M. S. Sardar, S. Zafar, and Z. Zahid, "Computing topological indices of the line graphs of banana tree graph and firecracker graph," *Applied Mathematics and Nonlinear Sciences*, vol. 2, no. 1, pp. 83–92, 2017.

[16] B. Basavanagoud, V. R. Desai, and S. Patil, "(β, α)–connectivity index of graphs," *Applied Mathematics and Nonlinear Sciences*, vol. 2, no. 1, pp. 21–30, 2017.

[17] H. S. Ramane and R. B. Jummannaver, "Note on forgotten topological index of chemical structure in drugs," *Applied Mathematics and Nonlinear Sciences*, vol. 1, no. 2, pp. 369–374, 2016.

[18] J.-B. Liu, C. Wang, S. Wang, and B. Wei, "Zagreb indices and multiplicative zagreb indices of eulerian graphs," *Bulletin of the Malaysian Mathematical Sciences Society*, vol. 42, no. 1, pp. 67–78, 2019.

[19] J.-B. Liu, X.-F. Pan, F.-T. Hu, and F.-F. Hu, "Asymptotic laplacian-energy-like invariant of lattices," *Applied Mathematics and Computation*, vol. 253, pp. 205–214, 2015.

[20] J.-B. Liu and X.-F. Pan, "Minimizing kirchhoff index among graphs with a given vertex bipartiteness," *Applied Mathematics and Computation*, vol. 291, pp. 84–88, 2016.

[21] H. Liu, Y. Pan, and J. Cao, "Composite learning adaptive dynamic surface control of fractional-order nonlinear systems," *IEEE Transactions on Cybernetics*, vol. 50, no. 6, pp. 2557–2567, 2020.

[22] H. Liu, H. Wang, J. Cao, A. Alsaedi, and T. Hayat, "Composite learning adaptive sliding mode control of fractional-order nonlinear systems with actuator faults," *Journal of the Franklin Institute*, vol. 356, no. 16, pp. 9580–9599, 2019.

Hindawi
Journal of Chemistry
Volume 2020, Article ID 8453405, 8 pages
https://doi.org/10.1155/2020/8453405

Research Article

Large Data Technology-Based Analysis Method of Sudden Eco-Environmental Toxic Pollution

Guilan He[1] **and Junping Yao**[2]

[1]*School of Artificial Intelligence and Big Data, Chongqing College of Electronic Engineering, Chongqing, China*
[2]*School of Electronic and Information Engineering, Chongqing Radio & TV University, Chongqing, China*

Correspondence should be addressed to Guilan He; heguilan83@163.com

Received 1 November 2019; Accepted 24 December 2019; Published 2 June 2020

Academic Editor: Jia-Bao Liu

Sudden environmental toxic pollution accidents occur from time to time at home and abroad, seriously affecting the safety of the ecological environment. Different environmental factors affect the use of manual inspection and analysis methods, causing inaccurate results of inspection and analysis. In view of this problem, a large data technology-based analysis of sudden ecological environmental toxic pollution is proposed. *Method*. The genome and proteome in different environments were analyzed, and the target organisms were strictly defined to determine the effect of the molecular toxicity of pollution factors on the ecological environment. According to the molecular toxicity, the sudden eco-environmental toxicity pollution was analyzed using large data technology. Under the action of different particle sizes, dosages, and adsorption times of activated carbon, the experiments confirmed that the results of large data technology analysis are more accurate, which have provided necessary means for the protection of the ecological environment.

1. Introduction

Recently, sudden environmental toxic pollution accidents have occurred in China from time to time, seriously affecting China's economic development and people's daily life [1]. The research on this issue has become a front-burner issue in the field of environmental protection in China. Sudden ecological environmental toxic pollution indicates that water quality in the water protection area is polluted instantaneously by sudden pollutant leakage, which seriously threatens the safety of water source area [2]. The main reasons for this sudden pollution include illegal discharge of conventional pollution sources, entry of urban and rural nonpoint source pollution into river ways by rain wash, oil spill, abrupt change of water quality, abrupt change of climate, and man-made poisoning [3]. Sudden pollution phenomena are mainly reflected in water pollution; its uncertainties of occurrence, development, and harm cause serious water quality safety and ecological safety problems in China; frequent environmental pollution accidents are caused by chemicals, uncertainty of emergency objects, and so on, which not only brings huge economic loss but also results in the serious damage of ecological environment [4]. The sudden ecological environmental pollution accidents have become a potential threat to China's water source safety and environmental quality [5]. In order to prevent the sudden water pollution accidents, it is particularly necessary and urgent to analyze the sudden ecological environmental toxic pollution.

With long incubation period and no fixed treatment way, sudden ecological environmental toxic pollution accidents seriously harm the ecological environment. Therefore, correct methods shall be selected to treat sudden ecological environmental toxic pollution accidents. Previous methods used to treat sudden ecological environmental toxic pollution accidents mainly included physical, chemical, and physicochemical methods. Among them, in terms of physical method, physical separation is applied to separate nonsoluble substances from water and make the discharge of petrochemical wastewater meet the national discharge

standard; in respect of chemical method, chemical reaction is used to treat dissolved substances in sewage, so as to improve water quality; with regard to physical-chemical method, the metabolism of microorganisms is used to treat organic pollutants suspended in water [6]. Among the above three analysis methods, the chemical method will cause secondary pollution easily, the physicochemical method takes a long time for analysis without reaching the emergency treatment effect, and the physical method is relatively safe and will not cause secondary pollution to the ecological environment [7].

With the support of physical analysis method, the research made by big data technology will undoubtedly improve the efficiency of treating sudden ecological environmental toxic pollution, so it is of great significance to promote the future development of pollution treatment plants [8].

2. Target Organism Definition of Environmental Genome and Proteome

As an integrated product of proteome and environmental science genome, ecological environmental proteome mainly studies the biomolecular toxicity caused by environmental pollution factors; the interaction law among pollutants, proteome, and genome; and the pollution analysis methods.

2.1. Genome. As a general term for a living entity's genes, genome is an important tool to carry information with the characteristics of uniqueness and stability. Environmental genome refers to the sum of genes responding to environmental factors, which is gradually formed with the research progress of genes responding to environmental factors. The effect of pollution factors on genes is detected to explain the molecular genetic toxicity mechanism of sudden ecological environmental toxic pollutants and the interference principle that different living entities bear different pollution factors, predict the consequences caused by pollution, and provide targeted solutions [9].

Environmental genome and proteome depend on each other [10]. The theory of environmental genome is mastered to research all cells in a living entity, and the same set of characteristic genomes is used to study the genomic gene under different pollution factors, different time conditions, and different intensity processes [11], so as to understand proteins with different polymorphism and pleiotropy. In the process of researching environmental genome, it is necessary to strictly define the target organisms and external environmental factors [12].

2.2. Proteome. Proteome is a general term of all proteins expressed by genome [13]. Protein identification technology is applied on a large scale to study the structure of genomic proteins and construct functional patterns. Currently, proteome is mainly used to study dynamic proteome with high activity, large-scale protein separation, and identification [14]. In a complex environment, the dynamic process of proteome is analyzed to provide direct evidence for the study of molecular toxicity of pollutants [15]. The invasion of exogenous pollutants threatens the living entity, directly acts on the body protein, changes the normal functions of protein, and affects the output and activity of genetic protein [16].

Environmental proteome is used to study the interaction between proteome and environmental pollution, find the markers of protein molecules of pollutant targets by applying the proteome theory, so as to analyze the effect of environmental pollution on the expression features of protein, determine the molecular toxicity caused by the action of sudden environmental toxic pollution factors on proteome, and avoid the threat to human health through the definition of target organism and external environment factors [17].

3. Analysis of Sudden Ecological Environmental Pollution Situation

The molecular toxicity of sudden environmental pollution was analyzed based on the above-determined proteome and genomic target organisms [18]. The molecular toxicity of pollution is shown in Figure 1.

The average value and relative pollution intensity of the polluted ecological environment were calculated according to the molecular toxicity compound [19]. The specific calculation formula is shown as follows:

$$Z = \frac{X_1 + X_2 + X_3 + \cdots + X_n}{2}, \tag{1}$$

$$P = \frac{Z_1}{Z_2} \times 100\%. \tag{2}$$

In (1) and (2), X expresses the polluted area;Z_1 represents the analysis value of relative pollution intensity under the research content of proteome; andZ_2 represents the analysis value of relative pollution intensity under the research content of proteome.

Changing situation of target organisms in the polluted ecological environment is shown in Figure 2.

According to different isoelectric points of proteins, the sample proteins were focused under the PH density gradient, and the proteins with different isoelectric points were obtained by the first electrophoretic separation. For the products after first electrophoretic separation [20], two-dimensional gel electrophoresis was used to obtain proteins with different molecular toxicity. After ionizing the protein sample, the molecular structure was determined according to the difference in the mass-to-charge ratio of different ions [21]. Environmental proteomics was used to analyze environmental internal-secretion interfering-substance and various diseases of the reproductive system, including spermoblasts, quality of male organisms, and disproportionality between male and female organisms. Big data technology with high throughput and high sensitivity was used to analyze the corresponding location of specific proteins and determine the molecular structure of specific proteins accordingly, so as to analyze the molecular toxicity of sudden ecological environmental pollution.

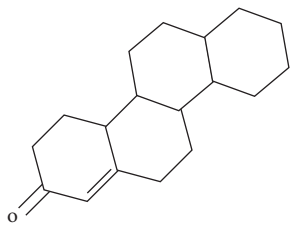

Figure 1: Molecular toxicity compound of pollution.

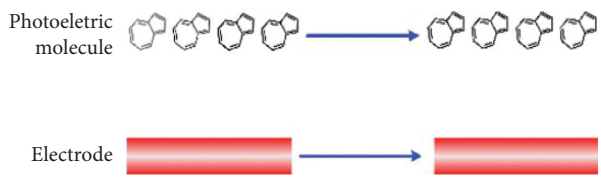

Figure 2: Changing situation of target organisms in the polluted ecological environment.

4. Large Data Technology-Based Analysis of Sudden Ecological Environmental Toxic Pollution

With strong decision-making ability and insight, big data technology is used to collect data within a certain time range by conventional software. The features of big data can be described by volume, variety, value, and speed. With large data size, volume is usually represented by P; data are widely diverse; value refers to relatively low data value density; and speed means quick big data processing, which is a distinguishing feature used to distinguish big data technology from traditional technology. Used to better dig and store relevant governance data, big data technology is of great significance to break through the sudden ecological environmental toxic pollution in China when combined with physical methods [22].

With good adsorption effect, fruit-peel activated carbon is suitable for the analysis of sudden ecological environmental toxic pollution. Therefore, fruit-peel activated carbon was used to treat the ecological environmental pollution. Main activities of fruit-peel activated carbon are shown in Table 1.

In order to prevent activated carbon from being interfered by other impurities, the activated carbon shall be soaked in ultrapure water to remove the impurities attached to the activated carbon, dried at the temperature of 120°C, and aired for standby application.

4.1. Particle Size of Activated Carbon. The volume and speed characteristics of big data technology were used to determine the optimal particle size of activated carbon. After adding the activated carbon of 2 g, 4 g, 6 g, 8 g, and 10 g with intermediate particle size to a solution of 200 mL, the basic water sample, the solution was stirred in the blender at a temperature of 30°C and speed of 150 r/min, so as to investigate the probability of removing sudden ecological environmental toxic pollution by activated carbon with different particle sizes. The results of investigation are shown in Figure 3.

Table 1: Main activities of fruit-peel activated carbon.

Parameter	Indicator
Weight of iodine	1000 (mg/g)
Adsorption rate of methylene blue	12.0 (mg/L)
Superficial area	400–800 (m^2/g)
Density	1.5 (g/mL)
Particle size	0.65–4.35 nm
Moisture	15%
pH	5-6

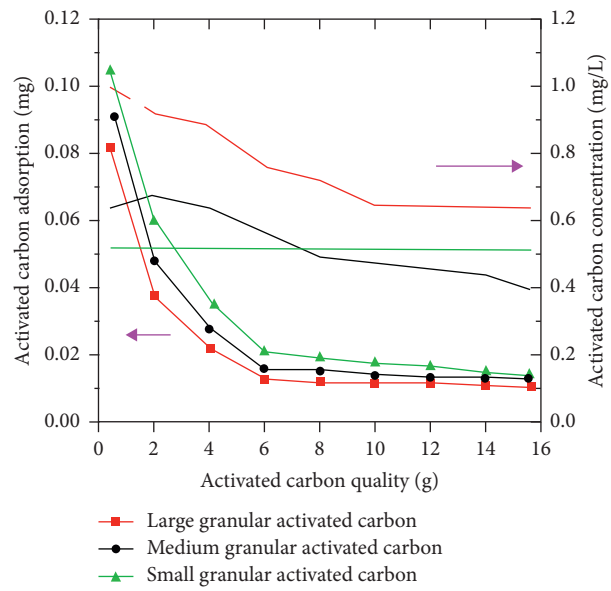

Figure 3: Adsorption capacity of activated carbon with different particle sizes.

Figure 3 shows that low-mass activated carbon has large capacity to absorb molecular toxicity of sudden ecological environmental pollution, and its adsorption capacity is increasingly gentle as the mass increases. Activated carbon with large particle size has relatively high rate of removing molecular toxicity of sudden ecological environmental pollution and relatively stable removal effect, which laid a foundation for the emergency treatment of molecular toxicity of sudden ecological environmental pollution.

4.2. Dosage of Activated Carbon. By using the speed characteristic of big data technology, the amount of activated carbon that has reached the test standard was found, and the gradient value of the dosage of activated carbon was determined. The initial reaction conditions were designed and controlled to ensure that the stirring time was 2 h and 24 h, so as to fully observe the mass of activated carbon. Through analyzing the removal rate and adsorption capacity of activated carbon numerically, the gradient value of the dosage of activated carbon was determined.

From Figure 4, the dosage of activated carbon with different masses has an obvious effect on the treatment of

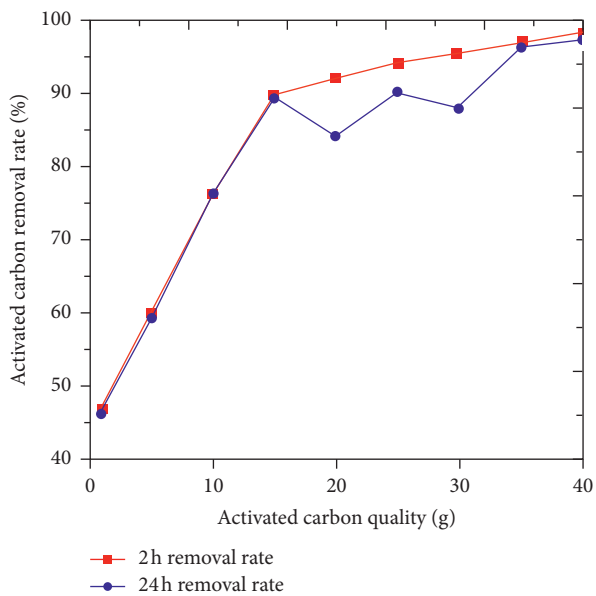

Figure 4: Removal rate of pollutant toxicity of activated carbon with different masses.

sudden ecological environmental toxic pollution. With the increase of the dosage of activated carbon, the removal rate rose rapidly at first and then tended to rise gently:

(1) For the removal rate of 24 h, when the mass of activated carbon was 5, 10, and 15 g, the removal rate of activated carbon was 60%, 76%, and 91%, respectively. When the mass of activated carbon was 20, 25, 30, 35, and 40 g, the removal rate of activated carbon was 86%, 89%, 84%, 96%, and 97%, respectively.

(2) For the removal rate of 2 h, when the mass of activated carbon was 5, 10, and 15 g, the removal rate of activated carbon was 60%, 76%, and 91%, respectively. When the mass of activated carbon was 20, 25, 30, 35, and 40 g, the removal rate of activated carbon was 93%, 95%, 96%, 97%, and 98%, respectively.

Activated carbon which has adsorbed in water sample for 2 h and 24 h has basically the same removal efficiency. Because activated carbon almost reached the saturated state after having adsorbed for 2 h, adsorption time shall be less than or equal to 2 h; in this way, the gradient value of activated carbon dosage was determined, and the level of sudden ecological environmental toxic pollution was analyzed based on the dosage of activated carbon at 2 h.

4.3. Adsorption Time of Activated Carbon. Selected by using the volume characteristic of big data technology, the adsorption time of activated carbon shall be more than 10 min, and too short adsorption time of activated carbon put repeatedly and manually shall be avoided. In order to avoid serious pollution caused by excessive flow velocity, the adsorption time of activated carbon shall not be too long; besides, because activated carbon almost reaches the saturation state after 2 h, the minimum adsorption time of activated carbon shall be set as 10 min, so as to investigate the probability of removing sudden ecological environmental toxic pollution by activated carbon at different adsorption time. The research results are shown in Figure 5.

Figure 5 shows that activated carbon with different masses has obvious effect on the treatment of sudden ecological environmental toxic pollution. As time goes by, three broken lines show different states:

(1) The removal rate of activated carbon with small particle size has been 92% from 10 min to 70 min but increased to 99% from 70 min to 80 min.

(2) The removal rate of activated carbon with medium particle size was 60%, 76%, and 84%, respectively, at 10, 20, and 30 min. The broken line of the removal rate of activated carbon showed a slow rising trend at 40, 50, 60, 70, and 80 min.

(3) The removal rate of activated carbon with large particle size was 52% and 69%, respectively, at 10 and 20 minutes. The broken line of the removal rate of activated carbon also showed a slow rising trend at 40, 50, 60, 70, and 80 min.

With the increase of adsorption time, the optimal adsorption time of activated carbon with different particle sizes was different: 70 min with small particle size, 30 min with medium particle size, and 20 min with large particle size. The optimal adsorption time of activated carbon with different particle sizes can be determined by using big data technology, so as to analyze the degree of sudden toxic pollution of ecological environment.

Through analyzing the adsorption time of activated carbon with different particle sizes and dosages, the big data technology was used to study the sudden ecological environmental toxic pollution. According to the research results, activated carbon with large particle size has high rate of removing molecular toxicity of sudden ecological environmental pollution, with relatively stable removal effect; at 2 h, the activated carbon almost reached the saturated state, and the gradient value of the dosage of activated carbon was determined by taking the dosage of activated carbon dosage at 2 h as the standard; the activated carbon with different particle sizes has different optimal adsorption time. According to the analysis content, the optimal adsorption time of activated carbon with different particle sizes was determined to ensure the stable effect of removing molecular toxicity of sudden ecological environmental pollution.

5. Analysis of Experimental Verification

In order to further verify the feasibility and stability of the analysis methods of sudden ecological environmental toxic pollution based on big data technology, further experimental verification and analysis of this technology shall be made.

5.1. Experimental Environment. In the laboratory, the software and hardware environment constructed by existing experimental conditions were used to test the sudden ecological environmental toxic pollution analysis methods

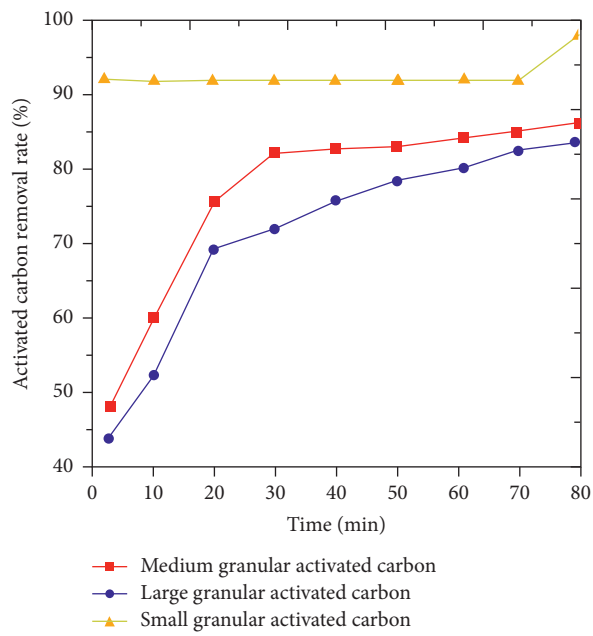

Figure 5: Removal rate of activated carbon at different time.

based on big data technology. The test equipment included 3 PC main engines, 1 communication server, and 1 database server. The specific configuration parameters are shown in Table 2.

The list of software version numbers is shown in Table 3.

The database was deployed on the database server, and the related programs were deployed on the application server.

Table 2: Table of configuration parameters.

Hardware	Equipment	Parameter explanation
CPU	Main engine	Intel Pentium(*R*) dual-core CPU E5400
	Data communication server	I3-6100/8 G/1 T
	Database server	I3-6100/8 G/1 T
Internal storage	Main engine	4 G
	Data communication server	16 G
	Database server	16 G
Hardware	Main engine	500 G
	Data communication server	1 T
	Database server	1 T

Table 3: List of software version numbers.

Name	Version no.
Ubuntu	11.05
JDK	1.6.0_64
Hadoop	1.1.2
Sqoop	1.4.4
Hive	0.11.1

5.2. Analysis and Discussion of Experimental Results

5.2.1. Changing the Particle Size of Activated Carbon. In this experiment, during the process of treating the molecular toxicity of sudden ecological environmental pollution, we only needed to change the particle size of activated carbon and divide it into large, medium, and small with the ranges of 5–8 mesh, 8–21 mesh, and >21 mesh, successively. The activated carbon with the dosage of 15 g and the concentration of 45 g/L was selected to be absorbed in water for about one day, so as to obtain the water samples of the molecular toxicity of sudden ecological environmental pollution with different concentrations. The concentrations of water samples are shown in Table 4.

Based on Table 4, manual analysis method, chemical analysis method, and big data technology analysis method were used to verify and analyze the degree of molecular toxicity of sudden ecological environmental pollution.

(1) Large Particle Size. Changing situation of the toxicity of pollutants with large particle size under different analysis methods is shown in Figure 6.

From Figure 6, with the increase of time, the toxicity of pollutants changed from high toxicity of 0.32 mg/L to low toxicity of 0.22 mg/L by manual analysis method; the toxicity of pollutants changed from high toxicity of 0.32 mg/L to low toxicity of 0.20 mg/L by chemical method; and the toxicity of pollutants changed from high toxicity of 0.32 mg/L to low toxicity of 0.06 mg/L by big data technology, which showed that the physical separation method in the big data technology analysis method can be used to remove a large amount of biological toxicity of pollutants with large particle size.

(2) Medium Particle Size. Changing situation of the toxicity of pollutants with medium particle size under different analysis methods is shown in Figure 7.

The toxicity of pollutants changed from high toxicity of 0.21 mg/L to medium toxicity of 0.14 mg/L by manual analysis; the toxicity of pollutants changed from high toxicity of 0.21 mg/L to low toxicity of 0.12 mg/L by chemical method; and the toxicity of pollutants changed from high toxicity of 0.32 mg/L to low toxicity of 0.02 mg/L by big data technology, which showed that the physical separation method in the big data technology analysis method can be used to remove a large amount of biological toxicity of pollutants with medium particle size.

(3) Small Particle Size. Changing situation of the toxicity of pollutants with small particle size under different analysis methods is shown in Figure 8.

The toxicity of pollutants changed from high toxicity of 0.20 mg/L to medium toxicity of 0.13 mg/L by manual analysis method; the toxicity of pollutants changed from high toxicity of 0.20 mg/L to medium toxicity of 0.10 mg/L by chemical method; and the toxicity of pollutants changed from high toxicity of 0.20 mg/L to low toxicity of 0.02 mg/L by big data technology, which showed that the physical

Table 4: Samples with different particle sizes of molecular toxicity of ecological environmental pollution.

Particle size of activated carbon	Large-sized particle	Medium-sized particle	Small-sized particle
Effluent concentration of samples (mg/L)	0.32	0.21	0.20
Relative pollution intensity	0.10	0.15	0.16
Toxicity level	Highly toxic	Highly toxic	Highly toxic

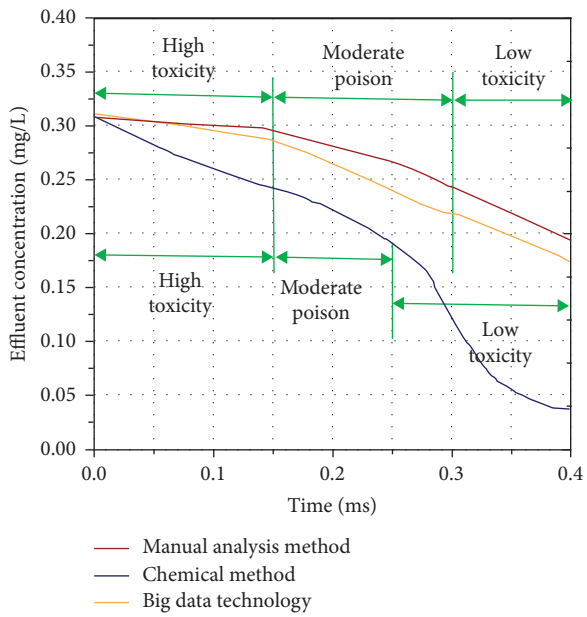

Figure 6: Changing situation of the toxicity of pollutants with large particle size under different analysis methods.

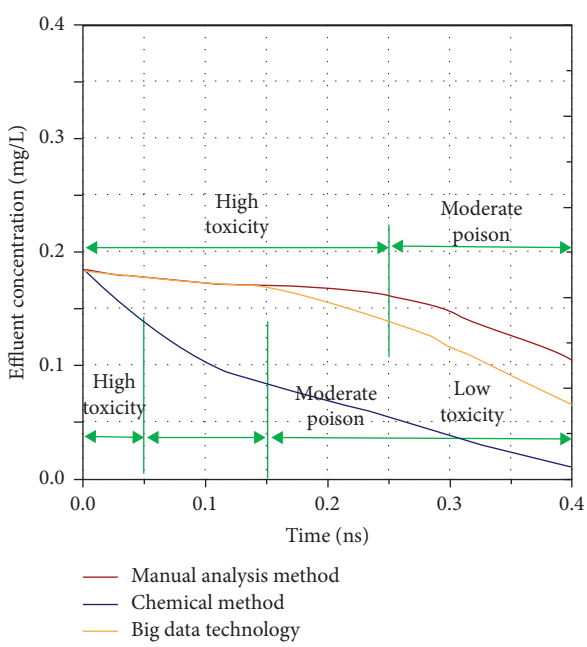

Figure 7: Changing situation of the toxicity of pollutants with medium particle size under different analysis methods.

separation method in the big data technology analysis method can be used to remove a large amount of biological toxicity of pollutants with small particle size.

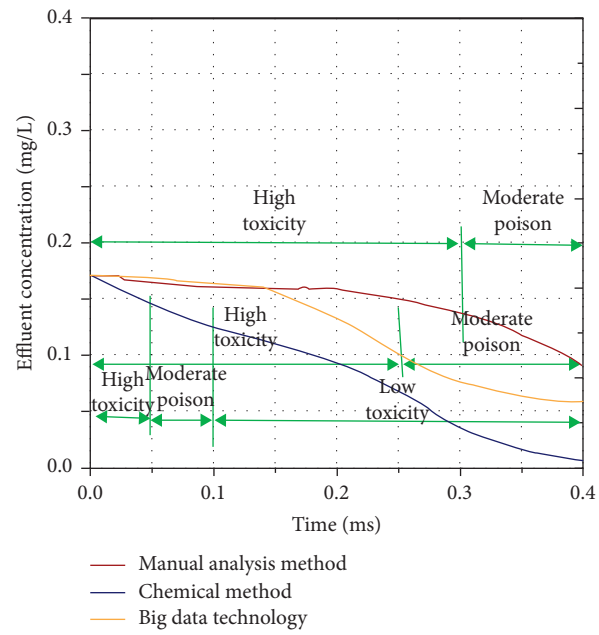

Figure 8: Changing situation of the toxicity of pollutants with small particle size under different analysis methods.

5.2.2. Changing the Dosage of Activated Carbon. In this experiment, during the process of treating the molecular toxicity of sudden ecological environmental pollution, we only needed to change the dosage of activated carbon and keep other conditions unchanged. The effluent concentration is shown in Table 5.

Based on Table 5, three analysis methods were used to verify and analyze the level of molecular toxicity of sudden ecological environmental pollution, which is shown in Table 6.

From Table 6, by the manual analysis method, activated carbon with different dosages has different levels of molecular toxicity of sudden ecological environmental pollution. The activated carbon with the dosage of 2 g, 4 g, 6 g, 8 g, 20 g, and 40 g was consistent with the original toxicity level; by the chemical analysis method, the activated carbon with the dosage of 2 g, 4 g, 20 g, and 40 g was consistent with the original toxicity level; by the big data analysis method, activated carbon with different dosages had different levels of molecular toxicity of sudden ecological environmental pollution and was consistent with the original toxicity level, which showed that big data analysis method can achieve more accurate analyzing results.

5.2.3. Changing the Adsorption Time of Activated Carbon. In this experiment, during the process of treating molecular toxicity of sudden ecological environmental pollution, we only needed to change the adsorption time of activated carbon. The effluent concentration is shown in Table 7.

Table 5: Samples with different dosages of molecular toxicity of sudden ecological environmental pollution.

Dosage (g)	Concentration of activated carbon (g/L)	Relative pollution intensity	Toxicity level
2	14	0.25	Highly toxic
4	28	0.29	Highly toxic
6	42	0.33	Heavily toxic
8	56	0.35	Heavily toxic
10	70	0.40	Heavily toxic
20	140	0.40	Medium toxic
40	280	0.45	Medium toxic
80	560	0.55	Low toxic
100	700	0.65	Low toxic

Table 6: Three analysis methods to verify the pollution level of molecular toxicity.

Dosage of activated carbon (g)	Manual analysis method	Chemical analysis method	Big data technology analysis
2	Highly toxic	Highly toxic	Highly toxic
4	Highly toxic	Highly toxic	Highly toxic
6	Heavily toxic	Highly toxic	Heavily toxic
8	Heavily toxic	Highly toxic	Heavily toxic
10	Medium toxic	Medium toxic	Heavily toxic
20	Medium toxic	Medium toxic	Medium toxic
40	Medium toxic	Medium toxic	Medium toxic
80	Medium toxic	Medium toxic	Low toxic
100	Medium toxic	Medium toxic	Low toxic

Table 7: Samples with different adsorption time of molecular toxicity of sudden ecological environmental pollution.

Adsorption time (h)	Concentration of activated carbon (mg/L)	Relative pollution intensity	Toxicity level
0	0.23	0.10	Acutely toxic
0.2	0.21	0.11	Acutely toxic
0.4	0.19	0.18	Highly toxic
0.6	0.18	0.25	Highly toxic
0.8	0.15	0.32	Heavily toxic
1.0	0.12	0.11	Medium toxic
1.2	0.9	0.18	Medium toxic
1.4	0.08	0.22	Medium toxic
1.6	0.04	0.25	Medium toxic
1.8	0.02	0.24	Medium toxic

Based on Table 7, three analysis methods were used to verify and analyze the level of molecular toxicity of sudden ecological environmental pollution, which is shown in Figure 9.

From Figure 9, with the increase of adsorption time, by big data technology, activated carbon was consistent with the actual concentration; however, the concentrations obtained by manual analysis method and chemical method were greatly different from the actual concentration.

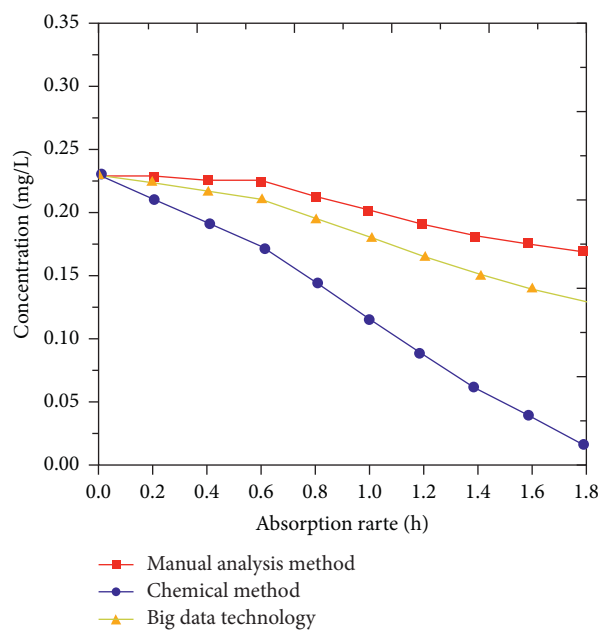

Figure 9: Different analysis methods to verify the pollution level of molecular toxicity.

In conclusion, the analysis results of sudden ecological environmental toxic pollution by using the combination of big data technology with physical methods were accurate and consistent with the actual results.

6. Conclusion

Starting from the subjects of environmental proteome and genome, the research on the molecular toxicity of sudden

ecological environmental pollution is applicable to the analysis techniques of environment with different pollution levels. Taking the database of environmental proteome as the center, the molecular toxicity was detected and analyzed by big data technology. During the process of analyzing the molecular toxicity of sudden ecological environmental pollution, big data technology can be used to successfully analyze the damage situation of molecular genome as a simple tool to supervise and assess molecular toxicity, which is expected to be applied in the field of environmental pollutant toxicity detection.

Due to the restrictions on experimental environment, the big data technology involved in the research content is only supported by relevant theories and simple equipment. This means that the content of the article is more theoretical. In terms of detecting the existing pollution molecules, the research on the molecular toxicity of sudden ecological environmental pollution plays a certain guiding role in protecting the environment, but there are still some limitations. Therefore, in the follow-up research process, it is necessary to combine practice with experiment, improve the experimental conditions, and increase the treatment efficiency of pollution molecules.

Data Availability

No data were used to support this study.

Conflicts of Interest

The authors declare that they have no conflicts of interest.

References

[1] A. M. Wu, X. L. Zhao, Y. Feng et al., "The enlightenment of American ecotoxicology database to Chinese database construction," *Environmental Science Research*, vol. 30, no. 4, pp. 636–644, 2017.

[2] Z. Wang, "Research hotspot and frontal analysis of mine ecological environmental restoration—big data visualization research based on vosviewer and citespace," *Geological Bulletin of China*, vol. 37, no. 12, pp. 2144–2153, 2018.

[3] M. M. Zhao, S. C. Zhao, and L. Y. Zhao, "Application progress and prospect of big data in the field of ecological environment," *Journal of Applied Ecology*, vol. 28, no. 5, pp. 1727–1734, 2017.

[4] W. Tang, Q. Yang, C. Huang et al., "Research on the change features of automobile pollutant emission in hangzhou based on big data analysis and IVE model," *Journal of Environmental Sciences*, vol. 38, no. 1, pp. 71–78, 2018.

[5] Y. Li, J. Yang, and J. Du, "Prospect of medical disruptive technologies," *Chinese Journal of Engineering Science*, vol. 20, no. 6, pp. 64–56, 2018.

[6] Y. Xia, Q. Yang, C. Xu et al., "Research on high-resolution ammonia emission inventory from agricultural sources in hangzhou based on big data analysis," *Journal of Environmental Sciences*, vol. 38, no. 2, pp. 661–668, 2018.

[7] W. Liu, J. Yang, H. Gui, P. Xie, R. Liu, and J. Wei, "Study on the development of multi perception system for "internet plus" smart environmental protection," *Chinese Journal of Engineering Science*, vol. 20, no. 2, pp. 111–119, 2018.

[8] Q. Q. Chen and S. Y. Yang, "Aquatic ecotoxicity and carrier function of microplastics pollution," *Asian Journal of Ecotoxicology*, vol. 19, no. 1, pp. 16–30, 2018.

[9] Y. W. Wang, Y. Wang, and G. B. Jiang, "Analysis method, pollution status and toxicity effect of short-chain chlorinated paraffin," *Progress in Chemistry*, vol. 32, no. 9, pp. 919–929, 2017.

[10] Q. Q. Zhang, M. Qiao, and H. F. Chi, "Review of test methods for soil ecotoxicity," *Asian Journal of Ecotoxicology*, vol. 12, no. 4, pp. 76–97, 2017.

[11] Q. L. Bao, W. H. Li, Y. Z. Huang et al., "Ecotoxicity of soil Cd pollution to springtail folsomia candida," *Asian Journal of Ecotoxicology*, vol. 12, no. 2, pp. 169–176, 2017.

[12] Z. C. Ma, "Preliminary application of mix index in the research on combined toxicity of environmental mixtures," *Asian Journal of Ecotoxicology*, vol. 16, no. 3, pp. 62–71, 2017.

[13] L. P. Guo, T. T. Liu, H. R. Li et al., "Change characteristics of environmental meteorological conditions of "sudden" severe air pollution in langfang," *Environmental Pollution and Prevention*, vol. 22, no. 4, p. 120, 2017.

[14] H. Li, "Research progress on environmental exposure, environmental behavior and toxic effects of organophosphate fire retardants," *Environmental Engineering*, vol. 36, no. 9, pp. 185–189, 2018.

[15] Z. Q. Zhang, "Analysis of bacteriostatic activity, cytotoxicity and safety of acetone extracts from five medicinal plants," *Molecular Plant Breeding*, vol. 16, no. 23, pp. 7849–7855, 2018.

[16] M. M. Wang, "Screening of watershed priority pollutant based on environmental risk ranking," *Environmental Science*, vol. 39, no. 10, pp. 82–88, 2018.

[17] Y. Luo, B. Q. Zhang, X. Q. Ren et al., "Pollution status and toxicity research progress of CL-pahs," *Asian Journal of Ecotoxicology*, vol. 12, no. 3, pp. 120–134, 2017.

[18] Y. D. Zou, Q. Q. Xu, G. Zhang et al., "Research progress on the joint toxic effects of microplastics and pesticide pollution," *Asian Journal of Ecotoxicology*, vol. 12, no. 4, pp. 25–33, 2017.

[19] Y. Z. Pan, H. Y. Sun, D. L. Wang, Z. F. Lin, C. S. Yin, and X. D. Wu, "Research progress on the inter-related phenomenon between the model curve of joint toxicity evaluation of mixed pollutants and the actual concentration effect curve," *Asian Journal of Ecotoxicology*, vol. 32, no. 3, pp. 72–85, 2017.

[20] N. N. Lu, W. C. Song, M. Q. Wang, S. H. Sun, and R. B. Jia, "Research on the behavioral toxicity of acute exposure of malathion to zebrafish," *Asian Journal of Ecotoxicology*, vol. 12, no. 4, pp. 249–254, 2017.

[21] M. Y. Wang, "Pollution and ecological toxicity of antidepressants in water environment," *Journal of Chemical Engineering of Chinese University*, vol. 30, no. 5, pp. 1009–1027, 2017.

[22] J.-B. Liu, J. Zhao, H. He, and Z. Shao, "Valency-based topological descriptors and structural property of the generalized sierpiński networks," *Journal of Statistical Physics*, vol. 177, no. 6, pp. 1131–1147, 2019.

Hindawi
Journal of Chemistry
Volume 2020, Article ID 8616309, 17 pages
https://doi.org/10.1155/2020/8616309

Research Article

Valency-Based Descriptors for Silicon Carbides, Bismuth(III) Iodide, and Dendrimers in Drug Applications

Qi-Zhao Li,[1] Abaid ur Rehman Virk,[2] Kashif Nazar,[3] Imran Ahmed,[3] and Iskander Tlili[4,5]

[1]*School of Pharmacy, Anhui Xinhua University, Hefei 230088, China*
[2]*Department of Mathematics, University of Management and Technology, Lahore 54000, Pakistan*
[3]*Department of Mathematics, COMSATS University of Islamabad, Lahore Campus, Lahore 54000, Pakistan*
[4]*Department for Management of Science and Technology Development, Ton Duc Thang University, Ho Chi Minh City, Vietnam*
[5]*Faculty of Applied Sciences, Ton Duc Thang University, Ho Chi Minh City, Vietnam*

Correspondence should be addressed to Iskander Tlili; iskander.tlili@tdtu.edu.vn

Received 20 October 2019; Revised 3 December 2019; Accepted 18 December 2019; Published 28 May 2020

Guest Editor: Shaohui Wang

Silicon carbide (SiC), also called carborundum, is a semiconductor containing silicon and carbon. Dendrimers are repetitively branched molecules that are typically symmetric around the core and often adopt a spherical three-dimensional morphology. Bismuth(III) iodide is an inorganic compound with the formula BiI_3. This gray-black solid is the product of the reaction between bismuth and iodine, which once was of interest in qualitative inorganic analysis. In chemical graph theory, we associate a graph to a compound and compute topological indices that help us in guessing properties of the understudy compound. A topological index is the graph invariant number, calculated from a graph representing a molecule. Most of the proposed topological indices are related either to a vertex adjacency relationship (atom-atom connectivity) in the graph or to topological distances in the graph. In this paper, we aim to compute the first and second Gourava indices and hyper-Gourava indices for silicon carbides, bismuth(III) iodide, and dendrimers.

1. Introduction

Mathematical chemistry provides tools such as polynomials and functions that depend upon the information hidden in the symmetry of graphs of chemical compounds and helps to predict properties of the understudy molecular compound without the use of quantum mechanics. A topological index is a numerical parameter of a graph and depicts its topology. It describes the structure of molecules numerically and are used in the development of qualitative structure activity relationships (QSARs). There are three kinds of topological indices, namely, degree-based, distance-based, and surface-based topological indices. Lot of research has been done on degree-based topological indices, for example, see [1–9]. Degree-based topological indices correlate the structure of the molecular compound with its various physical properties, biological activities, and chemical reactivity [10–14]. Boiling point, heat of formation, fracture toughness, strain energy, and rigidity of a molecule are strongly connected to its graphical structure.

The first topological index was introduced by Wiener when he was studying the boiling point of alkanes [15], which is now known as the Wiener index [16–20]. In 1975, Milan Randić introduced a simple topological index called the Randić index [21]. Many research papers and survey papers have been written on this graph invariant due to its interesting mathematical properties and valuable applications in chemistry [22–27]. The other oldest topological indices are Zagreb indices defined by Gutman and Trinajstic in [28] and are one of the most studied topological indices [29–33]. Topological indices are helpful in guessing properties of concerned compounds and are used in QSPRs [34–37]. There are more than 148 topological indices in the literature [38–42], but none of them are able to guess all the

properties of the concerned compound (together they do it to some extent). Therefore, there is always room to define new topological indices [43]. Recently, in 2017, the first and second Gourava indices [44] were defined as

$$\begin{aligned} GO_1(G) &= \sum_{uv\epsilon E(G)} [(d_u + d_v) + (d_u.d_v)], \\ GO_2(G) &= \sum_{uv\epsilon E(G)} [(d_u + d_v).(d_u.d_v)]. \end{aligned} \tag{1}$$

In the same year, the first and second hyper-Gourava indices [45] have been defined as

$$\begin{aligned} HGO_1(G) &= \sum_{uv\epsilon E(G)} [(d_u + d_v) + (d_u.d_v)]^2, \\ HGO_2(G) &= \sum_{uv\epsilon E(G)} [(d_u + d_v).(d_u.d_v)]^2. \end{aligned} \tag{2}$$

Note that $GO_1(G) = M_1(G) + M_2(G)$, $GO_2(G) = M_1(G)M_2(G)$, $HGO_1(G) = H_1(G) + H_2(G) + 2M_1(G) + M_2(G)$, and $HGO_2(G) = H_1(G)H_2(G)$. In this paper, the aim is to compute Gourava indices and hyper-Gourava indices for silicone carbides, bismuth triiodide, and dendrimers and their graphical representations.

2. Methodology

To compute our results, first we constructed the graph of the concerned molecular compounds and counted the total number of vertices and edges. Secondly, we divided the edge set of concerned graphs into different classes based on the degrees of end vertices. By applying definitions of Gourava indices, we computed our desired results. We plotted our computed results by using Maple 2015 to see their dependencies on the involved parameters.

3. Gourava Indices

In this section, we present our main computational results. This section consists of three subsections. In Section 3.1, we present results about silicone carbides $Si_2C_3 - I[p,q]$, $Si_2C_3 - II[p,q]$, $Si_2C_3 - III[p,q]$, and $SiC_3 - III[p,q]$. In Section 3.2, we give results about the bismuth triiodide chain $m - BiI_3$ and the bismuth triiodide sheet $BiI_3(m \times n)$. In Section 3.3, we present results about four dendrimer structures: porphyrin dendrimer D_nP_n, propyl ether imine dendrimer (PETIM), zinc-porphyrin dendrimer DPZ_n, and Poly(EThyleneAmidoAmine) dendrimer (PETAA).

3.1. Gourava Indices for Silicon Carbides. Silicon carbide (SiC), also called carborundum, is a semiconductor containing silicon and carbon. It occurs in nature as the incredibly uncommon mineral Moissanite. Manufactured SiC powder has been created in mass since 1893 for use as an abrasive. Grains of silicon carbide are reinforced together by sintering to shape extremely hard ceramic production that are generally utilized in applications requiring high continuance, for example, vehicle brakes, vehicle clutches, and ceramic plates in impenetrable vests. Electronic utilizations of silicon carbide, for example, light-emitting diodes (LEDs) and locators in early radios, were first exhibited around 1907. SiC is utilized in semiconductor electronic devices that work at high temperatures or high voltages, or both. Huge single crystals of silicon carbide can be developed by the Lely technique, and they can be cut into gems known as manufactured Moissanite. SiC with a high surface zone can be created from SiO_2 contained in the plant material. Due to huge amount of application, silicone carbides have been studied extensively [6, 42]. In this section, we computed Gourava indices for silicon carbides $Si_2C_3 - I[p,q]$, $Si_2C_3 - II[p,q]$, $Si_2C_3 - III[p,q]$, and $SiC_3 - III[p,q]$.

3.1.1. Gourava Indices for Silicon Carbide $Si_2C_3 - I[p,q]$. The molecular graphs of silicon carbide $Si_2C_3 - I[p,q]$ are shown in Figures 1–4, where Figure 1 shows the unit cell of silicone carbide, Figure 2 shows $Si_2C_3I[p,q]$ for $p = 4, q = 3$, Figure 3 shows $Si_2C_3I[p,q]$ for $p = 4$, $q = 1$, and Figure 4 shows $Si_2C_3I[p,q]$ for $p = 4, q = 3$. The edge partition of the edge set of $Si_2C_3 - I[p,q]$ based on the degree of the end vertex is given in Table 1.

Theorem 1. *Let G be the graph of silicon carbide $Si_2C_3I[p,q]$. Then, the first and second Gourava indices are*

(1) $GO_1(G) = 225pq - 61p - 91q + 18$,

(2) $GO_2(G) = 810pq - 290p - 430q + 126$.

Proof. From the edge partition of $Si_2C_3I[p,q]$ given in Table 1, we have

(1) The first Gourava index for $Si_2C_3I[p,q]$ is

$$\begin{aligned} GO_1(G) &= \sum_{uv\epsilon E(G)} [(d_u + d_v) + (d_u.d_v)] \\ &= [(1+2) + (1\times 2)](1) + [(1+3) + (1\times 3)](1) \\ &\quad + [(2+2) + (2\times 2)](p + 2q) \\ &\quad + [(2+3) + (2\times 3)](6p + 8q - 9) \\ &\quad + [(3+3) + (3\times 3)](15pq - 9p - 13q + 7) \\ &= 225pq - 61p - 91q + 18. \end{aligned} \tag{3}$$

(2) The second Gourava index for $Si_2C_3I[p,q]$ is

$$\begin{aligned} GO_2(G) &= \sum_{uv\epsilon E(G)} [(d_u + d_v).(d_u.d_v)] \\ &= [(1+2)\times(1+2)](1) + [(1+3)\times(1+3)](1) \\ &\quad + [(2+2)\times(2+2)](p + 2q) \\ &\quad + [(2+3)\times(2\times 3)](6p + 8q - 9) \\ &\quad + [(3+3)\times(3+3)](15pq - 9p - 13q + 7) \\ &= 810pq - 290p - 430q + 126. \end{aligned} \tag{4}$$

□

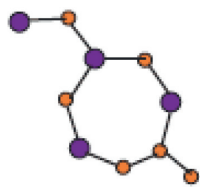

Figure 1: Unit cell of $Si_2C_3I[p,q]$.

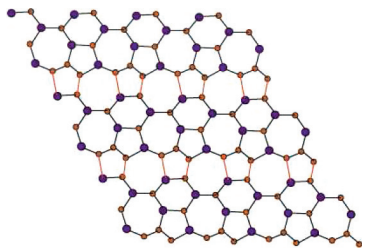

Figure 2: $Si_2C_3I[p,q]$ for $p = 4$, $q = 3$.

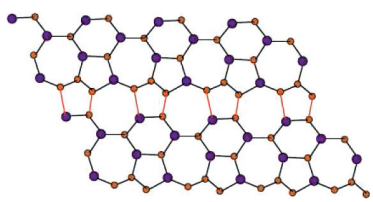

Figure 3: $Si_2C_3I[p,q]$ for $p = 4$, $q = 1$.

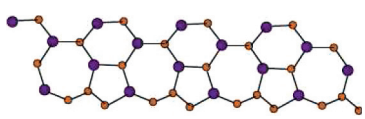

Figure 4: $Si_2C_3I[p,q]$ for $p = 4$, $q = 3$.

Table 1: Degree-based edge partition of $Si_2C_3I[p,q]$.

(d_u, d_v)	Frequency
$(1,2)$	1
$(1,3)$	1
$(2,2)$	$p+2q$
$(2,3)$	$6p-1+8(q-1)$
$(3,3)$	$15pq-9p-13q+7$

Theorem 2. *Let G be the graph of silicon carbide $Si_2C_3I[p,q]$. Then, the first and second hyper-Gourava indices are*

(1) $HGO_1(G) = 3375pq - 1235p - 1829q + 566$,

(2) $HGO_2(G) = 43740pq - 20588p - 30196q + 12492$.

Proof. From the edge partition of $Si_2C_3I[p,q]$ given in Table 1, we have

(1) The first hyper-Gourava index for $Si_2C_3I[p,q]$ is

$$\begin{aligned}
HGO_1(G) &= \sum_{uv\in E(G)} \left[(d_u + d_v) + (d_u.d_v)^2\right] \\
&= [(1\times 2) + (1\times 2)]^2 (1) + [(1+3) + (1\times 3)]^2 (1) \\
&\quad + [(2+2) + (2\times 2)]^2 (p+2q) \\
&\quad + [(2+3) + (2\times 3)]^2 (6p+8q-9) \\
&\quad + [(3+3) + (3\times 3)]^2 (15pq-9p-13q+7) \\
&= 3375pq - 1235p - 1829q + 566.
\end{aligned} \tag{5}$$

(2) The second hyper-Gourava index for $Si_2C_3I[p,q]$ is

$$\begin{aligned}
HGO_2(G) &= \sum_{uv\in E(G)} \left[(d_u + d_v).(d_u.d_v)^2\right] \\
&= [(1+2)\times(1+2)]^2 (1) + [(1+3)\times(1+3)]^2 (1) \\
&\quad + [(2+2)\times(2+2)]^2 (p+2q) \\
&\quad + [(2+3)\times(2+3)]^2 (6p+8q-9) \\
&\quad + [(3+3)\times(3\times 3)]^2 (15pq-9p-13q+7) \\
&= 43740pq - 20588p - 30196q + 12492.
\end{aligned} \tag{6}$$

□

3.1.2. Gourava Indices for Silicon Carbide $Si_2C_3 - II[p,q]$. The molecular graphs of silicon carbide $Si_2C_3 - II[p,q]$ are shown in Figures 5–8, where Figure 5 shows the unit cell of $Si_2C_3 - II[p,q]$, Figure 6 shows $Si_2C_3 - II[p,q]$ for $p = 3$, $q = 3$, Figure 7 shows $Si_2C_3 - II[p,q]$ for $p = 5$, $q = 1$, and Figure 8 shows $Si_2C_3 - II[p,q]$ for $p = 5$, $q = 2$. The edge partition of the edge set of $Si_2C_3 - II[p,q]$ based on the degree of the end vertex is given in Table 2.

Theorem 3. *Let G be the graph of silicon carbide $Si_2C_3 - II[p,q]$. Then, the first and second Gourava indices are*

(1) $GO_1(G) = 225pq - 91p - 91q + 28$,

(2) $GO_2(G) = 810pq - 430p - 430q + 198$.

Proof. From the edge partition of $Si_2C_3 - II[p,q]$ given in Table 2, we have

(1) The first Gourava index for $Si_2C_3I[p,q]$ is

$$\begin{aligned}
GO_1(G) &= \sum_{uv\in E(G)} \left[(d_u + d_v) + (d_u.d_v)\right] \\
&= [(1+2) + (1\times 2)](2) + [(1+3) + (1\times 3)](1) \\
&\quad + [(2+2) + (2\times 2)](2p+2q) \\
&\quad + [(2+3) + (2\times 3)](8p+8q-14) \\
&\quad + [(3+3) + (3\times 3)](15pq-13p-13q+11) \\
&= 225pq - 91p - 91q + 28.
\end{aligned} \tag{7}$$

Figure 5: Unit cell of $Si_2C_3 - II[p,q]$.

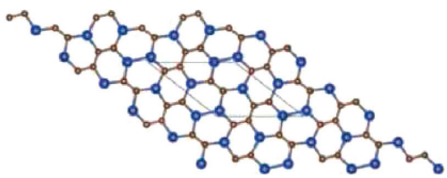

Figure 6: $Si_2C_3 - II[p,q]$ for $p = 3$, $q = 3$.

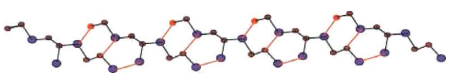

Figure 7: $Si_2C_3 - II[p,q]$ for $p = 5$, $q = 1$.

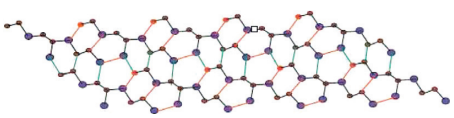

Figure 8: $Si_2C_3 - II[p,q]$ for $p = 5$, $q = 2$.

Table 2: Degree-based edge partition of $Si_2C_3 - II[p,q]$.

(d_u, d_v)	Frequency
$(1,2)$	2
$(1,3)$	1
$(2,2)$	$2p + 2q$
$(2,3)$	$8p + 8q - 14$
$(3,3)$	$15pq - 13p - 13q + 11$

(2) The second Gourava index for $Si_2C_3 - II[p,q]$ is

$$\begin{aligned} GO_2(G) &= \sum_{uv\epsilon E(G)} [(d_u + d_v).(d_u.d_v)] \\ &= [(1+2)\times(1\times 2)](2) + [(1+3)\times(1\times 3)](1) \\ &\quad + [(2+2)\times(2\times 2)](2p+2q) \\ &\quad + [(2+3)\times(2\times 3)](8p+8q-14) \\ &\quad + [(3+3)\times(3\times 3)](15pq-13p-13q+11) \\ &= 1080pq - 680p - 680q + 396. \end{aligned} \tag{8}$$

□

Theorem 4. *Let G be the graph of silicon carbide $Si_2C_3 - II[p,q]$. Then, the first and second hyper-Gourava indices are*

(1) $HGO_1(G) = 3375pq - 1829p - 1829q + 880$,

(2) $HGO_2(G) = 43740pq - 30196p - 30196q + 19692$.

Proof. From the edge partition of $Si_2C_3 - II[p,q]$ given in Table 2, we have

(1) The first hyper-Gourava index for $Si_2C_3 - II[p,q]$ is

$$\begin{aligned} HGO_1(G) &= \sum_{uv\epsilon E(G)} [(d_u + d_v) + (d_u.d_v)]^2 \\ &= [(1+2)+(1\times 2)]^2(2) + [(1+3)+(1\times 3)]^2(1) \\ &\quad + [(2+2)+(2\times 2)]^2(2p+2q) \\ &\quad + [(2+3)+(2\times 3)]^2(8p+8q-14) \\ &\quad + [(3+3)+(3\times 3)]^2(15pq-3p-13q+11) \\ &= 3375pq - 1829p - 1829q + 880. \end{aligned} \tag{9}$$

(2) The second hyper-Gourava index for $Si_2C_3 - II[p,q]$ is

$$\begin{aligned} HGO_2(G) &= \sum_{uv\epsilon E(G)} [(d_u + d_v).(d_u.d_v)]^2 \\ &= [(1+2)\times(1\times 2)]^2(2) + [(1+3)\times(1\times 3)]^2(1) \\ &\quad + [(2+2)\times(2\times 2)]^2(2p+2q) \\ &\quad + [(2+3)\times(2\times 3)]^2(8p+8q-14) \\ &\quad + [(3+3)\times(3\times 3)]^2(15pq-13p-13q+11) \\ &= 43740pq - 30196p - 30196q + 19692. \end{aligned} \tag{10}$$

□

3.1.3. Gourava Indices for Silicon Carbide $Si_2C_3 - III[p,q]$. The unit cell of $Si_2C_3III[p,q]$ is shown in Figure 9. The 2D lattice graphs of $Si_2C_3 - I[5,1]$, $Si_2C_3 - I[5,2]$, and $Si_2C_3 - I[5,4]$ are shown in Figures 10–12, respectively. The edge partition of the edge set of $Si_2C_3III[p,q]$ based on the degrees of end vertices is given in Table 3.

Theorem 5. *Let G be the graph of silicon carbide $Si_2C_3III[p,q]$. Then, the first and second Gourava indices are*

(1) $GO_1(G) = 225pq - 62p - 91q + 18$,

(2) $GO_2(G) = 810pq - 300p - 430q + 128$.

Proof. From the edge partition of $Si_2C_3III[p,q]$ given in Table 3, we have

(1) The first Gourava index for $Si_2C_3III[p,q]$ is

$$\begin{aligned} GO_1(G) &= \sum_{uv\epsilon E(G)} [(d_u + d_v) + (d_u.d_v)] \\ &= (1\times 3)](1) + [(2+2)+(2\times 2)](2p+2q) \\ &\quad + [(2+3)+(2\times 3)](8p+8q-14) \\ &\quad + [(3+3)+(3\times 3)](15pq-13p-13q+11) \\ &= 225pq - 62p - 91q + 18. \end{aligned} \tag{11}$$

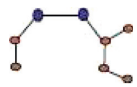

Figure 9: Unit cell.

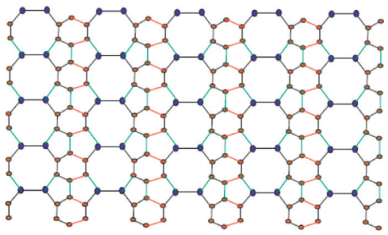

Figure 10: $Si_2C_3 - I[5,1]$.

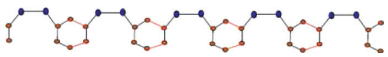

Figure 11: $Si_2C_3 - I[5,2]$.

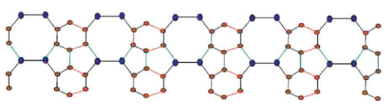

Figure 12: $Si_2C_3 - I[5,4]$.

Table 3: Degree-based edge partition of $Si_2C_3III[p,q]$.

(d_u, d_v)	Frequency
$(1,3)$	2
$(2,2)$	$2q+2$
$(2,3)$	$8p+8q-12$
$(3,3)$	$15pq-10p-13q+8$

(2) The second Gourava index for $Si_2C_3III[p,q]$ is

$$\begin{aligned} GO_2(G) &= \sum_{uv\epsilon E(G)} [(d_u+d_v).(d_u.d_v)] \\ &= [(1+3)\times(1\times3)](1) + [(2+2)\times(2\times2)](2p+2q) \\ &\quad + [(2+3)\times(2\times3)](8p+8q-14) \\ &\quad + [(3+3)\times(3\times3)](15pq-13p-13q+11) \\ &= 810pq-300p-430q+128. \end{aligned} \tag{12}$$

□

Theorem 6. *Let G be the graph of silicon carbide $Si_2C_3III[p,q]$. Then, the first and second hyper-Gourava indices are*

(1) $HGO_1(G) = 3375pq - 1282p - 1829q + 500$,

(2) $HGO_2(G) = 43740pq - 21960p - 30196q + 13328$.

Proof. From the edge partition of $Si_2C_3III[p,q]$ given in Table 3, we have

(1) The first hyper-Gourava index for $Si_2C_3III[p,q]$ is

$$\begin{aligned} HGO_1(G) &= \sum_{uv\epsilon E(G)} [(d_u+d_v)+(d_u.d_v)]^2 \\ &= [(1+3)+(1\times3)]^2(1) + [(2+2)+(2\times2)]^2(2p+2q) \\ &\quad + [(2+3)+(2\times3)]^2(8p+8q-14) \\ &\quad + [(3+3)+(3\times3)]^2(15pq-3p-13q+11) \\ &= 3375pq-1282p-1829q+500. \end{aligned} \tag{13}$$

(2) The second hyper-Gourava index for $Si_2C_3III[p,q]$ is

$$\begin{aligned} HGO_2(G) &= \sum_{uv\epsilon E(G)} [(d_u+d_v).(d_u.d_v)]^2 \\ &= [(1+3)\times(1\times3)]^2(1) + [(2+2)\times(2\times2)]^2(2p+2q) \\ &\quad + [(2+3)\times(2\times3)]^2(8p+8q-14) \\ &\quad + [(3+3)\times(3\times3)]^2(15pq-13p-13q+11) \\ &= 43740pq-21960p-30196q+13328. \end{aligned} \tag{14}$$

□

3.1.4. Gourava Indices for Silicon Carbide $SiC_3 - III[p,q]$. The unit cell of $SiC_3 - III[p,q]$ is shown in Figure 13. The 2D lattice graphs of $SiC_3 - III[5,1]$, $SiC_3 - III[5,2]$, and $SiC_3 - III[5,4]$ are shown in Figures 14–16, respectively. The edge partition of the edge set of $SiC_3 - III[p,q]$ based on the degrees of end vertices is given in Table 4.

Theorem 7. *Let G be the graph of silicon carbide $SiC_3III[p,q]$. Then, the first and second Gourava indices are*

(1) $GO_1(G) = 480pq - 90p - 60q + 25$,

(2) $GO_2(G) = 648pq - 420p - 280q + 168$.

Proof. From the edge partition of the edge set of $SiC_3III[p,q]$ given in Table 4, we have

(1) The first Gourava index for $SiC_3III[p,q]$ is

$$\begin{aligned} GO_1(G) &= \sum_{uv\epsilon E(G)} [(d_u+d_v)+(d_u.d_v)] \\ &= [(1+2)+(1\times2)](2) + [(1+3)+(1\times3)](1) \\ &\quad + [(2+2)+(2\times2)](3p+2q-3) \\ &\quad + [(2+3)+(2\times3)](6p+4q-8) \\ &\quad + [(3+3)+(3\times3)](12pq-12p-8q+8) \\ &= 480pq-90p-60q+25. \end{aligned} \tag{15}$$

(2) The second Gourava index for $SiC_3III[p,q]$ is

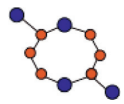

Figure 13: Unit cell.

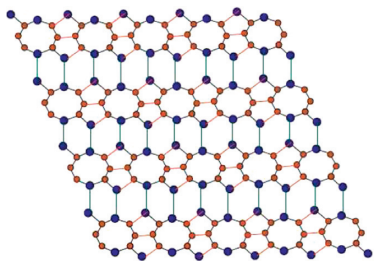

Figure 14: $SiC_3 - III[5,1]$.

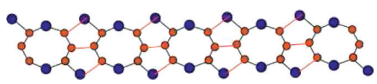

Figure 15: $SiC_3 - III[5,2]$.

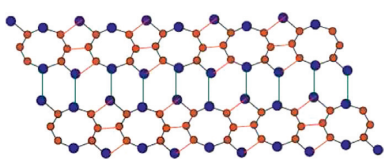

Figure 16: $SiC_3 - III[5,4]$.

Table 4: Degree-based edge partition of $SiC_3III[p,q]$.

(d_u, d_v)	Frequency
$(1,2)$	2
$(1,3)$	1
$(2,2)$	$3p+2q-3$
$(2,3)$	$6p+4q-8$
$(3,3)$	$12pq-12p-8q+8$

$$\begin{aligned} GO_2(G) &= \sum_{uv\epsilon E(G)} [(d_u+d_v).(d_u.d_v)] \\ &= [(1+2)\times(1\times 2)](2) + [(1+3)\times(1\times 3)](1) \\ &\quad + [(2+2)\times(2\times 2)](3p+2q-3) \\ &\quad + [(2+3)\times(2\times 3)](6p+4q-8) \\ &\quad + [(3+3)\times(3\times 3)](12pq-12p-8q+8) \\ &= 648pq-420p-280q+168. \end{aligned} \tag{16}$$

□

Theorem 8. *Let G be the graph of silicon carbide $SiC_3III[p,q]$. Then, the first and second hyper-Gourava indices are*

(1) $HGO_1(G) = 2700pq - 1782p - 118q + 739$,

(2) $HGO_2(G) = 34992pq - 28824p - 19216q + 15576$.

Proof. From the edge partition of the edge set of SiC_3 $III[p,q]$ given in Table 4, we have

(1) The first hyper-Gourava index for $SiC_3III[p,q]$ is

$$\begin{aligned} HGO_1(G) &= \sum_{uv\epsilon E(G)} [(d_u+d_v)+(d_u.d_v)]^2 \\ &= [(1+2)+(1\times 2)]^2(2) + [(1+3)+(1\times 3)]^2(1) \\ &\quad + [(2+2)+(2\times 2)]^2(2p+2q) \\ &\quad + [(2+3)+(2\times 3)]^2(8p+8q-14) \\ &\quad + [(3+3)+(3\times 3)]^2(15pq-3p-13q+11) \\ &= 2700pq-1782p-118q+739. \end{aligned} \tag{17}$$

(2) The second hyper-Gourava index for $SiC_3III[p,q]$ is

$$\begin{aligned} HGO_2(G) &= \sum_{uv\epsilon E(G)} [(d_u+d_v).(d_u.d_v)]^2 \\ &= [(1+2)\times(1\times 2)]^2(2) + [(1+3)\times(1\times 3)]^2(1) \\ &\quad + [(2+2)\times(2\times 2)]^2(2p+2q) \\ &\quad + [(2+3)\times(2\times 3)]^2(8p+8q-14) \\ &\quad + [(3+3)\times(3\times 3)]^2(15pq-13p-13q+11) \\ &= 34992pq-28824p-19216q+15576. \end{aligned} \tag{18}$$

□

3.1.5. Graphical Comparison of Results of Silicone Carbides. In Figures 17–20, we can observe that the behavior of all indices is exponentially increasing with respect to the involved parameters.

Codes for plotting the first and second Gourava indices for silicon carbide $Si_2C_3I[p,r]$ are given as follows:

```
plot3d(225 * p * q − 61 * p − 91 * q + 18, p = 0..1, q = 0..1,
  colour = red),
plot3d(810 * p * q − 290 * p − 430 * q + 126, p = 0..1, q = 0..1,
  colour = green).
```

(19)

3.2. Gourava Indices for Bismuth Triiodide. BiI_3 is an inorganic compound which is the result of the reaction between iodine and bismuth, which inspired the enthusiasm for subjective inorganic investigations [46]. BiI_3 is an excellent inorganic compound and is very useful in qualitative inorganic analysis [47]. It has been proven that Bi-doped glass optical strands are one of the most promising dynamic laser media. Different kinds of Bi-doped fiber strands have been created and have been used to construct Bi-doped fiber lasers and optical loudspeakers [48]. Layered BiI_3 gemstones are considered to be a three-layered stack structure in which a plane of bismuth atoms is sandwiched between iodide

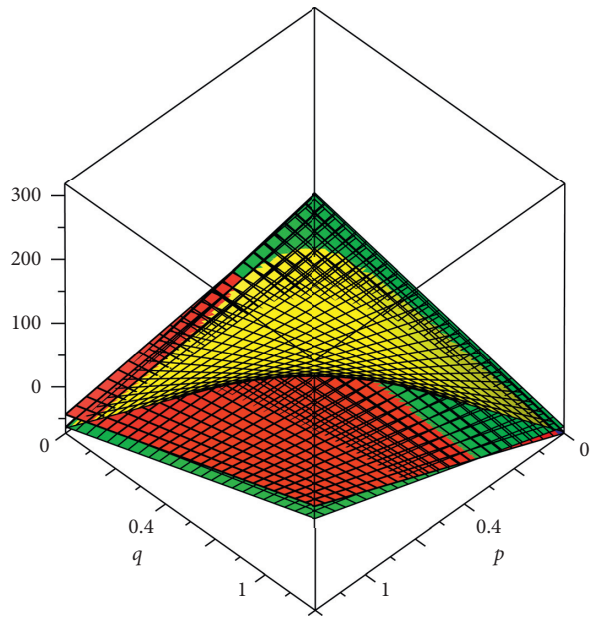

Figure 17: Comparison of the first Gourava index.

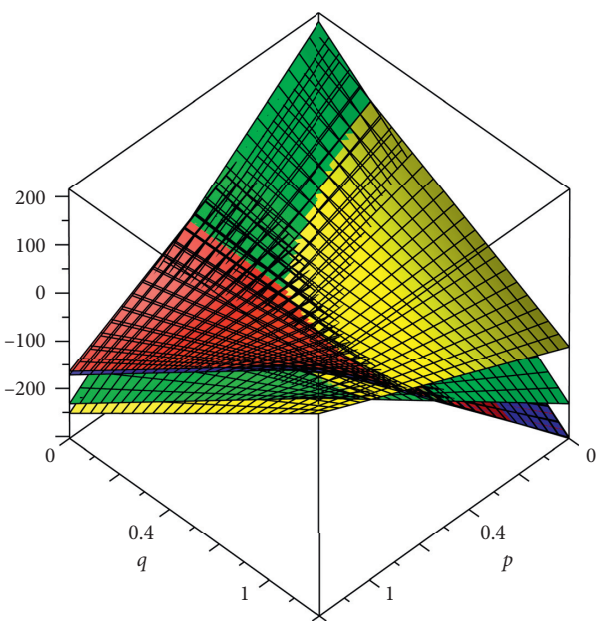

Figure 18: Comparison of the second Gourava index.

particle planes to form a continuous plane [49]. The periodic superposition of the three layers forms diamond-shaped BiI_3 crystals with $R-3$ symmetry [50, 51]. A progressive stack of I − Bi − I layers forms a hexagonal structure with symmetry [52]. A jewel of BiI_3 has been integrated in [46]. We referred to [6] for the topological study of bismuth triiodide.

3.2.1. Bismuth Triiodide Chain $m-BiI_3$. The molecular graph of the unit cell of $m-BiI_3$ is shown in Figure 21. From Figure 22, we can see that the molecular graph of $m-BiI_3$ has two types of edge sets. The edge partition of the edge set of $m-BiI_3$ is given in Table 5.

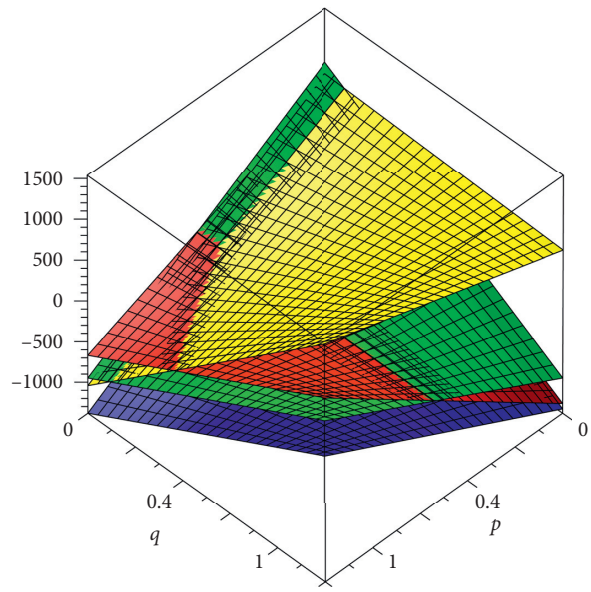

Figure 19: Comparison of the first hyper-Gourava index.

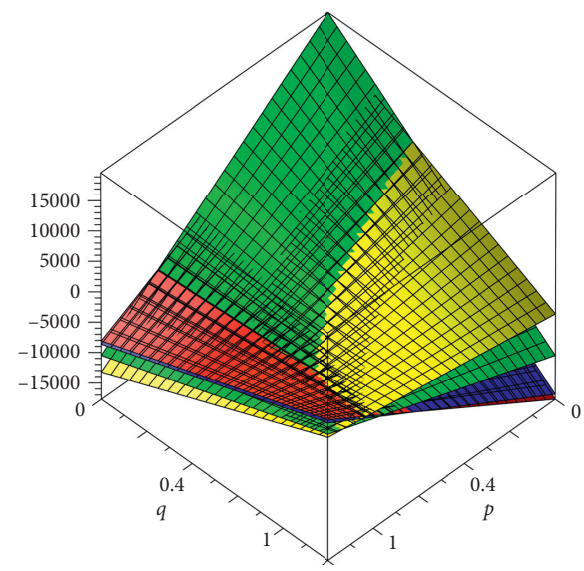

Figure 20: Comparison of the second hyper-Gourava index.

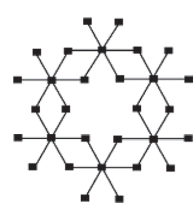

Figure 21: Unit cell (bismuth triiodide).

Theorem 9. *Let G be the graph of the bismuth triiodide chain $m-BiI_3$. Then, the first and second Gourava indices are*

(1) $GO_1(G) = 452m + 184$,

(2) $GO_2(G) = 2088m + 720$.

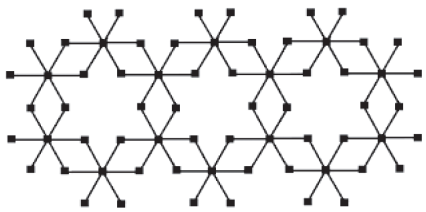

Figure 22: The chain for $m = 3$ (bismuth triiodide).

Table 5: Degree-based edge partition of $m - \mathrm{BiI}_3[m,n]$ of end vertices of each edge.

(d_u, d_v)	Frequency
$(1,6)$	$4m+8$
$(2,6)$	$20m+4$

Proof. From the edge partition of the edge set of $m - \mathrm{BiI}_3$ given in Table 5, we have

(1) The first Gourava index for $m - \mathrm{BiI}_3$ is

$$\begin{aligned} \mathrm{GO}_1(G) &= \sum_{uv\epsilon E(G)} [(d_u + d_v) + (d_u.d_v)] \\ &= [(1+6)+(1\times 6)](4m+8) \\ &\quad + [(2+6)+(2\times 6)](20m+4) \\ &= 452m + 184. \end{aligned} \tag{20}$$

(2) The second Gourava index for $m - \mathrm{BiI}_3$ is

$$\begin{aligned} \mathrm{GO}_2(G) &= \sum_{uv\epsilon E(G)} [(d_u + d_v).(d_u.d_v)] \\ &= [(1+6)\times(1\times 6)](4m+8) \\ &\quad + [(2+6)\times(2\times 6)](20m+4) \\ &= 2088m + 720. \end{aligned} \tag{21}$$

□

Theorem 10. *Let G be the graph of the bismuth triiodide chain $m - BiI_3$. Then, the first and second hyper-Gourava indices are*

(1) $HGO_1(G) = 8676m + 2952$,

(2) $HGO_2(G) = 191376m + 93376$.

Proof. From the edge partition of the edge set of $m - \mathrm{BiI}_3$ given in Table 5, we have

(1) The first hyper-Gourava index for $m - \mathrm{BiI}_3$ is

$$\begin{aligned} \mathrm{HGO}_1(G) &= \sum_{uv\epsilon E(G)} [(d_u + d_v) + (d_u.d_v)]^2 \\ &= [(1+6)+(1\times 6)]^2(4m+8) \\ &\quad + [(2+6)+(2\times 6)]^2(20m+4) \\ &= 8676m + 2952. \end{aligned} \tag{22}$$

(2) The second hyper-Gourava index for $m - \mathrm{BiI}_3$ is

$$\begin{aligned} \mathrm{HGO}_2(G) &= \sum_{uv\epsilon E(G)} [(d_u + d_v).(d_u.d_v)]^2 \\ &= [(1+6)\times(1\times 6)]^2(4m+8) \\ &\quad + [(2+6)\times(2\times 6)]^2(20m+4) \\ &= 191376m + 93376. \end{aligned} \tag{23}$$

□

3.2.2. Bismuth Triiodide Sheet $BiI_3(m \times n)$. The molecular graph of the bismuth triiodide sheet $\mathrm{BiI}_3(m \times n)$ is shown in Figure 23. It can be observed from Figure 23 that the edge set of the bismuth triiodide sheet $\mathrm{BiI}_3(m \times n)$ can be divided into three classes based on the degrees of end vertices as shown in Table 6.

Theorem 11. *Let G be the graph of the bismuth triiodide sheet $BiI_3(m \times n)$. Then, the first and second Gourava indices are*

(1) $GO_1(G) = 402mn + 212m + 50n - 28$,

(2) $GO_2(G) = 2124mn + 936m - 36n - 216$.

Proof. From the edge partition of the edge set of the bismuth triiodide sheet $\mathrm{BiI}_3(m \times n)$ given in Table 6, we have

(1) The first Gourava index for $\mathrm{BiI}_3(m \times n)$ is

$$\begin{aligned} \mathrm{GO}_1(G) &= \sum_{uv\epsilon E(G)} [(d_u + d_v) + (d_u.d_v)] \\ &= [(1+6)+(1\times 6)](4m+4n+4) \\ &\quad + [(2+6)+(2\times 6)](12mn+8m+8n-4) \\ &\quad + [(3+6)+(3\times 6)](6mn-6n) \\ &= 402mn + 212m + 50n - 28. \end{aligned} \tag{24}$$

(2) The second Gourava index for $\mathrm{BiI}_3(m \times n)$ is

$$\begin{aligned} \mathrm{GO}_2(G) &= \sum_{uv\epsilon E(G)} [(d_u + d_v).(d_u.d_v)] \\ &= [(1+6)\times(1\times 6)](4m+4n+4) \\ &\quad + [(2+6)\times(2\times 6)](12mn+8m+8n-4) \\ &\quad + [(3+6)\times(3\times 6)](6mn-6n) \\ &= 2124mn + 936m - 36n - 216. \end{aligned} \tag{25}$$

□

Theorem 12. *Let G be the graph of the bismuth triiodide sheet $BiI_3(m \times n)$. Then, the first and second hyperGourava indices are*

(1) $HGO_1(G) = 9174mn + 3876m - 498n - 924$,

(2) $HGO_2(G) = 268056mn + 80784m - 143036n - 29808$.

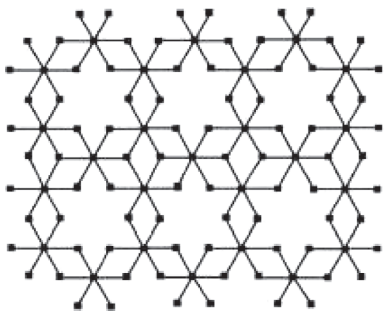

Figure 23: Bismuth triiodide sheet.

Table 6: Degree-based edge partition of $BiI_3\,(m \times n)$.

(d_u, d_v)	Frequency
$(1, 6)$	$4(m + n + 1)$
$(2, 6)$	$4(3mn + 2m + 2n - 1)$
$(3, 6)$	$6n(m - 1)$

Proof. From the edge partition of the edge set of the bismuth triiodide sheet $BiI_3\,(m \times n)$ given in Table 6, we have

(1) The first hyper-Gourava index for $BiI_3\,(m \times n)$ is

$$\begin{aligned} HGO_1(G) &= \sum_{uv \in E(G)} \left[(d_u + d_v) + (d_u.d_v)\right]^2 \\ &= [(1+6) + (1 \times 6)]^2 (4m + 4n + 4) \\ &\quad + [(2+6) + (2 \times 6)]^2 (12mn + 8m + 8n - 4) \\ &\quad + [(3+6) + (3 \times 6)]^2 (6mn - 6n) \\ &= 9174mn + 3876m - 498n - 924. \end{aligned} \tag{26}$$

(2) The second hyper-Gourava index for $BiI_3\,(m \times n)$ is

$$\begin{aligned} HGO_2(G) &= \sum_{uv \in E(G)} \left[(d_u + d_v).(d_u.d_v)\right]^2 \\ &= [(1+6) \times (1 \times 6)]^2 (4m + 4n + 4) \\ &\quad + [(2+6) \times (2 \times 6)]^2 (12mn + 8m + 8n - 4) \\ &\quad + [(3+6) \times (3 \times 6)]^2 (6mn - 6n) \\ &= 268056mn + 80784m - 143036n - 29808. \end{aligned} \tag{27}$$

□

3.3. Graphical Representation. Graphical representation of computed topological indices for the bismuth triiodide chain is shown in Figures 24–27, and the graphical representation of the bismuth triiodide sheet is shown in Figures 28–31.

3.4. Gourava Indices for Dendrimers. In the medication mathematical model, the structure of the drug is addressed as an undirected graph, where each vertex exhibits a molecule and each edge addresses a bond between atoms. A huge number of new drugs have been made each year. From this time forward, it asks for a giant measure of work to choose the pharmacological compound and organic qualities of these new drugs, and such remaining tasks at hand end up being progressively specific and grouped. It requires enough reagent rigging and accomplices to test the exhibitions and the responses of new drugs. Nevertheless, in cut down poor countries and locales (for instance, certain urban networks and countries in South America, Southeast Asia, Africa, and India), there is no sufficient money to settle reagents and apparatus which can be used to gauge the biochemical properties. For topological study of dendrimers, we refer [53–66].

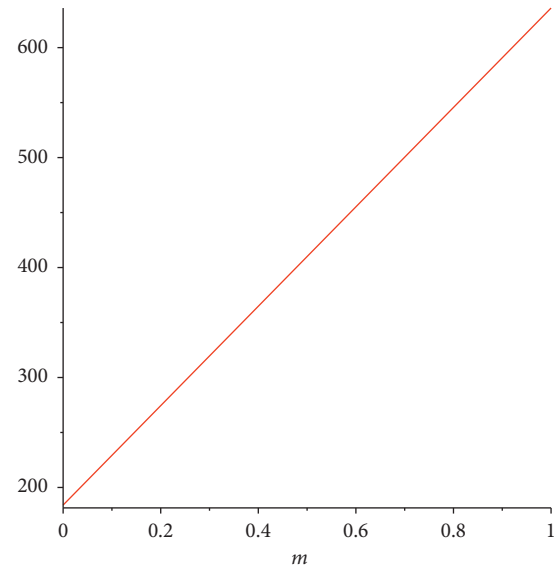

Figure 24: Plots of the first Gourava index for $m - BiI_3$.

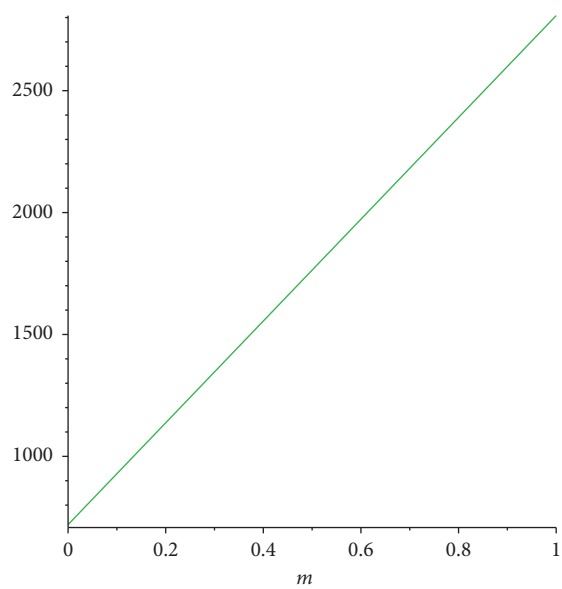

Figure 25: Plots of the second Gourava index for $m - BiI_3$.

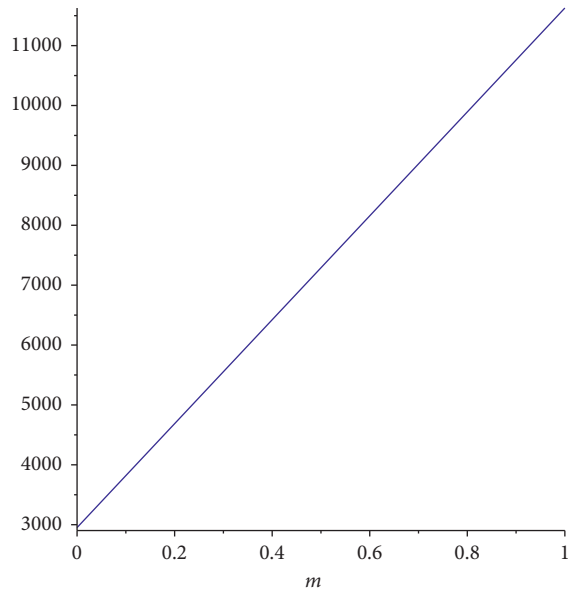

Figure 26: Plots of the first hyper-Gourava index for $m - \mathrm{Bil}_3$.

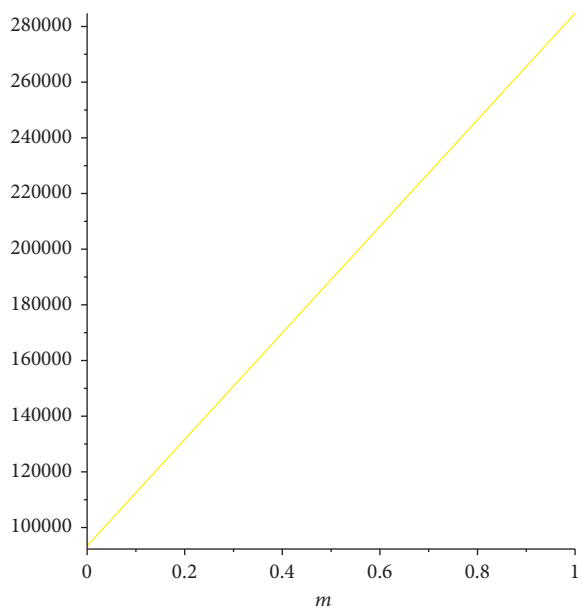

Figure 27: Plots of the second hyper-Gourava index for $m - \mathrm{Bil}_3$.

3.4.1. Gourava Indices of Porphyrin Dendrimer D_nP_n. The algebraic graph of porphyrin dendrimer $\mathrm{D}_n\mathrm{P}_n$ is shown in Figure 32. For porphyrin dendrimer $\mathrm{D}_n\mathrm{P}_n$, $|V(\mathrm{D}_n\mathrm{P}_n)| = 96n - 10$ and $|E(\mathrm{D}_n\mathrm{P}_n)| = 105n - 11$. There are six type of edges in the edge set of porphyrin dendrimer, based on the degree of end vertices. Degree-based partition of edges of porphyrin dendrimer $\mathrm{D}_n\mathrm{P}_n$ is given in Table 7.

Theorem 13. *Let G be the graph of porphyrin dendrimer D_nP_n. Then, the first and second Gourava indices are*

(1) $GO_1(G) = 1169n - 106$,

(2) $GO_2(G) = 3478n - 260$.

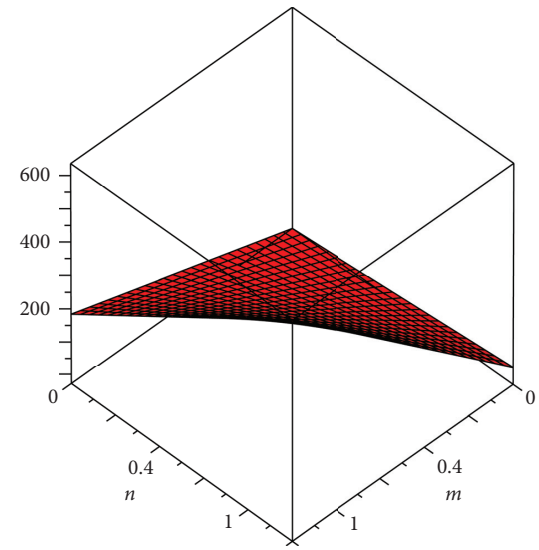

Figure 28: Plots of the first Gourava index for $\mathrm{Bil}_3(m \times n)$.

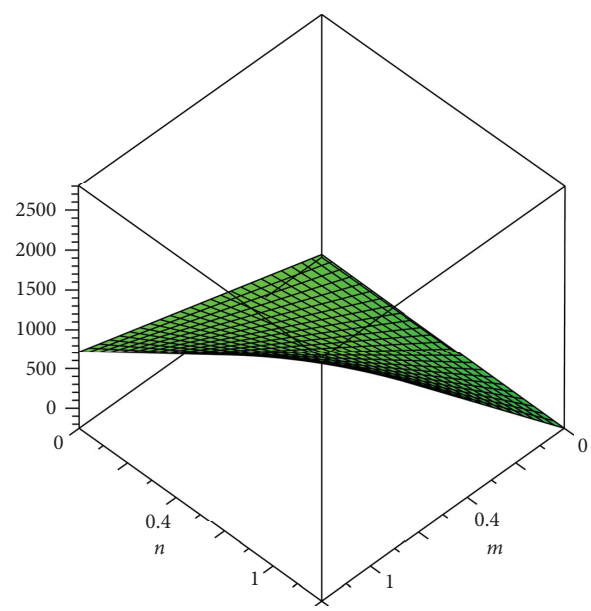

Figure 29: Plots of the second Gourava index for $\mathrm{Bil}_3(m \times n)$.

Proof. From the edge partition of $\mathrm{D}_n\mathrm{P}_n$ given in Table 7, we have

(1) The first Gourava index for $\mathrm{D}_n\mathrm{P}_n$ is

$$\begin{aligned}
\mathrm{GO}_1(G) &= \sum_{uv \in E(G)} [(d_u + d_v) + (d_u . d_v)] \\
&= [(1+3) + (1 \times 3)](2n) + [(1+4) + (1 \times 4)](24n) \\
&\quad + [(2+2) + (2 \times 2)](10n - 5) \\
&\quad + [(2+3) + (2 \times 3)](48n - 6) \\
&\quad + [(3+3) + (3 \times 3)](13n) + [(3+4) + (3 \times 4)](8n) \\
&= 1169n - 106.
\end{aligned} \tag{28}$$

(2) The second Gourava index for $\mathrm{D}_n\mathrm{P}_n$ is

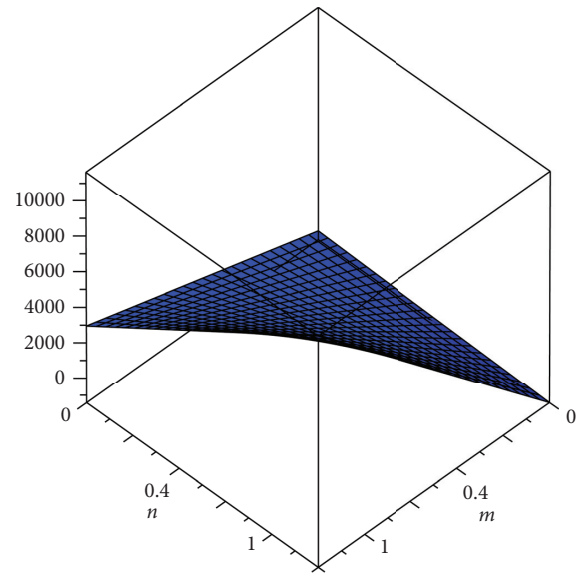

Figure 30: Plots of the first hyper-Gourava index for $\mathrm{Bil}_3\,(m \times n)$.

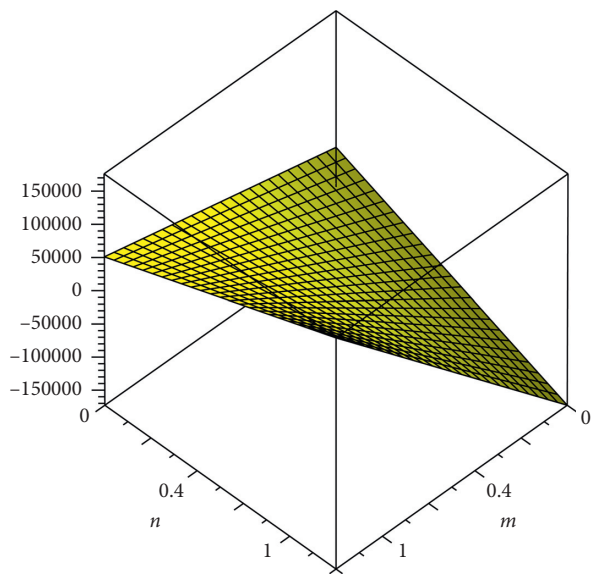

Figure 31: Plots of the second hyper-Gourava index for $\mathrm{Bil}_3\,(m \times n)$.

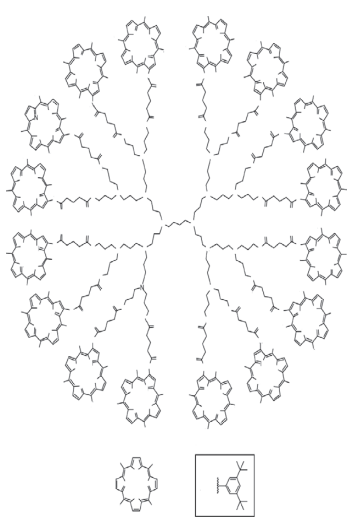

Figure 32: Porphyrin dendrimer $\mathrm{D}_n\mathrm{P}_n$.

Table 7: Degree-based edge partition of $\mathrm{D}_n\mathrm{P}_n$.

(d_u, d_v)	Frequency
$(1,3)$	$2n$
$(1,4)$	$124n$
$(2,2)$	$10n-5$
$(2,3)$	$48n-6$
$(3,3)$	$13n$
$(3,4)$	$8n$

$$\begin{aligned}
\mathrm{GO}_2(\mathrm{D}_n\mathrm{P}_n) &= \sum_{uv\epsilon E(G)} [(d_u + d_v).(d_u.d_v)] \\
&= [(1+3)\times(1\times 3)](2n) + [(1+4)\times(1\times 4)](24n) \\
&\quad + [(2+2)\times(2\times 2)](10n-5) \\
&\quad + [(2+3)\times(2\times 3)](48n-6) \\
&\quad + [(3+3)\times(3\times 3)](13n) + [(3+4)\times(3\times 4)](8n) \\
&= 3478n - 260.
\end{aligned} \tag{29}$$

□

Theorem 14. *Let G be the graph of porphyrin dendrimer D_nP_n. Then, the first and second hyper-Gourava indices are*

(1) $HGO_1(G) = 13727n - 1046$,

(2) $HGO_2(G) = 150004n - 6680$.

Proof. From the edge partition of $\mathrm{D}_n\mathrm{P}_n$ given in Table 7, we have

(1) The first hyper-Gourava index for $\mathrm{D}_n\mathrm{P}_n$ is

$$\begin{aligned}
\mathrm{HGO}_1(G) &= \sum_{uv\epsilon E(G)} [(d_u + d_v) + (d_u.d_v)]^2 \\
&= [(1+3)+(1\times 3)]^2(2n) + [(1+4)+(1\times 4)]^2(24n) \\
&\quad + [(2+2)+(2\times 2)]^2(10n-5) \\
&\quad + [(2+3)+(2\times 3)]^2(48n-6) \\
&\quad + [(3+3)+(3\times 3)]^2(13n) + [(3+4)+(3\times 4)]^2(8n) \\
&= 13727n - 1046.
\end{aligned} \tag{30}$$

(2) The second hyper-Gourava index for $\mathrm{D}_n\mathrm{P}_n$ is

$$\begin{aligned}
\mathrm{HGO}_2(G) &= \sum_{uv\epsilon E(G)} [(d_u + d_v).(d_u.d_v)]^2 \\
&= [(1+3)\times(1\times 3)]^2(2n) + [(1+4)\times(1\times 4)]^2(24n) \\
&\quad + [(2+2)\times(2\times 2)]^2(10n-5) \\
&\quad + [(2+3)\times(2\times 3)]^2(48n-6) \\
&\quad + [(3+3)\times(3\times 3)]^2(13n) + [(3+4)\times(3\times 4)]^{(8n)} \\
&= 150004n - 6680.
\end{aligned} \tag{31}$$

□

3.4.2. Propyl Ether Imine Dendrimer (PETIM). The algebraic graph of propyl ether imine dendrimer (PETIM) is shown in Figure 33. For propyl ether imine dendrimer (PETIM), $|V(\text{PETIM})| = 24.2^n - 23$ and $|E(\text{PETIM})| = 24.2^n - 24$. There are six type of edges in the edge set of porphyrin dendrimer, based on the degree of end vertices. Degree-based partition of edges of propyl ether imine dendrimer (PETIM) is given in Table 8.

Theorem 15. *Let G be the graph of propyl ether imine dendrimer (PETIM). Then, the first and second Gourava indices are*

(1) $GO_1(G) = 66.2^n + 5n^{n+1} + 8.2^{n+4} - 232$,

(2) $GO_2(G) = 18.2^n + 6.n^{n+1} + 16.2^{n+4} - 528$.

Proof. From the edge partition of PETIM given in Table 8, we have

(1) The first Gourava index for PETIM is

$$\begin{aligned} \mathrm{GO}_1(G) &= \sum_{uv\epsilon E(G)} [(d_u + d_v) + (d_u.d_v)] \\ &= [(1+2) + (1\times 2)]\left(2^{n+1}\right) \\ &\quad + [(2+2) + (2\times 2)]\left(2^{n+4} - 18\right) \\ &\quad + [(2+3) + (2\times 3)](6.2^n - 6) \\ &= 66.2^n + 5n^{n+1} + 8.2^{n+4} - 232. \end{aligned} \tag{32}$$

(2) The second Gourava index for PETIM is

$$\begin{aligned} \mathrm{GO}_2(\text{PETIM}) &= \sum_{uv\epsilon E(G)} [(d_u + d_v).(d_u.d_v)] \\ &= [(1+2)\times(1\times 2)]\left(2^{n+1}\right) \\ &\quad + [(2+2)\times(2\times 2)]\left(2^{n+4} - 18\right) \\ &\quad + [(2+3)\times(2\times 3)](6.2^n - 6) \\ &= 18.2^n + 6.n^{n+1} + 16.2^{n+4} - 528. \end{aligned} \tag{33}$$

□

Theorem 16. *Let G be the graph of propyl ether imine dendrimer (PETIM). Then, the first and second hyper-Gourava indices are*

(1) $HGO_1(G) = 726.2^n + 25.n^{n+1} + 64.2^{n+4} - 2120$,

(2) $HGO_2(G) = 5400.2^n + 36.n^{n+1} + 256.2^{n+4} - 11808$.

Proof. From the edge partition of PETIM given in Table 8, we have

(1) The first hyper-Gourava index for PETIM is

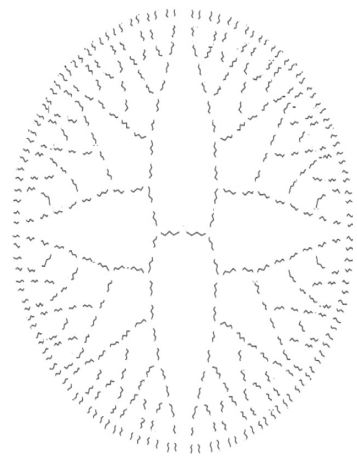

Figure 33: Propyl ether imine dendrimer (PETIM).

Table 8: Degree-based edge partition of (PETIM).

(d_u, d_v)	Frequency
$(1,2)$	2^{n+1}
$(2,2)$	$2^{n+4} - 18$
$(2,3)$	$6.2^n - 6$

$$\begin{aligned} \mathrm{HGO}_1(G) &= \sum_{uv\epsilon E(G)} [(d_u + d_v) + (d_u.d_v)]^2 \\ &= [(1+2) + (1\times 2)]^2\left(2^{n+1}\right) \\ &\quad + [(2+2) + (2\times 2)]^2\left(2^{n+4} - 18\right) \\ &\quad + [(2+3) + (2\times 3)]^2(6.2^n - 6) \\ &= 726.2^n + 25.n^{n+1} + 64.2^{n+4} - 2120. \end{aligned} \tag{34}$$

(2) The second hyper-Gourava index for PETIM is

$$\begin{aligned} \mathrm{HGO}_2(G) &= \sum_{uv\epsilon E(G)} [(d_u + d_v).(d_u.d_v)]^2 \\ &= [(1+2)\times(1\times 2)]^2\left(2^{n+1}\right) \\ &\quad + [(2+2)\times(2\times 2)]^2\left(2^{n+4} - 18\right) \\ &\quad + [(2+3)\times(2\times 3)]^{(6.2^n - 6)} \\ &= 5400.2^n + 36.n^{n+1} + 256.2^{n+4} - 11808. \end{aligned} \tag{35}$$

□

3.4.3. Zinc-Porphyrin Dendrimer DPZ_n. The algebraic graph of zinc-porphyrin dendrimer DPZ_n is shown in Figure 34. There are six type of edges in the edge set of porphyrin dendrimer, based on the degree of end vertices. Degree-based partition of edges of zinc-porphyrin dendrimer DPZ_n is given in Table 9.

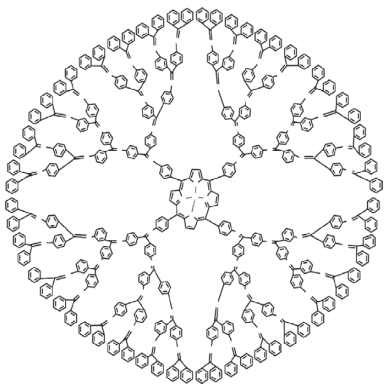

Figure 34: Zinc-porphyrin dendrimer DPZ_n.

Table 9: Degree-based edge partition of DPZ_n.

(d_u, d_v)	Frequency
$(2,2)$	$16.2^n - 4$
$(2,3)$	$40.2^n - 16$
$(3,3)$	$8.2^n - 16$
$(3,4)$	4

Theorem 17. *Let G be the graph of zinc-porphyrin dendrimer DPZ_n. Then, the first and second Gourava indices are*

(1) $GO_1(G) = 688.2^n - 372$,

(2) $GO_2(G) = 1888.2^n - 1072$.

Proof. From the edge partition of DPZ_n given in Table 9, we have

(1) The first Gourava index for DPZ_n is

$$\begin{aligned} GO_1(G) &= \sum_{uv\epsilon E(G)} [(d_u + d_v) + (d_u.d_v)] \\ &= [(2+2) + (2\times 2)](16.2^n - 4) \\ &\quad + [(2+3) + (2\times 3)](40.2^n - 16) \\ &\quad + [(3+3) + (3\times 3)](8.2^n - 16) \\ &\quad + [(3+4) + (3\times 4)](4) \\ &= 688.2^n - 372. \end{aligned} \tag{36}$$

(2) The second Gourava index for DPZ_n is

$$\begin{aligned} GO_2(G) &= \sum_{uv\epsilon E(G)} [(d_u + d_v).(d_u.d_v)] \\ &= [(2+2)\times(2\times 2)](16.2^n - 4) \\ &\quad + [(2+3)\times(2\times 3)](40.2^n - 16) \\ &\quad + [(3+3)\times(3\times 3)](8.2^n - 16) \\ &\quad + [(3+4)\times(3\times 4)](4) \\ &= 1888.2^n - 1072. \end{aligned} \tag{37}$$

□

Theorem 18. *Let G be the graph of zinc-porphyrin dendrimer DPZ_n. Then, the first and second hyper-Gourava indices are*

(1) $HGO_1(G) = 7664n^n - 5716$,

(2) $HGO_2(G) = 63424.2^n - 33856$.

Proof. From the edge partition of DPZ_n given in Table 9, we have

(1) The first hyper-Gourava index for DPZ_n is

$$\begin{aligned} HGO_1(G) &= \sum_{uv\epsilon E(G)} [(d_u + d_v) + (d_u.d_v)]^2 \\ &= [(2+2) + (2\times 2)]^2(16.2^n - 4) \\ &\quad + [(2+3) + (2\times 3)]^2(40.2^n - 16) \\ &\quad + [(3+3) + (3\times 3)]^2(8.2^n - 16) \\ &\quad + [(3+4) + (3\times 4)]^2(4) \\ &= 7664n^n - 5716. \end{aligned} \tag{38}$$

(2) The second hyper-Gourava index for DPZ_n is

$$\begin{aligned} HGO_2(G) &= \sum_{uv\epsilon E(G)} [(d_u + d_v).(d_u.d_v)]^2 \\ &= [(2+2)\times(2\times 2)]^2(16.2^n - 4) \\ &\quad + [(2+3)\times(2\times 3)]^2(40.2^n - 16) \\ &\quad + [(3+3)\times(3\times 3)]^2(8.2^n - 16) \\ &\quad + [(3+4)\times(3\times 4)]^2(4) \\ &= 63424.2^n - 33856. \end{aligned} \tag{39}$$

□

3.4.4. Poly(EThyleneAmidoAmine) Dendrimer (PETAA). The algebraic graph of Poly(EThyleneAmidoAmine) dendrimer (PETAA) is shown in Figure 35. For Poly(EThyleneAmidoAmine) dendrimer (PETAA), $|V(\text{PETAA})| = 44.2^n - 18$ and $|E(\text{PETAA})| = 44.2^n - 19$. There are six type of edges in the edge set of porphyrin dendrimer, based on the degree of end vertices. Degree-based partition of edges of Poly(EThyleneAmidoAmine) dendrimer (PETAA) is given in Table 10.

Theorem 19. *Let G be the graph of Poly(EThylene Amide Amine) dendrimer (PETAA). Then, the first and second Gourava indices are*

(1) $GO_1(G) = 369.2^n - 177$,

(2) $GO_2(G) = 928.2^n - 422$.

Proof. From the edge partition of PETAA given in Table 10, we have

(1) The first Gourava index for PETAA is

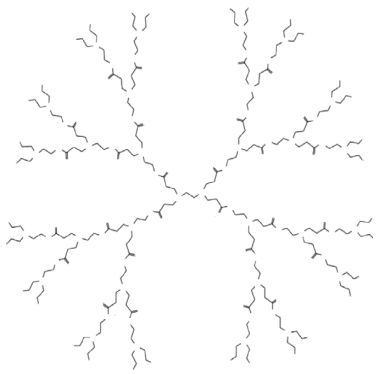

Figure 35: Poly(EThylene amide amine) dendrimer (PETAA).

Table 10: Degree-based edge partition of (PETAA).

(d_u, d_v)	Frequency
$(1,2)$	4.2^n
$(1,3)$	$4.2^n - 2$
$(2,2)$	$16.2^n - 8$
$(2,3)$	$20.2^n - 9$

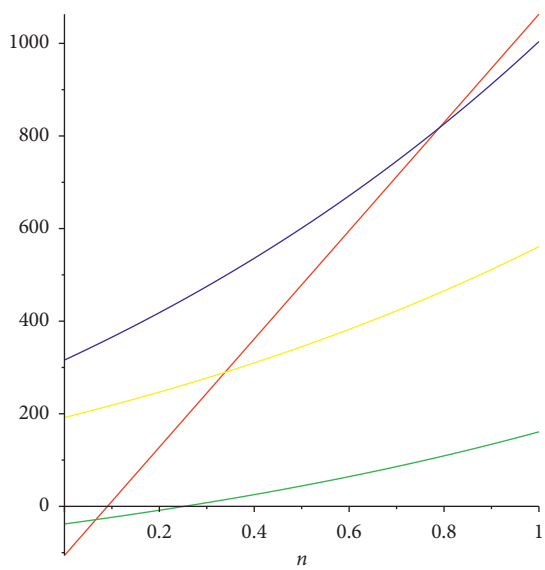

Figure 36: First Gourava index.

$$\begin{aligned} GO_1(G) &= \sum_{uv\epsilon E(G)} [(d_u + d_v) + (d_u.d_v)] \\ &= [(1+2) + (1\times 2)](4.2^n) \\ &\quad + [(1+3) + (1\times 3)](4.2^n - 2) \\ &\quad + [(2+2) + (2\times 2)](16.2^n - 8) \\ &\quad + [(2+3) + (2\times 3)](20.2^n - 9) \\ &= 369.2^n - 177. \end{aligned} \tag{40}$$

(2) The second Gourava index for PETAA is

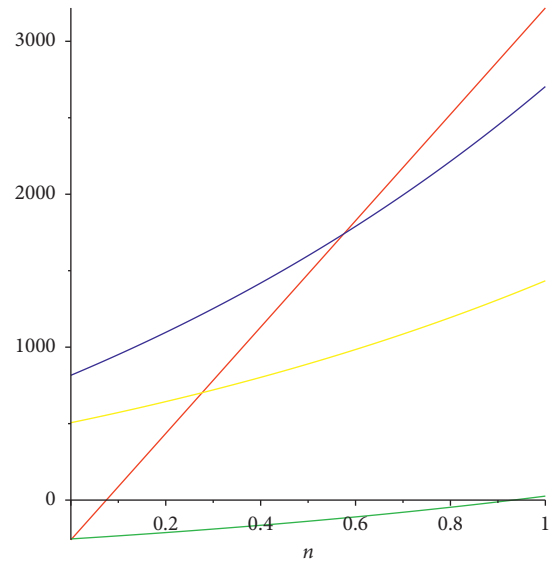

Figure 37: Second Gourava index.

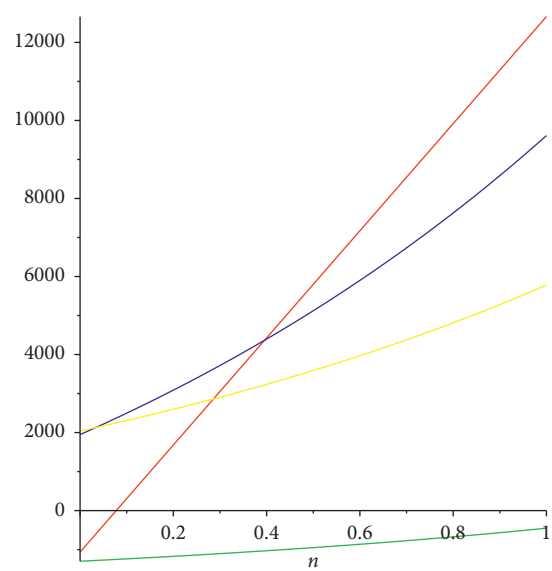

Figure 38: First hyper-Gourava index.

$$\begin{aligned} GO_2(PETAA) &= \sum_{uv\epsilon E(G)} [(d_u + d_v).(d_u.d_v)] \\ &= [(1+2)\times(1\times 2)](4.2^n) \\ &\quad + [(1+3)\times(1\times 3)](4.2^n - 2) \\ &\quad + [(2+2)\times(2\times 2)](16.2^n - 8) \\ &\quad + [(2+3)\times(2\times 3)](20.2^n - 9) \\ &= 928.2^n - 422. \end{aligned} \tag{41}$$

□

Theorem 20. *Let G be the graph of Poly(EThylene Amide Amine) dendrimer (PETAA). Then, the first and second hyper-Gourava indices are*

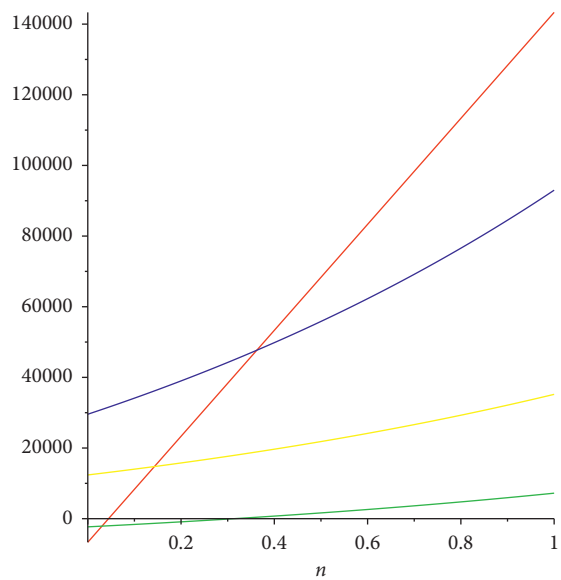

Figure 39: Second hyper-Gourava index.

(1) $HGO_1(G) = 3740.2^n - 1699$,

(2) $HGO_2(G) = 22816.2^n - 10436$.

Proof. From the edge partition of PETAA given in Table 10, we have

(1) The first hyper-Gourava index for PETAA is

$$\begin{aligned} \mathrm{HGO}_1(G) &= \sum_{uv\in E(G)} \left[(d_u + d_v) + (d_u.d_v)\right]^2 \\ &= [(1+2) + (1\times 2)]^2 (4.2^n) \\ &\quad + \left[(1+3) + (1\times 3)^2 (4.2^n - 2)\right. \\ &\quad + [(2+2) + (2\times 2)]^2 (16.2^n - 8) \\ &\quad + [(2+3) + (2\times 3)]^2 (20.2^n - 9) \\ &= 3740.2^n - 1699. \end{aligned} \tag{42}$$

(2) The second hyper-Gourava index for PETAA is

$$\begin{aligned} \mathrm{HGO}_2(G) &= \sum_{uv\in E(G)} \left[(d_u + d_v).(d_u.d_v)\right]^2 \\ &= [(1+2)\times(1\times 2)]^2 (4.2^n) \\ &\quad + [(1+3)\times(1\times 3)]^2 (4.2^n - 2) \\ &\quad + [(2+2)\times(2\times 2)]^2 (16.2^n - 8) \\ &\quad + [(2+3)\times(2\times 3)]^2 (20.2^n - 9) \\ &= 22816.2^n - 10436. \end{aligned} \tag{43}$$

□

3.4.5. Graphical Comparison. In this section, we will present the graphical comparison of first, second, first hyper-, and second hyper-Gourava indices for porphyrin dendrimer D_nP_n, propyl ether imine dendrimer (PETIM), zinc-porphyrin dendrimer DPZ_n and Poly(EThyleneAmidoAmine) dendrimer (PETAA). Figures 36–39 show the all indices are linearly increasing with respect to involved parameters.

4. Conclusions and Future Works

It is important to calculate topological indices of dendrimers because it is a proved fact that topological indices help to predict many properties without going to the wet lab. There are more than around 148 topological indices, but none of them can completely describe all properties of a chemical compound. Therefore, there is always room to define and study new topological indices. Gourava indices are one step in this direction and are very close to Zagreb indices. Zagreb indices are very well studied by chemists and mathematicians due to their huge applications in chemistry. It is an interesting problem for researchers to study chemical properties and bonds of Gourava indices.

Data Availability

The data used to support the findings of this study are included within the article.

Conflicts of Interest

The authors of this paper declare that they have no conflicts of interest.

Authors' Contributions

All authors have equal contribution.

Acknowledgments

This paper was supported by the Educational Commission of Anhui Province of China, under Grant no. KJ2017A627, Quality Engineering Project of Anhui Province, under Grant no. 2016sxzx021, and Quality Engineering Project of Anhui Xinhua University, under Grant nos. 2015xqjdx04; 2015xxk06; AH20171221607.

References

[1] M. Munir, W. Nazeer, S. Rafique, and S. Kang, "M-polynomial and related topological indices of Nanostar dendrimers," *Symmetry*, vol. 8, no. 9, p. 97, 2016.

[2] M. Munir, W. Nazeer, A. Nizami, S. Rafique, and S. Kang, "M-polynomials and topological indices of titania nanotubes," *Symmetry*, vol. 8, no. 11, p. 117, 2016.

[3] Y. Kwun, M. Munir, W. Nazeer, S. Rafique, and S. M. Kang, "M-polynomial and degree-based topological indices of V-phenalinic nanotubes and nanotori," *Scientific Reports*, vol. 7, no. 1, p. 8756, 2017.

[4] M. Munir, W. Nazeer, S. Rafique, A. Nizami, and S. Kang, "Some computational aspects of boron triangular nanotubes," *Symmetry*, vol. 9, no. 1, p. 6, 2016.

[5] M. Munir, W. Nazeer, S. Rafique, and S. Kang, "M-polynomial and degree-based topological indices of polyhex nanotubes," *Symmetry*, vol. 8, no. 12, p. 149, 2016.

[6] M. Imran, M. Siddiqui, M. Naeem, and M. Iqbal, "On topological properties of symmetric chemical structures," *Symmetry*, vol. 10, no. 5, p. 173, 2018.

[7] M. Alaeiyan, M. R. Farahani, and M. K. Jamil, "Computation of the fifth geometric-arithmetic index for polycyclic aromatic hydrocarbons pahk," *Applied Mathematics and Nonlinear Sciences*, vol. 1, no. 1, pp. 283–290, 2016.

[8] M. K. Jamil, M. R. Farahani, M. Imran, and M. Ali Malik, "Computing eccentric version of second zagreb index of polycyclic aromatic hydrocarbons (PAHk)," *Applied Mathematics and Nonlinear Sciences*, vol. 1, no. 1, pp. 247–252, 2016.

[9] M. R. Farahani, M. K. Jamil, and M. Imran, "Vertex PIv topological index of titania carbon nanotubes $TiO_2(m, n)$," *Applied Mathematics and Nonlinear Sciences*, vol. 1, no. 1, pp. 175–182, 2016.

[10] G. Rücker and C. Rücker, "On topological indices, boiling points, and cycloalkanes," *Journal of Chemical Information and Computer Sciences*, vol. 39, no. 5, pp. 788–802, 1999.

[11] S. Klavžar and I. Gutman, "A comparison of the Schultz molecular topological index with the Wiener index," *Journal of Chemical Information and Computer Sciences*, vol. 36, no. 5, pp. 1001–1003, 1996.

[12] F. M. Brückler, T. Došlić, A. Graovac, and I. Gutman, "On a class of distance-based molecular structure descriptors," *Chemical Physics Letters*, vol. 503, no. 4–6, pp. 336–338, 2011.

[13] H. Deng, J. Yang, and F. Xia, "A general modeling of some vertex-degree based topological indices in benzenoid systems and phenylenes," *Computers & Mathematics with Applications*, vol. 61, no. 10, pp. 3017–3023, 2011.

[14] H. Zhang and F. Zhang, "The Clar covering polynomial of hexagonal systems I," *Discrete Applied Mathematics*, vol. 69, no. 1-2, pp. 147–167, 1996.

[15] H. Wiener, "Structural determination of paraffin boiling points," *Journal of the American Chemical Society*, vol. 69, no. 1, pp. 17–20, 1947.

[16] A. A. Dobrynin, R. Entringer, and I. Gutman, "Wiener index of trees: theory and applications," *Acta Applicandae Mathematicae*, vol. 66, no. 3, pp. 211–249, 2001.

[17] A. A. Dobrynin, I. Gutman, S. Klavžar, and P. Žigert, "Wiener index of hexagonal systems," *Acta Applicandae Mathematicae*, vol. 72, no. 3, pp. 247–294, 2002.

[18] W. Gao and L. Shi, "Wiener index of gear fan graph and gear wheel graph," *Asian Journal of Chemistry*, vol. 26, no. 11, 2014.

[19] W. F. Xi and W. Gao, "λ-modified extremal hyper-Wiener index of molecular graphs," *Journal of Applied Computer Science & Mathematics*, vol. 18, no. 8, pp. 43–46, 2014.

[20] W. Gao and W. Wang, "The vertex version of weighted Wiener number for bicyclic molecular structures," *Computational and Mathematical Methods in Medicine*, vol. 2015, Article ID 418106, 10 pages, 2015.

[21] M. Randic, "Characterization of molecular branching," *Journal of the American Chemical Society*, vol. 97, no. 23, pp. 6609–6615, 1975.

[22] M. Randic, "On history of the Randic index and emerging hostility toward chemical graph theory," *MATCH Communications in Mathematical and in Computer Chemistry*, vol. 59, pp. 5–124, 2008.

[23] X. Li and Y. Shi, "A survey on the Randic index," *MATCH Communications in Mathematical and in Computer Chemistry*, vol. 59, no. 1, pp. 127–156, 2008.

[24] S. B. Bozkurt, A. D. Gungor, I. Gutman, and A. S. Cevik, "Randic matrix and Randic energy," *MATCH Communications in Mathematical and in Computer Chemistry*, vol. 64, pp. 239–250, 2010.

[25] C. Delorme, O. Favaron, and D. Rautenbach, "On the Randić index," *Discrete Mathematics*, vol. 257, no. 1, pp. 29–38, 2002.

[26] Y. Hu, X. Li, Y. Shi, T. Xu, and I. Gutman, "On molecular graphs with smallest and greatest zeroth-order general Randic index," *MATCH Communications in Mathematical and in Computer Chemistry*, vol. 54, no. 2, pp. 425–434, 2005.

[27] M. Cavers, S. Fallat, and S. Kirkland, "On the normalized Laplacian energy and general Randić index," *Linear Algebra and Its Applications*, vol. 433, no. 1, pp. 172–190, 2010.

[28] I. Gutman and N. Trinajstic, "Graph theory and molecular orbitals. Total π-electron energy of alternant hydrocarbons," *Chemical Physics Letters*, vol. 17, no. 4, pp. 535–538, 1972.

[29] B. Zhou and I. Gutman, "Further properties of Zagreb indices," *MATCH Communications in Mathematical and in Computer Chemistry*, vol. 54, no. 1, pp. 233–239, 2005.

[30] I. Gutman, B. Furtula, Z. K. Vukicevic, and G. Popivoda, "On Zagreb indices and coindices," *MATCH Communications in Mathematical and in Computer Chemistry*, vol. 74, no. 1, pp. 5–16, 2015.

[31] I. Gutman, "Multiplicative Zagreb indices of trees," *Bulletin of Society of Mathematicians Banja Luka*, vol. 18, pp. 17–23, 2011.

[32] B. Zhou and I. Gutman, "Relations between wiener, hyper-wiener and zagreb indices," *Chemical Physics Letters*, vol. 394, no. 1–3, pp. 93–95, 2004.

[33] I. Gutman, "An exceptional property of first Zagreb index," *MATCH Communications in Mathematical and in Computer Chemistry*, vol. 72, no. 3, pp. 733–740, 2014.

[34] W. Gao, M. R. Farahani, and L. Shi, "Forgotten topological index of some drug structures," *Acta Medica Mediterranea*, vol. 32, no. 1, pp. 579–585, 2016.

[35] W. Gao, M. K. Siddiqui, M. Imran, M. K. Jamil, and M. R. Farahani, "Forgotten topological index of chemical structure in drugs," *Saudi Pharmaceutical Journal*, vol. 24, no. 3, pp. 258–264, 2016.

[36] W. Gao, W. Wang, and M. R. Farahani, "Topological indices study of molecular structure in anticancer drugs," *Journal of Chemistry*, vol. 2016, Article ID 3216327, 8 pages, 2016.

[37] W. Gao, Y. Wang, W. Wang, and L. Shi, "The first multiplication atom-bond connectivity index of molecular structures in drugs," *Saudi Pharmaceutical Journal*, vol. 25, no. 4, pp. 548–555, 2017.

[38] S. Hayat and M. Imran, "Computation of certain topological indices of nanotubes covered by C_5 and C_7," *Journal of Computational and Theoretical Nanoscience*, vol. 12, no. 4, pp. 533–541, 2015.

[39] S. Hayat and M. Imran, "Computation of topological indices of certain networks," *Applied Mathematics and Computation*, vol. 240, pp. 213–228, 2014.

[40] W. Gao, M. Siddiqui, M. Naeem, and N. Rehman, "Topological characterization of carbon graphite and crystal cubic carbon structures," *Molecules*, vol. 22, no. 9, p. 1496, 2017.

[41] M. Imran, M. Siddiqui, A. Abunamous, D. Adi, S. Rafique, and A. Baig, "Eccentricity based topological indices of an oxide network," *Mathematics*, vol. 6, no. 7, p. 126, 2018.

[42] Y. Kwun, A. Virk, W. Nazeer, M. Rehman, and S. Kang, "On the multiplicative degree-based topological indices of silicon-carbon Si_2C_3-I$[p, q]$ and Si_2C_3-II$[p, q]$," *Symmetry*, vol. 10, no. 8, p. 320, 2018.

[43] W. Gao, M. Younas, A. Farooq, A. Mahboob, and W. Nazeer, "M-polynomials and degree-based topological indices of the crystallographic structure of molecules," *Biomolecules*, vol. 8, no. 4, p. 107, 2018.

[44] V. R. Kulli, "The Gourava indices and coindices of graphs," *Annals of Pure and Applied Mathematics*, vol. 14, no. 1, pp. 33–38, 2017.
[45] V. R. Kulli, "Computation of some Gourava indices of titania nanotubes," *International Journal of Fuzzy Mathematical Archive*, vol. 12, no. 2, pp. 75–81, 2017.
[46] M. Imran, M. A. Ali, S. Ahmad, M. K. Siddiqui, and A. Q. Baig, "Topological characterization of the symmetrical structure of bismuth tri-iodide," *Symmetry*, vol. 10, no. 6, p. 201, 2018.
[47] B. Iodide, *McGraw-Hill Dictionary of Scientific and Technical Terms*, McGraw-Hill, New York, NY, USA, 2003.
[48] R. A. Mackay and W. Henderson, *Introduction to Modern Inorganic Chemistry*, CRC Press, Boca Raton, FL, USA, 2002.
[49] L. Smart and A. M. Elaine, *Solid State Chemistry: An Introduction*, CRC Press, Boca Raton, FL, USA, 2005.
[50] K. Watanabe, T. Karasawa, T. Komatsu, and Y. Kaifu, "Optical properties of extrinsic two-dimensional excitons in BiI_3 single crystals," *Journal of the Physical Society of Japan*, vol. 55, no. 3, pp. 897–907, 1986.
[51] R. W. G. Wyckoff, *Crystal Structures*, John Wiley & Sons, Inc., New York, NY, USA, 2nd edition, 1964.
[52] H. Yorikawa and S. Muramatsu, "Theoretical study of crystal and electronic structures of BiI_3," *Journal of Physics: Condensed Matter*, vol. 20, pp. 325–335, 2008.
[53] M. Imran, M. Siddiqui, A. Ahmad, U. Ali, and N. Hanif, "On the degree-based topological indices of the Tickysim SpiNNaker model," *Axioms*, vol. 7, no. 4, p. 73, 2018.
[54] S. Imran, M. Siddiqui, M. Imran, and M. Nadeem, "Computing topological indices and polynomials for line graphs," *Mathematics*, vol. 6, no. 8, p. 137, 2018.
[55] Z. Shao, M. Siddiqui, and M. Muhammad, "Computing zagreb indices and zagreb polynomials for symmetrical nanotubes," *Symmetry*, vol. 10, no. 7, p. 244, 2018.
[56] J. B. Liu, M. Siddiqui, M. Zahid, M. Naeem, and A. Baig, "Topological properties of crystallographic structure of molecules," *Symmetry*, vol. 10, no. 7, p. 265, 2018.
[57] W. Gao, M. Younas, A. Farooq, A. Virk, and W. Nazeer, "Some reverse degree-based topological indices and polynomials of dendrimers," *Mathematics*, vol. 6, no. 10, p. 214, 2018.
[58] Z. Hussain, M. Munir, S. Rafique, and S. Min Kang, "Topological characterizations and index-analysis of new degree-based descriptors of honeycomb networks," *Symmetry*, vol. 10, no. 10, p. 478, 2018.
[59] M. Salaheldeen Abdelgader, C. Wang, and S. Abdalrhman Mohammed, "Computation of topological indices of some special graphs," *Mathematics*, vol. 6, no. 3, p. 33, 2018.
[60] X. Zhang, M. Siddiqui, M. Naeem, and A. Baig, "Computing eccentricity based topological indices of octagonal grid O nm," *Mathematics*, vol. 6, no. 9, p. 153, 2018.
[61] J. B. Liu, H. Ali, M. Shafiq, and U. Munir, "On degree-based topological indices of symmetric chemical structures," *Symmetry*, vol. 10, no. 11, p. 619, 2018.
[62] W. Nazeer, A. Farooq, M. Younas, M. Munir, and S. Kang, "On molecular descriptors of carbon nanocones," *Biomolecules*, vol. 8, no. 3, p. 92, 2018.
[63] M. Zahid, A. Baig, M. Naeem, and M. Azhar, "Eccentricity-based topological indices of a cyclic octahedron structure," *Mathematics*, vol. 6, no. 8, p. 141, 2018.
[64] H. Yang, M. Siddiqui, M. Arshad, and M. Naeem, "Degree-distance based topological indices of crystal cubic carbon structure," *Atoms*, vol. 6, no. 4, p. 62, 2018.
[65] Z. Shao, Pu Wu, X. Zhang, D. Dimitrov, and J.-B. Liu, "On the maximum ABC index of graphs with prescribed size and without pendent vertices," *IEEE Access*, vol. 6, pp. 27604–27616, 2018.
[66] Z. Shao, Pu Wu, Y. Gao, I. Gutman, and X. Zhang, "On the maximum ABC index of graphs without pendent vertices," *Applied Mathematics and Computation*, vol. 315, pp. 298–312, 2017.

Hindawi
Journal of Chemistry
Volume 2020, Article ID 6294613, 12 pages
https://doi.org/10.1155/2020/6294613

Research Article

TRIZ Theory and the Method of Cancer Document Selection for Chemical Complexes and Innovation Schemes of Meta-Analysis with Lymphomas as an Example

Yan Huiquan,[1,2] Lyu Penghui,[2] Wang Ling,[3] and Yu Zhiming[4]

[1]*Novelty Retrieving Center of National Education Department, Hefei University of Technology, Hefei, Anhui, China*
[2]*School of Management, Hefei University of Technology, Hefei, Anhui, China*
[3]*No. 24 Patient Ward, The First Affiliated Hospital of Anhui University of Chinese Medicine, Hefei, China*
[4]*Department of Biological and Environmental Sciences, Hefei University, Hefei, China*

Correspondence should be addressed to Lyu Penghui; lyu@hfut.edu.cn

Received 12 October 2019; Accepted 28 February 2020; Published 22 May 2020

Academic Editor: Jia-Bao Liu

In the face of the growing incidence of malignant tumors (about 3.929 million, data issued in January 2019) and the death rate (about 2.338 million, data issued in January 2019) and the limitation of the application of informatics in cancer treatment, this paper tried to use TRIZ theory to deduce new ideas about cancer treatments, perform literature analysis on schemes, and make retrieval strategy for meta-analyses on cancer therapy. By using TRIZ theory and information to analyze the fields of cancers, the research schemes for selecting documents on cancer therapy were presented. After retrieving the documents, we exported all those articles in text format. We further analyzed the research status with the software CiteSpace and Bibliographic Information Mining System (BICOMS) by using different keywords, regions, countries, schools, authors, geography, institutes, etc. We also performed the cluster analysis by using Statistical Package for the Social Sciences (SPSS) software and performed two-way cluster analysis by using Gluto software. The hot areas of research and their tendency or distribution were analyzed. The search strategy was set and the retrieving results were tried.

1. Introduction to TRIZ

1.1. The Origin of TRIZ and Its Definition. TRIZ theory provided systematic theoretical and methodological tools for finding and solving problems creatively. TRIZ theory was the theory of inventive problem solving and was developed by the Soviet engineer Genrich Altshuller and his colleagues in 1946. Altshuller and his colleagues studied more than 300,000 patents and developed inventive principles which had been often presented in the most successful cases. According to TRIZ, universal principles of creativity form the basis of innovation. TRIZ identified and codified these principles and used them to make the creative process more predictable. In other words, whatever the problems you are facing, somebody, somewhere, had already solved them. Creative problem solution involved finding the solution and adapting it to your problems.

TRIZ was most useful in roles such as product development, design engineering, and process management. For example, Six Sigma quality improvement processes often made use of TRIZ. TRIZ theory was often accepted as a problem-solving analysis and forecast tool derived from the study of patterns of invention in the global patent literature. TRIZ theory consisted of 840 principles of invention, a table of 39 contradictions, 76 standard solutions, 8 rules of technological evolution systems, the final IFR ideal solution, and so on [1].

1.2. The Key TRIZ Tools and Steps. Let us look at two of the central concepts behind TRIZ: generalizing problems and solutions and eliminating contradictions.

1.2.1. Generalizing Problems and Solutions. The primary findings of TRIZ research were as follows:

(i) Problems and solutions were repeated across industries and sciences. By representing a problem as a "contradiction" (we explored this later in this article), you could predict creative solutions to that problem. Patterns of technical evolution tended to repeat themselves across industries and sciences.

(ii) Creative innovations often used scientific effects outside the field where they were developed. Using TRIZ consisted of learning these repeating patterns of problems and solutions, understanding the contradictions present in a situation, and developing new methods of using scientific effects. You then applied the general TRIZ patterns to the specific situation that confronted you and discovered a generalized version of the problem.

Using Figure 1 you might take the specific problems that you faced and generalize them to one of the TRIZ general problems. From the TRIZ general problems, you identified the general TRIZ solution you needed and then considered how you could apply it to your specific problems. The TRIZ databases were actually a collection of "open source" resources compiled by users and aficionados of the system (such as the 40 principles and 76 standard solutions).

1.2.2. Eliminating Contradictions. Another fundamental TRIZ concept was that there were fundamental contradictions at the root of most problems. In many cases, a reliable way to solve a problem was to eliminate these contradictions. TRIZ recognized two categories of contradictions and technical contradictions. These were classical engineering "trade-offs," where you could not reach the desired state because something else in the system prevented it. In other words, when something got better, something else automatically got worse. For example, the product got stronger (good) but the weight increased (bad). Service was customized to each customer (good), but the service delivery system got complicated (bad). Training was comprehensive (good), but it kept employees away from their assignments (bad). The key technical contradictions were summarized in the TRIZ contradiction matrix. As with all TRIZ resources, it takes time and study to become familiar with the contradiction matrix physical (or "inherent") contradictions. These were situations in which an object or system suffers contradictory, opposite requirements. The opposite requirements could be imported into the matrix to deduce the novelty schemes for designing new products. Everyday examples included software that should be complex (to have many features) but also simple (to be easy to learn). All examples above showed us different requirements for products which could enable us to use matrix to deduce the design for products. You could solve physical contradictions with the TRIZ separation principles. These separated your requirements according to basic categories of space, time, and scale.

1.2.3. Key Points. TRIZ was a system of creative problem solving, commonly used in engineering and process management. It followed four basic steps:

(i) Defined your specific problems.

(ii) Find the TRIZ generalized problems which match them.

(iii) Find the generalized solution that solves the generalized problems.

(iv) Adapt the generalized solution to solve your specific problems.

Most problems stemmed from technical or physical contradictions. After applying one of hundreds of TRIZ principles and laws to eliminate these contradictions, you could solve the problems.

2. Background

The latest national cancer report in January 2019, national cancer statistics, was released by the National Cancer Center. Malignant tumors (cancers) have become one of the major public health problems that seriously threaten the health of the Chinese population. Malignant tumors accounted for the majority of deaths. 23.91% of the total deaths were caused by malignant tumors, and the incidence and mortality of malignant tumors have been rising continuously in the recent ten years. Malignant tumor occurrence every year would lead medical costs to exceed 220 billion. In 2015, the incidence of malignant tumors was about 3.929 million, and the death rate was about 2.338 million. On average more than 10,000 people were diagnosed with cancer every day. Over the past 10 years, the malignant incidence of female tumors increased by about 3.9%, and the mortality rate increased by 2.5% annually. The cancer types of males by order were lung cancers, liver cancers, gastric cancers, esophageal cancers, and colorectal cancers in turn. The top 10 malignant tumors in males accounted for 87.60% of all malignant tumors in males. Death causes of major malignant tumors in women were lung cancers, gastric cancers, liver cancers, colorectal cancers, and breast cancers, in order. The top 10 malignant tumors in women accounted for about all malignant tumors, 80.50%, of the patients who died of female tumors. At present, the 5-year relative survival rate of malignant tumors in China was increasing to 40.5%, but there was still a big gap with developed countries. It is estimated that, in 2015, the number of new malignant tumors in China was about 3.929 million, including 21.551 million males and 1.788 million females. On average, 7.5 people are diagnosed with cancer every minute [2, 3]. The incidence of lymphomas in China was about 9/100,000 for males, 8/100,000 for females, and about 2/100,000 for Hodgkin's lymphomas. In different clinical stages of Hodgkin's lymphomas, the 5-year survival rate was 92.5% in stage I, 86.3% in stage II, 69.5% in stage III, and 31.9% in stage IV. The prognosis of non-Hodgkin's lymphomas was related to pathological types and stages. The 6-year survival rate was 61% for those with good diffuse lymphocyte differentiation, 42% for those with poor diffuse lymphocyte differentiation, and only 30% for those with lymphoblastic lymphomas [4]. The latest national cancer report showed us that the situation of prevention and control was severe. The most schemes of

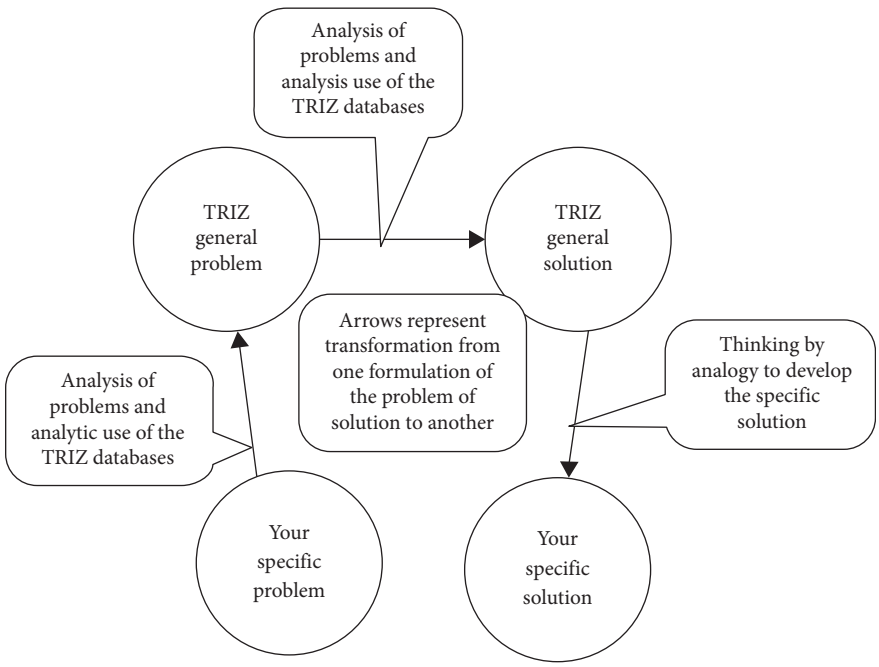

Figure 1: The TRIZ problem-solving method.

cancer therapy had their limitation especially when the patients suffered terminal cancers. The low 5-year survival ratio, the high occurrence of malignant tumors, and high costs of cancer therapy always lead to and appeal for the revolution on present conventional therapy for cancers. Many new treatments and researches had been continuously set to try new breakthrough in relative areas. The innovations and their methods for selecting documents to verify research value were very important in cancer treatments. The conventional flow of retrieving information for meta-analyses had its own limitation in control fields and output results. There were also blindness areas to documents distribution in relative fields like authors and keywords. There was no process of visual analysis (bibliometrics) in formulating retrieval strategies at the areas of traditional literature retrieval. There was also no bibliometric analysis to formulate retrieval terms in meta-analyses. Thus, in this article, we combined TRIZ to filter and screen innovation points and visual analysis of bibliometrics to make the innovation of retrieval literature more efficient and reliable.

3. The Methods of TRIZ and Bibliometrics

By limiting the retrieval database in the core database, the search strategy was used as "TITLE: (Therap* OR treat*) AND TITLE: (lymph cancer OR lymphadenocarcinoma OR lymphadenoma OR adenolymphoma OR lymph-gland tumor OR lymphoma*) AND TITLE: (magnet* OR electr* OR therm* OR evironmen* OR internal environment OR body fluid)". After retrieving the documents, we exported all those articles into text format. Then, we further analyzed the research status with CiteSpace software using different keywords, regions, countries, schools, and co-citation fields, respectively. We also used the Bibliographic Information Mining System (BICOMS) to handle the exported documents and export the field matrix including keywords, authors, title, geography, institutes, etc. We then used the Statistical Package for the Social Sciences (SPSS) software to perform the analysis of system cluster. The unified formula of system cluster was developed using Lance and Williams model as follows:

$$D_{kr}^2 = \alpha_p D_{kp}^2 + \alpha_q D_{kp}^2 + \beta D_{pq}^2 + \gamma \left| D_{kp}^2 - D_{kp}^2 \right|, \quad (1)$$

where $\alpha_p, \alpha_q, \gamma$, and β are parameters.

In the next step, we performed two-way cluster analysis using the Gluto software. The formula of two-way cluster was developed using Plaid model as follows:

$$Y_{ij} = \left(\mu_0 + \alpha_{i0} + \beta_{j0}\right) \sum_{k=1}^{K} \left(\mu_k + \alpha_{ik} + \beta_{jk}\right) \rho_{ik} \kappa_{jk} + \varepsilon_{ij} \Bigg), \quad (2)$$

where μ, α, and β represent mean values and ρ and κ represent a row or layers.

3.1. The Reasoning Process for the Schemes of Finding Novelty in Cancer Research. We used the table of 39 contradictions to give us a thinking path for cancer therapy. TRIZ theory provided us with very different methods from the present general ones of treating cancers which might enlighten us for future research on cancers. We took the steps of using the contradictions matrix to determine possible schemes for treating cancer. Firstly, the popular treating schemes had some effects (killing cancer cells while killing normal cells) on patients' health. The opposite requirements which could be imported into the matrix were side effects and functioning properly. Thus, we chose transverse characteristics (improving factors) as object-

generated harmful factors (AG 31) and lengthwise characteristics (worsening factors) to ease many factures (32) to form our matrix selection. We ascertained the contradiction matrix as per the following table to determine the schemes for treating cancers.

We listed all schemes from the matrix above in Table 1, respectively, as 21, 23, 33, 1, 34, 40, 11, and 12. We compared and reviewed each scheme from the contradiction matrix, respectively, with present popular schemes for treating cancers and tried to provide new views, methods, and thinking paths for treating cancers.

4. Objective

Through the use of TRIZ matrix, we could select the possible novelty options for the researches on treating cancers. We then analyzed the various options offered in the matrix by comparing all current treatment options. We classified and analyzed some schemes of cancers in order to find common points including common shortcomings and advantages. We then scanned and filtered the schemes and ideas by principles of TRIZ theory according to innovation points and tried to find out the new measures from TRIZ that differed from present general schemes of cancers. We then analyzed the documents to form the search strategy according to relevant fields of bibliometrics including keywords, subject hotspots, institutions, citations, magazines, etc. Through combining TRIZ theory and bibliometrics, the search strategy for literature on cancer treatment with innovation would be provided, which is shown in Figures 2 and 3.

5. Results

5.1. Comparing and Screening Schemes for Innovation in Cancer Research by the Principles of TRIZ Matrix. The content for the schemes of cancer treatment listed above could be explained by the following principles.

5.1.1. Principle 21: Skipping. We might deduce that cancer patients should be checked and diagnosed by regular convention medical checking which might require a lot of time for treating cancers. This was often stressed by the difference of survival ratio of most cases with the length of time ahead for surgical operations. The difference of the survival ratio between US and Chinses cancer patients was partially at the length of time and early check-ups or early therapy. We released chemotherapeutic drugs at lesion areas or released capsules by treating plans and time tables to enhance therapeutic effect for patients. The three main methods for treating cancers were operation, chemotherapy, and radiotherapy by Principle 21, skipping, which could be explained as early as possible after diagnosis. Other therapies such as proton therapy, cryotherapy, laser treatment, electrocautery, heavy ion therapy, and cyberknife could all be classified by this principle.

5.1.2. Principle 23: Feedback. We classified present biological treating and immunotherapy as Principle 23. We knew that the IFN-a, IFN-b, TNF-a, IL-2, G-CSF, GM-CSF, and EPO had been approved or used for treating cancers by NF-kB single path. The nutlins had been used to treat cancers by disturbing the gene regulation of P53 and MDM2. Rapamycin could be used on PC-3 SC by significant growth inhibition with rapamycin. The additive effect of IRS-1 ASO and IHC-20% could decrease in proliferative index by rapamycin. The recent development of gene treatment of IL-2/LAK therapy for refractory acute monoblastic leukemia relapsing has been reported. The CAR-T (chimeric antigen receptor) antibodies Ipilimumab and Tremelimumab have been developed to treat melanoma, kidney cancer, prostate cancer, lung cancer, and other clinical cases. Targeted drugs for lymphomas such as Lenalidomide, Idelalisib, Obinutuzumab, Rituximab, Ibritumomab Tiuxetan, Nivolumab, Pembrolizumab, Bortezomib, Ibrutinib, Lenalidomide, Temsirolimus, and Axicabtagene Ciloleucel have been used in clinical treatment. All the above schemes could be thought of as a feedback principle. There were nearly two thousand targets in the reports about target factors or therapy points as targets.

5.1.3. Principle 33: Homogeneity. This scheme provided us with some novel views for treating cancers. In general expression, cancers were considered "toxicants" by traditional Chinese medicine views, and consequently removal was usually wanted. However, from another perspective, the scheme of inducing some homogeneity into cancer patients' bodies was much different from present treatment schemes. We found some presently accepted treating schemes with this idea from Chinese medicine. As3O2 (arsenic) has been used to treat cancers in traditional Chinses medicine for a long time and is now widely accepted as a very effective medicine for treating leukemia. A report about CTL019 methods treating leukemia and saving the life of a US girl was published by scientists in 2015. This principle of homogeneity might enlighten creative ideas or thinking paths in applying magnetic fields or electric flow to deal with cancer cells or cancerous tissue using Principle 33.

5.1.4. Principle 1: Segmentation. Principle 1 could be used to classify present popular therapy methods immunotherapy and target therapy alongside segmentation. The main cancer therapy of operations, chemotherapy, or radiotherapy could be included as resection of cancer and removal from the body of harmful parts.

5.1.5. Principle 34: Discarding and Recovering. This principle could be used to set a research target for treating cancers with a special novel angle beyond the popular present treatment. We discovered that these schemes are different from traditional methods. Discarding usually was not seen as useful or valuable for treating cancers, but we collected some special cases which showed discarding as a creative new thinking path. We might try to search the cases of self-healing of cancers. A report was presented where a boy with a tumor in Sichuan province (in Western China) has

Table 1: The contradiction matrix of TRIZ theory.

TRIZ	Worsening factors					
Improving factors	AB	AC	AD	AE	AF	AG
22	19, 3, 10, 5, 28	35, 31, 40, 1, 34	37, 32, 28, 26, 1	17, 3, 2, 5, 9, 4, 3	2, 40, 15, 19, 4	35, 40, 3, 10, 25
23	35, 24, 10, 16, 5	5, 24, 3, 15, 4, 1	24, 10, 32, 7, 31	18, 31, 24, 9, 7	1, 15, 24, 21, 12,	24, 35, 40, 1, 39
24	19, 9, 35, 3, 21	35, 21, 24, 38, 3	35, 9, 24, 7, 32	35, 13, 39, 18, 2	3, 19, 15, 2, 18	35, 2, 25, 22, 10
25	19, 1, 26, 35, 17	19, 1, 35, 24, 13	32, 13, 4, 1, 14	35, 28, 39, 2, 9	35, 19, 40, 2, 15	35, 32, 19, 3, 39
26	3, 14, 28, 15, 24	3, 4, 31, 19, 15	3, 4, 19, 15, 32,	14, 9, 3, 4, 1, 2, 1	35, 24, 18, 28, 2	19, 15, 4, 33, 3
27	35, 15, 2, 18, 28	19, 38, 35, 27, 3	32, 40, 1, 10, 3	35, 17, 7, 2, 28	13, 2, 24, 35, 28,	3, 1, 15, 14, 29
28	10, 35, 28, 3, 5	5, 18, 35, 19, 1	24, 28, 32, 2, 26	9, 31, 14, 18, 19	1, 35, 21, 18, 5	35, 24, 14, 39, 2
29	10, 18, 7, 4, 32	35, 19, 3, 2, 28	19, 10, 4, 37, 1	28, 35, 14, 28, 2	2, 1, 21, 19, 3, 3	4, 35, 21, 24, 2
30	25, 22, 10, 24, 26, 28, 32, 23	24, 34, 19, 10, 7, 13	24, 10, 7, 25, 3, 28, 2, 32	2, 37, 3, 10, 25	7, 1, 13, 21, 35	7, 10, 31, 27, 21, 40, 6
31	35, 28, 19, 25, 3	3, 15, 9, 31, 35	10, 23, 2, 3, 26	3, 9, 35, 14, 2, 3	5, 2, 35, 19, 9, 2	28, 2, 18, 29, 3
32	2, 10, 35, 36, 21, 3	10, 18, 13, 2, 21, 35, 3, 1	9, 16, 13, 2, 4, 23	18, 35, 28, 14, 3, 1, 16	35, 1, 2, 10, 3, 19, 24, 18	21, 23, 33, 1, 34, 40, 12, 11

discarded the hope for recovery and forced himself to eat mud. This special behavior of madly eating mud helped the child to gradually recover from tumor illness with unknown mechanism. However, this special phenomenon has not been explained convincingly especially when we looked up for novelty on promoting the effectiveness of cancer treatment. We found that some methods of folk therapy usually do not use accepted scientific routes. Some cases might imply or contain some mechanism of new scientific discovery previously unknown or might arouse a new scientific revolution in therapy areas. For example, in Chinese folk sayings, there were many reports of drinking fresh human urine to keep people healthy, which can be included as recovery by the discarding for cancer patients. In these papers, the discarding was mainly in the form of serious prescriptions including components of metabolic products (discarding) such as medicine Wulingzhi and feces. The example above could be explained by the idea that rare elements could be supplied by eating mud which could change the inner physiological electrolyte environment and metabolic microenvironment of human beings.

5.1.6. Principle 40: Composite Materials. This principle made us think of Dr. David Ho and his invention of a cocktail therapy for AIDS by CD8 which could effectively fight HIV. Using this principle, several of the present cancer treating methods might be used in combination. For example, we might combine thermotherapy, chemotherapy, and blood therapy to treat digestive tract cancers at different stages with different composite strategies. We might also apply combined treatment with multiple targets together.

5.1.7. Principle 11: Beforehand Cushioning. This principle could be used to prepare for all kinds of cancer therapies which might increase the treating effect and speed patients' recovery. Cancer patients in China were usually diagnosed by a series of tests, and they then began to accept further treating schemes, mainly involving surgical treatment, chemotherapy, or radiotherapy. However, a belief in traditional Chinses medicine stressed that the patient should be made stronger by taking traditional tonics ahead of treatment with chemotherapy or radiotherapy.

By using this principle, we allowed patients to take thermal conductive agents or heating absorbers to multiply the effect of thermotherapy. Another example of beforehand cushioning (Principle 11) was when Angelina Jolie actively required a mastectomy because she had the BRCA1 gene defect.

5.1.8. Principle 12: Equipotentiality. Principle 12 enabled us to focus on physicotherapeutics. We could reach equipotentiality by using electric field therapy. Thermotherapy was also a treating measure by equipotentiality. Hyperbaric oxygen therapy could also be considered an equipotentiality scheme but there was no consensus about the therapy effect on cancers.

In summary, by the analysis above we knew that most of the principles from TRIZ theory that have been used correspond with all the present schemes or might be in researches listed above. We might focus on the principle which was a minor method for the novelty in possible research on curing cancers, which was Principle 34 from TRIZ, and combine bibliometrics to form strategy for selecting documents for meta-analyses.

5.2. The Rough Retrieval Choice of Research Directions with Innovation. In view of the high mortality of cancers and incidence of lymphomas, we might formulate corresponding retrieval strategies (by the data of national cancer statistics) in relative fields. We now focus on Principle 34 which was a minor method for treating cancers and involves a novel search strategy: (Therap* OR cur* OR recov* OR heal* OR treat*) AND (lymph cancer OR lymphadenocarcinoma OR lymphadenoma OR adenolymphoma OR lymph-gland tumor OR lymphoma*) AND (magnet* OR electr* OR therm* OR evironmen* OR internal environment OR body fluid).

A total of 193 articles (2 from WOS databases) were retrieved using the search strategy above. Then, the exported results of the 193 articles were further analyzed by bioinformatics methods to limit the range of keywords, authors,

countries, institutes, etc. to ascertain the best search strategy for selecting papers on meta-analyses [5–12].

5.3. Visual Fields' Election and Search Strategy Revision on Bibliometrics for Cancer Researches. In order to perform meta-analyses, we used the retrieving strategy outlined in the following sections and exported the retrieved papers. We further analyzed the exported literature using different phrases or keywords such as countries, institutes, and journals. We performed two-way clusters and system clusters to determine the "hot" areas and trends of research on lymphomas. Thus, we further made a search strategy to find novel treatments for lymphomas [13–15].

5.3.1. Keywords Analyses. The graph in Figure 2 was the result of keyword cluster analyses. Table 2 presents a list of the frequency and centrality of keywords.

There was also a list of keyword frequency and centrality in Table 2. Through keyword analyses, the keywords which ranked highest in frequency were MRI, carcinoma, lymphomas, magnetic resonance imaging, diagnosis, radiotherapy, radiation therapy, etc. The main point about lymphomas was the tools of diagnosis, and the main therapy method was radiation. We could also see from word frequency that the focus of most studies was metastatic cancer, non-Hodgkin lymphomas, and lymph node metastasis. Breast cancer and rectal cancer had the highest rankings. In the following position came Sezary syndrome. The words which ranked highest in diagnosis were chemotherapy, position emission tomography, and PET/CT sample biopsy. The words mycosis fungoides had centrality of 0.01, which suggests that fungal or antifungal related agents had the same effectiveness in the treatment of lymph adenocarcinoma or lymphoid. The retrieval field of keywords could provide a new direction and a new mechanism for the study of drugs for lymphomas.

5.3.2. Author Analyses. From the author's frequency in Table 3, we could see that Eich HT and Li Y were the most active scholars in the field of lymphomas. The frequency values of literature by Eich and Li were both five. The next highest author frequency was that of Elsayad and Ota with four papers each; Bischof, Patti, Moustakis, and Iversen all had three papers. Using the analyses in Figure 3, we knew that Ota published three articles in 2016. The authors who ranked the second position and published two papers were, respectively, Walter in 2015, Huang in 2016, Papaioannou in 2011, Rossi in 2009, Hennenfent in 2017, and Rummeny in 2014. From the table and figure above, we could find that the research on lymphatic cancer was hotter in 2015–2017 than in other years.

5.3.3. Countries Analyses. Table 4 represents the nations of the lymphomas researchers. The ranking from the highest to the lowest by number of documents was the United States, Japan, Germany, China, UK, and Italy. The United States ranked the first with 30 papers mainly published in 2005. Japan was listed second with 24, Germany third with 21 papers, and China fourth with 20. British authors had 8 published papers and Italians 4. This also showed us that the numbers of documents from Sweden, India, Taiwan, and Finland were all low, with 2 each. This clearly showed us that the number of documents was rather concentrated in certain countries especially in the first four countries.

5.3.4. Institutes Analyses. Table 4 and Table 5 demonstrate that the United States, Japan, and Germany ranked the highest three by the number of documents published on lymphomas. China ranked fourth, and Britain, Italy, and Sweden ranked 4th-6th. In comparison with the table of research institutes, the highest three rankings were those of Yokohama City University, Exeter University, and Oxford University, in order of number of papers.

Japan research institutions on lymphomas were Tokyo Medical and Dental University, Tokyo Women's Medical University, and Ming Chi University of Technology. China institution was Hunan Cancer Hospital. The UK research institutions on lymphomas were University of Oxford, University of Cambridge, University of Sheffield, and Exeter University.

5.3.5. Journal Analyses. Table 6 shows that the journal with the most citations was Radiology, cited 80 times. The second highest number of citations was that of Journal of Clinical Oncology, with 70 citations. In the third position came American Journal Roentgenology with 55 citations. In fourth and fifth position were European Radiology and European Journal of Radiology with 42 and 40 citations, respectively. The International Journal of Radiology Oncology ranked sixth with 39 citations. From the tables above, it could be clearly seen that the hot point for lymphatic cancer was radiotherapy but the journals which ranked the second and the third were comprehensive journals. The journals which ranked second, seventh, and eleventh were all highly influential and famous comprehensive magazines.

5.3.6. Cited References and Author Citation. From Table 7 we could find that the most cited author was Kwee TC, followed in descending order by Koh DM, Harisinghani MG, Cheson BD, Brown G, etc. We might focus on the articles listed ahead and follow the most active researchers in order to grasp the trend and research direction for cancer therapy on lymphomas (on the subtypes of lymphomas by the data of national cancer statistics) [16, 17].

5.3.7. Two-Way Cluster and System Cluster for Keywords. Figure 4 shows that the hot spots of research on lymphomas were pararectal lymph node, chronic lymphocytic leukemia, and malignant lymphomas. The most clusters of words in hot spots were diffusion weighted magnetic resonance imaging (MRI), diffusion weighted MR imaging, computed monitoring, apparent diffusion coefficient, whole-body diffusion MRI, biphase pulse, laser microdissection, superparamagnetic iron oxide, segmentation, sentinel node

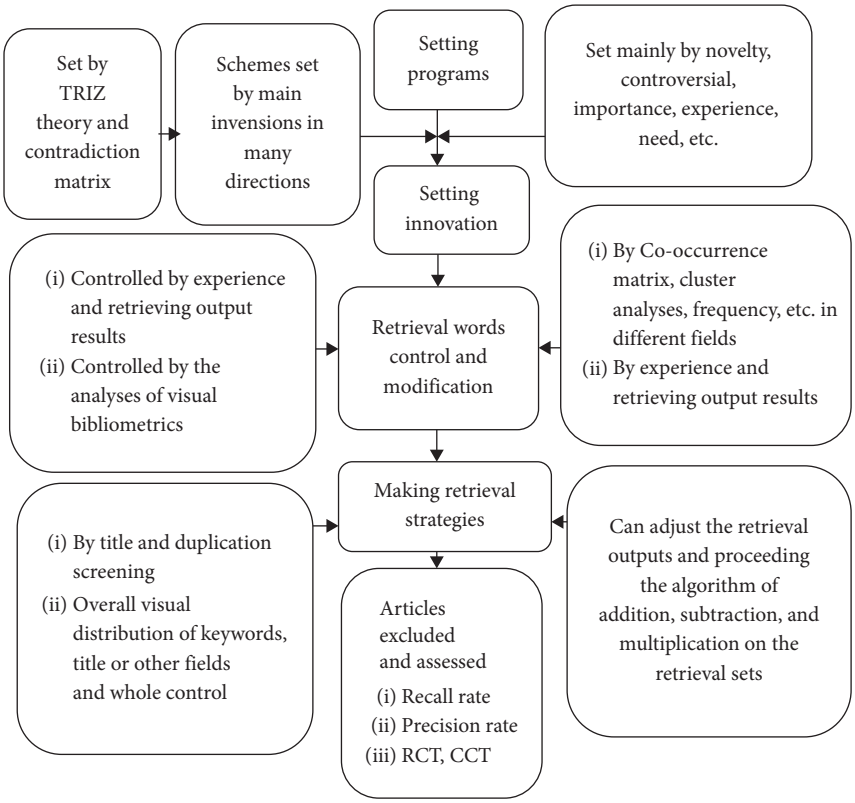

Figure 2: The flow of retrieval information for meta-analyses by TRIZ and bibliometrics.

Table 2: The list of keywords and terms.

Count	Centrality	Year	Keywords/noun phrases
34	0.48	2006	MRI
18	0.15	2003	Lymphoma
18	0.23	2006	Carcinoma
13	0.02	2008	Magnetic resonance imaging
12	0.01	2005	Diagnosis
9	0.04	2010	Radiation therapy
9	0.2	2007	Radiotherapy
9	0.2	209	Disease
8	0.03	2007	Therapy
8	0.03	2011	Breast cancer
7	.0.03	2005	Malignant lymphoma
7	0.05	2005	Lesion
7	0.12	2006	Metastases
7	0.05	2014	Tumor
7	0.23	2011	Biopsy
7	0.04	2013	Cancer
6	0.06	201	Dissection
6	0.03	2015	Metastasis
6	0.17	2012	Lymph node
5	0.06	2009	Positron emission tomography
5	0.01	2015	Sezary syndrome
5	0.01	2015	Mycosis fungoides
4	0.00	2015	In vivo
4	0.00	2015	Rectal cancer
4	0.01	2012	PET/CT
4	0.10	2005	Chemotherapy
4	0.01	2016	Survival

navigation, surgery, etc. From the cluster in Figure 5, it could be seen that there were three types of documents in the literature. Among them were three peaks and research hot areas, while other parts were not academic hotspots obviously. The peak boundary of the literature was very mild. The three peaks of literature indicated that the hot spots were not obvious or very sharp. We could see the key points in the literature and judge hot areas of literature by cluster [18–20].

The main means of detection of literature were image retrieval, mainly in chemistry. From the innovative view we might focus on sparse areas of less cluster density such as the signal channel therapy, field therapy, high heat physical therapy, and immune cell therapy which had low literature density.

There was less aggregation of papers in these fields which were not consistent with the current mainstream of treatments. Regarding innovation and diversity, even though the literature above might be seen as cold areas by most people, these papers might represent future novel directions, including the study of cerebral glioma, acute phrase protein, antioxidants, hypoxic condition, carnosol, electrons, and B cell. Contrary to those very cold areas, the literature on image diagnosis was very hot. We could follow these hot spots for treatment by verifying the evidence-based methods by high density clusters. We could also do research according to the cold distribution especially choosing the direction of low cluster density as an innovative choice for research designs [21–23].

Table 3: The list of authors.

Order	Authors	Frequency	Ratio	Percentage
1	Eich, HT	5	0.3566	0.566
2	Li, Y	5	0.3566	0.7133
3	Elsayad, K	4	0.2853	0.9986
4	Ota, M	4	0.2853	1.2839
5	Bischof, M	3	0.2140	1.4979
6	Patti, C	3	0.2140	1.7118
7	Moustakis, C	3	0.2140	1.9258
8	Iversen, L	3	0.2140	2.1398
9	Hennenfent, K	3	0.2140	2.3538
10	Gniadecki, R	3	0.2140	2.5679
11	Meng, Y	3	0.2140	2.7817
12	Galia, M	3	0.2140	2.9957
13	Kamstrup, MR	3	0.2140	3.2097
14	Ugurel, S	3	0.2140	3.4237
15	Galaznik, A	3	0.2140	3.6377
16	Brocker, EB	3	0.2140	3.8516
17	Ike, H	3	0.2140	4.0656
18	Kinugasa, T	3	0.2140	4.2796
19	Sugihara, K	3	0.2140	4.4936
20	Becker, JC	3	0.2140	4.7076
21	Bell, J	3	0.2140	4.9215
22	Haverkamp, U	3	0.2140	5.1355
23	Mule, A	3	0.2140	5.3495
24	Debus, J	3	0.2140	5.5635
25	Brualla, L	3	0.2140	5.7775
26	Sauerwein, W	3	0.2140	5.9914
27	Albano, D	3	0.2140	6.2054
28	Eadd, M	3	0.2140	6.4194
29	Shou, Y	3	0.2140	6.6334
30	Specht, L	3	0.2140	6.8474

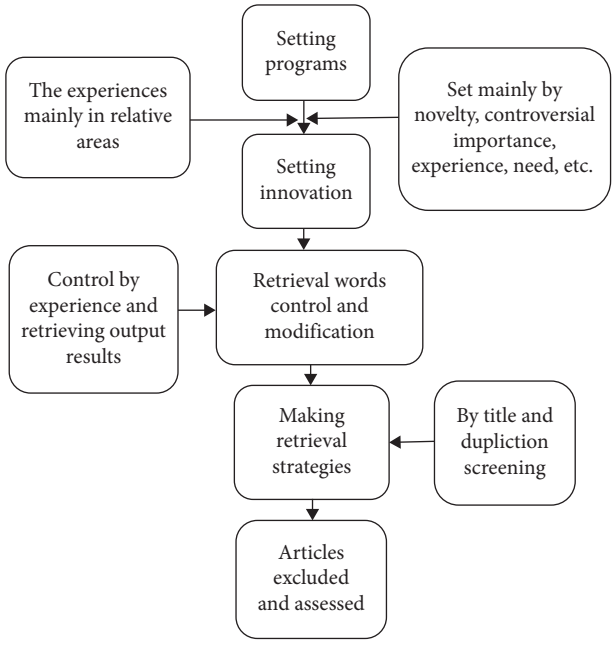

Figure 3: The conventional flow of retrieval information for meta-analyses.

Table 4: The list of countries.

Count	Centrality	Year	Countries
30	0.09	2005	USA
24	0.00	2005	Japan
21	0.00	2003	Germany
20	0.00	2010	China
8	0.15	2011	England
4	0.00	2009	Italy
2	0.00	2017	Sweden
2	0.00	2009	Finland
2	0.00	2017	Taiwan
2	0.00	2012	France
2	0.00	2011	Denmark
2	0.00	2015	Wales
2	0.00	2016	India

Table 5: The list of institutions.

Count	Centrality	Year	Institutions
3	0	2016	Yokohama City University
2	0	2015	University of Exeter
2	0	2015	University of Oxford
2	0	2009	Tampere University of Technology
2	0	2009	Essen University Hospital
2	0	2016	Tokyo Medical and Dental University
2	0	2017	Ming Chi University Hospital
2	0	2017	Chettinad Academy of Research and Education
2	0	2009	Muenster University Hospital
2	0	2016	Tokyo Women's Medical University
2	0	2017	Saiseikai Yokohamashi Nanbu Hospital
2	0	2016	Hunan Cancer Hospital
2	0	2016	Madurai Kamaraj University
2	0	2016	University of Cambridge
2	0	2016	National Defense Medical College
2	0	2015	Millennium Pharmaceuticals, Inc.
2	0	2016	University of Sheffield
2	0	2017	Karolinska University Hospital
2	0	2011	Central University
2	0	2009	Copenhagen University
2	0	2016	Technical University of Munich
2	0	2011	Tampere University
2	0	2014	Bangor University
2	0	2009	Kindai University
2	0	2015	Kurume University

From the analyses of different phrases above, we might choose the proper words for a retrieving strategy. We might choose hot words for treating schemes and cold words for research with novelty. We might also limit the retrieving areas to select papers for meta-analyses [24–26]. We might limit the geographic area such as the US, Japan, Germany, China, and England by the nations corresponding to analyses. We might also select from a limited range of journals such *as Radiology, Journal of Clinical Oncology, American Journal of Roentgenology, European Radiology, European Journal Radiative Oncology, Cancer, New England Journal of*

Table 6: The list of journals.

Count	Centrality	Year	Cited Journals
80	0.13	2003	Radiology
70	0.16	2003	J Clin Oncol
55	0.13	2003	Am J Roentgenol
42	0.04	2005	Eur Radiol
40	0.16	2005	Eur J Radiol
39	0.06	2005	Int J Radiat Oncol
36	0.01	2005	Cancer
35	0.06	2005	New Engl J Med
34	0.28	2005	Blood
33	0.01	2008	J Magn Reson Imaging
25	0.05	2005	Ann Oncol
18	0.03	2011	Ann Surg Oncol
18	0.06	2009	Lancet Oncol
17	0.07	2011	J Nucl Med
17	0.01	2005	Am J Neuroradiol
15	0.00	2005	Acta Radiol
14	0.01	2009	J Comput Assist Tomo
14	0.07	2011	Ann Surg
13	0.03	2008	Invest Radiol
13	0.02	2005	Proc Natl Acad Sci USA
13	0.04	2011	CA Cancer J Clin
13	0.06	2007	Magn Reson Med
13	0.03	2011	Clin Radiol
13	0.02	2013	Clin Cancer Res
12	0.06	2009	Eur J Nucl Med Mol
12	0.00	2016	PLOS One
12	0.12	2005	Cancer Res
12	0.06	2005	Brit J Cancer
12	0.00	2009	Cancer Imaging

Medicine, Blood, Ann Oncology, Surgical Oncology, or *Lancet Oncology*.

5.4. The Search Strategy and Result. We might choose the cold words for novelty schemes with limitations such as "glioma, acute phrase protein, antioxidants, hypoxic condition, carnosol, electrons, or B Cell." We might also choose the hot words for meta-analyses limited to "perirectal lymph node, chronic lymphocytic leukemia, or malignant lymphomas" or the hot spot of research on T-cell lymphomas. The most clusters of words in hot spots were "diffusion weighted magnetic resonance imaging (MRI), diffusion weighted MR imaging, computed monitoring, apparent diffusion coefficient, whole-body diffusion MRI, biphase pulse, laser microdissection, superparamagnetic iron oxide, segmentation, sentinel node navigation, surgery, etc." Thus, we might select the documents of hot areas with the retrieving strategy and search results as follows [27–29]:

(1) Result: 156

(2) Search strategy: subject: (non-Hodgkin's lymphomas OR Hodgkin's lymphomas OR perirectal lymph node OR chronic lymphocytic leukemia OR malignant lymphomas OR hot spot of the research on T-cell lymphomas OR diffusion weighted magnetic resonance imaging (MRI) OR diffusion weight MR imaging OR computed monitoring OR apparent diffusion coefficient OR whole-body diffusion MRI OR biphase pulse OR laser microdissection OR superparamagnetic iron oxide OR segmentation OR sentinel node navigation OR surgery) AND subject: (lymph cancer OR lymphadenocarcinoma OR lymphadenoma OR adenolymphoma OR lymph-gland tumor OR lymphoma*) AND subject: (Therap* OR cur* OR recov* OR heal* OR treat*) AND subject: (magnet* OR electr* OR therm* OR evironmen* OR internal environment OR body fluid) AND address: (US OR China OR Japan OR Germany OR England) AND publication source: (Radiology OR J Clin Oncol OR Am J Roentgenol OR Eur Radiol OR Eur J Radiol OR Cancer OR New Engl J Med OR Blood OR Ann Oncol OR Ann Surg Oncol OR Lancet Oncol) [156 results].

Table 7: The list of cited references.

Order	Cited authors	Frequency	Ratio	Percentage
1	Kwee, TC	30	0.5730	0.5730
2	Koh, DM	18	0.3438	0.9167
3	Harisinghani, MG	17	0.3247	1.2414
4	[Anonymous]	16	0.3056	1.5470
5	Cheson, BD	15	0.2665	1.8335
6	Brown, G	14	0.2674	2.1008
7	Lin, C	13	0.2483	2.3491
8	Kamstrup, MR	12	0.2292	2.5783
9	Willemze, R	12	0.2292	2.8075
10	Kim, YH	11	0.2292	3.0367
11	Oshrakh, MI	11	0.2101	3.2468
12	Vandecaveye, V	11	0.2101	3.4568
13	Hoppe, RT	10	0.2101	3.6669
14	Sumi, M	10	0.1910	3.8579
15	Cancer Research UK	9	0.1910	4.0489
16	Thoeny, HC	9	0.1910	4.2399
17	Veronesi, U	9	0.1719	4.4118
18	Jones, OW	8	0.1719	4.5837
19	Yang, F	8	0.1719	4.7555
20	Elsayad, K	8	0.1719	4.9274
21	Olsen, E	8	0.1528	5.0802
22	Shaikh, SR	8	0.1528	5.2330
23	Harrison, C	8	0.1528	5.3858
24	Wu, XC	8	0.1528	5.5386
25	Navi, D	8	0.1528	5.6914
26	Kim, CK	8	0.1528	5.8442
27	Choi, HJ	8	0.1528	5.9969
28	Duvic, M	8	0.1528	6.1497
29	Toh, CH	7	0.1337	6.2834
30	Haldorsen, IS	7	0.1337	6.4171
31	Weissleder, R	7	0.1337	6.5508
32	Jones, GW	7	0.1337	6.6845
33	Hoppe, RT	7	0.1337	6.8182
34	Wilson, LD	7	0.1337	6.9519
35	Ng, AD	7	0.1337	7.0856
36	King, AD	7	0.1337	7.2193
37	Winter, A	7	0.1337	7.3529
38	Akiyoshi, T	7	0.1337	7.4866
39	Briganti, A	7	0.1337	7.6203
40	Cha, S	7	0.1337	7.7540

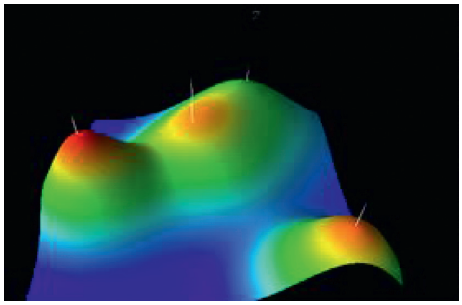

Figure 4: System cluster of keywords.

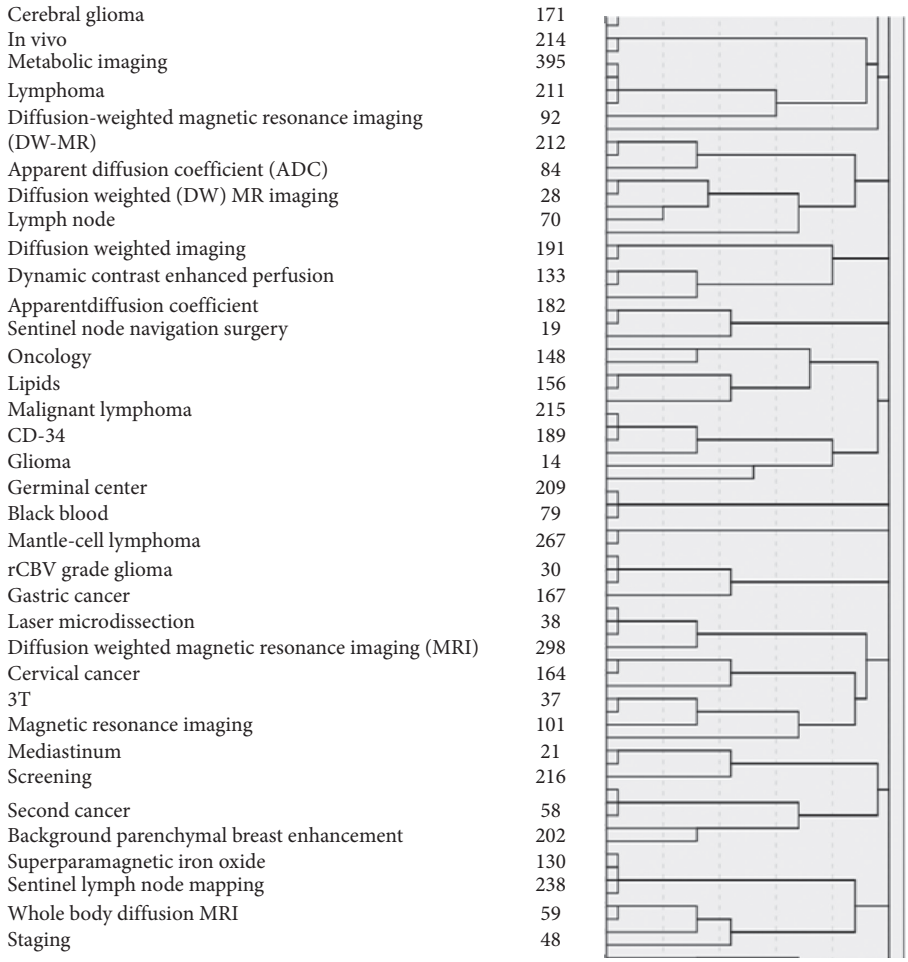

Figure 5: Two-way cluster of keywords.

Thus we might select the documents of cold areas with the retrieving strategy and search result as follows:

(1) Result: 184 (from WOS databases)

(2) Search strategy: subject: (glioma OR acute phrase protein OR antioxidants OR hypoxic condition OR carnosol OR electrons OR B Cell) AND subject: (lymph cancer OR lymphadenocarcinoma OR lymphadenoma OR adenolymphoma OR lymph-gland tumor OR lymphomas or non-Hodgkin's lymphomas or Hodgkin's lymphomas) AND subject: (Therap* OR cur* OR recov* OR heal* OR treat*) AND subject: (magnet* OR electr* OR therm* OR evironmen* OR Internal environment OR body fluid) AND address: (US OR China OR Japan OR Germany OR England) AND publication source: (Radiology OR J Clin Oncol OR Am J Roentgenol OR Eur Radiol OR Eur J Radiol OR Cancer OR New Engl J Med OR Blood OR Ann Oncol OR Ann Surg Oncol OR Lancet Oncol) [184 results].

(1) Result: 106 (from WOS databases)

(2) Search strategy: (canci* OR cancer OR tumor* OR onclog* OR lymph cancer OR lymphadenocarcinoma

OR lymphadenoma OR adenolymphoma OR lymph-gland tumor OR lymphoma*) AND (cur* or recov* or kill* or heal* or treat* or Therapeutic* or therap*) AND (urine OR waste OR urine OR defecate OR shit OR dung OR cow dung OR camel urine OR cat feces coffee OR civet coffee OR disinfection urine OR urea or uric acid).

(1) Result: 15 (from WOS databases and CNKI databases)

(2) Search strategy: (Wulingzhi OR Mochizuki sand OR night sand OR ambergris OR white cloves OR chicken vera OR white lilac OR silkworm OR insect tea OR cow dung OR camel urine OR cat feces coffee OR civet coffee OR disinfection urine OR stool Or urea or uric acid OR muscle liver OR hippuric acid OR oxalic acid OR urine blue mother) AND (canci* OR cancer OR tumor* OR lymph cancer OR lymphadenocarcinoma OR lymphadenoma OR adenolymphoma OR lymph-gland tumor OR lymphoma*) AND (cur* OR recov* OR kill* OR treat*) [15 results].

As a comparison, we could see that the number and domain of retrieval documents cannot be controlled without the modification by bibliometric analysis. The distribution of their various subfields of retrieval output could not be known by conventional meta-analyses. The following were the retrieval results by conventional meta-analyses without modification by bibliometrics (with title field).

(1) Result: 2166 (from WOS databases)

(2) Search strategy: Title: (non-Hodgkin's lymphomas OR Hodgkin's lymphomas OR perirectal lymph node OR Chronic lymphocytic leukemia OR malignant lymphomas OR hot spot of the research on T-cell lymphomas OR diffusion weighted magnetic resonance imaging (MRI) OR diffusion weight MR imaging OR computed monitoring OR apparent diffusion coefficient OR whole-body diffusion MRI OR biphase pulse OR laser microdissection OR superparamagnetic iron oxide OR segmentation OR sentinel node navigation OR surgery) AND subject: (lymph cancer OR lymphadenocarcinoma OR lymphadenoma OR adenolymphoma OR lymph-gland tumor OR lymphoma*) AND subject: (Therap* OR cur* OR recov* OR heal* OR treat*) [2166]

6. Conclusion

This article tried to apply new method for novelty on doing research by TRIZ and combine bibliometrics to visualize the retrieving process. Using TRIZ theory we could compare the schemes of conventional therapy and select the innovation in cancer researches. Then we could add the idea to the searching strategy to select documents. Using bibliometrics, we could freely select the words for searching strategy by the graph of system cluster and two-way cluster of keywords. We could also know all the hot areas of research and their tendency or distribution. At the same time, the analyses of bibliometrics could also provide us with tools and total vision on keywords distribution, units distribution, journal distribution, author distribution, etc. Thus, we could collect all the possible synonyms and high frequency words to construct search strategy and also ensured precision rate and recall rate, which were very important factors in bibliometrics for searching literature. We could flexibly adjust the search strategy to meet the search objectives, whether they were on research or on clinical treatment, by visualizing any field and setting the threshold for any field. Thus we could make our schemes of researches on cancers more novel and make our schemes of clinical treatment more effective.

In summary, we could reason out novelty from Principle 34 of TRIZ and focus on this principle to form strategy by combining bibliometrics. This article could provide a new method of the application of the interdisciplinary of bibliometrics, TRIZ, and meta-analysis and visualize the retrieving process. The interdisciplinary application above would offer the possibility of freely choosing search strategy in any fields with controlled fields and direction for documents on cancer treatment [30, 31].

Data Availability

The data used to support the findings of this study are included within the article.

Conflicts of Interest

The authors declare that there are no conflicts of interest regarding the publication of this paper.

Acknowledgments

This work was supported by MOE (Ministry of Education in China) Project of Humanities and Social Sciences (No.19YJC630116), Medical and Health Data Extraction and Evaluation for Meta-Analysis under Big Data Environment, and Major Project for Science and Technology Innovation Strategy and Soft Science Research in Anhui Province (No. 201806A02020005).

References

[1] "TRIZ"[OL], https://baike.baidu.com/item/triz/3516799?fr=aladdin.

[2] "The latest issue of National Cancer Center: National Cancer Report 2019"[OL] http://www.sohu.com/a/296354370_707276.

[3] "According to the Latest Cancer Data in 2019, 3.93 Million New Cancers Are Reported Every Year, with 7.5 Cancers Per Minute."[OL] http://www.sohu.com/a/292526227_120047572.

[4] "A Comparative Analysis of the Incidence and Survival Rates of Lymphoma between China and the United States"[OL] http://cancer.39.net/a/140312/4353102.html.

[5] Z. Y. Pu, S. X. Jin, and M. Tao, "Treatment of 92 cases of advanced gastric cancer with traditional Chinese medicine combined with chemotherapy," *Guangming Chinese Medicine*, vol. 28, no. 11, pp. 2359-2360, 2013.

[6] J. Wang and Y. L. Ren, "Experimental study on the inhibition of proliferation and induction of A549 human lung adenocarcinoma cells by Wulingzhi mixture," *Chinese Journal of Chinese Materia Medica*, vol. 31, no. 7, pp. 585–587, 2006.

[7] S. M. Chen, D. J. Wang, and M. X. Huang, "22 cases of precancerous lesion of gastric cancer treated with Ping Wei Decoction," *Fujian Journal of TCM*, vol. 28, no. 3, p. 21, 1997.

[8] J. B. Yuan, "Interventional therapy combined with Fuzheng soup in the treatment of 24 cases of liver cancer," *New Journal of Traditional Chinese Medicine*, vol. 37, no. 3, pp. 63–65, 2005.

[9] Z. Z. Tang and C. Y. Sun, "Therapeutic effect of Rebirth oral liquid on HBV related liver cancer," *Chinese Traditional Patent Medicine*, vol. 33, no. 6, pp. 929–931, 2011.

[10] M. Y. Wang and Q. T. Chen, "Randomized parallel controlled study of the combination of Shixiao Powder with three steps for analgesic, omitting, and stasis type of advanced cancer pain," *Journal of Practical Traditional Chinese Internal Medicine*, vol. 27, no. 6, pp. 79-80, 2013.

[11] S. J. Yang, "Randomized parallel controlled study of syndrome differentiation combined with western medicine in the treatment of advanced gastric cancer," *Journal Practical Traditional Chinese Internal Medicine*, vol. 29, no. 6, pp. 99–101, 2015.

[12] L. B. Zhu, L. R. Li, Y. S. Li, J. Wang, and Q. Wang, "Chinese herbal medicine as an adjunctive therapy for breast cancer: a systematic review and meta-analysis," *Evidence-based Complementary and Alternative Medicine*, vol. 2016, Article ID 9469276, 17 pages, 2016.

[13] G. W. Gu and X.-C. Li, "Meta-analysis of the efficacy of transcatheter arterial chemoembolization combined with percutaneous ethanol injection in treating unresectable primary liver cancer," *Zhonghua Yi Xue Za Zhi*, vol. 89, no. 12, pp. 805–809, 2009.

[14] Q. Wang, X. R. He, J. H. Tian et al., "A meta analysis of aidi injection plus taxotere and cisplatin in the treatment of non-small cell lung cancer," *Chinese Journal of Lung Cancer*, vol. 13, no. 11, pp. 1027–1034, 2010.

[15] R. Z. Xu, L. B. Lin, Y. Li, and Y. Li, "ShenQi FuZheng Injection combined with chemotherapy in the treatment of colorectal cancer: a meta-analysis," *Plos One*, vol. 12, no. 9, 2017.

[16] M. A. Kharfan-Dabaja, T. Reljic, J. El-Asmar et al., "Reduced-intensity or myeloablative allogeneic hematopoietic cell transplantation for mantle cell lymphoma: a systematic review," *Future Oncology*, vol. 12, no. 22, pp. 2631–2642, 2016.

[17] J. Wei, J. Xu, Y. Cao, J. Zhou, and Y. Zhang, "Allogeneic stem-cell transplantation for peripheral T-cell lymphoma: a systemic review and meta-analysis," *ACTA Haematologica*, vol. 133, no. 2, pp. 136–144, 2015.

[18] K. Fernandes, J. S. Cardoso, and J. Fernandes, "Automated methods for the decision support of cervical cancer screening using digital colposcopies," *IEEE Access*, vol. 6, pp. 33910–33927, 2018.

[19] M. Sajjad, S. Khan, Z. Jan et al., "Leukocytes classification and segmentation in microscopic blood smear: a resource-aware healthcare service in smart cities," *IEEE Access*, vol. 5, pp. 3475–3489, 2017.

[20] A. Kwok, T. Lam, P. Katelaris, and R. W. Leong, "Helicobacter pylorieradication therapy: indications, efficacy and safety," *Expert Opinion on Drug Safety*, vol. 7, no. 3, pp. 271–281, 2008.

[21] P. J. Brockelmann, D. A. Eichenauer, T. Jakob, M. Follmann, A. Engert, and N. Skoetz, "Hodgkin lymphoma in adults," *Deutsches Arzteblatt International*, vol. 115, no. 31-32, pp. 535–539, 2018.

[22] L. Specht, "Very long-term follow-up of the Danish National Hodgkin S Group's randomized trial of radiotherapy (RT) alone vs. combined modality treatment (CMT) for early stage Hodgkin lymphoma, with special reference to second tumours and overall survival," *Blood*, vol. 102, no. 11, pp. 635A–637A, 2003.

[23] J.-Q. Huang and R. H. Hunt, "Review: eradication of *Helicobacter pylori*. Problems and recommendations," *Journal of Gastroenterology and Hepatology*, vol. 12, no. 8, pp. 590–598, 1997.

[24] L. Brandt, E. Kimby, P. Nygren, and B. Glimelius, "A systematic overview of chemotherapy effects in Hodgkin's disease," *Acta Oncologica (Stockholm, Sweden)*, vol. 40, no. 2-3, pp. 185–197, 2001.

[25] A. Colosia, P. C. Trask, R. Olivares et al., "Efficacy and safety of treatments for relapsed or refractory DLBCL: results of a systematic literature review," *Blood*, vol. 122, no. 21, 2013.

[26] G. H. Lyman and N. M. Kuderer, "Gene expression profile signatures to predict survival in diffuse large B-cell lymphoma: a meta-analysis of early results," *Blood*, vol. 104, no. 11, pp. 624A–626A, 2004.

[27] M. T. Sickinger, B. Von Tresckow, C. Kobe, A. Engert, P. Borchmann, and N. Skoetz, "Positron emission tomography-adapted therapy for first-line treatment in individuals with Hodgkin lymphoma," *The Cochrane Database of Systematic Reviews*, vol. 1, no. 10, pp. 533–537, 2015.

[28] Z. Si, H. Yu, and Z. Ma, "Learning deep features for DNA methylation data analysis," *IEEE Access*, vol. 4, pp. 2732–2737, 2016.

[29] J. B. Spinelli, H. Yoon, A. E. Ringel, S. Jeanfavre, C. B. Clish, and M. C. Haigis, "Metabolic recycling of ammonia via glutamate dehydrogenase supports breast cancer biomass," *Science*, vol. 358, no. 6365, pp. 941–946, 2017.

[30] J.-B. Liu, Y.-S. Ding, Y. Zhang et al., "Anti-inflammatory hydrolyzable tannins fromMyricaria bracteata," *Journal of Natural Products*, vol. 78, no. 5, pp. 1015–1025, 2015.

[31] L. D. Chong, "Exploiting cancer metabolism," *Science*, vol. 355, no. 6329, p. 1036, 2017.

Hindawi
Journal of Chemistry
Volume 2020, Article ID 5343619, 7 pages
https://doi.org/10.1155/2020/5343619

Research Article

The Neuroprotective Effects of Astragaloside IV against H_2O_2-Induced Damage in SH-SY5Y Cells are Associated with Synaptic Plasticity

Zurong Song and Ali Tao

College of Pharmacy, Anhui Xinhua University, Hefei 230088, Anhui, China

Correspondence should be addressed to Ali Tao; taoali84@163.com

Received 17 October 2019; Accepted 16 November 2019; Published 13 May 2020

Guest Editor: Shaohui Wang

The aim of this study was to investigate whether the neuroprotective effects of astragaloside IV (AS-IV) against hydrogen peroxide (H_2O_2)-induced damage on human neuroblastoma cell line (SH-SY5Y) are associated with synaptic plasticity. The concentration screening of AS-IV and H_2O_2 on SH-SY5Y cells and the protective effects of AS-IV on SH-SY5Y cells under H_2O_2 stress were all determined by MTT assay. The expression of postsynaptic density 95 (PSD-95) and growth-associated protein 43 (GAP-43) were measured by western blot (WB) and inmunofluorescence staining assay under the same treatment conditions. According to the MTT results, the concentration of H_2O_2 at 50 μmol/L for 3 h was used for the cell damage model, and various concentrations of AS-IV (0.1, 0.2, 0.3, and 0.4 μmol/L) were used to affect SH-SY5Y cells. The MTT results showed that pretreatment of SH-SY5Y cells with AS-IV (0.1, 0.2, 0.3, and 0.4 μmol/L) attenuated the damage induced by H_2O_2 (50 μmol/L, 51.62% cell viability) and increased cell viability to 64.19, 63.48, 65.86, and 65.81%, respectively. Western blot analysis and immunofluorescence staining showed that the protective effects of AS-IV against SH-SY5Y cell damage caused by H_2O_2 resulted in reduced expression of PSD-95 and increased expression of GAP-43 in comparison with the H_2O_2 treatment group. The conclusion shows that AS-IV protected SH-SY5Y cells and enhanced their viability under H_2O_2 stress. AS-IV may facilitate presynaptic and postsynaptic plasticity to exert protective effects against oxidative damage of SH-SY5Y cells.

1. Introduction

Synaptic plasticity is the process by which neurons and neural circuits undergo adaptive changes to maintain relative stability in the external environment, as well as the molecular basis for learning and memory [1, 2]. Changes in synaptic plasticity, including those associated with particular diseases, can affect signal transduction in the nervous system [3]. Many important functions of the nervous system are dependent on synaptic plasticity.

Synaptic plasticity can occur as presynaptic plasticity and postsynaptic plasticity [4]. Recent research on the mechanisms of synaptic plasticity has been focused mainly on the functions of proteins involved in presynaptic and postsynaptic plasticity, as well as neural cytoskeletal proteins in key signaling pathways. Growth-associated protein 43 (GAP-43) and postsynaptic density 95 (PSD-95) are two synaptic protein markers distributing on presynaptic and postsynaptic membranes, respectively. Research had confirmed that these marker proteins could directly reflect the changes of synaptic morphology and functions of synaptic biology. Compelling evidence demonstrates that high expression levels of GAP-43 facilitate the construction of new synaptic connections and axonal growth during the process of neuronal growth coneformation [5]. PSD-95 is a prominent organizing protein in PSD complexes, which couple the C terminus of the modulatory NMDAR [6] subunit to various cytoplasmic proteins and enzymes [7].

Synaptic plasticity reflects the ability of the nervous system to adapt to internal and external environmental stimuli via dynamic changes in structure or function, which often involve compensation for damaged nerves and neural

circuits, as well as repair of nerve injuries, such as those caused by oxidative stress. Oxidative stress caused by the accumulation of reactive oxygen species can overwhelm the capacity of the cell to eliminate toxic reactive intermediates and repair the damage induced by such intermediates [8]. In the laboratory, oxidative stress is induced in vitro by adding H_2O_2 to the cell culture medium [9, 10].

Emotional and cognitive disorders seriously affect human life and health [11, 12]. In recent years, increasing attention has been paid to the neuroprotective effects of natural substances extracted from plants on the central nervous system. For example, natural substances such as curcuma [13], resveratrol [14], and ginsenosides [15] have been the focus of studies on their antioxidant properties and effects on synaptic plasticity. Astragaloside IV (AS-IV) is extracted from *Astragalus membranaceus* and frequently used as an herbal medicine. Based on its history as a traditional Chinese medicine and recent studies, AS-IV is known to be a free radical scavenger with many positive pharmacological effects, including antioxidant, anti-inflammatory, and antihypertensive effects [16–20]. Although AS-IV is used as a traditional therapy for degenerative diseases in China, a few studies have investigated the effects of AS-IV on synaptic plasticity. Moreover, further research is required in order to fully examine the neuroprotective effects of AS-IV.

Therefore, the aim of the present study was to evaluate the effects of AS-IV on synaptic plasticity in vitro using SH-SY5Y cells exposed to H_2O_2, as well as to measure changes in the protein expression levels of PSD-95 and GAP-43 associated with the protective effects of AS-IV. We found that AS-IV might protect cells from oxidative damage by regulating synaptic plasticity. Our experiments suggest that the protective effects of AS-IV are mediated by downregulation of PSD-95 expression and upregulation of GAP-43 expression. Our findings provide a foundation for further research on the neuroprotective effects of AS-IV, which could lead to the development of new therapies for diseases associated with changes in synaptic plasticity using AS-IV or similar molecules.

2. Methods

2.1. Cell Culture. SH-SY5Y cells were stored in liquid nitrogen, thawed rapidly at 37°C, and centrifuged at 1000 rpm for 4 min. The medium was removed and replaced by DMEM (Gibco, USA) supplemented with 10% fetal bovine serum (FBS, HyClone, New Zealand) and 0.2% penicillin/streptomycin/amphotericin B solution (Sangon Biotech, Shanghai). The cells were grown in an incubator (ThermoFisher, USA) at 37°C with an atmosphere containing 5% CO_2. The cells were transferred to new plates after 1~2 generations to restore growth.

2.2. Assay of Cell Viability. Firstly, the toxicity of AS-IV and H_2O_2 was assessed by the MTT assay. The SH-SY5Y cell line (5000 cells/well) was plated in 96-well microplates, adhered for 24 h, and then treated with H_2O_2 (25~300 μmol/L) for 2, 3, and 4 h and AS-IV (EDQM, European) (0~5 μmol/L) for 24 h, separately. The medium was replaced with 180 μL of fresh medium containing MTT (Sigma, USA) solution (5 mg/mL). The cells were incubated in an incubator (37°C, 5% CO_2) for 4~6 h, after which formazan was dissolved in 150 μL DMSO (Sigma, USA). The optical density of the samples was detected at 490 nm by a microplate reader (BioTek, USA). Untreated cells were used as a control group.

Secondly, the neuroprotective effects of different concentrations of AS-IV (0.1~0.4 μmol/L) on cell viability under H_2O_2 (50 μmol/L) stress were also measured by the MTT assay. SH-SY5Y cells (5000 cells/well) were plated in 96-well microplates and allowed to adhere for 24 h. Various concentrations of AS-IV (0.1~0.4 μmol/L) were used to pretreat the cells for 2 h, after which H_2O_2 (50 μmol/L) was added for 3 h. Cell viability was assessed using the MTT assay. Untreated SH-SY5Y cells were used as a control group, whereas H_2O_2-treated cells were used as a negative control group [21].

2.3. Cell Morphological Observation. Various concentrations of AS-IV (0.1~0.4 μmol/L) were used to pretreat SH-SY5Y cells for 2 h, followed by treatment with 50 μmol/L H_2O_2 for 3 h. Finally, the cells were observed under a microscope (OLYMPUS, Japan).

2.4. Western Blot Analysis. SH-SY5Y cells (3×104 cells/mL) were seeded in 12-well microplates for 24 h and pretreated with AS-IV (0.1~0.4 μmol/L) for 2 h prior to exposure to H_2O_2 (50 μmol/L) for 3 h. The treated cells were lysed in RIPA buffer with phosphatase inhibitor tablets and protease inhibitor cocktail on ice for 30 min. The resulting suspension was centrifuged at 12000 rpm for 15 min at 4°C, and the supernatant was collected. The protein in each sample was resuspended in an equal volume of $2 \times$ loading buffer, followed by protein denaturing in boiling water for 10 min. Finally, the protein samples were cooled at room temperature and stored at −80°C.

Equal amounts of protein were subjected to 12% sodium-dodecyl sulfate-polyacrylamide gel electrophoresis (SDS-PAGE) and transferred to polyvinylidene fluoride (PVDF) microporous membranes (MERCK). The samples were blocked with 5% nonfat dry milk in TBS containing 0.1% Tween-20 for 1 h at room temperature, followed by incubation with GAP-43 (Abcam, Britain), PSD-95 (Abcam, Britain), and GAPDH antibodies at a 1/800, 1/1000, and 1/2000 dilutions, respectively, for 20 h at 4°C. Next, the membranes were incubated with rabbit IgG secondary antibodies (Promega, USA) for 1 h at room temperature. Proteins were detected using enhanced chemiluminescence solution (ECL, BIO-RAD) with an Image Ware System.

2.5. Immunofluorescence Staining. The treated SH-SY5Y cells were fixed with 4% paraformaldehyde for 15 min on the ice and permeabilised with 0.3% triton X-100 and 0.3% H_2O_2 in PBS for 30 min at room temperature. The background was blocked with 5% donkey serum in PBS for 1 h

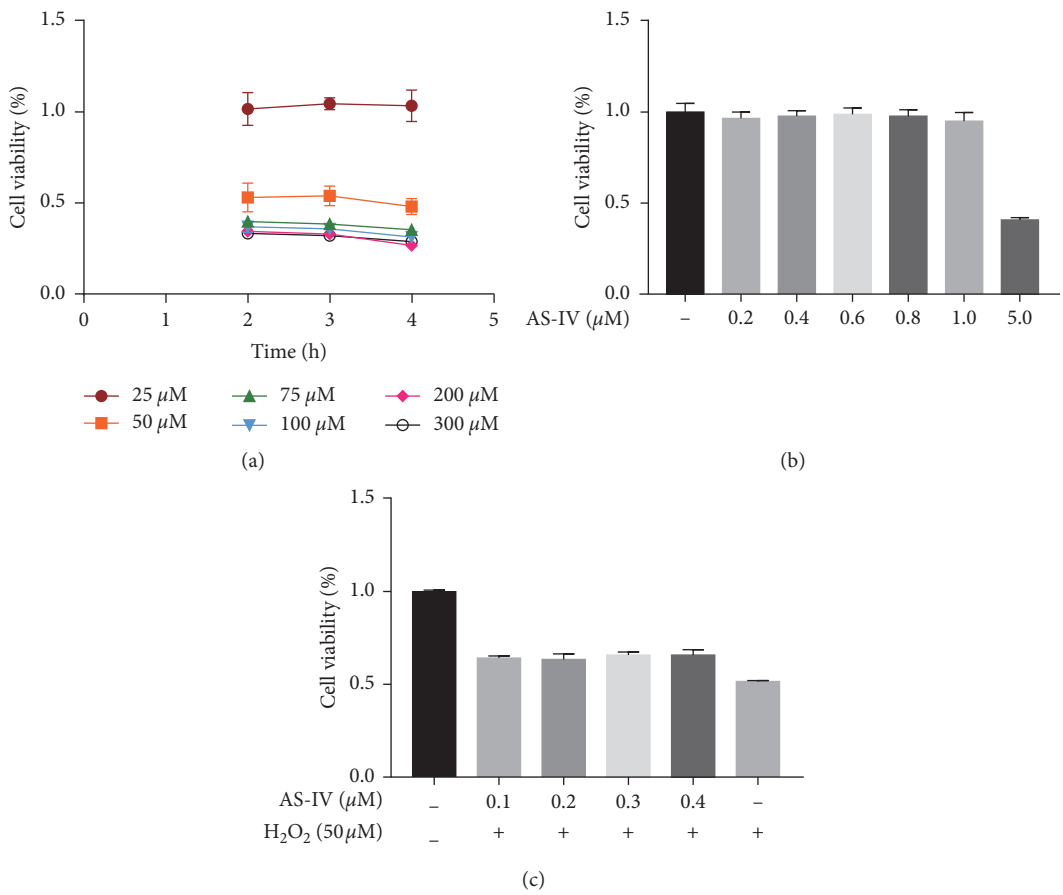

Figure 1: MTT assay for SH-SY5Y cells viability: (a) viability detection of SH-SY5Y cells treated with H_2O_2 (25~300 μmol·L^{-1}) for 2, 3, and 4 h. (b) Viability detection of SH-SY5Y cells treated with AS-IV (0.2~5 μmol·L^{-1}) for 24 h (c) Viability detection of SH-SY5Y cells under H_2O_2 (50 μmol·L^{-1}) treatment for 3 h after AS-IV (0.1~0.4 μmol·L^{-1}) pretreatment for 2 h.

beforeincubation with the primary antibodies. The primary antibodies for PSD-95 (1/1000) and GAP-43 (1/800) were diluted with PBS, followed by incubation with the cells for 90 min at 37°C and at 4°C overnight. The secondary antibodies (green) (Alexa Fluor 488 donkey-anti-rabbit, 1/200, Jackson ImmunoResearch Laboratories) were diluted in PBS for 1 h at room temperature. Finally, the cells were stained with DAPI (1/1000) for 10 min, mounted with 80% glycerol, and stored at 4°C for confocal microscopy (OLYMPUS, Japan) detection.

3. Results

3.1. The Protective Effects of AS-IV against H_2O_2-Induced Damage in SH-SY5Y Cells. Firstly, we detected the viability of SH-SY5Y cells by MTT assay (Figure 1) after treating the cells with H_2O_2 for 2, 3, or 4 h in the presence or absence of AS-IV for 2 h. As shown in Figure 1(a), the cell viability of SH-SY5Y cells treated with H_2O_2 showed a gradual decreasing trend that was time-dependent and dose-dependent. The cell viability was approximately 53.97% of the value of the control group following treatment with 50 μmol/L H_2O_2 for 3 h. Therefore, for the subsequent experiments, treatment with 50 μmol/L H_2O_2 for 3 h was used to induce cell damage.

As shown in Figure 1(b), SH-SY5Y cells were not affected by treatment with 0.2, 0.4, 0.6, 0.8, and 1 μmol/L AS-IV for 24 h. As shown in Figure 1(c), SH-SY5Y cells were pretreated with different concentrations of AS-IV (0.1, 0.2, 0.3, and 0.4 μmol/L) for 2 h, followed by treatment with H_2O_2 (50 μmol/L) for 3 h. The cell viability of the AS-IV treatment group was increased in comparison with that of the H_2O_2 treatment group, but it was lower than that of the control group. The cell viability of the group treated with H_2O_2 (50 μmol/L) for 3 h was 51.62% of that of the control group. However, cell viability of the cells pretreated with AS-IV (0.1, 0.2, 0.3, and 0.4 μmol/L) for 2 h prior to H_2O_2 increased to 64.19, 63.48, 65.86, and 65.81%, respectively. So, as a conclusion, AS-IV was effective in reducing the damage of H_2O_2 on SH-SY5Y cells to protect cells.

3.2. Morphology of Treated SH-SY5Y Cells. As shown in Figure 2, treatment with H_2O_2 (50 μmol/L) for 3 h resulted in shrinkage and aggregation of cell bodies. However, treatment with AS-IV (0.1~0.4 μmol/L) prior to H_2O_2 treatment significantly attenuated the morphological manifestations of cell damage. These results suggest that AS-IV can inhibit or prevent the morphological changes shown by SH-SY5Y cells under H_2O_2 stress.

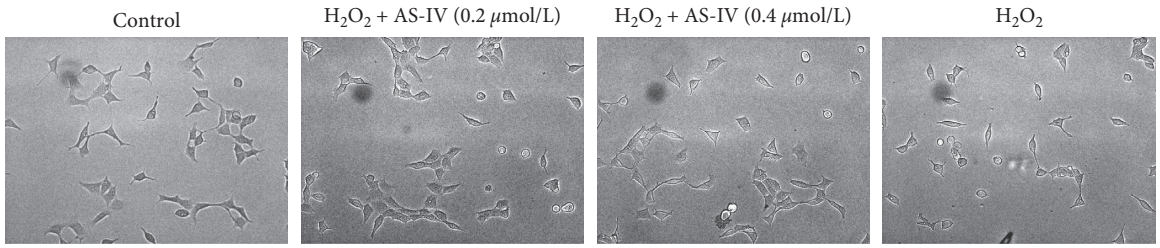

Figure 2: Morphological observation of SH-SY5Y cells under H_2O_2 (50 μmol·L^{-1}) treatment 3 h after AS-IV (0.1~0.4 μmol·L^{-1}) pretreatment for 2 h.

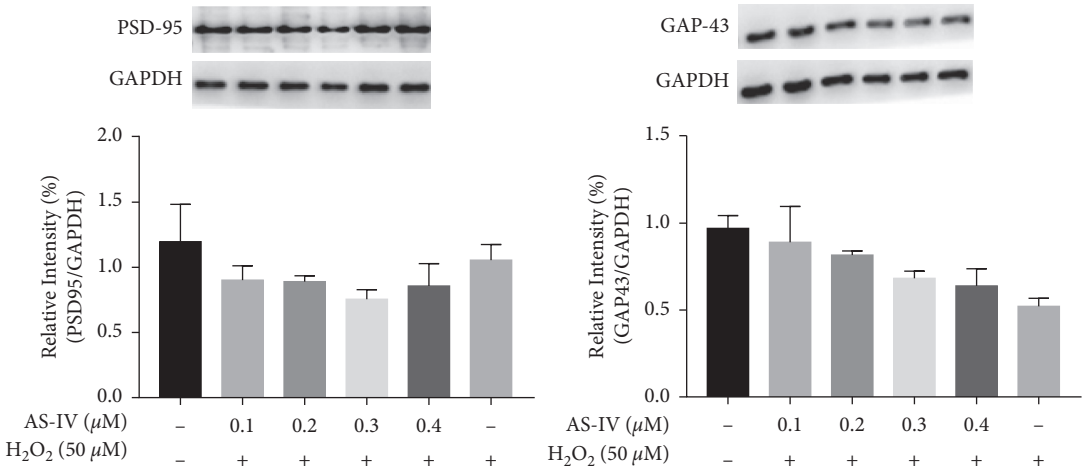

Figure 3: Protein expression of PSD-95 and GAP-43 in SH-SY5Y cells under stress conditions. (a) Expression of PSD-95 under H_2O_2 (50 μmol·L^{-1}) treatment for 3 h after AS-IV (0.1~0.4 μmol·L^{-1}) pretreatment for 2 h. (b) Expression of GAP-43 under H_2O_2 (50 μmol L^{-1}) treatment 3 h after AS-IV (0.1~0.4 μmol L^{-1}) pretreatment for 2 h untreated, and H_2O_2-treatment cells were used as blank and negative controls, respectively.

3.3. Analysis of PSD-95 and GAP-43 Expression by Western Blot. We detected the expression levels of PSD-95 and GAP-43 proteins by western blot analysis to determine the relationship between the neuroprotective effects of AS-IV under H_2O_2 stress and synaptic plasticity. Western blot analysis was performed using a polyclonal rabbit antibody against PSD-95 and a monoclonal rabbit antibody against GAP-43. As shown in Figure 3(a), when SH-SY5Y cells were treated with H_2O_2 (50 μmol/L) for 3 h, PSD-95 expression was decreased by 11.84% in comparison with that of the control group. In contrast, following AS-IV (0.1, 0.2, 0.3 and 0.4 μmol/L) pretreatment for 2 h, PSD-95 protein expression levels were decreased by 24.67%, 25.66%, 39.96%, and 28.35%, respectively.

As shown in Figure 3(b), the protein expression level of GAP-43 was decreased to 46% of that of the control group following treatment with H_2O_2 (50 μmol/L) for 3 h. In comparison, pretreatment with 0.1, 0.2, 0.3, or 0.4 μmol/L AS-IV increased the expression level of GAP-43 by 36.95%, 30.42%, 11.54%, and 12.62%, respectively, in comparison with that of the H_2O_2-exposed cells. Therefore, we speculate that the neuroprotective effects of AS-IV under H_2O_2 stress were mediated by reducing the protein expression level of PSD-95 and increasing that of GAP-43 in comparison with the H_2O_2-exposed group.

3.4. Analysis of PSD-95 and GAP-43 Expression by Immunofluorescence Assay. We performed immunofluorescence assays using a polyclonal rabbit antibody against PSD-95 and a monoclonal rabbit antibody against GAP-43 to further investigate the neuroprotective effects of AS-IV in the context of regulation of synaptic plasticity. As shown in Figure 4, the immunofluorescence analysis was consistent with the western blot analysis. However, DAPI staining revealed that nuclear condensation and fragmentation occurred after the SH-SY5Y cells were treated with H_2O_2 (50 μmol/L) for 3 h; however, pretreatment with AS-IV prevent the nuclear damage induced by H_2O_2.

4. Discussion

Synaptic plasticity plays a role in learning and memory and is the basis for many important functions of the nervous system. Recent results have shown that oxidative stress is involved in the pathological mechanisms of several neurodegenerative diseases, including Alzheimer's disease and Parkinson's disease [22–24]. Treatment with H_2O_2 is widely used in cellular models to induce oxidative stress [25, 26], and the SH-SY5Y cell line is extensively used as a cell model for studying neuronal cell death [27]. In our study, SH-SY5Y cells were subjected to H_2O_2-induced oxidative stress to induce H_2O_2-induced neurotoxicity and reveal the relationship between the neuroprotective effects of AS-IV and synaptic plasticity.

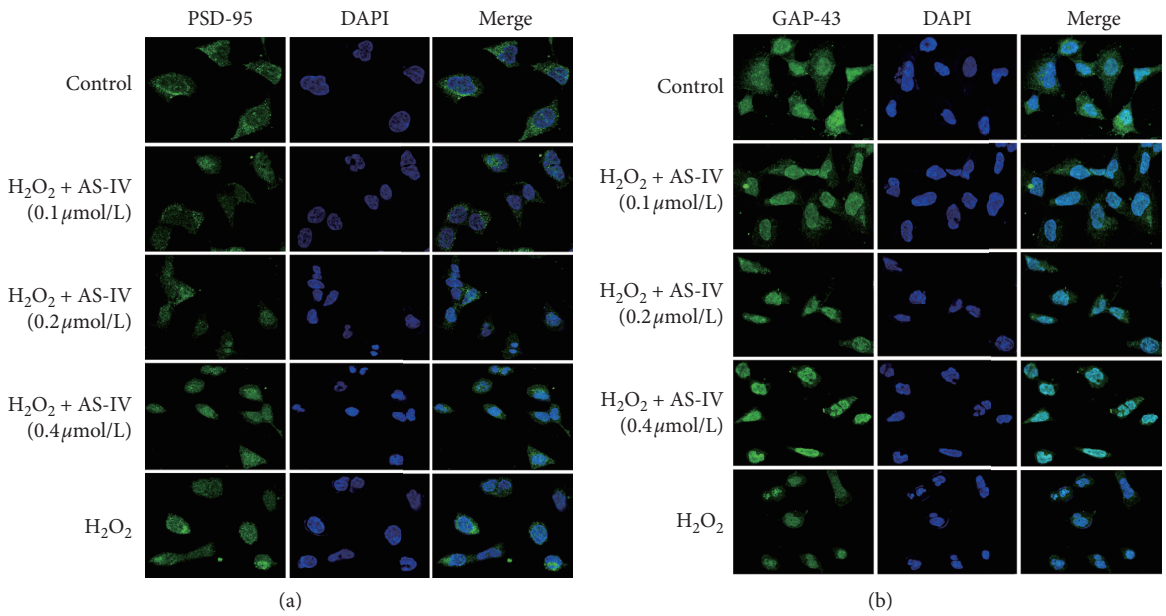

Figure 4: Immunofluorescence expressions of synaptic markers PSD-95 and GAP-43. (a) Expression of PSD-95 under H_2O_2 (50 μmol·L^{-1}) treatment 3 h after AS-IV (0.1~0.4 μmol·L^{-1}) pretreatment for 2 h. (b) Expression of GAP-43 under H_2O_2 (50 μmol·L^{-1}) treatment 3 h after AS-IV (0.1~0.4 μmol·L^{-1}) pretreatment for 2 h.

Although antioxidant agents represent potentially effective treatments for neurodegenerative diseases [28], the relationship between their beneficial effects and synaptic plasticity are unclear. AS-IV, the main active component of astragalus, has several beneficial pharmacological effects that are useful for treating particular pathophysiological conditions. Recent studies of AS-IV have demonstrated its antioxidant and antiaging effects [29–31], as well as positive effects on learning and memory [32]. In this study, we demonstrated that AS-IV protected SH-SY5Y cells from H_2O_2-induced cell damage and increased their cell viability in comparison with that of the H_2O_2-exposed group.

In our study, H_2O_2 was used to stimulate cells to allow us to explore the relationship between synaptic plasticity and the neuroprotective effects of AS-IV. We found that the protective effects of AS-IV against H_2O_2-induced damage might be mediated by decreased expression of PSD-95. PSD-95, a scaffold protein of the PSD, plays a role in signal transduction by linking the NMDAR to downstream enzymes and regulating the activity of signaling enzymes through its binding domains [33]. NMDA receptors function in synaptic plasticity by regulating the concentration of Ca^{2+} in postsynaptic cells, mediating some intracellular signaling pathways, and ultimately affecting long-term potentiation and long-term depression of synaptic transmission. However, overactivation of NMDA receptors is a major cause of ischemic cell injury [34]. NMDA receptors consist of principal NR1 and NR2 subunits [35], and tyrosine phosphorylation of NR2 (particularly NR2A and NR2B) upregulates the function of NMDA receptors [36]. Recently, it has been reported that NR2A-PSD-95-Src is a signal transduction module that promotes overactivation of NR2A and NMDA receptors [37]. In addition, excessive activation of NMDA receptor activated another signaling molecule, neuronal nitric oxide synthase (nNOS), which binding to the PDZ2 domain of PSD-95 [38], subsequently catalyzed the excessive production of highly reactive nitric oxide (NO) and induced NO toxicity [39]. Our results show that AS-IV decreased the expression level of PSD-95, which may have prevented the interaction of NR2A-PSD-95-Src that leads to NMDA receptor phosphorylation and increased the phosphorylation level of nNOS, thus protecting SH-SY5Y cells under H_2O_2-induced stress [40].

GAP-43 is a specific neuronal phosphoprotein. Expression of GAP-43 promotes the neuron growth, development and axon regeneration during development of the nervous system, as well as regeneration after injury [41]. GAP-43 is a repository of calmodulin that releases calmodulin due to the action of a second messenger molecule, leading to phosphorylation of GAP-43 and ultimately affecting the release of synaptic transmitters. Dephosphorylated GAP-43 recombines with calmodulin to form a feedback loop. Activated GAP-43 interacts with cytoskeletal components to regulate the activity of nerve endings, thereby altering cell morphology [42]. In this study, we found that AS-IV increased the expression level of GAP-43 in comparison with that of cells treated with H_2O_2. Therefore, we speculate that H_2O_2 exposure leads to GAP-43 phosphorylation, whereas AS-IV leads to dephosphorylation of GAP-43, which facilitates repair of oxidative damage, thereby protecting SH-SY5Y cells.

In conclusion, AS-IV protects cells under H_2O_2-induced injury in a manner that may be related to changes in the expression levels of PSD-95 and GAP-43. Furthermore, the neuroprotective effects of AS-IV against H_2O_2-induced damage in SH-SY5Y cells may be associated with synaptic plasticity. Our study may provide a therapeutic strategy for nervous system diseases, although further research into the

mechanisms through which AS-IV mediates synaptic plasticity is necessary.

Data Availability

The data used to support the findings of this study are available from the corresponding author upon request.

Conflicts of Interest

The authors declare that there are no conflicts of interest regarding the publication of this paper.

Acknowledgments

This work was supported by the National Undergraduate Innovation and Entrepreneurship Project (201712216034), Outstanding Young and Middle-Aged Talents in Colleges and Universities (gxfxZD2016295), School-level Scientific Research Projects(2017zr010), and the Natural Science Research Foundation of the Department of Education of Anhui Province (nos. KJ2019A0874 and KJ2018A0583).

References

[1] M.-H. Wang, N. Chen, and J.-H. Wang, "The coupling features of electrical synapses modulate neuronal synchrony in hypothalamic superachiasmatic nucleus," *Brain Research*, vol. 1550, pp. 9–17, 2014.

[2] A. Hasan, M. A. Nitsche, B. Rein et al., "Dysfunctional long-term potentiation-like plasticity in schizophrenia revealed by transcranial direct current stimulation," *Behavioural Brain Research*, vol. 224, no. 1, pp. 15–22, 2011.

[3] M. Guo and G. Li, "An update on key proteins involved in synaptic plasticity," *Acata Neuro Pharmacologica*, vol. 3, no. 6, pp. 57–64, 2013.

[4] G. Thomas, W. Valentina, D. Valentyna, A. Verena, and M.-K. Denise, "Altered neuronal excitability underlies impaired hippocampal function in an animal model of psychosis," *Frontiers Behavioral Neuroscience*, vol. 9, pp. 117–126, 2015.

[5] N. O. Al-Harbi, F. Imam, M. M. Al-Harbi et al., "Rutin inhibits carfilzomib-induced oxidative stress and inflammation via the NOS-mediated NF-κb signaling pathway," *Inflammopharmacology*, vol. 27, no. 4, pp. 1–10, 2019.

[6] M. Hamid, D. Liu, Y. Abdulrahim et al., "Amelioration of CCl 4 -induced liver injury in rats by selenizing astragalus polysaccharides: role of proinflammatory cytokines, oxidative stress and hepatic stellate cells," *Research in Veterinary Science*, vol. 114, pp. 202–211, 2017.

[7] W. Teng, T. Wulin, Y. Haiyang, S. Guoxi, and X. Guanghong, "Protective effects of phillyrin on H_2O_2-induced oxidative stress and apoptosis in PC12 cells," *Cellular & Molecular Neurobiology*, vol. 34, no. 8, pp. 1165–1173, 2014.

[8] D. Marina, P. Katarina, and S. Aleksandra, "Involvement of bradykinin in brain edema development after ischemic stroke," *Pflügers Archiv—European Journal of Physiology*, vol. 467, no. 2, pp. 201–212, 2015.

[9] G. M. Hautbergue, L. M. Castelli, L. Ferraiuolo et al., "SRSF1-dependent nuclear export inhibition of C_9ORF_{72} repeat transcripts prevents neurodegeneration and associated motor deficits," *Nature Communications*, vol. 8, pp. 16063–16080, 2017.

[10] X. Liu, J. Zhang, S. B. Wang, J. F. Qiu, and Y. U. Chao, "Astragaloside IV attenuatesthe H_2O_2-induced apoptosis of neuronal cells by inhibiting α-synuclein expression via the p38 MAPK pathway," *International Journal of Molecular Medicine*, vol. 40, no. 6, pp. 1772–1880, 2017.

[11] B. Michel, "Increased serotonin transporter expression reduces fear and recruitment of parvalbumin interneurons of the amygdale," *Neuropsychopharmacology*, vol. 40, no. 13, pp. 3015–3026, 2015.

[12] K. M. Choudhary, A. Mishra, and V. Poroikov, "Ameliorative effect of curcumin on seizure severity, depression like behavior, learning and memory deficit in post-pentylenetetrazole kindled mice," *European Journal of Pharmacology*, vol. 704, no. 3, pp. 33–40, 2013.

[13] J. Q. Yang, S. L. Song, and T. Liang, "Neuroprotective effect of curcumin on hippocampal injury in 6-OHDA-induced parkinson's disease rat," *Pathology Research and Practice*, vol. 210, no. 6, pp. 357–362, 2013.

[14] J. Li, L. Feng, Y. Xing et al., "Radioprotective and antioxidant effect of resveratrol in hippocampus by activating sirt1," *International Journal of Molecular Sciences*, vol. 15, no. 4, pp. 5928–5939, 2014.

[15] W. Wu, X. H. Chen, J. Q. Yang, and X. T. Wang, "Study on the effect and mechanism of ginsenoside Rg1 on survival and differentiation of implanted BMSCs in dementia model rats," *Journal of Wenzhou Medical University*, vol. 44, no. 9, pp. 637–640, 2014.

[16] H. Leila, M. Alireza, A. Farahnaz, E. S. Ahmad, and M. Mahdi, "The protective effect of different extracts of three artemisia species against H_2O_2-induced oxidative stress and apoptosis in PC12 neuronal cells," *Pharmacognosy Research*, vol. 10, no. 1, pp. 64–71, 2018.

[17] V. Umashankar, R. S. Baarathi, K. Kaviarasan, M. Jithu, and N. Angayarkanni, "Agonistic effect of polyunsaturated fatty acids (PUFAs) and its metabolites on brain-derived neurotrophic factor (BDNF) through molecular docking simulation," *Lipids in Health & Disease*, vol. 11, no. 1, pp. 109–115, 2012.

[18] L. Bin, W. Fei, L. N. Tao, S. Wen, and H. Tao, "Astragaloside IV inhibits progression of glioma via blocking MAPK/ERK signaling pathway," *Biochemical & Biophysical Research Communications*, vol. 491, no. 1, pp. 98–103, 2017.

[19] C. Byoung-Ok, R. Hyung-Won, L. Chang-Wook et al., "Protective effects of new blackberry cultivar MNU-32 extracts against H_2O_2-induced oxidative stress in $HepG_2$ cells," *Food Science & Biotechnology*, vol. 24, no. 2, pp. 643–650, 2015.

[20] D. Marina, Š. Katarina, G. Dunja et al., "Urodilatin reverses the detrimental influence of bradykinin in acute ischemic stroke," *Experimental Neurology*, vol. 284, pp. 1–10, 2016.

[21] I. T. Schiefer, L. Vandevrede, M. Fa, O. Arancio, and G. R. J. Thatcher, "Furoxans (1,2,5-oxadiazole-N-oxides) as novel NO mimetic neuroprotective and procognitive agents," *Journal of Medicinal Chemistry*, vol. 55, no. 7, pp. 3076–3087, 2012.

[22] M. Sharma, J. Burre, and T. C. Sudhof, "Proteasome inhibition alleviates SNARE-dependent neurodegeneration," *Science Translational Medicine*, vol. 4, no. 147, p. 147ra113, 2012.

[23] D. M. Small, C. Morais, J. S. Coombes, N. C. Bennett, D. W. Johnson, and G. C. Gobe, "Oxidative stress-induced alterations in PPAR-γ and associated mitochondrial destabilization contribute to kidney cell apoptosis," *American Journal of Physiology-Renal Physiology*, vol. 307, no. 7, pp. F814–F822, 2014.

[24] R. Niranjan, "The role of inflammatory and oxidative stress mechanisms in the pathogenesis of Parkinson's disease: focus on astrocytes," *Molecular Neurobiology*, vol. 49, no. 1, pp. 28–38, 2014.

[25] T. Nesil, A. Ü. Şendemir, and E. Bedir, "Protective effects of astragaloside IV and cycloastragenol in 6-hydroxydopamin (6-ohda)-induced neurotoxicity in PC12 cells," *Molecular Medicine Reports*, vol. 77, no. 12, pp. 1444–1456, 2011.

[26] X.-J. Wu, Y.-J. Zheng, Y.-Y. Cui, L. Zhu, Y. Lu, and H.-Z. Chen, "Propofol attenuates oxidative stress-induced PC12 cell injury via p38 MAP kinase dependent pathway," *Acta Pharmacologica Sinica*, vol. 28, no. 8, pp. 1123–1128, 2007.

[27] Y. Xiong, H. Ding, M. Xu, and J. Gao, "Protective effects of asiatic acid on rotenone- or H2O2-induced injury in SH-SY5Y cells," *Neurochemical Research*, vol. 34, no. 4, pp. 746–754, 2009.

[28] H. Yuan, J.-C. Zheng, P. Liu, S.-F. Zhang, J.-Y. Xu, and L.-M. Bai, "Pathogenesis of Parkinson's disease: oxidative stress, environmental impact factors and inflammatory processes," *Neuroscience Bulletin*, vol. 23, no. 2, pp. 125–130, 2007.

[29] M. Shabzad, D. M. Small, C. Morais, K. Wojcikowski, A. Shabbir, and G. C. Gobe, "Protection against oxidative stress-induced apoptosis in kidney epithelium by Angelica and Astragalus," *Journal of Ethnopharmacology*, vol. 179, no. 6, pp. 412–419, 2016.

[30] H. Xue, F. Gan, Z. Zhang, J. Hu, X. Chen, and K. Huang, "Astragalus polysaccharides inhibits PCV2 replication by inhibiting oxidative stress and blocking NF-κB pathway," *International Journal of Biological Macromolecules*, vol. 81, no. 7, pp. 22–30, 2015.

[31] F.-Y. Guan, S.-J. Yang, J. Liu, and S.-R. Yang, "Effect of astragaloside IV against rat myocardial cell apoptosis induced by oxidative stress via mitochondrial ATP-sensitive potassium channels," *Molecular Medicine Reports*, vol. 12, no. 1, pp. 371–376, 2015.

[32] Q. Sun, N. Jia, W. Wang, H. Jin, J. Xu, and H. Hu, "Protective effects of astragaloside IV against amyloid betal-42 neurotoxicity by inhibiting the mitochondrial permeability transition pore opening," *PLoS One*, vol. 9, no. 6, pp. 1371–1380, 2014.

[33] E. Hiley, R. Mcmullan, and S. J. Nurrish, "The Gα12-RGS rhogef-rhoa signalling pathway regulates neurotransmitter release in *C. elegans*," *The EMBO Journal*, vol. 25, no. 24, pp. 5884–5895, 2014.

[34] M. Takashi, S. Liana, T. Reuben et al., "Phosphorylation of tau at Y18, but not tau-fyn binding, is required for tau to modulate NMDA receptor-dependent excitotoxicity in primary neuronal culture," *Molecular Neurodegeneration*, vol. 12, no. 1, pp. 41–59, 2017.

[35] C. H. Trepanier, M. F. Jackson, and J. F. MacDonald, "Regulation of NMDA receptors by the tyrosine kinase Fyn," *FEBS Journal*, vol. 279, no. 1, pp. 12–19, 2012.

[36] M. A. Beazely, M. Weerapura, and J. F. MacDonald, "Abelson tyrosine kinase links PDGFbeta receptor activation to cytoskeletal regulation of NMDA receptors in CA1 hippocampal neurons," *Molecular Brain*, vol. 1, no. 1, pp. 20–30, 2008.

[37] J. Yang, H. X. Wang, Y. J. Zhang, J. Zhang, and S. T. Li, "Inhibition of astragaloside IV against isoproterenol-induced myocardial hypertrophy in neonatal rats and its mechanism," *Chinese Traditional & Herbal Drugs*, vol. 44, no. 21, pp. 3018–3023, 2013.

[38] S. D. Rosé, D. M. Byers, S. C. Morash, S. Fedoroff, and H. W. Cook, "Lipopolysaccharide stimulates differential expression of myristoylated protein kinase C substrates in murine microglia," *Journal of Neuroscience Research*, vol. 44, no. 3, pp. 235–242, 1996.

[39] R. K. Mcnamara and R. H. Lenox, "Distribution of the protein kinase C substrates MARCKS and MRP in the postnatal developing rat brain," *Journal of Comparative Neurology*, vol. 397, no. 3, pp. 337–356, 2015.

[40] S. Shansher and K. Puneet, "Neuroprotective potential of curcumin in combination with piperine against 6-hydroxy dopamine induced motor deficit and neurochemical alterations in rats," *Inflammopharmacology*, vol. 25, no. 1, pp. 69–79, 2017.

[41] K. M. Robert and H. L. Rober, "Comparative distribution of myristoylated alanine-rich C kinase substrate (MARCKS) and F1/GAP-43 gene expression in the adult rat brain," *Journal of Comparative Neurology*, vol. 379, no. 1, pp. 48–71, 2015.

[42] F. M. Zakharova and V. V. Zakharov, "Identification of brain proteins BASP1 and GAP-43 in mouse oocytes and zygotes," *Russian Journal of Developmental Biology*, vol. 48, no. 3, pp. 159–168, 2017.

Hindawi
Journal of Chemistry
Volume 2020, Article ID 2936932, 11 pages
https://doi.org/10.1155/2020/2936932

Research Article

Study on Mechanical Behavior of Jurassic Frozen Sandstone in Western China Based on NMR Porosity

Maoyan Ma,[1] **Yishun Huang**,[2] **Guangyong Cao**,[1] **Jian Lin**,[1] **and Shiliang Xu**[1]

[1]*Anhui Key Laboratory of Building Structure and Underground Engineering, Anhui Jianzhu University, Hefei 230601, China*
[2]*Chendu JZFZ Architectural Design Co. Ltd., Hefei 230031, China*

Correspondence should be addressed to Guangyong Cao; caogy1973@ahjzu.edu.cn

Received 18 October 2019; Accepted 27 November 2019; Published 30 April 2020

Guest Editor: Shaohui Wang

Study of frozen rock mechanical properties is necessary for safe application of the artificial ground freezing method in excavation of Chinese western water-rich soft rock layers. Triaxial compression tests and NMR test for samples from the western Jurassic sandstone were performed to investigate rock mechanical properties affected by low temperature and confining pressure. The results show mechanical parameters such as peak strength, cohesion, internal friction angle, residual strength, and elasticity modulus increased with the decreasing temperature under stable pressure, and the above parameters increased with the increasing confining pressure at a certain temperature. In particular, the growth rate of the rock strength would decline when the temperature was below −10°C in this study. Strength attenuation coefficients increased with the decreasing temperature, which indicated higher brittleness, whereas plastic characters got more obvious with the increasing confining pressure at a stable temperature. Furthermore, during the first two freezing stages, porosity decreased sharply with obvious increase of pore (crack) ice content, while porosity varied little at the third stage, which was the reason for the growth rate of rock strength declining with continuous low temperature from microcosmic point of view.

1. Introduction

During the "Thirteenth Five-Year Plan" period, China will reduce the total coal production of eastern, central, and northeastern areas and promote the base construction of western coal fields gradually. Western China, including Inner Mongolia, Shanxi, Xinjiang, Ningxia, Gansu, and other provinces and autonomous regions, has a huge amount of coal resources. Coal beds mainly distributed in Jurassic and Cretaceous water-rich soft rock layers are weakly cemented. Moreover, water-rich soft rock layers are ready to hydrolyze with sharply dropped strength when exposed to hydrodynamic erosion. Meanwhile, coal-bearing layers here usually have large unit water inflow and high permeability [1–6]. Therefore, artificial ground freezing method is still the key method used in the mine construction of Western China. At low temperature, rocks show mechanical properties which are different from those at normal temperature and mechanical properties at low temperature are the basic data of freeze sinking, so the mechanical properties of the frozen soft rock in Jurassic and Cretaceous layers in Western China are important to guide effectively the design and construction of frozen wells of western mines. It is also critical to the safety of other cold area engineering construction. Therefore, more and more attention has been paid to the mechanical properties of frozen rocks.

Studies of mechanical properties of rocks at low temperature have been widely carried out with the large number of artificial freezing engineering and other geotechnical engineering actions in cold regions. It is revealed that the rock with different water saturation has different performance in uniaxial compressive strength, tensile strength, and fracture toughness at low temperature [7–11]. Different kinds of rocks such as red sandstone, shale, and silty mudstone show different mechanical performance at different temperature [12, 13]. Loading rate also has effect on the mechanical properties of frozen rocks [14]. Mechanical properties of coal, sandstone, and sandy mudstone have been studied considering different pressure and temperature [15–22]. Besides, confining pressure and temperature, the

impact of cracks on the mechanical properties of the frozen rock should be considered [23]. Due to the extremely rich resources in Western China, the mechanical properties of rocks from Western China have always been one of the research hotspots. A large number of studies on Cretaceous rocks from Western China have shown that temperature, confining pressure, water-saturated state, and other conditions can lead to different mechanical properties and damage processes [24–28]. Recently, acoustic emission technology has been used to investigate the cause of physical mechanics properties change of the frozen rock, and it is proved that the damage process of the frozen rock is related to the freezing process [29].

In general, mechanical properties of the rocks at low temperature vary with lithology, microstructure of rocks, and water content. Due to the limitations of instrumentation and detection technology, it is still impossible to understand the physical and mechanical properties of rocks at low temperature comprehensively and accurately now. Systematic research studies on mechanical properties of frozen rocks are still necessary. In addition, former studies are mainly focused on the mechanical properties of Cretaceous frozen rocks of Western China. Studies on that of western Jurassic rocks are also necessary. Therefore, the mechanical properties of the Jurassic sandstone in Western China were studied under different conditions considering temperature and confining pressure in the current paper. The effects of temperature and confining pressure on the mechanical properties of Jurassic rocks were investigated, and an explanation was given from a microcosmic point of view based on the NMR test.

2. Materials and Methods

2.1. Sample Preparation. The rock samples were obtained from the Jurassic Zhiluo Formation in Balasu mine, Yulin city, Shaanxi province, China. Samples were standardized to the size of $\Phi 50 \times 100$ mm (Figure 1). A HC-F800 acoustic wave tester was used to make sure that samples for each testing group were in good consistency, and the difference of the longitudinal wave velocity was less than 0.5 km/s. The physical parameters of rock sampling depth and normal temperature are shown in Table 1.

Clastic grains of the sample are mainly highly sorted feldspar, quartz, and mica with poor roundness cemented by clay minerals and the secondary enlargement of quartz (Figure 2). Feldspar is mainly alkaline feldspar with high level kaolinization. The contact forms are mainly point-to-surface and surface-to-surface. The rocks are poor in their stability.

2.2. Test Scheme and Process. Triaxial compression tests were performed under different conditions with a temperature of 25°C, −5°C, −10°C, and −15°C and confining pressure of 0, 4, 6, and 8 MPa, respectively. Three rock samples were tested under each temperature and pressure condition, and the results from the three samples were averaged. Meanwhile, one sample was tested for NMR porosity at different temperatures of 25°C, −5°C, −10°C, and −15°C. The test process was as follows:

(1) Immerse the samples in a closed water cylinder without air for 24 hours.

(2) Place the water-saturated rock samples in a low temperature thermostat with preset temperature (25°C, −5°C, −10°C, and −15°C, respectively), and set the freezing rate at 1°C/h.

(3) After freezing for 48 hours at a specified temperature, cover the samples with rubber and put them into the MTS-816.02 electro-hydraulic servo mechanical test system for triaxial compression tests under different confining pressure.

MesoMR23-060H-I was used for NMR microstructure analysis. The samples were maintained at 1 MPa in the vacuum pressure saturation equipment and saturated for 24 h before they were put into the NMR equipment to measure the changes of porosity at 25°C, −5°C, −10°C, and −15°C.

3. Results and Analysis

3.1. Results under Different Conditions of Temperature and Confining Pressure. Stress-strain curves of the Jurassic sandstone under different conditions considering temperature and confining pressure were obtained by compression tests (Figure 3). It is observed that the failure process of Jurassic sandstone has four stages which include compaction stage, linear elasticity stage, yield stage, and failure stage. Confining pressure and temperature have great effects on the strength. Under stable confining pressure, the strength of the rock increases with the decreasing temperature. With the reduction of temperature, the compaction stage can be shortened and the slope of the elastic stage increases, and then yield phenomenon becomes more and more unobvious, which means increases in elastic modulus and brittleness. At a specified temperature, with the increasing confining pressure, the compaction stage is shortened, the slope of the elastic stage increases, and rock strength increases, but the yield phenomenon before reaching the peak value is more and more obvious, which indicates that increasing confining pressure can lead to an increase in rock plasticity.

3.2. Fracture Patterns of Jurassic Sandstone. The development of cracks and joints in rocks has effect on fracture patterns. The fracture modes of some samples in tests are shown in Figure 4. There are three types of damage: (1) tension failure, which occurs in the same direction as the maximum principal stress (Figure 4(a)); (2) shear failure, which forms one or more shear failure surfaces along the diagonal direction (Figure 4(b)); and (3) coupled tension and shear failure (Figure 4(c)). Shear failure is the primary type of damage, and temperature affects the roughness of the shear surfaces. As the temperature decreases, the shear surfaces will become smoother.

(a) (b)

Figure 1: Rock samples: (a) standard rock sample and (b) sample preparation.

Table 1: Rock physical properties.

Lithology	Density (g/cm^3)	Water content (%)	Porosity (%)
Medium sandstone	2.37	9.13	9.33

3.3. Strength Characteristics of Jurassic Sandstone at Low Temperature

3.3.1. Peak Strength. Results of rock peak strength for the tests under different temperature and confining pressure are shown in Figure 5. Results from the test at 25°C are also shown for comparison. It is found that lower temperature leads to higher peak strength, while the peak strength growth rate declines at colder temperature. At the temperature of −5°C, the peak strength increases by 100.98%, 95.44%, 90.13%, and 86.67%, respectively, under the confining pressure of 0, 4, 6, and 8 MPa compared to that of 25°C. The peak strength is nearly doubled under the confining pressure of 0 MPa. However, when the temperature is below 10°C, the growth rate declines (Figure 5(a)). In addition, the peak strength shows a positive relation with the confining pressure at a stable temperature (Figure 5(b)). When confining pressure increases from 0 to 8 MPa, the peak strength increases by 39.13%, 34.81%, and 37.43% at −5°C, −10°C, and −15°C, respectively. It indicates that the strength of the Jurassic sandstone is affected by both low temperature and confining pressure.

3.3.2. Shear Strength. Shear failure is the main fracture mode of tested Jurassic sandstones, so values of the cohesion and internal friction angle can be calculated based on the Mohr–Coulomb criterion. The relation curves of maximum principal stress and minimum principal stress were fitted by test results, and the cohesion and internal friction angle are obtained as given in Table 2.

Cohesion and internal friction angle at different temperature are shown in Figure 6. The values of cohesion and internal friction angle of the Jurassic sandstone increase with the decreasing temperature. When the temperature decreases from 25°C to −15°C, the cohesion increases from 6.82 MPa to 10.02 MPa with an increment of 46.92%. However, when the temperature reduces to about −10°C, the growth rate of cohesion slows down. The value of cohesion increases by 14.02% when the temperature decreases from −5°C to −10°C, and only 2.84% when the temperature decreases from −10°C to −15°C. In terms of the internal friction angle, it increases from 22.58° to 28.99° with an increment of 28.39% when the temperature decreases from 25°C to −15°C. Therefore, low temperature has more influence on cohesion than the internal friction angle of the Jurassic sandstone. In other words, pore (crack) ice plays a key role in enhancing cohesion of the rock at low temperature by cementing rock grains, which ultimately leads to the increase of the shear strength.

3.3.3. Residual Strength. Residual strength is shown in Figure 7. Under stable confining pressure, the residual strength of the Jurassic sandstone increases with the decreasing temperature and shows significant growth at subzero temperatures (Figure 7(a)). When the temperature drops to −15°C from 25°C, the residual strength increases by 151.15%, 123.9%, and 132.43%, respectively, under the confining pressure of 4, 6, and 8 MPa. When the temperature drops to −10°C from −5°C, the residual strength increases by 33.21%, 23.45%, and 12.05%, respectively, whereas when the temperature drops to −15°C from −10°C, the residual strength increases by 22.38%, 21.11%, and 11.75%, respectively, under the confining pressure of 4, 6, and 8 MPa. Therefore, the growth rate of the residual strength slows down at colder temperature (below −10°C). Figure 7(b) shows that the residual strength of the Jurassic sandstone increases when the confining pressure increases at a specified temperature. When the confining pressure rises from 4 MPa to 8 MPa, the residual strength increases by 96.51%, 69.06%, 42.21%, and 29.86%, respectively, at 25°C, −5°C, −10°C, and −15°C.

3.4. Deformation Characteristics of Jurassic Sandstone at Low Temperature

3.4.1. Elastic Modulus. According to stress-strain curves (Figure 3), the elastic modulus under different conditions can be obtained as shown in Figure 8. Figure 8(a) shows that

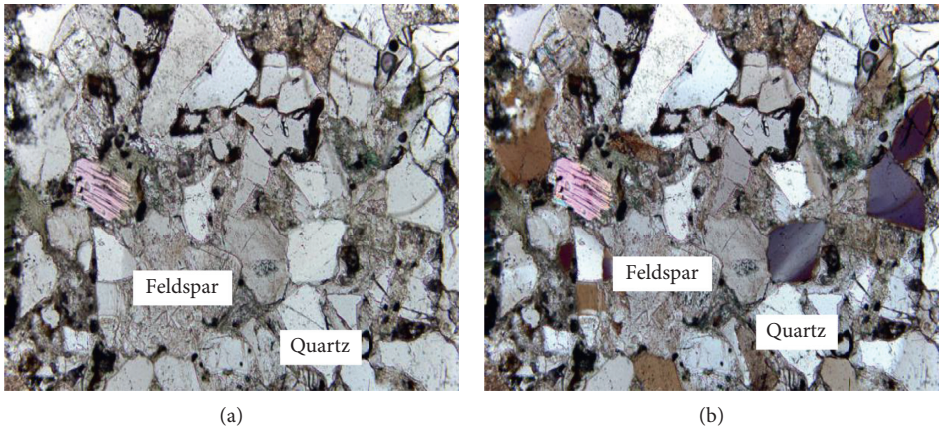

Figure 2: Microstructure of Jurassic sandstone (8x magnification): (a) plane polarized light, and (b) perpendicular polarized light.

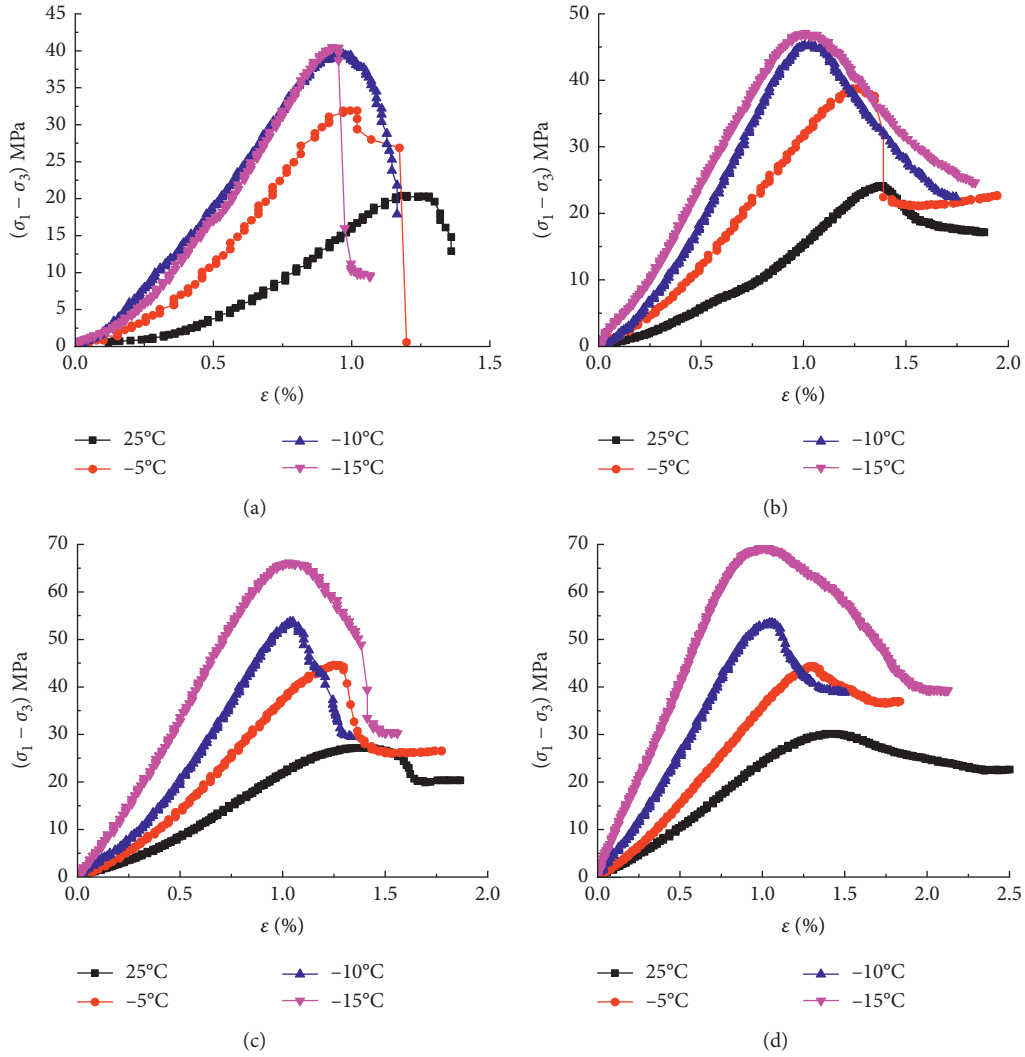

Figure 3: Stress-strain curves with different confining pressures: (a) 0 MPa, (b) 4 MPa, (c) 6 MPa, and (d) 8 MPa.

the value of elastic modulus is greatly affected by temperature. Under stable confining pressure, the elastic modulus gradually increases with the decreasing temperature, while the growth rate declines at colder temperature (below 10°C). The elastic modulus increases by 175.49% when the temperature decreases from 25°C to −5°C, 31.87% when the

(a) (b) (c)

Figure 4: Fracture modes of samples: (a) tension failure, (b) shear failure, and (c) coupled failure.

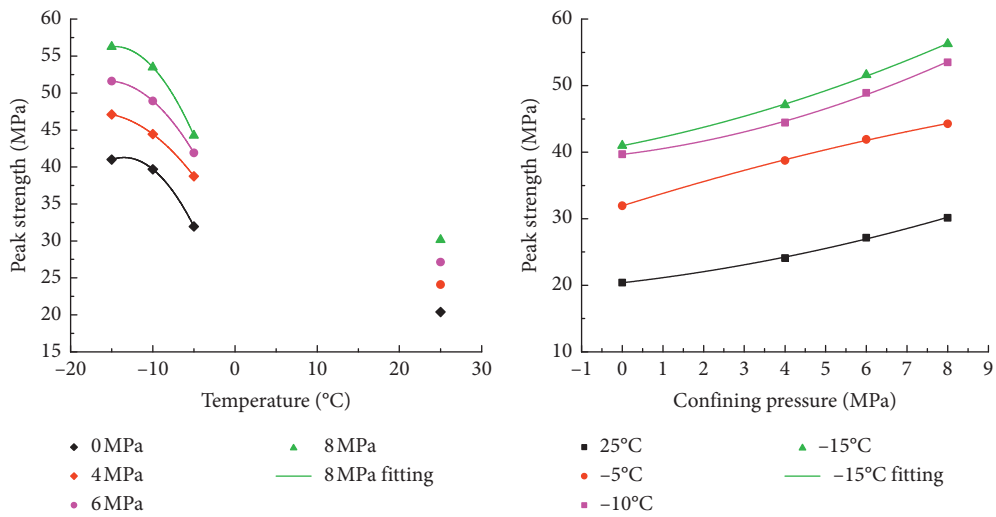

(a) (b)

Figure 5: Peak strength curves under different conditions: (a) temperature and (b) confining pressure.

Table 2: Cohesion and internal friction angle at different temperature.

Temperature (°C)	c (MPa)	Φ (°)
25	6.82	22.58
−5	10.02	26.14
−10	11.93	27.28
−15	11.96	28.99

temperature decreases from −5°C to −10°C, and 10.51% from −10°C to −15°C (taking the pressure of 5 MPa as an example). On the other hand, confining pressure also has a great influence on the elastic modulus (Figure 8(b)). At a stable temperature, the elastic modulus increases with confining pressure. For example, at −5°C when the confining pressure increases, the elastic modulus increases by 35.07%, 27.48%, and 11.92% successively under the testing pressure intervals.

3.4.2. Maximum Axial Strains. Figure 9(a) shows that the maximum axial strain is greatly affected by temperature. Under stable confining pressure, the maximum axial strain decreases and brittleness is getting more and more obvious with the decreasing temperature. Under the condition of 0 MPa, when the temperature decreases from 25°C to −15°C, the maximum axial strain decreases from 1.24% to 0.93% with a reduction of 25.56%. Similarly, the maximum axial strain decreases by 29.78%, 28.87%, and 27.56%, respectively, under the pressure of 4, 6, and 8 MPa at the same temperature interval. However, the reduction rate declines with continuous decrease of temperature (below −10°C) under the condition of given confining pressure. Under the confining pressure of 0, 4, 6, and 8 MPa, when the temperature decreases from −5°C to −10°C, the maximum axial strain decreases by 11.76%, 16.12%, 16.41%, and 16.03%, respectively, whereas when the temperature decreases from −10°C to −15°C, it decreases by 2.11%, 4.81%, 5.61%, and 6.36%, respectively. Confining pressure also

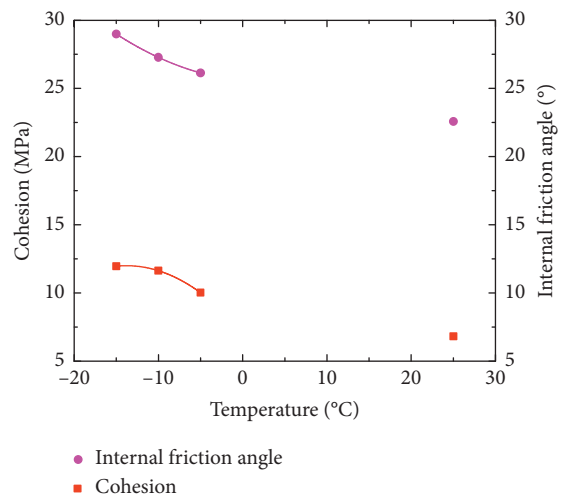

Figure 6: Cohesion and internal friction angle curves at different temperature.

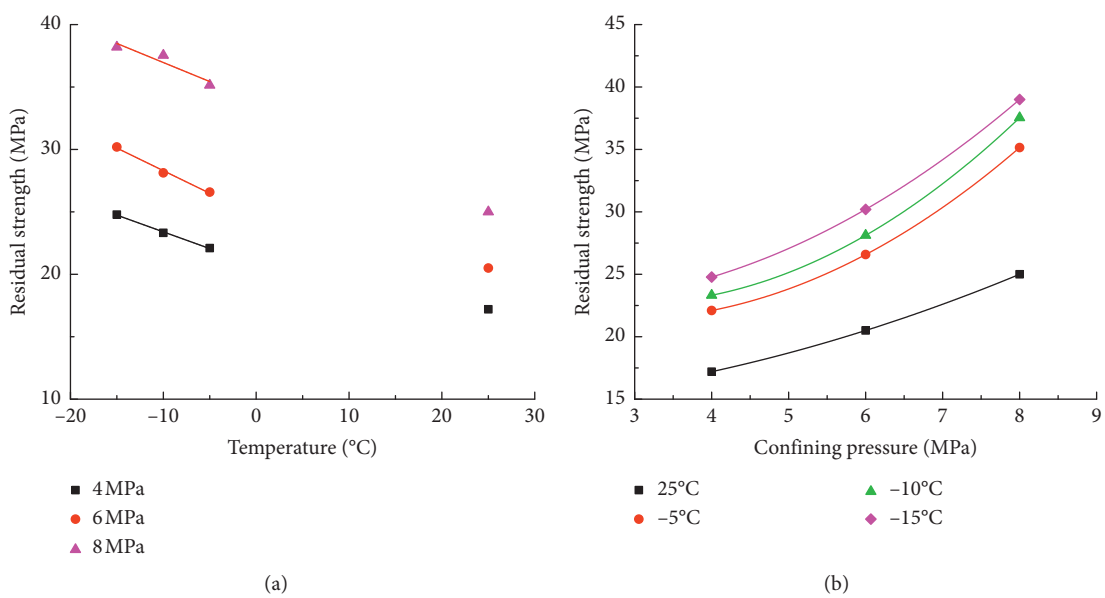

Figure 7: Residual strength curves under different conditions: (a) temperature and (b) confining pressure.

affects the maximum strain (Figure 9(b)). At a given temperature, the increase of confining pressure leads to a larger maximum strain with a time lag and lower brittleness. At the temperature of −5°C, the maximum axial strain increases by 24.43% and by 15.79% and 10.75% at −10°C and −15°C, respectively, when the confining pressure increases from 0 to 8 MPa.

3.4.3. Strength Attenuation Behavior. Strength attenuation behavior of rocks can be described by the attenuation coefficient D_a [30] as follows:

$$D_a = \frac{\sigma_p - \sigma_r}{\sigma_p} = \frac{\delta\sigma}{\sigma_p}, \quad (1)$$

where σ_p, σ_r, and $\delta\sigma$ are the peak strength, residual strength, and strength attenuation of the rock, respectively. The strength attenuation coefficient of the rock under uniaxial compression is called the initial intensity attenuation coefficient and can be denoted as D_{a0}, which can be expressed as follows:

$$D_{a0} = \frac{\delta\sigma_u}{\sigma_c}, \quad (2)$$

where $\delta\sigma_u$ and σ_c are the strength attenuation under uniaxial compression and the uniaxial compressive strength of the rock, respectively. The value of strength attenuation under uniaxial compression is large, so that D_{a0} can be considered to be close to 1. The larger the attenuation coefficient of rock strength is, the greater the difference from peak strength to residual strength will be. On the contrary, the smaller the strength attenuation coefficient of the rock is, the lower the brittleness of the rock will be. So, to some extent, the attenuation coefficient of rock strength can reflect the brittleness of the rock.

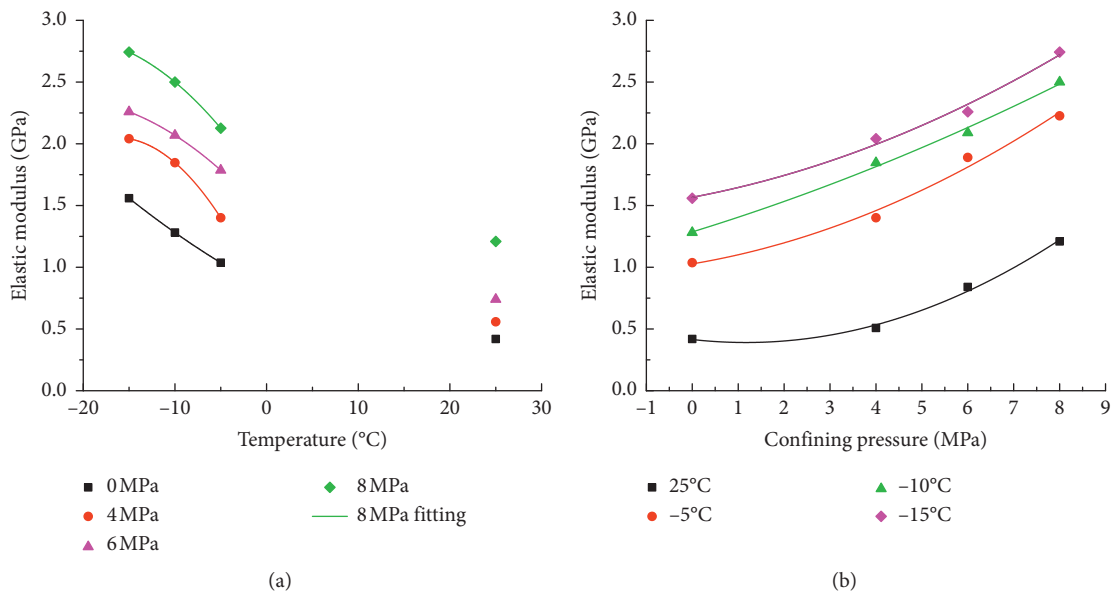

Figure 8: Elastic modulus curves under different conditions: (a) temperature and (b) confining pressure.

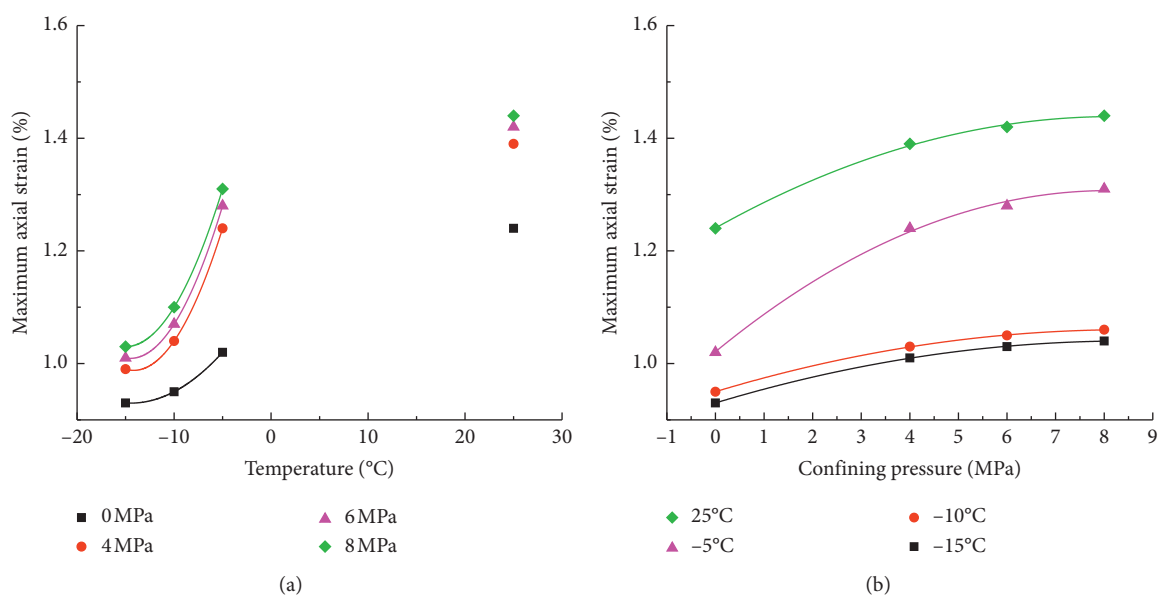

Figure 9: Maximum axial strain curves under different conditions: (a) temperature, and (b) confining pressure.

Based on the test results, according to equations (1) and (2), rock strength attenuation coefficients for different temperature and confining pressure can be obtained as given in Table 3.

Table 3 shows that freezing can promote brittleness of the Jurassic sandstone. At 25°C, the range of rock strength attenuation coefficient is 0.171–1 with an average value of 0.426. At −15°C, the range is 0.333–1 with an average value of 0.561. When the temperature decreases from 25°C to −15°C, the average strength attenuation coefficient increases from 0.426 to 0.561. The relationship between them is shown in Figure 10(a), and can be expressed by a polynomial equation. On the contrary, the brittleness of the Jurassic sandstone is reduced with increasing confining pressure. At 25°C, −5°C, −10°C, and −15°C, when the confining pressure rises from 0 to 8 MPa, the strength attenuation coefficient decreases by 0.829, 0.794, 0.701, and 0.667, respectively. A polynomial relationship can also be found between the strength attenuation coefficient and confining pressure (Figure 10(b)), which can be expressed as follows:

$$D_a = a + b \cdot p + c \cdot p^2, \tag{3}$$

where D_a and p are the strength attenuation coefficient and confining pressure of the sample, respectively, and a, b, and c are the fitting coefficients summarized in Table 4.

When temperature decreases, strength of the Jurassic sandstone increases, but the strength attenuation coefficient increases also. It means the plastic stage is shortened with

Table 3: Rock strength attenuation coefficients of Jurassic sandstones.

Temperature (°C)	Confining pressure (MPa)	$\delta\sigma$ (MPa)	σ_p (MPa)	D_a	$\overline{D_a}$
25	0	20.4	20.4	1.000	0.426
	4	6.9	24.1	0.286	
	6	6.65	27.15	0.245	
	8	5.15	30.15	0.171	
−5	0	31.96	31.96	1.000	0.500
	4	16.65	38.76	0.430	
	6	15.34	41.92	0.366	
	8	9.12	44.27	0.206	
−10	0	39.7	39.7	1.000	0.548
	4	20.78	44.1	0.471	
	6	20.38	48.5	0.420	
	8	16	53.5	0.299	
−15	0	41	41	1.000	0.561
	4	23.4	48.1	0.486	
	6	22.42	52.62	0.426	
	8	19.08	57.28	0.333	

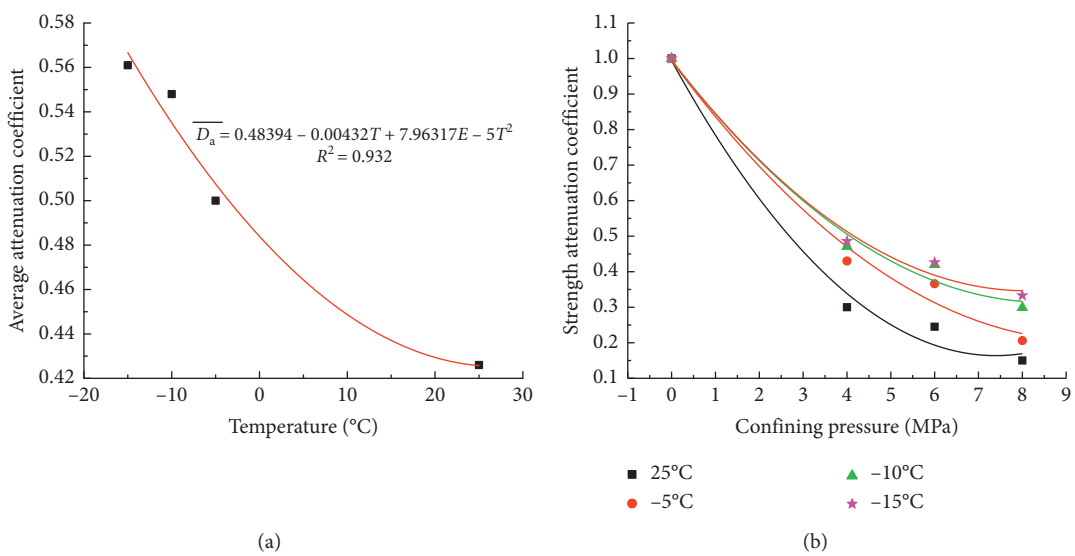

Figure 10: Attenuation coefficients curves under different conditions: (a) temperature, and (b) confining pressure.

higher brittleness and insufficient capacity of the plastic deformation reserve. Once the rock enters the plastic stage, it will be destroyed easily. Therefore, more attention should be paid in the design of freezing engineering.

4. Micromechanism Analysis of the Changes in Mechanical Properties of Jurassic Sandstone

4.1. Porosity Based on NMR Test. The pore-throat size plays an important role in the freezing of sandstone. The values of porosity and pore-throat size distribution of saturated samples at different temperature are shown in Table 5.

Table 5 shows porosity decreases with the decreasing temperature. The value of porosity is 1.17% with 1.12% small pore-throats and 0.05% large pore-throats at −10°C, and large pore-throats vanish at −15°C. Porosity decreases sharply when the temperature decreases from 25°C to −10°C; meanwhile, the peak strength increases greatly, while the reduction rate and the growth rate both decline when the temperature decreases from −10°C to −15°C. So, changes in porosity bring the changes in strength of the frozen rock.

4.2. Formation of Pore (Crack) Ice Crystals. The microstructure evolution is manifested by macrocosmic mechanical properties [31]. Internal pores and pore-throat size affect the freezing process of liquid water in rocks. The freezing process of rock can be divided into different stages according to the increment of ice crystals in pore-throats [32]. Based on microcharacteristics of the rock samples (Figure 3), the sketch of microstructure could be obtained (Figure 11(a)). Based on NMR test results (Table 5), the freezing process of water in pore-throats can go through three stages: (1) rapid freeze stage with the temperature range of 0 to −5°C. During this stage, violent phase transitions of water may occur inside rocks. Porosity decreases and larger pore-throat size disappears rapidly. Most of the

Table 4: Fitting coefficients for the strength attenuation coefficient at different temperatures.

Temperature (°C)	a	b	c	R^2
25	0.9941	−0.2242	0.0158	0.994
−5	0.9934	−0.1658	0.0089	0.959
−10	0.9943	−0.1589	0.0090	0.962
−15	0.9961	−0.1602	0.0097	0.975

Table 5: Porosity and pore-throat size distribution and peak strength.

Temperature (°C)	Peak strength (8 MPa)	Porosity (%)	Pore-throat size distribution (%)	
			0–1000 μm	>1000 μm
25	30.02	9.33	8.17	1.16
−5	44.24	4.01	3.77	0.24
−10	53.10	1.17	1.12	0.05
−15	56.32	1.11	1.11	0

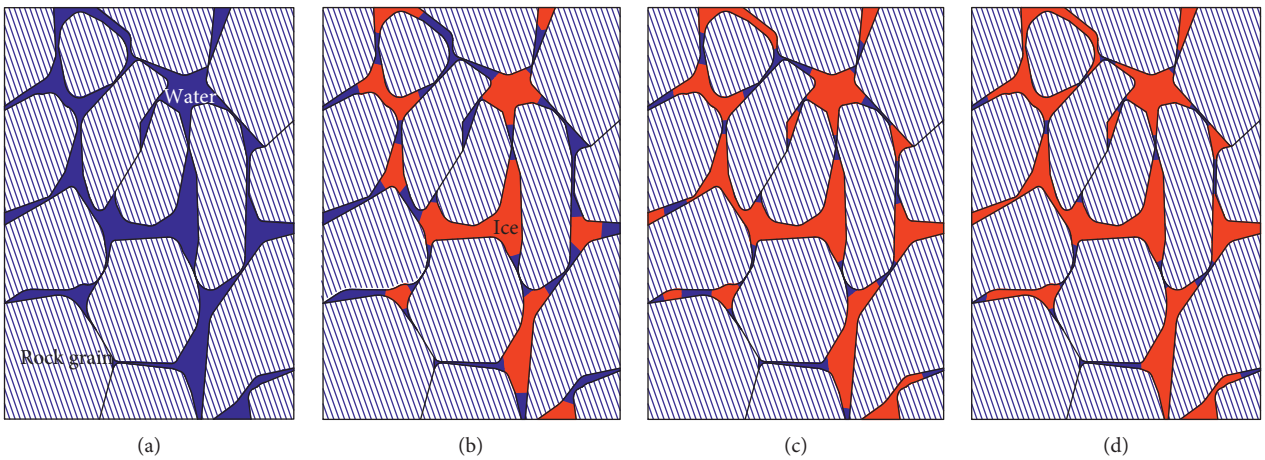

Figure 11: Formation process of pore (crack) ice during freezing: (a) 25°C, (b) −5°C, (c) −10°C, and (d) −15°C.

liquid water mainly in the large pore-throats has been turned into ice. The ice crystal content of pores (cracks) increases rapidly (Figure 11(b)). (2) Freeze developing stage with the corresponding temperature range of −5°C to −10°C. During this stage, liquid water in small pore-throats and some fine (micro) pore-throats has been turned into ice and ice crystal content in pores (cracks) continues to increase, but the growth rate declines (Figure 11(c)). The porosity and the mount of small pore-throats decrease continuously. (3) Freezing stable stage with the temperature below −10°C. During this stage, porosity and pore-throat size distribution vary little because most liquid water in the pore (crack) has been frozen; however, due to capillary force and surface adsorption of mineral grains, there is still water which cannot be frozen with relatively lower freezing point. Therefore, even if some liquid water mainly in fine (micro) pore-throats continues to be frozen, the increment of pore (crack) ice crystals is very small (Figure 11(d)).

4.3. Microcosmic Interpretation of Changes in Rock Mechanical Properties. It is revealed by the test results that temperature, especially subzero temperature, has a great impact on the strength and deformation characteristics of the Jurassic sandstone. Figure 11 shows that freezing process is substantially correlated to the variation of the pore-throat size. During the rapid freeze stage and the freeze developing stage, the pores (cracks) are filled with a large number of ice crystals, so the pore-throat radius decreases significantly. Rock grains are connected tightly with high cohesive force, which improves the rock's ability to resist deformation. In addition, the strength of ice crystals contributes to the rock strength. Therefore, elastic modulus and strength are greatly increased. During the third stage with temperature below −10°C, the increment of ice is very small and porosity and pore-throat size vary little (Figures 11(c) vs. 11(d)). The effect of grains shrinkage is not obvious at the same time. The increase of rock strength as one of the macrocosmic performance tends to slow down and be stable eventually. Different confining pressure and temperature may lead to different friction effect on rock grains and ice crystals, which causes diverse fracture patterns of testing samples. The rise of confining pressure may limit the expansion of internal cracks in rocks, enhance the closure effect of cracks, and

reduce the slip between grains, which may contribute to the rise of elastic modulus and strength. Meanwhile, the rise of confining pressure also can delay the peak strength and result in an increasing maximum axial strain.

Low temperature and confining pressure can greatly change microstructure characteristics of rock, which leads to the diversity of macromechanical properties.

5. Conclusions

Taking the Jurassic sandstone in Western China as an example, rock strength and deformation characteristics as well as the influencing mechanism of confining pressure and temperature were analyzed by the triaxial compression test and NMR test under different conditions.

(1) Strength parameters such as peak strength, residual strength, cohesion, and internal friction angle tended to increase with the decreasing temperature when the confining pressure was fixed. Similarly, the above parameters increased with the confining pressure at a specified temperature. The increment appeared to be especially obvious at subzero temperature, while the strength growth rate declined at colder temperature (below −10°C).

(2) Elastic modulus increased with the decreasing temperature under stable confining pressure, while the growth rate declined at colder temperature (below −10°C). There is a positive correlation between elastic modulus and confining pressure at a stable temperature. Under stable confining pressure, the maximum axial strain decreased and brittleness increased with the decrease of temperature. At a stable temperature, the increase in confining pressure led to a larger maximum strain with a time lag and lower brittleness.

(3) Average strength attenuation coefficients increased from 0.426 to 0.561 when the temperature decreased from 25°C to −15°C, while strength attenuation coefficients decreased with the increasing confining pressure at a certain temperature.

(4) During the first two stages of freezing, pores (cracks) of the rock were filled with a large number of ice crystals with significant decrease of porosity and pore-throat radius, whereas the increment of ice is very small during the third stage with the temperature below −10°C, which could explain why the growth rate of rock strength would slow down at colder temperature.

Data Availability

The data used to support the finding of this study are provided in this paper.

Conflicts of Interest

The authors declare no conflicts of interest regarding this paper.

Acknowledgments

This research was supported by the National Natural Science Foundation of China (grant no. 51874005) and the Educational Commission of Anhui Province of China (KJ2019A0739).

References

[1] Z. M. Xu, S. Gao, Y. J. Sun et al., "A study of conditions of water bearing media and water dynamics in typical Jurassic coal rich regions in Western," *China Journal of China Coal Society*, vol. 42, no. 2, pp. 444–451, 2017.

[2] L. M. Fan and X. D. Ma, "Research progress of water inrush hazard in shallow buried coal seam mine," *Coal Science and Technology*, vol. 44, no. 1, pp. 8–12, 2016.

[3] Q. B. Meng, L. J. Han, H. Pu et al., "Research and monitoring analysis of coal roadway bolting system in very weakly cemented stratum," *Journal of China Coal Society*, vol. 41, no. 1, pp. 234–245, 2016.

[4] L. H. Sun, H. G. Ji, and B. S. Yang, "Physical and mechanical characteristic of rocks with weakly cemented strata in Western representative mining," *Journal of China Coal Society*, vol. 44, no. 3, pp. 865–873, 2019.

[5] J. B. Liu, J. Zhao, and Z. X. Zhu, "On the number of spanning trees and normalized Laplacian of linear octagonal-quadrilateral networks," *International Journal of Quantum Chemistry*, vol. 119, no. 17, Article ID e25971, 2019.

[6] J.-B. Liu, J. Zhao, and Z.-Q. Cai, "On the generalized adjacency, Laplacian and signless Laplacian spectra of the weighted edge corona networks," *Physica A: Statistical Mechanics and Its Applications*, vol. 540, Article ID 123073, 2020.

[7] T. Yamabe and K. M. Neaupane, "Determination of some thermo-mechanical properties of Sirahama sandstone under subzero temperature condition," *International Journal of Rock Mechanics and Mining Sciences*, vol. 38, no. 7, pp. 1029–1034, 2001.

[8] C. Park, J. H. Synn, H. S. Shin, D. S. Cheon, H. D. Lim, and S. W. Jeon, "Experimental study on the thermal characteristics of rock at low temperatures," *International Journal of Rock Mechanics and Mining Sciences*, vol. 41, no. 1, pp. 81–86, 2004.

[9] G. M. Xu, Q. S. Liu, W. W. Peng, and X. X. Chang, "Experimental study on basic mechanical behaviors of rocks under low temperatures," *Chinese Journal of Rock Mechanics and Engineering*, vol. 25, no. 12, pp. 2502–2508, 2006.

[10] Q. S. Liu, G. M. Xu, Y. H. Hu, and X. Chang, "Study on basic mechanical behaviors of rocks at low temperatures," *Key Engineering Materials*, vol. 306–308, pp. 1479–1484, 2006.

[11] Y. P. Li and Z. Y. Wang, "Uniaxial compressive mechanical properties of rock at low temperature," *Journal of University of Science and Technology Beijing*, vol. 33, no. 6, pp. 671–675, 2011.

[12] Y. P. Li and Z. Y. Wang, "Study of parameters and strength of thermal effects for granite under low temperature," *Rock and Soil Mechanics*, vol. 33, no. 2, pp. 321–326, 2012.

[13] J. Kodama, T. Goto, Y. Fujii, and P. Hagan, "The effects of water content, temperature and loading rate on strength and failure process of frozen rocks," *International Journal of Rock Mechanics and Mining Sciences*, vol. 62, no. 2, pp. 1–13, 2013.

[14] G. S. Yang, Q. S. Zhang, and Y. B. Pu, "Preliminary study on meso-damage propagation characteristics of rock under condition of freezing temperature," *Rock and Soil Mechanics*, vol. 25, no. 9, pp. 1409–1412, 2004.

[15] G. S. Yang, J. M. Xi, H. J. Li, and L. Cheng, "Experimental study of rock mechanical properties under triaxial compressive and frozen conditions," *Chinese Journal of Rock Mechanics and Engineering*, vol. 29, no. 3, pp. 459–464, 2010.

[16] G. S. Yang, J. M. Xi, X. M. Shao, H. J. Li, and L. Cheng, "Experimental study on rock strength properties under freezing conditions," *Journal of Xi'an University of Science and Technology*, vol. 30, no. 1, pp. 14–18, 2010.

[17] G. S. Yang, J. M. Xi, Z. J. Wang, L. Cheng, and H. J. Li, "Study on rock mechanical properties of frozen wall of main shaft in Hujiahe coal mine," *Journal of China Coal Society*, vol. 35, no. 4, pp. 565–570, 2010.

[18] G. S. Yang and L. X. Tao, "Experimental study on the sandy mudstone mechanical properties of shaft sidewalls under the frozen conditions," *Journal of Mining & Safety Engineering*, vol. 29, no. 4, pp. 492–496, 2012.

[19] G. S. Yang, J. M. Xi, H. J. Li, L. Cheng, and X. T. Lv, "Experimental study on the mechanical properties of soft rock of coal mine shaft sidewalls under the frozen conditions," *Chinese Journal of Underground Space and Engineering*, vol. 8, no. 4, pp. 690–687, 2012.

[20] G. S. Yang, Y. L. Qu, and X. J. Mi, "Study of mechanical properties and temperature field of frozen wall in Cretaceous strata," *Chinese Journal of Rock Mechanics and Engineering*, vol. 33, no. 9, pp. 1873–1879, 2014.

[21] G. S. Yang, Y. Wei, Y. J. Shen et al., "Mechanical behavior and strength forecast model of frozen saturated sandstone under triaxial compression," *Chinese Journal of Rock Mechanics and Engineering*, vol. 38, no. 4, pp. 683–694, 2019.

[22] D. W. Li, R. H. Wang, and J. H. Fan, "Nonlinear rheological model for frozen soft rock during Cretaceous period," *Chinese Journal of Geotechnical Engineering*, vol. 33, no. 3, pp. 98–403, 2011.

[23] Y. Liu, R. H. Wang, and J. H. Chen, "Experiment study on physical mechanics performances of Cretaceous system rock under minus temperature," *Coal Mine Engineering*, vol. 1, pp. 82–84, 2011.

[24] J. M. Xi, G. S. Yang, L. Pang, X. T. Lv, and F. L. Liu, "Experimental study on basic mechanical behaviors of sandy mudstone under low freezing temperature," *Journal of China Coal Society*, vol. 39, no. 7, pp. 1262–1268, 2014.

[25] F. Zi, G. S. Yang, and H. L. Jia, "Influence of saturation degree on the mechanical properties of frozen argillaceous siltstone," *Journal of Glaciology and Geocryology*, vol. 40, no. 4, pp. 748–755, 2018.

[26] B. Liu, Y. J. Ma, H. L. Sheng, H. L. Deng, Q. Han, and Y. J. Cao, "Experimental study on mechanical properties of cretaceous red sandstone under different freezing temperatures and confining pressures," *Chinese Journal of Rock Mechanics and Engineering*, vol. 38, no. 3, pp. 455–465, 2019.

[27] G. Zhang, B. Liu, Y. J. Ma, and Y. C. Liu, "Mechanical analysis on sandy mudstone in uniaxial compression and acoustic emission test through artificial freezing method," *Chinese Journal of Underground Space and Engineering*, vol. 15, no. 3, pp. 699–706, 2019.

[28] A. Török, A. Ficsor, M. Davarpanah, and B. Vásárhelyi, "Comparison of mechanical properties of dry, Saturated and frozen porous rocks," in *IAEG/AEG Annual Meeting Proceedings, San Francisco, California, 2018—Volume 6*, A. Shakoor and K. Cato, Eds., Springer, Cham, Switzerland, pp. 455–465, 2018.

[29] H. Yang, J. X. Zhang, R. L. Shan, F. M. Wu, and Z. M. Guo, "Experimental study on mechanical properties of frozen saturated single fractured rock mass," *Rock and Soil Mechanics*, vol. 39, no. 4, pp. 1245–1255, 2018.

[30] J. Peng, G. Rong, M. Cai, and K. Peng, "Determination of residual strength of rocks by a brittle index," *Rock and Soil Mechanics*, vol. 36, no. 2, pp. 403–408, 2015.

[31] Z. L. Zhang and Z. D. Cui, "Analysis of microscopic pore structures of the silty clay before and after freezing–thawing under the subway vibration loading," *Environmental Earth Sciences*, vol. 76, no. 15, p. 528, 2017.

[32] H. Liu, G. S. Yang, H. L. Jia et al., "Experimental study on meso-structure of rock in the process of crack (pore) water freezing," *Chinese Journal of Rock Mechanics and Engineering*, vol. 35, no. 12, pp. 2516–2524, 2016.

Hindawi
Journal of Chemistry
Volume 2020, Article ID 1280632, 12 pages
https://doi.org/10.1155/2020/1280632

Research Article

Topological Properties of Nanostar Dendrimer and Smart Polymer

Muhammad Aamer Rashid,[1] **Sarfraz Ahmad**,[1] **Murat Cancan**,[2] **and Mehwish Hussain Muhammad**[3]

[1]*Department of Mathematics, COMSATS University Islamabad, Lahore Campus, Lahore 54000, Pakistan*
[2]*Faculty of Education, Van Yuzuncu Yil University, Van, Turkey*
[3]*College of Chemistry and Molecular Engineering, Zhengzhou University, Zhengzhou, 450001, China*

Correspondence should be addressed to Muhammad Aamer Rashid; aamerrasheed7869@gmail.com

Received 25 July 2019; Accepted 28 February 2020; Published 21 April 2020

Guest Editor: Shaohui Wang

The nanostar dendrimers are a piece of another gathering of macromolecules that seem, by all accounts, to be photon pipes simply like counterfeit reception apparatuses. In addition, nanostar dendrimers are one of the fundamental stuffs of nanobiotechnology. The smart polymers are large-scale particles that show an emotional physioconcoction change because of little changes in their condition, for example, temperature, pH, light, attractive field, and ionic variables. A topological record of a graph G is a numeric quantity notorious with G which portrays subatomic diagram G. In this paper, we decide first and second Zagreb indices, hyper-Zagreb index, first multiple Zagreb index, second numerous Zagreb index, and Zagreb polynomials for nanostar dendrimer and smart polymer.

1. Introduction

Scientific science is a part of hypothetical science where we examine and anticipate the compound erection by exploiting arithmetical devices. Substance diagram hypothesis is a part of scientific science wherein we apply apparatuses of chart hypothesis to display the synthetic marvel scientifically. This hypothesis contributes an unmistakable job in the fields of concoction sciences.

A nanostructure is an object of middle of the road size among minute and atomic structures. This is approximately due to a physical measurement lesser than 100 nanometers, extending from groups of iotas to dimensional layers. Nanobiotechnology is a hurriedly boosting territory of logical and mechanical open door that applies the apparatuses and procedures of nanofabrication to fabricate gadgets for examining biosystems.

From a polymer science perspective, dendrimers are almost immaculate monodisperse macromolecules with a customary and exceptionally fanned three-dimensional design. The nanostar dendrimer is a piece of another gathering of macroparticles that seem, by all accounts, to be photon channels simply like counterfeit reception apparatuses. These macromolecules and all those more absolutely containing phosphorus are utilized in the development of nanotubes, smaller scale macrocapsules, nanolatex, shaded glasses, concoction sensors, and adjusted terminals [1].

A topological index is a numeric amount related with a graph which portrays the topology of chart and is invariant under diagram automorphism. A topological record $\mathrm{Top}(G)$ of a graph G is a number with the property that, for each chart H isomorphic to G, $\mathrm{Top}(H) = \mathrm{Top}(G)$. The idea of topological record originated from work done by Wiener [2], while he was taking a shot at breaking point of paraffin. He named this record as *way number*. Later on, the way number was renamed as *Wiener index*. The Wiener list is the first and most concentrated topological file, both from hypothetical perspective and applications, and characterized as the whole of separations between all sets of vertices in G, see [3, 4]for subtleties.

One of the most seasoned topological files is the primary Zagreb list presented by Gutman and Trinajstic in 1972 [5] based on the level of vertices of G, and the first and second Zagreb indices are characterized as

$$M_1(G) = \sum_{\widehat{e}\widehat{f}\in E(G)} [\Omega(\widehat{e}) + \widehat{f}], \tag{1}$$

$$M_2(G) = \sum_{\widehat{e}\widehat{f}\in E(G)} [\Omega(\widehat{e}) \times \Omega(\widehat{f})]. \tag{2}$$

In 2013, Shirdel et al. [6] introduced a new degree-based Zagreb index named "hyper-Zagreb index" as

$$HM(G) = \sum_{\widehat{e}\widehat{f}\in E(G)} [\Omega(\widehat{e}) + \Omega(\widehat{f})]^2. \tag{3}$$

In 2012, Ghorbani and Azimi [7] characterized two new forms of Zagreb lists of a diagram G. The first multiple Zagreb index $PM_1(G)$, the second multiple Zagreb index $PM_2(G)$, and these are characterized as

$$PM_1(G) = \prod_{\widehat{e}\widehat{f}\in E(G)} [\Omega(\widehat{e}) + \Omega(\widehat{f})], \tag{4}$$

$$PM_2(G) = \prod_{\widehat{e}\widehat{f}\in E(G)} [\Omega(\widehat{e}) + \Omega(\widehat{f})]. \tag{5}$$

In [8], the Zagreb polynomials are characterized as

$$M_1(G,x) = \sum_{\widehat{e}\widehat{f}\in E(G)} x^{[\Omega(\widehat{e})+\Omega(\widehat{f})]}, \tag{6}$$

$$M_2(G,x) = \sum_{\widehat{e}\widehat{f}\in E(G)} x^{[\Omega(\widehat{e})+\Omega(\widehat{f})]}. \tag{7}$$

For further investigation of topological files of different chart families, see [5, 6, 9–23].

2. Nanostar Dendrimers $NSC_5C_6[n]$ and $NSD[n]$

Nanostar dendrimers are one of the fundamental objects of nanobiotechnology. They have an all-around characterized subatomic topology. Their progression insightful development pursues a scientific movement. In a precise expression, nanostar dendrimers are hyperbranched macromolecules, demonstrating a thorough, tastefully engaging engineering. The nanostar dendrimer is a piece of another gathering of macromolecules having extraordinary applications [1]. In 2012, Rostamia et al. [24] figured first geometric-number juggling list, Randic file, and entirely available file for nanostar dendrimer $NSC_5C_6[n]$ and $NSD[n]$. In this segment, we process first and Second Zagreb lists, hyper-Zagreb list, first different Zagreb record, second various Zagreb file, and Zagreb polynomials for nanostar dendrimers $NSC_5C_6[n]$ and $NSD[n]$.

2.1. Methodology and Construction of Nanostar Dendrimers $NSC_5C_6[n]$ Formulas. Consider the atomic chart $NSC_5C_6[n]$, where n are ventures of development in this kind of nanostar dendrimer (see Figure 1). It is anything but difficult to compute that the quantity of vertices in $NSC_5C_6[n]$ is $9\cdot 2^{n+2} - 44$ and the quantity of edges is $10\cdot 2^{n+2} - 50$, see likewise [24].

Moreover, there are seven types of edges in $NSC_5C_6[n]$. To compute the above results, we define seven partitions of edge set $E(NSC_5C_6[n])$ and compute their cardinalities in the following way:

$$\begin{aligned}
&E_1(NSC_5C_6[n]) = \{\widehat{e}\widehat{f} \in E(NSC_5C_6[n]) \mid \Omega(\widehat{e}) = 1, \Omega(\widehat{f}) = 3\},\\
&|E_1(NSC_5C_6[n])| = 2^{n+2} - 6,\\
&E_2(NSC_5C_6[n]) = \{\widehat{e}\widehat{f} \in E(NSC_5C_6[n]) \mid \Omega(\widehat{e}) = 1, \Omega(\widehat{f}) = 4\},\\
&|E_2(NSC_5C_6[n])| = 2^{n+2},\\
&E_3(NSC_5C_6[n]) = \{\widehat{e}\widehat{f} \in E(NSC_5C_6[n]) \mid \Omega(\widehat{e}) = 2, \Omega(\widehat{f}) = 2\},\\
&|E_3(NSC_5C_6[n])| = 2^{n+2} - 6,\\
&E_4(NSC_5C_6[n]) = \{\widehat{e}\widehat{f} \in E(NSC_5C_6[n]) \mid \Omega(\widehat{e}) = 2, \Omega(\widehat{f}) = 3\},\\
&|E_4(NSC_5C_6[n])| = 9\cdot 2^{n+2} - 28,\\
&E_5(NSC_5C_6[n]) = \{\widehat{e}\widehat{f} \in E(NSC_5C_6[n]) \mid \Omega(\widehat{e}) = 2, \Omega(\widehat{f}) = 4\},\\
&|E_5(NSC_5C_6[n])| = 2^{n+1},\\
&E_6(NSC_5C_6[n]) = \{\widehat{e}\widehat{f} \in E(NSC_5C_6[n]) \mid \Omega(\widehat{e}) = 3, \Omega(\widehat{f}) = 3\},\\
&|E_6(NSC_5C_6[n])| = 3\cdot 2^{n} - 10,\\
&E_7(NSC_5C_6[n]) = \{\widehat{e}\widehat{f} \in E(NSC_5C_6[n]) \mid \Omega(\widehat{e}) = 4, \Omega(\widehat{f}) = 4\},\\
&|E_7(NSC_5C_6[n])| = 2^{n}.
\end{aligned} \tag{8}$$

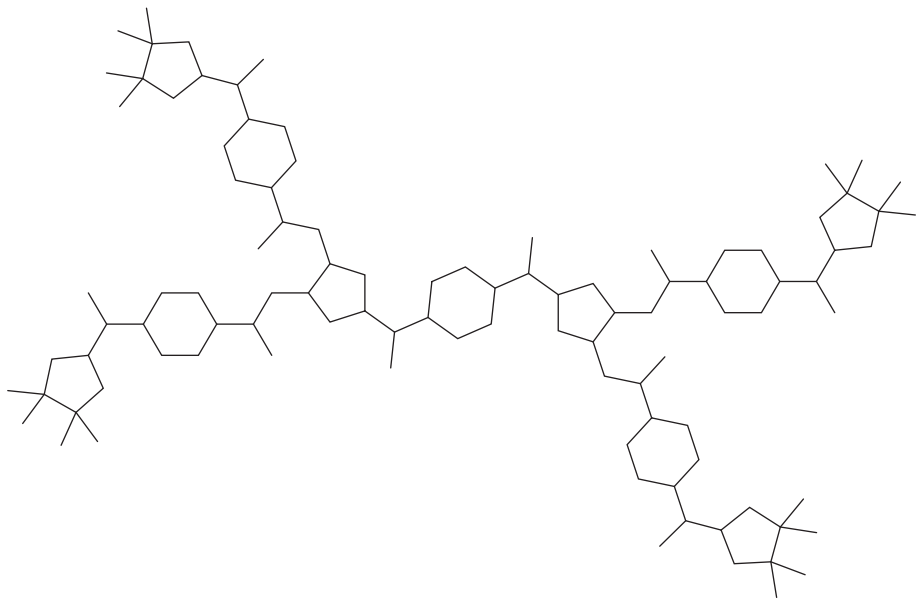

Figure 1: The nanostar dendrimer $NSC_5C_6[2]$.

Now using equations (1)–(7), we have the following results.

2.1.1. First and Second Zagreb Index

$$
\begin{aligned}
M_1(G) &= \sum_{\widehat{e}\widehat{f}\in E(G)} [\Omega(\widehat{e}) + \Omega(\widehat{f})],\\
M_1(NSC_5C_6[n]) &= \sum_{\widehat{e}\widehat{f}\in E_1} [\Omega(\widehat{e}) + \Omega(\widehat{f})] + \sum_{\widehat{e}\widehat{f}\in E_2} [\Omega(\widehat{e}) + \Omega(\widehat{f})] + \sum_{\widehat{e}\widehat{f}\in E_3} [\Omega(\widehat{e}) + \Omega(\widehat{f})]\\
&\quad + \sum_{\widehat{e}\widehat{f}\in E_4} [\Omega(\widehat{e}) + \Omega(\widehat{f})] + \sum_{\widehat{e}\widehat{f}\in E_5} [\Omega(\widehat{e}) + \Omega(\widehat{f})] + \sum_{\widehat{e}\widehat{f}\in E_6} [\Omega(\widehat{e}) + \Omega(\widehat{f})] + \sum_{\widehat{e}\widehat{f}\in E_7} [\Omega(\widehat{e}) + \Omega(\widehat{f})]\\
&= 4|E_1| + 5|E_2| + 4|E_3| + 5|E_4| + 6|E_5| + 6|E_6| + 8|E_7|\\
&= 4\left(2^{n+2} - 6\right) + 5\left(2^{n+2}\right) + 4\left(2^{n+2} - 6\right) + 5\left(9 \cdot 2^{n+2} - 28\right) + 6\left(2^{n+1}\right) + 6\left(3 \cdot 2^n - 10\right) + 8\left(2^n\right),\\
M_2(G) &= \sum_{\widehat{e}\widehat{f}\in E(G)} [\Omega(\widehat{e}) \times \Omega(\widehat{f})],\\
M_2(NSC_5C_6[n]) &= \sum_{\widehat{e}\widehat{f}\in E_1} [\Omega(\widehat{e}) \times \Omega(\widehat{f})] + \sum_{\widehat{e}\widehat{f}\in E_2} [\Omega(\widehat{e}) \times \Omega(\widehat{f})] + \sum_{\widehat{e}\widehat{f}\in E_3} [\Omega(\widehat{e}) \times \Omega(\widehat{f})]\\
&\quad + \sum_{\widehat{e}\widehat{f}\in E_4} [\Omega(\widehat{e}) \times \Omega(\widehat{f})] + \sum_{\widehat{e}\widehat{f}\in E_5} [\Omega(\widehat{e}) \times \Omega(\widehat{f})] + \sum_{\widehat{e}\widehat{f}\in E_6} [\Omega(\widehat{e}) \times \Omega(\widehat{f})] + \sum_{\widehat{e}\widehat{f}\in E_7} [\Omega(\widehat{e}) \times \Omega(\widehat{f})]\\
&= 3|E_1| + 4|E_2| + 4|E_3| + 6|E_4| + 8|E_5| + 9|E_6| + 16|E_7|\\
&= 3\left(2^{n+2} - 6\right) + 4\left(2^{n+2}\right) + 4\left(2^{n+2} - 6\right) + 6\left(9 \cdot 2^{n+2} - 28\right) + 8\left(2^{n+1}\right) + 9\left(3 \cdot 2^n - 10\right) + 16\left(2^n\right).
\end{aligned}
\tag{9}
$$

2.1.2. Hyper-Zagreb Index

$$
\begin{aligned}
HM(G) &= \sum_{\widehat{ef} \in E(G)} [\Omega(\widehat{e}) + \Omega(\widehat{f})]^2, \\
HM(NSC_5C_6[n]) &= \sum_{\widehat{ef}\in E_1} [\Omega(\widehat{e}) + \Omega(\widehat{f})]^2 + \sum_{\widehat{ef}\in E_2} [\Omega(\widehat{e}) + \Omega(\widehat{f})]^2 + \sum_{\widehat{ef}\in E_3} [\Omega(\widehat{e}) + \Omega(\widehat{f})]^2 \\
&\quad + \sum_{\widehat{ef}\in E_4} [\Omega(\widehat{e}) + \Omega(\widehat{f})]^2 + \sum_{\widehat{ef}\in E_5} [\Omega(\widehat{e}) + \Omega(\widehat{f})]^2 + \sum_{\widehat{ef}\in E_6} [\Omega(\widehat{e}) + \Omega(\widehat{f})]^2 + \sum_{\widehat{ef}\in E_7} [\Omega(\widehat{e}) + \Omega(\widehat{f})]^2 \\
&= 16|E_1| + 25|E_2| + 16|E_3| + 25|E_4| + 36|E_5| + 36|E_6| + 64|E_7| \\
&= 16\left(2^{n+2} - 6\right) + 25\left(2^{n+2}\right) + 16\left(2^{n+2} - 6\right) + 25\left(9 \cdot 2^{n+2} - 28\right) + 36\left(2^{n+1}\right) + 36\left(3 \cdot 2^n - 10\right) + 64\left(2^n\right).
\end{aligned}
\tag{10}
$$

2.1.3. First and Second Multiple Zagreb Index

$$
\begin{aligned}
PM_1(G) &= \prod_{\widehat{ef}\in E(G)} [\Omega(\widehat{e}) + \Omega(\widehat{f})], \\
PM_1(NSC_5C_6[n]) &= \prod_{\widehat{ef}\in E_1} [\Omega(\widehat{e}) + \Omega(\widehat{f})] \times \prod_{\widehat{ef}\in E_2} [\Omega(\widehat{e}) + \Omega(\widehat{f})] \times \prod_{\widehat{ef}\in E_3} [\Omega(\widehat{e}) + \Omega(\widehat{f})] \\
&\quad \times \prod_{\widehat{ef}\in E_4} [\Omega(\widehat{e}) + \Omega(\widehat{f})] \times \prod_{\widehat{ef}\in E_5} [\Omega(\widehat{e}) + \Omega(\widehat{f})] \times \prod_{\widehat{ef}\in E_6} [\Omega(\widehat{e}) + \Omega(\widehat{f})] \times \prod_{\widehat{ef}\in E_7} [\Omega(\widehat{e}) + \Omega(\widehat{f})] \\
&= 4^{|E_1|} \times 5^{|E_2|} \times 4^{|E_3|} \times 5^{|E_4|} \times 6^{|E_5|} \times 6^{|E_6|} \times 8^{|E_7|} \\
&= 4^{\left(2^{n+2}-6\right)} \times 5^{\left(2^{n+2}\right)} \times 4^{\left(2^{n+2}-6\right)} \times 5^{\left(9\cdot 2^{n+2}-28\right)} \times 6^{\left(2^{n+1}\right)} \times 6^{\left(3\cdot 2^n-10\right)} \times 8^{\left(2^n\right)}, \\
PM_2(G) &= \prod_{\widehat{ef}\in E(G)} [\Omega(\widehat{e}) \times \Omega(\widehat{f})], \\
PM_2(NSC_5C_6[n]) &= \prod_{\widehat{ef}\in E_1} [\Omega(\widehat{e}) \times \Omega(\widehat{f})] \times \prod_{\widehat{ef}\in E_2} [\Omega(\widehat{e}) \times \Omega(\widehat{f})] \times \prod_{\widehat{ef}\in E_3} [\Omega(\widehat{e}) \times \Omega(\widehat{f})] \\
&\quad \times \prod_{\widehat{ef}\in E_4} [\Omega(\widehat{e}) \times \Omega(\widehat{f})] \times \prod_{\widehat{ef}\in E_5} [\Omega(\widehat{e}) \times \Omega(\widehat{f})] \times \prod_{\widehat{ef}\in E_6} [\Omega(\widehat{e}) \times \Omega(\widehat{f})] \times \prod_{\widehat{ef}\in E_7} [\Omega(\widehat{e}) \times \Omega(\widehat{f})] \\
&= 3^{|E_1|} \times 4^{|E_2|} \times 4^{|E_3|} \times 6^{|E_4|} \times 8^{|E_5|} \times 9^{|E_6|} \times 16^{|E_7|} \\
&= 3^{\left(2^{n+2}-6\right)} \times 4^{\left(2^{n+2}\right)} \times 4^{\left(2^{n+2}-6\right)} \times 6^{\left(9\cdot 2^{n+2}-28\right)} \times 8^{\left(2^{n+1}\right)} \times 9^{\left(3\cdot 2^n-10\right)} \times 16^{\left(2^n\right)}.
\end{aligned}
\tag{11}
$$

2.1.4. First and Second Zagreb Polynomial

$$
\begin{aligned}
M_1(G,x) &= \sum_{\widehat{e}\widehat{f}\in E(G)} x^{[\Omega(\widehat{e})+\Omega(\widehat{f})]},\\
M_1(NSC_5C_6[n],x) &= \sum_{\widehat{e}\widehat{f}\in E_1} x^{[\Omega(\widehat{e})+\Omega(\widehat{f})]} + \sum_{\widehat{e}\widehat{f}\in E_2} x^{[\Omega(\widehat{e})+\Omega(\widehat{f})]} + \sum_{\widehat{e}\widehat{f}\in E_3} x^{[\Omega(\widehat{e})+\Omega(\widehat{f})]}\\
&\quad + \sum_{\widehat{e}\widehat{f}\in E_4} x^{[\Omega(\widehat{e})+\Omega(\widehat{f})]} + \sum_{\widehat{e}\widehat{f}\in E_5} x^{[\Omega(\widehat{e})+\Omega(\widehat{f})]} + \sum_{\widehat{e}\widehat{f}\in E_6} x^{[\Omega(\widehat{e})+\Omega(\widehat{f})]} + \sum_{\widehat{e}\widehat{f}\in E_7} x^{[\Omega(\widehat{e})+\Omega(\widehat{f})]}\\
&= |E_1|x^4 + |E_2|x^5 + |E_3|x^4 + |E_4|x^5 + |E_5|x^6 + |E_6|x^6 + |E_7|x^8\\
&= \left(2^{n+2}-6\right)x^4 + \left(2^{n+2}\right)x^5 + \left(2^{n+2}-6\right)x^4 + \left(9\cdot 2^{n+2}-28\right)x^5 + \left(2^{n+1}\right)x^6 + \left(3\cdot 2^n-10\right)x^6 + \left(2^n\right)x^8,\\
M_2(G,x) &= \sum_{\widehat{e}\widehat{f}\in E(G)} x^{[\Omega(\widehat{e})\times\Omega(\widehat{f})]},\\
M_2(NSC_5C_6[n],x) &= \sum_{\widehat{e}\widehat{f}\in E_1} x^{[\Omega(\widehat{e})\times\Omega(\widehat{f})]} + \sum_{\widehat{e}\widehat{f}\in E_2} x^{[\Omega(\widehat{e})\times\Omega(\widehat{f})]} + \sum_{\widehat{e}\widehat{f}\in E_3} x^{[\Omega(\widehat{e})\times\Omega(\widehat{f})]}\\
&\quad + \sum_{\widehat{e}\widehat{f}\in E_4} x^{[\Omega(\widehat{e})\times\Omega(\widehat{f})]} + \sum_{\widehat{e}\widehat{f}\in E_5} x^{[\Omega(\widehat{e})\times\Omega(\widehat{f})]} + \sum_{\widehat{e}\widehat{f}\in E_6} x^{[\Omega(\widehat{e})\times\Omega(\widehat{f})]} + \sum_{\widehat{e}\widehat{f}\in E_7} x^{[\Omega(\widehat{e})\times\Omega(\widehat{f})]}\\
&= |E_1|x^3 + |E_2|x^4 + |E_3|x^4 + |E_4|x^6 + |E_5|x^8 + |E_6|x^9 + |E_7|x^{16}\\
&= \left(2^{n+2}-6\right)x^3 + \left(2^{n+2}\right)x^4 + \left(2^{n+2}-6\right)x^4 + \left(9\cdot 2^{n+2}-28\right)x^6 + \left(2^{n+1}\right)^8 + \left(3\cdot 2^n-10\right)x^9 + \left(2^n\right)x^{16}.
\end{aligned}
\tag{12}
$$

2.2. Graphical Representation and Discussion of Results. In Figure 2(a), comparison of $M_1(NSC_5C_6[n],x)$ and $M_2(NSC_5C_6[n],x)$ polynomials of $NSC_5C_6[n]$ is given with $M_1(NSC_5C_6[n],x)$ in red and $M_2(NSC_5C_6[n],x)$ in blue. In Figure 2(b), we compare the indices $PM_1(NSC_5C_6[n])$ and $PM_2(NSC_5C_6[n])$ with $PM_1(NSC_5C_6[n])$ in red and $PM_2(NSC_5C_6[n])$ in blue. In Figure 2(c), we compare the indices $M_1(NSC_5C_6[n])$, $M_2(NSC_5C_6[n])$, and $HM(NSC_5C_6[n])$ with $M_1(NSC_5C_6[n])$ in red, $PM_2(NSC_5C_6[n])$ in blue, and $HM(NSC_5C_6[n])$ in black. It merits referencing that above-plotted charts demonstrate the reliance of each topological list on n. From these figures, one can envision that each topological file acts uniquely in contrast to other against parameters.

2.3. Methodology and Construction of Nanostar Dendrimers $NSD[n]$ Formulas. Consider the subatomic diagram $NSD[n]$, where n are ventures of development in this sort of nanostar dendrimer (see Figure 3). It is anything but difficult to ascertain that the quantity of vertices in $NSD[n]$ is $120\cdot 2^n-108$ and the quantity of edges is $140\cdot 2^n-127$, see likewise [24]. Moreover, there are three types of edges in $NSD[n]$ based on degrees of end vertices of each edge. To compute the above results, we define three partitions of edge set $E(NSD[n])$ and compute their cardinalities in the following way:

$$
\begin{aligned}
E_1(NSD[n]) &= \left\{\widehat{e}\widehat{f}\in E(NSD[n]) \mid \Omega(\widehat{e})=2, \Omega(\widehat{f})=2\right\},\\
\left|E_1(NSD[n])\right| &= 52\cdot 2^n-48,\\
E_2(NSD[n]) &= \left\{\widehat{e}\widehat{f}\in E(NSD[n]) \mid \Omega(\widehat{e})=2, \Omega(\widehat{f})=3\right\},\\
\left|E_2(NSD[n])\right| &= 48\cdot 2^n-44,\\
E_3(NSD[n]) &= \left\{\widehat{e}\widehat{f}\in E(NSD[n]) \mid \Omega(\widehat{e})=3, \Omega(\widehat{f})=3\right\},\\
\left|E_3(NSD[n])\right| &= 36\cdot 2^n-35.
\end{aligned}
\tag{13}
$$

Now using equations (1)–(7), we have the following results.

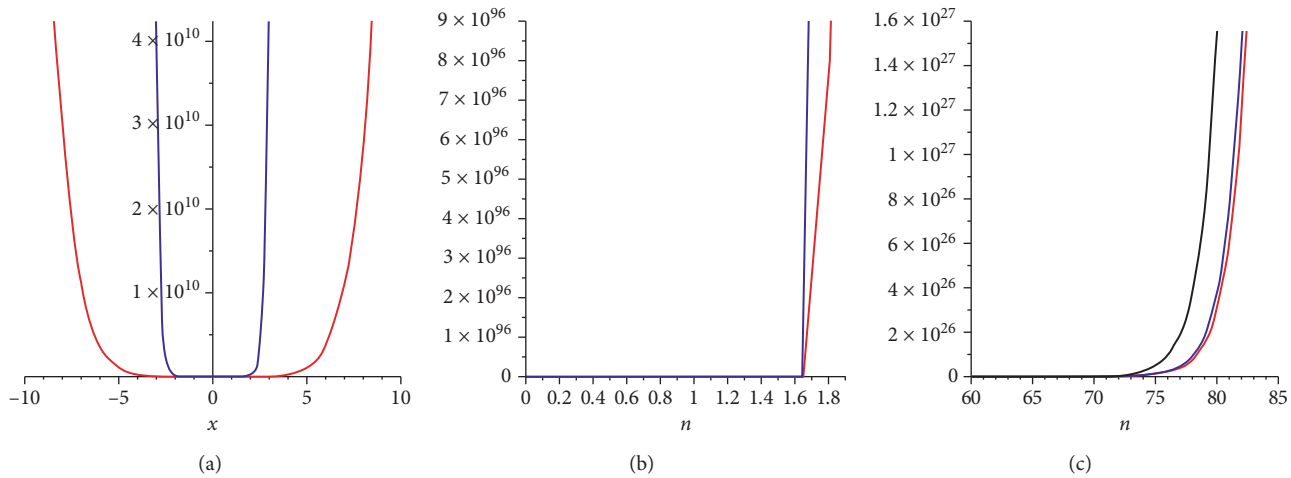

Figure 2: Comparison of topological indices and polynomials for $NSC_5C_6[n]$.

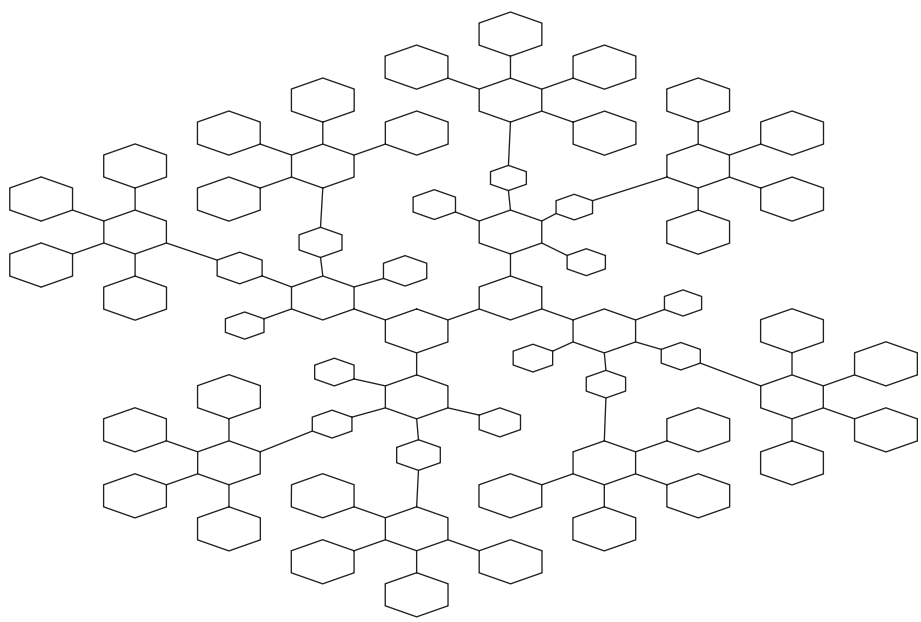

Figure 3: The nanostar dendrimer $NSD[n]$.

2.3.1. First and Second Zagreb Index

$$
\begin{aligned}
M_1(G) &= \sum_{\widehat{e}\widehat{f}\in E(G)} [\Omega(\widehat{e}) + \Omega(\widehat{f})],\\
M_1(NSD[n]) &= \sum_{\widehat{e}\widehat{f}\in E_1} [\Omega(\widehat{e}) + \Omega(\widehat{f})] + \sum_{\widehat{e}\widehat{f}\in E_2} [\Omega(\widehat{e}) + \Omega(\widehat{f})] + \sum_{\widehat{e}\widehat{f}\in E_3} [\Omega(\widehat{e}) + \Omega(\widehat{f})]\\
&= 4|E_1| + 5|E_2| + 6|E_3| = 4(52\cdot 2^n - 48) + 5(48\cdot 2^n - 44) + 6(36\cdot 2^n - 35),\\
M_2(G) &= \sum_{\widehat{e}\widehat{f}\in E(G)} [\Omega(\widehat{e}) + \Omega(\widehat{f})],\\
M_2(NSD[n]) &= \sum_{\widehat{e}\widehat{f}\in E_1} [\Omega(\widehat{e}) + \Omega(\widehat{f})] + \sum_{\widehat{e}\widehat{f}\in E_2} [\Omega(\widehat{e}) + \Omega(\widehat{f})] + \sum_{\widehat{e}\widehat{f}\in E_3} [\Omega(\widehat{e}) + \Omega(\widehat{f})]\\
&= 4|E_1| + 6|E_2| + 9|E_3| = 4(52\cdot 2^n - 48) + 6(48\cdot 2^n - 44) + 9(36\cdot 2^n - 35).
\end{aligned}
\tag{14}
$$

2.3.2. Hyper-Zagreb Index

$$\begin{aligned} HM(G) &= \sum_{\widehat{e}\widehat{f}\in E(G)} [\Omega(\widehat{e}) + \Omega(\widehat{f})]^2, \\ HM(NSD[n]) &= \sum_{\widehat{e}\widehat{f}\in E_1} [\Omega(\widehat{e}) + \Omega(\widehat{f})]^2 + \sum_{\widehat{e}\widehat{f}\in E_2} [\Omega(\widehat{e}) + \Omega(\widehat{f})]^2 + \sum_{\widehat{e}\widehat{f}\in E_3} [\Omega(\widehat{e}) + \Omega(\widehat{f})]^2 \\ &= 16|E_1| + 25|E_2| + 36|E_3| = 16(52\cdot 2^n - 48) + 25(48\cdot 2^n - 44) + 36(36\cdot 2^n - 35). \end{aligned} \tag{15}$$

2.3.3. First and Second Multiple Zagreb Index

$$\begin{aligned} PM_1(G) &= \prod_{\widehat{e}\widehat{f}\in E(G)} [\Omega(\widehat{e}) + \Omega(\widehat{f})], \\ PM_1(NSD[n]) &= \prod_{\widehat{e}\widehat{f}\in E_1} [\Omega(\widehat{e}) + \Omega(\widehat{f})] + \prod_{\widehat{e}\widehat{f}\in E_2} [\Omega(\widehat{e}) + \Omega(\widehat{f})] + \prod_{\widehat{e}\widehat{f}\in E_3} [\Omega(\widehat{e}) + \Omega(\widehat{f})] \\ &= 4^{|E_1|} \times 5^{|E_2|} \times 6^{|E_3|} = 4^{(52\cdot 2^n - 48)} \times 5^{(48\cdot 2^n - 44)} \times 6^{(36\cdot 2^n - 35)}, \\ PM_2(G) &= \prod_{\widehat{e}\widehat{f}\in E(G)} [\Omega(\widehat{e}) + \Omega(\widehat{f})], \\ PM_2(NSD[n]) &= \prod_{\widehat{e}\widehat{f}\in E_1} [\Omega(\widehat{e}) + \Omega(\widehat{f})] + \prod_{\widehat{e}\widehat{f}\in E_2} [\Omega(\widehat{e}) + \Omega(\widehat{f})] + \prod_{\widehat{e}\widehat{f}\in E_3} [\Omega(\widehat{e}) + \Omega(\widehat{f})] \\ &= 4^{|E_1|} \times 6^{|E_2|} \times 9^{|E_3|} = 4^{(52\cdot 2^n - 48)} \times 6^{(48\cdot 2^n - 44)} \times 9^{(36\cdot 2^n - 35)}. \end{aligned} \tag{16}$$

2.3.4. First and Second Zagreb Polynomial

$$\begin{aligned} M_1(G,x) &= \sum_{\widehat{e}\widehat{f}\in E(G)} x^{[\Omega(\widehat{e})+\Omega(\widehat{f})]}, \\ M_1(NSD[n],x) &= \sum_{\widehat{e}\widehat{f}\in E_1} x^{[\Omega(\widehat{e})+\Omega(\widehat{f})]} + \sum_{\widehat{e}\widehat{f}\in E_2} x^{[\Omega(\widehat{e})+\Omega(\widehat{f})]} + \sum_{\widehat{e}\widehat{f}\in E_3} x^{[\Omega(\widehat{e})+\Omega(\widehat{f})]} \\ &= |E_1|x^4 + |E_2|x^5 + |E_3|x^6 = (52\cdot 2^n - 48)x^4 + (48\cdot 2^n - 44)x^5 + (36\cdot 2^n - 35)x^6, \\ M_2(G,x) &= \sum_{\widehat{e}\widehat{f}\in E(G)} x^{[\Omega(\widehat{e})+\Omega(\widehat{f})]}, \\ M_2(NSD[n],x) &= \sum_{\widehat{e}\widehat{f}\in E_1} x^{[\Omega(\widehat{e})+\Omega(\widehat{f})]} + \sum_{\widehat{e}\widehat{f}\in E_2} x^{[\Omega(\widehat{e})+\Omega(\widehat{f})]} + \sum_{\widehat{e}\widehat{f}\in E_3} x^{[\Omega(\widehat{e})+\Omega(\widehat{f})]} \\ &= |E_1|x^4 + |E_2|x^6 + |E_3|x^9 = (52\cdot 2^n - 48)x^4 + (48\cdot 2^n - 44)x^6 + (36\cdot 2^n - 35)x^9. \end{aligned} \tag{17}$$

2.4. Graphical Representation and Discussion of Results. In Figure 4(a), comparison of $M_1(NSD[n],x)$ and $M_2(NSD[n],x)$ polynomials of $NSD[n]$ is given with $M_1(NSD[n],x)$ in red and $M_2(NSD[n],x)$ in blue. In Figure 4(b), we compare the indices $PM_1(NSD[n])$ and $PM_2(NSD[n])$ with $PM_1(NSD[n])$ in red and $PM_2(NSD[n])$ in blue. In Figure 4(c), we compare the indices $M_1(NSD[n])$, $M_2(NSD[n])$, and $HM(NSD[n])$ with $M_1(NSD[n])$ in red, $PM_2(NSD[n])$ in blue, and $HM(NSD[n])$ in black. These figures also give us some extreme values of the certain topological index. Moreover, these graphs give an insight view to control the values of topological indices with m and n.

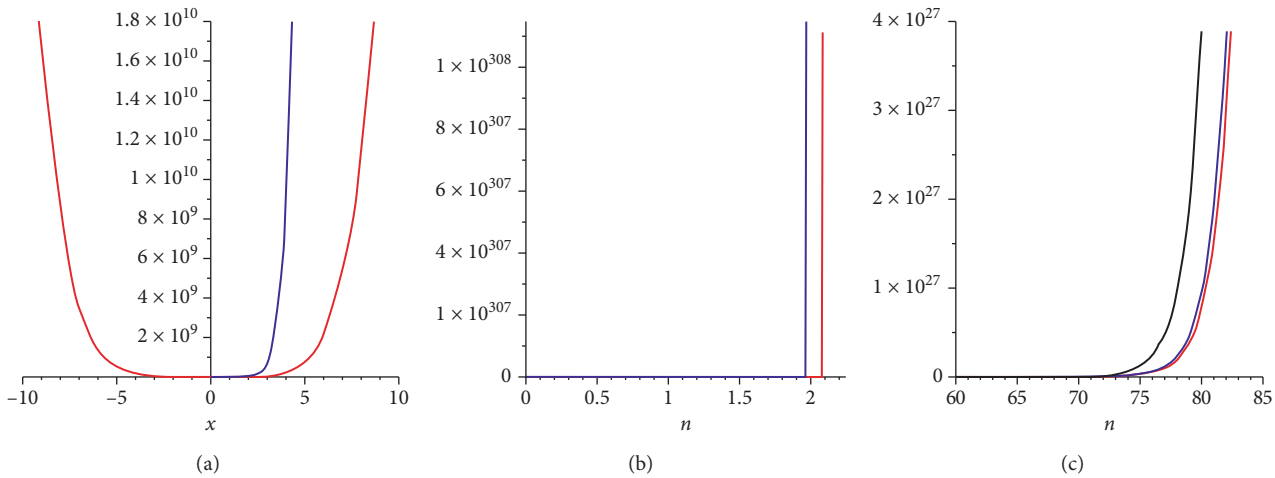

Figure 4: Comparison of topological indices and polynomials for $NSD[n]$.

3. Smart Polymer $SP[n]$

Keen polymers are characterized as the macromolecules that show a sensational physiochemical change because of little changes in their condition, for example, temperature, pH, light, attractive field, and ionic variables [25]. Shrewd polymers are additionally called as upgrades responsive or smart or naturally responsive frameworks. Shrewd polymers have different applications in biomedical field as conveyance frameworks like brilliant polymers with protein or nucleic corrosive conveyance to intracellular targets, for example, ribosome or core and in tissue designing [26, 27]. Polymeric micelles are one of the sorts of savvy polymers, which is accustomed to conveying hostile to malignant growth tranquilize, for instance, Dox-conjugated PEG-b-poly (aspartate) (PEG-PAsp) square copolymers [28]. In 2012, Shettya et al. [29] figured Randic record, first and second Zagreb lists, Geometric-math list, and atomic bond connectivity file of brilliant polymer.

In this area, we register hyper-Zagreb list, first various Zagreb file, second numerous Zagreb list, and Zagreb polynomials for the class of the shrewd polymer Dox-stacked micelle including PEG-PAsp square copolymer with artificially conjugated Dox $SP[n]$ (see Figure 5).

3.1. Methodology and Construction of Smart Polymer $SP[n]$ Formulas. Consider the atomic chart $SP[n]$, where n are ventures of development in this sort of polymers (see Figure 5). It is anything but difficult to ascertain that the quantity of vertices in $SP[n]$ is $49n+6$ and the quantity of edges is $54n+5$, see likewise [29]. Moreover, there are eight types of edges in $SP[n]$ based on degrees of end vertices of each edge. To compute the above results, we define eight partitions of edge set $E(SP[n])$ and compute their cardinalities in the following way:

$$\begin{aligned}
E_1(SP[n]) &= \{\widehat{e}\widehat{f} \in E(SP[n]) \mid \Omega(\widehat{e}) = 1, \Omega(\widehat{f}) = 2\},\\
|E_1(SP[n])| &= 2n+1,\\
E_2(SP[n]) &= \{\widehat{e}\widehat{f} \in E(SP[n]) \mid \Omega(\widehat{e}) = 1, \Omega(\widehat{f}) = 3\},\\
|E_2(SP[n])| &= 9n+1,\\
E_3(SP[n]) &= \{\widehat{e}\widehat{f} \in E(SP[n]) \mid \Omega(\widehat{e}) = 1, \Omega(\widehat{f}) = 4\},\\
|E_3(SP[n])| &= n,\\
E_4(SP[n]) &= \{\widehat{e}\widehat{f} \in E(SP[n]) \mid \Omega(\widehat{e}) = 2, \Omega(\widehat{f}) = 2\},\\
|E_4(SP[n])| &= 5n+4,\\
E_5(SP[n]) &= \{\widehat{e}\widehat{f} \in E(SP[n]) \mid \Omega(\widehat{e}) = 2, \Omega(\widehat{f}) = 3\},\\
|E_5(SP[n])| &= 18n-1,\\
E_6(SP[n]) &= \{\widehat{e}\widehat{f} \in E(SP[n]) \mid \Omega(\widehat{e}) = 2, \Omega(\widehat{f}) = 4\},\\
|E_6(SP[n])| &= 2n,\\
E_7(SP[n]) &= \{\widehat{e}\widehat{f} \in E(SP[n]) \mid \Omega(\widehat{e}) = 3, \Omega(\widehat{f}) = 3\},\\
|E_7(SP[n])| &= 16n,\\
E_8(SP[n]) &= \{\widehat{e}\widehat{f} \in E(SP[n]) \mid \Omega(\widehat{e}) = 3, \Omega(\widehat{f}) = 4\},\\
|E_8(SP[n])| &= n.
\end{aligned} \tag{18}$$

Now using equations (1)–(7), we have the following results.

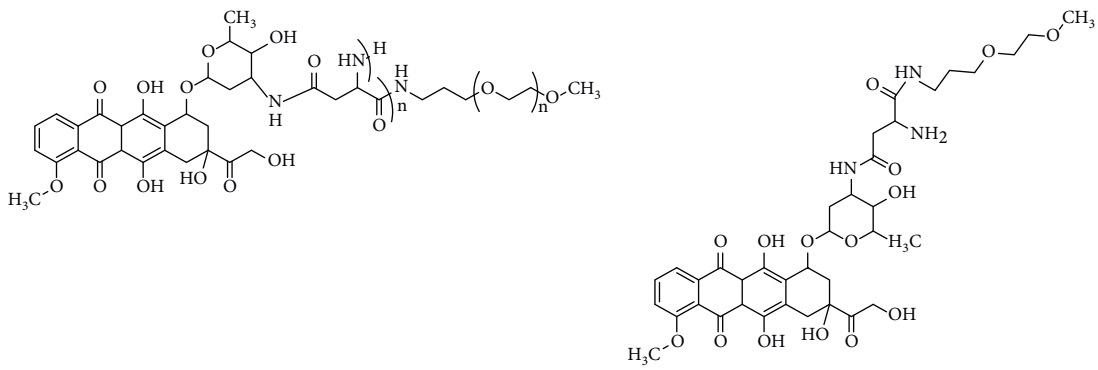

(a) (b)

Figure 5: (a) The smart polymer $SP[n]$. (b) The smart polymer $SP[1]$.

3.1.1. Hyper-Zagreb Index

$$
\begin{aligned}
HM(G) &= \sum_{\widehat{e}\widehat{f}\in E(G)} [\Omega(\widehat{e})+\Omega(\widehat{f})]^2,\\
HM(SP[n]) &= \sum_{\widehat{e}\widehat{f}\in E_1} [\Omega(\widehat{e})+\Omega(\widehat{f})]^2 + \sum_{\widehat{e}\widehat{f}\in E_2} [\Omega(\widehat{e})+\Omega(\widehat{f})]^2 + \sum_{\widehat{e}\widehat{f}\in E_3} [\Omega(\widehat{e})+\Omega(\widehat{f})]^2 + \sum_{\widehat{e}\widehat{f}\in E_4} [\Omega(\widehat{e})+\Omega(\widehat{f})]^2\\
&\quad + \sum_{\widehat{e}\widehat{f}\in E_5} [\Omega(\widehat{e})+\Omega(\widehat{f})]^2 + \sum_{\widehat{e}\widehat{f}\in E_6} [\Omega(\widehat{e})+\Omega(\widehat{f})]^2 + \sum_{\widehat{e}\widehat{f}\in E_7} [\Omega(\widehat{e})+\Omega(\widehat{f})]^2 + \sum_{\widehat{e}\widehat{f}\in E_8} [\Omega(\widehat{e})+\Omega(\widehat{f})]^2\\
&= 9|E_1| + 16|E_2| + 25|E_3| + 16|E_4| + 25|E_5| + 36|E_6| + 36|E_7| + 49|E_8|\\
&= 9(2n+1) + 16(9n+1) + 25n + 16(5n+4) + 25(18n-1) + 72n + 36(16n) + 49n.
\end{aligned}
\tag{19}
$$

3.1.2. First and Second Multiple Zagreb Index

$$
\begin{aligned}
PM_1(G) &= \prod_{\widehat{e}\widehat{f}\in E(G)} [\Omega(\widehat{e})+\Omega(\widehat{f})],\\
PM_1(SP[n]) &= \prod_{\widehat{e}\widehat{f}\in E_1} [\Omega(\widehat{e})+\Omega(\widehat{f})] \times \prod_{\widehat{e}\widehat{f}\in E_2} [\Omega(\widehat{e})+\Omega(\widehat{f})] \times \prod_{\widehat{e}\widehat{f}\in E_3} [\Omega(\widehat{e})+\Omega(\widehat{f})] \times \prod_{\widehat{e}\widehat{f}\in E_4} [\Omega(\widehat{e})+\Omega(\widehat{f})]\\
&\quad \times \prod_{\widehat{e}\widehat{f}\in E_5} [\Omega(\widehat{e})+\Omega(\widehat{f})] \times \prod_{\widehat{e}\widehat{f}\in E_6} [\Omega(\widehat{e})+\Omega(\widehat{f})] \times \prod_{\widehat{e}\widehat{f}\in E_7} [\Omega(\widehat{e})+\Omega(\widehat{f})] \times \prod_{\widehat{e}\widehat{f}\in E_8} [\Omega(\widehat{e})+\Omega(\widehat{f})]\\
&= 3^{|E_1|} \times 4^{|E_2|} \times 5^{|E_3|} \times 4^{|E_4|} \times 5^{|E_5|} \times 6^{|E_6|} \times 6^{|E_7|} \times 7^{|E_8|}\\
&= 3^{(2n+1)} \times 4^{(9n+1)} \times 5^{n} \times 4^{(5n+4)} \times 5^{(18n-1)} \times 6^{2n} \times 6^{16n} \times 7^{n},\\
PM_2(G) &= \prod_{\widehat{e}\widehat{f}\in E(G)} [\Omega(\widehat{e})\times\Omega(\widehat{f})],\\
PM_2(SP[n]) &= \prod_{\widehat{e}\widehat{f}\in E_1} [\Omega(\widehat{e})\times\Omega(\widehat{f})] \times \prod_{\widehat{e}\widehat{f}\in E_2} [\Omega(\widehat{e})\times\Omega(\widehat{f})] \times \prod_{\widehat{e}\widehat{f}\in E_3} [\Omega(\widehat{e})\times\Omega(\widehat{f})] \times \prod_{\widehat{e}\widehat{f}\in E_4} [\Omega(\widehat{e})\times\Omega(\widehat{f})]\\
&\quad \times \prod_{\widehat{e}\widehat{f}\in E_5} [\Omega(\widehat{e})\times\Omega(\widehat{f})] \times \prod_{\widehat{e}\widehat{f}\in E_6} [\Omega(\widehat{e})\times\Omega(\widehat{f})] \times \prod_{\widehat{e}\widehat{f}\in E_7} [\Omega(\widehat{e})\times\Omega(\widehat{f})] \times \prod_{\widehat{e}\widehat{f}\in E_8} [\Omega(\widehat{e})\times\Omega(\widehat{f})]\\
&= 2^{|E_1|} \times 3^{|E_2|} \times 4^{|E_3|} \times 4^{|E_4|} \times 6^{|E_5|} \times 8^{|E_6|} \times 9^{|E_7|} \times 12^{|E_8|}\\
&= 2^{(2n+1)} \times 3^{(9n+1)} \times 4^{n} \times 4^{(5n+4)} \times 6^{(18n-1)} \times 4^{2n} \times 9^{16n} \times 12^{n}.
\end{aligned}
\tag{20}
$$

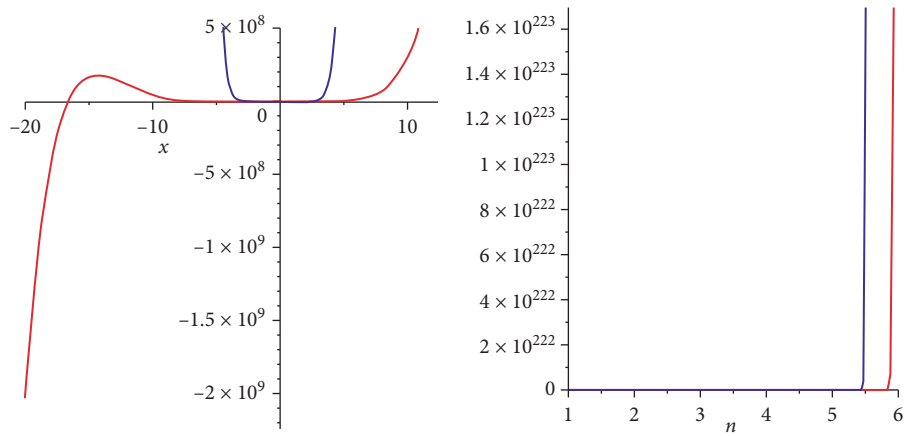

(a) (b)

Figure 6: Comparison of topological indices and polynomials for $SP[n]$.

3.1.3. First and Second Zagreb Polynomial

$$
\begin{aligned}
M_1(G,x) &= \sum_{\widehat{e}\widehat{f}\in E(G)} x^{[\Omega(\widehat{e})+\Omega(\widehat{f})]},\\
M_1(SP[n],x) &= \sum_{\widehat{e}\widehat{f}\in E_1} x^{[\Omega(\widehat{e})+\Omega(\widehat{f})]} + \sum_{\widehat{e}\widehat{f}\in E_2} x^{[\Omega(\widehat{e})+\Omega(\widehat{f})]} + \sum_{\widehat{e}\widehat{f}\in E_3} x^{[\Omega(\widehat{e})+\Omega(\widehat{f})]} + \sum_{\widehat{e}\widehat{f}\in E_4} x^{[\Omega(\widehat{e})+\Omega(\widehat{f})]}\\
&\quad + \sum_{\widehat{e}\widehat{f}\in E_5} x^{[\Omega(\widehat{e})+\Omega(\widehat{f})]} + \sum_{\widehat{e}\widehat{f}\in E_6} x^{[\Omega(\widehat{e})+\Omega(\widehat{f})]} + \sum_{\widehat{e}\widehat{f}\in E_7} x^{[\Omega(\widehat{e})+\Omega(\widehat{f})]} + \sum_{\widehat{e}\widehat{f}\in E_8} x^{[\Omega(\widehat{e})+\Omega(\widehat{f})]}\\
&= (2n+1)x^3 + (9n+1)x^4 + nx^5 + (5n+4)x^5 + (18n-1)x^5 + 2nx^6 + 16nx^6 + nx^7,\\
M_2(G,x) &= \sum_{\widehat{e}\widehat{f}\in E(G)} x^{[\Omega(\widehat{e})\times\Omega(\widehat{f})]},\\
M_2(SP[n],x) &= \sum_{\widehat{e}\widehat{f}\in E_1} x^{[\Omega(\widehat{e})\times\Omega(\widehat{f})]} + \sum_{\widehat{e}\widehat{f}\in E_2} x^{[\Omega(\widehat{e})\times\Omega(\widehat{f})]} + \sum_{\widehat{e}\widehat{f}\in E_3} x^{[\Omega(\widehat{e})\times\Omega(\widehat{f})]} + \sum_{\widehat{e}\widehat{f}\in E_4} x^{[\Omega(\widehat{e})\times\Omega(\widehat{f})]}\\
&\quad + \sum_{\widehat{e}\widehat{f}\in E_5} x^{[\Omega(\widehat{e})\times\Omega(\widehat{f})]} + \sum_{\widehat{e}\widehat{f}\in E_6} x^{[\Omega(\widehat{e})\times\Omega(\widehat{f})]} + \sum_{\widehat{e}\widehat{f}\in E_7} x^{[\Omega(\widehat{e})\times\Omega(\widehat{f})]} + \sum_{\widehat{e}\widehat{f}\in E_8} x^{[\Omega(\widehat{e})\times\Omega(\widehat{f})]}\\
&= |E_1|x^2 + |E_2|x^3 + |E_3|x^4 + |E_4|x^4 + |E_5|x^6 + |E_6|x^8 + |E_7|x^9 + |E_8|x^{12}\\
&= (2n+1)x^2 + (9n+1)x^3 + nx^4 + (5n+4)x^4 + (18n-1)x^6 + 2nx^8 + 16nx^9 + nx^{12}.
\end{aligned}
\tag{21}
$$

3.2. Graphical Representation and Discussion of Results. In Figure 6(a), comparison of $M_1(SP[n],x)$ and $M_2(SP[n],x)$ polynomials of $SP[n]$ is given with $M_1(SP[n],x)$ in red and $M_2(SP[n],x)$ in blue. In Figure 6(b), we compare the indices $PM_1(SP[n])$ and $PM_2(SP[n])$ with $PM_1(SP[n])$ in red and $PM_2(SP[n])$ in blue.

4. Comparison of Topological Indices and Polynomials

The graphical representations of topological indices $M_1(G)$, $M_2(G)$, and $HM(G)$ for G equivalent $NSC_5C_6[n]$, $NSD[n]$, and $SP[n]$ are depicted in Figures 2(c), 4(c), and 6(b) for certain values of n. For a better view to the reader, we have

joined all the terms of the sequence points in the graphs by curves, so one can see that the graphs are increasing. By varying the values of n, the topological indices behave differently.

The graphical representations of topological indices $PM_1(G)$ and $PM_2(G)$ for G equivalent $NSC_5C_6[n]$ and $NSD[n]$ are depicted in Figures 2(b) and 4(b) for certain values of n. For a better view to the reader, we have joined all the terms of the sequence points in the graphs by curves, so one can see that the graphs are increasing. One can see that, by varying the values of n, the topological indices behave differently.

The comparisons of Zagreb polynomials $M_1(G,x)$ and $M_2(G,x)$ for G equivalent $NSC_5C_6[n]$, $NSD[n]$, and $SP[n]$ are depicted in Figures 2(a), 4(a), and 6(a) for certain values of x and for fix $n = 10$. We can see from the graphs in Figure 2 that $M_1(G,x)$ and $M_2(G,x)$ are decreasing and increasing on $(-\infty, 0]$ and $[0, \infty)$, respectively. By varying the values of x, the polynomials behave differently. In Figure 4, the $M_1(G,x)$ and $M_2(G,x)$ behave differently and $M_1(NSD[n],x)$ is decreasing and increasing on $(-\infty, 0]$ and $[0, \infty)$, respectively, whereas $M_2(NSD[n],x)$ is increasing on $(-\infty, \infty)$. In Figure 6, the $M_1(G,x)$ and $M_2(G,x)$ behave differently and $M_1(SP[n],x)$ is decreasing and increasing on $[-14, 0]$ and $(-\infty, 14] \cup [0, \infty)$, respectively, whereas $M_2(SP[n],x)$ is decreasing and increasing on $(-\infty, 0]$ and $[0, \infty)$.

5. Conclusion

In this paper, we have managed nanostar dendrimers and star polymer and concentrated their topological records. We decide first and second Zagreb files, hyper-Zagreb record, first different Zagreb file, second numerous Zagreb file, and Zagreb polynomials for nanostar dendrimer and smart polymer. Toward the end, we give a graphical portrayal of all records and polynomials. In future, we are intrigued to register topological records for some new concoction diagrams.

Data Availability

The data used to support the findings of this study are available from the corresponding author upon request.

Conflicts of Interest

The authors declare that there are no conflicts of interest regarding the publication of this paper.

Acknowledgments

This research was supported by the Higher Education Commission of Pakistan under NRPU project "Properties of Ranking Ideals" via Grant no. 20–3665/R&D/HEC/14/699.

References

[1] M. V. Diudea and G. Katona, "Molecular topology of dendrimers," in *Advances in Dendritic Macromolecules*, G. A. Newkome, Ed., vol. 4, pp. 135–201, 1999.

[2] H. Wiener, "Structural determination of paraffin boiling points," *Journal of the American Chemical Society*, vol. 69, no. 1, pp. 17–20, 1947.

[3] A. A. Dobrynin, R. Entringer, and I. Gutman, "Wiener index of trees: theory and applications," *Acta Applicandae Mathematicae*, vol. 66, no. 3, pp. 211–249, 2001.

[4] I. Gutman and O. E. Polansky, *Mathematical Concepts in Organic Chemistry*, Springer-Verlag, Berlin, Germany, 1986.

[5] I. Gutman and N. Trinajstić, "Graph theory and molecular orbitals. Total φ-electron energy of alternant hydrocarbons," *Chemical Physics Letters*, vol. 17, no. 4, pp. 535–538, 1972.

[6] G. H. Shirdel, H. RezaPour, and A. M. Sayadi, "The hyper-zagreb index of graph operations," *Iranian Journal of Mathematical Chemistry*, vol. 4, no. 2, pp. 213–220, 2013.

[7] M. Ghorbani and N. Azimi, "Note on multiple Zagreb indices," *Iranian Journal of Mathematical Chemistry*, vol. 3, no. 2, pp. 137–143, 2012.

[8] I. Gutman and K. C. Das, "Some properties of the second Zagreb index," *MATCH Communications in Mathematical and in Computer*, vol. 50, pp. 103–112, 2004.

[9] M. Bača, J. Horváthová, M. Mokrišová, and A. Suhányiová, "On topological indices of fullerenes," *Applied Mathematics and Computation*, vol. 251, pp. 154–161, 2015.

[10] M. Bača, J. Horváthová, M. Mokrišová, A. Semanicov-Fenovckov, and A. Suhányiová, "On topological indices of a carbon nanotube network," *Canadian Journal of Chemistry*, vol. 93, no. 10, pp. 1157–1160, 2015.

[11] J.-B. Liu, C. Wang, S. Wang, and B. Wei, "Zagreb indices and multiplicative Zagreb indices of eulerian graphs," *Bulletin of the Malaysian Mathematical Sciences Society*, vol. 42, no. 1, pp. 67–78, 2019.

[12] J.-B. Liu, X.-F. Pan, F.-T. Hu, and F.-F. Hu, "Asymptotic Laplacian-energy-like invariant of lattices," *Applied Mathematics and Computation*, vol. 253, pp. 205–214, 2015.

[13] J.-B. Liu and X.-F. Pan, "Minimizing Kirchhoff index among graphs with a given vertex bipartiteness," *Applied Mathematics and Computation*, vol. 291, pp. 84–88, 2016.

[14] J. B. Liu, J. Zhao, and Z. Zhu, "On the number of spanning trees and normalized Laplacian of linear octagonal-quadrilateral networks," *International Journal of Quantum Chemistry*, vol. 119, no. 17, Article ID e25971, 2019.

[15] W. Gao, M. K. Siddiqui, M. Imran, M. K. Jamil, and M. R. Farahani, "Forgotten topological index of chemical structure in drugs," *Saudi Pharmaceutical Journal*, vol. 24, no. 3, pp. 258–264, 2016.

[16] W. Gao and M. K. Siddiqui, "Molecular descriptors of nanotube, oxide, silicate, and triangulene networks," *Journal of Chemistry*, vol. 2017, Article ID 6540754, 10 pages, 2017.

[17] W. Gharibi, A. Ahmad, and M. K. Siddiqui, "On Zagreb indices, Zagreb polynomials of nanocone and nanotubes," *Journal of Computational and Theoretical Nanoscience*, vol. 13, no. 8, pp. 5086–5092, 2016.

[18] I. Gutman, "Degree-based topological indices," *Croatica Chemica Acta*, vol. 86, no. 4, pp. 351–361, 2013.

[19] M. Imran, S. Hayat, and M. Y. H. Mailk, "On topological indices of certain interconnection networks," *Applied Mathematics and Computation*, vol. 244, pp. 936–951, 2014.

[20] M. Imran, M. Siddiqui, M. Naeem, and M. Iqbal, "On topological properties of symmetric chemical structures," *Symmetry*, vol. 10, no. 5, p. 173, 2018.

[21] M. K. Siddiqui, M. Imran, and A. Ahmad, "On Zagreb indices, Zagreb polynomials of some nanostar dendrimers," *Applied Mathematics and Computation*, vol. 280, pp. 132–139, 2016.

[22] M. K. Siddiqui and W. Gharibi, "On Zagreb indices, Zagreb polynomials of mesh derived networks," *Journal of Computational and Theoretical Nanoscience*, vol. 13, no. 11, pp. 8683–8688, 2016.

[23] M. K. Siddiqui, M. Naeem, N. A. Rahman, and M. Imran, "Computing topological indicesof certain networks," *Journal Optoelectronics and Advanced Materials*, vol. 18, no. 9, pp. 884–892, 2016.

[24] M. Rostamia, M. Habanianb, and H. Moghanianc, "Some topological indices for theoretical study of two types of Nanostar Denderimers," *Digest Journal of Nanomaterials and Biostructures*, vol. 7, no. 1, pp. 247–252, 2012.

[25] J. Singh and K. A. Tahami, "Smart polymer based delivery systems for peptides and proteins," *Recent Patents on Drug Delivery and Formulation*, vol. 1, no. 1, pp. 65–71, 2007.

[26] R. Freitag, *Synthetic Polymers for Biotechnology and Medicine, Biotechnology Intelligence Unit 4*, CRC Press, Boca Raton, FL, USA, 2003.

[27] S. S. Kulkarni and N. H. Aloorkar, "Smart polymers in drug delivery: an overview," *Journal of Pharmacy Research*, vol. 3, no. 1, pp. 100–108, 2010.

[28] K. Osada, R. J. Christie, and K. Kataoka, "Polymeric micelles from poly(ethylene glycol)-poly(amino acid) block copolymer for drug and gene delivery," *Journal of The Royal Society Interface*, vol. 6, pp. 325–339, 2009.

[29] B. S. Shettya, V. Lokeshab, P. S. Ranjinic, and K. C. Dasd, "Computing some topological indices of smart polymer," *Digest Journal of Nanomaterials and Biostructures*, vol. 7, no. 3, pp. 1097–1102, 2012.

Hindawi
Journal of Chemistry
Volume 2020, Article ID 4565094, 11 pages
https://doi.org/10.1155/2020/4565094

Research Article

Research on the Mechanism of Cold Chain Logistics Subsidy

Nai-Ru Xu [1] **and Zheng-Qun Cai** [2]

[1] *School of Business, Anhui Xinhua University, Hefei 230088, China*
[2] *School of Foreign Studies, Anhui Jianzhu University, Hefei 230601, China*

Correspondence should be addressed to Zheng-Qun Cai; caizhengqun1983@163.com

Received 31 October 2019; Accepted 12 March 2020; Published 19 April 2020

Guest Editor: Shaohui Wang

Considering the coexistence of cold chain agro-products and ordinary agro-products in the market, the research object is the cold chain logistics subsidy. It is designed that a supply chain system consisting of duopoly upstream agro-products suppliers and a downstream agro-products retailer for research. The mechanism of cold chain logistics subsidy is studied by analyzing the influence of cold chain subsidy on pricing behavior and cold chain decision-making of cold chain agro-products and ordinary agro-products. Based on the decentralized decision-making model without government subsidy, a differential pricing model for cold chain agro-products and ordinary agro-products with government subsidy is established in order to reduce the cost of cold chain agro-products. The optimal pricing strategy of two agro-products suppliers and their downstream retailer can be obtained by solving this problem. The research finds that differential pricing caused by government subsidy can achieve profit Pareto improvement of suppliers, retailer, and supply chain system of cold chain agro-products, but cannot achieve the optimal profit of the whole supply chain. Therefore, in view of the loss of supply chain efficiency caused by decentralized decision-making, the Shapley value method is used to make coordination, and the contract coordination mechanism is designed. Finally, the sensitivity of parameters is analyzed by a numerical example.

1. Introduction

Cold chain logistics generally refers to a systematic engineering in which the refrigerated and frozen food is always in the specified low-temperature environment in the segments of production, transportation, storage, and sale, as well as consumption, in order to ensure food quality and reduce the loss. With China's economic and social development and the continuous improvement of people's living level, consumers are increasingly demanding high-quality fresh products and the demand for cold chain logistics is becoming more and more vigorous.

However, due to its late start and weak foundation, China's cold chain logistics industry still has some problems, such as incomplete standard system, relatively backward infrastructure, low specialization level, and insufficient effective supervision. The development of cold chain logistics lags behind that of developed countries [1, 2]. In order to promote the development of cold chain logistics in China, the government should present supportive policies, such as cold chain logistics subsidy, in order to induce enterprises to increase investment in cold chain logistics, and raise the proportion of cold chain processing of agricultural products.

2. Research Status at Home and Abroad

With regard to subsidy for cold chain logistics and related research, scholars at home and abroad have made some achievements in this field. Considering the bankruptcy risk in the financing of agricultural enterprises, Huang et al. construct a three-stage Stackelberg game model of government, retailers, and agricultural enterprises on the base of the existing government subsidy mechanism. They propose the government subsidy mechanism to maximize social welfare, and analyze the influence of government subsidy on the interests of all participants in supply chain [3]. Xiong et al. construct the profit models of two supply chain organizational modes, apply the freshness loss compensation

plan of agricultural products to the elastic quantity contract to form a relationship contract, analyze the influence of cold chain facility subsidy mode on the stability of relationship contract in different organizational modes, and propose that choosing the appropriate cold chain facility subsidy mode can improve the freshness level of agricultural products and the farmers' profit, so as to enhance the stability of the supply chain relationship contract of fresh agricultural products [4]. Li et al. build an evolutionary game model of logistics resource input between suppliers and producers under government supervision. When the input and output of logistics resources of suppliers and producers are constantly changing, a variety of evolutionary stabilization strategies can be obtained. If the free-rider behavior obtains great benefits from the other participants' resource input, it will greatly damp the enthusiasm for cold chain logistics investment of suppliers and producers. It is found that when the punishment or subsidy of the government exceeds the threshold level, the cold chain logistics investment will become the evolutionary stabilization strategy of suppliers and producers [5]. Mancur analyzes the positive external effect of cold chain logistics investment and propose a punishment and subsidy mechanism for the free-rider behavior of the participants in the cold chain [6]. Zhu and Dou build a three-stage game model in green supply chain management with considering product greenness degree and government subsidy. Through the simulation analysis of the three parameters including the subsidy coefficient per unit product, the greenness degree of the final manufacturer's products, and the price of the final manufacturer's products, it provides a reference for the decision-making of the government and the final manufacturer in the green supply chain management. This study adds consumer preference for environmental protection to the model and provides a reference for analyzing the impact of cold chain logistics subsidy mechanism on consumers [7].

The above research focuses on the influence mechanism of cold chain logistics subsidy on the supply chain, including three aspects. Firstly, through the construction of a subsidy mechanism, we can coordinate the interests of participants in the supply chain, so as to maximize social welfare. Secondly, through the design of the subsidy mechanism, we can improve the freshness degree of fresh products and the stability of supply chain relationship. Thirdly, through the design of the subsidy mechanism, members of the fresh product supply chain should be encouraged to invest in the cold chain, including suppliers and producers, so as to avoid free-rider behavior. These studies provide references for the study of the subsidy mechanism of cold chain logistics, but do not consider the preference of consumers.

This paper analyzes the cold chain subsidy mechanism affecting the differential pricing behavior of cold chain agro-products and ordinary agro-products and studies the influence of cold chain subsidy on the pricing of upstream and downstream members in the supply chain from the perspective of supply chain coordination under the background of coexistence of two kinds of products in the market. This study has reference value for two types of enterprises to formulate their own pricing strategies in practice. On this basis, the reasonable scope of government subsidy is given through calculation, which can provide some theoretical references for the formulation of government subsidy policy.

3. Problem Description and Model Construction

3.1. Problem Description. Cold chain agro-products refer to the products which are processed through the cold chain measures adopted by agro-products suppliers in the process of production, transportation, storage, and sale, such as refrigeration and freezing, so as to preserve the freshness of agro-products and improve the quality of agro-products. Ordinary agro-products need operators of agro-products to take the normal temperature measures to preserve the freshness and quality of agro-products in the operation process. Cold chain agro-products suppliers and ordinary agro-products suppliers will not take cold chain measures at the same time due to differences in operating costs and business philosophy. The coexistence of cold chain agro-products and ordinary agro-products is a common phenomenon in the market. Cold chain agro-products suppliers hope to gain the product quality competitiveness in the agro-products market through cold chain measures, win the recognition of the public and consumers, and establish a good corporate image. Ordinary agro-products suppliers hope to operate at normal temperatures, avoid high operation costs, and gain competitive advantage through price advantage.

It is presented a supply chain system consisting of two agro-products suppliers including a cold chain agro-products supplier, an ordinary agro-products supplier, and a retailer. Two agro-products suppliers produce the same variety of agricultural products and sell them through the same retailer. In order to encourage the agro-products cold chain operation, the government will subsidize the suppliers of cold chain agro-products. Firstly, this paper studies the cold chain and price decision-making of the two agro-products suppliers and the price decision-making of the agro-products retailer when there is no government subsidy. Then, it studies the influence of government's cold chain subsidy on cold chain and price decision-making of supply chain members. Finally, it analyzes the coordination strategy of the supply chain under centralized decision-making condition.

3.2. Symbol Explanation. The symbols and explanations are described in the following text:

v_C: wholesale price of cold chain agro-products. It is a decision variable of the cold chain agro-products suppliers. The agro-products suppliers include various organizations engaged in agricultural production activities such as agricultural companies and farmers.

v_O: wholesale price of ordinary agro-products. It is a decision variable of the ordinary agro-products supplier.

P_C: retail price of cold chain agro-products. It is a decision variable of the agro-products retailer.

P_O: retail price of ordinary agro-products. It is a decision variable of agro-products retailers.

α: freshness-keeping rate of cold chain agro-products. It is a decision variable of cold chain agro-products suppliers.

β: subsidy coefficient of the cold chain agro-products decided by the government.

γ: freshness-keeping difficulty coefficient of the cold chain agro-products suppliers.

3.3. Model Hypothesis

(1) Assuming that cold chain agro-products and ordinary agro-products can be substituted for each other in basic functions. Both have the same demand function $d(p)$, and $P_C > P_O$, $d(p)$ satisfies first-order linear function, which is $q = d(p) = a - b(p)$, a and b are constants, $a, b > 0$, a represents market capacity, and b represents the sensitivity of consumers to price. Consumers check the freshness degree of agricultural products through packaging labels and on-site inspection. Consumers with sufficient payment ability and high freshness degree requirement will not buy ordinary agro-products. There are two types of consumers in the market. One is the consumer who buys cold chain agro-products, and the other is the consumer who buys ordinary agro-products.

Market demand of cold chain agro-products,

$$q_C = d_C(p) = a - bp_C. \tag{1}$$

Market demand of ordinary agro-products,

$$q_O = d_O(p) = b(p_C - p_O). \tag{2}$$

When the prices of cold chain agro-products and ordinary agro-products are equal, the demand for ordinary agro-products is 0, and ordinary agro-products will withdraw from the market. According to this hypothesis, the demand for cold chain agro-products and ordinary agro-products is shown in Figure 1.

(2) The suppliers of cold chain agro-products take measures such as cold chain transportation, cold chain storage, and sale to improve the freshness-keeping rate of agro-products α and pay the corresponding cost $g(\alpha)$, such as the cost of using refrigerated trucks, refrigerated cabinets, and temperature or humidity control equipment. This cost increases with the increase of freshness-keeping rate. It means $g'(\alpha) > 0$. The increased speed is accelerating; it means $g''(\alpha) > 0$. This characteristic is similar to which of R&D cost. Therefore, this paper assumes a quadratic relationship between freshness-keeping cost and freshness-keeping rate, and $g(\alpha) = (1/2)\gamma\alpha^2$.

(3) In order to improve the freshness degree of agro-products, the government encourages the suppliers of agro-products to carry out cold chain transportation. In order to subsidize the suppliers of cold chain agro-products directly, the amount of subsidy is related to the freshness-keeping rate of agro-products. Assume $\beta = \lambda\alpha$ is the subsidy coefficient of per agro-product decided by the government. λ is the adjustment factor of the subsidy coefficient.

(4) Assuming that the retailer can buy cold chain agro-products and ordinary agro-products only through these two suppliers, the suppliers are in the leading position in the supply chain, and the two suppliers have the same status. For the same reason [8, 9], it is assumed that the marginal production cost of the agro-products is 0 for convenience of analysis.

4. Differential Pricing Model Analysis

4.1. Decentralized Decision-Making without Government Subsidy. In the supply chain of decentralized decision-making, the retailer and two suppliers make decisions in the view of their respective profit maximization. π_C, π_O, π_R, and π_S, respectively, represent the profit of cold chain agro-products supplier, ordinary agro-products supplier, the retailer, and supply chain. The superscript $*$ denotes optimum. Therefore, the profit function without government subsidy is as follows:

$$\pi_C = v_C(a - bp_C) - \frac{1}{2}\gamma\alpha^2, \tag{3}$$

$$\pi_O = v_O b(p_C - p_O), \tag{4}$$

$$\pi_R = (p_C - v_C)(a - bp_C) + b(p_O - v_O)(p_C - p_O). \tag{5}$$

In the model without government subsidy, the profit function of cold chain agro-products supplier consists of two parts, the wholesale price from the retailer and cold chain freshness-keeping cost. Stackelberg dynamic game of simultaneous selection takes place between two suppliers and the retailer in the supplier-led supply chain. In the first stage, the cold chain agro-products supplier decides the wholesale price v_C and freshness-keeping rate α of cold chain agro-products. Ordinary agro-products supplier decides wholesale price of ordinary agro-products v_O. In the second stage, in the condition of given (v_C, v_O, α), the retailer chooses the retail prices (P_C, P_O) of two products, and backward induction is adopted to find the solution of subgame perfect Nash equilibrium.

Superscript N means without government subsidy. Given the decision (v_C, v_O, α) of the two suppliers, the optimization problem of the retailer is given by

$$\begin{aligned}&\max_{p_C, p_O} \pi_R^N\left(p_C, p_O \mid v_C, v_O, \alpha\right)\\&\quad = (p_C - v_C)(a - bp_C) + b(p_O - v_O)(p_C - p_O).\end{aligned} \tag{6}$$

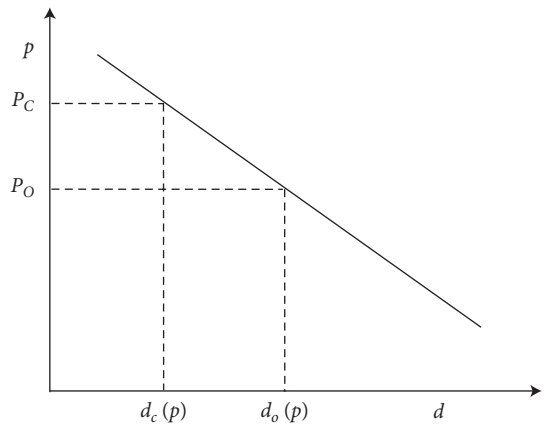

Figure 1: Market demand in differential pricing of cold chain agro-products.

Obviously, $\pi_R^N(p_C, p_O)$ is a joint concave function on (p_C, p_O). According to the first-order optimal condition, the retailer's response function can be obtained:

$$P_C = \frac{2a + 2bv_C - bv_O}{3b},$$
$$P_O = \frac{a + bv_C + bv_O}{3b}. \tag{7}$$

The response function indicates that the retail price of cold chain agro-products decreases with the increase of the wholesale price of ordinary agro-products, and this is due to the price competition effect. According to the hypothesis (1), the retail price of cold chain agro-products is higher than that of ordinary agro-products. The retailer's response function is substituted into formulae (1) and (2), and we can get

$$q_C = \frac{a - 2bv_C + bv_O}{3},$$
$$q_O = \frac{a + bv_C - 2bv_O}{3b}. \tag{8}$$

Under the price competition effect, the sale volume of cold chain agro-products increases with the increase of the wholesale price of ordinary agro-products and decreases with the increase of their own wholesale price. The same rule exists for ordinary agro-products.

By substituting q_C and q_O into formula (4), the optimization results of cold chain agro-products supplier and ordinary agro-products supplier can be obtained:

$$\max_{v_C,\alpha} \pi_C^N(v_C, \alpha) = v_C q_C - \frac{1}{2}\gamma\alpha^2, \tag{9}$$

$$\max_{v_O} \pi_O^N(v_O) = v_O q_C. \tag{10}$$

Obviously, $\max_{v_C,\alpha}\pi_C^N(v_C, \alpha)$ is a concave function on (v_C, α), and $\max_{v_O}\pi_O^N(v_O)$ is a concave function on v_O. From the first-order condition, we can get optimal (v_C^{N*}, α^{N*}) of cold chain agro-products supplier and optimal v_O^{N*} of ordinary agro-products supplier. The equilibrium results are shown in Proposition 1.

Proposition 1. *Conclusions without government subsidy:*

(1) The cold chain agro-products supplier decides the optimal wholesale price and freshness-keeping rate, and the ordinary agro-products supplier decides the optimal wholesale price, $v_C^{N*} = (a/3b)$, $\alpha^{N*} = 0$, and $v_O^{N*} = (a/3b)$

(2) The retailer decides the optimal retail prices of cold chain agro-products and ordinary agro-products, $p_C^{N*} = (7a/9b)$ and $p_O^{N*} = (5a/9b)$

(3) The sale volumes of cold chain agro-products and ordinary agro-products are as follows: $q_C^{N*} = (2a/9)$ and $q_O^{N*} = (2a/9)$

(4) The profit of cold chain agro-products supplier, ordinary agro-products supplier, retailer, and supply chain is $\pi_C^{N*} = (2a^2/27b)$, $\pi_O^{N*} = (2a^2/27b)$, $\pi_R^{N*} = (4a^2/27b)$, and $\pi_S^{N*} = (8a^2/27b)$, respectively.

According to Proposition 1, because of the freshness-keeping cost, the freshness-keeping rate of cold chain agro-products supplier without government subsidy α^{N*} is 0, and the market is divided equally by the two kinds of products, $q_C^{N*} = q_O^{N*}$. The government needs to take measures such as cold chain subsidy to promote the cold chain business of agro-products suppliers.

4.2. Decentralized Decision-Making with Government Subsidy. When the government directly subsidizes the cold-chain agro-products supplier, the profit function of cold chain agro-products supplier, ordinary agro-products supplier, and the retailer is, respectively, as follows:

$$\pi_C = (v_C + \lambda\alpha)(a - bp_C) - \frac{1}{2}\gamma\alpha^2, \tag{11}$$

$$\pi_O = v_O b(p_C - p_O), \tag{12}$$

$$\pi_R = (p_C - v_C)(a - bp_C) + b(p_O - v_O)(p_C - p_O). \tag{13}$$

The profit of cold chain agro-products supplier consists of three parts: wholesale price $v_C(a - bp_C)$, freshness-keeping subsidy $\lambda\alpha(a - bp_C)$ from the government, and freshness-keeping cost $(1/2)\gamma\alpha^2$. The profit structure of supplier and retailer of ordinary agro-products does not change. The optimal decision strategy (v_C, v_O, α) of two suppliers is presented, superscript B represents government subsidy, and the optimal solution of the retailer is as follows:

$$\max_{p_C,p_O} \pi_R^B\left(p_C, p_O \mid v_c, v_o, \alpha\right) = (p_C - v_c)(a - bp_C) + b(p_O - v_O)(p_C - p_O). \tag{14}$$

Obviously, $\pi_R^B(p_C, p_O)$ is a joint concave function on (p_C, p_O), and according to the first-order optimal condition, the retailer's response function can be obtained:

$$P_C(v_C, v_O, \alpha) = \frac{2a + 2bv_C - bv_O}{3b},$$
$$P_O(v_C, v_O, \alpha) = \frac{a + bv_C + bv_O}{3b}. \tag{15}$$

By substituting the retailer's response function into formulae (13) and (14), the optimal solutions of cold chain agro-products supplier and ordinary agro-products supplier can be obtained, respectively:

$$\max_{v_C,\alpha} \pi_C(v_C, \alpha) = (v_C + \lambda\alpha)(a - bp_C) - \frac{1}{2}\gamma\alpha^2, \tag{16}$$

$$\max_{v_O} \pi_O(v_O) = v_O b(p_C - p_O). \tag{17}$$

When $3\gamma > b\lambda^2$, $\max_{v_C,\alpha}\pi_C^B(v_C, \alpha)$ is a concave function on (v_C, α). $\max_{v_O}\pi_O^B(v_O)$ is a concave function on v_O. From the first-order condition, we can obtain the optimal solution (v_C^{B*}, α^{B*}) of cold chain agro-products supplier and obtain the optimal solution v_O^{B*} of ordinary agro-products supplier. The equilibrium results are shown in Proposition 2.

Proposition 2. *When the government presents cold chain subsidy policy, the following conclusions are drawn:*

(1) The optimal freshness-keeping rate decided by cold chain agro-products supplier is greater than 0, and the wholesale prices of cold chain agro-products and ordinary agro-products are lower than those without government subsidy:

$$v_C^{B*} = \frac{5a(3\gamma - 2b\lambda^2)}{b(45\gamma - 14b\lambda^2)} < v_C^{N*},$$
$$\alpha^{B*} = \frac{10a\lambda}{45\gamma - 14b\lambda^2} > 0, \tag{18}$$
$$v_O^{B*} = \frac{3a(5\gamma - 2b\lambda^2)}{b(45\gamma - 14b\lambda^2)} < v_O^{N*}.$$

(2) The optimal retail prices of cold chain agro-products and ordinary agro-products with government subsidy are lower than the retail prices without government subsidy:

$$p_C^{B*} = \frac{35a\gamma - 14ab\lambda^2)}{b(45\gamma - 14b\lambda^2)} < p_C^{N*},$$
$$p_O^{B*} = \frac{25a\gamma - 10ab\lambda^2}{b(45\gamma - 14b\lambda^2)} < p_O^{N*}. \tag{19}$$

(3) The sale volume of cold chain agro-products with government subsidy is larger than that without government subsidy, while the sale volume of ordinary agro-products is the opposite:

$$q_C^{B*} = \frac{10a\gamma}{45\gamma - 14b\lambda^2)} > q_C^{N*},$$
$$q_O^{B*} = \frac{10a\gamma - 4ab\lambda^2}{45\gamma - 14b\lambda^2)} < q_O^{N*}. \tag{20}$$

(4) The profit of cold chain agro-products supplier, ordinary agro-products supplier, the retailer, and supply chain is compared with those in decentralized decision-making condition, and the results are as follows:

$$\pi_C^{B*} = \frac{50a^2\gamma(3\gamma - b\lambda^2)}{b(45\gamma - 14b\lambda^2)^2} > \pi_C^{N*},$$
$$\pi_O^{B*} = \frac{6a^2(25\gamma^2 - 20b\gamma\lambda^2 + 4b^2\lambda^2)}{b(45\gamma - 14b\lambda^2)^2} < \pi_O^{N*},$$
$$\pi_R^{B*} = \frac{4a^2(75\gamma^2 - 30b\gamma\lambda^2 + 4b^2\lambda^2)}{b(45\gamma - 14b\lambda^2)^2} > \pi_R^{N*}, \tag{21}$$
$$\pi_S^{B*} = \frac{10a^2(60\gamma^2 - 29b\gamma\lambda^2 + 4b^2\lambda^2)}{b(45\gamma - 14b\lambda^2)^2} > \pi_S^{N*}.$$

According to Proposition 2, the following corollaries are obtained.

Corollary 1

(1) We have

$$\frac{\delta\alpha^{B*}}{\delta\lambda} = \frac{10a}{45\gamma - 14b\lambda^2} + \frac{280ab\lambda^2}{(45\gamma - 14b\lambda^2)^2} > 0,$$
$$\frac{\delta\alpha^{B*}}{\delta\gamma} = \frac{-450a\lambda}{(45\gamma - 14b\lambda^2)^2} < 0. \tag{22}$$

(2) We have

$$q_C^{B*} - q_O^{B*} = \frac{4ab\lambda^2}{45\gamma - 14b\lambda^2} > 0. \tag{23}$$

From Proposition 2 and Corollary 1, (1) under the government subsidy policy, the cold chain agro-products supplier begins to implement the cold chain freshness-keeping operation. The freshness-keeping rate is positively correlated with λ, the adjustment factor of government subsidy coefficient, and negatively correlated with γ, the difficulty coefficient of freshness-keeping. This is because the adjustment factor of government subsidy coefficient directly affects the profit of cold chain agro-products supplier. The higher the freshness-keeping rate is, the more subsidies the government provides. Freshness-

keeping difficulty coefficient directly affects the cost of cold chain agro-products supplier. The bigger the difficulty coefficient, the higher the freshness-keeping cost, the more reluctant the agro-products supplier is to improve the freshness-keeping rate. In addition, because the freshness-keeping rate of cold chain agro-products supplier cannot exceed 1, and therefore, the government should decide the subsidy scope according to the condition $0 < \alpha^{B*} < 1$, *when they formulate the subsidy policy. In the decentralized system with government subsidy, the reasonable scope of subsidy is* $0 < \lambda < ((\sqrt{5(5a^2 + 126b\gamma)} - 5a)/14b)$. *When* $\lambda \leq 0$, *enterprises will not have the motivation to implement cold chain operation.*

When $\lambda > ((\sqrt{5(5a^2 + 126bm)} - 5a)/14b)$, the excess subsidy provided by the government no longer improves the freshness-keeping rate. (2) The government subsidizes the cold chain agro-products supplier, which not only reduces the wholesale price and retail price of cold chain agro-products, but also reduces the wholesale price and retail price of ordinary agro-products due to the existence of price competition between two kinds of agro-products. (3) After subsidy, the cold chain agro-products supplier gains the greater price advantage, and their market share increases correspondingly, while the market share of ordinary agro-products decreases correspondingly. The final result is that the market share of cold chain agro-products supplier is larger than that of ordinary agro-products. In view of the above, we can know that the government can effectively control the proportion of cold-chain agro-products and ordinary agro-products in the market by means of subsidy policy. (4) The government subsidy for cold chain agro-products not only increases the profit of cold chain agro-products supplier, but also increases the profits of the retailer and the whole supply chain due to the sale increase of cold chain agro-products. Only the profit of ordinary agro-products supplier decreases after the subsidy.

This shows that the increase of the overall supply chain profit caused by the increase of the cold chain agro-products market share exceeds the decrease of the profit of the overall supply chain caused by the decrease of the ordinary agro-products market share.

4.3. Centralized Decision-Making with Government Subsidy. In the market economy system, if the upstream and downstream enterprises of supply chain belong to different economic entities, respectively, there is no central decision-maker aiming at maximizing the benefit of the overall supply chain. However, the optimal decision-making in the centralized decision-making system can be used as a benchmark to study the effect of contract coordination. Articles such as Cachon and Zhang assume that the upstream and downstream of the supply chain are vertically integrated, and the profit maximization of the supply chain is used as a benchmark to study the coordination of the supply chain [10, 11]. In the centralized decision-making system, it is assumed that there is a central decision-maker whose decision variables are P_L, P_H, and τ, superscript C represents centralized decision-making. Therefore, in the centralized decision-making system with government subsidy, the optimization solution is given by

$$\max_{p_C, p_O, \alpha} \pi_I^C = (p_C + \lambda\alpha)(a - bp_C) + p_O b(p_C - p_O) - \frac{1}{2}\gamma\alpha^2. \tag{24}$$

According to the Hesse matrix, when $3\gamma > b\lambda^2$, $\max_{p_C, p_O, \alpha} \pi_I^C$ is a joint concave function on P_C, P_O, α. Make use of the first-order condition of P_C, P_O, and α, we can figure out p_C^{C*}, p_O^{C*}, and α^{C*}, superscript C^* denotes the optimal result, and the equilibrium result is shown in Proposition 3.

Proposition 3. *In the centralized decision-making system with government subsidy, the following conclusions are drawn:*

(1) The retail price of cold chain agro-products and the retail price of ordinary agro-products are the lowest in the centralized decision-making system with government subsidy:

$$\begin{aligned} p_C^{C*} &= \frac{2a(\gamma - b\lambda^2)}{b(3\gamma - 2b\lambda^2)} < p_C^{B*} < p_C^{N*}, \\ p_O^{C*} &= \frac{a(\gamma - b\lambda^2)}{b(3\gamma - 2b\lambda^2)} < p_O^{B*} < p_O^{N*}. \end{aligned} \tag{25}$$

(2) The freshness-keeping rate of cold chain agro-products is the highest in the centralized decision-making system with government subsidy:

$$\alpha^{C*} = \frac{a\lambda}{3\gamma - 2b\lambda^2} > \alpha^{B*} > \alpha^{N*}. \tag{26}$$

(3) In the centralized decision-making system with government subsidy, the sale volume of cold chain agro-products is the largest, and the sale volume of ordinary agro-products is higher than that of the decentralized decision-making system:

$$\begin{aligned} q_C^{C*} &= \frac{a\gamma}{3\gamma - 2b\lambda^2} > q_C^{B*} > q_C^{N*}, \\ q_O^{C*} &= \frac{a\gamma - ab\lambda^2}{3\gamma - 2b\lambda^2} > q_O^{B*}. \end{aligned} \tag{27}$$

(4) The profit of the overall supply chain in the centralized decision-making system with government subsidy is as follows:

$$\pi_I^{C2} = \frac{6a^2\gamma^2 - 7a^2b\gamma\lambda^2 + 2a^2b^2\lambda^4}{2b(3\gamma - 2b\lambda^2)^2}. \tag{28}$$

Proposition 3 shows that there is only one decision-maker which can eliminate the "double marginalization effect," and the retail prices of cold chain agro-products and ordinary agro-products are the lowest, while the freshness-keeping rate of cold chain agro-products is the highest at this time. In addition, according to $0 < \alpha^{B*} < 1$, the scope of

subsidy decided by the government, the reasonable subsidy in centralized decision-making system is as follows:

$$0 < \lambda < \left(\frac{\sqrt{a^2 + 24b\gamma} - a}{14b}\right),$$
$$\left(\frac{\sqrt{a^2 + 24b\gamma} - a}{4bb}\right) < \frac{\sqrt{5\left(5a^2 + 126b\gamma\right)} - 5a}{14b}. \tag{29}$$

Therefore, in the centralized decision-making system, the government can get the better subsidy effect by subsidizing enterprises.

The abovementioned content analyzes the differential pricing decision and cold chain decision of cold chain agro-products and ordinary agro-products under the three models. Through the comparative analysis of the three models, it is found that, compared with the nongovernment subsidy, the price of cold chain agro-products decreases, the freshness-keeping rate increases, and the profit and market share also increase in the condition of the government subsidy. Therefore, government subsidy can play a positive role in encouraging agro-products suppliers to implement cold chain freshness-keeping operation. By comparing the centralized and decentralized decision-making system with government subsidy, the centralized decision-making system eliminates the "double marginalization effect." The retail price of agro-products is low and the profit of the overall supply chain is optimal.

Therefore, both cold chain agro-products supplier and ordinary agro-products supplier have the motivation to design an incentive mechanism of coordinating the supply chain to achieve the optimal effect of centralized decision-making. The retailer sets a retail price in the condition of centralized decision-making. The supplier of cold chain agro-products decides the optimal freshness-keeping rate in accordance with the freshness-keeping rate of centralized decision-making. The principle of win-win is adopted to ensure the participation and restraint of all participants involved in cooperation.

5. Supply Chain Coordination Based on Shapley Value Method

5.1. Introduction of Shapley Value Method. From the above analysis, we know that noncooperative decentralized decision-making leads to "double marginalization effect" which will reduce the profit of the whole supply chain. In order to protect the benefit of supply chain from loss, the coordination of the supply chain should be considered.

Shapley value method fairly and effectively distributes the benefit among the alliance members according to their contribution [12]. The basic principle of the Shapley value method is as follows: $I = \{1, 2, ..., n\}$ denotes the aggregation of all players, and z denotes an alliance, that is, in a multiplayer game, some players unite to choose strategies like one player, which is called alliance. Obviously, alliance z is a subset of the set I of players, $z \subseteq I$.

When several players unite to form an alliance z, they can obtain the maximum return value in this game, $v(z)$, if the revenue function $v(z)$ satisfies the following equation:

$$v(\phi) = 0,$$
$$v(z_1 \cup z_2) \geq v(z_1) + v(z_2), z_1 \cap z_2 = \phi, \tag{30}$$

where $v(z)$ is defined as a characteristic function of I and represents the benefit of cooperation alliance z. The above two formulas embody the system thought of "$1 + 1 > 2$" and satisfy the superadditivity, which means that their interests are the greatest and the maximum benefit of cooperation is $v(I)$ when players cooperate.

Let $\mu_i\,(i = 1, 2, \ldots, n)$ denote the benefit of member i of I from the maximum benefit of cooperation $v(I)$, then the distribution of the maximum benefit of cooperation can be described as $\mu(v) = (\mu_1(v), \mu_2(v), \ldots, \mu_n(v))$. At the same time, the following requirements need to be satisfied:

$$\sum_{i=1}^{n} \mu_i(v) = v(I)\mu_i(v) > v(i), \quad i = 1, 2, \ldots, n. \tag{31}$$

When all members of I choose to cooperate, the Shapley value of benefit distribution among the members of the supply chain is given by

$$\mu_i(v) = \sum_{i \in z(i)} w(z)\left[v(z) - v(z \backslash i)\right], \quad i = 1, 2, \ldots, n,$$
$$w(|z|) = \frac{(n - |z|)!\,(|z| - 1)!}{n!}, \tag{32}$$

where $z(i)$ denotes all subsets of set I which contain player i, $|z|$ is the number of elements in the subset z, n is the number of elements in the set I, and $w(|z|)$ is the weighting factor; it is the probability that the players make a contribution to the alliance. $v(z)$ represents the benefit of subset z, and $v(z \backslash i)$ is the benefit of subset z removing player i.

5.2. Partial Alliance. When the cold chain agro-products supplier and ordinary agro-products supplier build an alliance,

$$\max_{p_C, p_O, \alpha} \pi_{CO} = (v_C + \lambda\alpha)(a - bp_C) + v_O b(p_C - p_O) - \frac{1}{2}\gamma\alpha^2$$
$$\text{s.t.} \max_{p_C, p_O} \pi_R = (p_C - v_C)(a - bp_C) + (p_O - v_O)b(p_C - p_O). \tag{33}$$

Solution available:

$$v_C^* = \frac{3a\left(2\gamma - b\lambda^2\right)}{4b\left(3\gamma - b\lambda^2\right)},$$

$$v_O^* = \frac{a}{2b},$$

$$\alpha^* = \frac{a\lambda}{2\left(3\gamma - b\lambda^2\right)},$$

$$p_C^* = \frac{5a\gamma - 2ab\lambda^2}{2b\left(3\gamma - b\lambda^2\right)},$$

$$p_O^* = \frac{8a\gamma - 3ab\lambda^2}{4b\left(3\gamma - b\lambda^2\right)},$$

$$\pi_{CO}^* = \left(v_C^* + \lambda\alpha^*\right)\left(a - bp_C^*\right) + v_O^* b\left(p_C^* - p_O^*\right) - \frac{1}{2}\gamma\alpha^{*2}. \tag{34}$$

When the cold chain agro-products supplier and the retailer build an alliance,

$$\max_{p_C, p_O, \alpha} \pi_{CR} = \left(p_C + \lambda\alpha\right)\left(a - bp_C\right) + \left(p_O - v_O\right)b\left(p_C - p_O\right) - \frac{1}{2}\gamma\alpha^2$$

$$\text{s.t. } \max_{v_O} \pi_O = v_O b\left(p_C - p_O\right). \tag{35}$$

Solution available:

$$w_O^* = \frac{a\left(\gamma - b\lambda^2\right)}{2b\left(2\gamma - b\lambda^2\right)},$$

$$\alpha^* = \frac{a\lambda\left(5\gamma - 3b\lambda^2\right)}{2\left(3\gamma - 2b\lambda^2\right)\left(2\gamma - b\lambda^2\right)},$$

$$p_C^* = \frac{\left(a\gamma - ab\lambda^2\right)\left(7\gamma - 4b\lambda^2\right)}{2b\left(3\gamma - 2b\lambda^2\right)\left(2\gamma - b\lambda^2\right)},$$

$$p_O^* = \frac{\left(a\gamma - ab\lambda^2\right)\left(3\gamma - b\lambda^2\right)}{2b\left(3\gamma - 2b\lambda^2\right)\left(2\gamma - b\lambda^2\right)},$$

$$\pi_{CR}^* = \left(p_C^* + \lambda\tau^*\right)\left(a - bp_C^*\right) + \left(p_O^* - v_O^*\right)b\left(p_C^* - p_O^*\right) - \frac{1}{2}\gamma\alpha^{*2}. \tag{36}$$

When the ordinary agro-products supplier and the retailer build an alliance,

$$\max_{p_C, p_O} \pi_{OR} = \left(p_C - w_C\right)\left(a - bp_C\right) + p_O b\left(p_C - p_O\right),$$

$$\max_{v_C, \alpha} \pi_C = \left(v_C + \lambda\alpha\right)\left(a - bp_C\right) - \frac{1}{2}\gamma\alpha^2. \tag{37}$$

Solution available:

$$v_C^* = \frac{a\left(3\gamma - 2b\lambda^2\right)}{4b\left(3\gamma - b\lambda^2\right)},$$

$$\alpha^* = \frac{a\lambda}{2\left(3\gamma - 2b\lambda^2\right)},$$

$$p_C^* = \frac{2a}{3b} + \frac{a\left(3\gamma - 2b\lambda^2\right)}{6b\left(3\gamma - b\lambda^2\right)},$$

$$p_O^* = \frac{a}{3b} + \frac{a\left(3\gamma - 2b\lambda^2\right)}{12b\left(3\gamma - b\lambda^2\right)},$$

$$\pi_{OR}^* = \left(p_C^* - v_C^*\right)\left(a - bp_C^*\right) + p_O^* b\left(p_C^* - p_O^*\right), \tag{38}$$

According to Table 1, the benefit distribution of the cold chain agro-products supplier is as follows:

$$\mu_C^*(v) = \frac{1}{3}\pi_C^* + \frac{1}{6}\left[\pi_{CO}^* - \pi_O^*\right] + \frac{1}{6}\left[\pi_{CR}^* - \pi_R^*\right] + \frac{1}{3}\left[\pi_{COR}^* - \pi_{OR}^*\right]. \tag{39}$$

For the same reason, the benefit distribution between the ordinary agro-products supplier and the retailer is as follows:

$$\mu_O^*(v) = \frac{1}{3}\pi_O^* + \frac{1}{6}\left[\pi_{CO}^* - \pi_O^*\right] + \frac{1}{6}\left[\pi_{OR}^* - \pi_R^*\right] + \frac{1}{3}\left[\pi_{COR}^* - \pi_{CR}^*\right],$$

$$\mu_R^*(v) = \frac{1}{3}\pi_R^* + \frac{1}{6}\left[\pi_{CR}^* - \pi_C^*\right] + \frac{1}{6}\left[\pi_{OR}^* - \pi_O^*\right] + \frac{1}{3}\left[\pi_{COR}^* - \pi_{CO}^*\right]. \tag{40}$$

The decentralized decision-making supply chain sets the price and decides the freshness-keeping rate based on $(p_C^{D*}, p_O^{D*}, \alpha^{D*})$ and then redistributes the profit through Shapley value method. The profit distribution means $(\mu_C^*(v), \mu_O^*(v)\mu_R^*(v))$ and finally achieves supply chain coordination.

6. Numerical Example

Set $a = 50$, $b = 6$, $\gamma = 150$, and $\lambda = 2$. Contrast the profit of each member in the supply chain with government subsidy and the one without government subsidy, and use the Shapley value method to coordinate each member in the supply chain with government subsidy, as shown in Table 2. Table 2 shows that (1) compare the profit distribution of the decentralized decision-making with government subsidy with the one without government subsidy, the profit of supplier and retailer and the profit of overall supply chain of cold chain agro-products all increase, while the profit of ordinary agro-products supplier decreases. This is because the government subsidy strengthens the price advantage of cold chain agro-products and indirectly weakens the competitiveness of ordinary agro-products, so that the profit of ordinary agro-products supplier decreases, which is conducive to the government's control of cold chain agro-products and ordinary agro-products. (2) In the condition of government subsidy, after coordination on profit distribution in the case of the centralized decision-making by means of Shapley value method, the profit of each member in the

Table 1: Calculation of Shapley value of cold chain agro-products supplier.

z	C	CO	CR	COR
$v(z)$	π_C^*	π_{CO}^*	π_{CR}^*	π_{COR}^*
$v(z\backslash C)$	0	π_O^*	π_{CR}^*	π_{OR}^*
$v(s)-v(z\backslash C)$	π_C^*	$\pi_{CO}^*-\pi_O^*$	$\pi_{CR}^*-\pi_{CR}^*$	$\pi_{COR}^*-\pi_{OR}^*$
$\lvert z\rvert$	1	2	2	3
$v(\lvert z\rvert)$	1/3	1/6	1/6	1/3
$v(\lvert z\rvert)[v(z)-v(z\backslash C)]$	$(1/3)\pi_C^*$	$(1/6)\ [\pi_{CO}^*-\pi_O^*]$	$(1/6)\ [\pi_{CR}^*-\pi_R^*]$	$(1/3)\ [\pi_{COR}^*-\pi_{OR}^*]$

Table 2: Comparison of profits of members in supply chain in various conditions.

Decision-making types under subsidy policy	π_C^*	π_O^*	π_R^*	Gross profit
Decentralized decision-making without government subsidy	30.86	30.86	61.73	123.46
Decentralized decision-making with government subsidy	32.36	29.95	64.08	126.39
Centralized decision-making coordination with government subsidy	35.27	34.92	72.85	143.03

Table 3: Sensitivity analysis of parameters.

Parameter	value	Optimal value					
		Retail price of cold chain products p_C^{D*}	Retail price of common products p_O^{D*}	Fresh-keeping rate of cold chain products (%) α^{D*}	Profit of cold chain supplier π_C^*	Profit of common product supplier π_O^*	Retailer profit π_R^*
	1	5.48	2.74	11.42	32.76	37.08	70
λ	2	5.22	2.61	24.88	35.27	34.92	72.85
	3	4.68	2.34	43.86	40.19	31.13	78.53
	100	5.03	2.51	39.68	37.11	33.43	74.96
γ	150	5.22	2.61	24.88	35.27	34.92	72.85
	200	5.31	2.66	18.11	34.40	35.65	71.86
	30	3.13	1.57	14.93	12.7	12.57	26.22
a	50	5.22	2.61	24.88	35.27	34.92	72.85
	70	7.31	3.66	34.83	69.13	68.44	142.78
	5	6.34	3.17	24.39	41.63	42.49	86.62
b	6	5.22	2.61	24.88	35.27	34.92	72.85
	7	4.42	2.21	25.38	30.74	29.51	63.03

supply chain is greater than the one in the decentralized decision-making system, which satisfies the participation constraints of each member in the supply chain and meanwhile optimizes the profit of the whole supply chain.

In addition, the influence of the difficulty coefficient of freshness-keeping and the adjustment coefficient of government subsidy on decision variables and profits are shown in Table 3.

According to Table 3,

(1) With the increase of government subsidy, the retail prices of cold chain agro-products and ordinary agro-products will decrease, the freshness-keeping rate of cold chain agro-products will increase, the profits of cold chain agro-products supplier and retailer will increase, and the profit of ordinary agro-products supplier will decrease. According to these characteristics, the government indirectly controls the freshness-keeping rate of cold chain agro-products, meanwhile, it also achieves the goal of improving the enthusiasm of cold chain agro-products supplier and retailer to produce or sell cold chain agro-products. This is the main reason why the government makes policy subsidizing cold chain agro-products.

(2) With the increasing freshness-keeping difficulty of cold chain agro-products, the freshness-keeping rate of cold chain agro-products decreases, the retail prices of cold chain agro-products and ordinary agro-products increase, and the profits of cold chain agro-products supplier and retailer decrease. Only the profit of ordinary agro-products supplier increases. This is because the more difficult it is to keep freshness, the higher the cost that the cold chain agro-products supplier pays for keeping freshness, which leads to the increase of wholesale price and retail price of cold chain agro-products, and the increase of prices leads to the decrease of sale volume and ultimately leads to the decrease of profits of both cold chain agro-products supplier and retailer. At this time, due to the relative price advantage of ordinary agro-products, ordinary agro-products supplier gets more profit. This is the main reason that the difficulty of keeping freshness restricts the cold chain operation.

(3) With the increase of market capacity, the retail prices of two kinds of agro-products, the freshness-keeping rate of cold chain agro-products, and the profit of each member in the supply chain increase. This is the result of the interaction between supply and demand in the market and conforms to the market rules.

(4) The more sensitive the consumers are to prices, the lower the retail prices of both kinds of agro-products and the lower the profit of each member in the supply chain. This sensitivity can be evaluated to provide a reference for making price [13]. If we want to improve the profit of each member in the supply chain, we need to use nonprice characteristics to change consumers' price sensitivity.

7. Conclusion and Prospect

In view of the policy support of the government's cold chain subsidy and consumers' increasing preference for cold chain keeping freshness, more and more agro-products enterprises implement cold chain operation. It is a remarkable characteristic of the market that the same variety of agro-products implements cold chain operation and ordinary operation in the market at the same time. Based on this, this paper chooses the supply chain system composed of cold chain agro-products supplier, ordinary agro-products supplier, and retailer as the research object, studies the differential pricing strategies of supply chain members, introduces government subsidy to indirectly reduce the cost of cold chain agro-products, and builds a differential pricing model for upstream and downstream members in supply chain with government subsidy. By solving the model and comparing it with the one with centralized decision-making, the following conclusions are found. First of all, the government subsidy policy can reduce the wholesale price and retail price of cold chain agro-products and ordinary agro-products at the same time; however, cold chain agro-products have greater competitive advantages because of being backed by government subsidy, and market share will increase correspondingly and ultimately lead to the increase of profits of supplier and retailer of cold chain agro-products. This also indirectly shows that government subsidy for cold chain agro-products can promote the development of cold chain agro-products. In addition, through calculation, we can find that the government subsidy policy has a certain scope of validity, and only in this scope can the subsidy policy play an active role in promoting cold chain business. This conclusion can provide a theoretical basis for the formulation of government policy. Secondly, by comparing with centralized decision-making, it is found that although the government subsidy policy can improve the competitiveness of cold chain agro-products and increase the profit of cold chain agro-products supplier and supply chain system, the decentralized decision-making cannot coordinate the supply chain, which results in the loss of supply chain efficiency. In view of the loss of supply chain efficiency caused by decentralized decision-making, this paper chooses Shapley value method with strong operability and good stability to coordinate the supply chain. After coordination, the efficiency of supply chain can be improved to achieve the effect of centralized decision-making. This conclusion can provide theoretical guidance for joint pricing in practice. Finally, a numerical example is given to validate the proposition in this paper, and sensitivity analysis is made on the adjustment factor of government subsidy coefficient, the freshness-keeping difficulty coefficient, market capacity, and consumer price sensitivity.

This paper focuses on the cold chain operation management and pricing decision-making of enterprises with the government's cold chain subsidy. The government's cold chain subsidy is related to the freshness-keeping rate of enterprises. The higher the freshness-keeping rate, the more the cold chain subsidy provided by the government. The government subsidy plays a role in encouraging enterprises to implement cold chain operation and improving freshness-keeping rate. However, there is no specific target of freshness-keeping rate in the text. In the future, it will be one of our further research directions to add the target of freshness-keeping rate and cold chain efficiency when the government formulates the cold chain policy. In addition, the impact of the supply chain network structure on the mechanism of cold chain logistics subsidy is also worthy of consideration [14–16].

Data Availability

The data used to support the findings of the study are available within the article.

Conflicts of Interest

The authors declare no conflicts of interest regarding the content and implications of this manuscript.

Acknowledgments

This work was supported by the Key Project of Humanities and Social Sciences of Anhui Xinhua University under Grant no. 2018rw002 and supported in part by Anhui Provincial Quality Project in Colleges and Universities under Grant no. 2018ylzy074.

References

[1] X. G. Yuan, P. Zou, J. Zhu, and D. Wu, "Development trend problems and countermeasures for cold chain logistics industry in China," *Journal of Agricultural Science and Technology*, vol. 17, no. 1, pp. 7–14, 2015.

[2] J. L. Yang and H. P. Hou, "Research on real-time monitoring optimization of cold-chain logistics big data," *Science and Technology Management Research*, vol. 6, pp. 198–203, 2017.

[3] J. H. Huang, F. Ye, and Q. Lin, "Government subsidy mechanism in agricultural supply chain considering capital constrain under random yield," *Chinese Journal of Management*, vol. 14, no. 2, pp. 277–285, 2017.

[4] F. Xiong, J. Peng, P. Jin, X. Y. Zhang, and Y. Qiu, "The impact of relational contracts stability about fresh agricultural product supply chain study: from the perspective of cold chain

facilities subsidy mode," *Chinese Journal of Management Science*, vol. 23, no. 8, pp. 102–111, 2015.

[5] C. B. Li, E. J. Wang, and Y. Yang, "An evolutionary game study on cold chain logistics resource allocation under government supervision," *Journal of Beijing Jiaotong University (Social Sciences Edition)*, vol. 16, no. 3, pp. 108–118, 2017.

[6] O. J. Mancur, *The Logic of Collective Action: Public Goods and the Theory of Groups*, Harvard University Press, Cambridge, MA, USA, 1965.

[7] Q. H. Zhu and Y. J. Dou, "A game model for green supply chain management based on government subsidies," *Journal of Management Sciences in China*, vol. 14, no. 16, pp. 86–95, 2011.

[8] A. Arya, B. Mittendorf, and D. E. M. Sappington, "The bright side of supplier encroachment," *Marketing Science*, vol. 26, no. 5, pp. 651–659, 2007.

[9] A. Dumrongsiri, M. Fan, A. Jain, and K. Moinzadeh, "A supply chain model with direct and retail channels," *European Journal of Operational Research*, vol. 187, no. 3, pp. 691–718, 2008.

[10] G. P. Cachon, "Supply chain coordination with contracts," in *Handbooks in Operations Research and Management Science: Supply Chain Management, Chapter 6*, S. Graves and T. de Kok, Eds., Elsevier, Amsterdam, Netherlands, 2003.

[11] J. Zhang, Q. Gou, L. Liang, and Z. Huang, "Supply chain coordination through cooperative advertising with reference price effect," *Omega*, vol. 41, no. 2, pp. 345–353, 2013.

[12] Y. D. Gong, B. Y. Li, and T. Liu, "Supply chain coordination strategy based on Shapley value and the same profit increase rate," *Journal of Systems & Management*, vol. 18, no. 1, pp. 61–66, 2009.

[13] N. R. Xu and J. B. Liu, "Research on evaluation on agility of agile supply chain network based on complex network theory," *Mathematical Problems in Engineering*, vol. 2015, Article ID 707459, 10 pages, 2015.

[14] J.-B. Liu, J. Zhao, J. Min, and J. Cao, "The Hosoya index of graphs formed by a fractal graph," *Fractals*, vol. 27, no. 8, p. 1950135, 2019.

[15] J.-B. Liu, J. Zhao, and Z.-Q. Cai, "On the generalized adjacency, Laplacian and signless Laplacian spectra of the weighted edge corona networks," *Physica A: Statistical Mechanics and Its Applications*, vol. 540, Article ID 123073, 2020.

[16] J.-B. Liu, J. Zhao, H. He, and Z. Shao, "Valency-based topological descriptors and structural property of the generalized sierpiński networks," *Journal of Statistical Physics*, vol. 177, no. 6, pp. 1131–1147, 2019.

Hindawi
Journal of Chemistry
Volume 2020, Article ID 2878901, 8 pages
https://doi.org/10.1155/2020/2878901

Research Article

Unicyclic Graphs with the Fourth Extremal Wiener Indices

Guangfu Wang,[1] Yujun Yang,[2] Yuliang Cao,[2] and Shoujun Xu[3]

[1]*School of Science, East China Jiaotong University, Nanchang, Jiangxi 330013, China*
[2]*School of Mathematics and Information Sciences, Yantai University, Yantai, Shandong 264005, China*
[3]*School of Mathematics and Statistics, Lanzhou University, Lanzhou, Gansu 730000, China*

Correspondence should be addressed to Yujun Yang; yangyj@yahoo.com

Received 30 August 2019; Accepted 21 November 2019; Published 15 April 2020

Guest Editor: Jia-Bao Liu

A graph is called unicyclic if the graph contains exactly one cycle. Unicyclic graphs with the fourth extremal Wiener indices are characterized. It is shown that, among all unicyclic graphs with $n \geq 8$ vertices, $C_5(S_{n-4})$ and $C_2^{u_1,u_2}(S_3, S_{n-4})$ attain the fourth minimum Wiener index, whereas $C_3^{u_1,u_2}(P_3, P_{n-4})$ attains the fourth maximum Wiener index.

1. Introduction

Let $G = (V(G), E(G))$ be a connected (molecular) graph with vertex set $V(G)$ and edge set $E(G)$. For any two vertices $u, v \in V(G)$, the distance $d_G(u, v)$ between them is defined as the number of edges in a shortest path connecting them. The distance of a vertex $u \in V(G)$, denoted by $d_G(u)$, is the sum of distances between u and all other vertices of G, i.e., $d_G(u) = \sum_{v \in V(G)} d_G(u, v)$. The famous Wiener index of G, denoted by $W(G)$, is defined as

$$W(G) = \sum_{\{u,v\} \subseteq V(G)} d_G(u, v) = \frac{1}{2} \sum_{u \in V(G)} d_G(u). \quad (1)$$

The Wiener index of a graph is a well-known topological index, and it seems that Wiener [1] was the first who considered it. Wiener himself used the name path number and conceived $W(G)$ only for acyclic molecules. The definition of the Wiener index in terms of distances between vertices of a graph, such as in equation (1), was first given by Hosoya [2]. Since the middle of the 1970s, the Wiener index has been extensively studied. For research development on the Wiener index, the readers are referred to [3–7] and two special issues of MATCH [8] and Discrete Appl. Math. [9]. Analogous to the Wiener index, some other topological indices are introduced and studied (for example, see [10–13]).

As summarized in [14–16], studies on the Wiener index mainly focus on trees and hexagonal systems. Recently, Wiener indices of unicyclic graphs (i.e., connected graphs containing exactly one cycle) have attracted much attention. Studies along this line include relations between Wiener and Szeged indices of unicyclic graphs [17], minimum Wiener indices of unicyclic graphs of given order, cycle length and number of penden vertices [18], minimum Wiener indices of unicyclic graphs of given matching number [19], Wiener indices of unicyclic graphs with given girth [20], minimum Wiener indices of unicyclic graphs of order n with girth g and the matching number $\beta \geq 3g/2$ [21], minimum Wiener indices of unicyclic graphs of order n and girth g with k pendent vertices [22], minimum Wiener index of unicyclic graphs with given bipartition [23], and so on. In [24], Tang and Deng considered unicyclic graphs with the first three smallest and largest Wiener indices. However, their characterization turned out to be incomplete and two extremal graphs were missed. Later, Nasiri et al. [25] filled the gap and presented a complete characterization to these extremal graphs. On the basis of the previous work, in this paper, we characterize unicyclic graphs with the fourth smallest and largest Wiener indices.

2. Notations and Lemmas

Throughout the paper, the path, star, and cycle graphs on n vertices are denoted by P_n, S_n, and C_n, respectively. Let G be a unicyclic graph of order n with its unique cycle $C_m = v_1v_2\dots v_mv_1$ of length m. Suppose that $T_1, T_2, \dots, T_k$ $(0 \le k \le m)$ are all the nontrivial components (they are all nontrivial trees) of $G - E(C_m)$, and u_i is the common vertex of T_i and C_m, $i = 1, 2, \dots, k$. Such a unicyclic graph is denoted by $C_m^{u_1,u_2,\dots,u_k}(T_1, T_2, \dots, T_k)$. Specially, $G = C_n$ for $k = 0$. And if $k = 1$, we write $C_m(T_1)$ for $C_m^{u_1}(T_1)$. Let $|V(T_i)| = l_i + 1$, $i = 1, 2, \dots, k$. Then, $l = l_1 + l_2 + \dots + l_k = n - m$. Denote by $\mathcal{T}_n$ the set of all trees of order n.

In the following, we summarize some known results concerning Wiener indices of unicyclic graphs which will be used in the later.

Lemma 1 (see [24]). *Let $G = C_m^{u_1,u_2,\dots,u_k}(T_1, T_2, \dots, T_k)$ be a unicyclic graph. Then,*

$$W(G) = W(C_m) + (n-m)\omega + (m-1)\sum_{i=1}^{k}\omega_i + \sum_{i=1}^{k} W(T_i) + \sum_{i=1}^{k-1}\sum_{j=i+1}^{k}\left(l_i\omega_j + l_il_jd_{C_m}(u_i, u_j) + l_j\omega_i\right), \tag{2}$$

where $\omega_i = d_{T_i}(u_i)$, $\omega = d_{C_m}(u)$, and $u \in C_m$.

Lemma 2 (see [24]). *Let $G_1 = C_m^{u_1,u_2,\dots,u_k}(S_{l_1+1}, S_{l_2+1}, \dots, S_{l_k+1})$ and $G_2 = C_m^{u_1,u_2,\dots,u_k}(P_{l_1+1}, P_{l_2+1}, \dots, P_{l_k+1})$, where $u_1, u_2, \dots, u_k$ are the centers of $S_{l_1+1}, S_{l_2+1}, \dots, S_{l_k+1}$, respectively, in G_1 and $u_1, u_2, \dots, u_k$ are the pendent vertices of $P_{l_1+1}, P_{l_2+1}, \dots, P_{l_k+1}$, respectively, in G_2. Then,*

$$W(G_1) \le W(G) \le W(G_2), \tag{3}$$

for any graph $G = C_m^{u_1,u_2,\dots,u_k}(T_1, T_2, \dots, T_k)$ and $|V(T_i)| = l_i + 1$, $i = 1, 2, \dots, k$, with the equality on the left (or on the right) if and only if $G \cong G_1$ (or $G \cong G_2$).

Lemma 3 (see [24]). *Let $G_1 = C_m^{u_1,u_2,\dots,u_k}(S_{l_1+1}, S_{l_2+1}, \dots, S_{l_k+1})$ and $l_i = n(T_i)$, $i = 1, 2, \dots, k$. If $k \ge 1$, then*

$$W(G_1) \ge W(C_m(S_{l+1})), \tag{4}$$

with the equality if and only if $G_1 \cong C_m(S_{l+1})$, where $l = l_1 + l_2 + \dots + l_k = n - m$.

Lemma 4 (see [24]). *Let $G_2 = C_m^{u_1,u_2,\dots,u_k}(P_{l_1+1}, P_{l_2+1}, \dots, P_{l_k+1})$ and $l_i = n(T_i)$, $i = 1, 2, \dots, k$. If $k \ge 1$, then*

$$W(G_2) \ge W(C_m(P_{l+1})), \tag{5}$$

with the equality if and only if $G_1 \cong C_m(P_{l+1})$, where $l = l_1 + l_2 + \dots + l_k = n - m$.

Lemma 5 (see [25]). *If $n \ge 8$ and $m \ge 3$, then $W(C_m(S_{n-m+1})) - W(C_{m-1}(S_{n-m+2})) > 0$.*

Besides, we also need the following result.

Lemma 6 (see [22]). *Let H, X, and Y be three connected pairwise vertex-set disjoint graphs. Suppose that u and v are the two vertices of H, v' is a vertex of X, and u' is a vertex of Y. Let G be the graph obtained from H, X, and Y by identifying v with v' and u with u', respectively. Let G_1^* be the graph obtained from H, X, and Y by identifying vertices v, v', and u', and let G_2^* be the graph obtained from H, X, and Y by identifying vertices u, v', u'. Then,*

$$W(G_1^*) < W(G) \text{ or } W(G_2^*) < W(G). \tag{6}$$

3. Results

3.1. Unicyclic Graphs with the Fourth Minimum Wiener Index. Let $C_3(T_{n-5,1}^1)$ be the unicyclic graph as shown in Figure 1(a). Then, unicyclic graphs with the first smallest Wiener indices are completely characterized in the following result.

Theorem 1 (see [25]). *Suppose $G = C_m^{u_1,u_2,\dots,u_k}(T_1, T_2, \dots, T_k)$ is a unicyclic graph of order n, with $n \ge 7$. If $G \ncong S_n + e$, $C_4(S_{n-3}), C_3^{u_1,u_2}(S_2, S_{n-3})$, then*

$$\begin{aligned} W(S_n + e) &< W(C_4(S_{n-3})) = W(C_3^{u_1,u_2}(S_2, S_{n-3})) \\ &< W\left(C_3\left(T_{n-5,1}^1\right)\right) \le W(G), \end{aligned} \tag{7}$$

with equality if and only if

$$G \cong \begin{cases} C_3\left(T_{n-5,1}^1\right), & \text{if } n > 7, \\ C_3^{u_1,u_2}(S_3, S_3) \text{ or } C_5(S_3), & \text{if } n = 7. \end{cases} \tag{8}$$

As illustrated in the following theorem, we show that $C_5(S_{n-4})$ and $C_3^{u_1,u_2}(S_3, S_{n-4})$ have the fourth smallest Wiener indices.

Theorem 2. *Suppose $G = C_m^{u_1,u_2,\dots,u_k}(T_1, T_2, \dots, T_k)$ is a unicyclic graph of order n, with $n \ge 8$. If $G \ncong S_n + e$, $C_4(S_{n-3}), C_3^{u_1,u_2}(S_2, S_{n-3}), C_3(T_{n-5,1}^1)$, then*

$$\begin{aligned} W(S_n + e) &< W(C_4(S_{n-3})) = W(C_3^{u_1,u_2}(S_2, S_{n-3})) \\ &< W\left(C_3\left(T_{n-5,1}^1\right)\right) \\ &< W(C_5(S_{n-4})) = W(C_3^{u_1,u_2}(S_3, S_{n-4})) \le W(G), \end{aligned} \tag{9}$$

with equality if and only if $G \cong C_5(S_{n-4})$ or $C_3^{u_1,u_2}(S_3, S_{n-4})$.

Proof. By Lemma 1,

$$\begin{aligned} W(S_n + e) &< W(C_4(S_{n-3})) = W(C_3^{u_1,u_2}(S_2, S_{n-3})) \\ &< W\left(C_3\left(T_{n-5,1}^1\right)\right) = n^2 - n - 3. \end{aligned} \tag{10}$$

On the other hand, by Lemma 1, it is easily computed that

$$W(C_5(S_{n-4})) = W(C_3^{u_1,u_2}(S_3, S_{n-4})) = n^2 - 10. \quad (11)$$

Hence, for $n \geq 8$, $W(S_n + e) < W(C_4(S_{n-3})) = W(C_3^{u_1,} u^2 (S_2, S_{n-3})) < W(C_3(T_{n-5,1}^1)) < W(C_5(S_{n-4})) = W(C_3^{u_1,u_2}(S_3, S_{n-4}))$. So, it suffices to show that if G is a n-vertex unicyclic graph ($n \geq 8$), such that $G \ncong S_n + e, C_4(S_{n-3}), C_3^{u_1,u_2}(S_2, S_{n-3}), C_3(T_{n-5,1}^1)$, then $W(C_5(S_{n-4})) \leq W(G)$, with equality if and only if $G \cong C_5(S_{n-4})$ or $C_3^{u_1,u_2}(S_3, S_{n-4})$. To this end, for convenience, we distinguish three cases that $m = 3, 4$ or $m \geq 5$. □

Case 1 ($m \geq 5$). If $k = 0$, then $G = C_n$. It is well known that

$$W(C_n) = \begin{cases} \frac{1}{8}n^3, & \text{if } n \text{ is even,} \\ \frac{1}{8}n(n^2 - 1), & \text{otherwise.} \end{cases} \quad (12)$$

Hence, if n is even, then

$$W(G) - W(C_5(S_{n-4})) = \frac{1}{8}n^3 - (n^2 - 10) = \frac{1}{8}n^3 - n^2 + 10 > 0, \quad (13)$$

and if n is odd, then

$$\begin{aligned} W(G) - W(C_5(S_{n-4})) &= \frac{1}{8}n(n^2 - 1) - (n^2 - 10) \\ &= \frac{1}{8}n^3 - \frac{9}{8}n^2 + 10 > 0, \end{aligned} \quad (14)$$

as desired.

Now assume that $k \geq 1$. Then, by Lemmas 2, 3, and 5,

$$\begin{aligned} W(G) &\geq W(C_m^{u_1,u_2,\ldots,u_k}(S_{l_1+1}, S_{l_2+1}, \ldots, S_{l_k+1})) \\ &\geq W(C_m(S_{n-m+1})) \geq W(C_5(S_{n-4})), \end{aligned} \quad (15)$$

with equality if and only if $G \cong C_5(S_{n-4})$.

Case 2 ($m = 4$). In this case, we consider four subcases that k = 1, 2, 3, or 4.

Subcase 1 ($k = 1$). In this case, $G = C_4(T_1)$. Since $G = C_4(T_1) \ncong C_4(S_{n-3})$, it has been shown in [25] that

$$W(G) \geq W(C_4(T_{n-6,1}^1)) = n^2 - 7. \quad (16)$$

Hence, $W(G) \geq W(C_4(T_{n-6,1}^1)) = n^2 - 7 > n^2 - 10 = W(C_5(S_{n-4}))$, as desired.

Subcase 2 ($k = 2$). In this case, $G = C_4^{u_1,u_2}(T_1, T_2)$. It has been shown in [24] that

$$\begin{aligned} W(G) &= W(C_4^{u_1,u_2}(T_1, T_2)) \geq W(C_4^{u_1,u_2}(S_{l_1+1}, S_{l_2+1})) \\ &= n^2 - n - 4 + \alpha l_1 l_2, \end{aligned} \quad (17)$$

where $\alpha = 1$ if u_1 and u_2 are adjacent in C_4; otherwise, $\alpha = 2$. Noticing that $l_1 + l_2 = n - 4$, we have

$$\begin{aligned} W(G) - W(C_5(S_{n-4})) &\geq n^2 - n - 4 + \alpha l_1 l_2 - (n^2 - 10) \\ &= \alpha l_1 l_2 - n + 6 \\ &\geq 1 \times (n - 5) - n + 6 > 0. \end{aligned} \quad (18)$$

Subcase 3 ($k = 3$). In this case, $G = C_4^{u_1,u_2,u_3}(T_1, T_2, T_3)$. Let G_1^* be the graph obtained from G by first removing T_1 from G and then identifying the root of T_1 with u_2, and let G_2^* be the graph obtained from G by first removing T_2 from G and then identifying the root of T_2 with u_1. Then, by Lemma 6, $W(G_1^*) < W(G)$ or $W(G_2^*) < W(G)$. Suppose that $W(G_1^*) < W(G)$. Then, according to the proof of Subcase 2, we know that $W(G_1^*) > W(C_5(S_{n-4}))$. Hence, we have $W(G) > W(C_5(S_{n-4}))$, as desired.

Subcase 4 ($k = 4$). The same argument as Subcase 3 shows that

$$W(G) = W(C_4^{u_1,u_2,u_3,u_4})(T_1, T_2, T_3, T_4) > W(C_5(S_{n-4})). \quad (19)$$

Case 3 ($m = 3$). For convenience, we distinguish the following three cases.

Subcase 5 ($k = 1$). In this case, $G = C_3(T_1)$. Let $C_3(T_{n-6,1}^2)$ be the graph shown in Figure 1(b) . Then, it is well known that S_{n-3}, $T_{n-5,1}^1$, and $T_{n-6,1}^2$ has the minimum, second minimum, and third minimum of Wiener index in $\mathcal{T}_{n-2}$. Since $G \ncong S_n + e, C_3(T_{n-5,1}^1)$, we know $T_1 \ncong S_{n-2}, T_{n-5,1}^1$. By Lemma 1,

$$\begin{aligned} W(G) &= W(C_3(T_1)) = W(C_3) + (n - 3)d_u(C_3) \\ &\quad + 3d_{u_1}(T_1) + W(T_1). \end{aligned} \quad (20)$$

Noticing that $W(T_1) \geq W(T_{n-6,1}^2)$ and $d_{u_1}(T_1) \geq d_{u_1}(T_{n-6,1}^2)$, we readily have

$$W(G) \geq W(C_3(T_{n-6,1}^2)) = n^2 - 8 > W(C_5(S_{n-4})). \quad (21)$$

Subcase 6 ($k = 2$). In this case, $G = C_3^{u_1,u_2}(T_1, T_2)$. Without loss of generality, we assume that $l_1 \leq l_2$. Now, we consider the following two cases:

(1) $l_1 = 1$. In this case, $T_1 \cong S_2$. By Lemma 1,

$$\begin{aligned} W(G) &= W(C_3^{u_1,u_2}(S_2, T_2)) = W(C_3) + (n - 3)\omega + (m - 1) \\ &\quad \cdot (d_{u_1}(S_2) + d_{u_2}(T_2)) + W(S_2) + W(T_2) \\ &\quad + l_1 d_{u_2}(T_2) + l_1 l_2 d_{C_3}(u_1, u_2) + l_2 d_{u_1}(S_2). \end{aligned} \quad (22)$$

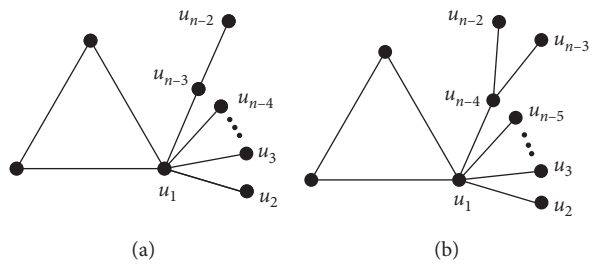

Figure 1: Unicyclic graphs $C_3(T^1_{n-5,1})$ (a) and $C_3(T^1_{n-6,2})$ (b).

Since $G \ncong C_3^{u_1,u_2}(S_2, S_{n-3})$, we have $T_2 \ncong S_{n-3}$. So $W(T_2) \geq W(T^1_{n-6,1})$ and $d_{u_2}(T_2) \geq d_{u_2}(T^1_{n-6,1})$. It thus follows that

$$W(G) = W(C_3^{u_1,u_2}(S_2, T_2)) \geq W\left(C_3^{u_1,u_2}\left(S_2, T^1_{n-6,1}\right)\right). \tag{23}$$

Again By Lemma 1, simple computation shows that $W(C_3^{u_1,u_2}(S_2, T^1_{n-6,1})) = n^2 - 7$. Hence, we have $W(G) \geq W(C_3^{u_1,u_2}(S_2, T^1_{n-6,1})) = n^2 - 7 > n^2 - 10 = W(C_5(S_{n-4}))$.

(2) $l_1 \geq 2$. In this case, it is obvious that $G \ncong C_3^{u_1,u_2}(S_2, S_{n-3})$. By Lemma 2,

$$W(G) = W(C_3^{u_1,u_2}(T_1, T_2)) \geq W\left(C_3^{u_1,u_2}\left(S_{l_1+1}, S_{l_2+1}\right)\right). \tag{24}$$

It has been computed in [24] that

$$W\left(C_3^{u_1,u_2}\left(S_{l_1+1}, S_{l_2+1}\right)\right) = n^2 - 2n + l_1 l_2. \tag{25}$$

Bearing in mind that $l_1 \geq 2$ and $l_1 + l_2 = n - 3$, we readily have

$$\begin{aligned} W\left(C_3^{u_1,u_2}\left(S_{l_1+1}, S_{l_2+1}\right)\right) &= n^2 - 2n + l_1 l_2 \geq n^2 - 2n \\ &\quad + 2(n-5) = n^2 - 10, \end{aligned} \tag{26}$$

with equality if and only if $l_1 = 2$ and $l_2 = n - 5$. Hence,

$$\begin{aligned} W(G) &= W(C_3^{u_1,u_2}(T_1, T_2)) \geq W\left(C_3^{u_1,u_2}\left(S_{l_1+1}, S_{l_2+1}\right)\right) \\ &\geq W(C_3^{u_1,u_2}(S_3, S_{n-4})) = n^2 - 10, \end{aligned} \tag{27}$$

with equality if and only if $G \cong C_3^{u_1,u_2}(S_3, S_{n-4})$.

Subcase 7 ($k = 3$). In this case, $G = C_3^{u_1,u_2,u_3}(T_1, T_2, T_3)$. It has been shown in [24] that

$$W(G) \geq W\left(C_3^{u_1,u_2,u_3}\left(S_{l_1+1}, S_{l_2+1}, S_{l_3+1}\right)\right) = n^2 - 2n + l_1 l_2 + l_1 l_3 + l_2 l_3. \tag{28}$$

Since $l_1 + l_2 + l_3 = n - 3$, we have

$$\begin{aligned} l_1 l_2 + l_1 l_3 + l_2 l_3 &= l_1 l_2 + (l_1 + l_2) l_3 = l_1 l_2 + (l_1 + l_2) \\ &\quad \cdot (n - 3 - (l_1 + l_2)). \end{aligned} \tag{29}$$

If $l_1 + l_2 = n - 4$, then $l_1 l_2 \geq n - 5$ and thus $l_1 l_2 + l_1 l_3 + l_2 l_3 \geq n - 5 + (n-4)(n - 3 - (n-4)) = 2n - 9$; otherwise, $2 \leq l_1 + l_2 \leq n - 5$, then $l_1 l_2 \geq 1$ and thus $l_1 l_2 + l_1 l_3 + l_2 l_3 \geq 1 + (n-5)(n - 3 - (n-5)) = 2n - 9$. Hence, in both cases, we have $l_1 l_2 + l_1 l_3 + l_2 l_3 \geq 2n - 9$ and consequently,

$$\begin{aligned} W(G) &\geq W\left(C_3^{u_1,u_2,u_3}\left(S_{l_1+1}, S_{l_2+1}, S_{l_3+1}\right)\right) \geq n^2 - 2n \\ &\quad + (2n - 9) = n^2 - 9 > n^2 - 10. \end{aligned} \tag{30}$$

□

3.2. Unicyclic Graphs with the Fourth Maximum Wiener Index. Unicyclic graphs with the first three largest Wiener indices were first characterized by Tang and Deng [24], but one extremal graph was missed. Then, Nasiri et al. [25] gave a complete characterization.

Theorem 3 (see [25]). *Suppose $G = C_m^{u_1,u_2,\ldots,u_k}(T_1, T_2, \ldots, T_k)$ is a unicyclic graph of order n, with $n \geq 6$. If $G \ncong C_3(P_{n-2}), C_4(P_{n-3})$, and $C_3^{u_1,u_2}(P_2, P_{n-3})$, then*

$$\begin{aligned} W(G) &\leq W(C_3(T(n-5,1,1))) < W(C_4(P_{n-3})) \\ &= W(C_3^{u_1,u_2}(P_2, P_{n-3})) < W(C_3(P_{n-2})), \end{aligned} \tag{31}$$

with equality if and only if $G = C_3(T(n-5,1,1))$. Here, $T(n-5,1,1)$ is a unicyclic graph depicted in Figure 2(a).

Now, we characterize unicyclic graphs with the fourth largest Wiener indices.

Theorem 4. *Suppose that $G = C_m^{u_1,u_2,\ldots,u_k}(T_1, T_2, \ldots, T_k)$ is a unicyclic graph of order n, with $n \geq 8$. If $G \ncong C_3(P_{n-2}), C_4(P_{n-3}), C_3^{u_1,u_2}(P_2, P_{n-3})$, and $C_3(T(n-5,1,1))$, then*

$$\begin{aligned} W(G) &\leq W(C_3^{u_1,u_2}(P_3, P_{n-4})) < W(C_3(T(n-5,1,1))) \\ &< W(C_4(P_{n-3})) \\ &= W(C_3^{u_1,u_2}(P_2, P_{n-3})) < W(C_3(P_{n-2})), \end{aligned} \tag{32}$$

with equality if and only if $G = C_3^{u_1,u_2}(P_3, P_{n-4})$.

Proof. By Lemma 1, it is easily computed that for $n \geq 8$,

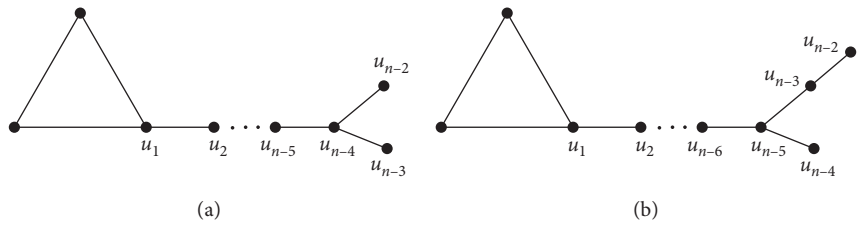

Figure 2: Unicyclic graphs $C_3(T(n-5,1,1))$ (a) and $C_3(T(n-6,1,2))$ (b).

$$\begin{aligned}\frac{1}{6}\left(n^3-19n+72\right) &= W\left(C_3^{u_1,u_2}\left(P_3,P_{n-4}\right)\right)\\ &< \frac{1}{6}\left(n^3-13n+30\right) = W\left(C_3\left(T\left(n-5,1,1\right)\right)\right).\end{aligned} \tag{33}$$

Hence, according to Theorem 4, we only need to show that for $n \geq 8$, if $G \ncong C_3(P_{n-2}), C_4(P_{n-3})$, $C_3^{u_1,u_2}(P_2,P_{n-3})$, and $C_3(T(n-5,1,1))$, then $W(G) \leq W(C_3^{u_1,u_2}(P_3,P_{n-4}))$, with equality if and only if $G \cong C_3^{u_1,u_2}(P_3,P_{n-4})$. To prove our result, we distinguish the following three cases according to m. □

Case 4 ($m \geq 5$). In this case, we consider two subcases that $k=0$ and $k \geq 1$.

Subcase 8 ($k=0$). In this case $G \cong C_n$. If n is even, then

$$\begin{aligned}W\left(C_n\right) - W\left(C_3^{u_1,u_2}\left(P_3,P_{n-4}\right)\right) &= \frac{1}{8}n^3 - \frac{1}{6}\left(n^3-19n+72\right)\\ &= -\frac{1}{24}n^3 + \frac{19}{6}n - 12 < 0.\end{aligned} \tag{34}$$

If n is odd, then

$$\begin{aligned}W\left(C_n\right) - W\left(C_3^{u_1,u_2}\left(P_3,P_{n-4}\right)\right) &= \frac{1}{8}n\left(n^2-1\right)\\ &- \frac{1}{6}\left(n^3-19n+72\right) = -\frac{1}{24}n^3 + \frac{73}{24}n - 12 < 0.\end{aligned} \tag{35}$$

Hence, $W(G) < W(C_3^{u_1,u_2}(P_3,P_{n-4}))$ as desired.

Subcase 9 ($k \geq 1$). By Lemmas 2 and 4,

$$W(G) \leq W\left(C_m^{u_1,u_2,\ldots,u_k}\left(P_{l_1+1},P_{l_2+1},\ldots,P_{l_k+1}\right)\right) \leq W\left(C_m\left(P_{l+1}\right)\right). \tag{36}$$

We now prove that $W(C_m(P_{l+1})) < W(C_3^{u_1,u_2}(P_3,P_{n-4}))$. We first assume that m is even. Then, $m \geq 6$ and by Lemma 1,

$$W\left(C_m\left(P_{l+1}\right)\right) = \frac{1}{6}\left[n^3 + \left(-\frac{3}{2}m^2+3m-1\right)n + \left(\frac{5}{4}m^3-3m^2+m\right)\right]. \tag{37}$$

Thus,

$$\begin{aligned}&W\left(C_3^{u_1,u_2}\left(P_3,P_{n-4}\right)\right) - W\left(C_m\left(P_{l+1}\right)\right)\\ &= \frac{1}{6}\left(n^3-19n+72\right) - \frac{1}{6}\left[n^3 + \left(-\frac{3}{2}m^2+3m-1\right)n\right.\\ &\quad \left. + \left(\frac{5}{4}m^3-3m^2+m\right)\right]\\ &= \frac{1}{4}\left(m^2-2m-12\right)n - \frac{1}{24}\left(5m^3-12m^2+4m-288\right)\\ &\geq \frac{1}{4}\left(m^2-2m-12\right)m - \frac{1}{24}\left(5m^3-12m^2+4m-288\right)\\ &= \frac{1}{24}m^3 - \frac{19}{6}m + 12 > 0.\end{aligned} \tag{38}$$

Now assume that m is odd. Then, $m \geq 5$ and by Lemma 1

$$\begin{aligned}W\left(C_m\left(P_{l+1}\right)\right) = \frac{1}{6}\left[n^3 + \left(-\frac{3}{2}m^2+3m-1\right)n + \left(\frac{5}{4}m^3-3m^2+m\right)\right.\\ \left. - \frac{1}{4}n + \frac{1}{8}m\right].\end{aligned} \tag{39}$$

Thus,

$$\begin{aligned}&W\left(C_3^{u_1,u_2}\left(P_3,P_{n-4}\right)\right) - W\left(C_m\left(P_{l+1}\right)\right)\\ &= \frac{1}{6}\left(n^3-19n+72\right) - \frac{1}{6}\left[n^3 + \left(-\frac{3}{2}m^2+3m-1\right)n\right.\\ &\quad \left. + \left(\frac{5}{4}m^3-3m^2+m\right)\right] + \frac{1}{4}n - \frac{1}{8}m\\ &= \frac{1}{4}\left(m^2-2m-11\right)n - \frac{1}{24}\left(5m^3-12m^2+7m-288\right)\\ &\geq \frac{1}{4}\left(m^2-2m-11\right)m - \frac{1}{24}\left(5m^3-12m^2+7m-288\right)\\ &= \frac{1}{24}m^3 - \frac{73}{24}m + 12 > 0.\end{aligned} \tag{40}$$

Therefore, we could conclude that $W(C_m(P_{l+1})) < W(C_3^{u_1,u_2}(P_3,P_{n-4}))$. □

Case 5 ($m=4$). We consider subcases that $k=1,2,3$, or 4.

Subcase 10 ($k = 1$). In this case, $G = C_4(T_1)$ with T_1 being a tree of order $n-3$. By assumption, $G \ncong C_4(P_{n-3})$ and so $T_1 \ncong P_{n-3}$. By Lemma 1,

$$W(G) = W(C_4(T_1)) = W(C_4) + (n-3)\omega + 3d_{u_1}(T_1) + W(T_1). \tag{41}$$

Noticing that $T(n-6,1,1)$ has the second maximum Wiener index in $\mathcal{T}_{n-3}$ and $d_{T_1}(u_1) \le d_{T(n-6,1,1)}(u_1)$, we have

$$\begin{aligned} W(G) &= W(C_4(T_1)) \le W(C_4(T(n-6,1,1))) \\ &= \frac{1}{6}\left(n^3 - 19n + 54\right). \end{aligned} \tag{42}$$

Thus, we have

$$\begin{aligned} W(G) &\le \frac{1}{6}\left(n^3 - 19n + 54\right) < \frac{1}{6}\left(n^3 - 19n + 72\right) \\ &= W(C_3^{u_1,u_2}(P_3, P_{n-4})), \end{aligned} \tag{43}$$

as desired.

Subcase 11 ($k = 2$). By Lemma 2, we have

$$W(G) = W(C_4^{u_1,u_2}(T_1,T_2)) \le W\left(C_4^{u_1,u_2}\left(P_{l_1+1}, P_{l_2+1}\right)\right). \tag{44}$$

In addition, it has been shown in [24] that

$$\begin{aligned} &W(C_3^{u_1,u_2}(P_3, P_{n-4})) - W\left(C_4^{u_1,u_2}\left(P_{l_1+1}, P_{l_2+1}\right)\right) \\ &\quad = (3-\alpha)l_1 l_2 - n + 6, \end{aligned} \tag{45}$$

where $\alpha = 1$ if u_1 and u_2 are adjacent and 2, otherwise. Bearing in mind that $l_1 + l_2 = n-4$, $l_1 l_2 \ge n-5$ and

$$\begin{aligned} &W(C_3^{u_1,u_2}(P_3, P_{n-4})) - W\left(C_4^{u_1,u_2}\left(P_{l_1+1}, P_{l_2+1}\right)\right) \\ &\quad > (3-2)(n-5) - n + 6 = 1 > 0. \end{aligned} \tag{46}$$

So we have $W(C_3^{u_1,u_2}(P_3, P_{n-4})) - W(G) > 0$ as desired.

Subcase 12 ($k = 3$ or $k = 4$). In this case, it has been shown in [24] that

$$\begin{aligned} W(C_4^{u_1,u_2,u_3})(T_1,T_2,T_3) &\le W(C_4^{u_1,u_2,u_3})\left(P_{l_1+1}, P_{l_2+1}, P_{l_3+1}\right) \\ &< W(C_4(T(n-6,1,1))), \\ W(C_4^{u_1,u_2,u_3,u_4})(T_1,T_2,T_3,T_4) &\le W(C_4^{u_1,u_2,u_3,u_4}) \\ &\quad \left(P_{l_1+1}, P_{l_2+1}, P_{l_3+1}, P_{l_4+1}\right) \\ &< W(C_4(T(n-6,1,1))). \end{aligned} \tag{47}$$

As shown in Subcase 10, $W(C_4(T(n-6,1,1))) < W(C_3^{u_1,u_2}(P_3, P_{n-4}))$. Thus, it is done.

Case 6 ($m = 3$). We distinguish three cases according to $k = 1, 2$, or 3.

Subcase 13 ($k = 1$). In this case, $G = C_3(T_1)$. By assumption, $C_3(T_1) \ncong C_3(P_{n-2}), C_3(T(n-5,1,1))$ and so $T_1 \ncong P_{n-2}, T(n-5,1,1)$. By Lemma 1,

$$W(C_3(T_1)) = W(C_3) + W(T_1) + 2(n-3) + 2d_{T_1}(u_1). \tag{48}$$

Since $T(n-6,1,2)$ has the third maximum Wiener index in $\mathcal{T}_{n-2}$ and $T_1 \ncong P_{n-2}, T(n-5,1,1)$, we readily have $W(C_3(T_1)) \le W(C_3(T(n-6,1,2)))$. It is easily verified that

$$\begin{aligned} W(C_3(T(n-6,1,2))) &= \frac{1}{6}\left(n^3 - 19n + 48\right) \\ &< W(C_3^{u_1,u_2}(P_3, P_{n-4})), \end{aligned} \tag{49}$$

as desired.

Subcase 14 ($k = 2$). In this case, $G = C_3^{u_1,u_2}(T_1,T_2)$. Without loss of generality, we suppose that $l_1 \le l_2$. For convenience, we distinguish the following two cases:

(1) $l_1 = 1$; that is, $T_1 \cong P_2$. Since $G \ncong C_3(P_2, P_{n-3})$, $T_2 \ncong P_{n-3}$. It is easy to compute that

$$W(C_3(P_2,T_2)) = W(C_3(P_2)) + W(T_2) + 3d_{T_2}(u_2) + 2(n-4). \tag{50}$$

Since $T(n-6,1,1)$ has the second maximum Wiener index in $\mathcal{T}_{n-3}$ and $T_2 \ncong P_{n-3}$, we have

$$W(C_3(P_2,T_2)) \le W(C_3(P_2, T(n-6,1,1))) = \frac{1}{6}\left(n^3 - 19n + 54\right). \tag{51}$$

Noticing that $W(C_3(P_2, T(n-6,1,1))) < W(C_3^{u_1,u_2}(P_3, P_{n-4}))$, we complete the proof.

(2) $l_1 \ge 2$. In this case, we have

$$W(G) = W(C_3^{u_1,u_2}(T_1,T_2)) \le W\left(C_3^{u_1,u_2}\left(P_{l_1+1}, P_{l_2+1}\right)\right). \tag{52}$$

By Lemma 1, simple calculation shows that

$$W\left(C_3^{u_1,u_2}\left(P_{l_1+1}, P_{l_2+1}\right)\right) = \frac{1}{6}n^3 - \frac{7}{6}n - l_1 l_2 + 2. \tag{53}$$

On the other hand,

$$\begin{aligned} &W\left(C_3^{u_1,u_2}\left(P_{l_1+1}, P_{l_2+1}\right)\right) - W(C_3^{u_1,u_2}(P_3, P_{n-4})) \\ &= \frac{1}{6}n^3 - \frac{7}{6}n - l_1 l_2 + 2 - \frac{1}{6}\left(n^3 - 19n + 72\right) \\ &= 2n - 10 - l_1 l_2 \le 2n - 10 - 2(n-5) = 0, \end{aligned} \tag{54}$$

with equality if and only if $l_1 = 2$ (and thus, $l_2 = n - 5$), that is, if and only if $C_3^{u_1,u_2}(P_{l_1+1}, P_{l_2+1}) \cong C_3^{u_1,u_2}(P_3, P_{n-4})$. Hence, $W(G) = W(C_3^{u_1,u_2}(T_1, T_2)) \leq W(C_3^{u_1,u_2}(P_3, P_{n-4}))$, with equality if and only if $G \cong C_3^{u_1,u_2}(P_3, P_{n-4})$.

Subcase 15 ($k = 3$). By Lemma 2, we have

$$\begin{aligned} W(G) &= W\left(C_3^{u_1,u_2,u_3}(T_1, T_2, T_3)\right) \\ &\leq W\left(C_3^{u_1,u_2,u_3}\left(P_{l_1+1}, P_{l_2+1}, P_{l_3+1}\right)\right). \end{aligned} \tag{55}$$

It has been shown in [25] that

$$\begin{aligned} W\left(C_3^{u_1,u_2,u_3}\left(P_{l_1+1}, P_{l_2+1}, P_{l_3+1}\right)\right) &= \frac{1}{6}n^3 - \frac{7}{6}n + 2 \\ &\quad - (l_1l_2l_3 + l_1l_2 + l_1l_3 + l_2l_3). \end{aligned} \tag{56}$$

Hence,

$$\begin{aligned} &W\left(C_3^{u_1,u_2,u_3}\left(P_{l_1+1}, P_{l_2+1}, P_{l_3+1}\right)\right) - W\left(C_3^{u_1,u_2}(P_3, P_{n-4})\right) \\ &= \frac{1}{6}n^3 - \frac{7}{6}n + 2 - (l_1l_2l_3 + l_1l_2 + l_1l_3 + l_2l_3) \\ &\quad - \frac{1}{6}\left(n^3 - 19n + 72\right) \\ &= 2n - 10 - (l_1l_2l_3 + l_1l_2 + l_1l_3 + l_2l_3). \end{aligned} \tag{57}$$

Since it has been shown in the proof of Theorem 2 that $l_1l_2 + l_1l_3 + l_2l_3 \geq 2n - 9$, it immediately follows that

$$W\left(C_3^{u_1,u_2,u_3}\left(P_{l_1+1}, P_{l_2+1}, P_{l_3+1}\right)\right) - W\left(C_3^{u_1,u_2}(P_3, P_{n-4})\right) < 0, \tag{58}$$

and the proof is complete. □

Data Availability

No data were used to support this study.

Conflicts of Interest

The authors declare no conflicts of interest.

Authors' Contributions

All authors contributed equally to this paper.

Acknowledgments

This research was funded by the National Natural Science Foundation of China (through grant nos. 116711347 and 11861032) and the project ZR2019YQ02 by the Shandong Provincial Natural Science Foundation.

References

[1] H. Wiener, "Structural determination of paraffin boiling points," *Journal of the American Chemical Society*, vol. 69, no. 1, pp. 17–20, 1947.

[2] H. Hosoya, "Topological index. A newly proposed quantity characterizing the topological nature of structural isomers of saturated hydrocarbons," *Bulletin of the Chemical Society of Japan*, vol. 44, no. 9, pp. 2332–2339, 1971.

[3] J. Devillers and A. T. Balaban, *Topological Indices and Related Descriptors in QSAR and QSPR*, Gordon & Breach, Amsterdam, Netherlands, 1999.

[4] M. V. Diudea, I. Gutman, and L. Jäntschi, *Molecular Topology*, Nova, Huntington, NY, USA, 2001.

[5] I. Gutman, Y. Yeh, S. Lee, and Y. Luo, "Some recents in the theory of the Wiener number," *Indian Journal of Chemistry*, vol. 32A, pp. 651–661, 1993.

[6] S. Nikolić, N. Trinajstć, and Z. Mihalić, "The Wiener index: developments and applications," *Croatica Chemica Acta*, vol. 68, pp. 105–129, 1995.

[7] K. Xu, M. Liu, K. Ch. Das, I. Gutman, and B. Furtula, "A survey on graphs extremal with respect to distance-based topological indices," *MATCH Communications in Mathematical and in Computer Chemistry*, vol. 71, no. 3, pp. 461–508, 2014.

[8] I. Gutman, S. Klavžar, and B. Mohar, "Fifty years of the Wiener index," *MATCH Communications in Mathematical and in Computer Chemistry*, vol. 35, 1997.

[9] I. Gutman, S. Klavžar, and B. Mohar, "Fiftieth anniversary of the Wiener index," *Discrete Applied Mathematics*, vol. 80, 1997.

[10] J.-B. Liu, C. Wang, S. Wang, and B. Wei, "Zagreb indices and multiplicative zagreb indices of eulerian graphs," *Bulletin of the Malaysian Mathematical Sciences Society*, vol. 42, no. 1, pp. 67–78, 2019.

[11] J.-B. Liu, X.-F. Pan, F.-T. Hu, and F.-F. Hu, "Asymptotic Laplacian-energy-like invariant of lattices," *Applied Mathematics and Computation*, vol. 253, pp. 205–214, 2015.

[12] J.-B. Liu and X.-F. Pan, "Minimizing Kirchhoff index among graphs with a given vertex bipartiteness," *Applied Mathematics and Computation*, vol. 291, pp. 84–88, 2016.

[13] Y. Yang and D. J. Klein, "Resistance distance-based graph invariants of subdivisions and triangulations of graphs," *Discrete Applied Mathematics*, vol. 181, pp. 260–274, 2015.

[14] A. A. Dobrymin, I. Gutman, S. Klavžar, and P. Žigert, "Wiener index of hexagonal systems," *Acta Applicandae Mathematica*, vol. 72, no. 3, pp. 247–294, 2002.

[15] A. A. Dobrymin, R. Entriger, and I. Gutman, "Wiener index of trees: theory and applications," *Acta Applicandae Mathematica*, vol. 66, no. 3, pp. 211–249, 2001.

[16] M. Fischermann, I. Gutman, A. Hoffmann, D. Rautenbach, D. Vidovića, and L. Volkmann, "Extremal chemical trees," *Zeitschrift für Naturforschung A*, vol. 57, no. 9-10, pp. 49–51, 2002.

[17] I. Gutman, L. Popovic, P. V. Khadikar, S. Karmarkar, S. Joshi, and M. Mandloi, "Relations between Wiener and Szeged indices of monocyclic molecules," *MATCH Communications in Mathematical and in Computer Chemistry*, vol. 35, pp. 91–103, 1997.

[18] Z. Du and B. Zhou, "A note on Wiener indices of unicyclic graphs," *Ars Combinatoria*, vol. 93, pp. 97–103, 2009.

[19] Z. Du and B. Zhou, "Minimum Wiener indices of trees and unicyclic graphs of given matching number," *MATCH*

Communications in Mathematical and in Computer Chemistry, vol. 63, no. 1, pp. 101–112, 2010.

[20] G. Yu and L. Feng, "On the Wiener index of unicyclic graphs with given girth," *Ars Combinatoria*, vol. 94, pp. 361–369, 2010.

[21] Y. Chen and X. Zhang, "The Wiener index of unicyclic graphs with girth and the matching number," *Mathematics*, vol. 2, pp. 1–15, 2011.

[22] Y. Hong, H. Liu, and X. Wu, "On the Wiener index of unicyclic graphs," *Hacettepe Journal of Mathematics and Statistics*, vol. 40, no. 1, pp. 63–68, 2011.

[23] Z. Du, "Wiener indices of trees and monocyclic graphs with given bipartition," *International Journal of Quantum Chemistry*, vol. 112, no. 6, pp. 1598–1605, 2012.

[24] Z. Tang and H. Deng, "The (n, n)-graphs with the first three extremal Wiener indices," *Journal of Mathematical Chemistry*, vol. 43, no. 1, pp. 60–74, 2008.

[25] R. Nasiri, H. Yousefi-Azari, M. R. Darafsheh, and A. R. Ashrafi, "Remarks on the Wiener index of unicyclic graphs," *Journal of Applied Mathematics and Computing*, vol. 41, no. 1-2, pp. 49–59, 2013.

Hindawi
Journal of Chemistry
Volume 2020, Article ID 5398109, 14 pages
https://doi.org/10.1155/2020/5398109

Research Article

Hosoya and Harary Polynomials of Hourglass and Rhombic Benzenoid Systems

Zhong-Lin Cheng,[1] Ashaq Ali,[2] Haseeb Ahmad,[3,4] Asim Naseem,[5] and Maqbool Ahmad Chaudhary[2]

[1]*Teaching Department of Public Basic Course, Anhui International Studies University, Hefei 231201, China*
[2]*Department of Mathematics and Statistics, University of Lahore, Lahore 54000, Pakistan*
[3]*Department of Mathematics, Lahore Leads University, Lahore, Pakistan*
[4]*Department of Mathematics, COMSATS University Islamabad, Lahore Campus, Lahore, Pakistan*
[5]*Department of Mathematics, Government College University, Lahore, Pakistan*

Correspondence should be addressed to Haseeb Ahmad; haseeb.ahmad@leads.edu.pk

Received 25 September 2019; Accepted 5 December 2019; Published 9 April 2020

Guest Editor: Shaohui Wang

In the fields of chemical graph theory, topological index is a type of a molecular descriptor that is calculated based on the graph of a chemical compound. In 1947, Harry Wiener introduced "path number" which is now known as Wiener index and is the oldest topological index related to molecular branching. Hosoya polynomial plays a vital role in determining Wiener index. In this report, we compute the Hosoya polynomials for hourglass and rhombic benzenoid systems and recover Wiener and hyper-Wiener indices from them.

1. Introduction

Cheminformatics is a new branch of science which relates chemistry, mathematics, and computer sciences. Quantitative structure-activity (QSAR) and structure-property relationships (QSPR) are the main components of cheminformatics which are helpful to study physicochemical properties of chemical compounds [1–3].

A topological index is a numeric quantity associated with a graph which characterizes the topology of graph and is invariant under graph automorphism [4–8]. There are numerous applications of graph theory in the field of structural chemistry. The first well-known use of a topological index in chemistry was by Wiener in the study of paraffin boiling points [9]. After that, in order to explain physicochemical properties, various topological indices have been introduced.

The Hosoya polynomial of a graph is a generating function about distance distribution, introduced by *Haruo Hosoya* in 1988 [10]. This polynomial has many chemical applications [11]; in particular, Wiener index can be directly obtained from the polynomial and studied extensively [12–14].

The Wiener index was first introduced by Harold Wiener in 1947 to study the boiling points of paraffin [9]. It plays an important role in the so-called inverse structure-property relationship problems [15]. For more details about this topological polynomial and index, see the paper series and the references therein [16–20]. In this report, we study Hosoya polynomials, Wiener index, and hyper-Wiener index of hourglass and rhombic benzenoid systems.

2. Preliminaries

Definition 1 (simple graph). A simple graph $G = (V, E)$ is a finite nonempty set $V(G)$ of objects called vertices together with a (possibly empty) set $E(G)$ of unordered pairs of distinct vertices of G called edges.

Definition 2 (Hosoya polynomial [10]). The Hosoya polynomial of a connected graph G is denoted by $H(G,x)$ and defined as follows:

$$H(G,x)=\frac{1}{2}\sum_{v\in V(G)}\sum_{u\in V(G)}x^{d(v,u)}, \tag{1}$$

where $d(u,v)$ denotes the distance between vertices u and v.

Definition 3 (Wiener index [9]). The Wiener index of a connected graph G is denoted by $W(G)$ and defined as the sum of distances between all pairs of vertices in G, i.e., it can be formulated as follows:

$$W(G)=\frac{1}{2}\sum_{v\in V(G)}\sum_{u\in V(G)}d(u,v). \tag{2}$$

Note that the first derivative of the Hosoya polynomial at $x=1$ is equal to the Wiener index:

$$W(G)=\left.\frac{\partial H(G)}{\partial x}\right|_{x=1}. \tag{3}$$

Definition 4 (modified Wiener index). The modified Wiener index of a connected graph G is denoted by $W_\lambda(G)$ and defined as the sum of λ power distances between all pairs of vertices in G, where $\lambda=1,2,3,4,\ldots$ i.e., it can be formulated as follows:

$$W(G)=\frac{1}{2}\sum_{v\in V(G)}\sum_{u\in V(G)}d(u,v)^{\lambda}. \tag{4}$$

For detailed survey about this index, see [21–23].

Definition 5 (hyper-Wiener index). Hyper-Wiener index is another distance-based graph invariants used for predicting physicochemical properties of organic compounds [24]. The hyper-Wiener index was introduced by Randić [25] as follows:

$$WW(G)=\frac{1}{2}\sum_{v\in V(G)}\sum_{u\in V(G)}\left(d(u,v)+d(u,v)^2\right). \tag{5}$$

Definition 6 (modified hyper-Wiener index). Modified hyper-Wiener index (see [26, 27]) of a connected graph G is denoted by $WW_\lambda(G)$ and defined as follows:

$$WW_\lambda(G)=\frac{1}{2}\sum_{v\in V(G)}\sum_{u\in V(G)}\left(d(u,v)^{\lambda}+d(u,v)^{2\lambda}\right), \tag{6}$$

where $\lambda=1,2,3,4,\ldots$.

Definition 7 (Harary polynomial). The Harary polynomial (see [28, 29]) of a connected graph G is denoted by $h(G)$ and defined as follows:

$$h(G)=\sum_{v\in V(G)}\sum_{u\in V(G)}\frac{1}{d(v,u)}x^{d(v,u)}. \tag{7}$$

Definition 8 (generalized Harary index). The generalized Harary index (see [30, 31]) of a connected graph G is denoted by $h_t(G)$ and defined as follows:

$$h_t(G)=\sum_{v\in V(G)}\sum_{u\in V(G)}\frac{1}{d(v,u)}+t, \tag{8}$$

where $t=1,2,3,4,\ldots$.

Definition 9 (multiplicative Wiener index). The multiplicative wiener index (see [32, 33]) of a connected graph G is denoted by $\pi(G)$ and defined as follows:

$$\pi(G)=\prod_{u,v\subseteq V(G)}d(u,v). \tag{9}$$

For detailed applications of topological indices in chemistry, we refer [34–41] and the references therein.

3. Methodology

To compute the Hosoya polynomial of a graph G, we need to compute number of pairs of vertices at distance $1,2,3,\ldots\operatorname{dia}(G)$, where $\operatorname{dia}(G)=\max\{d(u,v);u,v\in V(G)\}$. For this purpose, we use mathematical induction. Here, the $\operatorname{dia}(X_n)=4n-1$ and $\operatorname{dia}(R_n)=2n+1$. The general view of Hosoya polynomial is as below, where d is the diameter of graph.

$$H(G;x)=a_0(n)x^0+a_1(n)x^1+a_2(n)x^2+\cdots+a_d(n)x^d. \tag{10}$$

4. Computational Results

Benzenoid hydrocarbons play a vital role in our environment and in the food and chemical industries. Benzenoid molecular graphs are systems with deleted hydrogens. It is a connected geometric figure obtained by arranging congruent regular hexagons in a plane, so that two hexagons are either disjoint or have a common edge. This figure divides the plane into one infinite (external) region and a number of finite (internal) regions. All internal regions must be regular hexagons. Benzenoid systems are of considerable importance in theoretical chemistry because they are the natural graph representation of benzenoid hydrocarbons. A vertex of a hexagonal system belongs to, at most, three hexagons. A vertex shared by three hexagons is called an internal vertex.

Definition 10 (benzenoid hourglass system). Let X_n denotes the benzenoid hourglass, which is obtained from two copies of a triangular benzenoid T_n by overlapping their external hexagons (Figure 1).

4.1. Results for Benzenoid Hourglass System. The benzenoid hourglass system has $2(n^2+4n-2)$ vertices and $3n^2+9n-6$ edges.

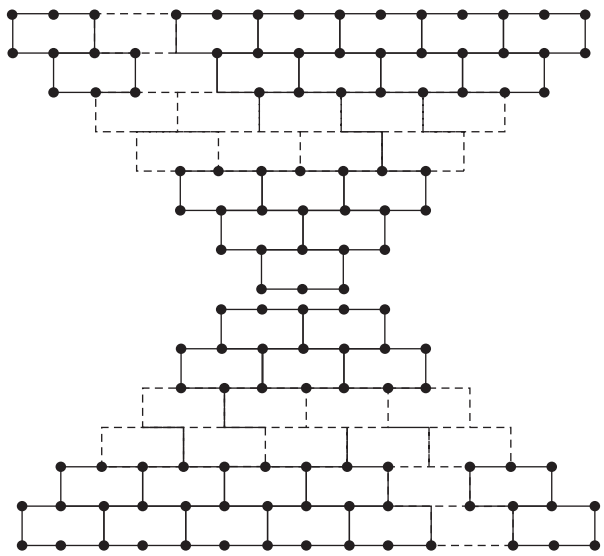

Figure 1: Benzenoid hourglass system X_n.

Theorem 1. *For the benzenoid hourglass system X_n, we have*

$$\begin{aligned} H(X_n;x) &= 2\left(n^2+4n-2\right)+\left(3n^2+9n-6\right)+\left(6n^2+12n-12\right)x^2 \\ &+\sum_{m\equiv 1\bmod(2),1<m\le 2n}\left(\frac{19m^3}{24}-3m^2n-5m^2+3mn^2+12mn+\frac{221m}{24}-17\right)x^m \\ &+\sum_{m\equiv 0\bmod(2),2<m\le 2n}\left(\frac{19m^3}{24}-3m^2n-5m^2+3mn^2+12mn+\frac{59m}{6}-20\right)x^m \\ &+\sum_{m\equiv 0\bmod(2),2\le m\le 2n-2}\left(-\frac{m^3}{24}-\frac{m^2n}{4}+\frac{mn^2}{2}+\frac{n^3}{3}-m^2+4n^2-\frac{35m}{6}+\frac{23n}{3}-4\right)x^{2n+m} \\ &+\sum_{m\equiv 1\bmod(2),3\le m\le 2n-2}\left(\frac{m^3}{24}-\frac{m^2n}{4}-m^2+\frac{mn^2}{2}-\frac{143m}{24}+\frac{n^3}{3}+4n^2+\frac{101n}{12}-5\right)x^{2n+m} \\ &+\left(\frac{133n}{6}+\frac{11(n-1)^2}{2}+\frac{(n-1)^3}{3}-\frac{127}{6}\right)x^{2n+1}+\left(n^2+2\right)x^{4n-1}. \end{aligned} \tag{11}$$

Proof. To prove this theorem, we need to compute $|a_m(n)|$ where $m=1,2,3,\ldots,4n-1$. It is easy to verify that

$$\begin{aligned} \left|a_0(n)\right| &= |V| = 2\left(n^2+4n-2\right), \\ \left|a_1(n)\right| &= |E| = 3n^2+9n-6, \\ \left|a_2(n)\right| &= 6n^2+12n-12. \end{aligned} \tag{12}$$

The remaining proof is divided into six parts which are according to the parity of m. □

Case 1. $m\equiv 1\bmod(2)$, $1<m\le 2n$.

It can be observed from Figure 1 that

$$\begin{aligned} \left|a_3(1)\right| &= 0, \\ \left|a_3(2)\right| &= 41, \\ \left|a_3(3)\right| &= 95, \\ \left|a_3(4)\right| &= 167, \\ \left|a_3(5)\right| &= 257. \end{aligned} \tag{13}$$

Now, one can conclude that

$$\left|a_3(n)\right| = 9(n-1)^2+27(n-1)+5. \tag{14}$$

Using a similar fashion, we have

$$\begin{aligned}|a_5(1)| &= 0,\\ |a_5(2)| &= 0,\\ |a_5(3)| &= 93,\\ |a_5(4)| &= 183,\\ |a_5(5)| &= 303,\\ |a_5(6)| &= 453.\end{aligned} \tag{15}$$

It implies that

$$|a_5(n)| = 15(n-2)^2 + 45(n-2) + 33. \tag{16}$$

In a similar fashion, we infer

$$\begin{aligned}|a_7(n)| &= 21(n-3)^2 + 63(n-3) + 74,\\ |a_9(n)| &= 27(n-4)^2 + 81(n-4) + 130,\\ |a_{11}(n)| &= 33(n-5)^2 + 99(n-5) + 203,\\ &\cdots.\end{aligned} \tag{17}$$

In terms of mathematical induction, we yield

$$\begin{aligned}|a_m(n)| &= 3m\left(n - \frac{m}{2} + \frac{1}{2}\right)^2 + 9m\left(n - \frac{m}{2} + \frac{1}{2}\right)\\ &\quad + \frac{9((m/2) - (1/2))^2}{2} + \frac{((m/2) - (1/2))^3}{3}\\ &\quad - \frac{217}{12} + \frac{73m}{12},\\ |a_m(n)| &= \frac{19m^2}{24} - 3m^2n - 5m^2 + 3mn^2 + 12mn + \frac{221m}{24} - 17.\end{aligned} \tag{18}$$

Case 2. $m \equiv 0 \bmod (2), 2 < m \le 2n$.

It can be observed from Figure 1 that

$$\begin{aligned}|a_4(1)| &= 0,\\ |a_4(2)| &= 38,\\ |a_4(3)| &= 98,\\ |a_4(4)| &= 182,\\ |a_4(5)| &= 290.\end{aligned} \tag{19}$$

Now, one can conclude that

$$|a_4(n)| = 12(n-1)^2 + 24(n-1) + 2. \tag{20}$$

By means of the same trick, we obtain

$$\begin{aligned}|a_6(1)| &= 0,\\ |a_6(2)| &= 0,\\ |a_6(3)| &= 84,\\ |a_6(4)| &= 174,\\ |a_6(5)| &= 300,\\ |a_6(6)| &= 462,\end{aligned} \tag{21}$$

which reveals that

$$|a_6(n)| = 18(n-2)^2 + 36(n-2) + 30. \tag{22}$$

In light of the similar approach, we get

$$\begin{aligned}|a_8(n)| &= 24(n-3)^2 + 48(n-3) + 72,\\ |a_{10}(n)| &= 30(n-4)^2 + 60(n-4) + 130,\\ |a_{12}(n)| &= 36(n-5)^2 + 72(n-5) + 206,\\ &\cdots.\end{aligned} \tag{23}$$

Hence, by mathematical induction, we have

$$\begin{aligned}|a_m(n)| &= 3m\left(n - \frac{m}{2} + 1\right)^2 + 6m\left(n - \frac{m}{2} + 1\right)^2\\ &\quad + 5\left(\frac{m}{2} - 1\right)^2 + \frac{((m/2) - 1)^3}{3} - \frac{74}{3} + \frac{16m}{3},\\ |a_m(n)| &= \frac{19m^3}{24} - 3m^2n - 5m^2 + 3mn^2 + 12mn + \frac{59m}{6} - 20.\end{aligned} \tag{24}$$

Case 3. $m \equiv 1 \bmod (2), 3 \le m \le 2n - 2$.

It can be observed from Figure 1 that

$$\begin{aligned}|a_5(1)| &= 0,\\ |a_7(2)| &= 0,\\ |a_9(3)| &= 44,\\ |a_{11}(4)| &= 41,\\ |a_{13}(5)| &= 101,\\ |a_{15}(6)| &= 177,\\ |a_{17}(7)| &= 274.\end{aligned} \tag{25}$$

Now, one can conclude that

$$|a_{2n+m}(n)| = \frac{(n-2)^3}{3} + \frac{15}{2}(n-2)^2 + \frac{193}{6}(n-2) + 4. \tag{26}$$

Using a similar fashion, we have

$$\begin{aligned}|a_5(1)| &= 0,\\ |a_7(2)| &= 0,\\ |a_9(3)| &= 0,\\ |a_{11}(4)| &= 0,\\ |a_{13}(5)| &= 101,\\ |a_{15}(6)| &= 150,\\ |a_{17}(7)| &= 254,\\ |a_{19}(8)| &= 383,\\ |a_{21}(9)| &= 539.\end{aligned} \tag{27}$$

It implies that

$$\left|a_{2n+m}(n)\right| = \frac{(n-3)^3}{3} + \frac{19}{2}(n-3)^2 + \frac{301}{6}(n-3) + 9. \tag{28}$$

In a similar fashion, we infer

$$\begin{aligned}
\left|a_{2n+m}(n)\right| &= \frac{(n-4)^3}{3} + \frac{23}{2}(n-4)^2 + \frac{433}{6}(n-4) + 16,\\
\left|a_{2n+m}(n)\right| &= \frac{(n-5)^3}{3} + \frac{27}{2}(n-5)^2 + \frac{589}{6}(n-5) + 25,\\
\left|a_{2n+m}(n)\right| &= \frac{(n-6)^3}{3} + \frac{31}{2}(n-6)^2 + \frac{769}{6}(n-6) + 36,\\
&\ldots.
\end{aligned} \tag{29}$$

In terms of mathematical induction, we yield

$$\begin{aligned}
\left|a_{2n+m}(n)\right| = &\left(\frac{(n-((m+1)/2))^3}{3} + \frac{1}{2}\left(4\left(\frac{m-1}{2}\right) + 11\right)\right.\\
&\cdot\left(n - \left(\frac{m+1}{2}\right)\right)^2 + \left(\frac{1}{6}\right)\left(12\left(\frac{m-1}{2}\right)^2\right.\\
&\left. + 72\left(\frac{m-1}{2}\right) + 109\right)\left(n - \left(\frac{m+1}{2}\right)\right)\\
&\left. + \left(\frac{m-1}{2}\right)^2 + 2\left(\frac{m-1}{2}\right) + 1\right),\\
\left|a_{2n+m}(n)\right| = &-\frac{m^3}{24} - \frac{m^2 n}{4} - m^2 + \frac{mn^2}{2} - \frac{143m}{24} + \frac{n^3}{3}\\
&+ 4n^2 + \frac{101n}{12} - 5.
\end{aligned} \tag{30}$$

Case 4. $m \equiv 0 \bmod (2), 2 \le m \le 2n-2$.

It can be observed from Figure 1 that

$$\begin{aligned}
\left|a_4(1)\right| &= 0,\\
\left|a_6(2)\right| &= 16,\\
\left|a_8(3)\right| &= 108,\\
\left|a_{10}(4)\right| &= 41,\\
\left|a_{12}(5)\right| &= 180,\\
\left|a_{14}(6)\right| &= 272,\\
\left|a_{16}(7)\right| &= 386.
\end{aligned} \tag{31}$$

Now, one can conclude that

$$\left|a_{2n+m}(n)\right| = \frac{(n-1)^3}{3} + 6(n-1)^2 + \frac{53}{3}(n-1) - 8. \tag{32}$$

Using a similar fashion, we have

$$\begin{aligned}
\left|a_4(1)\right| &= 0,\\
\left|a_6(2)\right| &= 0,\\
\left|a_8(3)\right| &= 0,\\
\left|a_{10}(4)\right| &= 28,\\
\left|a_{12}(5)\right| &= 86,\\
\left|a_{14}(6)\right| &= 164,\\
\left|a_{16}(7)\right| &= 264.
\end{aligned} \tag{33}$$

It implies that

$$\left|a_{2n+m}(n)\right| = \frac{(n-2)^3}{3} + 8(n-2)^2 + \frac{95}{3}(n-2) - 12. \tag{34}$$

In a similar fashion, we infer

$$\begin{aligned}
\left|a_{2n+m}(n)\right| &= \frac{(n-3)^3}{3} + 10(n-3)^2 + \frac{149}{3}(n-4) - 16,\\
\left|a_{2n+m}(n)\right| &= \frac{(n-4)^3}{3} + 12(n-4)^2 + \frac{215}{3}(n-5) - 20,\\
\left|a_{2n+m}(n)\right| &= \frac{(n-5)^3}{3} + 14(n-5)^2 + \frac{293}{3}(n-6) - 24,\\
&\ldots.
\end{aligned} \tag{35}$$

In terms of mathematical induction, we yield

$$\begin{aligned}
|a_{2n+m}(n)| = &\left(\frac{(n-(m/2))^3}{3} + \left(2\left(\frac{m}{2}\right) + 4\right)\left(n - \left(\frac{m}{2}\right)\right)^2\right.\\
&+ \left(\frac{6(m/2)^2 + 24(m/2) + 23}{3}\right)\left(n - \left(\frac{m}{2}\right)\right)\\
&\left. - 4\left(\frac{m}{2}\right) - 4\right),\\
\left|a_{2n+m}(n)\right| = &(m+4)\left(\frac{m}{2} - n\right)^2 - \left(\frac{(m/2) - n}{2}\right)^3\\
&- 2m - \left(\frac{m}{2} - n\right)\left(\frac{m^2}{2} + 4m + \frac{23}{3}\right) - 4,\\
\left|a_{2n+m}(n)\right| = &-\frac{m^3}{24} - \frac{m^2 n}{4} + \frac{mn^2}{2} + \frac{n^3}{3} - m^2 + 4n^2\\
&- \frac{35m}{6} + \frac{23n}{3} - 4.
\end{aligned} \tag{36}$$

Case 5. $m = 2n+1$.

It can be observed from Figure 1 that

$$\begin{aligned}|a_5(1)| &= 0,\\ |a_7(2)| &= 29,\\ |a_9(3)| &= 70,\\ |a_{11}(4)| &= 126,\\ |a_{13}(5)| &= 199,\\ |a_{15}(6)| &= 291,\\ |a_{17}(7)| &= 404.\end{aligned} \tag{37}$$

Now, one can conclude that

$$\begin{aligned}|a_{2n+1}(n)| &= \frac{(n-1)^3}{3} + \frac{11}{2}(n-1)^2 + \frac{133}{6}(n-1) + 1,\\ |a_{2n+1}(n)| &= \frac{133n}{6} + \frac{11(n-1)^2}{2} + \frac{(n-1)^3}{3} - \frac{127}{6}.\end{aligned} \tag{38}$$

Case 6. $m = 4n - 1$.

It can be observed from Figure 1 that

$$\begin{aligned}|a_3(1)| &= 3,\\ |a_7(2)| &= 6,\\ |a_{11}(3)| &= 11,\\ |a_{15}(4)| &= 18,\\ |a_{19}(5)| &= 27,\\ |a_{23}(6)| &= 38,\\ |a_{27}(7)| &= 51.\end{aligned} \tag{39}$$

Now, one can conclude that

$$|a_{4n-1}(n)| = n^2 + 2. \tag{40}$$

By what have been mentioned above, we get our required result.

Theorem 2. *For the benzenoid hourglass system X_n, the Harary polynomial is given by*

$$\begin{aligned}h(X_n;x) &= \left(3n^2 + 9n - 6\right)x + \left(3n^2 + 6n - 6\right)x^2\\ &+ \sum_{m\equiv 1 \bmod (2), 1<m\le 2n} \frac{1}{m}\left(\frac{19m^3}{24} - 3m^2n - 5m^2 + 3mn^2 + 12mn + \frac{221m}{24} - 17\right)x^m\\ &+ \sum_{m\equiv 0 \bmod (2), 2<m\le 2n} \frac{1}{m}\left(\frac{19m^3}{24} - 3m^2n - 5m^2 + 3mn^2 + 12mn + \frac{59m}{6} - 20\right)x^m\\ &+ \sum_{m\equiv 0 \bmod (2), 2\le m\le 2n-2} \frac{1}{2n+m}\left((m+4)\left(\frac{m}{2} - n\right)^2 - \frac{((m/2)-n)^3}{3} - 2m - \left(\frac{m}{2} - n\right)\left(\frac{m^2}{2} + 4m + \frac{23}{3}\right) - 4\right)x^{2n+m}\\ &+ \sum_{m\equiv 1 \bmod (2), 3\le m\le 2n-2} \frac{1}{2n+m}\left(-\frac{m^3}{24} - \frac{m^2n}{4} - m^2 + \frac{mn^2}{2} - \frac{143m}{24} + \frac{n^3}{3} + 4n^2 + \frac{101n}{12} - 5\right)x^{2n+m}\\ &+ \frac{1}{2n+1}\left(\frac{133n}{6} + \frac{11(n-1)^2}{2} + \frac{(n-1)^3}{3} - \frac{127}{6}\right)x^{2n+1} + \frac{1}{4n-1}\left(n^2 + 2\right)x^{4n-1}.\end{aligned} \tag{41}$$

Proof. From the information about the number of pairs of vertices at different distances given in Theorem 1, it is easy to get our desired result. □

Theorem 3. *For the benzenoid hourglass system X_n, we have*

(i) $W_\lambda(X_n) = (3n^2 + 9n - 6) + (6n^2 + 12n - 12)2^\lambda + \sum_{m\equiv 1 \bmod (2), 1<m\le 2n}((19m^3/24) - 3m^2n - 5m^2 + 3mn^2 + 12mn + (221m/24) - 17)m^\lambda + \sum_{m\equiv 0 \bmod (2), 2<m\le 2n}((19m^3/24) - 3m^2n - 5m^2 + 3mn^2 + 12mn + (59m/6) - 20)m^\lambda + \sum_{m\equiv 0 \bmod (2), 2\le m\le 2n-2}((m+4)((m/2)-n)^2 - (((m/2)-n)^3/3) - 2m - ((m/2)-n)((m^2/2) + 4m + (23/3)) - 4(2n+m)^\lambda) + + \sum_{m\equiv 1 \bmod (2), 3\le m\le 2n-2}(-(m^3/24) - (m^2n/4) - m^2 + (mn^2/2) - (143m/24) + (n^3/3) + 4n^2 + (101n/12) - 5)(2n+m)^\lambda + ((133n/6) + (11(n-1)^2/2) + ((n-1)^3/3) - (127/6))(2n+1)^\lambda + (n^2+2)(4n-1)^\lambda.$

(ii) $WW_\lambda(X_n) = (3n^2 + 9n - 6)(1^\lambda + 1^{2\lambda}) + (6n^2 + 12n - 12)(2^\lambda + 2^{2\lambda}) + \sum_{m\equiv 1 \bmod (2), 1<m\le 2n}((19m^3/24) - 3m^2n - 5m^2 + 3mn^2 + 12mn + (221m/24) - 17)(m^\lambda + m^{2\lambda}) +$

$\sum_{m\equiv 0\bmod(2),2<m\leq 2n}(((19m^3/24)-3m^2n-5m^2+3mn^2+12mn+(59m/6)-20)(m^{\lambda}+m^{2\lambda}))+\sum_{m\equiv 0\bmod(2),2\leq m\leq 2n-2}((m+4)((m/2)-n)^2-(((m/2)-n)^3/3)-2m-((m/2)-n)((m^2/2)+4m+(23/3))-4)((2n+m)^{\lambda}+(2n+m)^{2\lambda})+\sum_{m\equiv 1\bmod(2),3\leq m\leq 2n-2}(-(m^3/24)-(m^2n/4)-m^2+(mn^2/2)-(143m/24)+(n^3/3)+4n^2+(101n/12)-5)((2n+m)^{\lambda}+(2n+m)^{2\lambda})+((133n/6)+(11(n-1)^2/2+((n-1)^3/3))-(127/6))((2n+1)^{\lambda}+(2n+1)^{2\lambda})+(n^2+2)((4n-1)^{\lambda}+(4n-1)^{2\lambda})$.

(iii) $H_t(X_n)=(3n^2+9n-6)(1/(1+t))+(6n^2+12n-12)(1/(2+t))+\sum_{m\equiv 1\bmod(2),1<m\leq 2n}((19m^3/24)-3m^2n-5m^2+3mn^2+12mn+(221m/24)-17)(1/m+t)+\sum_{m\equiv 0\bmod(2),2<m\leq 2n}((19m^3/24)-3m^2n-5m^2+3mn^2+12mn+(59m/6)-20)(1/m+t)+\sum_{m\equiv 0\bmod(2),2\leq m\leq 2n-2}((m+4)((m/2)-n)^2-((m/2)-n)^3/3)-2m((m/2)-n)((m/2)-n)((m^2/2)4m+(23/3)-4)(1/2n+m+t)+\sum_{m\equiv 1\bmod(2),3\leq m\leq 2n-2}(-(m^3/24)-(m^2n/4)-m^2+(mn^2/2)-(143m/24)+(n^3/3)+4n^2+(101n/12)-5)(1/2n+m+t)+((133n/6)+(11(n-1)^2/2)+((n-1)^3/3)-(127/6))(1/2n+1+t)+(n^2+2)(1/4n-1+t)$.

(iv) $\pi(X_n)=1^{(3n^2+9n-6)}\times 2^{(6n^2+12n-12)}\times\prod_{m\equiv 1\bmod(2),1<m\leq 2n}m^{((19m^3/24)-3m^2n-5m^2+3mn^2+12mn+(221m/24)-17)}\times\prod_{m\equiv 0\bmod(2),2<m\leq 2n}m^{((19m^3/24)-3m^2n-5m^2+3mn^2+12mn+(59m/6)-20)}\times\prod_{m\equiv 0\bmod(2),2\leq m\leq 2n-2}(2n+m)^{((m+4)((m/2)-n)^2-(((m/2)-n)^3/3)-2m-((m/2)-n)((m^2/2)+4m+(23/3))-4)}\times\prod_{m\equiv 1\bmod(2),3\leq m\leq 2n-2}(2n+m)^{(-(m^3/24)-(m^2n/4)-m^2+(mn^2/2)-(143m/24)+(n^3/3)+4n^2+(101n/12)-5)}\times(2n+1)^{((133n/6)+(11(n-1)^2/2)+((n-1)^3/3)-(127/6))}\times(4n-1)^{(n^2+2)}$.

From the above theorem, we get the following results immediately.

Corollary 1. *For the benzenoid hourglass system X_n, we have*

$$W(X_n)=\frac{52n^5}{15}+\frac{80n^4}{3}+34n^3-\frac{116n^2}{3}-\frac{37n}{15}+4. \tag{42}$$

Corollary 2. *For the benzenoid hourglass system X_n, we have*

$$\begin{aligned}WW(X_n)=&\frac{4n^5}{3}+36n^4+\frac{217n^3}{3}+92n^2+\frac{31n}{3}-116\\&+\sum_{m\equiv 1\bmod(2),1<m\leq 2n}m(m+1)\left(\frac{19m^3}{24}-3m^2n-5m^2+3mn^2+12mn+\frac{221m}{24}-17\right)\\&+\sum_{m\equiv 0\bmod(2),2<m\leq 2n}m(m+1)\left(\frac{19m^3}{24}-3m^2n-5m^2+3mn^2+12mn+\frac{59m}{6}-20\right)\\&+\sum_{m\equiv 0\bmod(2),2\leq m\leq 2n-2}\left(2n+m+(2n+m)^2\right)\left((m+4)\left(\frac{m}{2}-n\right)^2-\frac{((m/2)-n)^3}{3}-2m-\left(\frac{m}{2}-n\right)\left(\frac{m^2}{2}+4m+\frac{23}{3}\right)-4\right)\\&+\sum_{m\equiv 1\bmod(2),3\leq m\leq 2n-2}\left(2n+m+(2n+m)^2\right)\left(-\frac{m^3}{24}-\frac{m^2n}{4}-m^2+\frac{mn^2}{2}-\frac{143m}{24}+\frac{n^3}{3}+4n^2+\frac{101n}{12}-5\right).\end{aligned} \tag{43}$$

Corollary 3. *The Harary index of benzenoid hourglass graph X_n is as follows:*

$$\begin{aligned} h(X_n) = {} & \frac{296n^4 + 910n^3 - 161n^2 - 667n + 180}{6(8n^2 + 2n - 1)} \\ & + \sum_{m \equiv 1 \bmod (2), 1 < m \le 2n} \frac{1}{m}\left(\frac{19m^3}{24} - 3m^2 n - 5m^2 + 3mn^2 + 12mn + \frac{221m}{24} - 17\right) \\ & + \sum_{m \equiv 0 \bmod (2), 2 < m \le 2n} \frac{1}{m}\left(\frac{19m^3}{24} - 3m^2 n - 5m^2 + 3mn^2 + 12mn + \frac{59m}{6} - 20\right) \\ & + \sum_{m \equiv 0 \bmod (2), 2 \le m \le 2n-2} \frac{1}{2n+m}\left((m+4)\left(\frac{m}{2} - n\right)^2 - \frac{((m/2) - n)^3}{3} - 2m - \left(\frac{m}{2} - n\right)\left(\frac{m^2}{2} + 4m + \frac{23}{3}\right) - 4\right) \\ & + \sum_{m \equiv 1 \bmod (2), 3 \le m \le 2n-2} \frac{1}{2n+m}\left(-\frac{m^3}{24} - \frac{m^2 n}{4} - m^2 + \frac{mn^2}{2} - \frac{143m}{24} + \frac{n^3}{3} + 4n^2 + \frac{101n}{12} - 5\right). \end{aligned} \tag{44}$$

4.2. Benzenoid Rhombus System. Consider a benzenoid system in which hexagons are arranged to form a rhombic shape, say, R_n, where n represents number of hexagons along each boundary of the rhombic as given in Figure 2.

Lemma 1. *The benzenoid rhombus system has $2n^2 + 4n$ vertices and $3n^2 + 4n - 1$ edges.*

Theorem 4. *For the benzenoid rhombus system R_n, we have*

$$\begin{aligned} H(R_n; x) = {} & 2n^2 + 4n + \left(3n^2 + 4n - 1\right)x + \left(6n^2 + 4n - 4\right)x^2 \\ & + \sum_{m \equiv 1 \bmod (2), 1 < m \le 2n+1} \left(3mn^2 - 2m^2 n + \frac{7m^3}{24} + 6mn - 2m^2 + \frac{41m}{24} - 1\right)x^m \\ & + \sum_{m \equiv 0 \bmod (2), 2 < m \le 2n} \left(3mn^2 - 2m^n + \frac{7m^3}{24} + 6mn - 2m^2 + \frac{11m}{6} - 2\right)x^m \\ & + \sum_{m \equiv 1 \bmod (2), 1 \le m \le 2n-3} \left(\frac{(-m + 2n - 2)^3}{24} + \frac{(-m + 2n - 2)^2}{2} + \frac{23(-m + 2n - 2)}{24} - \frac{1}{2}\right)x^{2n+m+2} \\ & + \sum_{m \equiv 0 \bmod (2), 2 \le m \le 2n-2} \frac{(-m + 2n)^3}{24}\left(+\frac{(-m + 2n)^2}{2} + \frac{5(-m + 2n)}{6}\right)x^{2n+m}. \end{aligned} \tag{45}$$

Proof. To prove this theorem, we need to compute $|a_m(n)|$ where $p = 1, 2, 3, \ldots, 2n + 1$. It is easy to verify that

$$\begin{aligned} |a_0(n)| &= |V| = 2n^2 + 4n, \\ |a_1(n)| &= |E| = 3n^2 + 4n - 1, \\ |a_2(n)| &= 6n^2 + 4n - 4. \end{aligned} \tag{46}$$

The remaining proof is divided into two parts which are according to the parity of m. □

Case 7. $m \equiv 1 \bmod (2), 1 < m \le 2n + 1$.

It can be observed from Figure 2 that

$$\begin{aligned} |a_3(1)| &= 3, \\ |a_3(2)| &= 30, \\ |a_3(3)| &= 75, \\ |a_3(4)| &= 138, \\ |a_3(5)| &= 219. \end{aligned} \tag{47}$$

Now, one can conclude that

$$|a_3(n)| = 9n^2 - 6. \tag{48}$$

In a similar fashion, we have

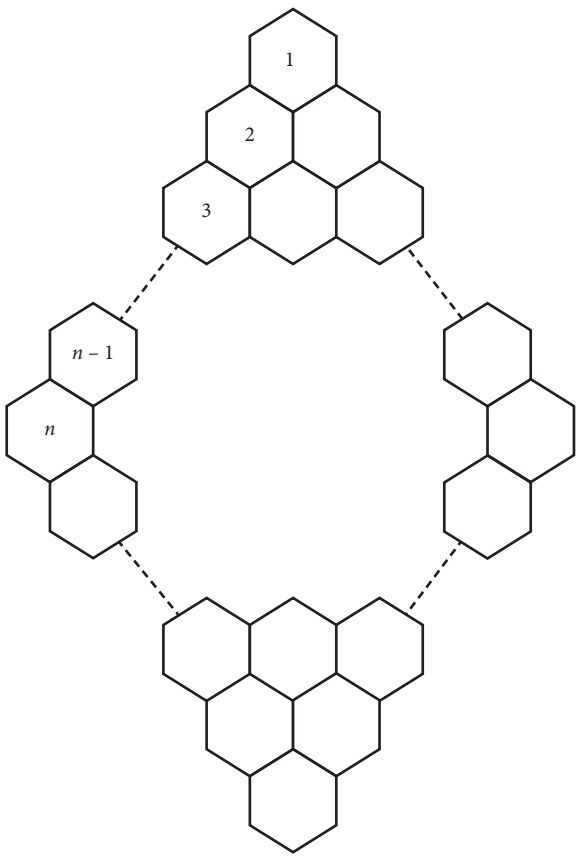

Figure 2: Benzenoid rhombus system R_n.

$$\begin{aligned} |a_5(1)| &= 0, \\ |a_5(2)| &= 24, \\ |a_5(3)| &= 76, \\ |a_5(4)| &= 152, \\ |a_5(5)| &= 252, \\ |a_5(6)| &= 376. \end{aligned} \tag{49}$$

It implies that

$$|a_5(n)| = 15(n-1)^2 + 10(n-1) - 11. \tag{50}$$

In a similar fashion, we infer

$$\begin{aligned} |a_7(n)| &= 21(n-2)^2 + 28(n-2) - 15, \\ |a_9(n)| &= 27(n-3)^2 + 54(n-3) - 16, \\ |a_{11}(n)| &= 33(n-4)^2 + 88(n-4) - 12, \\ &\cdots. \end{aligned} \tag{51}$$

In terms of mathematical induction, we yield

$$\begin{aligned} |a_m(n)| &= 3m\left(n - \left(\frac{m-3}{2}\right)\right)^2 \\ &\quad + \left(m^2 - 3m\right)\left(n - \left(\frac{m-3}{2}\right)\right) \\ &\quad + \frac{1}{24}m^3 - \frac{1}{2}m^2 - \frac{13}{24}m - 1, \\ |a_m(n)| &= 3mn^2 - 2m^2 n + \frac{7m^3}{24} + 6mn - 2m^2 + \frac{41m}{24} - 1. \end{aligned} \tag{52}$$

Case 8. $m \equiv 0 \bmod (2), 2 < m \leq 2n$.

It can be observed from Figure 2 that

$$\begin{aligned} |a_4(1)| &= 0, \\ |a_4(2)| &= 24, \\ |a_4(3)| &= 76, \\ |a_4(4)| &= 152, \\ |a_4(5)| &= 252. \end{aligned} \tag{53}$$

Now, one can conclude that

$$|a_4(n)| = 12(n-1)^2 + 16(n-1) - 4. \tag{54}$$

By means of the same trick, we obtain

$$\begin{aligned} |a_6(1)| &= 0, \\ |a_6(2)| &= 0, \\ |a_6(3)| &= 54, \\ |a_6(4)| &= 144, \\ |a_6(5)| &= 270, \\ |a_6(5)| &= 432, \end{aligned} \tag{55}$$

which reveals that

$$|a_6(n)| = 18(n-2)^2 + 36 * (n-2). \tag{56}$$

In light of the similar approach, we get

$$\begin{aligned} |a_8(n)| &= 24(n-3)^2 + 64(n-3) + 10, \\ |a_{10}(n)| &= 30(n-4)^2 + 100(n-4) + 28, \\ |a_{12}(n)| &= 36(n-5)^2 + 144(n-5) + 56, \\ &\cdots. \end{aligned} \tag{57}$$

Hence, by mathematical induction, we have

$$\begin{aligned} |a_m(n)| &= 3m\left(n - \frac{m}{2} + 1\right)^2 + m^2\left(n - \frac{m}{2} + 1\right) \\ &\quad + \frac{1}{24}m^3 - \frac{7}{6}m - 2, \\ |a_m(n)| &= 3mn^2 - 2m^n + \frac{7m^3}{24} + 6mn - 2m^2 + \frac{11m}{6} - 2. \end{aligned} \tag{58}$$

Now for $m = 2n + 2$ to $m = 4n - 1$, we will generalize in this way. By observing Table 1, values in italics show the distances from $2n + 2$ to $4n - 1$, but the values in the table are in descending order, so first we generalized this in ascending order and then reverse its order as required, let p_i be the values in ascending order as follows (from Table 1).

$$\begin{aligned} p_1 &= 1, \\ p_2 &= 4, \\ p_3 &= 8, \\ p_4 &= 14, \\ p_5 &= 22, \\ p_6 &= 32, \\ p_7 &= 45, \\ p_8 &= 60, \\ p_9 &= 79, \\ p_{10} &= 100. \end{aligned} \tag{59}$$

Case 9. $i \equiv 1 \bmod (2)$.

Hence, one can conclude that

$$p_i = \frac{i^3}{24} + \frac{i^2}{2} + \frac{23i}{24} - \frac{1}{2}. \tag{60}$$

For $m \equiv 1 \bmod (2), 1 \le m \le 2n - 3$.

So to reverse its order put $i = (-m + 2n - 2)$, we get

$$\left|a_m(n)\right| = \frac{(-m+2n-2)^3}{24} + \frac{(-m+2n-2)^2}{2} + \frac{23(-m+2n-2)}{24} - \frac{1}{2}. \tag{61}$$

Case 10. $i \equiv 0 \bmod (2)$.

Hence, one can conclude that

$$p_i = \frac{i^3}{24} + \frac{i^2}{2} + \frac{5i}{6}. \tag{62}$$

For $m \equiv 0 \bmod (2), 2 \le m \le 2n - 2$.

So to reverse its order put $i = (-m + 2n)$, we get

$$\left|a_m(n)\right| = \frac{(-m+2n)^3}{24} + \frac{(-m+2n)^2}{2} + \frac{5(-m+2n)}{6}. \tag{63}$$

By what has been mentioned above, we get our desired result.

Theorem 5. *For the benzenoid rhombus system R_n, the Harary polynomial is as follows:*

$$\begin{aligned} h(R_n; x) = {} & \left(3n^2 + 4n - 1\right)x + \left(3n^2 + 2n - 2\right)x^2 \\ & + \sum_{m \equiv 1 \bmod (2), 1 < m \le 2n+1} \frac{1}{m}\left(3mn^2 - 2m^2 n + \frac{7m^3}{24} + 6mn - 2m^2 + \frac{41m}{24} - 1\right)x^m \\ & + \sum_{m \equiv 0 \bmod (2), 2 < m \le 2n} \frac{1}{m}\left(3mn^2 - 2m^n + \frac{7m^3}{24} + 6mn - 2m^2 + \frac{11m}{6} - 2\right)x^m \\ & + \sum_{m \equiv 1 \bmod (2), 1 \le m \le 2n-3} \frac{1}{2n+m+2}\left(\frac{(-m+2n-2)^3}{24} + \frac{(-m+2n-2)^2}{2} + \frac{23(-m+2n-2)}{24} - \frac{1}{2}\right)x^{2n+m+2} \\ & + \sum_{m \equiv 0 \bmod (2), 2 \le m \le 2n-2} \frac{1}{2n+m}\left(\frac{(-m+2n)^3}{24} + \frac{(-m+2n)^2}{2} + \frac{5(-m+2n)}{6}\right)x^{2n+m}. \end{aligned} \tag{64}$$

Proof. From the information about the number of pairs of vertices at different distances given in Theorem 4, one can easily get this result. □

Theorem 6. *For the benzenoid rhombus system R_n, we have*

(i) $W_\lambda(R_n) = (3n^2 + 4n - 1) + (6n^2 + 4n - 4)2^\lambda + \sum_{m \equiv 1 \bmod (2), 1 < m \le 2n+1} (3mn^2 - 2m^2 n + (7m^3/24) + 6mn - 2m^2 + (41m/24) - 1)m^\lambda + \sum_{m \equiv 0 \bmod (2), 2 < m \le 2n} (3mn^2 - 2m^n + (7m^3/24) + 6mn - 2m^2 + 11m/6 - 2)m^\lambda + \sum_{m \equiv 1 \bmod (2), 1 \le m \le 2n-3} (((-m+2n-2)^3/24) + ((-m+2n-2)^2/2) + (23(-m+2n-2)/24) - (1/2))(2n+m+2)^\lambda + \sum_{m \equiv 0 \bmod (2), 2 \le m \le 2n-2} (((-m+2n)^3/24) + ((-m+2n)^2/2) + (5(-m+2n)/6))(2n+m)^\lambda$.

(ii) $WW_\lambda(R_n) = (3n^2 + 4n - 1)(1^\lambda + 1^{2\lambda}) + (6n^2 + 4n - 4)(2^\lambda + 2^{2\lambda}) + \sum_{m \equiv 1 \bmod (2), 1 < m \le 2n+1} (3mn^2 - 2m^2 n + (7m^3/24) + 6mn - 2m^2 + (41m/24) - 1)(m^\lambda + m^{2\lambda}) + \sum_{m \equiv 0 \bmod (2), 2 < m \le 2n} (3mn^2 - 2m^n + (7m^3/24) + 6mn -$

Table 1: Number of pair of vertices at different distances.

Distance (m)	n					
	2	3	4	5	6	7
1	19	38	63	94	131	174
2	28	62	108	166	236	318
3	30	75	138	219	318	435
4	24	76	152	252	376	524
5	14	69	154	269	414	589
6	*4*	54	144	270	432	630
7	*1*	34	125	258	433	650
8		*14*	98	234	418	650
9		*8*	65	200	389	632
10		*4*	*32*	158	348	598
11		*1*	*22*	109	296	549
12			*14*	*60*	236	488
13			*8*	*45*	168	415
14			*4*	*32*	*100*	334
15			*1*	*22*	*79*	244
16				*14*	*60*	*154*
17				*8*	*45*	*126*
18				*4*	*32*	*100*
19				*1*	*22*	*79*
20					*14*	*60*
21					*8*	*45*
22					*4*	*32*
23					1	*22*
24						*14*
25						*8*
26						*4*
27						*1*

$2m^2 + (11m/6) - 2)(m^{\lambda} + m^{2\lambda}) + \sum_{m\equiv 1 \bmod (2),\, 1\le m\le 2n-3} (((-m+2n-2)^3/24) + ((-m+2n-2)^2/2) + (23(-m+2n-2)/24) - (1/2)((2n+m+2)^{\lambda} + (2n+m+2)^{\lambda}) + \sum_{m\equiv 0 \bmod (2),\, 2\le m\le 2n-2} (((-m+2n)^3/24) + ((-m+2n)^2/2) + 5(-m+2n)/6)((2n+m)^{\lambda} + (2n+m)^{\lambda})$

(iii) $h_t(R_n) = (3n^2 + 4n - 1)(1/(1+t)) + (6n^2 + 4n - 4)(1/(2+t)) + \sum_{m\equiv 1 \bmod (2),\, 1<m\le 2n+1} (3mn^2 - 2m^2 n + (7m^3/24) + 6mn - 2m^2 + (41m/24) - 1)(1/(m+t)) + \sum_{m\equiv 0 \bmod (2),\, 2<m\le 2n} (3mn^2 - 2m^n + (7m^3/24) + 6mn - 2m^2 + (11m/6) - 2)(1/(m+t)) + \sum_{m\equiv 1 \bmod (2),\, 1\le m\le 2n-3} (((-m+2n-2)^3/24) + ((-m+2n-2)^2/2) + (23(-m+2n-2)/24) - (1/2))(1/(2n+m+2+t)) + \sum_{m\equiv 0 \bmod (2),\, 2\le m\le 2n-2} (((-m+2n)^3/24) + ((-m+2n)^2/2) + (5(-m+2n)/6))(1/(2n+m+t))$.

(iv) $\pi(R_n) = 1^{(3n^2+4n-1)} \times 2^{(6n^2+4n-4)} \prod_{m\equiv 1 \bmod (2),\, 1<m\le 2n+1}^{+} m^{(3mn^2 - 2m^2 n + (7m^3/24) + 6mn - 2m^2 + (41m/24) - 1)} \times \prod_{m\equiv 0 \bmod (2),\, 2<m\le 2n} m^{(3mn^2 - 2m^n + (7m^3/24) + 6mn - 2m^2 + (11m/6) - 2)} \times \prod_{m\equiv 1 \bmod (2),\, 1\le m\le 2n-3} (2n+m+2)^{(((-m+2n-2)^3/24) + ((-m+2n-2)^2/2) + (23(-m+2n-2)/24) - (1/2))} \times \prod_{m\equiv 0 \bmod (2),\, 2\le m\le 2n-2} (2n+m)^{(((-m+2n)^3/24) + ((-m+2n)^2/2) + 5(-m+2n)/6)}$.

From the above results, we get following results immediately.

Corollary 4. *For the benzenoid rhombus system R_n, we have*

$$W(R_n) = \frac{34n^5}{15} + \frac{34n^4}{3} + \frac{40n^3}{3} + \frac{2n^2}{3} - \frac{3n}{5}. \tag{65}$$

Corollary 5. *For the benzenoid rhombus system R_n, we have*

$$\begin{aligned} WW(R_n) &= 42n^2 + 32n - 26 \\ &+ \sum_{m\equiv 1 \bmod (2),\, 1<m\le 2n+1} m(m+1)\left(3mn^2 - 2m^2 n + \frac{7m^3}{24} + 6mn - 2m^2 + \frac{41m}{24} - 1\right) \\ &+ \sum_{m\equiv 0 \bmod (2),\, 2<m\le 2n} m(m+1)\left(3mn^2 - 2m^n + \frac{7m^3}{24} + 6mn - 2m^2 + \frac{11m}{6} - 2\right) \\ &+ \sum_{m\equiv 1 \bmod (2),\, 1\le m\le 2n-3} \left(2n+m+2+(2n+m+2)^2\right) \times \left(\frac{(-m+2n-2)^3}{24} + \frac{(-m+2n-2)^2}{2} + \frac{23(-m+2n-2)}{24} - \frac{1}{2}\right) \\ &+ \sum_{m\equiv 0 \bmod (2),\, 2\le m\le 2n-2} \left(2n+m+(2n+m)^2\right)\left(\frac{(-m+2n)^3}{24} + \frac{(-m+2n)^2}{2} + \frac{5(-m+2n)}{6}\right). \end{aligned} \tag{66}$$

Corollary 6. *The Harary index of benzenoid rhombus graph R_n is as follows:*

$$\begin{aligned} h(R_n) = 6n^2 + 6n - 3 &+ \sum_{m \equiv 1 \bmod (2), 1 < m \le 2n+1} \frac{1}{m}\left(3mn^2 - 2m^2 n + \frac{7m^3}{24} + 6mn - 2m^2 + \frac{41m}{24} - 1\right) \\ &+ \sum_{m \equiv 0 \bmod (2), 2 < m \le 2n} \frac{1}{m}\left(3mn^2 - 2m^n + \frac{7m^3}{24} + 6mn - 2m^2 + \frac{11m}{6} - 2\right) \\ &+ \sum_{m \equiv 1 \bmod (2), 1 \le m \le 2n-3} \frac{1}{2n+m+2}\left(\frac{(-m+2n-2)^3}{24} + \frac{(-m+2n-2)^2}{2} + \frac{23(-m+2n-2)}{24} - \frac{1}{2}\right) \\ &+ \sum_{m \equiv 0 \bmod (2), 2 \le m \le 2n-2} \frac{1}{2n+m}\left(\frac{(-m+2n)^3}{24} + \frac{(-m+2n)^2}{2} + \frac{5(-m+2n)}{6}\right). \end{aligned} \tag{67}$$

5. Conclusions

Wiener demonstrated that the Wiener index is firmly connected to the boiling point of alkane. Later work on quantitative structure-activity connections demonstrated that it is additionally corresponded to different amounts including the parameters of its basic point the thickness, surface strain, and consistency of its fluid stage and the van der Waals surface territory of the molecules. Wiener index is a valuable topological index in the structure-property relationship since it is the measurement of compactness of particle regarding its basic characteristics, for example, spreading and cyclicity. Utilizations of benzene follow a long history. In the nineteenth and midtwentieth centuries, benzene was utilized as an aftershave lotion due to its wonderful smell. Before the 1920s, benzene was as often as possible utilized as a modern dissolvable, particularly to degrease metal. As its lethality wound up self-evident, benzene was displaced by different solvents, particularly toluene (methylbenzene), which has comparable physical properties yet is not as cancer-causing. In 1903, Ludwig Roselius promoted the utilization of benzene to decaffeinate espresso. This disclosure prompted the creation of Sanka. This procedure was later ended. Benzene was generally utilized as a noteworthy part in numerous shopper items, for example, Liquid Wrench, a few paint strippers, elastic concretes, spot removers, and different items. Produce of a portion of these benzene-containing details stopped in around 1950, albeit Liquid Wrench kept on containing critical measures of benzene until the late 1970s. In this present paper, we computed Hosoya polynomial, Wiener index, and hyper-Wiener index of zigzag and benzenoid rhombus systems. It is an interesting problem to find out distance-based topological indices for the families of graphs studied in [42–47].

Data Availability

All the data are included within this paper.

Conflicts of Interest

The authors of this paper declare that they have no conflicts of interest.

Authors' Contributions

All authors have equal contribution.

Acknowledgments

This research was funded by the Anhui Provincial Department of Education Natural Science Foundation (Project code: KJ2017A739).

References

[1] J.-B. Liu, C. Wang, S. Wang, and B. Wei, "Zagreb indices and multiplicative Zagreb indices of eulerian graphs," *Bulletin of the Malaysian Mathematical Sciences Society*, vol. 42, no. 1, pp. 67–78, 2019.

[2] J.-B. Liu, X.-F. Pan, F.-T. Hu, and F.-F. Hu, "Asymptotic Laplacian-energy-like invariant of lattices," *Applied Mathematics and Computation*, vol. 253, pp. 205–214, 2015.

[3] J.-B. Liu and X.-F. Pan, "Minimizing Kirchhoff index among graphs with a given vertex bipartiteness," *Applied Mathematics and Computation*, vol. 291, pp. 84–88, 2016.

[4] M. Munir, W. Nazeer, S. Rafique, and S. Kang, "M-polynomial and degree-based topological indices of polyhex nanotubes," *Symmetry*, vol. 8, no. 12, p. 149, 2016.

[5] S. Kang, Z. Iqbal, M. Ishaq, R. Sarfraz, A. Aslam, and W. Nazeer, "On eccentricity-based topological indices and polynomials of phosphorus-containing dendrimers," *Symmetry*, vol. 10, no. 7, p. 237, 2018.

[6] M. Ajmal, W. Nazeer, M. Munir, S. Kang, and Y. Kwun, "Some algebraic polynomials and topological indices of

generalized prism and toroidal polyhex networks," *Symmetry*, vol. 9, no. 1, p. 5, 2016.

[7] A. Ali, W. Nazeer, M. Munir, and S. Min Kang, "M-polynomials and topological indices of zigzag and rhombic benzenoid systems," *Open Chemistry*, vol. 16, no. 1, pp. 73–78, 2018.

[8] W. Gao, B. Muzaffar, and W. Nazeer, "K-Banhatti and K-hyper Banhatti indices of dominating David derived network," *Open Journal of Mathematical Analysis*, vol. 2017, no. 1, pp. 13–24, 2017.

[9] H. Wiener, "Structural determination of paraffin boiling points," *Journal of the American Chemical Society*, vol. 69, no. 1, pp. 17–20, 1947.

[10] H. Hosoya, "On some counting polynomials in chemistry," *Discrete Applied Mathematics*, vol. 19, no. 1–3, pp. 239–257, 1988.

[11] I. Gutman, S. Klavzar, M. Petkovsek, and P. Zigert, "On Hosoya polynomials of benzenoid graphs," *MATCH Communications in Mathematical and in Computer Chemistry*, vol. 43, pp. 49–66, 2001.

[12] G. G. Cash, "Relationship between the Hosoya polynomial and the hyper-Wiener index," *Applied Mathematics Letters*, vol. 15, no. 7, pp. 893–895, 2002.

[13] W. Yan, B.-Y. Yang, and Y.-N. Yeh, "The behavior of Wiener indices and polynomials of graphs under five graph decorations," *Applied Mathematics Letters*, vol. 20, no. 3, pp. 290–295, 2007.

[14] M. R. Farahani, "On the Schultz polynomial and Hosoya polynomial of circumcoronene series of benzenoid," *Journal of Applied Mathematics & Informatics*, vol. 31, no. 5-6, pp. 595–608, 2013.

[15] J.-B. Liu, J. Zhao, and Z. Zhu, "On the number of spanning trees and normalized Laplacian of linear octagonal-quadrilateral networks," *International Journal of Quantum Chemistry*, vol. 119, no. 17, Article ID e25971, 2019.

[16] J. Cao, J.-B. Liu, and S. Wang, "Resistance distances in corona and neighborhood corona networks based on Laplacian generalized inverse approach," *Journal of Algebra and Its Applications*, vol. 18, no. 3, Article ID 1950053,12 pages, 2019.

[17] J.-B. Liu, J. Zhao, J. Min, and J. Cao, "On the Hosoya index of graphs formed by a fractal graph," *Fractals*, vol. 27, no. 8, Article ID 1950135, 2019.

[18] Z. Zhu and J.-B. Liu, "The normalized Laplacian, degree-Kirchhoff index and the spanning tree numbers of generalized phenylenes," *Discrete Applied Mathematics*, vol. 254, pp. 256–267, 2019.

[19] J.-B. Liu, S. Javed, M. Javaid, and K. Shabbir, "Computing first general Zagreb index of operations on graphs," *IEEE Access*, vol. 7, pp. 47494–47502, 2019.

[20] J. B. Liu, M. F. Nadeem, H. M. A. Siddiqui, and W. Nazir, "Computing metric dimension of certain families of Toeplitz graphs," *IEEE Access*, vol. 4, pp. 1–8, 2019.

[21] S. Nikolić, N. Trinajstić, and M. Randić, "Wiener index revisited," *Chemical Physics Letters*, vol. 333, no. 3-4, pp. 319–321, 2001.

[22] M. Ghorbani and S. Klavžar, "Modified Wiener index via canonical metric representation, and some fullerene patches," *Ars Mathematica Contemporanea*, vol. 11, no. 2, pp. 247–254, 2015.

[23] H. Shabani and A. R. Ashrafi, "The modified Wiener index of some graph operations," *Ars Mathematica Contemporanea*, vol. 11, no. 2, pp. 277–284, 2015.

[24] I. Lukovits and W. Linert, "A novel definition of the hyper-Wiener index for cycles," *Journal of Chemical Information and Modeling*, vol. 34, no. 4, pp. 899–902, 1994.

[25] M. Randić, "On generalization of Wiener index for cyclic structures," *Acta Chimica Slovenica*, vol. 49, no. 3, pp. 483–496, 2002.

[26] G. Cash, S. Klavžar, and M. Petkovšek, "Three methods for calculation of the hyper-Wiener index of molecular graphs," *Journal of Chemical Information and Computer Sciences*, vol. 42, no. 3, pp. 571–576, 2002.

[27] W. F. Xi and W. Gao, "λ-modified extremal hyper-Wiener index of molecular graphs," *Journal of Applied Computer Science & Mathematics*, vol. 18, no. 8, pp. 43–46, 2014.

[28] E. J. Farrell, "An introduction to matching polynomials," *Journal of Combinatorial Theory, Series B*, vol. 27, no. 1, pp. 75–86, 1979.

[29] M. R. Farahani, "On the Schultz and modified Schultz polynomials of some Harary graphs," *International Journal of Applications of Discrete Mathematics*, vol. 1, no. 1, pp. 1–8, 2013.

[30] S. Wagner, H. Wang, and X.-D. Zhang, "Distance-based graph invariants of trees and the Harary index," *Filomat*, vol. 27, no. 1, pp. 41–50, 2013.

[31] E. Estrada, "Three-dimensional generalized graph matrix, Harary descriptors, and a generalized interatomic Lennard-Jones potential," *The Journal of Physical Chemistry A*, vol. 108, no. 25, pp. 5468–5473, 2004.

[32] I. Gutman, W. Linert, I. Lukovits, and Ž. Tomović, "The multiplicative version of the Wiener index," *Journal of Chemical Information and Computer Sciences*, vol. 40, no. 1, pp. 113–116, 2000.

[33] I. Gutman, W. Linert, I. Lukovits, and Ž. Tomović, "On the multiplicative Wiener index and its possible chemical applications," *Chemical Monthly*, vol. 131, no. 5, pp. 421–427, 2000.

[34] M. S. Anjum and M. U. Safdar, "K Banhatti and K hyper-Banhatti indices of nanotubes," *Engineering and Applied Science Letters*, vol. 2, no. 1, pp. 19–37, 2019.

[35] Z. Shao, A. R. Virk, M. S. Javed, M. A. Rehman, and M. R. Farahani, "Degree based graph invariants for the molecular graph of Bismuth tri-iodide," *Engineering and Applied Science*, vol. 2, no. 1, pp. 1–11, 2019.

[36] A. U. R. Virk, M. N. Jhangeer, and M. A. Rehman, "Reverse zagreb and reverse hyper-Zagreb indices for silicon carbide $Si_2C_3I[r, s]$ and $Si_2C_3II[r, s]$," *Engineering and Applied Science Letters*, vol. 1, no. 2, pp. 37–50, 2018.

[37] N. De, "Computing reformulated first Zagreb index of some chemical graphs as an application of generalized hierarchical product of graphs," *Open Journal of Mathematical Sciences*, vol. 2, no. 1, pp. 338–350, 2018.

[38] L. Yan, M. R. Farahani, and W. Gao, "Distance-based indices computation of symmetry molecular structures," *Open Journal of Mathematical Sciences*, vol. 2, no. 1, pp. 323–337, 2018.

[39] M. Imran, A. Asghar, and A. Q. Baig, "On graph invariants of oxide network," *Engineering and Applied Science Letters*, vol. 1, no. 1, pp. 23–28, 2018.

[40] W. Gao, A. Asghar, and W. Nazeer, "Computing degree-based topological indices of Jahangir graph," *Engineering and Applied Science Letters*, vol. 1, no. 1, pp. 16–22, 2018.

[41] R. Kanabu and S. Hosamani, "Some numerical invariants associated with V-phenylenic nanotube and nanotori," *Engineering and Applied Science Letters*, vol. 1, no. 1, pp. 1–9, 2018.

[42] G. Liu, Z. Jia, and W. Gao, "Ontology similarity computing based on stochastic primal dual coordinate technique," *Open Journal of Mathematical Sciences*, vol. 2, no. 1, pp. 221–227, 2018.

[43] S. Noreen and A. Mahmood, "Zagreb polynomials and redefined Zagreb indices for the line graph of carbon nanocones," *Open Journal of Mathematical Analysis*, vol. 2, no. 1, pp. 66–73, 2018.

[44] Z. Tang, L. Liang, and W. Gao, "Wiener polarity index of quasi-tree molecular structures," *Open Journal of Mathematical Sciences*, vol. 2, no. 1, pp. 73–83, 2018.

[45] M. Riaz, W. Gao, and A. Qudair Baig, "M-polynomials and degree-based topological indices of some families of convex polytopes," *Open Journal of Mathematical Sciences*, vol. 2, no. 1, pp. 18–28, 2018.

[46] N. De, "Hyper Zagreb index of bridge and chain graphs," *Open Journal of Mathematical Sciences*, vol. 2, no. 1, pp. 1–17, 2018.

[47] H. Siddiqui and M. R. Farahani, "Forgotten polynomial and forgotten index of certain interconnection networks," *Open Journal of Mathematical Analysis*, vol. 1, no. 1, pp. 44–59, 2017.

Hindawi
Journal of Chemistry
Volume 2020, Article ID 2328171, 8 pages
https://doi.org/10.1155/2020/2328171

Research Article

The Impact of Venture Capital on the Growth of Small- and Medium-Sized Enterprises in Agriculture

Junjuan Du [1] **and Zheng-Qun Cai** [2]

[1] *School of Accounting and Finance, Anhui Xinhua University, Hefei 230088, China*
[2] *School of Foreign Studies, Anhui Jianzhu University, Hefei 230601, China*

Correspondence should be addressed to Zheng-Qun Cai; caizhengqun1983@163.com

Received 8 October 2019; Revised 28 November 2019; Accepted 6 March 2020; Published 30 March 2020

Guest Editor: Shaohui Wang

Small- and medium-sized enterprises (SMEs) are considered to have potential innovation capabilities and can create new market opportunities. Venture capital can financially support entrepreneurial activities for economic growth and governs and nurtures the growth of the SMEs. The aim of this study is to investigate the influence mechanism of venture capital on the development of SMEs in agri-food industry. Based on the enterprise growth theory, this study constructed an evaluation model, consisting of technological innovation, profitability, development capability, and solvency, to examine the effect of venture capital on the growth of agricultural SMEs. Using data of 40 agricultural SEMs from the SME and ChiNext boards in China, the empirical analysis has been conducted with the multivariate regression analysis method. The results show that the venture capital can significantly improve the technology innovation, profitability, and growth ability of SMEs. For the solvency of SMEs, the promoting role of venture capital is not obvious. Finally, the practical implications of this study for venture capitalists, entrepreneurs, and regulators are discussed.

1. Introduction

Small- and medium-sized enterprises (SMEs) are of great value to the stable and sustainable development of the economy and attracted high attention from governments worldwide. SMEs are viewed as a trigger of innovation and economic development, which can promote economic growth, urbanization, employment, technological innovation, social harmony, and stability. Data collected by Ayyagari et al. from 76 developing and developed countries show that SMEs account for nearly 60% of manufacturing employment on average [1]. Recently, many policies have been intensively formulated to stimulate the development of SMEs, such as preferential taxation policies in China [2, 3]. According to data from the National Bureau of Statistics, there are 369,000 SMEs at the end of 2018 in China, accounting for 97.6% of the total number of industrial enterprises above the designated size. The main business income of SMEs reached 57.9 trillion Yuan, accounting for 56.7% of the regular main business income. The total profit of SMEs was 3.4 trillion Yuan, accounting for 51.6% of the total profits of the enterprises. SMEs play a significant role in contributing to the national goal of wealth creation and making China an industrialized country [4].

The lack of credit is a main constraint inhibiting the growth of SMEs. Due to unreliable security coupled with an unsound system of legislation and management, SMEs cannot get financial support. Financing channels and costs are often listed as one of the most restrictive characteristics of SMEs in the business environment. The lack of access to finance is considered as major constraint by about 30% of SMEs, which is similar to economic policy uncertainty and corruption [5]. The financing barriers faced by SMEs are always higher than those of lager enterprises, such as high transaction costs, information asymmetry, inferior position in credit filtration, and greater risks in operation. The relative surplus of macro economy has led to the slow growth of SMEs. Difficulties in credit accumulation lead to the lack of

financing channels for SMEs [6]. Formal financial institutions considered SMEs as highly risky and difficult to survive commercially. Then, many SMEs could not get sufficient loans from banks. Even though some traditional financial institutions are optimistic about the development of SMEs, they are not willing to provide loans to SMEs without effective guaranty. Due to the insufficient provision of financial services to SMEs, financial constraints are likely to affect business creation and improvement of SMEs [7].

Financial support is the cornerstones for rapid growth of SMEs. As one source of nonbank financing, venture capital is quite prevalent in developed financial markets, which provide an initial capital for the development of many large companies, such as FedEx. King pointed out that venture capital firms operate in a rapidly changing environment [8]. Venture capital funds generally invest in those technology-based private firms that are likely to go public or being acquired at a premium within a few years. The entrepreneurs could obtain venture capital financing at different stages, including seed, start-up, expansion, development, or bridge finance. Venture capitalists can provide financial resources, managerial skills, and technical expertise to the investing enterprises through detailed preliminary research [9]. The providers of venture capital would actively take an ownership stake in the business, provide the needed capital, and share the risk when they considered that a business idea is promising. In other words, the venture capital has been another source of finance for SMEs, which has winning but risky business proposals and a shortage of capital. By providing equity capital, venture capital plays an important role in enhancing growth of SMEs [9]. Currently, SMEs receive more serious financing constraints under the background of "state advanced and private retreats" in China, which seriously restrict the development and transformation of enterprises. For SMEs, the first priority is to make full use of venture capital to promote the growth of SMEs.

Based on enterprise growth theory, this study compared the differences in the economic value added between venture-capital-backed and non-venture-capital-backed SMEs. The promoting role of venture capital on the growth of SMEs in agri-food industry is assessed by an evaluation model consisted of technological innovation, profitability, development capability, and solvency. Finally, this study proposed the practical implications for venture capitalists, SMEs owners, and regulators. We make two major contributions to the literature. First, we constructed a research model to conduct a comparative study on the economic value added of venture capital. Second, the empirical study reveals the mechanism of venture capital influencing the growth of SMEs in agri-food industry.

This paper is organized as follows. Section 2 discusses the literature on the impact of venture capital on growth of SMEs and provides hypotheses. Section 3 introduces variables, data, and research model. Section 4 conducts a comparative static analysis on the effects of venture capital on growth of SMEs by using the multivariate regression analysis method. Finally, we present conclusions, implications, and suggestions for future research.

2. Theory and Hypotheses

SMEs account for a large share of employment and a large share of enterprises in the private sector, which have played important roles in the development of developing countries, such as driving innovation and competition [10]. There are four type issues affecting the SMEs: poor funding, worst business environment, lack of access to modern technology, and low managerial skills [11]. To promote the growth of SMEs, proper financing of SMEs is essential. By identifying, financially supporting, and cultivating the growing enterprises with entrepreneurial tenacity, venture capital has showed a promoting role in the development of SMEs, which mainly reflect in the improvement of technological innovation, profitability, development capability, and solvency.

2.1. Impact of Venture Capital on the Technological Innovation Ability of SMEs. One of the inherent pursuits of venture capital is to obtain high returns. The improvement in technological innovation can enhance productivity and profit of SMEs, which help to achieve the investment objectives of venture capital. Ueda and Hirukawa revealed that venture capital has significant positive effect on the number of patents [12]. Venckuviene and Saboniene pointed out that the value-added services of venture capital can improve the innovation capabilities of enterprises [13]. Wang found that there is a significant positive correlation between venture capital and technological innovation, which vary among different regions in China [14]. Previous studies indicated that venture capital can provide substantial financial support for technological innovation of SMEs. Based on the discussion of this section, we propose the following hypothesis:

(i) H1a: SMEs with the participation of venture capital have better technological innovation capacities than those without the participation of venture capital

(ii) H1b: venture capital has a positive effect on the improvement of technological innovation capacity of SMEs

2.2. Impact of Venture Capital on the Profitability of SMEs. Profitability is an important indicator to evaluate the development of SMEs, which is also a growing concern for venture capitalists. Chahine et al. found that enterprises supported by venture capital have good profitability and market performance [15]. Audretsch and Lehmann proposed that venture capital has a positive effect on enterprise performance, which is complementary to bank loans [16]. Sun suggested that enterprises supported by venture capital have good performance in the first year after initial public offering, which is better than those of enterprises without venture capital [17]. On the contrary, other researchers concluded that venture capital has a nonpositive effect on enterprise performance. For SMEs, the introduction of venture capital can raise the urgently needed capital for promoting the development and improving the performance of enterprises. By raising the share of capital, venture capitalists can exert more influences on the management of

SMEs and obtain better returns. Therefore, based on the above discussion, the following hypotheses have been put forward:

(i) H2a: SMEs with the participation of venture capital have higher profitability level than those without the participation of venture capital

(ii) H2b: venture capital has a positive effect on the improvement of profitability level of SMEs

2.3. Impact of Venture Capital on the Development Capability of SMEs. When selecting investment object, the potential growth of enterprises is the focus of venture capitalists. With the support of venture capital, the development capability of SEMs can be greatly improved. Davila et al. suggested that the most attractive enterprises to venture capital are SMEs with good development prospects [18]. These enterprises can attract outstanding talents and high-tech to prompt the growth of enterprises. From the perspective of value-added services, Chemmanur and Loutskina proved that excellent venture capital can bring first-class brokers and institutional investors to enterprises, which plays a positive role in promoting the development of enterprises [19]. Rosenbusch et al. confirmed that venture capital has a significantly positive impact on the growth ability of enterprises [20]. According to the above analyses, the following hypotheses have been introduced:

(i) H3a: SMEs with the participation of venture capital have higher development capability than those without the participation of venture capital

(ii) H3b: venture capital has a positive effect on the improvement of development capability of SMEs

2.4. Impact of Venture Capital on the Solvency of SMEs. When investing, venture capitalist can provide intellectual capital, professional relationships, management guidance, business development, and business model consulting for SMEs. Jain and Kini found that there is an increase in sales volume and sales growth rate for SMEs with venture capital after being listed [21]. Nahata concluded that venture capital with higher reputation can significantly improve the solvency of SMEs [22]. Chaopeng et al. confirmed that venture capital can suppress excessive investment of the enterprise in free cash, enlarge short-term debt and equity financing, and alleviate the shortage of cash flow to a certain extent [23]. For SMEs with poor solvency, the introduction of venture capital can drive other social capital to invest in enterprises. The following hypotheses have been put forward according to the above-mentioned analyses:

(i) H4a: SMEs with the participation of venture capital have higher solvency than those without the participation of venture capital

(ii) H4b: venture capital has a positive effect on the improvement of solvency of SMEs

From enterprise growth theory, the enterprise growth can be defined as a process in which enterprises grow from small to large and from weak to strong and constantly realize scale expansion in market competition. The scale expansion includes output scale expansion, input scale expansion, profit scale expansion, and value scale expansion. In this study, we selected four indicators, including technological innovation ability, enterprise profitability, enterprise development ability, and enterprise solvency ability, to measure the growth of enterprises, especially for SMEs. The influences of venture capital on the growth of SMEs are conducted from the two perspectives of the context of venture and the degree of participation of venture capital. To reflect the effect of environmental factors, the control variables are introduced into the empirical process. The research conceptual model in this paper has been constructed, as shown in Figure 1.

3. Data and Methodology

3.1. Data. Data for this study were derived from 40 agricultural SMEs on the SME and ChiNext boards in China by the end of 2018. In view of complexity of data and samples of discrete, the data on investment time of venture capital, institutional background, and financial status are all from the prospectuses and listing financial reports of GEM companies. Other data that cannot be directly collected are obtained by calculation. Referring to the method adopted by Chaopeng et al. [23], the SMEs that meet the following criteria are considered to have venture capital background: the names of top 10 major shareholders including "entrepreneurship investment," "venture capital," and "science and technology investment," or a venture capital share of more than 5%. According to this criterion, the selected 40 SMEs were divided into two categories: 20 SMEs with the context of venture capital and 20 SMEs without the context of venture capital.

3.2. Methodology. Using the multivariate regression analysis method, this paper studies the promoting role of venture capital on the growth of SMEs in agriculture. Table 1 displays the descriptions of the variables. Among dependent variables, the technological innovation ability of SMEs is reflected by the variables R&D investment intensity (*RDINV*). The profitability of SMEs is reflected by the operating profit margin (*OPGR*) and the rate of return on net assets (*NAIR*). To evaluate the development ability of SMEs, we choose two variables of the operating income growth rate (*OIGR*) and the growth rate of total assets (*TAGR*). Finally, the solvency of SMEs is reflected by the cash flow ratio (*CASHCL*) and the current ratio (*CR*). The independent variables are a mix of categorical and continuous variables. The independent variable is represented by *DumVC*, *DumVC1*, *DumVC2*, *DumVC3*, and *DumVC4*. Among independent variables, the variable *DumVC* reflects the context of venture capital and the variables *DumVC1*, *DumVC2*, *DumVC3*, and *DumVC4* reflect the degree of participation of venture capital in SMEs. In addition, we take into account the influence of enterprise's own

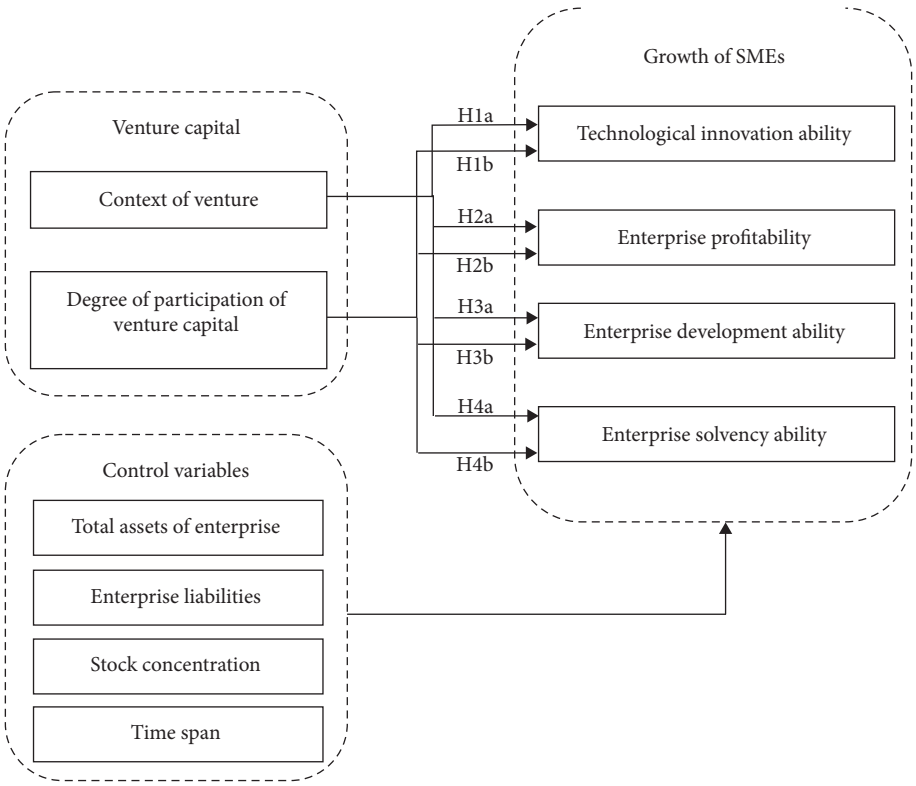

Figure 1: The research conceptual model.

Table 1: Description of variables and values assigned.

Variables		Symbol	Description
Dependent variables	R&D investment intensity	*RDINV*	Expenditures by a firm on its research and development divided by the firm's sales.
	Operating profit margin	*OPGR*	It is calculated by dividing the operating profit by total revenue.
	Rate of return on net assets	*NAIR*	A ratio of net income to the average total assets.
	Operating income growth rate	*OIGR*	Ratio of increase in operating revenue of current period to prior current period.
	Growth rate of total assets	*TAGR*	Ratio of increase in total assets to total assets.
	Cash flow ratio	*CASHCL*	Ratio of net cash flow from operating activities to incur debts.
	Current ratio	*CR*	Ratio of current assets to current liabilities.
Independent variables	Context of venture capital	*DumVC*	*DumVC* = 1 if the names of top 10 shareholders including "entrepreneurship investment," "venture capital," and "science and technology investment," or a venture capital share of more than 5%, otherwise 0.
	Degree of participation of venture capital	*DumVC1*	*DumVC1* = 1 if the share ratio of venture capital ranges between 5% and 15% (inclusive of 5% and 15%), otherwise 0.
		DumVC2	*DumVC2* = 1 if the share ratio of venture capital ranges between 15% and 25% (inclusive of 25%), otherwise 0.
		DumVC3	*DumVC3* = 1 if the share ratio of the venture capital ranges between 25% and 35% (inclusive of 35%), otherwise 0.
		DumVC4	*DumVC2* = 1 if the share ratio of venture capital is greater than 35%, otherwise 0.
Control variables	Total assets	*TA*	Total assets of enterprise.
	Enterprise liabilities	*ALR*	Ratio of total liabilities to total assets.
	Ownership structure	*Zindex*	Ratio of the percentage of the first major stockholder to the percentage of the second major stockholder.
	Time span	*Time*	Time it takes for a SME to go IPOs from start-ups.

characteristics on the relation between venture capital and the growth of SMEs. Control variables, including *TA*, *ALR*, *Zindex*, and *Time*, are selected to evaluate this impact of enterprise's own characteristics.

3.3. Model. To test our hypotheses related to the effects of venture capital on the growth of SMEs, the multiple linear regression models are constructed. These models are expressed by

$$y_i = \alpha_{0i} + \alpha_{1i}DumVC + \alpha_{2i}TA + \alpha_{3i}ALR + \alpha_{4i}Zindex + \alpha_{5i}Time + \varepsilon_i,$$
$$y_i = \beta_{0i} + \beta_{1i}DumVC1 + \beta_{2i}DumVC2 + \beta_{3i}DumVC3 + \beta_{4i}DumVC4 + \beta_{5i}TA + \beta_{6i}ALR + \beta_{7i}Zindex + \beta_{8i}Time + \varepsilon_i, \quad (1)$$

where $y\,(i = 1, 2, \ldots, 7)$ represents the dependent variables, including R&D input intensity, operating profit margin, rate of return on net assets, operating income growth rate, growth rate of total assets, cash flow ratio, and current ratio; α_0, β_0, and λ_0 are the intercept of models; α_i ($i = 1, 2, \ldots, 12$) and β_i ($i = 1, 2, \ldots, 12$) are the coefficients of models; and ε_i are the random error terms.

4. Results

4.1. Descriptive Statistics. The statistical results show that venture capitalist prefers to invest in SMEs which have relatively stable income. The shareholding ratio of venture capital has influences on the operation of SMEs. The rational shareholding ratio of venture capital can effectively improve the technological innovation and the operating performance of SMEs. Ruhnka and Young proposed that the optimum share ratio of venture capital in SMEs is 30% [24]. Currently, the share ratio of venture capital of 65% SMEs in China is less than 25%. Meanwhile, the venture capitalists prefer a long-established company. The data show that 80% SMEs without venture capital have less than 10 years from establishment to listing. Correspondingly, 55% of SMEs with venture capital context took more than 10 years to listing. Figure 2 shows the distribution of the dependant variables and control variables of all collected sample enterprises. Compared to SMEs without venture capital, SMEs with venture capital have better performances in terms of technological innovation investment intensity, operating profit margin, return on net assets, operating income growth rate, growth rate of total assets, cash flow ratio, and current ratio. To ensure investment income, venture capitalists tend to invest in a large-scale, long-established, low-leverage, and high-return SME in the agri-food industry.

4.2. Regression Analysis and Hypothesis Testing. Using SPSS 21, the Pearson correlation test is performed. The results indicate that the pairwise correlation between the variables is weak (the Pearson correlation coefficients are less than 0.5). The variance inflation factors of all variables are less than 2, which reveal that the effect of multicollinearity among variables is not significant. In addition to categorical variables and ordinal variables, other variables are processed by multiple regressions after logarithmic treatment. The regression results are shown in Table 2–5, respectively.

As shown in Table 2, the coefficient of *DumVC* in model 1 is 0.012, which indicates the significantly positive influence of venture capital on R&D investment intensity (*RDINV*) at the level of 1%. Meanwhile, the total assets (*TA*) show a positive correlation with R&D investment intensity (*RDINV*), and the enterprise liabilities (*ALR*) have a negative effect on R&D investment intensity (*RDINV*). The regression results show that the scale of technological innovation investment of SMEs with venture capital is more than that of SMEs without venture capital. Large enterprises can provide more capital for technological innovation. The improvement of enterprise's sustainable development ability can bring generous returns to venture capitalists, thus supporting H1a. The variables of share ratio of venture capital, including *DumVC1*, *DumVC2*, *DumVC3*, and *DumVC4*, have different influences on R&D investment intensity (*RDINV*). The share ratio of venture capital has a positive influence on R&D expenditure of SMEs, which supports hypothesis H1b.

Table 3 shows the regression results of effects of venture capital on profitability of SMEs. The coefficients between venture capital and dependant variables (*OPGR* and *NAIR*) are 0.022 and 0.126 respectively, which support hypothesis H2a. The regression results of the shareholding ratio of venture capital (including *DumVC1*, *DumVC2*, *DumVC3*, and *DumVC4*) on operating profit margin (*OPGR*) show that *DumVC1* has no influence on *OPGR*, and the coefficients of *DumVC2*, *DumVC3*, and *DumVC4* on *OPGR* are 0.05, 0.049, and 0.086 at the level of 5%, respectively. The coefficients of *DumVC1*, *DumVC2*, *DumVC3*, and *DumVC4* on profit margin of net assets (*NAIR*) are 0.098, 0.151, 0.213, and 0.31 at the level of 1%, respectively. Hypothesis H2b is supported. The results illustrate that the influences of venture capital institutions on SMEs management can improve the operation efficiency of assets and optimize the capital structure of the invested SMEs. Increasing the shareholding ratio of venture capital can strengthen SMEs' adaptability to market changes and competitiveness, improve the profitability, and obtain high returns.

The regression results of venture capital on development ability of SMEs are shown in Table 4. In model 1, the regression coefficients of venture capital background (*DumVC*) on the operating income growth rate (*OIGR*) and the growth rate of total assets (*TAGR*) are 0.199 and 0.438, respectively, which prove the role of venture capital on the growth ability of SMEs and support hypothesis H3a. In terms of the influences of shareholding ratio of venture capital on development ability of SMEs, the regression results show that only *DumVC4* is correlated with the operating income growth rate (*OIGR*) and the growth rate of total assets (*TAGR*). The coefficients are 0.721 and 1.045 at the level of 1%, respectively, thereby supporting H3b. The improvement of the shareholding ratio can enhance the influence of venture capital institutions on SMEs' decision-making and management and promote the ability of enterprise resources integration and the development of SMEs. The SMEs are successfully listed with the assistance of venture capitalists, who will withdraw from the enterprises after obtaining the final income.

The regression results in Table 5 show that the venture capital has no correlation with the cash flow rate (*CASHCL*). The share ratio of venture capital (including *DumVC*, *DumVC1*, *DumVC2*, *DumVC3* and *DumVC4*) has positive effects on the current ratio (*CR*) at the level of 10%. The

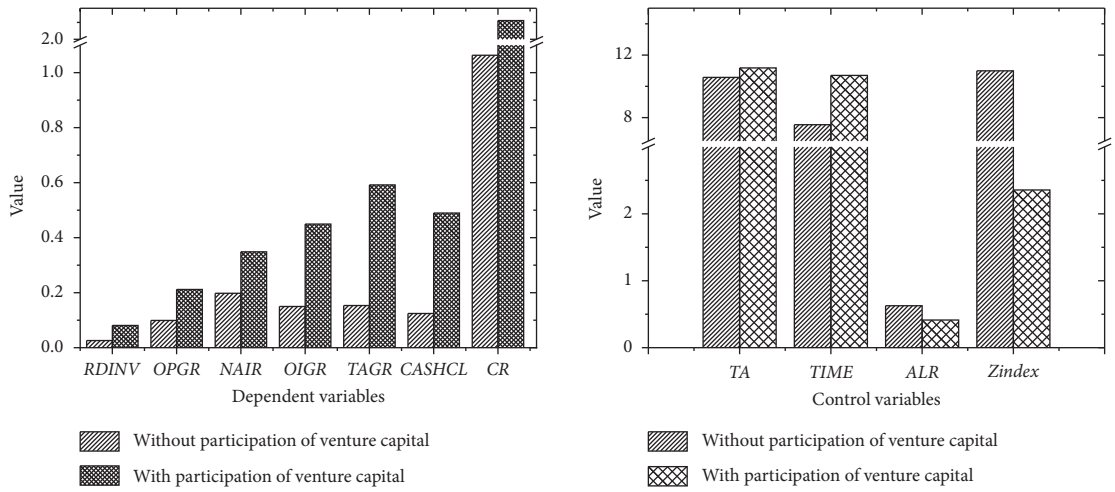

Figure 2: The mean value comparisons of development indicators of SMEs with or without venture capital.

Table 2: Effects of venture capital on the technological innovation of SMEs.

Dependant variable	*RDINV*	
	Model 1	Model 2
Constant	0.038*** (0.565)	−0.033*** (−0.523)
DumVC	0.012*** (2.025)	—
DumVC1	—	—
DumVC2	—	0.026*** (3.195)
DumVC3	—	0.049*** (5.008)
DumVC4	—	0.051*** (6.500)
TA	0.009* (1.771)	0.011* (2.550)
Time	—	—
ALR	−0.175* (−6.923)	−0.099* (−3.601)
Zindex	—	—
F value	106.080***	138.264***
Adjusted R^2	0.890	0.946

Note. * $p < 0.1$; ** $p < 0.05$; *** $p < 0.01$. Source: authors' elaboration.

Table 3: Effects of venture capital on the profitability of SMEs.

Dependant variable	*OPGR*		*NAIR*	
	Model 1	Model 2	Model 1	Model 2
Constant	0.038** (0.265)	−0.117** (−0.726)	0.324*** (6.617)	0.163*** (9.357)
DumVC	0.022*** (1.782)	—	0.126*** (4.411)	—
DumVC1	—	—	—	0.098*** (3.994)
DumVC2	—	0.05*** (2.378)	—	0.151*** (5.798)
DumVC3	—	0.049*** (1.928)	—	0.213*** (5.349)
DumVC4	—	0.086*** (4.232)	—	0.31*** (10.975)
TA	0.026** (2.449)	0.034** (2.896)	—	—
Time	—	—	—	—
ALR	−0.348** (−6.616)	−0.220* (−3.100)	−0.269* (−3.572)	
Zindex	—	—	0.004** (2.407)	0.003** (2.716)
F value	108.643***	89.574***	21.273***	28.325***
Adjusted R^2	0.892	0.919	0.609	0.778

Note. * $p < 0.1$; ** $p < 0.05$; *** $p < 0.01$. Source: authors' elaboration.

Table 4: Effect of venture capital on the development ability of SMEs.

Dependent variable	*OIGR*		*TAGR*	
	Model 1	Model 2	Model 1	Model 2
Constant	−1.594** (−2.033)	0.209*** (4.171)	0.153** (1.527)	0.242*** (4.023)
DumVC	0.199** (1.729)		0.438** (3.088)	
DumVC1	—	—	—	—
DumVC2	—	—	—	—
DumVC3	—	—	—	—
DumVC4	—	0.721*** (5.079)		1.045*** (6.143)
TA	0.165* (2.235)	—	—	—
Time	—	—	—	—
ALR	—	—	—	—
Zindex	—	—	—	—
F value	6.480***	25.793***	9.536***	37.733***
Adjusted R^2	0.219	0.389	0.180	0.485

Note. * $p < 0.1$; ** $p < 0.05$; *** $p < 0.01$. Source: authors' elaboration.

Table 5: Effect of venture capital on the solvency of SMEs.

Dependant variable	*CASHCL*		*CR*	
	Model 1	Model 2	Model 1	Model 2
Constant	1.112*** (16.538)	1.112*** (16.538)	2.444*** (5.621)	1.201*** (11.579)
DumVC	—	—	0.743* (3.094)	
DumVC1	—	—	—	0.386* (2.640)
DumVC2	—	—	—	0.741* (4.762)
DumVC3	—	—	—	1.21* (5.088)
DumVC4	—	—	—	2.514* (14.912)
TA	—	—	—	—
Time	—	—	—	—
ALR	−1.548** (−12.691)	−1.548** (−12.691)	−2.199* (−3.347)	—
Zindex	—	—	—	−0.013* (−1.775)
F value	161.055***	161.055***	25.148***	62.545***
Adjusted R^2	0.804	0.804	0.553	0.888

Note. * $p < 0.1$; ** $p < 0.05$; *** $p < 0.01$. Source: authors' elaboration.

hypotheses H4a and H4b are partially supported. The venture capitalists in China are intended to invest the SMEs with guaranteed income, low current rate, and high solvency.

5. Conclusions and Implications

5.1. Conclusions. This review created an evaluation model to investigate the impact of venture capital and the share ratio of venture capital on the growth of SMEs in agriculture based on enterprise growth theory. These findings can help the entrepreneurs of SMEs set a reasonable development plan to attract venture capital. We found that the venture capital in China has its own characteristics in selecting investee and promoting the development of SMEs. First, the venture capitalists prefer to invest in large-scale SMEs with stable operation, low debt ratio, low ownership concentration, and stable returns. Second, the venture capital can improve the technological innovation, the profitability, and the development ability of SMEs. Third, the venture capital has no significant impact on the solvency of SMEs.

5.2. Implications. This study sought to further develop enterprise growth theory. It provides theoretical basis and practical reference for encouraging venture capital to invest in SMEs, solving the financing constraints on SMEs, and improving the growth of SMEs. From a practical perspective, this study provides some suggestions for SMEs in China who want to obtain financial support from venture capital for their own growth. First, the entrepreneurs should formulate a scientific and standardized management system and establish an internal organization with clear responsibility in SMEs, based on the concept of modern corporate governance. Under the premise of protecting their own rights and interests, the entrepreneurs should increase the share of venture capitalists in the business income to attract the investment of venture capital. In addition, some measurements should be adopted to encourage the venture capitalists to participate in the management of SMEs, so as to improve the value-added service level of venture capital. Second, the venture capitalists should actively learn some Chinese laws about financial investment, enterprise management, and operation and fully understand the huge development potential of

SMEs in China. Setting a reasonable investment plan of venture capital is necessary for supporting the rapid growth of SMEs in technology, management, etc. Third, the regulators should set perfect financing policy and scientific credit supervision mechanism to guarantee revenue for venture capitalists. A series of preferential policies, such as investment subsidies, price subsidies, tax credit, and R&D supports, should be adopted to improve the profitability of SMEs and the investment income of venture capital. A seed fund with government capital as the main body should be established to introduce venture capital into the high-risk and high-yield SMEs.

Data Availability

All data generated or analyzed during this study are included in this published article and are available upon request from the corresponding author.

Conflicts of Interest

The authors declare that there are no conflicts of interest.

Acknowledgments

This study was supported by the Foundation for Planning of Philosophy and Social Sciences of Anhui Province (Award Number: AHSKF2018D62). Gratitude is also extended to all authors of the literature cited by this article.

References

[1] M. Ayyagari, T. Beck, and A. Demirguc-Kunt, "Small and medium enterprises across the globe," *Small Business Economics*, vol. 29, no. 4, pp. 415–434, 2007.

[2] Y. Zhu, X. Wittmann, and M. W. Peng, "Institution-based barriers to innovation in SMEs in China," *Asia Pacific Journal of Management*, vol. 29, no. 4, pp. 1131–1142, 2012.

[3] T. George, "Fair competition and preferential taxation policy for small & medium retail stores in China: a comparative study," *Journal of Chinese Tax and Policy*, vol. 3, no. 3, pp. 140–164, 2013.

[4] J. Yu and J. N. B. Bell, "Building a sustainable business in china's small and medium-sized enterprises (SMEs)," *Journal of Environmental Assessment Policy and Management*, vol. 9, no. 1, pp. 19–43, 2007.

[5] F. Olawale and D. Garwe, "Obstacles to the growth of new SMEs in South Africa: a principal component analysis approach," *African Journal of Business Management*, vol. 4, no. 5, pp. 729–738, 2010.

[6] J. Jiang, Z. Li, and C. Lin, "Financing difficulties of SMEs from its financing sources in China," *Journal of Service Science and Management*, vol. 7, no. 3, pp. 196–200, 2014.

[7] S. F. Memba, W. R. Gakure, and K. Karanja, "Venture capital (VC): its impact on growth of small and medium enterprises in Kenya," *International Journal of Business and Social Science*, vol. 3, no. 6, pp. 32–38, 2012.

[8] B. L. King, "Strategizing at leading venture capital firms: of planning, opportunism and deliberate emergence," *Long Range Planning*, vol. 41, no. 3, pp. 345–366, 2008.

[9] A. A. Eniola, "The role of SME firm performance in Nigeria," *Oman Chapter of Arabian Jou 10.12816/0016552 rnal of Business and Management Review*, vol. 3, no. 12, pp. 33–47, 2014.

[10] R. U. Etuk, G. R. Etuk, and B. Michael, "Small and medium scale enterprises (SMEs) and Nigeria's economic development," *Mediterranean Journal of Social Sciences*, vol. 5, no. 7, pp. 656–662, 2014.

[11] O. O. Fatoki, A. Van, and A. Smit, "Constraints to credit access by new SMEs in South Africa: a supply-side analysis," *African Journal of Business Management*, vol. 5, no. 4, pp. 1413–1425, 2011.

[12] M. Ueda and M. Hirukawa, "Venture capital and industrial innovation," *SSRN Electronic Journal*, vol. 2008, 2008.

[13] V. Venckuviene and A. Saboniene, "Implications for mitigating human resource and labor market restriction in low-tech sector," *Procedia—Social and Behavioral Sciences*, vol. 213, pp. 192–197, 2015.

[14] T. Wang, "Effect of VC to technology innovation based on regional perspective," *Studies in Science of Science*, vol. 34, no. 10, pp. 1576–1582, 2016, in Chinese.

[15] S. Chahine, J. D. Arthurs, I. Filatotchev, and R. E. Hoskisson, "The effects of venture capital syndicate diversity on earnings management and performance of IPOs in the US and UK: an institutional perspective," *Journal of Corporate Finance*, vol. 18, no. 1, pp. 179–192, 2012.

[16] D. B. Audretsch and E. E. Lehmann, "Financing high-tech growth: the role of banks and venture capitalists," *Schmalenbach Business Review*, vol. 56, no. 4, pp. 340–357, 2004.

[17] J. h. Sun, "Empirical support of decline in enterprises' operating performance after the IPO from the perspective of venture capital," *Finance & Economics*, vol. 8, pp. 67–78, 2015, in Chinese.

[18] A. Davila, G. Foster, and M. Gupta, "Venture capital financing and the growth of startup firms," *Journal of Business Venturing*, vol. 18, no. 6, pp. 689–708, 2003.

[19] T. J. Chemmanur and E. Loutskina, "The role of venture capital backing in initial public offerings: certification, screening, or market power?" in *Proceedings of the EFA 2005 Moscow Meetings*, Moscow, Russia, September 2006.

[20] N. Rosenbusch, J. Brinckmann, and V. Müller, "Does acquiring venture capital pay off for the funded firms? a meta-analysis on the relationship between venture capital investment and funded firm financial performance," *Journal of Business Venturing*, vol. 28, no. 3, pp. 335–353, 2013.

[21] B. A. Jain and O. Kini, "Venture capitalist participation and the post-issue operating performance of IPO firms," *Managerial and Decision Economics*, vol. 16, no. 6, pp. 593–606, 1995.

[22] R. Nahata, "Venture capital reputation and investment performance☆," *Journal of Financial Economics*, vol. 90, no. 2, pp. 127–151, 2008.

[23] W. Chaopeng, W. Shinong, C. Jingya, and W. Lu, "The role of venture capital in the investment and financing behavior of listed companies: evidence from China," *Economic Research Journal*, vol. 1, pp. 105–119, 2012, in Chinese.

[24] J. C. Ruhnka and J. E. Young, "Some hypotheses about risk in venture capital investing," *Journal of Business Venturing*, vol. 6, no. 2, pp. 115–133, 1991.

Hindawi
Journal of Chemistry
Volume 2020, Article ID 8474636, 8 pages
https://doi.org/10.1155/2020/8474636

Research Article

Optimizing Spatial Distribution of Urban Green Spaces by Balancing Supply and Demand for Ecosystem Services

Yi-Wen Ji,[1,2] Lang Zhang,[2] Jie Liu,[1] Qicheng Zhong,[2] and Xinxin Zhang[1]

[1]*College of Landscape Architecture, Nanjing Forestry University, Nanjing 210037, China*
[2]*Shanghai Academy of Landscape Architecture Science and Planning, Shanghai 200232, China*

Correspondence should be addressed to Lang Zhang; 1132467518@qq.com

Received 29 October 2019; Accepted 5 December 2019; Published 26 March 2020

Guest Editor: Jia-Bao Liu

The capacity and ecological flows of ecosystem services as well as the demand for them are key areas of urban and rural ecological planning that have been studied using the spatial-explicit model as a decision support tool. This study develops a framework for mapping the relationships among the capacity of and demand for ecosystem services, ecological flows, and planning management. This is done by estimating the ecosystem services based on the space for recreation and environmental conditions and assessing planning for green spaces using the spatial-explicit model. The results show that the carrying capacity of green recreational space was high in the northwest, southwest, and southeast parts of the city of Hefei in China, where this space was highly sustainable in the northwest and southwest. The data also show that the carrying capacity for air purification was higher in the northwest, southwest, and southeast suburbs of Hefei, while areas with high demand for air purification were mainly located in the northeast. The spatial variation in the flows of supply and demand for ecosystem services remained high and unbalanced in the northeast and southwest of Hefei. The excessive use of ecosystem services was concentrated in the urban center while their use in suburban areas was sustainable. The results show that the gap between the supply and demand of space for recreation increased with distance while that between the supply and demand of air purification decreased with increasing distance. The results of assessment based on spatial visualization show that green space was abundant in areas with low demand for it, while those with high demand for it tended to have limited green space in Hefei. This analysis shows that indices for the demand for green spaces in the context of ecosystem services can be improved via public participation, interactions between different scales of ecosystem services for green space, and use of decision support in urban and rural planning systems. These areas will form important directions for future research.

1. Introduction

With rapid urbanization and the attendant increase in urban population, the ecosystem of urban green space has been significantly influenced by the activities of humans and undergone major changes [1]. A growing number of problems with the urban ecological environment, such as soil erosion, loss of biodiversity, erosion of green land, and air pollution, have significantly reduced the benefits of the ecosystem services provided by urban green spaces [2]. Green spaces are an important part of the urban ecosystem, which contribute to the human health, recreation, and survival. Important challenges in this context include finding ways to assess the balance of urban green spaces, considering the relationship between supply and demand for such spaces and better coupling the recreational activities of urban residents and the function of urban green spaces.

The term "ecosystem services" refers to the provision, regulation, and support provided by nature for humans [2, 3]. The provision of ecosystem services depends on the ecological and socioeconomic conditions (of urban areas) [4–6]. Against the backdrop of rapid urbanization, ecosystem services provided by urban green spaces have generated a great deal of interest in academia. Work on the

evaluation of ecosystem services provided by urban green spaces has emphasized the value of carrying capacity and supply-demand relationships [5–7].

The assessment of ecosystem services from a static perspective, in the absence of considerations of dynamic delivery, is absent from previous work [8]. Ecological flow is a functional dynamic that is indicative of the relationships among material metabolism, energy conversion, information exchange, increases and decreases in value, and biological migration within ecological systems, all of which are concrete manifestations of ecological processes [9]. It is the movement of ecosystem services from source to sink in time and space driven by nature and human beings. Assessing the flow of ecosystem services is an important issue in the relevant research, which is in its incipient stage. The concept of ecosystem service flow is vague, and research has yielded two main interpretations: (1) the process of service transfer from the ecosystem to humans; (2) a of ecosystem services used to advance the well-being of humans [10, 11]. Both interpretations emphasize the flow of materials and energy of the ecosystem to service people, rather than the operation and dissipation of other aspects of the ecosystem. Based on the concept of ecosystem service flow, Baró et al. conducted a quantitative study on outdoor leisure and air purification in Barcelona, Spain, in 2016. They identified areas where the supply and demand of ecosystem services did not match [12]. Ecological carrying capacity refers to the ability of an ecosystem to develop in a healthy and orderly fashion to provide goods and services [13]. Ecological demand refers to socioeconomic system requirements with respect to the dynamic delivery of ecosystem services and ecological environmental resources within natural ecosystems in light of economic activities [14]. These are inseparable within the ecological system of urban green space with respect to ecological flows and carrying capacity and demand [15]. This is indicative of the sustainable development of ecosystem dynamics, flows, and demand as well as the supply and demand of goods and services within dynamic ecological systems [16]. These variables also provide a breakthrough in the dynamic evaluation of ecosystem services. Scholars divide the ecosystem services of urban green spaces into three levels: carrying capacity, flows, and demand [17–20]. This has enabled a dynamic evaluation of the sustainability of the ecosystem services of urban green spaces as well as the supply and demand for them [21]. The area chosen for this study is the city of Hefei, China. A framework is proposed to map the relationships among carrying capacity, ecosystem service flows, and demand for green spaces [22, 23]. Planning for green spaces in urban areas is evaluated using the results of the spatial-explicit model [24–26].

2. Research Area and Methods

2.1. Concepts and Frameworks. A conceptual framework for the assessment of ecosystem services based on capacity, flows, and demand is indicative of the relationship between ecosystem characteristics, functions, services, benefits, and human preferences [27]. Ecosystem service capacity is therefore defined as the ability of an ecosystem to provide services on the basis of biophysical characteristics, social conditions, and ecological functions even though service flows are services that are actually produced that people use or experience. At the same time, ecosystem service demand refers to the amount of services required or expected by society [28]. This approach can be further developed into an operational framework (Figure 1) that represents the degree of mismatch between ecosystem services, and how this influences decision making based on the relationships among capacity, flow, and demand [29–31]. In cases where the carrying capacity of ecosystem services is smaller than the flow, overuse or unsustainability is implied [20]. When the flow does not meet social demands, the ecosystem services remain incompletely utilized [29].

2.2. Summary of Research Area. The area used for this study is located in Hefei city in Anhui Province, China (Figure 2). Hefei is the political, economic, and cultural center of Anhui Province as well as an important national scientific, and educational center, modern manufacturing base, and regional transportation junction. It is between the Yangtze and Huaihe Rivers on the shore of Chaohu Lake (31°31′N–32°37 N, 116°40′E–117°52′E). Hefei has a number of important regional advantages, including linking east and west and connecting north to south. It covers an area of 7,047 km^2 consisting mainly of low hills and plains. The region has a subtropical humid monsoonal climate, with an annual average temperature of 15.7°C and annual average precipitation of 1000 mm. Its population is 7.86 million, including a central urban zone with a population of 3.6 million. The population continues to grow because of the rapid economic development of Hefei. The area of urban construction land in this region has expanded significantly in recent years and has had a significant impact on the urban green space system. This study chose the central urban area of Hefei. The central urban area is divided into four administrative regions: Shushan, Baohe, Luyang, and Yaohai districts (Figure 2).

2.3. Methods

2.3.1. Models

(1) Ecosystem Services. In the context of ecosystem services, recreational functions are helpful for improving the physical and mental health of citizens [32–34]. Recreational space (i.e., urban green space) is used in this analysis to evaluate the functions of ecosystems of green spaces in Hefei.

In the context of functions regulating ecosystem services, air purification is among the most important ones [35]. Vegetation in the urban green space can absorb pollutants and improve air quality. Sulfur dioxide (SO_2) was used as exemplar to calculate the annual volume of standard pollutants absorbed by vegetation.

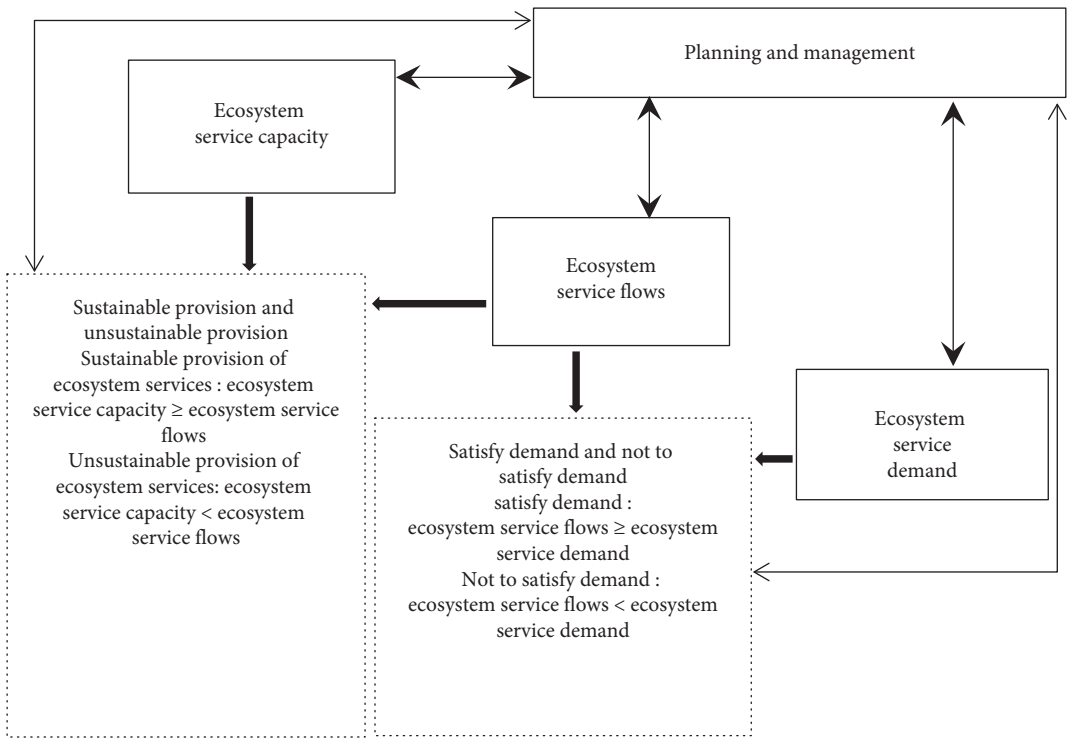

Figure 1: Flow chart of relationships among ecosystem service capacity, traffic, demand, and planning management.

(2) Indicators Used for Assessment of Ecosystem Services. An evaluation index along with the relevant data were used to assess the ecosystem services provided by urban green spaces, as summarized in Table 1.

(3) Standardized Treatment. To compare data in different dimensions, the results of the calculated recreational space, capacity for air purification, flow, demand, sustainable supply, and unmet demand were standardized. The formula used is as follows:

$$x' = \frac{x - x_{\min}}{x_{\max} - x_{\min}}, \tag{1}$$

where x' denotes the standardized value, $x_{\max}$ denotes the maximum value of the sampled data, $x_{\min}$ denotes its minimum value, and x denotes the original data.

2.3.2. Recreational Space. The model used to evaluate recreational space emphasizes natural recreation in daily life. The carrying capacity of green spaces was evaluated using the attraction model [38], where the area occupied by green spaces and the distance to these areas were key factors. The area of green spaces was calculated using the software package ArcGIS [36], as was the distance between the green space and the center of each block within Hefei. The attraction was calculated as follows:

$$F_{kl} = \frac{a_k}{d_{kl}^2}, \tag{2}$$

where F_{kl} denotes the attraction of green space K at point l, a_k denotes the area of green space K (m^2), and d_{kl} is the linear distance between green space K and point l (m).

The flow of recreational space was derived using a 1 km distance threshold for green space, which denotes daily outdoor activities in close proximity. ArcGIS was used to build a 1 km buffer zone with green space as source. These data were then superimposed onto a population density grid to calculate the number of residents arriving at green spaces as a measure of the flow of recreational space [33]. The results of the calculation of carrying capacity and flow of recreational space were divided into grades 1–5 using the natural fracture method of ArcGIS.

The demand for recreational space was evaluated based on an intersection matrix of the distance between the center of each block and the green space and the population density of the block. Thus, given the assumption that all residents have similar aspirations for their daily recreational spaces, spatial intersection was performed using the Euclidean distance between each reclassified block and the recreational space and the population density grid.

The sustainable supply and unmet demand of recreational space were evaluated using the conceptual framework outlined in Table 1. The results were divided into grades 1–5 using the natural fracture method. The sustainability of recreational spaces was calculated as follows:

$$V_{sr} = V_{cr} - V_{fr}, \tag{3}$$

where V_{sr} denotes the sustainable supply of recreational space, V_{cr} is the carrying capacity of such space, and V_{fr} denotes the flow of recreational space. This means that, if $V_{sr} \geq 0$, the recreational space was considered to have been used sustainably, but if $V_{sr} < 0$, it was being used excessively.

The area of the recreational space that did not meet the above demand was calculated as follows:

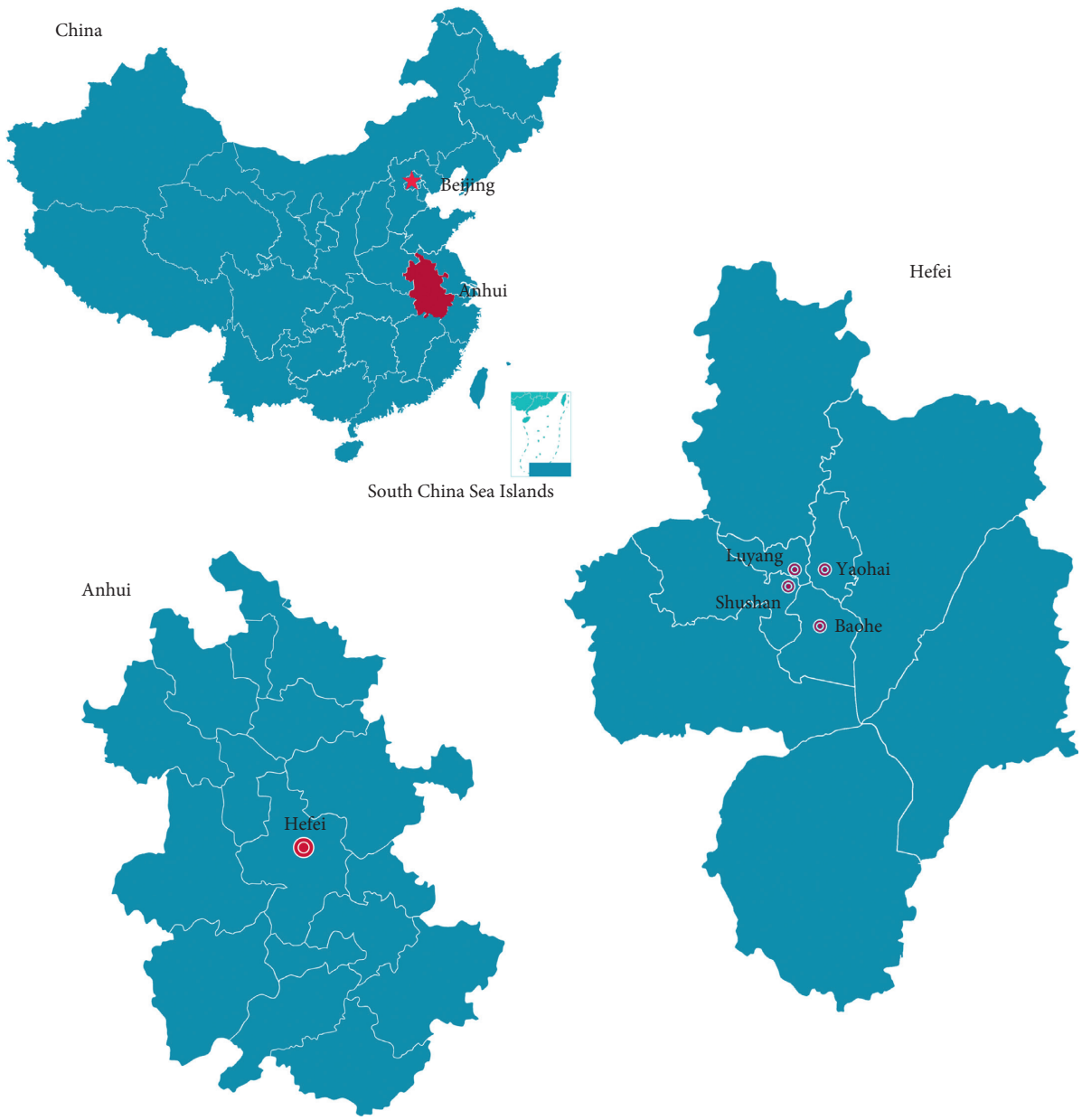

Figure 2: The study area: Hefei in Anhui Province, China.

$$V_{ur} = V_{fr} - V_{dr}, \tag{4}$$

where V_{ur} denotes the extent to which the given recreational space failed to meet demand, V_{fr} is the flow of recreational space, and V_{dr} is demand for it. If $V_{ur} \geq 0$, the recreational space was considered to have met demand, whereas if $V_{ur} < 0$, the demand was not met.

2.3.3. Air Purification (SO_2). This research focuses on SO_2 as air pollutant. In terms of evaluating the carrying capacity of air purification, the literature suggests that the maximum threshold of the absorption of SO_2 per unit area of green space is 88.65 kg·hm^{-2}·a^{-1} [37] as follows:

$$V_{ca} = 88.65 \times \frac{S_{sub}}{S}, \tag{5}$$

where V_{ca} denotes the carrying capacity of air purification, S_{sub} is the area of green space, and S is the area of green space.

A review of the literature on the flow evaluation of air purification shows that the annual volume of SO_2 absorbed through woodlands and grasslands is 123.5 t/hm^2 and 7.92 t/hm^2, respectively [37]:

$$V_{fa} = A_g \times 7.92 + A_f \times 123.5, \tag{6}$$

where V_{fa} denotes flow rate of air purification, A_g is the area of grassland within a green space system, and A_f denotes forested area.

Table 1: Standards and data used to evaluate ecosystem service models.

Function	Composition	Indicators	Data sources
Recreational function (daily life)	Capacity of recreational space	Recreational area and distance from street center	Landsat8 remote sensing (RS) image
	Recreational space flows	Number of residents visiting recreational space	Demographic data from the Hefei Civil Affairs Bureau
	The demand for recreational space	Distance of recreational area from street center and population density	Demographic data from the Hefei Civil Affairs Bureau
	Sustainable supply of recreational space	Carrying capacity minus flow is greater than or equal to zero: sustainable supply of recreational space Carrying capacity minus flows is less than zero: unsustainable provision of recreational space	Landsat8 RS image Demographic data from the Hefei Civil Affairs Bureau
	Supply and demand of recreational space	Flow minus demand is greater than or equal to zero: satisfy demand of recreational space Flows minus demand is less than zero: not to satisfy demand for recreational space	Landsat8 RS image Demographic data from the Hefei Civil Affairs Bureau
Air purification (SO_2)	Air purification capacity	Maximum annual absorption of SO_2 by vegetation	Reference [36]
	Air purification flows	Actual annual SO_2 uptake by vegetation	Reference [37]
	Air purification demand	SO_2 average concentration and population density of blocks	Monitoring data from the Hefei Environmental Protection Bureau
	Sustainable supply of air purification	Carrying capacity minus flows is greater than or equal to zero: sustainable supply of air purification Carrying capacity minus flow is less than zero: unsustainable provision of air purification	Reference [36, 37]
	Supply-demand relationship of air purification	Flows minus demand is greater than or equal to zero: satisfy demand of air purification Flows minus demand is less than zero: does not satisfy the demand for air purification	Reference [37], monitoring data from the Hefei Environmental Protection Bureau

The demand for air purification was evaluated based on the concentration levels of SO_2 in each block as well as population density. The spatial intersection between variables was evaluated using the same method as that used to calculate demand for recreational space. Thus, the obtained indices represent the demand for air purification in the range from 1 (low demand) to 5 (very high demand).

The sustainable supply of air purification and unmet demand were calculated using the conceptual framework outlined in Table 1. Sustainable air purification was calculated as follows:

$$V_{sa} = V_{ca} - V_{fa}, \tag{7}$$

where V_{sa} denotes a sustainable supply for air purification, V_{ca} is carrying capacity, and $V_{fa.}$ is the flow rate of air purification. $V_{sa} \geq 0$ implies the sustainable use of air purification, whereas $V_{sa} < 0$ implies excessive use.

The formula used to calculate the level of air purification that does not meet demand is as follows:

$$V_{ua} = V_{fa} - V_{da}, \tag{8}$$

where V_{ua} denotes the degree to which air purification cannot meet demand, V_{fa} refers to the flow of air purification, and V_{da}denotes demand for air purification. If $V_{ua} \geq 0$, air purification meets demand, whereas if $V_{ua} < 0$, it does not.

3. Results and Analysis

3.1. Capacity, Flow, and Supply and Demand for Ecosystem Services

3.1.1. Recreation. The ecosystem services evaluation model was used to obtain the carrying capacity, flow, and supply and demand for Hefei. These data show that the carrying capacities of recreational green space in the northwest, southwest, and southeast of the city were relatively high, including the Dongpu and Dafangying reservoirs as well as urban forests and the Binhu Wetland Park. Scores of the carrying capacity for green spaces in this area were 2.34, 2.11, 1.79, and 1.17; the data suggest that the carrying capacity of green spaces in parks in the central urban area of Hefei was moderate and included Swan Lake, Around the City Park, and Hefei Nanyanhu, with scores of 0.73, 0.64, and 0.45, respectively. Recreational spaces featuring significant activity included Around the City Park, Swan Lake, and Binhu Wetland Park. The data showed a highly sustainable supply of recreational space in the northwest and southwest of the city, while the supply of green space along Changjiang Road and Huizhou Avenue had low sustainability. The main reason for this result is that the parkland area around these roads was small, while the surrounding residential areas were large and housed a large population. At the same time,

the space for recreational activity was large, and areas with high demand for recreational space were mainly located in the east and southwest of Hefei. On the whole, the demand was greater than the supply. The relationship between supply and demand in this region was moderate and thus unsatisfactory.

3.1.2. Air Purification. The capacity of green spaces for air purification in the northwest, southwest, and southeast suburbs of Hefei was high. The scores of green space for the Dongpu reservoir, Dafangying reservoir, Urban Forest Park, and Binhu Wetland Park were 3.02, 1.68, 1.34, and 4.38, respectively. The capacity for air purification of green space in the city center was moderate, while scores for Tangxihe Park, Feicui Lake, and Hefei Nanyanhu were 0.79, 0.84, and 0.88, respectively. The air purification capacities of suburban green spaces were higher than those of their central urban counterparts. Areas with the highest flow of air purification were in the northwest, southwest, and southeast of Hefei and included the Dongpu and Dafangying reservoirs, Urban Forest Park, and Binhu Wetland Park. These green spaces absorbed more SO_2 because of the high vegetation coverage in their suburban areas, whereas the flow of air purification in park green spaces and protected green spaces was low. Areas with the highest demand for air purification in Hefei were mainly located in the northeast. It is an old city containing an industrial zone with high population density and a high concentration of SO_2. The capacity for air purification was inadequate in the northeast and southwest of Hefei.

In general, spatial differences in the flow of supply and demand for in green spaces were significant in Hefei. However, the northeast and southwest remained unbalanced with respect to supply and demand. The most significant factors controlling these differences were small green areas, high population density, and concentration of pollutants.

4. Discussion

4.1. Detecting Unsustainable Use of Green Spaces. A visual analysis of the flow of supply and demand for urban green spaces as ecosystem services shows that they were not fully coincident with the planning for urban green systems, and the local green space system with high demand is not perfect. To make planning more effective, the function of ecosystem services should be applied, especially because it is important for the use of resources and fairness. Such a plan can support urban green spaces for ecosystem services in a comprehensive way. A strategic and comprehensive process can help ensure the provision of ecosystem services owing to urban green space. The model to evaluate these ecosystem services provides a flexible tool to optimize the spatial layout of green space by assessing the supply and demand for them. This can help implement comprehensive land use governance to enhance the potential of multifunctional ecosystem services by balancing the supply and demand for green ecosystem services. Although the model can be used for spatial planning based on spatial restoration, it should not be considered an analysis of the suitability of land because it does not consider specific plots, land use, cost, and other effects on the green space. Public participation can also be used to improve the index of the demand for green space, interaction of ecosystem services at different scales, and decision support for urban and rural planning systems [39].

At present, the suburban green space is divided into the urban green space system in the urban and rural planning, and the suburban green space has the risk of destruction in the future urbanization process. Therefore, planning for Hefei should seek to protect the carrying capacity and discharge of ecosystem services in these sensitive areas. The demand for recreational spaces was mainly located in the eastern part of the city, close to the center. To address unsatisfactory demand, green infrastructure planning should be implemented to protect green spaces and develop ways to restore them or to create new green space. The assessments of air purification show that reducing or limiting private traffic in certain areas, encouraging the use of public transport and nonmotorized or low-emission vehicles, strengthening transport planning to achieve shorter commuting needs through tree planting or the selection of strategies such as trees with high air pollution removal capacity, and policy interventions can help solve the mismatch between the flow of air purification and demand for it [40].

5. Conclusions

The results of this study validate the relationships among the capacity, flow, and demand for ecosystem services as well as their applicability to a system of planning for urban green spaces. They also show a significant spatial difference in the flow of supply and demand for ecosystem services owing to green space within Hefei. The data show that the northeast and southwest of the city were significantly unbalanced with respect to supply and demand, where the excessive use of such services was concentrated in the urban center but was sustainable in suburban areas. The gap between the supply and demand for recreational space increased in concert with distance, whereas the gap between variables influencing air purification decreased with distance [41, 42].

The limitations of the proposed method are its suitable indicators of the unsustainable use of green spaces. Policies implemented in the future should seek to harmonize different components of this framework based on the characteristics of the city or area of interest. Urban policies for air purification should focus on reducing the concentration of pollutants, while the optimization of recreational spaces relies on planning tools to maintain and promote the carrying capacity and flow of ecosystem services. A combination of regulatory policies (e.g., enforcement caps and stricter green infrastructure ratios) as well as economic incentives (e.g., environmental taxes, subsidies, and payments) are feasible options.

Future work in this area should emphasize improvements in the service demand index of green space ecosystems by means of public participation, interactions among green space ecosystem services at different scales, and decision support for urban and rural planning systems.

Data Availability

The data used to support the findings of this study are available from the corresponding author upon request.

Conflicts of Interest

The authors declare that there are no conflicts of interest regarding the publication of this paper.

Acknowledgments

This work was supported by the National Key R&D Program of China (2017YFC0505706).

References

[1] E. Gómez-Baggethun, R. de Groot, P. L. Lomas, and C. Montes, "The history of ecosystem services in economic theory and practice: from early notions to markets and payment schemes," *Ecological Economics*, vol. 69, no. 6, pp. 1209–1218, 2010.

[2] R. Costanza, R. D'Arge, R. D. Groot et al., "The value of the world's ecosystem services and natural capital," *World Environment*, vol. 25, no. 1, pp. 3–15, 1997.

[3] J. Wu, "Landscape sustainability science: ecosystem services and human well-being in changing landscapes," *Landscape Ecology*, vol. 28, no. 6, pp. 123–135, 2013.

[4] E. Andersson, S. Barthel, S. Borgström et al., "Reconnecting cities to the biosphere: stewardship of green infrastructure and urban ecosystem services," *Ambio*, vol. 43, no. 4, pp. 445–453, 2014.

[5] C. Kambites and S. Owen, "Renewed prospects for green infrastructure planning in the UK," *Planning Practice and Research*, vol. 21, no. 4, pp. 483–496, 2006.

[6] T. Hooper, N. Beaumont, C. Griffiths, O. Langmead, and P. J. Somerfield, "Assessing the sensitivity of ecosystem services to changing pressures," *Ecosystem Services*, vol. 24, pp. 160–169, 2017.

[7] B. Zhang, Y.-T. Shi, J.-H. Liu, J. Xu, and G.-D. Xie, "Economic values and dominant providers of key ecosystem services of wetlands in Beijing, China," *Ecological Indicators*, vol. 77, pp. 48–58, 2017.

[8] L. Ma, S. Lu, Y. Lu, M. Wang, and L. Ma, "Evaluation of ecosystem services function of the north shore of west Dianchi lake Wetland park," *Science & Technology Review*, vol. 34, no. 18, pp. 156–161, 2016.

[9] Y. Yan, J. Y. Zhu, G. Wu, and Y. J. Zhan, "Review and prospective applications of demand, supply, and consumption of ecosystem services," *Acta Ecologica Sinica*, vol. 37, no. 8, pp. 2489–2496, 2017.

[10] E. S. V. D. Meulen, L. C. Braat, and J. M. Brils, "Abiotic flows should be inherent part of ecosystem services classification," *Ecosystem Services*, vol. 19, no. 19, pp. 1–5, 2016.

[11] J. Brils, P. de Boer, J. Mulder, and E. de Boer, "Reuse of dredged material as a way to tackle societal challenges," *Journal of Soils and Sediments*, vol. 14, no. 9, pp. 1638–1641, 2014.

[12] F. Baró, I. Palomo, G. Zulian, P. Vizcaino, D. Haase, and E. Gómez-Baggethun, "Mapping ecosystem service capacity, flow and demand for landscape and urban planning: a case study in the Barcelona metropolitan region," *Land Use Policy*, vol. 57, pp. 405–417, 2016.

[13] K. K. Gu, "Concepts and assessment methods of ecological carrying capacity," *Ecology and Environmental Sciences*, vol. 21, no. 2, pp. 389–396, 2012.

[14] O. Bastian, R.-U. Syrbe, M. Rosenberg, D. Rahe, and K. Grunewald, "The five pillar EPPS framework for quantifying, mapping and managing ecosystem services," *Ecosystem Services*, vol. 4, no. 4, pp. 15–24, 2013.

[15] P. Matos, J. Vieira, B. Rocha, C. Branquinho, and P. Pinho, "Modeling the provision of air-quality regulation ecosystem service provided by urban green spaces using lichens as ecological indicators," *Science of the Total Environment*, vol. 665, pp. 521–530, 2019.

[16] T. M. Anderson and S. Dragićević, "Network-agent based model for simulating the dynamic spatial network structure of complex ecological systems," *Ecological Modelling*, vol. 389, pp. 19–32, 2018.

[17] B. Danley and C. Widmark, "Evaluating conceptual definitions of ecosystem services and their implications," *Ecological Economics*, vol. 126, pp. 132–138, 2016.

[18] W. Verhagen, A. S. Kukkala, A. Moilanen, A. J. A. van Teeffelen, and P. H. Verburg, "Use of demand for and spatial flow of ecosystem services to identify priority areas," *Conservation Biology*, vol. 31, no. 4, pp. 860–871, 2017.

[19] B. Burkhard, M. Kandziora, Y. Hou, and F. Müller, "Ecosystem service potentials, flows and demands-concepts for spatial localisation, indication and quantification," *Landscape Online*, vol. 34, no. 1, pp. 1–32, 2014.

[20] M. Schröter, D. N. Barton, R. P. Remme, and L. Hein, "Accounting for capacity and flow of ecosystem services: a conceptual model and a case study for Telemark, Norway," *Ecological Indicators*, vol. 36, no. 1, pp. 539–551, 2014.

[21] F. Baró, D. Haase, E. Gómez-Baggethun, and N. Frantzeskaki, "Mismatches between ecosystem services supply and demand in urban areas: a quantitative assessment in five European cities," *Ecological Indicators*, vol. 55, pp. 146–158, 2015.

[22] L. Xu, H. You, D. Li, and K. Yu, "Urban green spaces, their spatial pattern, and ecosystem service value: the case of Beijing," *Habitat International*, vol. 56, pp. 84–95, 2016.

[23] P. Stessens, A. Z. Khan, M. Huysmans, and F. Canters, "Analysing urban green space accessibility and quality: a GIS-based model as spatial decision support for urban ecosystem services in Brussels," *Ecosystem Services*, vol. 28, pp. 328–340, 2017.

[24] C. L. Ana, B. Maartje, A. Cristiana et al., "Should I stay or should I go? Modelling the fluxes of urban residents to visit green spaces," *Urban Forestry & Urban Greening*, vol. 40, pp. 195–203, 2019.

[25] O. Barbosa, J. A. Tratalos, P. R. Armsworth et al., "Who benefits from access to green space? A case study from Sheffield, UK," *Landscape and Urban Planning*, vol. 83, no. 2-3, pp. 187–195, 2007.

[26] N. Kabisch and D. Haase, "Green justice or just green? Provision of urban green spaces in Berlin, Germany," *Landscape and Urban Planning*, vol. 122, pp. 129–139, 2014.

[27] R. Haines-Young and M. Potschin, "The links between biodiversity, ecosystem service and human well-being," in *Ecosystem Ecology: A New Synthesis*, Cambridge University Press, Cambridge, UK, 2009.

[28] A. M. Villamagna, P. L. Angermeier, and E. M. Bennett, "Capacity, pressure, demand, and flow: a conceptual framework for analyzing ecosystem service provision and delivery," *Ecological Complexity*, vol. 15, no. 5, pp. 114–121, 2013.

[29] W. Verhagen, A. J. A. Van Teeffelen, A. B. Compagnucci, L. Poggio, A. Gimona, and H. L. Peter, "Effects of landscape

configuration on mapping ecosystem service capacity: a review of evidence and a case study in Scotland," *Landscape Ecology*, vol. 31, no. 7, pp. 1457–1479, 2016.

[30] Y. Depietri, G. Kallis, F. Baró, and C. Cattaneo, "The urban political ecology of ecosystem services: the case of Barcelona," *Ecological Economics*, vol. 125, pp. 83–100, 2016.

[31] I. R. Geijzendorffer, B. Martín-López, and P. K. Roche, "Improving the identification of mismatches in ecosystem services assessments," *Ecological Indicators*, vol. 52, no. 52, pp. 320–331, 2015.

[32] A. Chiesura, "The role of urban parks for the sustainable city," *Landscape and Urban Planning*, vol. 68, no. 1, pp. 129–138, 2004.

[33] E. Gómez-Baggethun and D. N. Barton, "Classifying and valuing ecosystem services for urban planning," *Ecological Economics*, vol. 86, no. 1, pp. 235–245, 2013.

[34] M. Triguero-Mas, P. Dadvand, M. Cirach et al., "Natural outdoor environments and mental and physical health: relationships and mechanisms," *Environment International*, vol. 77, pp. 35–41, 2015.

[35] M. L. Paracchini, G. Zulian, L. Kopperoinen et al., "Mapping cultural ecosystem services: a framework to assess the potential for outdoor recreation across the EU," *Ecological Indicators*, vol. 45, no. 5, pp. 371–385, 2014.

[36] G. Zulian, C. Polce, and J. Maes, "ESTIMAP: a GIS-based model to map ecosystem services in the European Union," *Annali Di Botanica*, vol. 4, pp. 1–7, 2014.

[37] Z. M. Xiao, L. H. Wang, L. Hao, and L. Y. Wu, "Environment purification service value of urban green space ecosystem in Weifang City," *Acta Ecologica Sinica*, vol. 31, no. 9, pp. 2576–2584, 2011.

[38] E. Bukvareva, D. Zamolodchikov, G. Kraev, K. Grunewald, and A. Narykov, "Supplied, demanded and consumed ecosystem services: prospects for national assessment in Russia," *Ecological Indicators*, vol. 78, pp. 351–360, 2017.

[39] G. Pulighe, F. Fava, and F. Lupia, "Insights and opportunities from mapping ecosystem services of urban green spaces and potentials in planning," *Ecosystem Services*, vol. 22, pp. 1–10, 2016.

[40] I. Palomo, B. Martín-López, P. Zorrilla-Miras, D. García Del Amo, and C. Montes, "Deliberative mapping of ecosystem services within and around Doñana National Park (SW Spain) in relation to land use change," *Regional Environmental Change*, vol. 14, no. 1, pp. 237–251, 2014.

[41] J. B. Liu, J. Zhao, and Z. X. Zhu, "On the number of spanning trees and normalized Laplacian of linear octagonal-quadrilateral networks," *International Journal of Quantum Chemistry*, vol. 119, no. 17, Article ID e25971, 2019.

[42] J.-B. Liu, J. Zhao, and Z.-Q. Cai, "On the generalized adjacency, Laplacian and signless Laplacian spectra of the weighted edge corona networks," *Physica A: Statistical Mechanics and Its Applications*, vol. 540, p. 123073, 2020.

Hindawi
Journal of Chemistry
Volume 2020, Article ID 9805829, 12 pages
https://doi.org/10.1155/2020/9805829

Research Article

Reverse Zagreb and Reverse Hyper-Zagreb Indices for Crystallographic Structure of Molecules

Zhen Wang,[1] Faryal Chaudhry,[2] Maria Naseem,[3] and Adnan Asghar[2]

[1]*School of Computer Engineering, Anhui Wonder University of Information Engineering, Hefei 231201, China*
[2]*The University of Lahore, Lahore, Pakistan*
[3]*University of Central Punjab, Lahore, Pakistan*

Correspondence should be addressed to Adnan Asghar; adnan.asghar@math.uol.edu.pk

Received 9 October 2019; Accepted 8 February 2020; Published 13 March 2020

Academic Editor: Jia-Bao Liu

In the fields of chemical graph theory, topological index is a type of a molecular descriptor that is calculated based on the graph of a chemical compound. Topological indices help us collect information about algebraic graphs and give us mathematical approach to understand the properties of algebraic structures. With the help of topological indices, we can guess the properties of chemical compounds without performing experiments in wet lab. There are more than 148 topological indices in the literature, but none of them completely give all properties of under study compounds. Together, they do it to some extent; hence, there is always room to introduce new indices. In this paper, we present first and second reserve Zagreb indices and first reverse hyper-Zagreb indices, reverse GA index, and reverse atomic bond connectivity index for the crystallographic structure of molecules. We also present first and second reverse Zagreb polynomials and first and second reverse hyper-Zagreb polynomials for the crystallographic structure of molecules.

1. Introduction

Topological indices enable us to collect information about algebraic structures and give us a mathematical approach to understand the properties of algebraic structures. Here, we will discuss some newly introduced first and second reverse Zagreb indices, hyper-Zagreb indices, and their polynomials for the crystallographic structure of molecules [1–9].

A graph having no loop or multiple edges is known as simple graph. A molecular graph is a simple graph in which atoms and bonds are represented by vertex and edge sets, respectively. The vertex degree is the number of edges attached to that vertex [10–16]. The maximum degree of vertex among the vertices of a graph is denoted by $\Delta(G)$. Kulli et al. [17] introduce the concept of reverse vertex degree C_y, defined as $C_y = \Delta(G) - d_g(v) + 1$.

In discrete mathematics, graph theory in general is not only the study of different properties of objects but it also tells us about objects having same properties as investigating object. These properties of different objects are of main interest. In particular, graph polynomials related to graph are rich in information. Mathematical tools like polynomials and topological-based numbers have significant importance to collect information about the properties of chemical compounds. We can find out many hidden information about compounds through these tools. Multifold graph polynomials are present in the literature. Actually, topological indices are numeric quantities that tell us about the whole structure of graph. There are many topological indices [18, 19] that help us to study physical, chemical reactivities, and biological properties. Wiener, in 1947 [20], firstly introduce the concept of topological index while working on boiling point. In particular, Hosoya polynomial [21] plays an important in the area of distance-based topological indices; we can find out Wiener index, hyper-Wiener index, and Tratch–Stankevich–Zefirov index by Hosoya polynomial [22, 23]. Other well-established polynomials are Zagreb and hyper-Zagreb polynomials introduced by Gao.

The first and second reverse Zagreb indices are as follows:

$$\begin{aligned} CM_1(G) &= \sum_{uv\epsilon E(G)} (c_u + c_v), \\ CM_2(G) &= \sum_{uv\epsilon E(G)} (c_u.c_v). \end{aligned} \tag{1}$$

Now, the first and second reverse hyper-Zagreb indices are given by

$$\begin{aligned} HCM_1(G) &= \sum_{uv\epsilon E(G)} (c_u + c_v)^2, \\ HCM_2(G) &= \sum_{uv\epsilon E(G)} (c_u.c_v)^2. \end{aligned} \tag{2}$$

Atom-bond connectivity index can be abbreviated as ABC index. It is defined as follows:

$$ABC(G) = \sum_{uv\epsilon E(G)} \sqrt{\frac{d_u(G) + d_v(G) - 2}{d_u(G).d_v(G)}}. \tag{3}$$

Another degree-based topological index that utilizes the difference between the geometric and arithmetic means was invented by Vukicevic and Furtula, namely, geometric-arithmetic index and is defined as follows:

$$GA(G) = \sum_{uv\epsilon E(G)} \frac{\sqrt{d_u(G).d_v(G)}}{(1/2)[d_u(G) + d_v(G)]}. \tag{4}$$

With the help of reverse Zagreb and hyper-Zagreb indices, we are now able to write the reverse Zagreb and hyper Zagreb polynomials:

$$\begin{aligned} CM_1(G,x) &= \sum_{uv\epsilon E(G)} x^{(c_u+c_v)}, \\ CM_2(G,x) &= \sum_{uv\epsilon E(G)} x^{(c_u.c_v)}, \\ HCM_1(G,x) &= \sum_{uv\epsilon E(G)} x^{(c_u+c_v)^2}, \\ HCM_2(G,x) &= \sum_{uv\epsilon E(G)} x^{(c_u.c_v)^2}. \end{aligned} \tag{5}$$

We introduce the idea of reverse atom-bond connectivity index and reverse geometric-arithmetic index, and it is defined as follows:

$$\begin{aligned} CABC(G) &= \sum_{uv\epsilon E(G)} \sqrt{\frac{c_u(G) + c_v(G) - 2}{c_u(G).c_v(G)}}, \\ CGA(G) &= \sum_{uv\epsilon E(G)} \frac{\sqrt{c_u(G).c_v(G)}}{(1/2)[c_u(G) + c_v(G)]}. \end{aligned} \tag{6}$$

2. Main Results

Here, we will compute reverse Zagreb and reverse hyper-Zagreb indices for the crystallographic structure of molecules.

2.1. Crystallographic Structure of the Molecule Cu_2O. The unit cell of the crystallographic structure of the molecule Cu_2O is given in Figure 1 and the crystal structure of Cu_2O [3, 3, 3] is given in Figure 2.

Theorem 1. *Let G be the chemical graph of Cu_2O, with m, α, t ≥ 1. The first and second reverse Zagreb indices are as follows:*

(1) $CM_1(Cu_2O) = 32m\alpha t + 20m\alpha + 20mt + 20\alpha t + 36 - 28m - 28\alpha - 28t$

(2) $CM_2(Cu_2O) = 24m\alpha t + 24m\alpha + 24mt + 24\alpha t - 12m - 12\alpha - 12t$

Proof. From Figure 2, we can say that there are 3 types of edges in Cu_2O:

$$\begin{aligned} E_1(Cu_2O) &= \{uv \epsilon E(Cu_2O); d_u = 1, d_v = 2\}, \\ E_2(Cu_2O) &= \{uv \epsilon E(Cu_2O); d_u = 2, d_v = 2\}, \\ E_3(Cu_2O) &= \{uv \epsilon E(Cu_2O); d_u = 2, d_v = 4\}. \end{aligned} \tag{7}$$

We have $|E_1(Cu_2O)| = 4\alpha + 4m + 4t - 8$, $|E_2(Cu_2O)| = 4\alpha m + 4\alpha t + 4mt - 8\alpha - 8m - 8t + 12$, and $|E_3(Cu_2O)| = 4(2\alpha mt - \alpha m - \alpha t - mt + \alpha + m + t - 1)$. In this structure, the maximum edge degree is 4, and then, the reverse edges are given as follows:

$$c_u = \Delta(G) - d_G(u) + 1 = 5 - d_G(u). \tag{8}$$

The reverse edge set of Cu_2O is given as follows:

$$\begin{aligned} CE_1(Cu_2O) &= \{uv \epsilon E(Cu_2O); c_u = 4, c_v = 3\}, \\ CE_2(Cu_2O) &= \{uv \epsilon E(Cu_2O); c_u = 3, c_v = 3\}, \\ CE_3(Cu_2O) &= \{uv \epsilon E(Cu_2O); c_u = 3, c_v = 1\}. \end{aligned} \tag{9}$$

We have $|CE_1(Cu_2O)| = 4\alpha + 4m + 4t - 8$, $|CE_2(Cu_2O)| = 4\alpha m + 4\alpha t + 4mt - 8\alpha - 8m - 8t + 12$, and $|CE_3(Cu_2O)| = 4(2\alpha mt - \alpha m - \alpha t - mt + \alpha + m + t - 1)$.

(i) The first reverse ZI for Cu_2O is given by

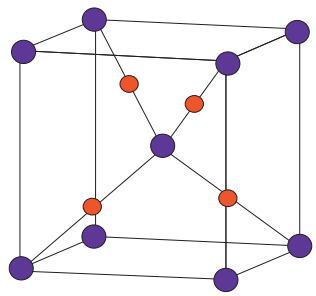

Figure 1: Unit cell of Cu_2O [1, 1, 1].

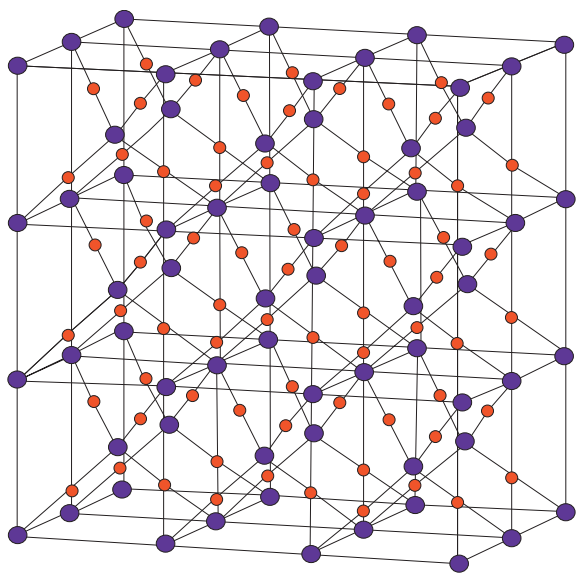

Figure 2: Crystal structure of Cu_2O [3, 3, 3].

$$\begin{aligned} CM_1(Cu_2O) &= \sum_{uv\epsilon E(G)} (c_u + c_v) \\ &= (4+3)(4\alpha + 4m + 4t - 8) + (3+3)(4\alpha m + 4\alpha t + 4mt - 8\alpha - 8m - 8t + 12) + (3+1) \\ &\quad \cdot (4(2\alpha mt - \alpha m - \alpha t - mt + \alpha + m + t - 1)) \\ &= 32m\alpha t + 20m\alpha + 20mt + 20\alpha t + 36 - 28m - 28\alpha - 28t. \end{aligned} \tag{10}$$

(ii) The second reverse ZI for Cu_2O is given by

$$\begin{aligned} CM_2(Cu_2O) &= \sum_{uv\epsilon E(G)} (c_u . c_v) \\ &= (4\times 3)(4\alpha + 4m + 4t - 8) + (3\times 3)(4\alpha m + 4\alpha t + 4mt - 8\alpha - 8m - 8t + 12) \\ &\quad + (3\times 1)(4(2\alpha mt - \alpha m - \alpha t - mt + \alpha + m + t - 1)) \\ &= 24m\alpha t + 24m\alpha + 24mt + 24\alpha t - 12m - 12\alpha - 12t. \end{aligned} \tag{11}$$

□

Theorem 2. *The first and second reverse Zagreb polynomials for Cu_2O with $m, n, t \geq 1$ are as follows:*

$$\begin{aligned} 1.\mathrm{CM}_1(\mathrm{Cu}_2\mathrm{O}, x) &= x^7(4\alpha + 4m + 4t - 8) + x^6(4\alpha m + 4\alpha t + 4mt - 8\alpha - 8m - 8t + 12) \\ &\quad + x^4(4(2\alpha mt - \alpha m - \alpha t - mt + \alpha + m + t - 1), \\ 2.\mathrm{CM}_2(\mathrm{Cu}_2\mathrm{O}, x) &= x^{12}(4\alpha + 4m + 4t - 8) + x^9(4\alpha m + 4\alpha t + 4mt - 8\alpha - 8m - 8t + 12) \\ &\quad + x^3(4(2\alpha mt - \alpha m - \alpha t - mt + \alpha + m + t - 1). \end{aligned} \tag{12}$$

Proof. Now, by the reverse edge partitions of Cu_2O, we have the following results:

(i) The first reverse Zagreb polynomial for Cu_2O is given as follows:

$$\begin{aligned} \mathrm{CM}_1(\mathrm{Cu}_2\mathrm{O}, x) &= \sum_{uv\epsilon E(G)} x^{(c_u + c_v)} \\ &= (4\alpha + 4m + 4t - 8)x^{(3+4)} + (4\alpha m + 4\alpha t + 4mt - 8\alpha - 8m - 8t + 12)x^{(3+3)} \\ &\quad + \left(4(2\alpha mt - \alpha m - \alpha t - mt + \alpha + m + t - 1)x^{(3+1)}\right. \\ &= x^7(4\alpha + 4m + 4t - 8) + x^6(4\alpha m + 4\alpha t + 4mt - 8\alpha - 8m - 8t + 12) \\ &\quad + x^4(4(2\alpha mt - \alpha m - \alpha t - mt + \alpha + m + t - 1). \end{aligned} \tag{13}$$

(ii) The second reverse Zagreb polynomial for Cu_2O, with $m, \alpha, t \geq 1$, is given as follows:

$$\begin{aligned} \mathrm{CM}_2(\mathrm{Cu}_2\mathrm{O}, x) &= \sum_{uv\epsilon E(G)} x^{(c_u \cdot c_v)} \\ &= (4\alpha + 4m + 4t - 8)x^{(3\times 4)} + (4\alpha m + 4\alpha t + 4mt - 8\alpha - 8m - 8t + 12)x^{(3\times 3)} \\ &\quad + \left(4(2\alpha mt - \alpha m - \alpha t - mt + \alpha + m + t - 1)x^{(3\times 1)}\right. \\ &= x^{12}(4\alpha + 4m + 4t - 8) + x^9(4\alpha m + 4\alpha t + 4mt - 8\alpha - 8m - 8t + 12) \\ &\quad + x^3(4(2\alpha mt - \alpha m - \alpha t - mt + \alpha + m + t - 1). \end{aligned} \tag{14}$$

□

Theorem 3. *The first and second reverse hyper-Zagreb indices of silicon-carbon Cu_2O with $m, \alpha, t \geq 1$ are as follows:*

(1) $HCM_1(Cu_2O) = 32m\alpha t + 128m\alpha + 128mt + 128\alpha t - 76m - 76\alpha - 76t + 24$

(2) $HCM_2(Cu_2O) = 18m\alpha t + 315m\alpha + 315mt + 315\alpha t - 63m - 63\alpha - 63t - 189$

Proof. Let G be a graph of Cu_2O. Then, by reverse edge partition and definition of reverse hyper-Zagreb indices, we have the following results:

(i) The first reverse hyper-ZI for Cu_2O is given by

$$\begin{aligned} \mathrm{CM}_1(\mathrm{Cu}_2\mathrm{O}) &= \sum_{uv\epsilon E(G)} (c_u + c_v)^2 \\ &= (4+3)^2(4\alpha + 4m + 4t - 8) + (3+3)^2(4\alpha m + 4\alpha t + 4mt - 8\alpha - 8m - 8t + 12) \\ &\quad + (3+1)^2(4(2\alpha mt - \alpha m - \alpha t - mt + \alpha + m + t - 1)) \\ &= 32m\alpha t + 128m\alpha + 128mt + 128\alpha t - 76m - 76\alpha - 76t + 24. \end{aligned} \tag{15}$$

(ii) The second reverse hyper-ZI for Cu_2O is given by

$$\begin{aligned} CM_2(Cu_2O) &= \sum_{uv\epsilon E(G)} (c_u.c_v)^2 \\ &= (4\times 3)^2(4\alpha+4m+4t-8)+(3\times 3)^2(4\alpha m+4\alpha t+4mt-8\alpha-8m-8t+12) \\ &\quad +(3\times 1)^2(4(2\alpha mt-\alpha m-\alpha t-mt+\alpha+m+t-1)) \\ &= 18m\alpha t+315m\alpha+315mt+315\alpha t-63m-63\alpha-63t-189. \end{aligned} \tag{16}$$

□

Theorem 4. *The first and second reverse hyper-Zagreb polynomials of Cu_2O with $m, \alpha, t \geq 1$ are as follows:*

$$\begin{aligned} 1.HCM_1(Cu_2O,x) &= x^{144}(4\alpha+4m+4t-8)+x^{81}(4\alpha m+4\alpha t+4mt-8\alpha-8m-8t+12) \\ &\quad +x^{9}(4(2\alpha mt-\alpha m-\alpha t-mt+\alpha+m+t-1), \\ 2.HCM_1(Cu_2O,x) &= x^{144}(4\alpha+4m+4t-8)+x^{81}(4\alpha m+4\alpha t+4mt-8\alpha-8m-8t+12) \\ &\quad +x^{9}(4(2\alpha mt-\alpha m-\alpha t-mt+\alpha+m+t-1). \end{aligned} \tag{17}$$

Proof. Now, by the reverse edge partitions for Cu_2O, we have the following results:

(i) The first reverse Zagreb polynomial for Cu_2O is given as follows:

$$\begin{aligned} HCM_1(Cu_2O,x) &= \sum_{uv\epsilon E(G)} x^{(c_u+c_v)^2} \\ &= (4\alpha+4m+4t-8)x^{(3+4)^2}+(4\alpha m+4\alpha t+4mt-8\alpha-8m-8t+12)x^{(3+3)^2} \\ &\quad +\left(4(2\alpha mt-\alpha m-\alpha t-mt+\alpha+m+t-1)x^{(3+1)^2}\right. \\ &= x^{49}(4\alpha+4m+4t-8)+x^{36}(4\alpha m+4\alpha t+4mt-8\alpha-8m-8t+12) \\ &\quad +x^{16}(4(2\alpha mt-\alpha m-\alpha t-mt+\alpha+m+t-1). \end{aligned} \tag{18}$$

(ii) The second reverse Zagreb polynomial for Cu_2O is given as follows:

$$\begin{aligned} HCM_2(Cu_2O,x) &= \sum_{uv\epsilon E(G)} x^{(c_u.c_v)^2} \\ &= (4\alpha+4m+4t-8)x^{(3\times 4)^2}+(4\alpha m+4\alpha t+4mt-8\alpha-8m-8t+12)x^{(3\times 3)^2} \\ &\quad +\left(4(2\alpha mt-\alpha m-\alpha t-mt+\alpha+m+t-1)x^{(3\times 1)^2}\right. \\ &= x^{144}(4\alpha+4m+4t-8)+x^{81}(4\alpha m+4\alpha t+4mt-8\alpha-8m-8t+12) \\ &\quad +x^{9}(4(2\alpha mt-\alpha m-\alpha t-mt+\alpha+m+t-1). \end{aligned} \tag{19}$$

□

Theorem 5. *Let G be the graph of Cu_2O with m, α, t ≥ 1. The reverse atom-bond connectivity index and reverse geometric-arithmetic index for Cu_2O with m, α, t ≥ 1 are as follows:*

$$1.\mathrm{CABC}(\mathrm{Cu_2O}) = \frac{1}{3}\left[(8\sqrt{6})m\alpha t + (8-32\sqrt{6})(m\alpha + mt + \alpha t) + (2\sqrt{15} - 16 + 32\sqrt{6})(m+\alpha+t) + (24 - 16\sqrt{15} - 32\sqrt{6})\right],$$

$$2.\mathrm{CGA}(\mathrm{Cu_2O}) = \frac{1}{14}\left[(56\sqrt{3})m\alpha t + (56-28\sqrt{3})(m\alpha + \alpha t + mt) + (-112 + 39\sqrt{3})(m+\alpha+t) + (168 - 71\sqrt{3})\right]. \tag{20}$$

Proof. By the reverse edge partition, we have the following results:

(i) The reverse atom-bond connectivity index for Cu_2O is given by

$$\begin{aligned}
\mathrm{CABC}(\mathrm{Cu_2O}) &= \sum_{uv\epsilon E(G)} \sqrt{\frac{c_u(G) + c_v(G) - 2}{c_u(G).c_v(G)}} \\
&= [4m + 4\alpha + 4t - 8]\left[\sqrt{\frac{4+3-2}{4\times 3}}\right] + [4m\alpha + 4\alpha t + 4mt - 8m - 8\alpha - 8t + 12]\left[\sqrt{\frac{3+3-2}{3\times 3}}\right] \\
&\quad + [4(2m\alpha t - m\alpha - mt - \alpha t + m + \alpha + t - 1)]\left[\sqrt{\frac{3+1-2}{3\times 1}}\right] \\
&= \frac{1}{3}\left[(8\sqrt{6})m\alpha t + (8-32\sqrt{6})(m\alpha + mt + \alpha t) + (2\sqrt{15} - 16 + 32\sqrt{6})(m+\alpha+t) + (24 - 16\sqrt{15} - 32\sqrt{6})\right].
\end{aligned} \tag{21}$$

(ii) The reverse geometric-arithmetic index for Cu_2O is given by

$$\begin{aligned}
\mathrm{CGA}(\mathrm{Cu_2O}) &= \sum_{uv\epsilon E(G)} \frac{\sqrt{c_u(G).c_v(G)}}{(1/2)[c_u(G) + c_v(G)]} \\
&= [4m + 4\alpha + 4t - 8]\left[\frac{\sqrt{4\times 3}}{(1/2)[4+3]}\right] + [4m\alpha + 4\alpha t + 4mt - 8m - 8\alpha - 8t + 12]\left[\frac{\sqrt{3\times 3}}{(1/2)[3+3]}\right] \\
&\quad + [4(2m\alpha t - m\alpha - mt - \alpha t + m + \alpha + t - 1)]\left[\frac{\sqrt{3\times 1}}{(1/2)[3+1]}\right] \\
&= \frac{1}{14}\left[(56\sqrt{3})m\alpha t + (56-28\sqrt{3})(m\alpha + \alpha t + mt) + (-112 + 39\sqrt{3})(m+\alpha+t) + (168 - 71\sqrt{3})\right].
\end{aligned} \tag{22}$$

□

The values of calculated topological indices of Cu_2O at different levels are given in Table 1.

2.2. Titanium Difluoride $TiF_2[m, \alpha, t]$. The unit cell of crystallographic structure of titanium difluoride $TiF_2[m, \alpha, t]$ is given in Figure 3 and the crystal structure of TiF_2 [1, 2, 4] is given in Figure 4.

Theorem 6. *Let G be the graph of titanium difluoride $TiF_2[m, \alpha, t]$, with m, α, t ≥ 1. The first and second reverse Zagreb indices are as follows:*

(1) $CM_1(TiF_2[m, \alpha, t]) = 192m\alpha t + 64m\alpha + 64mt + 64\alpha t - 16m - 16\alpha - 16t + 8$

(2) $CM_2(TiF_2[m, \alpha, t]) = 160m\alpha t + 320m\alpha + 320mt + 320\alpha t - 80m - 80\alpha - 80t + 40$

Table 1: Values of calculated topological indices of Cu_2O at different levels.

	m = 1 α = 1 t = 1	m = 2 α = 2 t = 2	m = 3 α = 3 t = 3	m = 1 α = 2 t = 3	m = 3 α = 2 t = 1	m = 3 α = 4 m = 5	m = 2 α = 4 t = 6
First reverse ZI	44	364	1188	280	280	2560	2116
Second reverse ZI	60	408	1188	336	336	2424	2064
First reverse hyper-ZI	212	1360	3660	1168	1168	7048	6280
Second reverse hyper-ZI	585	3357	8235	3006	3006	14940	13779
Reverse ABC index	−252.9	−117.5	−285.5	−117.4	−117.4	−469.1	−430.1
Reverse GA index	222	46.02	176.17	31.63	31.63	405.96	321.24

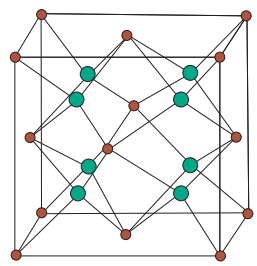

Figure 3: Unit cell of $TiF_2[m, \alpha, t]$.

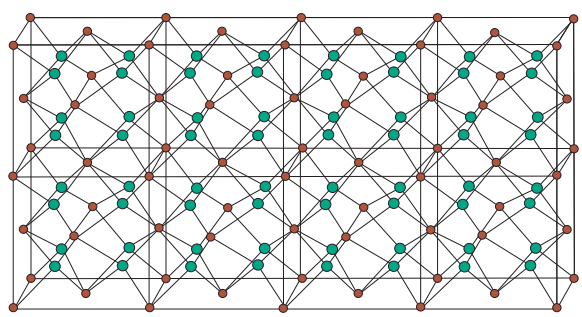

Figure 4: Crystal structure of TiF_2 [1, 2, 4].

Proof. Let G be a graph of titanium difluoride $TiF_2[m, \alpha, t]$. The vertex and edge sets of titanium difluoride $TiF_2[m, \alpha, t]$ are $|V(TiF_2[m, \alpha, t])| = 12m\alpha t + 2m\alpha + 2mt + 2\alpha t + m + \alpha + t + 1$ and $|E(TiF_2[m, \alpha, t])| = 32m\alpha t$, respectively. From Figure 4, we can say that there are five type of edges in $TiF_2[m, \alpha, t]$. The edge set of $|TiF_2[m, \alpha, t]| = 32m\alpha t$ is portioned into four edge sets:

$$\begin{aligned} E_1(TiF_2[m,\alpha,t]) &= \{uv\epsilon E(TiF_2[m,\alpha,t]); d_u = 1, d_v = 4\}, \\ E_2(TiF_2[m,\alpha,t]) &= \{uv\epsilon E(TiF_2[m,\alpha,t]); d_u = 2, d_v = 4\}, \\ E_3(TiF_2[m,\alpha,t]) &= \{uv\epsilon E(TiF_2[m,\alpha,t]); d_u = 4, d_v = 4\}, \\ E_4(TiF_2[m,\alpha,t]) &= \{uv\epsilon E(TiF_2[m,\alpha,t]); d_u = 4, d_v = 8\}. \end{aligned} \tag{23}$$

We have $|E_1(TiF_2[m, \alpha, t])| = 8$, $|E_2(TiF_2[m, \alpha, t])| = 8(m + \alpha + t - 3)$, $|E_3(TiF_2[m, \alpha, t])| = 16(m\alpha + \alpha t + mt) - 16(m + \alpha + t) + 24$, and $|E_4(TiF_2[m, \alpha, t])| = 32m\alpha t - 16(mt + m\alpha + \alpha t) + 8(m + \alpha + t) - 8$. The maximum edge degree is 8; then, the reverse edges are given as follows:

$$c_u = \Delta(G) - d_G(u) + 1 = 9 - d_G(u). \tag{24}$$

The reverse edge set of $TiF_2[m, \alpha, t]$ is given as follows:

$$\begin{aligned} CE_1(TiF_2[m,\alpha,t]) &= \{uv\epsilon E(TiF_2[m,\alpha,t]); c_u = 8, c_v = 5\}, \\ CE_2(TiF_2[m,\alpha,t]) &= \{uv\epsilon E(TiF_2[m,\alpha,t]); c_u = 7, c_v = 5\}, \\ CE_3(TiF_2[m,\alpha,t]) &= \{uv\epsilon E(TiF_2[m,\alpha,t]); c_u = 5, c_v = 5\}, \\ CE_4(TiF_2[m,\alpha,t]) &= \{uv\epsilon E(TiF_2[m,\alpha,t]); c_u = 5, c_v = 1\}. \end{aligned} \tag{25}$$

We have $|E_1(\mathrm{TiF}_2[m, \alpha, t])| = 8$, $|E_2(\mathrm{TiF}_2[m, \alpha, t])| = 8(m + \alpha + t - 3)$, $|E_3(\mathrm{TiF}_2[m, \alpha, t])| = 16(m\alpha + \alpha t + mt) - 16(m + \alpha + t) + 24$, and $|E_4(\mathrm{TiF}_2[m, \alpha, t])| = 32m\alpha t - 16(mt + m\alpha + \alpha t) + 8(m + \alpha + t) - 8$.

(i) The first reverse ZI for $\mathrm{TiF}_2[m, \alpha, t]$ is given by

$$\begin{aligned}\mathrm{CM}_1(\mathrm{TiF}_2[m,\alpha,t]) &= \sum_{uv\epsilon E(G)} (c_u + c_v)\\ &= (8+5)(8) + (7+5)[8(m+\alpha+t-3)] + (5+5)[16(mn+\alpha t+mt) - 16(m+\alpha+t) + 24]\\ &\quad + (5+1)[32m\alpha t - 16(mt+m\alpha+\alpha t) + 8(m+\alpha+t) - 8]\\ &= 192m\alpha t + 64m\alpha + 64mt + 64\alpha t - 16m - 16\alpha - 16t + 8.\end{aligned} \tag{26}$$

(ii) The second reverse ZI for $\mathrm{TiF}_2[m, \alpha, t]$ is given by

$$\begin{aligned}\mathrm{CM}_2(\mathrm{TiF}_2[m,\alpha,t]) &= \sum_{uv\epsilon E(G)} (c_u . c_v)\\ &= (8\times 5)(8) + (7\times 5)[8(m+\alpha+t-3)] + (5\times 5)[16(m\alpha+\alpha t+mt) - 16(m+\alpha+t) + 24]\\ &\quad + (5\times 1)[32m\alpha t - 16(mt+m\alpha+\alpha t) + 8(m+\alpha+t) - 8]\\ &= 160m\alpha t + 320m\alpha + 320mt + 320\alpha t - 80m - 80\alpha - 80t + 40.\end{aligned} \tag{27}$$

□

Theorem 7. *The first and second reverse Zagreb polynomials for $TiF_2[m, \alpha, t]$ are as follows:*

(1) $CM_1(TiF_2[m, \alpha, t], x) = 8x^{13} + [8(m + \alpha + t - 3)]x^{12} + [16(m\alpha + \alpha t + mt) - 16(m + \alpha + t) + 24]x^{10} + [32m\alpha t - 16(mt + m\alpha + \alpha t) + 8(m + \alpha + t) - 8]x^6$

(2) $CM_2(TiF_2[m, \alpha, t], x) = 8x^{40} + [8(m + \alpha + t - 3)]x^{35} + [16(m\alpha + \alpha t + mt) - 16(m + \alpha + t) + 24]x^{25} + [32m\alpha t - 16(mt + m\alpha + \alpha t) + 8(m + \alpha + t) - 8]x^5$

Proof. Now, by the reverse edge partitions for $\mathrm{TiF}_2[m, \alpha, t]$, we have the following results:

(i) The first reverse Zagreb polynomial for $\mathrm{TiF}_2[m, \alpha, t]$ is given as follows:

$$\begin{aligned}\mathrm{CM}_1(\mathrm{TiF}_2[m,\alpha,t],x) &= \sum_{uv\epsilon E(G)} x^{(c_u+c_v)}\\ &= (8)x^{(8+5)} + [8(m+\alpha+t-3)]x^{(7+5)} + [16(m\alpha+\alpha t+mt) - 16(m+\alpha+t) + 24]x^{(5+5)}\\ &\quad + [32m\alpha t - 16(mt+m\alpha+\alpha t) + 8(m+\alpha+t) - 8]x^{(5+1)}\\ &= 8x^{13} + [8(m+\alpha+t-3)]x^{12} + [16(m\alpha+\alpha t+mt) - 16(m+\alpha+t) + 24]x^{10}\\ &\quad + [32m\alpha t - 16(mt+m\alpha+\alpha t) + 8(m+\alpha+t) - 8]x^6.\end{aligned} \tag{28}$$

(ii) The second reverse Zagreb polynomial for $\mathrm{TiF}_2[m, \alpha, t]$ is given as follows:

$$\begin{aligned}\mathrm{CM}_2(\mathrm{TiF}_2[m,\alpha,t],x) &= \sum_{uv\epsilon E(G)} x^{(c_u.c_v)}\\ &= (8)x^{(8\times 5)} + [8(m+\alpha+t-3)]x^{(7\times 5)} + [16(m\alpha+\alpha t+mt) - 16(m+\alpha+t) + 24]x^{(5\times 5)}\\ &\quad + [32m\alpha t - 16(mt+m\alpha+\alpha t) + 8(m+\alpha+t) - 8]x^{(5\times 1)}\\ &= 8x^{40} + [8(m+\alpha+t-3)]x^{35} + [16(m\alpha+\alpha t+mt) - 16(m+\alpha+t) + 24]x^{25}\\ &\quad + [32m\alpha t - 16(mt+m\alpha+\alpha t) + 8(m+\alpha+t) - 8]x^5.\end{aligned} \tag{29}$$

□

Theorem 8. *The first and second reverse hyper-Zagreb indices of $TiF_2[m, \alpha, t]$ are as follows:*

(1) $HCM_1(TiF_2[m, \alpha, t]) = 1152m\alpha t - 160(m + \alpha + t) + 1024(m\alpha + \alpha t + mt) - 2152$

(2) $HCM_2(TiF_2[m, \alpha, t]) = 800m\alpha t + 9600(m\alpha + \alpha t + mt) - 14600$

Proof. Let G be a graph of silicon-carbon $TiF_2[m, \alpha, t]$. Then, by reverse edge partition and definition of reverse hyper-Zagreb indices, we have the following results:

(i) The first reverse hyper-ZI for $TiF_2[m, \alpha, t]$ is given by

$$\begin{aligned} CM_1(TiF_2[m,\alpha,t]) &= \sum_{uv\epsilon E(G)} (c_u + c_v)^2 \\ &= (8+5)^2(8) + (7+5)^2[8(m+\alpha+t-3)] + (5+5)^2[16(m\alpha+\alpha t+mt) - 16(m+\alpha+t) + 24] \\ &\quad + (5+1)^2[32m\alpha t - 16(mt+m\alpha+\alpha t) + 8(m+\alpha+t) - 8] \\ &= 1152m\alpha t - 160(m+\alpha+t) + 1024(m\alpha+\alpha t+mt) - 2152. \end{aligned} \tag{30}$$

(ii) The second reverse hyper-ZI for $TiF_2[m, \alpha, t]$ is given by

$$\begin{aligned} CM_2(TiF_2[m,\alpha,t]) &= \sum_{uv\epsilon E(G)} (c_u . c_v)^2 \\ &= (8\times 5)^2(8) + (7\times 5)^2[8(m+\alpha+t-3)] + (5\times 5)^2[16(m\alpha+\alpha t+mt) - 16(m+\alpha+t) + 24] \\ &\quad + (5\times 1)^2[32m\alpha t - 16(mt+m\alpha+\alpha t) + 8(m+\alpha+t) - 8] \\ &= 800m\alpha t + 9600(m\alpha+\alpha t+mt) - 14600. \end{aligned} \tag{31}$$

□

Theorem 9. *The first and second reverse hyper-Zagreb polynomials of $TiF_2[m, \alpha, t]$ are as follows:*

(1) $HCM_1(TiF_2[m, \alpha, t], x) = 8x^{169} + [8(m + \alpha + t - 3)]x^{144} + [16(m\alpha + \alpha t + mt) - 16(m + \alpha + t) + 24]x^{100} + [32m\alpha t - 16(mt + m\alpha + \alpha t) + 8(m + \alpha + t) - 8]x^{36}$

(2) $HCM_1(TiF_2[m, \alpha, t], x) = 8x^{1600} + [8(m + \alpha + t - 3)]x^{1225} + [16(m\alpha + \alpha t + mt) - 16(m + \alpha + t) + 24]x^{625} + [32m\alpha t - 16(mt + m\alpha + \alpha t) + 8(m + \alpha + t) - 8]x^{25}$

Proof. Now, by the reverse edge partitions for $TiF_2[m, \alpha, t]$, we have the following results:

(i) The first reverse Zagreb polynomial for $TiF_2[m, \alpha, t]$ is given as follows:

$$\begin{aligned} CM_1(TiF_2[m,\alpha,t],x) &= \sum_{uv\epsilon E(G)} x^{(c_u+c_v)^2} \\ &= (8)x^{(8+5)^2} + [8(m+\alpha+t-3)]x^{(7+5)^2} + [16(m\alpha+\alpha t+mt) - 16(m+\alpha+t) + 24]x^{(5+5)^2} \\ &\quad + [32m\alpha t - 16(mt+m\alpha+\alpha t) + 8(m+\alpha+t) - 8]x^{(5+1)^2} \\ &= 8x^{169} + [8(m+\alpha+t-3)]x^{144} + [16(m\alpha+\alpha t+mt) - 16(m+\alpha+t) + 24]x^{100} \\ &\quad + [32m\alpha t - 16(mt+m\alpha+\alpha t) + 8(m+\alpha+t) - 8]x^{36}. \end{aligned} \tag{32}$$

(ii) The second reverse Zagreb polynomial for $TiF_2[m, \alpha, t]$ is given as follows:

$$\begin{aligned}
CM_2\left(TiF_2[m,\alpha,t],x\right) &= \sum_{uv\epsilon E(G)} x^{\left(c_u.c_v\right)^2} \\
&= (8)x^{(8\times5)^2} + [8(m+\alpha+t-3)]x^{(7\times5)^2} + [16(m\alpha+\alpha t+mt) - 16(m+\alpha+t) + 24]x^{(5\times5)^2} \\
&\quad + [32m\alpha t - 16(mt+m\alpha+\alpha t) + 8(m+\alpha+t) - 8]x^{(5\times1)^2} \\
&= 8x^{1600} + [8(m+\alpha+t-3)]x^{1225} + [16(m\alpha+\alpha t+mt) - 16(m+\alpha+t) + 24]x^{625} \\
&\quad + [32m\alpha t - 16(mt+m\alpha+\alpha t) + 8(m+\alpha+t) - 8]x^{25}.
\end{aligned} \tag{33}$$

□

Theorem 10. *Let G be the graph of Cu_2O with $m, \alpha, t \geq 1$. The reverse atom-bond connectivity index and reverse geometric-arithmetic index for Cu_2O with $m, \alpha, t \geq 1$ are given by*

$$\begin{aligned}
(1)\mathrm{CABC}\left(TiF_2[m,\alpha,t]\right) &= \frac{1}{175}[(2240\sqrt{5})m\alpha t + (1225\sqrt{2} - 1225\sqrt{5})(m\alpha+mt+\alpha t) + (40\sqrt{350} - 224\sqrt{50} \\
&\quad + 560\sqrt{5})(m+\alpha+t) + (70\sqrt{110} - 6000\sqrt{14} + 1680\sqrt{2} - 2800\sqrt{5})], \\
(2)\mathrm{CGA}\left(TiF_2[m,\alpha,t]\right) &= \frac{1}{3}[(32\sqrt{5})m\alpha t + (48 - 16\sqrt{5})(m\alpha+mt+\alpha t) + (4\sqrt{35} + 8\sqrt{5} - 48)(m+\alpha+t)] \\
&\quad + \frac{1}{39}(96\sqrt{10} - 104\sqrt{5} + 156\sqrt{35} + 936).
\end{aligned} \tag{34}$$

Proof. By the reverse edge partition, we have the following results:

(i) The reverse atom-bond connectivity index for $TiF_2[m, \alpha, t]$ is given by

$$\begin{aligned}
\mathrm{CABC}\left(TiF_2[m,\alpha,t]\right) &= \sum_{uv\epsilon E(G)} \sqrt{\frac{c_u(G)+c_v(G)-2}{c_u(G).c_v(G)}} \\
&= [8]\left[\sqrt{\frac{8+5-2}{8\times5}}\right] + [8(m+\alpha+t-3)]\left[\sqrt{\frac{7+5-2}{7\times5}}\right] + [16(m\alpha+\alpha t+mt) - 16(m+\alpha+t) + 24] \\
&\quad \cdot \left[\sqrt{\frac{5+5-2}{5\times5}}\right] + [32m\alpha t - 16(m\alpha+mt+\alpha t) + 8(m+\alpha+t) - 8]\left[\sqrt{\frac{5+1-2}{5\times1}}\right] \\
&= \frac{1}{175}[(2240\sqrt{5})m\alpha t + (1225\sqrt{2} - 1225\sqrt{5})(m\alpha+mt+\alpha t) + (40\sqrt{350} - 224\sqrt{50} + 560\sqrt{5}) \\
&\quad \cdot (m+\alpha+t) + (70\sqrt{110} - 6000\sqrt{14} + 1680\sqrt{2} - 2800\sqrt{5})].
\end{aligned} \tag{35}$$

Table 2: Values of calculated topological indices of $TiF_2[m, \alpha, t]$ at different levels.

	m = 1 α = 1 t = 1	m = 2 α = 2 t = 2	m = 3 α = 3 t = 3	m = 1 α = 2 t = 3	m = 3 α = 2 t = 1	m = 3 α = 4 m = 5	m = 2 α = 4 t = 6
First reverse ZI	344	2216	6776	1768	1768	14344	11848
Second reverse ZI	920	4680	12280	4040	4040	23720	20840
First reverse hyper-ZI	1592	18392	55160	15064	15064	113176	96280
Second reverse hyper-ZI	15000	107000	266200	95800	95800	484600	446200
Reverse ABC index	-127.8	27.9	492.6	-23.57	-23.6	1346.4	860.3
Reverse GA index	79.1	276.3	784.1	224.5	224.5	1634.1	1241.3

(ii) The reverse geometric-arithmetic index for $TiF_2[m, \alpha, t]$ is given by

$$\begin{aligned}
\mathrm{CGA}\left(\mathrm{TiF}_2[m,\alpha,t]\right) &= \sum_{uv\in E(G)} \frac{\sqrt{c_u(G).c_v(G)}}{(1/2)\left[c_u(G)+c_v(G)\right]} \\
&= [8]\left[\frac{\sqrt{8\times 5}}{(1/2)[8+5]}\right] + [8(m+\alpha+t-3)]\left[\frac{\sqrt{7\times 5}}{(1/2)[7+5]}\right] + [16(m\alpha+\alpha t+mt)-16(m+\alpha+t)+24] \\
&\quad \cdot\left[\frac{\sqrt{5\times 5}}{(1/2)[5+5]}\right] + [32m\alpha t-16(m\alpha+mt+\alpha t)+8(m+\alpha+t)-8]\left[\frac{\sqrt{5\times 1}}{(1/2)[5+1]}\right] \\
&= \frac{1}{3}\left[(32\sqrt{5})m\alpha t+(48-16\sqrt{5})(m\alpha+mt+\alpha t)+(4\sqrt{35}+8\sqrt{5}-48)(m+\alpha+t)\right] \\
&\quad + \frac{1}{39}(96\sqrt{10}-104\sqrt{5}+156\sqrt{35}+936).
\end{aligned} \tag{36}$$

□

The values of calculated topological indices at different levels are given in Table 2.

3. Conclusion

In this paper, we computed first and second reverse Zagreb indices, first and second reverse hyper-Zagreb indices, reverse GA index, reverse atomic bond connectivity index, first and second reverse Zagreb polynomials, and first and second reverse hyper-Zagreb polynomials for the crystallographic structure of molecules [24, 25]. Our results are important to guess the properties [26–28] and study the topology of the crystallographic structure of molecules and can be used in drug delivery [29–31].

Data Availability

All data required for this paper are included within this paper.

Conflicts of Interest

The authors declare that they have no conflicts of interest.

Authors' Contributions

All authors contributed equally to this paper.

Acknowledgments

This research was supported by the Natural Science Fund of Anhui Wenda University of Information Engineering (Grant no. XZR2019A10).

References

[1] M. S. Anjum, M. U. Lingua, and M. U. Safdar, "K Banhatti and K hyper-Banhatti indices of nanotubes," *Engineering and Applied Science Letters*, vol. 2, no. 1, pp. 19–37, 2019.

[2] Z. Shao, A. R. Virk, M. S. Javed, M. A. Rehman, and M. R. Farahani, "Degree based graph invariants for the molecular graph of Bismuth Tri-Iodide," *Journal of Engineering and Applied Sciences*, vol. 2, no. 1, pp. 1–11, 2019.

[3] A. Shah, S. A. U. H. Lingua, and S. A. U. H. Bokhary, "On chromatic polynomial of certain families of dendrimer graphs," *Open Journal of Mathematical Sciences*, vol. 3, no. 1, pp. 404–416, 2019.

[4] N. De, "Computing reformulated first zagreb index of some chemical graphs as an application of generalized hierarchical

product of graphs," *Open Journal of Mathematical Sciences*, vol. 2018, no. 2, pp. 338–350, 2018.

[5] J.-B. Liu, C. Wang, S. Wang, and B. Wei, "Zagreb indices and multiplicative zagreb indices of eulerian graphs," *Bulletin of the Malaysian Mathematical Sciences Society*, vol. 42, no. 1, pp. 67–78, 2019.

[6] J.-B. Liu, J. Zhao, and Z. X. Zhu, "On the number of spanning trees and normalized Laplacian of linear octagonal quadrilateral networks," *International Journal of Quantum Chemistry*, vol. 119, 2019.

[7] B. Liu, J. Zhao, J. Min, and J. D. Cao, "On the hosoya index of graphs formed by a fractal graph," *Fractals-Complex Geometry Patterns and Scaling in Nature and Society*, vol. 10, 2019.

[8] J.-B. Liu, J. Zhao, and Z.-Q. Cai, "On the generalized adjacency, Laplacian and signless Laplacian spectra of the weighted edge corona networks," *Physica A: Statistical Mechanics and Its Applications*, vol. 540, 2020.

[9] J.-B. Liu, J. Zhao, H. He, and Z. Shao, "Valency-based topological descriptors and structural property of the generalized sierpiński networks," *Journal of Statistical Physics*, vol. 177, no. 6, pp. 1131–1147, 2019.

[10] A. Tabassum, M. A. Lingua, M. A. Umar et al., "Antimagicness of subdivided fans," *Open Journal of Mathematical Sciences*, vol. 4, no. 1, pp. 18–22, 2020.

[11] E. Zhu, C. Lingua, and C. Liu, "On smarandachely adjacent vertex total coloring of subcubic graphs," *Open Journal of Mathematical Sciences*, vol. 3, no. 1, pp. 390–397, 2019.

[12] C. P. Panchanathan, "On codes over $\mathbb{R} = \mathbb{Z}_2 + \mathrm{u}\mathbb{Z}_2 + \mathrm{u}^2\mathbb{Z}_2$ where $u^3 = 0$ and its related parameters," *Open Journal of Mathematical Sciences*, vol. 3, no. 1, pp. 256–261, 2019.

[13] M. A. Umar and N. Ali, "Book graphs are cycle antimagic," *Open Journal of Mathematical Sciences*, vol. 3, no. 1, pp. 184–190, 2019.

[14] M. A. Umar, "Cyclic-antimagic construction of ladders," *Engineering and Applied Science Letters*, vol. 2, no. 2, pp. 43–47, 2019.

[15] L. Chen and H. Jiang, "Dominator and total dominator colorings in vague graphs," *Engineering and Applied Science Letters*, vol. 2, no. 2, pp. 10–17, 2019.

[16] F. Aslam, Z. Zahid, and S. Zafar, "3-total edge mean cordial labeling of some standard graphs," *Open Journal of Mathematical Sciences*, vol. 2019, no. 3, pp. 129–138, 2019.

[17] V. R. Kulli, B. Chaluvaraju, and H. S. Boregowda, "Some degree based connectivity indices of Kulli cycle windmill graphs," *South Asian Journal of Mathematics*, vol. 6, no. 6, pp. 263–268, 2016.

[18] S. Noreen and A. Mahmood, "Zagreb polynomials and redefined zagreb indices for the line graph of carbon nanocones," *Open Journal of Mathematical Analysis*, vol. 2018, no. 1, pp. 66–73, 2018.

[19] H. Siddiqui and M. R. Farahani, "Forgotten polynomial and forgotten index of certain interconnection networks," *Open Journal of Mathematical Analysis*, vol. 2017, no. 1, pp. 44–59, 2017.

[20] H. Wiener, "Structural determination of paraffin boiling points," *Journal of the American Chemical Society*, vol. 69, no. 1, pp. 17–20, 1947.

[21] H. Hosoya, "On some counting polynomials in chemistry," *Discrete Applied Mathematics*, vol. 19, no. 1–3, pp. 239–257, 1988.

[22] G. Liu, Z. Jia, and W. Gao, "Ontology similarity computing based on stochastic primal dual coordinate technique," *Open Journal of Mathematical Sciences*, vol. 2018, no. 1, pp. 221–227, 2018.

[23] Z. Tang, L. Liang, and W. Gao, "Wiener polarity index of quasi-tree molecular structures," *Open Journal of Mathematical Sciences*, vol. 2, no. 1, pp. 73–83, 2018.

[24] K. C. Das and I. Gutman, "Some properties of the second Zi. Match Communication," *Mathematical and in Computer Chemistry*, vol. 52, no. 1, pp. 3–1, 2004.

[25] M. Randić, "The connectivity index 25 years after," *Journal of Molecular Graphics and Modelling*, vol. 20, no. 1, pp. 19–35, 2001.

[26] Y. Hu, X. Li, Y. Shi, T. Xu, and I. Gutman, "On molecular graphs with smallest and greatest zeroth-order general Randic index," *MATCH Communications in Mathematical and in Computer Chemistry*, vol. 4, no. 2, pp. 425–434, 2005.

[27] L. Pogliani, "From molecular connectivity indices to semiempirical connectivity terms: recent trends in graph theoretical descriptors," *Chemical Reviews*, vol. 100, no. 10, pp. 3827–3858, 2000.

[28] W. Gao, M. R. Farahani, and L. Shi, "Forgotten topological index of some drug structures," *Acta Medica Mediterranea*, vol. 32, no. 1, pp. 579–585, 2016.

[29] W. Gao, M. K. Siddiqui, M. Imran, M. K. Jamil, and M. R. Farahani, "Forgotten topological index of chemical structure in drugs," *Saudi Pharmaceutical Journal*, vol. 24, no. 3, pp. 258–264, 2016.

[30] A. Aslam, J. L. G. I. Guirao, S. Ahmad, and W. Gao, "Topological indices of the line graph of subdivision graph of complete bipartite graphs," *Applied Mathematics & Information Sciences*, vol. 11, no. 6, pp. 1631–1636, 2017.

[31] N. De, "Hyper zagreb index of bridge and chain graphs," *Open Journal of Mathematical Sciences*, vol. 2, no. 1, pp. 1–17, 2018.

Hindawi
Journal of Chemistry
Volume 2020, Article ID 6289518, 13 pages
https://doi.org/10.1155/2020/6289518

Research Article

Some Topological Invariants of Graphs Associated with the Group of Symmetries

Chang-Cheng Wei,[1] Muhammad Salman,[2] Usman Ali,[3,4] Masood Ur Rehman,[5,6] Muhammad Aqeel Ahmad Khan,[7] Muhammad Hasanain Chaudary,[8] and Farooq Ahmad[8]

[1]*Department of Mathematics and Computer Science, Anhui TongLing University, Tongling 244061, China*
[2]*Department of Mathematics, The Islamia University of Bahawalpur, Bahawalpur, Pakistan*
[3]*Centre for Advanced Studies in Pure and Applied Mathematics (CASPAM), Bahauddin Zakaryia University, Multan, Pakistan*
[4]*Institut de Mathématiques de Jussieu-Paris Rive Gauche, Paris, France*
[5]*Department of Mathematics, Abbottabad University of Science and Technology, Abbottabad, Pakistan*
[6]*Department of Basic Sciences, Balochistan University of Engineering and Technology, Khuzdar, Balochistan, Pakistan*
[7]*Department of Mathematics, COMSATS University Islamabad, Lahore Campus, Lahore, Pakistan*
[8]*Department of Computer Science, COMSATS University Islamabad, Lahore Campus, Lahore, Pakistan*

Correspondence should be addressed to Usman Ali; uali@bzu.edu.pk and Masood Ur Rehman; masood@mail.ustc.edu.cn

Received 21 August 2019; Accepted 9 October 2019; Published 9 March 2020

Academic Editor: Teodorico C. Ramalho

A topological index is a quantity that is somehow calculated from a graph (molecular structure), which reflects relevant structural features of the underlying molecule. It is, in fact, a numerical value associated with the chemical constitution for the correlation of chemical structures with various physical properties, chemical reactivity, or biological activity. A large number of properties like physicochemical properties, thermodynamic properties, chemical activity, and biological activity can be determined with the help of various topological indices such as atom-bond connectivity indices, Randić index, and geometric arithmetic indices. In this paper, we investigate topological properties of two graphs (commuting and noncommuting) associated with an algebraic structure by determining their Randić index, geometric arithmetic indices, atomic bond connectivity indices, harmonic index, Wiener index, reciprocal complementary Wiener index, Schultz molecular topological index, and Harary index.

1. Introduction

In quantitative structure-activity relationship (QSAR)/quantitative structure-property relationship (QSPR) study, physicochemical properties and topological indices such as Randić index, atom-bond connectivity (ABC) index, and geometric-arithmetic (GA) index are used to predict the bioactivity of chemical compounds. A topological index is actually designed by transforming a chemical structure into a numerical number. It correlates certain physicochemical properties such as boiling point, stability, and strain energy of chemical compounds of a molecular structure (graph). It is a numeric quantity associated with a chemical structure (graph), which characterizes the topology of the structure and is invariant under a structure-preserving mapping [1]. In 1947, Wiener [2] introduced the concept of (distance-based) topological index while working on the boiling point of paraffin. He named this index as the path number. Later on, the path number was renamed as the Wiener index [2], and then, the theory of topological indices started. Nowadays, a number of distance-based and degree-based topological indices have been introduced and computed (see for example [3–15], and the references therein).

We consider simple and connected graph (chemical structure) G with vertex set $V(G)$ and edge set $E(G)$. We denote the two adjacent vertices u and v in G as $u \sim v$ and nonadjacent vertices as $u \nsim v$. The number d_v denotes the degree of a vertex $v \in V(G)$ and $S_v = \sum_{u \in N(v)} d_u$ is the

Table 1: List of under consideration topological indices.

Name of the index	Notation	Formula
Wiener index [2]	$W(G)$	$\sum_{\{u,v\}\in V(G)} d(u,v)$
Reciprocal complementary Wiener index [21]	$\mathrm{RCW}(G)$	$\sum_{\{u,v\}\in V(G)} 1/(D(G)+1-d(u,v))$
Schultz molecular topological index [22]	$\mathrm{MTI}(G)$	$\sum_{\{u,v\}\in V(G)} (d_u+d_v)d(u,v)+\sum_{v\in V(G)} d^{2/v}$
Harary index [23, 24]	$H(G)$	$\sum_{\{u\neq v\}\in V(G)} 1/(d(u,v))$
Randić index [10]	$R_{-1/2}(G)$	$\sum_{u\sim v} 1/(\sqrt{d_u\times d_v})$
General Randić index [11, 12]	$R_\alpha(G)$	$\sum_{u\sim v}(d_u\times d_v)^\alpha$
Geometric arithmetic (GA) index [13]	$\mathrm{GA}(G)$	s
Fifth version of GA index [4]	$\mathrm{GA}_5(G)$	$\sum_{u\sim v}(2\sqrt{S_u\times S_v})/(S_u+S_v)$
Atomic bond connectivity (ABC) index [14]	$\mathrm{ABC}(G)$	$\sum_{u\sim v}\sqrt{(d_u+d_v-2)/(d_u\times d_v)}$
Fourth version of ABC index [5]	$\mathrm{ABC}_4(G)$	$\sum_{u\sim v}\sqrt{(S_u+S_v-2)/(S_u\times S_v)}$
Harmonic index [15]	$H_r(G)$	$\sum_{u\sim v} 2/(d_u+d_v)$

All the notations used in formulas are defined in Section 1.

degrees sum of v, where $N(v)=\{u\in V(G)\mid u\sim v \text{ in } G\}$ is the neighborhood of v. The number $d(u,v)$ denotes the length of a geodesic between u and v in G and is called the distance between u and v. The eccentricity of a vertex v in G, denoted by $\mathrm{ecc}(v)$, is the maximum distance between v and any other vertex of G. The minimum eccentricity amongst the vertices of G is called the radius of G, denoted by $\mathrm{rad}(G)$. The diameter of a graph G is the maximum eccentricity in G, denoted by $D(G)$. A vertex v in G is said to be a central vertex if $\mathrm{ecc}(v)=\mathrm{rad}(G)$, and the subgraph of G induced by central vertices of G is called the center of G. A vertex v in a graph G is called a peripheral vertex if $\mathrm{ecc}(v)=D(G)$, and the subgraph of G induced by peripheral vertices is called the periphery of G. The sum of two graphs G_1 and G_2, denoted by G_1+G_2, is a graph with vertex set $V(G_1)\cup V(G_2)$ and an edge set $E(G_1)\cup E(G_2)\cup\{u\sim v\colon u\in V(G_1)\wedge v\in V(G_2)\}$.

Let Γ be a group. The set $\zeta(\Gamma)=\{x\colon x\in\Gamma\wedge xy=yx\forall y\in\Gamma\}$ is called the center of the group Γ. Then, commuting and noncommuting graphs of Γ are defined as follows:

(i) The commuting graph of a nonabelian group Γ is denoted by $\Gamma_G=C(\Gamma,\Omega)$ with vertex set $\Omega\subseteq\Gamma$. For two distinct elements $x,y\in\Omega$, $x\sim y$ in Γ_G (x and y form an edge in Γ_G) if and only if $xy=yx$ in Γ. The concept of commuting graphs on noncentral elements of a group has been studied by various researchers (see [16, 17]).

(ii) The noncommuting graph of a nonabelian group G_Γ is a graph with vertex set $V(G_1)\cup V(G_2)$, and two distinct vertices u and v in G_Γ form an edge if $uv\neq vu$ in Γ. The study of noncommuting graphs of groups was initiated in 1975 by Neumann [18] who posed the problem regarding the clique number of a noncommuting graph. Noncommuting graphs on noncentral elements of a group have also been studied by various other researchers [19, 20].

The following useful property for a noncommuting graph was proposed in [19].

Proposition 1 (see [19]). *For any nonabelian group Γ, $D(G_\Gamma)=2$.*

A graph G is said to be self-centered if $\mathrm{rad}(G)=D(G)$. Since $\mathrm{ecc}(v)\leq 2$ for every $v\in G_\Gamma$, so we have the following straightforward proposition:

Proposition 2. *A noncommuting graph G_Γ of any nonabelian finite group Γ is self-centered if for each $v\in G_\Gamma$, $ecc(v)=2$. Otherwise, it is the sum of the center and the periphery of G_Γ.*

This paper aimed at investigating all the topological properties (listed in Table 1) of commuting and noncommuting graphs associated with the group of symmetries. The rest of the paper consists of five sections. In the next section, we illustrate the group of symmetries and associate commuting and noncommuting graphs to this group. In Section 3, some useful constructions to investigate our main results of Sections 4 and 5 are provided.

2. Group of Symmetries and Associated Graphs

Group of symmetries finds its remarkable use in the theory of electron structures and molecular vibrations. Due to their significant employment in chemical structures, in the context of topological indices, we consider the group of symmetries of a regular polygon (also called a regular n-gon for $n\geq 2$) in this paper. A regular n-gon is a geometrical figure all of whose sides have the same length and all the angles are of equal measurement. Each internal angle of a n-gon is of $\pi-(2\pi)/(n)$ radian. The group of symmetries of a n-gon consists of $2n$ elements, which are n rotations ($r_0=e,r_1,r_2,\ldots,r_{n-1}$ about its center through an angle of $(2k\pi)/n$ radian, where $k=0,1,\ldots,n-1$, either all clockwise or all anticlockwise) and n reflections (for even n, the reflections through a line joining the midpoints of the opposite sides or through a line joining two opposite vertices, and for odd n, the reflections through those lines which join a vertex with the midpoint of the opposite side). The group of symmetries is denoted by D_n and is called the dihedral group of order $2n$. If we denote a rotation by "a" and a reflection by "b," then $2n$ elements of D_n are $a,a^2,\ldots,a^{n-1},a^n=e$ and $b,ab,a^2b,\ldots,a^{n-1}b$, where e is the identical rotation. The general representation of D_n is given by

Table 2: Vertex partition of Γ_G for each vertex $v \in V(\Gamma_G)$.

n is	d_v	$D(v \mid \Gamma_G)$	$D_s(v \mid \Gamma_G)$	$D_r(v \mid \Gamma_G)$	Number of vertices
Odd	$n-1$	$3n-1$	$(1/2)(3n-1)$	$(1/2)(3n-2)$	$n-1$
Odd	$2n-1$	$2n-1$	$(1/2)(2n-1)$	$2n-1$	1
Odd	1	$4n-3$	$(1/2)(4n-3)$	n	n
Even	$n-1$	$3n-1$	$(1/2)(3n-1)$	$(1/2)(3n-2)$	$n-2$
Even	$2n-1$	$2n-1$	$(1/2)(2n-1)$	$2n-1$	2
Even	3	$4n-5$	$(1/2)(4n-5)$	$n+1$	n

$$D_n = \langle a, b \mid a^n = b^2 = e, ab = ba^{-1} \rangle, \tag{1}$$

with the center

$$\zeta(D_n) = \begin{cases} \{e\}, & \text{when } n \text{ is odd}, \\ \{e, a^{n/2}\}, & \text{when } n \text{ is even}. \end{cases} \tag{2}$$

Let $\Omega_1 = \{e, a, a^2, \ldots, a^{n-1}\}$, $\Omega_2 = \{b, ab, a^2b, \ldots, a^{n-1}b\}$, and $\Omega_3 = \Omega_1 - \zeta(D_n)$. Then $|\Omega_1| = n = |\Omega_2|$ and

$$|\Omega_3| = \begin{cases} n-1, & \text{when } n \text{ is odd}, \\ n-2, & \text{when } n \text{ is even}. \end{cases} \tag{3}$$

In the case of even value of $n \geq 4$, we partitioned Ω_2 into $n/2$ two element subsets $\Omega_2^i = \{a^ib, a^{((n/2)+i)}b\}$, $0 \leq i \leq (n/2) - 1$, so that $\Omega_2 = \cap_{i=0}^{(n/2)-1} \Omega_2^i$.

Remark 1. In the dihedral group D_n, we have

(i) $xy = yx$ for all $x, y \in D_2$

(ii) $a^ib = ba^{n-i}$ for $i = 1, 2, \ldots, n-1$

(iii) For odd values of $n \geq 3$, $xy \neq yx$ for distinct $x, y \in \Omega_2$

(iv) For even values of $n \geq 4$, and for any distinct $x, y \in \Omega_2$, $xy = yx$ if and only if $x, y \in \Omega_2^i$, $0 \leq i \leq (n/2) - 1$

(v) For any distinct $x, y \in \Omega_3$, $xy = yx$

(vi) For each pair $(x, y) \in \Omega_2 \times \Omega_3$, $xy \neq yx$

According to Remark 1, the commuting graph on D_n is defined in the following result.

Proposition 3 (see [16]). *For all $n \geq 3$, let $\Gamma_G = \mathscr{C}(D_n, D_n)$ be a commuting graph on D_n, then*

$$\Gamma_G = \begin{cases} K_1 + \left(K_{|\Omega_3|} \cup N_{|\Omega_1|}\right), & \text{when } n \text{ is odd}, \\ K_2 + \left(K_{|\Omega_3|} \cup \frac{n}{2} K_2\right), & \text{when } n \text{ is even}. \end{cases} \tag{4}$$

Here, K_1 is the trivial graph, K_p is a complete graph on p vertices, N_t is a null (empty) graph on t vertices, and $(n/2)K_2$ is the union of $(n/2)$ copies of K_2.

Let $\Gamma = D_n, n \geq 3$, and G_Γ be the corresponding non-commuting graph. Then, according to Remark 1, we have the following points:

When $n \geq 3$ is odd, then

(1) For $u, v \in V(G_\Gamma), u \sim v$ whenever $u, v \in \Omega_2$.

(2) For $u, v \in V(G_\Gamma), u \sim v$ whenever $u, v \in \Omega_3$.

(3) For $u, v \in V(G_\Gamma), u \sim v$ whenever $u \in \Omega_2$ and $v \in \Omega_3$.

(4) In G_Γ, it can be seen that $\mathrm{ecc}(v) = 1$ for all $v \in \Omega_2$, and $\mathrm{ecc}(v) = 2$ for all $v \in \Omega_3$. It follows that Ω_2 induces the center of G_Γ, which is a complete graph $K_{|\Omega_2|}$ on $|\Omega_2|$ vertices, and Ω_3 induces the periphery of G_Γ, which is a null graph $N_{|\Omega_3|}$ on $|\Omega_3|$ vertices.

When $n \geq 4$ is even, then

(1) For $u, v \in V(G_\Gamma), u \nsim v$ whenever $u, v \in \Omega_2^i$ for any $0 \leq i \leq (n/2) - 1$.

(2) For $u, v \in V(G_\Gamma), u \nsim v$ whenever $u, v \in \Omega_3$.

(3) For $u, v \in V(G_\Gamma), u \sim v$ whenever $u \in \Omega_2$ and $v \in \Omega_3$.

(4) For $u, v \in V(G_\Gamma), u \sim v$ whenever $u \in \Omega_2^i$ and $v \in \Omega_2^j$ with $0 \leq i, j \leq (n/2) - 1$ and $i \neq j$.

(5) In G_Γ, it can be seen that $\mathrm{ecc}(v) = 2$ for all $v \in \Omega_2 \cup \Omega_3$. It follows that G_Γ is a self-centered graph, which is a complete multipartite graph $K_{\underbrace{2, 2, \ldots, 2}_{(n/2)-\text{times}}, |\Omega_3|}$ with $n/2$ partite sets $\Omega_2^i, 0 \leq i \leq (n/2) - 1$, and one partite set Ω_3.

Hence, by Proposition 2, we deduce the following result.

Proposition 4. *For $n \geq 3$, let $\Gamma = D_n$. Then, the non-commuting graph G_Γ of D_n is given by*

$$G_\Gamma = \begin{cases} K_{\Omega_2} + N_{\Omega_3}, & \text{when } n \text{ is odd}, \\ K_{\underbrace{2, 2, \ldots, 2}_{(n/2)-\text{times}}, |\Omega_3|}, & \text{when } n \text{ is even}. \end{cases} \tag{5}$$

3. Construction of Vertex and Edge Partitions

First we define some useful parameters, which support in the investigation of some predefined (in Table 1) topological indices. For any vertex v of G, these parameters are defined as follows:

(i) The distance number of v in G is $D(v \mid G) = \sum_{u \in V(G)} d(u, v)$

(ii) The sum distance number of v in G is $D_s(v \mid G) = \sum_{u \in V(G) - \{v\}} 1/(D(G) + 1 - d(u, v))$

(iii) The reciprocal distance number of v in G is $D_r(v \mid G) = \sum_{u \in V(G)} 1/(d(u, v))$

According to these parameters, the distance-based topological indices, listed in Table 1, become

Table 3: Edge partition of Γ_G for each edge $u \sim v \in E(\Gamma_G)$.

n is	(d_u, d_v) type edges	(S_u, S_v) type edges	Number of edges
Odd	$(n-1, n-1)$	(n^2-n+1, n^2-n+1)	$((n-1)(n-2))/2$
Odd	$(n-1, 2n-1)$	(n^2-n+1, n^2-n+1)	$n-1$
Odd	$(1, 2n-1)$	$(2n-n, n^2-n+1)$	n
Even	$(n-1, n-1)$	(n^2+1, n^2+1)	$((n-2)(n-3))/2$
Even	$(n-1, 2n-1)$	$(n^2+1, (n+1)^2)$	$2(n-2)$
Even	$(2n-1, 2n-1)$	$((n+1)^2, (n+1)^2)$	1
Even	$(2n-1, 3)$	$((n+1)^2, 4n+1)$	$2n$
Even	$(3, 3)$	$(4n+1, 4n+1)$	$n/2$

Note: (d_u, d_v) denotes the type of edge $u \sim v$ according to degrees of the end vertices, and (S_u, S_v) denotes the type of edge $u \sim v$ according to degrees sum of the end vertices.

Table 4: Vertex partition of G_Γ for each vertex $v \in V(G_\Gamma)$.

n is	d_v	$\mathrm{ecc}(v)$	$D(v \mid G_\Gamma)$	$D_s(v \mid G_\Gamma)$	$D_r(v \mid G_\Gamma)$	Number of vertices
Odd	$2n-2$	1	$2n-2$	$n-1$	$2n-2$	n
Odd	n	2	$3n-4$	$(1/2)(3n-4)$	$(1/2)(3n-1)$	$n-1$
Even	$2n-2$	2	$2n-2$	$n-1$	$(1/2)(4n-7)$	n
Even	n	2	$3n-6$	$(3/2)(n-2)$	$(3/2)(n-1)$	$n-2$

Table 5: Edge partition of G_Γ for each edge $u \sim v \in E(G_\Gamma)$.

n is	(d_u, d_v) type edges	(S_u, S_v) type edges	Number of edges
Odd	$(n, 2n-2)$	$(2n(n-1), (n-1)(3n-2))$	$n(n-1)$
Odd	$(2n-2, 2n-2)$	$((n-1)(3n-2), (n-1)(3n-2))$	$(n(n-1))/2$
Even	$(n, 2n-4)$	$(2n(n-2), (n-2)(3n-4))$	$n(n-2)$
Even	$(2n-4, 2n-4)$	$((n-2)(3n-4), (n-2)(3n-4))$	$(n(n-2))/2$

Note: (d_u, d_v) denotes the type of edge $u \sim v$ according to degrees of the end vertices, and (S_u, S_v) denotes the type of edge $u \sim v$ according to degrees sum of the end vertices.

$$W(G) = \frac{1}{2} \sum_{v \in V(G)} D(v \mid G), \tag{6}$$

$$\mathrm{RCW}(G) = \frac{|G|}{D(G)+1} + \frac{1}{2} \sum_{v \in V(G)} D_s(v \mid G), \tag{7}$$

$$\mathrm{MTI}(G) = \sum_{v \in V(G)} (d(v))^2 + \sum_{v \in V(G)} d(v) D(v \mid G), \tag{8}$$

$$H(G) = \frac{1}{2} \sum_{v \in V(G)} D_r(v \mid G). \tag{9}$$

Let Γ_G be a commuting graph of the dihedral group D_n. In Γ_G, there are $2n$ vertices. The number of edges in Γ_G is $(n(n+1))/2$ when n is odd and is $(n(n+4))/2$ when n is even. Based on the degree, distance number, sum distance number, and reciprocal distance number of each vertex of Γ_G, the useful vertex partition is given in Table 2. Based on degrees and degrees sum of the end vertices of each edge of Γ_G, the useful edge partition is given in Table 3.

Let G_Γ be a non-commuting graph of the dihedral group D_n. In G_Γ,

(1) There are $2n-1$ vertices and $(3/2)n(n-1)$ edges when n is odd

(2) There are $2n-2$ vertices and $(3/2)n(n-2)$ edges when n is even

Based on the degree, eccentricity, distance number, sum distance number, and reciprocal distance number of each vertex of G_Γ, the useful vertex partition is given in Table 4. Based on degrees and degrees sum of the end vertices of each edge of G_Γ, the useful edge partition is given in Table 5.

4. Topological Properties of Commuting Graph Γ_G

In this section, we compute the Wiener, reciprocal complementary Wiener, MTI, Harary general Randić, ABC, ABC_4, GA, GA_5, and harmonic indices of Γ_G. Throughout this section, in each of the two-row equation arrays, the first row corresponds to odd values of n, while the second corresponds to even values of n.

Theorem 1. *For $n \geq 3$, let Γ_G be a commuting graph on D_n, then*

$$W(\Gamma_G) = \begin{cases} \frac{n}{2}(7n-5), & \text{when } n \text{ is odd,} \\ \frac{n}{2}(7n-8), & \text{when } n \text{ is even.} \end{cases} \tag{10}$$

Proof. Using the vertex partition, given in Table 2, in formula (6) of the Wiener index, we have

$$W(\Gamma_G) = \begin{cases} \frac{(n-1)(3n-1)+(2n-1)+n(4n-3)}{2}, & \text{when } n \text{ is odd,} \\ \frac{(n-2)(3n-1)+2(2n-1)+n(4n-5)}{2}, & \text{when } n \text{ is even.} \end{cases} \tag{11}$$

Now, the required Wiener index can be obtained after some simplifications. □

Theorem 2. *For $n \geq 3$, let Γ_G be a commuting graph on D_n, then*

$$\mathrm{RCW}(\Gamma_G) = \begin{cases} \frac{7n}{12}(3n-1), & \text{when } n \text{ is odd,} \\ \frac{n}{12}(21n-16), & \text{when } n \text{ is even.} \end{cases} \tag{12}$$

Proof. Since the diameter of G_Γ is 2, so by using the vertex partition, given in Table 4, in formula (7) of the reciprocal complimentary Wiener index, we have

$$\mathrm{RCW}(\Gamma_G) = \begin{cases} \frac{2n}{3} + \frac{1}{2}\left(\frac{n}{2}(4n-3) + \frac{1}{2}(2n-1) + \frac{1}{2}(n-1)(3n-1)\right), & \text{when } n \text{ is odd,} \\ \frac{2n}{3} + \frac{1}{2}\left(\frac{n}{2}(4n-5) + (2n-1) + \frac{1}{2}(n-2)(3n-1)\right), & \text{when } n \text{ is even.} \end{cases} \tag{13}$$

Now, the required index can be easily found by performing some simplifications. □

Theorem 3. *For $n \geq 3$, let Γ_G be a commuting graph on D_n, then*

$$\mathrm{MTI}(\Gamma_G) = \begin{cases} 2n(2n-1)(n+1), & \text{when } n \text{ is odd,} \\ 2n(2n-1)(n+4), & \text{when } n \text{ is even.} \end{cases} \tag{14}$$

Proof. By applying formula (8) of the Schultz molecular topological index using the vertex partition, given in Table 2, we have when n is odd

$$\begin{aligned} \mathrm{MTI}(\Gamma_G) &= (n-1)^3 + (2n-1)^2 + n + (n-1)^2(3n-1) \\ &\quad + (2n-1)^2 + n(4n-3) \\ &= 2n(2n-1)(n+1), \end{aligned} \tag{15}$$

and when n is even

$$\begin{aligned} \mathrm{MTI}(\Gamma_G) &= (n-2)(n-1)^2 + 2(2n-1)^2 + n(3)^2 \\ &\quad + (n-2)(n-1)(3n-1) + 2(2n-1)^2 \\ &\quad + 3n(4n-5) = 2n(2n-1)(n+4). \end{aligned} \tag{16}$$

□

Theorem 4. *For $n \geq 3$, let Γ_G be a commuting graph on D_n, then*

$$H(\Gamma_G) = \begin{cases} \frac{n}{4}(5n-1), & \text{when } n \text{ is odd,} \\ \frac{n}{4}(5n+2), & \text{when } n \text{ is even.} \end{cases} \tag{17}$$

Proof. Using the vertex partitions, given in Table 2, in formula (9) of the Harary index, we have

$$H(\Gamma_G) = \begin{cases} \frac{1}{2}\left(\frac{(n-1)(3n-2)}{2} + 2n - 1 + n^2\right), & \text{when } n \text{ is odd,} \\ \frac{1}{2}\left(\frac{(n-2)(3n-2)}{2} + 2(2n-1) + n(n+1)\right), & \text{when } n \text{ is even.} \end{cases} \tag{18}$$

Some easy simplifications yield the required Harary index. □

Theorem 5. *For $n \geq 3$, let Γ_G be a commuting graph of $\Gamma = D_n$. Then, for odd values of n,*

$$R_\alpha(\Gamma_G) = \begin{cases} \frac{n}{2}\left(n^3 - n^2 + 3n - 1\right), & \text{for } \alpha = 1, \\ \frac{n(4n-5)}{(2n-2)(2n-1)}, & \text{for } \alpha = -1, \\ \frac{(n-1)^2(n-2) + 2(n-1)\sqrt{(n-1)(2n-1)} + 2n\sqrt{2n-1}}{2}, & \text{for } \alpha = \frac{1}{2}, \\ \frac{n - 2\sqrt{2n-1} + 2\sqrt{n-1} + 2n}{2\sqrt{2n-1}}, & \text{for } \alpha = -\frac{1}{2}, \end{cases} \tag{19}$$

and for even values of n,

$$R_\alpha(\Gamma_G) = \begin{cases} \frac{1}{2}\left((n-1)^2\left(n^2 - 5n + 6\right) + 2(2n-1)\left(2n^2 + 2n + 3\right) + 9n\right), & \text{for } \alpha = 1, \\ \frac{9(2n-1)\left(2n^3 - 7n^2 + 5n + 2\right)^2\left(4n^3 + 20n^2 - 11n + 18\right)}{18(n-1)^2(2n-1)^2}, & \text{for } \alpha = -1, \\ \frac{(n-1)(n-2)(n-3) + 7n - 2 + 4\sqrt{2n-1}\left((n-2)\sqrt{n-1} + n\sqrt{3}\right)}{2}, & \text{for } \alpha = \frac{1}{2}, \\ \frac{2n(n-1)(2n-7) + 3(5n-4)}{3(n-1)(2n-1)} + \frac{2(n-2)\sqrt{3} + 2n\sqrt{n-1}}{\sqrt{3(2n-1)(n-1)}}, & \text{for } \alpha = -\frac{1}{2}. \end{cases} \tag{20}$$

Proof. Using the edge partition, given in Table 3, in the formula of general Randić index R_α for $\alpha = 1, -1, (1/2), -(1/2)$, we have

$$R_1(\Gamma_G)=\begin{cases}\dfrac{(n-1)^3(n-2)}{2}+(n-1)^2(2n-1)+n(2n-1),\\[2ex] \dfrac{(n-2)(n-3)(n-1)^2}{2}+2(n-2)(n-1)(2n-1)+(2n-1)^2+6n(2n-1)+\dfrac{9n}{2},\end{cases}$$

$$R_{-1}(\Gamma_G)=\begin{cases}\dfrac{(n-2)}{2(n-1)}+\dfrac{1}{2n-1}+\dfrac{n}{2n-1},\\[2ex] \dfrac{(n-2)(n-3)}{2(n-1)^2}+\dfrac{2(n-2)}{(n-1)(2n-1)}+\dfrac{1}{(2n-1)^2}+\dfrac{2n}{3(2n-1)}+\dfrac{n}{18},\end{cases}$$

$$R_{1/2}(\Gamma_G)=\begin{cases}\dfrac{(n-1)(n-2)\sqrt{(n-1)^2}}{2}+(n-1)\sqrt{(n-1)(2n-1)}+n\sqrt{2n-1},\\[2ex] \dfrac{(n-2)(n-3)(n-1)}{2}+2(n-2)\sqrt{(n-1)(2n-1)}+2n-1+2n\sqrt{3(2n-1)}+\dfrac{3n}{2},\end{cases} \tag{21}$$

$$R_{-(1/2)}(\Gamma_G)=\begin{cases}\dfrac{(n-1)(n-2)}{2\sqrt{(n-1)(n-1)}}+\dfrac{(n-1)}{\sqrt{(n-1)(2n-1)}}+\dfrac{n}{\sqrt{2n-1}},\\[2ex] \dfrac{(n-2)(n-3)}{2(n-1)}+\dfrac{2(n-2)}{\sqrt{(n-1)(2n-1)}}+\dfrac{1}{2n-1}+\dfrac{2n}{\sqrt{3(2n-1)}}+\dfrac{n}{6}.\end{cases}$$

After a minor simplification, we get our required result. □

Theorem 6. *For $n\geq 3$, let Γ_G be a commuting graph of $\Gamma=D_n$, then*

$$\mathrm{GA}(\Gamma_G)=\begin{cases}\dfrac{(n-1)(n-2)}{2}+\dfrac{2(n-1)\sqrt{(n-1)(2n-1)}}{3n-2}+\sqrt{2n-1},\\[2ex] \dfrac{n^2-4n+8}{2}+\dfrac{4(n^2-n-2)\sqrt{2n^2-3n+1}+2n(3n-2)\sqrt{3(2n-1)}}{(n+1)(3n-2)},\end{cases}$$

$$\mathrm{GA}_5(\Gamma_G)=\begin{cases}\dfrac{n(n^2-1)+4\sqrt{n^3+(n-1)^3}}{2(n+1)},\\[2ex] \dfrac{n^2-4n+8}{2}+\dfrac{2(n-2)(n+1)\sqrt{n^2+1}}{n^2+n+1}+\dfrac{4n(n+1)\sqrt{4n+1}}{n^2+6n+2}.\end{cases} \tag{22}$$

Proof. Applying formulas of the geometric arithmetic index and its fifth version, using the edge partition given in Table 3, we have

$$\mathrm{GA}(\Gamma_G)=\begin{cases}\dfrac{2(n-1)^2(n-2)}{2(2n-2)}+\dfrac{2(n-1)\sqrt{(n-1)(2n-1)}}{3n-2}+\dfrac{2n\sqrt{2n-1}}{2n},\\[2ex] \dfrac{(n-2)(n-3)}{2}+\dfrac{4(n-2)\sqrt{(n-1)(2n-1)}}{3n-2}+1+\dfrac{2n\sqrt{3(2n-1)}}{n+1}+\dfrac{n}{2},\end{cases}$$
$$\mathrm{GA}_5(\Gamma_G)=\begin{cases}\dfrac{2n(n-1)\sqrt{(n^2-n+1)^2}}{4(n^2-n+1)}+\dfrac{2n\sqrt{(n^2-n+1)(2n-1)}}{n(n+1)},\\[2ex] \dfrac{(n-2)(n-3)}{2}+\dfrac{4(n-2)\sqrt{(n^2+1)(n+1)^2}}{2n^2+2n+2}+1+\dfrac{4n\sqrt{(n+1)^2(4n+1)}}{n^2+6n+2}+\dfrac{n}{2}.\end{cases}\tag{23}$$

The required values of the geometric arithmetic index and its fifth version can be obtained after some simplifications. □

Theorem 7. *For $n\geq 3$, let Γ_G be a commuting graph of $\Gamma = D_n$, then*

$$\mathrm{ABC}(\Gamma_G)=\begin{cases}\dfrac{(n-2)\sqrt{(n-2)(2n-1)}+\sqrt{2(n-1)(3n-4)}+2n\sqrt{n-1}}{\sqrt{2(2n-1)}},\\[2ex] \dfrac{(n-2)(n-3)\sqrt{2(n-2)}}{2(n-1)}+\dfrac{2\sqrt{n-1}}{(2n-1)}+\dfrac{n}{3}+\dfrac{2n\sqrt{2n(n-1)}+2(n-2)\sqrt{3(3n-4)}}{\sqrt{3(n-1)(2n-1)}},\end{cases}$$
$$\mathrm{ABC}_4(\Gamma_G)=\begin{cases}\dfrac{n(n-1)\sqrt{2n(n-1)}}{2(n^2-n+1)}+n\sqrt{\dfrac{n^2+n-2}{(2n-1)(n^2-n+1)}},\\[2ex] \dfrac{n(n-2)(n-3)\sqrt{2}}{2(n^2+1)}+\dfrac{2(n-2)}{n+1}\sqrt{\dfrac{2n(n+1)}{n^2+1}}+\dfrac{\sqrt{2n(n+2)}}{(n+1)^2}+\dfrac{2n}{n+1}\sqrt{\dfrac{n(n+6)}{4n+1}}+\dfrac{n\sqrt{2n}}{4n+1}.\end{cases}\tag{24}$$

Proof. By using the edge partition, given in Table 3, in formulas of ABC and ABC_4 indices, we have

$$\mathrm{ABC}(\Gamma_G)=\begin{cases}\dfrac{(n-2)\sqrt{2(n-2)}}{2}+(n-1)\sqrt{\dfrac{3n-4}{(n-1)(2n-1)}}+n\sqrt{\dfrac{2(n-1)}{2n-1}},\\[2ex] \dfrac{(n-2)(n-3)\sqrt{2(n-2)}}{2(n-1)}+2(n-2)\sqrt{\dfrac{3n-4}{(n-1)(2n-1)}}+\dfrac{2\sqrt{n-1}}{2n-1}+\dfrac{n}{3}+2n\sqrt{\dfrac{2n}{3(2n-1)}}.\end{cases}\tag{25}$$

Also, for odd values of n, we have

$$\mathrm{ABC}_4(\Gamma_G)=\frac{n(n-1)}{2}\sqrt{\frac{(n^2-n+1)+(n^2-n+1)-2}{(n^2-n+1)(n^2-n+1)}}+n\sqrt{\frac{(n^2-n+1)+(2n-1)-2}{(n^2-n+1)(2n-1)}},\tag{26}$$

and for even values of n, we have

$$\mathrm{ABC}_4(\Gamma_G)=\frac{(n-2)(n-3)\sqrt{2n^2}}{2(n^2+1)}+\frac{2(n-2)}{n+1}\sqrt{\frac{2n^2+2n}{n^2+1}}+\frac{\sqrt{2n^2+4n}}{(n+1)^2}+\frac{2n}{n+1}\sqrt{\frac{n^2+6n}{4n+1}}+\frac{n\sqrt{8n}}{2(4n+1)}.\tag{27}$$

The required formulas for both the indices one can get by performing an easy simplification. □

Theorem 8. *For $n \geq 3$, let Γ_G be a commuting graph of $\Gamma = D_n$, then*

$$H_r(\Gamma_G) = \begin{cases} \dfrac{3n^2 + 2n - 4}{2(3n-2)}, \\ \dfrac{(n-2)(3n^2 - 3n - 2)}{2(n-1)(3n-2)} + \dfrac{6(n+1) + n(2n-1)(n+13)}{6(n+1)(2n-1)}. \end{cases} \tag{28}$$

Proof. By applying the formula of the harmonic index, using the edge partition given in Table 3, we have

$$H_r(\Gamma_G) = \begin{cases} \dfrac{(n-1)(n-2)}{2(n-1)} + \dfrac{2(n-1)}{3n-2} + 1, \\ \dfrac{(n-2)(n-3)}{2(n-1)} + \dfrac{4(n-2)}{3n-2} + \dfrac{1}{2n-1} + \dfrac{2n}{n+1} + \dfrac{n}{6}. \end{cases} \tag{29}$$

Some simplifications yield the required values of the harmonic index. □

5. Topological Properties of Noncommuting Graph G_Γ

In this section, we compute the reciprocal complementary Wiener, Harary, general Randić, ABC, ABC_4, GA, GA_5, and harmonic indices of G_Γ.

Theorem 9. *For $n \geq 3$, let G_Γ be a noncommuting graph of $\Gamma = D_n$, then*

$$\mathrm{RCW}(G_\Gamma) = \begin{cases} \dfrac{1}{12}\left(15n^2 - 19n + 4\right), & \text{when } n \text{ is odd}, \\ \dfrac{1}{12}\left(15n^2 - 34n + 28\right), & \text{when } n \text{ is even}. \end{cases} \tag{30}$$

Proof. Since the diameter of G_Γ is 2, so by sing the vertex partition, given in Table 4, in formula (7) of the reciprocal complimentary Wiener index, we have

$$\mathrm{RCW}(G_\Gamma) = \begin{cases} \dfrac{2n-1}{3} + \dfrac{n(n-1)}{2} + \dfrac{(n-1)(3n-4)}{4}, & \text{when } n \text{ is odd}, \\ \dfrac{2n-2}{3} + \dfrac{n(n-1)}{2} + \dfrac{3(n-2)(n-2)}{4}, & \text{when } n \text{ is even}. \end{cases} \tag{31}$$

Exact values for this index are due to some easy calculations. □

Theorem 10. *For $n \geq 3$, let G_Γ be a noncommuting graph of $\Gamma = D_n$, then*

$$H(G_\Gamma) = \begin{cases} \dfrac{1}{4}\left(7n^2 - 8n + 1\right), & \text{when } n \text{ is odd}, \\ \dfrac{1}{4}\left(7n^2 - 16n + 6\right), & \text{when } n \text{ is even}. \end{cases} \tag{32}$$

Proof. By sing the vertex partition, given in Table 4, in formula (9) of the Harary index, we have

$$H(G_\Gamma) = \begin{cases} \dfrac{n(2n-2)}{2} + \dfrac{(n-1)(3n-1)}{4}, & \text{when } n \text{ is odd}, \\ \dfrac{n(4n-7)}{4} + \dfrac{3(n-2)(n-1)}{4}, & \text{when } n \text{ is even}. \end{cases} \tag{33}$$

By performing some algebraic computations, one can obtain the required Harary index. □

Theorem 11. *For $n \geq 3$, let G_Γ be a noncommuting graph of $\Gamma = D_n$. Then, for odd values of n,*

$$R_\alpha(G_\Gamma) = \begin{cases} 2n(n-1)^2(2n-1), & \text{for } \alpha = 1, \\ \dfrac{5n-4}{8(n-1)}, & \text{for } \alpha = -1, \\ n(n-1)\sqrt{2n(n-1)} + n - 1, & \text{for } \alpha = \dfrac{1}{2}, \\ \sqrt{\dfrac{n(n-1)}{2}} + \dfrac{n}{4}, & \text{for } \alpha = -\dfrac{1}{2}, \end{cases} \tag{34}$$

and for even values of n,

$$R_\alpha(G_\Gamma) = \begin{cases} 4n(n-2)^2(n-1), & \text{for } \alpha = 1, \\ \dfrac{10n-16}{16n-32}, & \text{for } \alpha = -1, \\ n(n-2)\sqrt{n(2n-4)} + n(n-2)^2, & \text{for } \alpha = \dfrac{1}{2}, \\ \dfrac{4n(n-2) + n\sqrt{2n(n-2)}}{4\sqrt{2n(n-2)}}, & \text{for } \alpha = -\dfrac{1}{2}. \end{cases} \tag{35}$$

Proof. Using the edge partition, given in Table 5, in the formula of general Randić index R_α for $\alpha = 1, -1, 1/2, -(1/2)$, we have

$$\begin{aligned} R_1(G_\Gamma) &= \begin{cases} n^2(n-1)(2n-2) + \dfrac{n(n-1)(2n-2)^2}{2}, & \text{when } n \text{ is odd}, \\ n^2(n-2)(2n-4) + \dfrac{n(n-2)(2n-4)^2}{2}, & \text{when } n \text{ is even}, \end{cases} \\ R_{-1}(G_\Gamma) &= \begin{cases} \dfrac{n(n-1)}{n(2n-2)} + \dfrac{n(n-1)}{2(2n-2)^2}, & \text{when } n \text{ is odd}, \\ \dfrac{n(n-2)}{n(2n-4)} + \dfrac{n(n-2)}{2(2n-4)^2}, & \text{when } n \text{ is even}, \end{cases} \\ R_{1/2}(G_\Gamma) &= \begin{cases} n(n-1)\sqrt{n(2n-2)} + \dfrac{n(n-1)(2n-2)}{2}, & \text{when } n \text{ is odd}, \\ n(n-2)\sqrt{n(2n-4)} + \dfrac{n(n-2)(2n-4)}{2}, & \text{when } n \text{ is even}, \end{cases} \\ R_{-(1/2)}(G_\Gamma) &= \begin{cases} \dfrac{n(n-1)}{\sqrt{n(2n-2)}} + \dfrac{n(n-1)}{2(2n-2)}, & \text{when } n \text{ is odd}, \\ \dfrac{n(n-2)}{\sqrt{n(2n-4)}} + \dfrac{n(n-2)}{2(2n-4)}, & \text{when } n \text{ is even}. \end{cases} \end{aligned} \tag{36}$$

By performing some simplifications, we get the required results. □

Theorem 12. *Let G_Γ be a noncommuting graph of $\Gamma = D_n$, for $n \geq 3$, then*

$$\mathrm{GA}(G_\Gamma) = \begin{cases} \dfrac{2(2n(n-1))^{3/2} + n(n-1)(3n-2)}{2(3n-2)}, & \text{when } n \text{ is odd,} \\ \dfrac{2(2n(n-2))^{3/2} + n(n-2)(3n-4)}{2(3n-4)}, & \text{when } n \text{ is even,} \end{cases}$$
$$\mathrm{GA}_5(G_\Gamma) = \begin{cases} \dfrac{4n\sqrt{2n(n-1)^2(3n-2)} + n(n-1)(5n-2)}{10n-4}, & \text{when } n \text{ is odd,} \\ \dfrac{n(n-2)(5n-4+\sqrt{32n(3n-4)})}{10n-8}, & \text{when } n \text{ is even.} \end{cases} \tag{37}$$

Proof. Applying formulas of the geometric arithmetic index and its fifth version, using the edge partition given in Table 5, we have

$$\mathrm{GA}(G_\Gamma) = \begin{cases} \dfrac{2n(n-1)\sqrt{n(2n-2)}}{3n-2} + \dfrac{n(n-1)}{2}, & \text{when } n \text{ is odd,} \\ \dfrac{2n(n-2)\sqrt{n(2n-4)}}{3n-4} + \dfrac{n(n-2)}{2}, & \text{when } n \text{ is even,} \end{cases}$$
$$\mathrm{GA}_5(G_\Gamma) = \begin{cases} \dfrac{2n(n-1)\sqrt{2n(n-1)^2(3n-2)}}{2n(n-1)+(n-1)(3n-2)} + \dfrac{n(n-1)}{2}, & \text{when } n \text{ is odd,} \\ \dfrac{2n(n-2)\sqrt{2n(n-2)^2(3n-4)}}{2n(n-2)+(n-2)(3n-4)} + \dfrac{n(n-2)}{2}, & \text{when } n \text{ is even.} \end{cases} \tag{38}$$

The required values of the geometric arithmetic index and its fifth version can be obtained after some simplifications. □

Theorem 13. *For $n \geq 3$, let G_Γ be a noncommuting graph of $\Gamma = D_n$, then*

$$\mathrm{ABC}(G_\Gamma) = \begin{cases} \sqrt{\dfrac{n(n-1)(3n-4)}{2}} + \sqrt{\dfrac{n^2(2n-3)}{8}}, & \text{when } n \text{ is odd,} \\ \sqrt{\dfrac{n(n-2)(3n-6)}{2}} + \dfrac{n\sqrt{4n-10}}{4}, & \text{when } n \text{ is even,} \end{cases}$$
$$\mathrm{ABC}_4(G_\Gamma) = \begin{cases} \sqrt{\dfrac{n^2(n-1)^2(5n^2-7n)}{6n^4-16n^3+14n^2-4n}} + \dfrac{\sqrt{n^2(6n^2-10n+2)}}{2(3n-2)}, & \text{when } n \text{ is odd,} \\ \sqrt{\dfrac{5n^3-14n^2+6n}{3n-4}} + \dfrac{\sqrt{2n^2(n-1)(3n-7)}}{2(3n-4)}, & \text{when } n \text{ is even.} \end{cases} \tag{39}$$

Proof. By using the edge partition, given in Table 5, in formulas of ABC and ABC_4 indices, we have

$$\mathrm{ABC}(G_\Gamma) = \begin{cases} n(n-1)\sqrt{\dfrac{3n-4}{2n(n-1)}} + \dfrac{n(n-1)\sqrt{4n-6}}{2(2n-2)}, & \text{when } n \text{ is odd,} \\ n(n-2)\sqrt{\dfrac{3n-6}{n(2n-4)}} + \dfrac{n(n-2)\sqrt{4n-10}}{2(2n-4)}, & \text{when } n \text{ is even.} \end{cases} \tag{40}$$

Also, for odd values of n, we have

$$\mathrm{ABC}_4(G_\Gamma) = n(n-1)\sqrt{\frac{2n(n-1)+(n-1)(3n-2)-2}{2n(n-1)^2(3n-2)}} + \frac{n(n-1)}{2}\sqrt{\frac{2(n-1)(3n-2)-2}{((n-1)(3n-2))^2}}, \tag{41}$$

and for even values of n, we have

$$\mathrm{ABC}_4(G_\Gamma) = n(n-2)\sqrt{\frac{2n(n-2)+(n-2)(3n-4)-2}{2n(n-2)^2(3n-4)}} + \frac{n(n-2)\sqrt{2(n-2)(3n-4)-2}}{2(n-2)(3n-4)}. \tag{42}$$

The required formulas for both the indices one can get by performing an easy simplification. □

Theorem 14. *For $n \geq 3$, let G_Γ be a noncommuting graph of $\Gamma = D_n$, then*

$$H_r(G_\Gamma) = \begin{cases} \dfrac{n(11n-10)}{4(3n-2)}, & \text{when } n \text{ is odd,} \\ \dfrac{n(11n-20)}{4(3n-4)}, & \text{when } n \text{ is even.} \end{cases} \tag{43}$$

Proof. By applying the formula of the harmonic index, using the edge partition given in Table 5, we have

$$H_r(G_\Gamma) = \begin{cases} \dfrac{2n(n-1)}{3n-2} + \dfrac{n(n-1)}{2(2n-2)}, & \text{when } n \text{ is odd,} \\ \dfrac{2n(n-2)}{3n-4} + \dfrac{n(n-2)}{2(2n-4)}, & \text{when } n \text{ is even.} \end{cases} \tag{44}$$

Some simplifications yield the required values of the harmonic index. □

6. Concluding Remarks

An algebraic structure plays a vital role in chemistry to form chemical compound structures and in investigating various chemical properties of chemical compounds in these structures. Here, we considered a very well-known algebraic structure, called the group of symmetries of regular gons (the dihedral group), which has remarkable contribution in the theory of electron structures and molecular vibrations. We considered one algebraic property, namely, commutation property, on the dihedral group and associated two graphs (chemical structure) with the group of symmetries. We computed some distance-based and degree-based topological properties of these associated graphs by computing the exact formulae of the Wiener index, reciprocal complementary Wiener index, Schultz molecular topological index, Harary index, Randić index, geometric arithmetic indices, atomic bond connectivity indices, and harmonic index. All the indices are numeric quantities and, in fact, this work is a theoretical contribution in the theory of topological indices with the unique algebraic structure, and it can be very helpful to predict the bioactivity of chemical compounds using physicochemical properties in QSAR/QSPR studied.

Data Availability

The data used to support the findings of this study are included within the article.

Conflicts of Interest

The authors declare that they have no conflicts of interest.

Acknowledgments

This work was supported by Top-Notch Talents Cultivation Project of Anhui Higher Education (Grant no. gxyq2017081) and Natural Science Fund of Education Department of Anhui Province (Grant no. KJ2017A4691).

References

[1] M. Mirzargar and A. R. Ashrafi, "Some distance-based topological indices of a non-commuting graph," *Hacettepe Journal of Mathematics and Statistics*, vol. 41, no. 4, pp. 515–526, 2012.

[2] H. Wiener, "Structural determination of paraffin boiling points," *Journal of the American Chemical Society*, vol. 69, no. 1, pp. 17–20, 1947.

[3] G. Caporossi, I. Gutman, P. Hansen, and L. Pavlović, "Graphs with maximum connectivity index," *Computational Biology and Chemistry*, vol. 27, no. 1, pp. 85–90, 2003.

[4] A. Graovac, M. Ghorbani, and M. A. Hosseinzadeh, "Computing fifth goemetric-arithmetic index for nanostar dendrimers," *Journal of Mathematical Nanoscience*, vol. 1, pp. 33–42, 2011.

[5] M. Ghorbani and M. A. Hosseinzadeh, "Computing ABC_4 index of nanostar dendrimers," *Advanced Materials—Rapid Communications*, vol. 4, pp. 1419–1422, 2010.

[6] I. Gutman, "Degree-based topological indices," *Croatica Chemica Acta*, vol. 86, no. 4, pp. 351–361, 2013.

[7] S. Hayat and M. Imran, "Computation of topological indices of certain networks," *Applied Mathematics and Computation*, vol. 240, pp. 213–228, 2014.

[8] M. Imran, S. Hayat, and M. Y. H. Mailk, "On topological indices of certain interconnection networks," *Applied Mathematics and Computation*, vol. 244, pp. 936–951, 2014.

[9] K. Xu, M. Liu, K. C. Das, I. Gutman, and B. Furtula, "A survey on graphs extremal with respect to distance-based topological indices," *MATCH Communications in Mathematical and in Computer Chemistry*, vol. 71, pp. 461–508, 2014.

[10] S. Hayat, M. Imran, and J.-B. Liu, "An efficient computational technique for degree and distance based topological descriptors with applications," *IEEE Access*, vol. 7, pp. 32276–32296, 2019.

[11] S. Hayat, S. Wang, and J.-B. Liu, "Valency-based topological descriptors of chemical networks and their applications," *Applied Mathematical Modelling*, vol. 60, pp. 164–178, 2018.

[12] S. Hayat, "Computing distance-based topological descriptors of complex chemical networks: new theoretical techniques," *Chemical Physics Letters*, vol. 688, pp. 51–58, 2017.

[13] J.-B. Liu, C. Wang, S. Wang, and B. Wei, "Zagreb indices and multiplicative Zagreb indices of Eulerian graphs," *Bulletin of the Malaysian Mathematical Sciences Society*, vol. 42, no. 1, pp. 67–78, 2019.

[14] J.-B. Liu and X.-F. Pan, "Minimizing Kirchhoff index among graphs with a given vertex bipartiteness," *Applied Mathematics and Computation*, vol. 291, pp. 84–88, 2016.

[15] J.-B. Liu, X.-F. Pan, F.-T. Hu, and F.-F. Hu, "Asymptotic Laplacian-energy-like invariant of lattices," *Applied Mathematics and Computation*, vol. 253, pp. 205–214, 2015.

[16] F. Ali, M. Salman, and S. Huang, "On the commuting graph of dihedral group," *Communications in Algebra*, vol. 44, no. 6, pp. 2389–2401, 2016.

[17] D. Bunday, "The connectivity of commuting graphs," *Journal of Combinatorial Theory, Series A*, vol. 113, no. 6, pp. 995–1007, 2006.

[18] B. H. Neumann, "A problem of Paul Erdös on groups," *Journal of the Australian Mathematical Society*, vol. 21, no. 4, pp. 467–472, 1976.

[19] A. Abdollahi, S. Akbari, and H. R. Maimani, "Non-commuting graph of a group," *Journal of Algebra*, vol. 298, no. 2, pp. 468–492, 2006.

[20] A. R. Moghaddamfar, W. J. Shi, W. Zhou, and A. R. Zokayi, "On the noncommuting graph associated with a finite group," *Siberian Mathematical Journal*, vol. 46, no. 2, pp. 325–332, 2005.

[21] O. Ivancivc, "QSAR comparative study of Wiener descriptors for weighted molecular graphs," *Journal of Chemical Information and Computer Sciences*, vol. 40, no. 6, pp. 1412–1422, 2000.

[22] H. P. Schultz, "Topological organic chemistry. 1. graph theory and topological indices of alkanes," *Journal of Chemical Information and Modeling*, vol. 29, no. 3, pp. 227-228, 1989.

[23] O. Ivancivc, T. S. Balaban, and A. T. Balaban, "Design of topological indices. Part 4. Reciprocal distance matrix, related local vertex invariants and topological indices," *Journal of Mathematical Chemistry*, vol. 12, no. 1, pp. 309–318, 1993.

[24] D. Plavšić, S. Nikolić, N. Trinajstić, and Z. Mihalić, "On the Harary index for the characterization of chemical graphs," *Journal of Mathematical Chemistry*, vol. 12, no. 1, pp. 235–250, 1993.

[25] M. Randic, "Characterization of molecular branching," *Journal of the American Chemical Society*, vol. 97, no. 23, pp. 6609–6615, 1975.

[26] D. Amić, D. Bešlo, B. Lučić, S. Nikolić, and N. Trinajstić, "The vertex-connectivity index revisited," *Journal of Chemical Information and Computer Sciences*, vol. 38, no. 5, pp. 819–822, 1998.

[27] B. Bollobás and P. Erdös, "Graph of extremal weights," *Ars Combinatoria*, vol. 50, pp. 225–233, 1998.

[28] D. Vukičević and B. Furtula, "Topological index based on the ratios of geometrical and arithmetical means of end-vertex degrees of edges," *Journal of Mathematical Chemistry*, vol. 46, no. 4, pp. 1369–1376, 2009.

[29] E. Estrada, L. Torres, L. Rodríguez, and I. Gutman, "An atom-bond connectivity index: modelling the enthalpy of formation of alkanes," *Indian Journal of Chemistry*, vol. 37, no. 10, pp. 849–855, 1998.

[30] S. Fajtlowicz, "On conjectures of Grafitti II," *Congress Numer*, vol. 60, pp. 189–197, 1987.

Hindawi
Journal of Chemistry
Volume 2020, Article ID 1237034, 6 pages
https://doi.org/10.1155/2020/1237034

Research Article

Research on Noise Reduction Scheme of Heat Pump Unit in a Square

Xueyong Zhang,[1,2,3] **Yuanyuan Hu**,[1,3] **Shengyuan Geng**,[2] **Qianyong Hu**,[1] **and Huanbao Wang**[1,3]

[1]*School of Mathematics and Physics, Institute of Acoustics, Anhui Jianzhu University, Hefei 230601, China*
[2]*Anhui Province Key Laboratory of Intelligent Building & Building Energy Saving, Hefei 230022, China*
[3]*Key Laboratory of Architectural Acoustic Environment of Anhui Higher Education Institutes, Hefei 230601, China*

Correspondence should be addressed to Xueyong Zhang; xyzhang_aua@126.com

Received 30 October 2019; Revised 16 December 2019; Accepted 7 January 2020; Published 9 March 2020

Guest Editor: Shaohui Wang

Heat pump unit is a host device located in the central air-conditioning terminal, providing cold and hot water. Heat pump unit has the advantages of energy saving, environmental protection, easy maintenance, and so on. It is adopted to solve the problems of refrigeration and heating in ventilation and air conditioning from many engineering projects in China. When the equipment is turned on, however, the high noise generated by the heat pump unit has a very negative impact on the life and work of the surrounding residents. Therefore, noise reduction is needed to improve the environment quality. In this paper, the noise of the air-cooled heat pump unit of the square area in Shanghai was detected, the noise source was analyzed, and the corresponding noise reduction scheme was proposed. After the completion of the scheme, measurements indicate that A-weighted sound pressure level is less than or equal to 60 dB (A) during the day and less than or equal to 50 dB (A) at night, which meets the relevant national noise limit emission standards and conforms to the second-class quality standard of the acoustic environment.

1. Introduction

Statistics released by China's ministry of ecology and environment protection show that, by February 2019, the hotline 12369 had received noise pollution accounted for 32 percent of reports. Noise has gradually become one of the biggest public hazards in recent years [1–5]. Among them, the impact of the heat pump unit on the surrounding environment is a universal environmental pollution problem that the city faces and needs to be solved [6, 7]. Effective control noise is, therefore, very urgent and necessary.

The air-cooled heat pump unit is widely used in the projects with its advantages, such as dual functions of cooling and heating, simple operation, convenient management, and maintenance [8, 9]. In order to reduce the noise of the heat pump unit and thus providing a more comfortable living environment for people, a reasonable implementation scheme should be adopted in several projects. In this paper, the acoustic environment of the heat pump unit of the square in Shanghai is taken as the main research area. First, the sound environment is tested. Then, according to the noise evaluation standards in China [10–12], a reasonable implementation scheme is developed and given to solve the noise disturbance of heat pump units in the square.

2. Methods

2.1. Project Overview. The air-cooled heat pump unit equipment (model: AEH1080E, unit weight: 6900 kg, rated refrigeration/heat: 180/179 kw, China) has a total of four units and a supporting water pump, which are located in the iron fence area beside the road in a square. The main body of the equipment is 2,300 mm away from the other side enclosing wall, and the height of the wall is 1,900 mm. The ground between the wall and the main part of the equipment is mainly paved with equipment pipelines. The heat pump unit has 40 fans at the top, the chassis is not fully closed, and

the compressor is all supported on the steel frame. The heat pump unit is surrounded by high-rise residential buildings, only 8 m from the nearest west side residence as shown in Figure 1.

The units operate 24 hours without stopping. When the equipment is in operation, the sound pressure level is high. When the noise generated by the heat pump unit exceed the emission limit of the corresponding area stipulated in the national standard "acoustic environment quality standard" (GB-3096, China), effective measures should be taken immediately to reduce the noise.

2.2. Noise Sources. From the analysis of the overall structure of the heat pump unit, the noise radiated by the equipment during operation can be divided into two parts. When the heat pump unit is running, its steel structure will have a slight vibration, and this vibration will produce noise; the other is generated by the compressor and the exhaust fan of the heat pump unit. The latter may be the main part of the noise of the heat pump unit.

According to the field investigation, the noise area emitted by the heat pump unit is very large. Because the two sides and the top of the unit emit noise outwards, the noise of the heat pump unit is open. In addition, the compressor is supported fully on the steel frame, and the noise of the heat pump unit also spreads down from the bottom.

2.3. Acoustic Measurements. In order to evaluate the acoustic quality of the square and to solve the noise disturbance of heat pump units, acoustic measurements were carried out. A hand-held analyzer type 2250 (Brüel & Kjær Sound & Vibration Measurement A/S, Nærum, Denmark) was used in this study. This sound level meter was calibrated before measurement. The noise measured values were characterized by equivalent continuous A sound pressure level (see equations (1) and (2). The time recording characteristic of the instrument was "slow" response. 100 values were read continuously. The interval of reading the instantaneous value of the measuring point was 5 seconds. In order to improve the precision, several cares were taken, such as good weather conditions. The measurement time, place, and temperature were accurately recorded. In this current study, the temperature measured was 20 to 26 degrees Celsius, and the weather was clear. In addition, the microphone diaphragm of the sound level meter should be clean during measurement. In order to reduce the influence of wind on noise measurement results, when the wind speed is greater than 3 m/s, the microphone should be timely covered with a windshield; when the wind speed is greater than 5 m/s, the measurement should be stopped immediately. During measurement, the microphone should be far away from other reflective surfaces, and the vertical distance from the ground should be greater than 1.2 m. Finally, safety should be observed during measurement to avoid obstructing the passage of vehicles and pedestrians.

When the four heat pump units are all working, the noise of the unit itself and the interior of the west residential building is measured at eleven o'clock in the day time. The measurement points and test data are shown in Tables 1 and 2, respectively.

2.4. Theoretical Model of Sound Source Attenuation. The attenuation of point sound source can be given by the following equation:

$$L_A(r) = L_A(r_0) - 20\log\left(\frac{r}{r_0}\right) - \Delta L, \tag{1}$$

where $L_A(r)$ is A-weighted sound pressure level (SPL (A)) at r distance from the sound source, in units of dB (A). $L_A(r_0)$ is the A-weighted sound pressure level at the point r_0 and $r_0 = 1$ m from the sound source, in units of dB (A). ΔL is the amount of attenuation caused by various factors, including shielding, air absorption, and ground effect, and the unit is dB (A).

In the current study, noise sources are varied. According to the superposition theorem of sound sources, the equivalent sound pressure level at any point in the sound field can be given by the following equation:

$$L_{\text{eqA}} = 10\log\left(\frac{1}{N}\sum_{i=1}^{N} 10^{(L_{Ai}/10)}\right), \tag{2}$$

where L_{eqA} is the equivalent A sound pressure level in dB (A). L_{Ai} is the ith A sound pressure level in dB (A). N is the total number of sources.

2.5. Noise Reduction Measures. For noise reduction of the air-cooled heat pump unit, we mainly design a closed noise reduction structure, that is, steel structure beams and columns are designed on the periphery of the heat pump unit, and the sound insulation plate is used to seal the air-cooled heat pump unit on three sides, forming a large sound insulation space. At the same time, the muffler is installed in the inlet and outlet of the heat pump unit to avoid secondary noise pollution.

In order to prevent the vibration of the heat pump unit and the pump from being transmitted to other places through the pipeline, we installed the vibration absorption and vibration isolation devices at the base of the heat pump unit and the inlet and outlet water pipes, respectively, and installed the vibration absorption support at the main pipeline.

3. Results and Discussion

3.1. Sound Pressure Level. Before noise modification, the measurement data of sound pressure level of the noise from heat pump units are shown in Table 1, and the measurements of equivalent sound pressure level in the west residential building with windows closed are shown in Table 2.

In Table 1, it can be found that the noise generated by the air-cooled heat pump unit during operation is about 80 dB (A), and the maximum noise value reaches 92 dB (A). The huge noise generated by the heat pump unit causes noise pollution to the adjacent floors and affects the lives of the residents.

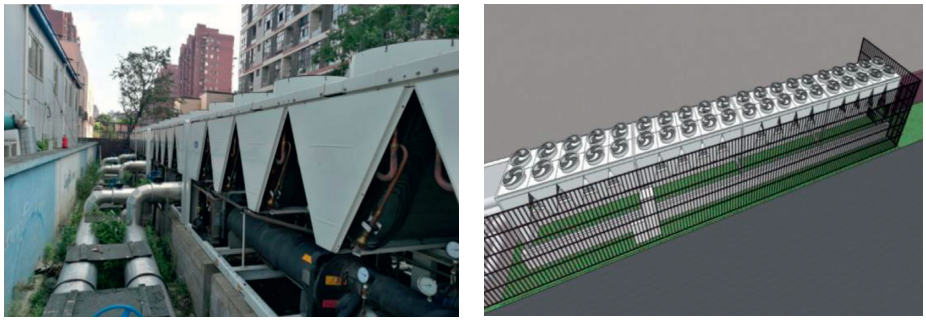

(a) (b)

Figure 1: The air-cooled heat pump unit before noise reduction treatment: (a) left, photograph; (b) right, schematic diagram.

Table 1: Sound pressure levels of the noise from heat pump units before noise modification.

Serial number	Noise source	Measuring point	Sound pressure level (dB) (A)
1	Heat pump unit	Next to the unit	89
2	Heat pump unit outlet	Beside air outlet	92
3	Water pump	Near the water pump	84
4	Heat pump unit and water pump	In front of the residential building on the south side	74
5	Heat pump unit and water pump	In front of the west side residential building	72
6	Heat pump unit outlet	West side residential building 4-5 floors outside the window	77
7	Heat pump unit outlet	South side residential building 4-5 floors outside the window	75

Table 2: Sound pressure levels in the west residential building with windows closed before noise modification.

Measuring point	Time (s)	Leq, T (dB) (A)	Frequency (Hz)						
			125	250	500	1k	2k	4k	8k
8F, room 831	37	46.3	56.2	52.3	38.8	31.9	35.6	23.8	19.3
8F, room 822	45	46.3	54.5	51.6	40.8	38.4	36.2	24	19.8
7F, room 731	51	49.1	57.4	54.7	43.6	41.7	40.2	27.3	21.5
7F, room 722	33	48.9	58.4	55.9	41.7	35.3	35.5	29.1	23.9
6F, room 622	30	50.9	49.7	48.2	39.2	36.9	36	27.3	22.5
5F, room 522	30	49.7	47.3	46	37.8	41.9	39.4	29.5	22.8

As can be seen in Table 2, the noise generated by the heat pump unit presents a mid-low frequency characteristic. Because the low-frequency noise has strong penetration, wide frequency band, slow distance attenuation, and wide influence range, the fifth and sixth floors are the areas most affected by the noise. The equivalent sound pressure levels are 49.7 dB (A) and 50.9 dB (A), respectively. To create a comfortable living environment, noise must be controlled.

3.2. Overall Noise Reduction Scheme. Generally, there are three ways to consider for noise reduction of the heat pump unit: first, sound source management. Because the unit is not easy to reform, sound source management has operational disadvantages, and it is difficult to achieve; second, the noise transmission way to control, such as sound insulation, noise reduction, and vibration reduction methods for noise control; and third, on the receiver side, the noise-sensitive people should wear earmuffs and other labor protection measures to indirectly prevent and control noise [13, 14]. In the current study, the second noise reduction method is adopted.

Considering that the noise mainly comes from the compressor and the exhaust fan during the operation of the heat pump unit, the exhaust air of the heat pump unit, and the running water pump, we use the overall sound insulation cover design for the heat pump unit, that is, the heat pump unit area is closed and isolated. In order to facilitate the ventilation and heat dissipation of the equipment, we set up an inlet and outlet air channel on the sound insulation cover and further apply a muffler in the inlet and outlet air channel for noise elimination. The schematic diagram of the sound shield for the heat pump unit is shown in Figure 2. It should be mentioned here that, in order to improve the sound insulation effect of the sound enclosure, sealing materials are

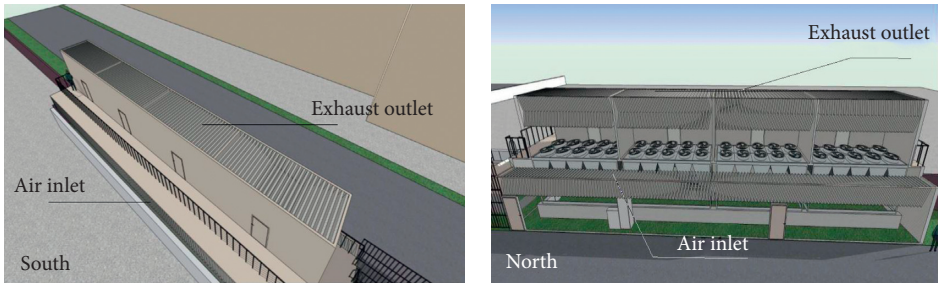

(a) (b)

Figure 2: The schematic diagram of the sound shield for the heat pump unit.

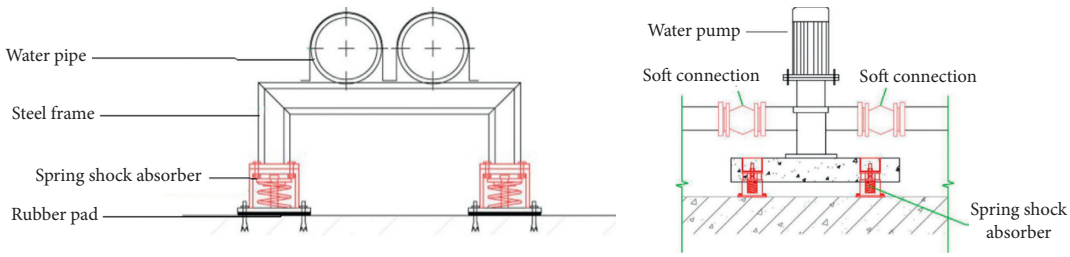

(a) (b)

Figure 3: The schematic diagram of vibration isolation of the water pipe and the water pump.

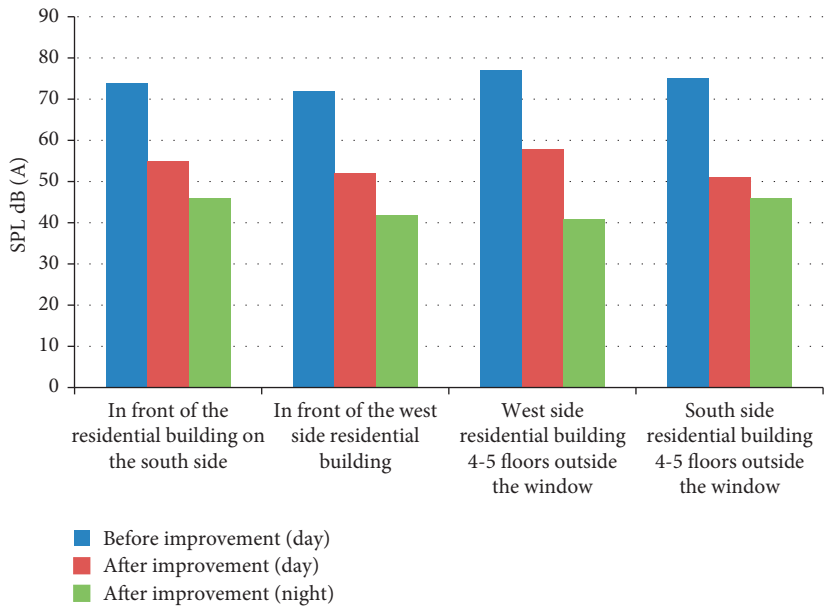

Figure 4: Sound pressure levels of the noise outside the window of the building before and after improvement.

used between the sound enclosure modules. In particular, when installing the sound insulation cover, rubber damping pad should be installed between the module and the ground to prevent rigid sound transmission.

As for the air inlet design, due to the limited space in the region, a vertical direct-insert muffler with a size of 1,500 mm * 1,000 mm is adopted for the air inlet on the south side and the north side of the unit, which is installed at a tilt of 15°, as shown in Figure 2. In this way, the labyrinth channel is formed to ensure that the heat pump unit can enter the air and achieve the best noise reduction effect. Considering the top air exhaust muffler, we use half bending muffler insert and use professional sound-absorbing wall to block the equipment exhaust outlet. In this way, after the exhaust area of each equipment is separated by the sound-absorbing wall, the exhaust air of the heat pump unit will form an independent space. The lower part of the independent space is the slow flow area of exhaust air, which is mainly used for static pressure and rectification of the exhaust

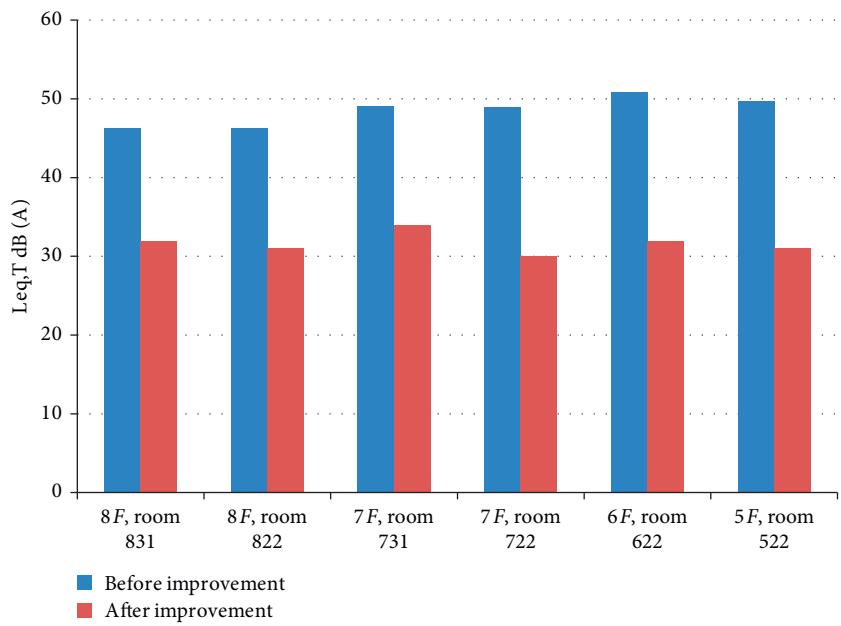

Figure 5: Sound pressure levels in the west residential building with windows closed before and after improvement.

air. The upper part is the muffler channel composed of two-sided metal perforated plate filled with environmentally friendly sound-absorbing cotton, which has dual functions of resistance muffler and reactive muffler. For the muffling of the top exhaust air, we adopt the half-folded muffler insert, which has been proved to be effective in multifrequency and wide-band muffling. The upper and lower parts constitute the exhaust muffler of the heat pump unit (noise attenuation: 24 dB (A)), which can effectively control the influence of exhaust noise on the surrounding environment.

As shown in Figure 3, in order to prevent the noise from being transmitted to other places through the pipe vibration, we install the vibration absorption and vibration isolation devices on the base of the heat pump unit and the inlet and outlet water pipes, respectively. To overcome the vibration of the heat pump unit, the concrete approach is to add a steel frame base on its side and then to install a spring shock absorber with deformation of 50 mm under the steel frame base. Meanwhile, 25 mm spring shock absorber is installed in the ground riser of the heat pump unit. The spring shock absorbers are all provided with 8 mm thick shock absorbent rubber pads. To reduce the vibration of the water pump, a spring shock absorber should be added on the side of the base of the steel frame. Soft connection is installed on both ends of the inlet and the outlet, and the concentricity should be adjusted [15, 16]. Current practice shows that these methods are very effective in reducing noise transmission.

Before and after improvement, sound pressure levels of the noise outside the window of the building are shown in Figure 4. The noise interference generated by sound superposition outside the window of the affected building is no more than 60 dB (A) during day time and no more than 50 dB (A) at night. In the west residential building, the sound pressure levels after closing the window are shown in Figure 5. It can be found that the sound pressure level is less than or equal to 35 dB (A) after noise improvement.

4. Conclusions

The noise of the air-cooled heat pump unit of a square area in Shanghai was detected, the source of the noise was analyzed, and the corresponding noise reduction scheme was proposed. Noise reduction construction was carried out with the scheme. The scheme is simple in construction and nice in design. After the completion of the scheme, the heat pump unit has smooth ventilation and heat dissipation and runs normally. Measurements indicate that the designed schemes meet the relevant national noise limit emission standards, which conform to the second-class quality standard of acoustic environment (SPL (A) ≤60 dB (A) during the day and ≤50 dB (A) at night) in China. In addition, on the premise of ensuring the noise reduction effect, the scheme can be well integrated with the environment and has a good landscape effect.

Data Availability

The data used to support the findings of this study are available from the corresponding author upon request.

Conflicts of Interest

All authors declare no conflicts of interest regarding the content and implications of this manuscript.

Acknowledgments

This work was sponsored by the Open Foundation of Anhui Province Key Laboratory of Intelligent Building & Building Energy Saving (no. IBBE2018KX04) and the National

Natural Science Foundation of China (no. 61471003). The authors are grateful for the supports of Z-X He for her contributions to the study.

References

[1] Y. De Kluizenaar, S. A. Janssen, F. J. Van Lenthe, H. M. E. Miedema, and J. P. Mackenbach, "Long-term road traffic noise exposure is associated with an increase in morning tiredness," *The Journal of the Acoustical Society of America*, vol. 126, no. 2, pp. 626–633, 2009.

[2] G. Licitra, L. Fredianelli, D. Petri, and M. A. Vigotti, "Annoyance evaluation due to overall railway noise and vibration in Pisa urban areas," *Science of The Total Environment*, vol. 568, pp. 1315–1325, 2016.

[3] G. Bluhm and C. Eriksson, "Cardiovascular effects of environmental noise: research in Sweden," *Noise and Health*, vol. 13, no. 52, pp. 212–216, 2011.

[4] T. N. Le, L. V. Straatman, J. Lea, and B. Westerberg, "Current insights in noise-induced hearing loss: a literature review of the underlying mechanism, pathophysiology, asymmetry, and management options," *Journal of Otolaryngology—Head & Neck Surgery*, vol. 46, no. 1, p. 41, 2017.

[5] P. Lercher, G. W. Evans, and M. Meis, "Ambient noise and cognitive processes among primary school children," *Environment and Behavior*, vol. 35, no. 6, pp. 725–735, 2003.

[6] C. Bai, Z. Han, H. Wei, X. Ju, X. Meng, and Q. Fu, "Simulation study on performance of a dual-source hybrid heat pump unit with alternative refrigerants," *Energy and Built Environment*, vol. 1, no. 1, pp. 1–10, 2020.

[7] M. Dongellini and G. L. Morini, "On-off cycling losses of reversible air-to-water heat pump systems as a function of the unit power modulation capacity," *Energy Conversion and Management*, vol. 196, no. 15, pp. 966–978, 2019.

[8] S. Li, G. Gong, and J. Peng, "Dynamic coupling method between air-source heat pumps and buildings in China's hot-summer/cold-winter zone," *Applied Energy*, vol. 254, no. 15, Article ID 113664, 2019.

[9] Y. Cai, D.-D. Zhang, D. Liu, F.-Y. Zhao, and H.-Q. Wang, "Air source thermoelectric heat pump for simultaneous cold air delivery and hot water supply: full modeling and performance evaluation," *Renewable Energy*, vol. 130, pp. 968–981, 2019.

[10] GB 22337, *Noise Emission from Social Life*, China Environmental Science Press, Beijing, China, 2008.

[11] GB/T 50121, *Evaluation Standard for Sound Insulation of Buildings*, China Building Industry Press, Beijing, China, 2005.

[12] GBJ 50118, *Code for Sound Insulation Design of Civil Buildings*, China Building Industry Press, Beijing, China, 2010.

[13] O. Gustafsson, C. Haglund Stignor, and J.-O. Dalenbäck, "Heat exchanger design aspects related to noise in heat pump applications," *Applied Thermal Engineering*, vol. 93, no. 25, pp. 742–749, 2016.

[14] O. Gustafsson, H. Hellgren, C. H. Stignor, M. Axell, K. Larsson, and C. Teuillieres, "Flat tube heat exchangers—direct and indirect noise levels in heat pump applications," *Applied Thermal Engineering*, vol. 66, no. 1-2, pp. 104–112, 2014.

[15] D. Yano, S. Ishikawa, K. Tanaka, and S. Kijimoto, "Vibration analysis of viscoelastic damping material attached to a cylindrical pipe by added mass and added damping," *Journal of Sound and Vibration*, vol. 454, no. 18, pp. 14–31, 2019.

[16] K. Bi and H. Hao, "Using pipe-in-pipe systems for subsea pipeline vibration control," *Engineering Structures*, vol. 109, no. 15, pp. 75–84, 2016.

Hindawi
Journal of Chemistry
Volume 2020, Article ID 7390545, 7 pages
https://doi.org/10.1155/2020/7390545

Research Article

Research on Quantitative Remote Sensing Monitoring Algorithm of Air Pollution Based on Artificial Intelligence

Yun Liu,[1] Yuqin Jing,[2] and Yinan Lu[3]

[1]*School of Information Engineering, Chaohu University, Chaohu, China*
[2]*School of Electronic Information Engineering, Chongqing Technology and Business Institute, Chongqing, China*
[3]*School of Information Engineering, Nanchang University, Nanchang, China*

Correspondence should be addressed to Yinan Lu; luyinan250@163.com

Received 1 November 2019; Accepted 30 November 2019; Published 4 March 2020

Guest Editor: Jia-Bao Liu

When the current algorithm is used for quantitative remote sensing monitoring of air pollution, it takes a long time to monitor the air pollution data, and the obtained range coefficient is small. The error between the monitoring result and the actual result is large, and the monitoring efficiency is low, the monitoring range is small, and the monitoring accuracy rate is low. An artificial intelligence-based quantitative monitoring algorithm for air pollution is proposed. The basic theory of atmospheric radiation transmission is analyzed by atmospheric radiation transfer equation, Beer–Bouguer–Lambert law, parallel plane atmospheric radiation theory, atmospheric radiation transmission model, and electromagnetic radiation transmission model. Quantitative remote sensing monitoring of air pollution provides relevant information. The simultaneous equations are constructed on the basis of multiband satellite remote sensing data through pixel information, and the aerosol turbidity of the atmosphere is calculated by the equation decomposition of the pixel information. The quantitative remote sensing monitoring of air pollution is realized according to the calculated aerosol turbidity. The experimental results show that the proposed algorithm has high monitoring efficiency, wide monitoring range, and high monitoring accuracy.

1. Introduction

With the improvement of people's material living conditions, the advancement of science and technology, and the increased consumption of energy, the air pollution and living environment are getting worse and worse [1]. As a result, the air pollution has widened the gap between people's economic living conditions and quality of life. Since the atmospheric environment monitoring technology in China started late with the problem of slow development, the quantitative remote sensing monitoring of air pollution has become a hot spot [2]. The excessive pollution incidents that happened frequently in China has gradually received people's attentions to explore air pollution monitoring technology and awareness of protecting the environment. Therefore, improving air quality and protecting the environment are the urgent demand [3].

At present, the commonly used air pollution monitoring methods including satellite remote sensing monitoring, ground-based remote sensing monitoring, and manual instrument monitoring are currently used [4]. As for the manual instrument monitoring, it has the shortcomings of cumbersome operation and small monitoring area. The ground-based remote sensing monitoring is generally applied to monitor the local range, and it is only located in some regions. With the rapid development of aerospace technology, satellite remote sensing monitoring technology, as a new type of artificial intelligence technology, has been widely adopted in quantitative remote sensing monitoring of air pollution by virtue of its good real-time performance, strong periodicity, and wide coverage [5]. Considering the defects of the quantitative remote sensing monitoring algorithm of air pollution, such as low monitoring efficiency, small monitoring range, and low monitoring accuracy, it is

necessary to study the quantitative remote sensing monitoring algorithm of air pollution.

According to the quantitative monitoring algorithm of air pollution based on geostationary satellite GOCI sensor proposed by Zhang et al., this algorithm, by combining with the theory of atmospheric aerosol change with time, the minimum fitting method, and time series iterative algorithm, mines the data of aerosol optical thickness and realizes the quantitative remote sensing monitoring of air pollution. However, in this algorithm, the monitoring time is long and there are many errors in the obtained monitoring results, so the monitoring efficiency and monitoring accuracy are low [6]. Zhang et al. proposed a quantitative remote sensing monitoring algorithm of air pollution based on MODIS data. By means of the 6S model, this algorithm calculates the radiation transmission model equation under different aerosol optical thickness conditions, obtains the original spectral band information, and then acquires the surface reflectance information through pixel method [7]. In this way, it calculates the aerosol optical thickness so as to realize the remote sensing monitoring of air pollution. But this algorithm has the weaknesses of small monitoring coefficient as well as narrow monitoring range [8].

For the sake of solving the problems existing in the abovementioned algorithms, a quantitative monitoring algorithm of pollution based on artificial intelligence is proposed.

2. Basic Theory of Atmospheric Radiation Transmission

2.1. Equation of Atmospheric Radiation Transmission. In an uneven air medium, the interaction between light will affect the radiation intensity of light propagation [8].

Let λ be the wavelength, I_λ stand for the radiation intensity, and $I_\lambda + dI_\lambda$ stand for the radiation intensity corresponding to I_λ after passing through the path in length ofds, then there is an equation as follows:

$$\mathrm{d}I_\lambda = -k_\lambda \rho \times I_\lambda \mathrm{d}s, \tag{1}$$

where k_λ represents the mass extinction cross section corresponding to the radiation wavelength λ and the transmission medium and ρ represents the density corresponding to the transmission medium. As can be learned from above formula, the radiated electromagnetic wave will increase or decrease under the influence of different concentrations of aerosol [9]. The strength can be increased through the following equation:

$$\mathrm{d}I_\lambda = j_\lambda \rho \mathrm{d}s, \tag{2}$$

where j_λ represents the source function coefficient and its physical meaning is similar to the mass extinction cross section; then, there is equation as follows:

$$\mathrm{d}I_\lambda = -k_\lambda \rho \times I_\lambda \mathrm{d}s + j_\lambda \rho \mathrm{d}s. \tag{3}$$

The above equation can be transformed into

$$\frac{dI_\lambda}{k_\lambda \rho \mathrm{d}s} = -I_\lambda + J_\lambda. \tag{4}$$

There is no particularity in the above radiation transmission equation, and all coordinate systems are available.

2.2. Beer–Bouguer–Lambert Law. Without regard to the influence of multiple scattering and emission on the radiation intensity during the research path and assume that the radiation transmission is a uniform medium, then there will be Beer–Bouguer–Lambert law [10].

Based on the Beer–Bouguer–Lambert law, the radiation transmission equation can be simplified as follows:

$$\frac{\mathrm{d}I_\lambda}{k_\lambda \rho \mathrm{d}s} = -I_\lambda. \tag{5}$$

If the intensity $I_\lambda(0)$ is incident on $s = 0$, the corresponding scattering intensity at s_1 can be obtained via the integration of above equation:

$$I_\lambda(s_1) = I_\lambda(0)\exp\left(-\int_0^{s_1} k_\lambda \rho \mathrm{d}s\right). \tag{6}$$

Assume k_λ does not depend on the distance s; that is, the medium extinction cross section is uniform and constant; let u stand for the path length; then, the equation is as follows:

$$u = \int_0^{s_1} \rho \mathrm{d}s. \tag{7}$$

Then, there is the following equation:

$$I_\lambda(s_1) = I_\lambda(0)\exp(-k_\lambda u). \tag{8}$$

Let τ_λ be the dielectric thickness of the medium existing betweens_1 and s_2; then, its equation is as follows:

$$\tau_\lambda = -\int_{s_1}^{s_2} k_\lambda \rho \mathrm{d}s'. \tag{9}$$

2.3. Parallel Plane Atmospheric Radiation Theory. If the medium is divided, an infinite or several mutually parallel planes can be obtained, the light propagation planes are parallel, the internal properties of the layers in the plane are uniform, and the layers have different properties in the plane [11]. Let z represent the linear distance corresponding to the vertical layered plane; then, the expression of the atmospheric radiation transmission equation without considering the monochromatic light wavelength variable is as follows:

$$\cos\theta \frac{\mathrm{d}I(z,\theta,\phi)}{k\rho \mathrm{d}z} = -I(z,\theta,\phi) + J(z,\theta,\phi), \tag{10}$$

where θ describes the angle of inclination with the upward perpendicular and ϕ describes the azimuth.

Let τ describe the vertical extinction thickness measured from the upper boundary of the atmosphere to the plane parallel atmosphere. When the entire extinction degree of the atmosphere can be expressed by τ, τ becomes the optical thickness corresponding to the atmosphere. The equation is as follows:

$$\tau(z) = \int_z^{\infty} k\rho \mathrm{d}z'. \tag{11}$$

In combination of equations (4) and (11), then

$$\mu \frac{\mathrm{d}I(\tau,\theta,\phi)}{\mathrm{d}\tau} = I(\tau,\theta,\phi) - J(\tau,\theta,\phi), \quad \mu = \cos\theta. \tag{12}$$

Without considering the infrared heat radiation problem, the scattering expression existing in the source function is the sum of multiple scattering and single scattering of solar radiation [12], and its calculation equation is as follows:

$$J(\tau,\Omega) = \frac{\omega}{4\pi} F_0 e^{-e/\mu_0} p(\Omega,\Omega_0) + \frac{\omega}{4\pi}\int_{4\pi} I(\tau,\Omega') p(\Omega,\Omega') \mathrm{d}\Omega', \tag{13}$$

where the first item on the right describes the contribution of the single scattering of direct solar radiation in the direction $\Omega(\theta,\phi)$, the second item describes the contribution of the multiple scattering of the atmosphere, ω represents the reflection of the single scattering rate, F_0 represents the solar constant, p represents the scattering phase function, and μ_0 represents the cosine corresponding to the solar zenith angle.

By expanding the radiation transmission equation, the following formula is obtained:

$$\mu \frac{\mathrm{d}I(\tau,\theta,\phi)}{\mathrm{d}\tau} = I(z,\theta,\phi) - \frac{\omega}{4\pi} F_0 e^{-e/\mu_0} p(\Omega,\Omega_0) - \frac{\omega}{4\pi}\int_{4\pi} I(\tau,\Omega') p(\Omega,\Omega') \mathrm{d}\Omega. \tag{14}$$

2.4. Atmospheric Radiation Transmission Model. The positive and negative changes in solar radiant energy during atmospheric transmission can be expressed by processes such as atmospheric emission, absorption, and scattering [9]. The above processes usually produce a continuous spectrum, which is widely used in atmospheric environment monitoring based on the ability to avoid large quantitative errors appearing in the spectral inversion.

The expression formula of the 6S atmospheric transmission model is as follows:

$$\rho_T(\theta_s,\theta_v) = T_g(\theta_s,\theta_v)\left[\rho_{R+a} + T(\theta_s)T(\theta_v)\frac{\rho_s}{1 - s\rho_s}\right], \tag{15}$$

wherein ρ_T represents the total reflectivity corresponding to atmospheric transmission; $T_g(\theta_s,\theta_v)$ represents the transmittance, which is formed by atmospheric absorption; ρ_{R+a} describes the reflectance of the radiation path formed by aerosol particles and molecular scattering; $T(\theta_s)$ represents the straight transmittance of the ground target and the solar path; $T(\theta_v)$ represents the linear transmittance of the sensor and the ground target path; s represents the atmospheric hemispheric albedo; and ρ_s represents the surface diffuse reflectance.

2.5. Electromagnetic Radiation Transmission Model. The complex process formed by the interaction between different media and electromagnetic waves is electromagnetic radiation transmission [13]. Solar radiations, such as radiation from the atmosphere and radiation from the ground, belong to the electromagnetic radiation received by the satellite sensor.

The radiance corresponding to the ground target recorded by a remote sensor is affected by the atmosphere. The scattering and absorption of the atmosphere will attenuate the electromagnetic radiation energy, while the path radiation of radiator can increase the electromagnetic radiation energy. Radiation transmission model generally describes the basic equation of electromagnetic radiation during atmospheric transmission. During atmospheric radiation transmission, the positive and negative changes in electromagnetic radiation energy can be expressed by the equation as follows.

(1) Atmospheric attenuation:

$$\Delta I = -\rho \times k \times I \times \mathrm{d}s, \tag{16}$$

where I describes the emission energy and reflected energy corresponding to the ground object, that is, the incident brightness; ΔI describes the amount of energy change; ρ describes the density corresponding to the scattering material or the absorbing material; k is the sum of scattering coefficient and absorption coefficient, that is, the extinction coefficient; and ds describes the length of the optical path.

(2) Atmospheric heat radiation:

$$\Delta I = \rho \times J \times \mathrm{d}s = \rho^2 \times B(T) \times \mathrm{d}s, \tag{17}$$

where ρ describes the density corresponding to the absorbing material, J describes the emission coefficient, T is the thermodynamic temperature corresponding to the atmosphere, and B is the Planck function.

(3) Atmospheric path radiation, which is equal to sky radiation:

$$\Delta I = \omega_0 \frac{K}{4\pi}\rho^2 \times \mathrm{d}s \int_0^{4\pi} P(\Omega,\Omega') \times I(\Omega') \times \mathrm{d}\Omega' - \rho \times k \times I, \tag{18}$$

where ω_0 describes a single scattering albedo, P describes the scattering phase function of the scattering field angle distribution, and Ω describes the solid angle corresponding to the incident direction.

The influence of atmosphere on electromagnetic radiation includes refraction, absorption, reflection, and scattering. Due to the atmospheric influence, there is absorption effect existing in some bands of electromagnetic waves when the solar radiation passes through the atmosphere. Then, the

radiation energy, which is affected by the absorption, will become the internal energy of the molecules, thereby causing the attenuation of solar radiation intensity in these bands.

Let E_0 represent the solar irradiance; the irradiance after atmospheric attenuation and by passing through the atmosphere path x is E^*, and the formula is as follows:

$$E^* = E_0 e^{-kx}, \tag{19}$$

where k describes the extinction coefficient, that is, the attenuation coefficient and kx describes the optical thickness.

The electromagnetic wavelength and the atmospheric state determine the value of atmospheric attenuation. Let L represent the total radiance obtained by the airborne remote sensor. The formula is as follows:

$$L = L_G \tau + L_P, \tag{20}$$

where τ represents the atmospheric transmittance, L_P represents the path radiation corresponding to the atmosphere, and L_G represents the brightness corresponding to ground target after atmospheric attenuation; the calculation formula is as follows:

$$L_G = \frac{E\rho}{\pi}, \tag{21}$$

where E represents the irradiance corresponding to the ground target. On the basis of equation (21), the following formula is obtained:

$$L_G = \frac{E\rho}{\pi} + L_P, \tag{22}$$

where parameter E is related to atmospheric thickness and weather conditions; its calculation formula is as follows:

$$E = \frac{E_0}{D^2} \times \cos(\theta) \times \tau, \tag{23}$$

where D represents the solar-ratio distance, which usually refers to the daily average distance; E_0 represents the solar constant; and E_0 represents the corresponding transmittance of the atmosphere.

3. Quantitative Remote Sensing Monitoring Algorithm of Air Pollution

In the near-infrared and visible-light bands, the pixel spectrum of satellite data includes two parts: surface reflected light and sky scattered light. Let I represent the reflection spectrum received by the sensor; then, the expression formula is as follows:

$$I = [I_0 (T_a T_m T_b)^u + I_m + I_{bd} + I_{ad}] R_g T_a T_m T_b + I_a + I_m + I_b, \tag{24}$$

where I_0 represents the incident light intensity, T_a represents the transmittance corresponding to anthropogenic aerosol, T_m describes the transmittance of the atmospheric molecules, T_b represents the transmittance of the background aerosol, I_m represents the upward scattered light intensity of the atmospheric molecules, I_{bd} represents the downward scattered light intensity corresponding to the background aerosol, I_{ad} represents the downward scattered light intensity corresponding to the anthropogenic aerosol, R_g represents the ground reflectivity, and I_a represents the upward scattered light intensity corresponding to the anthropogenic aerosol.

Based on dividing by I_0 with the two sides of above equation, the following formula can be obtained:

$$R_g = \frac{R - \omega_a - \omega_m - \omega_b}{[I_0 (T_a T_m T_b)^u + \omega_m + \omega_{bd} + \omega_{ad}] T_a T_m T_b}, \tag{25}$$

where R represents the pixel comprehensive reflectivity, ω_a represents the upward scattering rate corresponding to the anthropogenic aerosol, ω_b represents the upward scattering rate of the background aerosol, ω_m represents the upward scattering rate of the atmospheric molecule, ω_{bd} represents the downward scattering rate corresponding to the background aerosol, and ω_{ad} represents the downward scattering rate corresponding to the anthropogenic aerosol.

It can be deemed that the background aerosol is horizontally uniform within a scale of tens of miles, and the factors of season and geographical location will affect the type of background aerosol [14–17]. Based on the above analysis, the function of aerosol turbidity $\beta_1 + \beta_2$ and β_3, as well as the pixel comprehensive reflectivity R and the ground reflectivity, is obtained:

$$R_g(R, \beta_1 + \beta_2, \beta_3) = \frac{R - \omega_a - \omega_m - \omega_b}{[[I_0 (T_a T_m T_b)^u + \omega_m + \omega_{bd} + \omega_{ad}] T_a T_m T_b]}. \tag{26}$$

When the single leaf reflectance, water absorption rate, dry soil reflectance parameters, the direction of observation, and the direction of incidence are known, the pixel reflectance is a function of soil water content V_{ws}, vegetation leaf area index L, and wavelength. The expression formula is as follows:

$$R_g(\lambda, V_{ws}, L) = R_p(\lambda, L) + R_s'(\lambda, V_{ws}, L). \tag{27}$$

According to formula (27), the equation below is obtained:

$$R_g(\lambda, V_{ws}, L) = R_g(R, \beta_1 + \beta_2, \beta_3). \tag{28}$$

By introducing the remote sensing data into the following equation, the only solution obtained is the aerosol turbidity:

$$\begin{cases} R_g(\lambda_1, \beta_{1+2}, \beta_3) = R_g(R_1, V_{ws}, L), \\ R_g(\lambda_2, \beta_{1+2}, \beta_3) = R_g(R_2, V_{ws}, L), \\ R_g(\lambda_3, \beta_{1+2}, \beta_3) = R_g(R_3, V_{ws}, L), \\ R_g(\lambda_4, \beta_{1+2}, \beta_3) = R_g(R_4, V_{ws}, L). \end{cases} \tag{29}$$

The quantitative remote sensing monitoring of air pollution can be realized through the aerosol turbidity.

4. Experiment and Analysis

In order to verify the overall effectiveness of the artificial intelligence-based quantitative remote sensing monitoring

Table 1: Monitoring time of three different algorithms.

DD	JC		
	RG	JZ	SJ
1	0.2	0.6	1.1
2	0.3	0.8	1.0
3	0.2	0.7	1.2
4	0.4	0.7	1.3
5	0.3	0.8	1.3
PJ	0.28	0.72	1.18

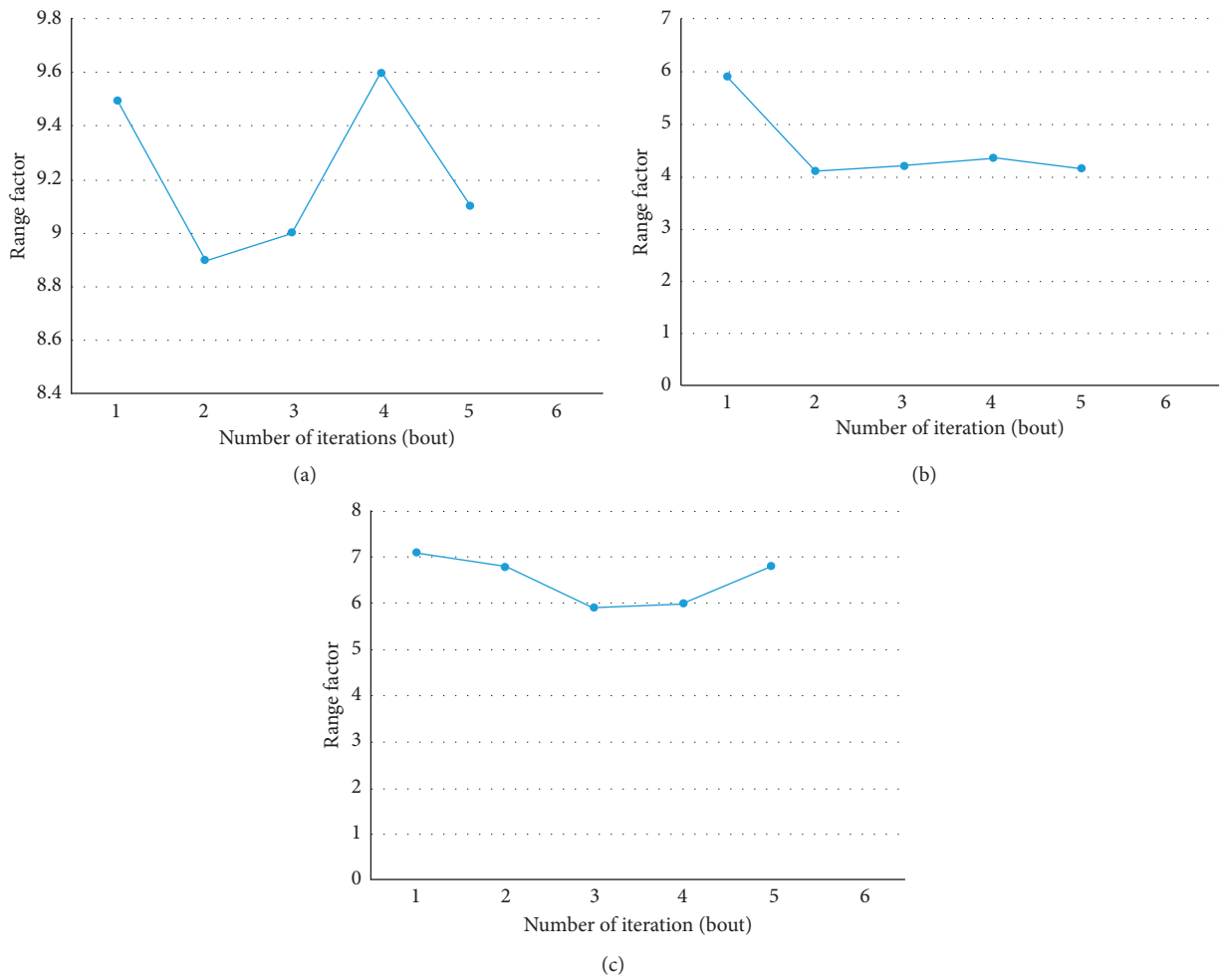

Figure 1: Range coefficient of (a) proposed algorithm, (b) algorithm based on geostationary satellite GOCI sensor, and (c) algorithm based on MODIS data.

algorithm of air pollution, a test is completed in the Linux platform. The monitoring times of three different algorithms of artificial intelligence-based quantitative remote sensing monitoring algorithm of air pollution, the geostationary satellite GOCI sensor-based quantitative remote sensing monitoring algorithm of air pollution, and MODIS data-based quantitative remote sensing monitoring algorithm of air pollution are compared. The test results are shown in Table 1.

In Table 1, DD represents the number of iterations of three different algorithms; JC represents the monitoring time of three algorithms, and the unit is s; RG represents the quantitative remote sensing monitoring algorithm of air pollution based on artificial intelligence; JZ represents the quantitative monitoring algorithm of air pollution based on geostationary satellite GOCI sensor; and SJ represents the quantitative remote sensing monitoring algorithm of air pollution based on MODIS data.

Analysis of the data in Table 1 shows that, in five iterations, the average monitoring time of the quantitative remote sensing monitoring algorithm of air pollution based on artificial intelligence is 0.28 s; the quantitative monitoring algorithm of air pollution based on geostationary satellite GOCI sensor is 0.72 s; and the quantitative remote sensing monitoring algorithm of air pollution based on MODIS data

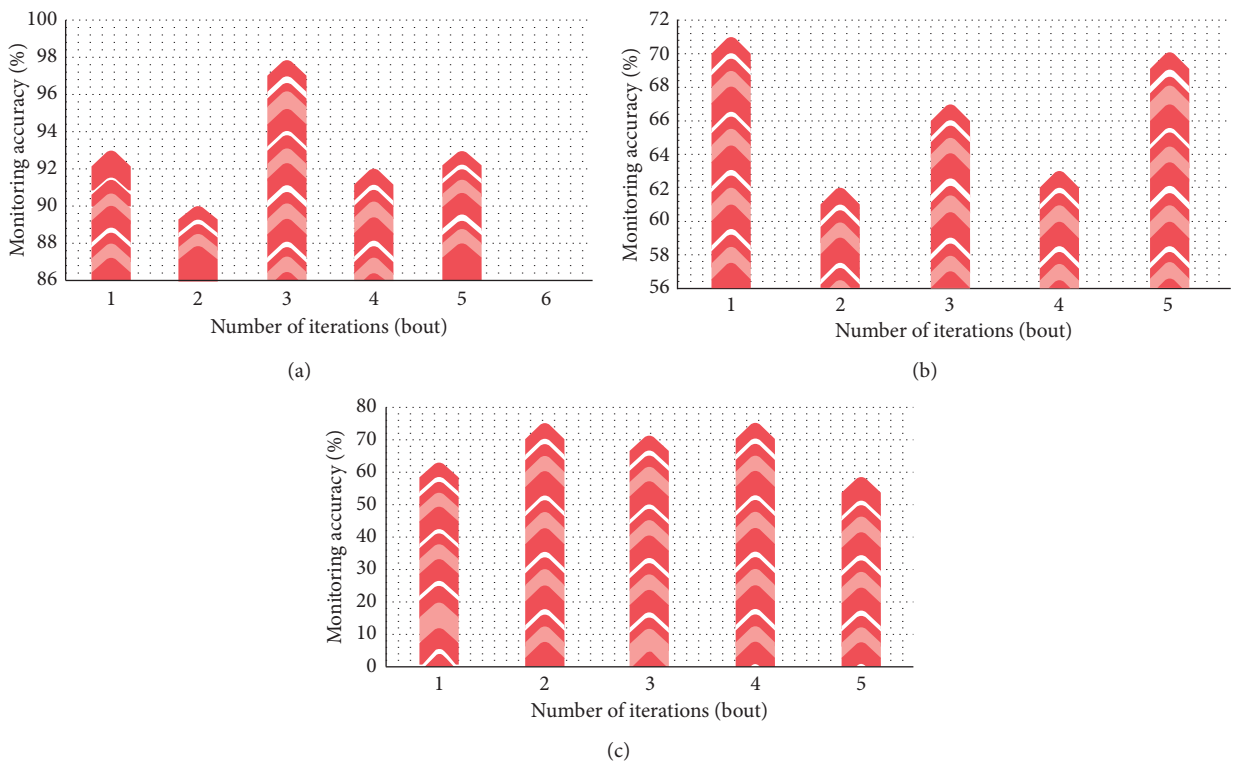

Figure 2: Monitoring accuracy of (a) proposed algorithm, (b) algorithm based on geostationary satellite GOCI, and (c) algorithm based on MODIS data.

is 1.18 s. According to the comparison of the test results of three different algorithms, the quantitative remote sensing monitoring algorithm of air pollution based on artificial intelligence uses the shorted monitoring time. This is because the characteristics of atmospheric radiation transmission, Beer–Bouguer–Lambert law, parallel plane atmospheric radiation theory, and electromagnetic radiation transmission characteristics are analyzed before the quantitative monitoring, which have provided relevant information for quantitative remote sensing monitoring of air pollution, reduced the monitoring time, and improved the monitoring efficiency of quantitative remote sensing monitoring algorithm of air pollution based on artificial intelligence.

Let δ represent the range coefficient that takes value in the interval [0, 10]. The larger the range coefficient, the larger the monitoring range of the algorithm. Based on taking range coefficient δ as a test index, the quantitative remote sensing monitoring algorithm of air pollution based on artificial intelligence, the quantitative monitoring algorithm of air pollution based on geostationary satellite GOCI sensor, and the quantitative remote sensing monitoring algorithm of air pollution based on MODIS data is tested. The results of comparing the monitoring scope of three algorithms are shown below.

Figure 1(a) is the test result of the quantitative remote sensing monitoring algorithm of air pollution based on artificial intelligence, which shows that the range coefficient of the quantitative remote sensing monitoring algorithm of air pollution based on artificial intelligence is above 8; Figure 1(b) is the test result of the quantitative monitoring algorithm of air pollution based on geostationary satellite GOCI sensor; Figure 1(c) is the test result of the quantitative remote sensing monitoring algorithm of air pollution based on MODIS data. The analysis of Figures 1(b) and 1(c) found that the range coefficients of the quantitative monitoring algorithm of air pollution based on geostationary satellite GOCI sensor and the quantitative remote sensing monitoring algorithm of air pollution based on MODIS data fluctuate around 5 and 7, respectively. As can be observed from comparing the results of the above algorithms, the range coefficient of the quantitative remote sensing monitoring algorithm of air pollution based on artificial intelligence is higher. Since the higher the range coefficient, the wider the monitoring range of the algorithm, and the monitoring range of the quantitative remote sensing monitoring algorithm of air pollution based on artificial intelligence is wider.

The quantitative remote sensing monitoring algorithm of air pollution based on artificial intelligence, the quantitative monitoring algorithm of air pollution based on geostationary satellite GOCI sensor, and the quantitative remote sensing monitoring algorithm of air pollution based on MODIS data are tested and compared in the monitoring accuracy. The results are shown below.

It can be seen from Figure 2 that, in multiple iterations, the monitoring accuracy of the quantitative remote sensing monitoring algorithm of air pollution based on artificial intelligence is higher than that of the quantitative monitoring algorithm of air pollution based on geostationary satellite GOCI sensor and the quantitative remote sensing

monitoring algorithm of air pollution based on MODIS data. This is because the quantitative remote sensing monitoring algorithm of air pollution based on artificial intelligence constructs the pixel element combination simultaneous equation, which helps calculate the atmospheric aerosol turbidity and then realize the quantitative remote sensing monitoring of air pollution through the calculated aerosol turbidity. Therefore, this improved the monitoring accuracy of the quantitative remote sensing monitoring algorithm of air pollution based on artificial intelligence.

5. Conclusions

The rapid urbanization over the past years has increased energy consumption, worsened the air quality, and seriously threatened people's physical and mental health. Therefore, how to enhance air quality and protect the environment in fierce competition and development has become the main problem faced by the society. Urban environment is the result of urban construction and industrial production, and the urban air environment is receiving more attention since discovering its dangers. The premise of environmental governance and protection is environmental testing. However, the monitoring cost and station distribution will affect the routine monitoring of air pollution, making it difficult to obtain long-term and large-scale air pollution information. On this consideration, the sensing data have been widely used in the field of air pollution monitoring because it is economical and macroscopic.

At present, the quantitative remote sensing monitoring algorithm of air pollution has the shortcomings of low monitoring efficiency, small monitoring range, and low monitoring accuracy. The proposed quantitative remote sensing monitoring algorithm based on artificial intelligence is proposed and can accurately detect a wide range of air pollution data within a short time, which has solved the problems existing in the current algorithm and laid a foundation for the development of quantitative remote sensing monitoring technology of air pollution.

Data Availability

We use simulation data, and our model and related hyperparameters are provided in our paper.

Conflicts of Interest

The authors declare that they have no conflicts of interest.

Acknowledgments

This work was supported by the Key Research Project of Natural Science in Anhui Province (KJ2019 A0681).

References

[1] W. Q. Liu, Z. Y. Chen, and J. G. Liu, "Air pollution optical remote sensing technology and development tendency," *Environmental Monitoring in China*, vol. 34, no. 2, pp. 1–9, 2018.

[2] Z. Yu, S. D. Liu, and Y. W. Wang, "Observation and analysis of variation characteristics of air pollutant concentration in urban area of Hangzhou city in 2014," *Science Technology and Engineering*, vol. 16, no. 16, pp. 95–104, 2016.

[3] N. Wang, T. R. He, and J. P. Liu, "Analysis on effect of summer precipitation in removing atmospheric pollutants in chongqing urban area," *Environmental Engineering*, vol. 35, no. 4, pp. 69–73, 2017.

[4] X. X. Zhang, Z. B. Yuan, and J. Y. Zhen, "Establishment of uncertainty evaluation method system for air pollutant monitoring data and analysis of its impact on PMF source analysis," *Acta Scientiae Circumstantiate*, vol. 39, no. 1, pp. 97–106, 2019.

[5] A. X. Cao, M. Ao, and L. C. Liang, "Mercury content in natural stone moss and biological indications of air pollution," *Environmental Chemistry*, vol. 35, no. 10, pp. 2204–2210, 2016.

[6] Y. H. Zhang, H. Q. Mao, and Q. Li, "Air pollution process AOD monitoring based on geostationary satellite GOCI sensor," *China Environmental Science*, vol. 38, no. 10, pp. 49–55, 2018.

[7] Z. H. Zhang, B. Mu, and H. You, "Application of PM2.5 retrieval in air pollution monitoring with MODIS data," *Science of Surveying and Mapping*, vol. 41, no. 9, pp. 42–46, 2016.

[8] F. Wang, Y. L. Han, and Y. Zhao, "Study on law of multi-time scale change of atmospheric particles PM10 and PM2.5 in Taiyuan city," *Ecology and Environment*, vol. 26, no. 9, pp. 1521–1528, 2017.

[9] F. Li, X. Tang, and Z. F. Wang, "Representative error estimation of ground observation of atmospheric pollutant concentration based on Beijing-Tianjin-Hebei high density ground observation network," *Chinese Journal of Atmospheric Sciences*, vol. 43, no. 2, pp. 277–284, 2019.

[10] L. Wang, B. L. Zi Bi, Y. Si Ma, and S. T. Yang, "Analysis of air pollution status in major cities in northern Xinjiang," *Journal of Arid Land Resources and Environment*, vol. 32, no. 6, pp. 182–186, 2018.

[11] M. H. Wang, W. C. Fu, and Z. P. Zhu, "Analysis of atmospheric visibility change characteristics in hangzhou from 1957 to 2016," *Journal of Sichuan Agricultural University*, vol. 35, no. 3, pp. 396–400, 2017.

[12] Z. M. Guo, Y. Liu, and X. F. Gao, "Absence from school in smog weather and analysis of influencing factors in chengdu primary school students," *Chinese Journal of School Health*, vol. 39, no. 11, pp. 84–87, 2018.

[13] Y. S. Lu, Y. X. Li, and B. Liu, "Hyper-spectral remote sensing smog monitoring based on deep residual network," *Acta Optical Sinica*, vol. 37, no. 11, pp. 314–324, 2017.

[14] J. B. Liu, J. Zhao, and Z. X. Zhu, "On the number of spanning trees and normalized Laplacian of linear octagonal-quadrilateral networks," *International Journal of Quantum Chemistry*, vol. 119, no. 17, Article ID e25971, 2019.

[15] J.-B. Liu, J. Zhao, and Z.-Q. Cai, "On the generalized adjacency, Laplacian and signless Laplacian spectra of the weighted edge corona networks," *Physica A: Statistical Mechanics and Its Applications*, vol. 540, p. 123073, 2020.

[16] J.-B. Liu, J. Zhao, H. He, and Z. Shao, "Valency-based topological descriptors and structural property of the generalized sierpiński networks," *Journal of Statistical Physics*, vol. 177, no. 6, pp. 1131–1147, 2019.

[17] J. L. Gu, H. S. Tang, and M. Liu, "Correlation analysis between mass concentration of atmospheric pollutants and aerosol optical thickness in Dalian," *Scientia Geographical Sonica*, vol. 39, no. 3, pp. 516–523, 2019.

Hindawi
Journal of Chemistry
Volume 2020, Article ID 7472954, 8 pages
https://doi.org/10.1155/2020/7472954

Research Article

Prediction of Chemical Gas Emissions Based on Ecological Environment

Guobin Chen[1] and Shijin Li[2]

[1]*Chongqing Key Laboratory of Spatial Data Mining and Big Data Integration for Ecology and Environment, Rongzhi College of Chongqing Technology and Business University, Chongqing 401320, China*
[2]*Academic Affairs Office, Yunnan University of Finance and Economics, Kunming, Yunnan 650221, China*

Correspondence should be addressed to Shijin Li; lee_shijin@sina.com

Received 23 October 2019; Accepted 6 December 2019; Published 4 March 2020

Guest Editor: Jia-Bao Liu

With the serious pollution of the ecological environment, there are a large number of harmful gases in the chemical gases emitted by the industry. Relevant intelligent chemical algorithms control the emission of chemical gases, which can effectively reduce emissions and predict emissions more accurately. This paper proposes a gray wolf optimization algorithm based on chaotic search strategy combined with extreme learning machine to predict chemical emission gases, taking a 330 MW pulverized coal-fired boiler as a test object and establishing chemical emissions of CNGWO-ELM. The prediction model, by using the relevant data collected by DCS as training samples and test samples, trains and tests the model. Simulation experiments show that the chemical emission prediction model of CNGWO-ELM has better accuracy and stronger generalization ability, with higher practical value.

1. Introduction

In recent years, with the release of chemical gases, environmental pollution problems have become increasingly serious [1, 2]. In order to effectively control environmental pollution, it is necessary to monitor the degree of environmental pollution in a timely manner and analyze the composition of environmental pollutants in order to better solve environmental pollution problems. More and more experts and scholars have found that analytical chemistry is an important way to effectively monitor the environment and is of great significance to environmental protection.

With the continuous advancement of industrialization, the dependence of economic and social development on energy will be further increased. Strengthening the alternative strategic research on fossil energy such as coal, oil, and natural gas is a necessary measure to solve energy supply shortage and promote economic development and environmental friendliness. Among the chemical emissions emitted from the ecological environment, circulating fluidized bed (CFB) combustion is one of the main coal combustion methods in China. It has the advantages of wide fuel application range, good load regulation performance, low pollutant discharge, and easy utilization of ash [2–4]. The combination of CFB combustion mode and ultra-supercritical parameter technology will be the inevitable development direction of CFB boilers in the future. The original NO_X emission concentration of conventional CFB boilers is between 100 and 300 mg/Nm^3 [5, 6], which cannot meet the national standard limit of NO_X emission concentration below 100 mg/Nm^3, and the NO_X emission concentration in some areas is lower than 50 mg/Nm^3. The ultralow emission standards, CFB boilers face the problem of having to further reduce NO_x emissions.

Many scholars at home and abroad have devoted themselves to the study of optimizing combustion conditions to control NO_x formation. Rajan and Wen [7] first established a comprehensive model of fluidized bed coal combustion chamber (FBC) simulation. The model can predict combustion efficiency, particle size distribution of coke and limestone, slag discharge rate of bed material, bed temperature change, and the distribution of SO_2, NO_x, O_2, CO, CO_2, and volatile matter along the furnace height. The factors influencing NO_x emission from the CFB boiler are

combustion temperature and uniformity, excess air coefficient, staged combustion, and so on [8, 9]. In addition, the study of deep reduction of NO_x in the CFB boiler with the selective noncatalytic reduction (SNCR) technology as the mainstream is also affected by reductant type, reaction temperature, ammonia-nitrogen ratio, and other factors [10–12]. Edelman et al. added the dynamic mathematical model of a steam-water system to the overall mathematical model of a circulating fluidized bed boiler on the basis of the Wei model [13] and Muir model [14]. The dynamic models of combustion chamber temperature, heat transfer rate of heat exchanger, and oxygen content in flue gas in circulating fluidized bed (CFB) were established, and the dynamic predictions were made.

The structure of this paper is as follows. Firstly, the basic algorithm of CWO is explained and a chaotic nonlinear grey wolf optimization algorithm is proposed. Secondly, an ELM optimization model is proposed. Finally, the CNGWO-ELM algorithm proposed in this paper is tested to achieve the prediction effect and the relevant evaluation indicators are given.

2. Standard Gray Wolf Optimization Algorithm

The grey wolf optimization algorithm (GWO) is a group intelligence algorithm proposed by Mirjalili et al. in 2014 for the inspired grey wolf predation behavior [15]. The gray wolf group has a 4-layer hierarchical mechanism of α, β, δ, and ω. Among them, α wolf is the leader with the best fitness in the grey wolf group; β and δ are the two individuals with the second best fitness, and their task is to assist the α wolf in the management and hunting of the wolves; ω is the remaining common wolves. The predation process is described as follows: first, the α wolf leads the gray wolf group to search, track, and approach the prey; then, the β and δ wolves attack the prey under the command of the wolf and summon the ordinary wolf to attack the prey until the prey is captured. The GWO algorithm completes the predation behavior by simulating predation behaviors such as gray wolf enveloping, hunt, and attack, thus achieving a global optimization process.

Assume that, in the dimensional space, the gray wolf group $\{X_i, i = 1, 2, \ldots, N\}$ consists of N gray wolves. The GWO algorithm is described as follows.

Surrounding stage: after the wolves determine the position of the prey, they first surround the prey. The mathematical description is as follows:

$$\begin{aligned} D &= \left|C \cdot X_p(t) - X(t)\right|, \\ X(t+1) &= X_p(t) - A \cdot D, \end{aligned} \tag{1}$$

where D is the distance between the grey wolf and the prey, $X_p(t)$ is the position of the prey after the t-th iteration (current optimal solution), $X(t)$ is the position of the grey wolf after the t-th iteration (feasible solution), and A and C are coefficient factors, defined as follows:

$$\begin{cases} A = 2a \times r_1 - a, \\ C = 2 \times r_2, \end{cases} \tag{2}$$

where r_1 and r_2 are random numbers in $[0, 1]$ and a is a convergence factor, which decreases linearly from 2 to 0 as the number of iterations increases.

Hunting phase: after the encirclement phase is completed, a wolf leads β and δ wolves to hunt down the prey. During the hunt, the individual positions of the wolves move as the prey escapes:

$$\begin{cases} X_1 = X_\alpha - A_1\left|C_1 X_\alpha(t) - X(t)\right|, \\ X_2 = X_\beta - A_2\left|C_2 X_\beta(t) - X(t)\right|, \\ X_3 = X_\delta - A_3\left|C_3 X_\delta(t) - X(t)\right|, \end{cases} \tag{3}$$

where X_α, X_β, and X_δ represent the current position of α, β, and δ wolves, $X(t)$ represents the current gray wolf position, and C_1, C_2, and C_3 are random vectors.

Update the location of ω wolf as follows:

$$X(t+1) = \frac{X_1 + X_2 + X_3}{3}. \tag{4}$$

2.1. Chaotic Nonlinear Grey Wolf Optimization Algorithm. The literature [16] pointed out that the optimization process of the GWO algorithm is essentially dominated by three optimal solutions, α, β, and δ wolves, which easily cause the algorithm to prematurely converge and fall into local optimum. Chaos is a kind of nonlinear linearity with phase space ergodicity and inherent randomness. Combining chaotic variables for optimal search can effectively jump out of local optimum and achieve global optimization. The literature [17] pointed out that Kent chaotic maps have better performance than logistic chaotic maps. Therefore, the introduction of Kent chaos optimization strategy in the basic GWO algorithm to optimize the solution that falls into the local optimum will effectively help the algorithm find a better solution. In addition, the introduction of nonlinear dynamic weighting strategy in the GWO algorithm will effectively balance the development and exploration capabilities of the algorithm and further improve the global optimization performance of the GWO algorithm.

2.1.1. Kent Chaotic Search Strategy. The Kent chaotic map model is described as follows:

$$Z^{t+1} = \begin{cases} \dfrac{Z^t}{a}, & 0 < Z^t \le a, \\ \dfrac{1 - Z^t}{1 - a}, & a < Z^t < 1, \end{cases} \tag{5}$$

where the control parameter $a \in (0, 1)$ and the Lyapunov exponent of the Kent map is greater than 0 which is in a chaotic state. In this paper, the probability density function obeys a uniform distribution in (0, 1), that is, $\rho(Z) = 1$. The Lyapunov exponent can be used to characterize the divergence ratio of the initial state of small uncertainty. The Lyapunov exponent of Kent chaos is 0.696, which is greater than the classical logistic of 0.693.

In the chaotic search process, the ergodicity of the chaotic motion is used to generate the chaotic series based on the solution of the current search stagnation. The optimal solution in the sequence is taken as the global optimal solution, which makes it jump out of the local optimum. In the GWO algorithm, it is assumed that the solution does not improve significantly after continuous limit iterative search, indicating that the solution falls into local optimum, so Kent is used to optimize chaos. Chaos optimization is performed on α, β, and δ wolves of the GWO algorithm. The solution space of the optimization problem is $[X_{\min}, X_{\max}]$. The Kent chaos optimization steps are as follows:

Step 1: use equation (3) X_α, X_β, and X_δ to map into the domain $[0, 1]$ of the Kent:

$$Z^0 = \frac{X_\alpha - X_{\min}}{X_{\max} - X_{\min}}. \tag{6}$$

Step 2: generate chaotic sequences. Iteratively generate $C_{\max}$ chaotic variable sequences by Kent equation $Z_k\,(k = 1, 2, \ldots, C_{\max})$.

Step 3: using the carrier operation, Z_k is first amplified and then loaded onto the gray wolf individual X_α, X_β, and X_δ to be searched so that the new gray wolf individual position U_k in the field of the original solution space after the chaotic operator operation is obtained from formula (7), where $k = 1, 2, \ldots, C_{\max}$:

$$U_k = X_{\alpha,\beta,\delta} + \frac{X_{\max} - X_{\min}}{2} \times (2Z_k - 1). \tag{7}$$

Step 4: calculate the fitness value $f(U_k)$ of U_k and compare it with the fitness value $f(X)$ of X to retain the best solution.

2.1.2. Nonlinear Dynamic Weights. For the GWO algorithm, global exploration capabilities mean detecting a wider range of search areas, while local development emphasizes the use of existing information to perform detailed searches on certain areas of the group. There is no doubt that how the GWO algorithm seeks the balance between global exploration and local development is the key to ensuring the global search performance of the algorithm. In the GWO algorithm, A adjusts the balance between global exploration and local development. From equation (6), it can be found that the value of A changes with the change of control parameter α. Therefore, the control parameters largely determine the global balance between exploration and local development.

In the standard GWO algorithm, the control parameter A decreases linearly from 2 to 0 as the number of iterations increases. However, this linearly decreasing strategy cannot fully reflect the actual complex optimization process of the algorithm. The nonlinear control parameters obtained better performance than the linear decreasing strategy. Based on this, the following nonlinear exponential decreasing strategy is proposed:

$$\alpha = \alpha_{\text{end}} \left(\frac{\alpha_{\text{start}}}{\alpha_{\text{end}}} \right)^{1/\left((1+10t)/t_{\max}\right)^2}, \tag{8}$$

where $\alpha_{\text{start}} = 2$, $\alpha_{\text{end}} = 0.01$, and $t = 0$ and the weight in equation (8) is $\alpha = \alpha_{\text{start}} = 2$. When $t = t_{\max}$, α converges to 0.01. In the initial stage, α has a large weight and α weight decreases rapidly with the increase of the number of iterations. In the latter part of the iteration, the descending speed gradually slows down, compared with the linear decreasing adjustment scheme, the weighting strategy of the nonlinear exponential decreasing. It can improve the optimization performance of the GWO algorithm.

2.2. CNGWO Algorithm Steps. The following are the basic steps of the CNGWO algorithm, as shown in Algorithm 1.

3. Extreme Learning Machine Optimization Model

3.1. Fundamental Principles of Extreme Learning Machine (ELM). ELM is a new single hidden layer forward neural network learning algorithm that has received extensive attention in recent years. The difference from traditional neural network training is that the ELM hidden layer does not need to be iterated and the input weight and hidden layer node offset are randomly selected. With the minimum training error as the goal, the hidden layer output weight is finally determined. The algorithm is described as follows.

Let m, M, and n be the number of nodes in the network input layer, hidden layer, and output layer, respectively, $g(x)$ is the activation function of the hidden layer neurons, and b_i is the threshold. Let N samples be $(\mathbf{x}_i, \mathbf{t}_i)$, where $x_i = [x_{i1}, x_{i2}, \ldots, x_{im}]^T \in R^m$ is the network input vector and $\mathbf{t}_i = [t_{i1}, t_{i2}, \ldots, t_{in}]^T \in R^n$ is the target output vector.

The ELM model is described as follows:

$$\sum_{i=1}^{M} \boldsymbol{\beta}_i g(\boldsymbol{\omega}_i \cdot \mathbf{x}_i + b_i) = \mathbf{o}_j, \quad j = 1, 2, \ldots, N, \tag{9}$$

where $\boldsymbol{\omega}_i = [\omega_{1i}, \omega_{2i}, \ldots, \omega_{mi}]$ represents the input weight vector connecting the network input layer node and the first hidden layer node, $\boldsymbol{\beta}_i = [\beta_{i1}, \beta_{i2}, \ldots, \beta_{in}]^T$ represents the output weight vector connecting the first hidden layer node and the network output layer node, and $\mathbf{o}_j = [o_{j1}, o_{j2}, \ldots, o_{jn}]^T$ represents the network output value.

$\mathbf{S} = (\omega_i, b_i, i = 1, 2, \ldots, M)$ contains the network input weight and the hidden layer node threshold. ELM's training goal is to find the optimal $\mathbf{S}, \boldsymbol{\beta}$. $\min(E(\mathbf{S}, \boldsymbol{\beta}))$ can be further described as follows:

$$\min E = \min \|\mathbf{H}(\boldsymbol{\omega}, b, \mathbf{x})\boldsymbol{\beta} - \mathbf{T}\|, \tag{10}$$

where $\mathbf{H}$ represents the hidden layer output matrix of the network with respect to the sample, $\boldsymbol{\beta}$ represents the output weight matrix, and $\mathbf{T}$ represents the target value matrix of the sample set. $\mathbf{H}, \boldsymbol{\beta}$, and $\mathbf{T}$ are defined as follows:

Step 1: algorithm parameter setting: gray wolf group size N, maximum iteration number $t_{\max}$, iteration number t.
Step 2: randomly initialize the population and order.
While $(t < t_{\max})$ do
  Calculate the fitness value of the gray wolf group, update the α, β, δ wolf according to the fitness value, and record the positions X_a, X_b, and X_δ.
  For $i = 1$ to N do
    Calculate the value of the control parameter Aaccording to equation (7).
    Update the values of parameters A, C according to equation (2).
    Update the position of the remaining ω wolves according to equations (3) and (4).
    Update the position of α, β, δ wolf.
    According to Kent chaotic search strategy.
  End for
  $t = t + 1$
End while

Algorithm 1: CNGWO algorithm flow (CNGWO algorithm pseudocode).

$$\mathbf{H}(\boldsymbol{\omega}, b, \mathbf{x}) = \begin{bmatrix} g(\boldsymbol{\omega}_1\mathbf{x}_1 + b_1) & \cdots & g(\boldsymbol{\omega}_M\mathbf{x}_1 + b_M) \\ \vdots & & \vdots \\ g(\boldsymbol{\omega}_1\mathbf{x}_N + b_1) & \cdots & g(\boldsymbol{\omega}_M\mathbf{x}_N + b_M) \end{bmatrix}_{N\times M},$$
$$\boldsymbol{\beta} = \begin{bmatrix} \boldsymbol{\beta}_1^T \\ \vdots \\ \boldsymbol{\beta}_M^T \end{bmatrix}_{M\times n},$$
$$\mathbf{T} = \begin{bmatrix} \mathbf{t}_1^T \\ \vdots \\ \mathbf{t}_N^T \end{bmatrix}_{N\times n}. \tag{11}$$

The ELM network training process can be reduced to a nonlinear optimization problem. When the activation function $g(x)$ is infinitely divisible, the network input weight $\boldsymbol{\omega}_i$ and the threshold b_i can be randomly assigned. At this time, the matrix $\mathbf{H}$ is a constant matrix and the learning process of the extreme learning machine can be equivalent to obtaining the linear system $\mathbf{H}\boldsymbol{\beta} = \mathbf{T}$. The least squares solution of the minimum norm $\widehat{\boldsymbol{\beta}}$ is calculated as follows:

$$\widehat{\boldsymbol{\beta}} = \mathbf{H}^{\dagger}\mathbf{T}, \tag{12}$$

where $\mathbf{H}^{\dagger}$ is the Moore–Penrose generalized inverse of the hidden layer output matrix $\mathbf{H}$; after $\widehat{\boldsymbol{\beta}}$ is solved, ELM's network training process is completed. The implementation steps of the ELM algorithm are as follows:

Step 1: given a training set $(\mathbf{x}_i, \mathbf{t}_i)$, the activation function $g(x)$, and the number of hidden layer nodes M, randomly generate the input weight $\boldsymbol{\omega}_i$ and the threshold b_i

Step 2: calculate the hidden layer output matrix $\mathbf{H}$

Step 3: calculate the output weight $\boldsymbol{\beta}$ from formula (12)

3.2. ELM Optimization Model. Although the ELM learning algorithm has certain advantages in the computational performance and accuracy of the regression problem, the ELM lacks the a priori knowledge to randomly determine the input weight and the hidden layer threshold and obtain the output weight of the network. If the input weight and hidden layer threshold are not properly selected, it will affect the prediction accuracy and generalization ability of the ELM. Aiming at this problem, the CNGWO algorithm is used to optimize the extreme learning machine prediction model (CNGWO-ELM). The core idea is to use the sample data as the input of ELM and search and adjust the CNGWO optimization algorithm to get the best input weight and hidden layer node threshold. The regression effect of the ELM algorithm is best when the hidden layer nodes are as small as possible, and the output weight $\boldsymbol{\beta}$ is obtained by parsing the MP generalized inverse. Figure 1 depicts the process by which CNGWO optimizes ELM model parameters.

The specific steps of CNGWO to optimize ELM model parameters are as follows:

Step 1: population initialization: randomly generate a population consisting of N individuals, each consisting of input weights and thresholds, encoded according to $\mathbf{x}_j = (\omega_{11}, \ldots, \omega_{1M}, \omega_{21}, \omega_{22}, \ldots, \omega_{m1}, \ldots, \omega_{mM}, b_1, b_2, \ldots, b_M)$.

Step 2: variable selection and data acquisition: when modeling gas emissions, select reasonable input and output modes, collect and process operational data related to modeling from the combustion system, and divide into training data sets and test data sets.

Step 3: determine the fitness function J defined as follows:

$$J = \frac{1}{1 + \sqrt{\left(\sum_{j=1}^{N}\left\|\mathbf{o}_j - \mathbf{t}_j\right\|_2^2\right)\Big/ nN}}, \tag{13}$$

where $\mathbf{t}_i = [t_{i1}, t_{i2}, \ldots, t_{in}]^T$ is the target output vector and $\mathbf{o}_i = [o_{i1}, o_{i2}, \ldots, o_{in}]^T$ is the network predicted output value.

Step 4: model selection: the random initialization method generates the initial population, establishes the gas emission prediction model according to the initial

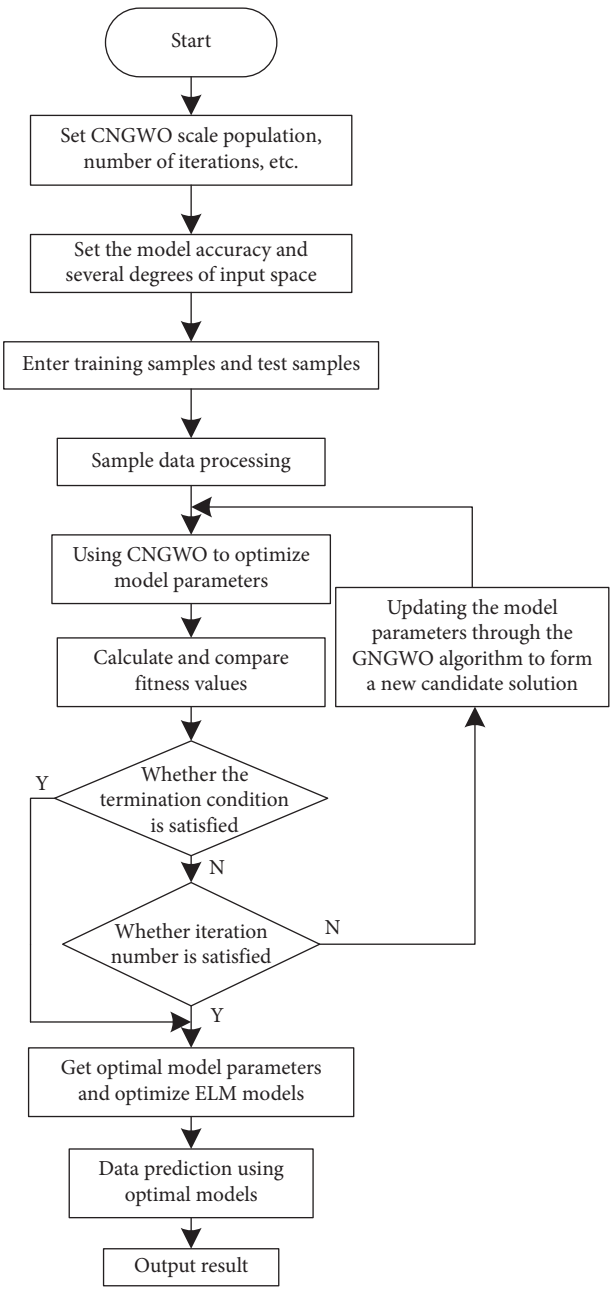

Figure 1: Optimized parameters of ELM by CNGWO.

population $(\omega_{11}, \ldots, \omega_{1M}, \omega_{21}, \omega_{22}, \ldots, \omega_{m1}, \ldots, \omega_{mM}, b_1, b_2, \ldots, b_M)$, and calculates the fitness value. If the fitness value does not meet the requirements, the CNGWO algorithm is used to optimize the model parameters of the ELM until satisfactory. As a result, the CNGWO-ELM model was established.

Step 5: model validation: validate model performance using test data.

4. Experimental Comparative

4.1. Experimental Index. The CFB boiler adopts a single furnace, single air distribution plate, M-type arrangement structure, and circulating fluidized bed combustion mode.

Table 1: CFB boiler design indicators and parameters.

Item	Value
Stand-alone capacity (MW)	660
Main steam pressure (MPa)	29.4
Main steam temperature (°C)	605
Reheat steam temperature (°C)	623
Boiler efficiency (%)	>93.5
Coal consumption for power supply (g/(kWh)	<290
SO_2 emission concentration (mg/Nm^3)	<35
NO_X emission concentration (mg/Nm^3)	<50
Dust emission concentration (mg/Nm^3)	<10

The boiler consists of 1 furnace, 4 steam-cooled cyclones, 4 return valves, 4 external heat exchangers, 8 slag coolers, and 2 rotary air preheaters. The tail is double flue. The preheater adopts the baffle to adjust the temperature, and the mechanical feeding mode of the starting bed material adding system is shown in Table 1.

The CFB boiler burns coal blended with coal slime, vermiculite, and terminal coal. The mixing ratio of designed coal slime, vermiculite, and terminal coal is 55 : 20 : 25; the ratio of coal mine slime, vermiculite, and end coal is 35 : 35 : 30. The specific coal quality information is shown in Table 2.

The boiler design has low nitrogen content in the coal quality, which reduces the formation of fuel-type NO_X, but its high volatile content is not conducive to controlling NO_X emissions. Data modeling and the modeling method proposed above are used to establish a CNGWO-ELM-based NO_x emission prediction model and a boiler load prediction model. Among them, the boiler load prediction model includes 9 input characteristics, corrected total fuel quantity, feed water flow rate, A coal mill inlet air volume, B coal mill inlet air volume, D coal mill inlet air volume, E coal mill inlet air volume, the total primary air volume, the total secondary air volume, and the boiler load per unit time before the measurement time, and the boiler load as the output. The NO_x emission prediction model includes 16 input characteristics, corrected total fuel quantity, main feed water flow rate, A coal mill inlet air volume, B coal mill inlet air volume, D coal mill inlet air volume, E coal mill inlet air volume, total primary air volume, total secondary air volume, furnace pressure, A coal mill inlet primary air temperature, B coal mill inlet primary air temperature, D coal mill inlet primary air temperature, E coal mill inlet primary air temperature, front wall outlet flue gas oxygen content, rear wall outlet flue gas oxygen content, and measurement time. The experimental data are the output values of each NO_x emission index, as shown in Table 3.

4.2. Comparison of Model Prediction Control Results. The comparison results of the CNGWO-ELM predictive control and the widely used actual values of the power plant proposed in this paper are shown in Figures 2 and 3. It can be seen from Figure 2 that there is a high degree of consistency between the load predicted value and the actual load value and the accuracy of the data higher. In Figure 3, the chemical gas emission prediction model proposed in this paper compares the actual emission with

Table 2: CFB boiler burning coal quality data.

Item	Chemical symbol	Unit	Design coal type	Check coal type
Full moisture	M_t	%	19.1	14
Air drying base moisture	M_{ad}	%	2.41	2.32
Receiving base ash	A_{ar}	%	31.34	37.18
Dry ashless base volatiles	V_{daf}	%	33.52	35.37
Receiving fixed carbon	F_{Car}	%	32.95	31.55
Receiving base carbon	C_{ar}	%	39.51	37.96
Receiving hydrogen	H_{ar}	%	2.21	2.28
Receiving base nitrogen	N_{ar}	%	0.4	0.39
Receiving oxygen	O_{ar}	%	6.81	7.39
Received total sulfur	$S_{t,ar}$	%	0.63	0.8
Received low base heat	$Q_{net,v,ar}$	MJ/kg	14.52	13.99

Table 3: Overview of experimental data.

Project	Value
Boiler load (MW)	450~850
NO_x concentration before denitration (mg/m^3)	403~773
Total fuel quantity (t/h)	133~188
Main feed water flow (t/h)	862~1125
Coal mill inlet air volume (A, B, D, E) (t/h)	67~93
Total primary air volume (t/h)	305~362
Total secondary air volume (t/h)	1083~1089
Furnace pressure (Pa)	−144~−6
Primary air temperature at the coal mill inlet (A, B, D, E) (°C)	187~258
Front wall outlet flue gas oxygen content (%)	3~6
After the wall outlet flue gas oxygen content (%)	3~6
Flue gas temperature (°C)	102~106

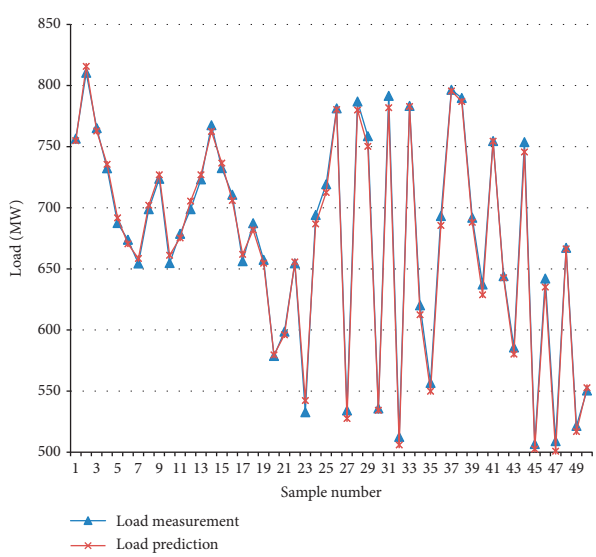

Figure 2: Comparisons and load measured value.

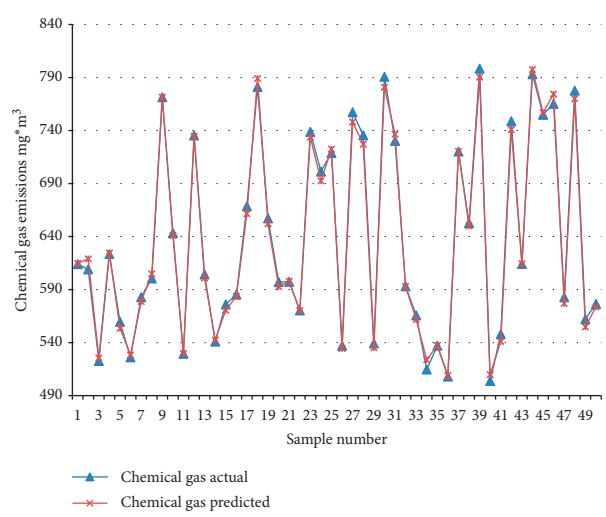

Figure 3: Comparison of chemical gas emission forecast with actual values.

the predicted value, which shows that the effect of the gas emission prediction model is better and the error between the actual value and the predicted value is small. At the same time, the model's generalization ability test results show that the maximum relative error of chemical gas emissions is 3.56%, indicating that the model has strong generalization ability.

In order to better understand the algorithm applied in this paper, other methods are used to compare the predicted values. Figure 4 shows the prediction results of 50 models with heat consumption rate of 3 models. It can be seen that the CNGWO-ELM model can predict the test samples well. Compared with the other two models, the prediction accuracy is higher, indicating that CNGWO-ELM model has strong generalization ability.

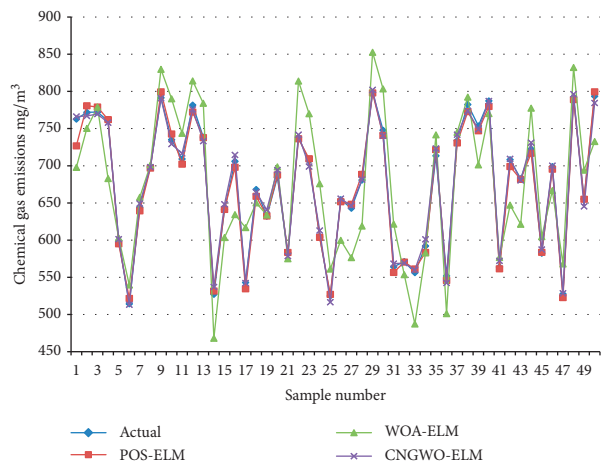

Figure 4: Comparison of CNGWO-ELM with other algorithms.

Table 4: Precision analysis of forecast results of 3 algorithms for testing set.

Sample no.	POS-ELM			WOA-ELM			CNGWO-ELM		
	RMSE	MRE %	R^2	RMSE	MRE%	R^2	RMSE	MRE %	R^2
10	24.321	6.342	0.864	33.22	8.212	0.786	5.321	2.232	0.923
30	22.216	7.433	0.885	30.87	10.651	0.793	3.234	2.013	0.942
50	18.987	9.547	0.892	27.65	11.562	0.821	3.126	1.245	0.981

4.3. Performance Comparison. In order to facilitate the evaluation of the performance of the model, this paper defines root mean squared errors (RMSE), mean relative error (MRE), and decision coefficient R^2 as follows:

$$\text{RMSE} = \sqrt{\frac{\sum_{i=1}^{n}\left(y_i' - y_i\right)^2}{n}},$$
$$\text{MRE} = \frac{1}{n}\sum_{i=1}^{n}\left|\frac{y_i' - y_i}{y_i}\right| * 100\%, \quad (14)$$
$$R^2 = 1 - \frac{\left(y_i' - y_i\right)^2}{\sum_{i=1}^{n}\left(y_i - \overline{y}_i\right)^2}.$$

where n is the number of samples, y_i is the actual measured value, y_i' is the corresponding predicted value, and $\overline{y}_i$ is the average of the actual measured values.

It can be seen that the predicted value and the true value are roughly distributed in the CNGWO-ELM model, which is relatively close to the one mentioned in the paper, indicating that the model can better predict the chemical gas. The effect is shown in Table 4.

The CNGWO-ELM model has smaller RMSE and MRE for the training samples and the least error for the test samples, which indicates that the generalization ability of the CNGWO-ELM model will be better when the input variables are larger. As the sample size changes, the values of RMSM, MRE, and R^2 also have related changes, and the values also change well. In the optimization process of the ELM algorithm, the relevant data can be optimized and analyzed.

5. Conclusions

The characteristics of chemical gas emissions are affected by many factors, and the influence relationship is complex. In order to accurately predict the chemical gas emissions, a prediction model based on improved standard gray wolf optimization algorithm (GWO) and extreme learning machine (ELM) is proposed. CNGWO-ELM is used to preselect ELM model parameters to improve the accuracy and generalization capabilities of the predictive model. Taking a 330 MW pulverized coal-fired boiler as a test object and establishing a predictive model of chemical emissions of CNGWO-ELM, the model was trained and tested by using the relevant data collected by DCS as training samples and test samples. Simulation experiments show that CNGWO-ELM's chemical emission prediction model has good accuracy and strong generalization ability and has higher practical value. In the future, other optimization algorithms will be introduced to achieve fast and accurate prediction and improve the global optimization effect.

Data Availability

The data used in this article are available in https://pan.baidu.com/s/1YHr7hRz25evFtIB1iNIpYw. Download code: dju4.

Conflicts of Interest

The authors declare that they have no conflicts of interest.

Authors' Contributions

All the authors contributed equally to the writing of this paper and read and approved the final manuscript.

Acknowledgments

This work was supported by the Science and Technology Research Program of Chongqing Municipal Education Commission (Grant no. KJZD-K201902101) and the Open Fund of Chongqing Key Laboratory of Spatial Data Mining and Big Data Integration for Ecology and Environment.

References

[1] J. Liu, X. Chen, and R. Wei, "Socioeconomic drivers of environmental pollution in China: a spatial econometric analysis," *Discrete Dynamics in Nature and Society*, vol. 2017, Article ID 4673262, 13 pages, 2017.

[2] W. Jiang, D. R. Carter, H. L. Fu et al., "The impact of the biomass crop assistance program on the United States forest products market: an application of the global forest products model," *Forests*, vol. 10, no. 3, p. 215, 2019.

[3] J. B. Liu, J. Zhao, and Z. X. Zhu, "On the number of spanning trees and normalized Laplacian of linear octagonal-quadrilateral networks," *International Journal of Quantum Chemistry*, vol. 119, no. 17, pp. 1–21, 2019.

[4] J. B. Liu, J. Zhao, and Z. Cai, "On the generalized adjacency, Laplacian and signless Laplacian spectra of the weighted edge corona networks," *Physica A: Statistical Mechanics and its Applications*, vol. 540, Article ID 123073, 2020.

[5] B. A. Nault, J. L. Laughner, P. J. Wooldridge et al., "Lightning NO_x Emissions: reconciling measured and modeled estimates with updated NO_x chemistry," *Geophysical Research Letters*, vol. 44, no. 18, pp. 9479–9488, 2017.

[6] J. Duan, F. Liu, Z. Yang, B. Sun, W. Chen, and L. Wang, "Study on the NO_x emissions mechanism of an HICE under high load," *International Journal of Hydrogen Energy*, vol. 42, no. 34, pp. 22027–22035, 2017.

[7] R. R. Rajan and C. Y. Wen, "A comprehensive model for fluidized bed coal combustors," *AIChE Journal*, vol. 26, no. 4, pp. 642–655, 2010.

[8] G. Q. Li, X. B. Qi, B. Chen et al., "Modeling research of a CFB boiler combustion system based on neural network," *Journal of Chinese Society of Power Engineering*, vol. 38, no. 6, pp. 440–446, 2018, in Chinese.

[9] T. Zhou, Q. Lu, Y. Cao, G. Wu, and S. Li, "Study on the combustion and NO_x emission characteristics of low rank coal in a circulating fluidized bed with post combustion," *The Canadian Journal of Chemical Engineering*, vol. 95, no. 12, pp. 2333–2340, 2017.

[10] Z. Kang, Q. Yuan, L. Zhao, Y. Dai, B. Sun, and T. Wang, "Study of the performance, simplification and characteristics of SNCR de-NO_x in large-scale cyclone separator," *Applied Thermal Engineering*, vol. 123, no. 8, pp. 635–645, 2017.

[11] C. Locci, L. Vervisch, B. Farcy, P. Domingo, and N. Perret, "Selective non-catalytic reduction (SNCR) of nitrogen oxide emissions: a perspective from numerical modeling," *Flow, Turbulence & Combustion*, vol. 100, no. 2, pp. 1–40, 2017.

[12] S. D. Park, D. W. Lee, D. J. Kim, and S. Cho, "Numerical investigation on cooling performance of breeding zone in HCCR TBM," *Fusion Science & Technology*, vol. 72, no. 4, pp. 801–806, 2017.

[13] H. Xu, J. Ma, and H. Zhao, "Macroscopic fuel reactor modelling of a 5 kWth, interconnected fluidized bed for in-situ gasification chemical looping combustion of coal," *Chemical Engineering Journal*, vol. 348, no. 9, pp. 978–991, 2018.

[14] J. R. Muir, C. Brereton, J. R. Grace, and C. J. Lim, "Dynamic modeling for simulation and control of a circulating fluidized-bed combustor," *AIChE Journal*, vol. 43, no. 5, pp. 1141–1152, 1997.

[15] S. Mirjalili, S. M. Mirjalili, and A. Lewis, "Grey wolf optimizer," *Advances in Engineering Software*, vol. 69, no. 7, pp. 46–61, 2014.

[16] Z.-j. Teng, J.-l. Lv, and L.-w. Guo, "An improved hybrid grey wolf optimization algorithm," *Soft Computing*, vol. 23, no. 15, pp. 6617–6631, 2019.

[17] F. Zhao, Z. Shao, J. Wang, and C. Zhang, "A hybrid optimization algorithm based on chaotic differential evolution and estimation of distribution," *Computational and Applied Mathematics*, vol. 36, no. 1, pp. 433–458, 2017.

Hindawi
Journal of Chemistry
Volume 2020, Article ID 6210758, 4 pages
https://doi.org/10.1155/2020/6210758

Research Article

A Geometric Property of the Laplacian matrix of a Connected Nonsingular Mixed Graph

Zheng-Da Zhou and Shi-Cai Gong

School of Science, Zhejiang University of Science and Technology, Hangzhou 310023, China

Correspondence should be addressed to Shi-Cai Gong; scgong@zafu.edu.cn

Received 5 August 2019; Accepted 29 October 2019; Published 28 February 2020

Guest Editor: Jia-Bao Liu

In this paper, we give a geometric interpretation of the Laplacian matrix of a connected nonsingular mixed graph which generalizes the results of M. Fiedler (M. Fiedler, Geometry of the Laplacian, *Linear Algebra Appl.*, 2005, 403: 409–413). In addition, the relations of geometric properties between a connected (singular or nonsingular) mixed graph, and all its resigned graphs will be characterized.

1. Introduction

Let $G = (V, E)$ be a *mixed graph* with vertex set $V = V(G) = \{v_1, v_2, \ldots, v_n\}$ and edge set $E = E(G) = \{e_1, e_2, \ldots, e_m\}$, which is obtained from an undirected simple graph by orienting some (possibly none or all) of its edges such that one of its endpoint forms a head and the another one is a tail. The *incidence matrix* of G is an $n \times m$ matrix $M = M(G) = (m_{ij})$ whose entries are defined by $m_{ij} = 1$ if e_j is an unoriented edge incident to v_i or e_j is an oriented edge with head v_i, $m_{ij} = -1$ if e_j is an oriented edge with tail v_i, and $m_{ij} = 0$ otherwise. The *Laplacian matrix* of G is defined as $L(G) = (l_{ij})_{n\times n} = MM^T$ (see [1–4]), where the matrix M^T denotes the transpose of M. Obviously $L(G)$ is a Gram matrix and thus is positive semidefinite. G is called *singular* (or *nonsingular*) if $L(G)$ is singular (or nonsingular).

A mixed graph is called *quasi-bipartite* if it does not contain a nonsingular cycle, or equivalently, it contains no cycles with an odd number of unoriented edges (see (1, Lemma 1)). The all-oriented graph obtained from the mixed graph G by arbitrarily orienting every unoriented edge of G (if one exists) will be denoted by $\overrightarrow{G}$, the *signature matrix* with 1 or -1 along its diagonal of a diagonal matrix will be denoted by D. A graph is called a *resigned graph* of G if it is obtained from G by resigning under the signature matrix D, and that the labelling of the vertices is the same as that of G, denoted by ${}^{D}G$. Then each resigned graph of G gives a resigning of the edges of G (that is, some oriented edges of G may turn to be unoriented and vice versa), and $L({}^{D}G) = D^T L(G) D$. The following results are well known.

Lemma 1 (see [3], Lemma 2.2, and [5], Lemma 5). *Let G be a connected mixed graph. Then, G is singular if and only if G is quasi-bipartite.*

Theorem 1 (see [1], Theorem 4). *Let G be a connected mixed graph. Then, G is quasi-bipartite if and only if there exists a signature matrix D such that $D^T L(G) D = L(\overrightarrow{G})$.*

In this paper, we firstly give a geometric interpretation of the Laplacian matrix of a connected nonsingular mixed graph which generalizes the results of Fiedler [6] from undirected graphs to mixed graphs. Finally, the relations of geometric properties between a connected (singular or nonsingular) mixed graph and its resigned graphs will be characterized.

2. Geometric Properties

2.1. Nonsingular Mixed Graphs. Let $L = L(G) = (l_{ij})_{n\times n}$ be the Laplacian matrix of a connected nonsingular mixed graph on $n (n \geq 3)$ vertices. Then, $\operatorname{rank}(L) = n$. By the well-known equivalence of positive definite and Gram matrices, there exists uniquely n linear independent vectors denoted

by $u_1, \ldots, u_n$, in a Euclidean space E_n of dimension n, such that the inner products of the vectors u_i satisfy

$$\left(u_i, u_j\right) = l_{ij} \quad \text{for all } 1 \le i,\ j \le n. \tag{1}$$

Observe that the vectors u_i and u_j $(i \neq j)$ are orthogonal if and only if there is no edge in G between the vertices i and j. If $(i, j) \in E(G)$, then the angle between u_i and u_j is obtuse if (i, j) is oriented, the angle is acute otherwise.

Let $U = (u_1, \ldots, u_n) \in E_n$, then we have the following geometric interpretation of $L(G)$.

Theorem 2. *Let $L = L(G) = (l_{ij})_{n\times n}$ be the Laplacian matrix of a connected nonsingular mixed graph G on $n (n \ge 3)$ vertices. Then, there exists a unique quadric Q:*

$$x^T K^{-1} x = 1, \tag{2}$$

such that

(i) Q contains all the end-points of the vectors u_i, and

(ii) The tangent hyperplane at each of these end-points is parallel to the hyperplane containing the remaining $n-1$ vectors,

From the above equation, x means the column vector of orthonormal coordinates in E_n and $K = UU^T$.

Proof. Note that $K^{-1} = (UU^T)^{-1} = (U^T)^{-1}U^{-1}$, then $Z = U^T K^{-1} U = I_n$. Thus, all diagonal entries of Z are equal to 1, i.e.,

$$u_i^T K^{-1} u_i = 1, \quad i = 1, 2, \ldots, n, \tag{3}$$

and all nondiagonal entries of Z are 0, which proves that quadric equation (2) contains all the end-points of the vectors u_i.

The equation of the tangent hyperplane at the end-points of u_k to the quadric equation (2) is

$$\frac{1}{2}\left(x^T K^{-1} u_k + u_k^T K^{-1} x\right) = 1. \tag{4}$$

Note that $(x^T K^{-1} u_k)^T = u_k^T K^{-1} x$, then

$$x^T K^{-1} u_k = 1. \tag{5}$$

On the contrary, the hyperplane containing all vectors u_i for $i \neq k$ satisfies the relation:

$$x^T K^{-1} u_k = 0, \tag{6}$$

since $u_i^T K^{-1} u_k = (Z)_{ik} = 0$ for $i \neq k$. Thus, both the hyperplanes are parallel, and equation (2) is indeed the equation of Q.

Assume there exists another quadric Q':

$$x^T B x = 1, \tag{7}$$

which holds properties (i) and (ii) mentioned above. Then, by property (i), we have

$$u_i^T B u_i = 1, \quad \text{for } i = 1, \ldots, n. \tag{8}$$

Thus, the equation of the tangent hyperplane at the end-points of u_k to the quadric equation (2) is

$$x^T B u_k = 1. \tag{9}$$

Consequently, by property (ii), the equation of the hyperplane containing all the remaining $n-1$ vectors is

$$x^T B u_k = 0, \tag{10}$$

since, for each i, the vector u_i contains the origin as one end-point.

Associating equations (3) and (6), we have

$$U^T B U = I. \tag{11}$$

Then, $B = K^{-1}$. Hence, the uniqueness follows.

The quadric Q is an ellipsoid, usually called the *Steiner circumscribed ellipsoid* of the simplex with vertices in the end-points of the vector u_i.

Now, suppose that v is an eigenvector of L corresponding to the eigenvalue λ. We have $U^T U v = \lambda v$. Consequently, $UU^T U v = \lambda U v$. The vector $z = Uv$ is thus an eigenvector of K as well as K^{-1} corresponding to the same λ and is thus the direction of an axis of the quadric Q. Indeed, the halfline $x = \mu z$, $\mu \ge 0$, meets the quadric in the point in which the tangent is parallel to $x^T z = 0$, thus orthogonal to z. We have thus a correspondence Γ between the eigenvector of L and the axis of Q. If the eigenvector corresponds to the eigenvalue λ, then the length of the corresponding half axis is $\sqrt{\lambda}$. Applying the method similar to that of Theorem 1 in [6], we have the following. □

Theorem 3. *The coordinates of the eigenvector v of the Laplacian matrix L are proportioned to the Euclidean coordinates of the points on the one-dimensional line generated by the vector z (corresponding in Γ) obtained as orthogonal projections of the vectors u_i on z.*

Let us transform the original orthogonal coordinate system in E_n into an other orthogonal coordinate system in which the axes coincide with the axes of the quadric Q. This will be performed algebraically as follows.

The matrix K can be written as $O\Lambda O^T$, where O is an orthogonal matrix and Λ is a diagonal matrix of the eigenvalues of K. Since $K^{-1} = O\Lambda^{-1}O^T$, equation (2) of Q will be transformed into

$$\begin{gathered} x^T O \Lambda^{-1} O^T x = 1 \\ \text{or } y^T \Lambda^{-1} y = 1, \end{gathered} \tag{12}$$

where $y = O^T x$ is again the column vector of orthogonal coordinates in the transformed system. Then, in the new system, the quadric Q has the equation:

$$\sum_{i=1}^{n} \frac{y_i^2}{d_i} = 1. \tag{13}$$

Of course, the numbers d_i are positive. They are equal to the eigenvalues of L. Let $d(G) = \max\{d_i \mid i = 1, \ldots, n\}$ and $\alpha(G) = \min\{d_i \mid i = 1, \ldots, n\}$. Then, $\sqrt{d(G)}$ (respectively, $\sqrt{\alpha(G)}$) is the semimajor (respectively, semiminor) axis of the quadric. On the contrary, $d(G)$ is the spectral radius of

$L(G)$, and $\alpha(G)$ is the smallest eigenvalue of $L(G)$. Then, the radius of the externally tangent circle of Q is $\sqrt{d(G)}$, and the radius of the internally tangent circle of Q is $\sqrt{\alpha(G)}$.

Then, the vector u_i transforms into the vector $w_i = O^T u_i$ for $i = 1$ to n. The following result seems interesting, we say as usual that an *affine transformation* is such a linear transformation which transforms points at infinity into points at infinity.

Theorem 4. *Let A be the affine transformation in E_n which transforms the ellipsoid Q into a hypersphere:*

$$y_i = \sqrt{d_i} Y_i. \tag{14}$$

Then, A transforms the vector w_i into vector $W_i = d_i^{(-1/2)} w_i$ which form an eutactic star, being all of equal length and spanning equal mutual angles.

Proof. By equation (14), we obtain the matrix form

$$y = \Lambda^{(-1/2)} Y, \tag{15}$$

where Λ was defined earlier. Since $w_i = O^T u_i$ and $W_i = \Lambda^{(-1/2)} w_i$, we have for the matrix W whose columns are the coordinates of the vectors W_i, $W = \Lambda^{(-1/2)} O^T U$. Therefore, the Gram matrix of the vectors W_i is

$$W^T W = U^T O \Lambda^{-1} O T U = U^T K^{-1} U = U^T \left(UU^T\right)^{-1} U = I_n, \tag{16}$$

since this is the matrix Z mentioned above. Immediately, the last matrix is the Gram matrix of an eutactic star. □

2.2. Mixed Graphs with the Same Underlying. In this section, we will characterize the relations of geometric properties between the graph G (singular or nonsingular) and all its resigned graphs ${}^D G$.

Denoted by $K^{-1}(G)$, the matrix of quadric corresponding to the graph G, by ${}^D u_i$ the column vector of the matrix $U\ D$ since more than one graph is under discussion. Assume $L = L(G) = (l_{ij})_{n\times n}$ be the Laplacian matrix of a connected mixed graph G on n vertices. Let $\aleph(G)$ be the set of all resigned graphs of a mixed graph G. Obviously, $\aleph(G)$ has the following properties:

(i) $G \in \aleph(G)$

(ii) All elements of $\aleph(G)$ have the same singularity as that of the graph G

(iii) All elements of $\aleph(G)$ can be considered as the resigned graphs of a (arbitrary) element of $\aleph(G)$

By Lemma 1 and Theorem 1, if G is nonsingular, we have

$$L({}^D G) = D^T L(G) D = D^T U^T U\ D = (U\ D)^T U\ D. \tag{17}$$

Thus,

$$K^{-1}({}^D G) = \left(U\ D (U\ D)^T\right)^{-1} = \left(UU^T\right)^{-1} = K^{-1}(G), \tag{18}$$

where $U = (u_1, \ldots, u_n)$ has been defined above.

Consequently, we have the following.

Theorem 5. *Let G be a connected nonsingular mixed graph on n vertices, and let $\aleph(G)$ be the set of all its resigned graphs. Then, there exists a unique quadric Q:*

$$x^T K^{-1}(G) x = 1, \tag{19}$$

such that, for all ${}^D G \in \aleph(G)$, the quadric Q contains all the endpoints of the vectors ${}^D u_i$ of ${}^D G$, and the tangent hyperplane at each of these endpoints is parallel to the hyperplane containing the remaining $n-1$ vectors, where $K^{-1}(G) = UU^T \in E_n$ has been defined above.

Similarly, by the result of [6], we have the following.

Theorem 6. *Let G be a connected singular mixed graph on n vertices, and let $\aleph(G)$ be the set of all its resigned graphs. Then, there exists a unique quadric Q:*

$$x^T K^{-1}(G) x = \frac{n-1}{n}, \tag{20}$$

such that, for all ${}^D G \in \aleph(G)$, the quadric Q contains all the endpoints of the vectors ${}^D u_i$ of ${}^D G$, and the tangent hyperplane at each of these endpoints is parallel to the hyperplane containing the endpoints of the remaining $n-1$ vectors, , where $K^{-1}(G) = UU^T \in E_{n-1}$, $U = (u_1, u_2, \ldots, u_n)$ which holds that $\sum_{i=1}^n u_i = 0$ and $U^T U = L(G')$ the Laplacian matrix of the undirected graph G' with the same underlying graph as that of G.

Proof. Let G be a connected singular mixed graph, then $\overrightarrow{G} \in \aleph(G)$. By Lemma 1 and Theorem 1 and by the definition of the Laplacian matrix, the matrix $L(\overrightarrow{G})$ is the same as that of the undirected graph G' with the same underlying graph. To graph G', by [6], there exists n vectors, $u_1, \ldots, u_n$, in a Euclidean space E_{n-1} of dimension $n-1$, such that

$$\begin{gathered} \sum_{i=1}^n u_i = 0, \\ L(G') = U^T U, \end{gathered} \tag{21}$$

where $U = (u_1, \ldots, u_n)$

And by [6], there exists a unique quadric Q:

$$x^T K^{-1}(G') x - \frac{n-1}{n} = 0, \tag{22}$$

such that the quadric Q contains all the endpoints of the vectors u_i, and the tangent hyperplane at each of these endpoints is parallel to the hyperplane containing the endpoints of the remaining $n-1$ vectors, where $K^{-1}(G') = UU^T \in E_{n-1}$.

Let ${}^D G$ be a arbitrary element of $\aleph(G)$; now, we discuss the relation of the matrices between $K^{-1}({}^D G)$ and $K^{-1}(G')$. By Lemma 1 and Theorem 1, there exists a signature matrix D such that

$$L({}^D G) = D^T L(G') D = D^T U^T U\ D = (U\ D)^T U\ D. \tag{23}$$

Thus,

$$K^{-1}({}^{D}G) = \left(U\ D(U\ D)^{T}\right)^{-1} = \left(UU^{T}\right)^{-1} = K^{-1}(G'). \quad (24)$$

The result follows immediately. □

Data Availability

The data used to support this study are available from the corresponding author upon request.

Conflicts of Interest

The authors declare no conflicts of interest.

Authors' Contributions

S. C. Gong provided the idea of the paper and the sketchy proof of theorems; Z. D. Zhou wrote the paper.

Acknowledgments

This work was supported by the National Natural Science Foundation of China (no. 11571315) and Zhejiang Provincial Natural Science Foundation of China (no. LY20A010005).

References

[1] R. B. Bapat, J. W. Grossman, and D. M. Kulkarni, "Generalized matrix tree theorem for mixed graphs," *Linear and Multilinear Algebra*, vol. 46, no. 4, pp. 299–312, 1999.
[2] R. Merris, "Laplacian matrices of graphs: a survey," *Linear Algebra and Its Applications*, vol. 197-198, pp. 143–176, 1994.
[3] X.-D. Zhang and J.-S. Li, "The Laplacian spectrum of a mixed graph," *Linear Algebra and Its Applications*, vol. 353, no. 1–3, pp. 11–20, 2002.
[4] X.-D. Zhang and R. Luo, "The Laplacian eigenvalues of mixed graphs," *Linear Algebra and Its Applications*, vol. 362, pp. 109–119, 2003.
[5] Y. Fan and J. Li, "On graphs with small number of Laplacian eigenvalues greater than two," *Linear Algebra and Its Applications*, vol. 360, pp. 207–213, 2003.
[6] M. Fiedler, "Geometry of the Laplacian," *Linear Algebra and Its Applications*, vol. 403, pp. 409–413, 2005.

Hindawi
Journal of Chemistry
Volume 2020, Article ID 9437612, 12 pages
https://doi.org/10.1155/2020/9437612

Research Article

Molecular Irregularity Indices of Nanostar, Fullerene, and Polymer Dendrimers

Xie Qing,[1] Zhen Wang,[1] Mobeen Munir,[2] and Haseeb Ahmad[2]

[1]*School of Computer Engineering, Anhui Wenda University of Information Engineering, Hefei 230032, China*
[2]*Department of Mathematics, Division of Science and Technology, University of Education, Lahore 54000, Pakistan*

Correspondence should be addressed to Mobeen Munir; mmunir@ue.edu.pk

Received 21 July 2019; Accepted 17 December 2019; Published 28 February 2020

Academic Editor: Juan L. G. Guirao

Dendrimers are highly branched organic macromolecules with successive layers of branch units surrounding a central core. Some properties like toxicity, entropy, and heats of vaporization of these dendrimers can be forecasted using topological indices. The present article is devoted to study of irregularity indices of three well-known classes of dendrimers, namely, nanostar dendrimer D$[p]$, fullerene dendrimer $NS_4[p]$, and polymer dendrimer$NS_5[p]$, where p is the step size. We also see the relation of irregularity of these dendrimers on the step size graphically.

1. Introduction

Dendrimers are nanosized, gradually well-formed molecules with precise, homogeneous, and monodispersed structure consisting of tree-like arms or branches used as anticancer drug [1]. These molecules were formed initially in 1978, by D. Tomalia and coworkers in the early 1980s and at the same time independently by George. Dendrimers might be labeled as "cascade molecules," but this term is not fixed as dendrimers [2–4]. Dendrimers are approximately monodisperse macromolecules consisting of symmetric branched units constructed around a small molecule or a linear polymer core [5–7]. Dendrimers are used in supermolecular chemistry, especially in hot-guest reactions and self-assembly processes. These are eminently defined artificial macromolecules, which are described by a combination of a high number of functional groups and a compact molecular structure [3]. These materials are fresh addition in a class of macromolecular nanoscale delivery devices [8]. In Figure 1, the main three general parts of a dendrimer are elaborated.

The formations of dendrimer molecules start with the central atom or group of atoms called core [5, 9–12]. There is a debate about the exact arrangement of dendrimers, whether they are fully enlarged with high density at the surface or whether the end-groups bend back into a closely packed interior [5, 11, 12]. Dendrimers have several applications in different fields of medicines like anticancer drugs in biomedical fields, a transdermal drug delivery, and gene delivery and as a magnetic resonance imaging contrast agent and as a dendritic sensor [13–15].

The subject matter of the present article is degree-based irregularity indices of some dendrimers. We are interested in the study of irregularity determinants of some famous dendrimers, namely, nanostar dendrimer D$[p]$, fullerene dendrimer $NS_4[p]$, and polymer dendrimer $NS_5[p]$. It has been keenly observed that the geometry and pattern of chemical systems characterize its physical aspects [16–24].

2. Preliminaries and Notations

Let G be a simple connected graph with vertex V and edge set E, and d_u be the degree of vertices u. A topological invariant is an isomorphism of the graph that preserves the topology of the graph. A graph is said to be regular if every vertex of the graph has the same degree. A topological invariant is called an irregularity index if this index vanishes for a regular graph and is nonzero for a nonregular graph. Regular graphs have been extensively investigated, particularly in mathematics. Their applications in chemical graph theory came to be known after the discovery of nanotubes and fullerenes.

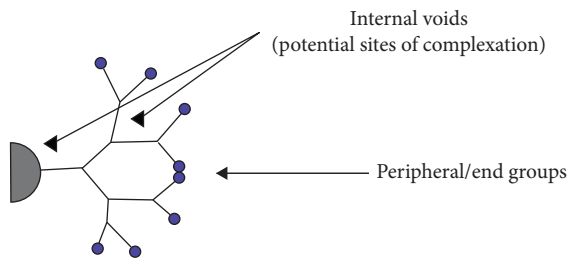

Figure 1: Three main parts of a dendrimer.

Paul Erdos emphasized this in the study of irregular graphs for the first time in history in [25]. In the Second Krakow Conference on Graph Theory, Erdos officially posed an open problem to " determine the extreme size of highly irregular graphs of given order" [26–28]. Since then, irregular graphs and the degree of irregularity have become one of the core open problems of graph theory. A graph in which each vertex has a different degree than the other vertices is known as a perfect graph. The authors of [27] demonstrated that there does not exist any perfect graph. The graphs lying in between are called quasiperfect graphs, in which all except two vertices have different degrees [29]. Irregularity of networks is discussed in [30]. Simplified ways of expressing the irregularities are irregularity indices. These irregularity indices have been studied recently in a novel way [31–33]. The first such irregularity index was introduced in [32]. Most of these indices used the concept of the imbalance of an edge defined as $\mathrm{imball}_{uv} = |\mathrm{d}u - \mathrm{d}v|$ [33]. The Albertson index, AL(G), was defined by Albertson in [32] as $\mathrm{AL}(G) = \sum_{UV\in E}|d_u - d_v|$. In this index, the imbalance of edges is computed. The irregularity indices IRL(G) and IRLU(G) are introduced by Vukičević and Graovac [33] as $\mathrm{IRL}(G) = \sum_{UV\in E}|\ln d_u - \ln d_v|$ and $\mathrm{IRLU}(G) = \sum_{UV\in E}(|d_u - t\, d_v|/\min n(d_{u,}d_v))$. Recently, Abdo et al. introduced the new term "total irregularity measure of a graph G", which is defined as $\mathrm{IRR}_t(G) = 1/2\sum_{UV\in E}|d_u - d_v|$ [34–36]. Recently, Gutman introduced the IRF(G) irregularity index of the graph G, which is described as $\mathrm{IRF}(G) = \sum_{UV\in E}(d_u - d_v)^2$ in [37]. The Randic index itself is directly related to an irregularity measure, which is described as $\mathrm{IRA}(G) = \sum_{UV\in E}(d_u^{(-1t/2)} - td_v^{(-1/2)})^2$ in [38]. Further irregularity indices of similar nature can be traced in [37, 39] in detail. These indices are given as $\mathrm{IRDIF}(G) = \sum_{UV\in E}|(d_u/d_v) - t\,(d_v/d_v)|$, $\mathrm{IRLF}(G) = \sum_{UV\in E}(|d_u - d_v|/\sqrt{(d_u d_v)})$, $\mathrm{LA}(G) = 2\sum_{UV\in E}(|d_u - d_v|/(d_u + d_v))$, $\mathrm{IRD1} = \sum_{UV\in E}\ln\{1 + |d_v - d_v|\}$, $\mathrm{IRGA}(G) = \sum_{UV\in E}\ln(d_u + d_v/2\sqrt{(d_u d_v)})$, and $\mathrm{IRB}(G) = \sum_{UV\in E}(d_u^{(1/2)} - d_v^{(1/2)})^2$. Recently, Zahid et al. computed the irregularity indices of a nanotube [40]. Gao et al. recently computed irregularity measures of some dendrimer structures in [41] and molecular structures in [42]. Hussain et al. discussed irregularity indices of some well-known benzenoid systems in [43] and some classes of nanostar dendrimers $\mathrm{NS}_1[p]$, $\mathrm{NS}_2[p]$, and $\mathrm{NS}_3[p]$ in [44]. Liu et al. computed Zagreb and multiple Zagreb indices of Eulerian graphs in [45] and number of spanning trees and normalized Laplacian of some network in [46].

In the current article, we are interested in finding the degree of irregularity of the nanostar dendrimers $D[p]$, fullerene dendrimer$\mathrm{NS}_4[p]$, and polymer dendrimer$\mathrm{NS}_5[p]$. Figures 2–4 represent molecular graphs of these three systems. The main motivation comes from the fact that graphs of the irregularity indices show close and accurate results about properties like entropy, standard enthalpy, vaporization, and acentric factors of octane isomers [39]. The molecular pattern and topology of these three dendrimers are shown in these figures. Figure 2 represents the structure of $D[p]$ nanostar dendrimer. In Figures 3 and 4, structure of $\mathrm{NS}_4[p]$ fullerene dendrimers and $\mathrm{NS}_5[p]$ polymer dendrimer is shown, respectively.

3. Main Results

In this section, we present our main theoretical results.

Theorem 1. *Let D_p be the nanostar dendrimer, then the irregularity indices of D_p are as follows:*

(1) $IRDIF(D[p]) = 5(5 \times 2^{p-1} - 4)$.

(2) $IRR(D[p]) = 6(5 \times 2^{p-1} - 4)$.

(3) $IRL(D[p]) = 2.432790649(5 \times 2^{p-1} - 4)$.

(4) $IRLU(D[p]) = 3(5 \times 2^{p-1} - 4)$.

(5) $IRLF(D[p]) = 2.449489743(5 \times 2^{p-1} - 4)$.

(6) $\sigma(D[p]) = 6(5 \times 2^{p-1} - 4)$.

(7) $IRLA(D[p]) = 2.4(5 \times 2^{p-1} - 4)$.

(8) $IRD1 = 4.158883083(5 \times 2^{p-1} - 4)$.

(9) $IRA(D[p]) = 0.1010205144(5 \times 2^{p-1} - 4)$.

(10) $IRGA(D[p]) = 0.1224659836(5 \times 2^{p-1} - 4)$.

(11) $IRB(D[p]) = 0.6061230866(5 \times 2^{p-1} - 4)$.

(12) $IRR_t(D[p]) = 3(5 \times 2^{p-1} - 4)$.

Proof. In order to prove the above theorem, we have to consider Figure 2 along with Table 1.

Now using Table 1 and the above definitions, we have

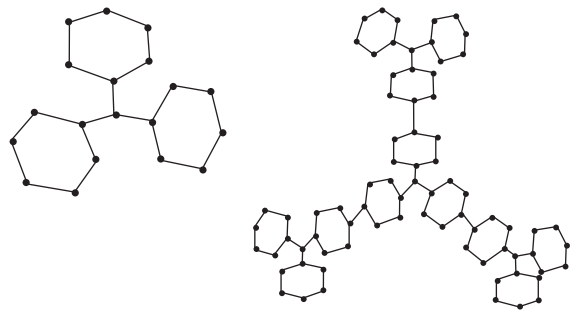

(a) (b)

Figure 2: The nanostar dendrimer D_p for $p = 1$ shown in (a) and for $p = 2$ shown in (b).

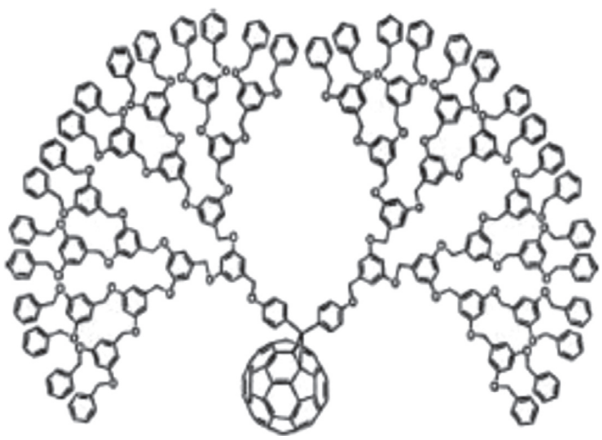

Figure 3: Fullerene dendrimer $NS_4[p]$.

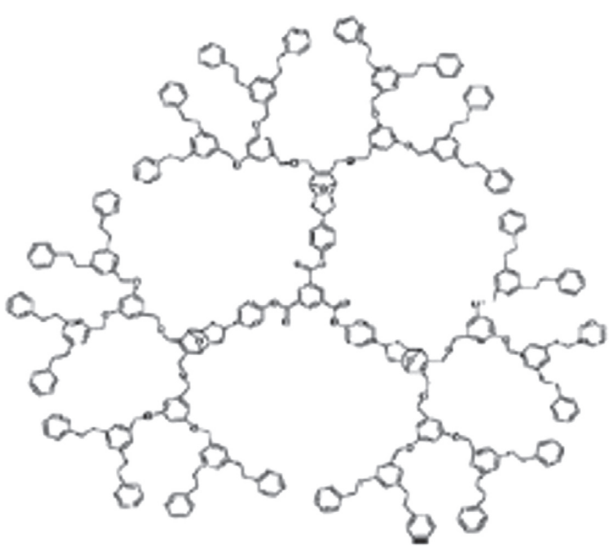

Figure 4: Polymer dendrimer $NS_5[p]$.

$$\mathrm{IRDIF}(G) = \sum_{UV\in E}\left|\frac{d_u}{d_v}-\frac{d_v}{d_v}\right|,$$

$$\begin{aligned}\mathrm{IRR}(D_p,x,y) &= 12\left(2\times 2^{p-1}-1\right)\left|\frac{2}{2}-\frac{2}{2}\right| \\ &\quad + 6\left(5\times 2^{p-1}-4\right)\left|\frac{3}{2}-\frac{2}{3}\right| \\ &\quad + 6\left(12\times 2^{p-1}-9\right)\left|\frac{3}{3}-\frac{3}{3}\right| \\ &= 6\left(5\times 2^{p-1}-4\right)\left|\frac{3}{2}-\frac{2}{3}\right|,\end{aligned} \tag{1}$$

$$\begin{aligned}\mathrm{IRR}(G) &= \sum_{UV\in E}\mathrm{imb}(e) \quad \left(\therefore \mathrm{imb}(e) = \left|d_u - d_v\right|\right), \\ \mathrm{IRR}(D_p,x,y) &= 12\left(2\times 2^{p-1}-1\right)|2-2| \\ &\quad + 6\left(5\times 2^{p-1}-4\right)|3-2| \\ &\quad + 6\left(12\times 2^{p-1}-9\right)|3-3| \\ &= 6\left(5\times 2^{p-1}-4\right)|3-2|,\end{aligned} \tag{2}$$

$$\begin{aligned}\mathrm{IRL}(G) &= \sum_{UV\in E}\left|\ln \mathrm{d}_u - \ln \mathrm{d}_v\right|, \\ \mathrm{IRL}(D_p,x,y) &= \left(2\times 2^{p-1}-1\right)|\ln 2-\ln 2| \\ &\quad + 6\left(5\times 2^{p-1}-4\right)|\ln 3-\ln 2| \\ &\quad + 6\left(12\times 2^{p-1}-9\right)|\ln 3-\ln 3| \\ &= 6\left(5\times 2^{p-1}-4\right)\left|\ln\frac{3}{2}\right|,\end{aligned} \tag{3}$$

Table 1: Edge partition of nanostar dendrimer D_p.

Number of edges (d_u, d_v)	Number of indices
(2,2)	$12(2\times 2^{p-1}-1)$
(2,3)	$6(5\times 2^{p-1}-4)$
(3,3)	$6(12\times 2^{p-1}-9)$

$$\begin{aligned}\mathrm{IRLU}(G) &= \sum_{UV\in E}\frac{|d_u-d_v|}{\min(d_u,d_v)},\\ \mathrm{IRLU}(D_p,x,y) &= (2\times 2^{p-1}-1)\frac{|2-2|}{2}\\ &\quad+6(5\times 2^{p-1}-4)\frac{|3-2|}{2}\\ &\quad+6(12\times 2^{p-1}-9)\frac{|3-3|}{3}\\ &= 6(5\times 2^{p-1}-4)\frac{|3-2|}{2},\end{aligned}\tag{4}$$

$$\begin{aligned}\mathrm{IRLF}(G) &= \sum_{UV\in E}\frac{|d_u-d_v|}{\sqrt{(d_ud_v)}},\\ \mathrm{IRLF}(D_p,x,y) &= (2\times 2^{p-1}-1)\frac{|2-2|}{\sqrt{4}}\\ &\quad+6(5\times 2^{p-1}-4)\frac{|3-2|}{\sqrt{6}}\\ &\quad+6(12\times 2^{p-1}-9)\frac{|3-3|}{\sqrt{9}}\\ &= 6(5\times 2^{p-1}-4)\frac{|3-2|}{\sqrt{6}},\end{aligned}\tag{5}$$

$$\begin{aligned}\sigma(G) &= \sum_{UV\in E}(d_u-d_v)^2,\\ \sigma(D_p,x,y) &= (2\times 2^{p-1}-1)(2-2)^2\\ &\quad+6(5\times 2^{p-1}-4)(3-2)^2\\ &\quad+6(12\times 2^{p-1}-9)(3-3)^2\left(\frac{\varepsilon}{2}\right)\\ &= 6(5\times 2^{p-1}-4)(3-2)^2,\end{aligned}\tag{6}$$

$$\begin{aligned}\mathrm{IRLA}(G) &= 2\sum_{UV\in E}\frac{|d_u-d_v|}{(d_u+d_v)},\\ \mathrm{IRLA}(D_p,x,y) &= 2\Big[(2\times 2^{p-1}-1)\frac{|2-2|}{4}\\ &\quad+6(5\times 2^{p-1}-4)\frac{|3-2|}{5}\\ &\quad+6(12\times 2^{p-1}-9)\frac{|3-3|}{6}\Big]\\ &= 2\left[6(5\times 2^{p-1}-4)\frac{|3-2|}{5}\right],\end{aligned}\tag{7}$$

$$\begin{aligned}\mathrm{IRD1} &= \sum_{UV\in E}\ln\{1+|d_v-d_v|\},\\ \mathrm{IRD1}(D_p,x,y) &= (2\times 2^{p-1}-1)\ln\{1+|2-2|\}\\ &\quad+6(5\times 2^{p-1}-4)\ln\{1+|3-2|\}\\ &\quad+6(12\times 2^{p-1}-9)\ln\{1+|3-3|\}\\ &= 6(5\times 2^{p-1}-4)\ln 2,\end{aligned}\tag{8}$$

$$\begin{aligned}\mathrm{IRA}(G) &= \sum_{UV\in E}\left(d_u^{(-1/2)}-d_v^{(-1/2)}\right)^2,\\ \mathrm{IRA}(D_p,x,y) &= (2\times 2^{p-1}-1)\left(\frac{1}{\sqrt{2}}-\frac{1}{\sqrt{2}}\right)^2\\ &\quad+6(5\times 2^{p-1}-4)\left(\frac{1}{\sqrt{3}}-\frac{1}{\sqrt{2}}\right)^2\\ &\quad+6(12\times 2^{p-1}-9)\left(\frac{1}{\sqrt{3}}-\frac{1}{\sqrt{3}}\right)^2\\ &= 6(5\times 2^{p-1}-4)\left(\frac{1}{\sqrt{3}}-\frac{1}{\sqrt{2}}\right)^2,\end{aligned}\tag{9}$$

$$\begin{aligned}\mathrm{IRGA}(G) &= \sum_{UV\in E}\ln\frac{d_u+d_v}{2\sqrt{(d_ud_v)}},\\ \mathrm{IRGA}(D_p,x,y) &= (2\times 2^{p-1}-1)\ln\frac{|2+2|}{2\sqrt{4}}\\ &\quad+6(5\times 2^{p-1}-4)\ln\frac{|3+2|}{2\sqrt{6}}\\ &\quad+6(12\times 2^{p-1}-9)\ln\frac{|3+3|}{2\sqrt{9}}\\ &= 6(5\times 2^{p-1}-4)\ln\frac{|3+2|}{2\sqrt{6}},\end{aligned}\tag{10}$$

$$\begin{aligned}\mathrm{IRB}(G) &= \sum_{UV\in E}\left(d_u^{(1/2)}-d_v^{(1/2)}\right)^2,\\ \mathrm{IRB}(D_p,x,y) &= (2\times 2^{p-1}-1)(\sqrt{2}-\sqrt{2})^2\\ &\quad+6(5\times 2^{p-1}-4)(\sqrt{3}-\sqrt{2})^2+\\ &\quad 6(12\times 2^{p-1}-9)(\sqrt{3}-\sqrt{3})^2\\ &= 6(5\times 2^{p-1}-4)(\sqrt{3}-\sqrt{2})^2,\end{aligned}\tag{11}$$

$$\begin{aligned}\mathrm{IRR}_t(G) &= \frac{1}{2}\sum_{u,v\in V(G)}|d_u-d_v|,\\ \mathrm{IRR}_t(D_p,x,y) &= \frac{1}{2}\big[12(2\times 2^{p-1}-1)|2-2|\\ &\quad+6(5\times 2^{p-1}-4)|3-2|\\ &\quad+6(12\times 2^{p-1}-9)|3-3|\big]\\ &= 3(5\times 2^{p-1}-4).\end{aligned}\tag{12}$$

Table 2 shows the values of these irregularity indices for some test values of parameter p. □

Theorem 2. *Let $NS_4[p]$ be the fullerene dendrimer, then the irregularity indices of $NS_4[p]$ are as follows:*

(1) $IRDIF(NS_4[p]) = 26.666.2^{p-1} + 2.66667.2^{p+1} - 0.6664$.
(2) $IRR(NS_4[p]) = 32.2^{p-1} + 2.2^{p+1} - 2$.
(3) $IRL(NS_4[p]) = 12.97488.2^{p-1} + 1.6986.2^{p+1} - 1.517628$.
(4) $IRLU(NS_4[p]) = 16.2^{p-1} + 2.\,2^{p+1} - 2$.
(5) $IRLF(NS_4[p]) = 13.063936.2^{p-1} + 1.1547.2^{p+1} - 1.533934$.
(6) $\sigma(NS_4[p]) = 32.2^{p-1} + 4.2^{p+1} - 2$.
(7) $IRLA(NS_4[p]) = 12.8.2^{p-1} + 2^{p+1} - 1.485714$.
(8) $IRD1 = 22.180704.2^{p-1} + 1.098612.2^{p+1} - 1.386294$.
(9) $IRA(NS_4\quad[p]) = 0.538784.2^{p-1} + 0.17863322^{p+1} - 0.128713$.
(10) $IRGA(NS_4[p]) = 57.242453.2^{p-1} + 1.242453.2^{p-1} + 0.473936$.
(11) $IRB(NS_4[p]) = 3.232672.2^{p-1} + 0.535898.2^{p+1} - 0.377386$.
(12) $IRR_t(NS_4[p]) = 16.2^{p-1} + 2^{p+1} - 1$.

Proof. In order to prove the above theorem, we have to consider Figure 3 and Table 3.

Now using Table 3 and the above definitions, we have

$$\begin{aligned}
\mathrm{IRDIF}(G) &= \sum_{UV\in E}\left|\frac{\mathrm{d}_u}{\mathrm{d}_v}-\frac{\mathrm{d}_v}{\mathrm{d}_v}\right|,\\
\mathrm{IRDIF}(\mathrm{NS}_4[p],x,y) &= 32.2^{p-1} - 8\left|\frac{3}{2}-\frac{2}{3}\right| + 2^{p+1}\\
&\quad + 2\left|\frac{2}{2}-\frac{2}{2}\right| + 2^{p+1}\left|\frac{3}{1}-\frac{1}{3}\right|\\
&\quad + 86.\left|\frac{3}{3}-\frac{3}{3}\right| + 6\left|\frac{4}{3}-\frac{3}{4}\right| + 3\left|\frac{4}{4}-\frac{4}{4}\right|\\
&= 32.2^{p-1} - 8\left|\frac{3}{2}-\frac{2}{3}\right|\\
&\quad + 2^{p+1}\left|\frac{3}{1}-\frac{1}{3}\right| + 6\left|\frac{4}{3}-\frac{3}{4}\right|,
\end{aligned} \tag{13}$$

$$\begin{aligned}
\mathrm{IRR}(G) &= \sum_{UV\in E}\mathrm{imb}(e) \quad \therefore \mathrm{imb}(e) = |d_u - d_v|,\\
\mathrm{IRR}(\mathrm{NS}_4[p],x,y) &= 32.2^{p-1} - 8\,|3-2| + 2^{p+1} + 2|2-2|\\
&\quad + 2^{p+1}|3-1| + 86.|3-3|\\
&\quad + 6|4-3| + 3|4-4|\\
&= 32.2^{p-1} - 8 + 2.2^{p+1} + 6,
\end{aligned} \tag{14}$$

$$\begin{aligned}
\mathrm{IRL}(G) &= \sum_{UV\in E}\left|\ln \mathrm{d}_u - \ln \mathrm{d}_v\right|,\\
\mathrm{IRL}(\mathrm{NS}_4[p],x,y) &= 32.2^{p-1} - 8\,|\ln 3 - \ln 2| + 2^{p+1}\\
&\quad + 2|\ln 2 - \ln 2| + 2^{p+1}|\ln 3 - \ln 1|\\
&\quad + 86.|\ln 3 - \ln 3| + 6|\ln 4 - \ln 3|\\
&\quad + 3|\ln 4 - \ln 4|\\
&= 32.2^{p-1} - 8\ln\frac{3}{2} + 2^{p+1}\ln\frac{3}{1}\\
&\quad + 6.\ln\frac{4}{3},
\end{aligned} \tag{15}$$

$$\begin{aligned}
\mathrm{IRLU}(G) &= \sum_{UV\in E}\frac{\left|\mathrm{d}_u - \mathrm{d}_v\right|}{\min(d_u d_v)},\\
\mathrm{IRLU}(\mathrm{NS}_4[p],x,y) &= 32.2^{p-1} - 8\frac{|3-2|}{2} + 2^{p+1}\\
&\quad + 2\frac{|2-2|}{2}\\
&\quad + 2^{p+1}\frac{|3-1|}{1} + 86.\frac{|3-3|}{3}\\
&\quad + 6.\frac{|4-3|}{3} + 3.\frac{|4-4|}{4}\\
&= \frac{32.2^{p-1}-8}{2} + 2, 2^{p+1} + 2,
\end{aligned} \tag{16}$$

$$\begin{aligned}
\mathrm{IRLF}(G) &= \sum_{UV\in E}\frac{\left|\mathrm{d}_u - \mathrm{d}_v\right|}{\sqrt{(\mathrm{d}_u\mathrm{d}_v)}},\\
\mathrm{IRLF}(\mathrm{NS}_4[p],x,y) &= 32.2^{p-1} - 8\frac{|3-2|}{\sqrt{6}} + 2^{p+1}\\
&\quad + 2\frac{|2-2|}{\sqrt{4}} + 2^{p+1}\frac{|3-1|}{\sqrt{3}}\\
&\quad + 86.\frac{|3-3|}{\sqrt{9}}\\
&\quad + 6.\frac{|4-3|}{\sqrt{12}} + 3.\frac{|4-4|}{\sqrt{16}}\\
&= \frac{32.2^{p-1}-8}{\sqrt{6}} + \frac{2.2^{p+1}}{\sqrt{3}} + \frac{6}{\sqrt{12}},
\end{aligned} \tag{17}$$

$$\begin{aligned}
\sigma(G) &= \sum_{UV\in E}(d_u - d_v)^2,\\
\sigma(\mathrm{NS}_4[p],x,y) &= 32.2^{p-1} - 8(3-2)^2 + 2^{p+1}\\
&\quad + 2(2-2)^2 + 2^{p+1}(3-1)^2\\
&\quad + 86.(3-3)^2 + 6.(4-3)^2\\
&\quad + 3.(4-4)^2\\
&= 32.2^{p-1} - 8 + 4.2^{p+1} + 6,
\end{aligned} \tag{18}$$

Table 2: Irregularity indices for nanostar dendrimer D_p.

Irregularity indices	$p = 1$	$p = 2$	$p = 3$	$p = 4$	$p = 5$
$\mathrm{IRDIF}(G) = \sum_{UV\in E} \lvert (d_u/d_v) - (d_v/d_v) \rvert$	5	30	80	180	380
$\mathrm{AL}(G) = \sum_{UV\in E} \lvert d_u - d_v \rvert$	6	36	96	216	456
$\mathrm{IRL}(G) = \sum_{UV\in E} \lvert \ln \mathrm{d}_u - \ln \mathrm{d}_v \rvert$	2.4328	14.5968	38.9246	87.5805	184.8921
$\mathrm{IRLU}(G) = \sum_{UV\in E} (\lvert d_u - d_v \rvert / \min(d_u, d_v))$	3	18	48	108	228
$\mathrm{IRLU}(G) = \sum_{UV\in E} (\lvert d_u - d_v \rvert / \sqrt{(d_u d_v)})$	2.4495	14.6969	39.1918	88.1816	186.1612
$\mathrm{IRF}(G) = \sum_{UV\in E} (d_u - d_v)^2$	6	36	96	216	456
$\mathrm{IRLA}(G) = 2\sum_{UV\in E} (\lvert d_u - d_v \rvert / (d_u + d_v))$	2.4	14.4	38.4	86.4	182.4
$\mathrm{IRD1} = \sum_{UV\in E} \ln\{1 + \lvert d_v - d_v \rvert\}$	4.1589	24.9533	66.5422	149.7198	316.0751
$\mathrm{IRA}(G) = \sum_{UV\in E} (d_u^{(-1/2)} - d_v^{(-1/2)})^2$	0.10102	0.6061	1.6163	3.6367	7.6775
$\mathrm{IRGA}(G) = \sum_{UV\in E} \ln(d_u + d_v / 2\sqrt{(d_u d_v)})$	0.1225	0.73479	1.9594	4.4087	9.3074
$\mathrm{IRB}(G) = \sum_{UV\in E} (d_u^{(1/2)} - d_v^{(1/2)})^2$	0.6061	3.6367	9.6979	21.8204	46.0653
$\mathrm{IRR}_t(G) = (1/2)\sum_{UV\in E} \lvert d_u - d_v \rvert$	3	18	48	108	228

Table 3: Edge partition of fullerene dendrimers.

Number of edges (d_u, d_v)	Number of indices
(2,3)	$32.2^{p-1} - 8$
(2,2)	$2^{p+1} + 2$
(1,3)	2^{p+1}
(3,3)	86
(3,4)	6
(4,4)	3

$$\begin{aligned}
\mathrm{IRLA}(G) &= 2\sum_{UV\in E} \frac{\lvert d_u - d_v \rvert}{(d_u + d_v)}, \\
\mathrm{IRLA}(\mathrm{NS}_3[p], x, y) &= 2\left[32.2^{p-1} - 8\frac{\lvert 3-2 \rvert}{5} + 2^{p+1}\right. \\
&\quad + 2\frac{\lvert 2-2 \rvert}{4} + 2^{p+1}\frac{\lvert 3-1 \rvert}{4} + 86.\frac{\lvert 3-3 \rvert}{6} \\
&\quad \left. + 6.\frac{\lvert 4-3 \rvert}{7} + 3.\frac{\lvert 4-4 \rvert}{8}\right] \\
&= 2\left[\frac{32.2^{p-1} - 8}{5} + \frac{2^{p+1}}{2} + \frac{6}{7}\right],
\end{aligned} \tag{19}$$

$$\begin{aligned}
\mathrm{IRD1} &= \sum_{UV\in E} \ln\left\{1 + \lvert d_v - d_v \rvert\right\}, \\
\mathrm{IRD1}(\mathrm{NS}_4[n], x, y) &= 32.2^{p-1} - 8\ln\{1 + \lvert 3-2 \rvert\} \\
&\quad + 2^{p+1} + 2\ln\{1 + \lvert 2-2 \rvert\} \\
&\quad + 2^{p+1}\ln\{1 + \lvert 3-1 \rvert\} \\
&\quad + 86\ln\{1 + \lvert 3-3 \rvert\} \\
&\quad + 6\ln\{1 + \lvert 4-3 \rvert\} \\
&\quad + 3\ln\{1 + \lvert 4-4 \rvert\} \\
&= 32.2^{p-1} - 8\ln 2 \\
&\quad + 2^{p+1}\ln 3 + 6\ln 2,
\end{aligned} \tag{20}$$

$$\begin{aligned}
\mathrm{IRA}(G) &= \sum_{UV\in E} \left(d_u^{(-1/2)} - d_v^{(-1/2)}\right)^2, \\
\mathrm{IRA}(\mathrm{NS}_4[p], x, y) &= 32.2^{p-1} - 8\left(\frac{1}{\sqrt{3}} - \frac{1}{\sqrt{2}}\right)^2 + 2^{p+1} \\
&\quad + 2\left(\frac{1}{\sqrt{2}} - \frac{1}{\sqrt{2}}\right)^2 + 2^{p+1}\left(\frac{1}{\sqrt{3}} - \frac{1}{\sqrt{1}}\right)^2 \\
&\quad + 86\left(\frac{1}{\sqrt{3}} - \frac{1}{\sqrt{3}}\right)^2 + 6\left(\frac{1}{\sqrt{4}} - \frac{1}{\sqrt{3}}\right)^2 \\
&\quad + 3\left(\frac{1}{\sqrt{4}} - \frac{1}{\sqrt{4}}\right)^2 \\
&= 32.2^{p-1} - 8\left(\frac{1}{\sqrt{3}} - \frac{1}{\sqrt{2}}\right)^2 \\
&\quad + 2^{p+1}\left(\frac{1}{\sqrt{3}} - \frac{1}{\sqrt{1}}\right)^2 + 6\left(\frac{1}{\sqrt{4}} - \frac{1}{\sqrt{3}}\right)^2,
\end{aligned} \tag{21}$$

$$\begin{aligned}
\mathrm{IRGA}(G) &= \sum_{UV\in E} \ln\frac{d_u + d_v}{2\sqrt{(d_u d_v)}}, \\
\mathrm{IRGA}(\mathrm{NS}_4[p], x, y) &= 32.2^{p-1} - 8\ln\frac{\lvert 3+2 \rvert}{2\sqrt{6}} + 2^{p+1} \\
&\quad + 2\ln\frac{\lvert 2+2 \rvert}{2\sqrt{4}} + 2^{p+1}\ln\frac{\lvert 3+1 \rvert}{2\sqrt{3}} \\
&\quad + 86\ln\frac{\lvert 3+3 \rvert}{2\sqrt{9}} + 6\ln\frac{\lvert 4+3 \rvert}{2\sqrt{12}} \\
&\quad + 3\ln\frac{\lvert 4+4 \rvert}{2\sqrt{16}} \\
&= 32.2^{p-1} - 8\ln\frac{5}{2\sqrt{6}} \\
&\quad + 2^{p+1}\ln\frac{4}{2\sqrt{3}} + 6\ln\frac{7}{2\sqrt{12}},
\end{aligned} \tag{22}$$

$$\begin{aligned}
\mathrm{IRB}(G) &= \sum_{UV\in E}\left(d_u^{(1/2)} - d_v^{(1/2)}\right)^2,\\
\mathrm{IRB}(\mathrm{NS}_4[p], x, y) &= 32.2^{p-1} - 8(\sqrt{3}-\sqrt{2})^2 + 2^{p+1}\\
&\quad + 2(\sqrt{2}-\sqrt{2})^2 + 2^{p+1}(\sqrt{3}-\sqrt{1})^2\\
&\quad + 86(\sqrt{3}-\sqrt{3})^2 + 6(\sqrt{4}-\sqrt{3})^2\\
&\quad + 3(\sqrt{4}-\sqrt{4})^2\\
&= 32.2^{p-1} - 8(\sqrt{3}-\sqrt{2})^2\\
&\quad + 2^{p+1}(\sqrt{3}-\sqrt{1})^2 + 6(\sqrt{4}-\sqrt{3})^2,
\end{aligned} \tag{23}$$

$$\begin{aligned}
\mathrm{IRR}_t(G) &= \frac{1}{2}\sum_{UV\in E}\left|d_u - d_v\right|,\\
\mathrm{IRR}_t(\mathrm{NS}_4[p], x, y) &= \frac{1}{2}\left[32.2^{p-1} - 8|3-2| + 2^{p+1}\right.\\
&\quad + 2|2-2| + 2^{p+1}|3-1|\\
&\quad \left. + 86|3-3| + 6|4-3| + 3|4-4|\right]\\
&= \frac{1}{2}\left[32.2^{p-1} - 8 + 2.2^{p+1} + 6\right].
\end{aligned} \tag{24}$$

Table 4 demonstrates the values of these irregularity indices of fullerene dendrimers for some test values of parameter p. □

Theorem 3. *Let $NS_5[p]$ be the polymer dendrimer, then the irregularity indices of $NS_5[p]$ are as follows:*

(1) $IRDIF(NS_5[p]) = 4.999998.2^{p+3} + 8.2^{p+1} + 3$.
(2) $IRR(NS_5[p]) = 6.2^{p+3} + 6.2^{p+1}$.
(3) $IRL(NS_5[p]) = 2.43279.2^{p+3} + 3.295836.2^{p+1} + 0.8630546$.
(4) $IRLU(NS_5[p]) = 3.2^{p+3} + 6.2^{p+1} + 3$.
(5) $IRLF(NS_5[p]) = 4.242641.2^{p+3} + 2.44949.2^{p+1} - 1.793151$.
(6) $\sigma(NS_5[p]) = 6.2^{p+3} + 12.2^{p+1} + 6$.
(7) $IRLA(NS_5[p]) = 2.4.2^{p+3} + 3.2^{p+1} + 0.6$.
(8) $IRD1 = 4.158882.2^{p+3} + 3.295836.2^{p+1} - 0.863046$.
(9) $IRA(NS_5[p]) = 0.101022.2^{p+3} + 0.535899.2^{p+1} + 0.434877$.
(10) $IRGA(NS_5[p]) = 10.87302.2^{p+3} + 3.727359.2^{p+1} - 7.145661$.
(11) $IRB(NS_5[p]) = 0.606126.2^{p+3} + 1.607694.2^{p+1} + 1.001568$.
(12) $IRR_t(NS_5[p]) = 3.2^{p+3} + 3.2^{p+1}$.

Proof. In order to prove the above theorem, we have to consider Figure 4 and Table 5.

Now, using Table 5 and the above definitions, we have

$$\begin{aligned}
\mathrm{IRDIF}(G) &= \sum_{UV\in E}\left|\frac{d_u}{d_v} - \frac{d_v}{d_v}\right|,\\
\mathrm{IRDIF}(\mathrm{NS}_5[p], x, y) &= 6\left(2^{p+3}-1\right)\left|\frac{3}{2}-\frac{2}{3}\right| + 6\left(2^{p+1}\right)\left|\frac{2}{2}-\frac{2}{2}\right|\\
&\quad + (24)\left|\frac{3}{3}-\frac{3}{3}\right| + 3\left(2^{p+1}+1\right)\left|\frac{3}{1}-\frac{1}{3}\right|\\
&= 6\left(2^{p+3}-1\right)\left|\frac{3}{2}-\frac{2}{3}\right|\\
&\quad + 3\left(2^{p+1}+1\right)\left|\frac{3}{1}-\frac{1}{3}\right|,
\end{aligned} \tag{25}$$

$$\begin{aligned}
\mathrm{IRR}(G) &= \sum_{UV\in E}\mathrm{imb}(e) \quad \therefore \mathrm{imb}(e)\\
\mathrm{IRR}(\mathrm{NS}_5[p], x, y) &= 6\left(2^{p+3}-1\right)|3-2|\\
&\quad + 6\left(2^{p+1}\right)|2-2| + (24)|3-3|\\
&\quad + 3\left(2^{p+1}+1\right)|3-1|\\
&= 6\left(2^{p+3}-1\right) + 6\left(2^{p+1}+1\right),
\end{aligned} \tag{26}$$

$$\begin{aligned}
\mathrm{IRL}(G) &= \sum_{UV\in E}\left|\ln \mathrm{d}_u - \ln \mathrm{d}_v\right|,\\
\mathrm{IRL}(NS_5[p], x, y) &= 6\left(2^{p+3}-1\right)|\ln 3 - \ln 2|\\
&\quad + 6\left(2^{p+1}\right)|\ln 2 - \ln 2| + (24)|\ln 3 - \ln 3|\\
&\quad + 3\left(2^{p+1}+1\right)|\ln 3 - \ln 1|\\
&= 6\left(2^{p+3}-1\right)\ln\frac{3}{2} + 3\left(2^{p+1}+1\right)\ln\frac{3}{1},
\end{aligned} \tag{27}$$

$$\begin{aligned}
\mathrm{IRLU}(G) &= \sum_{UV\in E}\frac{\left|d_u - d_v\right|}{\min\left(d_u d_v\right)},\\
\mathrm{IRLU}(\mathrm{NS}_5[p], x, y) &= 6\left(2^{p+3}-1\right)\frac{|3-2|}{2}\\
&\quad + 6\left(2^{p+1}\right)\frac{|2-2|}{2} + 24.\frac{|3-3|}{3}\\
&\quad + 3\left(2^{p+1}+1\right)\frac{|3-1|}{1}\\
&= 3\left(2^{p+3}-1\right) + 6\left(2^{p+1}+1\right),
\end{aligned} \tag{28}$$

$$\begin{aligned}
\mathrm{IRLF}(G) &= \sum_{UV\in E}\frac{\left|d_u - d_v\right|}{\sqrt{\left(d_u d_v\right)}},\\
\mathrm{IRLF}(\mathrm{NS}_5[p], x, y) &= 6\left(2^{p+3}-1\right)\frac{|3-2|}{\sqrt{6}}\\
&\quad + 6\left(2^{p+1}\right)\frac{|2-2|}{\sqrt{4}} + 24\frac{|3-3|}{\sqrt{9}}\\
&\quad + 3\left(2^{p+1}+1\right)\frac{|3-1|}{\sqrt{3}}\\
&= \frac{6\left(2^{p+3}-1\right)}{\sqrt{2}} + \frac{6\left(2^{p+1}+1\right)}{\sqrt{6}},
\end{aligned} \tag{29}$$

Table 4: Irregularity indices for fullerene dendrimer $NS_4[p]$.

Irregularity indices	$p=1$	$p=2$	$p=3$	$p=4$	$p=5$
$IRDIF(G)=\sum_{UV\in E}\lvert(d_u/d_v)-t(d_v/d_v)\rvert$	36.66628	73.99896	148.66432	297.99504	596.65648
$AL(G)=\sum_{UV\in E}\lvert d_u-d_v\rvert$	38	78	158	318	638
$IRL(G)=\sum_{UV\in E}\lvert \ln d_u-\ln d_v\rvert$	18.251652	38.0209	77.5594	156.636	314.7908
$IRLU(G)=\sum_{UV\in E}\lvert d_u-d_v\rvert/\min(d_u,d_v)$	22	46	94	190	382
$IRLU(G)=\sum_{UV\in E}(\lvert d_u-td_v\rvert/\sqrt{(d_ud_v)})$	16.148802	33.83153	69.197010	139.92795	281.38984
$IRF(G)=\sum_{UV\in E}(d_u-d_v)^2$	46	94	190	382	766
$IRLA(G)=2\sum_{UV\in E}(\lvert d_u-td_v\rvert/(d_u+d_v))$	15.31428	32.11428	65.714286	132.91428	267.31428
$IRD1=\sum_{UV\in E}\ln\{1+\lvert d_v-d_v\rvert\}$	25.18885	51.7640	104.9143	211.2149	423.8161
$IRA(G)=\sum_{UV\in E}(d_u^{(-1/2)}-d_v^{(-1t/2)})^2$	1.1246038	2.3779206	4.8845542	9.8978214	19.924355
$IRGA(G)=\sum_{UV\in E}\ln(d_u+td_vn/2\sqrt{(d_ud_v)})$	58.958842	117.44374	234.4135	468.3531	936.2324
$IRB(G)=\sum_{UV\in E}(d_u^{(1/2)}-d_v^{(1/2)})^2$	4.99887	10.375142	21.127670	42.6327	85.642838
$IRR_t(G)=(1/2)\sum_{UV\in E}\lvert d_u-d_v\rvert$	19	39	79	159	319

Table 5: Edge partition of polymer dendrimer $NS_5[p]$.

Number of edges (d_u,d_v)	Number of indices
(2,3)	$6(2^{p+3}-1)$
(2,2)	$6(2^{p+1})$
(3,3)	24
(1,3)	$3(2^{p+1}+1)$

$$\begin{aligned}\sigma(G)&=\sum_{UV\in E}(d_u-d_v)^2,\\ \sigma(NS_5[p],x,y)&=6\left(2^{p+3}-1\right)(3-2)^2\\ &\quad+6\left(2^{p+1}\right)(2-2)^2+24.(3-3)^2\\ &\quad+3\left(2^{p+1}+1\right)(3-1)^2\\ &=6\left(2^{p+1}-1\right)+12\left(2^{p+1}+1\right),\end{aligned}\tag{30}$$

$$\begin{aligned}IRLA(G)&=2\sum_{UV\in E}\frac{\lvert d_u-d_v\rvert}{(d_u+d_v)},\\ IRLA(NS_5[p],x,y)&=2\left[6\left(2^{p+3}-1\right)\frac{\lvert 3-2\rvert}{(3+2)}\right.\\ &\quad+6\left(2^{p+1}\right)\frac{\lvert 2-2\rvert}{(2+2)}+24.\frac{\lvert 3-3\rvert}{(3+3)}\\ &\quad\left.+3\left(2^{p+1}+1\right)\frac{\lvert 3-1\rvert}{(3+1)}\right]\\ &=2\left[\frac{6(2^{p+3}-1)}{5}+\frac{6(2^{p+1}+1)}{4}\right],\end{aligned}\tag{31}$$

$$\begin{aligned}IRD1&=\sum_{UV\in E}\ln\left\{1+\lvert d_v-d_v\rvert\right\},\\ IRD1(NS_5[n],x,y)&=6\left(2^{p+3}-1\right)\ln\{1+\lvert 3-2\rvert\}\\ &\quad+6\left(2^{p+1}\right)\ln\{1+\lvert 2-2\rvert\}\\ &\quad+24.\ln\{1+\lvert 3-3\rvert\}\\ &\quad+3\left(2^{p+1}+1\right)\ln\{1+\lvert 3-1\rvert\}\\ &=6\left(2^{p+3}-1\right)\ln 2\\ &\quad+3\left(2^{p+1}+1\right)\ln 3,\end{aligned}\tag{32}$$

$$\begin{aligned}IRA(G)&=\sum_{UV\in E}\left(d_u^{(-1t/2)}-d_v^{(-1/2)}\right)^2,\\ IRA(NS_5[p],x,y)&=6\left(2^{p+3}-1\right)\left(\frac{1}{\sqrt{3}}-\frac{1}{\sqrt{2}}\right)^2\\ &\quad+6\left(2^{p+1}\right)\left(\frac{1}{\sqrt{2}}-\frac{1}{\sqrt{2}}\right)^2\\ &\quad+24.\left(\frac{1}{\sqrt{3}}-\frac{1}{\sqrt{3}}\right)^2\\ &\quad+3\left(2^{p+1}+1\right)\left(\frac{1}{\sqrt{3}}-\frac{1}{\sqrt{1}}\right)^2\\ &=6\left(2^{p+3}-1\right)\left(\frac{1}{\sqrt{3}}-\frac{1}{\sqrt{2}}\right)^2\\ &\quad+3\left(2^{p+1}+1\right)\left(\frac{1}{\sqrt{3}}-\frac{1}{\sqrt{1}}\right)^2,\end{aligned}\tag{33}$$

$$\begin{aligned}IRGA(G)&=\sum_{UV\in E}\ln\frac{d_u+d_v}{2\sqrt{(d_ud_v)}},\\ IRGA(NS_5[p],x,y)&=6\left(2^{p+3}-1\right)\ln\frac{\lvert 3+2\rvert}{2\sqrt{6}}\\ &\quad+6\left(2^{p+1}\right)\ln\frac{\lvert 2+2\rvert}{2\sqrt{4}}\\ &\quad+24.\ln\frac{\lvert 3+3\rvert}{2\sqrt{9}}\\ &\quad+3\left(2^{p+1}+1\right)\ln\frac{\lvert 3+1\rvert}{2\sqrt{3}}\\ &=6\left(2^{p+3}-1\right)\ln\frac{5}{2\sqrt{6}}\\ &\quad+3\left(2^{p+1}+1\right)\ln\frac{4}{2\sqrt{3}},\end{aligned}\tag{34}$$

Table 6: Irregularity indices for polymer dendrimer $NS_5[p]$.

Irregularity indices	$p = 1$	$p = 2$	$p = 3$	$p = 4$	$p = 5$
$\mathrm{IRDIF}(G) = \sum_{UV\in E}\lvert(d_u/d_v) - t(d_v/d_v)\rvert$	114.9999	226.999	450.99	898.999	1794.99
$\mathrm{AL}(G) = \sum_{UV\in E}\lvert d_u - d_v\rvert$	120	240	480	960	1920
$\mathrm{IRL}(G) = \sum_{UV\in E}\lvert\ln d_u - \ln d_v\rvert$	52.97103	105.0790	209.2949	417.7269	834.5907
$\mathrm{IRLU}(G) = \sum_{UV\in E}(\lvert d_u - td_v\rvert/\min n(d_u, d_v))$	75	147	291	579	1155
$\mathrm{IRLU}(G) = \sum_{UV\in E}(\lvert d_u - td_v\rvert/\sqrt{(d_u d_v)})$	75.8870	153.567	308.9277	619.648	1241.090
$\mathrm{IRF}(G) = \sum_{UV\in E}(d_u - d_v)^2$	150	294	582	1158	2310
$\mathrm{IRLA}(G) = 2\sum_{UV\in E}(\lvert d_u - td_v\rvert/(d_u + d_v))$	51	101.4	202.2	403.8	807
$\mathrm{IRD1} = \sum_{UV\in E}\ln\{1 + \lvert d_v - d_v\rvert\}$	78.8624	158.5878	318.038	636.9406	1274.744
$\mathrm{IRA}(G) = \sum_{UV\in E}(d_u^{(-1t/2)} - d_v^{(-1t/2)})^2$	4.19482	7.95477	15.47466	30.514461	60.59404
$\mathrm{IRGA}(G) = \sum_{UV\in E}(\ln d_u + d_v/2\sqrt{(d_u d_v)})$	181.73209	370.6098	748.3653	1503.876	3014.898
$\mathrm{IRB}(G) = \sum_{UV\in E}(d_u^{(1/2)} - d_v^{(1/2)})^2$	17.1303	33.2591	65.5167	130.0319	259.062
$\mathrm{IRR}_t(G) = (1/2)\sum_{UV\in E}\lvert d_u - d_v\rvert$	60	120	240	480	960

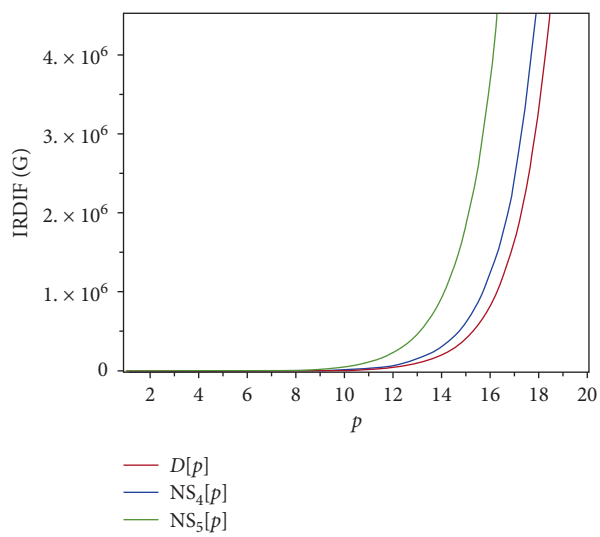

Figure 5: Graphs of irregularity index IRDIF.

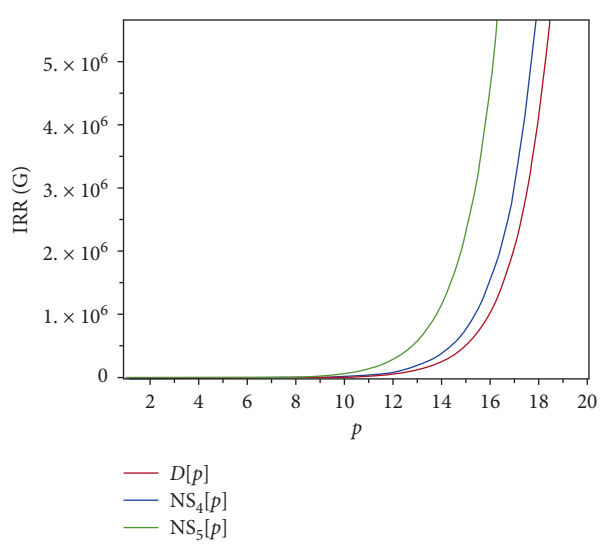

Figure 6: Curves of irregularity index IRR.

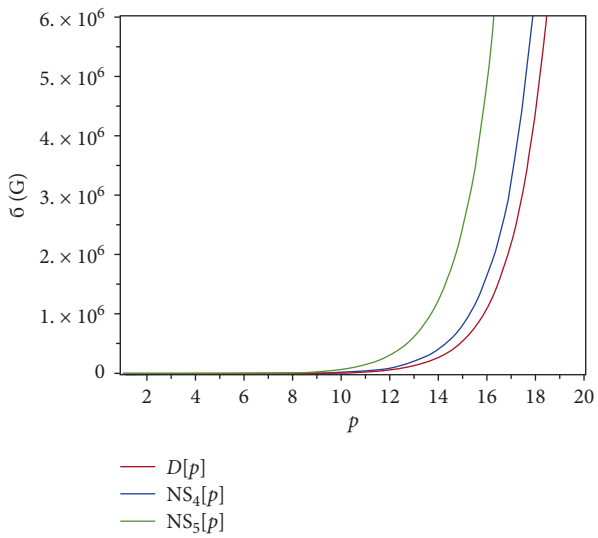

Figure 7: Curves of irregularity index σ.

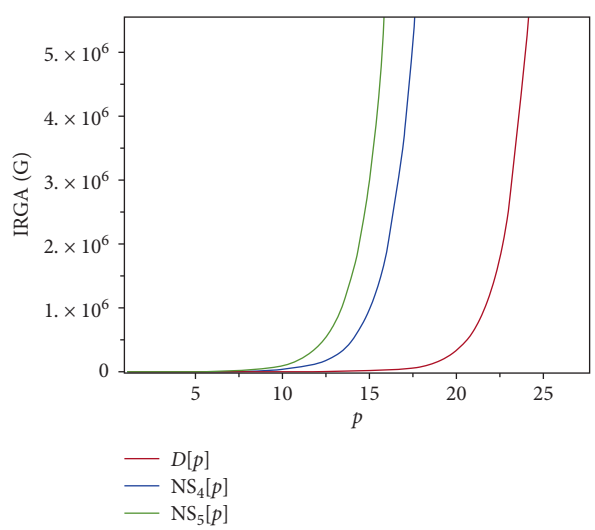

Figure 8: Curves of irregularity index IRGA.

$$\begin{aligned}
\mathrm{IRB}(G) &= \sum_{UV\in E}\left(d_u^{(1/2)} - d_v^{(1/2)}\right)^2,\\
\mathrm{IRB}(\mathrm{NS}_5[p], x, y) &= 6\left(2^{p+3}-1\right)(\sqrt{3}-\sqrt{2})^2\\
&\quad + 6\left(2^{p+1}\right)(\sqrt{2}-\sqrt{2})^2\\
&\quad + 24.(\sqrt{3}-\sqrt{3})^2\\
&\quad + 3\left(2^{p+1}+1\right)(\sqrt{3}-\sqrt{1})^2\\
&= 6\left(2^{p+3}-1\right)(\sqrt{3}-\sqrt{2})^2\\
&\quad + 3\left(2^{p+1}+1\right)(\sqrt{3}-\sqrt{1})^2,
\end{aligned} \tag{35}$$

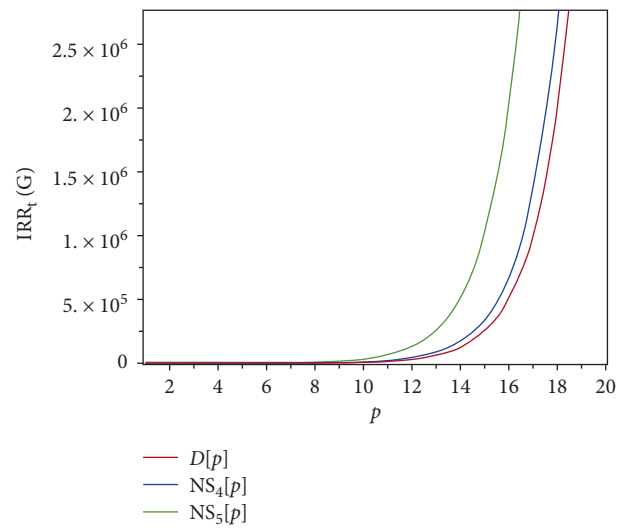

Figure 9: Curves of irregularity index IRR_t.

$$\begin{aligned}
\mathrm{IRR}_t(G) &= \frac{1}{2}\sum_{UV\in E}|d_u - d_v|,\\
\mathrm{IRR}_t(\mathrm{NS}_5[p], x, y) &= \frac{1}{2}\Big[6\left(2^{p+3}-1\right)|3-2|\\
&\quad + 6\left(2^{p+1}\right)|2-2| + 24.|3-3|\\
&\quad + 3\left(2^{p+1}+1\right)|3-1|\Big]\\
&= \frac{1}{2}\left[6\left(2^{p+3}-1\right) + 6\left(2^{p+1}+1\right)\right].
\end{aligned} \tag{36}$$

Table 6 depicts the values of these irregularity indices for some test values of parameter p. □

4. Graphical Analysis, Discussions, and Conclusions

In the present section, we give the graphical analysis of the irregularity measures of the above three classes of dendrimer structures. We summarize our findings in terms of graphs of irregularity indices against the step size p from 1 to 30.

Figure 5 presents three different curves for the values of irregularity index IRDIF against the step size p. It can be demonstrated that irregularity of all three dendrimers tends to increase with increase in step size. It is noticeable that for $p > 16$, IRDIF rises sharply showing that irregularity is nonuniform.

In Figure 6, curves of irregularity index IRR have been drawn against step size p and behavior of this index is similar to IRIDF.

All irregularity indices show the similar pattern for three dendrimers, as indicated in Figures 7–9.

From the above discussion, it can be concluded that $\mathrm{NS}_5[p]$ is relatively more irregular than $\mathrm{NS}_4[p]$ and $\mathrm{D}[p]$ is

most regular in these three dendrimers. The dependence of irregularity of structures on step size could be a potential information career for modelling nanoscale drugs and devices.

Data Availability

No such data are associated with this article.

Conflicts of Interest

The authors declare no conflicts of interest.

Authors' Contributions

M. M. gave the idea, and H. A., Q. X., and Z. W. wrote the article.

Acknowledgments

This research was supported by the Natural Science Fund of Anhui Wenda University of Information Engineering (Grant no. XZR2019A10) and Quality Engineering Fund of Anhui Education Department (Project code: 2018jyxm1318).

References

[1] S. Gopalan and Y. KJ, "Nanotechnologies for the life sciences," *Dendrimers in Cancer Treatment and Diagnosis*, Vol. 7, Wiley, New York, NY, USA, 2007.

[2] B. Klajnert and M. Bryszewska, "Dendrimers: properties and applications," *Acta Biochimica Polonica*, vol. 48, no. 1, pp. 199–208, 2001.

[3] D. A. Tomalia and J. M. J. Fréchet, "Discovery of dendrimers and dendritic polymers: a brief historical perspective," *Journal of Polymer Science Part A: Polymer Chemistry*, vol. 40, no. 16, pp. 2719–2728, 2002.

[4] D. A. Tomalia, "The dendritic state," *Materials Today*, vol. 8, no. 3, pp. 34–46, 2005.

[5] D. A. Tomalia, H. Baker, J. Dewald et al., "A new class of polymers: starburst-dendritic macromolecules," *Polymer Journal*, vol. 17, no. 1, pp. 117–132, 1985.

[6] G. R. Newkome, Z. Yao, G. R. Baker, and V. K. Gupta, "Micelles. Part 1. Cascade molecules: a new approach to micelles. A [27]-arborol," *The Journal of Organic Chemistry*, vol. 50, no. 11, pp. 2003-2004, 1985.

[7] C. J. Hawker and J. M. J. Frechet, "Preparation of polymers with controlled molecular architecture. A new convergent approach to dendritic macromolecules," *Journal of the American Chemical Society*, vol. 112, no. 21, pp. 7638–7647, 1990.

[8] J. Wolinsky and M. Grinstaff, "Therapeutic and diagnostic applications of dendrimers for cancer treatment," *Advanced Drug Delivery Reviews*, vol. 60, no. 9, pp. 1037–1055, 2008.

[9] S. C. Zimmerman, "Dendrimers in molecular recognition and self-assembly," *Current Opinion in Colloid & Interface Science*, vol. 2, no. 1, pp. 89–99, 1997.

[10] F. Zeng and S. C. Zimmerman, "Dendrimers in supramolecular chemistry: from molecular recognition to self-assembly," *Chemical Reviews*, vol. 97, no. 5, pp. 1681–1712, 1997.

[11] D. Boris and M. Rubinstein, "A self-consistent mean field model of a starburst dendrimer: dense core vs dense shell," *Macromolecules*, vol. 29, no. 22, pp. 7251–7260, 1996.

[12] G. Spataro, F. Malecaze, C.-O. Turrin et al., "Designing dendrimers for ocular drug delivery," *European Journal of Medicinal Chemistry*, vol. 45, no. 1, pp. 326–334, 2010.

[13] H. Patel and P. DRPM, "Dendrimer applications—a review," *International Journal of Pharma and Bio Sciences*, vol. 4, no. 2, pp. 454–463, 2013.

[14] D. Ruth and I. Lorella, "Dendrimer biocompatibility and toxicity," *Advanced Drug Delivery Reviews*, vol. 57, pp. 2215–2237, 2005.

[15] S. Sampathkumar and K. Yarema, "Chapter 1, dendrimers in cancer treatment and diagnosis," in *Nanotechnologies for the Life Sciences*, Vol. 6, Springer, Berlin, Germany, 2007.

[16] V. Bezugly, J. Kunstmann, and B. Grundkötter-Stock, T. Stock, T. Frauenheim, G. Cuniberti, and G. Cuniberti, Highly conductive boron nanotubes: transport properties, work functions, and structural stabilities," *ACS Nano*, vol. 5, no. 6, pp. 4997–5005, 2011.

[17] F. M. Brückler, T. Došlić, A. Graovac, and I. Gutman, "On a class of distance-based molecular structure descriptors," *Chemical Physics Letters*, vol. 503, no. 4–6, pp. 336–338, 2011.

[18] H. Deng, J. Yang, and F. Xia, "A general modeling of some vertex-degree based topological indices in benzenoid systems and phenylenes," *Computers & Mathematics with Applications*, vol. 61, no. 10, pp. 3017–3023, 2011.

[19] E. Deutsch and S. Klavzar, "M-Polynomial, and degree based topological indices," *Iranian Journal of Mathematical Chemistry*, vol. 6, pp. 93–102, 2015.

[20] M. Munir, W. Nazeer, A. Nizami, S. Rafique, and S. Kang, "M-polynomials and topological indices of titania nanotubes," *Symmetry*, vol. 8, no. 11, p. 117, 2016.

[21] M. Munir, W. Nazeer, S. Rafique, and S. Kang, "M-polynomial and degree-based topological indices of polyhex nanotubes," *Symmetry*, vol. 8, no. 12, p. 149, 2016.

[22] M. Ajmal, W. Nazeer, M. Munir, S. M. Kang, and Y. C. Kwun, "M-polynomials and topological indices of generalized prism and toroidal polyhex networks," *Symmetry Under Review*, vol. 9, 2016.

[23] M. Munir, W. Nazeer, Z. Shahzadi, and S. Kang, "Some invariants of circulant graphs," *Symmetry*, vol. 8, no. 11, p. 134, 2016.

[24] H. Wiener, "Structural determination of paraffin boiling points," *Journal of the American Chemical Society*, vol. 69, no. 1, pp. 17–20, 1947.

[25] G. Chartrand, P. Erdös, and O. R. Oellermann, "How to define an irregular graph," *The College Mathematics Journal*, vol. 19, no. 1, pp. 36–42, 1988.

[26] Z. Majcher and J. Michael, "Highly irregular graphs with extreme numbers of edges," *Discrete Mathematics*, vol. 164, no. 1–3, pp. 237–242, 1997.

[27] M. Behzad and G. Chartrand, "No graph is perfect," *The American Mathematical Monthly*, vol. 74, no. 8, pp. 962-963, 1967.

[28] B. Horoldagva, L. Buyantogtokh, S. Dorjsembe, and I. Gutman, "Maximum sizeof maximally irregular graphs," *MATCH Communications in Mathematical and in Computer Chemistry*, vol. 76, pp. 81–98, 2016.

[29] F. Liu, Z. Zhang, and J. Meng, "The size of maximally irregular graphs and maximally irregular triangle-free graphs," *Graphs and Combinatorics*, vol. 30, no. 3, pp. 699–705, 2014.

[30] L. Collatz and U. Sinogowitz, "Spektren endlicher graphen," *Abhandlungen aus dem Mathematischen Seminar der Universität Hamburg*, vol. 21, pp. 63–77, 1957.
[31] F. K. Bell, "A note on the irregularity of graphs," *Linear Algebra and Its Applications*, vol. 161, pp. 45–54, 1992.
[32] M. Albertson, "The irregularity of a graph," *Ars Combinatoria*, vol. 46, pp. 219–225, 1997.
[33] D. Vukičević and A. Graovac, "Valence connectivities versus Randić, Zagreb and modified Zagreb index: A.linear algorithm to check discriminative properties of indices in acyclic molecular graphs," *Croatica Chemica Acta*, vol. 77, pp. 501–508, 2004.
[34] H. Abdo, S. Brandt, and D. Dimitrov, "The total irregularity of a graph," *Discrete Mathematics & Theoretical Computer Science*, vol. 16, pp. 201–206, 2014.
[35] H. Abdo and D. Dimitrov, "The total irregularity of graphs under graph operations," *Miskolc Mathematical Notes*, vol. 15, no. 1, pp. 3–17, 2014.
[36] H. Abdo and D. Dimitrov, "The irregularity of graphs under graph operations," *Discussiones Mathematicae Graph Theory*, vol. 34, no. 2, pp. 263–278, 2014.
[37] I. Gutman, "Topological indices and irregularity measures," *Bulletin of Society of Mathematicians*, vol. 8, pp. 469–475, 2018.
[38] X. Li and I. Gutman, "Mathematical aspects of Randic, type molecular structure descriptors," in *Mathematical Chemistry Monographs*, University of Kragujevac and Faculty of Science Kragujevac, Kragujevac, Serbia, 2006.
[39] T. Reti, R. Sharfdini, A. Dregelyi-Kiss, and H. Hagobin, "Graph irregularity indices used as molecular discriptors in QSPR studies," *MATCH Communications in Mathematical and in Computer Chemistry*, vol. 79, 2018.
[40] J.-B. Liu, J. Zhao, and Z.-Q. Cai, "On the generalized adjacency, Laplacian and signless Laplacian spectra of the weighted edge corona networks," *Physica A: Statistical Mechanics and Its Applications*, vol. 540, p. 123073, 2020.
[41] W. Gao, M. Aamir, Z. Iqbal, M. Ishaq, and A. Aslam, "On irregularity measures of some dendrimers structures," *Mathematics*, vol. 7, no. 3, p. 271, 2019.
[42] J.-B. Liu, J. Zhao, H. He, Z. Shao, and Shao, "Valency-based topological descriptors and structural property of the generalized sierpiński networks," *Journal of Statistical Physics*, vol. 177, no. 6, pp. 1131–1147, 2019.
[43] Z. Hussain, S. Rafique, M. Munir et al., "Irregularity molecular descriptors of hourglass, jagged-rectangle, and triangular benzenoid systems," *Processes*, vol. 7, no. 7, p. 413, 2019.
[44] Z. Hussain, S. Rafique, M. Munir et al., "Irregularity molecular descriptors of some nanostar dendrimers," *Processes*, vol. 7, no. 8, p. 517, 2019.
[45] J.-B. Liu, C. Wang, S. Wang, and B. Wei, "Zagreb indices and multiplicative Zagreb indices of eulerian graphs," *Bulletin of the Malaysian Mathematical Sciences Society*, vol. 42, no. 1, pp. 67–78, 2019.
[46] J. Liu, Z. Jing, and Z. Zhongxun, "On the number of spanning trees and normalized Laplacian of linear octagonal-quadrilateral networks," *International Journal of Quantum Chemistry*, vol. 119, no. 17, Article ID e25971, 2019.

Hindawi
Journal of Chemistry
Volume 2020, Article ID 3236813, 7 pages
https://doi.org/10.1155/2020/3236813

Research Article

The Cardinal Spline Methods for the Numerical Solution of Nonlinear Integral Equations

Xiaoyan Liu,[1] **Jin Xie**,[2] **Zhi Liu**,[3] **and Jiahuan Huang**[1]

[1]*Department of Mathematic, University of La Verne, La Verne, CA 91750, USA*
[2]*School of Artificial Intelligence and Big Data, Hefei University, Hefei 230601, China*
[3]*School of Mathematic, Hefei University of Technology, Hefei 230001, China*

Correspondence should be addressed to Jin Xie; xiejin@hfuu.edu.cn

Received 20 October 2019; Revised 27 December 2019; Accepted 6 January 2020; Published 12 February 2020

Guest Editor: Shaohui Wang

In this study, an effective technique is presented for solving nonlinear Volterra integral equations. The method is based on application of cardinal spline functions on small compact supports. The integral equation is reduced to a system of algebra equations. Since the matrix for the system is triangular, it is relatively straightforward to solve for the unknowns and an approximation of the original solution with high accuracy is accomplished. Several cardinal splines are employed in the paper to enhance the accuracy. The sufficient condition for the existence of the inverse matrix is examined, and the convergence rate is analyzed. We compare our method with other methods proposed in recent papers and demonstrated the advantage of our method with several examples.

1. Introduction

Integral equations appear in many fields, including dynamic systems, mathematical applications in economics, communication theory, optimization and optimal control systems, biology and population growth, continuum and quantum mechanics, kinetic theory of gases, electricity and magnetism, potential theory, geophysics, and theoretical-model chemistry. Many differential equations with boundary values can be reformulated as integral equations. There are also some problems that can be expressed only in terms of integral equations. Many differential equations with boundary values can be reformulated as integral equations; for example, for chemical integral equations with boundaries, Polyanin summarized different solutions of integral equations in [1–3], published in 2013 and 2016. In [4–6], we discussed numerical methods using cardinal splines in solving systems of linear integral equations. In this paper, we are going to explore the applications of cardinal splines in solving nonlinear integral equations.

We are interested in the Volterra integral equations of the second kind:

$$y(x) = g(x) + \int_a^x K(x,t,y(t))\mathrm{d}t, \quad x \in (a,b), \tag{1}$$

where the kernel $K(x,t,y)$ and $g(x)$ are known functions and $y(x)$ is to be determined.

This paper is divided into six sections. In Sections 2 and 3, two univariate cardinal continuous splines on small compact supports are constructed and properties are given. In Section 4, the applications of cardinal splines on solving integral equations are explored. The unknown function is expressed as a linear combination of horizontal translations of a cardinal spline function. Then, a system of equations on the coefficients are deducted. We can solve the system, and a good approximation of the original solution is obtained. The sufficient condition for the existence of the inverse matrix is discussed, and the convergence is investigated. In Section 5, the numerical examples are given. The nonlinear system on unknowns is solved, and an accurate approximation of the

original solution is obtained in each case. Section 6 contains the conclusion remarks.

2. Cardinal Splines with Small Compact Supports

Since the paper [7] by Schoenberg published in 1946, spline functions have been studied by many scholars. Spline functions have excellent properties, and applications are endless (for examples, cf [2]). The spline functions on uniform partitions are simple to construct and easy to apply and are sufficient for a variety of applications.

The starting point is frequently the zero degree polynomial B-spline (see Figure 1), with the integral iteration formula

$$B_0(x) = \begin{cases} 1, & -\frac{1}{2} < x < \frac{1}{2}, \\ 0, & \text{elsewhere}, \end{cases} \tag{2}$$

$$B_n(x) = \int_{-(1/2)}^{1/2} B_{n-1}(x+t)\mathrm{d}t, \quad n = 1, 2, 3, \ldots.$$

We could construct higher-order polynomial spline functions with a higher degree of smoothness. More specifically, $B_1(x)$ has the expression (see Figure 2) as follows:

$$B_1(x) = \frac{1}{2}|x-1| + \frac{1}{2}|x+1| - |x|. \tag{3}$$

$B_n(x)$ are called one-dimensional B-splines, which are polynomial splines and have small supports $(-((n+1)/2), (n+1)/2)$,i.e., $B_n(x) = 0$ for $x > (n+1)/2$ or $< -((n+1)/2)$ and excellent traits (cf [8]). In my previous papers [4, 5], low-degree orthonormal spline and cardinal spline functions with small compact supports were applied in solving the second kind of Volterra integral equations. In this paper, we use the notation $\|u\|_A = \max_{x\in A}|u(x)|$.

Let $B_{1,h}(x) = B_1(x/h)$. It is proved that

$$\sum_{m=-\infty}^{\infty} (a + bmh) B_{1,h}(x - mh) = (a + bx). \tag{4}$$

Note that this particular B-spline is also a cardinal spline; therefore, it is straightforward to apply it in interpolations. As far as the convergence rate of interpolation is concerned, we have the following proposition (cf [9–12]).

Proposition 1. *Given that $f(x) \in C[a,b]$, $f'(x)$ exists and is bounded in $[a,b]$. Let n be an integer; $h = (b-a)/n$; let $x_i = a + ih$; $f_i = f(x_i)$, $i = 0, 1, 2, \ldots, n$, as follows:*

$$\Omega f(x) = \sum_{k=0}^{n} f_k B_{1,h}(x - kh). \tag{5}$$

Then,

$$\|\Omega f(x) - f(x)\|_{[a,b]} \le 3\|f'(x)\|_{[a,b]} h^2, \tag{6}$$

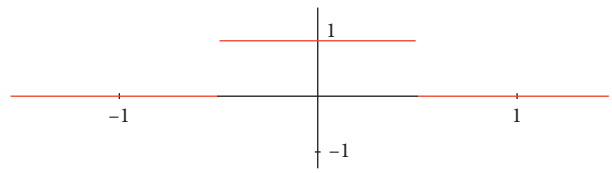

Figure 1: The graph of $B_0(x)$.

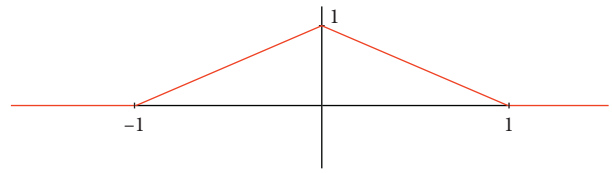

Figure 2: The graph of $B_1(x)$.

where Ω denotes the approximation polynomial of $f(x)$.

If $f(x) \in C(-\infty, \infty)$ and $f'(x)$ exists and is bounded, let h be a real number, and let $f_i = f(ih)$, $i = 0, 1, 2, \ldots$:

$$\Omega f(x) = \sum_{k=-\infty}^{\infty} f_k B_{1,h}(x - kh). \tag{7}$$

Then,

$$\|\Omega f(x) - f(x)\|_{(-\infty,\infty)} \le 3\|f'(x)\|_{(-\infty,\infty)} h^2. \tag{8}$$

3. A Univariate C^2 Cardinal Spline

By cardinal conditions (cf [13]), we mean that let $L(x)$ be a function, $\{x_i\}$, $i = 0, \pm1, \pm2, \pm3, \ldots$ be interpolation points; then,

$$L(x_i) = \begin{cases} 1, & i = 0, \\ 0, & i \ne 0, \end{cases} \quad i = 0, \pm1, \pm2, \pm3, \pm4, \ldots. \tag{9}$$

The cardinal spline that was originally given in [10] is based on $B_3(x)$ using the similar process as in Section 2. Let

$$\begin{aligned} L_3(x) &= 6B_3(x) - 60\int_{-(1/2)}^{1/2} t^2 B_2(x+t)\mathrm{d}t \\ &= \int_{-(1/2)}^{1/2} \left(6 - 60t^2\right) B_2(x+t)\mathrm{d}t. \end{aligned} \tag{10}$$

Figure 3 shows the graph of $L_3(x)$.

Then, $L_3(x/h)$ satisfies the above cardinal condition when $x_i = ih$, $i = 0, \pm1, \pm2, \pm3, \ldots$. Notice that by the construction $L_3(x) \in C^2(-\infty, \infty)$. $L_3(x) = 0$ for $x \in (-\infty, -2) \cup (2, \infty)$. $L_3(x)$ is a polynomial of degree ≤ 5 in each subinterval $(-2, -1)$, $(-1, 0)$, $(0, 1)$, and $(1, 2)$ of its support.

Furthermore, from direct calculation, we deduct the following two propositions (cf [10]).

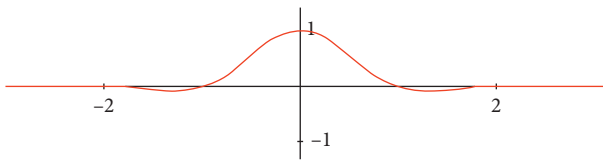

Figure 3: The graph of $L_3(x)$.

Proposition 2. *Let $L_3(x)$ be the cardinal spline constructed above; then,*

$$\sum_{m=-\infty}^{\infty} L_3\left(\frac{x}{h}-m\right)\left(\alpha(ih)^2+\beta(ih)+\gamma\right)=\alpha x^2+\beta x+\gamma,$$
$$\left\|\sum_{m=-\infty}^{\infty} L_3\left(\frac{x}{h}-m\right)(ih)^3-x^3\right\|\le\frac{1}{6}h^3, \tag{11}$$

where α,β, and γ are any complex number.

Proposition 3. *If $f(x)\in C^3[a,b]$, let $h=(b-a)/n$,n be an integer; let $f_i=f(a+ih)$, $i=0,1,2,\ldots$:*

$$\Omega f(x)=(3f_0-3f_1+f_2)L_3\left(\frac{x}{h}+1\right)+\sum_{k=0}^{n} fL_3\left(\frac{x}{h}-k\right)_i$$
$$+(3f_n-3f_{n-1}+f_{n-2})L_3\left(\frac{x}{h}-n-1\right). \tag{12}$$

Then,

$$\|\Omega f(x)-f(x)\|_{[a,b]}\le 7\|f'''(x)\|_{[a,b]}h^3. \tag{13}$$

If $f(x)\in C^3(-\infty,\infty)$ and is bounded, let h be a real number; let $f_i=f(ih)$, $i=0,1,2,\ldots$:

$$\Omega f(x)=\sum_{k=-\infty}^{\infty} f_k L_3\left(\frac{x}{h}-k\right). \tag{14}$$

Then,

$$\|\Omega f(x)-f(x)\|_{(-\infty,\infty)}\le 7\|f'''(x)\|_{(-\infty,\infty)}h^3. \tag{15}$$

4. Numerical Methods Solving Integral Equations

4.1. Method 1-V for Solving the Volterra Integral Equation. As for the Volterra integral equations (1), we solve it in an interval $[a,b]$. Again, we let $h=(b-a)/n$ and $x_i=a+ih$, $i=0,1,\ldots,n$. Furthermore, plugging $f(x)=\sum_{k=0}^{n}c_kB_{1,h}(x-x_k)$,$K(x,t,y(t))=\sum_{i=0}^{n}\sum_{j=0}^{n}K(x_i,x_j,c_j)B_{1,h}(x-x_i)B_{1,h}(t-x_j)$, and $g(x)=\sum_{k=0}^{n}g(x_k)B_{1,h}(x-x_k)$, we get

$$\sum_{k=0}^{n}c_kB_{1,h}(x-x_k)-\sum_{i=0}^{n}\sum_{j=0}^{n}B_{1,h}(x-x_i)\int_a^x K(x_i,x_j,c_j)\cdot B_{1,h}(t-x_j)\mathrm{d}t=\sum_{k=0}^{n}g(x_k)B_{1,h}(x-x_k). \tag{16}$$

Let $x=x_s$; we arrive at

$$c_s-\sum_{j=0}^{n}K(x_s,x_j,c_j)\int_a^{x_s}B_{1,h}(t-x_j)\mathrm{d}t=g(x_s),\quad s=0,1,2,3,4,\ldots,n, \tag{17}$$

which is a simple system of $n+1$ nonlinear equations of unknowns $\{c_0,c_1,\ldots,c_n\}$. Notice that this is a triangular system and it is solvable (the solution may not be unique because it is not linear):

$$\begin{aligned}
&c_0=g(x_0),\\
&c_1-\frac{h}{2}\sum_{j=0}^{1}K(x_1,x_j,c_j)=g(x_1),\\
&c_s-\frac{h}{2}\left(K(x_s,x_0,c_0)+2\sum_{j=1}^{s-1}K(x_s,x_j,c_j)\right.\\
&\quad\left.+K(x_s,x_s,c_s)\right)=g(x_s),\quad s=2,3,4,\ldots,n.
\end{aligned} \tag{18}$$

Proposition 4. *Given equation (1) and that $f(x)$, $g(x)\in C[a,b]$, $f'(x)$ and $g'(x)$ exist and are bounded in $[a,b]$, $K(x,y,u)\in C[a,b]\times[a,b]\times[a,b]$ and $(\partial/\partial x)(K(x,y,u))$ and $(\partial/\partial y)(K(x,y,u))$ exist and are bounded in $[a,b]\times[a,b]\times[a,b]$. Furthermore, $K(x,y,u)$ satisfies the following condition:*

$$\left|\int_a^b(K(x,t,f(t))-K(x,t,u(t)))\mathrm{d}t\right|<LM\max_{x\in[a,b]}|f(x)-u(x)|, \tag{19}$$

where $|LM|<1$. Let n be an integer, $h=(b-a)/n$; let $x_i=a+ih$, $f_i=f(x_i)$, $i=0,1,2,\ldots,n.c_0,c_1,\ldots,c_n$ satisfies the nonlinear system (17):

$$f^*(x)=\sum_{k=0}^{n}c_iB_{1,h}(x-kh). \tag{20}$$

Then,

$$\left\| f^{*}(x) - f(x) \right\|_{[a,b]} = O\left(h^{2}\right), \tag{21}$$

where $f(x)$ is the exact solution of equation (1).

4.2. Method 2-V for Solving the Volterra Integral Equation. For more accurate solution, we apply $L_3(x/h)$. Again, we let $h = (b-a)/n$ and $x_i = a + ih$, $i = -1, 0, \ldots, n+1$

Furthermore, let $L_{3,h}(x) = L_3(x/h)$ be the cardinal spline given in Section 3, and

$$\begin{aligned} f(x) &= \sum_{k=-1}^{n+1} c_k L_{3,h}(x - x_k), K(x,t,y(t)), \\ K(x,t,y(t)) &= \sum_{i=-1}^{n+1} \sum_{j=-1}^{n+1} K\left(x_i, x_j, c_j\right) L_{3,h}(x - x_i) L_{3,h}\left(t - x_j\right), \\ g(x) &= \sum_{k=-1}^{n+1} g(x_k) L_{3,h}(x - x_k). \end{aligned} \tag{22}$$

Since the support of $L_{3,h}(x - x_{-1})$ and $L_{3,h}(x - x_{n+1})$ is wider than $[a,b]$, we need values that define

$$\begin{aligned} K\left(x_{-1}, x_j\right) &= 3K\left(x_0, x_j\right) - 3K\left(x_1, x_j\right) + K\left(x_2, x_j\right), \quad j = 0, 1, \ldots, n, \\ K(x_i, x_{-1}) &= 3K(x_i, x_0) - 3K(x_i, x_1) + K(x_i, x_2), \quad i = 0, 1, \ldots, n, \\ K(x_{-1}, x_{-1}) &= 3K(x_0, x_0) - 3K(x_1, x_0) + K(x_2, x_0) + 3K(x_0, x_1) - 3K(x_1, x_1) \\ &\quad + K(x_2, x_1) - (3K(x_0, x_2) - 3K(x_1, x_2) + K(x_2, x_2)), \\ g(x_{-1}) &= 3g(x_0) - 3g(x_1) + g(x_2), \\ K\left(x_{n+1}, x_j\right) &= 3K\left(x_n, x_j\right) - 3K\left(x_{n-1}, x_j\right) + K\left(x_{n-2}, x_j\right), \quad j = 0, 1, \ldots, n, \\ K(x_i, x_{n+1}) &= 3K(x_i, x_n) - 3K(x_i, x_{n-1}) + K(x_i, x_2), \quad i = 0, 1, \ldots, n, \\ K(x_{n+1}, x_{n+1}) &= 3K(x_n, x_n) - 3K(x_{n-1}, x_n) + K(x_{n-2}, x_n) + 3K(x_n, x_{n-1}) - 3K(x_{n-1}, x_{n-1}) \\ &\quad + K(x_{n-2}, x_{n-1}) - (3K(x_n, x_{n-2}) - 3K(x_{n-1}, x_{n-2}) + K(x_{n-2}, x_{n-2})), \\ g(x_{n+1}) &= 3g(x_n) - 3g(x_{n-1}) + g(x_{n-2}). \end{aligned} \tag{23}$$

Let $\{c_0, c_1, \ldots, c_n\}$ be the unknown coefficients to be determined and $c_{-1} = 3c_0 - 3c_1 + c_2$ and $c_{n+1} = 3c_n - 3c_{n-1} + c_{n-2}$. Plug into the integral equation (1); then, we have

$$\begin{aligned} &\sum_{k=-1}^{n+1} c_k L_{3,h}(x - x_k) - \lambda \int_a^x \sum_{i=-1}^{n+1} \sum_{j=-1}^{n+1} K\left(x_i, x_j, c_j\right) L_{3,h} \\ &\quad (x - x_i) L_{3,h}\left(t - x_j\right) \mathrm{d}t = \sum_{k=-1}^{n+1} g(x_k) L_{3,h}(x - x_k), \quad x \in [a,b]. \end{aligned} \tag{24}$$

Let $x = x_i$; we arrive at

$$\begin{aligned} c_s - \sum_{j=-1}^{n+1} K\left(x_s, x_j, c_j\right) \int_a^{x_s} L_{3,h}\left(t - x_j\right) \mathrm{d}t \\ = g(x_s), \quad s = 0, 1, 2, 3, 4, \ldots, n, \end{aligned} \tag{25}$$

which is still a relatively simple system of equations. For the convergence rate of solution of Volterra integral equation (1), we have a similar result.

Proposition 5. *Given that $f(x)$, $g(x) \in C^3[a,b]$, $f^{(4)}(x)$ and $g^{(4)}(x)$ exist and are bounded in $[a,b]$, $K(x,t,y) \in C^3([a,b] \times [a,b] \times [c,d])$. Furthermore, $K(x,t,y)$ satisfies the following condition:*

$$\left| \int_a^b (K(x,t,f(t)) - K(x,t,u(t))) \mathrm{d}t \right| < LM \max_{x \in [a,b]} |f(x) - u(x)|. \tag{26}$$

where $|LM| < 1$. Let n be an integer, $h = (b-a)/n$; let $x_i = a + ih$, $f_i = f(x_i)$, $i = 0, 1, 2, \ldots, n$. $c_0, c_1, \ldots, c_n$ satisfies system (35):

$$f^{*}(x) = \sum_{k=-1}^{n+1} c_k L_{3,h}(x - x_k). \tag{27}$$

Then,

$$\begin{aligned} \left\| f^{*}(x) - f(x) \right\|_{[a,b\%]} &= O\left(h^{3}\right), \\ f^{*}(x) - f(x)_{[a,b]} &= O\left(h^{3}\right), \end{aligned} \tag{28}$$

where $f(x)$ is the exact solution of equation (1).

5. Numerical Examples

Example 1 (from [1]). Solve

$$u(x) = f(x) + \int_0^x \frac{e^x u^2(t)}{1+e^{x+t}}\,\mathrm{d}t, \tag{29}$$

where $f(x) = e^{x/2} - \ln((1+e^{2x})/(1+e^x))$. For comparison, we found that the exact solution is $u(x) = e^{x/2}$.

To find the numerical solution in $[0,1]$, we let $h = 0.1$, $n = 10$, $x_i = ih$, $i = 0,1,2,\ldots,10$, $r(x,t) = (e^x/1 + e^{x+t})$, $K(x,t,u(t)) = (e^x \quad u^2(t)/1+e^{x+t}) = \sum_{k=0}^{10}\sum_{j=0}^{10} r(x_k, t_j)c_j^2 B_{1,h}\%(x-x_k)\cdot B_{1,h}(t-x_j)$, and $f(x) = \sum_{k=0}^{10} f(x_k)B_{1,h}(x-x_k)$, $u(x) = \sum_{k=0}^{10} c_k B_{1,h}(x-x_k)$. Plug into integral equation (29), and let $x = x_i$; we obtain the following nonlinear system:

$$c_i = f(x_i) + \int_0^{x_i} \sum_{j=0}^{10} r(x_i,t_j)c_j^2 \cdot B_{1,h}(t-x_j)\,\mathrm{d}t, \quad i = 0,1,2,\ldots,10. \tag{30}$$

Since it is a triangular system, which means, the first equation only contains c_0 and the ith equation only contains $c_0, c_1, \ldots, c_{n-1}$, $i = 0,1,2,\ldots,10$, it is relatively easy to solve; the solution is not unique because the quadratic nature c_0 is unique, so we choose solution c_1 that is close to c_0, and so on. We arrive at $[c_0,c_1,c_2,c_3,c_4,c_5,c_6,c_7,c_8,c_9,c_{10}] = [1, 1.05127, 1.10516, 1.16182, 1.221378, 1.28399, 1.34980, 1.41899, 1.49173, 1.568120, 1.64859]$, with error: $|c_i - e^{x_i/2}| < 1.5\times 10^{-4}$.

Let $h = (1/20)$, $n = 20, x_i = ih$, $i = 0,1,2,\ldots,20$, $r(x,t) = (e^x/1+e^{x+t})$, $K(x,t,u(t)) = (e^x u^2(t)/1+e^{x+t}) = \sum_{k=0}^{20}\sum_{j=0}^{20} r(x_k,t_j)c_j^2\ B_{1,h}(x-x_k)\cdot B_{1,h}(t-x_j)$, $f(x) = \sum_{k=0}^{20} f(x_k)B_{1,h}(x-x_k)$, and $u(x) = \sum_{k=0}^{20} c_k B_{1,h}(x-x_k)$; plug into integral equation (29) and let $x = x_i$; we obtain the following nonlinear system:

$$c_i = f(x_i) + \int_0^{x_i} \sum_{j=0}^{20} r(x_i,t_j)c_j^2 \cdot B_{1,h}(t-x_j)\,\mathrm{d}t, \quad i = 0,1,2,\ldots,20. \tag{31}$$

Since it is still a triangular system, it is relatively easy to solve; the solution is not unique because the quadratic nature c_0 is unique, so we choose solution c_1 that is close to c_0, and so on. We arrive at $[c_0,c_1,c_2,c_3,c_4,c_5,c_6,c_7,c_8,c_9,c_{10},c_{11},c_{12},c_{13},c_{14},c_{15},c_{16},c_{17},c_{18},c_{19},c_{20}] = [1, 1.025315, 1.051271, 1.077883, 1.105169, 1.133146, 1.161831, 1.191241, 1.221396, 1.252315, 1.284015, 1.316519, 1.349845, 1.384014, 1.419049, 1.454971, 1.491801, 1.529565, 1.568284, 1.607983, 1.648688]$ with error $< 3.6\times 10^{-5}$.

Example 2 (from [1]). Solve

$$u(x) = f(x) - \int_0^x \left(u^2(t) + u(t)\right)\mathrm{d}t, \tag{32}$$

where $f(x) = (3/2) - (1/2)e^{-2x}$ and the exact solution is $u(x) = e^{-x}$.

To find the numerical solution in $[0,1]$, we let $h = 0.1$, $n = 10$, $x_i = ih$, $i = 0,1,2,\ldots,10$, $r(x,t) = 1$, $K(x,t,u(t)) = \sum_{k=0}^{10}\sum_{j=0}^{10} r(x_k,t_j)(\ c_j^2 + c_j)B_{1,h}(x-x_k)\cdot B_{1,h}(t-x_j)$, $f(x) = \sum_{k=0}^{10} f(x_k)B_{1,h}(x-x_k)$,and $u(x) = \sum_{k=0}^{n+1} c_k B_{1,h}(x-x_k)$; plug into integral equation (32), and let $x = x_i$; we obtain the following nonlinear system:

$$c_i = f(x_i) - \int_0^{x_i} \sum_{j=0}^{10} r(x_i,t_j)\left(c_j^2 + c_j\right) \cdot B_{1,h}(t-x_j)\,\mathrm{d}t, \quad i = 0,1,2,\ldots,10. \tag{33}$$

It is a triangular system again, so it is relatively easy to solve. We arrive at $[c_0,c_1,c_2,c_3,c_4,c_5,c_6,c_7,c_8,c_9,c_{10}] = [1, 0.904602, 0.818183, 0.740144, 0.669608, 0.605795, 0.548075, 0.495864, 0.448631, 0.405902, 0.367245\ ]$, with the error: $|c_i - u(x_i)| < 8\times 10^{-4}$ (in the paper [1], the error was 10^{-3} for much smaller h).

Let $h = 0.05$, $n = 20$, $x_i = ih$, $i = 0,1,2,\ldots,20$, $r(x,t) = (\sin(x-t)+1)$, $f(x) = \cos x + (1/2)\sin x + (1/2)x\cos x$, $K(x,t,u(t)) = \sum_{k=\ 0}^{20}\sum_{j=0}^{10} r(x_k,t_j)(c_j)B_{1,h}(x-x_k)\cdot B_{1,h}(t-x_j)$, $f(x) = \sum_{k=0}^{20} f(x_k)B_{1,h}(x-x_k)$, and $u(x) = \sum_{k=0}^{20} c_k B_{1,h}(x-x_k)$; plug into integral equation (33) and let $x = x_i$; we obtain the following nonlinear system:

$$c_i = f(x_i) - \int_0^{x_i} \sum_{j=0}^{20} r(x_i,t_j)(c_j) \cdot B_{1,h}(t-x_j)\,\mathrm{d}t, \quad i = 0,1,2,\ldots,10. \tag{34}$$

We arrive at $[c_0,c_1,c_2,c_3,c_4,c_5,c_6,c_7,c_8,c_9,c_{10},c_{11},c_{12},c_{13},c_{14},c_{15},c_{16},c_{17},c_{18},c_{19},c_{20}] = [1, 0.951144, 0.904745, 0.860597, 0.818598, 0.778651, 0.740656, 0.704517, 0.670143, 0.637447, 0.606348, 0.576766, 0.548628, 0.521864, 0.496405, 0.472189, 0.449155, 0.427245, 0.406403, 0.386579, 0.367721]$ with error $<2\times 10^{-4}$.

Example 3 (from [3]). Solve $\int_0^x (\sin(x-t)+1)\cos(y(t))\mathrm{d}t = (1/2)x\sin x + \sin x$, $0 \le x \le 1$.

By solving $u(x) = \cos(y(x))$ first, it becomes a linear equation. To change it into Volterra integral equation of the second kind, we differentiate the equation and obtain the following:

$$u(x) + \int_0^x \cos(x-t)u(t)\mathrm{d}t = \cos x + \frac{1}{2}\sin x + \frac{1}{2}x\cos x. \tag{35}$$

To find the numerical solution in $[0,1]$, we let $h = 0.05$, $n = 20$, $x_i = ih$, $i = 0,1,2,\ldots,20$, $r(x,t) = \cos(x-t)$, $f(x) = \cos x + (1/2)\sin x + (1/2)x\cos x$, $K(x,t,u(t)) = \sum_{k=0}^{20}\sum_{j=0}^{20} r(x_k,t_j)(c_j)B_{1,h}(x-x_k)\cdot B_{1,h}(t-x_j)$, $f(x) = \sum_{k=0}^{20} f(x_k)B_{1,h}(x-x_k)$, and $u(x) = \sum_{k=0}^{20} c_k B_{1,h}(x-x_k)$; plug into integral equation (35), and let $x = x_i$; we obtain the following nonlinear system:

$$c_i = f(x_i) - \int_0^{x_i} \sum_{j=0}^{20} r(x_i,t_j)(c_j) \cdot B_{1,h}(t-x_j)\,\mathrm{d}t, \quad i = 0,1,2,\ldots,10. \tag{36}$$

We arrive at $[c_0,c_1,c_2,c_3,c_4,c_5,c_6,c_7,c_8,c_9,c_{10},c_{11},c_{12},c_{13},c_{14},c_{15},c_{16},c_{17},c_{18},c_{19},c_{20}] = [1, 0.999166, 0.994962, 0.989190, 0.979979, 0.969336, 0.955202, 0.939805, 0.920877,$

0.900891, 0.877347, 0.852984, 0.825046, 0.796563, 0.764495, 0.732193, 0.696299, 0.660518, 0.621139, 0.582251, 0.539763]. The error $|c_i - u(x_i)| < 5.4 \times 10^{-4}$.

Applying L_3, we still let $h = 0.1$, $n = 10$, $x_i = ih$, $i = 0, 1, 2, \ldots, 10$, $r(x,t) = (\sin(x-t) + 1)$, $f(x) = \cos x + (1/2)\sin x + (1/2)x\cos x$, $K(x,t,u(t)) = \sum_{k=-1}^{11}\sum_{j=-1}^{11} r(x_k,t_j)(c_j) L_{3,h}(x-x_k)\cdot L_{3,h}(t-x_j)$, $f(x) = \sum_{k=-1}^{11} f(x_k)L_{3,h}(x-x_k)$, and $u(x) = \sum_{k=-1}^{11} c_k L_{3,h}(x-x_k)$; plug into integral equation (35), and let $x = x_i$, we obtain the following nonlinear system:

$$\sum_{k=-1}^{11} c_k L_{3,h}(x-x_k) - \int_a^x \sum_{k=-1}^{11}\sum_{j=-1}^{11} r(x_k,t_j)c_j \cdot L_{3,h}(x-x_k)L_{3,h}(t-x_j)\mathrm{d}t = \sum_{k=-1}^{n+1} g(x_k)L_{3,h}(x-x_k), \quad x \in [a,b], \tag{37}$$

where $c_{-1} = 3c_0 - 3c_1 + c_2$ and $c_{n+1} = 3c_n - 3c_{n-1} + c_{n-2}$; we achieve $[c_0, c_1, c_2, c_3, c_4, c_5, c_6, c_7, c_8, c_9, c_{10}] = [1, 0.99501, 0.98007, 0.95534, 0.92107, 0.87759, 0.82534, 0.76485, 0.69671, 0.62162, 0.54031]$ with error $|c_i - u(x_i)| < 1.2 \times 10^{-5}$.

We use the same process, and let $h = 0.05$ and $x_i = ih$, $i = 0, 1, 2, \ldots, 20$, the result is $[c_0, c_1, c_2, c_3, c_4, c_5, c_6, c_7, c_8, c_9, c_{10}, c_{11}, c_{12}, c_{13}, c_{14}, c_{15}, c_{16}, c_{17}, c_{18}, c_{19}, c_{20}] = [1.0, 0.99875, 0.995, 0.98877, 0.98007, 0.96891, 0.95534, 0.93937, 0.92106, 0.90045, 0.87758, 0.85252, 0.82534, 0.79608, 0.76484, 0.73169, 0.69671, 0.65998, 0.62161, 0.58168, 0.5403]$ with error: $< 4.6 \times 10^{-4}$.

Example 4 (from [3]). $\int_0^x e^{x-t}\ln(y(t))\mathrm{d}t = e^x - x - 1$, $0 \le x \le 1$. $(y(x) = e^x)$

We change it to the linear Volterra integral equation of second kind:

$$w(x) + \int_0^x e^{x-t} w(t)\mathrm{d}t = e^x - 1, \quad 0 \le x \le 1, \tag{38}$$

where $w(t) = \ln(y(t))$.

Let $h = 0.1$, $n = 10$, $x_i = ih$, $i = 0, 1, 2, \ldots, 10$, $r(x,t) = e^{x-t}$, $f(x) = e^x - 1$, $K(x,t,u(t)) = \sum_{k=0}^{10}\sum_{j=0}^{10} r(x_k,t_j)(c_j) B_{1,h}(x-x_k)\cdot B_{1,h}(t-x_j)$, $f(x) = \sum_{k=0}^{10} f(x_k)B_{1,h}(x-x_k)$, and $u(x) = \sum_{k=0}^{n+1} c_k B_{1,h}(x-x_k)$; plug into integral equation (38), and let $x = x_i$; we obtain the following nonlinear system:

$$c_i = f(x_i) - \int_0^{x_i} \sum_{j=0}^{10} r(x_i,t_j)(c_j)\cdot B_{1,h}(t-x_j)\mathrm{d}t, \quad i = 0, 1, 2, \ldots, 10. \tag{39}$$

We arrive at $[c_0, c_1, c_2, c_3, c_4, c_5, c_6, c_7, c_8, c_9, c_{10}] = [0, 0.100163, 0.200317, 0.300463, 0.400601, 0.500730, 0.600851, 0.700964, 0.801068, 0.901164, 1.00125]$. The error $|c_i - u(x_i)| < 4 \times 10^{-3}$.

Using the same process, let $h = 0.05$, $n = 20$, $x_i = ih$, $i = 0, 1, 2, \ldots, 20$, $r(x,t) = e^{x-t}$, $f(x) = e^x - x - 1$, $K(x,t,u(t)) = \sum_{k=0}^{20}\sum_{j=0}^{20} r(x_k,t_j)(c_j)B_{1,h}(x-x_k)\cdot B_{1,h}(t-x_j)$, $f(x) = \sum_{k=0}^{20} f(x_k)B_{1,h}(x-x_k)$, and $u(x) = \sum_{k=0}^{n+1} c_k B_{1,h}(x-x_k)$; plug into integral equation (38), and let $x = x_i$; we obtain the following nonlinear system:

$$c_i = f(x_i) - \int_0^{x_i} \sum_{j=0}^{20} r(x_i,t_j)(c_j)\cdot B_{1,h}(t-x_j)\mathrm{d}t, \quad i = 0, 1, 2, \ldots, 20. \tag{40}$$

We arrive at $[c_{01}, c_2, c_3, c_4, c_5, c_6, c_7, c_8, c_9, c_{10}, c_{11}, c_{12}, c_{13}, c_{14}, c_{15}, c_{16}, c_{17}, c_{18}, c_{19}, c_{20}] = [0, 0.0500206, 0.100041, 0.150060, 0.200079, 0.250098, 0.300116, 0.350133, 0.400150, 0.450166, 0.50018, 0.550198, 0.600213, 0.650227, 0.700241, 0.750254, 0.800267, 0.850279, 0.900291, 0.950302, 1.00031]$. The error: $|c_i - u(x_i)| < 8.5 \times 10^{-4}$.

Applying L_3, we still let $h = 0.05$, $n = 20$, $x_i = ih$, $i = 0, 1, 2, \ldots, 20$, $r(x,t) = \sin(x-t) + 1 f(x) = \cos x + (1/2)\sin x + (1/2)x\cos x$, $K(x,t,u(t)) = \sum_{k=-1}^{21}\sum_{j=-1}^{21} r(x_k,t_j)(c_j) L_{3,h}(x-x_k)\cdot L_{3,h}(t-x_j)$, $f(x) = \sum_{k=-1}^{21} f(x_k)L_{3,h}(x-x_k)$, and $u(x) = \sum_{k=-1}^{21} c_k L_{3,h}(x-x_k)$; plug into integral equation (38), and let $x = x_i$; we obtain the following nonlinear system:

$$\sum_{k=-1}^{21} c_k L_{3,h}(x-x_k) - \int_a^x \sum_{k=-1}^{21}\sum_{j=-1}^{21} r(x_k,t_j)c_j \cdot L_{3,h}(x-x_k)L_{3,h}(t-x_j)\mathrm{d}t = \sum_{k=-1}^{21} g(x_k)L_{3,h}(x-x_k), \quad x \in [a,b], \tag{41}$$

where $c_{-1} = 3c_0 - 3c_1 + c_2$ and $c_{n+1} = 3c_n - 3c_{n-1} + c_{n-2}$; we achieve $[c_0, c_1, c_2, c_3, c_4, c_5, c_6, c_7, c_8, c_9, c_{10}, c_{11}, c_{12}, c_{13}, c_{14}, c_{15}, c_{16}, c_{17}, c_{18}, c_{19}, c_{20}] = [0.0, 0.04, 0.999998, 0.09999996, 0.1499999, 0.1999999, 0.2499999, 0.2999999, 0.3499999, 0.39999986, 0.44999984, 0.49999982, 0.54999980, 0.59999979, 0.64999977, 0.69999976, 0.74999974, 0.79999972, 0.84999971, 0.89999969, 0.94999968, 0.99999967]$. The error $|c_i - u(x_i)| < 3.5 \times 10^{-7}$ (in paper [1], the error was 10^{-4} for a much smaller $h = (1/32)$, they achieve the error 4.7×10^{-7} with $h = (1/512)$).

6. Conclusion

The proposed method is a simple and effective procedure for solving nonlinear Volterra integral equations of the second kind. The methods can be adapted easily to the Volterra integral equations of the first kind. The methods can also be extended to the Fredholm and Volterra integral equations of the first kind or the second kind, where the integral is on an infinite set. When the higher degree cardinal splines are applied to nonlinear integral equations, the resulting system of coefficients will be a little more complicated nonlinear

system, which takes more time and effort to solve. Compared with the recent papers [1] and [3], our method is more effective and efficient. Furthermore, we could use higher dimensional spline functions to solve higher dimensional integral equations.

Data Availability

The data used to support the findings of this study are available from the corresponding author upon request.

Conflicts of Interest

The authors declare that there are no conflicts of interest regarding the publication of this paper.

Acknowledgments

The work was funded by the Fostering Master's Degree Empowerment Point Project of Hefei University under Grant no. 2018xs03 and the Project Foundation of Scientific Research, Education Department of Anhui Province, under Grant no. KJ2019A0846. This research was partially supported by the research funds of the University of La Verne. Ms. Jiahuan Huang was an undergraduate student at the University of La Verne, who did some numerical calculations. The authors thank the organizers of the 8th International Conference on Computational Methods for accepting this paper for presentation.

References

[1] I. Aziz and Siraj-ul-Islam, "New algorithms for the numerical solution of nonlinear Fredholm and Volterra integral equations using Haar wavelets," *Journal of Computational and Applied Mathematics*, vol. 239, pp. 333–345, 2013.

[2] A. D. Polyanin, *Handbook of Integral Equations*, CRC Press LLC, Boca Raton, FL, USA, 1998.

[3] I. Singh and S. Kumar, "Haar wavelet method for some nonlinear Volterra integral equations of the first kind," *Journal of Computational and Applied Mathematics*, vol. 292, pp. 541–552, 2016.

[4] X. Liu and J. Xie, "Numerical methods for solving systems of Fredholm integral equations with cardinal splines," *AIP Conference Proceedings*, vol. 1637, p. 590, 2014.

[5] X. Liu, Z. Liu, and J. Xie, "Solving systems of Volterra integral equations with cardinal splines," *Journal of Applied Mathematics and Physics (JAMP)*, vol. 3, no. 11, pp. 1422–1430, 2015.

[6] J.-B. Liu, C. Wang, S. Wang, and B. Wei, "Zagreb indices and multiplicative zagreb indices of eulerian graphs," *Bulletin of the Malaysian Mathematical Sciences Society*, vol. 42, no. 1, pp. 67–78, 2019.

[7] I. J. Schoenberg, "Contributions to the problem of approximation of equidistant data by analytic functions," *Quarterly of Applied Mathematics*, vol. 4, pp. 45–99, 1946.

[8] C. K. Chui, *Multivariate Splines*, SIAM, Philadelphia, PA, USA, 1988.

[9] X. Liu, "Bivariate cardinal spline functions for digital signal processing," in *Trends in Approximation Theory*, K. Kopotum, T. Lyche, and M. Neamtu, Eds., pp. 261–271, Vanderbilt University, Nashville, TN, USA, 2001.

[10] X. Liu, "Univariate and bivariate orthornormal splines and cardinal splines on compact supports," *Journal of Computational and Applied Mathematics*, vol. 195, no. 1-2, pp. 93–105, 2006.

[11] X. Liu, "Interpolation by cardinal exponential splines," *The Journal of Information and Computational Science*, vol. 4, no. 1, pp. 179–194, 2007.

[12] X. Liu, "Interpolation by cardinal trigonometric splines," *International Journal of Pure and Applied Mathematics*, vol. 40, no. 1, pp. 115–122, 2007.

[13] I. Schoenberg, "On trigonometric spline functions," *Indiana University Mathematics Journal*, vol. 13, no. 5, pp. 795–825, 1964.

Hindawi
Journal of Chemistry
Volume 2020, Article ID 4860327, 4 pages
https://doi.org/10.1155/2020/4860327

Research Article

Note on the Reformulated Zagreb Indices of Two Classes of Graphs

Tongkun Qu, Mengya He, Shengjin Ji, and Xia Li

School of Science, Shandong University of Technology, Zibo, Shandong 255000, China

Correspondence should be addressed to Shengjin Ji; jishengjin2013@163.com

Received 6 October 2019; Revised 26 November 2019; Accepted 5 December 2019; Published 10 February 2020

Academic Editor: Juan L. G. Guirao

The reformulated Zagreb indices of a graph are obtained from the original Zagreb indices by replacing vertex degrees with edge degrees, where the degree of an edge is taken as the sum of degrees of its two end vertices minus 2. In this paper, we obtain two upper bounds of the first reformulated Zagreb index among all graphs with p pendant vertices and all graphs having key vertices for which they will become trees after deleting their one key vertex. Moreover, the corresponding extremal graphs which attained these bounds are characterized.

1. Introduction

Some constants are used to characterize some properties of the graph of a molecule, which are usually called topological indices. One of the most famous topological indices is the Randić index (Randić connectivity index), proposed by Randic [1] in 1975 (for details, see [2, 3]). Soon later, a lot of mathematicians focused on the structure and application of Randić connectivity index. In 1977, Kier and Kall [4] extended the concept of molecular connectivity index and defined the zeroth-order general Randić index. Note that the first Zagreb index is the zeroth-order general Randić index for $\alpha = 2$. For more results of the zeroth-order general Randić index and first Zagreb index, we refer to [5, 6, 7]. In addition, Zagreb indices have been explored as molecular descriptors in QSPR and QSAR (see [8, 9, 10, 11, 12, 13, 14, 15, 16, 17–20]). For a graph G, the first Zagreb index M_1 and the second Zagreb index M_2 [21] are defined as

$$\begin{aligned} M_1 = M_1(G) &= \sum_{v\in V(G)} d(v)^2, \\ M_2 = M_2(G) &= \sum_{uv\in E} d(u)d(v). \end{aligned} \tag{1}$$

For an edge $e = uv$, the edge degree of e is referred as the sum of degrees of its two end vertices minus 2 and is denoted by $d(e) = d(u) + d(v) - 2$. $e \sim f$ indicates the edges e and f are adjacent.

For a given G, let $L(G)$ be its line graph. Observe that two edges are adjacent in G if and only if the corresponding two vertices are adjacent in $\mathrm{L}(\mathrm{G})$. The edge version of the Zagreb indices [22], motivated by the above property, was proposed by Miličeviv et al. in 2004 through the edge degree instead of vertex degree, that is,

$$\begin{aligned} \mathrm{EM}_1(G) &= \sum_{e\in E} d(e)^2, \\ \mathrm{EM}_2(G) &= \sum_{e\sim f} d(e)\cdot d(f). \end{aligned} \tag{2}$$

The reformulated Zagreb indices, particularly its bounds, have attracted recently the attention of many mathematicians (see, [12, 22–30]).

In order to describe this more clearly in the sequel, we now introduce some notations. Let G_n^p be the set of connected graphs with $p(\geq 2)$ pendant vertices. Evidently, if $G \in \mathrm{G}_n^p$, then there will be a connected subgraph H_0 with order $n - p$ for which G can be reconstructed by linking p vertices to some vertices H_0. For convenience, we call H_1 as the *core* of G. Since H_0 is connected, it has two extremal cases, i.e., $H_0 \cong K_{n-p}$ and $H_0 \cong T_{n-p}$. Let $A_n \in \mathrm{G}_n^p$ be the graph with core K_{n-p}, and let all pendants of A_n have a common neighbor in K_{n-p}. Let B_n be the set of all graphs for which each of its element will be changed to a tree by deleting some of its vertex. That is to say, if G belongs to B_n, then there is a vertex $v_0 \in V(G)$ such that $G - v_0$ is

isomorphic to a tree. We call the vertex v_0 as the *key* of G. Note that, for a given graph, its key may not be unique, e.g., G is a cycle, and every vertex is a key of G. Let B_n be the graph with two vertices having degree $n-1$ and other vertices owning degree 2. Obviously, $B_n \in \mathrm{B}_n$ and the two vertices possessing degree $n-1$ are keys.

In this paper, we determined the two upper bounds of reformulated Zagreb indices of two kinds of graphs and characterized completely extremal graphs.

2. Main Results

In the section, we will research the maximal properties regarding the reformulated Zagreb index on G_n^p and B_n, respectively. Meanwhile, the graphs attaining the bounds are obtained.

Based on the definition of EM_1, the following result holds obviously.

Proposition 1. *Let G be a connected graph.*

(i) If $e \in E(G)$, then $EM_1(G) > EM_1(G-e)$

(ii) If $e \notin E(G)$, then $EM_1(G) < EM_1(G+e)$

Lemma 1. *G and G' denote the two graphs as shown in Figure 1, and G' is regarded as the graph from G by shifting all pendants of v_s to v_t. If $d_G(v_t) \geq d_G(v_s)$ and $d_G(v_s) \geq n-p$, then $EM_1(G') > EM_1(G)$.*

Proof. Let G and G' be the two graphs as shown in Figure 1, and v_s and v_t be two vertices owning ℓ pendants and k pendants, respectively. The common neighbors of v_s and v_t are labeled as $u_1, u_2, \ldots, u_{n-p-2}$, and these $n-p$ vertices induce a complete subgraph K_{n-p} of G. We write $r = n-p-2$ for short. Obviously, $d_G(v_t) = k+r+1$, $d_G(v_s) = \ell+r+1$, $d_{G'}(v_t) = k+\ell+r+1$, and $d_{G'}(v_s) = r+1$. In order to show $\mathrm{EM}_1(G') > \mathrm{EM}_1(G)$, we can confirm that $\mathrm{EM}_1(G') - \mathrm{EM}_1(G) > 0$. In fact, we arrive at

$$\begin{aligned}
\mathrm{EM}_1(G') - \mathrm{EM}_1(G) &= \sum_{i=1}^{r} \left(d_{G'}(v_t) + d_{G'}(u_i) - 2\right)^2 + \sum_{i=1}^{r} \left(d_{G'}(v_s) + d_{G'}(u_i) - 2\right)^2 \\
&\quad + \sum_{i=1}^{k+\ell} \left(d_{G'}(v_t) - 1\right)^2 + \left(d_{G'}(v_t) + d_{G'}(v_s) - 2\right)^2 \\
&\quad - \sum_{i=1}^{r} \left(d_G(v_t) + d_G(u_i) - 2\right)^2 - \sum_{i=1}^{r} \left(d_G(v_s) + d_G(u_i) - 2\right)^2 \\
&\quad - \sum_{i=1}^{k} \left(d_G(v_t) - 1\right)^2 - \sum_{i=1}^{\ell} \left(d_G(v_s) - 1\right)^2 - \left(d_G(v_t) + d_G(v_s) - 2\right)^2 \\
&= r(2r)^2 + r(k+\ell+2r)^2 + (k+\ell)(k+\ell+r)^2 \\
&\quad - r(\ell+2r)^2 + r(k+2r)^2 + k(k+r)^2 + \ell(\ell+r)^2 \\
&> 2rk\ell > 0.
\end{aligned} \tag{3}$$

The proof hence is complete. □

Theorem 1. *If $G \in \mathrm{G}_n^p$, then $EM_1(G) \leq \binom{n-p-1}{2}(2n-2p-4)^2 + (n-p-1)(2n-p-4)^2 + p(n-2)^2$. Furthermore, the above equality is attained only if $G \cong A_n$.*

Proof. Let G be a graph with n vertices and p pendants and having the maximum with respect to EM_1. Let H_0 denote the core of G. Clearly, H_0 is connected. In fact, $H_0 \cong K_{n-p}$. On the contrary, suppose that H_0 is not a complete subgraph of G. That is to say, there are some nonadjacent vertex pairs in H_0. After connecting these pairs of H_0, we obtain a new graph G_1. Evidently, $G_1 \in \mathrm{G}_n^p$. From Proposition 1, $\mathrm{EM}_1(G_1) > \mathrm{EM}_1(G)$, which is contradicted with the maximum of G.

We now show that all pendants of G are adjacent to the same vertex in H_0. If not, assume that there are two vertices $v_s, v_t \in V(H_0)$ possessing pendants. In other words, $d(v_s), d(v_t) \geq n-p$. We obtain a new graph $G' \in \mathrm{G}_n^p$ by removing all pendants of v_s and joining them to v_t. Then, by Lemma 1, $\mathrm{EM}_1(G') > \mathrm{EM}_1(G)$. Hence, all pendants in G own a common neighbor. In other words, $G \cong A_n$. In addition, by calculation,

$$\begin{aligned}
\mathrm{EM}_1(A_n) = &\binom{n-p-1}{2}(2n-2p-4)^2 + (n-p-1) \\
&\cdot (2n-p-4)^2 + p(n-2)^2.
\end{aligned} \tag{4}$$

Therefore, we complete the proof. □

Lemma 2. *Let G be a graph with key v_0, and let $T = G - v_0$ be a tree having an edge $e = v_s v_t$ with $d_T(v_t) \geq d_T(v_s) \geq 2$. If*

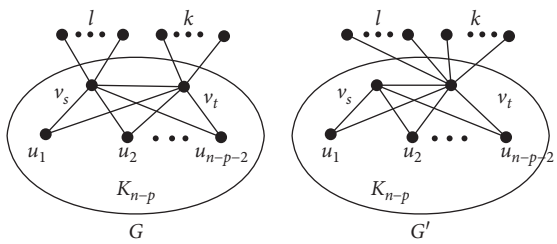

Figure 1: G and G' used in Lemma 1.

G' is obtained by deleting the ℓ branches of v_s and adding them to v_t, then $EM_1(G') > EM_1(G)$.

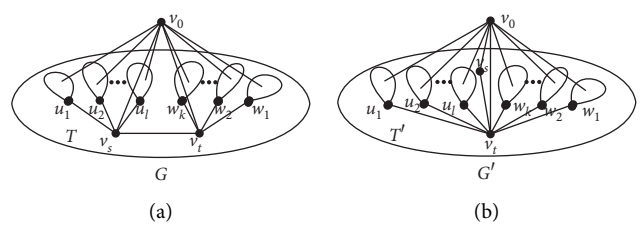

Figure 2: G and G' used in Lemma 2.

Proof. Let G and G' are two graphs with n vertices as shown in Figure 2. Suppose that $d_T(v_t) \geq d_T(v_s) \geq 2$. It is clear that $d_T(v_s) = \ell + 1$, $d_T(v_t) = k + 1$, $d_{T'}(v_t) = d_T(v_t) + \ell$, and $d_{T'}(v_s) = 1$. We now consider the difference $\mathrm{EM}_1(G') - \mathrm{EM}_1(G)$ and deduce that

$$\begin{aligned}
\mathrm{EM}_1(G') - \mathrm{EM}_1(G) &= \sum_{i=1}^{k} \left(d_{G'}(v_t) + d_{G'}(w_i) - 2\right)^2 + \sum_{i=1}^{\ell} \left(d_{G'}(v_t) + d_{G'}(u_i) - 2\right)^2 \\
&\quad + \left(d_{G'}(v_t) + d_{G'}(v_s) - 2\right)^2 + \left(d_{G'}(v_0) + d_{G'}(v_s) - 2\right)^2 \\
&\quad + \left(d_{G'}(v_t) + d_{G'}(v_0) - 2\right)^2 - \left(d_G(v_t) + d_G(v_0) - 2\right)^2 \\
&\quad - \left(d_G(v_t) + d_G(v_s) - 2\right)^2 - \left(d_G(v_0) + d_G(v_s) - 2\right)^2 \\
&\quad - \sum_{i=1}^{k} \left(d_G(v_t) + d_G(w_i) - 2\right)^2 - \sum_{i=1}^{\ell} \left(d_G(v_s) + d_G(u_i) - 2\right)^2 \\
&\quad > (n-1)^2 + (k + \ell + n - 1)^2 - (n - 1 + \ell)^2 - (k + n - 1)^2 \\
&= 2k\ell > 0.
\end{aligned} \tag{5}$$

Therefore, the result holds. □

Theorem 2. *Let $G \in \mathrm{B}_n$. Then, $EM_1(G) \leq 2n^3 - 4n^2 - 10n + 12$ with equality if and only if $G \cong B_n$.*

Proof. Let G be a graph in B_n. Hence, there is a vertex $v_0 \in V(G)$ such that $T = G - v_0$ is a tree with $n - 1$ vertices. Assume that G is the maximal graph with respect to EM_1. We firstly claim that $d_G(v_0) = n - 1$. Otherwise, if $G - v_0$ is a tree for $v_0 \in V(G)$, we have $d_G(v_0) < n - 1$. Let the new graph G_1 is obtained from G by connecting v_0 to all of its nonadjacent vertices in G. Hence, by Proposition 1, $\mathrm{EM}_1(G_1) > \mathrm{EM}_1(G)$, which is contradicted with the choice of G.

We next claim that the tree T is isomorphic to a star with $n - 1$ vertices. If not, we find an edge $e = v_s v_t$ in $E(T)$ such that $d_T(v_t), d_T(v_s) \geq 2$. Suppose now that $d_T(v_t) \geq d_T(v_s)$. From Lemma 2, we will obtain a new graph $G_2 \in \mathrm{B}_n$ and $\mathrm{EM}_1(G_2)$ is more than $\mathrm{EM}_1(G)$, a contradiction. Based on the above discussion, we deduce that $G \cong B_n$. Furthermore, by direct calculation, $\mathrm{EM}_1(B_n) = 2n^3 - 4n^2 - 10n + 12$.

Consequently, the proof is complete. □

Data Availability

The data used to support the findings of this study are included within the article.

Conflicts of Interest

The authors declare that they have no conflicts of interest.

Acknowledgments

This work was supported by the National Natural Science Foundation of China (Grant nos. 11401348 and 11561032), Shandong Provincial Natural Science Foundation (no. ZR201807061145), and Postdoctoral Science Foundation of China.

References

[1] M. Randic, "Characterization of molecular branching," *Journal of the American Chemical Society*, vol. 97, no. 23, pp. 6609–6615, 1975.

[2] I. Gutman, B. Furtula, and C. Elphick, "Three new/old vertex-degree-based topological indices," *MATCH Communications*

in Mathematical and in Computer Chemistry, vol. 72, pp. 617–632, 2014.

[3] J. Rada and R. Cruz, "Vertex-degree-based topological indices over graphs," *MATCH Communications in Mathematical and in Computer Chemistry*, vol. 72, pp. 603–616, 2014.

[4] L. B. Kier and L. H. Hall, *Molecular Connectivity in Chemistry and Drug Research*, Academic Press, New York, NY, USA, 1976.

[5] X. Li and Y. Shi, "A survey on the Randić index," *MATCH Communications in Mathematical and in Computer Chemistry*, vol. 59, no. 1, pp. 127–156, 2008.

[6] X. Li and Y. Shi, "On a relation between the Randić index and the chromatic number," *Discrete Mathematics*, vol. 310, no. 17-18, pp. 2448–2451, 2010.

[7] Y. Shi, "Note on two generalizations of the Randić index," *Applied Mathematics and Computation*, vol. 265, pp. 1019–1025, 2015.

[8] H. Abdo, D. Dimitrov, T. Reti, and D. Stevanović, "Estimating the spectral radius of a graph by the second Zagreb index," *MATCH Communications in Mathematical and in Computer Chemistry*, vol. 72, no. 3, pp. 741–751, 2014.

[9] D. de Caen, "An upper bound on the sum of squares of degrees in a graph," *Discrete Mathematics*, vol. 185, no. 1–3, pp. 245–248, 1998.

[10] I. Gutman, "An exceptional property of first Zagreb index," *MATCH Communications in Mathematical and in Computer Chemistry*, vol. 72, pp. 733–740, 2014.

[11] A. Hamzeh and T. Reti, "An analogue of Zagreb index inequality obtained from graph irregularity measures," *MATCH Communications in Mathematical and in Computer Chemistry*, vol. 72, no. 3, pp. 669–683, 2014.

[12] S. Ji and S. Wang, "On the sharp lower bounds of Zagreb indices of graphs with given number of cut vertices," *Journal of Mathematical Analysis and Applications*, vol. 458, no. 1, pp. 21–29, 2018.

[13] R. Kazemi, "The second Zagreb index of molecular graphs with tree structure," *MATCH Communications in Mathematical and in Computer Chemistry*, vol. 72, no. 3, pp. 753–760, 2014.

[14] H. Lin, "Vertices of degree two and the first Zagreb index of trees," *MATCH Communications in Mathematical and in Computer Chemistry*, vol. 72, pp. 825–834, 2014.

[15] A. Vasilyev, R. Darda, and D. Stevanović, "Trees of given order and independence number with minimal first Zagreb index," *MATCH Communications in Mathematical and in Computer Chemistry*, vol. 72, pp. 775–782, 2014.

[16] K. Xu, K. C. Das, and S. Balachandran, "Maximizing the Zagreb indices of (n, m)-graphs," *MATCH Communications in Mathematical and in Computer Chemistry*, vol. 72, pp. 641–654, 2014.

[17] C. S. Edwards, "The largest vertex degree sum for a triangle in a graph," *Bulletin of the London Mathematical Society*, vol. 9, no. 2, pp. 203–208, 1977.

[18] A. Ilić and D. Stevanović, "On comparing Zagreb indices," *MATCH Communications in Mathematical and in Computer Chemistry*, vol. 62, pp. 681–687, 2009.

[19] J. B. Liu, J. Zhao, and Z. X. Zhu, "On the number of spanning trees and normalized Laplacian of linear octagonal-quadrilateral networks," *International Journal of Quantum Chemistry*, vol. 119, no. 17, Article ID e25971, 2019.

[20] J.-B. Liu, J. Zhao, and Z.-Q. Cai, "On the generalized adjacency, Laplacian and signless Laplacian spectra of the weighted edge corona networks," *Physica A: Statistical Mechanics and Its Applications*, vol. 540, Article ID 123073, 2020.

[21] I. Gutman and N. Trinajstić, "Graph theory and molecular orbitals. Total φ-electron energy of alternant hydrocarbons," *Chemical Physics Letters*, vol. 17, no. 4, pp. 535–538, 1972.

[22] A. Milicević, S. Nikolić, and N. Trinajstić, "On reformulated Zagreb indices," *Molecular Diversity*, vol. 8, no. 4, pp. 393–399, 2004.

[23] D. Andrica and C. Badea, "Grüss' inequality for positive linear functionals," *Periodica Mathematica Hungarica*, vol. 19, no. 2, pp. 155–167, 1988.

[24] N. De, "Some bounds of reformulated Zagreb indices," *International Journal of Applied Mathematical Sciences*, vol. 6, no. 101, pp. 5005–5012, 2012.

[25] B. Furtula and I. Gutman, "A forgotten topological index," *Journal of Mathematical Chemistry*, vol. 53, no. 4, pp. 1184–1190, 2015.

[26] A. Ilić and B. Zhou, "On reformulated Zagreb indices," *Discrete Applied Mathematics*, vol. 160, pp. 204–209, 2012.

[27] D. S. Mitrinović and P. M. Vasić, *Analytic Inequalities*, Springer-Verlag, Berlin, Germany, 1970.

[28] D. S. Mitrinović, J. E. Pecarić, and A. M. Fink, *Classical and New Inequalities in Analysis*, Kluwer Academic Publishers, Dordrecht, Netherlands, 1993.

[29] G. Su, L. Xiong, L. Xu, and B. Ma, "On the maximum and minimum first reformulated Zagreb index of graphs with connectivity at most k," *Filomat*, vol. 25, no. 4, pp. 75–83, 2011.

[30] B. Zhou and N. Trinajstić, "Some properties of the reformulated Zagreb indices," *Journal of Mathematical Chemistry*, vol. 48, no. 3, pp. 714–719, 2010.

Hindawi
Journal of Chemistry
Volume 2020, Article ID 6161343, 10 pages
https://doi.org/10.1155/2020/6161343

Research Article

An Integrated Slacks-Based Measure of Super-Efficiency with Input Saving and Output Surplus Scaling Factors and its Application in Paper Chemical Mills

Dong Guo[1] and Zheng-Qun Cai[2]

[1]*School of Mathematics and Physics, Anhui Jianzhu University, Hefei 230601, China*
[2]*School of Foreign Studies, Anhui Jianzhu University, Hefei 230601, China*

Correspondence should be addressed to Zheng-Qun Cai; caizhengqun1983@163.com

Received 29 October 2019; Accepted 18 January 2020; Published 8 February 2020

Guest Editor: Shaohui Wang

Data envelopment analysis (DEA) as a nonparametric programming approach has been widely extended and applied in many areas. Conventional DEA models can well measure the efficiency of inefficient decision-making units (DMUs) but cannot further discriminate the efficient DMUs. A lot of methods are proposed to address this problem. One of the most important methods is the slacks-based measure of super-efficiency model (S-SBM model) developed by Tone in 2002. However, the projection for a DMU on the efficient frontier identified by S-SBM model may not be strongly Pareto-efficient that makes the super-efficiency score misestimated. This paper revises the usual slacks-based measure of super-efficiency by incorporating input saving and output surplus scaling factors into the objection function for measuring DMUs. We integrate SBM model and S-SBM model effectively and yield input saving and output surplus scaling factors as well as input and output slacks under only one integrated model. According to the study, the projection reference point identified by our method is strongly Pareto-efficient. Meanwhile, how each decision variable influences the efficiency score for a specific DMU is revealed and illustrated through two numerical examples and an empirical study in paper chemical mills.

1. Introduction

Over the past several decades, the data envelopment analysis (DEA) initially proposed by Charnes et al. has proved to be an effective data-oriented programming method for measuring the efficiencies of a group of homogenous decision making units (DMUs) [1]. The technique of DEA depicts a best-practice production efficient frontier formed by observed DMUs and provides a benchmark or reference point on this frontier for each DMU to compute its efficiency score. Using DEA does not assume any production function or presuppose any specific weight restriction to inputs and outputs. So in the recent years, DEA has been widely extended and applied in many fields [2]. The efficiency value obtained by the classic CCR model indicates how efficiently a DMU has performed when compared with other DMUs so as to determine its efficient level within the group of all DMUs. The CCR model works as a radial model and has both input- and output-orientation styles which permits the DMU under assessment to proportionally reduce all its inputs for producing its given outputs, or to proportionally expand all its outputs by using its given inputs.

However, when the evaluation target group includes a considerable number of DMUs, more than one unit will always get the same efficient score of unity. In this case, the CCR model cannot further differentiate the efficiency performances of these DMUs and cannot provide more recognizing information on them. For example, it does not detect whether the evaluated DMU is weakly efficient. As Chen pointed out, the "radial" efficiency model may make some DMU measured against a weakly efficient point on the efficient frontier in the production possibility set [3].

Specifically, the weakly efficient reference point for the current evaluated DMU may still have a positive amount of input excesses or output shortfalls, for it is not the strongly Pareto-efficient reference point. From the view of DEA, the efficiency score obtained by the weakly efficient reference point makes the evaluated DMU misestimated with respect to its strongly Pareto-efficient reference point on the efficient frontier.

So far, many methods have been developed and studied in order to enhance the cognition levels and discrimination abilities to distinguish DMUs, such as the cross-efficiency technique [4, 5], the benchmark ranking method, and others [6]. These newly developed methods are mainly built to solve problems resulting from the original CCR model in a certain aspect. Therein, Andersen and Petersen creatively developed the first radial super-efficiency model under the assumption of constant returns to scale (CRS) to reassess the efficient DMUs under CCR model [7]. They exclude the DMUs being evaluated from the reference set by the envelopment linear program so as to retrieve the called super-efficiency scores for those efficient DMUs, while, for the variable returns to scale (VRS) super-efficiency model, Seiford and Zhu found that the problem of infeasibility may occur [8]. Chen further ascribed the sources of super-efficiency for an efficient DMU to its achieved positive amounts of input saving and output surplus regarding its efficient reference point on the super-efficiency frontier [9]. Cook et al. derived a revised VRS super-efficiency model which could generate optimal solutions for some efficient DMUs that is infeasible in the original VRS super-efficiency model [10]. The resulting super-efficiency scores gained by their model could be described from both inputs and outputs aspects to some degree. Later, Lee et al. introduced a two-stage process to address the infeasibility issue under VRS [11]. Next, this two-stage process was merged into a single linear program by the work of Chen and Liang [12]. More recently, Lee and Zhu settled the infeasibility caused by zero input data and decompose the acquired super-efficiency score into three indices: radial efficiency index, input saving index, and output surplus index [13].

The above super-efficiency models are all of a radial type and they all have both input- and output-oriented forms. Tone built a popular nonradial model named slacks-based measure (SBM), which uses a fractional objection function depending on input and output slacks instead of a simple radial efficiency variable [14]. The SBM model only has one style, for there is no distinction between input-orientation and output-orientation under SBM. The efficiency score computed by the SBM model is also between 0 and 1. Compared to the traditional radial super-efficiency DEA models under CRS, the SBM model avoids the problem of infeasibility. Moreover, input slacks and output slacks in the SBM model can be utilized to detect the input excesses and output shortfalls of a given DMU, respectively. However, for SBM-efficient DMUs, Tone designed a super-efficiency model (S-SBM model) to examine their super-efficiency scores in order to allow SBM-efficient DMUs to be also ranked and compared [15]. Liu and Chen developed a HypoSBM model to distinguish the worst-performance DMUs from the bad ones [16]. Du et al. extended the SBM super-efficiency model to the additive slacks-based DEA model [17]. Fang et al. established a two-stage process, which was an alternative disposal treatment for the SBM method proposed by Tone [18]. They demonstrated that their two-stage approach generated the same results as Tone's models. Chen indicated that there exists a discontinuous gap between the SBM score and S-SBM score for a DMU who has a weakly reference point under S-SBM model [3]. In his study, an ambidextrous joint computation model (J-SBM model) for slacks-based measure was provided.

However, J-SBM model has two noted shortcomings. First, it fails to represent all input saving and output surplus scaling factors explicitly for each DMU. Second, it has a more complicated operational procedure and needs a three-stage computational process. The current paper further investigates this topic and presents a modified slacks-based measure of super-efficiency with input saving and output surplus scaling factors to reevaluate these DMUs. Our approach is devoted to detecting the specific scaling factors for each input and output as well as input and output slacks explicitly by one integrated model. Meanwhile, the phenomenon of discontinuousness between SBM score and S-SBM score for the same DMU can be eliminated. The results indicate that the projection obtained through our proposed model is strongly Pareto-efficient. And in this approach, we can see clearly how each decision variable influences the final efficiency score for a specific DMU.

The structure of this paper is organized as follows. Section 2 briefly reviews several kinds of slacks-based models. Section 3 presents a modified slacks-based measure of super-efficiency with input saving and output surplus scaling factors to determine DMUs' efficiency scores. In Section 4, two numerical examples are applied to compare our approach with the previous models. Section 5 applies our approach to an empirical example where the performance of 32 paper chemical mills in China is evaluated. The main conclusions and remarks are given in Section 6.

2. Preliminaries

Suppose there are n DMUs, $\{\mathrm{DMU}_k\,(k = 1, 2, \ldots, n)\}$. Let $x_k = (x_{1k}, \ldots, x_{mk})$ and $y_k = (y_{1k}, \ldots, y_{sk})$ denote the input and output vectors of the kth DMU. The ith input of the kth DMU is denoted as x_{ik} and the rth output of the kth DMU is denoted as y_{rk}, respectively. λ_j is the intensity coefficient for the kth DMU which means its contribution to forming the efficient frontier. Assume that all input and output data are positive.

2.1. Tone's SBM Measure. Tone developed the following SBM model to evaluate the relative efficiency of DMU_k [14], where input and output slacks are denoted, respectively, as $z_i^-\,(i = 1, \ldots, m)$ and $z_r^+\,(r = 1, \ldots, s)$. Unlike the CCR

model, the objective function in SBM model has a fractional form which directly includes input and output slacks.

$$\begin{aligned}
\rho_k^* &= \min \frac{1-(1/m)\sum_{i=1}^m z_i^-/x_{ik}}{1+(1/s)\sum_{r=1}^s z_r^+/y_{rk}}, \\
\text{s.t.} \quad & \sum_{j=1}^n \lambda_j x_{ij} = x_{ik} - z_i^-, \quad i=1,\ldots,m, \\
& \sum_{j=1}^n \lambda_j y_{rj} = y_{rk} + z_r^+, \quad r=1,\ldots,s, \\
& \lambda_j \geq 0, \quad j=1,\ldots,n, \\
& z_i^- \geq 0, \quad i=1,\ldots,m, \\
& z_r^+ \geq 0, \quad r=1,\ldots,s,
\end{aligned} \tag{1}$$

where DMU_k is called SBM-efficient if and only if $z_i^- = z_r^+ = 0$ for all i and r, that is, $\rho_k^* = 1$; otherwise, it is called SBM-inefficient. In order to further discriminate SBM-efficient DMUs with the same SBM efficiency score of 1, Tone introduced a SBM super-efficiency model which was referred to as S-SBM model in the following formula [15].

$$\begin{aligned}
\delta_k^* &= \min \frac{(1/m)\sum_{i=1}^m \overline{x}_{ik}/x_{ik}}{(1/s)\sum_{r=1}^s \overline{y}_{rk}/y_{rk}}, \\
\text{s.t.} \quad & \sum_{\substack{j=1 \\ j\neq k}}^n \lambda_j x_{ij} \leq \overline{x}_{ik}, \quad i=1,\ldots,m, \\
& \sum_{\substack{j=1 \\ j\neq k}}^n \lambda_j y_{rj} \geq \overline{y}_{rk}, \quad r=1,\ldots,s, \\
& \overline{x}_{ik} \geq x_{ik}, \quad i=1,\ldots,m, \\
& \overline{y}_{rk} \leq y_{rk}, \quad r=1,\ldots,s, \\
& \lambda_j, \overline{y}_{rk} \geq 0, \quad j\neq k, j=1,\ldots,n, i=1,\ldots,s.
\end{aligned} \tag{2}$$

It should be noticed that the S-SBM model can only be used for the DMU whose SBM efficiency score $\rho^* = 1$. Through model (2), these SBM-efficient DMUs get its super-efficiency scores. However, model (2) cannot discriminate SBM-inefficient DMUs for they will get the same efficiency score of 1.

2.2. Fang's Models. Fang et al. provided a two-stage process which brings in the same efficiency scores as those obtained by Tone's two models [18]. In the first stage, they replace $\overline{x}_{ik}$, $\overline{y}_{rk}$ with $x_{ik} + w_i^-$, $y_{rk} + w_r^+$ to form model (3) for detecting both input savings and output surpluses for all DMUs first.

$$\begin{aligned}
\delta_k^* &= \min \frac{1+(1/m)\sum_{i=1}^m w_i^-/x_{ik}}{1-(1/s)\sum_{r=1}^s w_r^+/y_{rk}}, \\
\text{s.t.} \quad & \sum_{\substack{j=1 \\ j\neq k}}^n \lambda_j x_{ij} \leq x_{ik} + w_i^-, \quad i=1,\ldots,m, \\
& \sum_{\substack{j=1 \\ j\neq k}}^n \lambda_j y_{rj} \geq y_{rk} - w_r^+, \quad r=1,\ldots,s, \\
& \lambda_j \geq 0, \quad j\neq k, j=1,\ldots,n, \\
& w_i^- \geq 0, \quad i=1,\ldots,m, \\
& w_r^+ \geq 0, w_r^+ \leq y_{rk}, \quad r=1,\ldots,s.
\end{aligned} \tag{3}$$

Through Model (3), the optimal w_i^{-*} and w_r^{+*} for each input and output for all DMUs can be obtained. For SBM-efficient DMUs in model (1), there will exist at least one i or r, so that $w_i^{-*} > 0$ or $w_r^{+*} > 0$ in model (3), while, for SBM-inefficient DMUs in model (1), they have no positive input saving and output surplus for each corresponding input and output at all. So these DMUs will get $w_i^- = w_r^+ = 0$ for all i and r. Then, plug w_i^{-*} and w_r^{+*} into the following model, and a slacks-based measure is reconstructed as model (4) exhibits.

$$\begin{aligned}
\rho_k^* &= \min \frac{1-(1/m)\sum_{i=1}^m s_i^-/x_{ik}}{1+(1/s)\sum_{r=1}^s s_r^+/y_{rk}}, \\
\text{s.t.} \quad & \sum_{\substack{j=1 \\ j\neq k}}^n \lambda_j x_{ij} = x_{ik} + w_i^{-*} - s_i^-, \quad i=1,\ldots,m, \\
& \sum_{\substack{j=1 \\ j\neq k}}^n \lambda_j y_{rj} = y_{rk} - w_r^{+*} + s_r^+, \quad r=1,\ldots,s, \\
& \lambda_j \geq 0, \quad j\neq k, j=1,\ldots,n, \\
& s_i^- \geq 0, \quad i=1,\ldots,m, \\
& s_r^+ \geq 0, \quad r=1,\ldots,s.
\end{aligned} \tag{4}$$

Obviously, model (3) is equivalent to model (2). So model (3) also determines the super-efficiency scores for SBM-efficient DMUs. The optimal SBM efficiency scores and the optimal slacks (s_i^{-*}, s_r^{+*}) for SBM-inefficient DMUs can be computed based on the optimal (w_i^{-*}, w_i^{+*}) by model (4).

At last, the final efficiency score for DMU_k based on SBM is defined as

$$\varphi_k^* = \begin{cases} \dfrac{1+(1/m)\sum_{i=1}^m w_i^{-*}/x_{ik}}{1-(1/s)\sum_{r=1}^s w_r^{+*}/y_{rk}}, & \text{if } \dfrac{1+(1/m)\sum_{i=1}^m w_i^{-*}/x_{ik}}{1-(1/s)\sum_{r=1}^s w_r^{+*}/y_{rk}} > 1, \\ \dfrac{1-(1/m)\sum_{i=1}^m s_i^{-*}/x_{ik}}{1+(1/s)\sum_{r=1}^s s_r^{+*}/y_{rk}}, & \text{otherwise.} \end{cases} \tag{5}$$

2.3. Chen's Model. Chen investigated a data set in Tone's which can be seen in Table 1 and found the reference points generated by model (2) or (3) might not be Pareto-efficient [3]. This resulted in a discontinuous gap between the SBM score and S-SBM score. The author indicated that the issue of discontinuity makes troubles to rationalize the efficiency score. So he established an ambidextrous joint computation model (6) (J-SBM model) to find the Pareto-efficient point for each DMU.

$$\begin{aligned}
&\min \quad \phi_k = \frac{\mathrm{JSBM}_k^x}{\mathrm{JSBM}_k^x} - M\left(b_1 + (1-b_1)b_2\right), \\
&\text{s.t.} \quad \mathrm{JSBM}_k^x = 1 - \frac{1}{m}\left[b_1\left(\sum_{i=1}^m \frac{s_i^-}{x_{ik}}\right) - (1-b_1)b_2\left(\sum_{i=1}^m \frac{s_i^-}{x_{ik}}\right) + (1-b_1)(1-b_2)\left(\sum_{i=1}^m \frac{\tilde{s}_i^-}{x_{ik}}\right)\right], \\
&\qquad \mathrm{JSBM}_k^y = 1 + \frac{1}{s}\left[b_1\left(\sum_{r=1}^s \frac{s_r^+}{y_{rk}}\right) - (1-b_1)b_2\left(\sum_{r=1}^s \frac{s_r^+}{y_{rk}}\right) + (1-b_1)(1-b_2)\left(\sum_{r=1}^s \frac{\tilde{s}_r^+}{y_{rk}}\right)\right], \\
&(6.1)\begin{cases} b_1\left(\sum_{j=1,j\neq k}^n \lambda_j x_{ij}\right) = b_1\left(x_{ik} - s_i^-\right), & i = 1,\ldots,m, \\ b_1\left(\sum_{j=1,j\neq k}^n \lambda_j y_{rj}\right) = b_1\left(y_{rk} + s_r^+\right), & r = 1,\ldots,s, \end{cases} \\
&(6.2)\begin{cases} (1-b_1)b_2\left(\sum_{j=1,j\neq k}^n \lambda_j x_{ij}\right) = (1-b_1)b_2\left(x_{ik} + s_i^-\right), & i = 1,\ldots,m, \\ (1-b_1)b_2\left(\sum_{j=1,j\neq k}^n \lambda_j y_{rj}\right) = (1-b_1)b_2\left(y_{rk} - s_r^+\right), & r = 1,\ldots,s, \end{cases} \\
&(6.3)\begin{cases} (1-b_1)(1-b_2)\left(\sum_{j=1,j\neq k}^n \lambda_j x_{ij}\right) = (1-b_1)(1-b_2)\left(x_{ik} - \tilde{s}_i^-\right), & i = 1,\ldots,m, \\ (1-b_1)(1-b_2)\left(\sum_{j=1,j\neq k}^n \lambda_j y_{rj}\right) = (1-b_1)(1-b_2)\left(y_{rk} + \tilde{s}_r^+\right), & r = 1,\ldots,s, \end{cases} \\
&\lambda_j \geq 0, \quad j = 1,\ldots,n, \\
&s_i^- \geq 0, \quad \tilde{s}_i^- \text{ free for } i = 1,\ldots,m, \\
&s_r^+ \geq 0, \quad \tilde{s}_r^+ \text{ free for } r = 1,\ldots,s, \\
&b_1, b_2 \in \{0,1\}, \\
&M \text{ is a large enough positive number.}
\end{aligned} \tag{6}$$

In model (6), b_1 and b_2 are two binary variables that are used to control which one of the three kinds of constraint conditions (6.1), (6.2), and (6.3) is chosen. For the SBM-inefficient DMUs, $b_1 = b_2 = 1$, constraint condition (6.1) is active; now model (6) works as the SBM model. For SBM-efficient DMUs, model (6) first acts as the S-SBM model under active constraint condition (6.2) when $b_1 = 0, b_2 = 1$. In the meantime, if the super-efficiency reference point is

Table 1: Data set 1 from Tone [15].

DMU	x_1	x_2	y_1	Tone's or Fang's approach S-SBM δ_k^*	SBM ρ_k^*	SBM φ_k^*	Chen's approach J-SBM ϕ_k^*	Our approach Integrated model (10) ψ_k^*
A	4	3	1	1	0.833	0.833	0.833	0.833
B	7	3	1	1	0.619	0.619	0.619	0.619
C	8	1	1	1.125	1	1.125	1.125	1.125
D	4	2	1	1.25	1	1.25	1.25	1.25
E	2	4	1	1.5	1	1.5	1.25	1.25
F	10	1	1	1	0.9	0.9	0.9	0.9
G	12	1	1	1	0.833	0.833	0.833	0.833

not Pareto-efficient for the evaluated DMU, model (6) will activate constraint condition (6.3), and the corresponding super-efficiency score will be corrected for the DMU. Additionally, Chen further proved that the reference points for all DMUs under model (6) are Pareto-efficient [3].

As can be seen from the above procedures in operating model (6), the constraint condition (6.3) is set intentionally to correct the misestimated efficiency score due to the less Pareto-efficient reference point caused by the S-SBM model (2) or (3). For these DMUs who have a weakly efficient reference point under model (2) or (3), however, the achievement of its super-efficiency needs a three-stage process. For instance, when $\mathrm{DMU_E}$ in Table 1 gets its super-efficiency of 1.25 under the constraint condition (6.3), the constraint conditions (6.1), (6.2) have been inspected before.

3. A Modified Slacks-Based Measure of Super-efficiency

In this section, we first establish an equivalent form of S-SBM model, which explicitly contains input saving and output surplus scaling factors. Note that $\overline{x}_{ik} \geq x_{ik}$ for all i and $\overline{y}_{rk} \leq y_{rk}$ for all r in model (2). Let $\overline{x}_{ik} = x_{ik} + t_i x_{ik}$, $t_i \geq 0$ and $\overline{y}_{rk} = y_{rk} - \beta_r y_{rk} \geq 0$, $0 \leq \beta_r \leq 1$, or $w_i^- = x_{ik} + t_i x_{ik}$, $t_i \geq 0$ and $w_r^+ = y_{rk} - \beta_r y_{rk} \geq 0$, $0 \leq \beta_r \leq 1$; then model (2) or model (3) will become the following model (7).

$$\begin{aligned}
\delta_k^* &= \min \frac{1 + (1/m)\sum_{i=1}^m t_i}{1 - (1/s)\sum_{r=1}^s \beta_r}, \\
\text{s.t.} \quad & \sum_{\substack{j=1 \\ j\neq k}}^n \lambda_j x_{ij} \leq (1 + t_i) x_{ik}, \quad i = 1, \ldots, m, \\
& \sum_{\substack{j=1 \\ j\neq k}}^n \lambda_j y_{rj} \geq (1 - \beta_r) y_{rk}, \quad r = 1, \ldots, s, \\
& \lambda_j \geq 0, \quad j \neq k, j = 1, \ldots, n, \\
& t_i \geq 0, \quad i = 1, \ldots, m, \\
& 0 \leq \beta_r \leq 1, \quad r = 1, \ldots, s.
\end{aligned} \tag{7}$$

The difference between models (7) and (3) is that model (7) can not only measure the input saving $t_i x_{ik}$ and the output surplus $\beta_r y_{rk}$, but also present the specific scaling factors t_i for x_{ik} and β_r for y_{rk} of DMU_k.

Let (t_i^*, β_r^*) be the optimal solution of model (7). Based on model (7), the standard SBM model (1) can be revised as follows:

$$\begin{aligned}
\rho_k^* &= \min \frac{1 - (1/m)\sum_{i=1}^m s_i^- / x_{ik}}{1 + (1/s)\sum_{r=1}^s s_r^+ / y_{rk}}, \\
\text{s.t.} \quad & \sum_{\substack{j=1 \\ j\neq k}}^n \lambda_j x_{ij} = (1 + t_i^*) x_{ik} - s_i^-, \quad i = 1, \ldots, m, \\
& \sum_{\substack{j=1 \\ j\neq k}}^n \lambda_j y_{rj} = (1 - \beta_r^*) y_{rk} + s_r^+, \quad r = 1, \ldots, s, \\
& \lambda_j \geq 0, \quad j \neq k, j = 1, \ldots, n, \\
& s_i^- \geq 0, \quad i = 1, \ldots, m, \\
& s_r^+ \geq 0, \quad r = 1, \ldots, s.
\end{aligned} \tag{8}$$

Similarly, we apply model (7) to all DMUs before the utilization of model (8) on inefficient DMUs. We define the final efficiency score for DMU_k based on SBM with the following piecewise function:

$$\varphi_k^* = \begin{cases} \dfrac{1 + (1/m)\sum_{i=1}^m t_i^*}{1 - (1/s)\sum_{r=1}^s \beta_r^*}, & \text{if } \dfrac{1 + (1/m)\sum_{i=1}^m t_i^*}{1 - (1/s)\sum_{r=1}^s \beta_r^*} > 1, \\[2ex] \dfrac{1 - (1/m)\sum_{i=1}^m s_i^{-*} / x_{ik}}{1 + (1/s)\sum_{r=1}^s s_r^{+*} / y_{rk}}, & \text{otherwise}, \end{cases} \tag{9}$$

where (s_i^{-*}, s_i^{+*}) is the optimal solution in model (8).

The above two-stage process is identical to that of Fang et al. Model (7) may also suffer from the problem that the projection reference point for a specific DMU may not be Pareto-efficient. As Chen mentioned, the SBM and S-SBM efficiency scores are calculated in two separate models with two different objection functions that have two different projecting styles for the evaluated DMU [3]. The SBM scores are achieved by their input and output slacks, while the S-SBM scores depend only on the reference point (may not be Pareto-efficient) on the super-efficiency frontier. Therefore, the whole evaluation system is not an integrated one

and is divided into two styles, which results in the problem of a discontinuous gap.

In order to integrate the whole evaluation system, we maintain the basic sense of SBM model and S-SBM model into one model and ensure that the desired model has the uniform projecting way for the evaluated DMU. So, we develop the following modified SBM measure based on model (7).

$$\begin{aligned}
&\mathrm{SE} = \min \frac{1-(1/m)\sum_{i=1}^{m}\left((s_i^-/x_{ik})-t_i\right)}{1+(1/s)\sum_{r=1}^{s}\left((s_r^+/y_{rk})-\beta_r\right)} + M\times\left(\frac{1+(1/m)\sum_{i=1}^{m}t_i}{1-(1/s)\sum_{r=1}^{s}\beta_r}\right),\\
&\text{s.t.}\quad \sum_{\substack{j=1\\ j\neq k}}^{n}\lambda_j x_{ij} = (1+t_i)x_{ik} - s_i^-, \quad i=1,\ldots,m,\\
&\qquad \sum_{\substack{j=1\\ j\neq k}}^{n}\lambda_j y_{rj} = (1-\beta_r)y_{rk} + s_r^+, \quad r=1,\ldots,s,\\
&\qquad \lambda_j \geq 0, \quad j\neq k, j=1,\ldots,n,\\
&\qquad s_i^- \geq 0, \quad i=1,\ldots,m,\\
&\qquad s_r^+ \geq 0, \quad r=1,\ldots,s,\\
&\qquad t_i \geq 0, \quad i=1,\ldots,m,\\
&\qquad 0\leq \beta_r < 1, \quad r=1,\ldots,s.
\end{aligned} \tag{10}$$

The logic behind model (10) is based on two major attributes. First, the measure we modified as $(1-(1/m)\sum_{i=1}^{m}((s_i^-/x_{ik})-t_i))/(1+(1/s)\sum_{r=1}^{s}((s_r^+/y_{rk})-\beta_r))$, which not only includes the input and output slacks in SBM measure, but also includes input saving and output surplus scaling factors in S-SBM model. It is able to comprehensively explain the reason for the resulting efficiency scores; that is to say, when input saving scaling factors or output surplus scaling factors appear together with input or output slacks, they all contribute to the efficiency score.

Hence, the efficiency score can be defined as

$$\begin{aligned}
\psi_k^* &= \frac{1-(1/m)\sum_{i=1}^{m}\left((s_i^{-*}/x_{ik})-t_i^*\right)}{1+(1/s)\sum_{r=1}^{s}\left(s_r^{+*}/y_{rk}\right)-\beta_r^*}\\
&= \frac{1-(1/m)\sum_{i=1}^{m}s_i^{-*}/x_{ik}+(1/m)\sum_{i=1}^{m}t_i^*}{1+(1/s)\sum_{r=1}^{s}s_r^{+*}/y_{rk}-(1/s)\sum_{r=1}^{s}\beta_r^*},
\end{aligned} \tag{11}$$

where $(t_i^*, \beta_r^*, s_i^{-*}, s_i^{+*})$ is the optimal solution of model (10).

Second, we integrate SBM model and S-SBM model under the rule that the evaluated DMU must have the minimum super-efficiency score if it has at least one $t_i^* > 0$ or $\beta_r^* > 0$. So we add the controllable term of $M\times(1+(1/m)\sum_{i=1}^{m}t_i/1-(1/s)\sum_{r=1}^{s}\beta_r)$ to the objective function so as to make t_i and β_r as small as possible for all i and r.

Here, M (we set it 10^7 so as to make it large enough in the empirical study) is a predetermined large number used mainly for magnifying the effect of input saving and output surplus scaling factors on the objective function under the condition of minimum S-SBM score. Simultaneously, it can control the optimal values of decision variables. Note the constraints in model (10):

$$\begin{aligned}
&\sum_{\substack{j=1\\ j\neq k}}^{n}\lambda_j x_{ij} = (1+t_i)x_{ik} - s_i^-, \quad i=1,\ldots,m,\\
&\sum_{\substack{j=1\\ j\neq k}}^{n}\lambda_j y_{rj} = (1-\beta_r)y_{rk} + s_r^+, \quad r=1,\ldots,s.
\end{aligned} \tag{12}$$

A severe problem which may occur is that when $t_i > 0$ and $s_i^- > 0$ for a certain i (or $\beta_r > 0$ and $s_r^+ > 0$ for a certain r) simultaneously exist, there is an offsetting contradiction between $t_i x_{ik}$ and s_i^- (or $\beta_r y_{rk}$ and s_r^+). To avoid this kind of situation, the controllable term of $M\times((1+(1/m)\sum_{i=1}^{m}t_i)/(1-(1/s)\sum_{r=1}^{s}\beta_r))$ added to the objective function is able to ensure that either $t_i^* > 0$ or $s_i^{-*} > 0$ for a certain i (either $\beta_r^* > 0$ or $s_r^{+*} > 0$ for a certain r) and both of them are not in existence.

Model (10) has close connections with the SBM model and S-SBM model.

Theorem 1. *For any SBM-inefficient DMU$_k$, $\psi_k^* = \rho_k^*$.*

Proof. For SBM-inefficient DMU$_k$, there must be $t_i^* = 0$ and $\beta_r^* = 0$ for all i and r in model (10). In this case, model (10) degenerates into SBM model (1). □

Theorem 2. *For SBM-efficient DMU$_k$, if the reference point under S-SBM model for DMU$_k$ is Pareto-efficient, $\psi_k^* = \delta_k^*$.*

Proof. For SBM-inefficient DMU$_k$, suppose the reference point of DMU$_k$ in S-SBM model is Pareto-efficient, there must be s_i^{-*} and $s_r^{+*} = 0$ for all i and r in model (10). At this moment, model (10) degenerates into model (7) which is equivalent to S-SBM model (2).

However, for other SBM-efficient DMUs, if the reference point under S-SBM model is not Pareto-efficient, model (10) will revise the super-efficiency score obtained by S-SBM model (7) but just make sure that model (10) can identify the Pareto-efficient reference for these DMUs. □

Theorem 3. *The reference point identified by model (10) is Pareto-efficient.*

Proof. For a SBM-inefficient DMU, model (10) serves as the standard SBM model (1); the reference point identified the standard SBM model as Pareto-efficient, and so does model (10).

For a SBM-efficient DMU, there at least exists one input $i \in \{1,\ldots,m\}$ or one output $r \in \{1,\ldots,s\}$ such that at least one scaling factor $t_i^* > 0$ or $\beta_r^* > 0$. Meanwhile, the existence of input and output slacks allows the evaluated DMU to decrease its inputs and increase its outputs. Thus, the reference point identified by model (10) is as follows:

$$\sum_{\substack{j=1\\ j\neq k}}^{n} \lambda_j^* x_{ij} = (1+t_i^*)x_{ik} - s_i^{-*}, \quad i=1,\ldots,m,$$
$$\sum_{\substack{j=1\\ j\neq k}}^{n} \lambda_j^* y_{rj} = (1-\beta_r^*)y_{rk} + s_r^{+*}, \quad r=1,\ldots,s. \tag{13}$$

If $((1+t_i^*)x_{ik}, (1-\beta_r^*)y_{rk})$ is not a Pareto-efficient reference point, then it moves s_i^{-*} leftward and s_r^{+*} upward to reach the Pareto-efficient reference points.

However, it should be noted that model (10) is a quite different optimization design because the objective function and constraints are quite different to the standard SBM and S-SBM models. Although the projection identified by model (10) is Pareto-efficient, for SBM-efficient DMUs, the projected reference point by model (10) may not coincide with that by S-SBM model or J-SBM model (see examples in Section 4).

Clearly, the modified measurement ψ_k has the unit-invariant property. □

Theorem 4. *ψ_k is unit-invariant.*

The fractional programming (10) can be transformed into a linear programming problem through the following Charnes-Cooper transformation by setting $w_1 = (1/(1+(1/s)\sum_{r=1}^{s}(s_r^+/y_{rk}) - \beta_r))$, $w_2 = 1/(1-(1/s)\sum_{r=1}^{s}\beta_r)$ $(w_1 \le w_2)$, $\lambda_j' = w_1 \cdot \lambda_j$, $s_i'^- = w_1 \cdot s_i^-$, $s_r'^+ = w_1 \cdot s_r^+$, $t_i' = w_1 \cdot t_i$, $\beta_r' = w_1\beta_r$, $t_i'' = w_2 \cdot t_i$, $\beta_r'' = w_2\beta_r$; then model (10) will become the following linear programming:

$$\begin{aligned}
\min \quad & w_1 - \frac{1}{m}\sum_{i=1}^{m}\left(\frac{s_i'^-}{x_{ik}} - t_i'\right) + M \times \left(w_2 + \frac{1}{m}\sum_{i=1}^{m} t_i''\right),\\
\text{s.t.} \quad & w_1 + \frac{1}{s}\sum_{r=1}^{s}\left(\frac{s_r'^+}{y_{rk}} - \beta_r'\right) = 1,\\
& w_2 - \frac{1}{s}\sum_{r=1}^{s}\beta_r'' = 1,\\
& \sum_{\substack{j=1\\ j\neq k}}^{n} \lambda_j' x_{ij} = w_1 x_{ik} + t_i' x_{ik} - s_i'^-, \quad i=1,\ldots,m,\\
& \sum_{\substack{j=1\\ j\neq k}}^{n} \lambda_j' y_{rj} = w_1 y_{rk} - \beta_r' y_{rk} + s_r'^+, \quad r=1,\ldots,s,\\
& \lambda_j' \ge 0, \quad j\neq k, j=1,\ldots,n,\\
& s_i'^- \ge 0, \quad i=1,\ldots,m,\\
& s_r'^+ \ge 0, \quad r=1,\ldots,s,\\
& 0 \le t_i' \le t_i'', \quad i=1,\ldots,m,\\
& 0 \le \beta_r' \le w_1, \beta_r' \le \beta_r'', \quad r=1,\ldots,s,\\
& 0 \le w_1 \le w.
\end{aligned} \tag{14}$$

Suppose $(w_1^*, t_i'^*, \beta_r'^*, s_i'^{-*}, s_r'^+)$ is the optimal solution of model (11), then $(t_i^* = t_i'^*/w_1^*, \beta_r^* = \beta_r'^*/w_1^*, s_i^{-*} = s_i'^{-*}/w_1^*, s_r^{+*} = s_r'^{+*}/w_1^*)$ is the optimal solution of model (10).

4. Illustration Examples

Two numerical examples from Tone are used to verify our approach through comparing with the SBM model, S-SBM model, and J-SBM model. In Table 1, the efficiency scores derived by the SBM model, S-SBM model, and J-SBM model are presented and those identified through our approach are listed in the last column. Table 2 shows detailed optimal solutions under J-SBM model (6) and we rewrite them in the form of input and output surplus scaling factors so as to facilitate comparison. Table 3 presents detailed optimal solutions under our model (10). As shown in Tables 2 and 3, these DMUs get the same efficiency scores but may be a different optimal solution for each decision variable. For example, DMU_D gets the super-efficiency score of 1.25 under J-SBM model (6), and the achievement of super-efficiency score seems reflected in its input saving scaling factors $t_1^* = 0.234$ and $t_2^* = 0.266$, while under our model (10) it not only owns input saving scaling factors $t_1^* = 0.137$ and $t_2^* = 0.163$, but also has the output surplus scaling factor $\beta_1^* = 0.08$. The reason is that due to the different projecting style of these two models, DMU_D gets different reference points, which are both Pareto-efficient projected points. And for DMU_E, J-SBM model (6) and our model (10) identified the same Pareto-efficient reference point. Our model also overcomes the problem of the discontinuous gap and finds its input saving scaling factor $t_1^* = 1$ and input slack $s_2^{-*} = 2$, so the rational super-efficiency score is

$$\begin{aligned}
\psi_k^* &= \frac{1-(1/m)\sum_{i=1}^{m}\left((s_i^{-*}/x_{ik}) - t_i^*\right)}{1+(1/s)\sum_{r=1}^{s}\left((s_r^{+*}/y_{rk}) - \beta_r^*\right)}\\
&= \frac{1-(1/2)\times(1/2)+(1/2)\times 1}{1} = 1.25.
\end{aligned} \tag{15}$$

In Table 4, we mainly compare the approach from Tone's or Fang's and ours using data set 2 from Tone. For the first four DMUs (1–4), two approaches gain the same efficiency scores. But for DMU_5, our approach detects that it has both input saving scaling factor $t_1^* = 0.4$ and output surplus scaling factor $\beta_2^* = 0.475$. Besides, it has input slack $s_2^{-*} = 1.9$ and output slack $s_1^{+*} = 0.4$. This situation means that S-SBM model does not project DMU_5 at a Pareto-efficient targeted point and its efficiency score should be revised. According to our approach, the efficiency score should be modified as

$$\begin{aligned}
\psi_k^* &= \frac{1-(1/m)\sum_{i=1}^{m}\left((s_i^{-*}/x_{ik}) - t_i^*\right)}{1+(1/s)\sum_{r=1}^{s}\left((s_r^{+*}/y_{rk}) - \beta_r^*\right)}\\
&= \frac{1-(1/2)\times(1.711/4)+(1/2)\times 0.526}{1+(1/2)\times 0.526-(1/2)\times 0.428} = 1.0001.
\end{aligned} \tag{16}$$

Table 2: Results from J-SBM model (6).

DMU	x_1	x_2	y_1	φ_k^*	t_1^*	t_2^*	β_1^*	s_1^{-*}	s_2^{-*}	s_1^{+*}
A	4	3	1	0.833	0	0	0	0	1	0
B	7	3	1	0.619	0	0	0	2.895	0.948	0.026
C	8	1	1	1.125	0.25	0	0	0	0	0
D	4	2	1	1.25	0.234	0.266	0	0	0	0
E	2	4	1	1.25	1	0	0	0	2	0
F	10	1	1	0.9	0	0	0	2	0	0
G	12	1	1	0.833	0	0	0	4	0	0

Table 3: Results from our model (10).

DMU	x_1	x_2	y_1	ψ_k^*	t_1^*	t_2^*	β_1^*	s_1^{-*}	s_2^{-*}	s_1^{+*}
A	4	3	1	0.833	0	0	0	0	1	0
B	7	3	1	0.619	0	0	0	1.706	0.353	0.324
C	8	1	1	1.125	0.25	0	0	0	0	0
D	4	2	1	1.25	0.137	0.163	0.08	0	0	0
E	2	4	1	1.25	1	0	0	0	2	0
F	10	1	1	0.9	0	0	0	2	0	0
G	12	1	1	0.833	0	0	0	4	0	0

Table 4: Data set 2 from Tone [14] and results from our approach.

DMU	x_1	x_2	y_1	y_2	Tone's or Fang's approach	Our approach									
					φ_k^*	ψ_k^*	t_1^*	t_2^*	β_1^*	β_2^*	s_1^{-*}	s_2^{-*}	s_1^{+*}	s_2^{+*}
1	4	3	2	3	0.7980	0.7980	0	0	0	0	0	0.357	0.714	0
2	6	3	2	3	0.5682	0.5682	0	0	0	0	0	0.643	2.286	0
3	8	1	6	2	1.3333	1.3333	0	0	0	0.5	0	0	0	0
4	8	1	6	1	0.6667	0.6667	0	0	0	0	0	0	0	1
5	2	4	1	4	1.4545	1.0001	0.526	0	0	0.428	0	1.711	0.526	0

5. An Empirical Study

After high speed development on industries and economics during the past several decades, China has accumulated a lot of air environment problems and the Chinese government is paying more and more attention to ecological and environmental assessment. Recent years have seen a lot of studies based on DEA to measure China's environmental pollution problems. For example, Zhou et al. [19, 20] construct a set of DEA models with the integral and zero-sum gain constraints for calculating air quality and a new nonradial directional distance function to scale the performance of water use and wastewater emission, respectively.

In this section, the method that we have developed is applied to examine the efficiencies and rankings of 32 paper chemical mills along the Huai River in China. In this empirical study, four input and output variables are considered to evaluate each mill's performance. The inputs of each paper mill include labor and capital, and good output as paper products as well as bad output as biochemical oxygen demand (BOD). The detailed data set of these 32 paper chemical mills is shown in Table 5.

In papermaking industry, the good products are always produced with bad products and it is impossible to increase good outputs and decrease bad outputs meanwhile. First, the attribute of "the smaller the better" for bad outputs is consistent with inputs. Second, bad outputs cannot create any new profit and dealing with them (such as sewage treatment and air purification) always comes at a price which the mill should afford [21]. Therefore, here we simply treat the bad outputs as inputs from the cost point of view.

We use model (10) to assess the performance of 32 paper chemical mills and the computed efficiency scores and ranking results are also displayed in Table 5. The last column gives their ranks according to efficiency scores obtained by our method. Of the 32 paper mills, only three mills, named mills 9, 12, and 25, are identified to obtain super-efficiency scores and they are ranked as the top three accordingly. For example, mill 9 and 12 get super-efficiency of 1.0734 and 1.4546, respectively, due to that the scaling factor of output surplus in one good output (paper) is 0.0734 and 0.4546 separately and there exist no slacks in all inputs and outputs. In contrast, 29 mills fail to get super-efficiency scores. For instance, mill 6 ranks dead last because it does not have any scaling factor of each input or output. Meanwhile, positive slacks are found to exist in two inputs and one bad output. Although mill 31 achieves the input saving scaling factor of 0.0229 in the first input (labor) and the output surplus scaling factor of 0.1077 in the good output (paper), its efficiency score is identified as 0.8538 and is ranked eighth finally. The reason for this is that there exists a slack amount of 13.7051 in the bad output (BOD), which brings more negative impact to efficiency scores than the positive effect brought by input and output scaling factors.

Table 5: The Data set and efficiency results of 32 paper mills.

Paper mills	Inputs		Bad output	Good output	ψ_k^*	Rank
	Labor (person)	Capital (¥10000)	BOD (ton)	Paper (ton)		
1	1077	2959.9	21.4290	27582	0.9005	5
2	452	3589	19.8062	29514	0.8544	7
3	319	5901.9	12.3287	14700	0.3590	26
4	1075	4892.8	9.1559	22354	0.4337	16
5	813	4079.7	11.9146	20669	0.4328	17
6	850	5239.6	5.2037	8222	0.2019	32
7	1090	3022.8	3.6054	15066	0.5286	12
8	122	3173.1	3.7278	8066	0.4937	14
9	297	2277.4	8.0765	19125	1.0734	3
10	1047	1491.9	8.9060	7601	0.3141	30
11	1010	3940.1	4.8940	11579	0.3184	28
12	262	3236.5	4.0835	23216	1.4546	1
13	551	4448.6	4.8750	21698	0.6357	10
14	671	1789.7	4.5334	8127	0.3617	25
15	577	2310.9	6.1362	11549	0.4179	20
16	208	3398.2	7.0186	10295	0.4130	21
17	667	5331.9	28.4877	29881	0.4904	15
18	878	3450.4	13.1680	19076	0.4236	19
19	640	3109.8	6.1616	12176	0.3694	24
20	927	3345.2	1.4533	5187	0.3024	31
21	167	4329.7	22.5809	24005	0.8937	6
22	903	3855.2	26.3390	23085	0.4258	18
23	720	1908.3	3.0787	6545	0.3182	29
24	629	3468.2	21.7332	27599	0.6853	9
25	152	5571.7	5.3061	23748	1.2256	2
26	1010	4647.1	9.1360	17323	0.3489	27
27	578	2513.3	5.0049	10617	0.3898	23
28	384	2247.4	4.4373	9083	0.3968	22
29	166	3968.1	10.6127	15151	0.5997	11
30	894	1368.5	4.7758	9911	0.5089	13
31	143	5350.2	17.4677	25260	0.8538	8
32	879	2873.2	26.9134	27721	0.9464	4

Source: Anhui Environmental Protection Bureau, the Fuyang Environmental Protection Bureau, and the Huainan Environmental Protection Bureau.

As can be seen from Table 5, the efficiency score or the super-efficiency score for each mill can be obtained by the integrated model (10). This course by our method prevents transformations among three submodels of the method by Chen. The final efficiency scores $\psi_k^*\,(k = 1, \ldots, 32)$ are affected synthetically by all decision variables that include input saving and output surplus scaling factors, input and output slacks. So we can fully differentiate the performances of all 32 paper mills and can provide a complete ranking criterion for all DMUs to be compared with regard to these efficiency scores.

6. Conclusions and Remarks

The classic SBM model proposed by Tone projects the DMU under evaluation at a Pareto-efficient reference point on the production frontier, while the S-SBM model proposed by Tone may not apply and the reference point on the super-efficiency frontier by S-SBM model may not be Pareto-efficient. Chen found an approach through transformations among three submodels to handle this issue.

In the present paper, we build a universal model to realize the integration of SBM model and S-SBM model. Our approach not only shows the specific scaling factors for each input and output of a specific DMU explicitly, but also provides input saving, output surplus, and slacks information simultaneously only in one model. And we can see clearly how the efficiency scores are obtained by the optimal value for each decision making variable. Thus, more recognizing information on DMUs is revealed via two numerical examples and an empirical study in paper chemical mills. The composite efficiency scores for 32 mills are represented and ranked by integrating the effect of all decision variables, which include input saving, output surplus scaling factors, and input and output slacks.

The current paper also overcomes the problem of a discontinuous gap between SBM score and S-SBM score found by Chen. Model (10) is proved to make sure that for each DMU under evaluation it supplies a Pareto-efficient reference point on the efficient frontier. This is achieved by incorporating input and output slacks into S-SBM model and controlling optimal values for each variable through the use of big M. For one specific input (output), input saving scaling factor (output surplus scaling factor) and input slack (output slack) are not permitted to appear at the same time. Especially, for a certain DMU, we can judge whether the

reference point in S-SBM model is Pareto-efficient through our model. That is, the reference point $((1+t_i^*)x_{ik}, (1-\beta_r^*)y_{rk})$ for DMU_k in S-SBM model (7) is not Pareto-efficient if and only if there exists $s_i^{-*} > 0$ $(i' \neq i \in (1, \ldots, m))$ or $s_{r'}^{+*} > 0$ $(r' \neq r \in (1, \ldots, m))$ under model (10).

Data Availability

The data used to support the findings of this study are available from the corresponding author upon request.

Conflicts of Interest

The authors declare no conflicts of interest.

Acknowledgments

This work was supported by the Start-up Scientific Research Foundation of Anhui Jianzhu University (2019QDZ09).

References

[1] A. Charnes, W. W. Cooper, and E. Rhodes, "Measuring the efficiency of decision making units," *European Journal of Operational Research*, vol. 2, no. 6, pp. 429–444, 1978.

[2] W. W. Cooper, L. M. Seiford, and J. Zhu, *Handbook on Data Envelopment Analysis*, Springer, Berlin, Germany, 2011.

[3] C.-M. Chen, "Super efficiencies or super inefficiencies? Insights from a joint computation model for slacks-based measures in DEA," *European Journal of Operational Research*, vol. 226, no. 2, pp. 258–267, 2013.

[4] T. R. Sexton, R. H. Silkman, and A. J. Hogan, "Data envelopment analysis: critique and extensions," in *Measuring Efficiency: An Assessment of Data Envelopment Analysis*, R. H. Silkman, Ed., pp. 73–105, Jossey-Bass, San Francisco, CA, USA, 1986.

[5] L. Liang, J. Wu, W. D. Cook, and J. Zhu, "The DEA game cross-efficiency model and its nash equilibrium," *Operations Research*, vol. 56, no. 5, pp. 1278–1288, 2008.

[6] A. M. Torgersen, F. R. Førsund, and S. A. C. Kittelsen, "Slack-adjusted efficiency measures and ranking of efficient units," *Journal of Productivity Analysis*, vol. 7, no. 4, pp. 379–398, 1996.

[7] P. Andersen and N. C. Petersen, "A procedure for ranking efficient units in data envelopment analysis," *Management Science*, vol. 39, no. 10, pp. 1261–1264, 1993.

[8] L. M. Seiford and J. Zhu, "Infeasibility of super-efficiency data envelopment analysis models," *INFOR: Information Systems and Operational Research*, vol. 37, no. 2, pp. 174–187, 1999.

[9] Y. Chen, "Measuring super-efficiency in DEA in the presence of infeasibility," *European Journal of Operational Research*, vol. 161, no. 2, pp. 545–551, 2005.

[10] W. D. Cook, L. Liang, Y. Zha, and J. Zhu, "A Modified super-efficiency DEA model for infeasibility," *Journal of the Operational Research Society*, vol. 60, no. 2, pp. 276–281, 2009.

[11] H.-S. Lee, C.-W. Chu, and J. Zhu, "Super-efficiency DEA in the presence of infeasibility," *European Journal of Operational Research*, vol. 212, no. 1, pp. 141–147, 2011.

[12] Y. Chen and L. Liang, "Super-efficiency DEA in the presence of infeasibility: one model approach," *European Journal of Operational Research*, vol. 213, no. 1, pp. 359-360, 2011.

[13] H.-S. Lee and J. Zhu, "Super-efficiency infeasibility and zero data in DEA," *European Journal of Operational Research*, vol. 216, no. 2, pp. 429–433, 2012.

[14] K. Tone, "A slacks-based measure of efficiency in data envelopment analysis," *European Journal of Operational Research*, vol. 130, no. 3, pp. 498–509, 2001.

[15] K. Tone, "A slacks-based measure of super-efficiency in data envelopment analysis," *European Journal of Operational Research*, vol. 143, no. 1, pp. 32–41, 2002.

[16] F.-H. F. Liu and C.-L. Chen, "The worst-practice DEA model with slack-based measurement," *Computers & Industrial Engineering*, vol. 57, no. 2, pp. 496–505, 2009.

[17] J. Du, L. Liang, and J. Zhu, "A slacks-based measure of super-efficiency in data envelopment analysis: a comment," *European Journal of Operational Research*, vol. 204, no. 3, pp. 694–697, 2010.

[18] H.-H. Fang, H.-S. Lee, S.-N. Hwang, and C.-C. Chung, "A slacks-based measure of super-efficiency in data envelopment analysis: an alternative approach," *Omega*, vol. 41, no. 4, pp. 731–734, 2013.

[19] Z. Zhou, X. Guo, H. Wu, and J. Yu, "Evaluating air quality in China based on daily data: application of integer data envelopment analysis," *Journal of Cleaner Production*, vol. 198, pp. 304–311, 2018.

[20] Z. Zhou, H. Wu, and P. Song, "Measuring the resource and environmental efficiency of industrial water consumption in China: a non-radial directional distance function," *Journal of Cleaner Production*, vol. 240, Article ID 118169, 2019.

[21] D. Guo and J. Wu, "A complete ranking of DMUs with undesirable outputs using restrictions in DEA models," *Mathematical and Computer Modelling*, vol. 58, no. 5-6, pp. 1102–1109, 2013.

Hindawi
Journal of Chemistry
Volume 2019, Article ID 9846913, 14 pages
https://doi.org/10.1155/2019/9846913

Research Article

Zagreb Connection Indices of Subdivision and Semi-Total Point Operations on Graphs

Jiang-Hua Tang,[1] Usman Ali,[2] Muhammad Javaid,[2] and Khurram Shabbir[3]

[1]*Department of General Education, Anhui Xinhua University, Hefei 230088, China*
[2]*Department of Mathematics, School of Science, University of Management and Technology, Lahore, Pakistan*
[3]*Department of Mathematics, GC University, Lahore, Pakistan*

Correspondence should be addressed to Khurram Shabbir; khurramsms@gmail.com

Received 29 October 2019; Accepted 9 December 2019; Published 28 December 2019

Academic Editor: Juan L. G. Guirao

Representation or coding of the molecular graphs with the help of numerical numbers plays a vital role in the studies of physicochemical and structural properties of the chemical compounds that are involved in the molecular graphs. For the first time, the modified first Zagreb connection index appeared in the paper by Gutman and Trinajstic (1972) to compute total electron energy of the alternant hydrocarbons, but after that, for a long time, it has not been studied. Recently, Ali and Trinajstic (2018) restudied the first Zagreb connection index (ZC_1), the second Zagreb connection index (ZC_2), and the modified first Zagreb connection index (ZC_1^*) to find entropy and acentric factor of the octane isomers. They also reported that the values provided by the International Academy of Mathematical Chemistry show better chemical capability of the Zagreb connection indices than the ordinary Zagreb indices. Assume that S_1 and S_2 denote the operations of subdivision and semitotal point, respectively. Then, the S-sum graphs $Q_1 +_S Q_2$ are obtained by the cartesian product of $S(Q_1)$ and Q_2, where $S \in \{S_1, S_2\}$, Q_1 and Q_2 are any connected graphs, and $S(Q_1)$ is a graph obtained after applying the operation S on Q_1. In this paper, we compute the Zagreb connection indices (ZC_1, ZC_2, and ZC_1^*) of the S-sum graphs in terms of various topological indices of their factor graphs. At the end, as an application of the computed results, the Zagreb connection indices of the S-sum graphs obtained by the particular classes of alkanes are also included.

1. Introduction

The importance of graph theory [1] is increased day by day in the various disciplines of science, especially in the field of chemistry and information science [2–5]. In view of Todeschini et al. [6], a topological invariant (TI) is the final outcome of a logical, systematic, and mathematical process that transforms features encoded in a molecular graph to a fixed real number. These TIs predict the chemical and physical features of the molecular graphs just on solubility, weight, connectivity, polarizability, surface tension, critical temperature, freezing, melting and boiling point, heat of evaporation, and heat of formation. A number of drugs, micromaterials, and crystalline materials which are strongly applied in several industrial networks and pharmaceutical fields are studied and evaluated on the basis or frame provided by the TIs (see [7–10]).

Moreover, TIs are presented into useful identity in the study of the quantitative structure activity relationships (QSARs) and quantitative structure property relationships (QSPRs), which connect the molecular graphs to their biological behaviour [11–16]. Mathematically, we represent this link as $T = \chi(U)$, where χ is the real-valued function, U is the molecular structure, and T is a real value that depends upon U. For more details, we refer to [17, 18, 19, 20]. The first TI was defined by Wiener in 1947 working on the boiling point of paraffin [21]. In 1972, Gutman and Trinajstić [22] defined degree-based TIs named as first Zagreb index and second Zagreb index. In the same paper, another TI is also defined, which got less tension of the researchers. Furtula and Gutman

[23] reinvestigated this index with its various basic properties and called it by the name of forgotten index. Nowadays, many extended studies have been delivered on these invariants. For more study, we refer to [6, 24–27]. In brief, to date, many TIs with various properties have been defined (see [6, 27]). These TIs have been classified into various classes, but degree-based TIs are more popular than others (see [7–9, 28, 29]).

Also another TI is defined in the same paper [22] of Gutman and Trinajstić, but there is no more attention or study on this predictor for a long time. In 2018, Ali and Trinajstic [30] reinvestigated this topological index and called it modified first Zagreb connection index (ZC_1^*). They also reported (as per data provided by the International Academy of Mathematical Chemistry) that its chemical capability has more precise correlation coefficient values for the following thirteen physicochemical properties of octane isomers: density, heat capacity at temperature, standard enthalpy of vaporization, boiling point, heat capacity at pressure, enthalpy of vaporization, entropy, acentric factor, molar volume, total surface area, enthalpy of formation, standard enthalpy of formation, and octanol water partition coefficient. Du et al. [31] determined extremal alkanes by using modified first Zagreb connection index. In the same year, Ducoffe et al. [32] also characterized extremal graphs with respect to the modified first Zagreb connection index for trees and unicyclic graphs with or without a fixed girth. Shao et al. [33] also used the same molecular descriptor to find the extremal graphs in the class of alkanes and cycloalkanes under certain conditions.

In the computational graph theory, the operations on graphs played an important role in the studies of graph invariants in the complex structures into their factors. For the purpose, Yan et al. [34] defined the operations of subdivision and semitotal point on graphs and obtained the Wiener index of the resultant graphs. Eliasi and Taeri [35] used these operations to construct new families of S-sum graphs. Deng and Akhter [36, 37] computed the first Zagreb index (M_1), second Zagreb index (M_2), and forgotten index (M_3) of the S-sum graphs. Liu et al. [38] derived the exact formulas for the first general Zagreb index (M^α) on the S-sum graphs, where α is a real number. For more details about TIs and their applications, we refer to [39–48] and the references therein.

In this paper, we extend this study and compute Zagreb connection indices such as first Zagreb connection index (ZC_1), second Zagreb connection index (ZC_2), and modified first Zagreb connection index (ZC_1^*) of the S-sum graphs $Q_1 +_S Q_2$, which are obtained by the cartesian product of $S(Q_1)$ and Q_2, where $S \in \{S_1, S_2\}$, Q_1 and Q_2 are any connected graphs, and $S(Q_1)$ is a graph obtained after applying the operations S on Q_1. The rest of the paper is organized as follows: Section 2 covers the preliminary definitions of the Zagreb indices and Zagreb connection indices. Section 3 presents the main results, and Section 4 includes the conclusion.

2. Preliminaries

Let $Q = (V(Q), E(Q))$ be a simple and connected graph with vertex set $V(Q)$ and edge set $E(Q) \subseteq V(Q) \times V(Q)$ such that their cardinalities are called order and size of Q, respectively. Todesehini et al. [6] defined the generalized form of the degrees of vertices of the graph Q as ${}^k f_Q(b) = |{}^k N_Q(b)|$, where ${}^k N_Q(b) = \{a \in V(Q): d(a,b) = k\}$. For $k = 1$ and $k = 2$, ${}^1 f_Q(b) = d_Q(b)$ and ${}^2 f_Q(b) = \tau_Q(b)$ are called the degree and connection number of the vertex b in the graph Q. In chemical modeling of molecular descriptors [49], chemical terms atom and bond are equal to graphical terms vertex and edge, respectively. For further basic terminologies of graphs, we refer to [50].

Definition 1. For a graph Q, the first Zagreb index ($M_1(Q)$), second Zagreb index ($M_2(Q)$), and forgotten index ($F(Q)$) are defined as

$$\begin{aligned} M_1(Q) &= \sum_{b\in V(Q)} \left[d_Q(b)\right]^2 = \sum_{ab\in E(Q)} \left[d_Q(a) + d_Q(b)\right], \\ M_2(Q) &= \sum_{ab\in E(Q)} \left[d_Q(a) \times d_Q(b)\right], \\ F(Q) &= \sum_{b\in V(Q)} \left[d_Q(b)\right]^3 = \sum_{ab\in V(Q)} \left[d_Q^2(a) + d_Q^2(b)\right]. \end{aligned} \tag{1}$$

These degree-based indices are defined by Gutman, Trinajstic, Ruscic, and Furtula (see [22, 23, 51]). These are frequently used to predict better outcomes in molecular structures such as entropy, heat capacity, ZE isomerism, acentric factor, and absolute value of correlation coefficient [52]. These indices also played an important role in the study of QSPR and QSAR (see [18, 19, 49]).

Corresponding to these degree-based TIs, the connection-based TIs are defined in Definition 2. For further studies of connection-based TIs, see [30, 53].

Definition 2. For a graph Q, the first Zagreb connection index ($ZC_1(Q)$), second Zagreb connection index ($ZC_2(Q)$), and modified first Zagreb connection index $ZC_1^*(Q)$ are defined as

$$\begin{aligned} ZC_1(Q) &= \sum_{b\in V(Q)} \left[\tau_Q(b)\right]^2, \\ ZC_2(Q) &= \sum_{ab\in E(Q)} \left[\tau_Q(a) \times \tau_Q(b)\right], \\ ZC_1^*(Q) &= \sum_{b\in V(Q)} d_Q(b)\tau_Q(b) = \sum_{ab\in E(Q)} \left[\tau_Q(a) + \tau_Q(b)\right]. \end{aligned} \tag{2}$$

Now, we describe the subdivision and semitotal point operations on graphs as follows: (a) $S_1(Q)$ is a graph that is obtained by including a new vertex between each edge of the graph Q; (b) $S_2(Q)$ is a graph that is obtained from $S_1(Q)$ by adding the edges between old vertices which are adjacent in Q. More details of these operations can be found in [34, 35, 54, 55]. For further understanding, see Figure 1. The concept of S-sum graphs is defined as in Definition 3.

Definition 3. For $i \in \{1, 2\}$ and $S \in \{S_i\}$, assume that Q_i are connected graphs and the graph $S(Q_1)$ with vertex set

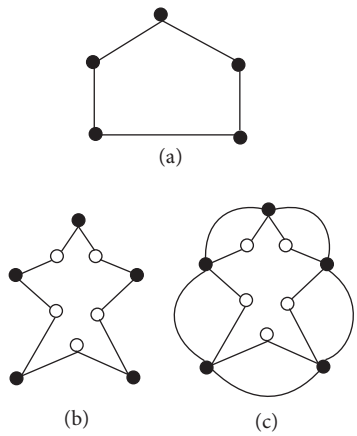

Figure 1: (a) Q, (b) $S_1(Q)$, and (c) $S_2(Q)$.

$V(S(Q_1))$ and edge set $E(S(Q_1))$ is obtained after applying the operation S on Q_1. Then, the graphs $Q_1 +_S Q_2$ with vertex set $V(Q_1 +_S Q_2) = V(S(Q_1)) \times (V_2) = V_1 \cup E_1 \times (V_2)$ and edge set $E(Q_1 +_S Q_2)$ are called S-sum graphs if for $(a_1, b_1)(a_2, b_2) \in E(Q_1 +_s Q_2)$ either $a_1 = a_2$ in $V(Q_1)$ and $b_1 b_2 \in E(Q_2)$ or $b_1 = b_2$ in $V(Q_2)$ and $a_1 a_2 \in E(S(Q_1))$, where (a_1, b_1), $(a_2, b_2) \in V(Q_1 +_S Q_2)$. For more clearance, see Figures 2 and 3.

Now, we present some important results which are used in the main results.

Lemma 1 (see [56]). *Let Q be a connected graph with n vertices and m edges. Then, $\tau_Q(a) + d_Q(a) \le \sum_{b \in N_Q(a)} (d_Q(b))$, where equality holds if and only if Q is a $\{C_3, C_4\}$–free graph.*

Lemma 2. *Let Q be a connected and $\{C_3, C_4\}$–free graph with n vertices and m edges. Then, $\sum_{a \in V(Q)} \tau_Q(a) = M_1(Q) - 2m$.*

Proof. Proof is obvious using Hand-Shaking Lemma and Lemma 1. □

3. Main Results

This section contains the main results of the first Zagreb connection index (ZC_1), second Zagreb connection index (ZC_2), and modified first Zagreb connection index (ZC_1^*) on the S-sum graphs under the operations of subdivision and semitotal point.

Theorem 1. *Let Q_1 and Q_2 be two connected and $\{C_3, C_4\}$–free graphs. Then, the first Zagreb connection indices of their S-sum graphs under the operations of subdivision and semitotal point are*

$$\begin{aligned} ZC_1\left(Q_1 +_{S_1} Q_2\right) &= 4e_1 ZC_1^*(Q_2) + n_1 ZC_1(G_2) + n_2 F(Q_1) \\ &\quad + 2n_2 M_2(Q_1) + 3M_1(Q_1)(4e_2 - n_2) \\ &\quad + M_1(Q_2)[8e_1 + M_1(Q_1)] + 4e_1(n_2 - 6e_2), \end{aligned} \tag{3}$$

$$\begin{aligned} ZC_1\left(Q_1 +_{S_2} Q_2\right) &= 16e_2 ZC_1^*(Q_1) + 8e_1 ZC_1^*(Q_2) \\ &\quad + 4n_2 ZC_1(Q_1) + n_1 ZC_1(Q_2) + n_2 F(Q_1) \\ &\quad + 2n_2[M_2(Q_1) - M_1(Q_1)] \\ &\quad + 4M_1(Q_2)[2M_1(Q_1) - e_1] \\ &\quad + e_1(n_2 + 8e_2). \end{aligned} \tag{4}$$

Proof. (a) Let $\tau(a,b) = \tau_{Q_1 +_{S_1} Q_2}(a,b)$ be a connection number of the vertex (a,b) in the graph $Q_1 +_{S_1} Q_2$. Then,

$$\begin{aligned} ZC_1\left(Q_1 +_{S_1} Q_2\right) &= \sum_{(a,b) \in V\left(Q_1 +_{S_1} Q_2\right)} [\tau(a,b)]^2 \\ &= \sum_{a \in V(Q_1)} \sum_{b \in V(Q_2)} [\tau(a,b)]^2 + \sum_{b \in V(Q_2)} \sum_{a_1 a_2 \in E(Q_1)} \left[\tau(a,b)^2\right]. \end{aligned} \tag{5}$$

Consider

$$\begin{aligned} \sum_{a \in V(Q_1)} \sum_{b \in V(Q_2)} [\tau(a,b)]^2 &= \sum_{a \in V(Q_1)} \sum_{b \in V(Q_2)} \left[d_{Q_1}(a) + d_{Q_1}(a) d_{Q_2}(b) + \tau_{Q_2}(b)\right]^2 \\ &= \sum_{a \in V(Q_1)} \sum_{b \in V(Q_2)} \left[d_{Q_1}^2(a) + d_{Q_1}^2(a) d_{Q_2}^2(b) + \tau_{Q_2}^2(b) + 2d_{Q1}^2(a) d_{Q_2}(b)\right. \\ &\quad \left. + 2d_{Q_1}(a) d_{Q_2}(b) \tau_{Q_2}(b) + 2d_{Q_1}(a) \tau_{Q_2}(b)\right]. \end{aligned} \tag{6}$$

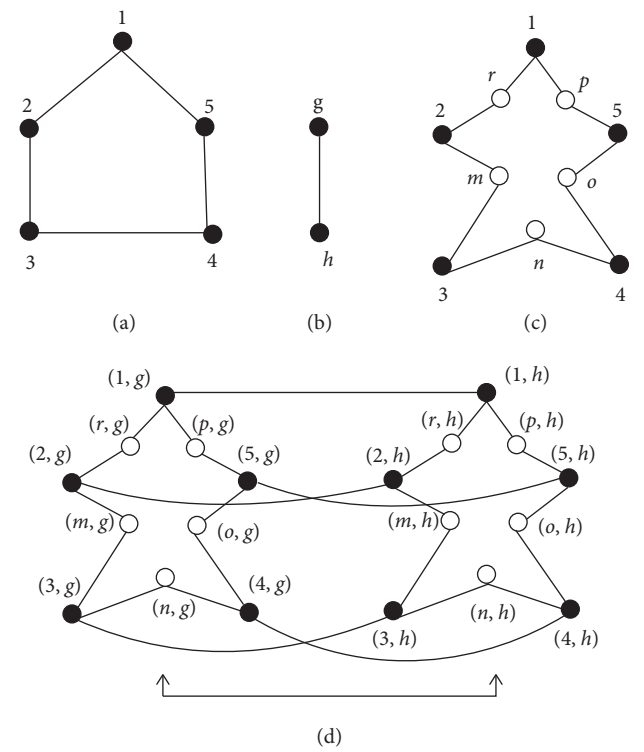

Figure 2: (a) $Q_1 \cong C_5$, (b) $Q_2 \cong P_2$, (c) $S_1(Q_1)$, and (d) $Q_1 +_s Q_2$ iff $S = S_1$.

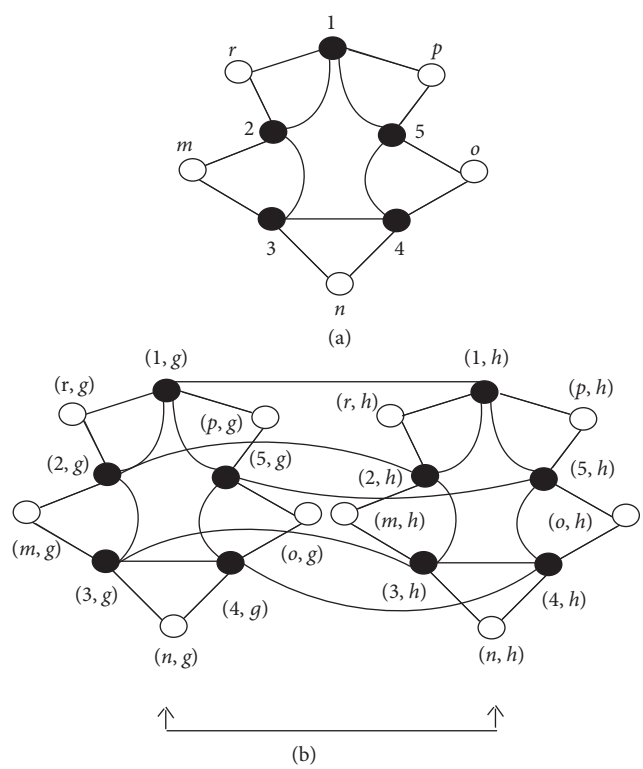

Figure 3: (a) $S_2(Q_1)$ and (b) $Q_1 +_s Q_2$ iff $S = S_2$.

By Lemma 2 $\sum_{b\in V(Q_2)} \tau_{Q_2}(b) = M_1(Q_2) - 2e_2$, we have

$$= n_2 M_1(Q_1) + M_1(Q_1) M_1(Q_2) + n_1 \mathrm{ZC}_1(Q_2) + 4e_2 M_1(Q_1) + 4e_1 \mathrm{ZC}_1^*(Q_2) + 4e_1 (M_1(Q_2) - 2e_2). \tag{7}$$

Since $r(a,b) = [d_{Q_1}(a_1) + 2(d_{Q_2}(b) - 1) + d_{Q_1}(a_2)]^2$, we have

$$\begin{aligned}\sum_{b\in V(Q_2)} \sum_{a_1a_2\in E(Q_1)} [\tau(a,b)]^2 &= \sum_{b\in V(Q_2)} \sum_{a_1a_2\in E(Q_1)} \Big[d_{Q_1}^2(a_1) + 4\big(d_{Q_2}(b) - 1\big)^2 + d_{Q_1}^2(a_2) + 4d_{Q_1}(a_1)\big(d_{Q_2}(b) - 1\big) \\ &\quad + 4d_{Q_1}(a_2)\big(d_{Q_2}(b) - 1\big) + 2d_{Q_1}(a_1)d_{Q_1}(a_2)\Big] \\ &= \sum_{b\in V(Q_2)} \sum_{a_1a_2\in E(Q_1)} \Big[d_{Q_1}^2(a_1) + d_{Q_1}^2(a_2) + 4d_{Q_2}^2(b) - 8d_{Q_2}(b) \\ &\quad + 4d_{Q_2}(b)\big(d_{Q_1}(a_1) + d_{Q_1}(a_2)\big) - 4\big(d_{Q_1}(a_1) + d_{Q_1}(a_2)\big) + 2d_{Q_1}(a_1)d_{Q_1}(a_2) + 4\Big].\end{aligned} \tag{8}$$

By Definition 1 $F(Q_1) = \sum_{a_1a_2\in E(Q_1)} (d_{Q_1}^2(a_1) + d_{Q_1}^2(a_2))$, we have

$$\begin{aligned}&= \sum_{b\in V(Q_2)} \Big[F(Q_1) + 4e_1 d_{Q_2}^2(b) - 8e_1 d_{Q_2}(b) \\ &\quad + 4d_{Q_2}(b)(M_1(Q_1)) - 4M_1(Q_1) + 2M_2(Q_1) + 4e_1\Big] \\ &= n_2 F(Q_1) + 4e_1 M_1(Q_2) - 16e_1e_2 + 8e_2 M_1(Q_1) \\ &\quad - 4n_2 M_1(Q_1) + 2n_2 M_2(Q_1) + 4n_2 e_1.\end{aligned} \tag{9}$$

Finally, we obtain

$$\begin{aligned}\mathrm{ZC}_1\big(Q_1 +_{S_1} Q_2\big) &= 4e_1 \mathrm{ZC}_1^*(Q_2) + n_1 \mathrm{ZC}_1(Q_2) + n_2 F(Q_1) \\ &\quad + 2n_2 M_2(Q_1) + 3M_1(Q_1)(4e_2 - n_2) \\ &\quad + M_1(Q_2)[8e_1 + M_1(Q_1)] + 4e_1(n_2 - 6e_2).\end{aligned} \tag{10}$$

□

Proof. (b) Let $\tau(a,b) = \tau_{Q_1 +_{S_2} Q_2}(a,b)$ be a connection number of the vertex (a,b) in the graph $Q_1 +_{S_2} Q_2$. Then,

$$\mathrm{ZC}_1\left(Q_1 +_{S_2} Q_2\right) = \sum_{(a,b)\in V\left(Q_1 +_{S_2} Q_2\right)} [\tau(a,b)]^2 = \sum_{a\in V(Q_1)} \sum_{b\in V(Q_2)} [\tau(a,b)]^2 + \sum_{b\in V(Q_2)} \sum_{a_1a_2\in E(S_2(Q_1))} [\tau(a,b)]^2. \tag{11}$$

Consider

$$\begin{aligned}\sum_{a\in V(Q_1)} \sum_{b\in V(Q_2)} [\tau(a,b)]^2 &= \sum_{a\in V(Q_1)} \sum_{b\in V(Q_2)} \left[2\tau_{Q_1}(a) + \tau_{Q_2}(b) + 2d_{Q_1}(a)d_{Q_2}(b)^2\right] \\ &= \sum_{a\in V(Q_1)} \sum_{b\in V(G_2)} \left[4\tau_{Q_1}^2(a) + \tau_{Q_2}^2(b) + 4d_{Q_1}^2(a)d_{Q_2}^2(b) + 4\tau_{Q1}(a)\tau_{Q_2}(b)\right. \\ &\quad \left. + 4d_{Q_1}(a)d_{Q_2}(b)\tau_{Q_2}(b) + 8d_{Q_2}(b)d_{Q_1}(a)\tau_{Q_1}(a)\right].\end{aligned} \tag{12}$$

Using Definition 2 and Lemma 2, we have

$$\begin{aligned}&= 4n_2\mathrm{ZC}_1(Q_1) + n_1\mathrm{ZC}_1(Q_2) + 4M_1(Q_1)M_1(Q_2) + 4\left[\sum_{a\in V(Q_1)} \tau_{Q_1}(a)\right]\left[\sum_{b\in V(Q_2)} \tau_{Q_2}(b)\right] + 8e_1\mathrm{ZC}_1^*(Q_2) + 8e_2\mathrm{ZC}_1^*(Q_1) \\ &= 4n_2\mathrm{ZC}_1(Q_1) + n_1\mathrm{ZC}_1(Q_2) + 8M_1(Q_1)M_1(Q_2) - 8e_2M_1(Q_1) - 8e_1M_1(Q_2) + 16e_1e_2 + 8e_1\mathrm{ZC}_1^*(Q_2) + 16e_2\mathrm{ZC}_1^*(Q_1).\end{aligned} \tag{13}$$

Also, consider

$$\begin{aligned}\sum_{b\in V(Q_2)} \sum_{a_1a_2\in E(S_2(Q_1))} [\tau(a,b)]^2 &= \sum_{b\in V(Q_2)} \sum_{a_1a_2\in E(Q_1)} \left[d_{Q_1}(a_1) + \left(2d_{Q_2}(b) - 1\right) + d_{Q_1}(a_2)\right]^2 \\ &= \sum_{b\in V(Q_2)} \sum_{a_1a_2\in E(Q_1)} \left[d_{Q_1}^2(a_1) + \left(2d_{Q_2}(b) - 1\right)^2 + d_{Q_1}^2(a_2) + 2d_{Q_1}(a_1)\left(2d_{Q_2}(b) - 1\right)\right. \\ &\quad \left. + 2d_{Q_1}(a_2)\left(2d_{Q_2}(b) - 1\right) + 2d_{Q_1}(a_1)d_{Q_1}(a_2)\right] \\ &= \sum_{b\in V(Q_2)} \left[F(Q_1) + 4e_1d_{Q_2}^2(b) - 4e_1d_{Q_2}(b) + 4M_1(Q_1)d_{Q_2}(b) - 2M_1(Q_1) + 2M_2(Q_1) + e_1\right] \\ &= n_2F(Q_1) + 4e_1M_1(Q_2) - 8e_1e_2 + 8e_2M_1(Q_1) - 2n_2M_1(Q_1) + 2n_2M_2(Q_1) + n_2e_1.\end{aligned} \tag{14}$$

Finally, we obtain

$$\begin{aligned}\mathrm{ZC}_1\left(Q_1 +_{S_2} Q_2\right) &= 16e_2\mathrm{ZC}_1^*(Q_1) + 8e_1\mathrm{ZC}_1^*(Q_2) + 4n_2\mathrm{ZC}_1(Q_1) + n_1\mathrm{ZC}_1(Q_2) \\ &\quad + n_2F(Q_1) + 2n_2\left[M_2(Q_1) - M_1(Q_1)\right] + 4M_1(Q_2)\left[2M_1(Q_1) - e_1\right] + e_1(n_2 + 8e_2).\end{aligned} \tag{15}$$

□

Theorem 2. *Let Q_1 and Q_2 be two connected and $\{C_3, C_4\}$–free graphs. Then, the second Zagreb connection indices of their S-sum graphs under the operations of subdivision and semitotal point are*

$$\begin{aligned}\mathrm{ZC}_2\left(G_1 +_{S_1} Q_2\right) &= 6e_1\mathrm{ZC}_1^*(Q_2) + n_1\mathrm{ZC}_2(Q_2) + (n_2 + 2e_2)[M_3(Q_1) + 2M_2(Q_1)] - (2n_2 + 3e_2)M_1(Q_1)\\ &\quad - 4e_1M_1(Q_2) + [5M_1(Q_2) + M_2(Q_2)]M_1(Q_1) + 8e_1e_2 + 2e_1\sum_{b_1b_2\in E(Q_2)}\left[d_{Q_2}(b_1)\tau_{Q_2}(b_2) + d_{Q_2}(b_2)\tau_{Q_2}(b_1)\right],\end{aligned} \tag{16}$$

$$\begin{aligned}\mathrm{ZC}_2\left(Q_1 +_{S_2} Q_2\right) &= [6M_1(Q_2) + 4e_2 - 2n_2]\mathrm{ZC}_1^*(Q_1) + 4M_1(Q_1)\mathrm{ZC}_1^*(Q_2) + n_1\mathrm{ZC}_2(Q_2) + 4n_2\mathrm{ZC}_2(Q_1) + 4e_2\mathrm{ZC}_1(Q_1)\\ &\quad + e_1\mathrm{ZC}_1(Q_2) + 4e_2M_3(Q_1) + 8e_2[M_2(Q_1) - M_1(Q_1)] - 2e_1M_1(Q_2) + 2M_1(Q_1)[2M_2(Q_2) + 3M_1(Q_2)]\\ &\quad + 4M_1(Q_2)M_2(Q_1) + 4e_1\sum_{b_1b_2\in E(Q_2)}\left[d_{Q_2}(b_2)\tau_{Q_2}(b_1) + d_{Q_2}(b_1)\tau_{Q_2}(b_2)\right] + 2(n_2 + 4e_2)\\ &\quad \cdot\sum_{a_1a_2\in E(Q_1)}\left[d_{Q_1}(a_2)\tau_{Q_1}(a_1) + d_{Q_1}(a_1)\tau_{Q_1}(a_2)\right] + 2n_2\sum_{a_1a_2\in E(Q_1)}\left[d_{Q_1}(a_1)\tau_{Q_1}(a_1) + d_{Q_1}(a_2)\tau_{Q_1}(a_2)\right] + 4e_1e_2.\end{aligned} \tag{17}$$

Proof. (a) Let $\tau(a,b) = \tau_{Q_1+_{S_1}Q_2}(a,b)$ be a connection number of the vertex (a,b) in the graph $Q_1+_{S_1}Q_2$. Then,

$$\begin{aligned}\mathrm{ZC}_2\left(Q_1 +_{S_1} Q_2\right) &= \sum_{(a_1,b_1)(a_2,b_2)\in E\left(Q_1+_{S_1}Q_2\right)}[\tau(a_1,b_1)\times\tau(a_2,b_2)]\\ &= \sum_{a\in V(Q_1)}\sum_{b_1b_2\in E(Q_2)}[\tau(a,b_1)\times\tau(a,b_2)] + \sum_{b\in V(Q_2)}\sum_{a_1a_2\in E(S_1(G_1))}[\tau(a_1,b)\times\tau(a_2,b)].\end{aligned} \tag{18}$$

Consider

$$\begin{aligned}&\sum_{a\in V(Q_1)}\sum_{b_1b_2\in E(Q_2)}[\tau(a,b_1)\times\tau(a,b_2)]\\ &= \sum_{a\in V(Q_1)}\sum_{b_1b_2\in E(Q_2)}\left[d_{Q_1}(a) + d_{Q_1}(a)d_{Q_2}(b_1) + \tau_{Q_2}(b_1)\right]\times\left[d_{Q_1}(a) + d_{Q_1}(a)d_{Q_2}(b_2) + \tau_{Q_2}(b_2)\right]\\ &= \sum_{a\in V(Q_1)}\sum_{b_1b_2\in E(Q_2)}\left[d_{Q_1}^2(a) + d_{Q_1}^2(a)d_{Q_2}(b_2) + d_{Q_1}(a)\tau_{Q_2}(b_2) + d_{Q_1}^2(a)d_{Q_2}(b_1) + d_{Q_1}^2(a)d_{Q_2}(b_1)d_{Q_2}(b_2)\right.\\ &\quad \left. + d_{Q_1}(a)d_{Q_2}(b_1)\tau_{Q_2}(b_2) + d_{Q_1}(a)\tau_{Q_2}(b_1) + d_{Q_1}(a)\tau_{Q_2}(b_1)d_{Q_2}(b_2) + \tau_{Q_2}(b_1)\tau_{Q_2}(b_2)\right]\\ &= \sum_{a\in V(Q_1)}\sum_{b_1b_2\in E(Q_2)}\left[d_{Q_1}^2(a) + d_{Q_1}^2(a)\left\{d_{Q_2}(b_1) + d_{Q_2}(b_2)\right\} + d_{Q_1}(a)\left\{\tau_{Q_2}(b_1) + \tau_{Q_2}(b_2)\right\} + d_{Q_1}^2(a)\left\{d_{Q_2}(b_1)d_{Q_2}(b_2)\right\}\right.\\ &\quad \left. + d_{Q_1}(a)\left\{d_{Q_2}(b_1)\tau_{Q_2}(b_2) + d_{Q_2}(b_2)\tau_{Q_2}(b_1)\right\} + \tau_{Q_2}(b_1)\tau_{Q_2}(b_2)\right]\\ &= \sum_{a\in V(Q_1)}\left[e_2d_{Q_1}^2(a) + M_1(Q_2)d_{Q_1}^2(a) + \mathrm{ZC}_1^*(Q_2)d_{Q_1}(a) + M_2(Q_2)d_{Q_1}^2(a)\right.\\ &\quad \left. + d_{Q_1}(a)\sum_{b_1b_2\in E(Q_2)}\left\{d_{Q_2}(b_1)\tau_{Q_2}(b_2) + d_{Q_2}(b_2)\tau_{Q_2}(b_1)\right\} + \mathrm{ZC}_2(Q_2)\right]\\ &= e_2M_1(Q_1) + M_1(Q_1)M_1(Q_2) + 2e_1\mathrm{ZC}_1^*(Q_2) + M_1(Q_1)M_2(Q_2) + n_1\mathrm{ZC}_2(Q_2)\\ &\quad + 2e_1\sum_{b_1b_2\in E(Q_2)}\left\{d_{Q_2}(b_1)\tau_{Q_2}(b_2) + d_{Q_2}(b_2)\tau_{Q_2}(b_1)\right\}.\end{aligned} \tag{19}$$

Also, consider

$$\begin{aligned}
&\sum_{b\in V(Q_2)}\sum_{a_1a_2\in E(S_1(Q_1))}[\tau(a_1,b)\times\tau(a_2,b)]\\
&=\sum_{b\in V(Q_2)}\sum_{a_1a_2\in E(Q_1)}\left[d_{Q_1}(a_1)+d_{Q_1}(a_1)d_{Q_2}(b)+2\tau_{Q_2}(b)+d_{Q_1}(a_2)+d_{Q_1}(a_2)d_{Q_2}(b)\right]\times\left[d_{Q_1}(a_1)+d_{Q_1}(a_2)+2d_{Q_2}(b)-2\right]\\
&=\sum_{b\in V(Q_2)}\sum_{a_1a_2\in E(Q_1)}\left[d^2_{Q_1}(a_1)+d_{Q_1}(a_1)d_{Q_1}(a_2)+2d_{Q_1}(a_1)d_{Q_2}(b)-2d_{Q_1}(a_1)+d^2_{Q_1}(a_1)d_{Q_2}(b)+d_{Q_1}(a_1)d_{Q_1}(a_2)d_{Q_2}(b)\right.\\
&\quad+2d_{Q_1}(a_1)d^2_{Q_2}(b)-2d_{Q_1}(a_1)d_{Q_2}(b)+2d_{Q_1}(a_1)\tau_{Q_2}(b)+2d_{Q_1}(a_2)\tau_{Q_2}(b)+4d_{Q_2}(b)\tau_{Q_2}(b)-4\tau_{Q_2}(b)+d_{Q_1}(a_1)d_{Q_1}(a_2)\\
&\quad\left.+d^2_{Q_1}(a_2)+2d_{Q_1}(a_2)d_{Q_2}(b)-2d_{Q_1}(a_2)+d_{Q_1}(a_1)d_{Q_1}(a_2)d_{Q_2}(b)+d^2_{Q_1}(a_2)d_{Q_2}(b)+2d_{Q_1}(a_2)d^2_{Q_2}(b)-2d_{Q_1}(a_2)d_{Q_2}(b)\right]\\
&=\sum_{b\in V(Q_2)}\sum_{a_1a_2\in E(Q_1)}\left[\left\{d^2_{Q_1}(a_1)+d^2_{Q_1}(a_2)\right\}+d_{Q_1}(a_1)d_{Q_1}(a_2)-2\left\{d_{Q_1}(a_1)+d_{Q_1}(a_2)\right\}+d_{Q_2}(b)\left\{d^2_{Q_1}(a_1)+d^2_{Q_1}(a_2)\right\}\right.\\
&\quad+2d_{Q_1}(a_1)d_{Q_1}(a_2)d_{Q_2}(b)+2d^2_{Q_2}(b)\left\{d_{Q_1}(a_1)+d_{Q_1}(a_2)\right\}+2\tau_{Q_2}(b)\left\{d_{Q_1}(a_1)+d_{Q_1}(a_2)\right\}\\
&\quad\left.+4d_{Q_2}(b)\tau_{Q_2}(b)-4\tau_{Q_2}(b)+d_{Q_1}(a_1)d_{Q_1}(a_2)\right]\\
&=\sum_{b\in V(Q_2)}\left[M_3(Q_1)+M_2(Q_1)-2M_1(Q_1)+M_3(Q_1)d_{Q_2}(b)+2M_2(Q_1)d_{Q_2}(b)+2M_1(Q_1)d^2_{Q_2}(b)\right.\\
&\quad\left.+2M_1(Q_1)\tau_{Q_2}(b)+4e_1d_{Q_2}(b)\tau_{G_2}(b)-4e_1\tau_{Q_2}(b)+M_2(Q_1)\right]\\
&=n_2M_3(Q_1)+n_2M_2(Q_1)-2n_2M_1(Q_1)+2e_2M_3(Q_1)+4e_2M_2(Q_1)+2M_1(Q_1)M_1(Q_2)\\
&\quad+2M_1(Q_1)\{M_1(Q_2)-2e_2\}+4e_1ZC^*_1(Q_2)-4e_1\{M_1(Q_2)-2e_2\}+n_2M_2(Q_1)\\
&=n_2M_3(Q_1)+2n_2M_2(Q_1)-2n_2M_1(Q_1)+2e_2M_3(Q_1)+4e_2M_2(Q_1)+4M_1(Q_1)M_1(Q_2)\\
&\quad-4e_2M_1(Q_1)+4e_1ZC^*_1(Q_2)-4e_1M_1(Q_2)+8e_1e_2.
\end{aligned}\tag{20}$$

Therefore,

$$\begin{aligned}
ZC_2\left(G_1+_{S_1}Q_2\right)&=6e_1ZC^*_1(Q_2)+n_1ZC_2(Q_2)+(n_2+2e_2)[M_3(Q_1)+2M_2(Q_1)]-(2n_2+3e_2)M_1(Q_1)-4e_1M_1(Q_2)\\
&\quad+[5M_1(Q_2)+M_2(Q_2)]M_1(Q_1)+8e_1e_2+2e_1\sum_{b_1b_2\in E(Q_2)}\left[d_{Q_2}(b_1)\tau_{Q_2}(b_2)+d_{Q_2}(b_2)\tau_{Q_2}(b_1)\right].
\end{aligned}\tag{21}$$

□

proof. (b) Let $\tau(a,b)=\tau_{Q_1+_{S_2}Q_2}(a,b)$ be a connection number of the vertex (a,b) in the graph $Q_1+_{S_2}Q_2$. Then,

$$ZC_2\left(Q_1 +_{S_2} Q_2\right) = \sum_{(a_1,b_1)(a_2,b_2)\in E\left(Q_1+_{S_2}Q_2\right)} \left[\tau(a_1,b_1)\times\tau(a_2,b_2)\right]$$
$$= \sum_{a\in V(Q_1)}\sum_{b_1b_2\in E(Q_2)} \left[\tau(a,b_1)\times\tau(a,b_2)\right] + \sum_{b\in V(Q_2)}\sum_{a_1a_2\in E(S_2(G_1))} \left[\tau(a_1,b)\times\tau(a_2,b)\right]. \tag{22}$$

Consider

$$\begin{aligned}
\sum 1 &= \sum_{a\in V(Q_1)}\sum_{b_1b_2\in E(Q_2)} \left[\tau(a,b_1)\times\tau(a,b_2)\right] \\
&= \sum_{a\in V(Q_1)}\sum_{b_1b_2\in E(G_2)} \left[2\tau_{Q_1}(a)+\tau_{Q_2}(b_1)+2d_{Q_1}(a)d_{Q_2}(b_1)\right]\times\left[2\tau_{Q_1}(a)+\tau_{Q_2}(b_2)+2d_{Q_1}(a)d_{Q_2}(b_2)\right] \\
&= \sum_{a\in V(Q_1)}\sum_{b_1v_2\in E(Q_2)} \Big[4\tau_{Q_1}^2(a)+2\tau_{Q_1}(a)\tau_{Q_2}(b_2)+4d_{Q_1}(a)\tau_{Q_1}(a)d_{Q_2}(b_2)+2\tau_{Q_1}(a)\tau_{Q_2}(b_1)+\tau_{Q_2}(b_1)\tau_{G_2}(b_2) \\
&\quad + 2d_{Q_1}(a)d_{Q_2}(b_2)\tau_{Q_2}(b_1)+4d_{Q_1}(a)\tau_{Q_1}(a)d_{Q_2}(b_1)+2d_{Q_1}(a)d_{Q_2}(b_1)\tau_{Q_2}(b_2)+4d_{Q_1}^2(a)d_{Q_2}(b_1)d_{Q_2}(b_2)\Big] \\
&= \sum_{a\in V(Q_1)}\sum_{b_1v_2\in E(Q_2)} \Big[4\tau_{Q_1}^2(a)+2\tau_{Q_1}(a)\left\{\tau_{Q_2}(b_1)\tau_{Q_2}(b_2)\right\}+4d_{Q_1}(a)\tau_{Q_1}(a)\left\{d_{Q_2}(b_1)+d_{Q_2}(b_2)\right\}+\tau_{Q_2}(b_1)\tau_{Q_2}(b_2) \\
&\quad + 2d_{Q_1}(u)d_{Q_2}(v_2)\tau_{Q_2}(v_1)+2d_{Q_1}(u)d_{Q_2}(v_1)\tau_{Q_2}(b_2)+4d_{Q_1}^2(a)d_{Q_2}(b_1)d_{Q_2}(b_2)\Big] \\
&= \sum_{a\in V(Q_1)}\Bigg[4e_2\tau_{Q_1}^2(a)+2ZC_1^*(Q_2)\tau_{Q_1}(a)+4M_1(Q_2)d_{Q_1}(a)\tau_{Q_1}(a)+ZC_2(Q_2)+2d_{Q_1}(a)\sum_{b_1b_2\in E(Q_2)} d_{Q_2}(b_2)\tau_{Q_2}(b_1) \\
&\quad + 2d_{Q_1}(a)\sum_{b_1b_2\in E(Q_2)} d_{Q_2}(b_1)\tau_{Q_2}(b_2)+4M_2(Q_2)d_{Q_1}^2(a)\Bigg] \\
&= 4e_2ZC_1(Q_1)+2ZC_1^*(Q_2)\{M_1(Q_1)-2e_1\}+4M_1(Q_2)ZC_1^*(Q_1)+n_1ZC_2(Q_2)+4e_1\sum_{v_1v_2\in E(Q_2)} d_{Q_2}(b_2)\tau_{Q_2}(b_1) \\
&\quad + 4e_1\sum_{b_1b_2\in E(Q_2)} d_{Q_2}(b_1)\tau_{Q_2}(b_2)+4M_1(Q_1)M_2(Q_2) \\
&= 4e_2ZC_1(Q_1)+2M_1(Q_1)ZC_1^*(Q_2)-4e_1ZC_1^*(Q_2)+4M_1(Q_2)ZC_1^*(Q_1)+n_1ZC_2(Q_2) \\
&\quad + 4M_1(Q_1)M_2(Q_2)+4e_1\sum_{b_1b_2\in E(Q_2)}\left\{d_{Q_2}(b_2)\tau_{Q_2}(b_1)+d_{Q_2}(b_1)\tau_{Q_2}(b_2)\right\}.
\end{aligned} \tag{23}$$

Also, consider

$$
\begin{aligned}
&\sum_{b\in V(Q_2)}\sum_{a_1a_2\in E(S_2(G_1))}\left[\tau(a_1,b)\times\tau(a_2,b)\right]=\sum 2+\sum 3\\
&\sum 2=\sum_{b\in V(Q_2)}\sum_{a_1a_2\in E(Q_1)}\left[2\tau_{Q_1}(a_1)+\tau_{Q_2}(b)+2d_{Q_1}(a_1)d_{Q_2}(b)\right]\times\left[2\tau_{Q_1}(a_2)+\tau_{Q_2}(b)+2d_{Q_1}(a_2)d_{Q_2}(b)\right]\\
&\quad=\sum_{b\in V(Q_2)}\sum_{a_1a_2\in E(G_1)}\left[4\tau_{Q_1}(a_1)\tau_{Q_1}(a_2)+2\tau_{Q_1}(a_1)\tau_{Q_2}(b)+4d_{Q_1}(a_2)\tau_{Q_1}(a_1)d_{Q_2}(b)+2\tau_{Q_1}(a_2)\tau_{Q_2}(b)+\tau_{Q_2}^2(b)\right.\\
&\qquad\left.+2d_{Q_1}(a_2)d_{Q_2}(b)\tau_{Q_2}(b)+4d_{Q_1}(a_1)\tau_{Q_1}(a_2)d_{Q_2}(b)+2d_{Q_1}(a_1)d_{Q_2}(b)\tau_{Q_2}(b)+4d_{Q_1}(a_1)d_{Q_1}(a_2)d_{Q_2}^2(b)\right]\\
&\quad=\sum_{b\in V(Q_2)}\sum_{a_1a_2\in E(Q_1)}\left[4\tau_{Q_1}(a_1)\tau_{Q_1}(a_2)+2\tau_{Q_2}(b)\left\{\tau_{Q_1}(a_1)+\tau_{Q_1}(a_2)\right\}+\tau_{Q_2}^2(b)+2d_{Q_2}(b)\tau_{Q_2}(b)\left\{d_{Q_1}(a_1)+d_{Q_1}(a_2)\right\}\right.\\
&\qquad\left.+4d_{Q_1}(a_1)d_{Q_1}(a_2)d_{Q_2}^2(b)+4d_{Q_1}(a_2)\tau_{Q_1}(a_1)d_{Q_2}(b)+4d_{Q_1}(a_1)\tau_{Q_1}(a_2)d_{Q_2}(b)\right]\\
&\quad=\sum_{b\in V(Q_2)}\left[4ZC_2(Q_1)+2ZC_1^*(Q_1)\tau_{Q_2}(b)+e_1\tau_{Q_2}^2(b)+2M_1(Q_1)d_{Q_2}(b)\tau_{Q_2}(b)+4M_2(Q_1)d_{Q_2}^2(b)\right.\\
&\qquad\left.+4d_{Q_2}(b)\sum_{a_1a_2\in E(Q_1)}d_{Q_1}(a_2)\tau_{Q_1}(a_1)+4d_{Q_2}(b)\sum_{a_1a_2\in E(Q_1)}d_{Q_1}(a_1)\tau_{Q_1}(a_2)\right]\\
&\quad=4n_2ZC_2(Q_1)+2ZC_1^*(Q_1)\{M_1(Q_2)-2e_2\}+e_1ZC_1(Q_2)+2M_1(Q_1)ZC_1^*(Q_2)+4M_2(Q_1)M_1(Q_2)\\
&\qquad+8e_2\sum_{u_1u_2\in E(Q_1)}d_{Q_1}(a_2)\tau_{Q_1}(a_1)+8e_2\sum_{a_1a_2\in E(Q_1)}d_{Q_1}(a_1)\tau_{Q_1}(a_2)\\
&\quad=4n_2ZC_2(Q_1)+2M_1(Q_2)ZC_1^*(Q_1)-4e_2ZC_1^*(Q_1)+e_1ZC_1(Q_2)+2M_1(Q_1)ZC_1^*(Q_2)+4M_2(Q_1)M_1(Q_2)\\
&\qquad+8e_2\sum_{a_1a_2\in E(Q_1)}\left[d_{Q_1}(a_2)\tau_{Q_1}(a_1)+d_{Q_1}(a_1)\tau_{Q_1}(a_2)\right],\\
&\sum 3=\sum_{b\in V(Q_2)}\sum_{a_1a_2\in E(Q_1)}\left[2\tau_{Q_1}(a_1)+2\tau_{Q_2}(b)+2d_{Q_1}(a_1)d_{Q_2}(b)+2\tau_{Q_1}(a_2)+2d_{Q_1}(a_2)d_{Q_2}(b)\right]\\
&\qquad\times\left[d_{Q_1}(a_1)+d_{Q_1}(a_2)+2d_{Q_2}(b)-1\right]\\
&\quad=\sum_{b\in V(Q_2)}\sum_{a_1a_2\in E(Q_1)}\left[2d_{Q_1}(a_1)\tau_{Q_1}(a_1)+2d_{Q_1}(a_2)\tau_{Q_1}(a_1)+4\tau_{Q_1}(a_1)d_{Q_2}(b)-2\tau_{Q_1}(a_1)+2d_{Q_1}(a_1)\tau_{Q_2}(b)\right.\\
&\qquad+2d_{Q_1}(a_2)\tau_{Q_2}(b)+4d_{Q_2}(b)\tau_{Q_2}(b)-2\tau_{Q_2}(b)+2d_{Q_1}^2(a_1)d_{Q_2}(b)+2d_{Q_1}(a_1)d_{Q_1}(a_2)d_{Q_2}(b)+4d_{Q_1}(a_1)d_{Q_2}^2(b)\\
&\qquad-2d_{Q_1}(a_1)d_{Q_2}(b)+2d_{Q_1}(a_1)\tau_{Q_1}(a_2)+2d_{Q_1}(a_2)\tau_{Q_1}(a_2)+4\tau_{Q_1}(a_2)d_{Q_2}(b)-2\tau_{Q_1}(a_2)\\
&\qquad\left.+2d_{Q_1}(a_1)d_{Q_1}(a_2)d_{Q_2}(b)+2d_{Q_1}^2(a_2)d_{Q_2}(b)+4d_{Q_1}(a_2)d_{Q_2}^2(b)-2d_{Q_1}(a_2)d_{Q_2}(b)\right]\\
&\quad=\sum_{b\in V(Q_2)}\sum_{a_1a_2\in E(G_1)}\left[4d_{Q_2}(b)\left\{\tau_{Q_1}(a_1)+\tau_{Q_1}(a_2)\right\}-2\left\{\tau_{Q_1}(a_1)+\tau_{Q_1}(a_2)\right\}+2\tau_{Q_2}(b)\left\{d_{Q_1}(a_1)+d_{Q_1}(a_1)\right\}\right.\\
&\qquad+4d_{Q_2}(b)\tau_{Q_2}(b)-2\tau_{Q_2}(b)+2d_{Q_2}(b)\left\{d_{Q_1}^2(a_1)+d_{Q_1}^2(a_2)\right\}+4d_{Q_1}(a_1)d_{Q_1}(a_2)d_{Q_2}(b)+4d_{Q_2}^2(b)\left\{d_{Q_1}(a_1)+d_{Q_1}(a_2)\right\}\\
&\qquad\left.-2d_{Q_2}(b)\left\{d_{Q_1}(a_1)+d_{Q_1}(a_2)\right\}+2d_{Q_1}(a_1)\tau_{Q_1}(a_1)+2d_{Q_1}(a_2)\tau_{Q_1}(a_1)+2d_{Q_1}(a_1)\tau_{Q_1}(a_2)+2d_{Q_1}(a_2)\tau_{Q_1}(a_2)\right]\\
&\quad=\sum_{b\in V(Q_2)}\left[4ZC_1^*(G_1)d_{Q_2}(b)-2ZC_1^*(Q_1)+2M_1(Q_1)\tau_{Q_2}(v)+4e_1d_{Q_2}(b)\tau_{Q_2}(b)-2e_1\tau_{Q_2}(b)+2M_3(Q_1)d_{Q_2}(b)\right.\\
&\qquad+4M_2(Q_1)d_{Q_2}(b)+4M_1(Q_1)d_{Q_2}^2(b)-2M_1(Q_1)d_{Q_2}(b)+2\sum_{a_1a_2\in E(Q_1)}d_{Q_1}(a_1)\tau_{G_1}(a_1)+2\sum_{a_1a_2\in E(G_1)}d_{G_1}(a_2)\tau_{G_1}(a_1)\\
&\qquad\left.+2\sum_{a_1a_2\in E(Q_1)}d_{Q_1}(a_1)\tau_{Q_1}(a_2)+2\sum_{a_1a_2\in E(Q_1)}d_{Q_1}(a_2)\tau_{Q_1}(a_2)\right]\\
&\quad=8e_2ZC_1^*(Q_1)-2n_2ZC_1^*(Q_1)+6M_1(Q_1)M_1(Q_2)-8e_2M_1(Q_1)+4e_1ZC_1^*(Q_2)-2e_1M_1(Q_2)+4e_1e_2+4e_2M_3(Q_1)\\
&\qquad+8e_2M_2(Q_1)+2n_2\sum_{a_1a_2\in E(Q_1)}\left[d_{Q_1}(a_1)\tau_{Q_1}(a_1)+d_{Q_1}(a_2)\tau_{Q_1}(a_2)\right]+2n_2\sum_{a_1a_2\in E(Q_1)}\left[d_{Q_1}(a_2)\tau_{Q_1}(a_1)+d_{Q_1}(a_1)\tau_{Q_1}(a_2)\right].
\end{aligned}
\tag{24}
$$

Consequently,

$$\begin{aligned}
\mathrm{ZC}_2\left(Q_1 +_{S_2} Q_2\right) &= \sum 1 + \sum 2 + \sum 3 \\
&= \left[6M_1\left(Q_2\right) + 4e_2 - 2n_2\right]\mathrm{ZC}_1^*\left(Q_1\right) + 4M_1\left(Q_1\right)\mathrm{ZC}_1^*\left(Q_2\right) + n_1\mathrm{ZC}_2\left(Q_2\right) + 4n_2\mathrm{ZC}_2\left(Q_1\right) + 4e_2\mathrm{ZC}_1\left(Q_1\right) \\
&\quad + e_1\mathrm{ZC}_1\left(Q_2\right) + 4e_2M_3\left(Q_1\right) + 8e_2\left[M_2\left(Q_1\right) - M_1\left(Q_1\right)\right] - 2e_1M_1\left(Q_2\right) + 2M_1\left(Q_1\right) \\
&\quad \cdot \left[2M_2\left(Q_2\right) + 3M_1\left(Q_2\right)\right] + 4M_1\left(Q_2\right)M_2\left(Q_1\right) + 4e_1 \sum_{b_1b_2\in E\left(Q_2\right)} \left[d_{Q_2}\left(b_2\right)\tau_{Q_2}\left(b_1\right) + d_{Q_2}\left(b_1\right)\tau_{Q_2}\left(b_2\right)\right] \\
&\quad + 2\left(n_2 + 4e_2\right) \sum_{a_1a_2\in E\left(Q_1\right)} \left[d_{Q_1}\left(a_2\right)\tau_{Q_1}\left(a_1\right) + d_{Q_1}\left(a_1\right)\tau_{Q_1}\left(a_2\right)\right] \\
&\quad + 2n_2 \sum_{a_1a_2\in E\left(Q_1\right)} \left[d_{Q_1}\left(a_1\right)\tau_{Q_1}\left(a_1\right) + d_{Q_1}\left(a_2\right)\tau_{Q_1}\left(a_2\right)\right] + 4e_1e_2.
\end{aligned} \tag{25}$$

Theorem 3. *Let Q_1 and Q_2 be two connected and $\{C_3, C_4\}$–free graphs. Then, the modified first Zagreb connection indices of their S-sum graphs under the operations of subdivision and semitotal point are*

$$\begin{aligned}
\mathrm{ZC}_1^*\left(Q_1 +_{S_1} Q_2\right) &= n_1\mathrm{ZC}_1^*\left(Q_2\right) + M_1\left(Q_1\right)\left(3n_2 + 2e_2\right) \\
&\quad + 4e_1M_1\left(Q_2\right) + 8e_1e_2 - 4n_2e_1,
\end{aligned} \tag{26}$$

$$\begin{aligned}
\mathrm{ZC}_1^*\left(Q_1 +_{S_2} Q_2\right) &= 4n_2\mathrm{ZC}_1^*\left(Q_1\right) + n_1\mathrm{ZC}_1^*\left(Q_2\right) \\
&\quad + 2M_1\left(Q_1\right)\left(n_2 + 6e_2\right) + 8e_1M_1\left(Q_2\right) \\
&\quad - 2e_1\left(n_2 + 4e_2\right).
\end{aligned} \tag{27}$$

Proof. (a) Let $\tau(a,b) = \tau_{Q_1+_{S_1}Q_2}(a,b)$ be a connection number of the vertex (a,b) in the graph $Q_1 +_{S_1} Q_2$. Then,

$$\begin{aligned}
\mathrm{ZC}_1^*\left(Q_1 +_{S_1} Q_2\right) &= \sum_{\left(a_1,b_1\right)\left(a_2,b_2\right)\in E\left(Q_1+_{S_1}Q_2\right)} \left[\tau\left(a_1,b_1\right) + \tau\left(a_2,b_2\right)\right] \\
&= \sum_{a\in V\left(Q_1\right)} \sum_{b_1b_2\in E\left(Q_2\right)} \left[\tau\left(a,b_1\right) + \tau\left(a,b_2\right)\right] \\
&\quad + \sum_{b\in V\left(Q_2\right)} \sum_{a_1b_2\in E\left(S_1\left(Q_1\right)\right)} \left[\tau\left(a_1,b\right) \times \tau\left(a_2,b\right)\right].
\end{aligned} \tag{28}$$

Consider

$$\begin{aligned}
\sum_{a\in V\left(Q_1\right)} \sum_{b_1b_2\in E\left(Q_2\right)} \left[\tau\left(a,b_1\right) + \tau\left(a,b_2\right)\right] &= \sum_{a\in V\left(Q_1\right)} \sum_{b_1b_2\in E\left(Q_2\right)} \left[d_{G_1}(a) + d_{Q_1}(a)d_{Q_2}\left(b_1\right) + \tau_{Q_2}\left(b_1\right)\right]] \\
&\quad + \left[d_{Q_1}(a) + d_{Q_1}(a)d_{Q_2}\left(b_2\right) + \tau_{Q_2}\left(b_2\right)\right] \\
&= \sum_{a\in V\left(Q_1\right)} \sum_{b_1b_2\in E\left(Q_2\right)} \left[2d_{Q_1}(a) + d_{Q_1}(a)\left\{d_{Q_2}\left(b_1\right) + d_{Q_2}\left(b_2\right)\right\} + \left\{\tau_{Q_2}\left(b_1\right) + \tau_{Q_2}\left(b_2\right)\right\}\right] \\
&= \sum_{a\in V\left(Q_1\right)} \left[2e_2d_{Q_1}(u) + M_1\left(Q_2\right)d_{Q_1}(u) + \mathrm{ZC}_1^*\left(Q_2\right)\right] \\
&= n_1\mathrm{ZC}_1^*\left(Q_2\right)2e_1M_1\left(Q_2\right) + 4e_1e_2.
\end{aligned} \tag{29}$$

Also, consider

$$\begin{aligned}\sum_{b\in V(Q_2)}\sum_{a_1a_2\in E(S_1(Q_1))}[\tau(a_1,b)+\tau(a_2,b)] &= \sum_{b\in V(Q_2)}\sum_{a_1a_2\in E(Q_1)}\Big[\big\{d_{Q_1}(a_1)+d_{Q_1}(a_1)d_{Q_2}(b)+\tau_{Q_2}(b)\big\}\\ &\quad+2\big\{d_{Q_1}(a_1)+d_{Q_1}(a_2)+2d_{Q_2}(b)-2\big\}+\big\{d_{Q_1}(a_2)+d_{Q_1}(a_2)d_{Q_2}(b)+\tau_{Q_2}(b)\big\}\Big]\\ &= \sum_{b\in V(Q_2)}\sum_{a_1a_2\in E(Q_1)}\Big[\big\{d_{Q_1}(a_1)+d_{Q_1}(a_2)\big\}+d_{Q_2}(b)\big\{d_{Q_1}(a_1)+d_{Q_1}(a_2)\big\}+2\tau_{Q_2}(b)\\ &\quad+2\big\{d_{Q_1}(a_1)+d_{Q_1}(a_2)\big\}+4d_{Q_2}(b)-4\Big].\\ &= \sum_{b\in V(Q_2)}\Big[M_1(Q_1)+M_1(Q_1)d_{Q_2}(b)+2e_1\tau_{Q_2}(b)+2M_1(Q_1)+4e_1d_{Q_2}(b)-4e_1\Big]\\ &= n_2M_1(Q_1)+M_1(Q_1)(2e_2)+2e_1\{M_1(Q_2)-2e_2\}+2n_2M_1(Q_1)+4e_1(2e_2)-4n_2e_1\\ &= M_1(Q_1)(3n_2+2e_2)+2e_1M_1(Q_2)+4e_1e_2-4n_2e_1.\end{aligned} \tag{30}$$

Finally, we obtain

$$\begin{aligned}ZC_1^*\left(Q_1+_{S_1}Q_2\right) &= n_1ZC_1^*(Q_2)+M_1(Q_1)(3n_2+2e_2)\\ &\quad+4e_1M_1(Q_2)+8e_1e_2-4n_2e_1.\end{aligned} \tag{31}$$

□

proof. (b) Let $\tau(a,b)=\tau_{Q_1+_{S_2}Q_2}(a,b)$ be a connection number of the vertex (a,b) in the graph $Q_1+_{S_2}Q_2$. Then,

$$\begin{aligned}&ZC_1^*\left(Q_1+_{S_2}Q_2\right)\sum_{(a_1,b_1)(a_2,b_2)\in E\left(Q_1+_{S_2}Q_2\right)}[\tau(a_1,b_1)+\tau(a_2,b_2)]\\ &\quad=\sum_{a\in V(Q_1)}\sum_{b_1b_2\in E(Q_2)}[\tau(a,b_1)+\tau(a,b_2)]+\sum_{b\in V(Q_2)}\sum_{a_1a_2\in E(S_2(Q_1))}[\tau(a_1,b)+\tau(a_2,b)].\end{aligned} \tag{32}$$

Consider

$$\begin{aligned}\sum A &= \sum_{a\in V(G_1)}\sum_{b_1b_2\in E(Q_2)}[\tau(a,b_1)+\tau(a,b_2)]\\ &= \sum_{a\in V(Q_1)}\sum_{b_1b_2\in E(Q_2)}\Big[2\tau_{Q_1}(a)+\tau_{Q_2}(b_1)+2d_{Q_1}(a)d_{Q_2}(b_1)\Big]+\Big[2\tau_{Q_1}(a)+\tau_{Q_2}(b_2)+2d_{Q_1}(a)d_{Q_2}(b_2)\Big]\\ &= \sum_{a\in V(Q_1)}\sum_{b_1b_2\in E(Q_2)}\Big[4\tau_{Q_1}(a)+\big\{\tau_{Q_2}(b_1)+\tau_{Q_2}(b_2)\big\}+2d_{Q_1}(a)\big\{d_{Q_2}(b_1)+d_{Q_2}(b_2)\big\}\Big]\\ &= \sum_{a\in V(Q_1)}\Big[4e_2\tau_{Q_1}(a)+ZC_1^*(Q_2)+2M_1(Q_2)d_{Q_1}(a)\Big]\\ &= 4e_2\{M_1(Q_1)-2e_1\}+n_1ZC_1^*(Q_2)+2M_1(Q_2)(2e_1)\\ &= n_1ZC_1^*(Q_2)+4e_2M_1(Q_1)+4e_1M_1(Q_2)-8e_1e_2.\end{aligned} \tag{33}$$

Also, consider

$$\begin{aligned}
&\sum_{b\in V(Q_2)}\sum_{a_1a_2\in E(S_2(Q_1))}\left[\tau(a_1,b)+\tau(a_2,b)\right]=\sum B+\sum C,\\
\sum B&=\sum_{b\in V(Q_2)}\sum_{a_1a_2\in E(Q_1)}\left[2\tau_{Q_1}(a_1)+\tau_{Q_2}(b)+2d_{Q_1}(a_1)d_{Q_2}(b)\right]+\left[2\tau_{Q_1}(a_2)+\tau_{Q_2}(b)+2d_{Q_1}(a_2)d_{Q_2}(b)\right]\\
&=\sum_{b\in V(Q_2)}\sum_{a_1a_2\in E(Q_1)}\left[2\left\{\tau_{Q_1}(a_1)+\tau_{Q_1}(a_2)\right\}+2\tau_{Q_2}(b)+2d_{Q_2}(b)\left\{d_{Q_1}(a_1)+d_{Q_1}(a_2)\right\}\right]\\
&=\sum_{b\in V(Q_2)}\left[2ZC_1^*(Q_1)+2e_1\tau_{Q_2}(b)+2M_1(Q_1)d_{Q_2}(b)\right]\\
&=2n_2ZC_1^*(Q_1)+4e_2M_1(Q_1)+2e_1M_1(Q_2)-4e_1e_2,\\
\sum C&=\sum_{b\in V(Q_2)}\sum_{a_1a_2\in E(Q_1)}\left[\left\{2\tau_{Q_1}(a_1)+\tau_{Q_2}(b)+2d_{Q_1}(a_1)d_{Q_2}(b)\right\}+\left\{2\tau_{Q_1}(a_2)+\tau_{Q_2}(b)+2d_{Q_1}(a_2)d_{Q_2}(b)\right\}\right.\\
&\quad\left.+2\left\{d_{Q_1}(a_1)+d_{Q_1}(a_2)+2d_{Q_2}(b)-1\right\}\right]\\
&=\sum_{b\in V(Q_2)}\sum_{a_1a_2\in E(Q_1)}\left[2\left\{\tau_{Q_1}(a_1)+\tau_{Q_1}(a_2)\right\}+2\tau_{Q_2}(b)+2d_{Q_2}(b)\left\{d_{Q_1}(a_1)+d_{Q_1}(a_2)\right\}\right.\\
&\quad\left.+2\left\{d_{Q_1}(a_1)+d_{Q_1}(a_2)\right\}+4d_{Q_2}(b)-2\right]\\
&=\sum_{b\in V(Q_2)}\left[2ZC_1^*(Q_1)+2e_1\tau_{Q_2}(b)+2M_1(Q_1)d_{Q_2}(b)+2M_1(Q_1)+4e_1d_{Q_2}(b)-2e_1\right]\\
&=2n_2ZC_1^*(Q_1)+2n_2M_1(Q_1)+4e_2M_1(Q_1)+2e_1M_1(Q_2)+4e_1e_2-2n_2e_1.
\end{aligned}\tag{34}$$

Consequently,

$$\begin{aligned}
ZC_1^*\left(Q_1+_{S_2}Q_2\right)&=\sum A+\sum B+\sum C\\
&=4n_2ZC_1^*(Q_1)+n_1ZC_1^*(Q_2)\\
&\quad+2M_1(Q_1)(n_2+6e_2)+8e_1M_1(Q_2)\\
&\quad-2e_1(n_2+4e_2).
\end{aligned}\tag{35}$$

□

4. Applications and Conclusion

Let $Q_1\cong P_m$ and $Q_2\cong P_n$ be two particular alkanes called by paths, where $m,n\geq 5$. Then, the Zagreb connection indices of their S-sum graphs as the consequences of the obtained main results are as follows:

(1) (a) $ZC_1(P_m+_{S_1}P_n)=100mn-148m-136n+172$,
(b) $ZC_1(P_m+_{S_2}P_n)=245mn-332m-443n+512$.

(2) (a) $ZC_2(P_m+_{S_1}P_n)=160mn-274m-236n+358$,
(b) $ZC_2(P_m+_{S_2}P_n)=588mn-906m-1196n+1628$.

(3) (a) $ZC_1^*(P_m+_{S_1}P_n)=44mn-50m-50n+44$,
(b) $ZC_1^*(P_m+_{S_2}P_n)=98mn-98m-146n+112$.

In this paper, we obtained the S-sum graphs using the operations of subdivision, semitotal point and cartesian product on two connected graphs in a certain order. Finally, we computed the first Zagreb connection index, second Zagreb connection index, and modified first Zagreb connection index of the obtained S-sum graphs in the terms of Zagreb indices and Zagreb connection indices of their factor graphs. Our results are interesting for pharmaceuticals [57–61]. Also, the problem is still open to compute the Zagreb connection indices for other families of graphs obtained by various operations on graphs.

Data Availability

The data used to support the findings of this study are cited at relevant places within the text as references.

Conflicts of Interest

The authors declare that they have no conflicts of interest.

Authors' Contributions

All authors contributed equally to this paper.

Acknowledgments

This work was jointly supported by the Natural Science Fund Project of Anhui Xinhua University (Grant no. 2017zr011).

References

[1] S. G. Shirinivas, S. Vetrivel, and N. M. Elango, "Application of graph theory in computer science an overview," *International Journal of Engineering*, vol. 2, no. 9, pp. 4610–4621, 2010.

[2] Z. Shao, A. R. Virk, M. S. Javed, M. A. Rehman, and M. R. Farahani, "Degree based graph invariants for the molecular graph of bismuth tri-iodide," *Engineering and Applied Science Letters*, vol. 2, no. 1, pp. 01–11, 2019.

[3] N. De, "Computing reformulated first Zagreb index of some chemical graphs as an application of generalized hierarchical product of graphs," *Open Journal of Mathematical Sciences*, vol. 2(2018), no. 1, pp. 338–350, 2018.

[4] L. Yan, M. R. Farahani, and W. Gao, "Distance-based indices computation of symmetry molecular structures," *Open Journal of Mathematical Sciences*, vol. 2(2018), no. 1, pp. 323–337, 2018.

[5] J. A. Aledo, L. G. Diaz, S. Martinez, and J. C. Valverde, "Predecessors and gardens of Eden in sequential dynamical systems over directed graphs," *Applied Mathematics and Nonlinear Sciences*, vol. 3, no. 2, pp. 593–602, 2018.

[6] R. Todeschini, V. Consonni, R. Mannhold, H. Kubinyi, and H. Timmerman, *Handbook of Molecular Descriptors*, Wiley-VCH, Weinheim; Germany, 2002.

[7] G. Rücker and C. Rücker, "On topological indices, boiling points, and cycloalkanes," *Journal of Chemical Information and Computer Sciences*, vol. 39, no. 5, pp. 788–802, 1999.

[8] M. Randic, "Characterization of molecular branching," *Journal of the American Chemical Society*, vol. 97, no. 23, pp. 6609–6615, 1975.

[9] A. R. Matamala and E. Estrada, "Generalised topological indices: optimisation methodology and physico-chemical interpretation," *Chemical Physics Letters*, vol. 410, no. 4–6, pp. 343–347, 2005.

[10] H. Gonzalez-Diaz, S. Vilar, L. Santana, and E. Uriarte, "Medicinal chemistry and bioinformatics—current trends in drugs discovery with networks topological indices," *Current Topics in Medicinal Chemistry*, vol. 7, no. 10, pp. 1015–1029, 2007.

[11] M. Imran, A. Asghar, and A. Q. Baig, "On graph invariants of oxide network," *Engineering and Applied Science Letters*, vol. 1(2018), no. 1, pp. 23–28, 2018.

[12] S. Noreen and A. Mahmood, "Zagreb polynomials and redefined Zagreb indices for the line graph of carbon nanocones," *Open Journal of Mathematical Analysis*, vol. 2(2018), no. 1, pp. 66–73, 2018.

[13] W. Gao, A. Asghar, and W. Nazeer, "Computing degree-based topological indices of Jahangir graph," *Engineering and Applied Science Letters*, vol. 1(2018), no. 1, pp. 16–22, 2018.

[14] B. Basavanagoud, W. Gao, S. Patil, V. R. Desai, K. G. Mirajkar, and B. Pooja, "Computing first Zagreb index and F-index of new C-products of graphs," *Applied Mathematics and Nonlinear Sciences*, vol. 2, no. 1, pp. 285–298, 2017.

[15] W. Gao, M. Asif, and W. Nazeer, "The study of honey comb derived network via topological indices," *Open Journal of Mathematical Analysis*, vol. 2(2018), no. 2, pp. 10–26, 2018.

[16] M. Riaz, W. Gao, and A. Qudair Baig, "M-polynomials and degree-based topological indices of some families of convex polytopes," *Open Journal of Mathematical Sciences*, vol. 2, no. 1, pp. 18–28, 2018.

[17] F. Yan, Q. Shang, S. Xia, Q. Wang, and P. Ma, "Application of topological index in predicting ionic liquids densities by the quantitative structure property relationship method," *Journal of Chemical & Engineering Data*, vol. 60, no. 3, pp. 734–739, 2015.

[18] M. V. Diudea, *QSPR/QSAR Studies by Molecular Descriptors*, NOVA, New York, NY, USA, 2001.

[19] J. Devillers and A. T. Balaban, *Topological Indices and Related Descriptors in QSAR and QSPR*, Gordon & Breach, Amsterdam, Netherlands, 1999.

[20] R. Gozalbes, J. Doucet, and F. Derouin, "Application of topological descriptors in QSAR and drug design: history and new trends," *Current Drug Target-Infectious Disorders*, vol. 2, no. 1, pp. 93–102, 2002.

[21] H. Wiener, "Structural determination of paraffin boiling points," *Journal of the American Chemical Society*, vol. 69, no. 1, pp. 17–20, 1947.

[22] I. Gutman and N. Trinajstić, "Graph theory and molecular orbitals: total φ-electron energy of alternant hydrocarbons," *Chemical Physics Letters*, vol. 17, no. 4, pp. 535–538, 1972.

[23] B. Furtula and I. Gutman, "A forgotten topological index," *Journal of Mathematical Chemistry*, vol. 53, no. 4, pp. 1184–1190, 2015.

[24] S. Nikolic and N. Trinajstic, "The Zagreb indices 30 years after," *Croatica Chemica Acta*, vol. 76, no. 2, pp. 113–124, 2003.

[25] K. C. Das and I. Gutman, "Some properties of the second Zagreb index," *Communications in Mathematical and in Computer Chemistry*, vol. 52, pp. 103–112, 2004.

[26] B. Borovicanin, K. C. Das, B. Furtula, and I. Gutman, "Bounds for Zagreb indices," *Communications in Mathematical and in Computer Chemistry*, vol. 158, pp. 1571–1578, 2010.

[27] I. Gutman and O. Polansky, *Mathematical Concepts in Organic Chemistry*, Springer-Verlag, Berlin, Germany, 1986.

[28] L. H. Hall and L. B. Kier, *Molecular Connectivity in Chemistry and Drug Research*, Academic Press, Boston, MA, USA, 1976.

[29] I. Gutman, "Degree-based topological indices," *Croatica Chemica Acta*, vol. 86, no. 4, pp. 351–361, 2013.

[30] A. Ali and N. Trinajstic, "A novel/old modification of the first Zagreb index," *Molecular Informatics*, vol. 37, no. 6-7, 2018.

[31] Z. Du, A. Ali, and N. Trinajstić, "Alkanes with the first three maximal/minimal modified first Zagreb connection indices," *Molecular Informatics*, vol. 38, no. 4, p. 1800116, 2019.

[32] G. Ducoffe, R. Marinescu-Ghemeci, C. Obeja, A. Popa, and R. M. Tache, "Extremal graphs with respect to the modified first Zagreb connection index," in *Proceedings of the 16th Cologne-Twente Workshop on Graphs and Combinatorial Optimization (CNAM)*, pp. 65–68, Paris, France, June 2018.

[33] Z. Shao, I. Gutman, Z. Li, S. Wang, and P. Wu, "Leap Zagreb indices of trees and unicyclic graphs," *Communications in Combinatorics and Optimization*, vol. 3, no. 2, pp. 179–194, 2018.

[34] W. Yan, B.-Y. Yang, and Y.-N. Yeh, "The behavior of Wiener indices and polynomials of graphs under five graph decorations," *Applied Mathematics Letters*, vol. 20, no. 3, pp. 290–295, 2007.

[35] M. Eliasi and B. Taeri, "Four new sums of graphs and their Wiener indices," *Discrete Applied Mathematics*, vol. 157, no. 4, pp. 794–803, 2009.

[36] H. Deng, D. Sarala, S. K. Ayyaswamy, and S. Balachandran, "The Zagreb indices of four operations on graphs," *Applied Mathematics and Computation*, vol. 275, pp. 422–431, 2016.

[37] S. Akhter and M. Imran, "Computing the forgotten topological index of four operations on graphs," *AKCE International Journal of Graphs and Combinatorics*, vol. 14, no. 1, pp. 70–79, 2017.

[38] J.-B. Liu, S. Javed, M. Javaid, and K. Shabbir, "Computing first general Zagreb index of operations on graphs," *IEEE Access*, vol. 7, pp. 47494–47502, 2019.

[39] D. Liu, C. Wang, and S. Wang, "Hamilton-connectivity of interconnection networks modeled by a product of graphs," *Applied Mathematics and Nonlinear Sciences*, vol. 3, no. 2, pp. 419–426, 2018.

[40] R. Kanabu and S. Hosamani, "Some numerical invariants associated with V-phenylenic nanotube and nanotori," *Engineering and Applied Science Letters*, vol. 1(2018), no. 1, pp. 1–9, 2018.

[41] Z. Tang, L. Liang, and W. Gao, "Wiener polarity index of quasi-tree molecular structures," *Open Journal of Mathematical Sciences*, vol. 2, no. 1, pp. 73–83, 2018.

[42] M. Knor, R. Škrekovski, and A. Tepeh, "Convexity result and trees with large Balaban index," *Applied Mathematics and Nonlinear Sciences*, vol. 3, no. 2, pp. 433–446, 2018.

[43] S. Shirakol, M. Kalyanshetti, and S. M. Hosamani, "QSPR analysis of certain distance based topological indices," *Applied Mathematics and Nonlinear Sciences*, vol. 4, no. 2, pp. 371–386, 2019.

[44] W. Gao, B. Muzaffar, and W. Nazeer, "K-Banhatti and K-hyper Banhatti indices of dominating David derived network," *Open Journal of Mathematical Analysis*, vol. 1(2017), no. 1, pp. 13–24, 2017.

[45] H. Siddiqui and M. R. Farahani, "Forgotten polynomial and forgotten index of certain interconnection networks," *Open Journal of Mathematical Analysis*, vol. 1(2017), no. 1, pp. 44–59, 2017.

[46] M. S. Anjum and M. U. Safdar, "K Banhatti and K hyper-Banhatti indices of nanotubes," *Engineering and Applied Science Letters*, vol. 2, no. 1, pp. 19–37, 2019.

[47] A. R. Virk, M. N. Jhangeer, and M. A. Rehman, "Reverse Zagreb and reverse hyper-Zagreb indices for silicon carbide $Si_2C_3I[r, s]$ and $Si_2C_3II[r, s]$," *Engineering and Applied Science Letters*, vol. 1(2018), no. 2, pp. 37–50, 2018.

[48] J.-B. Liu, M. Javaid, and H. M. Awais, "Computing Zagreb indices of the subdivision-related generalized operations of graphs," *IEEE Access*, vol. 7, pp. 105479–105488, 2019.

[49] M. Dehmer, K. Varmuza, and D. Bonchev, *Statistical Modeling of Molecular Descriptors in QSAR/QSPR*, Wiley-VCH, Weinheim, Germany, 2012.

[50] D. M. Cvetkovic, M. Doob, and H. Sachs, *Spectra of Graphs-Theory and Applications*, Academic Press, New York, NY, USA, 1980.

[51] I. Gutman, B. Ruscic, N. Trinajstic, and C. F. Wilson, "Graph theory and molecular orbitals. XII. Acyclic polyenes," *The Journal of Chemical Physics*, vol. 62, no. 9, pp. 3399–3405, 1975.

[52] I. Gutman and K. C. Das, "The first Zagreb index 30 years after," *MATCH Communications in Mathematical and in Computer Chemistry*, vol. 50, pp. 83–92, 2004.

[53] A. M. Naji, N. D. Soner, and I. Gutman, "On leap Zagreb indices of graphs," *Communications in Combinatorics and Optimization*, vol. 2, no. 2, pp. 99–117, 2017.

[54] F. Harary, *Graph Theory*, Addison-Wesley, Boston, MA, USA, 1969.

[55] E. Sampathkumar and S. B. Chikkodimath, "Semi-total graphs of a graph-1," *Journal of Karnataka University Science*, vol. 18, pp. 274–280, 1973.

[56] S. Yamaguchi, "Estimating the Zagreb indices and the spectral radius of triangle- and quadrangle-free connected graphs," *Chemical Physics Letters*, vol. 458, no. 4–6, pp. 396–398, 2008.

[57] J.-B. Liu, M. Younas, M. Habib, M. Yousaf, and W. Nazeer, "M-polynomials and degree-based topological indices of VC_5C_7[p,q] and HC_5C_7[p,q] nanotubes," *IEEE Access*, vol. 7, pp. 41125–41132, 2019.

[58] J.-B. Liu, C. Wang, S. Wang, and B. Wei, "Zagreb indices and multiplicative Zagreb indices of eulerian graphs," *Bulletin of the Malaysian Mathematical Sciences Society*, vol. 42, no. 1, pp. 67–78, 2019.

[59] J.-B. Liu, X.-F. Pan, F.-T. Hu, and F.-F. Hu, "Asymptotic Laplacian-energy-like invariant of lattices," *Applied Mathematics and Computation*, vol. 253, pp. 205–214, 2015.

[60] J.-B. Liu and X.-F. Pan, "Minimizing Kirchhoff index among graphs with a given vertex bipartiteness," *Applied Mathematics and Computation*, vol. 291, pp. 84–88, 2016.

[61] J.-B. Liu, J. Zhao, and Z. Zhu, "On the number of spanning trees and normalized Laplacian of linear octagonal-quadrilateral networks," *International Journal of Quantum Chemistry*, vol. 119, no. 17, Article ID e25971, 2019.

Hindawi
Journal of Chemistry
Volume 2019, Article ID 6720616, 7 pages
https://doi.org/10.1155/2019/6720616

Research Article

Molecular Interactions of Renin with Chikusetsusaponin IV and Momordin IIc

Hai-Ling Zhang,[1] Gui-Lan Zhu,[1] and Xiao-Tian Chen[2]

[1]*School of Life Sciences, Hefei Normal University, Hefei 230601, China*
[2]*Teaching Affairs Department, Anhui Jianzhu University, Hefei 230601, China*

Correspondence should be addressed to Xiao-Tian Chen; cxt214@126.com

Received 24 October 2019; Accepted 9 December 2019; Published 27 December 2019

Guest Editor: Shaohui Wang

The paper dealt with the molecular mechanism for the binding sites and driving forces of renin with chikusetsusaponin IV and momordin IIc by means of molecular docking and free energy calculation based on the crystal structure. The result showed that renin and the saponins fit well. As shown by LigPlot + software analyzing the hydrogen bonding and hydrophobic effect between renin and the saponins, the amino acid residues such as Ser230, Tyr85, and Tyr201 form the hydrogen bonds, with $S3^{sp}$, S3, and S2′ being the active pockets. In addition, there are relatively strong hydrophobic interactions of renin with saponins in $S3^{sp}$, S3, S2, S1, S1′, and S2′, with Gly228, Val36, Ala229, Gln19, Met303, Gln135, Ser41, Ile137, Asp38, Arg82, and Tyr83 being the key amino acids. The dynamics reached equilibration after about 1000 ps simulation with average root-mean-square deviations of 0.222 nm and 0.217 nm. The molecular mechanics Poisson–Boltzmann surface area (MM-PBSA) yielded −1.10812 kcal/mol and −39.0587 kcal/mol total binding energy for the two complexes, respectively, which were primarily contributed by electrostatic and van der Waals interaction energies, and the binding was strongly unfavored by polar solvation energy, a further confirmation that momordin IIc has stronger hydrogen bonding and hydrophobic effect in the inhibition of renin than the chikusetsusaponin IV.

1. Introduction

Complications such as hypertension, cardiovascular disease, and coronary heart disease are mostly caused by excessive activation of the renin-angiotensin system (RAS), which is mainly composed of angiotensinogen (AGT), renin, angiotensin-converting enzyme (ACE), angiotensin I (Ang I), angiotensin II (Ang II), and its receptors such as AT1 (AT1R) and AT2 (AT2R) [1, 2]. Angiotensinogen, under the effect of renin, is enzymatically hydrolyzed into a deficient Ang I which is cleaved by ACE. In addition, the hydroxy terminal residue is converted into an octapeptide Ang II which is secreted into the target tissue through the blood circulation. Because of its combination with receptors, resulting in vasoconstriction and regular changes in blood pressure, body fluid balance, and electrolyte balance [3], Ang II can be bound to AT1 to cause vasoconstriction and increase blood pressure. Therefore, Ang II is the active hormone in the process and its reduction is of great significance to treat the above-mentioned diseases. Renin, also known as angiotensinogenase or angiotensin-forming enzyme, is the crucial first rate-limiting enzyme that catalyzes the formation of Ang II, and confining its activity can block RAS and Ang II production.

The inhibitors interfere with not only renin but also the amplified physiological effects of prorenin, suggesting that they have unique physiological and pharmacological effects compared to other RAS inhibitors [4]. Although there has been advance in the study of inhibitors of renin in the past years, there has been little progress recently, which, Fisher and Hollenberg believe, is because of the failure to obtain highly active compounds due to the lack of structural system optimization based on the active site [5]. Although aliskiren was the first to be used in clinical practice because it can reduce the renin activity and, in turn, the blood pressure [6], its use has been restricted due to its side effects and inability

to be used on special populations [7]. This is why studies on inhibitors of renin and receptor blockers have been receiving much attention in recent years.

In 2010, Saori et al. [8] found out that there are some legumes that have the inhibitory effect on renin. The inhibitor isolated from soybean was identified as soyasaponin I, an oleanane-type pentacyclic triterpenoid glycoside compound, after the determination of its chemical structure composed of oligosaccharide chain and the nonpolar triterpene aglycone. Studies in China and other countries have confirmed that chikusetsusaponin is mainly composed of oleanane-type triterpene saponins [9]. Modern pharmacological studies have found that ginseng saponins have a variety of biological activities that have certain pharmacological effects on the cardiovascular system, kidney, myocardium, diabetes, and tumors [10, 11]. HPLC of the sample bamboo ginseng from different areas defines ginseng saponins mainly consist of chikusetsusaponin V, chikusetsusaponin IV, and chikusetsusaponin Iva [12], accounting for 3% to 7.9%, 0.2% to 8.6%, and 0.5% to 6.2%, respectively [13]. Although there have been some studies on the nutritional functions of chikusetsusaponin V and chikusetsusaponin IVa and their effects on the cardiovascular system [14–17], the biological activity of the bamboo chikusetsusaponin IV has not been studied, if not published. Some studies show that a dog has increased blood flow in its hind limbs after it is injected in its femoral artery momordica saponin whose leachate has a good antihypertensive effect on animals such as rabbits, dogs, and cats [18]. In addition, a rat experiences short-lived and excited breathing and significantly decreased blood pressure [19]. Momordin Ic and IIc were first isolated by Iwamoto et al. [20], the former of which has inhibition on renin [21], while the effect of the latter on renin remains undetermined.

As computers are widely being used in aiding the design of drugs, the three-dimensional structure of proteins is identified, and the data of the structure of receptors are being accumulated, which promotes the development of molecular docking [22]. With molecular docking and dynamic simulation being the proven methods for the design of drugs, especially based on the three-dimensional structure of receptors, the interaction between the receptor and the ligand [23] and between the small macromolecular protein receptor and the molecular ligand can be assessed through the study of the key residues of amino acids, interaction sites, and free binding energy in the docking [24]. The paper investigated the interactions of chikusetsusaponin IV and momordin IIc with renin through molecular docking and dynamic simulation.

2. Materials and Methods

2.1. The Structures of Renin and Saponins. The crystal structure with PDB ID 3OOT was retrieved from the Protein Data Bank (PDB) (http://www.rcsb.org/pdb/), and the ligand $C_8H_{15}NO_6$ was stripped out, using DS (Discovery Studio 3.0), to obtain the three-dimensional structure of renin. The three-dimensional structures of chikusetsusaponin IV and momordin IIc are drawn using PyMol [25] (http://pymol.org), as shown in Figure 1. Then the structures are charged on PRODRG (http://davapc1.bioch.dundee.ac.uk/cgi-bin/prodrg) and optimized for future treatment [26].

2.2. The Molecular Dockings of Renin and Saponins. The water molecules were removed first before the docking which was added the CHARMm force of Discovery Studio 3.0 (DS) for the combination of renin and the saponins. With the Thr85 residue of renin being the active center and a radius of 13 Å being the docking region, the Libdock was performed and its parameters are as follows: number of hotspots: 100; docking tolerance: 0.25; conformation method: FAST; parallel processing: false; docking preference: high quality.

Then, the molecular dockings were started, each producing a structure which was to be gathered using Libdock. The best-combined structures were chosen to obtain intermolecular interaction network using LigPlot+ [26]. The residues of amino acids that have hydrogen bonding and hydrophobic effect were analyzed and corresponded to the active pockets of renin by using DS. Finally, the spatial interaction between the pockets and the saponins was analyzed, considering the free binding energy.

2.3. The Molecular Dynamics Simulation of Docking Complexes. The dynamic simulation was carried out using GROMACS 4.0 [27]. In this experiment, it is the GROMOS 96 force field that was added to the docking complexes. In addition, the temperature was set to 300 K because a water model was added to the system for the solvation effect. Before the simulation, the spatial structures of the docked complexes were optimized twice, one being a 1000-step steepest descent and the other a 2000-step conjugate gradient. During the simulation, the solute molecules were stabilized within 100 ps while the temperature increased gradually from 0 K to 300 K. Then, they were stabilized within 5 ns after the restraint was released. In addition, the real-time structures were observed using VMD. Moreover, the integration step was set to 2 fs and the cutoff of the nonbond interaction 1.2 nm.

In order to reduce the errors caused by the vacuum environment, a certain amount of water was added to the spatial structure of renin using GROMACS and the capacity of the water box was defined by editconf in GROMACS, which was then run and water was added by the genbox command. In the system, the total number of charges was automatically calculated by GROMACS which applied the charges in the metal ion balance system to perform molecular dynamic simulations in a charge-balanced environment [28, 29]. Then, the systems were optimized twice with a 1000-step steepest descent and the other a 2000-step conjugate gradient, with and without the solutes being sterilized. Finally, the free binding energy in the system was calculated after the system was minimized using grompp and marum in GROMACS [30].

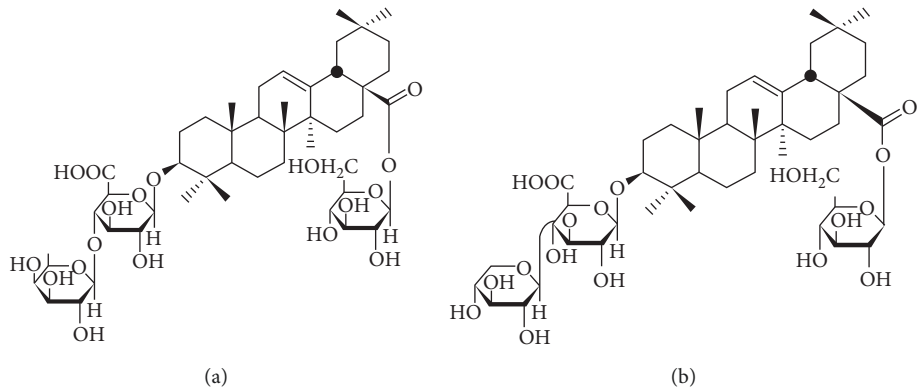

Figure 1: The structures of the saponins. (a) Chikusetsusaponin IV. (b) Momordin IIc.

2.4. The Calculation of Free Binding Energies of the Complexes. The calculation of the free binding energies in the interaction between the ligand and protein is the core issue to test the molecular docking. Using MM-PBSA, the free binding energies can be calculated after the solute molecules are removed in the regular dynamic simulation to obtain the structures that change with the passage of time [31, 32]. The calculation was defined in an attempt to obtain the contribution of each energy so as to have a better analysis of the interaction between renin and the saponins [33]. The equation is as follows:

$$\Delta G_{\text{bind}} = \Delta E_{\text{elec}} + \Delta E_{\text{vdW}} + \Delta G_{\text{pb}} + \Delta G_{\text{sur}}, \quad (1)$$

where ΔG_{bind} is the total free binding energy of the complexes; ΔE_{elec} is the electrostatic interaction; ΔE_{vdW} is the van der Waals interaction; ΔG_{pb} is the polar solvation energy; and ΔG_{sur} is the nonpolar solvation energy.

3. Results and Analysis

3.1. The Molecular Docking. The hydrogen bonding and hydrophobic effects can be calculated using HBPLUS of LigPlot+, a computational program for a statistical analysis of the interaction between receptors and ligands [34, 35]. A floor plan of the amino acids and hydrogen bonds in the interaction can prevent the overlapping and intersection of the bonds. The best docking structure was chosen to obtain the network of the interaction and calculate the amino acid residues because of the hydrogen bonding and hydrophobic effects so as to analyze the spatial forces of the complexes.

In the study, the complexes derived from the docking of the renin and saponins were uploaded in LigPlot+. The hydrogen bonding between momordin IIc and renin was stronger than that between chikusetsusaponin IV and renin, as shown in Table 1. A comparison of the residues of the amino acids in renin that interacted with the saponins showed that Ser230, Tyr85, and Tyr201 formed stable hydrogen bonds.

3.2. The Hydrogen Bonding of the Active Pockets in Renin. Renin is a highly selective aspartic protease with a diploblastic structure. There are active sites of renin in the fissures on each leaf such as $S3^{sp}$, S3, S2, S2′, S1, and S1′ [36]. After the docking, the amino acid residues in the interaction between renin and the saponins in the pockets were calculated , as shown in Figure 2.

Based on the analysis of the hydrogen bonding in the pockets as shown in Table 2, it was found out that the bonding between chikusetsusaponin IV and renin took place in all pockets except for S1 and S2 while the bonding between momordin IIc and renin in all pockets except for S1, which proved that the hydrogen bonding between momordin IIc and renin is stronger, verified in Section 2.1.

An analysis of the varieties of the amino acids in the active renin pockets showed that Ser230 interacts with chikusetsusaponin IV and momordin IIc in $S3^{sp}$ and S2, and Thr85 formed hydrogen bonds with both of the saponins in S3 and Trp201 in S2′.

Therefore, it can be concluded that renin mainly interacts with chikusetsusaponin IV in $S3^{sp}$, S3, and S2′ and with momordin IIc in $S3^{sp}$, S3, S2, and S2′, with $S3^{sp}$, S3, and S2′ being the active pockets. Moreover, Ser230, Tyr85, and Tyr201 are of primary importance for the formation of hydrogen bonds.

3.3. The Hydrogen Bonding and Hydrophobic Interaction in the Active Pockets in Renin. Analysis of the active pockets where the residues of amino acids existed showed that there were relatively strong hydrophobic interactions in $S3^{sp}$, S3, S2, S1, S1′, and S2′, as shown in Table 3.

Gly228 and Val36 formed a hydrophobic interaction with the saponins in $S3^{sp}$, Ala229 and Gln19 in S3, Met303 in S2, Gln135, Ser41, and Ile137 in S2′, Asp38 and Arg82 in S1, and Tyr83 in S1′. During the interaction, momordin IIc has one more Thr18, Gly40, and Asp226 than chikusetsusaponin IV in S3, S2′, and S1′. Therefore, it can be anticipated that momordin IIc inhibits the hydrophobic interaction more than chikusetsusaponin IV.

3.4. The Stability of Dynamic Trajectory. Root mean square deviation (RMSD) is an important indicator of whether the system has reached a steady state. In order to make sure whether the sampling of the simulations and the free binding energies are correct, the RMSD of the structures of the

Table 1: The hydrogen bonds in the complexes.

	Hydrogen bonds	Ligand atoms	Receptor atoms	Distance (Å)
Chikusetsusaponin IV	1	O78	Trp201-N	3.07
	2	O26	Thr85-OG1	2.88
	3	O48	Ser230-OG	2.68
Momordin IIc	1	O48	Tyr20-N	3.32
	2	O58	Tyr20-N	2.62
	3	O37	Ser230-N	2.37
	4	O36	Thr85-OG1	2.92
	5	O26	Thr85-OG1	2.49
	6	O4	Ser42-OH	2.57
	7	O2	Phe132-N	2.48
	8	O1	Trp201-N	2.89

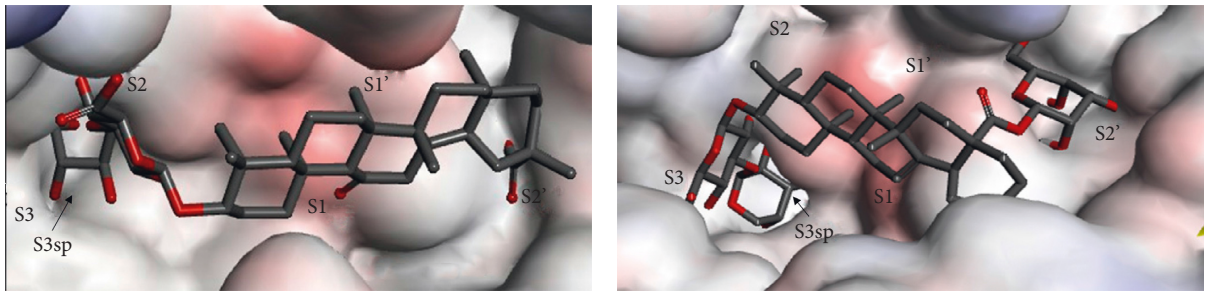

(a) (b)

Figure 2: Docking in the active pockets in renin. (a) Chikusetsusaponin IV. (b) Momordin IIc.

Table 2: Residues of amino acids with hydrogen bonding in the active pockets.

Saponin	$S3^{sp}$	S3	S2	S2′	S1
Chikusetsusaponin IV	Ser230	Thr85	—	Trp201	—
Momordin IIc	Tyr20	Thr85	Ser230	Ser42, Trp201, Phe132	—

Table 3: Residues of amino acids with hydrophobic interactions in the active pockets of renin.

Saponin	$S3^{sp}$	S3	S2	S2′	S1	S1′
Chikusetsusaponin IV	Val36, Gly228	Ala229, Gln19,	Met303	Gln135, Ser41, Ile137	Asp38, Arg82	Tyr83
Momordin IIc	Val36, Gly228	Ala229, Gln19, Thr18	Met303	Gly40, Gln135, Ser41, Ile137	Asp38, Arg82	Asp226, Tyr83

complexes and the root mean square fluctuations (RMSF) of the residues were calculated.

RMSF was used to determine the relatively flexible and stable areas in the simulation. In addition, the complexes existed in the active areas with low RMSF such as Thr39-Trp45, Met107-Thr112, Leu2224-Ser235, and Ala314-Thr318 where the renin and the saponins interacted. The RMSFs of the residues of amino acids were calculated, as shown in Figure 3, in order to describe the fluctuations of the complexes. As shown in Figure 4, RMSFs generally had large values, meaning that the molecular structure of renin had great flexibility.

The simulation went for 5000 ps and the RMSDs were obtained with the passage of time and compared to the initial frame. The dynamics reached equilibration with average RMSD of 0.2224 nm and 0.2169 nm because there were a few fluctuations after 3000 ps, as shown in Figure 4 and Table 4, proving it was reasonable to analyze the structures of the free binding energies.

3.5. The Calculation of the Free Binding Energy. The free binding energies were calculated using formula (1), as shown in Table 5. Both of the energies are below zero, with the one in the interaction between momordin IIc and renin being −39.0587 kcal/mol and the other −1.10812 kcal/mol, which indicated that both of the saponins have inhibitory effect on renin.

Although having similar van der Waals energy, polar solvation energy, and a nonpolar solvent with momordin IIc, chikusetsusaponin IV has much larger electrostatic energy which is −50.3008 kcal/mol, leading to less inhibitory effect.

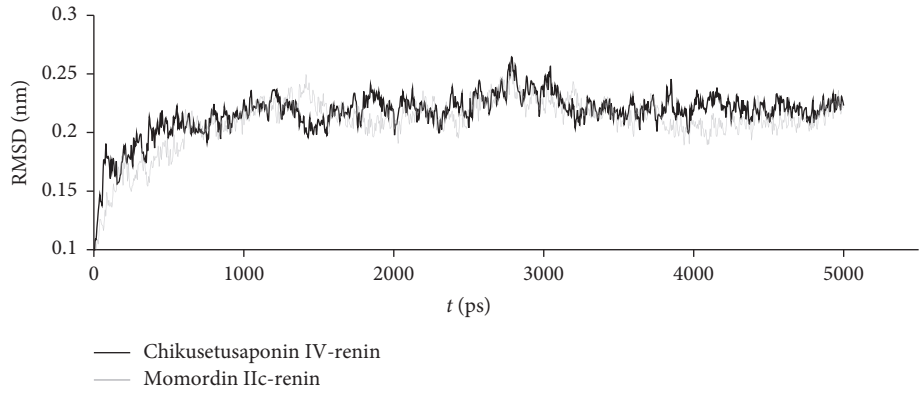

Figure 3: The RMSDs of complexes.

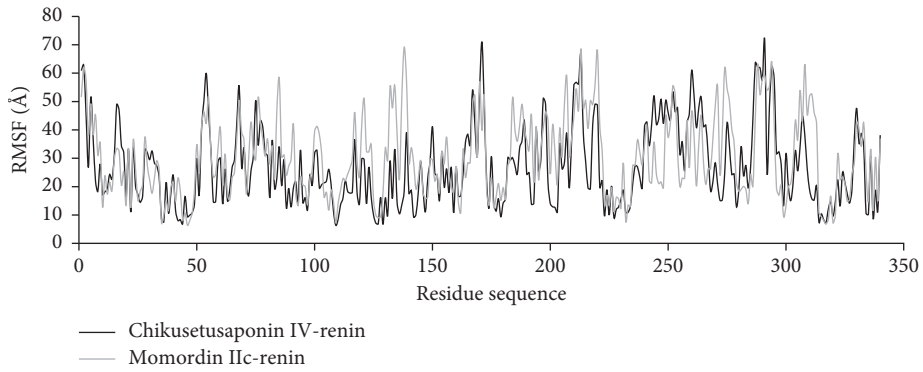

Figure 4: The RMSFs of complexes.

Table 4: The RMSDs of complexes after 3000 ps.

Complexes	RMSD average (nm)	Fluctuation range (nm)
Chikusetsusaponin IV-renin	0.2224	0.068
Momordin IIc-renin	0.2169	0.068

Table 5: Free binding energies of the complexes.

Complexes	ΔE_{vdw}	ΔE_{elec}	ΔG_{pb}	ΔG_{sur}	ΔG_{bind} (kcal/mol)
Chikusetsusaponin IV-renin	−94.587	−50.3008	153.2202	−9.44048	−1.10812
Momordin IIc-renin	−91.6879	−92.2665	154.1899	−9.29422	−39.0587

This proved the correctness of what was mentioned in Section 3.3.

4. Conclusions

In the study, chikusetsusaponin IV and momordin IIc were docked with renin. Based on the scoring of the results by Libdock, it was concluded that the overlapping is relatively good. The analysis of the hydrogen bonding of renin with the saponins showed that the residues of amino acids such as Ser230, Tyr85, and Tyr201 formed the hydrogen bonds, with $S3^{sp}$, S3, and S2′ being the active pockets. In addition, the analysis of hydrophobic interactions of renin with the saponins indicated that there are relatively strong hydrophobic interactions of the former with the latter in $S3^{sp}$, S3, S2, S1, S1′, and S2′, with Gly228, Val36, Ala229, Gln19, Met303, Gln135, Ser41, Ile137, Asp38, Arg82, and Tyr83 being the key amino acids. The dynamic simulation of the complexes revealed that the residues of the amino acids in renin that has strong hydrogen bonding with the saponins have low RMSF and the dynamics of the complexes reaches equilibration after about 1000 ps simulation with average root-mean-square deviations of 0.222 nm and 0.217 nm, respectively. In addition, the complexes existed in the active areas with low RMSF such as Thr39-Trp45, Met107-Thr112, Leu2224-Ser235, and Ala314-Thr318 where the renin and the saponins interacted.

The calculation of the free binding energies of chikusetsusaponin IV and momordin IIc with renin, which

were primarily contributed by electrostatic and van der Waals interaction energies, through MM-PBSA yielded −1.10812 kcal/mol and −39.0587 kcal/mol, respectively, further confirming that momordin IIc has stronger hydrogen bonding and hydrophobic effect in the inhibition of renin than chikusetsusaponin IV. In conclusion, the study proves the significance of further research on the structures and the catalytic mechanism of the saponins in the inhibition of renin.

Data Availability

The data used to support the findings of this study are available from the corresponding author upon request.

Conflicts of Interest

The authors declare no conflicts of interest regarding the content and implications of this manuscript.

Acknowledgments

This work was supported by the National Natural Science Foundation of China Youth Science Fund Project (31201289) and National Natural Science Foundation of China (31401657).

References

[1] V. Dzau, "The cardiovascular continuum and renin–angiotensin–aldosterone system blockade," *Journal of Hypertension. Supplement: Official Journal of the International Society of Hypertension*, vol. 23, no. 1, pp. S9–S17, 2005.

[2] V. J. Dzau, K. Bernstein, D. Celermajer et al., "The relevance of tissue angiotensin-converting enzyme: manifestations in mechanistic and endpoint data," *The American Journal of Cardiology*, vol. 88, no. 9, pp. 1–20, 2001.

[3] M. Sata and D. Fukuda, "Crucial role of renin-angiotensin system in the pathogenesis of atherosclerosis," *The Journal of Medical Investigation*, vol. 57, no. 1-2, pp. 12–25, 2010.

[4] D. L. Zhu, "Direct renin inhibitors and plasma renin activity and plasma renin concentration," *Chinese Journal of Internal Medicine*, vol. 49, no. 6, pp. 531-532, 2010.

[5] N. D. L. Fisher and N. K. Hollenberg, "Is there a future for renin inhibitors?" *Expert Opinion on Investigational Drugs*, vol. 10, no. 3, pp. 417–426, 2001.

[6] J. Sealey and J. Laragh, "Aliskiren, the first renin inhibitor for treating hypertension: reactive renin secretion may limit its effectiveness," *American Journal of Hypertension*, vol. 20, no. 5, pp. 587–597, 2007.

[7] H. Y. Wu and J. M. Zhou, "Renin inhibitor aliskiren," *Shanghai Medicine*, vol. 34, no. 17, pp. 6–9, 2013.

[8] T. Saori, H. Kazuyuki, H. Mika, G. Takeshi, and S. Toshihiro, "Inhibition of human renin activity by saponins," *Biomedical Research*, vol. 31, no. 2, pp. 155–159, 2010.

[9] J.-Y. Wang, X.-G. Li, Y.-N. Zheng, and X. W. Yang, "Isoginsenoside-Rh3, a new triterpenoid saponin from the fruits of *Panax ginseng* C. A. Mey," *Journal of Asian Natural Products Research*, vol. 6, no. 4, pp. 289–293, 2004.

[10] X. L. Yang and P. Chen, "Experimental study on the anti-hyperlipidemia effect of the total rhizoma panacis japonica saponins," *Acta Chinese Medicine and Pharmacology*, vol. 38, no. 6, pp. 22–24, 2010.

[11] H. Zhao, Q. X. Zhang, and Y. Mu, "Protective effect of total saponin of bamboo ginseng on focal cerebral ischemia rat model," *China Traditional Chinese Medicine Information Magazine*, vol. 2, no. 3, pp. 43-44, 2005.

[12] T. Morita, O. Tanaka, and H. Kohda, "Saponin composition of rhizomes of *Panax japonicus* collected in South Kyushu, Japan, and its significance in oriental traditional medicine," *Chemical & Pharmaceutical Bulletin*, vol. 33, no. 33, pp. 3852–3858, 1985.

[13] F. Jia, *Study on the Components of Saponins in Bamboo Ginseng*, Wuhan Institute of Technology, Wuhan, China, 2012.

[14] X. L. Hou, P. P. Zhou, and X. L. Yang, "Effects of ginsenoside V on fat accumulation of HepG2 cells induced by oleic acid," *Straits Pharmacy*, vol. 3, no. 29, pp. 38–40, 2017.

[15] G. B. Sun, H. B. Xu, and F. C. Wun, "Protective effect of saponin IVa on hypoxic and reoxygenated myocardial cell injury," *Chinese Journal of Pharmacology and Toxicology*, vol. 19, no. 6, pp. 424–427, 2005.

[16] G. B. Sun, H. B. Xu, and F. C. Wun, "Anti-arrhythmic effect of deglucose-chikusetsu-saponin IVa," *Chinese Journal of Pharmacology and Toxicology*, vol. 5, pp. 377–380, 2006.

[17] M. X. Pan, Y. Y. Dun, and J. Chen, "Effect of saponin IVa on the signal pathway of small intestinal stem cells and microenvironment Wnt/β-catenin in high-fat diet mice," *Chinese Herbal Medicine*, vol. 6, no. 40, pp. 1415–1418, 2017.

[18] C. L. Yang, *Poison Materia Medica*, China Traditional Chinese Medicine Press, Beijing, China, 1998.

[19] L. D. Kan, Q. Hu, and Z. M. Chao, "Study on the chemical constituents of non-saponification substances in fat oil of strychnine," *Chinese Traditional Chinese Medicine Magazine*, vol. 31, no. 17, pp. 1441–1444, 2006.

[20] M. Iwamoto, H. Okabe, T. Yamauchi et al., "Studies on the constituents of *Momordica cochinchinensis* Spreng. I. Isolation and characterization of the seed saponins, momordica saponins I and II," *Chemical & Pharmaceutical Bulletin*, vol. 33, no. 2, pp. 464–478, 1985.

[21] C. E. Guang, H. L. Zhang, J. Q. Wang, and R. Phillips, "Molecular interactions between renin and its inhibitor saponins from *Kochia scoparia* fruit," *Food Science*, vol. 38, no. 9, pp. 8–12, 2017.

[22] H. L. Zhang, C. E. Guang, and B. Jiang, "Molecular docking and binding energy analysis of saponin analogues and renin," *Journal of Food and Biotechnology*, vol. 33, no. 10, pp. 1056–1062, 2014.

[23] K. X. Chen, H. L. Jiang, and R. Y. Ji, *Computer-aided Drug Design: Principles, Methods and Applications*, Shanghai Science and Technology Press, Shanghai, China, 2000.

[24] X. L. Cai, Y. Z. Ma, and Z. X. Zhao, "Molecular docking, 3D-QSAR and molecular dynamics simulation studies of substituted pyrimidines as selective covalent janus kinase 3 inhibitors," *Chinese Journal of Structural Chemistry*, vol. 37, no. 6, pp. 839–853, 2018.

[25] L. Schrodinger, *The PyMOL Molecular Graphics System, Version 1. 3r1*, 2010.

[26] A. C. Wallace, R. A. Laskowski, and J. M. Thornton, "LIGPLOT: a program to generate schematic diagrams of protein-ligand interactions," *Protein Engineering, Design and Selection*, vol. 8, no. 2, pp. 127–134, 1995.

[27] J. Chen, J. Wang, B. Yin, L. Pang, W. Wang, and W. Zhu, "Molecular mechanism of binding selectivity of inhibitors toward BACE1 and BACE2 revealed by multiple short molecular dynamics simulations and free-energy predictions,"

ACS Chemical Neuroscience, vol. 10, no. 10, pp. 4303–4318, 2019.

[28] J.-B. Liu, J. Zhao, and Z.-Q. Cai, "On the generalized adjacency, Laplacian and signless Laplacian spectra of the weighted edge corona networks," *Physica A: Statistical Mechanics and Its Applications*, vol. 540, p. 123073, 2020.

[29] J. B. Liu, J. Zhao, and Z. X. Zhu, "On the number of spanning trees and normalized Laplacian of linear octagonal-quadrilateral networks," *International Journal of Quantum Chemistry*, vol. 119, no. 17, Article ID e25971, 2019.

[30] J. Chen, X. Wang, L. Pang, J. Z. H. Zhang, and T. Zhu, "Effect of mutations on binding of ligands to guanine riboswitch probed by free energy perturbation and molecular dynamics simulations," *Nucleic Acids Research*, vol. 47, no. 13, pp. 6618–6631, 2019.

[31] G. D. Hu, *Studies on Molecular Dynamics Simulation and Free Energy Calculation of Several Biological Systems*, Shandong Normal University, Shan Dong, China, 2011.

[32] Y. Zhang, D. Pan, Y. Shen, N. Jin, H. Liu, and X. Yao, "Understanding the molecular mechanism of the broad and potent neutralization of HIV-1 by antibody VRC01 from the perspective of molecular dynamics simulation and binding free energy calculations," *Journal of Molecular Modeling*, vol. 18, no. 9, pp. 4517–4527, 2012.

[33] J.-B. Liu, J. Zhao, H. He, and Z. Shao, "Valency-based topological descriptors and structural property of the generalized sierpiński networks," *Journal of Statistical Physics*, vol. 177, no. 6, pp. 1131–1147, 2019.

[34] I. K. Mcdonald and J. M. Thornton, "Satisfying hydrogen bonding potential in proteins," *Journal of Molecular Biology*, vol. 238, no. 5, pp. 777–793, 1994.

[35] R. A. Laskowski and M. B. Swindells, "LigPlot+: multiple ligand-protein interaction diagrams for drug discovery," *Journal of Chemical Information and Modeling*, vol. 51, no. 10, pp. 2778–2786, 2011.

[36] J. Rahuel, V. Rasetti, J. Maibaum et al., "Structure-based drug design: the discovery of novel nonpeptide orally active inhibitors of human renin," *Chemistry & Biology*, vol. 7, no. 7, pp. 493–504, 2000.

Hindawi
Journal of Chemistry
Volume 2019, Article ID 9296401, 6 pages
https://doi.org/10.1155/2019/9296401

Research Article

The Third Leap Zagreb Index for Trees

Jia-Ming Zhu,[1] Nasrin Dehgardi,[2] and Xiaoxin Li[3]

[1]*School of Statistics and Applied Mathematics, Anhui University of Finance and Economics, Bengbu 233030, China*
[2]*Department of Mathematics and Computer Science, Sirjan University of Technology, Sirjan, Iran*
[3]*School of Big Data and Artificial Intelligence, Chizhou University, Chizhou 247000, China*

Correspondence should be addressed to Xiaoxin Li; lxx@czu.edu.cn

Received 8 August 2019; Accepted 19 November 2019; Published 24 December 2019

Guest Editor: Shaohui Wang

The third leap Zagreb index is the sum of the products of vertex degrees and second degrees. In this paper, a lower bound on the third leap Zagreb index is established, and the extremal trees achieving this bound are characterized.

1. Introduction

In this paper, we consider simple and connected graphs. Let G be such a graph with vertex set $V = V(G)$ and edge set $E = E(G)$. The *order* $|V|$ of G is denoted by $n = n(G)$ and the *size* $|E|$ of G is denoted by $m = m(G)$. The *degree* of a vertex v in G is the number of edges incident to v and is denoted by $d(v/G)$. The *minimum* and *maximum degrees* of a graph G are denoted by $\delta = \delta(G)$ and $\Delta = \Delta(G)$, respectively.

The *distance* $d_G(u, v)$ between any two vertices u and v of a graph G is equal to the length of a shortest path connecting them. For a vertex $v \in V(G)$ and a positive integer k, the *open k-neighborhood* of v in the graph G, denoted by $N_k(v/G)$, is defined as $N_k(v/G) = \{u \in V(G): d(u, v) = k\}$. The *k-distance degree* of a vertex v in G, denoted by $d_k(v/G)$, is the number of k-neighbors of the vertex v in G, i.e., $d_k(v/G) = |N_k(v/G)|$. Evidently, $d_1(v/G) = d(v/G)$ for every $v \in V(G)$.

A *leaf* of a tree T is a vertex of degree one. A *stem* is a vertex adjacent to a leaf, and a *strong stem* is a stem adjacent to at least two leaves. An end stem is a stem whose all neighbors with exception at most one are leaves. Denote by $\ell(v)$ the number of leaves that are adjacent to the vertex v. A *rooted tree* is a directed tree having a distinguished vertex ω, called the *root*. For a vertex v in a rooted tree T, let $C(v)$ denote the set of children of v and $D(v)$ denote the set of descendants of v, whereas the depth of v, depth(v), is the largest distance from v to a vertex in $D(v)$.

The Zagreb indices are the oldest vertex-degree-based graph invariants. They were introduced in the 1970s [1, 2]. Details of their mathematical theory and chemical applications can be found in the surveys [3–12].

For a graph G, the first and second Zagreb indices are defined as

$$M_1 = M_1(G) = \sum_{v \in V(G)} d\left(\frac{v}{G}\right)^2,$$
$$M_2 = M_2(G) = \sum_{uv \in E(G)} d\left(\frac{u}{G}\right) d\left(\frac{v}{G}\right). \quad (1)$$

Note that $M_1(G) = \sum_{uv \in E(G)} [d(u/G) + d(v/G)]$.

In recent years, some novel variants of Zagreb indices have been put forward, such as Zagreb coindices [13, 14], reformulated Zagreb indices [15, 16, 17], Zagreb hyper indices [18, 19], multiplicative Zagreb indices [20], general Zagreb indices [21], multiplicative sum Zagreb indices [22, 23], multiplicative Zagreb coindices [24], etc.

Naji et al. [25] extended the concept of the Zagreb index to the second vertex degrees, conceiving the so-called *leap Zagreb indices*. For a graph G, the first, second, and third leap Zagreb indices are defined as follows:

$$\mathrm{LM}_1 = \mathrm{LM}_1(G) = \sum_{v\in V(G)} d_2\left(\frac{v}{G}\right)^2,$$

$$\mathrm{LM}_2 = \mathrm{LM}_2(G) = \sum_{uv\in E(G)} d_2\left(\frac{u}{G}\right)d_2\left(\frac{v}{G}\right), \tag{2}$$

$$\mathrm{LM}_3 = \mathrm{LM}_3(G) = \sum_{v\in V(G)} d\left(\frac{v}{G}\right)d_2\left(\frac{v}{G}\right).$$

In [25], the basic properties of these invariants were established, including bounds in terms of Zagreb indices, order, and the size of the underlying graph. In this paper, we establish a lower bound on the third leap Zagreb index and characterize the extremal trees achieving this bound.

2. A Lower Bound on the Third Leap Zagreb Index of Trees

In this section, we present a sharp lower bound for the third leap Zagreb index of trees in terms of their order and maximum degree and characterize all extremal trees.

Throughout this section, T denotes a rooted tree with root ω, where ω is a vertex of maximum degree and $N(\omega) = \{w_1, w_2, \ldots, w_\Delta\}$.

We start with some lemmas.

Lemma 1. *Let T be a tree of order n with maximum degree Δ. If T has a vertex u of degree at least three in maximum distance from ω, then there is a tree T' of order n with maximum degree Δ such that $LM_3(T') < LM_3(T)$.*

Proof. Let $u \neq \omega$ be a stem of T with $d(u) = \alpha \geq 3$ and let $N_T(u) = \{v, x_1, x_2, \ldots, x_{\alpha-1}\}$, where v is the parent of u. Assume $d(v) = \beta$. We consider the following cases.

Case 1. All neighbors of u except v are leaves.

Subcase 1. v is adjacent to a leaf z, and the variable v is preceded by a variable.

Let T' be the tree obtained from $T - \{x_1\}$ by attaching the path zx_1. Clearly, T' is a tree of order n with $\Delta(T) = \Delta(T')$ and $d(u/T) = d(u/T') + 1$, $d(z/T) = d(z/T') - 1$, $d_2(u/T) = d_2(u/T')$, $d_2(v/T) = d_2(v/T')$, $d_2(x_1/T) = d_2(x_1/T') + \alpha - 2 = \alpha - 1$, and $d_2(x_i/T) = d_2(x_i/T') + 1 = \alpha - 1$ for $2 \leq i \leq \alpha - 1$. By definitions, we have

$$\begin{aligned}
\mathrm{LM}_3(T') - \mathrm{LM}_3(T) &= \sum_{v\in V(T')} d\left(\frac{v}{T'}\right)d_2\left(\frac{v}{T'}\right) - \sum_{v\in V(T)} d\left(\frac{v}{T}\right)d_2\left(\frac{v}{T}\right) \\
&= \sum_{i=2}^{\alpha-1} d\left(\frac{x_i}{T'}\right)d_2\left(\frac{x_i}{T'}\right) + d\left(\frac{u}{T'}\right)d_2\left(\frac{u}{T'}\right) + d\left(\frac{z}{T'}\right)d_2\left(\frac{z}{T'}\right) + d\left(\frac{x_1}{T'}\right)d_2\left(\frac{x_1}{T'}\right) \\
&\quad - \sum_{i=2}^{\alpha-1} d\left(\frac{x_i}{T}\right)d_2\left(\frac{x_i}{T}\right) - d\left(\frac{u}{T}\right)d_2\left(\frac{u}{T}\right) - d\left(\frac{z}{T}\right)d_2\left(\frac{z}{T}\right) - d\left(\frac{x_1}{T}\right)d_2\left(\frac{x_1}{T}\right) \\
&= (\alpha-2)(\alpha-2) + (\alpha-1)(\beta-1) + 2(\beta-1) + 1 - (\alpha-2)(\alpha-1) - \alpha(\beta-1) - (\beta-1) - (\alpha-1) \\
&= -2\alpha + 4 < 0.
\end{aligned} \tag{3}$$

Subcase 2. v has no new leaf neighbor.

Let
$T' = (T - \{x_i u \mid 1 \leq i \leq \alpha - 2\}) \cup \{x_i x_{i+1} \mid 1 \leq i \leq \alpha - 2\}$.
Then,

$$\begin{aligned}
\mathrm{LM}_3(T') - \mathrm{LM}_3(T) &= \sum_{v\in V(T')} d\left(\frac{v}{T'}\right)d_2\left(\frac{v}{T'}\right) - \sum_{v\in V(T)} d\left(\frac{v}{T}\right)d_2\left(\frac{v}{T}\right) \\
&= \sum_{i=2}^{\alpha-1} d\left(\frac{x_i}{T'}\right)d_2\left(\frac{x_i}{T'}\right) + d\left(\frac{u}{T'}\right)d_2\left(\frac{u}{T'}\right) + d\left(\frac{v}{T'}\right)d_2\left(\frac{v}{T'}\right) \\
&\quad - \sum_{i=2}^{\alpha-1} d\left(\frac{x_i}{T}\right)d_2\left(\frac{x_i}{T}\right) - d\left(\frac{u}{T}\right)d_2\left(\frac{u}{T}\right) - d\left(\frac{v}{T}\right)d_2\left(\frac{v}{T}\right) \\
&= \beta(k+1) + 2\beta + 4(\alpha-2) + 2 + 1 - \beta(\alpha+k-1) - \alpha(\beta-1) - (\alpha-1)^2 \\
&= -\alpha^2 + 7\alpha - \alpha\beta - 6.
\end{aligned} \tag{4}$$

If $\alpha \geq 4$, then $\mathrm{LM}_3(T') - \mathrm{LM}_3(T) \leq -\alpha^2 + 7\alpha - 4\beta - 6 \leq \alpha^2 + 7\alpha - 14 < 0$.

If $\alpha = 3$ and $\beta \geq 3$, then $\mathrm{LM}_3(T') - \mathrm{LM}_3(T) = -3\beta + 6 < 0$.

If $\alpha = 3$ and $\beta = 2$, then $\mathrm{LM}_3(T') - \mathrm{LM}_3(T) = 2(k+1) + 6 - 2(k+2) - 7 = -3 < 0$.

Case 2. u is adjacent to a leaf x_1, and $uy_1y_2, \ldots, y_\ell$ is a path in T for $\ell \geq 2$.

If v is a stem, then the result is immediate as in Case 1. So assume that v is not a stem. Let T' be the tree obtained from $T - \{x_1\}$ by attaching the path $y_\ell x_1$. Then, $d_2(v/T) = d_2(v/T') + 1 = k + \alpha - 1$, $d_2(u/T) = d_2(u/T')$, $d_2(x_1/T) = d_2(x_1/T') + \alpha - 2$, $d_2(y_{\ell-1}/T) = d_2(y_{\ell-1}/T') - 1$, and $d_2(x_i/T) = d_2(x_i/T') + 1$, for $2 \leq i \leq \alpha - 1$. Let $d_2(u/T) = s$. Then,

$$\begin{aligned}
\mathrm{LM}_3(T') - \mathrm{LM}_3(T) &= \sum_{v\in V(T')} d\left(\frac{v}{T'}\right)d_2\left(\frac{v}{T'}\right) - \sum_{v\in V(T)} d\left(\frac{v}{T}\right)d_2\left(\frac{v}{T}\right) \\
&= \beta(k+\alpha-2) + (\alpha-1) + 2(\alpha-1) + 4(\ell-3) + 4 + 2 + 1 - \beta(k+\alpha-1) - \alpha s - 2\alpha \\
&\quad - (\alpha-1) - 4(\ell-3) - 2 - 1 \\
&= -\alpha - \beta - s + 3 < 0.
\end{aligned} \tag{5}$$

Case 3. u is not a stem, and $ux_1x_2, \ldots, x_\ell$ and $uy_1y_2, \ldots, y_t$ $(\ell, t \geq 2)$ are two paths in T.

Clearly $d_2(u/T) = \beta + \alpha - 2$, $d_2(v/T) = k + \alpha - 1$, and $d_2(z/T) = d(u) - 1 = \alpha - 1$ for $z \in N(u) - \{v\}$. Let T' be the tree obtained from $T - \{x_1\}$ by attaching the path $y_t x_1$. Then, $d_2(v/T') = k + \alpha - 2$, $d_2(u/T') = \beta + \alpha - 3$, and $d_2(z/T') = \alpha - 2$ for $z \in N(u) - \{x_1, y_1, v\}$. Also, we have $d_2(x_i/T) = d_2(x_i/T')$ for $2 \leq i \leq \ell$, $d_2(y_t/T) = d_2(y_{t-1}/T) = 1$, $d_2(x_1/T) = d_2(y_t/T') = d_2(y_{t-1}/T') = 2$, $d_2(y_j/T) = d_2(y_j/T')$ for $2 \leq j \leq t-2$, $d_2(x_1/T) = d_2(y_1/T) = \alpha - 1$, and $d_2(y_1/T') = \alpha - 2$. Now, we consider the following subcases.

Subcase 1. $\ell, t \geq 3$.

$$\begin{aligned}
\mathrm{LM}_3(T') - \mathrm{LM}_3(T) &= \sum_{v\in V(T')} d\left(\frac{v}{T'}\right)d_2\left(\frac{v}{T'}\right) - \sum_{v\in V(T)} d\left(\frac{v}{T}\right)d_2\left(\frac{v}{T}\right) \\
&= \beta(\alpha+k-2) + (\alpha-1)(s-1) + 2(\alpha-1) + 4(\ell+t-3) + 2 + 1 - \beta(\alpha+k-1) - \alpha s \\
&\quad - 2\alpha - 4(\ell+t-4) - 4 - 2 \\
&= -\beta - 3\alpha - s < 0.
\end{aligned} \tag{6}$$

Subcase 2. $\ell = 2, t \geq 3$.

$$\begin{aligned}\mathrm{LM}_3(T') - \mathrm{LM}_3(T) &= \sum_{v\in V(T')} d\left(\frac{v}{T'}\right)d_2\left(\frac{v}{T'}\right) - \sum_{v\in V(T)} d\left(\frac{v}{T}\right)d_2\left(\frac{v}{T}\right)\\ &= \beta(\alpha+k-2)+(\alpha-1)(s-1)+2(\alpha-1)+4(t-1)+3-\beta(\alpha+k-1)-\alpha s-2(\alpha-1)\\ &\quad -2\alpha-4(t-2)-2-2\\ &= -\beta-3\alpha-s+2<0.\end{aligned} \tag{7}$$

Subcase 3. $\ell = t = 2$.

$$\begin{aligned}\mathrm{LM}_3(T') - \mathrm{LM}_3(T) &= \sum_{v\in V(T')} d\left(\frac{v}{T'}\right)d_2\left(\frac{v}{T'}\right) - \sum_{v\in V(T)} d\left(\frac{v}{T}\right)d_2\left(\frac{v}{T}\right)\\ &= \beta(\alpha+k-2)+(\alpha-1)(s-1)+2(\alpha-1)+7-\beta(\alpha+k-1)-\alpha s-4(\alpha-1)-2\\ &= -\beta-3\alpha-s+8<0.\end{aligned} \tag{8}$$

A *spider* is a tree with at most one vertex of degree greater than 2, called the center of the spider. If there is no vertex of degree greater than two, then any vertex can be the considered as the center. A *leg* of the spider is a path from the center to a vertex of degree one. Thus, a star with k edges is a spider with k legs, each of length 1, and the path is a spider with 1 or 2 legs.

By Lemma 1, among all trees of order n with maximum degree Δ, the spiders have the minimum third leap Zagreb index. In what follows, we determine the spiders having minimum third leap Zagreb index. If $\Delta = 2$, then $T \cong P_n$. Therefore, let $\Delta \geq 3$. □

Lemma 2. *Let T be a spider of order n with $p \geq 3$ legs. If T has at least two legs of length at least 2, then there is a spider T' of order n with p legs such that $LM_3(T') < LM_3(T)$.*

Proof. Let ω be the center of T and let $\omega x_1 x_2, \ldots, x_\ell$, $\omega y_1 y_2, \ldots, y_t$ be two legs of length at least two in T. Let T' be the tree obtained from $T - \{x_1 x_2\}$ by attaching the path $y_t x_2$, and let $d_2(\omega/T) = k$. We consider the following cases.

Case 1. $\ell = t = 2$.

$$\begin{aligned}\mathrm{LM}_3(T') - \mathrm{LM}_3(T) &= \sum_{v\in V(T')} d\left(\frac{v}{T'}\right)d_2\left(\frac{v}{T'}\right) - \sum_{v\in V(T)} d\left(\frac{v}{T}\right)d_2\left(\frac{v}{T}\right)\\ &= \Delta(k-1)+\Delta-1+2\Delta+3-\Delta k-4(\Delta-1)-2\\ &= -2\Delta+4<0.\end{aligned} \tag{9}$$

Case 2. $\ell = 2, t \geq 3$.

$$\begin{aligned}\mathrm{LM}_3(T') - \mathrm{LM}_3(T) &= \sum_{v\in V(T')} d\left(\frac{v}{T'}\right)d_2\left(\frac{v}{T'}\right) - \sum_{v\in V(T)} d\left(\frac{v}{T}\right)d_2\left(\frac{v}{T}\right)\\ &= \Delta(k-1)+\Delta-1+2\Delta+4+3-\Delta k-2(\Delta-1)-2\Delta-3\\ &= -2\Delta+5<0.\end{aligned} \tag{10}$$

Case 3. $\ell, t \geq 3$.

$$\begin{aligned} \mathrm{LM}_3(T') - \mathrm{LM}_3(T) &= \sum_{v \in V(T')} d\left(\frac{v}{T'}\right) d_2\left(\frac{v}{T'}\right) - \sum_{v \in V(T)} d\left(\frac{v}{T}\right) d_2\left(\frac{v}{T}\right) \\ &= \Delta(k-1) + 2\Delta + \Delta - 1 + 4(t+\ell-4) + 3 - \Delta k - 2\Delta - 2\Delta - 4(t+\ell-6) - 4 - 2 \\ &= -2\Delta + 4 < 0. \end{aligned} \tag{11}$$

Now, we are ready to state our main result. □

Theorem 3. *For any tree T of order $n \geq 5$ with maximum degree Δ,*

$$\mathrm{LM}_3(T) \geq \begin{cases} \Delta^2 - 4\Delta + 4n - 9, & \text{if } \Delta < n-2, \\ \Delta^2 + \Delta, & \text{if } \Delta = n-2, \\ (\Delta - 1)^2, & \text{if } \Delta = n-1, \end{cases} \tag{12}$$

with equality if and only if T is a spider with at most one leg of length at least two.

Proof. Let T_1 be a tree of order $n \geq 2$ with maximum degree Δ such that

$$\mathrm{LM}_3(T_1) = \min\left\{\mathrm{LM}_3(T) \,\middle|\, T \text{ is a tree of order } n \text{ with maximum degree } \Delta\right\}. \tag{13}$$

Let v be a vertex with maximum degree Δ. Root T_1 at v. By the choice of T_1, we deduce from Lemma 1 that T_1 is a spider with center v. It follows from Lemma 2 and the choice of T_1 that T_1 has at most one leg of length at least two. First, let all legs of T_1 have length one. Then, T_1 is a star of order n and $\mathrm{LM}_3(T_1) = (n-1)^2$. Now, let T_1 have only one leg of length at least two. Then, $\mathrm{LM}_3(T_1) = \Delta^2 + \Delta$ when $\Delta = n-2$, and $\mathrm{LM}_3(T_1) = \Delta^2 - 4\Delta + 4n - 9$ when $\Delta < n-2$. This completes the proof. □

3. Conclusion

We continue the study of the third leap Zagreb index and establish the lower bound on the third leap Zagreb index of trees in terms of their order and maximum degree. Also, we characterize the extremal trees achieving this bound. We conclude this paper with two open problems.

Problem 1. Present sharp lower bounds for the first and second leap Zagreb indices of trees in terms of their order and maximum degree.

Problem 2. Present sharp upper bounds for the leap Zagreb indices of trees in terms of their order and maximum degree.

Data Availability

The data used to support the findings of this study are included within the article.

Conflicts of Interest

The authors declare that there are no conflicts of interest regarding the publication of this paper.

Acknowledgments

This study was supported by Humanities and Social Sciences Research Project of the Ministry of Education "Research on the Development of Chinese Family Policies at Low Fertility Levels" (No. 19YJCZH069) and Anhui Education Department Teaching and Research Fund Project (No. 2018jyxm1305); Anhui University of Finance and Economics School-Level Teaching and Research Fund Project (acxkjsjy201803zd and acjyyb2018006); and Chizhou University Teaching Team Project (2016XJXTD02).

References

[1] I. Gutman, B. Ruščić, N. Trinajstić, and C. F. Wilcox, "Graph theory and molecular orbitals. XII. Acyclic polyenes," *The Journal of Chemical Physics*, vol. 62, no. 9, pp. 3399–3405, 1975.

[2] I. Gutman and N. Trinajstić, "Graph theory and molecular orbitals. Total φ-electron energy of alternant hydrocarbons," *Chemical Physics Letters*, vol. 17, no. 4, pp. 535–538, 1972.

[3] H. Aram and N. Dehgardi, "Reformulated F-index of graph operations," *Communications in Combinatorics and Optimization*, vol. 2, no. 2, pp. 87–98, 2017.

[4] N. Dehgardi, "A note on revised Szeged index of graph operations," *Iranian Journal of Mathematical Chemistry*, vol. 9, pp. 57–63, 2018.

[5] N. Dehgardi and H. Aram, "Sharp bounds on the augmented Zagreb index of graph operations," *Kragujevac Journal of Mathematics*, vol. 44, pp. 509–522, 2020.

[6] S. Ji and S. Wang, "On the sharp lower bounds of Zagreb indices of graphs with given number of cut vertices," *Journal of Mathematical Analysis and Applications*, vol. 458, no. 1, pp. 21–29, 2018.
[7] J.-B. Liu, C. Wang, S. Wang, and B. Wei, "Zagreb indices and multiplicative Zagreb indices of Eulerian graphs," *Bulletin of the Malaysian Mathematical Sciences Society*, vol. 42, no. 1, pp. 67–78, 2019.
[8] J.-B. Liu, X.-F. Pan, F.-T. Hu, and F.-F. Hu, "Asymptotic Laplacian-energy-like invariant of lattices," *Applied Mathematics and Computation*, vol. 253, pp. 205–214, 2015.
[9] J.-B. Liu and X.-F. Pan, "Minimizing Kirchhoff index among graphs with a given vertex bipartiteness," *Applied Mathematics and Computation*, vol. 291, pp. 84–88, 2016.
[10] J. B. Liu, J. Zhao, and Z. Zhu, "On the number of spanning trees and normalized Laplacian of linear octagonal—quadrilateral networks," *International Journal of Quantum Chemistry*, vol. 119, no. 17, Article ID e25971, 2019.
[11] S. Nikolić, G. Kovačević, A. Miličević, and N. Trinajstić, "The Zagreb indices 30 years after," *Croatica Chemica Acta*, vol. 76, pp. 113–124, 2003.
[12] J. Xu, J.-B. Liu, A. Bilal et al., "Distance degree index of some derived graphs," *Mathematics*, vol. 7, no. 3, p. 283, 2019.
[13] A. R. Ashrafi, T. Došlić, and A. Hamzeh, "The Zagreb coindices of graph operations," *Discrete Applied Mathematics*, vol. 158, no. 15, pp. 1571–1578, 2010.
[14] T. Došlić, "Vertex-weighted Wiener polynomials for composite graphs," *ARS Mathematica Contemporanea*, vol. 1, pp. 66–80, 2008.
[15] A. Ilić and B. Zhou, "On reformulated Zagreb indices," *Discrete Applied Mathematics*, vol. 160, pp. 204–209, 2012.
[16] J.-B. Liu, B. Ali, M. A. Malik, H. M. A. Siddiqui, and M. Imran, "Reformulated zagreb indices of some derived graphs," *Mathematics*, vol. 7, no. 4, p. 366, 2019.
[17] A. Miličević, S. Nikolić, and N. Trinajstić, "On reformulated Zagreb indices," *Molecular Diversity*, vol. 8, no. 4, pp. 393–399, 2004.
[18] B. Basavanagoud and S. Patil, "A note on hyper-Zagreb index of graph operations, Iran," *Journal of Mathematical Chemistry*, vol. 7, pp. 89–92, 2016.
[19] K. Pattabiraman and M. Vijayaragavan, "Hyper Zagreb indices and its coindices of graphs," *Bulletin of the International Mathematical Virtual Institute*, vol. 7, pp. 31–41, 2017.
[20] K. Xu and H. Hua, "A unified approach to extremal multiplicative Zagreb indices for trees, unicyclic and bicyclic graphs," *MATCH Communications in Mathematical and in Computer Chemistry*, vol. 68, pp. 241–256, 2012.
[21] I. Gutman, N. Dehgardi, and H. Aram, "On general first Zagreb index of graphs with fixed maximum degree," *Bulletin of the International Mathematical Virtual Institute*, vol. 6, pp. 251–258, 2016.
[22] M. Eliasi, A. Iranmanesh, and I. Gutman, "Multiplicative versions of first Zagreb index," *MATCH Communications in Mathematical and in Computer Chemistry*, vol. 68, pp. 217–230, 2012.
[23] K. Xu and K. C. Das, "Trees, unicyclic, and bicyclic graphs extremal with respect to multiplicative sum Zagreb index," *MATCH Communications in Mathematical and in Computer Chemistry*, vol. 68, pp. 257–272, 2012.
[24] K. Xu, K. C. Das, and K. Tang, "On the multiplicative Zagreb coindex of graphs," *Opuscula Mathematica*, vol. 33, no. 1, pp. 191–204, 2013.
[25] A. M. Naji, N. D. Soner, and I. Gutman, "On leap Zagreb indices of graphs," *Communications in Combinatorics and Optimization*, vol. 2, pp. 99–117, 2017.

Hindawi
Journal of Chemistry
Volume 2019, Article ID 9089781, 8 pages
https://doi.org/10.1155/2019/9089781

Research Article

Dynamical Behavior of a Nonautonomous Stochastic Modified Bazykin Model

Zhangzhi Wei,[1,2] **Zheng Wu**,[1] **and Lianglong Wang**[1]

[1]*School of Mathematics and Statistics, Suzhou University, Suzhou 234000, China*
[2]*School of Mathematical Sciences, Anhui University, Hefei 230601, China*

Correspondence should be addressed to Lianglong Wang; wangll@ahu.edu.cn

Received 17 October 2019; Accepted 3 December 2019; Published 21 December 2019

Academic Editor: Juan L. G. Guirao

In this article, a nonautonomous stochastic modified Bazykin model is introduced. The positive solution is proved to be unique and global for any initial data via stochastic comparison theorem and Itô formula. Stochastic ultimate boundedness and stochastic permanence are also considered. Finally, some simulations are performed to verify the validity of results.

1. Introduction

The study on population systems is one of the hot topic in applied mathematics and ecology. Mathematical modelling and qualitative analysis have received much concern, such as the famous Lotka–Volterra model [1]. For more than a decade, predator-prey models with ration-dependent response function have been discussed extensively [2–4]. Today, most predator-prey models assume that the functional response function is a function of prey population density [5–7].

Considering the classical assumptions is not always appropriate which assume that predators encounter prey at random, and the functional response only depends on prey abundance. In 1998, Alexeev and Bazykin first proposed the following Bazykin's model [2].

$$\begin{aligned} \dot{N}(t) &= N(t)\left(a - bN(t) - \frac{cP(t)}{1 + AN(t)}\right), \\ \dot{P}(t) &= P(t)\left(-g - hP(t)\frac{fN(t)}{1 + AN(t)}\right), \end{aligned} \tag{1}$$

where $N(t)$ and $P(t)$ denote the number (or density) of prey species and predator species. The parameters a, b, c, g, f, and m are greater than zero with their usual ecological meanings (for details refer [2]). Many research studies about system (1) have been received, more about its generalization [8–11].

Taking the ratio-dependent of predator into account (more predators are good for hunting in serious situations), M. Haque remodeled a modified Bazykin model according to system (1)

$$\begin{aligned} \dot{N}(t) &= N(t)\left(a - bN(t) - \frac{cP(t)}{P(t) + AN(t)}\right), \\ \dot{P}(t) &= P(t)\left(-g - hP(t)\frac{fN(t)}{P(t) + AN(t)}\right), \end{aligned} \tag{2}$$

in which the analytical behavior of the system near origin is observed [1].

In the real environment, there is the interference of random factors everywhere, such as emergencies, weather changes, and disease spread, and then the actual observed data have some deviation from the results of the deterministic model. Therefore, the influence of the real random factors on the populations should be considered, and the stochastic model can describe the real situation better [12–16].

Considering that the parameters a and g are affected by white noise, the rates a and g can been replaced by $a \longrightarrow a + \sigma_1 \dot{w}_1(t)$, and $g \longrightarrow g + \sigma_2 \dot{w}_2(t)$, respectively, where $w_1(t)$ and $w_2(t)$ are Wiener process (or Brownian motion), and they are independent. σ_1 and σ_2 indicate the

intensities of white noise. The following autonomous stochastic model was built by Lv et al. [13]:

$$\dot{N}(t) = N(t)\left(a - bN(t) - \frac{cP(t)}{P(t) + AN(t)}\right) + \sigma_1 N(t)\mathrm{d}w_1(t),$$
$$\dot{P}(t) = P(t)\left(-g - hP(t)\frac{fN(t)}{P(t) + AN(t)}\right) - \sigma_2 P(t)\mathrm{d}w_2(t), \tag{3}$$

and has been investigated, and the system (3) is persistent in mean or die out under some conditions [13].

In this paper, we will consider the nonautonomous stochastic modified Bazykin model

$$\begin{aligned}\dot{N}(t) &= N(t)\left(a(t) - b(t)N(t) - \frac{c(t)P(t)}{P(t) + A(t)N(t)}\right) \\ &\quad + \sigma_1(t)N(t)\mathrm{d}w_1(t), \\ \dot{P}(t) &= P(t)\left(-g(t) - h(t)P(t)\frac{f(t)N(t)}{P(t) + A(t)N(t)}\right) \\ &\quad - \sigma_2(t)P(t)\mathrm{d}w_2(t),\end{aligned} \tag{4}$$

where $a(t), b(t), c(t), g(t), h(t), f(t), A(t)$, and $\sigma_1(t), \sigma_2(t)$ are assumed to be continuous and bounded.

It is important for population systems to keep permanence, which means that the species will not extinct in the future. Some definitions and conditions which guarantee that system (4) is stochastic permanent and boundedness are given as follows.

Without specification, $(N_0, P_0) \in R_+^2$ is an initial data by default in the full text, and $Y(t) = (N(t), P(t))$ is the solution of system (4) with an initial (N_0, P_0).

Definition 1 (see [15]). Assume any $0 < \epsilon < 1$, then $M > 0$ and $\eta > 0$, when following is hold:

$$\begin{aligned}\liminf_{t\longrightarrow+\infty} \mathbb{P}\{|Y(t)| \le M\} &\ge 1 - \epsilon, \\ \liminf_{t\longrightarrow+\infty} \mathbb{P}\{|Y(t)| \ge \eta\} &\ge 1 - \epsilon,\end{aligned} \tag{5}$$

so solution $Y(t) = (N(t), P(t))$ for system (4) is called stochastically permanent.

Definition 2 (see [15]). Assume any $0 < \epsilon < 1$, then $\eta > 0$, when following is hold

$$\limsup_{t\longrightarrow+\infty} \mathbb{P}\{|Y(t)| > \eta\} < \epsilon, \tag{6}$$

so solution $Y(t) = (N(t), P(t))$ for system (4) is called stochastically ultimately bounded.

In Section 2, main results about the existence and uniqueness of global positive solution and the properties of asymptotic bounded were introduced and then shows us that the solution of system (4) is stochastically ultimate bounded and stochastically permanent. In Section 3, we briefly give conclusions and remark. In Section 4, numerical simulations are carried out to illustrate our results. In the end, some lemmas and proofs of main results are given.

2. Main Results

2.1. Existence and Globality

Theorem 1. *Let $(N_0, P_0) \in R_+^2$ be initial value, then the positive solution $Y(t) = (N(t), P(t))$ to system (4) exists globally a.s.*

Corollary 1. *The solution $Y(t) = (N(t), P(t))$ of system (4) must stay in R_+^2 a.s., and that*

$$\begin{aligned}&N_1(t) \le N(t) \le N_2(t), \\ &P_1(t) \le P(t) \le P_2(t), \quad \text{a.s.},\end{aligned} \tag{7}$$

where upper-lower solutions are defined later in (20)–(22) and (51).

2.2. Dynamical Behavior of System (4).

In the following, we denote

$$\begin{aligned}\varphi^u &= \max_{t\in[0,+\infty)} \varphi(t), \\ \varphi_l &= \min_{t\in[0,+\infty)} \varphi(t), \\ q(t) &= a(t) - c(t) - \sigma_1^2(t), \\ \lambda(t) &= g(t) - \frac{f(t)}{A(t)} + \frac{1}{2}\sigma_2^2(t), \\ \nu(t) &= a(t) - c(t) - \frac{\sigma_1^2(t)}{2}, \\ \rho(t) &= a(t) - c(t) - \frac{3}{2}\sigma_1^2(t), \\ \sigma(t) &= \frac{f(t)}{A(t)} - g(t) - \frac{3}{2}\sigma_2^2(t).\end{aligned} \tag{8}$$

The functions above are bounded and continuous on $[0, +\infty)$.

Theorem 2. *If $b_l > 0$ and $g_l > 0$, the solution $(N(t), P(t))$ to system (4) satisfies*

$$\begin{aligned}\limsup_{t\longrightarrow+\infty} \mathbb{E}[N(t)] &\le \frac{a^u}{b_l}, \\ \limsup_{t\longrightarrow+\infty} \mathbb{E}\left[N(t) + \frac{c_l}{f^u}P(t)\right] &\le \frac{(a^u + g^u)^2}{4b_l g_l}.\end{aligned} \tag{9}$$

Furthermore,

$$\limsup_{t\longrightarrow+\infty} \mathbb{E}[P(t)] \le \frac{f^u(a^u + g^u)^2}{4b_l c_l g_l}, \tag{10}$$

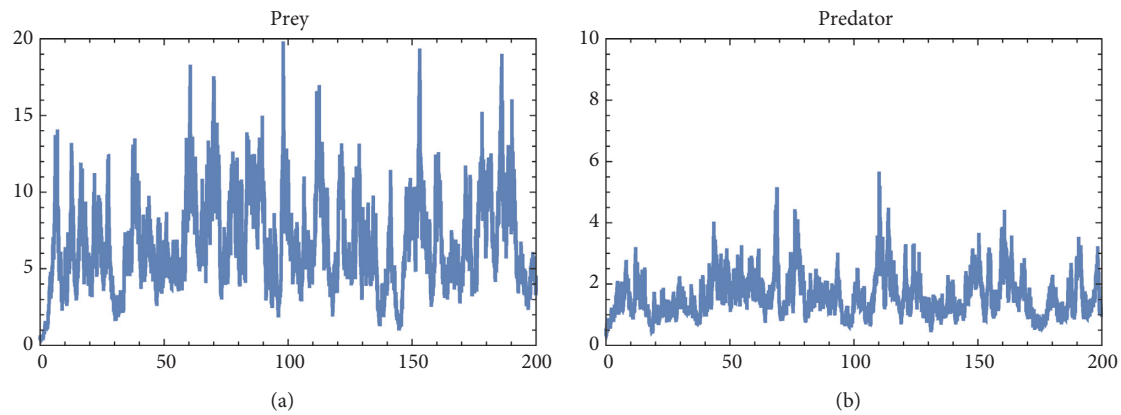

Figure 1: Solution is stochastically permanent if $b_l > 0, c_l > 0, g_l > 0, r_l > 0, \rho_l > 0$, and $\sigma_l > 0$.

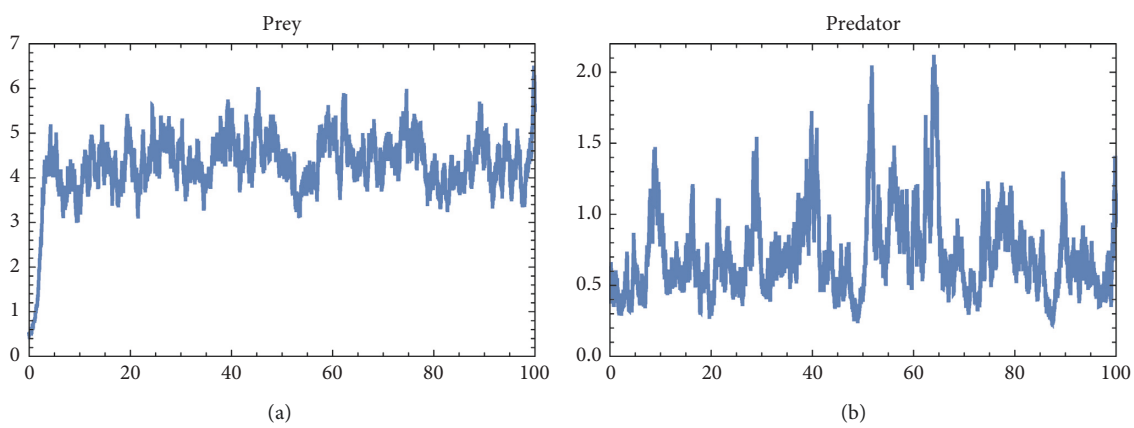

Figure 2: Solution is stochastically permanent if $b_l > 0, c_l > 0, g_l > 0$, and $r_l > 0$, but $\rho_l < 0$ and $\sigma_l < 0$.

when $c_l > 0$.

Theorem 3. *The solutions* $(N(t), P(t))$ *of system (4) are stochastically ultimately bounded when* $b_l > 0, c_l > 0$, *and* $g_l > 0$.

Theorem 4. *The solutions* $(N(t), P(t))$ *of system (4) are stochastically permanent, if* $b_l > 0, c_l > 0, g_l > 0$, *and* $q_l > 0$.

Theorem 5. *The solutions* $(N(t), P(t))$ *of system (4) are stochastically permanent, if* $b_l > 0, c_l > 0, g_l > 0, \rho_l > 0$, *and* $\sigma_l > 0$.

3. Conclusion

Theorem 5 shows that predator species is permanent a.s., if $b_l > 0, c_l > 0, g_l > 0, \rho_l > 0$, and $\sigma_l > 0$. It is clear that prey species is also permanent a.s., i.e., predator species and prey species are both stochastically permanent. Furthermore, under assumption of Theorem 5, system (4) is persistent according to Theorem 7 in [13]. By our Theorem 5, we can conclude that prey species and predator species in equation (4) are both stochastically permanent. Our work is based on the result of Lv et al. [13] and Wu et al. [15]. At the same time, we have achieved some results about the stochastic model with Markovian switching and Lévy jumps [17, 18].

4. Simulations

In this part, some numerical experiments are given to show that our main results as true. In Figure 1, we choose

$$\begin{aligned} a &= 0.8 + 0.1 \sin t, \\ b &= 0.1 + 0.05 \cos t, \\ c &= 0.2 + \sin t, \\ A &= 0.9 + 0.1 \sin t, \\ g &= 0.3 + 0.01 \sin t, \\ h &= 0.1, \\ f &= 0.9 + 0.1 \cos t, \\ \sigma_1 &= 0.49 + 0.01 \sin t, \\ \sigma_2 &= 0.49 + 0.1 \cos t. \end{aligned} \tag{11}$$

We notice that $b_l > 0, c_l > 0, g_l > 0, r_l > 0, \rho_l > 0$, and $\sigma_l > 0$, and then the solution of system (4) will be stochastically permanent by virtue of Theorem 5.

In Figure 2, we choose

$$\begin{aligned} a &= 0.8 + 0.1\sin t, \\ b &= 0.1 + 0.05\cos t, \\ c &= 0.2 + \sin t, \\ A &= 0.9 + 0.1\sin t, \\ g &= 0.3 + 0.01\sin t, \\ h &= 0.1, \\ f &= 0.9 + 0.1\cos t, \\ \sigma_1 &= 0.59 + 0.01\sin t, \\ \sigma_2 &= 0.59 + 0.1\cos t, \end{aligned} \tag{12}$$

where $r_l > 0, \rho_l < 0$, and $\sigma_l < 0$, and $b_l > 0, c_l > 0, g_l > 0$, and $r_l > 0$, but $\rho_l < 0$ and $\sigma_l < 0$. According to Theorem 4, we know that the solution of system (4) is also stochastically permanent.

5. Proofs of Main Results

Lemma 1 (see [16]). *Let $N_2(t)$ be a solution of equation (21). If $b_l > 0$, then*

$$\limsup_{t\longrightarrow+\infty} \mathbb{E}[N_2(t)] \le \frac{a^u}{b_l}. \tag{13}$$

Lemma 2 (see [16])

$$\mathbb{E}\left[\exp\left\{\int_{t_0}^{t} \sigma_1(s)\mathrm{d}w(s)\right\}\right] = \exp\left\{\frac{1}{2}\int_{t_0}^{t} \sigma_1^2(s)\mathrm{d}s\right\}, \quad 0 \le t_0 \le t. \tag{14}$$

Lemma 3. *If $q_l > 0$, then*

$$\limsup_{t\longrightarrow+\infty} \mathbb{E}\left[\frac{1}{N(t)}\right] \le \frac{b^u}{q_l}. \tag{15}$$

Lemma 4. *If $b_l > 0$ and $q_l > 0$, for every $\epsilon > 0$, there exists $M = > 0, \eta > 0$; then,*

$$\begin{aligned} \liminf_{t\longrightarrow+\infty} \mathbb{P}\{N(t) \le M\} &\ge 1 - \epsilon, \\ \liminf_{t\longrightarrow+\infty} \mathbb{P}\{N(t) \ge \eta\} &\ge 1 - \epsilon. \end{aligned} \tag{16}$$

Lemma 5. *If $\rho_l > 0$ and $\sigma_l > 0$, then*

$$\limsup_{t\longrightarrow+\infty} \mathbb{E}\left[\frac{1}{P(t)}\right] \le P(0)^{-1} + \sqrt{f^u m^u \left[2N(0)^{-1} + 2(b^u)^2 \rho_l^{-2}\right]}. \tag{17}$$

Proof of Theorem 1 and Corollary 1. The proof process is a standard operation and is omitted here (see [12, 13, 15]).

The following system is obtained by comparison

$$\begin{aligned} \mathrm{d}N_1(t) &= N_1(t)[a(t) - c(t) - b(t)N_1(t)]\mathrm{d}t \\ &\quad + \sigma_1(t)N_1(t)\mathrm{d}w_1(t), \\ N_1(0) &= N(0), \\ \mathrm{d}N_2(t) &= N_2(t)[a(t) - b(t)N_2]\mathrm{d}t + \sigma_1(t)N_2(t)\mathrm{d}w_1(t), \\ N_2(0) &= N(0), \\ \mathrm{d}P_1(t) &= P_1 t\left(\left(\frac{f(t)}{A(t)} - g(t)\right) - P_1(t)\left(h(t)\right.\right. \\ &\quad \left.\left. + \frac{f(t)}{A^2(t)P_1(t)}\right)\right)\mathrm{d}t - \sigma_2(t)P_1(t)\mathrm{d}w_2(t), \\ P_1(0) &= P(0), \\ \mathrm{d}P_2(t) &= P_2(t)\left(-h(t)P_2(t) + \left(\frac{f(t)}{A(t)} - g(t)\right)\right)\mathrm{d}t \\ &\quad - \sigma_2(t)P_2(t)\mathrm{d}w_2(t), P_2(0) = P(0). \end{aligned} \tag{18}$$

They have solutions as follows:

$$N_1(t) = \frac{\exp\left\{\int_0^t [a(s) - c(s) - (\sigma_1^2(s)/2)]\mathrm{d}s + \int_0^t \sigma_1(s)\mathrm{d}w_1(s)\right\}}{N(0)^{-1} + \int_0^t b(s)\exp\left\{\int_0^s [a(\tau) - c(\tau) - (\sigma_1^2(\tau)/2)]\mathrm{d}\tau + \int_0^s \sigma_1(\tau)\mathrm{d}w_1(\tau)\right\}\mathrm{d}s}, \tag{19}$$

$$N_2(t) = \frac{\exp\left\{\int_0^t [a(s) - (\sigma_1^2(s)/2)]\mathrm{d}s + \int_0^t \sigma_1(s)\mathrm{d}w_1(s)\right\}}{N(0)^{-1} + \int_0^t b(s)\exp\left\{\int_0^s [a(\tau) - (\sigma_1^2(\tau)/2)]\mathrm{d}\tau + \int_0^s \sigma_1(\tau)\mathrm{d}w_1(\tau)\right\}\mathrm{d}s}, \tag{20}$$

$$P_1(t) = \frac{\exp\left\{\int_0^t [(f(s)/A(s)) - g(s) - (\sigma_2^2(s)/2)]\mathrm{d}s - \int_0^t \sigma_2(s)\mathrm{d}w_2(s)\right\}}{P(0)^{-1} + \int_0^t h(s)\exp\left\{\int_0^s [(f(r)/A(r)) - g(r) - (\sigma_2^2(s)/2)]\mathrm{d}r - \int_0^s \sigma_2(r)\mathrm{d}w_2(r)\right\}\mathrm{d}s}, \tag{21}$$

$$P_2(t)=\frac{\exp\left\{\int_0^t[(f(s)/A(s))-g(s)-(\sigma_2^2(s)/2)]\mathrm{d}s-\int_0^t\sigma_2(s)\mathrm{d}w_2(s)\right\}}{P(0)^{-1}+\int_0^t\left(h(s)+\left(f(s)/A^2(s)N_1(s)\right)\right)\exp\left\{\int_0^s[(f(r)/A(r))-g(r)-(\sigma_2^2(s)/2)]\mathrm{d}r-\int_0^s\sigma_2(r)\mathrm{d}w_2(r)\right\}\mathrm{d}s}. \tag{22}$$

Consequently

$$\begin{aligned}&N_1(t)\le N(t)\le N_2(t),\quad \text{a.s.},\\&P_1(t)\le P(t)\le P_2(t),\quad \text{a.s.}\end{aligned} \tag{23}$$

□

Proof of Theorem 2. From $N(t)\le N_2(t)(t)$ a.s., and Lemma 1, one obtain that

$$\limsup_{t\longrightarrow+\infty}\mathbb{E}[N(t)]\le\frac{a^u}{b_l}. \tag{24}$$

Let

$$F(t)=N(t)+\frac{c_l}{f^u}P(t). \tag{25}$$

The derivative of $F(t)$ along system (4) can be obtained as follows:

$$\begin{aligned}\mathrm{d}F(t)=&\left((a(t)+g(t))N(t)-b(t)N^2(t)-g(t)F(t)\right)\mathrm{d}t\\&+\left(\left(-c(t)+\frac{c_l}{f^u}f(t)\right)\frac{N(t)P(t)}{y(t)+A(t)N(t)}-h(t)\frac{c_l}{f^u}P^2(t)\right)\mathrm{d}t\\&+\sigma_1(t)N(t)\mathrm{d}w_1(t)-\frac{c_l}{f^u}\sigma_2(t)P(t)\mathrm{d}w_2(t).\end{aligned} \tag{26}$$

Through calculating the integral, we have

$$\begin{aligned}F(t)=F(0)+\int_0^t\Bigg\{&[a(s)+g(s)]N(s)-b(s)N^2(s)\\&-g(s)F(s)-h(t)\frac{c_l}{f^u}P^2(t)+\left(-c(s)+\frac{c_l}{f^u}f(s)\right)\\&\cdot\frac{N(s)P(s)}{P(s)+A(s)N(s)}\Bigg\}\mathrm{d}s+\int_0^t\sigma_1(s)N(s)\mathrm{d}w_1(s)\\&-\int_0^t\frac{c_l}{f^u}\sigma_2(s)\mathrm{d}w_2(s).\end{aligned} \tag{27}$$

Then, we calculate the expectation

$$\begin{aligned}\mathbb{E}[F(t)]=F(0)+\mathbb{E}\int_0^t\Bigg\{&[a(s)+g(s)]x(s)-b(s)N^2(s)\\&-g(s)F(s)-h(t)\frac{c_l}{f^u}P^2(t)+\left(-c(s)+\frac{c_l}{f^u}f(s)\right)\\&\cdot\frac{N(s)P(s)}{P(s)+A(s)N(s)}\Bigg\}\mathrm{d}s.\end{aligned} \tag{28}$$

The following formula is easy to be obtained:

$$\begin{aligned}\frac{\mathrm{d}\mathbb{E}[F(t)]}{\mathrm{d}t}&=[a(t)+g(t)]\mathbb{E}[N(t)]-b(t)\mathbb{E}\left[N^2(t)\right]-g(t)\mathbb{E}[F(t)]-h(t)\frac{c_l}{f^u}\mathbb{E}\left[P^2(t)\right]\\&\quad+\left[-c(t)+\frac{c_l}{f^u}f(t)\right]\mathbb{E}\left[\frac{N(t)P(t)}{P(t)+A(t)N(t)}\right]\\&\le[a(t)+g(t)]\mathbb{E}[N(t)]-b(t)\mathbb{E}\left[N^2(t)\right]-g(t)\mathbb{E}[F(t)]\\&\le(a^u+g^u)\mathbb{E}[N(t)]-b_l(\mathbb{E}[N(t)])^2-g_l\mathbb{E}[F(t)].\end{aligned} \tag{29}$$

Note that inequality $K_1x-K_2x^2\le K_1^2/4K_2$, and then

$$\frac{\mathrm{d}\mathbb{E}[F(t)]}{\mathrm{d}t}\le\frac{(a^u+g^u)^2}{4b_l}-g_l\mathbb{E}[F(t)]. \tag{30}$$

Therefore, by basic theories of ordinary differential equation, we have

$$0\le\limsup_{t\longrightarrow+\infty}\mathbb{E}[F(t)]\le\frac{(a^u+g^u)^2}{4b_lg_l}. \tag{31}$$

According to the above equation, the following is obtained:

$$\limsup_{t\longrightarrow+\infty}\mathbb{E}[P(t)]\le-\mathbb{E}[N(t)]+\frac{f^u(a^u+g^u)^2}{4b_lc_lg_l}\le\frac{f^u(a^u+g^u)^2}{4b_lc_lg_l}. \tag{32}$$

□

Proof of Theorem 3. By Theorem 2,

$$\begin{aligned}&\limsup_{t\longrightarrow+\infty}\mathbb{E}[N(t)]\le\frac{a^u}{b_l},\\&\limsup_{t\longrightarrow+\infty}\mathbb{E}[P(t)]\le\frac{f_l(a^u+g^u)^2}{4b_lc_lg_l}.\end{aligned} \tag{33}$$

Now, for any $\epsilon > 0$, let $H_1 > (a^u/b_l\epsilon)$ and $H_2 > ((a^u + g^u)^2 f^u/4b_l c_l g_l \epsilon)$. Then, the following are obtained through the Chebyshev inequality

$$\mathbb{P}\{N(t) > H_1\} \le \frac{\mathbb{E}[N(t)]}{H_1} < \epsilon,$$
$$\mathbb{P}\{P(t) > H_2\} \le \frac{\mathbb{E}[P(t)]}{H_2} < \epsilon. \tag{34}$$

Taking $H = 2\max\{H_1, H_2\}$, it yields

$$\mathbb{P}\{|Y(t)| > H\} \le \mathbb{P}\{N(t) + P(t) > H\} \le \frac{\mathbb{E}[N(t) + P(t)]}{H} < \epsilon. \tag{35}$$

Then,

$$\limsup_{t\longrightarrow+\infty} \mathbb{P}\{|Y(t)| > H\} < \epsilon. \tag{36}$$

□

Proof of Lemma 3. Combing (21) with Lemma 2, we have

$$\begin{aligned} E\left[\frac{1}{N_1(t)}\right] &= N(0)^{-1}\exp\left\{-\int_0^t\left[a(s) - c(s) - \frac{\sigma_1^2(s)}{2}\right]\mathrm{d}s\right\}\mathbb{E}\left[\exp\left\{-\int_0^t \sigma_1(s)\mathrm{d}w_1(s)\right\}\right] \\ &\quad + \int_0^t b(s)\exp\left\{-\int_s^t\left[a(\tau) - c(\tau) - \frac{\sigma_1^2(\tau)}{2}\right]\mathrm{d}\tau\right\}\mathbb{E}\left[\exp\left\{-\int_s^t \sigma_1(\tau)\mathrm{d}w_1(\tau)\right\}\right]\mathrm{d}s \\ &= N(0)^{-1}\exp\left\{-\int_0^t q(s)\mathrm{d}s\right\} + \int_0^t b(s)\exp\left\{-\int_s^t q(\tau)\mathrm{d}\tau\right\}\mathrm{d}s \\ &\le N(0)^{-1}e^{-q_l t} + b^u\int_0^t e^{-q_l(t-s)}\mathrm{d}s \le N(0)^{-1}e^{-q_l t} + \frac{b^u}{q_l}. \end{aligned} \tag{37}$$

From Corollary 1, it has

$$\mathbb{E}\left[\frac{1}{N(t)}\right] \le \mathbb{E}\left[\frac{1}{N(t)}\right] \le N(0)^{-1}e^{-q_l t} + \frac{b^u}{q_l}. \tag{38}$$

Therefore, $\limsup_{t\longrightarrow+\infty}\mathbb{E}[1/N(t)] \le (b^u/q_l)$. □

Proof of Lemma 4. By Theorem 2, there exists $K > 0$ s.t. $\mathbb{E}[N(t)] \le K$. For each $\epsilon > 0$, denote $H = K/\epsilon$; hence, we have

$$\mathbb{P}\{N(t) > H\} \le \frac{\mathbb{E}[N(t)]}{H} \le \epsilon. \tag{39}$$

Then,

$$\mathbb{P}\{N(t) \le H\} \ge 1 - \epsilon. \tag{40}$$

By Lemma 3, we have

$$\limsup_{t\longrightarrow+\infty}\mathbb{E}\left[\frac{1}{N(t)}\right] \le \frac{b^u}{q_l}. \tag{41}$$

Therefore, for any $\epsilon > 0$, let $\delta = \epsilon r_l/b^u$, we have

$$\mathbb{P}\{N(t) < \delta\} = \mathbb{P}\left\{\frac{1}{N(t)} > \frac{1}{\delta}\right\} \le \frac{\mathbb{E}[1/N(t)]}{1/\delta} \le \delta\mathbb{E}[1/N(t)], \tag{42}$$

which yields

$$\limsup_{t\longrightarrow+\infty}\mathbb{P}[N(t) < \delta] \le \delta\mathbb{E}\left[\frac{1}{N(t)}\right] = \frac{\delta b^u}{q_l} = \frac{\epsilon q_l}{b^u}\cdot\frac{b^u}{q_l} = \epsilon. \tag{43}$$

This implies

$$\liminf_{t\longrightarrow+\infty}\mathbb{P}[N(t) \ge \delta] \ge 1 - \epsilon. \tag{44}$$

□

Proof of Theorem 4. According to the arguments in Lemma 4, we know that for any ϵ, existing $\delta > 0, M > 0$ and the following is true:

$$\liminf_{t\longrightarrow+\infty}\mathbb{P}\{N(t) \ge \delta\} \ge 1 - \epsilon. \tag{45}$$

Then, we get

$$\liminf_{t\longrightarrow+\infty}\mathbb{P}\{|Y(t)| \ge \delta\} \ge \liminf_{t\longrightarrow+\infty}\mathbb{P}\{N(t) \ge \delta\} \ge 1 - \epsilon. \tag{46}$$

Similarly, we have

$$\liminf_{t\longrightarrow+\infty}\mathbb{P}\{|Y(t)| \le M\} \ge 1 - \epsilon. \tag{47}$$

From Definition 1, we know the solution of system (4) is stochastically permanent. □

Proof of Lemma 5. By Corollary 1, it is easy to have

$$P_1(t) < P(t),$$

$$P_1(t) = \frac{\exp\left\{\int_0^t \left[(f(s)/A(s)) - g(s) - \left(\sigma_2^2(s)/2\right)\right]\mathrm{d}s - \int_0^t \sigma_2(s)\mathrm{d}w_2(s)\right\}}{P(0)^{-1} + \int_0^t \left[h(s) + \left(f(s)/A^2(s)\phi(s)\right)\right]\exp\left\{\int_0^s \left[(f(r)/A(r)) - g(r) - \left(\sigma_2^2(s)/2\right)\right]\mathrm{d}r - \int_0^s \sigma_2(r)\mathrm{d}w_2(r)\right\}\mathrm{d}s}. \tag{48}$$

So,

$$\begin{aligned} P_1^{-1}(t) = {} & P(0)^{-1}\exp\left\{\int_0^t \left[-\frac{f(s)}{A(s)} + g(s) + \left(\sigma_2^2\frac{(s)}{2}\right)\right]\mathrm{d}s + \int_0^t \sigma_2(s)\mathrm{d}w_2(s)\right\} \\ & + \int_0^t \left(h(s) + \frac{f(s)}{A^2(s)\phi(s)}\right)\exp\left\{\int_s^t \left[g(\tau) - \frac{f(\tau)}{A(\tau)} + \frac{1}{2}\sigma_2^2(\tau)\right]\mathrm{d}\tau + \int_s^t \sigma_2(\tau)\mathrm{d}w_2(\tau)\right\}\mathrm{d}s. \end{aligned} \tag{49}$$

By Lemma 2 and Hölder inequality, one has

$$\begin{aligned} \mathbb{E}\left[P_1^{-1}(t)\right] \le {} & P(0)^{-1}\exp\left\{\int_0^t \left[g(s) - \frac{f(s)}{A(s)} + \sigma_2^2(s)\right]\mathrm{d}s\right\} \\ & + \int_0^t \left[h(s) + \frac{f(s)}{A^2(s)\phi(s)}\right]\exp\left\{\int_s^t [d(\tau) \right. \\ & \left. - f(\tau) + \frac{3}{2}\sigma_2^2(\tau)\right]\mathrm{d}\tau\Bigg\}\left\{\mathbb{E}\left[\phi^{-2}(s)\right]\right\}^{1/2}\mathrm{d}s. \end{aligned} \tag{50}$$

Combiing inequality $(a+b)^2 \le 2(a^2+b^2)$ with (21), one can get

$$\begin{aligned} \mathbb{E}\left[N_1^{-2}(t)\right] \le {} & 2x_0^{-2}\mathbb{E}\left\{\exp\left\{-2\int_0^t \nu(s)\mathrm{d}s - 2\int_0^t \sigma_1(s)\mathrm{d}w_1(s)\right\}\right\} \\ & + 2\mathbb{E}\left\{\int_0^t b(s)\exp\left\{-\int_s^t \nu(\tau)\mathrm{d}\tau - \int_s^t \sigma_1(\tau)\mathrm{d}w_1(\tau)\right\}\mathrm{d}s\right\}^2. \end{aligned} \tag{51}$$

Meanwhile,

$$\begin{aligned} & \mathbb{E}\left\{\int_0^t b(s)\exp\left\{-\int_s^t \nu(\tau)\mathrm{d}\tau - \int_s^t \sigma_1(\tau)\mathrm{d}w_1(\tau)\right\}\mathrm{d}s\right\}^2 \\ & = \int_0^t\int_0^t b(s)b(u)\exp\left\{-\int_s^t \nu(\tau)\mathrm{d}\tau\right\}\exp\left\{-\int_s^t \nu(\tau)\mathrm{d}\tau\right\} \\ & \quad \cdot \mathbb{E}\left[\exp\left\{-\int_s^t \sigma_1(\tau)\mathrm{d}w_1(\tau)\right\}\exp\left\{-\int_u^t \sigma_1(\tau)\mathrm{d}w_1(\tau)\right\}\right]\mathrm{d}u\,\mathrm{d}s. \end{aligned} \tag{52}$$

Furthermore,

$$\begin{aligned} & \mathbb{E}\left[\exp\left\{-\int_s^t \sigma_1(\tau)\mathrm{d}w_1(\tau)\right\}\exp\left\{-\int_u^t \sigma_1(\tau)\mathrm{d}w_1(\tau)\right\}\right] \\ & \le \exp\left\{\int_s^t \sigma_1^2(\tau)\mathrm{d}\tau\right\}\exp\left\{\int_u^t \sigma_1^2(\tau)\mathrm{d}\tau\right\}. \end{aligned} \tag{53}$$

Substituting (53) into (52), we have

$$\begin{aligned} & \mathbb{E}\left\{\int_0^t b(s)\exp\left\{-\int_s^t \nu(\tau)\mathrm{d}\tau - \int_s^t \sigma_1(\tau)\mathrm{d}w_1(\tau)\right\}\mathrm{d}s\right\}^2 \\ & = \left\{\int_0^t b(s)\exp\left\{-\int_s^t \left[a(\tau) - \frac{c(\tau)}{m(\tau)} - \frac{3}{2}\sigma_1^2(\tau)\right]\mathrm{d}\tau\right\}\mathrm{d}s\right\}^2. \end{aligned} \tag{54}$$

Therefore, by (51) and (54), one can get

$$\begin{aligned} \mathbb{E}\left[N_1^{-2}(t)\right] & \le \frac{2}{N(0)}\exp\{-2\rho_l t\} + 2\left(\frac{b^u}{\rho_l}\right)^2 \\ & \le \frac{2}{N(0)} + 2\left(\frac{b^u}{\rho_l}\right)^2. \end{aligned} \tag{55}$$

Finally, we obtain the required assertion through substituting (55) into (51).

In summary, Theorem 5 has been obtained. □

Remark 1. It is clear that stochastic differential equation which is stochastically permanent implies that its solutions are stochastically ultimately bounded. Lemma 4 shows that the prey species will be permanent if $b_l > 0$ and $q_l > 0$, or it will be extinct. Theorem 4 shows that if $b_l > 0, c_l > 0, g_l > 0$ and $q_l > 0$, system (4) is permanent in probability 1, i.e., the number (or density) is bounded a.s.

Data Availability

The data used to support this study are provided in our paper.

Conflicts of Interest

The authors declare that they have no conflicts of interest.

Acknowledgments

This work was supported by the Natural Science Foundation of China (no. 11771001), Provincial Natural Science Research Project of Anhui Colleges (nos. KJ2019A0672 and

KJ2019A0666), Program for Excellent Young Talents in University of Anhui Province (no. gxyq2017092), and Key Teaching Research Project of Suzhou University (no. szxy2018jyxm12).

References

[1] M. Haque, "Ratio-dependent predator-prey models of interacting populations," *Bulletin of Mathematical Biology*, vol. 71, no. 2, pp. 430–452, 2009.

[2] A. D. Bazykin, A. I. Khibnik, and B. Krauskopf, *Nonlinear Dynamics of Interacting Populations*, World Scientific, Singapore, 1998.

[3] Y. Kuang and E. Beretta, "Global qualitative analysis of a ratio-dependent predator-prey system," *Journal of Mathematical Biology*, vol. 36, no. 4, pp. 389–406, 1998.

[4] H. R. Akcakaya, R. Arditi, and L. R. Ginzburg, "Ratio-dependent predation: an abstraction that works," *Ecology*, vol. 76, no. 3, pp. 995–1004, 1995.

[5] H.-B. Shi, S. Ruan, Y. Su, and J.-F. Zhang, "Spatiotemporal dynamics of a diffusive Leslie-Gower predator-prey model with ratio-dependent functional response," *International Journal of Bifurcation and Chaos*, vol. 25, no. 5, Article ID 1530014, 2015.

[6] J. Zhou, "Bifurcation analysis of a diffusive predator-prey model with ratio-dependent Holling type III functional response," *Nonlinear Dynamics*, vol. 81, no. 3, pp. 1535–1552, 2015.

[7] C. M. Heggerud and K. Lan, "Local stability analysis of ratio-dependent predator-prey models with predator harvesting rates," *Applied Mathematics and Computation*, vol. 270, pp. 349–357, 2015.

[8] M. Sen, M. Banerjee, and A. Morozov, "Bifurcation analysis of a ratio-dependent prey-predator model with the Allee effect," *Ecological Complexity*, vol. 11, pp. 12–27, 2012.

[9] M. Banerjee and S. Abbas, "Existence and non-existence of spatial patterns in a ratio-dependent predator-prey model," *Ecological Complexity*, vol. 21, pp. 199–214, 2015.

[10] C. Çelik, "Stability and Hopf bifurcation in a delayed ratio dependent Holling-Tanner type model," *Applied Mathematics and Computation*, vol. 255, pp. 228–237, 2015.

[11] D. Xiao and L. S. Jennings, "Bifurcations of a ratio-dependent predator-prey system with constant rate harvesting," *SIAM Journal on Applied Mathematics*, vol. 65, no. 3, pp. 737–753, 2005.

[12] C. Ji, D. Jiang, and X. Li, "Qualitative analysis of a stochastic ratio-dependent predator-prey system," *Journal of Computational and Applied Mathematics*, vol. 235, no. 5, pp. 1326–1341, 2011.

[13] J. Lv, K. Wang, and D. Chen, "Analysis on a stochastic two-species ratio-dependent predator-prey model," *Methodology and Computing in Applied Probability*, vol. 17, no. 2, pp. 403–418, 2015.

[14] X. Mao, *Stochastic Differential Equations and Their Applications*, Horwood Publishing, Chichester, UK, 2007.

[15] Z. Wu, H. Huang, and L. Wang, "Dynamical behavior of a stochastic ratio-dependent predator-prey system," *Journal of Applied Mathematics*, vol. 2012, Article ID 857134, 17 pages, 2012.

[16] D. Jiang and N. Shi, "A note on nonautonomous logistic equation with random perturbation," *Journal of Mathematical Analysis and Applications*, vol. 303, no. 1, pp. 164–172, 2005.

[17] Z. Wei, Z. Wu, L. Hu, and L. Wang, "Stochastic modified Bazykin predator-prey model with Markovian switching," *International Journal of Nonlinear Sciences and Numerical Simulation*, vol. 19, no. 6, pp. 573–581, 2018.

[18] Z. Wei, Z. Wu, L. Hu, and L. Wang, "Persistence and extinction of a stochastic modified Bazykin predator-prey system with Lévy jumps," *Discrete Dynamics in Nature and Society*, vol. 2018, Article ID 8479101, 7 pages, 2018.

Hindawi
Journal of Chemistry
Volume 2019, Article ID 1042308, 12 pages
https://doi.org/10.1155/2019/1042308

Research Article

Irregularity of Block Shift Networks and Hierarchical Hypercube Networks

Juanyan Fang,[1] Iftikhar Ahmed,[2,3] Abid Mehboob,[4] Kashif Nazar,[2] and Haseeb Ahmad[2,5]

[1]*Institute of Information Technology & Engineering Management, Tongling College, Tongling 244000, China*
[2]*Department of Mathematics, COMSATS University Islamabad, Lahore 54000, Pakistan*
[3]*Department of Mathematics, Riphah International University, Lahore 54000, Pakistan*
[4]*Department of Mathematics, Division of Science and Technology, University of Education, Lahore, Pakistan*
[5]*Department of Mathematics, Lahore Leads University, Lahore, Pakistan*

Correspondence should be addressed to Iftikhar Ahmed; iffi6301@gmail.com

Received 20 October 2019; Accepted 21 November 2019; Published 18 December 2019

Guest Editor: Jia-Bao Liu

There is extremely a great deal of mathematics associated with electrical and electronic engineering. It relies upon what zone of electrical and electronic engineering; for instance, there is much increasingly theoretical mathematics in communication theory, signal processing and networking, and so forth. Systems include hubs speaking with one another. A great deal of PCs connected together structure a system. Mobile phone clients structure a network. Networking includes the investigation of the most ideal method for executing a system. Graph theory has discovered a significant use in this zone of research. In this paper, we stretch out this examination to interconnection systems. Hierarchical interconnection systems (HINs) give a system to planning systems with diminished connection cost by exploiting the area of correspondence that exists in parallel applications. HINs utilize numerous levels. Lower-level systems give nearby correspondence, while more significant level systems encourage remote correspondence. HINs provide issue resilience within the sight of some defective nodes and additionally interfaces. Existing HINs can be comprehensively characterized into two classes: those that use nodes or potential interface replication and those that utilize reserve interface nodes.

1. Introduction

Graph theory has many applications in chemistry, physics, computer sciences, and other applied sciences [1–9]. Multiprocessor interconnection networks (MINs) are required to connect processor-memory pairs, each of which is known as the processing node. Design and usage of MINs have gained remarkable attention because of the availability of powerful microprocessors and memory chips and also due to its low cost [10, 11]. Hierarchical interconnection network (HIN) [12] is a framework for designing new networks that decrease link cost and has applications in parallel communications. The multistage networks have applications as communication networks for parallel computing [12–14]. For details about graph theory, we recommend the references [15–19].

Throughout this article, all graphs are finite, undirected, and simple. Let $G = (V(G), E(G))$ be such a graph with vertex set $V(G)$ and edge set $E(G)$. The order of G is the cardinality of its vertex set, and size is the cardinality of its edge set. In a network, the vertices of G correspond to node, and an edge between two vertices is the link between these vertices. The degree of a vertex u of a graph G is symbolized by d_u and is defined as the number of edges incident with u. A graph is said to be regular, if all its vertices have the same degree; otherwise, it is irregular.

For the first time in history, Chartrand et al. [20] underlined the study of irregular graphs. From that point forward, the irregularity degree and irregular graphs have turned into the essential open issue of graph theory. A graph is said to be a perfect graph if all the vertices have different

degrees (i.e., no two vertices have the same degree). The fact no graph is perfect is proved in [21]. The graphs lying in the middle are called semiperfect (quasiperfect) graphs, in which each, aside from the two vertices, has various degrees [22]. The irregularity indices give the best knowledge about the irregularity of graph and have been studied extensively in the literature [23, 24]. The primary irregularity index was presented in [25]. The Albertson index, $\mathrm{AL}(G)$, was introduced by Albertson in [26] as follows:

$$\mathrm{AL}(G) = \sum_{uv\in E(G)} \left|d_u - d_v\right|. \tag{1}$$

The irregularity indexes IRL (G) and IRLU (G) are defined by Vukičević and Graovac [27] as follows:

$$\begin{aligned} \mathrm{IRL}(G) &= \sum_{uv\in E(G)} \left|\ln(d_u) - \ln(d_v)\right|, \\ \mathrm{IRLU}(G) &= \sum_{uv\in E(G)} \frac{\left|(d_u) - (d_v)\right|}{\min(d_u, d_v)}. \end{aligned} \tag{2}$$

Recently, Abdo and Dimitrov [28] established the new idea of "total irregularity measure of a graph G," which was lately discussed in [29, 30]. The Randić index itself is directly associated with an irregularity determination [31] as follows:

$$\mathrm{IRA}(G) = \sum_{uv\in E(G)} \left(d_u^{-1/2} - d_v^{-1/2}\right)^2. \tag{3}$$

Further irregularity indices of comparative nature can be followed in [30] in detail, and for the applications of indices in chemistry, we refer [31–42]. In [43], irregularity indices of nanotubes were determined. Gao et al. [44] computed irregularity measures of some dendrimers, and the same was computed for different molecular structures in [45]. In [46], irregularity measures for some classes of benzenoid systems were computed.

Irregularity indices investigated in this paper are given in Table 1. For the undefined notion in Table 1, we refer [47–52]. All of them belong to the family of degree-based irregularity indices.

2. Methodology

Let $G = (V(G), E(G))$ be such a graph with vertex set $V(G)$ and edge set $E(G)$. We use edge partition to find irregularity indices, and edge partition depends on the degree of end vertices of edges. Edges are partitioned by the same and different degrees of vertices hold edges.

2.1. Results for Block Shift Network (BSN). The block shift network can be denoted by BSN and was firstly introduced in 1991 by Pan and Chuang [53]. These are interconnection networks, and due to its hypercube topology, it has many benefits. The idea to design this network is to have a linkage in certain dimensions in order to make it a comparable performance and reduce number of links. The topology of BSN fulfils the requirements of the communication algorithms. BSN surpasses the hypercube in several respects while retaining most of its advantages, especially when the traffic has the locality property [54]. Many existing networks can be considered as special cases of BSN. For example, $\mathrm{BSN}-1$ is the shuffle-exchange network with n-dimensional hypercube, while $\mathrm{BSN}-2$ is the complete network, as shown in Figures 1 and 2, respectively. Let G be a block shift network. It can be seen from Figure 1 that the number of vertices and edges in $\mathrm{BSN}-1$ are $16a^2$ and $24a^2-2$, respectively. From Figure 2, one can observe that the number of vertices and edges in $\mathrm{BSN}-2$ are $16a^2$ and $32a^2-2$, respectively.

Theorem 1. *For the block shift network BSN − 1, we have*

(1) $VAR(BSN-1) = (4a^2 - 1/16a^4)$

(2) $AL(BSN-1) = 8$

(3) $IR1(BSN-1) = (5(4a^2-1)/a^2)$

(4) $IR2(BSN-1) = \sqrt{6}\sqrt{(216a^2 - 42/6(24a^2-2))} - (48a^2 - 4/16a^2)$

(5) $IRF(BSN-1) = 8$

(6) $IRFW(BSN-1) = (4/108a^2 - 21)$

(7) $IRA(BSN-1) = (1213215869760357/9007199254740992)$

(8) $IRB(BSN-1) = (909911902320267/1125899906842624)$

(9) $IRC(BSN-1) = -(36a^2 - 16\sqrt{6}\,a^2 + 1/4a^2(12a^2-1))$

(10) $IRDIF(BSN-1) = (20/3)$

(11) $IRL(BSN-1) = (3652105019575333/1125899906842624)$

(12) $IRLU(BSN-1) = 4$

(13) $IRLF(BSN-1) = (4\sqrt{6}/3)$

(14) $IRLA(BSN-1) = (16/5)$

(15) $IRD1(BSN-1) = (6243314768165359/1125899906842624)$

(16) $IRGA(BSN-1) = (2941534708959071/18014398509481984)$

Proof. The order of graph is $n = |V(\mathrm{BSN}-1)| = 16a^2$, and its size is $m = |E(\mathrm{BSN}-1)| = 24a^2 - 2$. The vertex set of $\mathrm{BSN}-1$ can be divided into the following classes by means of degrees:

$$\begin{aligned} V_1(\mathrm{BSN}-1) &= \{v \in V(\mathrm{BSN}-1) : d_u = 2\}, \\ V_2(\mathrm{BSN}-1) &= \{v \in V(\mathrm{BSN}-1) : d_u = 3\}. \end{aligned} \tag{4}$$

The edge set of $\mathrm{BSN}-1$ can be divided into the following classes with respect to the degrees of end vertices:

$$\begin{aligned} E_1(\mathrm{BSN}-1) &= \{uv \in E(\mathrm{BSN}-1) : d_u = d_v = 3\}, \\ E_2(\mathrm{BSN}-1) &= \{uv \in E(\mathrm{BSN}-1) : d_u = 2, d_v = 3\}. \end{aligned} \tag{5}$$

And the cardinality of edges is as follows:

Table 1: Irregularity indices.

$\mathrm{VAR}(G) = (M_1(G)/n) - ((2m/n)^2)$	$\mathrm{IRC}(G) = (\mathrm{RR}(G)/m) - (2m/n)$
$\mathrm{AL}(G) = \sum_{uv\in E(G)} \lvert d_u - d_v \rvert$	$\mathrm{IRDIF}(G) = \sum_{uv\in E(G)} \lvert (d_u/d_v) - (d_v/d_u) \rvert$
$\mathrm{IR1}(G) = F(G) - (2m/n)M_1(G)$	$\mathrm{IRL}(G) = \sum_{uv\in E(G)} \lvert \ln(d_u) - \ln(d_v) \rvert$
$\mathrm{IR2}(G) = \sqrt{(M_2(G)/m)} - (2m/n)$	$\mathrm{IRLU}(G) = \sum_{uv\in E(G)} (\lvert (d_u) - (d_v) \rvert / \min(d_u, d_v))$
$\mathrm{IRF}(G) = F(G) - 2M_2(G)$	$\mathrm{IRLF}(G) = \sum_{uv\in E(G)} (\lvert d_u - d_v \rvert / \sqrt{(d_u \times d_v)})$
$\mathrm{IRFW}(G) = (\mathrm{IRF}(G)/M_2(G))$	$\mathrm{IRLA}(G) = \sum_{uv\in E(G)} 2(\lvert d_u - d_v \rvert / d_u + d_v)$
$\mathrm{IRA}(G) = \sum_{uv\in E(G)} (d_u^{-1/2} - d_v^{-1/2})^2$	$\mathrm{IRD1}(G) = \sum_{uv\in E(G)} \ln[1 + \lvert d_u - d_v \rvert]$
$\mathrm{IRB}(G) = \sum_{uv\in E(G)} (d_u^{1/2} - d_v^{1/2})^2$	$\mathrm{IRGA}(G) = \sum_{uv\in E(G)} \ln(d_u + d_v / 2\sqrt{(d_u \times d_v)})$

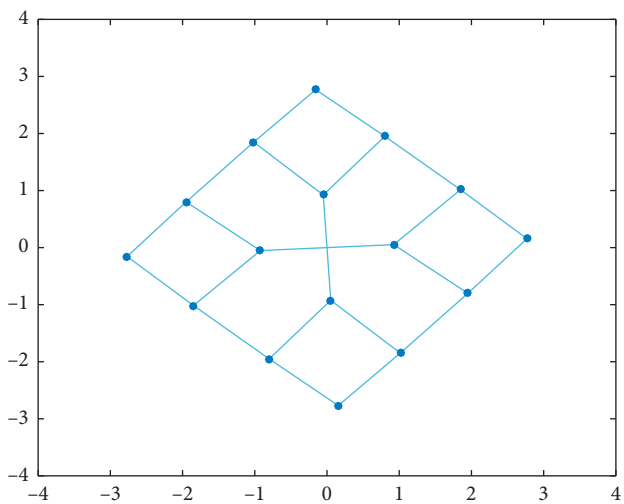

Figure 1: $(\mathrm{BSN}-1)_{(3\times3)}$.

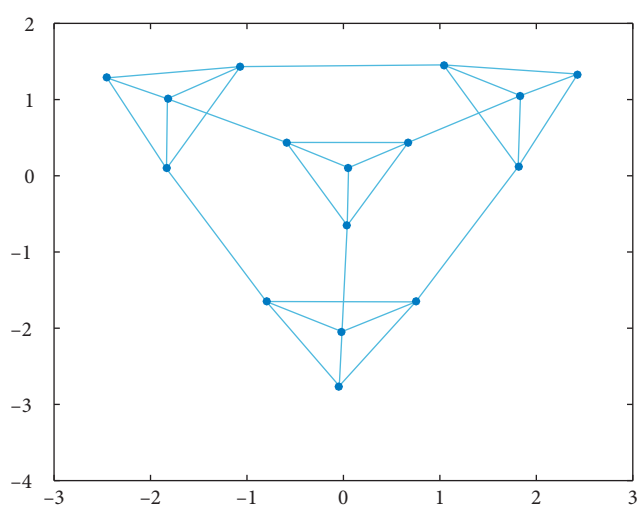

Figure 2: $(\mathrm{BSN}-2)_{(1\times1)}$.

$$\begin{aligned} \lvert E_1(\mathrm{BSN}-1) \rvert &= 24a^2 - 10, \\ \lvert E_2(\mathrm{BSN}-1) \rvert &= 8. \end{aligned} \tag{6}$$

First, we find some topological indices, which will be used in irregularity indices:

$$\begin{aligned} M_1(\mathrm{BSN}-1) &= 144a^2 - 20, \\ M_2(\mathrm{BSN}-1) &= 216a^2 - 42, \\ F(\mathrm{BSN}-1) &= 432a^2 - 76, \\ \mathrm{RR}(\mathrm{BSN}-1) &= 72a^2 + 8\sqrt{6} - 30. \end{aligned} \tag{7}$$

Now, by definitions given in Table 1, we have

$$\begin{aligned} \mathrm{VAR}(\mathrm{BSN}-1) &= \frac{M_1(\mathrm{BSN}-1)}{n} - \left(\frac{2m}{n}\right)^2 \\ &= \frac{144a^2 - 20}{16a^2} - \left(\frac{224a^2 - 2}{16a^2}\right)^2 \\ &= \frac{4a^2 - 1}{16a^4}. \end{aligned} \tag{8}$$

$$\begin{aligned} \mathrm{AL}(\mathrm{BSN}-1) &= \sum_{uv\in E(\mathrm{BSN}-1)} \lvert d_u - d_v \rvert \\ &= \sum_{uv\in E_1(\mathrm{BSN}-1)} (0) + \sum_{uv\in E_2(\mathrm{BSN}-1)} \lvert (2) - (3) \rvert \\ &= 8. \end{aligned} \tag{9}$$

$$\begin{aligned} \mathrm{IR1}(\mathrm{BSN}-1) &= F(\mathrm{BSN}-1) - \frac{2m}{n} M_1(\mathrm{BSN}-1) \\ &= 432a^2 - 76 - \frac{2(24a^2 - 2)}{16a^2} 144a^2 - 20 \\ &= \frac{5(4a^2 - 1)}{a^2}. \end{aligned} \tag{10}$$

$$\begin{aligned} \mathrm{IR2}(\mathrm{BSN}-1) &= \sqrt{\frac{M_2(\mathrm{BSN}-1)}{m}} - \frac{2m}{n} \\ &= \sqrt{\frac{216a^2 - 42}{24a^2 - 2}} - \frac{2(24a^2 - 2)}{16a^2} \\ &= \sqrt{6}\sqrt{\frac{216a^2 - 42}{6(24a^2 - 2)}} - \frac{48a^2 - 4}{16a^2}. \end{aligned} \tag{11}$$

$$\begin{aligned}\mathrm{IRF}(\mathrm{BSN}-1) &= F(\mathrm{BSN}-1) - 2M_2(\mathrm{BSN}-1)\\ &= 432a^2 - 76 - 2\left(216a^2 - 42\right)\\ &= 8.\end{aligned} \tag{12}$$

$$\begin{aligned}\mathrm{IRFW}(\mathrm{BSN}-1) &= \frac{\mathrm{IRF}(\mathrm{BSN}-1)}{M_2(\mathrm{BSN}-1)}\\ &= \frac{8}{216a^2 - 42}\\ &= 8.\end{aligned} \tag{13}$$

$$\begin{aligned}\mathrm{IRA}(\mathrm{BSN}-1) &= \sum_{uv\in E(\mathrm{BSN}-1)} \left(d_u^{-1/2} - d_v^{-1/2}\right)^2\\ &= \sum_{uv\in E_1(\mathrm{BSN}-1)} (0)\\ &\quad + \sum_{uv\in E_2(\mathrm{BSN}-1)} \left((2)^{-1/2} - (3)^{-1/2}\right)^2\\ &= \frac{1213215869760357}{9007199254740992}.\end{aligned} \tag{14}$$

$$\begin{aligned}\mathrm{IRB}(\mathrm{BSN}-1) &= \sum_{uv\in E(\mathrm{BSN}-1)} \left(d_u^{1/2} - d_v^{1/2}\right)^2\\ &= \sum_{uv\in E_1(\mathrm{BSN}-1)} (0)\\ &\quad + \sum_{uv\in E_2(\mathrm{BSN}-1)} \left((2)^{1/2} - (3)^{1/2}\right)^2\\ &= \frac{909911902320267}{1125899906842624}.\end{aligned} \tag{15}$$

$$\begin{aligned}\mathrm{IRC}(\mathrm{BSN}-1) &= \frac{\mathrm{RR}(\mathrm{BSN}-1)}{m} - \frac{2m}{n}\\ &= \frac{72a^2 + 8\sqrt{6} - 30}{24a^2 - 2} - \frac{2\left(24a^2 - 2\right)}{16a^2}\\ &= -\frac{36a^2 - 16\sqrt{6}a^2 + 1}{4a^2\left(12a^2 - 1\right)}.\end{aligned} \tag{16}$$

$$\begin{aligned}\mathrm{IRDIF}(\mathrm{BSN}-1) &= \sum_{uv\in E(\mathrm{BSN}-1)} \left|\frac{d_u}{d_v} - \frac{d_v}{d_u}\right|\\ &= \sum_{uv\in E_1(\mathrm{BSN}-1)} (0) + \sum_{uv\in E_2(\mathrm{BSN}-1)} \left|\frac{2}{3} - \frac{3}{2}\right|\\ &= \frac{20}{3}.\end{aligned} \tag{17}$$

$$\begin{aligned}\mathrm{IRL}(\mathrm{BSN}-1) &= \sum_{uv\in E(\mathrm{BSN}-1)} \left|\ln(d_u) - \ln(d_v)\right|\\ &= \sum_{uv\in E_1(\mathrm{BSN}-1)} (0)\\ &\quad + \sum_{uv\in E_2(\mathrm{BSN}-1)} \left|\ln(2) - \ln(3)\right|\\ &= \frac{3652105019575333}{1125899906842624}.\end{aligned} \tag{18}$$

$$\begin{aligned}\mathrm{IRLU}(\mathrm{BSN}-1) &= \sum_{uv\in E(\mathrm{BSN}-1)} \frac{\left|(d_u) - (d_v)\right|}{\min(d_u, d_v)}\\ &= \sum_{uv\in E_1(\mathrm{BSN}-1)} (0) + \sum_{uv\in E_2(\mathrm{BSN}-1)} \frac{|(2) - (3)|}{\min(2, 3)}\\ &= 4.\end{aligned} \tag{19}$$

$$\begin{aligned}\mathrm{IRLF}(\mathrm{BSN}-1) &= \sum_{uv\in E(\mathrm{BSN}-1)} \frac{\left|d_u - d_v\right|}{\sqrt{(d_u \times d_v)}}\\ &= \sum_{uv\in E_1(\mathrm{BSN}-1)} (0) + \sum_{uv\in E_2(\mathrm{BSN}-1)} \frac{|2-3|}{\sqrt{(2\times 3)}}\\ &= \frac{4\sqrt{6}}{3}.\end{aligned} \tag{20}$$

$$\begin{aligned}\mathrm{IRLA}(\mathrm{BSN}-1) &= \sum_{uv\in E(\mathrm{BSN}-1)} 2\frac{\left|d_u - d_v\right|}{d_u + d_v}\\ &= \sum_{uv\in E_1(\mathrm{BSN}-1)} (0) + \sum_{uv\in E_2(\mathrm{BSN}-1)} 2\frac{|2-3|}{2+3}\\ &= \frac{16}{5}.\end{aligned} \tag{21}$$

$$\begin{aligned}\mathrm{IRD1}(\mathrm{BSN}-1) &= \sum_{uv\in E(\mathrm{BSN}-1)} \ln\left[1 + \left|d_u - d_v\right|\right]\\ &= \sum_{uv\in E_1(\mathrm{BSN}-1)} (0)\\ &\quad + \sum_{uv\in E_2(\mathrm{BSN}-1)} \ln[1 + |(2) - (3)|]\\ &= \frac{6243314768165359}{1125899906842624}.\end{aligned} \tag{22}$$

$$\begin{aligned}\mathrm{IRGA}(\mathrm{BSN}-1) &= \sum_{uv\in E(\mathrm{BSN}-1)} \ln\left(\frac{d_u + d_v}{2\sqrt{(d_u \times d_v)}}\right)\\ &= \sum_{uv\in E_1(\mathrm{BSN}-1)} (0)\\ &\quad + \sum_{uv\in E_2(\mathrm{BSN}-1)} \ln\left(\frac{2+3}{2\sqrt{(2\times 3)}}\right)\\ &= \frac{2941534708959071}{18014398509481984}.\end{aligned} \tag{23}$$

□

Theorem 2. *For the block shift network BSN − 2, we have*

(1) $VAR(BSN-2) = (4a^2 - 1/16a^4)$

(2) $AL(BSN-2) = 12$

(3) $IR1(BSN-2) = (7(4a^2 - 1)/a^2)$

(4) $IR2(BSN-2) = 4\sqrt{(512a^2 - 80/16(32a^2-2))} - (64a^2 - 4/16a^2)$

(5) $IRF(BSN-2) = 12$

(6) $IRFW(BSN-2) = (3/128a^2 - 20)$

(7) $IRA(BSN-2) = (20694009944167803/288230376151711744)$

(8) $IRB(BSN-2) = (15520507458125877/18014398509481984)$

(9) $IRC(BSN-2) = -((80a^2 - 48\sqrt{3}\,a^2 + 1)/(4a^2(16a^2-1)))$

(10) $IRDIF(BSN-2) = 7$

(11) $IRL(BSN-2) = (3886814622885039/1125899906842624)$

(12) $IRLU(BSN-2) = 4$

(13) $IRLF(BSN-2) = 2\sqrt{3}$

(14) $IRLA(BSN-2) = (24/7)$

(15) $IRD1(BSN-2) = (18729944304496077/2251799813685248)$

(16) $IRGA(BSN-2) = (2228664339909267/18014398509481984)$

Proof. The order of graph is $n = |V(\mathrm{BSN}-2)| = 16a^2$, and its size is $m = |E(\mathrm{BSN}-2)| = 32a^2 - 2$. The vertex set of BSN − 2 can be divided into the following classes by means of degrees:

$$\begin{aligned} V_1(\mathrm{BSN}-2) &= \{v \in V(\mathrm{BSN}-2) : d_u = 3\}, \\ V_2(\mathrm{BSN}-2) &= \{v \in V(\mathrm{BSN}-2) : d_u = 4\}. \end{aligned} \tag{24}$$

The edge set of BSN − 2 can be divided into the following classes with respect to the degrees of end vertices:

$$\begin{aligned} E_1(\mathrm{BSN}-2) &= \{uv \in E(\mathrm{BSN}-2) : d_u = d_v = 4\}, \\ E_2(\mathrm{BSN}-2) &= \{uv \in E(\mathrm{BSN}-2) : d_u = 3, d_v = 4\}. \end{aligned} \tag{25}$$

And the cardinality of edges is as follows:

$$\begin{aligned} |E_1(\mathrm{BSN}-2)| &= 32a^2 - 14, \\ |E_2(\mathrm{BSN}-2)| &= 12. \end{aligned} \tag{26}$$

First, we find some topological indices, which will be used in irregularity indices:

$$\begin{aligned} M_1(\mathrm{BSN}-2) &= 256a^2 - 28, \\ M2(\mathrm{BSN}-2) &= 512a^2 - 80, \\ F(\mathrm{BSN}-2) &= 1024a^2 - 148, \\ \mathrm{RR}(\mathrm{BSN}-2) &= 128a^2 + 24\sqrt{3} - 56. \end{aligned} \tag{27}$$

Now, from the definitions given in Table 1, we have

$$\begin{aligned} \mathrm{VAR}(\mathrm{BSN}-2) &= \frac{M_1(\mathrm{BSN}-2)}{n} - \left(\frac{2m}{n}\right)^2 \\ &= \frac{256a^2 - 28}{16a^2} - \left(\frac{232a^2 - 2}{16a^2}\right)^2 \\ &= \frac{4a^2 - 1}{16a^4}. \end{aligned} \tag{28}$$

$$\begin{aligned} \mathrm{AL}(\mathrm{BSN}-2) &= \sum_{uv \in E(\mathrm{BSN}-2)} |d_u - d_v| \\ &= \sum_{uv \in E_1(\mathrm{BSN}-2)} (0) + \sum_{uv \in E_2(\mathrm{BSN}-2)} |(3) - (4)| \\ &= 12. \end{aligned} \tag{29}$$

$$\begin{aligned} \mathrm{IR1}(\mathrm{BSN}-2) &= F(\mathrm{BSN}-2) - \frac{2m}{n} M_1(\mathrm{BSN}-2) \\ &= 1024a^2 - 148 - \frac{2(32a^2-2)}{16a^2} 256a^2 - 28 \\ &= \frac{7(4a^2-1)}{a^2}. \end{aligned} \tag{30}$$

$$\begin{aligned} \mathrm{IR2}(\mathrm{BSN}-2) &= \sqrt{\frac{M_2(\mathrm{BSN}-2)}{m}} - \frac{2m}{n} \\ &= \sqrt{\frac{512a^2 - 80}{32a^2 - 2}} - \frac{2(32a^2-2)}{16a^2} \\ &= 4\sqrt{\frac{512a^2 - 80}{16(32a^2-2)}} - \frac{64a^2 - 4}{16a^2}. \end{aligned} \tag{31}$$

$$\begin{aligned} \mathrm{IRF}(\mathrm{BSN}-2) &= F(\mathrm{BSN}-2) - 2M_2(\mathrm{BSN}-2) \\ &= 1024a^2 - 148 - 2(512a^2 - 80) \\ &= 12. \end{aligned} \tag{32}$$

$$\begin{aligned} \mathrm{IRFW}(\mathrm{BSN}-2) &= \frac{\mathrm{IRF}(\mathrm{BSN}-2)}{M_2(\mathrm{BSN}-2)} \\ &= \frac{12}{512a^2 - 80} \\ &= 12. \end{aligned} \tag{33}$$

$$\begin{aligned} \mathrm{IRA}(\mathrm{BSN}-2) &= \sum_{uv \in E(\mathrm{BSN}-2)} \left(d_u^{-1/2} - d_v^{-1/2}\right)^2 \\ &= \sum_{uv \in E_1(\mathrm{BSN}-2)} (0) \\ &\quad + \sum_{uv \in E_2(\mathrm{BSN}-2)} \left((3)^{-1/2} - (4)^{-1/2}\right)^2 \\ &= \frac{20694009944167803}{288230376151711744}. \end{aligned} \tag{34}$$

$$\begin{aligned}\mathrm{IRB}(\mathrm{BSN}-2) &= \sum_{uv\in E(\mathrm{BSN}-2)} \left(d_u^{1/2}-d_v^{1/2}\right)^2 \\ &= \sum_{uv\in E_1(\mathrm{BSN}-2)} (0) \\ &\quad + \sum_{uv\in E_2(\mathrm{BSN}-2)} \left((3)^{1/2}-(4)^{1/2}\right)^2 \\ &= \frac{15520507458125877}{18014398509481984}.\end{aligned} \tag{35}$$

$$\begin{aligned}\mathrm{IRC}(\mathrm{BSN}-2) &= \frac{\mathrm{RR}(\mathrm{BSN}-2)}{m}-\frac{2m}{n} \\ &= \frac{128a^2+24\sqrt{3}-56}{32a^2-2}-\frac{2(32a^2-2)}{16a^2} \\ &= -\frac{80a^2-48\sqrt{3}a^2+1}{4a^2(16a^2-1)}.\end{aligned} \tag{36}$$

$$\begin{aligned}\mathrm{IRDIF}(\mathrm{BSN}-2) &= \sum_{uv\in E(\mathrm{BSN}-2)} \left|\frac{d_u}{d_v}-\frac{d_v}{d_u}\right| \\ &= \sum_{uv\in E_1(\mathrm{BSN}-2)} (0) \\ &\quad + \sum_{uv\in E_2(\mathrm{BSN}-2)} \left|\frac{3}{4}-\frac{4}{3}\right| \\ &= 7.\end{aligned} \tag{37}$$

$$\begin{aligned}\mathrm{IRL}(\mathrm{BSN}-2) &= \sum_{uv\in E(\mathrm{BSN}-2)} \left|\ln(d_u)-\ln(d_v)\right| \\ &= \sum_{uv\in E_1(\mathrm{BSN}-2)} (0) \\ &\quad + \sum_{uv\in E_2(\mathrm{BSN}-2)} |\ln(3)-\ln(4)| \\ &= \frac{3886814622885039}{1125899906842624}.\end{aligned} \tag{38}$$

$$\begin{aligned}\mathrm{IRLU}(\mathrm{BSN}-2) &= \sum_{uv\in E(\mathrm{BSN}-2)} \frac{|(d_u)-(d_v)|}{\min(d_u,d_v)} \\ &= \sum_{uv\in E_1(\mathrm{BSN}-2)} (0) + \sum_{uv\in E_2(\mathrm{BSN}-2)} \frac{|(3)-(4)|}{\min(3,4)} \\ &= 4.\end{aligned} \tag{39}$$

$$\begin{aligned}\mathrm{IRLF}(\mathrm{BSN}-2) &= \sum_{uv\in E(\mathrm{BSN}-2)} \frac{|d_u-d_v|}{\sqrt{(d_u\times d_v)}} \\ &= \sum_{uv\in E_1(\mathrm{BSN}-2)} (0) + \sum_{uv\in E_2(\mathrm{BSN}-2)} \frac{|3-4|}{\sqrt{(3\times 4)}} \\ &= 2\sqrt{3}.\end{aligned} \tag{40}$$

$$\begin{aligned}\mathrm{IRLA}(\mathrm{BSN}-2) &= \sum_{uv\in E(\mathrm{BSN}-2)} 2\frac{|d_u-d_v|}{d_u+d_v} \\ &= \sum_{uv\in E_1(\mathrm{BSN}-2)} (0) + \sum_{uv\in E_2(\mathrm{BSN}-2)} 2\frac{|3-4|}{3+4} \\ &= \frac{24}{7}.\end{aligned} \tag{41}$$

$$\begin{aligned}\mathrm{IRD1}(\mathrm{BSN}-2) &= \sum_{uv\in E(\mathrm{BSN}-2)} \ln\left[1+|d_u-d_v|\right] \\ &= \sum_{uv\in E_1(\mathrm{BSN}-2)} (0) \\ &\quad + \sum_{uv\in E_2(\mathrm{BSN}-2)} \ln[1+|(3)-(4)|] \\ &= \frac{18729944304496077}{2251799813685248}.\end{aligned} \tag{42}$$

$$\begin{aligned}\mathrm{IRGA}(\mathrm{BSN}-2) &= \sum_{uv\in E(\mathrm{BSN}-2)} \ln\left(\frac{d_u+d_v}{2\sqrt{(d_u\times d_v)}}\right) \\ &= \sum_{uv\in E_1(\mathrm{BSN}-2)} (0) \\ &\quad + \sum_{uv\in E_2(\mathrm{BSN}-2)} \ln\left(\frac{3+4}{2\sqrt{(3\times 4)}}\right) \\ &= \frac{2228664339909267}{18014398509481984}.\end{aligned} \tag{43}$$

□

2.2. Results for Hierarchical Hypercube Network (HHC). Hierarchical hypercube network (HHC) has many features, for example, symmetry and logarithmic diameter, which imply easy and fast algorithms for communication [55]. The structure of an n- (HHC) consists of three levels of hierarchy. At the lowest level of hierarchy, there is a pool of $2n$ nodes. These nodes are grouped into clusters of $2m$ nodes each, and the nodes in each cluster are interconnected to form an $m-$cube called the son cube or the S-cube. The set of the S-cubes constitutes the second level of hierarchy [56].

Due to the hierarchical structure, HHC has the advantages that are gained by hierarchy. "In addition, hierarchical structures are capable of exploiting the locality of reference (communication), and they are fault tolerant. Other attractive properties of the HHC structure are logarithmic diameter and a topology inherited from, and closely related to, the hypercube topology. The former property implies fast communication, and the latter implies easy mapping of operations from HC to HHC. The HHC can emulate the hypercube for a large class of problems (divide conquer), without a significant increase in processing time. The HHC can embed rings and HHCs of lower dimension. In addition, HHC embeds the cube connected cycles (CCC)

[57]." As a result, the performance of HHC is in the worst case equivalent to the performance of the CCC.

The number of vertices and edges in HHC − 1 are $16a + 16$ and $24a + 20$, respectively. The number of vertices and edges in HHC − 2 are $16a + 16$ and $32a + 28$, respectively. HHC − 1 and HHC − 2 are shown in Figures 3 and 4, respectively.

Theorem 3. *For the hierarchical hypercube network HHC − 1, we have*

(1) $VAR(HHC-1) = (2a + 1/4(a+1)^2)$

(2) $AL(HHC-1) = 16$

(3) $IR1(HHC-1) = (20(2a+1)/a+1)$

(4) $IR2(HHC-1) = 2\sqrt{3}\sqrt{(18a + 11/24a + 20)} - (6a + 5/2(a+1))$

(5) $IRF(HHC-1) = 16$

(6) $IRFW(HHC-1) = (4/54a + 33)$

(7) $IRA(HHC-1) = (1213215869760357/4503599627370496)$

(8) $IRB(HHC-1) = (909911902320267/562949953421312)$

(9) $IRC(HHC-1) = (72a + 16\sqrt{6} + 12/24a + 20) - (48a + 40/16a + 16)$

(10) $IRDIF(HHC-1) = (40/3)$

(11) $IRL(HHC-1) = (3652105019575333/562949953421312)$

(12) $IRLU(HHC-1) = 8$

(13) $IRLF(HHC-1) = (8\sqrt{6}/3)$

(14) $IRLA(HHC-1) = (32/5)$

(15) $IRD1(HHC-1) = (6243314768165359/562949953421312)$

(16) $IRGA(HHC-1) = (2941534708959071/9007199254740992)$

Proof. The order of graph is $n = |V(\text{HHC}-1)| = 16a + 16$, and its size is $m = |E(\text{HHC}-1)| = 24a + 20$. The vertex set of HHC − 1 can be divided into the following classes by means of degrees:

$$\begin{aligned} V_1(\text{HHC}-1) &= \{v \in V(\text{HHC}-1) : d_u = 2\}, \\ V_2(\text{HHC}-1) &= \{v \in V(\text{HHC}-1) : d_u = 3\}. \end{aligned} \tag{44}$$

The edge set of HHC − 1 can be divided into the following classes with respect to the degrees of end vertices:

$$\begin{aligned} E_1(\text{HHC}-1) &= \{uv \in E(\text{HHC}-1) : d_u = d_v = 3\}, \\ E_2(\text{HHC}-1) &= \{uv \in E(\text{HHC}-1) : d_u = 2, d_v = 3\}. \end{aligned} \tag{45}$$

And the cardinality of edges is as follows:

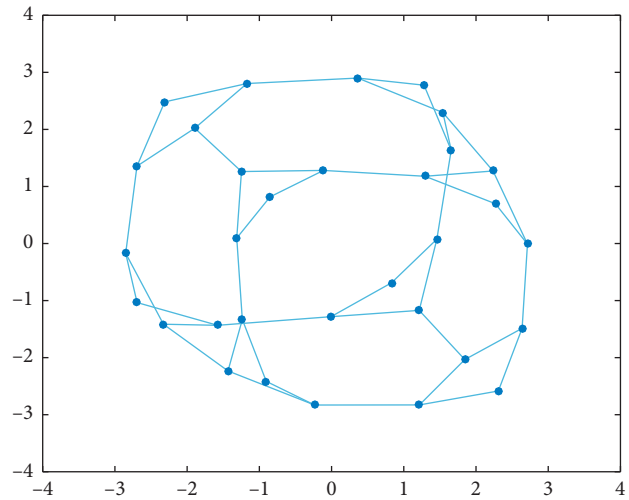

Figure 3: $(\text{HHC}-1)_{(1\times1)}$.

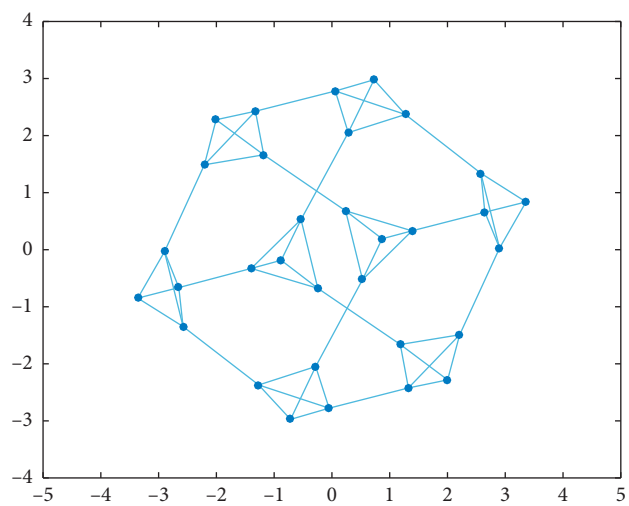

Figure 4: $(\text{HHC}-2)_{(1\times1)}$.

$$\begin{aligned} |E_1(\text{HHC}-1)| &= 24a + 4, \\ |E_2(\text{HHC}-1)| &= 16. \end{aligned} \tag{46}$$

First, we find some topological indices, which will be used in irregularity indices:

$$\begin{aligned} M_1(\text{HHC}-1) &= 144a + 104, \\ M2(\text{HHC}-1) &= 216a + 132, \\ F(\text{HHC}-1) &= 432a + 280, \\ \text{RR}(\text{HHC}-1) &= 72a + 16\sqrt{6} + 12. \end{aligned} \tag{47}$$

Now from definitions, we have

$$\begin{aligned}\mathrm{VAR}(\mathrm{HHC}-1) &= \frac{M_1(\mathrm{HHC}-1)}{n} - \left(\frac{2m}{n}\right)^2 \\ &= \frac{144a+104}{16a+16} - \left(\frac{224a+20}{16a+16}\right)^2 \\ &= \frac{2a+1}{4(a+1)^2}.\end{aligned} \tag{48}$$

$$\begin{aligned}\mathrm{AL}(\mathrm{HHC}-1) &= \sum_{uv\in E(\mathrm{HHC}-1)} \left|d_u - d_v\right| \\ &= \sum_{uv\in E_1(\mathrm{HHC}-1)} (0) + \sum_{uv\in E_2(\mathrm{HHC}-1)} |(2)-(3)| \\ &= 16.\end{aligned} \tag{49}$$

$$\begin{aligned}\mathrm{IR1}(\mathrm{HHC}-1) &= F(\mathrm{HHC}-1) - \frac{2m}{n} M_1(\mathrm{HHC}-1) \\ &= 432a+280 - \frac{2(24a+20)}{16a+16} 144a+104 \\ &= \frac{20(2a+1)}{a+1}.\end{aligned} \tag{50}$$

$$\begin{aligned}\mathrm{IR2}(\mathrm{HHC}-1) &= \sqrt{\frac{M_2(\mathrm{HHC}-1)}{m}} - \frac{2m}{n} \\ &= \sqrt{\frac{216a+132}{24a+20}} - \frac{2(24a+20)}{16a+16} \\ &= 2\sqrt{3}\sqrt{\frac{18a+11}{24a+20}} - \frac{6a+5}{2(a+1)}.\end{aligned} \tag{51}$$

$$\begin{aligned}\mathrm{IRF}(\mathrm{HHC}-1) &= F(\mathrm{HHC}-1) - 2M_2(\mathrm{HHC}-1) \\ &= 432a+280 - 2(216a+132) \\ &= 16.\end{aligned} \tag{52}$$

$$\begin{aligned}\mathrm{IRFW}(\mathrm{HHC}-1) &= \frac{\mathrm{IRF}(\mathrm{HHC}-1)}{M_2(\mathrm{HHC}-1)} \\ &= \frac{16}{216a+132} \\ &= 16.\end{aligned} \tag{53}$$

$$\begin{aligned}\mathrm{IRA}(\mathrm{HHC}-1) &= \sum_{uv\in E(\mathrm{HHC}-1)} \left(d_u^{-1/2} - d_v^{-1/2}\right)^2 \\ &= \sum_{uv\in E_1(\mathrm{HHC}-1)} (0) \\ &\quad + \sum_{uv\in E_2(\mathrm{HHC}-1)} \left((2)^{-1/2} - (3)^{-1/2}\right)^2 \\ &= \frac{1213215869760357}{4503599627370496}.\end{aligned} \tag{54}$$

$$\begin{aligned}\mathrm{IRC}(\mathrm{HHC}-1) &= \frac{\mathrm{RR}(\mathrm{HHC}-1)}{m} - \frac{2m}{n} \\ &= \frac{72a+16\sqrt{6}+12}{24a+20} - \frac{2(24a+20)}{16a+16} \\ &= \frac{72a+16\sqrt{6}+12}{24a+20} - \frac{48a+40}{16a+16}.\end{aligned} \tag{55}$$

$$\begin{aligned}\mathrm{IRDIF}(\mathrm{HHC}-1) &= \sum_{uv\in E(\mathrm{HHC}-1)} \left|\frac{d_u}{d_v} - \frac{d_v}{d_u}\right| \\ &= \sum_{uv\in E_1(\mathrm{HHC}-1)} (0) + \sum_{uv\in E_2(\mathrm{HHC}-1)} \left|\frac{2}{3} - \frac{3}{2}\right| \\ &= \frac{40}{3}.\end{aligned} \tag{56}$$

$$\begin{aligned}\mathrm{IRL}(\mathrm{HHC}-1) &= \sum_{uv\in E(\mathrm{HHC}-1)} \left|\ln(d_u) - \ln(d_v)\right| \\ &= \sum_{uv\in E_1(\mathrm{HHC}-1)} (0) \\ &\quad + \sum_{uv\in E_2(\mathrm{HHC}-1)} |\ln(2) - \ln(3)| \\ &= \frac{3652105019575333}{562949953421312}.\end{aligned} \tag{57}$$

$$\begin{aligned}\mathrm{IRLU}(\mathrm{HHC}-1) &= \sum_{uv\in E(\mathrm{HHC}-1)} \frac{\left|(d_u) - (d_v)\right|}{\min(d_u, d_v)} \\ &= \sum_{uv\in E_1(\mathrm{HHC}-1)} (0) + \sum_{uv\in E_2(\mathrm{HHC}-1)} \frac{|(2)-(3)|}{\min(2,3)} \\ &= 8.\end{aligned} \tag{58}$$

$$\begin{aligned}\mathrm{IRLF}(\mathrm{HHC}-1) &= \sum_{uv\in E(\mathrm{HHC}-1)} \frac{\left|d_u - d_v\right|}{\sqrt{(d_u \times d_v)}} \\ &= \sum_{uv\in E_1(\mathrm{HHC}-1)} (0) + \sum_{uv\in E_2(\mathrm{HHC}-1)} \frac{|2-3|}{\sqrt{(2\times 3)}} \\ &= \frac{8\sqrt{6}}{3}.\end{aligned} \tag{59}$$

$$\begin{aligned}\mathrm{IRLA}(\mathrm{HHC}-1) &= \sum_{uv\in E(\mathrm{HHC}-1)} 2\frac{\left|d_u - d_v\right|}{d_u + d_v} \\ &= \sum_{uv\in E_1(\mathrm{HHC}-1)} (0) + \sum_{uv\in E_2(\mathrm{HHC}-1)} 2\frac{|2-3|}{2+3} \\ &= \frac{32}{5}.\end{aligned} \tag{60}$$

$$\begin{aligned}\mathrm{IRD1}(\mathrm{HHC}-1) &= \sum_{uv\in E(\mathrm{HHC}-1)} \ln\left[1+\left|d_u-d_v\right|\right]\\ &= \sum_{uv\in E_1(\mathrm{HHC}-1)} (0)\\ &\quad+\sum_{uv\in E_2(\mathrm{HHC}-1)} \ln[1+|(2)-(3)|]\\ &= \frac{6243314768165359}{562949953421312}.\end{aligned} \tag{61}$$

$$\begin{aligned}\mathrm{IRGA}(\mathrm{HHC}-1) &= \sum_{uv\in E(\mathrm{HHC}-1)} \ln\left(\frac{d_u+d_v}{2\sqrt{(d_u\times d_v)}}\right)\\ &= \sum_{uv\in E_1(\mathrm{HHC}-1)} (0)\\ &\quad+\sum_{uv\in E_2(\mathrm{HHC}-1)} \ln\left(\frac{2+3}{2\sqrt{(2\times 3)}}\right)\\ &= \frac{2941534708959071}{9007199254740992}.\end{aligned} \tag{62}$$

□

Theorem 4. *For the hierarchical hypercube network HHC − 2, we have*

(1) $VAR(HHC-2) = (2a+1/4(a+1)^2)$
(2) $AL(HHC-2) = 24$
(3) $IR1(HHC-2) = (28(2a+1)/a+1)$
(4) $IR2(HHC-2) = 4\sqrt{2}\sqrt{(16a+11/32a+28)} - (8a+7/(2(a+1)))$
(5) $IRF(HHC-2) = 24$
(6) $IRFW(HHC-2) = (3/64a+44)$
(7) $IRA(HHC-2) = (20694009944167803/144115188075855872)$
(8) $IRB(HHC-2) = (15520507458125877/9007199254740992)$
(9) $IRC(HHC-2) = (128a+48\sqrt{3}+16/32a+28) - (64a+56/16a+16)$
(10) $IRDIF(HHC-2) = 14$
(11) $IRL(HHC-2) = (3886814622885039/562949953421312)$
(12) $IRLU(HHC-2) = 8$
(13) $IRLF(HHC-2) = 4\sqrt{3}$
(14) $IRLA(HHC-2) = (48/7)$
(15) $\mathrm{IRD1}(\mathrm{HHC}-2) = (18729944304496077/1125899906842624)$
(16) $IRGA(HHC-2) = (2228664339909267/9007199254740992)$

Proof. The order of graph is $n = |V(\mathrm{HHC}-2)| = 16a+16$, and its size is $m = |E(\mathrm{HHC}-2)| = 32a+28$. The vertex set of HHC − 2 can be divided into the following classes by means of degrees:

$$\begin{aligned}V_1(\mathrm{HHC}-2) &= \{v\in V(\mathrm{HHC}-2): d_u=3\},\\ V_2(\mathrm{HHC}-2) &= \{v\in V(\mathrm{HHC}-2): d_u=4\}.\end{aligned} \tag{63}$$

The edge set of HHC − 2 can be divided into the following classes with respect to the degrees of end vertices:

$$\begin{aligned}E_1(\mathrm{HHC}-2) &= \{uv\in E(\mathrm{HHC}-2): d_u=d_v=4\},\\ E_2(\mathrm{HHC}-2) &= \{uv\in E(\mathrm{HHC}-2): d_u=3, d_v=4\}.\end{aligned} \tag{64}$$

And the cardinality of edges is as follows:

$$\begin{aligned}\left|E_1(\mathrm{HHC}-2)\right| &= 32a+4,\\ \left|E_2(\mathrm{HHC}-2)\right| &= 24.\end{aligned} \tag{65}$$

First, we find some topological indices, which will be used in irregularity indices:

$$\begin{aligned}M_1(\mathrm{HHC}-2) &= 256a+200,\\ M2(\mathrm{HHC}-2) &= 512a+352,\\ F(\mathrm{HHC}-2) &= 1024a+728,\\ \mathrm{RR}(\mathrm{HHC}-2) &= 128a+48\sqrt{3}+16.\end{aligned} \tag{66}$$

Now, from definitions, we have

$$\begin{aligned}\mathrm{VAR}(\mathrm{HHC}-2) &= \frac{M_1(\mathrm{HHC}-2)}{n}-\left(\frac{2m}{n}\right)^2\\ &= \frac{256a+200}{16a+16}-\left(\frac{232a+28}{16a+16}\right)^2\\ &= \frac{2a+1}{4(a+1)^2}.\end{aligned} \tag{67}$$

$$\begin{aligned}\mathrm{AL}(\mathrm{HHC}-2) &= \sum_{uv\in E(\mathrm{HHC}-2)} \left|d_u-d_v\right|\\ &= \sum_{uv\in E_1(\mathrm{HHC}-2)} (0)+\sum_{uv\in E_2(\mathrm{HHC}-2)} |(3)-(4)|\\ &= 24.\end{aligned} \tag{68}$$

$$\begin{aligned}\mathrm{IR1}(\mathrm{HHC}-2) &= F(\mathrm{HHC}-2)-\frac{2m}{n}M_1(\mathrm{HHC}-2)\\ &= 1024a+728-\frac{2(32a+28)}{16a+16}256a+200\\ &= \frac{28(2a+1)}{a+1}.\end{aligned} \tag{69}$$

$$\begin{aligned}\mathrm{IR2}(\mathrm{HHC}-2) &= \sqrt{\frac{M_2(\mathrm{HHC}-2)}{m}}-\frac{2m}{n}\\ &= \sqrt{\frac{512a+352}{32a+28}}-\frac{2(32a+28)}{16a+16}\\ &= 4\sqrt{2}\sqrt{\frac{16a+11}{32a+28}}-\frac{8a+7}{2(a+1)}.\end{aligned} \tag{70}$$

$$\begin{aligned}\mathrm{IRF}(\mathrm{HHC}-2) &= F(\mathrm{HHC}-2) - 2M_2(\mathrm{HHC}-2)\\ &= 1024a + 728 - 2(512a + 352)\\ &= 24.\end{aligned} \tag{71}$$

$$\begin{aligned}\mathrm{IRFW}(\mathrm{HHC}-2) &= \frac{\mathrm{IRF}(\mathrm{HHC}-2)}{M_2(\mathrm{HHC}-2)}\\ &= \frac{24}{512a + 352}\\ &= 24.\end{aligned} \tag{72}$$

$$\begin{aligned}\mathrm{IRA}(\mathrm{HHC}-2) &= \sum_{uv\in E(\mathrm{HHC}-2)} \left(d_u^{-1/2} - d_v^{-1/2}\right)^2\\ &= \sum_{uv\in E_1(\mathrm{HHC}-2)} (0)\\ &\quad + \sum_{uv\in E_2(\mathrm{HHC}-2)} \left((3)^{-1/2} - (4)^{-1/2}\right)^2\\ &= \frac{20694009944167803}{144115188075855872}.\end{aligned} \tag{73}$$

$$\begin{aligned}\mathrm{IRB}(\mathrm{HHC}-2) &= \sum_{uv\in E(\mathrm{HHC}-2)} \left(d_u^{1/2} - d_v^{1/2}\right)^2\\ &= \sum_{uv\in E_1(\mathrm{HHC}-2)} (0)\\ &\quad + \sum_{uv\in E_2(\mathrm{HHC}-2)} \left((3)^{1/2} - (4)^{1/2}\right)^2\\ &= \frac{15520507458125877}{9007199254740992}.\end{aligned} \tag{74}$$

$$\begin{aligned}\mathrm{IRC}(\mathrm{HHC}-2) &= \frac{\mathrm{RR}(\mathrm{HHC}-2)}{m} - \frac{2m}{n}\\ &= \frac{128a + 48\sqrt{3} + 16}{32a + 28} - \frac{2(32a + 28)}{16a + 16}\\ &= \frac{128a + 48\sqrt{3} + 16}{32a + 28} - \frac{64a + 56}{16a + 16}.\end{aligned} \tag{75}$$

$$\begin{aligned}\mathrm{IRDIF}(\mathrm{HHC}-2) &= \sum_{uv\in E(\mathrm{HHC}-2)} \left|\frac{d_u}{d_v} - \frac{d_v}{d_u}\right|\\ &= \sum_{uv\in E_1(\mathrm{HHC}-2)} (0) + \sum_{uv\in E_2(\mathrm{HHC}-2)} \left|\frac{3}{4} - \frac{4}{3}\right|\\ &= 14.\end{aligned} \tag{76}$$

$$\begin{aligned}\mathrm{IRL}(\mathrm{HHC}-2) &= \sum_{uv\in E(\mathrm{HHC}-2)} \left|\ln(d_u) - \ln(d_v)\right|\\ &= \sum_{uv\in E_1(\mathrm{HHC}-2)} (0)\\ &\quad + \sum_{uv\in E_2(\mathrm{HHC}-2)} |\ln(3) - \ln(4)|\\ &= \frac{3886814622885039}{562949953421312}.\end{aligned} \tag{77}$$

$$\begin{aligned}\mathrm{IRLU}(\mathrm{HHC}-2) &= \sum_{uv\in E(\mathrm{HHC}-2)} \frac{|(d_u) - (d_v)|}{\min(d_u, d_v)}\\ &= \sum_{uv\in E_1(\mathrm{HHC}-2)} (0) + \sum_{uv\in E_2(\mathrm{HHC}-2)} \frac{|(3) - (4)|}{\min(3, 4)}\\ &= 8.\end{aligned} \tag{78}$$

$$\begin{aligned}\mathrm{IRLF}(\mathrm{HHC}-2) &= \sum_{uv\in E(\mathrm{HHC}-2)} \frac{|d_u - d_v|}{\sqrt{(d_u \times d_v)}}\\ &= \sum_{uv\in E_1(\mathrm{HHC}-2)} (0) + \sum_{uv\in E_2(\mathrm{HHC}-2)} \frac{|3 - 4|}{\sqrt{(3 \times 4)}}\\ &= 4\sqrt{3}.\end{aligned} \tag{79}$$

$$\begin{aligned}\mathrm{IRLA}(\mathrm{HHC}-2) &= \sum_{uv\in E(\mathrm{HHC}-2)} 2\frac{|d_u - d_v|}{d_u + d_v}\\ &= \sum_{uv\in E_1(\mathrm{HHC}-2)} (0) + \sum_{uv\in E_2(\mathrm{HHC}-2)} 2\frac{|3 - 4|}{3 + 4}\\ &= \frac{48}{7}.\end{aligned} \tag{80}$$

$$\begin{aligned}\mathrm{IRD1}(\mathrm{HHC}-2) &= \sum_{uv\in E(\mathrm{HHC}-2)} \ln\left[1 + |d_u - d_v|\right]\\ &= \sum_{uv\in E_1(\mathrm{HHC}-2)} (0)\\ &\quad + \sum_{uv\in E_2(\mathrm{HHC}-2)} \ln[1 + |(3) - (4)|]\\ &= \frac{18729944304496077}{1125899906842624}.\end{aligned} \tag{81}$$

$$\begin{aligned}\mathrm{IRGA}(\mathrm{HHC}-2) &= \sum_{uv\in E(\mathrm{HHC}-2)} \ln\left(\frac{d_u + d_v}{2\sqrt{(d_u \times d_v)}}\right)\\ &= \sum_{uv\in E_1(\mathrm{HHC}-2)} (0)\\ &\quad + \sum_{uv\in E_2(\mathrm{HHC}-2)} \ln\left(\frac{3 + 4}{2\sqrt{(3 \times 4)}}\right)\\ &= \frac{2228664339909267}{9007199254740992}.\end{aligned} \tag{82}$$

□

3. Conclusion

In this paper, we have computed several degree-based irregularity indices of block shift networks and hierarchical hypercube networks. Our results are applicable in chemistry, physics, and other applied sciences. Topological indices help us to understand structural properties of understudy

networks [58–63]. The computed results give understanding about the irregularities of understudy networks.

Data Availability

The data used to support the findings of this study are included within the article.

Conflicts of Interest

The authors declare that there are no conflicts of interest regarding the publication of this paper.

Authors' Contributions

All authors contributed equally to this work.

Acknowledgments

This paper was supported by the Anhui Natural Science Research Project (2017) under Grant no. KJ2017A469, Scientific Research Project (2018) of Tongling University under Grant no. 2017tlxyzd5, and Top-Notch Talents Cultivation Project of Anhui Higher Education under Grant no. gxgnfx2018044.

References

[1] J.-B. Liu, C. Wang, S. Wang, and B. Wei, "Zagreb indices and multiplicative zagreb indices of eulerian graphs," *Bulletin of the Malaysian Mathematical Sciences Society*, vol. 42, no. 1, pp. 67–78, 2019.

[2] M. C. M. Kumar and H. M. Nagesh, "Directed pathos total digraph of an arborescence," *Engineering and Applied Science Letters*, vol. 1, no. 1, pp. 29–42, 2018.

[3] H. M. Nagesh and M. C. M. Kumar, "Block digraph of a directed graph," *Open Journal of Mathematical Sciences*, vol. 2, no. 1, pp. 202–208, 2018.

[4] G. V. Rajasekharaiah and U. P. Murthy, "Secure domination in lict graphs," *Open Journal of Mathematical Sciences*, vol. 2, no. 1, pp. 134–145, 2018.

[5] N. Ali, M. A. Umar, A. Tabassum, and A. Raheem, "Super (a, d)-C3-antimagicness of a corona graph," *Open Journal of Mathematical Sciences*, vol. 2, no. 1, pp. 371–278, 2018.

[6] J.-B. Liu, X.-F. Pan, F.-T. Hu, and F.-F. Hu, "Asymptotic Laplacian-energy-like invariant of lattices," *Applied Mathematics and Computation*, vol. 253, pp. 205–214, 2015.

[7] G. Liu, Z. Jia, and W. Gao, "Ontology similarity computing based on stochastic primal dual coordinate technique," *Open Journal of Mathematical Sciences*, vol. 2, no. 1, pp. 221–227, 2018.

[8] J.-B. Liu and X.-F. Pan, "Minimizing Kirchhoff index among graphs with a given vertex bipartiteness," *Applied Mathematics and Computation*, vol. 291, pp. 84–88, 2016.

[9] J. B. Liu, J. Zhao, and Z. Zhu, "On the number of spanning trees and normalized Laplacian of linear octagonal-quadrilateral networks," *International Journal of Quantum Chemistry*, vol. 59, Article ID e25971, 2019.

[10] L. N. Bhuyan, Q. Yang, and D. P. Agrawal, "Performance of multiprocessor interconnection networks," *Computer*, vol. 22, no. 2, pp. 25–37, 1989.

[11] T.-Y Feng, "A survey of interconnection networks," *Computer*, vol. 14, no. 12, pp. 12–27, 1981.

[12] J. M. Kumar and L. M. Patnaik, "Extended hypercube: a hierarchical interconnection network of hypercubes," *IEEE Transactions on Parallel and Distributed Systems*, vol. 3, no. 1, pp. 45–57, 1992.

[13] K. Ghose and K. R. Desai, "Hierarchical cubic networks," *IEEE Transactions on Parallel and Distributed Systems*, vol. 6, no. 4, pp. 427–435, 1995.

[14] S. Konstantinidou, "The selective extra stage buttery," *IEEE Transactions on Very Large Scale Integration (VLSI) Systems*, vol. 1, Article ID 502506, 1992.

[15] M. A. Umar, M. A. Javed, M. Hussain, and B. R. Ali, "Super (a, d)-C4-antimagicness of book graphs," *Open Journal of Mathematical Sciences*, vol. 2, no. 1, pp. 115–121, 2018.

[16] Z. Tang, L. Liang, and W. Gao, "Wiener polarity index of quasi-tree molecular structures," *Open Journal of Mathematical Sciences*, vol. 2, no. 1, pp. 73–83, 2018.

[17] M. S. Sardar, S. Zafar, and M. R. Farahani, "The generalized zagreb index of capra-designed planar benzenoid series $Ca_k (C_6)$," *Open Journal of Mathematical Sciences*, vol. 1, no. 1, pp. 44–51, 2017.

[18] S. Noreen and A. Mahmood, "Zagreb polynomials and redefined zagreb indices for the line graph of carbon nanocones," *Open Journal of Mathematical Analysis*, vol. 2, no. 1, pp. 66–73, 2018.

[19] M. S. Anjum and M. U. Safdar, "*K* Banhatti and *K* hyper-Banhatti indices of nanotubes," *Engineering and Applied Science Letters*, vol. 2, no. 1, pp. 19–37, 2019.

[20] G. Chartrand, P. Erdös, and O. R. Oellermann, "How to define an irregular graph," *The College Mathematics Journal*, vol. 19, no. 1, pp. 36–42, 1988.

[21] M. Behzad and G. Chartrand, "No graph is perfect," *The American Mathematical Monthly*, vol. 74, no. 8, pp. 962-963, 1967.

[22] B. Horoldagva, L. Buyantogtokh, S. Dorjsembe, and I. Gutman, "Maximum size of maximally irregular graphs," *MATCH Communications in Mathematical and in Computer Chemistry*, vol. 76, pp. 81–98, 2016.

[23] F. Liu, Z. Zhang, and J. Meng, "The size of maximally irregular graphs and maximally irregular triangle-free graphs," *Graphs and Combinatorics*, vol. 30, no. 3, pp. 699–705, 2014.

[24] L. Von Collatz and S. Ulrich, "Spektren endlicher grafen," *In Abhandlungen aus dem Mathematischen Seminar der Universitat Hamburg*, vol. 21, no. 1, pp. 63–77, 1957.

[25] F. K. Bell, "A note on the irregularity of graphs," *Linear Algebra and Its Applications*, vol. 161, pp. 45–54, 1992.

[26] M. O. Albertson, "The irregularity of a graph," *Ars Combinatoria*, vol. 46, pp. 219–225, 1997.

[27] D. Vukičević and A. Graovac, "Valence connectivity versus Randić, Zagreb and modified Zagreb index: a linear algorithm to check discriminative properties of indices in acyclic molecular graphs," *Croatica Chemica Acta*, vol. 77, no. 3, pp. 501–508, 2004.

[28] H. Abdo and D. Dimitrov, "The total irregularity of graphs under graph operations," *Miskolc Mathematical Notes*, vol. 15, no. 1, pp. 3–17, 2014.

[29] H. Abdo and D. Dimitrov, "The irregularity of graphs under graph operations," *Discussiones Mathematicae Graph Theory*, vol. 34, no. 2, pp. 263–278, 2014.

[30] I. Gutman, "Topological indices and irregularity measures," *John Bull*, vol. 8, pp. 469–475, 2018.

[31] Z. Shao, A. R. Virk, M. S. Javed, M. A. Rehman, and M. R. Farahani, "Degree based graph invariants for the molecular graph of Bismuth Tri-Iodide," *Engineering and Applied Science Letters*, vol. 2, no. 1, pp. 01–11, 2019.

[32] A. u. R. Virk, M. N. Jhangeer, and M. A. Rehman, "Reverse zagreb and reverse hyper-zagreb indices for silicon carbide \(Si_{2}C_{3}I[r, s]\) and \(Si_{2}C_{3}II[r, s]\)," *Engineering and Applied Science Letters*, vol. 1, no. 2, pp. 37–50, 2018.

[33] N. De, "Computing reformulated first zagreb index of some chemical graphs as an application of generalized hierarchical product of graphs," *Open Journal of Mathematical Sciences*, vol. 2, no. 1, pp. 338–350, 2018.

[34] L. Yan, M. R. Farahani, and W. Gao, "Distance-based indices computation of symmetry molecular structures," *Open Journal of Mathematical Sciences*, vol. 2, no. 1, pp. 323–337, 2018.

[35] W. Gao, A. Asghar, and W. Nazeer, "Computing degree-based topological indices of jahangir graph," *Engineering and Applied Science Letters*, vol. 1, no. 1, pp. 16–22, 2018.

[36] M. Riaz, W. Gao, and A. Qudair Baig, "*M*-polynomials and degree-based topological indices of some families of convex polytopes," *Open Journal of Mathematical Sciences*, vol. 2, no. 1, pp. 18–28, 2018.

[37] W. Gao, B. Muzaffar, and W. Nazeer, "*K*-Banhatti and *K*-hyper Banhatti indices of dominating David Derived network," *Open Journal of Mathematical Analysis*, vol. 1, no. 1, pp. 13–24, 2017.

[38] H. Siddiqui and M. R. Farahani, "Forgotten polynomial and forgotten index of certain interconnection networks," *Open Journal of Mathematical Analysis*, vol. 1, no. 1, pp. 44–59, 2017.

[39] M. S. Sardar and X.-F. Pan, "Computing sanskruti index of titania nanotubes," *Open Journal of Mathematical Sciences*, vol. 1, no. 1, pp. 126–131, 2017.

[40] H. M. U. Rehman, R. Sardar, and A. Raza, "Computing topological indices of Hex Board and its line graph," *Open Journal of Mathematical Sciences*, vol. 1, no. 1, pp. 62–71, 2017.

[41] M. Munir, W. Nazeer, S. Rafique, and S. Kang, "*M*-polynomial and related topological indices of Nanostar dendrimers," *Symmetry*, vol. 8, no. 9, p. 97, 2016.

[42] M. Ajmal, W. Nazeer, M. Munir, S. M. Kang, and Y. C. Kwun, "Some algebraic polynomials and topological indices of generalized prism and toroidal polyhex networks," *Symmetry*, vol. 9, no. 1, p. 5, 2017.

[43] Z. Iqbal, A. Aslam, M. Ishaq, and M. Aamir, "Characteristic study of irregularity measures of some nanotubes," *Canadian Journal of Physics*, vol. 97, 2019.

[44] W. Gao, M. Aamir, Z. Iqbal, M. Ishaq, and A. Aslam, "On irregularity measures of some dendrimers structures," *Mathematics*, vol. 7, no. 3, p. 271, 2019.

[45] H. Abdo, D. Dimitrov, and W. Gao, "On the irregularity of some molecular structures," *Canadian Journal of Chemistry*, vol. 95, no. 2, pp. 174–183, 2016.

[46] Z. Hussain, S. Rafique, and M. Munir, "Irregularity molecular descriptors of hourglass, jagged-rectangle, and triangular benzenoid systems," *Processes*, vol. 7, no. 7, p. 413, 2019.

[47] W. Gao, M. Asif, and W. Nazeer, "The study of honey comb derived network via topological indices," *Open Journal of Mathematical Analysis*, vol. 2, no. 2, pp. 10–26, 2018.

[48] R. Kanabu and S. Hosamani, "Some numerical invariants associated with *V*-phenylenic nanotube and nanotori," *Engineering and Applied Science Letters*, vol. 1, no. 1, pp. 1–9, 2018.

[49] N. De, "Hyper zagreb index of bridge and chain graphs," *Open Journal of Mathematical Sciences*, vol. 2, no. 1, pp. 1–17, 2018.

[50] M. Imran, A. Asghar, and A. Q. Baig, "On graph invariants of oxide network," *Engineering and Applied Science Letters*, vol. 1, no. 1, pp. 23–28, 2018.

[51] A. Ali, W. Nazeer, M. Munir, and S. M. Kang, "*M*-polynomials and topological indices of zigzag and rhombic benzenoid systems," *Open Chemistry*, vol. 16, no. 1, pp. 73–78, 2018.

[52] S. M. Kang, M. A. Zahid, A. U. R. Virk, W. Nazeer, and W. Gao, "Calculating the degree-based topological indices of dendrimers," *Open Chemistry*, vol. 16, no. 1, pp. 681–688, 2018.

[53] Y. Pan, *The Block Shift Network: Interconnection Strategies for Large Parallel Systems*, University of Pittsburgh, Pittsburgh, PA, USA, 1992.

[54] Y. Pan and H. Y. H. Chuang, "Properties and performance of the block shift network," *IEEE Transactions on Circuits and Systems I: Fundamental Theory and Applications*, vol. 44, no. 2, pp. 93–102, 1997.

[55] Q. M. Malluhi and M. A. Bayoumi, "The hierarchical hypercube: a new interconnection topology for massively parallel systems," *IEEE Transactions on Parallel and Distributed Systems*, vol. 5, no. 1, pp. 17–30, 1994.

[56] R.-Y. Wu, G.-H. Chen, Y.-L. Kuo, and G. J. Chang, "Node-disjoint paths in hierarchical hypercube networks," *Information Sciences*, vol. 177, no. 19, pp. 4200–4207, 2007.

[57] F. P. Preparata and J. Vuillemin, "The cube-connected cycles: a versatile network for parallel computation," *Communications of the ACM*, vol. 24, no. 5, pp. 300–309, 1981.

[58] W. Gao, M. Younas, A. Farooq, A. Virk, and W. Nazeer, "Some reverse degree-based topological indices and polynomials of dendrimers," *Mathematics*, vol. 6, no. 10, p. 214, 2018.

[59] S. M. Kang, W. Nazeer, M. A. Zahid, A. R. Nizami, A. Aslam, and M. Munir, "*M*-polynomials and topological indices of hex-derived networks," *Open Physics*, vol. 16, no. 1, pp. 394–403, 2018.

[60] W. Gao, M. Younas, A. Farooq, A. Mahboob, and W. Nazeer, "*M*-polynomials and degree-based topological indices of the crystallographic structure of molecules," *Biomolecules*, vol. 8, no. 4, p. 107, 2018.

[61] W. Gao, M. K. Jamil, W. Nazeer, and M. Amin, "Degree-based multiplicative atom-bond connectivity index of nanostructures," *International Journal of Applied Mathematics*, vol. 47, no. 4, 2017.

[62] M. S. Ahmad, W. Nazeer, S. M. Kang, M. Imran, and W. Gao, "Calculating degree-based topological indices of dominating David derived networks," *Open Physics*, vol. 15, no. 1, pp. 1015–1021, 2017.

[63] Y. Kwun, A. Virk, W. Nazeer, M. Rehman, and S. Kang, "On the multiplicative degree-based topological indices of silicon-carbon Si2C3-I[p, q] and Si2C3-II[p, q]," *Symmetry*, vol. 10, no. 8, p. 320, 2018.

Hindawi
Journal of Chemistry
Volume 2019, Article ID 2096019, 17 pages
https://doi.org/10.1155/2019/2096019

Research Article

Useful Irregularity Indices in QSPR Study for Bismuth Tri-Iodide

Abaid ur Rehman Virk,[1] **M. A. Rehman**,[1] **Ce Shi**,[2] **and Waqas Nazeer**[3]

[1]*Department of Mathematics, University of Management and Technology, Lahore 54000, Pakistan*
[2]*School of Statistics and Mathematics, Shanghai Lixin University of Accounting and Finance, Shanghai 201209, China*
[3]*Department of Mathematics, Government College University, Lahore 54000, Pakistan*

Correspondence should be addressed to Ce Shi; shice060@lixin.edu.cn

Received 6 July 2019; Accepted 5 September 2019; Published 12 December 2019

Academic Editor: Juan L. G. Guirao

Topological indices give us a mathematical language to study molecular structures. They convert a chemical compound into a single number which foresees properties, for example, boiling points, viscosity, and the radius of gyrations. Drugs and other chemical compounds are often modeled as various polygonal shapes, trees, and graphs. In this paper, we will compute some irregularity indices for bismuth tri-iodide chain and sheet that are useful in the quantitative structure-activity relationship.

1. Introduction

In discrete mathematics, graph theory in general not only is the study of different properties of objects but also tells us about objects having same properties as the investigating object. These properties of different objects are of main interest. In particular, graph polynomials related to graph are rich in information. Mathematical tools like polynomials and topological-based numbers [1–5] have significant importance to collect information about properties of chemical compounds. We can find out many hidden information about compounds through these tools. Multifold graph polynomials are presented in the literature. Actually, topological indices are numeric quantities that tell us about the whole structure of graph. There are many topological indices that help us to study physical and chemical reactivities and biological properties [6–12]. Wiener, in 1947, firstly introduced the concept of topological index while working on boiling point. In particular, Hosoya polynomial plays an important in the area of distance-based topological indices, and we can find out the Wiener index, hyper-Wiener index, and Tratch–Stankevich–Zefirov index by Hosoya polynomial. For more about topological indices, refer [5, 13–35].

BiI_3 is an inorganic compound which is the result of the reaction of iodine and bismuth, which inspired the enthusiasm for subjective inorganic investigations [36]. BiI_3 is an excellent inorganic compound and is very useful in "qualitative inorganic analysis" [37]. It was proved that Bi-doped glass optical strands are one of the most promising dynamic laser media. Different kinds of Bi-doped fiber strands have been created and have been used to construct Bi-doped fiber lasers and optical loudspeakers [38].

Layered BiI_3 gemstones are considered to be a three-layered stack structure in which a plane of bismuth atoms is sandwiched between iodide particle planes to form a continuous I-Bi-I plane [39]. The periodic superposition of the diamond-shaped three layers forms BiI_3 crystals with R-3 symmetry [40, 41]. A progressive stack of I-Bi-I layers forms a symmetric hexagonal structure [42], and jewel of BiI_3 was integrated in [43]. In Figures 1 and 2, main cycles are C_4^1 and C_4^2, central cycles are C_4^3 and C_4^6, and base cycles are C_4^4 and C_4^5.

TI is known as the irregularity index, [44] if TI of graph is greater than or equal to zero and TI of graph is equal to zero if and only if graph is regular. The irregularity indices are given below. All these irregularity indices belong to degree-based topological invariants except IRM2 (G) and are used in QSAR.

(1) $\mathrm{VAR}(G) = \sum_{u\epsilon V}(d_u - (2m/n))^2 = (M_1(G)/n) - (2m/n)^2$

(2) $\mathrm{AL}(G) = \sum_{uv\epsilon E(G)}|d_u - d_v|$

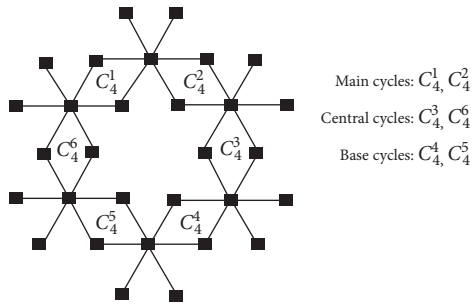

Figure 1: Unit cell (bismuth tri-iodide).

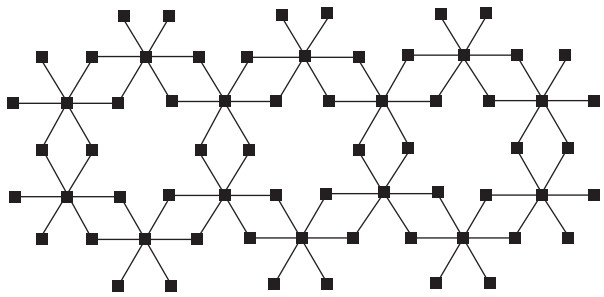

Figure 2: Chain for $m = 3$ (bismuth tri-iodide).

(3) $\mathrm{IR1}(G) = \sum_{u\in V}(d_u)^3 - (2m/n)\sum_{u\in V}(d_u)^2 = F(G) - (2m/n)M_1(G)$

(4) $\mathrm{IR2}(G) = \sqrt{(\sum_{uv\in E(G)} d_u d_v/m)} - (2m/n) = \sqrt{(M_2(G)/m)} - (2m/n)$

(5) $\mathrm{IRF}(G) = \sum_{uv\in E(G)}(d_u - d_v)^2 = F(G) - 2M_2(G)$

(6) $\mathrm{IRFW}(G) = (\mathrm{IRF}(G)/M_2(G))$

(7) $\mathrm{IRA}(G) = \sum_{uv\in E(G)}(d_u^{-1/2} - d_v^{-1/2})^2 = n - 2R(G)$

(8) $\mathrm{IRB}(G) = \sum_{uv\in E(G)}(d_u^{1/2} - d_v^{1/2})^2 = M_1(G) - 2\mathrm{RR}(G)$

(9) $\mathrm{IRC}(G) = (\sum_{uv\in E(G)}\sqrt{d_u d_v}/m) - (2m/n) = (\mathrm{RR}(G)/m) - (2m/n)$

(10) $\mathrm{IRDIF}(G) = \sum_{uv\in E(G)}|(d_u/d_v) - (d_v/d_u)| = \sum_{i<j} m_{i,j}((j/i) - (i/j))$

(11) $\mathrm{IRL}(G) = \sum_{uv\in E(G)}|\mathrm{lnd}_u - \mathrm{lnd}_v| = \sum_{i<j} m_{i,j} ln(j/i)$

(12) $\mathrm{IRLU}(G) = \sum_{uv\in E(G)}|d_u - d_v|/\min(d_u, d_v) = \sum_{i<j} m_{i,j}\ln((j-i)/i)$

(13) $\mathrm{IRLF}(G) = \sum_{uv\in E(G)}|d_u - d_v|/\sqrt{(d_u d_v)} = \sum_{i<j} m_{i,j}((j-i)/\sqrt{ij})$

(14) $\mathrm{IRLA}(G) = 2\sum_{uv\in E(G)}|d_u - d_v|/(d_u + d_v) = 2\sum_{i<j} m_{i,j}((j-i)/(i+j))$

(15) $\mathrm{IRD1}(G) = \sum_{uv\in E(G)}\ln 1 + |d_u - d_v| = \sum_{i<j} m_{i,j}\ln(i+j-1)$

(16) $\mathrm{IRGA}(G)\sum_{uv\in E(G)}\ln((d_u + d_v)/2\sqrt{d_u d_v})\sum_{i<j} m_{i,j}((i+j)/2\sqrt{ij})$

M_1, M_2, R, RR, and F are first Zagreb index, second Zagreb index, Randić index, reverse Randić index, and forgotten index, respectively [45–49]. It can be noted that many irregularity indices are constructed with the help of many known TIs.

2. Methodology

To compute our results, first we construct graphs of bismuth tri-iodides and count number of vertices and edges. Secondly, we divide the edge set into different classes with respect to the degrees of end vertices. By applying definitions and using edge division, we computed our results. Finally, we plotted our results to see the dependence on the involved parameters. We used Maple 2015 for plotting our results.

3. Irregularity Indices for Bismuth Tri-Iodide

3.1. Irregularity Indices for Bismuth Tri-Iodide Chain $m - BiI_3$. The unit cell of bismuth tri-iodide is given in Figure 1, and the algebraic graph of bismuth tri-iodide chain $m - \mathrm{BiI}_3$ is shown in Figure 2. For bismuth tri-iodide chain, $|V(m - \mathrm{BiI}_3)| = 6(3m+2)$ and $|E(m - \mathrm{BiI}_3)| = 12(2m+1)$. There are two types of edges in edge set present in the bismuth tri-iodide chain $m - \mathrm{BiI}_3$ given in Table 1.

Theorem 1. *Let $m - BiI_3$ be the bismuth tri-iodide chain. The irregularity indices are*

(1) $\mathrm{VAR}(m - \mathrm{BiI}_3) = 2(45m^2 + 64m + 20)/3(3m+2)^2$

(2) $\mathrm{AL}(m - \mathrm{BiI}_3) = 100m + 56$

Table 1: Partition of $E(m-\mathrm{BiI}_3)$.

(d_u, d_v)	Frequency
(1, 6)	$4m+8$
(2, 6)	$20m+4$

(3) $\mathrm{IR1}(m-\mathrm{BiI}_3) = 8(55m^2+151m+70)/(3m+2)$

(4) $\mathrm{IR2}(m-\mathrm{BiI}_3) = 1/(\sqrt{6m+3})(3m+2)((\sqrt{66m+24})(3m+2)-(8m+4)(\sqrt{6m+3}))$

(5) $\mathrm{IRF}(m-\mathrm{BiI}_3) = 120m+264$

(6) $\mathrm{IRFW}(m-\mathrm{BiI}_3) = (120m+264)/(264m+96)$

(7) $\mathrm{IRA}(m-\mathrm{BiI}_3) = (1/3)((24-20\sqrt{3}-4\sqrt{6})m+(36-4\sqrt{3}-8\sqrt{6}))$

(8) $\mathrm{IRB}(m-\mathrm{BiI}_3) = (188-8\sqrt{3}-8\sqrt{6})m+(88-16\sqrt{3}-16\sqrt{6})$

(9) $\mathrm{IRC}(m-\mathrm{BiI}_3) = (1/3)(2m+1)(3m+2)((3\sqrt{6}+30\sqrt{3}-48)m^2+(8\sqrt{6}+26\sqrt{3}-48)m+(4\sqrt{6}+4\sqrt{3}-12))$

(10) $\mathrm{IRDIF}(m-\mathrm{BiI}_3) = (1/3)(230m+172)$

(11) $\mathrm{IRL}(m-\mathrm{BiI}_3) = 28.96m+18.68$

(12) $\mathrm{IRLU}(m-\mathrm{BiI}_3) = 60m+48$

(13) $\mathrm{IRLF}(m-\mathrm{BiI}_3) = (1/6)[(20\sqrt{6}+80\sqrt{3})m+(40\sqrt{6}+16\sqrt{3})]$

(14) $\mathrm{IRLA}(m-\mathrm{BiI}_3) = (1/7)(180m+108)$

(15) $\mathrm{IRD1}(m-\mathrm{BiI}_3) = 39.16m+20.72$

(16) $\mathrm{IRGA}(m-\mathrm{BiI}_3) = 4m+3.32$

Proof

$$\begin{aligned}\mathrm{VAR}(m-\mathrm{BiI}_3) &= \sum_{u\epsilon V}\left(d_u-\frac{2m}{n}\right)^2 = \frac{M_1(m-BiI_3)}{n}-\left(\frac{2m}{n}\right)^2\\ &= \left(\frac{188m+88}{18m+12}\right)-\left(\frac{2(24m+12)}{(18m+12)}\right)^2\\ &= \frac{2(45m^2+64m+20)}{3(3m+2)^2},\end{aligned} \tag{1}$$

$$\begin{aligned}\mathrm{AL}(m-\mathrm{BiI}_3) &= \sum_{uv\epsilon E(m-\mathrm{BiI}_3)}|d_u-d_v|\\ &= |1-6|(4m+8)+|2-6|(20m+4)\\ &= 100m+56,\end{aligned} \tag{2}$$

$$\begin{aligned}\mathrm{IR1}(m-\mathrm{BiI}_3) &= \sum_{u\epsilon V} d_u^3-\frac{2m}{n}\sum_{u\epsilon V} d_u^2\\ &= F(G)-\left(\frac{2m}{n}\right)M_1(m-\mathrm{BiI}_3)\\ &= (948m+456)-\frac{2(24m+12)}{18m+12}(188m+88)\\ &= \frac{8(55m^2+151m+70)}{3m+2},\end{aligned} \tag{3}$$

$$\begin{aligned}\mathrm{IR2}(m-\mathrm{BiI}_3) &= \sqrt{\frac{\sum_{uv\epsilon E(m-\mathrm{BiI}_3)} d_u d_v}{m}}-\frac{2m}{n}\\ &= \sqrt{\frac{M_2(m-\mathrm{BiI}_3)}{m}}-\frac{2m}{n}\\ &= \sqrt{\frac{264m+96}{24m+12}}-\left(\frac{2(24m+12)}{18m+12}\right)\\ &= \frac{1}{(\sqrt{6m+3})(3m+2)}((\sqrt{66m+24})\\ &\quad\cdot(3m+2)-(8m+4)(\sqrt{6m+3})),\end{aligned} \tag{4}$$

$$\begin{aligned}\mathrm{IRF}(m-\mathrm{BiI}_3) &= \sum_{uv\epsilon E(m-\mathrm{BiI}_3)}(d_u-d_v)^2\\ &= (1-6)^2(4m+8)+(2-6)^2(20m+4)\\ &= 120m+264,\end{aligned} \tag{5}$$

$$\begin{aligned}\mathrm{IRFW}(m-\mathrm{BiI}_3) &= \frac{\mathrm{IRF}(m-\mathrm{BiI}_3)}{M_2(m-\mathrm{BiI}_3)}\\ &= \frac{120m+264}{264m+96},\end{aligned} \tag{6}$$

$$\begin{aligned}\mathrm{IRA}(m-\mathrm{BiI}_3) &= \sum_{uv\epsilon E(m-\mathrm{BiI}_3)}\left(d_u^{-1/2}-d_v^{-1/2}\right)^2\\ &= n-2R(m-\mathrm{BiI}_3)\\ &= (18m+12)-\left(\frac{1}{6}\sqrt{6}(4m+8)\right.\\ &\quad\left.+\frac{1}{6}\sqrt{3}(20m+4)\right)\\ &= \frac{1}{3}((24-20\sqrt{3}-4\sqrt{6})m\\ &\quad+(36-4\sqrt{3}-8\sqrt{6})),\end{aligned} \tag{7}$$

$$\begin{aligned}\mathrm{IRB}(m-\mathrm{BiI}_3) &= \sum_{uv\epsilon E(m-\mathrm{BiI}_3)} \left(d_u^{1/2}-d_v^{1/2}\right)^2 \\ &= M_1(D_nP_n) - 2\mathrm{RR}(m-\mathrm{BiI}_3) \\ &= (188m+88) - 2(\sqrt{6}\,(4m+8) \\ &\quad + 2\sqrt{3}\,(20m+4)) = (188-8\sqrt{3}-8\sqrt{6})m \\ &\quad + (88-16\sqrt{3}-16\sqrt{6}),\end{aligned} \tag{8}$$

$$\begin{aligned}\mathrm{IRC}(m-\mathrm{BiI}_3) &= \frac{\sum_{uv\epsilon E(m-\mathrm{BiI}_3)}\sqrt{d_ud_v}}{m} - \frac{2m}{n} \\ &= \frac{\mathrm{RR}(m-\mathrm{BiI}_3)}{m} - \frac{2m}{n} \\ &= \frac{\sqrt{6}(4m+8)+2\sqrt{3}(20m+4)}{24m+12} \\ &\quad - \frac{2(24m+12)}{18m+12} = \frac{1}{3(2m+1)(3m+2)} \\ &\quad \cdot \left((3\sqrt{6}+30\sqrt{3}-48)m^2\right. \\ &\quad + (8\sqrt{6}+26\sqrt{3}-48)m \\ &\quad \left. + (4\sqrt{6}+4\sqrt{3}-12)\right),\end{aligned} \tag{9}$$

$$\begin{aligned}\mathrm{IRDIF}(m-\mathrm{BiI}_3) &= \sum_{uv\epsilon E(m-\mathrm{BiI}_3)} \left|\frac{d_u}{d_v} - \frac{d_v}{d_u}\right| \\ &= \left(\left|\frac{1}{6}-\frac{6}{1}\right|\right)(4m+8) + \left(\left|\frac{2}{6}-\frac{6}{2}\right|\right)(20m+4) \\ &= \frac{1}{3}(230m+172),\end{aligned} \tag{10}$$

$$\begin{aligned}\mathrm{IRL}(m-\mathrm{BiI}_3) &= \sum_{uv\epsilon E(m-\mathrm{BiI}_3)} \left|\ln d_u - \ln d_v\right| \\ &= |\ln 1 - \ln 6|(4m+8) + |\ln 2 - \ln 6|(20m+4) \\ &= 28.96m + 18.68,\end{aligned} \tag{11}$$

$$\begin{aligned}\mathrm{IRLU}(m-\mathrm{BiI}_3) &= \sum_{uv\epsilon E(m-\mathrm{BiI}_3)} \frac{|d_u-d_v|}{\min(d_u,d_v)} \\ &= \left(\frac{|1-6|}{1}\right)(4m+8) + \left(\frac{|2-6|}{2}\right)(20m+8) \\ &= 60m+48,\end{aligned} \tag{12}$$

$$\begin{aligned}\mathrm{IRLF}(m-\mathrm{BiI}_3) &= \sum_{uv\epsilon E(m-\mathrm{BiI}_3)} \frac{|d_u-d_v|}{\sqrt{d_u\cdot d_v}} \\ &= \left(\frac{|1-6|}{\sqrt{6}}\right)(4m+8) + \left(\frac{|2-6|}{\sqrt{12}}\right)(20m+8) \\ &= \frac{1}{6}((20\sqrt{6}+80\sqrt{3})m + (40\sqrt{6}+16\sqrt{3})),\end{aligned} \tag{13}$$

$$\begin{aligned}\mathrm{IRLA}(m-\mathrm{BiI}_3) &= \sum_{uv\epsilon E(m-\mathrm{BiI}_3)} 2\frac{|d_u-d_v|}{(d_u+d_v)} \\ &= 2\left(\frac{|1-6|}{1+6}\right)(4m+8) + 2\left(\frac{|2-6|}{2+6}\right) \\ &\quad \cdot (20m+4) \\ &= \frac{1}{7}(180m+108),\end{aligned} \tag{14}$$

$$\begin{aligned}\mathrm{IRD1}(m-\mathrm{BiI}_3) &= \sum_{uv\epsilon E(m-\mathrm{BiI}_3)} \ln\left\{1+|d_u-d_v|\right\} \\ &= \ln\{1+|1-6|\}(4m+8) + \ln\{1+|2-6|\} \\ &\quad \cdot (20m+4) \\ &= 39.16m + 20.72,\end{aligned} \tag{15}$$

$$\begin{aligned}\mathrm{IRGA}(m-\mathrm{BiI}_3) &= \sum_{uv\epsilon E(m-\mathrm{BiI}_3)} \ln\left(\frac{d_u+d_v}{2\sqrt{d_ud_v}}\right) \\ &= \ln\left(\frac{1+6}{2\sqrt{1\times 6}}\right)(4m+8) + \ln\left(\frac{2+6}{2\sqrt{2\times 6}}\right) \\ &\quad \cdot (20m+4) \\ &= 4m+3.32.\end{aligned} \tag{16}$$

□

3.2. Graphical Representation of Bismuth Tri-Iodide Chain $m-BiI_3$. Here, we will graphically present results of irregularity indices for bismuth tri-iodide chain $m-\mathrm{BiI}_3$. From these plots, one can observe the behavior of computed results on the involved parameters (Figure 3).

4. Irregularity Indices for Bismuth Tri-Iodide Sheet BiI_3 $(m\times n)$

The algebraic graph of bismuth tri-iodide sheet BiI_3 $(m\times n)$ is shown in Figure 4. For bismuth tri-iodide sheet, $|V(\mathrm{BiI}_3(m\times$

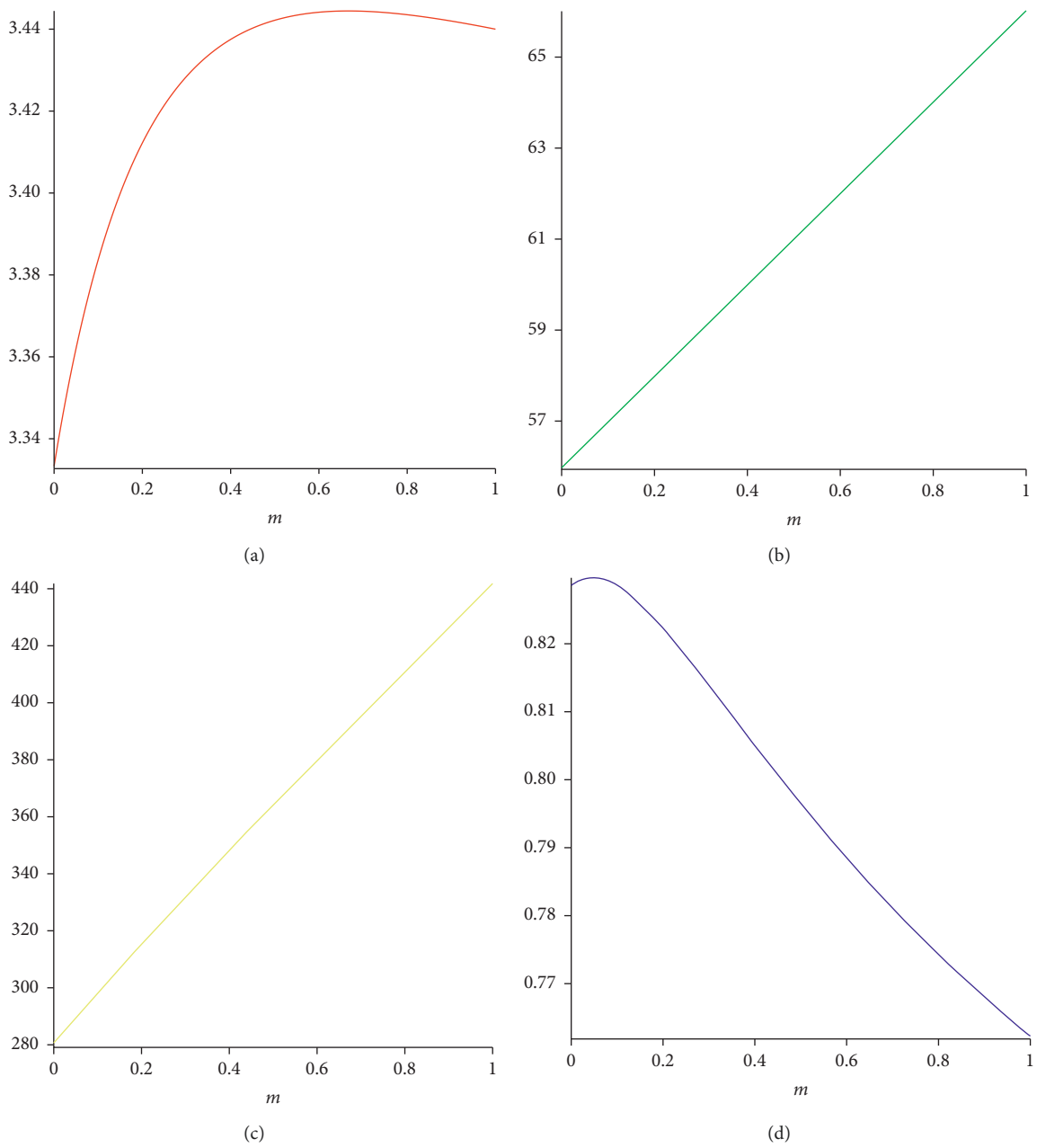

Figure 3: Continued.

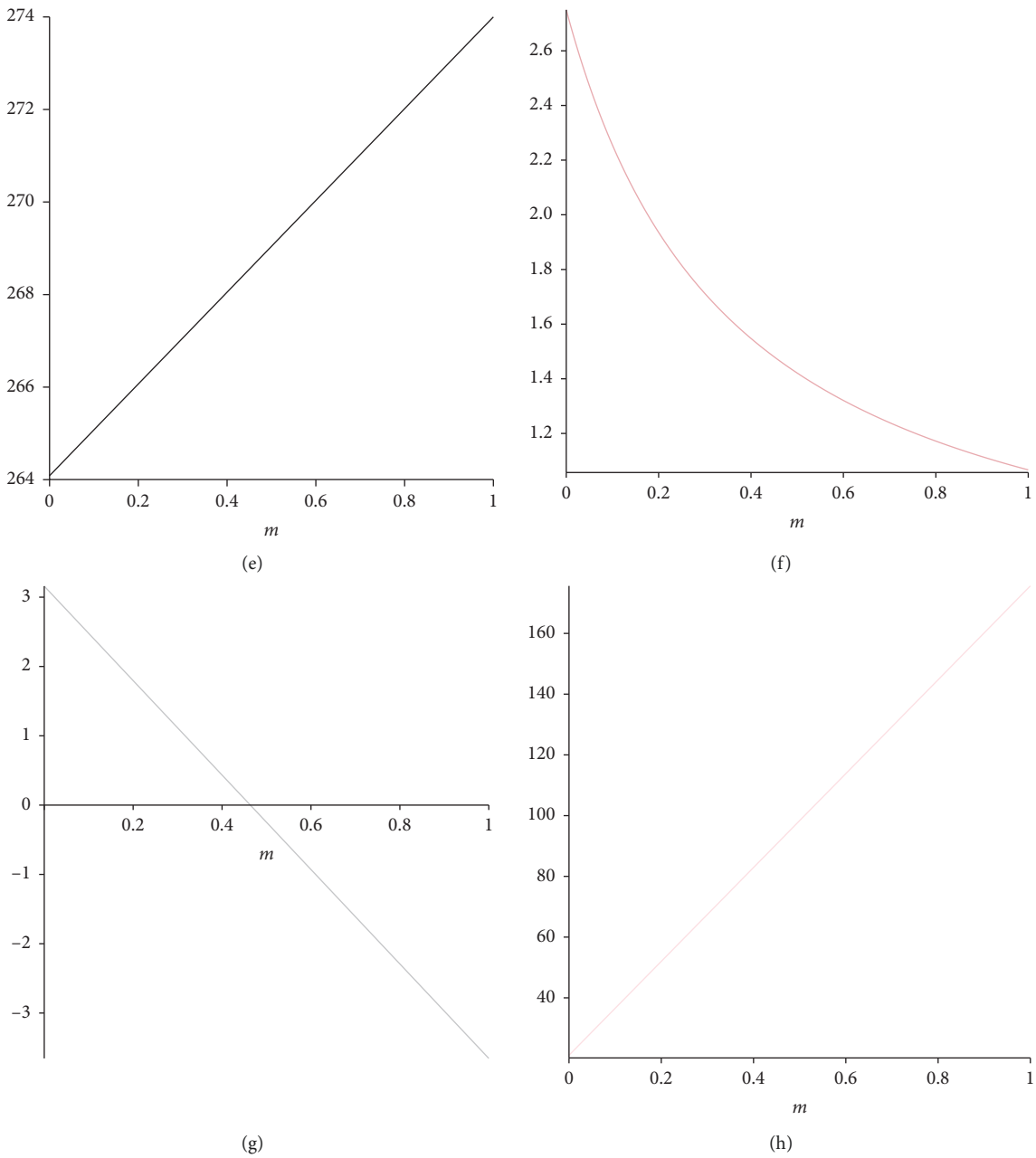

Figure 3: Continued.

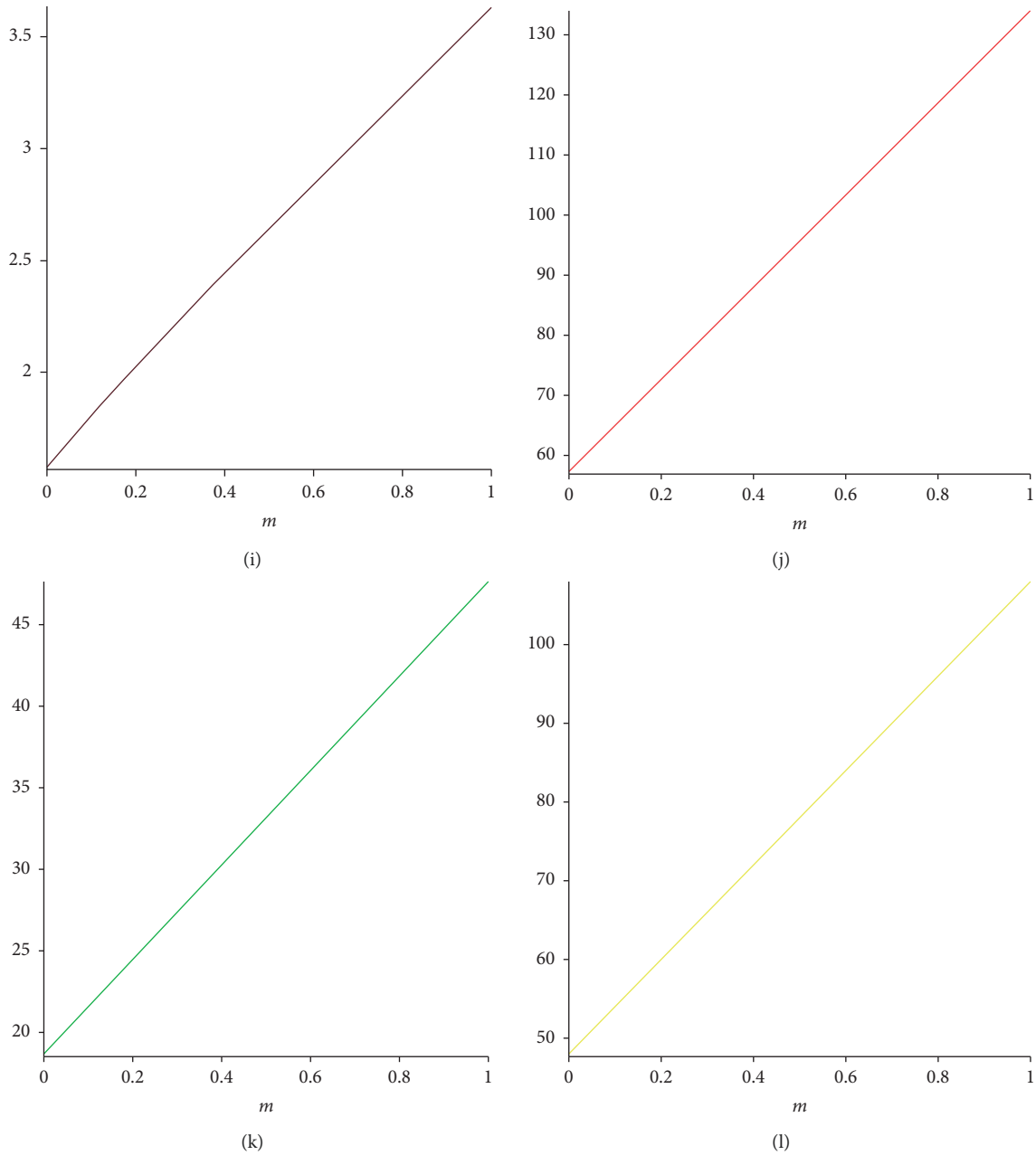

Figure 3: Continued.

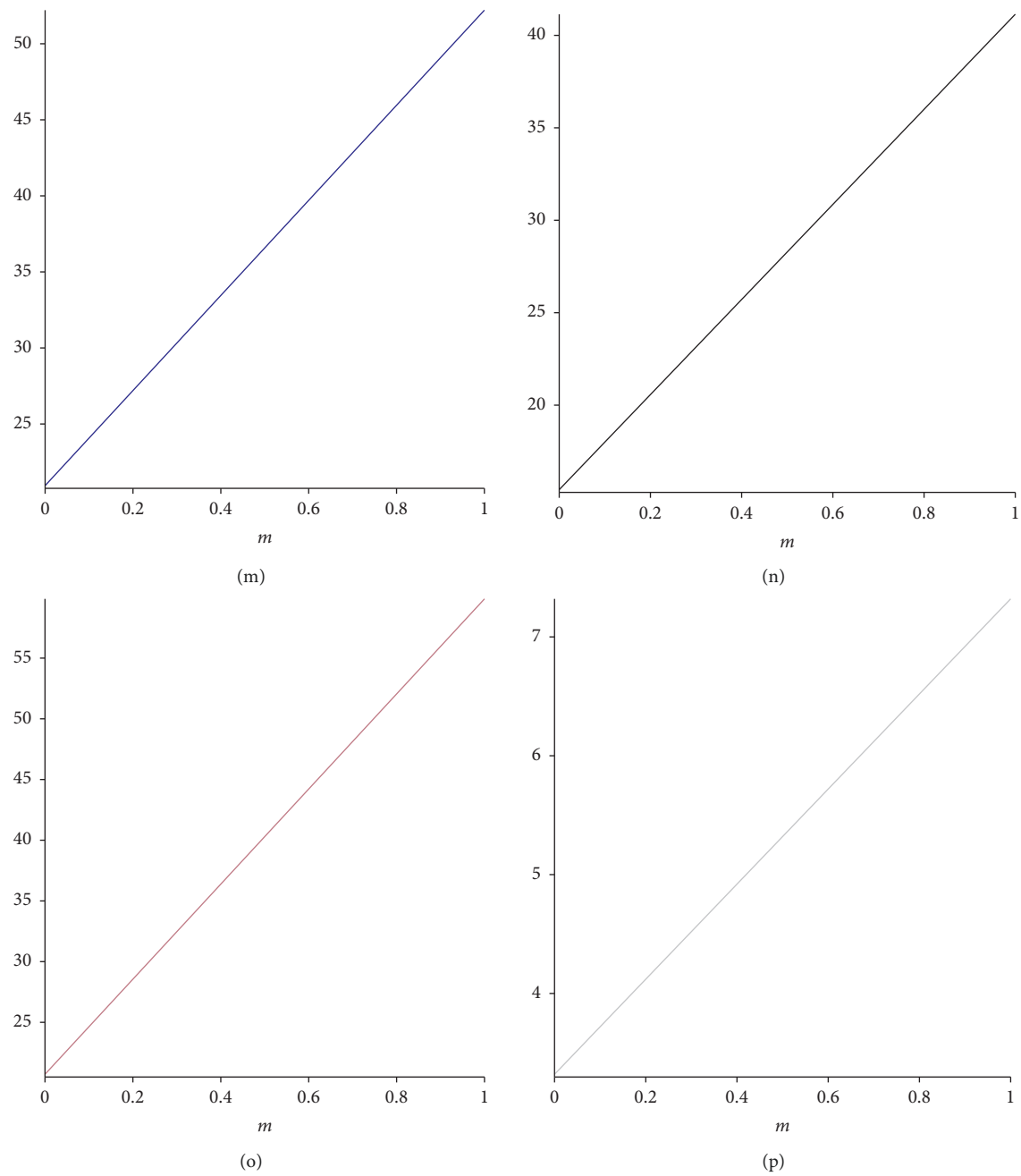

Figure 3: (a) VAR $(m - \mathrm{BiI}_3)$; (b) AL $(m - \mathrm{BiI}_3)$; (c) IR1 $(m - \mathrm{BiI}_3)$; (d) IR2 $(m - \mathrm{BiI}_3)$; (e) IRF $(m - \mathrm{BiI}_3)$; (f) IRFW $(m - \mathrm{BiI}_3)$; (g) IRA $(m - \mathrm{BiI}_3)$; (h) IRB $(m - \mathrm{BiI}_3)$; (i) IRC $(m - \mathrm{BiI}_3)$; (j) IRDIF $(m - \mathrm{BiI}_3)$; (k) IRL $(m - \mathrm{BiI}_3)$; (l) IRLU $(m - \mathrm{BiI}_3)$; (m) IRLF $(m - \mathrm{BiI}_3)$; (n) IRLA $(m - \mathrm{BiI}_3)$; (o) IRD1 $(m - \mathrm{BiI}_3)$; (p) IRGA $(m - \mathrm{BiI}_3)$.

$n))| = 11mn + 10m + 7n + 2$ and $|E(\mathrm{BiI}_3(m \times n))| = 18mn + 12m + 6n$. There are two types of edges in edge set present in bismuth tri-iodide sheet $\mathrm{BiI}_3(m \times n)$, as given in Table 2.

Theorem 2. *Let $BiI_3(m \times n)$ be the bismuth tri-iodide sheet. The irregularity indices are*

(1) $\mathrm{VAR}(\mathrm{BiI}_3(m \times n)) = 2(177m^2n^2 + 392m^2n - 402mn^2 + 172m^2 - 288mn - 387n^2 + 72m - 104n - 4)/(11mn + 10m + 7n + 2)^2$

(2) $\mathrm{AL}(\mathrm{BiI}_3(m \times n)) = 66mn + 52m - 30n + 4$

(3) $\mathrm{IR1}(\mathrm{BiI}_3(m \times n)) = 2(1425m^2n^2 + 2868m^2n + 914mn^2 + 1236m^2 + 712mn - 1007n^2 + 456m - 460n - 12)/(11mn + 10m + 7n + 2)$

(4) $\mathrm{IR2}(\mathrm{BiI}_3(m \times n)) = (1/(\sqrt{18mn + 12m + 6n})(11mn + 10m + 7n + 2))[(\sqrt{252mn + 468m - 442n - 12})(11mn + 10m + 7n + 2) - 2(18mn + 12m + 6n)(\sqrt{18mn + 12m + 6n})]$

(5) $\mathrm{IRF}(\mathrm{BiI}_3(m \times n)) = 246mn + 228m - 82n + 36$

(6) $\mathrm{IRFW}(\mathrm{BiI}_3(m \times n)) = (246mn + 228m - 82n + 36)/(252mn + 120m - 180n - 24)$

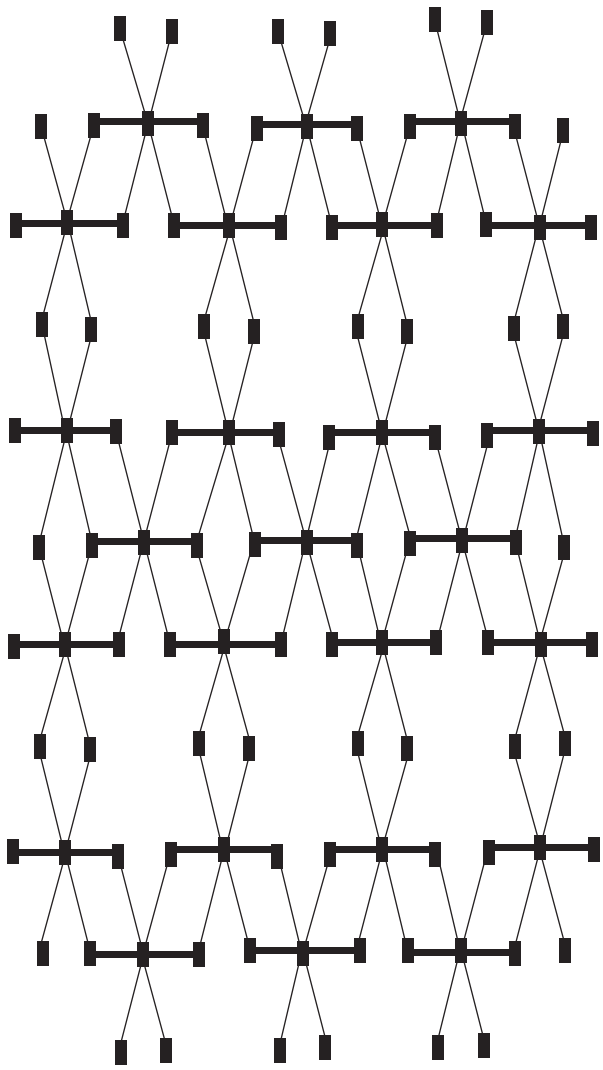

Figure 4: Sheet for $m = 2$ and $n = 3$ (bismuth tri-iodide).

Table 2: Partition of $E(\mathrm{BiI}_3(m \times n))$.

(d_u, d_v)	Frequency
(1, 6)	$4(m+n+1)$
(2, 6)	$4(3mn+2m+2n-1)$
(3, 6)	$6n(m-1)$

(7) $\mathrm{IRA}(\mathrm{BiI}_3(m \times n)) = (1/3)[(33 - 4\sqrt{3} - 2\sqrt{2})mn + (10 - 4\sqrt{6} - 8\sqrt{3})m + (21 - 2\sqrt{6} + 8\sqrt{3} + 5\sqrt{2})n + (6 - 2\sqrt{6} + 2\sqrt{3})]$

(8) $\mathrm{IRB}(\mathrm{BiI}_3(m \times n)) = (150 - 48\sqrt{3} - 36\sqrt{2})mn + (92 - 8\sqrt{3} - 4\sqrt{6})m - (90 - 4\sqrt{2} - 8\sqrt{3} + 2\sqrt{6})n - (4 - 2\sqrt{3} + 2\sqrt{6})$

(9) $\mathrm{IRC}(\mathrm{BiI}_3(m \times n)) = (((18\sqrt{(2)} + 24\sqrt{(3)})mn + (2\sqrt{(6)} + 4\sqrt{(3)})m - (2\sqrt{(2)} + 4\sqrt{(3)} - \sqrt{(6)})n + \sqrt{(6)} - \sqrt{(3)})/(18mn + 12m + 6n)) - (2(18mn + 12m + 6n)/(11mn + 10m + 7n + 2))$

(10) $\mathrm{IRDIF}(\mathrm{BiI}_3(m \times n)) = (1/3)(123mn + 134m - 21n + 38)$

(11) $\mathrm{IRL}(\mathrm{BiI}_3(m \times n)) = 17.22mn + 15.88m - 5.70n + 2.80$

(12) $\mathrm{IRLU}(\mathrm{BiI}_3(m \times n)) = 30mn + 36m - 2n + 12$

(13) $\mathrm{IRLF}(\mathrm{BiI}_3(m \times n)) = (1/3)[(9\sqrt{2} + 24\sqrt{3})mn + (10\sqrt{6} + 16\sqrt{3})m + (10\sqrt{6} - 16\sqrt{3} - 9\sqrt{2})n + (10\sqrt{6} - 8\sqrt{3})]$

(14) $\mathrm{IRLA}(\mathrm{BiI}_3(m \times n)) = (1/7)(112mn + 64m - 76n - 20)$

(15) $\mathrm{IRD1}(\mathrm{BiI}_3(m \times n)) = 27.48mn + 19.96m - 13.92n + 0.76$

(16) $\mathrm{IRGA}(\mathrm{BiI}_3(m \times n)) = 1.86mn + 2.44m + 0.06n + 0.88$

Proof

$$\begin{aligned}\mathrm{VAR}\left(\mathrm{BiI}_3\left(m\times n\right)\right) &= \sum_{u\in V}\left(d_u-\frac{2m}{n}\right)^2=\frac{M_1\left(\mathrm{BiI}_3\left(m\times n\right)\right)}{n}-\left(\frac{2m}{n}\right)^2\\ &=\left(\frac{150mn+92m-90n-4}{11mn+10m+7n+2}\right)-\left(\frac{2\left(18mn+12m+6n\right)}{11mn+10m+7n+2}\right)^2\\ &=\frac{1}{\left(11mn+10m+7n+2\right)^2}\left(2\left(177m^2n^2+392m^2n-402mn^2\right.\right.\\ &\quad\left.\left.+172m^2-288mn-387n^2+72m-104n-4\right)\right),\end{aligned} \tag{17}$$

$$\begin{aligned}\mathrm{AL}\left(\mathrm{BiI}_3\left(m\times n\right)\right) &= \sum_{uv\in E\left(\mathrm{BiI}_3\left(m\times n\right)\right)}\left|d_u-d_v\right|\\ &=\left|1-6\right|\left(4m+4n+4\right)+\left|1-3\right|\left(1\right)+\left|2-6\right|\left(12mn+8m+8n-4\right)\\ &\quad+\left|3-6\right|\left(6mn-6n\right)=66mn+52m-30n+4,\end{aligned} \tag{18}$$

$$\begin{aligned}\mathrm{IR1}\left(\mathrm{BiI}_3\left(m\times n\right)\right) &= \sum_{u\in V)}d_u^3-\frac{2m}{n}\sum_{u\in V)}d_u^2=F\left(G\right)-\frac{2m}{n}M_1\left(\mathrm{BiI}_3\left(m\times n\right)\right)\\ &=\left(750mn+468m-442n-12\right)\\ &\quad-\left(\frac{2\left(18mn+12m+6n\right)}{11mn+10m+7n+2}\right)\left(150mn+92m-90n-4\right)\\ &=\frac{1}{11mn+10m+7n+2}\left(2\left(1425m^2n^2+2868m^2n\right.\right.\\ &\quad\left.\left.+914mn^2+1236m^2+712mn-1007n^2+456m-460n-12\right)\right),\end{aligned} \tag{19}$$

$$\begin{aligned}\mathrm{IR2}\left(\mathrm{BiI}_3\left(m\times n\right)\right) &= \sqrt{\frac{\sum_{uv\in E\left(\mathrm{BiI}_3\left(m\times n\right)\right)}d_ud_v}{m}}-\frac{2m}{n}=\sqrt{\frac{M_2\left(\mathrm{BiI}_3\left(m\times n\right)\right)}{m}}-\frac{2m}{n}\\ &=\sqrt{\frac{252mn+120m+180n-24}{18mn+12m+6n}}-\frac{2\left(18mn+12m+6n\right)}{11mn+10m+7n+2}\\ &=\frac{1}{\left(\sqrt{18mn+12m+6n}\right)\left(11mn+10m+7n+2\right)}\\ &\quad\cdot\left[\left(\sqrt{252mn+468m-442n-12}\right)\left(11mn+10m+7n+2\right)\right.\\ &\quad\left.-2\left(18mn+12m+6n\right)\left(\sqrt{18mn+12m+6n}\right)\right],\end{aligned} \tag{20}$$

$$\begin{aligned}\mathrm{IRF}\left(\mathrm{BiI}_3\left(m\times n\right)\right) &= \sum_{uv\in E\left(\mathrm{BiI}_3\left(m\times n\right)\right)}\left(d_u-d_v\right)^2\\ &=\left(1-6\right)^2\left(4m+4n+4\right)+\left(2-6\right)^2\\ &\quad\cdot\left(12mn=8m+8n-4\right)+\left(3-6\right)^2\left(6mn-6n\right)\\ &=246mn+228m-82n+36,\end{aligned} \tag{21}$$

$$\begin{aligned}\mathrm{IRFW}\left(\mathrm{BiI}_3\left(m\times n\right)\right) &= \frac{\left(\mathrm{IRF}\left(m\times n\right)\right)}{M_2\left(\mathrm{BiI}_3\left(m\times n\right)\right)}\\ &=\frac{246mn+228m-82n+36}{252mn+120m-180-24},\end{aligned} \tag{22}$$

$$\begin{aligned}\mathrm{IRA}\left(\mathrm{BiI}_3(m\times n)\right) &= \sum_{uv\in E\left(\mathrm{BiI}_3(m\times n)\right)}\left(d_u^{-1/2}-d_v^{-1/2}\right)^2 = n-2R(G)\\ &= (11mn+10m+7n+2)-\frac{2}{3}\left((\sqrt{2}+2\sqrt{3})mn\right.\\ &\quad +(2\sqrt{6}+\sqrt{3})m-(2\sqrt{2}+4\sqrt{3}-\sqrt{6})n\\ &\quad \left.+(\sqrt{6}-\sqrt{3})\right)=\frac{1}{3}\left((33-4\sqrt{3}-2\sqrt{2})mn\right.\\ &\quad +(10-4\sqrt{6}-8\sqrt{3})m+(21-2\sqrt{6}+8\sqrt{3}\\ &\quad \left.+5\sqrt{2})n+(6-2\sqrt{6}+2\sqrt{3})\right),\end{aligned} \tag{23}$$

$$\begin{aligned}\mathrm{IRB}\left(\mathrm{BiI}_3(m\times n)\right) &= \sum_{uv\in E\left(\mathrm{BiI}_3(m\times n)\right)}\left(d_u^{1/2}-d_v^{1/2}\right)^2 = M_1(G)-2\mathrm{RR}(G)\\ &= (252mn+120m-180n-24)-[(24\sqrt{3}+18\sqrt{2})mn\\ &\quad +(4\sqrt{6}+16\sqrt{3})m+(4\sqrt{6}-16\sqrt{3}-18\sqrt{2})n\\ &\quad +(4\sqrt{6}-8\sqrt{3})]=(150-48\sqrt{3}-36\sqrt{2})mn\\ &\quad +(92-8\sqrt{3}-4\sqrt{6})m-(90-4\sqrt{2}-8\sqrt{3}\\ &\quad +2\sqrt{6})n-(4-2\sqrt{3}+2\sqrt{6}),\end{aligned} \tag{24}$$

$$\begin{aligned}\mathrm{IRC}\left(\mathrm{BiI}_3(m\times n)\right) &= \frac{\sum_{uv\in E\left(\mathrm{BiI}_3(m\times n)\right)}\sqrt{d_u d_v}}{m}-\frac{2m}{n}\\ &= \frac{\mathrm{RR}\left(\mathrm{BiI}_3(m\times n)\right)}{m}-\frac{2m}{n}\\ &= \frac{1}{18mn+12m+6n}\left((24\sqrt{3}+18\sqrt{2})mn+(4\sqrt{6}\right.\\ &\quad +16\sqrt{3})m+(4\sqrt{6}-16\sqrt{3}-18\sqrt{2})n\\ &\quad \left.+(4\sqrt{6}-8\sqrt{3})-\frac{2(18mn+12m+6n)}{11mn+10m+7n+2}\right),\end{aligned} \tag{25}$$

$$\begin{aligned}\mathrm{IRDIF}\left(\mathrm{BiI}_3(m\times n)\right) &= \sum_{uv\in E\left(\mathrm{BiI}_3(m\times n)\right)}\left|\frac{d_u}{d_v}-\frac{d_v}{d_u}\right|\\ &= \left|\frac{1}{6}-\frac{6}{1}\right|(4m+4n+4)+\left|\frac{2}{6}-\frac{6}{2}\right|(12mn\\ &\quad +8m+8n-4)+\left|\frac{3}{6}-\frac{6}{3}\right|(6mn\\ &\quad -6n)=\frac{1}{3}(123mn+134m-21n+38),\end{aligned} \tag{26}$$

$$\begin{aligned}\mathrm{IRL}\left(\mathrm{BiI}_3(m\times n)\right) &= \sum_{uv\in E\left(\mathrm{BiI}_3(m\times n)\right)}\left|\ln d_u-\ln d_v\right|\\ &= |\ln 1-\ln 6|(4m+4n+4)+|\ln 2-\ln 3|\\ &\quad \cdot(12mn+8m+8n-4)+|\ln 3-\ln 6|(6mn-6n)\\ &= 17.22mn+15.88m-5.70n+2.80,\end{aligned} \tag{27}$$

$$\begin{aligned}\mathrm{IRLU}\left(\mathrm{BiI}_3(m\times n)\right) &= \sum_{uv\in E\left(\mathrm{BiI}_3(m\times n)\right)} \frac{\left|d_u-d_v\right|}{\min\left(d_u,d_v\right)}\\ &= \left(\frac{|1-6|}{1}\right)(4m+4n+4)+\left(\frac{|2-6|}{2}\right)\\ &\quad\cdot(12mn+8m+8n-4)+\left(\frac{|3-6|}{3}\right)(6mn-6n)\\ &= 30mn+36m-2n+12,\end{aligned} \tag{28}$$

$$\begin{aligned}\mathrm{IRLF}\left(\mathrm{BiI}_3(m\times n)\right) &= \sum_{uv\in E\left(\mathrm{BiI}_3(m\times n)\right)} \frac{\left|d_u-d_v\right|}{\sqrt{d_u\cdot d_v}}\\ &= \left(\frac{|1-6|}{\sqrt{6}}\right)(4m+4n+4)+\left(\frac{|2-6|}{\sqrt{12}}\right)\\ &\quad\cdot(12mn+8m+8n-4)+\left(\frac{|3-6|}{\sqrt{18}}\right)(6mn-6n)\\ &= \frac{1}{3}\left[(9\sqrt{2}+24\sqrt{3})mn+(10\sqrt{6}+16\sqrt{3})m\right.\\ &\quad\left.+(10\sqrt{6}-16\sqrt{3}-9\sqrt{2})n+(10\sqrt{6}-8\sqrt{3})\right],\end{aligned} \tag{29}$$

$$\begin{aligned}\mathrm{IRLA}\left(\mathrm{BiI}_3(m\times n)\right) &= \sum_{uv\in E\left(\mathrm{BiI}_3(m\times n)\right)} 2\frac{\left|d_u-d_v\right|}{\left(d_u+d_v\right)}\\ &= 2\left(\frac{|1-6|}{1+6}\right)(4m+4n+4)+2\left(\frac{|2-6|}{2+6}\right)\\ &\quad\cdot(12mn+8m+8n-4)+2\left(\frac{|3-6|}{3+6}\right)(6mn-6n)\\ &= \frac{1}{7}(112mn+64m-76n-20),\end{aligned} \tag{30}$$

$$\begin{aligned}\mathrm{IRD1}\left(\mathrm{BiI}_3(m\times n)\right) &= \sum_{uv\in E\left(\mathrm{BiI}_3(m\times n)\right)} \ln\left\{1+\left|d_u-d_v\right|\right\}\\ &= \ln\{1+|1-6|\}(4m+4n+4)+\ln\{1+|2-6|\}\\ &\quad\cdot(12mn+8m+8n-4)+\ln\{1+|3-6|\}(6mn-6n)\\ &= 27.48mn+19.96m-13.92n+0.76,\end{aligned} \tag{31}$$

$$\begin{aligned}\mathrm{IRGA}\left(\mathrm{BiI}_3(m\times n)\right) &= \sum_{uv\in E\left(\mathrm{BiI}_3(m\times n)\right)} \ln\left(\frac{d_u+d_v}{2\sqrt{d_u d_v}}\right)\\ &= \ln\left(\frac{1+6}{2\sqrt{1\times 6}}\right)(4m+4m+4)+\ln\left(\frac{2+6}{2\sqrt{2\times 6}}\right)\\ &\quad\cdot(12mn+8m+8n-4)+\ln\left(\frac{3+6}{2}\sqrt{3\times 6}\right)(6mn-6n)\\ &= 1.86mn+2.44m+0.06n+0.88.\end{aligned} \tag{32}$$

□

4.1. Graphical Representation of Bismuth Tri-Iodide Sheet $BiI_3(m\times n)$. Here, we will graphically present results of irregularity indices for bismuth tri-iodide sheet $\mathrm{BiI}_3(m\times n)$. From these plots, one can observe the behavior of computed results on the involved parameters (Figure 5).

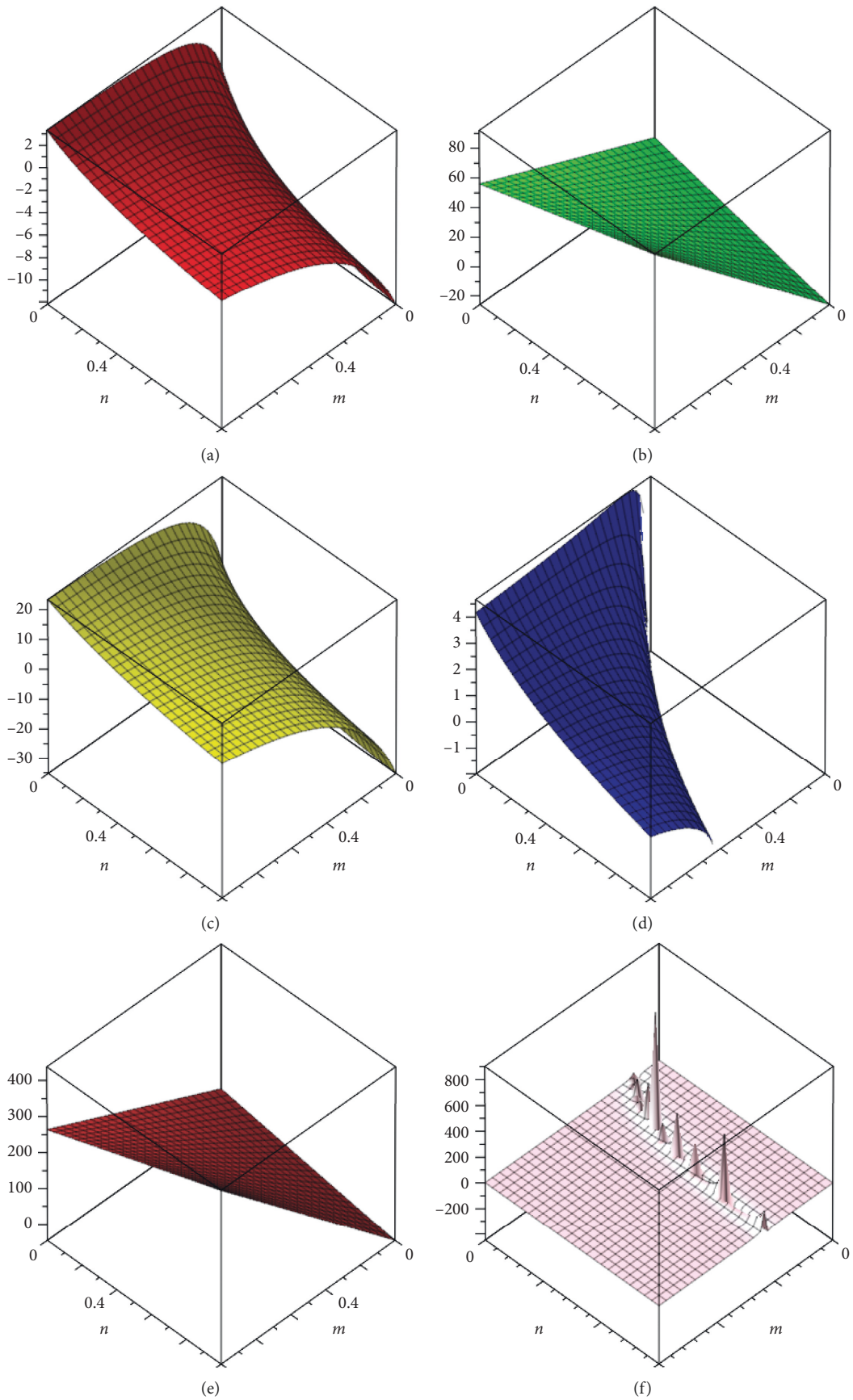

Figure 5: Continued.

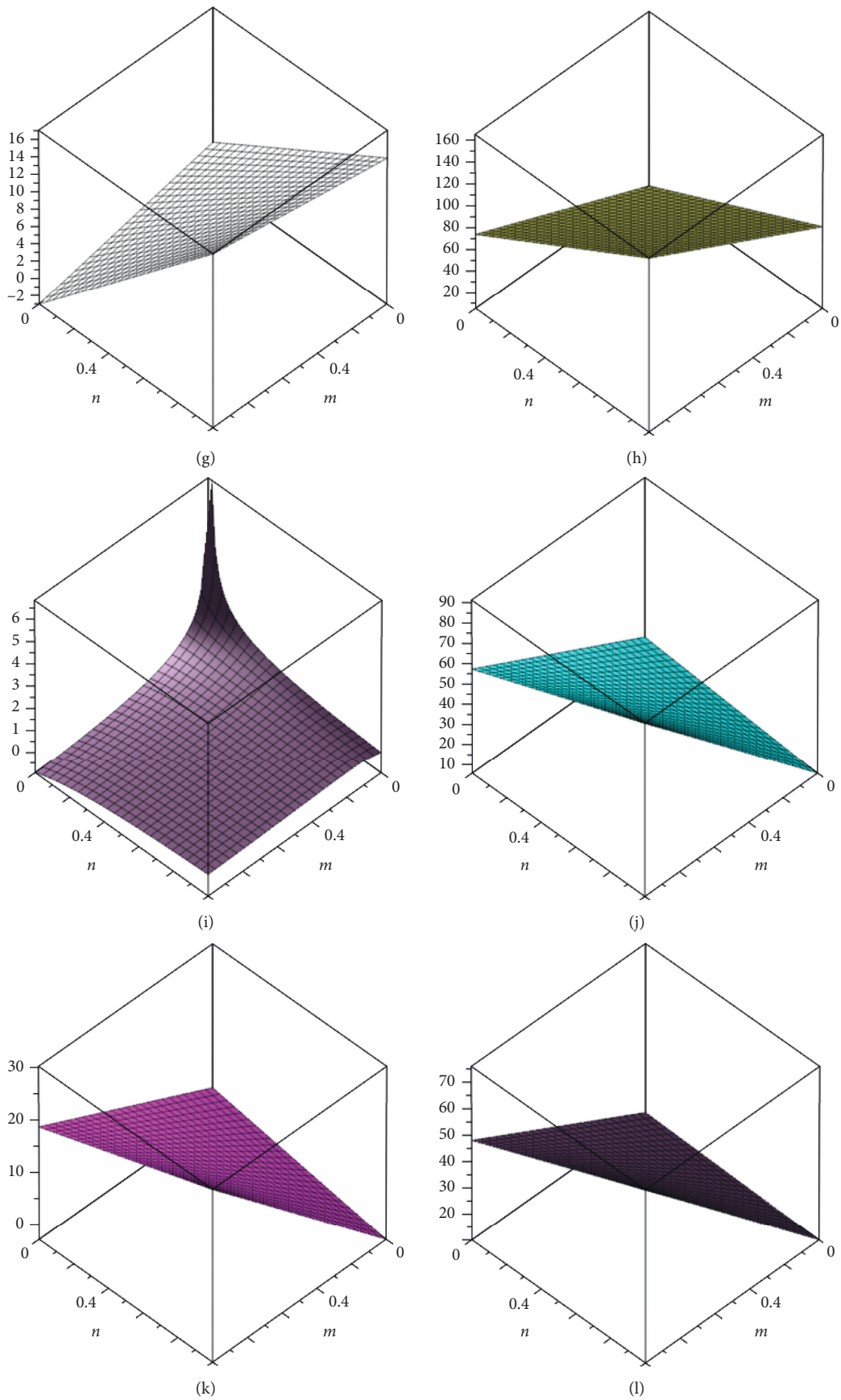

Figure 5: Continued.

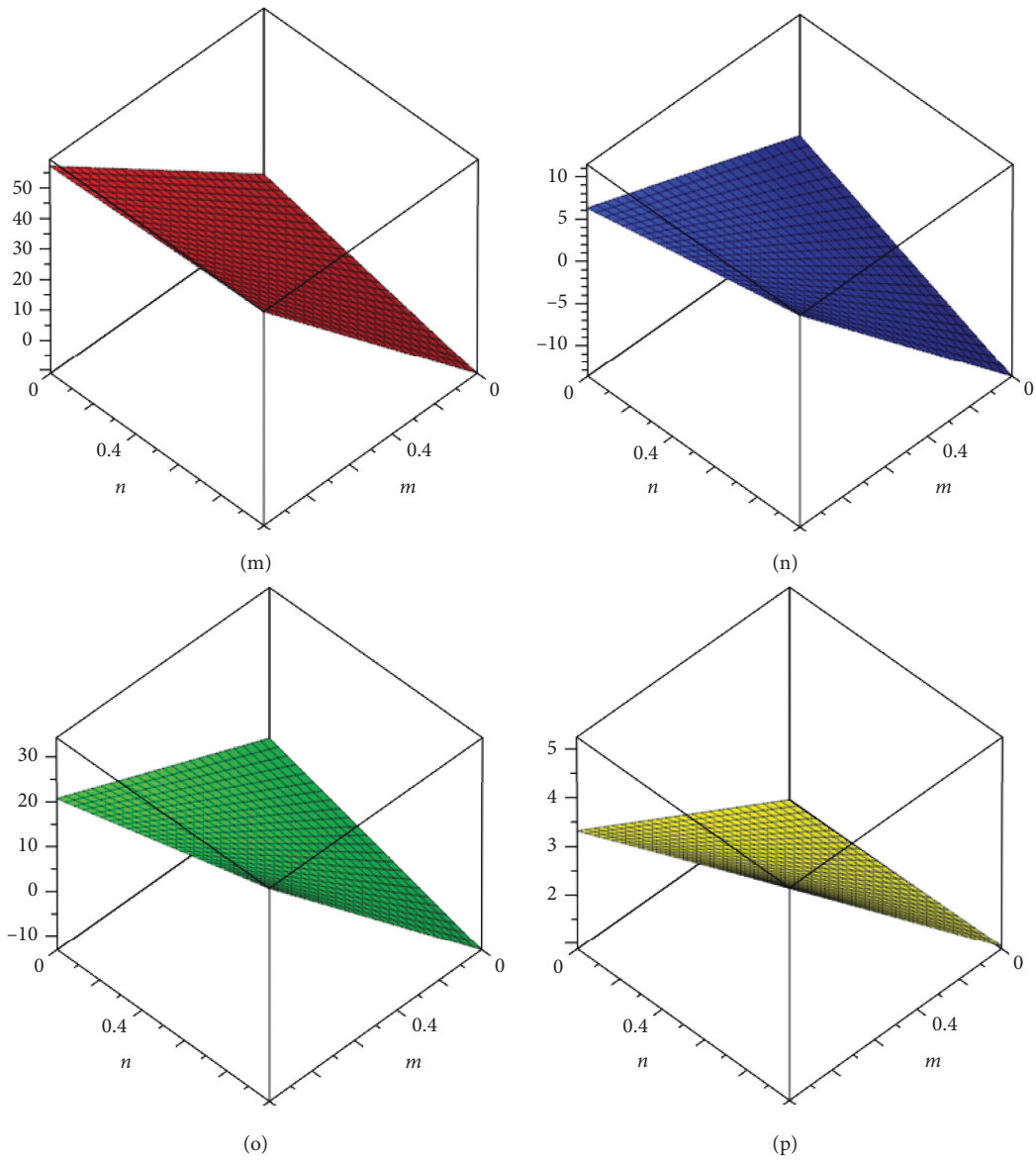

Figure 5: (a) VAR$(m-\mathrm{BiI_3})$; (b) AL$(m-\mathrm{BiI_3})$; (c) IR1$(m-\mathrm{BiI_3})$; (d) IR2$(m-\mathrm{BiI_3})$; (e) IRF$(m-\mathrm{BiI_3})$; (f) IRFW$(m-\mathrm{BiI_3})$; (g) IRA$(m-\mathrm{BiI_3})$; (h) IRB$(m-\mathrm{BiI_3})$; (i) IRC$(m-\mathrm{BiI_3})$; (j) IRDIF$(m-\mathrm{BiI_3})$; (k) IRL$(m-\mathrm{BiI_3})$; (l) IRLU$(m-\mathrm{BiI_3})$; (m) IRLF$(m-\mathrm{BiI_3})$; (n) IRLA$(m-\mathrm{BiI_3})$; (o) IRD1$(m-\mathrm{BiI_3})$; (p) IRGA$(m-\mathrm{BiI_3})$.

5. Conclusion

TIs are used to see the properties of concerned compound without going to wet lab. In the present paper, we have computed several degree-based TIs. All these indices are useful in QSPR and QSAR. Our results can help to guess properties of bismuth tri-iodide chain and sheet. Computing distance-based TIs is an interesting problem.

Data Availability

The data used to support the findings of this study are included within the article.

Conflicts of Interest

The authors declare that there are no conflicts of interest.

Authors' Contributions

All authors contributed equally in this paper.

Acknowledgments

The work was supported by the Natural Science Foundation of Shanghai (no. 17ZR1419900) and Xu Lun Scholars Programme, Shanghai Lixin University of Accounting and

Finance. The authors are thankful to Professor Chahn Yong Jung for his guidelines and expert opinion in writing this paper.

References

[1] W. Gao, H. Wu, M. K. Siddiqui, and A. Q. Baig, "Study of biological networks using graph theory," *Saudi Journal of Biological Sciences*, vol. 25, no. 6, pp. 1212–1219, 2018.

[2] K. Yang, Z. Yu, Y. Luo, Y. Yang, L. Zhao, and X. Zhou, "Spatial and temporal variations in the relationship between lake water surface temperatures and water quality—a case study of Dianchi Lake," *Science of the Total Environment*, vol. 624, pp. 859–871, 2018.

[3] W. Gao, W. Wang, D. Dimitrov, and Y. Wang, "Nano properties analysis via fourth multiplicative ABC indicator calculating," *Arabian Journal of Chemistry*, vol. 11, no. 6, pp. 793–801, 2018.

[4] W. Gao, J. L. G. Guirao, M. Abdel-Aty, and W. Xi, "An independent set degree condition for fractional critical deleted graphs," *Discrete and Continuous Dynamical Systems-S*, vol. 12, 2018.

[5] B. Bollobás and P. Erdös, "Graphs of extremal weights," *Ars Combinatoria*, vol. 50, pp. 225–233, 1998.

[6] W. Gao, W. Wang, M. K. Jamil, and M. R. Farahani, "Electron energy studying of molecular structures via forgotten topological index computation," *Journal of Chemistry*, vol. 2016, Article ID 1053183, 7 pages, 2016.

[7] M. Naeem, M. K. Siddiqui, J. L. G. Guirao, and W. Gao, "New and modified eccentric indices of octagonal grid Omn," *Applied Mathematics and Nonlinear Sciences*, vol. 3, no. 1, pp. 209–228, 2018.

[8] W. Gao and M. R. Farahani, "Degree-based indices computation for special chemical molecular structures using edge dividing method," *Applied Mathematics and Nonlinear Sciences*, vol. 1, no. 1, pp. 99–122, 2016.

[9] W. Gao, M. R. Farahani, and L. Shi, "Forgotten topological index of some drug structures," *Acta Medica Mediterranea*, vol. 32, no. 1, pp. 579–585, 2016.

[10] M. Ghorbani and M. Ghazi, "Computing some topological indices of Triangular Benzenoid," *Digest Journal of Nanomaterials and Biostructures*, vol. 5, no. 4, pp. 1107–1111, 2010.

[11] D. Amić, D. Bešlo, B. Lučić, S. Nikolić, and N. Trinajstic, "The vertex-connectivity index revisited," *Journal of Chemical Information and Computer Sciences*, vol. 38, no. 5, pp. 819–822, 1998.

[12] I. Gutman, "Some properties of the Wiener polynomial," *Graph Theory Notes New York*, vol. 125, pp. 13–18, 1993.

[13] E. Deutsch and S. Klavzar, "M-polynomial and degree-based topological indices," *Iranian Journal of Mathematical Chemistry*, vol. 6, pp. 93–102, 2015.

[14] M. Ajmal, W. Nazeer, M. Munir, S. M. Kang, and C. Y. Jung, "The M-polynomials and topological indices of generalized prism network," *International Journal of Mathematical Analysis*, vol. 11, no. 6, pp. 293–303, 2017.

[15] M. Munir, W. Nazeer, Z. Shahzadi, and S. Kang, "Some invariants of circulant graphs," *Symmetry*, vol. 8, no. 11, p. 134, 2016.

[16] H. Wiener, "Structural determination of paraffin boiling points," *Journal of the American Chemical Society*, vol. 69, no. 1, pp. 17–20, 1947.

[17] A. A. Dobrynin, R. Entringer, and I. Gutman, "Wiener index of trees: theory and applications," *Acta Applicandae Mathematicae*, vol. 66, no. 3, pp. 211–249, 2001.

[18] I. Gutman and O. E. Polansky, *Mathematical Concepts in Organic Chemistry*, Springer Science & Business Media, Berlin, Germany, 2012.

[19] M. Randic, "Characterization of molecular branching," *Journal of the American Chemical Society*, vol. 97, no. 23, pp. 6609–6615, 1975.

[20] D. Amic, D. Bešlo, B. Luccić, S. Nikolic, and N. Trinajstic, "The vertex-connectivity index revisited," *Journal of Chemical Information and Computer Sciences*, vol. 38, no. 5, pp. 819–822, 1998.

[21] Y. Hu, X. Li, Y. Shi, T. Xu, and I. Gutman, "On molecular graphs with smallest and greatest zeroth-order general Randić index," *MATCH Communications in Mathematical and in Computer Chemistry*, vol. 54, no. 2, pp. 425–434, 2005.

[22] G. Caporossi, I. Gutman, P. Hansen, and L. Pavlović, "Graphs with maximum connectivity index," *Computational Biology and Chemistry*, vol. 27, no. 1, pp. 85–90, 2003.

[23] X. Li and I. Gutman, *Mathematical Chemistry Monographs No. 1*, University of Kragujevac, Kragujevac, Serbia, 2006.

[24] X. Li, I. Gutman, and M. Randić, *Mathematical Aspects of Randić-Type Molecular Structure Descriptors*, University of Kragujevac and Faculty of Science Kragujevac, Kragujevac, Serbia, 2006.

[25] I. Gutman, B. Furtula, and C. Elphick, "Three new/old vertex-degree-based topological indices," *MATCH Communications in Mathematical and in Computer Chemistry*, vol. 72, no. 3, pp. 617–632, 2014.

[26] X. Li and Y. Shi, "A survey on the Randić index," *MATCH Communications in Mathematical and in Computer Chemistry*, vol. 59, no. 1, pp. 127–156, 2008.

[27] S. Nikolić, G. Kovačević, A. Miličević, and N. Trinajstic, "The Zagreb indices 30 years after," *Croatica Chemica Acta*, vol. 76, no. 2, pp. 113–124, 2003.

[28] I. Gutman and K. C. Das, "The first Zagreb index 30 years after," *MATCH Communications in Mathematical and in Computer Chemistry*, vol. 50, no. 1, pp. 83–92, 2004.

[29] W. Gao, Y. Wang, W. Wang, and L. Shi, "The first multiplication atom-bond connectivity index of molecular structures in drugs," *Saudi Pharmaceutical Journal*, vol. 25, no. 4, pp. 548–555, 2017.

[30] D. Vukičević and A. Graovac, "Valence connectivity versus Randić, Zagreb and modified Zagreb index: a linear algorithm to check discriminative properties of indices in acyclic molecular graphs," *Croatica Chemica Acta*, vol. 77, no. 3, pp. 501–508, 2004.

[31] A. Miličević, S. Nikolić, and N. Trinajstic, "On reformulated Zagreb indices," *Molecular Diversity*, vol. 8, no. 4, pp. 393–399, 2004.

[32] C. K. Gupta, V. Lokesha, S. B. Shwetha, and P. S. Ranjini, "On the symmetric division deg index of graph," *Southeast Asian Bulletin of Mathematics*, vol. 40, no. 1, 2016.

[33] O. Favaron, M. Mahéo, and J. F. Saclé, "Some eigenvalue properties in graphs (conjectures of Graffiti II)," *Discrete Mathematics*, vol. 111, no. 1–3, pp. 197–220, 1993.

[34] A. T. Balaban, "Highly discriminating distance-based topological index," *Chemical Physics Letters*, vol. 89, no. 5, pp. 399–404, 1982.

[35] S. M. Hosamani, V. Lokesha, I. N. Cangul, and K. M. Devendraiah, "On certain topological indices of the derived graphs of subdivision graphs," *TWMS Journal of Applied and Engineering Mathematics*, vol. 6, no. 2, p. 324, 2016.

[36] M. Imran, M. Ali, S. Ahmad, M. Siddiqui, and A. Baig, "Topological characterization of the symmetrical structure of bismuth tri-iodide," *Symmetry*, vol. 10, no. 6, p. 201, 2018.
[37] S. P. Parker, *McGraw-Hill Dictionary of Scientific and Technical Terms*, McGraw-Hill Book Co, New York, NY, USA, 1989.
[38] J.-B. Liu, M. Siddiqui, M. Zahid, M. Naeem, and A. Baig, "Topological properties of crystallographic structure of molecules," *Symmetry*, vol. 10, no. 7, p. 265, 2018.
[39] L. E. Smart and E. A. Moore, *Solid State Chemistry: An Introduction*, CRC Press, Boca Raton, FL, USA, 2016.
[40] K. Watanabe, T. Karasawa, T. Komatsu, and Y. Kaifu, "Optical properties of extrinsic two-dimensional excitons in BiI_3 single crystals," *Journal of the Physical Society of Japan*, vol. 55, no. 3, pp. 897–907, 1986.
[41] J. P. Glusker, M. Lewis, and M. Rossi, *Crystal Structure Analysis for Chemists and Biologists*, Vol. 16, John Wiley & Sons, Hoboken, NJ, USA, 1994.
[42] H. Yorikawa and S. Muramatsu, "Theoretical study of crystal and electronic structures of BiI_3," *Journal of Physics: Condensed Matter*, vol. 20, no. 32, Article ID 325220, 2008.
[43] D. Nason and L. Keller, "The growth and crystallography of bismuth tri-iodide crystals grown by vapor transport," *Journal of Crystal Growth*, vol. 156, no. 3, pp. 221–226, 1995.
[44] T. Réti, R. Sharafdini, A. Dregelyi-Kiss, and H. Haghbin, "Graph irregularity indices used as molecular descriptors in QSPR studies," *MATCH Communications in Mathematical and in Computer Chemistry*, vol. 79, pp. 509–524, 2018.
[45] B. Basavanagoud, W. Gao, S. Patil, V. R. Desai, K. G. Mirajkar, and B. Pooja, "Computing first Zagreb index and F-index of new C-products of graphs," *Applied Mathematics and Nonlinear Sciences*, vol. 2, no. 1, pp. 285–298, 2017.
[46] V. Lokesha, T. Deepika, P. S. Ranjini, and I. N. Cangul, "Operations of Nanostructures via SDD, ABC4 and GA5 indices indices," *Applied Mathematics and Nonlinear Sciences*, vol. 2, no. 1, pp. 173–180, 2017.
[47] S. M. Hosamani, B. B. Kulkarni, R. G. Boli, and V. M. Gadag, "QSPR analysis of certain graph theocratical matrices and their corresponding energy," *Applied Mathematics and Nonlinear Sciences*, vol. 2, no. 1, pp. 131–150, 2017.
[48] M. S. Sardar, S. Zafar, and Z. Zahid, "Computing topological indices of the line graphs of Banana tree graph and Firecracker graph," *Applied Mathematics and Nonlinear Sciences*, vol. 2, no. 1, pp. 83–92, 2017.
[49] B. Basavanagoud, V. R. Desai, and S. Patil, "(β, α)–connectivity index of graphs," *Applied Mathematics and Nonlinear Sciences*, vol. 2, no. 1, pp. 21–30, 2017.

Hindawi
Journal of Chemistry
Volume 2019, Article ID 5294198, 19 pages
https://doi.org/10.1155/2019/5294198

Research Article

Multiplicative Zagreb Indices of Molecular Graphs

Xiujun Zhang,[1] **H. M. Awais**,[2] **M. Javaid**,[2] **and Muhammad Kamran Siddiqui**[3]

[1]*School of Information Science and Engineering, Chengdu University, Chengdu 610106, China*
[2]*Department of Mathematics, School of Science, University of Management and Technology (UMT), Lahore 54770, Pakistan*
[3]*Department of Mathematics, COMSATS University Islamabad, Lahore Campus, Islamabad, Pakistan*

Correspondence should be addressed to M. Javaid; javaidmath@gmail.com

Received 1 November 2019; Accepted 19 November 2019; Published 6 December 2019

Academic Editor: Juan L. G. Guirao

Mathematical modeling with the help of numerical coding of graphs has been used in the different fields of science, especially in chemistry for the studies of the molecular structures. It also plays a vital role in the study of the quantitative structure activities relationship (QSAR) and quantitative structure properties relationship (QSPR) models. Todeshine et al. (2010) and Eliasi et al. (2012) defined two different versions of the 1st multiplicative Zagreb index as $\prod(\Gamma) = \prod_{p\in V(\Gamma)}[d_\Gamma(p)^2]$ and $\prod_1(\Gamma) = \prod_{pq\in E(\Gamma)}[d_\Gamma(p) + d_\Gamma(q)]$, respectively. In the same paper of Todeshine, they also defined the 2nd multiplicative Zagreb index as $\prod_2(\Gamma) = \prod_{pq\in E(\Gamma)}[d_\Gamma(p) \times d_\Gamma(q)]$. Recently, Liu et al. [IEEE Access; 7(2019); 105479–-105488] defined the generalized subdivision-related operations of graphs and obtained the generalized F-sum graphs using these operations. They also computed the first and second Zagreb indices of the newly defined generalized F-sum graphs. In this paper, we extend this study and compute the upper bonds of the first multiplicative Zagreb and second multiplicative Zagreb indices of the generalized F-sum graphs. At the end, some particular results as applications of the obtained results for alkane are also included.

1. Introduction

The numerical demonstration of a molecular graph can be assumed as a single number, commonly known as topological index (TI). There are many interesting and significant results about TIs to study the different properties of chemical compounds such as chromatographic retention times, heat of formation and evaporation, flash point, viscosity, freezing, boiling and melting point, octanol-water partition coefficient, surface tension, stability, temperature, density, weight, polarizability, connectivity, and solubility. Many medicines, crystalline and nanomaterials, that are used in numerous pharmaceutical industries are examined with the assistance of different TIs, see [1–7]. TIs also study QSPR and QSAR models that join molecular graphs to their molecular characteristics by means of statistical tools. For additional information, see [8–17].

In 1947, to investigate the paraffin's boiling point, Wiener utilized the distance-based TI [18]. Gutman and Trinajstić [19] determined a pair of degree-based first and second Zagreb indices. After this, different impressive TIs are introduced in molecular graph theory [20,21], but the degree-based TIs are famous than others, see [22].

In graph theory, the various operations on different graphs show an important role in the creation of advanced families of graphs, see [23,24]. Yan et al. [13] gave the idea of four operations S_1, R_1, Q_1, and T_1 of graphs and computed the Wiener index of the resultant graphs obtained by using these operations. Eliasi and Taeri [25] introduced the F_1-sum graphs $(\Gamma_{1+F_1}\Gamma_2)$ by using the cartesian product of graphs $F_1(\Gamma_1)$ and Γ_2, where Γ_1 and Γ_2 are the two simple graphs and $F_1(\Gamma_1)$ is obtained by using $F_1 \in \{S_1, R_1, Q_1, \& T_1\}$. They also determined the Wiener index of these F_1-sum graphs. Additionally, Deng et al. [26], Imran and Akhtar [27], Shirdel et al. [28], and Liu et al. [29] determined the 1st and 2nd Zagreb

indices, F-index, Hyper-Zagreb index, and the 1st general Zagreb index of F_1-sum graphs.

Recently, Liu et al. [30] defined the generalized form of the aforesaid four operations $\{S_k, R_k, Q_k,$ and T_k, for $k \geq 1$ integer$\}$. They also constructed the generalized F-sum graphs ($\Gamma_{1+F_k}\Gamma_2$ for $F_k \in \{S_k, R_k, Q_k, \& T_k\}$) and obtained the 1st and 2nd Zagreb indices. In this paper, we calculate the upper bounds of the 1st and 2nd multiplicative Zagreb indices of the F_k-sum graphs. The remaining article is organized as follows: Section 2 contains few definitions and terminologies, Section 3 covers the main results, and Section 4 includes applications and closing comments.

2. Preliminaries

A molecular graph $\Gamma = (V(\Gamma), E(\Gamma))$ has the node (vertex) set $V(\Gamma) = \{p_1, p_2, p_3, \ldots, p_n\}$ and the edge set $E(\Gamma) \subseteq V(\Gamma) \times V(\Gamma)$. The vertices in the molecular graphs are denoted as atoms, and bonds are denoted as edges. The order and size of a chemical structure is denoted as $|V(\Gamma)| = \mu$ and $|E(\Gamma)| = \omega$. The degree $(d_\Gamma(p))$ is the total edges that are incident on a node p. Throughout the paper, we study the finite, indirected, simple (without loops, isolated vertices, and multiple edges), and connected graphs. The well-known TIs are discussed as follows.

Definition 1. Let Γ be a graph, then the first and second Zagreb indices are defined as follows:

$$\begin{aligned} M_1(\Gamma) &= \sum_{pq \in E(\Gamma)} [d_\Gamma(p) + d_\Gamma(q)], \\ M_2(\Gamma) &= \sum_{pq \in E(\Gamma)} [d_\Gamma(p) \times d_\Gamma(q)]. \end{aligned} \tag{1}$$

Gutman and Trinajstić [19] defined these indices which are utilized to determine the structural base different characteristics of graphs like molecular complexity, energy, ZE-isomerism, chirality, connectivity, and heterosystems, as well as branching , see [15,31–36].

Definition 2. Let Γ be a graph, then the first and second multiplicative Zagreb indices are

$$\begin{aligned} \prod_1(\Gamma) &= \prod_{pq \in E(\Gamma)} [d_\Gamma(p) + d_\Gamma(q)], \\ \prod_2(\Gamma) &= \prod_{pq \in E(\Gamma)} [d_\Gamma(p) \times d_\Gamma(q)]. \end{aligned} \tag{2}$$

During the past two decades, various noteworthy applications regarding multiplicative Zagreb indices have been explained in detail, see [37–46] and the references cited therein. The resultant graphs under the four new generalized subdivision operations defined in [30] are given as follows:

(i) $S_k(\Gamma)$ is the generalized subdivided graph (Γ).

(ii) $R_k(\Gamma)$ is the generalized semitotal (point) graph.

(iii) $Q_k(\Gamma)$ is the generalized semitotal (line) graph.

(iv) $T_k(\Gamma)$ is the generalized total graph. For more details, see Figure 1.

Definition 3. Let Γ_1 and Γ_2 be two graphs, then$F_k \in \{S_k, R_k, Q_k, T_k\}$ and $F_k(\Gamma_1)$ be a new graph gained after using F_k on Γ_1 having an edge set $E(F_k(\Gamma_1))$ and vertex set $V(F_k(\Gamma_1))$. So, the generalized F-sum graph $(\Gamma_{1+F_k}\Gamma_2)$ is a graph having the vertex set $V(\Gamma_{1+F_k}\Gamma_2) = V(F_k(\Gamma_1)) \times V(\Gamma_2) = V(\Gamma_1) \cup E(\Gamma_1) \times V(\Gamma_2)$ in such a way that two vertices (p_1, q_1) and (p_2, q_2) of $V(\Gamma_{1+F_k}\Gamma_2)$ are adjacent if and only if $[p_1 = p_2 \in V(\Gamma_1)$ and $(q_1, q_2) \in E(\Gamma_2)]$ or $[q_1 = q_2 \in \Gamma_2$ and $(p_1, p_2) \in E(F_k(\Gamma_1))]$.

Thus, the generalized F-sum graph $\Gamma_{1+F_k}\Gamma_2$ contains $|V(\Gamma_2)|$ copies of new graphs $F_k(\Gamma_1)$ that are labeled with the vertex set of Γ_2. For further details, see Figures 2 and 3.

3. Main Results

Now, we calculate the key results of the multiplicative Zagreb indices for the different classes on graphs.

Theorem 1. *Let Γ_1, Γ_2 be two graphs with $|V(\Gamma_1)| = \mu_1$, $|V(\Gamma_2)| = \mu_2$, $|E(\Gamma_1)| = \omega_1$, and $|E(\Gamma_2)| = \omega_2$. For $\mu_1, \mu_2 \geq 4$and and $k \geq 1$, we have*

$$\begin{aligned} \prod_1(\Gamma_1 +_{S_k} \Gamma_2) &\leq \frac{1}{\mu_1\omega_2}[4\omega_1\omega_2 + \mu_1 M_1(\Gamma_2)]^{\mu_1\omega_2} \\ &\quad \times \frac{1}{2\omega_1\mu_2}[4\omega_1\omega_2 + \mu_2 M_1(S_1(\Gamma_1))]^{2\omega_1\mu_2} \\ &\quad \times \frac{1}{\omega_1\mu_2(k-1)}[4(k-1)\mu_2\omega_1]^{\omega_1\mu_2(k-1)}, \\ \prod_2(\Gamma_1 +_{S_k} \Gamma_2) &\leq \frac{1}{\mu_1\omega_2}[\omega_2 M_1(\Gamma_1) + 2\omega_1 M_1(\Gamma_2) + \mu_1 M_2(\Gamma_2)]^{\mu_1\omega_2} \\ &\quad \times \frac{1}{2\mu_2\omega_1}[\mu_2 M_2(S_1(\Gamma_1)) + 8\omega_1\omega_2]^{2\mu_2\omega_1} \\ &\quad \times \frac{1}{(k-1)\mu_2\omega_1}[4(k-1)\mu_2\omega_1]^{(k-1)\mu_2\omega_1}. \end{aligned} \tag{3}$$

Proof

(a) Consider $d(p,q) = d_{\Gamma_{1+S_k}}\Gamma_2(p,q)$ as a degree of a node (p,q) in $\Gamma_1 +_{S_k} \Gamma_2$.

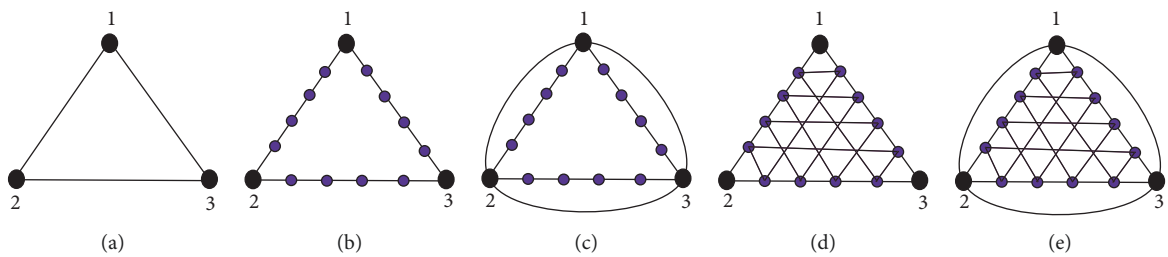

Figure 1: (a) Γ, (b) $S_4(\Gamma)$, (c) $R_4(\Gamma)$. (d) $Q_4(\Gamma)$, and (e) $T_4(\Gamma)$.

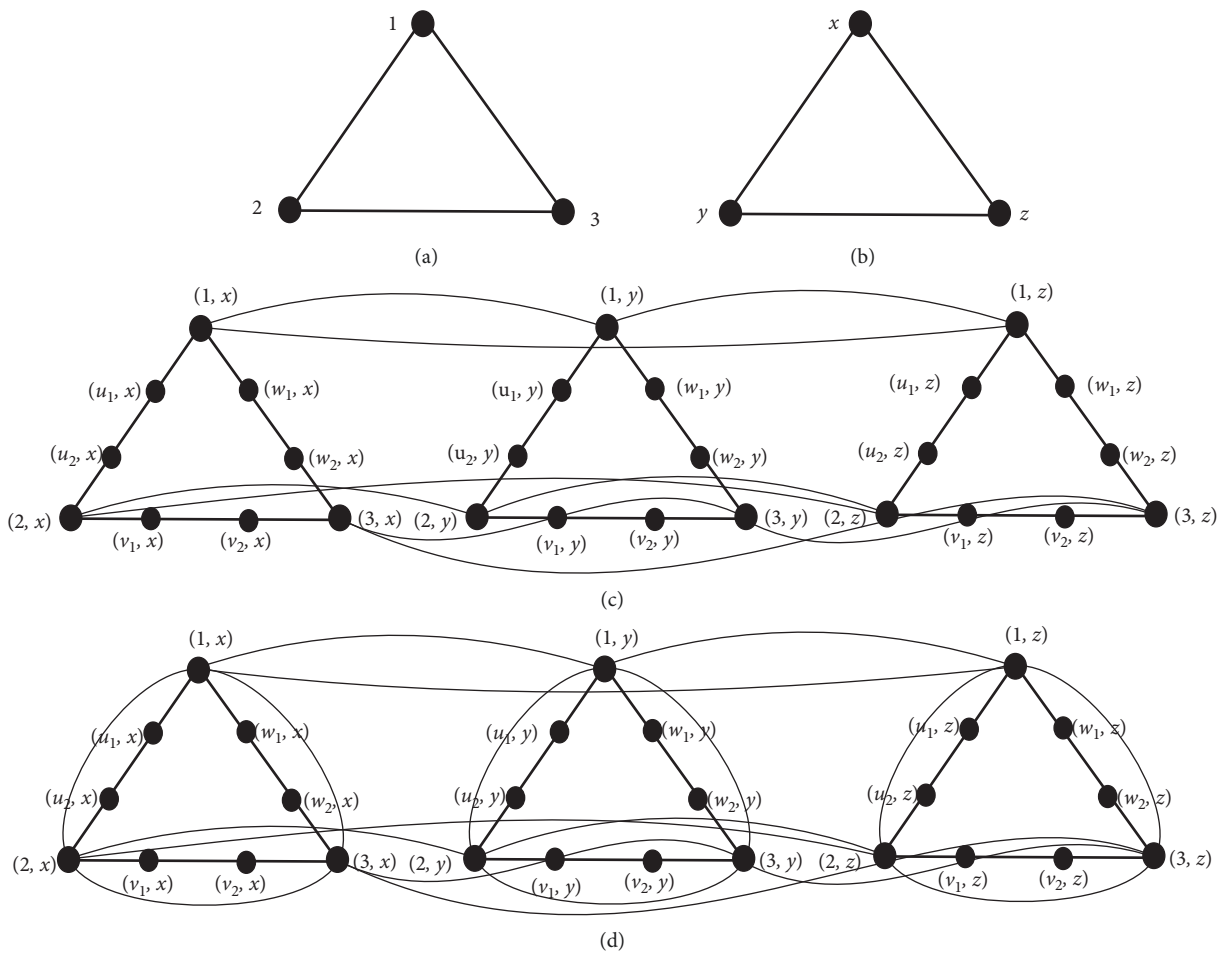

Figure 2: (a) $\Gamma_1 \cong C_3$, (b) $\Gamma_2 \cong C_3$, (c) $\Gamma_{1+S_2}\Gamma_2$, and (d) $\Gamma_{1+R_2}\Gamma_2$.

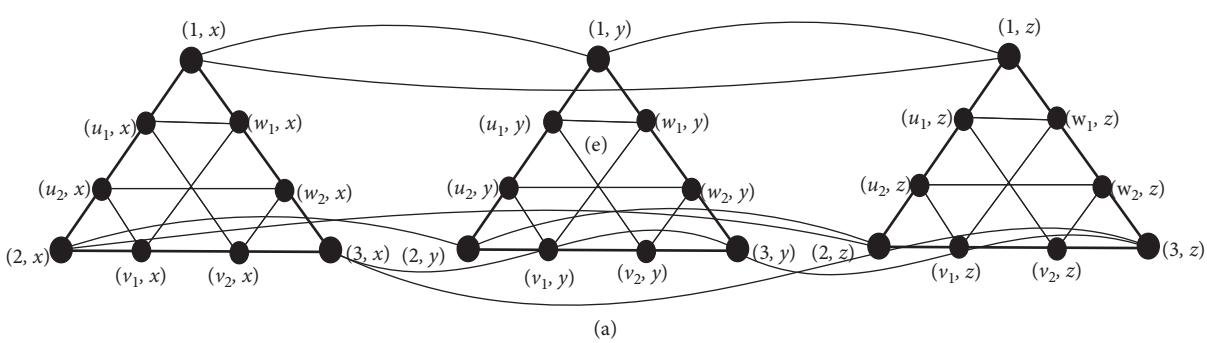

Figure 3: Continued.

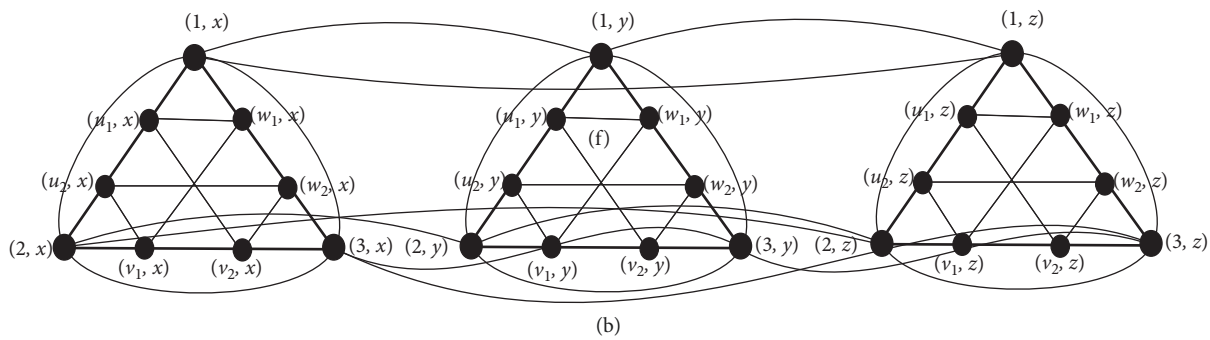

Figure 3: (a) $H_{1+Q_2}H_2$ and (b) $\Gamma_{1+T_2}\Gamma_2$.

$$\begin{aligned}
\prod_1\left(\Gamma_1 +_{S_k}\Gamma_2\right) &= \prod_{(p_1,q_1)(p_2,q_2)\in E\left(\Gamma_1+_{S_k}\Gamma_2\right)}\left[d(p_1,q_1)+d(p_2,q_2)\right] \\
&= \prod_{p\in V(\Gamma_1)}\prod_{q_1q_2\in E(\Gamma_2)}\left[d(p,q_1)+d(p,q_2)\right]\times\prod_{q\in V(\Gamma_2)}\prod_{\substack{p_1p_2\in E(S_k(\Gamma_1))\\ p_1\in V(\Gamma_1),p_2\in V(S_k(\Gamma_1)-\Gamma_1)}}\left[d(p_1,q)+d(p_2,q)\right] \\
&\quad\times\prod_{q\in V(\Gamma_2)}\prod_{\substack{p_1p_2\in E(S_k(\Gamma_1))\\ p_1,p_2\in V(S_k(\Gamma_1)-\Gamma_1)}}\left[d(p_1,q)+d(p_2,q)\right] \\
&= \prod 1\times\prod 2\times\prod 3.
\end{aligned} \tag{4}$$

Now,

$$\begin{aligned}
\prod 1 &= \prod_{p\in V(\Gamma_1)}\prod_{q_1q_2\in E(\Gamma_2)}\left[d(p,q_1)+d(p,q_2)\right] \le \frac{1}{\mu_1\omega_2}\left[\sum_{p\in V(\Gamma_1)}\sum_{q_1q_2\in E(\Gamma_2)}\left[d(p,q_1)+d(p,q_2)\right]\right]^{\mu_1\omega_2} \\
&= \frac{1}{\mu_1\omega_2}\left[\sum_{p\in V(\Gamma_1)}\sum_{q_1q_2\in E(\Gamma_2)}\left[2d_{\Gamma_1}(p)+d_{\Gamma_2}(q_1)+d_{\Gamma_2}(q_2)\right]\right]^{\mu_1\omega_2} = \frac{1}{\mu_1\omega_2}\left[4\omega_1\omega_2+\mu_1M_1(\Gamma_2)\right]^{\mu_1\omega_2},
\end{aligned}$$

$$\begin{aligned}
\prod 2 &= \prod_{q\in V(\Gamma_2)}\prod_{p_1p_2\in E(S_k(\Gamma_1))}\left[d(p_1,q)+d(p_2,q)\right] \le \frac{1}{2\omega_1\mu_2}\left[\sum_{q\in V(\Gamma_2)}\sum_{\substack{p_1p_2\in E(S_k(\Gamma_1))\\ p_1\in V(\Gamma_1),p_2\in V(S_k(\Gamma_1))-\mu(\Gamma_1)}}\left[d(p_1,q)+d(p_2,q)\right]\right]^{2\omega_1\mu_2} \\
&= \frac{1}{2\omega_1\mu_2}\left[\sum_{q\in V(\Gamma_2)}\sum_{\substack{p_1p_2\in E(S_k(\Gamma_1))\\ p_1\in V(\Gamma_1),p_2\in V(S_k(\Gamma_1))-\mu(\Gamma_1)}}\left[d_{S_k(\Gamma_1)}(p_1)+d_{\Gamma_2}(q)+d_{S_k(\Gamma_1)}(p_2)\right]\right]^{2\omega_1\mu_2} \\
&= \frac{1}{2\omega_1\mu_2}\left[4\omega_1\omega_2+\mu_2M_1(S_1(\Gamma_1))\right]^{2\omega_1\mu_2},
\end{aligned}$$

$$\begin{aligned}
\prod 3 &= \prod_{q\in V(\Gamma_2)} \prod_{\substack{p_1p_2\in E(S_k(\Gamma_1))\\ p_1,p_2\in V(S_k(\Gamma_1))-\Gamma_1}} [d(p_1,q)+d(p_2,q)] \\
&\le \frac{1}{\omega_1\mu_2(k-1)}\left[(k-1)\sum_{q\in V(\Gamma_2)} \sum_{\substack{p_1p_2\in E(S_k(\Gamma_1))\\ p_1,p_2\in V(S_k(\Gamma_1))-\mu(\Gamma_1)}} [d(p_1,q)+d(p_2,q)]\right]^{\omega_1\mu_2(k-1)} \\
&= \frac{1}{\omega_1\mu_2(k-1)}\left[(k-1)\sum_{q\in V(\Gamma_2)} \sum_{\substack{p_1p_2\in E(S_k(\Gamma_1))\\ p_1,p_2\in V(S_k(\Gamma_1))-\mu(\Gamma_1)}} [2+2]\right]^{\omega_1\mu_2(k-1)} = \frac{1}{\omega_1\mu_2(k-1)}\left[(k-1)\left|\omega(\Gamma_1)\right| \sum_{q\in V(\Gamma_2)} (4)\right]^{\omega_1\mu_2(k-1)} \\
&= \frac{1}{\omega_1\mu_2(k-1)}\left[4(k-1)\mu_2\omega_1\right]^{\omega_1\mu_2(k-1)}.
\end{aligned} \tag{5}$$

Hence,

$$\begin{aligned}
\prod_1\left(\Gamma_1 +_{S_k} \Gamma_2\right) &\le \frac{1}{\mu_1\omega_2}\left[4\omega_1\omega_2+\mu_1 M_1(\Gamma_2)\right]^{\mu_1\omega_2} \times \frac{1}{2\omega_1\mu_2}\left[4\omega_1\omega_2+\mu_2 M_1(S_1(\Gamma_1))\right]^{2\omega_1\mu_2} \\
&\quad \times \frac{1}{\omega_1\mu_2(k-1)}\left[4(k-1)\mu_2\omega_1\right]^{\omega_1\mu_2(k-1)}, \\
(b)\prod_2\left(\Gamma_1 +_{S_k} \Gamma_2\right) &= \prod_{(p_1,q_1)(p_2,q_2)\in E\left(\Gamma_1+_{S_k}\Gamma_2\right)} [d(p_1,q_1)d(p_2,q_2)] \\
&= \prod_{p\in V(\Gamma_1)} \prod_{q_1q_2\in E(\Gamma_2)} [d(p,q_1)d(p,q_2)] \\
&\quad \times \prod_{q\in V(\Gamma_2)} \prod_{\substack{p_1p_2\in E(S_k(\Gamma_1))\\ p_1,p_2\in V(S_k(\Gamma_1))-\mu(\Gamma_1)}} [d(p_1,q)d(p_2,q)]4 \\
&\quad \times \prod_{q\in V(\Gamma_2)} \prod_{\substack{p_1p_2\in E(S_k(\Gamma_1))\\ p_1\in V(\Gamma_1),p_2\in V(S_k(\Gamma_1))-\mu(\Gamma_1)}} [d(p_1,q)d(p_2,q)] \\
&= \prod 1 \times \prod 2 \times \prod 3.
\end{aligned} \tag{6}$$

Now,

$$\prod 1 = \prod_{p\in V(\Gamma_1)} \prod_{q_1q_2\in E(\Gamma_2)} [d(p,q_1)d(p,q_2)] \le \frac{1}{\mu_1\omega_2}\left[\sum_{p\in V(\Gamma_1)} \sum_{q_1q_2\in E(\Gamma_2)} [d(p,q_1)d(p,q_2)]\right]^{\mu_1\omega_2}$$

$$= \frac{1}{\mu_1\omega_2}\left[\sum_{p\in V(\Gamma_1)} \sum_{q_1q_2\in E(\Gamma_2)} \left[d_{\Gamma_1}(p)+d_{\Gamma_2}(q_1)\right]\left[d_{\Gamma_1}(p)+d_{\Gamma_2}(q_2)\right]\right]^{\mu_1\omega_2}$$

$$= \frac{1}{\mu_1\omega_2}\left[\omega_2 M_1(\Gamma_1) + 2\omega_1 M_1(\Gamma_2) + \mu_1 M_2(\Gamma_2)\right]^{\mu_1\omega_2},$$

$$\prod 2 = \prod_{q\in V(\Gamma_2)} \prod_{\substack{p_1p_2\in E(S_k(\Gamma_1)) \\ p_1\in V(\Gamma_1), p_2\in V(S_k(\Gamma_1))-\mu(\Gamma_1)}} [d(p_1,q)d(p_2,q)]$$

$$\le \frac{1}{2\mu_2\omega_1}\left[\sum_{q\in V(\Gamma_2)} \sum_{\substack{p_1p_2\in E(S_k(\Gamma)) \\ p_1\in V(\Gamma_1), p_2\in V(S_k(\Gamma_1))-\mu(\Gamma_1)}} [d(p_1,q)d(p_2,q)]\right]^{2\mu_2\omega_1}$$

$$= \frac{1}{2\mu_2\omega_1}\left[\sum_{q\in V(\Gamma_2)} \sum_{\substack{p_1p_2\in E(S_k(\Gamma_1)) \\ p_1\in V(\Gamma_1), p_2\in V(S_k(\Gamma_1))-\mu(\Gamma_1)}} \left[d_{S_k(\Gamma_1)}(p_1)+d_{\Gamma_2}(q)\right] d_{S_k(\Gamma_1)}(p_2)\right]^{2\mu_2\omega_1}, \tag{7}$$

$$\prod 3 = \sum_{q\in V(\Gamma_2)} \sum_{\substack{p_1p_2\in E(S_k(\Gamma_1)) \\ p_1\in V(\Gamma_1), p_2\in V(S_k(\Gamma_1))-\mu(\Gamma_1)}} [d(p_1,q)d(p_2,q)]$$

$$\le \frac{1}{(k-1)\mu_2\omega_1}\left[\prod_{q\in V(\Gamma_2)} \prod_{\substack{p_1p_2\in E(S_k(\Gamma_1)) \\ p_1,p_2\in V(S_k(\Gamma_1))-\mu(\Gamma_1)}} [d(p_1,q)d(p_2,q)]\right]^{(k-1)\mu_2\omega_1}$$

$$= \frac{1}{(k-1)\mu_2\omega_1}\left[\sum_{q\in V(\Gamma_2)} \sum_{\substack{p_1p_2\in E(S_k(\Gamma_1)) \\ p_1,p_2\in V(S_k(\Gamma_1))-\mu(\Gamma_1)}} [4]\right]^{(k-1)\mu_2\omega_1} = \frac{1}{(k-1)\mu_2\omega_1}\left[4(k-1)\mu_2\omega_1\right]^{(k-1)\mu_2\omega_1}.$$

Consequently,

$$\prod_2\left(\Gamma_1 +_{S_k} \Gamma_2\right) \le \frac{1}{\mu_1\omega_2}\left[\omega_2 M_1(\Gamma_1) + 2\omega_1 M_1(\Gamma_2) + \mu_1 M_2(\Gamma_2)\right]^{\mu_1\omega_2} \times \frac{1}{2\mu_2\omega_1}\left[\mu_2 M_2(S_1(\Gamma_1)) + 8\omega_1\omega_2\right]^{2\mu_2\omega_1} \times \frac{1}{(k-1)\mu_2\omega_1}\left[4(k-1)\mu_2\omega_1\right]^{(k-1)\mu_2\omega_1}. \tag{8}$$

□

Theorem 2. *Let Γ_1, Γ_2 be two graphs with $|V(\Gamma_1)| = \mu_1$, $|V(\Gamma_2)| = \mu_2$, $|E(\Gamma_1)| = \omega_1$, and $|E(\Gamma_2)| = \omega_2$. For $\mu_1, \mu_2 \ge 4$ and $k \ge 1$, we have*

$$\begin{aligned}
\prod_1\left(\Gamma_1 +_{R_k} \Gamma_2\right) &\le \frac{1}{\mu_1\omega_2}\left[\mu_1 M_1(\Gamma_2) + 8\omega_1\omega_2\right]^{\mu_1\omega_2} \times \frac{1}{\omega_1\mu_2}\left[4\omega_1\omega_2 + 2\mu_2 M_1(\Gamma_1)\right]^{\omega_1\mu_2} \\
&\quad \times \frac{1}{2\omega_1\mu_2}\left[4\omega_1\omega_2 + \mu_2\left(M_1 R_1(\Gamma_1) - 2M_1(\Gamma_1)\right)\right]^{2\omega_1\mu_2} \times \frac{1}{\omega_1\mu_2(k-1)}\left[4(k-1)\mu_2\omega_1\right]^{\omega_1\mu_2(k-1)}, \\
\prod_2\left(\Gamma_1 +_{R_k} \Gamma_2\right) &\le \frac{1}{\omega_2\mu_1}\left[4\omega_2 M_1(\Gamma_1) + 4\omega_1 M_1(\Gamma_2) + \mu_1 M_2(\Gamma_2)\right]^{\omega_2\mu_1} \\
&\quad \times \frac{1}{\omega_1\mu_2}\left[4\mu_2 M_2(\Gamma_1) + 4\omega_2 M_1(\Gamma_1) + \omega_1 M_1(\Gamma_2)\right]^{\omega_1\mu_2} \\
&\quad \times \frac{1}{2\omega_1\mu_2}\left[8\omega_1\omega_2 + \mu_2\left(M_2(R_1(\Gamma_1)) - 4M_2(\Gamma_1)\right)\right]^{2\omega_1\mu_2} \times \frac{1}{(k-1)\omega_1\mu_2}\left[4\mu_2\omega_1(k-1)\right]^{(k-1)\omega_1\mu_2}.
\end{aligned} \tag{9}$$

Proof

(a) Consider $d(p,q) = d_{(\Gamma_1 +_{R_k} \Gamma_2)}(p,q)$ as a degree of a node (p,q) in $\Gamma_1 +_{R_k} \Gamma_2$:

$$\begin{aligned}
\prod_1\left(\Gamma_1 +_{R_k} \Gamma_2\right) &= \prod_{(p_1,q_1)(p_2,q_2)\in E\left(\Gamma_1 +_{R_k} \Gamma_2\right)} \left[d(p_1,q_1) + d(p_2,q_2)\right] \\
&= \prod_{p\in V(\Gamma_1)} \prod_{q_1q_2\in E(\Gamma_2)} \left[d(p,q_1) + d(p,q_2)\right] \\
&\quad \times \prod_{q\in V(\Gamma_2)} \prod_{p_1p_2\in E(R_k(\Gamma_1))} \left[d(p_1,q) + d(p_2,q)\right] \\
&= \prod 1 \times \prod 2.
\end{aligned} \tag{10}$$

Now,

$$\begin{aligned}
\prod 1 &= \prod_{p\in V(\Gamma_1)} \prod_{q_1q_2\in E(\Gamma_2)} [d(p,q_1)+d(p,q_2)] \le \frac{1}{\mu_1\omega_2}\left[\sum_{p\in V(\Gamma_1)} \sum_{q_1q_2\in E(\Gamma_2)} [d(p,q_1)+d(p,q_2)]\right]^{\mu_1\omega_2} \\
&= \frac{1}{\mu_1\omega_2}\left[\sum_{p\in V(\Gamma_1)} \sum_{q_1q_2\in E(\Gamma_2)} \left[2d_{R_k(\Gamma_1)}(p)+d_{\Gamma_2}(q_1)+d_{\Gamma_2}(q_2)\right]\right]^{\mu_1\omega_2} \\
&= \frac{1}{\mu_1\omega_2}\left[\sum_{p\in V(\Gamma_1)} \sum_{q_1q_2\in E(\Gamma_2)} \left[4d_{\Gamma_1}(p)+d_{\Gamma_2}(q_1)+d_{\Gamma_2}(q_2)\right]\right]^{\mu_1\omega_2} = \frac{1}{\mu_1\omega_2}[\mu_1M_1(\Gamma_2)+8\omega_1\omega_2]^{\mu_1\omega_2}, \\
\prod 2 &= \prod_{q\in V(\Gamma_2)} \prod_{p_1p_2\in E(R_k(\Gamma_1))} [d(p_1,q)+d(p_2,q)] = \prod_{q\in V(\Gamma_2)} \prod_{\substack{p_1p_2\in E(R_k(\Gamma_1)) \\ p_1,p_2\in V(\Gamma_1)}} [d(p_1,q)+d(p_2,q)] \\
&\quad \times \prod_{q\in V(\Gamma_2)} \prod_{\substack{p_1p_2\in E(R_k(\Gamma_1)) \\ p_1\in V(\Gamma_1)}} [d(p_1,q)+d(p_2,q)] \times \prod_{q\in V(\Gamma_2)} \prod_{\substack{p_1p_2\in E(R_k(\Gamma_1)) \\ p_1,p_2\in V(R_k(\Gamma_1))-\mu(\Gamma_1)}} [d(p_1,q)+d(p_2,q)] \\
&= \prod{}' 2 \times \prod{}'' 2 \times \prod{}''' 2.
\end{aligned} \tag{11}$$

Now, for $p_1p_2 \in V(\Gamma_1)$, then $p_1p_2 \in E(R_k(\Gamma_1))$ if and only if $p_1p_2 \in E(\Gamma_1)$; for $p_1 \in V(\Gamma_1)$, we get $d_{R_k(\Gamma_1)}(p_1) = 2d_{\Gamma_1}(p_1)$ and for $p_2 \in V(R_k(\Gamma_1)) - \mu(\Gamma_1)$, we have $d_{R_k(\Gamma_1)}(p_2) = 2$. Now,

$$\begin{aligned}
\prod{}' 2 &= \prod_{q\in V(\Gamma_2)} \prod_{\substack{p_1p_2\in E(R_k(\Gamma_1)) \\ p_1,p_2\in V(\Gamma_1)}} [d(p_1,q)+d(p_2,q)] \le \frac{1}{\omega_1\mu_2}\left[\sum_{q\in V(\Gamma_2)} \sum_{\substack{p_1p_2\in E(R_k(\Gamma_1)) \\ p_1p_2\in V(\Gamma_1)}} [d(p_1,q)+d(p_2,q)]\right]^{\omega_1\mu_2} \\
&= \frac{1}{\omega_1\mu_2}\left[\sum_{q\in V(\Gamma_2)} \sum_{p_1p_2\in E(\Gamma_1)} \left[2d_{\Gamma_2}(q)\right] + \sum_{q\in V(\Gamma_2)} \sum_{p_1p_2\in E(\Gamma_1)} \left[d_{R_k(\Gamma_1)}(p_1)+d_{R_k(\Gamma_1)}(p_2)\right]\right]^{\omega_1\mu_2} = \frac{1}{\omega_1\mu_2}[4\omega_1\omega_2+2\mu_2M_1(\Gamma_1)]^{\omega_1\mu_2}, \\
\prod{}'' 2 &= \prod_{q\in V(\Gamma_2)} \prod_{\substack{p_1p_2\in E(R_k(\Gamma_1)) \\ p_1\in V(\Gamma_1)}} [d(p_1,q)+d(p_2,q)] \le \frac{1}{2\omega_1\mu_2}\left[\sum_{q\in V(\Gamma_2)} \sum_{\substack{p_1p_2\in E(R_k(\Gamma_1)) \\ p_1\in V(\Gamma_1)}} [d(p_1,q)+d(p_2,q)]\right]^{2\omega_1\mu_2} \\
&= \frac{1}{2\omega_1\mu_2}\left[\sum_{q\in V(\Gamma_2)} \sum_{\substack{p_1p_2\in E(R_k(\Gamma_1)) \\ p_1\in V(\Gamma_1)}} \left[d_{R_k(\Gamma_1)}(p_1)+d_{\Gamma_2}(q)+d_{R_k(\Gamma_1)}(p_2)\right]\right]^{2\omega_1\mu_2} = \frac{1}{2\omega_1\mu_2}[4\omega_1\omega_2+\mu_2(M_1R_1(\Gamma_1)-2M_1(\Gamma_1))]^{2\omega_1\mu_2}, \\
\prod{}''' 2 &= \prod_{q\in V(\Gamma_2)} \prod_{\substack{p_1p_2\in E(R_k(\Gamma_1)) \\ p_1,p_2\in V(R_k(\Gamma_1))-\mu(\Gamma_1)}} [d(p_1,q)+d(p_2,q)] \\
&\le \frac{1}{\omega_1\mu_2(k-1)}\left[\sum_{q\in V(\Gamma_2)} \sum_{\substack{p_1p_2\in E(R_k(\Gamma_1)) \\ p_1,p_2\in V(R_k(\Gamma_1))-\mu(\Gamma_1)}} [d(p_1,q)+d(p_2,q)]\right]^{\omega_1\mu_2(k-1)} = \frac{1}{\omega_1\mu_2(k-1)}[4(k-1)\mu_2\omega_1]^{\omega_1\mu_2(k-1)}.
\end{aligned} \tag{12}$$

Hence,

$$\prod_1\left(\Gamma_1 +_{R_k}\Gamma_2\right) \le \frac{1}{\mu_1\omega_2}\left[\mu_1 M_1\left(\Gamma_2\right) + 8\omega_1\omega_2\right]^{\mu_1\omega_2} \times \frac{1}{\omega_1\mu_2}\left[4\omega_1\omega_2 + 2\mu_2 M_1\left(\Gamma_1\right)\right]^{\omega_1\mu_2}$$

$$\times \frac{1}{2\omega_1\mu_2}\left[4\omega_1\omega_2 + \mu_2\left(M_1 R_1\left(\Gamma_1\right) - 2M_1\left(\Gamma_1\right)\right)\right]^{2\omega_1\mu_2} \times \frac{1}{\omega_1\mu_2\left(k-1\right)}\left[4\left(k-1\right)\mu_2\omega_1\right]^{\omega_1\mu_2\left(k-1\right)},$$

$$\text{(b)} \prod_2\left(\Gamma_1 +_{R_k}\Gamma_2\right) = \prod_{\left(p_1,q_1\right)\left(p_2,q_2\right).\in E\left(\Gamma_1 +_{R_k}\Gamma_2\right)}\left[d\left(p_1,q_1\right)d\left(p_2,q_2\right)\right]$$

$$= \prod_{p\in V\left(\Gamma_1\right)}\prod_{q_1q_2\in E\left(\Gamma_2\right)}\left[d\left(p,q_1\right)d\left(p,q_2\right)\right]$$

$$\times \prod_{q\in V\left(\Gamma_2\right)}\prod_{p_1p_2\in E\left(R_k\left(\Gamma_1\right)\right)}\left[d\left(p_1,q\right)d\left(p_2,q\right)\right] \tag{13}$$

$$= \prod 1 \times \prod 2.$$

Now,

$$\prod 1 = \prod_{p\in V\left(\Gamma_1\right)}\prod_{q_1q_2\in E\left(\Gamma_2\right)}\left[d\left(p,q_1\right)d\left(p,q_2\right)\right] \le \frac{1}{\omega_2\mu_1}\left[\sum_{p\in V\left(\Gamma_1\right)}\sum_{q_1q_2\in E\left(\Gamma_2\right)}\left[d\left(p,q_1\right)d\left(p,q_2\right)\right]\right]^{\omega_2\mu_1}$$

$$= \frac{1}{\omega_2\mu_1}\left[\sum_{p\in V\left(\Gamma_1\right)}\sum_{q_1q_2\in E\left(\Gamma_2\right)}\left[d_{R_k\left(\Gamma_1\right)}\left(p\right) + d_{\Gamma_2}\left(q_1\right)\right]\left[d_{R_k\left(\Gamma_1\right)}\left(p\right) + d_{\Gamma_2}\left(q_2\right)\right]\right]^{\omega_2\mu_1}$$

$$= \frac{1}{\omega_2\mu_1}\left[4\omega_2 M_1\left(\Gamma_1\right) + 4\omega_1 M_1\left(\Gamma_2\right) + \mu_1 M_2\left(\Gamma_2\right)\right]^{\omega_2\mu_1},$$

$$\prod 2 = \prod_{q\in V\left(\Gamma_2\right)}\prod_{p_1p_2\in E\left(R_k\left(\Gamma_1\right)\right)}\left[d\left(p_1,q\right)d\left(p_2,q\right)\right]$$

$$= \prod_{q\in V\left(\Gamma_2\right)}\prod_{\substack{p_1p_2\in E\left(R_k\left(\Gamma_1\right)\right)\\ p_1,p_2\in V\left(\Gamma_1\right)}}\left[d\left(p_1,q\right)d\left(p_2,q\right)\right] \times \prod_{q\in V\left(\Gamma_2\right)}\prod_{\substack{p_1p_2\in E\left(R_k\left(\Gamma_1\right)\right)\\ p_1\in V\left(\Gamma_1\right)\\ p_2\in V\left(R_k\left(\Gamma_1\right)\right)-\mu\left(\Gamma_2\right)}}\left[d\left(p_1,q\right)d\left(p_2,q\right)\right] \tag{14}$$

$$\times \prod_{q\in V\left(\Gamma_2\right)}\prod_{\substack{p_1p_2\in E\left(R_k\left(\Gamma_1\right)\right)\\ p_1,p_2\in V\left(R_k\left(\Gamma_1\right)\right)-\mu\left(\Gamma_1\right)}}\left[d\left(p_1,q\right)d\left(p_2,q\right)\right]$$

$$= \prod^{\prime} 2 \times \prod^{\prime\prime} 2 \times \prod^{\prime\prime\prime} 2.$$

Now, we consider

$$\prod_{2}^{\prime} = \prod_{q\in V(\Gamma_2)} \prod_{\substack{p_1p_2\in E(R_k(\Gamma_1))\\ p_1p_2\in V(\Gamma_1)}} [d(p_1,q)d(p_2,q)] = \prod_{q\in V(\Gamma_2)} \prod_{p_1p_2\in E(\Gamma_1)} [d(p_1,q)d(p_2,q)]$$

$$\leq \frac{1}{\omega_1\mu_2}\left[\sum_{q\in V(\Gamma_2)} \sum_{p_1p_2\in E(\Gamma_1)} [d(p_1,q)d(p_2,q)]\right]^{\omega_1\mu_2}$$

$$= \frac{1}{\omega_1\mu_2}\left[\sum_{q\in V(\Gamma_2)} \sum_{p_1p_2\in E(\Gamma_1)} \left[d_{R_k(\Gamma_1)}(p_1)+d_{\Gamma_2}(q)\right]\left[d_{R_k(\Gamma_1)}(p_2)+d_{\Gamma_2}(q)\right]\right]^{\omega_1\mu_2}$$

$$= \frac{1}{\omega_1\mu_2}[4\mu_2M_2(\Gamma_1)+4\omega_2M_1(\Gamma_1)+\omega_1M_1(\Gamma_2)]^{\omega_1\mu_2},$$

$$\prod_{2}^{\prime\prime} = \prod_{q\in V(\Gamma_2)} \prod_{\substack{p_1p_2\in E(R_k(\Gamma_1))\\ p_1\in V(\Gamma_1)}} [d(p_1,q)d(p_2,q)]$$

$$\leq \frac{1}{2\omega_1\mu_2}\left[\sum_{q\in V(\Gamma_2)} \sum_{\substack{p_1p_2\in E(R_k(\Gamma_1))\\ p_1\in V(\Gamma_1)}} [d(p_1,q)d(p_2,q)]\right]^{2\omega_1\mu_2} = \frac{1}{2\omega_1\mu_2}\left[\sum_{q\in V(\Gamma_2)} \sum_{\substack{p_1p_2\in E(R_k(\Gamma_1))\\ p_1\in V(\Gamma_1)}} \left[d_{R_k(\Gamma_1)}(p_1)+d_{\Gamma_2}(q)\right]\times 2\right]^{2\omega_1\mu_2}$$

$$= \frac{1}{2\omega_1\mu_2}[8\omega_1\omega_2+\mu_2(M_2(R_1(\Gamma_1))-4M_2(\Gamma_1))]^{2\omega_1\mu_2},$$

$$\prod_{2}^{\prime\prime\prime} = \prod_{q\in V(\Gamma_2)} \prod_{\substack{p_1p_2\in E(R_k(\Gamma_1))\\ p_1p_2\in V(R_k(\Gamma_1))-\mu(\Gamma_1)}} [d(p_1,q)d(p_2,q)]$$

$$\leq \frac{1}{(k-1)\omega_1\mu_2}\left[(k-1)\sum_{q\in V(\Gamma_2)} \sum_{\substack{p_1p_2\in E(R_k(\Gamma_1))\\ p_1p_2\in V(R_k(\Gamma_1))-\mu(\Gamma_1)}} [d(p_1,q)d(p_2,q)]\right]^{(k-1)\omega_1\mu_2} = \frac{1}{(k-1)\omega_1\mu_2}[4\mu_2\omega_1(k-1)]^{(k-1)\omega_1\mu_2}. \tag{15}$$

Therefore, we have

$$\begin{aligned}\prod_{2}(\Gamma_1 +_{R_k} \Gamma_2) \leq{}& \frac{1}{\omega_2\mu_1}[4\omega_2M_1(\Gamma_1)+4\omega_1M_1(\Gamma_2)+\mu_1M_2(\Gamma_2)]^{\omega_2\mu_1}\\ &\times \frac{1}{\omega_1\mu_2}[4\mu_2M_2(\Gamma_1)+4\omega_2M_1(\Gamma_1)+\omega_1M_1(\Gamma_2)]^{\omega_1\mu_2}\\ &\times \frac{1}{2\omega_1\mu_2}[8\omega_1\omega_2+\mu_2(M_2(R_1(\Gamma_1))-4M_2(\Gamma_1))]^{2\omega_1\mu_2} \times \frac{1}{(k-1)\omega_1\mu_2}[4\mu_2\omega_1(k-1)]^{(k-1)\omega_1\mu_2}.\end{aligned} \tag{16}$$

□

Theorem 3. *Let Γ_1, Γ_2 be two graphs with $|V(\Gamma_1)| = \mu_1$, $|V(\Gamma_2)| = \mu_2$, $|E(\Gamma_1)| = \omega_1$, and $|E(\Gamma_2)| = \omega_2$. For $\mu_1, \mu_2 \geq 4$ and and $k \geq 1$, we have*

$$\begin{aligned}
\prod_1 \left(\Gamma_1 +_{Q_k} \Gamma_2\right) \leq{}& \frac{1}{\mu_1\omega_2}\left[4\omega_1\omega_2 + \mu_1 M_1(\Gamma_2)\right]^{\mu_1\omega_2} \times \frac{1}{2\omega_1\mu_2}\left[4\omega_1\omega_2 + 3\mu_2 M_1(\Gamma_1)\right]^{2\omega_1\mu_2} \\
&\times \frac{1}{\omega_1\mu_2(k-1)}\left[2(k-1)\mu_2 M_1(\Gamma_1)\right]^{\omega_1\mu_2(k-1)} \\
&\times \frac{1}{k\mu_2(2\omega_1-\mu_1)}\left[(k)\mu_2\left[M_3(\Gamma_1) + 2M_2(\Gamma_1) - 2M_1(\Gamma_1)\right]\right]^{k\mu_2(2\omega_1-\mu_1)}, \\
\prod_2 \left(\Gamma_1 +_{Q_k} \Gamma_2\right) \leq{}& \frac{1}{\mu_1\omega_2}\left[\omega_2 M_1(\Gamma_1) + 2\omega_1 M_1(\Gamma_2) + \mu_1 M_2(\Gamma_2)\right]^{\mu_1\omega_2} \\
&\times \frac{1}{2\mu_2\omega_1}\left[4\omega_2 M_1(\Gamma_1) + \mu_2\left[M_3(\Gamma_1) + 2M_2(\Gamma_1)\right]\right]^{2\mu_2\omega_1} \\
&\times \frac{1}{(k-1)\mu_2\omega_1}\left[(k-1)\mu_2\left[2M_2(\Gamma_1) + M_3(\Gamma_1)\right]\right]^{(k-1)\mu_2\omega_1} \\
&\times \frac{1}{k\mu_2(2\omega_1-\mu_1)}\left[(k)\mu_2\left[\frac{1}{2}M_4(\Gamma_1) - \frac{1}{2}M_3(\Gamma_1)\right] + \sum_{uv\in V(\Gamma_1)} r d_{\Gamma_1}(u) d_{\Gamma_1}(v)\right]^{k\mu_2(2\omega_1-\mu_1)} \\
&+ \frac{1}{k\mu_2(2\omega_1-\mu_1)}\left[\sum_{v\in V(\Gamma_1)} d^2_{\Gamma_1}(v) \sum_{\substack{u\in V(\Gamma_1) \\ uv\in E(\Gamma_1)}} d_{\Gamma_1}(u) - 2M_2(\Gamma_1)\right]^{k\mu_2(2\omega_1-\mu_1)}.
\end{aligned} \tag{17}$$

Proof.

$$\begin{aligned}
\text{(a)} \prod_1 \left(\Gamma_1 +_{Q_k} \Gamma_2\right) &= \prod_{(p_1,q_1)(p_2,q_2)\in E\left(\Gamma_1 +_{Q_k} \Gamma_2\right)} \left[d(p_1,q_1) + d(p_2,q_2)\right] \\
&= \prod_{p\in V(\Gamma_1)} \prod_{q_1q_2\in E(\Gamma_2)} \left[d(p,q_1) + d(p,q_2)\right] \times \prod_{q\in V(\Gamma_2)} \prod_{p_1p_2\in E(Q_k(\Gamma_2))} \left[d(p_1,q) + d(p_2,q)\right] \\
&= \prod 1 \times \prod 2.
\end{aligned} \tag{18}$$

Now,

$$\begin{aligned}\prod 1 &= \prod_{p\in V(\Gamma_1)} \prod_{q_1q_2\in E(\Gamma_2)} [d(p,q_1)+d(p,q_2)]\\ &\le \frac{1}{\mu_1\omega_2}\left[\sum_{p\in V(\Gamma_1)} \sum_{q_1q_2\in E(\Gamma_2)} \left[2d_{\Gamma_1}(p)+d_{\Gamma_2}(q_1)+d_{\Gamma_2}(q_2)\right]\right]^{\mu_1\omega_2} = \frac{1}{\mu_1\omega_2}\left[4\omega_1\omega_2+\mu_1M_1(\Gamma_2)\right]^{\mu_1\omega_2},\\ \prod 2 &= \prod_{q\in V(\Gamma_2)} \prod_{p_1p_2\in E(Q_k(\Gamma_1))} [d(p_1,q)+d(p_2,q)] = q\in V(\Gamma_2) \prod_{q\in V(\Gamma_2)} \prod_{\substack{p_1p_2\in E(Q_k(\Gamma_1))\\ p_1\in V(\Gamma_1)\\ p_1p_2\in V(Q_k(\Gamma_1))-\mu(\Gamma_1)}} [d(p_1,q)+d(p_2,q)]\\ &\quad\times \prod_{q\in V(\Gamma_2)} \prod_{\substack{p_1p_2\in E(Q_k(\Gamma_1))\\ p_1p_2\in V(Q_k(\Gamma_1))-\mu(\Gamma_1)}} [d(p_1,q)+d(p_2,q)]\\ &= \prod{}' 2 \times \prod{}'' 2.\end{aligned} \tag{19}$$

Consider

$$\begin{aligned}\prod{}' 2 &= \prod_{q\in V(\Gamma_2)} \prod_{\substack{p_1p_2\in E(Q_k(\Gamma_1))\\ p_1\in V(\Gamma_1)\\ p_1p_2\in V(Q_k(\Gamma_1))-\mu(\Gamma_1)}} [d(p_1,q)+d(p_2,q)]\\ &\le \frac{1}{2\omega_1\mu_2}\left[\sum_{q\in V(\Gamma_2)} \sum_{\substack{p_1p_2\in E(Q_k(\Gamma_1))\\ p_1\in V(\Gamma_1)\\ p_1p_2\in V(Q_k(\Gamma_1))-\mu(\Gamma_1)}} \left[d_{Q_k(\Gamma_1)}(p_1)+d_{\Gamma_2}(q)+d_{Q_k(\Gamma_1)}(p_2)\right]\right]^{2\omega_1\mu_2}\\ &= \frac{1}{2\omega_1\mu_2}\left[\sum_{q\in V(\Gamma_2)} \sum_{p_1\in V(\Gamma_1)} \left[d_{\Gamma_1}(p_1)+d_{\Gamma_2}(q)\right]\right]^{2\omega_1\mu_2}\\ &\quad+\frac{1}{2\omega_1\mu_2}\left[\sum_{q\in V(\Gamma_2)} \prod_{\substack{p_1p_2\in E(Q_k(\Gamma_1))\\ p_1\in V(\Gamma_1)\\ p_1p_2\in V(Q_k(\Gamma_1))-\mu(\Gamma_1)}} \left[d_{Q_k(\Gamma_1)}(p_2)\right]\right]^{2\omega_1\mu_2}.\end{aligned} \tag{20}$$

Then,

$$\prod{}' 2 = \frac{1}{2\omega_1\mu_2}\left[4\omega_1\omega_2+3\mu_2M_1(\Gamma_1)\right]^{2\omega_1\mu_2}. \tag{21}$$

Now we take

$$\prod{}'' 2 = \prod_{q\in V(\Gamma_2)} \prod_{\substack{p_1p_2\in E(Q_k(\Gamma_1))\\ p_1p_2\in V(Q_k(\Gamma_1))-\mu(\Gamma_1)}} [d(p_1,q)+d(p_2,q)]. \tag{22}$$

Let $\prod'' 2 = \prod 3 \times \prod 4$, then

$$\begin{aligned}
\prod 3 &= \prod_{q\in V(\Gamma_2)} \prod_{\substack{p_1p_2\in E(Q_k(\Gamma_1)) \\ p_1p_2\in V(Q_k(\Gamma_1))-\mu(\Gamma_1)}} \left[d_{Q_k(\Gamma_1)}(p_1)+d_{Q_k(\Gamma_1)}(p_2)\right] \\
&\le \frac{1}{\omega_1\mu_2(k-1)}\left[2(k-1)\sum_{q\in V(\Gamma_2)}\sum_{uv\in E(\Gamma_1)}\left[d_{\Gamma_1}(u)+d_{\Gamma_1}(v)\right]\right]^{\omega_1\mu_2(k-1)} \\
&= \frac{1}{\omega_1\mu_2(k-1)}\left[2(k-1)\mu_2M_1(\Gamma_1)\right]^{\omega_1\mu_2(k-1)}, \\
\prod 4 &= \prod_{q\in V(\Gamma_2)} \prod_{\substack{p_1p_2\in E(Q_k(\Gamma_1)) \\ p_1p_2\in V(Q_k(\Gamma_1))-\mu(\Gamma_1)}} \left[d_{Q_k(\Gamma_1)}(p_1)+d_{Q_k(\Gamma_1)}(p_2)\right] \\
&\le \frac{1}{k\mu_2(2\omega_1-\mu_1)}\left[\sum_{q\in V(\Gamma_2)}\sum_{\substack{p_1p_2\in E(Q_k(\Gamma_1)) \\ p_1p_2\in V(Q_k(\Gamma_1))-\mu(\Gamma_1)}}\left[d_{Q_k(\Gamma_1)}(p_1)+d_{Q_k(\Gamma_1)}(p_2)\right]\right]^{k\mu_2(2\omega_1-\mu_1)} \\
&= \frac{1}{k\mu_2(2\omega_1-\mu_1)}\left[(k)\mu_2\left[M_3(\Gamma_1)+2M_2(\Gamma_1)-2M_1(\Gamma_1)\right]\right]^{k\mu_2(2\omega_1-\mu_1)}.
\end{aligned} \tag{23}$$

Therefore, we have

$$\begin{aligned}
\prod_1\left(\Gamma_1+{}_{Q_k}\Gamma_2\right) &\le \frac{1}{\mu_1\omega_2}\left[4\omega_1\omega_2+\mu_1M_1(\Gamma_2)\right]^{\mu_1\omega_2} \times \frac{1}{2\omega_1\mu_2}\left[4\omega_1\omega_2+3\mu_2M_1(\Gamma_1)\right]^{2\omega_1\mu_2} \\
&\times \frac{1}{\omega_1\mu_2(k-1)}\left[2(k-1)\mu_2M_1(\Gamma_1)\right]^{\omega_1\mu_2(k-1)} \\
&\times \frac{1}{k\mu_2(2\omega_1-\mu_1)}\left[(k)\mu_2\left[M_3(\Gamma_1)+2M_2(\Gamma_1)-2M_1(\Gamma_1)\right]\right]^{k\mu_2(2\omega_1-\mu_1)}.
\end{aligned} \tag{24}$$

Next,

$$\begin{aligned}
\prod_2\left(\Gamma_1+{}_{Q_k}\Gamma_2\right) &= \prod_{(p_1,q_1)(p_2,q_2)\in E\left(\Gamma_1+{}_{Q_k}\Gamma_2\right)}\left[d(p_1,q_1)+d(p_2,q_2)\right] \\
&= \prod_{p\in V(\Gamma_1)}\prod_{q_1q_2\in E(\Gamma_2)}\left[d(p,q_1)d(p,q_2)\right] \times \prod_{q\in V(\Gamma_2)}\prod_{p_1p_2\in E(Q_k(\Gamma_1))}\left[d(p_1,q)d(p_2,q)\right] \\
&= \prod 1 \times \prod 2.
\end{aligned} \tag{25}$$

Consider

$$\begin{aligned}
\prod 1 &= \prod_{p\in V(\Gamma_1)} \prod_{q_1q_2\in E(\Gamma_2)} [d(p,q_1)d(p,q_2)] \\
&\le \frac{1}{\mu_1\omega_2}\left[\sum_{p\in V(\Gamma_1)} \sum_{q_1q_2\in E(\Gamma_2)} [d(p,q_1)d(p,q_2)]\right]^{\mu_1\omega_2} \\
&= \frac{1}{\mu_1\omega_2}[\omega_2 M_1(\Gamma_1) + 2\omega_1 M_1(\Gamma_2) + \mu_1 M_2(\Gamma_2)]^{\mu_1\omega_2}, \\
\prod 2 &= \prod_{q\in V(\Gamma_2)} \prod_{p_1p_2\in E(Q_k(\Gamma_1))} [d(p_1,q)d(p_2,q)] \\
&= \prod_{q\in V(\Gamma_2)} \prod_{\substack{p_1p_2\in E(Q_k(\Gamma_1)) \\ p_1\in V(\Gamma_1)}} [d(p_1,q)d(p_2,q)] \\
&\quad \times \prod_{q\in V(\Gamma_2)} \prod_{\substack{p_1p_2\in E(Q_k(\Gamma_1)) \\ p_1p_2\in V(Q_k(\Gamma_1))-\mu(\Gamma_1)}} [d(p_1,q)d(p_2,q)] \\
&= \prod{}' 2 \times \prod{}'' 2.
\end{aligned} \tag{26}$$

Then,

$$\begin{aligned}
\prod{}' 2 &= \prod_{q\in V(\Gamma_2)} \prod_{\substack{p_1p_2\in E(Q_k(\Gamma_1)) \\ p_1\in V(\Gamma_1)}} [d(p_1,q)d(p_2,q)] \\
&\le \frac{1}{2\omega_1\mu_2}\left[\sum_{q\in V(\Gamma_2)} \sum_{\substack{p_1p_2\in E(Q_k(\Gamma_1)) \\ p_1\in V(\Gamma_1)}} [d(p_1,q)d(p_2,q)]\right]^{2\omega_1\mu_2} \\
&= \frac{1}{2\omega_1\mu_2}\left[\sum_{q\in V(\Gamma_2)} \sum_{\substack{p_1p_2\in E(Q_k(\Gamma_1)) \\ p_1\in V(\Gamma_1)}} \left[d_{\Gamma_1}(p_1) + d_{\Gamma_2}(q)\right] d_{Q_k(\Gamma_1)}(p_2)\right]^{2\omega_1\mu_2} \\
&= \frac{1}{2\omega_1\mu_2}[4\omega_2 M_1(\Gamma_1) + \mu_2[M_3(\Gamma_1) + 2M_2(\Gamma_1)]]^{2\omega_1\mu_2}, \\
\prod{}'' 2 &= \prod_{q\in V(\Gamma_2)} \prod_{\substack{p_1p_2\in E(Q_k(\Gamma_1)) \\ p_1p_2\in V(Q_k(\Gamma_1))-\mu(\Gamma_1)}} [d(p_1,q)d(p_2,q)].
\end{aligned} \tag{27}$$

Let $\prod'' 2 = \prod 3 \times \prod 4$, then

$$\prod 3 = \prod_{q\in V(\Gamma_2)} \prod_{\substack{p_1p_2\in E(Q_k(\Gamma_1)) \\ p_1p_2\in V(Q_k(\Gamma_1))-\mu(\Gamma_1)}} \left[d_{Q_k(\Gamma_1)}(p_1)d_{Q_k(\Gamma_1)}(p_2)\right]$$

$$\leq \frac{1}{(k-1)\mu_2\omega_1}\left[\sum_{q\in V(\Gamma_2)} \sum_{\substack{p_1p_2\in E(Q_k(\Gamma_1)) \\ p_1p_2\in V(Q_k(\Gamma_1))-\mu(\Gamma_1)}} \left[d_{Q_k(\Gamma_1)}(p_1)d_{Q_k(\Gamma_1)}(p_2)\right]\right]^{(k-1)\mu_2\omega_1}$$

$$= \frac{1}{(k-1)\mu_2\omega_1}\left[(k-1)\mu_2\left[2M_2(\Gamma_1)+M_3(\Gamma_1)\right]\right]^{(k-1)\mu_2\omega_1},$$

$$\prod 4 = \prod_{q\in V(\Gamma_2)} \prod_{\substack{p_1p_2\in E(Q_k(\Gamma_1)) \\ p_1p_2\in V(Q_k(\Gamma_1))-\mu(\Gamma_1)}} \left[d_{Q_k(\Gamma_1)}(p_1)d_{Q_k(\Gamma_1)}(p_2)\right]$$

$$\leq \frac{1}{k\mu_2(2\omega_1-\mu_1)}\left[\sum_{q\in V(\Gamma_2)} \sum_{\substack{p_1p_2\in E(Q_k(\Gamma_1)) \\ p_1p_2\in V(Q_k(\Gamma_1))-\mu(\Gamma_1)}} \left[d_{Q_k(\Gamma_1)}(p_1)d_{Q_k(\Gamma_1)}(p_2)\right]\right]^{k\mu_2(2\omega_1-\mu_1)} \tag{28}$$

$$= \frac{1}{k\mu_2(2\omega_1-\mu_1)}\left[(k)\sum_{q\in V(\Gamma_2)} \sum_{\substack{uv\in E(\Gamma_1) \\ vw\in E(\Gamma_2)}} \left[d_{\Gamma_1}(u)+d_{\Gamma_1}(v)\right]\left[d_{\Gamma_1}(v)+d_{\Gamma_1}(w)\right]\right]^{k\mu_2(2\omega_1-\mu_1)}$$

$$= \frac{1}{k\mu_2(2\omega_1-\mu_1)}\left[(k)\mu_2\left[\frac{1}{2}M_4(\Gamma_1)-\frac{1}{2}M_3(\Gamma_1)\right]+\sum_{uv\in V(\Gamma_1)} rd_{\Gamma_1}(u)d_{\Gamma_1}(v)\right]^{k\mu_2(2\omega_1-\mu_1)}$$

$$+\frac{1}{k\mu_2(2\omega_1-\mu_1)}\left[\sum_{v\in V(\Gamma_1)} d^2_{\Gamma_1}(v)\sum_{\substack{u\in V(\Gamma_1) \\ uv\in E(\Gamma_1)}} d_{\Gamma_1}(u)-2M_2(\Gamma_1)\right]^{k\mu_2(2\omega_1-\mu_1)},$$

where r is the total neighbors that we consider mutual nodes of u and v in (Γ_1).

Therefore,

$$\begin{aligned}\prod_2\left(\Gamma_1 +_{Q^k}\Gamma_2\right) \le{}& \frac{1}{\mu_1\omega_2}\left[\omega_2 M_1(\Gamma_1) + 2\omega_1 M_1(\Gamma_2) + \mu_1 M_2(\Gamma_2)\right]^{\mu_1\omega_2}\\ &\times \frac{1}{2\mu_2\omega_1}\left[4\omega_2 M_1(\Gamma_1) + \mu_2\left[M_3(\Gamma_1) + 2M_2(\Gamma_1)\right]\right]^{2\mu_2\omega_1}\\ &\times \frac{1}{(k-1)\mu_2\omega_1}\left[(k-1)\mu_2\left[2M_2(\Gamma_1) + M_3(\Gamma_1)\right]\right]^{(k-1)\mu_2\omega_1}\\ &\times \frac{1}{k\mu_2(2\omega_1-\mu_1)}\left[(k)\mu_2\left[\frac{1}{2}M_4(\Gamma_1) - \frac{1}{2}M_3(\Gamma_1)\right] + \sum_{uv\in V(\Gamma_1)} r d_{\Gamma_1}(u) d_{\Gamma_1}(v)\right]^{k\mu_2(2\omega_1-\mu_1)}\\ &+ \frac{1}{k\mu_2(2\omega_1-\mu_1)}\left[\sum_{v\in V(\Gamma_1)} d^2_{\Gamma_1}(v) \sum_{\substack{u\in V(\Gamma_1)\\ uv\in E(\Gamma_1)}} d_{\Gamma_1}(u) - 2M_2(\Gamma_1)\right]^{k\mu_2(2\omega_1-\mu_1)}.\end{aligned} \tag{29}$$

□

Theorem 4. *Let Γ_1, Γ_2 be two graphs with $|V(\Gamma_1)| = \mu_1$, $|V(\Gamma_2)| = \mu_2$, $|E(\Gamma_1)| = \omega_1$, and $|E(\Gamma_2)| = \omega_2$. For $\mu_1, \mu_2 \ge 4$ and and $k \ge 1$, we have*

$$\begin{aligned}\prod_1\left(\Gamma_1 +_{T_k}\Gamma_2\right) \le{}& \frac{1}{\mu_1\omega_2}\left[\mu_1 M_1(\Gamma_2) + 8\omega_1\omega_2\right]^{\mu_1\omega_2} \times \frac{1}{\omega_1\mu_2}\left[4\omega_1\omega_2 + 2\mu_2 M_1(\Gamma_1)\right]^{\omega_1\mu_2}\\ &\times \frac{1}{2\omega_1\mu_2}\left[4\omega_1\omega_2 + 4\mu_2 M_1(\Gamma_1)\right]^{2\omega_1\mu_2} \times \frac{1}{\omega_1\mu_2(k-1)}\left[2(k-1)\mu_2 M_1(\Gamma_1)\right]^{\omega_1\mu_2(k-1)}\\ &\times \frac{1}{k\mu_2(2\omega_1-\mu_1)}\left[(k)\mu_2\left[M_3(\Gamma_1) + 2M_2(\Gamma_1) - 2M_1(\Gamma_1)\right]\right]^{k\mu_2(2\omega_1-\mu_1)},\\ \prod_2\left(\Gamma_1 +_{T_k}\Gamma_2\right) \le{}& \frac{1}{\omega_2\mu_1}\left[4\omega_2 M_1(\Gamma_1) + 4\omega_1 M_1(\Gamma_2) + \mu_1 M_2(\Gamma_2)\right]^{\omega_2\mu_1} \times \frac{1}{\omega_1\mu_2}\left[4\mu_2 M_2(\Gamma_1) + 4\omega_2 M_1(\Gamma_1) + \omega_1 M_1(\Gamma_2)\right]^{\omega_1\mu_2}\\ &\times \frac{1}{2\mu_2\omega_1}\left[4\omega_2 M_1(\Gamma_1) + \mu_2\left[2M_3(\Gamma_1) + 4M_2(\Gamma_1)\right]\right]^{2\mu_2\omega_1} \times \frac{1}{(k-1)\mu_2\omega_1}\left[(k-1)\mu_2\left[2M_2(\Gamma_1) + M_3(\Gamma_1)\right]\right]^{(k-1)\mu_2\omega_1}\\ &\times \frac{1}{k\mu_2(2\omega_1-\mu_1)}\left[(k)\mu_2\left[\frac{1}{2}M_4(\Gamma_1) - \frac{1}{2}M_3(\Gamma_1)\right] + \sum_{uv\in V(\Gamma_1)} r d_{\Gamma_1}(u) d_{\Gamma_1}(v)\right]^{k\mu_2(2\omega_1-\mu_1)}\\ &+ \frac{1}{k\mu_2(2\omega_1-\mu_1)}\left[\sum_{v\in V(\Gamma_1)} d^2_{\Gamma_1}(v) \sum_{\substack{u\in V(\Gamma_1)\\ uv\in E(\Gamma_1)}} d_{\Gamma_1}(u) - 2M_2(\Gamma_1)\right]^{k\mu_2(2\omega_1-\mu_1)}.\end{aligned} \tag{30}$$

4. Conclusion

For $a, b \geq 4$ and $k = 4$, we consider that $\Gamma_1 = P_a$ and $\Gamma_2 = P_b$ are specific examples of alkane known as paths having orders a and b, respectively. Then, the following results are the direct outcomes of the above four theorems.

$$\prod_1\left(P_{a+S_4}P_b\right) = \frac{1}{ab-a}[8ab-10a-4a+4]^{ab-a} \times \frac{1}{2ab-2b}[12ab-4a-14b+4]^{2ab-2b} \times \frac{1}{3ab-3b}[12ab-12b]^{3ab-3b},$$

$$\prod_2\left(P_{a+S_4}P_b\right) = \frac{1}{ab-a}[16ab-24a-14b+18]^{ab-a} \times \frac{1}{2ab-2b}[16ab-8a-20b+8]^{2ab-2b} \times \frac{1}{3ab-3b}[12ab-12b]^{3ab-3b},$$

$$\prod_1\left(P_{a+R_4}P_b\right) = \frac{1}{ab-a}[12ab-14a-8b+8]^{ab-a} \times \frac{1}{ab-b}[12ab-4a-16b+4]^{ab-b} \times \frac{1}{2ab-2b}[16ab-4a-20b+4]^{2ab-2b} \times \frac{1}{3ab-3b}[12ab-12b]^{3ab-3b},$$

$$\prod_2\left(P_{a+R_4}P_b\right) = \frac{1}{ab-a}[36ab-48a-40b+48]^{ab-a} \times \frac{1}{ab-b}[36ab-22a-60b+30]^{ab-b} \times \frac{1}{2ab-2b}[24ab-8a-32b+8]^{2ab-2b} \times \frac{1}{3ab-3b}[12ab-12b]^{3ab-3b},$$

$$\prod_1\left(P_{a+Q_4}P_b\right) = \frac{1}{ab-a}[8ab-10a-4b+4]^{ab-a} \times \frac{1}{2ab-2b}[16ab-4a-22b+4]^{2ab-2b} \times \frac{1}{3ab-3b}[24ab-36b]^{3ab-3b} \times \frac{1}{4ab-8b}[32ab-72b]^{4ab-8b},$$

$$\prod_2\left(P_{a+Q_4}P_b\right) = \frac{1}{ab-a}[16ab-24a-14b+18]^{ab-a} \times \frac{1}{2ab-2b}[32ab-16a-54b+24]^{2ab-2b} \times \frac{1}{3ab-3b}[48ab-90b]^{3ab-3b} \times \frac{1}{4ab-8b}[64ab-160b]^{4ab-8b},$$

$$\prod_1\left(P_{a+T_4}P_b\right) = \frac{1}{ab-a}[12ab-14a-8b+8]^{ab-a} \times \frac{1}{ab-b}[12ab-4a-16b+4]^{ab-b} \times \frac{1}{2ab-2b}[20ab-4a-28b+4]^{2ab-2b} \times \frac{1}{4ab-8b}[24ab-36b]^{4ab-8b} \times \frac{1}{3ab-3b}[32ab-72b]^{3ab-3b},$$

$$\prod_2\left(P_{a+T_4}P_b\right) = \frac{1}{ab-a}[36ab-48a-40b+48]^{ab-a} \times \frac{1}{ab-b}[36ab-22a-60b+30]^{ab-b} \times \frac{1}{2ab-2b}[48ab-16a-84b+24]^{2ab-2b} \times \frac{1}{4ab-8b}[48ab-90b]^{4ab-8b} \times \frac{1}{3ab-3b}[64ab-160b]^{3ab-3b}, \tag{31}$$

In this paper, for the integer $k \geq 1$, we computed upper bonds of the 1st and 2nd multiplicative Zagreb indices of the generalized F-sum graphs $[(\Gamma_{1+F_k}\Gamma_2)$ for $F_k \in \{S_k, R_k, Q_k, \& T_k\}]$ that was defined by Liu et al. [30]. However, the problem is still open to compute the other topological indices of the generalized F-sum graphs.

Data Availability

The data used to support the findings of this study are cited at relevant places within the text as references.

Conflicts of Interest

The authors declare no conflicts of interest.

Authors' Contributions

All authors contributed equally to this work.

Acknowledgments

This research was supported by the Applied Basic Research (Key Project) of Sichuan Province under grant 2017JY0095 and the Soft Science Project of Sichuan Province under grant 2017ZR0041.

References

[1] G. Rücker and C. Rücker, "On topological indices, boiling points, and cycloalkanes," *Journal of Chemical Information and Computer Sciences*, vol. 39, no. 5, pp. 788–802, 1999.

[2] M. Randić, "On characterization of molecular branching," *Journal of the American Chemical Society*, vol. 97, pp. 6609–6615, 1975.

[3] A. R. Matamala and E. Estrada, "Generalised topological indices: optimisation methodology and physico-chemical interpretation," *Chemical Physics Letters*, vol. 410, no. 4–6, pp. 343–347, 2005.

[4] W. Yan, B.-Y. Yang, and Y.-N. Yeh, "The behavior of Wiener indices and polynomials of graphs under five graph decorations," *Applied Mathematics Letters*, vol. 20, no. 3, pp. 290–295, 2007.

[5] H. González-Dìaz, S. Vilar, L. Santana, and E. Uriarte, "Medicinal chemistry and bioinformatics—current trends in drugs discovery with networks topological indices," *Current Topics in Medicinal Chemistry*, vol. 7, no. 10, pp. 1015–1029, 2007.

[6] X. Li and J. Zheng, "A unified approach to the extremal trees for different indices," *MATCH-Communications in Mathematical and in Computer Chemistry*, vol. 54, pp. 195–208, 2005.

[7] J.-B. Liu, C. Wang, S. Wang, and B. Wei, "Zagreb indices and multiplicative Zagreb indices of eulerian graphs," *Bulletin of the Malaysian Mathematical Sciences Society*, vol. 42, no. 1, pp. 67–78, 2019.

[8] R. Todeschini and V. Consonni, "New local vertex invariants and molecular descriptors based on functions of the vertex degrees," *MATCH-Communications in Mathematical and in Computer Chemistry*, vol. 64, pp. 359–372, 2010.

[9] I. Gutman and B. Furtula, *Novel Molecular Structure Descriptors-Theory and Applications*, University of Kragujevac, Kragujevac, Serbia, 2010.

[10] Z. Shao, M. Siddiqui, and M. Muhammad, "Computing Zagreb indices and Zagreb polynomials for symmetrical nanotubes," *Symmetry*, vol. 10, no. 7, pp. 244–254, 2018.

[11] M. Eliasi, I. Gutman, and A. Iranmanesh, "Multiplicative versions of first Zagreb index," *MATCH-Communications in Mathematical and in Computer Chemistry*, vol. 68, pp. 217–230, 2012.

[12] M. Eliasi and D. Vukičević, "Comparing the multiplicative Zagreb indices," *Communications in Mathematical and in Computer Chemistry*, vol. 69, pp. 765–773, 2013.

[13] F. Yan, Q. Shang, S. Xia, Q. Wang, and P. Ma, "Application of topological index in predicting ionic liquids densities by the quantitative structure property relationship method," *Journal of Chemical & Engineering Data*, vol. 60, no. 3, pp. 734–739, 2015.

[14] M. V. Diudea, *QSPR/QSAR Studies by Molecular Descriptors*, NOVA, New York, NY, USA, 2001.

[15] J. Devillers and A. T. Balaban, *Topological Indices and Related Descriptors in QSAR and QSPR*, Gordon & Breach, Amsterdam, Netherlands, 1999.

[16] R. Gozalbes, J. Doucet, and F. Derouin, "Application of topological descriptors in QSAR and drug design: history and new trends," *Current Drug Target -Infectious Disorders*, vol. 2, no. 1, pp. 93–102, 2002.

[17] J.-B. Liu, J. Zhao, and Z. Zhu, "On the number of spanning trees and normalized Laplacian of linear octagonal-quadrilateral networks," *International Journal of Quantum Chemistry*, vol. 119, Article ID e25971, 2019.

[18] H. Wiener, "Structural determination of paraffin boiling points," *Journal of the American Chemical Society*, vol. 69, no. 1, pp. 17–20, 1947.

[19] I. Gutman and N. Trinajstić, "Graph theory and molecular orbitals. Total φ-electron energy of alternant hydrocarbons," *Chemical Physics Letters*, vol. 17, no. 4, pp. 535–538, 1972.

[20] R. Todeschini, V. Consonni, R. Mannhold, H. Kubinyi, and H. Timmerman, *Handbook of Molecular Descriptors*, Wiley VCH, Weinheim, Germany, 2002.

[21] I. Gutman and O. Polansky, *Mathematical Concepts in Organic Chemistry*, Springer-Verlag, Berlin, Germany, 1986.

[22] I. Gutman, "Degree-based topological indices," *Croatica Chemica Acta*, vol. 86, no. 4, pp. 351–361, 2013.

[23] Z. Shao, M. Liang, and X. Xu, "Some new optimal generalized Sidon sequences," *Ars Combinatoria*, vol. 107, pp. 369–378, 2012.

[24] D. M. Cvetkocić, M. Doob, and H. Sachs, *Spectra of Graphs: Theory and Application*, Academic Press, New York, NY, USA, 1980.

[25] M. Eliasi and B. Taeri, "Four new sums of graphs and their Wiener indices," *Discrete Applied Mathematics*, vol. 157, no. 4, pp. 794–803, 2009.

[26] H. Deng, D. Sarala, S. K. Ayyaswamy, and S. Balachandran, "The Zagreb indices of four operations on graphs," *Applied Mathematics and Computation*, vol. 275, pp. 422–431, 2016.

[27] S. Akhter and M. Imran, "Computing the forgotten topological index of four operations on graphs," *AKCE International Journal of Graphs and Combinatorics*, vol. 14, no. 1, pp. 70–79, 2017.

[28] G. H. Shirdel, H. Rezapour, and A. M. Sayadi, "Hyper-Zagreb index of graph operations," *Iranian Journal of Mathematical Chemistry*, vol. 4, no. 2, pp. 213–220, 2013.

[29] J.-B. Liu, S. Javed, M. Javaid, and K. Shabbir, "Computing first general Zagreb index of operations on graphs," *IEEE Access*, vol. 7, pp. 47494–47502, 2019.

[30] J.-B. Liu, M. Javaid, and H. M. Awais, "Computing Zagreb indices of the subdivision-related generalized operations of graphs," *IEEE Access*, vol. 7, pp. 105479–105488, 2019.
[31] M. Knor, R. Škrekovski, and A. Tepeh, "Convexity result and trees with large Balaban index," *Applied Mathematics and Nonlinear Sciences*, vol. 3, no. 2, pp. 433–446, 2018.
[32] Z. Shao, P. Wu, X. Zhang, D. Dimitrov, and J.-B. Liu, "On the maximum ABC index of graphs with prescribed size and without pendent vertices," *IEEE Access*, vol. 6, pp. 604–616, 2018.
[33] Z. Shao, P. Wu, Y. Gao, I. Gutman, and X. Zhang, "On the maximum ABC index of graphs without pendent vertices," *Applied Mathematics and Computation*, vol. 315, pp. 298–312, 2017.
[34] J. A. Aledo, L. G. Diaz, S. Martinez, and J. C. Valverde, "Predecessors and Gardens of Eden in sequential dynamical systems over directed graphs," *Applied Mathematics and Nonlinear Sciences*, vol. 3, no. 2, pp. 593–602, 2018.
[35] J.-B. Liu, X.-F. Pan, F.-T. Hu, and F.-F. Hu, "Asymptotic Laplacian-energy-like invariant of lattices," *Applied Mathematics and Computation*, vol. 253, pp. 205–214, 2015.
[36] J.-B. Liu and X.-F. Pan, "Minimizing Kirchhoffindex among graphs with a given vertex bipartiteness," *Applied Mathematics and Computation*, vol. 291, p. 8488, 2016.
[37] D. Liu, C. Wang, and S. Wang, "Hamilton-connectivity of interconnection networks modeled by a product of graphs," *Applied Mathematics and Nonlinear Sciences*, vol. 3, no. 2, pp. 419–426, 2018.
[38] S. Wang, Z. Shao, J.-B. Liu, and B. Wei, "The bounds of vertex Padmakar-Ivan index on k-trees," *Mathematics*, vol. 7, no. 4, pp. 324–334, 2019.
[39] B. Basavanagoud, W. Gao, S. Patil, V. R. Desai, K. G. Mirajkar, and B. Pooja, "Computing first Zagreb index and F-index of new C-products of graphs," *Applied Mathematics and Nonlinear Sciences*, vol. 2, no. 1, pp. 285–298, 2017.
[40] M. Azari and A. Iranmanesh, "Some inequalities for the multiplicative sum Zagreb index of graph operations," *Journal of Mathematical Inequalities*, vol. 9, no. 3, pp. 727–738, 2015.
[41] K. C. Das, A. Yurttas, M. Togan, A. S. Cevik, and I. N. Cangul, "The multiplicative Zagreb indices of graph operations," *Journal of Inequality and Applications*, vol. 90, pp. 1–14, 2013.
[42] J. Liu and Q. Zhang, "Sharp upper bounds for multiplicative Zagreb indices," *MATCH-Communications in Mathematical and in Computer Chemistry*, vol. 68, pp. 231–240, 2012.
[43] T. Réti and I. Gutman, "Relations between ordinary and multiplicative Zagreb indices," *Bulletin of International Mathematical Virtual Institute*, vol. 2, pp. 133–140, 2012.
[44] S. Wang and B. Wei, "Multiplicative Zagreb indices of k-tree," *Discrete Applied Mathematics*, vol. 180, pp. 168–175, 2015.
[45] K. Xu and K. C. Das, "Trees, unicyclic and bicyclic graphs extremal with respect to multiplicative sum Zagreb index," *MATCH-Communications in Mathematical and in Computer Chemistry*, vol. 68, pp. 257–272, 2012.
[46] K. Xu and H. Hua, "A unified approach to extremal multiplicative Zagreb indices for trees, unicyclic and bicyclic graphs," *MATCH-Communications in Mathematical and in Computer Chemistry*, vol. 68, pp. 241–256, 2012.

Hindawi
Journal of Chemistry
Volume 2019, Article ID 6073905, 7 pages
https://doi.org/10.1155/2019/6073905

Research Article

The Exact Controllability of the Molecular Graph Networks

Liang Wei,[1,2] **Faxu Li**,[3] **Haixing Zhao**,[3] **Bo Deng**,[2] **and Zhonglin Ye**[3]

[1]*School of Computer Science, Shaanxi Normal University, Xi'an 710062, China*
[2]*School of Mathematics and Statistics, Qinghai Normal University, Xining 810008, China*
[3]*College of Computer, Qinghai Normal University, Xining 810008, China*

Correspondence should be addressed to Faxu Li; lifaxu@qhnu.edu.cn

Received 30 July 2019; Accepted 18 October 2019; Published 30 November 2019

Guest Editor: Jia-Bao Liu

In this paper, we mainly study the exact controllability of several types of extended-path molecular graph networks. Based on the construction of extended-path molecular graph networks with C_3, C_4, or K_4, using the determinant operation of the matrix and the recursive method, the exact characteristic polynomial of these networks is deduced. According to the definition of minimum driver node number N_D, the exact controllability of these networks is obtained. Moreover, we give the minimum driver node sets of partial small networks.

1. Introduction

In recent years, the research on complex network is one of the hottest research fields, and controllability of complex network is a challenging problem in modern network science, such as molecular graph networks, computer networks, social networks, biological networks, and transportation networks [1–8]. The study of network structure has always been a basic object in complex network research. The majority of core issues of research in many fields are based on the structure of the networks, such as connectivity, robustness, and controllability of networks.

In chemical graph theory, the vertices represent each atom and the edges represent the bonds between them in the molecule, and the corresponding molecular graph represents different chemical structures when they represent different things. Figure 1(a) shows the representation of two small molecular structures. As the molecular scale increases, the molecular graph structure gradually becomes a complex system, an example as shown in Figure 1(b). Generally, researchers investigate the related problems of complex systems with large molecular structure by using methods of studying complex networks. In addition, molecular graphs can be used to express some topological properties of molecules. The topological properties of molecules with the same connected structure should be identical. The quantity describing the topological properties of molecules is topological invariants of molecular graphs, such as number of nodes, number of edges, shortest distance, and spectrum. In order to quantify the topological properties of molecules, researchers proposed a lot of indexes, such as Wiener index, Randic index, Hosoya index, Merrifield–Simmons index, and molecular information index.

With the development of network science, people begin to pay much attention to study how to control some nodes in the network to achieve the desirable goals, namely, making the network controllable. The structural controllability of molecular graphs is studied as a molecular topological index. Lin firstly gives the concept of structural controllability in the literature [9] and presents the structural controllability theorem. In the literature [10], the structural controllability theorem is applied to the directed and unweighted complex networks, and the maximum matching theory and the minimum input theorem of structural controllability are proposed.

However, when the edges of the networks are undirected or weighted, the previous theory is not suitable for this type of networks. Then, researchers present another theory framework, which is the exact controllability analysis of the complex network. Yuan et al. [11] proves

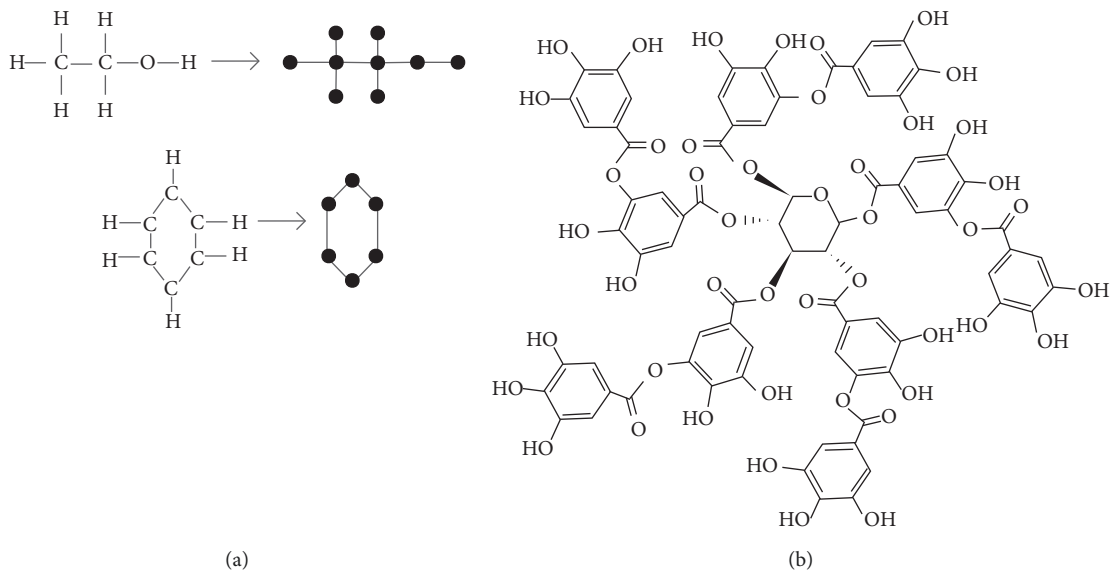

Figure 1: Transformation from molecular structure to molecular graph network. Representation of (a) two small molecular structures and (b) a large molecular structure.

that the number of driver nodes of a network is equal to the maximum geometric multiplicity and gives a method to solve the minimum set of driver nodes. In [12], Wu et al. constructs a star-type network and gives its characteristic polynomial, which directly expresses the exact controllability of this kind of complex networks. Furthermore, research on controllability of multilayer networks and fractal networks, which is common in the chemical system, has some results [13, 14].

In chemistry, hexagonal chain and polyomino chain are two kinds of classical linear systems. In order to observe different linear systems, we consider the controllability of complex networks with linear dynamics. A network with N nodes is described by the following set of ordinary differential equations [15]:

$$\dot{x} = A\mathbf{x} + B\mathbf{u}, \tag{1}$$

where $\mathbf{x} = (x_1, x_2, x_3 \ldots, x_N)^T$ is the status of nodes, $A \in R^{N\times N}$ denotes the coupling matrix of the system, in which a_{ij} represents the weight of a link (i, j) and $\mathbf{u} = (u_1, u_2, u_3 \ldots, u_M)^T$ is the status of M controllers, and B is the control matrix with the size of $N \times M$. In classic control theory, the system (1) can be controlled from any initial state to any final state with finite time if and only if

$$\operatorname{rank}\left(\left[B, AB, A^2B, \ldots, A^{N-1}B\right]\right) = N. \tag{2}$$

Generally, solving the controllability problems is to construct a suitable control matrix B, which consists of a minimum set of driver nodes for satisfying the Kalman rank condition [16]. And there are many possible control matrices B for system (1), which satisfies the controllable condition. The main task of exact controllability is to find a set of B corresponding to the minimum number N_{D} of controllers, which can control the whole network. Then, it is important to measure the exact controllability of the system (1). For undirected graphs, the system controllability can be given by the following terms:

$$N_{\mathrm{D}} = \max_i\{\delta(\lambda_i)\}, \tag{3}$$

where $\delta(\lambda_i)$ is the algebraic multiplicity of eigenvalue of matrix A. It is well known that the theory of graph spectra is related to the chemistry through the HMO (Huckel Molecular Orbital) theory [1]. At an early stage, it was supposed that HMO theory could be reduced to the study of graph spectra of the adjacency matrix of molecular graphs.

In subsequent sections, we mainly discuss the undirected graph with link unweight. Firstly, we give some construction methods of the extended-path molecular graph networks. By using the controllability theory in Sections 3 and 4, we then analyze the exact controllability of these networks and characterize all minimum sets of driver nodes of partial small networks by simulation.

2. Construction of the Extended-Path Networks

In real world, we can find a class of regular networks [17–19], which is constructed like a path network, and each component looks like a star, circle, or clique. In order to carry out our research, we must construct some networks with such characteristics.

Firstly, we give the construction method of the H-extended-path networks (H-EPN), which is composed of several subgraphs pasted together by one common node. As shown in Figure 2(b), H-EPN is composed of subgraph H, the number of H is N, and it satisfies that every two subgraph are connected by one common node. In other words, each edge of the path (Figure 2(a)) can be extended by a subgraph H, which can be connected to each other at a common node. We likewise construct several types of H-$EPNs$ as shown in Figures 3(a)–3(d).

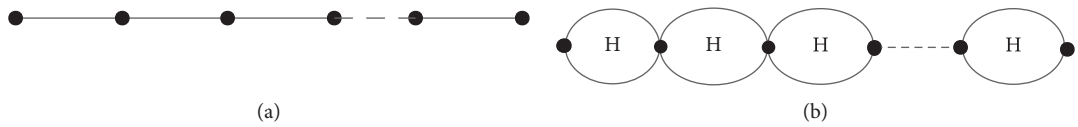

Figure 2: Construction of extended-path networks. (a) Path networks. (b) Extended-path networks.

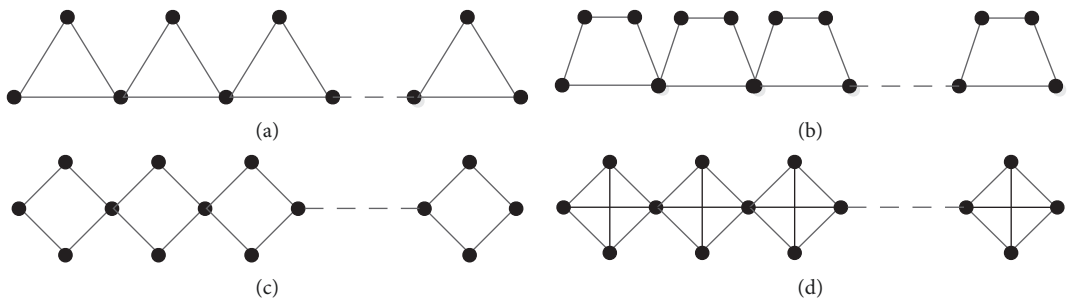

Figure 3: *H-EPN* extended by C_3, C_4, and K_4. (a) C_3-*EPN*. (b) C_4-*EPN*1. (c) C_4-*EPN*2. (d) K_4-*EPN*.

3. Main Results

In this section, we will study the exact controllability of several extended-path networks, which are extended by C_3, C_4, and K_4.

The adjacent matrix of C_3-*EPN* can be formalized as follows:

$$A = \begin{bmatrix} 0 & 1 & 1 & & & \\ 1 & 0 & 1 & & & \\ 1 & 1 & 0 & 1 & 1 & \\ & & 1 & 0 & 1 & \\ & & 1 & 1 & 0 & \\ & & & & & \cdots \end{bmatrix}. \tag{4}$$

Therefore, we can obtain the characteristic polynomial of the coupling matrix A of C_3-*EPN* with $2N+1$ nodes. For convenience, we use B_{2N+1} to represent the determinant of matrix $\lambda I - A$ as follows:

$$\begin{aligned} |\lambda I - A| = B_{2N+1} &= \begin{vmatrix} \lambda & -1 & -1 & & & \\ -1 & \lambda & -1 & & & \\ -1 & -1 & \lambda & -1 & -1 & \\ & & -1 & \lambda & -1 & \\ & & -1 & -1 & \lambda & \\ & & & & & \cdots \end{vmatrix} \\ &= \left(\lambda^2 - 1\right)B_{2N-1} - 2(\lambda+1)C_{2N-2}, \end{aligned} \tag{5}$$

where

$$C_{2N-2} = \begin{vmatrix} \lambda & -1 & & & \\ -1 & \lambda & -1 & -1 & \\ & -1 & \lambda & -1 & \\ & -1 & -1 & \lambda & \\ & & & & \cdots \end{vmatrix}. \tag{6}$$

Thus, it follows that

$$B_{2N+1} = \left(\lambda^2 - 1\right)B_{2N-1} - 2(\lambda+1)C_{2N-2}, \tag{7}$$

$$C_{2N-2} = \lambda B_{2N-3} + \lambda C_{2N-4}. \tag{8}$$

According to the equations (7) and (8), we have

$$B_{2N+1} - \left(\lambda^2 + \lambda - 1\right)B_{2N-1} + \left(\lambda^3 + 2\lambda^2 + \lambda\right)B_{2N-3} = 0. \tag{9}$$

For convenience of calculation, take $S_N = B_{2N+1}$. Then,

$$\begin{aligned} S_{N-1} &= B_{2N-1}, \\ S_{N-2} &= B_{2N-3}. \end{aligned} \tag{10}$$

So we have

$$S_N - \left(\lambda^2 + \lambda - 1\right)S_{N-1} + \left(\lambda^3 + 2\lambda^2 + \lambda\right)S_{N-2} = 0. \tag{11}$$

According to the recursive method in the theory of the determinant, the characteristic equation of recursive relations [11] is given by

$$m^2 - \left(\lambda^2 + \lambda - 1\right)m + \left(\lambda^3 + 2\lambda^2 + \lambda\right) = 0. \tag{12}$$

It is easy to get

$$\begin{aligned} m_1 &= \frac{\left(\lambda^2 + \lambda - 1\right) + p}{2}, \\ m_2 &= \frac{\left(\lambda^2 + \lambda - 1\right) - p}{2}, \end{aligned} \tag{13}$$

where $p = \sqrt{\lambda^4 - 2\lambda^3 - 9\lambda^2 - 6\lambda + 1}$.

Thus, we give the form of solution of S_N in the following expression:

$$S_N = k_1 m_1^N + k_2 m_2^N. \tag{14}$$

For $S_0 = B_1 = \lambda$ and $S_1 = B_3 = \lambda^3 - 3\lambda - 2$, we have $k_1 + k_2 = \lambda$ and $k_1 m_1 + k_2 m_2 = \lambda^3 - 3\lambda - 2$.

So we get

$$k_1 = \frac{\lambda^3 - 3\lambda - 2 - \lambda m_2}{m_1 - m_2} = \frac{1}{p}\left(\lambda^3 - 3\lambda - 2 - \lambda m_2\right),$$
$$k_2 = \frac{\lambda^3 - 3\lambda - 2 - \lambda m_1}{m_1 - m_2} = \frac{1}{p}\left(\lambda^3 - 3\lambda - 2 - \lambda m_1\right). \tag{15}$$

After an arrangement of equations (13)–(15), we have

$$S_N = k_1 m_1^N + k_2 m_2^N = \frac{1}{2p}(\lambda+1)^2\left[(\lambda-2)\left(m_1^N - m_2^N\right) - \lambda^2\left(m_1^{N-1} - m_2^{N-1}\right)\right]. \tag{16}$$

According to equations (5) and (10), the characteristic polynomial of matrix A is as follows:

$$|\lambda I - A| = B_{2N+1} = S_N = \frac{1}{2p}(\lambda+1)^2\left[(\lambda-2)\left(m_1^N - m_2^N\right) - \lambda^2\left(m_1^{N-1} - m_2^{N-1}\right)\right]. \tag{17}$$

Let $g(\lambda) = (\lambda-2)(m_1^N - m_2^N) - \lambda^2(m_1^{N-1} - m_2^{N-1})$, then it is easy to get that $g(-1) \neq 0$, $g(1) \neq 0$, and $g(0) \neq 0$. So the multiplicity of eigenvalue -1 is 2. Now, we discuss the multiplicity of the remaining eigenvalues. We all know from equations (7) and (9) that if there is an eigenvalue λ_0 making $B_{2N+1} = 0$ and suppose that $C_{2N-2} = 0$, then it must be $B_{2N-1} = 0$ and $B_{2N-3} = 0$ (note that 1 and 0 are not roots of the $B_{2N+1} = 0$), which is a contradiction with λ_0 being the root of all $B_{2i+1}(\lambda_0) = 0$, $(i = 1, 2, \ldots, N)$.

Now, we show that there is a principal minor determinant of order $2N$ for B_{2N+1} such that the value is not 0 as follows:

$$A' = \begin{vmatrix} \lambda & -1 & & & & & \\ -1 & \lambda & & & & & \\ & & \lambda & -1 & & & \\ & & -1 & \lambda & -1 & -1 & \\ & & & -1 & \lambda & -1 & \\ & & & -1 & -1 & \lambda & \\ & & & & & & \ldots \end{vmatrix} = \begin{vmatrix} \lambda & -1 \\ -1 & \lambda \end{vmatrix} C_{2N-2}, \tag{18}$$

which is constructed by deleting the 3th row and the 3th volume of B_{2N+1}. For $C_{2N-2} \neq 0$ and $\begin{vmatrix} \lambda & -1 \\ -1 & \lambda \end{vmatrix} \neq 0$ when $\lambda \neq -1$, we have $A' \neq 0$. By $B_{2N+1} = 0$ and $A' \neq 0$ in the case of $\lambda \neq -1$, we see that the rank of the corresponding matrix of B_{2N+1} is $2N$. Then, for all the eigenvalues $\lambda \neq -1$, its multiplicity is 1. So we know that all roots of $B_{2N+1} = 0$ are distinct except -1.

According to the above analysis, it can be known that the maximum multiplicity of the solution of the equation (17) is 2. Therefore, we get the minimum number of driver nodes in the C_3-EPN as follows:

$$N_D = 2. \tag{19}$$

Using the same way, we investigate the exact controllability of the C_4-$EPN1$. The adjacent matrix A of the C_4-$EPN1$ can be formalized as follows:

$$A = \begin{bmatrix} 0 & 1 & 0 & 1 & & & & \\ 1 & 0 & 1 & 0 & & & & \\ 0 & 1 & 0 & 1 & & & & \\ 1 & 0 & 1 & 0 & 1 & 0 & 1 & \\ & & & 1 & 0 & 1 & 0 & \\ & & & 0 & 1 & 0 & 1 & \\ & & & 1 & 0 & 1 & 0 & \\ & & & & & & & \ldots \end{bmatrix}. \tag{20}$$

We obtain the characteristic polynomial of the matrix A as follows:

$$|\lambda I - A| = \begin{vmatrix} \lambda & -1 & 0 & -1 & & & & \\ -1 & \lambda & -1 & 0 & & & & \\ 0 & -1 & \lambda & -1 & & & & \\ -1 & 0 & -1 & \lambda & -1 & 0 & -1 & \\ & & & -1 & \lambda & -1 & 0 & \\ & & & 0 & -1 & \lambda & -1 & \\ & & & -1 & 0 & -1 & \lambda & \\ & & & & & & & \ldots \end{vmatrix}. \tag{21}$$

Let $B_{3N+1} = |\lambda I - A|$, and taking a series of determinant operations, one gets the form as follows:

$$B_{3N+1} = |\lambda I - A| = \lambda^2 C_{3N-1} - 2\lambda B_{3N-2}, \tag{22}$$

$$C_{3N-1} = \lambda B_{3N-2} - 2D_{3N-3}, \tag{23}$$

$$D_{3N-3} = \left(\lambda^2 - 1\right)B_{3N-5} - \lambda D_{3N-6}, \tag{24}$$

where C_{3N-1} and D_{3N-3} are determinants with the size of $(3N-1) \times (3N-1)$ and $(3N-3) \times (3N-3)$, respectively. We can formalise them as follows:

$$C_{3N-1} = \begin{vmatrix} \lambda & -1 & & & & \\ -2 & \lambda & -1 & 0 & -1 & \\ & -1 & \lambda & -1 & 0 & \\ & 0 & -1 & \lambda & -1 & \\ & -1 & 0 & -1 & \lambda & \\ & & & & & \ldots \end{vmatrix},$$
$$D_{3N-3} = \begin{vmatrix} \lambda & -1 & 0 & & & & \\ -1 & \lambda & -1 & & & & \\ 0 & -1 & \lambda & -1 & 0 & -1 & \\ & & -1 & \lambda & -1 & 0 & \\ & & 0 & -1 & \lambda & -1 & \\ & & -1 & 0 & -1 & \lambda & \\ & & & & & & \ldots \end{vmatrix}. \tag{25}$$

Through the equations (22)–(24), we get the following form of recurrence relationship:

$$B_{3N+1} = \left(\lambda^3 - 3\lambda\right)B_{3N-2} - \lambda^4 B_{3N-5}. \quad (26)$$

Now, let us define $S_N = B_{3N+1}, S_{N-1} = B_{3N-2}$, and $S_{N-2} = B_{3N-5}$, then the equation (26) can be formalized as

$$S_N = \left(\lambda^3 - 3\lambda\right)S_{N-1} - \lambda^4 S_{N-2}. \quad (27)$$

According to the above definitions and equation (27), we have $S_0 = B_1 = \lambda$ and $S_1 = B_4 = \lambda^2(\lambda^2 - 4)$, so

$$S_2 = \left(\lambda^3 - 3\lambda\right)S_1 - \lambda^4 S_0 = \lambda^3\left(\lambda^4 - 8\lambda^2 + 12\right) = \lambda^3 f_2(\lambda), \quad (28)$$

where $f_i(x)$ represents the i-th polynomial about x, for which the lowest order is 0. Fox example, $f_0(\lambda) = 1$, $f_1(\lambda) = \lambda^2 - 4$, and $f_2(\lambda) = \lambda^4 - 8\lambda^2 + 12$. Obviously, we can get remaining items formalized as

$$\begin{aligned} S_3 &= \left(\lambda^3 - 3\lambda\right)S_2 - \lambda^4 S_1 = \lambda^4 f_3(\lambda), \\ S_4 &= \left(\lambda^3 - 3\lambda\right)S_3 - \lambda^4 S_2 = \lambda^5 f_4(\lambda), \\ &\ldots \\ S_N &= \left(\lambda^3 - 3\lambda\right)S_{N-1} - \lambda^4 S_{N-2} = \lambda^{N+1} f_N(\lambda). \end{aligned} \quad (29)$$

Using a simple induction and computation, we can easily get (29). That is to say, the lowest orders of polynomials S_0, $S_1, S_2, \ldots$, and S_N are $1, 2, 3, \ldots$, and $N + 1$, respectively, and the multiplicity of the eigenvalue 0 of S_N is $N + 1$. Since a connected graph with diameter D has at least $D + 1$ distinct eigenvalues, noticing that the network C_4-$EPN1$ with N cells has $3N + 1$ nodes and the diameter is $N + 2$, we have that C_4-$EPN1$ has at least $N + 3$ distinct eigenvalues. However, the eigenvalue 0 has a multiplicity of $N + 1$, and the remaining $2N$ eigenvalues have at least $N + 2$ distinct, namely, the maximum multiplicity of these eigenvalues shall not exceed $N - 1$. Therefore, the maximum multiplicity of C_4-$EPN1$'s eigenvalues is $N + 1$ (the eigenvalue is 0). Thus, the minimum number of driver nodes of the system corresponding to the graph C_4-$EPN1$ is as follows:

$$N_D = N + 1. \quad (30)$$

By the analytical method of the preceding part, we can obtain the recursive relations of characteristic polynomial of C_4-$EPN2$ and K_4-EPN (see (31) and (32)) as follows:

$$S_N = \left(\lambda^3 - 4\lambda\right)S_{N-1} - \lambda^4 S_{N-2} = \lambda^{N+1} f_N(\lambda), \quad (31)$$

$$\begin{aligned} S_N &= (\lambda + 1)\left(\lambda^2 - \lambda - 4\right)S_{N-1} - (\lambda + 1)^4 S_{N-2} \\ &= (\lambda + 1)^{N+2} f_N(\lambda + 1). \end{aligned} \quad (32)$$

Using a method similar to that of the C_3-EPN and C_4-$EPN1$, it is easy to get that the minimum number of driver nodes of C_4-$EPN2$ and K_4-EPN, shown in Table 1.

4. Characterization of Driver Nodes

The topology of the complex network determines the controllability, and the minimum driver nodes can quantitatively reflect the controllability of the network structures. Therefore, the minimum driver nodes are the key factors in the structural controllability analysis. In fact, evaluating the exact controllability of complex networks is to obtain the minimum driver nodes of networks.

Table 1: N_D of extended-path networks.

Networks	Number of cells	n	N_D
C_3-EPN	N	$2N + 1$	2
C_4-$EPN1$	N	$3N + 1$	$N + 1$
C_4-$EPN2$	N	$3N + 1$	$N + 1$
K_4-EPN	N	$3N + 1$	$N + 2$

Table 2: N_D and N_C of three kinds of situations.

Case	N_D	N_C
Zero row vector	x	1
Repetitive row vector	$\sum_{i=1}^{y}(r_i - 1)$	$\prod_{i=1}^{y}(C_{r_i}^{r_i-1})$
Correlation row vector	z	$\prod_{j=1}^{z}(C_{c_j}^{1})$

Using the method based on the PBH rank criterion [11, 20], we can characterize the minimum driver node set in detail. The condition of the full rank of the matrix $[\lambda I - A \;\; B]$ is

(1) Matrix $\lambda I - A$ avoids zero vector

(2) Matrix $\lambda I - A$ avoids repetitive vector

(3) Matrix $\lambda I - A$ avoids correlation vector

Because of the symmetry of graph structures, the minimum driver nodes set is not unique and its number is mainly determined by three factors such as zero row vector, repetitive row vector, and correlation row vector of $[\lambda I - A]$.

Let zero vector have x rows, repetitive row vector have y groups, in which each group has $r_1, r_2, \ldots, r_y$ rows, and the correlation row vectors have z groups, in which each group has $c_1, c_2, \ldots, c_z$ rows; then, the number of the minimum driver nodes N_D and the number of groups obtained N_C are shown in Table 2.

Based on the above conditions, we design a corresponding algorithm to obtain the minimum driver nodes set. Through simulation analysis of Matlab platform, we compute the controllability, and describe all sets of minimal driver nodes of C_3-EPN, C_4-EPN, and K_4-EPN(N= 4, 5), respectively; they are shown in Tables 3, 4 and 5; H-EPNs of $N = 4$ are shown in Figure 4.

The simulation results show that, in order to fully control these extended-path networks, the driver nodes selected are usually nodes with small degree, rather than the maximum degree nodes. The point is consistent with the conclusion in the literature [11]. And we can obtain from Table 3 that the C_3-EPN has a fixed number of minimum driver node set, which can be fully controlled by minimal cost. Namely, the C_3-EPN has higher controllability. In addition, although the structures of the C_4-$EPN1$ and C_4-$EPN2$ are different, we find that the controllability of the two networks is exactly the same in different network scales.

Table 3: Controllability of C_3-*EPN*, C_4-*EPN*, and K_4-*EPN* ($N = 4$, 5).

Networks	Number of cell (N)	Number of nodes (n)	Minimum driver node (N_D)	Controllability (N_D/n)
C_3-*EPN*	4	9	2	0.2222
C_4-*EPN*1	4	13	5	0.3846
C_4-*EPN*2	4	13	5	0.3846
K_4-*EPN*	4	13	6	0.4615
C_3-*EPN*	5	11	2	0.1818
C_4-*EPN*1	5	16	6	0.3750
C_4-*EPN*2	5	16	6	0.3750
K_4-*EPN*	5	16	7	0.4375

Table 4: Minimum driver nodes set of C_3-*EPN*, C_4-*EPN*, and K_4-*EPN* ($N = 4$).

Networks	Minimum driver node set
C_3-*EPN*	$\{(n1, n2) \mid n1 \in \{1, 2\}, n2 \in \{8, 9\}\}$
C_4-*EPN*1	$\{(1, n1, n2, n3, n4) \mid n1 \in \{2, 3\}, n2 \in \{5, 6\}, n3 \in \{8, 9\}, n4 \in \{11, 12\}\}$, or $\{(n1, n2, n3, n4, 13) \mid n1 \in \{2, 3\}, n2 \in \{5, 6\}, n3 \in \{8, 9\}, n4 \in \{11, 12\}\}$
C_4-*EPN*2	$\{(n1, 10, 11, 12, 13) \mid n1 \in \{1, 3\}\}$, or $\{(1, 2, 3, 4, n1) \mid n1 \in \{11, 13\}\}$
K_4-*EPN*	$\{(n1, n2, n3, n4, n5, n6) \mid n1 \in \{1, 2, 3\}, n2 \in \{1, 2, 3\}, n1 \neq n2, n3 \in \{5, 6\}, n4 \in \{8, 9\}, n5 \in \{11, 12, 13\}, n6 \in \{11, 12, 13\}, n5 \neq n6\}$

Table 5: Minimum driver node set of C_3-*EPN*, C_4-*EPN*, and K_4-*EPN* ($N = 5$).

Networks	Minimum driver node set
C_3-*EPN*	$\{(n1, n2) \mid n1 \in \{1, 2\}, n2 \in \{10, 11\}\}$
C_4-*EPN*1	$\{(1, n1, n2, n3, n4, n5) \mid n1 \in \{2, 3\}, n2 \in \{5, 6\}, n3 \in \{8, 9\}, n4 \in \{11, 12\}, n5 \in \{14, 15\}\}, n3 \in \{8, 9\}, n4 \in \{11, 12\}, n5 \in \{14, 15\}\}$
C_4-*EPN*2	$\{(n1, 12, 13, 14, 15, 16) \mid n1 \in \{1, 3\}\}$, or $\{(1, 2, 3, 4, 5, n1) \mid n2 \in \{14, 16\}\}$
K_4-*EPN*	$\{(n1, n2, n3, n4, n5, n6, n7) \mid n1 \in \{1, 2, 3\}, n2 \in \{1, 2, 3\}, n1 \neq n2, n3 \in \{5, 6\}, n4 \in \{8, 9\}, n5 \in \{11, 12\}, n6 \in \{14, 15, 16\}, n7 \in \{14, 15, 16\}, n6 \neq n7\}$

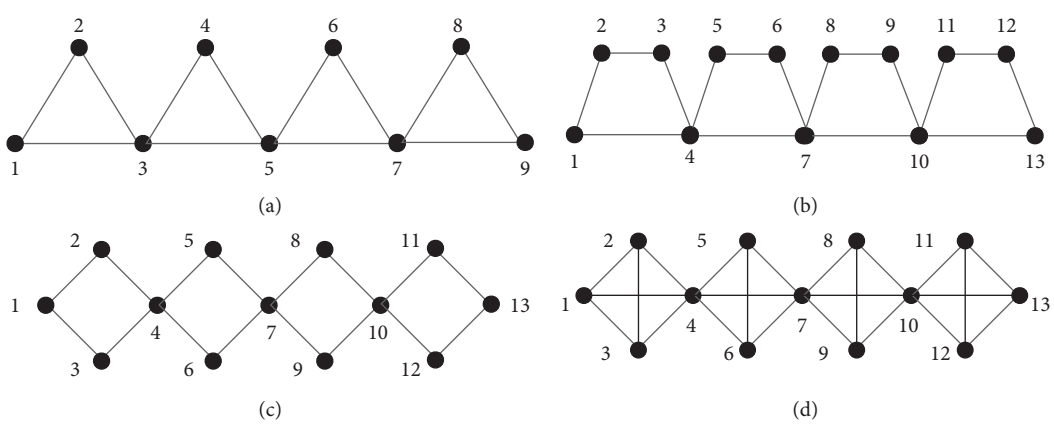

Figure 4: C_3-*EPN*, C_4-*EPN*, and K_4-*EPN* ($N = 4$).

5. Conclusion

To summarize, we mainly study the controllability of several types of the extended-path molecular graph networks. The structural characteristics of these networks are linearly connected by a cycle or complete graph. For these special network structures, we derive the general formula of the characteristic polynomial of the network's adjacent matrix. Furthermore, the exact controllability of these kinds of networks is analyzed, and some results are obtained. In addition, in order to directly reflect the concrete minimum driver node set of each network, we determine the distribution of the nodes by simulation.

Data Availability

All data, models, and codes generated or used during the study are available from the corresponding author upon request.

Conflicts of Interest

The authors declare that there are no conflicts of interest regarding the publication of this paper.

Acknowledgments

This work was supported by the Nature Science Foundation from Qinghai Province (No. 2018-ZJ-718), the Tibetan Information Processing and Machine Translation Key Laboratory of Qinghai Province, and the Key Laboratory of Tibetan Information Processing, Ministry of Education.

References

[1] A. Graovac, I. Gutman, and N. Trinajstic, *Topological Approach to the Chemistry of Conjugated Molecules*, Springer-Verlag, Berlin, Germany, 1977.

[2] A. Lombardi and M. Hornquist, "Controllability analysis of networks," *Physical Review E*, vol. 75, no. 5, Article ID 056110, 2007.

[3] X. F. Wang and G. R. Chen, "Pinning control of scale-free dynamical networks," *Physica A: Statistical Mechanics and its Applications*, vol. 310, no. 3-4, pp. 521–531, 2002.

[4] B. Liu, T. Chu, L. Wang, and G. Xie, "Controllability of a leader-follower dynamic network with switching topology," *IEEE Transactions on Automatic Control*, vol. 53, no. 4, pp. 1009–1013, 2008.

[5] A. Rahmani, M. Ji, M. Mesbahi, and M. Egerstedt, "Controllability of multi-agent systems from a graph-theoretic perspective," *SIAM Journal on Control and Optimization*, vol. 48, no. 1, pp. 162–186, 2009.

[6] G.-R. Chen, "Problems and challenges in control theory under complex dynamical network environments," *Acta Automatica Sinica*, vol. 39, no. 4, pp. 312–321, 2013.

[7] G. Chen, "Pinning control and synchronization on complex dynamical networks," *International Journal of Control, Automation and Systems*, vol. 12, no. 2, pp. 221–230, 2014.

[8] L. Hou, S. Y. Lao, Y. D. Xiao et al., "Recent progression controllability of complex network," *Acta Physica Sinica*, vol. 64, no. 18, pp. 188901_1–188901_11, 2015, (in Chinese).

[9] C. T. Lin, "Structural controllability," *IEEE Trans Automatic Control*, vol. 19, no. 3, pp. 201–208, 1974.

[10] Y.-Y. Liu, J.-J. Slotine, and A.-L. Barabási, "Controllability of complex networks," *Nature*, vol. 473, no. 7346, pp. 167–173, 2011.

[11] Z. Z. Yuan, C. Zhao, Z. R. Di et al., "Exact controllability of complex networks," *Nature Communications*, vol. 4, no. 1, p. 2447, 2013.

[12] L. P. Wu, J. K. Zhou, Z. Z. Yuan et al., "Exact controllability of a star-type network," in *Proceedings of the 27th Chinese Control and Decision Conference (2015 CCDC)*, Qingdao, China, May 2015, pp. 5187-5191, in Chinese.

[13] Z. Yuan, C. Zhao, W.-X. Wang, Z. Di, and Y.-C. Lai, "Exact controllability of multiplex networks," *New Journal of Physics*, vol. 16, no. 10, Article ID 103036, 2014.

[14] J. Li, Z. Yuan, Y. Fan, W.-X. Wang, and Z. Di, "Controllability of fractal networks: an analytical approach," *EPL (Europhysics Letters)*, vol. 105, no. 5, Article ID 58001, 2014.

[15] J. J. Slotine and W. Li, *Applied Nonlinear Control*, Prentice-Hall, Upper Saddle River, NJ, USA, 1991.

[16] R. E. Kalman, "Mathematical description of linear dynamical systems," *Journal of the Society for Industrial and Applied Mathematics Series A Control*, vol. 1, no. 2, pp. 152–192, 1963.

[17] A. Shafieinejad, F. Hendessi, and F. Fekri, "Star-structure network coding for multiple unicast sessions in wireless mesh networks," *Wireless Personal Communications*, vol. 72, no. 4, pp. 2185–2214, 2013.

[18] A. Jain, A. Vyas, and H. Yadav, "Analysis of ethernet load on various nodes of star network using opnet," *International Journal of Computer Science and Applications (TIJCSA)*, vol. 3, no. 1, 2014.

[19] X. J. Li and J. M. Xu, "Fault-tolerance of (n, k) star network," *Applied Mathematics and Computation*, vol. 248, pp. 525–530, 2014.

[20] X. K. Chen, Y. Lu, and L. Y. Chen, "Network structural controllability analysis based on PBH," *Journal of PLA University of Science and Technology (Natural Science Edition)*.

Hindawi
Journal of Chemistry
Volume 2019, Article ID 9259032, 9 pages
https://doi.org/10.1155/2019/9259032

Research Article

On Resolvability Parameters of Some Wheel-Related Graphs

Bin Yang,[1] Muhammad Rafiullah,[2] Hafiz Muhammad Afzal Siddiqui,[2] and Sarfraz Ahmad[2]

[1]*Department of Computer Science and Technology, Hefei University, Hefei 230601, Anhui, China*
[2]*Department of Mathematics, COMSATS University Islamabad, Lahore Campus, Lahore, Pakistan*

Correspondence should be addressed to Hafiz Muhammad Afzal Siddiqui; hmasiddiqui@gmail.com

Received 11 July 2019; Accepted 12 October 2019; Published 28 November 2019

Guest Editor: Shaohui Wang

Let $G = (V, E)$ be a simple connected graph, $w \in V$ be a vertex, and $e = uv \in E$ be an edge. The distance between the vertex w and edge e is given by $d(e, w) = \min\{d(w, u), d(w, v)\}$, A vertex w distinguishes two edges $e_1, e_2 \in E$ if $d(w, e_1) \neq d(w, e_2)$. A set S is said to be resolving if every pair of edges of G is distinguished by some vertices of S. A resolving set with minimum cardinality is the basis for G, and this cardinality is the edge metric dimension of G, denoted by $\operatorname{edim}(G)$. It has already been proved that the edge metric dimension is an NP-hard problem. The main objective of this article is to study the edge metric dimension of some families of wheel-related graphs and prove that these families have unbounded edge metric dimension. Moreover, the results are compared with the metric dimension of these graphs.

1. Introduction and Preliminary

The molecular structure of a chemical compound is known as molecular graph (or chemical graph). There are different structures of chemical compounds, and every structure correlated with many chemical properties, and these properties can be calculated through some specific mathematical formulas. Graph theory helps us to study and analyze these dense structures in detail. In graph theory, we consider every atom as a vertex and covalent bound between atoms as an edge. A *graph* G consists of a set of objects $V(G) = \{v_1, v_2, v_3, \ldots, v_n\}$ called vertices, set of connections between vertices called edges $E(G) = \{e_1, e_2, e_3, \ldots, e_m\}$, and graph G is usually denoted as $G = (V(G), E(G))$. The number of vertices in G denoted by $n = |V(G)|$ is often called the order of G, while the number of edges is known as size of G and denoted by $m = |E(G)|$. The concept of metric dimension was introduced by Slater in 1975 [1], and this concept independently was elaborated for graphs by Harary and Melter in 1976 [2]. After these two papers, lot of research papers have been published related to its theoretical properties and applications. The theoretical studies on metric dimension are highly contributed by several authors like, for instance, independent resolving sets [3], resolving dominating sets [4], strong resolving sets [5], local resolving sets [6], k-metric generators [7, 8], simultaneous metric generators [9], resolving partitions [10], strong resolving partitions [11], and k-antiresolving sets [12]. The metric dimension has many applications in the digital world and in mathematical chemistry such as network verification [13], robot navigation, image processing and pattern recognition [14], mastermind game [15], chemistry [16, 17, 18], and pharmaceutical chemistry [18].

If G is a simple connected graph and u and v are any two vertices of G, then the distance $d(u, v)$ is the length of a shortest path between u and v. Let $S = \{s_1, s_2, s_3, \ldots, s_k\}$ be an ordered set of vertices of G and let v be a vertex of G. The representation $r(v \mid S)$ of v with respect to S is the ordered k-tuple $(d(v, s_1), d(v, s_2), d(v, s_3), \ldots, d(v, s_k))$. If $d(x, v) \neq d(y, v)$, then we shall say that vertex v distinguishes two vertices x and y. If distinct vertices of G have distinct representations with respect to S, then S is called a resolving set for G. A resolving set of minimum cardinality is called a basis for G and the cardinality is known as metric dimension of G, and it is denoted as $\dim(G)$.

Let S be a set of vertices of a simple connected graph G. Then, S is called an edge metric generator for G if every two edges of G are distinguished by some vertices of S. The minimum cardinality of S is called the edge metric dimension, and it is denoted by $\operatorname{edim}(G)$. For an ordered set of vertices $S = \{s_1, s_2, \ldots, s_k\}$ of a graph G and any edge e in G, we refer to the k-vector (ordered k-tuple) $r(e \mid S) = (d(e, s_1), d(e, s_2), \ldots d(e, s_k))$ as the edge metric representation of e with respect to S. The set S is an edge metric generator for G if and only if for every pair of different edges e_1, e_2 of G, $r(e_1 \mid S) \neq r(e_2 \mid S)$.

Let $\mathscr{F} = (G_n)_{n \geq 1}$ be a family of connected graphs G_n of order $\varphi(n)$ for which $\lim \varphi(n)_{n \longrightarrow \infty} = \infty$. If there exists a constant $C > 0$ such that $\operatorname{edim}(G_n) \leq C$ for every $n \geq 1$, then we shall say that $\mathscr{F}$ has a bounded edge metric dimension, otherwise $\mathscr{F}$ has unbounded edge metric dimension. Moreover, if $\operatorname{edim}(G_n) = C$, $\forall n \geq 1$, then $\mathscr{F}$ has a constant edge metric dimension.

There is a controversy in the definition of edge resolving set and edge metric dimension. In the literature, another version of edge metric dimension exists, which is based on the distance between edges, denoted as $d(f, g)$. This version of edge metric dimension follows the following steps.

Step 1. Convert a graph G into a line graph $L(G)$.

Step 2. Find metric dimension, $\dim(L(G))$ of line graph $L(G)$.

According to the above steps, $\dim(L(G)) = \operatorname{edim}(G)$, for reference see [19]. But in our case, the distance is based on vertex to edge, $d(v, e)$, as defined by Kelenc et al. [20].

In 1979, Garey and Johnson [21] pointed out that the finding of the metric dimension of a graph is an NP-hard problem. In 1994, Khuller et al. [22] also showed by another construction that the metric dimension of a graph is an NP-hard problem.

Recently, Kelenc et al. [20] have introduced the notion of edge metric dimension of graph, denoted by $\operatorname{edim}(G)$, and they presented some results relating the notions of metric dimension and edge metric dimension for some families of graph such as for path P_n: $\operatorname{edim}(P_n) = \dim(P_n) = 1$ where $n \geq 2$, for cycle C_n: $\operatorname{edim}(C_n) = \dim(C_n) = 2$, for complete graph K_n: $\operatorname{edim}(K_n) = \dim(K_n) = n - 1$, where $n \geq 2$, for complete bipartite graph $K_{r,t}$: $\operatorname{edim}(K_{r,t}) = \dim(K_{r,t}) = r + t - 2$, where $r, t \geq 2$, for tree T_n which is not a path: $\operatorname{edim}(T) = \dim(T) = \sum_{v \in V, L_v > 1}(L_v - 1)$, for grid graph $G = P_r \square P_t$ (where $r \geq t \geq 2$): $\operatorname{edim}(G) = \dim(G) = 2$, for wheel graph ($G = S_{1,n}$): $\operatorname{edim}(G) > \dim(G)$, and for the grid graph $G = C_r \square C_t$: $\operatorname{edim}(C_r \square C_t) < \dim(C_r \square C_t)$. They also proved that the edge metric dimension is an NP-hard problem. Moreover, they have raised many open problems related to edge metric dimension. Furthermore, in 2019, Zubrilina has classified some graphs on the same topic which has the $\operatorname{edim}(G) = |V| - 1$ in her paper [23]. Recently, in 2019, Rafiullah et al. studied the edge metric dimensions of wheel-related convex polytopes in [24] and characterized these graphs.

This paper is based on the question raised in [20] to characterize the families of graphs which observe one of the relations $\dim(G) = \operatorname{edim}(G)$, $\dim(G) < \operatorname{edim}(G)$, or $\dim(G) > \operatorname{edim}(G)$.

We consider Jahangir graph J_{2n}, helm graph H_n, sunflower graph Sf_n, and friendship graph F_n for edge metric dimension (NP-hard problem). Our aim is to characterize these families with respect to the nature of edge metric dimension. Moreover, we present closed formulas for edge metric dimension of these graphs. For further reading on metric dimension and edge metric dimension, we refer [19, 24, 25, 26, 27].

2. Main Results

2.1. Jahangir Graph (J_{2n}). The *Jahangir graph* J_{2n} obtained from wheel graph W_{2n} by alternately deleting n spokes. The order of J_{2n} is $2n + 1$, and the size is $3n$. The Jahangir graph is also referred to as gear graph G_n [28]. The metric dimension of Jahangir graph $\dim(J_{2n})2n/3$ is given in [29]. Now, we present some observations for J_{2n} in the form of lemmas which help us to compute its edge metric dimension.

Lemma 1. *The central vertex v does not belong to any edge metric basis S of J_{2n}, for $n \geq 6$.*

Proof. Let $J_{2n} = C_{2n} + K_1$ be a gear graph of order $2n + 1$. The vertices of C_{2n} are labeled as $v_1, v_2, v_3, \ldots, v_{2n}$, and edges of J_{2n} are labeled as $e_j = vv_{2j-1}$ and $e_i' = v_i v_{i+1}$ for all $j \in \{1, 2, \ldots, n\}$ and $i \in \{1, 2, \ldots, 2n - 1\}$ as shown in Figure 1. The vertices v_{2j-1} and v_{2j} are named as major and minor vertices, respectively. Since $d(e_j, v) = 0$ and $d(e_i', v) = 1$, v does not belong to any basis of J_{2n}.

Let $S = \{v_{i_1}, v_{i_2}, \ldots, v_{i_r}\}$ be a basis of J_{2n} and $r = |S| \geq 2$ number of vertices on C_{2n} for $n \geq 6$. We say that the pairs of vertices $\{v_{i_a}, v_{i_a+1}\}$ for $1 \leq i \leq r - 1$ and $\{v_{i_r}, v_{i_1}\}$ are pair of neighboring vertices. We define the gap g_a for $1 \leq a \leq r - 1$ as the set of vertices $\{v_j | i_a < j < i_{a+1}\}$ and $g_r = \{v_j | 1 \leq j < i \text{ or } i_r < j \leq 2n\}$. The number of gaps is r and some of which may be empty. If $|a - b| = 1$ or $r - 1$, then the gaps g_a and g_b are known as the neighboring gaps. Let $d(u) = \alpha$ and $d(v) = \beta$ or $d(u) = \beta$ and $d(v) = \alpha$ with $\alpha \leq \beta$. Then, the gap between u and v is denoted by $\alpha - \beta$. The number of vertices between u and v is known as the size of gap. There are three types of gaps observed on C_{2n} of J_{2n}, which are $2 - 2$, $2 - 3$, and $3 - 3$. We represent the major vertices by $\overset{*}{x}$ in the following proofs. □

Lemma 2. *If S is a basis of J_{2n} ($n \geq 6$), then every $2 - 2$, $2 - 3$, and $3 - 3$ gap of S contains at most 5, 4, and 3 vertices, respectively.*

Proof. Let $e_i' = v_i v_{i+1}$ be edges on C_{2n} where $i \in \{1, 2, \ldots, 2n - 1\}$ and $e_j = vv_{2j-1}$ be spokes edges of J_{2n} where $j \in \{1, 2, \ldots, n\}$. Suppose that there is a $2 - 2$ gap of S containing seven consecutive vertices $\overset{*}{x}_{i+1}, x_{i+2}, \ldots, \overset{*}{x}_{i+7}$ of C_{2n}, determined by x_i and x_{i+8} with $d(\overset{*}{x}_{i+1}) = d(\overset{*}{x}_{i+7}) = 3$. Then, we have $r(e_{i+2} \mid S) = r(e_{i+3} \mid S)$, a contradiction. The existence of a $2 - 3$ gap containing six consecutive vertices of C_{2n}: $\overset{*}{x}_{i+1}, x_{i+2}, \ldots, x_{i+6}$, determined by x_i and $\overset{*}{x}_{i+7}$ with

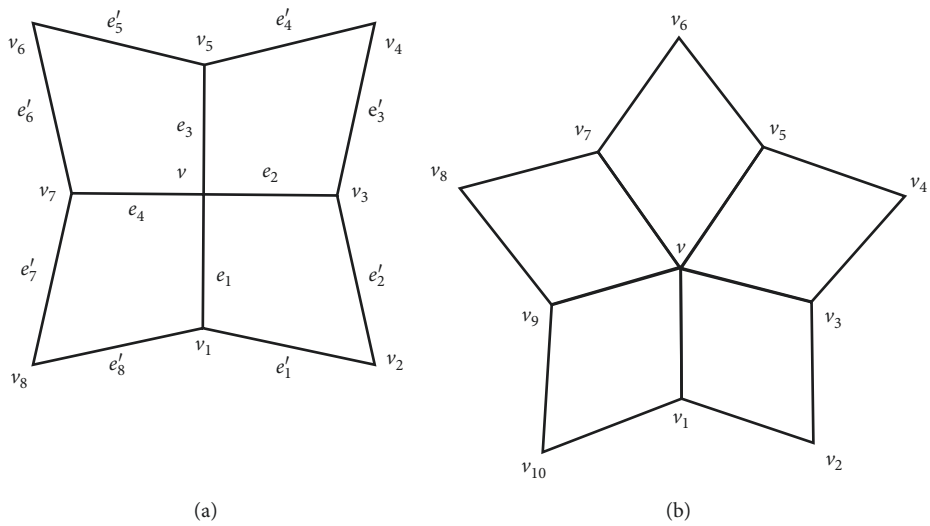

Figure 1: Jahangir graph (J_{2n}). (a) J_8. (b). J_{10}.

$d(\overset{*}{x}_{i+1}) = 3$ and $d(x_{i+6}) = 2$, it follows that $r(e'_{i+4} \mid S) = r(e'_{i+5} \mid S)$ and $r(e_i \mid S) = r(e_{i+1} \mid S)$.

If there is a $3-3$ gap of S containing five consecutive vertices $x_{i+1}, \overset{*}{x}_{i+2}, \ldots, x_{i+5}$ of C_{2n} and determined by $\overset{*}{x}_i$ and $\overset{*}{x}_{i+6}$ with $d(x_{i+1}) = d(x_{i+5}) = 2$ would imply $r(e_{i+1} \mid S) = r(e_{i+2} \mid S)$ and $r(e'_{i+2} \mid S) = r(e'_{i+3} \mid S)$, a contradiction.

Hence, it is proved that every $2-2$, $2-3$, and $3-3$ gap of S contains at most 5, 4, and 3 vertices, respectively.

Note that these $2-2$, $2-3$, and $3-3$ gaps are the known major gaps. □

Lemma 3. *If S is a basis of J_{2n} ($n \geq 6$), then it contains at most one major gap.*

Proof. Suppose that S contains two distinct major gaps g_a and g_b.

(i) $3-3$ and $3-3$: $x_{i+1}, \overset{*}{x}_{i+2}, x_{i+3}$ and $y_{j+1}, \overset{*}{y}_{j+2}, y_{j+3}$, it follows $r(e_{i+1} \mid S) = r(e_{i+3} \mid S)$ and $r(e'_{i+3} \mid S) = r(e'_{i+4} \mid S)$

(ii) $3-3$ and $2-2$: $x_{i+1}, \overset{*}{x}_{i+2}, x_{i+3}$ and $\overset{*}{y}_{j+1}, y_{j+2}, \overset{*}{y}_{j+3}, y_{j+4}, \overset{*}{y}_{j+5}$; in this case $r(e_{i+1} \mid S) = r(e_{i+4} \mid S)$

(iii) $3-3$ and $2-3$: $x_{i+1}, \overset{*}{x}_{i+2}, x_{i+3}$ and $\overset{*}{y}_{j+1}, y_{j+2}, \overset{*}{y}_{j+3}, y_{j+5}$; we have $r(e_{i+1} \mid S) = r(e_{i+3} \mid S)$ and $r(e'_{i+3} \mid S) = r(e'_{i+4} \mid S)$

(iv) $2-2$ and $2-2$: $\overset{*}{x}_{i+1}, x_{i+2}, \overset{*}{x}_{i+3}, x_{i+4}, \overset{*}{x}_{i+5}$ and $\overset{*}{y}_{j+1}, y_{j+2}, \overset{*}{y}_{j+3}, y_{j+4}, \overset{*}{y}_{j+5}$; in this case, $r(e_{i+2} \mid S) = r(e_{i+5} \mid S)$, $r(e_{i+3} \mid S) = r(e_{i+4} \mid S)$, and $r(e'_{i+4} \mid S) = r(e'_{i+9} \mid S)$

(v) $2-2$ and $2-3$: $\overset{*}{x}_{i+1}, x_{i+2}, \overset{*}{x}_{i+3}, x_{i+4}, \overset{*}{x}_{i+5}$ and $\overset{*}{y}_{j+1}, y_{j+2}, \overset{*}{y}_{j+3}, y_{j+4}$; in this case, $r(e_{i+2} \mid S) = r(e_{i+5} \mid S)$, $r(e_{i+3} \mid S) = r(e_{i+4} \mid S)$, and $r(e'_{i+4} \mid S) = r(e'_{i+9} \mid S)$

(vi) $2-3$ and $2-3$: $\overset{*}{x}_{i+1}, x_{i+2}, \overset{*}{x}_{i+3}, x_{i+4}$ and $\overset{*}{y}_{j+1}, y_{j+2}, \overset{*}{y}_{j+3}, y_{j+4}$; in this case, $r(e_i \mid S) = r(e_{i+1} \mid S)$, $r(e_{i+2} \mid S) = r(e_{i+5} \mid S)$, and $r(e'_i \mid S) = r(e'_{i+1} \mid S)$, which contradicts the hypothesis. □

Lemma 4. *If $n \geq 6$ and S be a basis of J_{2n}. Then, any two neighboring gaps, one of which being a major gap, contain together at most six vertices.*

Proof. If we take a $3-3$ gap which contains three vertices, then its neighboring gap should contain three vertices that is only possible when we take $3-3$ as a neighboring gap, which is not possible because Lemma 2 says that the basis only contains one major gap.

If we take major $2-2$ gap with five vertices, then the neighboring cannot be a minor $2-2$ gap with three vertices or minor $2-3$ gap with two vertices, we show them below case wise:

Case 1. The vertices of gaps g_a and g_b are $\overset{*}{x}_{i+1}, x_{i+2}, \overset{*}{x}_{i+3}, x_{i+4}, \overset{*}{x}_{i+5}$ and $\overset{*}{x}_{i+7}, x_{i+8}, x_{i+9}$, respectively, and determined by x_i, x_{i+6}, and x_{i+10}, then we have $r(e_{i+3} \mid S) = r(e_{i+4} \mid S)$ and $r(e'_{i+6} \mid S) = r(e'_{i+8} \mid S)$, a contradiction.

Case 2. The vertices of gaps g_a and g_b are $\overset{*}{x}_{i+1}, x_{i+2}, \overset{*}{x}_{i+3}, x_{i+4}, \overset{*}{x}_{i+5}$ and $\overset{*}{x}_{i+7}, x_{i+8}$, respectively, determined by x_i, x_{i+6}, and x_{i+9}, then we have $r(e_i \mid S) = r(e_{i+1} \mid S)$ and $r(e'_i \mid S) = r(e'_{i+1} \mid S)$.

If the gap is $2-3$ gap with four vertices, then Lemma 2 is sufficient to show the neighboring gap cannot be minor $2-2$ gap with three vertices. In this case, the gaps g_a and g_b vertices are $\overset{*}{x}_{i+1}, x_{i+2}, \overset{*}{x}_{i+3}, x_{i+4}$ and $\overset{*}{x}_{i-1}, x_{i-2}, \overset{*}{x}_{i-3}$, respectively, so $r(e_i \mid S) = r(e_{i+1} \mid S)$ and $r(e'_{i+2} \mid S) = r(e'_{i+3} \mid S)$. □

Lemma 5. *If S is a basis of J_{2n} ($n \geq 6$), then any two minor neighboring gaps contain together at most four vertices.*

Proof. Since by Lemma 2 any minor $2-2$, $2-3$, and $3-3$ gap contains 3, 2, and 1 vertexes, respectively, it is sufficient to consider the following cases:

Case 1. A $2-2$ gap with 3 vertices has a neighboring $2-2$ gap with 3 vertices.

Case 2. A $2-2$ gap with 3 vertices having a neighboring $2-3$ gap with 2 vertices cannot occur.

If Case 1 holds, then $r(e_i \mid S) = r(e_{i+1} \mid S)$ and $r(e'_i \mid S) = r(e'_{i+1} \mid S)$, and if Case 2 holds, then $r(e_i \mid S) = r(e_{i+1} \mid S)$ and $r(e'_i \mid S) = r(e'_{i+1} \mid S)$, so there are contradictions. □

Theorem 1. *If $n \geq 6$, then $edim(J_{2n}) = 2n/3$.*

Proof. We can easily see that $\operatorname{edim}(J_8) = 2$, in this case, the possible resolving sets are $\{v_2, v_4\}$, $\{v_4, v_6\}$, and $\{v_6, v_8\}$. Similarly, we can also see that $\operatorname{edim}(J_{10}) = 3$. First, we show that $\operatorname{edim}(J_{2n}) \leq 2n/3$ by constructing a resolving set in J_{2n} with $2n/3$ vertices. We consider three cases according to the residue classes of modulo 3, where n belongs to the following cases.

Case 1. $n \equiv 0 \pmod 3$. Let $2n = 3k$, where k is even, $k \geq 4$, and $2n/3 = k$. In this case, $S = \{v_{6i-4}, v_{6i} : 1 \leq i \leq k/2 - 1\} \cup \{v_1, v_{2n-4}\}$.

Case 2. $n \equiv 1 \pmod 3$. Let $2n = 3k + 2$, where k is even, $k \geq 4$, and $2n/3 = k$. We define $S = \{v_{6i-2}, v_{6i+2} : 1 \leq i \leq k/2 - 1\} \cup \{v_2, v_{2n-4}\}$.

Case 3. $n \equiv 2 \pmod 3$. Let $2n = 3k + 1$, where k is odd, $k \geq 5$, and $2n/3 = k$ and $S = \{v_{6i-2}, v_{6i} : 1 \leq i \leq (k-1)/2\} \cup \{v_1\}$.

The set S contains only one major gap, and remaining gaps are minor gaps which are $2-2$, $2-3$, and $3-3$ gaps containing 3, 2, and 1 number of vertices, respectively. The total number of vertices in any two neighboring gaps, one of which is major, are at most 6 (Lemma 4). Any two neighboring gaps contain at most 4 vertices (Lemma 5). Now, we show that $\operatorname{edim}(J_{2n}) \geq 2n/3$. Let S be a basis of J_{2n} and $|S| = r$. Then, S induces r gaps on C_{2n}, denoted as $g_1, \ldots, g_r$ such that g_i and g_{i+1} for every $1 \leq i \leq r-1$ and also g_1 and g_r are neighboring gaps. By Lemma 3, at most one of them, say g_1 is a major gap. By Lemma 4, we can write $|g_1| + |g_2| \leq 6$, $|g_r| + |g_1| \leq 6$, and by Lemma 5, the relation for the remaining neighboring gaps is $|g_i| + |g_{i+1}| \leq 4$ for every $i = 2, \ldots, r-1$.

So, we have

$$\begin{gathered} 2(2n - r) = 2\sum_{i=1}^{r} |g_i| \leq 4(r = 2) + 12, \\ 2(2n - r) \leq 4r + 4, \\ r \geq \frac{2n-2}{3} \geq \lfloor \frac{2n}{3} \rfloor. \end{gathered} \tag{1}$$

Since $r \in \mathbb{N}$, for each $n \equiv 0, 1 \text{ or } 2 \pmod 3$, we obtain $r \geq 2n/3$. □

2.2. Helm Graph (H_n). The *helm graph* H_n is obtained from wheel graph W_n by adding a single pendant edge at each vertex of cycle C_n. The number of vertices in the helm graph are $|V| = 2n + 1$, and the number of edges are $|E| = 3n$. We labeled the central vertex, cycle vertices, and pendant vertices as v, v_i, and v'_i, respectively, where $1 \leq i \leq n$. There are three types of edges, and we labeled them in such a way $e_i = vv_i$, $e'_i = v_i v_{i+1}$, and $e''_i = v_i v'_i$, see Figure 2.

In [30], it was proved that the metric dimension of the helm graph is unbounded, i.e., $\dim(H_n) = 2n + 2/5$.

Theorem 2. *Let H_n be a helm graph. Then,*

$$\operatorname{edim}(H_n) = \begin{cases} n, & n = 3, 4, \\ n - 1, & n \geq 5. \end{cases} \tag{2}$$

Proof. If $n = 3$ or 4, then the proof is simple. Let $n \geq 5$ and $V(H_n) = \{v, v_1, v_2, \ldots, v_n, v'_1, v'_2, \ldots, v'_n\}$, where $d(v) = n$, vertices v_i are on C_n and they have degree 4, i.e., $d(v_i) = 4$, and the v'_i are the pendant vertices having $d(v_i) = 1$. To prove that S is a minimum edge resolving set, we consider the following three cases:

(1) If $e_i = vv_i$, then e_i has distance 0 to v_i and distance 1 to v_j, where $j \in \{1, 2, \ldots, n\}$ and $j \neq i$, distance 1 to v'_i and distance 2 to v'_j, where $j \in \{1, 2, \ldots, n\}$ and $j \neq i$.

(2) If $e'_i = v_i v_{i+1}$, then e'_i has distance 0 to v_i and v_{i+1}, distance 1 to $\{v, v_{i-1}, v_{i+2}\}$, distance 2 to all other vertices on C_n, distance 1 to $\{v'_i, v'_{i+1}\}$, distance 2 to $\{v'_{i-1}, v'_{i+2}\}$, and distance 3 to all other pendant vertices.

(3) If $e''_i = v_i v'_i$, then e''_i has distance 0 to v_i and v'_i, distance 1 to $\{v, v_{i-1}, v_{i+1}\}$, distance 2 to $\{v'_{i-1}, v'_{i+1}\}$, and distance 3 to all other pendant vertices.

The above cases show that the edge metric representation with any $n-2$ vertices or less number of vertices of H_n is same for some edges. So, S is the edge metric generator with $n-1$ vertices, and therefore,

$$\operatorname{edim}(H_n) \leq n - 1. \tag{3}$$

We can also show that the $\operatorname{edim}(H_n) \nleq n - 2$ by considering S as a basis of H_n with $|S| = n - 2$. For this we have the following cases:

(i) If we take $S = \{v_i, v_{i+1}, \ldots, v_{n-2}\}$, then $r(e_{i-1} \mid S) = r(e_{n-1} \mid S)$.

(ii) If we suppose $S = \{v'_i, v'_{i+1}, \ldots, v'_{n-2}\}$, then $r(e_{i-1} \mid S) = r(e_{n-1} \mid S)$.

(iii) If we consider $S = \{v'_i, \ldots, v'_{i+n-4}, v'_{i+n-3}\}$ and $S = \{v'_i, v'_{i+1}, \ldots, v'_{i+n-3}\}$, then $r(e_i \mid S) = r(e'_i \mid S)$ and $r(e_{i+1} \mid S) = r(e_{i+2} \mid S)$, respectively.

So, set S is not the basis of H_n. This implies that

$$\operatorname{edim}(H_n) \geq n - 1. \tag{4}$$

Hence, from inequalities (3) and (4), we have $\operatorname{edim}(H_n) = n - 1$.

Note. The total number of edge resolving sets for the helm graph (H_n) is $n + 1$. □

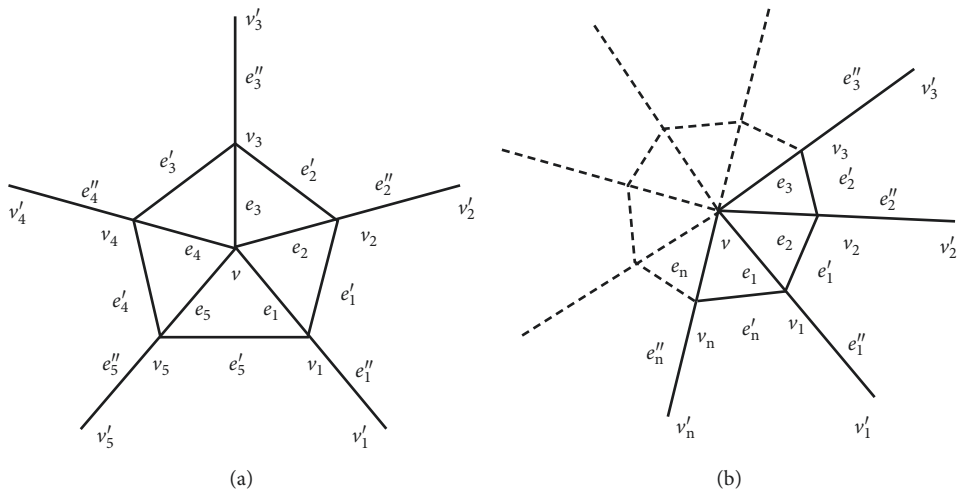

Figure 2: Helm graph (H_n). (a) H_5. (b). H_n.

2.3. Sunflower Graph (Sf_n). The *sunflower graph* Sf_n obtained from wheel graph (W_n) having a cycle C_n $(v_1, v_2, \ldots, v_n)$ and by adding n new vertices $v_1', v_2', \ldots, v_n'$ with new edges (v_i', v_i) and (v_i', v_{i+1}) where $1 \le i \le n$ are shown in Figure 3. The number of vertices in the sunflower graph are $|V| = 2n + 1$, and the number of edges are $|E| = 4n$. We labeled the central vertex, cycle vertices, and the newly added vertices by v, v_i, and v_i', respectively, where $1 \le i \le n$. We denote the cycle $v_1, v_1', v_2, v_2', \ldots, v_n', v_1$ by C_{2n}'. There are three types of edges and we label them in the following manner, $e_i = vv_i$, $e_i' = v_i v_{i+1}$, and $e_i'' = v_i v_i'$ or $e_i'' = v_{i+1} v_i'$, consider Figure 3 for reference.

The metric dimension of the sunflower graph for $n \ge 6$,

$$\dim(Sf_n) = \begin{cases} \dfrac{n}{3}, & n \equiv 0 \,(\mathrm{mod}3), \\ \left.\begin{array}{ll} \dfrac{n-1}{3}, & \text{if } n \text{ is odd}, \\ \dfrac{n+1}{3}, & \text{if } n \text{ is even}, \end{array}\right\}, & n \equiv 1 \,(\mathrm{mod}3), \\ \dfrac{n+1}{3}, & n \equiv 2 \,(\mathrm{mod}3). \end{cases} \tag{5}$$

Now, we present some observations for Sf_n to prove its edge metric dimension.

(i) There are two edge disjoint cycles: $C_n : v_1 e_1' v_2 e_2' v_3 \cdots e_{n-1}' v_n e_n' v_1$ and $C_{2n}' : v_1 e_1'' v_1' e_2'' v_2 \cdots v_n e_{2n-1}'' v_n' e_{2n}'' v_1$.

(ii) Every $2-2$ gap of S contains one vertex v_i or three vertices v_i, v_i', v_{i+1} of C_n and C_{2n}', respectively.

(iii) There are three types of gaps, namely, $2-2$, $2-5$, and $5-5$ with the maximum gap of sizes 3, 2, and 0, respectively.

(iv) The resolving set S contains two $2-5$ gaps of sizes 2 and 0, when $n \equiv 2\,(\mathrm{mod}3)$.

(v) The resolving set S mostly contains $2-2$ gaps.

(vi) Any two $2-2$ neighboring gaps contain together at most 4 number of vertices.

(vii) The neighboring $2-2$ and $2-5$ gaps contain together at most 3 number of vertices.

(viii) Only one vertex of degree 5 from C_n belongs to edge resolving set S of Sf_n, when $n \equiv 2\,(\mathrm{mod}3)$ and all remaining vertices belong to C_{2n}'. If we consider any two consecutive vertices of the degree 5 in basis set S such as v_i and v_{i+1}, then $r(e_{i+1}' \mid S) = r(e_{i+2}' \mid S) = (1, 0, 2, 3, \ldots, 3)$ and $r(e_i' \mid S) = r(e_{i-1} \mid S) = (0, 1, 3, \ldots, 3, 2)$. So, the $5-5$ gap is not possible in the sunflower graph for edge metric dimension.

(ix) Any two $2-5$ neighboring gaps contain together at most 2 vertices. If there are 4 vertices in $2-5$ neighboring gaps for $v_i \in S$ where $1 \le i \le 2n$, then $r(e_{i+1}' \mid S) = r(e_{i+3}' \mid S) = (1, 1, 2, \ldots, 2)$, $r(e_{i-1}' \mid S) = r(e_i' \mid S) = (1, 2, \ldots, 1, 2)$, and $r(e_{2n}'' \mid S) = r(e_n' \mid S) = (0, 2, 3, \ldots, 3)$.

(x) The central vertex v does not belong to any edge metric basis S of Sf_n because $d(e_i, v) = 0$, $d(e_i', v) = 1$, and $d(e_j'', v) = 1$ where $1 \le i \le n$ and $1 \le j \le 2n$.

We can also define the selection of basis S of Sf_n by the following Claims.

Claim 1. The resolving set S mostly contains $2-2$ gaps having one vertex.

If a gap g of the size 1 with vertex v_{i+1} on C_n and $v_i', v_{i+1}', v_{i+3}', v_{i+4}' \in S$, then g contains two edges $e_{i+1}'' = v_i' v_{i+1}$ and $e_{i+2}'' = v_{i+1} v_{i+1}'$ on C_{2n}'. If $z \in \{e_{i+1}'', e_{i+2}''\}$ then

$$\begin{aligned} r(z \mid S) &= (1, 0, 1, 2, \ldots, 2, \overline{0, 1, 2, 3, \ldots, 3, 2}), \\ r(z \mid S) &= (1, 0, 1, 2, \ldots, 2, \overline{1, 0, 2, 3, \ldots, 3, 2}), \end{aligned} \tag{6}$$

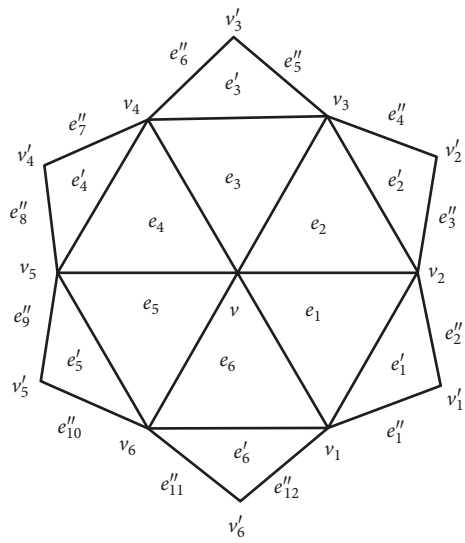

Figure 3: Sunflower graph (Sf_6).

where the normal part of the code and overlined part of the code represent the distance of z from v_i and v'_i types of vertices, respectively.

By observation v and Claim 1, there is no other edge in Sf_n having these types of codes.

Claim 2. At most one $2-2$ gap of S has at most 3 number of vertices.

If a gap g of the size 3 with vertices $v_{i+3}, v'_{i+3}, v_{i+4}$, on C'_{2n} and $v'_i, v'_{i+1}, v'_{i+2}, v'_{i+4}, v'_{i+5} \in S$, then the g contains 5 number of edges, one of them $e'_{i+3} = v_{i+3}v_{i+4}$ on C_n, and 4 of them $e''_{i+5} = v'_{i+2}v_{i+3}, e''_{i+6} = v_{i+3}v'_{i+3}, e''_{i+7} = v'_{i+3}v_{i+4}, e_{i+8} = v_{i+4}v'_{i+4}$ on C'_{2n}. If $z \in \{e'_{i+3}, e''_{i+5}, e''_{i+6}, e''_{i+7}, e''_{i+8}\}$, then

$$\begin{aligned}
r(z\mid S) &= (2,2,1,0,0,1,2,\ldots,2,\overline{3,2,1,1,1,2,3,\ldots,3}),\\
r(z\mid S) &= (2,2,1,0,1,2,\ldots,2,\overline{3,2,0,1,2,3,\ldots,3}),\\
r(z\mid S) &= (2,2,1,0,1,2,\ldots,2,\overline{3,2,1,0,2,3,\ldots,3}),\\
r(z\mid S) &= (2,2,2,1,0,1,2,\ldots,2,\overline{3,3,2,0,1,3,\ldots,3}),\\
r(z\mid S) &= (2,2,2,1,0,1,2,\ldots,2,\overline{3,3,2,1,0,2,3,\ldots,3}),
\end{aligned} \tag{7}$$

where the normal part of the code and overlined part of the code represent the distance of z from v_i and v'_i types of vertices, respectively.

By observation iii and Claim 2, there is no other edge in Sf_n with these types of codes.

Claim 3. At most one $2-5$ gap of S has 2 vertices.

If a gap g of the size 2 with vertices v_n,v'_n, and $v'_{n-7}, v'_{n-6}, v'_{n-4}, v'_{n-2}, v'_{n-1}, v_{n+1} = v_i \in S$, then the g contains 4 number of edges, one of them $e'_n = v_nv_{n+1}$ on C_n and 3 of them $e''_{2n-2} = v'_{n-1}v_n$, $e''_{2n-1} = v_nv'_n$, $e''_{2n-1} = v'_nv_{n+1}$ on C'_{2n}. If z $z \in \{e'_n, e''_{2n-2}, e''_{2n-1}, e''_{2n}\}$, then

$$\begin{aligned}
r(z\mid S) &= (0,1,2,\ldots,2,1,0,\overline{1,2,3,\ldots,3,2,1,1}),\\
r(z\mid S) &= (1,2,\ldots,2,1,0,\overline{2,3,\ldots,3,2,0,1}),\\
r(z\mid S) &= (1,2,\ldots,2,1,0,\overline{2,3,\ldots,3,2,1,0}),\\
r(z\mid S) &= (0,1,2,\ldots,2,0,1,\overline{1,2,3,\ldots,3,2,1}),
\end{aligned} \tag{8}$$

where the normal part of the code and overlined part of the code represent the distance of z from v_i and v'_i types of vertices, respectively.

By observations iii and iv and Claim 3, there is no other edge in Sf_n with these type of codes.

Claim 4. Any two, $2-2$ neighboring gaps contain together at most 4 number of vertices.

Let two $2-2$ neighboring gaps g_a and g_b have 1 and 3 number of vertices, respectively. The gaps g_a and g_b are determined by v'_i, v'_{i+2}, and v'_{i+3}. The gap g_a has one vertex v_{i+2} and two edges $e''_{i+3} = v'_{i+1}v_{i+2}$, $e''_{i+4} = v_{i+2}v'_{i+2}$ on C'_{2n}. The g_b has 3 vertices v_{i+3}, v'_{i+3}, and v_{i+4} and 5 number of edges, one of them $e'_{i+3} = v_{i+3}v_{i+4}$ on C_n and 4 of them $e''_{i+5} = v'_{i+2}v_{i+3}$, $e''_{i+6} = v_{i+3}v'_{i+3}$, $e''_{i+7} = v'_{i+3}v_{i+4}$, $e''_{i+8} = v_{i+4}v'_{i+4}$ on C'_{2n}. If $v'_i, v'_{i+1}, v'_{i+2}, v'_{i+4}, v'_{i+5} \in S$ and z $z \in \{e''_{i+3}, e'_{i+3}, e''_{i+4}, e'_{i+5}, e'_{i+6}, e'_{i+7}, e'_{i+8}\}$, then

$$\begin{aligned}
r(z\mid S) &= (2,1,0,1,2,\ldots,2,\overline{2,0,1,2,3,\ldots,3}),\\
r(z\mid S) &= (2,2,1,0,0,1,2,\ldots,2,\overline{3,2,1,1,1,2,3,\ldots,3}),\\
r(z\mid S) &= (2,1,0,1,2,\ldots.,2,\overline{2,1,0,2,3,\ldots,3}),\\
r(z\mid S) &= (2,2,1,0,1,2,\ldots,2,\overline{3,3,2,0,1,3,\ldots,3}),\\
r(z\mid S) &= (2,2,1,0,1,2,\ldots,2,\overline{3,2,1,0,2,3,\ldots,3}),\\
r(z\mid S) &= (2,2,2,1,0,1,2,\ldots,2,\overline{3,3,2,0,1,3,\ldots,3}),\\
r(z\mid S) &= (2,2,2,1,0,1,2,\ldots,2,\overline{3,3,2,1,0,2,3,\ldots,3}),
\end{aligned} \tag{9}$$

where the normal part of the code and overlined part of the code represent the distance of z from v_i and v'_i types of vertices, respectively.

By observations iii, v, and vi and Claim 4, there is no other edge in Sf_n having these types of codes.

Claim 5. The neighboring $2-2$ and $2-5$ gaps contain together at most 3 number of vertices.

Let g_a and g_b be $2-2$ and $2-5$ neighboring gaps having 1 and 2 vertices, respectively. These gaps can be determined by v'_{i-7}, v'_{n-1}, and v_{n+1}. The gap g_a has one vertex v_{n-1} on C_n or two edges $e''_{2n-3} = v'_{n-1}v_{n-1}$, $e''_{2n-4} = v_{n-1}v'_n$ on C'_{2n}. The g_b has 2 vertices v_n, v'_n and 4 number of edges, one of them $e'_n = v_nv_{n+1}$ on C_n and 3 of them $e''_{2n-2} = v_{n-1}'v_n$, $e''_{2n-1} = v_nv'_n$, and $e''_{2n} = v'_nv_{n+1}$ on C'_{2n}. If $v'_{n-7}, v'_{n-6}, v'_{n-4}, v'_{n-2}, v'_{n-1}, v'_{n+1} = v_i \in S$ and $z \in \{e'_n, e''_{2n-4}, e''_{2n-3}, e''_{2n-2}, e''_{2n-1}, e''_{2n}\}$, then

$$\begin{aligned}
r(z \mid S) &= (0,1,2,\ldots,2,1,0,\overline{1,2,3,\ldots,3,2,1,1}),\\
r(z \mid S) &= (2,\ldots,2,1,0,1,\overline{3,\ldots,3,2,0,1,2}),\\
r(z \mid S) &= (2,\ldots,2,1,0,1,1,0,\overline{3,\ldots,3,2,1,0,2}),\\
r(z \mid S) &= (1,2,\ldots,2,1,0,\overline{2,3,\ldots,3,2,0,1}),\\
r(z \mid S) &= (1,2,\ldots,2,1,0,\overline{2,3,\ldots,3,2,1,0}),\\
r(z \mid S) &= (0,1,2,\ldots,2,0,1,\overline{1,2,3,\ldots,3,2,1}),
\end{aligned} \tag{10}$$

where the normal part of the code and overlined part of the code represent distance of z from v_i and v_i' types of vertices, respectively.

By observations iii, v, and vii and Claim 5, there is no other edge in Sf_n with these types of codes.

Theorem 3. *If $n \geq 6$, then $edim(Sf_n) = 2n/3$.*

Proof. The resolving set for Sf_5 is $S = \{v_2, v_3, v_7, v_9, v_{10}\}$.

First, we show that $edim(Sf_n) \leq 2n/3$ for $n \geq 6$ by constructing a resolving set for Sf_n with $2n/3$ vertices. We consider three cases according to the residue class modulo 3 to which n belongs.

Case 1. $n \equiv 0 \pmod 3$. Let $2n = 3k$, where k is even, $k \geq 4$, and $2n/3 = k$. In this case, $S = \{v_{3i-1}', v_{3i}' : 1 \leq i \leq (k/2) - 1\} \cup \{v_{n-1}', v_n'\}$.

Case 2. $n \equiv 1 \pmod 3$. Let $2n = 3k + 2$, where k is even, $k \geq 4$, and $2n/3 = k$. We define $S = \{v_{3i}', v_{3i+1}' : 1 \leq i \leq (k/2) - 1\} \cup \{v_{n+2}'\}$.

Case 3. $n \equiv 2 \pmod 3$. Let $2n = 3k + 1$, where k is odd, $k \geq 5$, and $2n/3 = k$ and $S = \{v_{3i+2}', v_{3i+2}' : 1 \leq i \leq (k/2) - 1\} \cup \{v_{n+2}'\}$.

To show that $edim(Sf_n) \geq 2n/3$, we consider the aforementioned observations.

Let S be a basis of Sf_n and $|S| = r$. Then, S induces r gaps which are denoted as $g_1, \ldots, g_r$ such that g_i and g_{i+1} for every $1 \leq i \leq r - 1$ and also g_1 and g_r are neighboring gaps. We can write $|g_1| + |g_2| \leq 3$, $|g_r| + |g_1| \leq 3$ and the relation for the remaining neighboring gaps is $|g_i| + |g_{i+1}| \leq 3$ for every $i = 2, \ldots, r - 1$.

So, we have

$$\begin{aligned}
2(2n - r) &= 2\sum_{i=1}^{r} |g_i| \leq 4(r-2) + 6,\\
2(2n - r) &\leq 4r - 2,\\
r &\geq \frac{4n+2}{6} = \frac{2n}{3} + \frac{1}{3} \geq \left\lceil \frac{2n}{3} \right\rceil.
\end{aligned} \tag{11}$$

Since $r \in \mathbb{N}$, for each $n \equiv 0, 1$ *or* $2 \pmod 3$, we obtain $r \geq 2n/3$ Hence, the theorem is proved. □

2.4. Friendship Graph (F_n). The *friendship graph* F_n can be obtained from the wheel graph by removing the alternative edges of the C_n cycle of W_n. The number of vertices in the friendship graph are $|V| = 2n + 1$, and the number of edges are $|E| = 3n$. We label the central vertex and remaining vertices as v and v_i, respectively, where $1 \leq i \leq 2n$. There are two types of edges, and we label them in such a way $e_i = vv_i$ and $e_j' = v_{2j-1}v_{2j}$ where $j \in \{1, 2, \ldots, n\}$, for reference, see Figure 4

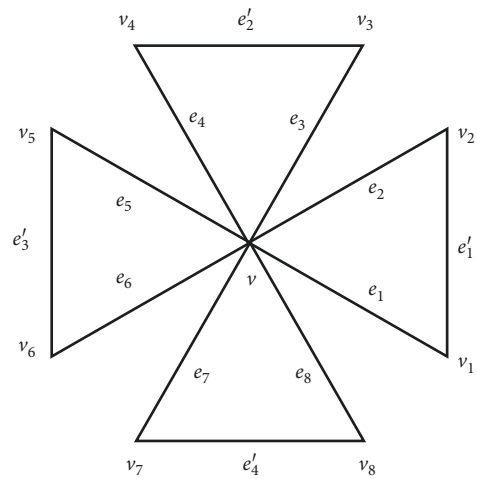

Figure 4: Friendship graph (F_4).

The metric dimension of friendship graph $\dim(F_n) = n$ for $n \geq 2$, computed by Mulyono and Wulandari in [31].

Theorem 4. *Let F_n be a friendship graph, then $edim(F_n) = 2n - 1$ for $n \geq 3$.*

Proof. Let $n \geq 3$ and $V(F_n) = \{v, v_1, v_2, \ldots, v_{2n}\}$, where $d(v) = 2n$ and $d(v_i) = 2$, where $i \in \{1, 2, \ldots, 2n\}$. To prove that S is a minimum edge resolving set, we consider the following three cases:

Case 1. If $e_i = vv_i$, then e_i has distance 0 to $\{v, v_i\}$ and distance 1 to all other vertices, where $i \in \{1, 2, \ldots, 2n\}$.

Case 2. If $e_i' = v_iv_{i+1}$, then e_i' has distance 0 to v_i and v_{i+1} distance 1 to v, distance 2 to all other vertices.

The above cases show that the edge metric representation of edges of $G \cong F_n$ with respect to a set with $2n - 2$ vertices is not distinct. So S can be edge metric generator if we take $2n - 1$ number of vertices. Therefore, the edge metric dimension of the friendship graph is $2n - 1$.

We also show that the by considering the resolving set, S of the size $2n - 2$. Let $S = \{v_i, v_{i+1}, \ldots, v_{2n-2}\}$, then $r(e_{n-1} \mid S) = r(e_n \mid S)$ or $r(e_i \mid S) = r(e_n \mid S)$. So set S is not the basis of F_n. Hence, it is proved that $edim(F_n) = 2n - 1$.

Note. The total number of edge resolving sets for a fan graph (F_n) is $2n$. □

3. Conclusion

In this article, the edge metric dimension for certain families of wheel-related graphs, like Jahangir graph J_{2n}, helm graph H_n, sunflower graph Sf_n, and friendship graph F_n, have been studied and proved that all these families have

unbounded edge metric dimensions. We also compared the results with their metric dimensions and concluded that $\dim(G) = \operatorname{edim}(G)$ if $G \cong J_{2n}, H_n$, and $\dim(G) < \operatorname{edim}(G)$ if $G \cong Sf_n, F_n$.

4. Open Problems

It is natural to ask about the characterization of the graph families on the bases of the nature of their edge metric dimension. To answer the aforementioned question, the readers are invited to study the following problems.

(1) Characterize the nanostructures, nanocones, nanotubes, nanotorus, and chemical trees on the basis of edge metric dimension.

(2) Is it the case that the other families of graphs generated by wheel also have unbounded edge metric dimension?

Data Availability

The data used to support the findings of this study are included within the article.

Conflicts of Interest

The authors declare no conflicts of interest.

Authors' Contributions

All the authors contributed equally to preparing this article.

Acknowledgments

The authors are grateful to Prof. Jia-Bao Liu for his useful suggestions and help to improve and complete this manuscript. This study was supported by Major University Science Research Project of Anhui Province (KJ2016A605) and Major Nature Science Project of Hefei University Research and Development Foundation (16ZR13ZDA).

References

[1] P. J. Slater, "Leaves of trees," *Congressus Numerantium*, vol. 14, pp. 549–559, 1975.

[2] F. Harary and R. A. Melter, "On the metric dimension of a graph," *Ars Combinatoria*, vol. 2, pp. 191–195, 1976.

[3] G. Chartrand, V. Saenpholphat, and P. Zhang, "The independent resolving number of a graph," *Mathematica Bohemica*, vol. 128, no. 4, pp. 379–393, 2003.

[4] R. C. Brigham, G. Chartrand, R. D. Dutton, and P. Zhang, "Resolving domination in graphs," *Mathematica Bohemica*, vol. 128, no. 1, pp. 25–36, 2003.

[5] O. R. Oellermann and J. Peters-Fransen, "The strong metric dimension of graphs and digraphs," *Discrete Applied Mathematics*, vol. 155, no. 3, pp. 356–364, 2007.

[6] F. Okamoto, S. Phinezyn, and P. Zhang, "The local metric dimension of a graph," *Mathematica Bohemica*, vol. 135, no. 3, pp. 239–255, 2010.

[7] A. Estrada-Moreno, J. A. Rodríguez-Velázquez, and I. G. Yero, "The k-metric dimension of a graph," *Applied Mathematics & Information Sciences*, vol. 9, no. 6, pp. 2829–2840, 2015.

[8] I. G. Yero, A. Estrada-Moreno, and J. A. Rodríguez-Velázquez, "Computing the k-metric dimension of graphs," *Applied Mathematics and Computation*, vol. 300, pp. 60–69, 2017.

[9] Y. Ramírez-Cruz, O. R. Oellermann, and J. A. Rodríguez-Velázquez, "The simultaneous metric dimension of graph families," *Discrete Applied Mathematics*, vol. 198, pp. 241–250, 2016.

[10] G. Chartrand, E. Salehi, and P. Zhang, "The partition dimension of a graph," *Aequationes Mathematicae*, vol. 59, no. 1, pp. 45–54, 2000.

[11] I. G. Yero, "On the strong partition dimension of graphs," *The Electronic Journal of Combinatorics*, vol. 21, no. 3, 3.14 pages, 2014.

[12] R. Trujillo-Rasua and I. G. Yero, "k-metric antidimension: a privacy measure for social graphs," *Information Sciences*, vol. 328, pp. 403–417, 2016.

[13] Z. Beerliova, F. Eberhard, T. Erlebach et al., "Network discovery and verification," *IEEE Journal on Selected Areas in Communications*, vol. 24, no. 12, pp. 2168–2181, 2006.

[14] R. A. Melter and I. Tomescu, "Metric bases in digital geometry," *Computer Vision, Graphics, and Image Processing*, vol. 25, no. 1, pp. 113–121, 1984.

[15] J. Cáceres, C. Hernando, M. Mora et al., "On the metric dimension of cartesian products of graphs," *SIAM Journal on Discrete Mathematics*, vol. 21, no. 2, pp. 423–441, 2007.

[16] G. Chartrand, L. Eroh, M. A. Johnson, and O. R. Oellermann, "Resolvability in graphs and the metric dimension of a graph," *Discrete Applied Mathematics*, vol. 105, no. 1–3, pp. 99–113, 2000.

[17] G. Chartrand, C. Poisson, and P. Zhang, "Resolvability and the upper dimension of graphs," *Computers & Mathematics with Applications*, vol. 39, no. 12, pp. 19–28, 2000.

[18] M. Johnson, "Structure-activity maps for visualizing the graph variables arising in drug design," *Journal of Biopharmaceutical Statistics*, vol. 3, no. 2, pp. 203–236, 1993.

[19] J.-B. Liu, Z. Zahid, R. Nasir, and W. Nazeer, "Edge version of metric dimension and doubly resolving sets of the necklace graph," *Mathematics*, vol. 6, no. 11, p. 243, 2018.

[20] A. Kelenc, N. Tratnik, and I. G. Yero, "Uniquely identifying the edges of a graph: the edge metric dimension," *Discrete Applied Mathematics*, vol. 251, pp. 204–220, 2018.

[21] M. R. Garey and D. S. Johnson, *Computers and Intractability: A Guide to the Theorey of NP-Completeness*, Freeman, New York, NY, USA, 1979.

[22] S. Khuller, B. Raghavachari, and A. Rosenfeld, "Landmarks in graphs," *Discrete Applied Mathematics*, vol. 70, no. 3, pp. 217–229, 1996.

[23] N. Zulbrilina, "On edge metric dimension of a graph," *Discrete Mathematics*, vol. 341, pp. 2083–2088, 2018.

[24] M. Rafiullah, H. M. A. Siddiqui, and A. Sarfraz, "Resolvability of some convex polytopes," *Utilitas Mathematica*, vol. 111, pp. 309–328, 2019.

[25] M. Imran and H. M. A. Siddiqui, "Computing the metric dimension of convex polytopes generated by wheel related graphs," *Acta Mathematica Hungarica*, vol. 149, no. 1, pp. 10–30, 2016.

[26] J.-B. Liu, A. Kashif, T. Rashid, and M. Javaid, "Fractional metric dimension of generalized jahangir graph," *Mathematics*, vol. 7, no. 1, p. 100, 2019.

[27] H. M. A. Siddiqui and M. Imran, "Computing the metric dimension of wheel related graphs," *Applied Mathematics and Computation*, vol. 242, pp. 624–632, 2014.
[28] J. A. Gallian, "A dynamic survey of graph labeling," *The Electronic Journal of Combinatorics*, vol. 16, no. 6, pp. 1–219, 2009.
[29] I. Tomescu and I. Javaid, "On the metric dimension of the Jahangir graph," *Bulletin mathématique de la Société des Sciences Mathématiques de Roumanie*, vol. 50, no. 98, pp. 371–376, 2007.
[30] I. Javaid, *On metric and partition dimension of some wheel related graphs*, Ph.D. thesis, GC University Lahore, Lahore, Pakistan, 2007.
[31] W. Mulyono, "The metric dimension of friendship graph F_n, lollipop graph $L_{m,n}$ and peterson graph, $P_{n,m}$.," *Bulletin of Mathematics*, vol. 8, no. 2, pp. 117–124, 2016.

Hindawi
Journal of Chemistry
Volume 2019, Article ID 7214047, 12 pages
https://doi.org/10.1155/2019/7214047

Research Article

Some New Results on Various Graph Energies of the Splitting Graph

Zheng-Qing Chu,[1] Saima Nazeer,[2] Tariq Javed Zia,[3] Imran Ahmed,[3] and Sana Shahid[2]

[1]*Department of Mathematics and Physics, Anhui Xinhua University, 230088 Hefei, China*
[2]*Lahore College for Women University, Lahore, Pakistan*
[3]*COMSATS University of Islamabad, Lahore Campus, Lahore 54000, Pakistan*

Correspondence should be addressed to Saima Nazeer; saimanazeer123@yahoo.com

Received 20 July 2019; Accepted 1 October 2019; Published 19 November 2019

Guest Editor: Shaohui Wang

The energy of a simple connected graph G is equal to the sum of the absolute value of eigenvalues of the graph G where the eigenvalue of a graph G is the eigenvalue of its adjacency matrix $A(G)$. Ultimately, scores of various graph energies have been originated. It has been shown in this paper that the different graph energies of the regular splitting graph $S'(G)$ is a multiple of corresponding energy of a given graph G.

1. Introduction

Let G be a simple, finite, and undirected graph and its vertex set and edge set are denoted by $V(G) = \{v_1, v_2, v_3, \ldots, v_p\}$ and $E(G) = \{e_1, e_2, e_3, \ldots, e_q\}$, respectively. Number of edges finishing at a vertex v of a graph G is named as degree of vertex v and is denoted by $d(v)$ or d_v.

The adjacency matrix of G, denoted by $A(G)$, is a square matrix $[a_{ij}]$ such that a_{ij} is equal to unity if $v_i v_j \in E(G)$ and is equal to zero otherwise. The eigenvalues of the adjacency matrix $A(G)$ are known as the eigenvalues of the graph G. Collection of eigenvalues of the graph G together with their multiplicities is called spectrum of the graph G.

Let $\mu_1, \mu_2, \mu_3, \ldots, \mu_p$ be eigenvalues of G and are assumed in nonincreasing order; then, Ivan Gutman in 1978 [1] defined the energy of the graph G as the sum of the absolute values of all eigenvalues of the graph G:

$$E(G) = \sum_{j=1}^{p} |\mu_j|. \tag{1}$$

The inspiration of description energy of graph happened from quantum Chemistry. During 1930s, E. Hückel presented chemical applications of graph theory in his molecular orbital theory where eigenvalues of graphs take place. In quantum chemistry, the skeleton of nonsaturated hydrocarbon is represented by a graph. The energy levels of electrons in such a molecule are eigenvalues of graph. The strength of particles is closely identified with the spectrum of its graph. The carbon atoms and chemical bond between them in a hydrocarbon system denote vertices and edges, respectively, in a molecular graph. A lot of work has been done on graph theory, special graph labeling [2–10], chemical graph theory and graph energies. In the thesis of Siraj [11], certain elementary results on the energy of the graph are also described.

The present work is considered to relate several energies of a graph to bigger graph acquired from the given graph with the help of some graph operations, namely, the splitting graph which is defined in [12]. For a graph G, the splitting graph $S'(G)$ is obtained by taking a new vertex v' corresponding to each vertex v of the graph G and then join v' to all vertices of G adjacent to v. In [13], it has been proven that $E(S'(G)) = \sqrt{5}E(G)$.

Let $A = [a_{ij}]$ and $B = [b_{ij}]$ be two matrices of order $a \times m$ and $b \times n$, respectively. Then, their tensor product, $A \otimes B$ is obtained from A when every element a_{ij} is replaced by the block $a_{ij}B$ and is of order $ab \times mn$.

Proposition 1 (see [14]). *Let $A \in M^q$ and $B \in M^p$. Also, let α be an eigenvalue of the matrix A with corresponding eigenvector y and β be an eigenvalue of the matrix B with corresponding eigenvector z. Then, $\alpha\beta$ is an eigenvalue of $A \otimes B$ with corresponding eigenvector yz.*

In recent times, comparable energies are being considered, based on eigenvalues of a variety of other graph matrices. Numerous matrices can be related to a graph, and their spectrums provide certain helpful information about the graph [15–18].

2. Maximum Degree Energy

The maximum degree energy E_M of a simple connected graph G in [19] is defined as the sum of the absolute values of eigenvalues of the maximum degree matrix $M(G)$ of a graph G. Then, $M(G) = [M_{ij}]$ where

$$M_{ij} = \begin{cases} \max\left(d_i, d_j\right), & \text{if } v_i, v_j \in E(G), \\ 0, & \text{otherwise}, \end{cases} \tag{2}$$

where d_i and d_j are the degrees of vertices v_i and v_j, respectively.

Theorem 1. *For a graph G,*

$$E_M\left(S'(G)\right) = 2E_M(G). \tag{3}$$

Proof. Let G be a graph with vertices $v_1, v_2, v_3, \ldots, v_p$. Then the maximum degree matrix $M(G)$ is

$$M(G) = \begin{array}{c} \\ v_1 \\ v_2 \\ v_3 \\ \vdots \\ v_p \end{array} \begin{array}{c} \begin{array}{ccccc} v_1 & v_2 & v_3 & \ldots & v_p \end{array} \\ \begin{bmatrix} 0 & d_{k_{12}} & d_{k_{13}} & \ldots & d_{k_{1p}} \\ d_{k_{21}} & 0 & d_{k_{23}} & \ldots & d_{k_{2p}} \\ d_{k_{31}} & d_{k_{32}} & 0 & \ldots & d_{k_{3p}} \\ \vdots & \vdots & \vdots & \ddots & \vdots \\ d_{k_{p1}} & d_{k_{p2}} & d_{k_{p3}} & \ldots & 0 \end{bmatrix} \end{array}, \tag{4}$$

where $d_{k_{ij}} = \max(d_i, d_j)$ and d_i and d_j are the degrees of vertices v_i and v_j, respectively, for $i = 1, 2, 3, \ldots, p$ and $j = 1, 2, 3, \ldots, p$.

Let $v_1', v_2', v_3', \ldots, v_p'$ be the vertices corresponding to $v_1, v_2, v_3, \ldots, v_p$ which are added in G to obtain $S'(G)$ such that $N(v_j) = N(v_j')$ for $j = 1, 2, 3, \ldots, p$. Then, the maximum degree matrix of $S'(G)$ is denoted by $M(S'(G))$ and can be written as a block matrix:

$$\begin{array}{c} \\ v_1 \\ v_2 \\ v_3 \\ \vdots \\ v_p \\ v_1' \\ v_2' \\ v_3' \\ \vdots \\ v_p' \end{array} \begin{array}{c} \begin{array}{cccccccccc} v_1 & v_2 & v_3 & \ldots & v_p & v_1' & v_2' & v_3' & \ldots & v_p' \end{array} \\ \begin{bmatrix} 0 & 2d_{k_{12}} & 2d_{k_{13}} & \ldots & 2d_{k_{1p}} & 0 & 2d_{k_{12}} & 2d_{k_{13}} & \ldots & 2d_{k_{1p}} \\ 2d_{k_{21}} & 0 & 2d_{k_{23}} & \ldots & 2d_{k_{2p}} & 2d_{k_{21}} & 0 & 2d_{k_{23}} & \ldots & 2d_{k_{2p}} \\ 2d_{k_{31}} & 2d_{k_{32}} & 0 & \ldots & 2d_{k_{3p}} & 2d_{k_{31}} & 2d_{k_{32}} & 0 & \ldots & 2d_{k_{3p}} \\ \vdots & \vdots & \vdots & \ddots & \vdots & \vdots & \vdots & \vdots & \ddots & \vdots \\ 2d_{k_{p1}} & 2d_{k_{p2}} & 2d_{k_{p3}} & \ldots & 0 & 2d_{k_{p1}} & 2d_{k_{p2}} & 2d_{k_{p3}} & \ldots & 0 \\ 0 & 2d_{k_{12}} & 2d_{k_{13}} & \ldots & 2d_{k_{1p}} & 0 & 0 & 0 & \ldots & 0 \\ 2d_{k_{21}} & 0 & 2d_{k_{23}} & \ldots & 2d_{k_{2p}} & 0 & 0 & 0 & \ldots & 0 \\ 2d_{k_{31}} & 2d_{k_{32}} & 0 & \ldots & 2d_{k_{3p}} & 0 & 0 & 0 & \ldots & 0 \\ \vdots & \vdots & \vdots & \ddots & \vdots & \vdots & \vdots & \vdots & \ddots & \vdots \\ 2d_{k_{p1}} & 2d_{k_{p2}} & 2d_{k_{p3}} & \ldots & 0 & 0 & 0 & 0 & \ldots & 0 \end{bmatrix} \end{array}. \tag{5}$$

That is

$$\begin{aligned} M\left(S'(G)\right) &= \begin{bmatrix} 2M(G) & 2M(G) \\ 2M(G) & 0 \end{bmatrix} \\ \text{or } &= \begin{bmatrix} 2 & 2 \\ 2 & 0 \end{bmatrix} \otimes M(G). \end{aligned} \tag{6}$$

Here, the maximum degree spectrum of $S'(G)$ is

$$\begin{pmatrix} (1+\sqrt{5})\mu_j & (1-\sqrt{5})\mu_j \\ p & p \end{pmatrix}, \tag{7}$$

where μ_j for $j = 1, 2, 3, \ldots, p$ are the eigenvalues of $M(G)$and $1 \pm \sqrt{5}$ are the eigenvalues of $\begin{bmatrix} 2 & 2 \\ 2 & 0 \end{bmatrix}$.

Here,

$$\begin{aligned} E_M\left(S'(G)\right) &= \sum_{j=1}^{j=p} \left|(1 \pm \sqrt{5})\mu_j\right| \\ &= \sum_{j=1}^{j=p} \left|\mu_j\right| (1 + \sqrt{5} + 1 - \sqrt{5}) \\ &= 2\sum_{j=1}^{j=p} \left|\mu_j\right| \\ &= 2E_M(G), \end{aligned} \tag{8}$$

which completes the proof. □

3. Minimum Degree Energy

In [20], the minimum degree energy E_m of a simple connected graph G is defined as the sum of the absolute values of eigenvalues of minimum degree matrix $m(G)$ of a graph G. Here, $m(G) = [m_{ij}]$ where

$$m_{ij} = \begin{cases} \min\left(d_i, d_j\right), & \text{if } v_i, v_j \epsilon E(G), \\ 0, & \text{otherwise}, \end{cases} \tag{9}$$

where d_i and d_j are the degrees of vertices v_i and v_j, respectively.

Theorem 2. *For a graph G,*

$$E_m\left(S'(G)\right) = 2E_m(G). \tag{10}$$

Proof. Let G be a graph with vertices $v_1, v_2, v_3, \ldots, v_p$. Then, the minimum degree matrix $m(G)$ is

$$m(G) = \begin{array}{c} \\ v_1 \\ v_2 \\ v_3 \\ \vdots \\ v_p \end{array} \begin{array}{c} \begin{array}{ccccc} v_1 & v_2 & v_3 & \ldots & v_p \end{array} \\ \begin{bmatrix} 0 & d_{k_{12}} & d_{k_{13}} & \ldots & d_{k_{1p}} \\ d_{k_{21}} & 0 & d_{k_{23}} & \ldots & d_{k_{2p}} \\ d_{k_{31}} & d_{k_{32}} & 0 & \ldots & d_{k_{3p}} \\ \vdots & \vdots & \vdots & \ddots & \vdots \\ d_{k_{p1}} & d_{k_{p2}} & d_{k_{p3}} & \ldots & 0 \end{bmatrix} \end{array}, \tag{11}$$

where $d_{k_{ij}} = \min(d_i, d_j)$ and d_i and d_j are the degrees of vertices v_i and v_j, respectively, for $i = 1, 2, 3, \ldots, p$ and $j = 1, 2, 3, \ldots, p$. Let $v_1', v_2', v_3', \ldots, v_p'$ be the vertices corresponding to $v_1, v_2, v_3, \ldots, v_p$ which are added in G to obtain $S'(G)$ such that $N(v_j) = N(v_j')$ for $j = 1, 2, 3, \ldots, p$. Then, the minimum degree matrix of splitting graph of G, denoted by $m(S'(G))$, can be defined as a block matrix as follows:

$$\begin{array}{c} \\ v_1 \\ v_2 \\ v_3 \\ \vdots \\ v_p \\ v_1' \\ v_2' \\ v_3' \\ \vdots \\ v_p' \end{array} \begin{array}{c} \begin{array}{cccccccccc} v_1 & v_2 & v_3 & \ldots & v_p & v_1' & v_2' & v_3' & \ldots & v_p' \end{array} \\ \begin{bmatrix} 0 & 2d_{k_{12}} & 2d_{k_{13}} & \ldots & 2d_{k_{1p}} & 0 & d_{k_{12}} & d_{k_{13}} & \ldots & d_{k_{1p}} \\ 2d_{k_{21}} & 0 & 2d_{k_{23}} & \ldots & 2d_{k_{2p}} & d_{k_{21}} & 0 & d_{k_{23}} & \ldots & d_{k_{2p}} \\ 2d_{k_{31}} & 2d_{k_{32}} & 0 & \ldots & 2d_{k_{3p}} & d_{k_{31}} & d_{k_{32}} & 0 & \ldots & d_{k_{3p}} \\ \vdots & \vdots & \vdots & \ddots & \vdots & \vdots & \vdots & \vdots & \ddots & \vdots \\ 2d_{k_{p1}} & 2d_{k_{p2}} & 2d_{k_{p3}} & \ldots & 0 & d_{k_{p1}} & d_{k_{p2}} & d_{k_{p3}} & \ldots & 0 \\ 0 & d_{k_{12}} & d_{k_{13}} & \ldots & d_{k_{1p}} & 0 & 0 & 0 & \ldots & 0 \\ d_{k_{21}} & 0 & d_{k_{23}} & \ldots & d_{k_{2p}} & 0 & 0 & 0 & \ldots & 0 \\ d_{k_{31}} & d_{k_{32}} & 0 & \ldots & d_{k_{3p}} & 0 & 0 & 0 & \ldots & 0 \\ \vdots & \vdots & \vdots & \ddots & \vdots & \vdots & \vdots & \vdots & \ddots & \vdots \\ d_{k_{p1}} & d_{k_{p2}} & d_{k_{p3}} & \ldots & 0 & 0 & 0 & 0 & \ldots & 0 \end{bmatrix} \end{array}. \tag{12}$$

That is

$$\begin{aligned} m\left(S'(G)\right) &= \begin{bmatrix} 2m(G) & m(G) \\ m(G) & 0 \end{bmatrix} \\ \text{or } &= \begin{bmatrix} 2 & 1 \\ 1 & 0 \end{bmatrix} \otimes m(G). \end{aligned} \tag{13}$$

Here, the minimum degree spectrum of $S'(G)$ is

$$\begin{pmatrix} (1+\sqrt{2})\nu_j & (1-\sqrt{2})\nu_j \\ p & p \end{pmatrix}, \tag{14}$$

where ν_j for $j = 1, 2, 3, \ldots, p$ are the eigenvalues of $m(G)$ and $1 \pm \sqrt{2}$ are the eigenvalues of $\begin{bmatrix} 2 & 1 \\ 1 & 0 \end{bmatrix}$.

Here,

$$\begin{aligned} E_m\left(S'(G)\right) &= \sum_{j=1}^{j=n} \left|(1 \pm \sqrt{2})\nu_j\right| \\ &= \sum_{j=1}^{j=p} \left|\nu_j\right| (1 + \sqrt{2} + 1 - \sqrt{2}) \\ &= 2\sum_{j=1}^{j=n} \left|\nu_j\right| \\ &= 2E_m(G), \end{aligned} \tag{15}$$

which is the required result. □

4. Randić Energy

The randić energy E_R of a simple connected graph G in [21] is the sum of the absolute values of eigenvalues of the randić matrix $R(G)$. Here, $R(G) = [r_{ij}]$ where

$$r_{ij} = \begin{cases} \dfrac{1}{\sqrt{d_i d_j}}, & \text{if } v_i, v_j \epsilon E(G), \\ 0, & \text{otherwise.} \end{cases} \tag{16}$$

Here, d_i and d_j are the degrees of vertices v_i and v_j, respectively.

Theorem 3. *For a graph G,*

$$E_R(S'(G)) = \frac{3}{2} E_R(G). \tag{17}$$

Proof. Let $x_1, x_2, x_3, \ldots, x_p$ be vertices of a graph G. Then, the randić matrix of G is denoted by $R(G)$ and is given as

$$R(G) = \begin{array}{c} \\ x_1 \\ x_2 \\ x_3 \\ \vdots \\ x_p \end{array} \begin{array}{c} \begin{array}{ccccc} x_1 & x_2 & x_3 & \cdots & x_p \end{array} \\ \begin{bmatrix} 0 & \frac{1}{d_1 d_2} & \frac{1}{d_1 d_3} & \cdots & \frac{1}{d_1 d_p} \\ \frac{1}{d_2 d_1} & 0 & \frac{1}{d_2 d_3} & \cdots & \frac{1}{d_2 d_p} \\ \frac{1}{d_3 d_1} & \frac{1}{d_3 d_2} & 0 & \cdots & \frac{1}{d_3 d_p} \\ \vdots & \vdots & \vdots & \ddots & \vdots \\ \frac{1}{d_p d_1} & \frac{1}{d_p d_2} & \frac{1}{d_p d_3} & \cdots & 0 \end{bmatrix} \end{array}. \tag{18}$$

Let $x_1', x_2', x_3', \ldots, x_p'$ be the vertices corresponding to $x_1, x_2, x_3, \ldots, x_p$ which are added in G to obtain $S'(G)$ such that $N(x_j) = N(x_j')$ for $j = 1, 2, 3, \ldots, p$. Then, the randić matrix of $S'(G)$ is denoted by $R(S'(G))$ and can be written as a block matrix as follows:

$$\begin{array}{c} \\ x_1 \\ x_2 \\ x_3 \\ \vdots \\ x_p \\ x_1' \\ x_2' \\ x_3' \\ \vdots \\ x_p' \end{array} \begin{array}{c} \begin{array}{cccccccccc} x_1 & x_2 & x_3 & \cdots & x_p & x_1' & x_2' & x_3' & \cdots & x_p' \end{array} \\ \begin{bmatrix} 0 & \frac{1}{d_1 d_2} & \frac{1}{d_1 d_3} & \cdots & \frac{1}{d_1 d_p} & 0 & \frac{1}{d_1 d_2} & \frac{1}{d_1 d_3} & \cdots & \frac{1}{d_1 d_p} \\ \frac{1}{d_2 d_1} & 0 & \frac{1}{d_2 d_3} & \cdots & \frac{1}{d_2 d_p} & \frac{1}{d_2 d_1} & 0 & \frac{1}{d_2 d_3} & \cdots & \frac{1}{d_2 d_p} \\ \frac{1}{d_3 d_1} & \frac{1}{d_3 d_2} & 0 & \cdots & \frac{1}{d_3 d_p} & \frac{1}{d_3 d_1} & \frac{1}{d_3 d_2} & 0 & \cdots & \frac{1}{d_3 d_p} \\ \vdots & \vdots & \vdots & \ddots & \vdots & \vdots & \vdots & \vdots & \ddots & \vdots \\ \frac{1}{d_p d_1} & \frac{1}{d_p d_2} & \frac{1}{d_p d_3} & \cdots & 0 & \frac{1}{d_p d_1} & \frac{1}{d_p d_2} & \frac{1}{d_p d_3} & \cdots & 0 \\ 0 & \frac{1}{d_1 d_2} & \frac{1}{d_1 d_3} & \cdots & \frac{1}{d_1 d_p} & 0 & 0 & 0 & \cdots & 0 \\ \frac{1}{d_2 d_1} & 0 & \frac{1}{d_2 d_3} & \cdots & \frac{1}{d_2 d_p} & 0 & 0 & 0 & \cdots & 0 \\ \frac{1}{d_3 d_1} & \frac{1}{d_3 d_2} & 0 & \cdots & \frac{1}{d_3 d_p} & 0 & 0 & 0 & \cdots & 0 \\ \vdots & \vdots & \vdots & \ddots & \vdots & \vdots & \vdots & \vdots & \ddots & \vdots \\ \frac{1}{d_p d_1} & \frac{1}{d_p d_2} & \frac{1}{d_p d_3} & \cdots & 0 & 0 & 0 & 0 & \cdots & 0 \end{bmatrix} \end{array}. \tag{19}$$

That is,

$$R(S'(G)) = \begin{bmatrix} \frac{1}{2} R(G) & \frac{1}{\sqrt{2}} R(G) \\ \frac{1}{\sqrt{2}} R(G) & 0 \end{bmatrix} = \begin{bmatrix} \frac{1}{2} & \frac{1}{\sqrt{2}} \\ \frac{1}{\sqrt{2}} & 0 \end{bmatrix} \otimes R(G). \tag{20}$$

Here, the randić spectrum of $S'(G)$ is

$$\begin{pmatrix} \left(\frac{-1}{2}\right)\rho_j & (1)\rho_j \\ p & p \end{pmatrix}, \tag{21}$$

where ρ_j for $j = 1, 2, 3, \ldots, p$ are the eigenvalues of $R(G)$and $-1/2$ and 1 are the eigenvalues of $\begin{bmatrix} 1/2 & 1/\sqrt{2} \\ 1/\sqrt{2} & 0 \end{bmatrix}$.

Here,

$$\begin{aligned} E_R(S'(G)) &= \sum_{j=1}^{j=p} \left| \left(\frac{-1}{2} + 1 \right) \rho_j \right| \\ &= \sum_{j=1}^{j=p} \left| \rho_j \right| \left(\frac{1}{2} + 1 \right) \\ &= \frac{3}{2} \sum_{j=1}^{j=p} \left| \rho_j \right| \\ &= \frac{3}{2} E_R(G). \end{aligned} \tag{22}$$

□

5. Seidel Energy

In [22], Haemers defined the Seidel energy E_{SE} of a simple connected graph G as the sum of the absolute values of eigenvalues of the seidel matrix $\mathrm{SE}(G)$ of G. Here, $\mathrm{SE}(G) = [s_{ij}]$ where

$$s_{ij} = \begin{cases} -1, & \text{if } v_i \text{ and } v_j \text{ are adjacent and } i \neq j, \\ 1, & \text{if } v_i \text{ and } v_j \text{ are non adjacent and } i \neq j, \\ 0, & \text{if } i = j. \end{cases} \tag{23}$$

Theorem 4. *For a s-regular graph G,*

$$E_{\mathrm{SE}}(S'(G)) \geq E_{\mathrm{SE}}(G). \tag{24}$$

Proof. Let G be a graph with vertices $v_1, v_2, v_3, \ldots, v_p$. Then, the seidel matrix $\mathrm{SE}(G)$ of G is

$$\mathrm{SE}(G) = \begin{array}{c} \\ v_1 \\ v_2 \\ v_3 \\ \vdots \\ v_p \end{array} \begin{array}{c} \begin{array}{ccccc} v_1 & v_2 & v_3 & \ldots & v_p \end{array} \\ \begin{bmatrix} 0 & s_{12} & s_{13} & \ldots & s_{1p} \\ s_{21} & 0 & s_{23} & \ldots & s_{2p} \\ s_{31} & s_{32} & 0 & \ldots & s_{3p} \\ \vdots & \vdots & \vdots & \ddots & \vdots \\ s_{p1} & s_{p2} & s_{p3} & \ldots & 0 \end{bmatrix} \end{array}. \tag{25}$$

Let $u_1, u_2, u_3, \ldots, u_p$ be the vertices corresponding to $v_1, v_2, v_3, \ldots, v_p$ which are added in G to obtain $S'(G)$. Then, the seidel matrix of $S'(G)$ is denoted by $\mathrm{SE}(S'(G))$ and can be written as a block matrix as follows:

$$\begin{array}{c} \\ v_1 \\ v_2 \\ v_3 \\ \vdots \\ v_p \\ u_1 \\ u_2 \\ u_3 \\ \vdots \\ u_p \end{array} \begin{array}{c} \begin{array}{ccccccccc} v_1 & v_2 & v_3 & \ldots & v_p & u_1 & u_2 & u_3 & \ldots & u_p \end{array} \\ \begin{bmatrix} 0 & s_{12} & s_{13} & \ldots & s_{1p} & 1 & s_{12} & s_{13} & \ldots & s_{1p} \\ s_{21} & 0 & s_{23} & \ldots & s_{2p} & s_{21} & 1 & s_{23} & \ldots & s_{2p} \\ s_{31} & s_{32} & 0 & \ldots & s_{3p} & s_{31} & s_{32} & 1 & \ldots & s_{3p} \\ \vdots & \vdots & \vdots & \ddots & \vdots & \vdots & \vdots & \vdots & \ddots & \vdots \\ s_{p1} & s_{p2} & s_{p3} & \ldots & 0 & s_{p1} & s_{p2} & s_{p3} & \ldots & 1 \\ 1 & s_{12} & s_{13} & \ldots & s_{1p} & 0 & 1 & 1 & \ldots & 1 \\ s_{21} & 1 & s_{23} & \ldots & s_{2p} & 1 & 0 & 1 & \ldots & 1 \\ s_{31} & s_{32} & 1 & \ldots & s_{3p} & 1 & 1 & 0 & \ldots & 1 \\ \vdots & \vdots & \vdots & \ddots & \vdots & \vdots & \vdots & \vdots & \ddots & \vdots \\ s_{p1} & s_{p2} & s_{p3} & \ldots & 1 & 1 & 1 & 1 & \ldots & 0 \end{bmatrix} \end{array}. \tag{26}$$

That is,

$$\begin{aligned} \mathrm{SE}(S'(G)) &= \begin{bmatrix} \mathrm{SE}(G) & \mathrm{SE}(G) + I_p \\ \mathrm{SE}(G) + I_p & J_p - I_p \end{bmatrix} \\ \text{or } &= \begin{bmatrix} \mathrm{SE}(G) & \mathrm{SE}(G) \\ \mathrm{SE}(G) & 0 \end{bmatrix} + \begin{bmatrix} 0I_p & I_p \\ I_p & J_p - I_p \end{bmatrix}. \end{aligned} \tag{27}$$

Hence,

$$\mathrm{SE}(S'(G)) \geq \begin{bmatrix} \mathrm{SE}(G) & \mathrm{SE}(G) \\ \mathrm{SE}(G) & 0 \end{bmatrix} = \begin{bmatrix} 1 & 1 \\ 1 & 0 \end{bmatrix} \otimes SE(G). \tag{28}$$

Here, the seidel spectrum of $S'(G)$ is greater than or equal to the spectrum

$$\begin{pmatrix} \frac{1}{2}(1 + \sqrt{5}) s_j & \frac{1}{2}(1 - \sqrt{5}) s_j \\ p & p \end{pmatrix}, \tag{29}$$

where s_j for $j = 1, 2, 3, \ldots, p$ are the eigenvalues of $\mathrm{SE}(G)$and $1/2(1 \pm \sqrt{5})$ are the eigenvalues of $\begin{bmatrix} 1 & 1 \\ 1 & 0 \end{bmatrix}$.

Thus,

$$\begin{aligned} E_{\mathrm{SE}}(S'(G)) &\geq \sum_{j=1}^{j=p} \left| \left(\frac{1}{2}(1 \pm \sqrt{5}) \right) s_j \right| \\ &= \sum_{j=1}^{j=p} \left| s_j \right| \left(\frac{1}{2} + \frac{\sqrt{5}}{2} + \frac{1}{2} - \frac{\sqrt{5}}{2} \right) \\ &= \left(\frac{1}{2} + \frac{1}{2} \right) \sum_{j=1}^{j=p} \left| s_j \right| \\ &= E_{\mathrm{SE}}(G). \end{aligned} \tag{30}$$

Hence,

$$E_{SE}(S'(G)) \geq E_{SE}(G). \tag{31}$$

□

6. Sum-Connectivity Energy

The sum-connectivity energy E_{SC} of a simple connected graph G in [23] is defined as the sum of the absolute values of eigenvalues of the sum-connectivity matrix $\mathrm{SC}(G)$. Here, $\mathrm{SC}(G) = [\mathrm{sc}_{ij}]$ where

$$\mathrm{sc}_{ij} = \begin{cases} \dfrac{1}{\sqrt{d_i + d_j}}, & \text{if } v_i, v_j \in E(G), \\ 0, & \text{otherwise.} \end{cases} \tag{32}$$

Here, d_i and d_j are the degrees of vertices v_i and v_j, respectively.

Theorem 5. *For a regular graph G,*

$$E_{\mathrm{SC}}(S'(G)) = \frac{1}{\sqrt{2}} E_{\mathrm{SC}}(G). \tag{33}$$

Proof. Let G be a graph with vertices $z_1, z_2, z_3, \ldots, z_p$. Then the sum-connectivity matrix of G is denoted by $\mathrm{SC}(G)$ and is defined as

$$\mathrm{SC}(G) = \begin{array}{c} \\ z_1 \\ z_2 \\ z_3 \\ \vdots \\ z_p \end{array} \begin{array}{c} \begin{array}{ccccc} z_1 & z_2 & z_3 & \cdots & z_p \end{array} \\ \begin{bmatrix} 0 & \frac{1}{\sqrt{d_1+d_2}} & \frac{1}{\sqrt{d_1+d_3}} & \cdots & \frac{1}{\sqrt{d_1+d_p}} \\ \frac{1}{\sqrt{d_2+d_1}} & 0 & \frac{1}{\sqrt{d_2+d_3}} & \cdots & \frac{1}{\sqrt{d_2+d_p}} \\ \frac{1}{\sqrt{d_3+d_1}} & \frac{1}{\sqrt{d_3+d_2}} & 0 & \cdots & \frac{1}{\sqrt{d_3+d_p}} \\ \vdots & \vdots & \vdots & \ddots & \vdots \\ \frac{1}{\sqrt{d_p+d_1}} & \frac{1}{\sqrt{d_p+d_2}} & \frac{1}{\sqrt{d_p+d_3}} & \cdots & 0 \end{bmatrix} \end{array}, \tag{34}$$

where d_j is the degree of vertex z_j for $j = 1, 2, 3, \ldots, p$. Let $z_1', z_2', z_3', \ldots, z_p'$ be the vertices that are added in G to acquire $S'(G)$ such that $N(z_j) = N(z_j')$. Then the sum-connectivity matrix of $S'(G)$ is denoted by $\mathrm{SC}(S'(G))$ and is defined as a block matrix as follows:

$$\begin{array}{c} \\ z_1 \\ z_2 \\ z_3 \\ \vdots \\ z_p \\ z_1' \\ z_2' \\ z_3' \\ \vdots \\ z_p' \end{array} \begin{array}{c} \begin{array}{cccccccccc} z_1 & z_2 & z_3 & \cdots & z_p & z_1' & z_2' & z_3' & \cdots & z_p' \end{array} \\ \begin{bmatrix} 0 & \frac{1}{\sqrt{d_1+d_2}} & \frac{1}{\sqrt{d_1+d_3}} & \cdots & \frac{1}{\sqrt{d_1+d_p}} & 0 & \frac{1}{\sqrt{d_1+d_2'}} & \frac{1}{\sqrt{d_1+d_3'}} & \cdots & \frac{1}{\sqrt{d_1+d_p'}} \\ \frac{1}{\sqrt{d_2+d_1}} & 0 & \frac{1}{\sqrt{d_2+d_3}} & \cdots & \frac{1}{\sqrt{d_2+d_p}} & \frac{1}{\sqrt{d_2+d_1'}} & 0 & \frac{1}{\sqrt{d_2+d_3'}} & \cdots & \frac{1}{\sqrt{d_2+d_p'}} \\ \frac{1}{\sqrt{d_3+d_1}} & \frac{1}{\sqrt{d_3+d_2}} & 0 & \cdots & \frac{1}{\sqrt{d_3+d_p}} & \frac{1}{\sqrt{d_3+d_1'}} & \frac{1}{\sqrt{d_3+d_2'}} & 0 & \cdots & \frac{1}{\sqrt{d_3+d_p'}} \\ \vdots & \vdots & \vdots & \ddots & \vdots & \vdots & \vdots & \vdots & \ddots & \vdots \\ \frac{1}{\sqrt{d_p+d_1}} & \frac{1}{\sqrt{d_p+d_2}} & \frac{1}{\sqrt{d_p+d_3}} & \cdots & 0 & \frac{1}{\sqrt{d_p+d_1'}} & \frac{1}{\sqrt{d_p+d_2'}} & \frac{1}{\sqrt{d_p+d_3'}} & \cdots & 0 \\ 0 & \frac{1}{\sqrt{d_1'+d_2}} & \frac{1}{\sqrt{d_1'+d_3}} & \cdots & \frac{1}{\sqrt{d_1'+d_p}} & 0 & 0 & 0 & \cdots & 0 \\ \frac{1}{\sqrt{d_2'+d_1}} & 0 & \frac{1}{\sqrt{d_2'+d_3}} & \cdots & \frac{1}{\sqrt{d_2'+d_p}} & 0 & 0 & 0 & \cdots & 0 \\ \frac{1}{\sqrt{d_3'+d_1}} & \frac{1}{\sqrt{d_3'+d_2}} & 0 & \cdots & \frac{1}{\sqrt{d_3'+d_p}} & 0 & 0 & 0 & \cdots & 0 \\ \vdots & \vdots & \vdots & \ddots & \vdots & \vdots & \vdots & \vdots & \ddots & \vdots \\ \frac{1}{\sqrt{d_p'+d_1}} & \frac{1}{\sqrt{d_p'+d_2}} & \frac{1}{\sqrt{d_p'+d_3}} & \cdots & 0\&0 & 0 & 0 & \cdots & 0 & \end{bmatrix} \end{array}, \tag{35}$$

where d'_j is the degree of vertex z'_j for $j = 1, 2, 3, \ldots, p$. Thus,

$$\mathrm{SC}(S'(G)) = \begin{bmatrix} \frac{1}{\sqrt{2}}\mathrm{SC}(G) & \sqrt{\frac{2}{3}}\mathrm{SC}(G) \\ \sqrt{\frac{2}{3}}\mathrm{SC}(G) & 0 \end{bmatrix}$$
$$\text{or} \Longrightarrow \mathrm{SC}(S'(G)) = \begin{bmatrix} \frac{1}{\sqrt{2}} & \sqrt{\frac{2}{3}} \\ \sqrt{\frac{2}{3}} & 0 \end{bmatrix} \otimes \mathrm{SC}(G). \tag{36}$$

Here, the sum-connectivity spectrum of $S'(G)$ is

$$\begin{pmatrix} \left(\frac{3\sqrt{2} + \sqrt{114}}{12}\right)\beta_j & \left(\frac{3\sqrt{2} - \sqrt{114}}{12}\right)\beta_j \\ p & p \end{pmatrix}, \tag{37}$$

where β_j, for $j = 1, 2, 3, \ldots, p$ are the eigenvalues of $\mathrm{SC}(G)$ and $(3\sqrt{2} \pm \sqrt{114})/12$ are the eigenvalues of $\begin{bmatrix} 1/\sqrt{2} & \sqrt{2/3} \\ \sqrt{2/3} & 0 \end{bmatrix}$.

Hence,

$$\begin{aligned} E_{\mathrm{SC}}(S'(G)) &= \sum_{j=1}^{j=p} \left| \left(\frac{3\sqrt{2} \pm \sqrt{114}}{12}\right)\beta_j \right| \\ &= \sum_{j=1}^{j=p} |\beta_j| \left(\frac{3\sqrt{2} + \sqrt{114}}{12} + \frac{3\sqrt{2} - \sqrt{114}}{12}\right) \\ &= \frac{6\sqrt{2}}{12} \sum_{j=1}^{j=p} |\beta_j| = \frac{1}{\sqrt{2}} E_{\mathrm{SC}}(G), \end{aligned} \tag{38}$$

which completes the proof. □

7. Degree Sum Energy

In [24], the degree sum energy E_{DS} of a simple connected graph G is defined as the sum of the absolute values of eigenvalues of the degree sum matrix $\mathrm{DS}(G)$ of G. Here, $\mathrm{DS}(G) = \mathrm{ds}_{ij}$ where

$$\mathrm{ds}_{ij} = \begin{cases} d_i + d_j, & \text{if } i \neq j, \\ 0, & \text{otherwise.} \end{cases} \tag{39}$$

Here, d_i and d_j are the degrees of vertices v_i and v_j, respectively.

Theorem 6. *For a s-regular graph G with order p,*

$$E_{\mathrm{DS}}(S'(G)) \leq 6s(3p - 2). \tag{40}$$

Proof. Let G be a s-regular graph with vertices $w_1, w_2, w_3, \ldots, w_p$. Then the degree sum matrix of G is denoted by $\mathrm{DS}(G)$ and is defined as

$$\mathrm{DS}(G) = \begin{array}{c} \\ w_1 \\ w_2 \\ w_3 \\ \vdots \\ w_p \end{array} \begin{array}{c} \begin{array}{ccccc} w_1 & w_2 & w_3 & \ldots & w_p \end{array} \\ \begin{bmatrix} 0 & d_1 + d_2 & d_1 + d_3 & \ldots & d_1 + d_p \\ d_2 + d_1 & 0 & d_2 + d_3 & \ldots & d_2 + d_p \\ d_3 + d_1 & d_3 + d_2 & 0 & \ldots & d_3 + d_p \\ \vdots & \vdots & \vdots & \ddots & \vdots \\ d_p + d_1 & d_p + d_2 & d_p + d_3 & \ldots & 0 \end{bmatrix} \end{array}, \tag{41}$$

where d_j is degree of vertex w_j for $j = 1, 2, 3, \ldots, p$. Let $w'_1, w'_2, w'_3, \ldots, w'_p$ be the vertices corresponding to vertices $w_1, w_2, w_3, \ldots, w_p$ that are added in G to get the splitting graph $S'(G)$. Then the degree sum matrix of $S'(G)$ is given as

$$\begin{array}{c} \\ w_1 \\ w_2 \\ w_3 \\ \vdots \\ w_p \\ w'_1 \\ w'_2 \\ w'_3 \\ \vdots \\ w'_p \end{array} \begin{array}{c} \begin{array}{ccccccccccc} w_1 & w_2 & w_3 & \ldots & w_p & w'_1 & w'_2 & w'_3 & \ldots & w'_p \end{array} \\ \begin{bmatrix} 0 & d_1 + d_2 & d_1 + d_3 & \ldots & d_1 + d_p & 0 & d_1 + d'_2 & d_1 + d'_3 & & d_1 + d'_p \\ d_2 + d_1 & 0 & d_2 + d_3 & \ldots & d_2 + d_p & d_2 + d'_1 & 0 & d_2 + d'_3 & \ldots & d_2 + d'_p \\ d_3 + d_1 & d_3 + d_2 & 0 & \ldots & d_3 + d_p & d_3 + d'_1 & d_3 + d'_2 & 0 & \ldots & d_3 + d'_p \\ \vdots & \vdots & \vdots & \ddots & \vdots & \vdots & \vdots & \vdots & \ddots & \vdots \\ d_p + d_1 & d_p + d_2 & d_p + d_3 & \ldots & 0 & d_p + d'_1 & d_p + d'_2 & d_p + d'_3 & \ldots & 0 \\ 0 & d'_1 + d_2 & d'_1 + d_3 & \ldots & d'_1 + d_p & 0 & d'_1 + d'_2 & d'_1 + d'_3 & \ldots & d'_1 + d'_p \\ d'_2 + d_1 & 0 & d'_2 + d_3 & \ldots & d'_2 + d_p & d'_2 + d'_1 & 0 & d'_2 + d'_3 & \ldots & d'_2 + d'_p \\ d'_3 + d_1 & d'_3 + d_2 & 0 & \ldots & d'_3 + d_p & d'_3 + d'_1 & d'_3 + d'_2 & 0 & \ldots & d'_3 + d'_p \\ \vdots & \vdots & \vdots & \ddots & \vdots & \vdots & \vdots & \vdots & \ddots & \vdots \\ d'_p + d_1 & d'_p + d_2 & d'_p + d_3 & \ldots & 0 & d'_p + d'_1 & d'_p + d'_2 & d'_p + d'_3 & \ldots & 0 \end{bmatrix} \end{array}, \tag{42}$$

where d'_j is the degree of vertex w'_j for $j = 1, 2, 3, \ldots, p$.

Note that

$$\mathrm{DS}(S'(G)) = \begin{bmatrix} 4s[J_p - I_p] & 3s[J_{p\times p}] \\ 3s[J_{p\times p}] & 2s[J_p - I_p] \end{bmatrix}. \tag{43}$$

Thus,

$$E_{\mathrm{DS}}(S'(G)) \leq \sum_{j=1}^{2p}\left|\mu_j\begin{bmatrix} 4s\left[J_p - I_p\right] & 0I_p \\ 0I_p & 0I_p \end{bmatrix}\right| + \sum_{j=1}^{2p}\left|\mu_j\begin{bmatrix} 0I_p & 3sJ_{p\times p} \\ 3sJ_{p\times p} & 0I_p \end{bmatrix}\right| + \sum_{j=1}^{2p}\left|\mu_j\begin{bmatrix} 0I_p & 0I_p \\ 0I_p & 4s\left[J_p - I_p\right] \end{bmatrix}\right|. \tag{44}$$

As

$$\begin{aligned} \sum_{j=1}^{2p}\left|\mu_j\begin{bmatrix} 4s\left[J_p - I_p\right] & 0I_p \\ 0I_p & 0I_p \end{bmatrix}\right| &= 8s(p-1), \\ \sum_{j=1}^{2p}\left|\mu_j\begin{bmatrix} 0I_p & 3sJ_{p\times p} \\ 3sJ_{p\times p} & 0I_p \end{bmatrix}\right| &= 6sp, \\ \sum_{j=1}^{2p}\left|\mu_j\begin{bmatrix} 0I_p & 0I_p \\ 0I_p & 4s\left[J_p - I_p\right] \end{bmatrix}\right| &= 4s(p-1). \end{aligned} \tag{45}$$

Hence,

$$\begin{aligned} E_{\mathrm{DS}}(S'(G)) &\leq 8s(p-1) + 6sp + 4s(p-1) \\ &= 12s(p-1) + 6sp \\ &= 18sp - 12s \\ &= 6s(3p-2), \end{aligned} \tag{46}$$

which is the required result. □

8. Degree Square Sum Energy

The degree square sum energy $E_{\mathrm{DSS}}(G)$ of a simple connected graph G in [25] is defined as the sum of the absolute values of eigenvalues of the degree square sum matrix $\mathrm{DSS}(G)$. Here, $\mathrm{DSS}(G) = [\mathrm{dss}_{ij}]$ where

$$\mathrm{dss}_{ij} = \begin{cases} d_i^2 + d_j^2, & \text{if } i \neq j, \\ 0, & \text{otherwise.} \end{cases} \tag{47}$$

Here, d_i and d_j are degrees of vertices v_i and v_j, respectively.

Theorem 7. *For a s-regular graph G with p vertices,*

$$E_{\mathrm{DSS}}(S'(G)) \leq 2s^2(14p - 9). \tag{48}$$

Proof. Let $x_1, x_2, x_3, \ldots, x_p$ be vertices of a s-regular graph G and $x_1', x_2', x_3', \ldots, x_p'$ be the vertices added in G corresponding to $x_1, x_2, x_3, \ldots, x_p$ to get the splitting graph $S'(G)$ such that for $j = 1, 2, 3, \ldots, p$, $N(x_j) = N(x_j')$. Then, the degree square sum matrix of G and $S'(G)$ are given as

$$\mathrm{DSS}(G) = \begin{array}{c} \\ x_1 \\ x_2 \\ x_3 \\ \vdots \\ x_p \end{array} \begin{array}{c} \begin{array}{ccccc} x_1 & x_2 & x_3 & \cdots & x_p \end{array} \\ \begin{bmatrix} 0 & d_1^2 + d_2^2 & d_1^2 + d_3^2 & \ldots & d_1^2 + d_p^2 \\ d_2^2 + d_1^2 & 0 & d_2^2 + d_3^2 & \ldots & d_2^2 + d_p^2 \\ d_3^2 + d_1^2 & d_3^2 + d_2^2 & 0 & \ldots & d_3^2 + d_p^2 \\ \vdots & \vdots & \vdots & \ddots & \vdots \\ d_p^2 + d_1^2 & d_p^2 + d_2^2 & d_p^2 + d_3^2 & \ldots & 0 \end{bmatrix} \end{array},$$

$$\begin{array}{c} \\ x_1 \\ x_2 \\ x_3 \\ \vdots \\ x_p \\ x_1' \\ x_2' \\ x_3' \\ \vdots \\ x_p' \end{array} \begin{array}{c} \begin{array}{ccccccccccc} x_1 & x_2 & x_3 & \cdots & x_p & x_1' & x_2' & x_3' & \cdots & x_p' \end{array} \\ \begin{bmatrix} 0 & d_1^2 + d_2^2 & d_1^2 + d_3^2 & \ldots & d_1^2 + d_p^2 & 0 & d_1^2 + d_2'^2 & d_1^2 + d_3'^2 & \ldots & d_1^2 + d_p'^2 \\ d_2^2 + d_1^2 & 0 & d_2^2 + d_3^2 & \ldots & d_2^2 + d_p^2 & d_2^2 + d_1'^2 & 0 & d_2^2 + d_3'^2 & \ldots & d_2^2 + d_p'^2 \\ d_3^2 + d_1^2 & d_3^2 + d_2^2 & 0 & \ldots & d_3^2 + d_p^2 & d_3^2 + d_1'^2 & d_3^2 + d_2'^2 & 0 & \ldots & d_3^2 + d_p'^2 \\ \vdots & \vdots & \vdots & \ddots & \vdots & \vdots & \vdots & \vdots & \ddots & \vdots \\ d_p^2 + d_1^2 & d_p^2 + d_2^2 & d_p^2 + d_3^2 & \ldots & 0 & d_p^2 + d_1'^2 & d_p^2 + d_2'^2 & d_p^2 + d_3'^2 & \ldots & 0 \\ 0 & d_1'^2 + d_2^2 & d_1'^2 + d_3^2 & \ldots & d_1'^2 + d_p^2 & 0 & d_1'^2 + d_2'^2 & d_1'^2 + d_3'^2 & \ldots & d_1'^2 + d_p'^2 \\ d_2'^2 + d_1^2 & 0 & d_2'^2 + d_3^2 & \ldots & d_2'^2 + d_p^2 & d_2'^2 + d_1'^2 & 0 & d_2'^2 + d_3'^2 & \ldots & d_2'^2 + d_p'^2 \\ d_3'^2 + d_1^2 & d_3'^2 + d_2^2 & 0 & \ldots & d_3'^2 + d_p^2 & d_3'^2 + d_1'^2 & d_3'^2 + d_2'^2 & 0 & \ldots & d_3'^2 + d_p'^2 \\ \vdots & \vdots & \vdots & \ddots & \vdots & \vdots & \vdots & \vdots & \ddots & \vdots \\ d_p'^2 + d_1^2 & d_p'^2 + d_2^2 & d_p'^2 + d_3^2 & \ldots & 0 & d_p'^2 + d_1'^2 & d_p'^2 + d_2'^2 & d_p'^2 + d_3'^2 & \ldots & 0 \end{bmatrix} \end{array}, \tag{49}$$

where d_i is the degree of vertex x_i and d_i' is the degree of vertex x_i', for $i = 1, 2, 3, \ldots, p$.

Note that

$$\mathrm{DSS}(S'(G)) = \begin{bmatrix} 8s^2\left[J_p - I_p\right] & 5s^2[J(p\times p)] \\ 5s^2[J(p\times p)] & 2s^2\left[J_p - I_p\right] \end{bmatrix}. \tag{50}$$

Thus,

$$\begin{aligned} E_{\mathrm{DSS}}(S'(G)) \le & \sum_{j=1}^{2p}\left|\mu_j\begin{bmatrix} 8s^2\left[J_p - I_p\right] & 0I_p \\ 0I_p & 0I_p \end{bmatrix}\right| \\ & + \sum_{j=1}^{2p}\left|\mu_j\begin{bmatrix} 0I_p & 5s^2[J(p\times p)] \\ 5s^2[J(p\times p)] & 0I_p \end{bmatrix}\right| + \sum_{j=1}^{2p}\left|\mu_j\begin{bmatrix} 0I_p & 0I_p \\ 0I_p & 2s^2\left[J_p - I_p\right] \end{bmatrix}\right|. \end{aligned} \tag{51}$$

As

$$\begin{aligned} \sum_{j=1}^{2p}\left|\mu_j\begin{bmatrix} 8s^2\left[J_p - I_p\right] & 0I_p \\ 0I_p & 0I_p \end{bmatrix}\right| &= 16s^2(p-1), \\ \sum_{j=1}^{2p}\left|\mu_j\begin{bmatrix} 0I_p & 5s^2[J(p\times p)] \\ 5s^2[J(p\times p)] & 0I_p \end{bmatrix}\right| &= 10s^2 p, \\ \sum_{j=1}^{2p}\left|\mu_j\begin{bmatrix} 0I_p & 0I_p \\ 0I_p & 2s^2\left[J_p - I_p\right] \end{bmatrix}\right| &= 4s^2(p-1). \end{aligned} \tag{52}$$

Hence,

$$\begin{aligned} E_{\mathrm{DSS}}(S'(G)) &\le 16s^2(p-1) + 10s^2 p + 4s^2(p-1) \\ &= 20s^2(p-1) + 10s^2 p \\ &= 30s^2 p - 20s^2 \\ &= 10s^2(3p-2), \end{aligned} \tag{53}$$

which completes the proof. □

9. First Zagreb Energy

In [26], the First zagreb energy ZE_1 of a simple connected graph G is defined as the sum of the absolute values of eigenvalues of first zagreb matrix $Z^{(1)}(G)$ of G where $Z^{(1)}(G) = [z_{ij}^{(1)}]$ where

$$z_{ij}^{(1)} = \begin{cases} d_i + d_j, & \text{if } v_i, v_j \in E(G), \\ 0, & \text{otherwise.} \end{cases} \tag{54}$$

Here, d_i and d_j are degrees of vertices v_i and v_j, respectively.

Theorem 8. *For a regular graph G,*

$$\mathrm{ZE}_1(S'(G)) = 2\mathrm{ZE}_1(G). \tag{55}$$

Proof. Let G be a graph with vertices $z_1, z_2, z_3, \ldots, z_p$. Then, the first zagreb matrix of G is denoted by $Z^{(1)}(G)$ and is defined as

$$Z^{(1)}(G) = \begin{array}{c} \\ z_1 \\ z_2 \\ z_3 \\ \vdots \\ z_p \end{array} \begin{array}{c} \begin{array}{ccccc} z_1 & z_2 & z_3 & \cdots & z_p \end{array} \\ \begin{bmatrix} 0 & d_1+d_2 & d_1+d_3 & \cdots & d_1+d_p \\ d_2+d_1 & 0 & d_2+d_3 & \cdots & d_2+d_p \\ d_3+d_1 & d_3+d_2 & 0 & \cdots & d_3+d_p \\ \vdots & \vdots & \vdots & \ddots & \vdots \\ d_p+d_1 & d_p+d_2 & d_p+d_3 & \cdots & 0 \end{bmatrix} \end{array}, \tag{56}$$

where d_j is the degree of vertex z_j for $j = 1, 2, 3, \ldots, p$. Let $z_1', z_2', z_3', \ldots, z_p''$ be vertices added in G corresponding to $z_1, z_2, z_3, \ldots, z_p$ to get $S'(G)$ such that $N(z_i) = N(z_i')$. Then, the first zagreb matrix of $S'(G)$ can be written as a block matrix as follows:

$$\begin{array}{c} \\ z_1 \\ z_2 \\ z_3 \\ \vdots \\ z_p \\ z_1' \\ z_2' \\ z_3' \\ \vdots \\ z_p' \end{array} \begin{array}{c} \begin{array}{cccccccccc} z_1 & z_2 & z_3 & \cdots & z_p & z_1' & z_2' & z_3' & \cdots & z_p' \end{array} \\ \begin{bmatrix} 0 & d_1+d_2 & d_1+d_3 & \cdots & d_1+d_p & 0 & d_1+d_2' & d_1+d_3' & \cdots & d_1+d_p' \\ d_2+d_1 & 0 & d_2+d_3 & \cdots & d_2+d_p & d_2+d_1' & 0 & d_2+d_3' & \cdots & d_2+d_p' \\ d_3+d_1 & d_3+d_2 & 0 & \cdots & d_3+d_p & d_3+d_1' & d_3+d_2' & 0 & \cdots & d_3+d_p' \\ \vdots & \vdots & \vdots & \ddots & \vdots & \vdots & \vdots & \vdots & \ddots & \vdots \\ d_p+d_1 & d_p+d_2 & d_p+d_3 & \cdots & 0 & d_p+d_1' & d_p+d_2' & d_p+d_3' & \cdots & 0 \\ 0 & d_1'+d_2 & d_1'+d_3 & \cdots & d_1'+d_p & 0 & 0 & 0 & \cdots & 0 \\ d_2'+d_1 & 0 & d_2'+d_3 & \cdots & d_2'+d_p & 0 & 0 & 0 & \cdots & 0 \\ d_3'+d_1 & d_3'+d_2 & 0 & \cdots & d_3'+d_p & 0 & 0 & 0 & \cdots & 0 \\ \vdots & \vdots & \vdots & \ddots & \vdots & \vdots & \vdots & \vdots & \ddots & \vdots \\ d_p'+d_1 & d_p'+d_2 & d_p'+d_3 & \cdots & 0 & 0 & 0 & 0 & \cdots & 0 \end{bmatrix} \end{array}, \tag{57}$$

where d_j' is the degree of vertex z_j' for $j = 1, 2, 3, \ldots, p$.

Here,

$$Z^{(1)}(S'(G)) = \begin{bmatrix} 2Z^{(1)}(G) & \frac{3}{2}Z^{(1)}(G) \\ \frac{3}{2}Z^{(1)}(G) & 0 \end{bmatrix}$$
$$\text{or } Z^{(1)}(S'(G)) = \begin{bmatrix} 2 & \frac{3}{2} \\ \frac{3}{2} & 0 \end{bmatrix} \otimes Z^{(1)}(G). \tag{58}$$

Here, the first zagreb spectrum of $S'(G)$ is

$$\begin{pmatrix} \left(\frac{2-\sqrt{13}}{2}\right)\zeta_j & \left(\frac{2+\sqrt{13}}{2}\right)\zeta_j \\ p & p \end{pmatrix}, \tag{59}$$

where ζ_j for $j = 1, 2, 3, \ldots, p$ are the eigenvalues of $Z^{(1)}(G)$and $((2 \pm \sqrt{13})/2)$ are the eigenvalues of $\begin{bmatrix} 2 & 3/2 \\ 3/2 & 0 \end{bmatrix}$. Hence,

$$\begin{aligned} \mathrm{ZE}_1(S'(G)) &= \sum_{j=1}^{j=p} \left| \left(\frac{2 \pm \sqrt{13}}{2}\right)\zeta_j \right| \\ &= \sum_{j=1}^{j=p} |\zeta_j| \left(\frac{2-\sqrt{13}}{2} + \frac{2+\sqrt{13}}{2}\right) \\ &= 2ZE_1(G). \end{aligned} \tag{60}$$

□

10. Second Zagreb Energy

The second zagreb energy ZE_2 of a simple connected graph G is defined in [26] as the sum of the absolute values of eigenvalues of the second zagreb matrix $Z^{(2)}(G)$ of G where $Z^{(2)}(G) = [z_{ij}^{(2)}]$, where

$$z_{ij}^{(2)} = \begin{cases} d_i \cdot d_j, & \text{if } v_i, v_j \epsilon E(G), \\ 0, & \text{otherwise.} \end{cases} \tag{61}$$

Here, d_i and d_j are the degrees of vertices v_i and v_j, respectively.

Theorem 9. *For a regular graph G,*

$$\mathrm{ZE}_2(S'(G)) = 4\mathrm{ZE}_2(G). \tag{62}$$

Proof. Let G be a graph with vertices $z_1, z_2, z_3, \ldots, z_p$. Then, the second zagreb matrix of G is denoted by $Z^{(2)}(G)$ and is defined as

$$Z^{(2)}(G) = \begin{array}{c} \\ z_1 \\ z_2 \\ z_3 \\ \vdots \\ z_p \end{array} \begin{array}{c} \begin{array}{ccccc} z_1 & z_2 & z_3 & \cdots & z_p \end{array} \\ \begin{bmatrix} 0 & d_1 \cdot d_2 & d_1 \cdot d_3 & \cdots & d_1 \cdot d_p \\ d_2 \cdot d_1 & 0 & d_2 \cdot d_3 & \cdots & d_2 \cdot d_p \\ d_3 \cdot d_1 & d_3 \cdot d_2 & 0 & \cdots & d_3 \cdot d_p \\ \vdots & \vdots & \vdots & \ddots & \vdots \\ d_p \cdot d_1 & d_p \cdot d_2 & d_p \cdot d_3 & \cdots & 0 \end{bmatrix} \end{array}, \tag{63}$$

where d_j is the degree of vertex z_j for $j = 1, 2, 3, \ldots, p$. Let $z_1', z_2', z_3', \ldots, z_p'$ be vertices added in G corresponding to $z_1, z_2, z_3, \ldots, z_p$ to get $S'(G)$ such that $N(z_j) = N(z_j')$. Then, the second Zagreb matrix of $S'(G)$ is denoted by $Z^{(2)}(S'(G))$ and can be written as a square matrix as follows:

$$\begin{array}{c} \\ z_1 \\ z_2 \\ z_3 \\ \vdots \\ z_p \\ z_1' \\ z_2' \\ z_3' \\ \vdots \\ z_p' \end{array} \begin{array}{c} \begin{array}{cccccccccc} z_1 & z_2 & z_3 & \cdots & z_p & z_1' & z_2' & z_3' & \cdots & z_p' \end{array} \\ \begin{bmatrix} 0 & d_1\cdot d_2 & d_1\cdot d_3 & \cdots & d_1\cdot d_p & 0 & d_1\cdot d_2' & d_1\cdot d_3' & \cdots & d_1\cdot d_p' \\ d_2\cdot d_1 & 0 & d_2\cdot d_3 & \cdots & d_2\cdot d_p & d_2\cdot d_1' & 0 & d_2\cdot d_3' & \cdots & d_2\cdot d_p' \\ d_3\cdot d_1 & d_3\cdot d_2 & 0 & \cdots & d_3\cdot d_p & d_3\cdot d_1' & d_3\cdot d_2' & 0 & \cdots & d_3\cdot d_p' \\ \vdots & \vdots & \vdots & \ddots & \vdots & \vdots & \vdots & \vdots & \ddots & \vdots \\ d_p\cdot d_1 & d_p\cdot d_2 & d_p\cdot d_3 & \cdots & 0 & d_p\cdot d_1' & d_p\cdot d_2' & d_p\cdot d_3' & \cdots & 0 \\ 0 & d_1'\cdot d_2 & d_1'\cdot d_3 & \cdots & d_1'\cdot d_p & 0 & 0 & 0 & \cdots & 0 \\ d_2'\cdot d_1 & 0 & d_2'\cdot d_3 & \cdots & d_2'\cdot d_p & 0 & 0 & 0 & \cdots & 0 \\ d_3'\cdot d_1 & d_3'\cdot d_2 & 0 & \cdots & d_3'\cdot d_p & 0 & 0 & 0 & \cdots & 0 \\ \vdots & \vdots & \vdots & \ddots & \vdots & \vdots & \vdots & \vdots & \ddots & \vdots \\ d_p'\cdot d_1 & d_p'\cdot d_2 & d_p'\cdot d_3 & \cdots & 0 & 0 & 0 & 0 & \cdots & 0 \end{bmatrix} \end{array}, \tag{64}$$

where d_j' is the degree of vertex z_j' for $j = 1, 2, 3, \ldots, p$.

Here,

$$\begin{aligned} Z^{(2)}(S'(G)) &= \begin{bmatrix} 4Z^{(2)}(G) & 2Z^{(2)}(G) \\ 2Z^{(2)}(G) & 0 \end{bmatrix}, \\ Z^{(2)}(S'(G)) &= \begin{bmatrix} 4 & 2 \\ 2 & 0 \end{bmatrix} \otimes Z^{(2)}(G). \end{aligned} \tag{65}$$

Here, the second zagreb spectrum of $S'(G)$ is

$$\begin{pmatrix} (2+2\sqrt{2})\eta_j & (2-2\sqrt{2})\eta_j \\ p & p \end{pmatrix}, \tag{66}$$

where η_j for $j = 1, 2, 3, \ldots, p$ are the eigenvalues of $Z^{(2)}(G)$and $2 \pm 2\sqrt{2}$ are the eigenvalues of $\begin{bmatrix} 4 & 2 \\ 2 & 0 \end{bmatrix}$. Hence,

$$\begin{aligned} \mathrm{ZE}_2(S'(G)) &= \sum_{j=1}^{j=p} \left|(2 \pm 2\sqrt{2})\eta_j\right| \\ &= \sum_{j=1}^{j=p} \left|\eta_i\right| (2+2\sqrt{2}+2-2\sqrt{2}) \\ &= \sum_{j=1}^{j=p} \left|\eta_i\right| (4) \\ &= 4\mathrm{ZE}_2(G). \end{aligned} \tag{67}$$

□

11. Conclusion

The energy of a graph is one of the important idea of spectral graph theory. This idea links organic chemistry to mathematics. Numerous graph energies established from the eigenvalues of a variety of graph matrices and their bounds has been discovered. In this paper, we give a relation of various graph energies between the regular graph and its splitting graph. It is interesting to compute graph energies for the families of graphs considered in [27–31].

Data Availability

All data are included within this paper.

Conflicts of Interest

The authors declare no conflicts of interests

Authors' Contributions

All authors contributed equally to this work.

Acknowledgments

The authors would like to express their sincere gratitude to the Natural Science Foundation for the Higher Education Institutions of Anhui Province of China (nos. KJ2019A0875 and KJ2019A0876) and the Quality Engineering Projects of Anhui Xinhua University of China (no. 2017jxtdx05).

References

[1] I. Gutman, "The energy of a graph," *Berichte der Mathematisch–Statistischen Sektion im Forschungszentrum Graz*, vol. 103, pp. 1–22, 1978.

[2] M. A. Umar, N. Ali, A. Tabassum, and B. R. Ali, "Book graphs are cycle antimagic," *Open Journal of Mathematical Sciences*, vol. 3, no. 1, pp. 184–190, 2019.

[3] M. A. Umar, "Cyclic-antimagic construction of ladders," *Engineering and Applied Science Letters*, vol. 2, no. 2, pp. 43–47, 2019.

[4] L. Chen, H. Jiang, Z. Shao, and M. Ivanović, "Dominator and total dominator colorings in vague graphs," *Engineering and Applied Science Letters*, vol. 2, no. 2, pp. 10–17, 2019.

[5] F. Aslam, Z. Zahid, and S. Zafar, "3-total edge mean cordial labeling of some standard graphs," *Open Journal of Mathematical Sciences*, vol. 3, no. 1, pp. 129–138, 2019.

[6] N. Ali, M. A. Umar, A. Tabassum, and A. Raheem, "Super (a, d)-C_3-antimagicness of a corona graph," *Open Journal of Mathematical Sciences*, vol. 2, no. 1, pp. 371–378, 2018.

[7] M. C. M. Kumar and H. M. Nagesh, "Directed pathos total digraph of an arborescence," *Engineering and Applied Science Letters*, vol. 1, no. 1, pp. 29–42, 2018.

[8] W. Gao, M. Asif, and W. Nazeer, "The study of honey comb derived network via topological indices," *Open Journal of Mathematical Analysis*, vol. 2, no. 2, pp. 10–26, 2018.

[9] H. M. Nagesh and M. C. M. Kumar, "Block digraph of a directed graph," *Open Journal of Mathematical Sciences*, vol. 2, no. 1, pp. 202–208, 2018.

[10] G. V. Rajasekharaiah and U. P. Murthy, "Secure domination in lict graphs," *Open Journal of Mathematical Sciences*, vol. 2, no. 1, pp. 134–145, 2018.

[11] M. A. Sriraj, *Some Studies on Energy of Graphs*, Ph.D. thesis, University of Mysore, Mysore, India, 2014.

[12] E. Sampathkumar and H. B. Walikar, "On the splitting graph of a graph," *Journal of the Karnatak University Science*, vol. 25, no. 13, pp. 13–16, 1980.

[13] S. K. Vaidya and K. M. Popat, "Some new results on energy of graphs," *MATCH Communications in Mathematical and in Computer Chemistry*, vol. 77, pp. 589–594, 2017.

[14] R. A. Horn and C. R. Johnson, *Topics in Matrix Analysis*, Cambridge University Press, Cambridge, UK, 1991.

[15] J.-B. Liu, C. Wang, S. Wang, and B. Wei, "Zagreb indices and multiplicative zagreb indices of eulerian graphs," *Bulletin of the Malaysian Mathematical Sciences Society*, vol. 42, no. 1, pp. 67–78, 2019.

[16] J.-B. Liu, X.-F. Pan, F.-T. Hu, and F.-F. Hu, "Asymptotic Laplacian-energy-like invariant of lattices," *Applied Mathematics and Computation*, vol. 253, pp. 205–214, 2015.

[17] J.-B. Liu and X.-F. Pan, "Minimizing Kirchhoff index among graphs with a given vertex bipartiteness," *Applied Mathematics and Computation*, vol. 291, pp. 84–88, 2016.

[18] J.-B. Liu, J. Zhao, and Z. Zhu, "On the number of spanning trees and normalized Laplacian of linear octagonal-quadrilateral networks," *International Journal of Quantum Chemistry*, vol. 119, no. 17, Article ID e25971, 2019.

[19] C. Adiga and M. Smitha, "On maximum degree energy of a graph," *International Journal of Contemporary Mathematical Sciences*, vol. 4, no. 8, pp. 385–396, 2009.

[20] C. Adiga and C. S. Swamy, "Bounds on the largest of minimum degree eigenvalues of graphs," *International Mathematical Forum*, vol. 5, no. 37, pp. 1823–1831, 2010.

[21] K. C. Das, S. Sorguna, and K. Xu, "On randic energy of graphs," *MATCH Communications in Mathematical and in Computer Chemistry*, vol. 72, no. 1, pp. 227–238, 2014.

[22] P. Nageswari and P. B. Sarasija, "Seidel energy and its bounds," *International Journal of Mathematical Analysis*, vol. 8, no. 58, pp. 2869–2871, 2014.

[23] B. Zhou and N. Trinajstic, "On the sum-connectivity matrix and sum-connectivity energy of (molecular) graphs," *Acta Chimica Slovenica*, vol. 57, no. 3, pp. 513–517, 2010.

[24] S. M. Hosamani and H. S. Ramane, "On degree sum energy of a graph," *European Journal of Pure and Applied Mathematics*, vol. 9, no. 3, pp. 340–345, 2016.

[25] B. Basavanagoud and E. Chitra, "Degree square sum energy of graphs," *International Journal of Mathematics and Its Applications*, vol. 6, no. 2B, pp. 193–205, 2018.

[26] N. J. Rad, A. Jahanbani, and I. Gutman, "Zagreb energy and Zagreb estrada index of graphs," *MATCH Communications in Mathematical and in Computer Chemistry*, vol. 79, pp. 371–386, 2018.

[27] H. Siddiqui and M. R. Farahani, "Forgotten polynomial and forgotten index of certain interconnection networks," *Open Journal of Mathematical Analysis*, vol. 1, no. 1, pp. 44–59, 2017.

[28] S. Noreen and A. Mahmood, "Zagreb polynomials and redefined Zagreb indices for the line graph of carbon nanocones," *Open Journal of Mathematical Analysis*, vol. 2, no. 1, pp. 66–73, 2018.

[29] Z. Tang, L. Liang, and W. Gao, "Wiener polarity index of quasi-tree molecular structures," *Open Journal of Mathematical Sciences*, vol. 2, no. 1, pp. 73–83, 2018.

[30] M. Imran, A. Asghar, and A. Q. Baig, "On graph invariants of oxide network," *Engineering and Applied Science Letters*, vol. 1, no. 1, pp. 23–28, 2018.

[31] W. Gao, A. Asghar, and W. Nazeer, "Computing degree-based topological indices of Jahangir graph," *Engineering and Applied Science Letters*, vol. 1, no. 1, pp. 16–22, 2018.

Hindawi
Journal of Chemistry
Volume 2019, Article ID 2047406, 9 pages
https://doi.org/10.1155/2019/2047406

Research Article

Sufficient Conditions for Hamiltonicity of Graphs with Respect to Wiener Index, Hyper-Wiener Index, and Harary Index

Guisheng Jiang,[1] Lifang Ren,[2] and Guidong Yu [2,3]

[1]*School of Physics and Electronic Engineering, Anqing Normal University, Anqing 246133, China*
[2]*School of Mathematics and Computation Sciences, Anqing Normal University, Anqing 246133, China*
[3]*Basic Department, Hefei Preschool Education College, Hefei 230013, China*

Correspondence should be addressed to Guidong Yu; guidongy@163.com

Received 30 June 2019; Revised 28 September 2019; Accepted 12 October 2019; Published 15 November 2019

Guest Editor: Jia-Bao Liu

In this paper, with respect to the Wiener index, hyper-Wiener index, and Harary index, it gives some sufficient conditions for some graphs to be traceable, Hamiltonian, Hamilton-connected, or traceable for every vertex. Firstly, we discuss balanced bipartite graphs with $\delta(G) \geq t$, where $\delta(G)$ is the minimum degree of G, and gain some sufficient conditions for the graphs to be traceable or Hamiltonian, respectively. Secondly, we discuss nearly balanced bipartite graphs with $\delta(G) \geq t$ and present some sufficient conditions for the graphs to be traceable. Thirdly, we discuss graphs with $\delta(G) \geq t$ and obtain some conditions for the graphs to be traceable or Hamiltonian, respectively. Finally, we discuss t-connected graphs and provide some conditions for the graphs to be Hamilton-connected or traceable for every vertex, respectively.

1. Introduction

We consider only a simple graph. For a graph $G = (V(G), E(G))$, we use n to denote $|V(G)|$ and $e(G)$ to $|E(G)|$. We write $d_G(x, y)$ as the minimum length of the paths between x and y in G, which is called the distance between two vertices x and y of G. Denote $\delta(G) = \min\{d_G(v), v \in V(G)\}$. For a bipartite graph $G = (X, Y; E)$, if $|X| = |Y|$, it is called a *balanced bipartite graph*; if $|X| = |Y| + 1$, it is called a *nearly balanced bipartite graph*. For disjoint graphs G_1 and G_2, the graph $G_1 + G_2$ is called the union of G_1 and G_2, where $V(G_1 + G_2) = V(G_1) \cup V(G_2)$ and $E(G_1 + G_2) = E(G_1) \cup E(G_2)$; the graph $G_1 \vee G_2$ is called the join of G_1 and G_2, where $V(G_1 \vee G_2) = V(G_1) \cup V(G_2)$ and $E(G_1 \vee G_2) = E(G_1 + G_2) \cup \{xy : \forall x \in V(G_1), \forall y \in V(G_2)\}$. For example, $K_{n,m} = O_n \vee O_m$. The graph $\overline{G} = (V(\overline{G}), E(\overline{G}))$ means the *complement* of G, where $V(\overline{G}) = V(G)$ and $E(\overline{G}) = \{xy : x, y \in V(G), xy \notin E(G)\}$. The graph $\widehat{G} := (X, Y; E')$, $E' = \{xy : x \in X, y \in Y, xy \notin E\}$ is called the *quasicomplement* of bipartite $G = (X, Y; E)$.

In [1], Wiener introduced the *Wiener index*, $W(G) = \sum_{v_i, v_j \in V(G)} d_G(v_i, v_j)$, for a connected graph G in 1947.

We denote $D_i(G) = \sum_{v_j \in V(G)} d_G(v_i, v_j)$; then,

$$W(G) = \frac{1}{2} \sum_{i=1}^{n} D_i(G). \tag{1}$$

For a connected graph G, $WW(G) = (1/2)(\sum_{v_i, v_j \in V(G)} d_G(v_i, v_j) + \sum_{v_i, v_j \in V(G)} d_G^2(v_i, v_j))$ is called its *hyper-Wiener index*, which is introduced by Klein et al. [2] in 1995.

We denote $DD_i(G) = \sum_{v_j \in V(G)} d_G^2(v_i, v_j)$; then,

$$WW(G) = \frac{1}{4} \sum_{i=1}^{n} (D_i(G) + DD_i(G)). \tag{2}$$

In [3, 4], Plavšić et al. and Ivanciuc et al. gave the *Harary* index, $H(G) = \sum_{v_i, v_j \in V(G)} 1/(d_G(v_i, v_j))$ for a connected graph G, independently.

We denote $\widetilde{D}_G(v_i) = \sum_{v_j \in V(G)} 1/(d_G(v_i, v_j))$; then,

$$H(G) = \frac{1}{2}\sum_{i=1}^{n} \widetilde{D}_G(v_i). \tag{3}$$

For a graph G, if it contains a path (cycle) containing all vertices of G, it is *traceable* (*Hamiltonian*); if there are paths containing all vertices of G between any two vertices in G, it is called to be *Hamilton-connected*; if there are paths containing all vertices of G from any vertex in G, it is called to be *traceable from every vertex*.

Topological indices have attracted much attention in the literature, and they are widely applied in various fields of science and technology. Recently, some interesting results have been obtained, see [5–11]. Especially, some topological indices are used to characterize the Hamiltonian property of graphs. We refer readers to see [2, 12–21]. Among them, Hua and Ning [15] gave Hamiltonian conditions for a balanced bipartite graph with respect to the Wiener index and Harary index. Cai et al. [13], by the hyper-Wiener index, gave conditions for a balanced bipartite graph to be traceable and Hamiltonian and a t-connected graph to be Hamiltonian, respectively. Li [18, 19] gave Hamitonian conditions for a t-connected graph with respect to the Wiener index and Harary index, respectively. With the Wiener index, hyper-Wiener index, and Harary index, Yu et al. [20] gave conditions for a t-connected graph to be Hamilton-connected and then got conditions for it to be traceable from every vertex, as well as gave conditions for a nearly balance bipartite graph to be traceable. Especially, Liu et al. [16, 17] studied the Hamiltonian property of graphs with respect to the Wiener index and Harary index of complement of graph or quasicomplement of bipartite graph, respectively. As a continuance of these results, we also study the similar problems.

In this paper, we discuss the hamiltonicity of graph by the Wiener index, hyper-Wiener index, and Harary index for quasicomplement or complement. In Section 2, we present some notations and some lemmas needed in the following. In Sections 3 and 4, we present some conditions for a balanced bipartite graph G with $\delta(G) \geq t$ to be traceable and Hamiltion, respectively. In Section 5, we give sufficient conditions for a nearly balanced bipartite graph G with $\delta(G) \geq t$ to be traceable. In Sections 6 and 7, we present some conditions for a graph G with $\delta(G) \geq t$ to be traceable and Hamiltonian, respectively. In Sections 8 and 9, we provide some conditions for a t-connected graph to be Hamilton-connected and traceable from every vertex, respectively.

2. Preliminaries

Especially, in the following, for bipartite graphs, we always fix their partite sets. For instance, $O_{s,t}$ and $O_{t,s}$ are seen as different bipartite graphs unless $s = t$.

A graph $G_1 \sqcup G_2$ is the graph obtained from $G_1 \vee G_2$ by deleting all possible edges between X_1 and X_2 and possible edges between Y_1 and Y_2, where $G_i(X_i, Y_i, E_i)$, $(i = 1, 2)$ be bipartite graphs. Next, we denote some special classes of graphs:

$$\begin{aligned}
B_n^t &= O_{t,n-t} \sqcup K_{n-t,t}\left(1 \leq t \leq \frac{n}{2}\right),\\
C_n^t &= O_{t,n-t} \sqcup K_{n-t-1,t}\left(1 \leq t \leq \frac{n}{2}\right),\\
R_n^t &= K_{t,t} + K_{n-t,n-t}\left(1 \leq t \leq \frac{n}{2}\right),\\
Q_n^t &= O_{t+1,n-t} \sqcup K_{n-t-1,t}\left(1 \leq t \leq \frac{n}{2}\right),\\
L_n^t &= K_1 \vee (K_t + K_{n-t-1}), \left(1 \leq t \leq \frac{(n-1)}{2}\right),\\
N_n^t &= K_t \vee (K_{n-2t} + tK_1), \left(1 \leq t \leq \frac{(n-1)}{2}\right),\\
\underline{L}_n^t &= K_{t+1} + K_{n-t-1}, \left(1 \leq t \leq \frac{(n-1)}{2}\right),\\
\underline{N}_n^t &= K_t \vee (K_{n-2t-1} + (t+1)K_1), \left(1 \leq t \leq \frac{(n-1)}{2}\right).
\end{aligned} \tag{4}$$

Note that $e(C_n^t) = n(n-t-1) + t^2$, and C_n^t is not traceable.

Lemma 1. *Denote $\widehat{G}$ as a quasicomplement of bipartite G with $2n$ vertices. If $\widehat{G}$ is a connected balanced bipartite graph, then*

$$W(\widehat{G}) \leq 2n^3 - 3n^2 + 2n + 2(n-1)e(G). \tag{5}$$

Proof. As $\widehat{G}$ is a quasicomplement,

$$\begin{aligned}
W(\widehat{G}) &= \sum_{v_i, v_j \in V(\widehat{G})} d_{\widehat{G}}(v_i, v_j),\\
&= \frac{1}{2}\sum_{j=1}^{2n} D_j(\widehat{G}),\\
&\leq \frac{1}{2}\left(\sum_{j=1}^{2n}\left(d_{\widehat{G}}(x_j) + (2n-1)\left(n - d_{\widehat{G}}(x_j)\right) + 2n^2\right.\right.\\
&\quad \left.\left. - 4n + 2\right)\right),\\
&= 4n^3 - 5n^2 + 2n + (1-n)\sum_{j=1}^{2n} d_{\widehat{G}}(x_j),\\
&= 4n^3 - 5n^2 + 2n + (1-n)\sum_{j=1}^{2n}\left(n - d_G(x_j)\right),\\
&= 2n^3 - 3n^2 + 2n + (n-1)\sum_{j=1}^{2n} d_G(x_j),\\
&= 2n^3 - 3n^2 + 2n + 2(n-1)e(G).
\end{aligned} \tag{6}$$

□

Lemma 2. *Let $\widehat{G}$ be a quasicomplement of bipartite G with $2n$ vertices. If $\widehat{G}$ is a connected balanced bipartite graph, then*

$$WW(\widehat{G}) \le 2n^4 - 5n^3 + 5n^2 - n + \left(2n^2 - n - 1\right)e(G). \quad (7)$$

Proof. As $\widehat{G}$ is a quasicomplement,

$$\begin{aligned}
WW(\widehat{G}) &= \frac{1}{2}\sum_{v_i,v_j\in V(\widehat{G})}\left(d_{\widehat{G}}(v_i,v_j) + d^2_{\widehat{G}}(v_i,v_j)\right),\\
&= \frac{1}{4}\sum_{j=1}^{2n}\left(D_j(\widehat{G}) + DD_j(\widehat{G})\right),\\
&\le \frac{1}{4}\sum_{j=1}^{2n}\left(d_{\widehat{G}}(x_j) + (2n-1)\left(n - d_{\widehat{G}}(x_j)\right)\right.\\
&\quad \left. + 2n^2 - 4n + 2\right)\\
&\quad + \frac{1}{4}\sum_{j=1}^{2n}\left(d_{\widehat{G}}(x_j) + \left(4n^2 - 4n + 1\right)\left(n - d_{\widehat{G}}(x_j)\right)\right.\\
&\quad \left. + 4(n-1)^3\right),\\
&= 4n^4 - 6n^3 + 4n^2 - n\\
&\quad -\left(n^2 - 0.5n - 0.5\right)\sum_{j=1}^{2n} d_{\widehat{G}}(x_j),\\
&= 4n^4 - 6n^3 + 4n^2 - n\\
&\quad -\left(n^2 - 0.5n - 0.5\right)\sum_{j=1}^{2n}\left(n - d_G(x_j)\right),\\
&= 2n^4 - 5n^3 + 5n^2 - n + \left(2n^2 - n - 1\right)e(G).
\end{aligned} \quad (8)$$

□

Lemma 3. *Let $\widehat{G}$ be a quasicomplement of bipartite G of order $2n$. If $\widehat{G}$ is a connected balanced bipartite graph, then*

$$H(\widehat{G}) \ge \frac{4n^3 - n}{4n - 2} - \frac{2n - 2}{2n - 1}e(G). \quad (9)$$

Proof. As $\widehat{G}$ is a quasicomplement,

$$\begin{aligned}
H(\widehat{G}) &= \sum_{v_i,v_j\in V(\widehat{G})}\frac{1}{d_{\widehat{G}}(v_i,v_j)},\\
&= \frac{1}{2}\sum_{j=1}^{2n}\widetilde{D}_{\widehat{G}}(v_j),\\
&\ge \frac{1}{2}\sum_{j=1}^{2n}\left(d_{\widehat{G}}(x_j) + \frac{1}{2n-1}\left(n - d_{\widehat{G}}(x_j)\right) + \frac{1}{2}\right),\\
&= \frac{n(4n-1)}{2(2n-1)} + \frac{n-1}{2n-1}\sum_{j=1}^{2n} d_{\widehat{G}}(x_j),\\
&= \frac{n(4n-1)}{2(2n-1)} + \frac{n-1}{2n-1}\sum_{j=1}^{2n}\left(n - d_G(x_j)\right),\\
&= \frac{4n^3 - n}{4n-2} - \frac{n-1}{2n-1}\sum_{j=1}^{2n} d_G(x_j),\\
&= \frac{4n^3 - n}{4n-2} - \frac{2n-2}{2n-1}e(G).
\end{aligned} \quad (10)$$

□

Lemma 4. *Let $\overline{G}$ be a complement of G with n vertices. If $\overline{G}$ is a connected graph, then*

$$W(\overline{G}) \le \frac{1}{2}n(n-1) + (n-2)e(G). \quad (11)$$

Proof.

$$\begin{aligned}
W(\overline{G}) &= \sum_{v_i,v_j\in V(\overline{G})} d_{\overline{G}}(v_i,v_j),\\
&= \frac{1}{2}\sum_{j=1}^{n} D_j(\overline{G}),\\
&\le \frac{1}{2}\sum_{j=1}^{n}\left(d_{\overline{G}}(x_j) + (n-1)\left(n - 1 - d_{\overline{G}}(x_j)\right)\right),\\
&= \frac{n}{2}\left(n^2 - 2n + 1\right) + \frac{n}{2}(2-n)\sum_{j=1}^{n} d_{\overline{G}}(x_j),\\
&= \frac{n}{2}\left(n^2 - 2n + 1\right) - \frac{n}{2}(n-2)\sum_{j=1}^{n}\left(n - 1 - d_G(x_j)\right),\\
&= \frac{n}{2}(n-1) + \frac{(n-2)}{2}\sum_{j=1}^{n} d_G(x_j),\\
&= \frac{1}{2}n(n-1) + (n-2)e(G).
\end{aligned} \quad (12)$$

□

Lemma 5. *Let $\overline{G}$ be a complement of G with n vertices. If $\overline{G}$ is a connected graph, then*

$$WW(\overline{G}) \le \frac{1}{2}n(n-1) + \frac{1}{2}\left(n^2 - n - 2\right)e(G). \tag{13}$$

Proof

$$\begin{aligned}
WW(\overline{G}) &= \frac{1}{2}\sum_{v_i,v_j\in V(\overline{G})}\left(d_{\overline{G}}(v_i,v_j) + d^2_{\overline{G}}(v_i,v_j)\right),\\
&= \frac{1}{4}\sum_{j=1}^{n}\left(D_j(\overline{G}) + DD_j(\overline{G})\right),\\
&\le \frac{1}{4}\sum_{j=1}^{n}\left(d_{\overline{G}}(x_j) + (n-1)\left(n-1-d_{\overline{G}}(x_j)\right)\right),\\
&\quad + \frac{1}{4}\sum_{j=1}^{n}\left(d_{\overline{G}}(x_j) + (n-1)^2\left(n-1-d_{\overline{G}}(x_j)\right)\right)\\
&= \frac{n^2}{4}\left(n^2-2n+1\right) + \frac{(2+n-n^2)}{4}\sum_{j=1}^{n}d_{\overline{G}}(x_j),\\
&= \frac{n^2}{4}\left(n^2-2n+1\right) + \frac{(2+n-n^2)}{4}\sum_{j=1}^{n}\left(n-1-d_G(x_j)\right),\\
&= \frac{n}{2}(n-1) + \frac{(n^2-n-2)}{4}\sum_{j=1}^{n}d_G(x_j),\\
&= \frac{1}{2}n(n-1) + \frac{1}{2}\left(n^2-n-2\right)e(G).
\end{aligned} \tag{14}$$

□

Lemma 6. *Let $\overline{G}$ be a complement of G with n vertices. If $\overline{G}$ is a connected graph, then*

$$H(\overline{G}) \ge \frac{1}{2}\left(n^2-n\right) - \frac{n-2}{n-1}e(G). \tag{15}$$

Proof

$$\begin{aligned}
H(\overline{G}) &= \sum_{v_i,v_j\in V(\overline{G})}\frac{1}{d_{\overline{G}}(v_i,v_j)},\\
&= \frac{1}{2}\sum_{j=1}^{n}\tilde{D}_{\overline{G}}(v_j),\\
&\ge \frac{1}{2}\sum_{j=1}^{n}\left(d_{\overline{G}}(x_j) + \frac{1}{n-1}\left(n-1-d_{\overline{G}}(x_j)\right)\right),\\
&= \frac{n}{2} + \frac{n-2}{2(n-1)}\sum_{j=1}^{n}d_{\overline{G}}(x_j),\\
&= \frac{n^2-n}{2} - \frac{n-2}{2(n-1)}\sum_{j=1}^{n}d_G(x_j),\\
&= \frac{1}{2}\left(n^2-n\right) - \frac{n-2}{n-1}e(G).
\end{aligned} \tag{16}$$

□

3. Traceable of Balanced Bipartite Graphs

Lemma 7 (see [22]). *Let G be a balanced bipartite graph with $2n$ vertices. If $\delta(G) \ge t \ge 1$, $n \ge 2t+3$, and*

$$e(G) > n^2 - nt - 2n + t^2 + 4t + 4, \tag{17}$$

for some integer t, then G is traceable or $G \subseteq Q_n^t$ or $t = 1$, $G \subseteq R_n^1$.

Theorem 1. *Let $\widehat{G}$ be a connected balanced bipartite graph with $2n$ vertices. If $\delta(G) \ge t \ge 1$, $n \ge 2t+3$, and*

$$W(\widehat{G}) > 4n^3 - (2t+9)n^2 + \left(2t^2+10t+14\right)n - 2(t+2)^2, \tag{18}$$

for some integer t, then G is traceable or $t = 1$ and $G \subseteq R_n^1$.

Proof. Since $W(\widehat{G}) > 4n^3 - (2t+9)n^2 + (2t^2+10t+14)n - 2(t+2)^2$, by Lemma 1, we get $e(G) > n^2 - nt - 2n + t^2 + 4t + 4$. By Lemma 7, we obtain that G is traceable or $G \subseteq Q_n^t$ or $t = 1$, $G \subseteq R_n^1$.

If $G \subseteq Q_n^t$: because $\widehat{G}$ is connected and $\delta(G) \ge t \ge 1$, we get $e(G) \le n^2 - nt - n + t^2 + t - (n-t-1) - t < n^2 - nt - 2n + t^2 + 4t + 4$. It is in contradiction with the above.

If $t = 1$: because $\widehat{G}$ is connected, $G \subseteq R_n^1$. □

Theorem 2. *Let $\widehat{G}$ be a connected balanced bipartite graph with $2n$ vertices. If $\delta(G) \ge t \ge 1$, $n \ge 2t+3$, and*

$$\begin{aligned}
WW(\widehat{G}) > {}& 4n^4 - (2t+10)n^3 + \left(2t^2+9t+14\right)n^2\\
&- \left(t^2+3t+3\right)n - (t+2)^2,
\end{aligned} \tag{19}$$

for some integer t, then G is traceable or $t = 1$, $G \subseteq R_n^1$.

Proof. Since $WW(\widehat{G}) > 4n^4 - (2t+10)n^3 + (2t^2+9t+14)n^2 - (t^2+3t+3)n - (t+2)^2$, by Lemma 2, $e(G) > n^2 - nt - 2n + t^2 + 4t + 4$. By Lemma 7, G is traceable or $G \subseteq Q_n^t$ or $t = 1$, $G \subseteq R_n^1$. By the same discussion as the proof of Theorem 1, the conclusion is established. □

Theorem 3. *Let G be a connected balanced bipartite graph with $2n$ vertices. If $\delta(G) \ge t \ge 1$, $n \ge 2t+3$, and*

$$H(\widehat{G}) < \frac{(4t+12)n^2 - \left(4t^2+20t-25\right)n + 4t^2 + 16t + 16}{4n-2}, \tag{20}$$

for some integer t, then G is traceable or $t = 1$, $G \subseteq R_n^1$.

Proof. Since $H(\widehat{G}) < ((4t+12)n^2 - (4t^2+20t-25)n + 4t^2 + 16t + 16)/(4n-2)$, by Lemma 3, we get $e(G) > n^2 - nt - 2n + t^2 + 4t + 4$. By Lemma 7, we obtain that G is traceable or $G \subseteq Q_n^t$ or $t = 1$, $G \subseteq R_n^1$. By the same discussion as the proof of Theorem 1, the conclusion is established. □

4. Hamiltonian of Balanced Bipartite Graphs

Lemma 8 (see [23]). *Let G be a balanced bipartite graph with $2n$ vertices. If $\delta(G) \geq t \geq 1$, $n \geq 2t+3$, and*

$$e(G) > n^2 - nt - n + t^2 + 2t + 1, \tag{21}$$

for some integer t, then G is Hamiltonian or $G \subseteq B_n^t$.

Theorem 4. *Let $\widehat{G}$ be a connected balanced bipartite graph with $2n$ vertices. If $\delta(G) \geq t \geq 1$, $n \geq 2t+3$, and*

$$W(\widehat{G}) > 4n^3 - (2t+7)n^2 + \left(2t + 2(t+1)^2 + 4\right)n - 2(t+1)^2, \tag{22}$$

for some integer t, then G is Hamiltonian.

Proof. Since $W(\widehat{G}) > 4n^3 - (2t+7)n^2 + (2t + 2(t+1)^2 + 4)n - 2(t+1)^2$, by Lemma 1, we get $e(G) > n^2 - nt - n + t^2 + 2t + 1$. By Lemma 8, G is Hamiltonian or $G \subseteq B_n^t$.

If $G \subseteq B_n^t$: because $\widehat{G}$ is connected and $\delta(G) \geq t \geq 1$, we get $e(G) \leq (n-t)^2 + nt - (n-t) - t < n^2 - nt - n + t^2 + 2t + 1$. It is in contradiction with the above. □

Theorem 5. *Let $\widehat{G}$ be a connected balanced bipartite graph with $2n$ vertices. If $\delta(G) \geq t \geq 1$, $n \geq 2t+3$, and*

$$\begin{aligned} WW(\widehat{G}) > {} & 4n^4 - (2t+8)n^3 + \left(2t^2 + 5t + 7\right)n^2 \\ & - \left(t^2 + t + 1\right)n - (t+1)^2, \end{aligned} \tag{23}$$

for some integer t, then G is Hamiltonian.

Proof. Since $WW(\widehat{G}) > 4n^4 - (2t+8)n^3 + (2t^2 + 5t + 7)n^2 - (t^2 + t + 1)n - (t+1)^2$, by Lemma 2, we get $e(G) > n^2 - nt - n + t^2 + 2t + 1$. By Lemma 8, G is Hamiltonian or $G \subseteq B_n^t$. By the same discussion as the proof of Theorem 4, the conclusion is established. □

Theorem 6. *Let $\widehat{G}$ be a connected balanced bipartite graph of with $2n$ vertices. If $\delta(G) \geq t \geq 1$, $n \geq 2t+3$, and*

$$H(\widehat{G}) < \frac{(4t+8)n^2 - \left(4t^2 + 12t + 9\right)n + 4t^2 + 8t + 4}{4n-2}, \tag{24}$$

for some integer t, then G is Hamiltonian.

Proof. Since $H(\widehat{G}) < (((4t+8)n^2 - (4t^2 + 12t + 9)n + 4t^2 + 8t + 4)/(4n-2))$, by Lemma 3, $e(G) > n^2 - nt - n + t^2 + 2t + 1$. By Lemma 8, G is Hamiltonian or $G \subseteq B_n^t$. By the same discussion as the proof of Theorem 4, the conclusion is established. □

5. Traceable of Nearly Balanced Bipartite Graphs

Lemma 9 (Yu, Fang, and Fan [24]). *Let G be a nearly balanced bipartite graph with $2n-1$ vertices. If $\delta(G) \geq t \geq 1$, $n \geq 2t+1$, and*

$$e(G) > n^2 - nt - 2n + t^2 + 2t + 1, \tag{25}$$

for some integer t, then G is traceable or $G \subseteq C_n^t$.

Theorem 7. *Let $\widehat{G}$ be a connected nearly balanced bipartite graph with $2n-1$ vertices. If $n \geq 2t+1$, $\delta(G) \geq t \geq 1$, and*

$$\begin{aligned} W(\widehat{G}) > {} & 4n^3 - (2t+14)n^2 + \left(4t + 2(t+1)^2 + 16\right)n \\ & - 4(t+1)^2 - 4, \end{aligned} \tag{26}$$

for some integer t, then G is traceable.

Proof. Let $G = G(X, Y; E)$, where $X = \{x_1, x_2, \ldots, x_n\}$ and $Y = \{y_1, y_2, \ldots, y_{n-1}\}$, then

$$\begin{aligned} W(\widehat{G}) &= \sum_{v_i, v_j \in V(\widehat{G})} d_{\widehat{G}}(v_i, v_j) \\ &= \frac{1}{2} \sum_{j=1}^{2n-1} D_j(\widehat{G}) \\ &\leq \frac{1}{2} \left(\sum_{j=1}^{n} \left(d_{\widehat{G}}(x_j) + (2n-3)\left(n - 1 - d_{\widehat{G}}(x_j)\right) \right.\right. \\ &\quad \left.\left. + 2\left(n^2 - 2n + 1\right)\right)\right) \\ &\quad + \frac{1}{2} \left(\sum_{j=1}^{n-1} \left(d_{\widehat{G}}(y_j) + (2n-3)\left(n - d_{\widehat{G}}(y_j)\right) \right.\right. \\ &\quad \left.\left. + 2\left(n^2 - 4n + 4\right)\right)\right) \\ &= 4n^3 - 12n^2 + 12n - 4 - (n-2) \\ &\quad \cdot \left(\sum_{j=1}^{n} d_{\widehat{G}}(x_j) + \sum_{j=1}^{n-1} d_{\widehat{G}}(y_j) \right) \\ &= 2n^3 - 6n^2 + 8n - 4 + (n-2) \\ &\quad \cdot \left(\sum_{j=1}^{n} d_G(x_j) + \sum_{j=1}^{n-1} d_G(y_j) \right) \\ &= 2n^3 - 6n^2 + 8n - 4 + 2(n-2)e(G), \end{aligned} \tag{27}$$

where $d_{\widehat{G}}(x_j) = n - 1 - d_G(x_j)$ and $d_{\widehat{G}}(y_j) = n - d_G(y_j)$. Because $W(\widehat{G}) > 4n^3 - (2t+14)n^2 + (4t + 2(t+1)^2 + 16)n - 4(t+1)^2 - 4$, we get $e(G) > n^2 - nt - 2n + t^2 + 2t + 1$. By Lemma 9, we get G is traceable or $G \subseteq C_n^t$.

If $G \subseteq C_n^t$: because $\widehat{G}$ is connected and $\delta(G) \geq t \geq 1$, we get $e(G) \leq t^2 + n(n-t-1) - (n-t-1) - t < n^2 - nt - 2n + t^2 + 2t + 1$. It is in contradiction with the above. □

Theorem 8. *Let $\widehat{G}$ be a connected nearly balanced bipartite graph with $2n-1$ vertices. If $n \geq 2t+1$, $\delta(G) \geq t \geq 1$, and*

$$WW(\widehat{G}) > 4n^4 - (2t+18)n^3 + \left(2t^2 + 9t + \frac{65}{2}\right)n^2 - \left(5t^2 + 12t + \frac{53}{2}\right)n + 2t^2 + 4t + 8, \tag{28}$$

for some integer t, then G is traceable.

Proof. Let $G = G(X, Y : E)$, where $X = \{x_1, x_2, \ldots, x_n\}$ and $Y = \{y_1, y_2, \ldots, y_{n-1}\}$, then

$$\begin{aligned}
WW(\widehat{G}) &= \frac{1}{2} \sum_{v_i, v_j \in V(\widehat{G})} \left(d_{\widehat{G}}(v_i, v_j) + d_{\widehat{G}}^2(v_i, v_j)\right) \\
&= \frac{1}{4} \sum_{j=1}^{2n-1} \left(D_j(\widehat{G}) + DD_j(\widehat{G})\right) \\
&\leq \frac{1}{4} \sum_{j=1}^{n} \left(d_{\widehat{G}}(x_j) + (2n-3)\left(n-1-d_{\widehat{G}}(x_j)\right)\right. \\
&\quad \left. + 2\left(n^2 - 2n + 1\right)\right) \\
&\quad + \frac{1}{4} \sum_{j=1}^{n} \left(d_{\widehat{G}}(x_j) + (2n-3)^2\left(n-1-d_{\widehat{G}}(x_j)\right)\right. \\
&\quad \left. + 4(n-1)^2(n-1)\right) \\
&\quad + \frac{1}{4} \sum_{j=1}^{n-1} \left(d_{\widehat{G}}(y_j) + (2n-3)\left(n-d_{\widehat{G}}(y_j)\right)\right. \\
&\quad \left. + (2n-4)(n-2)\right) \\
&\quad + \frac{1}{4} \sum_{j=1}^{n-1} \left(d_{\widehat{G}}(y_j) + (2n-3)^2\left(n-d_{\widehat{G}}(y_j)\right)\right. \\
&\quad \left. + (2n-4)^2(n-2)\right) \\
&= 4n^4 - 16n^3 + \frac{51}{2}n^2 - \frac{39}{2}n + 6 + \frac{1}{4}\left(-4n^2 + 10n - 4\right) \\
&\quad \cdot \left(\sum_{j=1}^{n} d_{\widehat{G}}(x_j) + \sum_{j=1}^{n-1} d_{\widehat{G}}(y_j)\right) \\
&= 2n^4 - 9n^3 + \frac{37}{2}n^2 - \frac{35}{2}n + 6 + \frac{1}{4}\left(4n^2 - 10n + 4\right) \\
&\quad \cdot \left(\sum_{j=1}^{n} d_G(x_j) + \sum_{j=1}^{n-1} d_G(y_j)\right) \\
&= 2n^4 - 9n^3 + \frac{37}{2}n^2 - \frac{35}{2}n + 6 + \left(2n^2 - 5n + 2\right)e(G),
\end{aligned} \tag{29}$$

where $d_{\widehat{G}}(x_j) = n - 1 - d_G(x_j)$ and $d_{\widehat{G}}(y_j) = n - d_G(y_j)$. Because $WW(\widehat{G}) > 4n^4 - (2t+18)n^3 + (2t^2 + 9t + (65/2))n^2 - (5t^2 + 12t + (53/2))n + 2t^2 + 4t + 8$, we get $e(G) > n^2 - nt - 2n + t^2 + 2t + 1$. By Lemma 9, we obtain that G is traceable or $G \subseteq C_n^t$. By the same discussion as the proof of Theorem 7, the conclusion is established. □

Theorem 9. *Let $\widehat{G}$ be a connected nearly balanced bipartite graph with $2n-1$ vertices. If $n \geq 2t+1$, $\delta(G) \geq t \geq 1$, and*

$$H(\widehat{G}) \leq \frac{(4t+8)n^2 - \left(4t^2 + 16t + 17\right)n + 8t^2 + 16t + 8}{4n-6}, \tag{30}$$

for some integer t, then G is traceable or $G \subseteq C_n^t$ $(t \leq 6)$.

Proof. Let $G = G(X, Y : E)$, where $X = \{x_1, x_2, \ldots, x_n\}$ and $Y = \{y_1, y_2, \ldots, y_{n-1}\}$, then

$$\begin{aligned}
H(\widehat{G}) &= \sum_{v_i, v_j \in V(G)} \frac{1}{d_{\widehat{G}}(v_i, v_j)} \\
&= \frac{1}{2} \sum_{j=1}^{n} \widetilde{D}_{\widehat{G}}(v_j) \\
&\geq \frac{1}{2} \sum_{j=1}^{n} \left(d_{\widehat{G}}(x_j) + \frac{1}{2n-3}\left(n-1-d_{\widehat{G}}(x_j)\right) + \frac{1}{2}\right) \\
&\quad + \frac{1}{2} \sum_{j=1}^{n-1} \left(d_{\widehat{G}}(y_j) + \frac{1}{2n-3}\left(n-d_{\widehat{G}}(y_j)\right) + \frac{1}{2}\right) \\
&= \frac{4n^2 - 5n}{4n-6} + \frac{n-2}{2n-3}\left(\sum_{j=1}^{n} d_{\widehat{G}}(x_j) + \sum_{j=1}^{n-1} d_{\widehat{G}}(y_j)\right) \\
&= \frac{4n^3 - 8n^2 + 3n}{4n-6} - \frac{n-2}{2n-3}\left(\sum_{j=1}^{n} d_G(x_j) + \sum_{j=1}^{n-1} d_G(y_j)\right) \\
&= \frac{4n^3 - 8n^2 + 3n}{4n-6} - \frac{2(n-2)}{2n-3} e(G),
\end{aligned} \tag{31}$$

where $d_{\widehat{G}}(x_j) = n - 1 - d_G(x_j)$ and $d_{\widehat{G}}(y_j) = n - d_G(y_j)$. Because

$$H(\widehat{G}) \leq \frac{(4t+8)n^2 - \left(4t^2 + 16t + 17\right)n + 8t^2 + 16t + 8}{4n-6}, \tag{32}$$

we get $e(G) > n^2 - nt - 2n + t^2 + 2t + 1$. By Lemma 9, we obtain that G is traceable or $G \subseteq C_n^t$. Note that $t \geq 7$ and $H(\widehat{C_n^t}) = (1/4)(n^2 + 2tn - n - 2t^2) > ((4t+8)n^3 - (4t^2 + 24t + 33)n^2 + (16t^2 + 48t + 44)n - 16t^2 - 32t - 19)/(4n^2 - 14n + 12)$. If $G \subseteq C_n^t$, then $H(\widehat{G}) > H(\widehat{C_n^t})$. The conclusion is established. □

6. Traceable of Graphs

Lemma 10 (see [23]). *Let G be a graph with $n(\geq 6t+10)$ vertices, where t is an integer. If $\delta(G)\geq t$ and $e(G)>\binom{n-t-2}{2}+t^2+3t+2$, then G is traceable unless $G\subseteq \underline{L}_n^t$ or $\underline{N}_n^t$.*

Theorem 10. *Let $\overline{G}$ be a connected graph with $n(\geq 6t+10)$ vertices, where t is an integer. If $\delta(G)\geq t$ and*

$$W(\overline{G})>\frac{1}{2}\left(n^3-(2t+6)n^2+\left(3t^2+15t+19\right)n-6t^2-22t-20\right), \tag{33}$$

then G is traceable.

Proof. Since $W(\overline{G})>(1/2)(n^3-(2t+6)n^2+(3t^2+15t+19)n-6t^2-22t-20)$, by Lemma 4, we get $e(G)>\binom{n-t-2}{2}+t^2+3t+2$. By Lemma 10, we obtain that G is traceable unless $G\subseteq \underline{L}_n^t$ or $\underline{N}_n^t$.

If $G\subseteq \underline{L}_n^t$: note that $W(\overline{\underline{L}_n^t})=n^2-2n-tn+t^2+2t+1$. Then, if $G\subseteq \underline{L}_n^t$, we have $W(\overline{G})\leq W(\overline{\underline{L}_n^t})<(1/2)(n^3-(2t+6)n^2+(3t^2+15t+19)n-6t^2-22t-20)$, a contradiction.

If $G\subseteq \underline{N}_n^t$: note that $W(\overline{\underline{N}_n^t})=(1/2)(2n^2-4n-6tn+5t^2+7t+2)$. Then, if $G\subseteq \underline{N}_n^t$, we have $W(\overline{G})\leq W(\overline{\underline{N}_n^t})<(1/2)(n^3-(2t+6)n^2+(3t^2+15t+19)n-6t^2-22t-20)$, a contradiction. □

Theorem 11. *Let $\overline{G}$ be a connected graph with $n(\geq 6t+10)$ vertices, where t is an integer. If $\delta(G)\geq t$ and*

$$WW(\overline{G})>\frac{1}{4}n^4-\left(\frac{1}{2}t+\frac{3}{2}\right)n^3+\left(\frac{3}{4}t^2+\frac{13}{4}t+\frac{15}{4}\right)n^2-\left(\frac{3}{4}t^2+\frac{7}{4}t+\frac{1}{2}\right)n-\frac{3}{2}t^2-\frac{11}{2}t-5, \tag{34}$$

then G is traceable.

Proof. Since $WW(\overline{G})>(1/4)n^4-((1/2)t+(3/2))n^3+((3/4)t^2+(13/4)t+(15/4))n^2-((3/4)t^2+(7/4)t+(1/2))n-(3/2)t^2-(11/2)t-5$, by Lemma 5, we get $e(G)>\binom{n-t-2}{2}+t^2+3t+2$. By Lemma 10, we obtain that G is traceable or $G\subseteq \underline{L}_n^t$ or $\underline{N}_n^t$.

If $G\subseteq \underline{L}_n^t$: note that $WW(\overline{\underline{L}_n^t})=(1/2)(3n^2-7n-4tn+4t^2+8t+4)$. Then, if $G\subseteq \underline{L}_n^t$, we have $WW(\overline{G})\leq WW(\overline{\underline{L}_n^t})<(1/4)n^4-((1/2)t+(3/2))n^3+((3/4)t^2+(13/4)t+(15/4))n^2-((3/4)t^2+(7/4)t+(1/2))n-(3/2)t^2-(11/2)t-5$, a contradiction.

If $G\subseteq \underline{N}_n^t$: note that $WW(\overline{\underline{N}_n^t})=3n^2-7n-10tn+9t^2+13t+4$. Then, if $G\subseteq \underline{N}_n^t$, we have $WW(\overline{G})\leq WW(\overline{\underline{N}_n^t})<(1/4)n^4-((1/2)t+(3/2))n^3+((3/4)t^2+(13/4)t+(15/4))n^2-((3/4)t^2+(7/4)t+(1/2))n-(3/2)t^2-(11/2)t-5$, a contradiction. □

Theorem 12. *Let $\overline{G}$ be a connected graph with $n(\geq 6t+10)$ vertices, where t is an integer. If $\delta(G)\geq t$ and*

$$H(\overline{G})<\frac{(2t+4)n^2-\left(3t^2+15t+18\right)n+6t^2+22t+20}{2n-2}, \tag{35}$$

then G is traceable.

Proof. Since $H(\overline{G})<(((2t+4)n^2-(3t^2+15t+18)n+6t^2+22t+20)/(2n-2))$, by Lemma 6, we get $e(G)>\binom{n-t-2}{2}+t^2+3t+2$. By Lemma 10, we obtain that G is traceable unless $G\subseteq \underline{L}_n^t$ or $\underline{N}_n^t$.

If $G\subseteq \underline{L}_n^t$: note that $H(\overline{\underline{L}_n^t})=(1/4)(n^2+n+2tn-2t^2-2)$. Then, if $G\subseteq \underline{L}_n^t$, we have $H(\overline{G})\geq H(\overline{\underline{L}_n^t})>(((2t+4)n^2-(3t^2+15t+18)n+6t^2+22t+20)/(2n-2))$, a contradiction.

If $G\subseteq \underline{N}_n{}^t$: note that $H(\overline{\underline{N}_n^t})=(1/4)(n^2+n+2tn-2t^2-6t-2)$. Then, if $G\subseteq \underline{N}_n^t$, we have $H(\overline{G})\geq H(\overline{\underline{N}_n^t})>(((2t+4)n^2-(3t^2+15t+18)n+6t^2+22t+20)/(2n-2))$, a contradiction. □

7. Hamiltonian of Graphs

Lemma 11 (see [23]). *Let G be a graph with $n(\geq 6t+5)$ vertices, where t is an integer. If $\delta(G)\geq t$ and*

$$e(G)>\binom{n-t-1}{2}+t^2+2t+1, \tag{36}$$

then G is Hamiltonian or $G\subseteq L_n^t$ or N_n^t.

Theorem 13. *Let $\overline{G}$ be a connected graph with $n(\geq 6t+5)$ vertices, where t is an integer. If $\delta(G)\geq t$ and*

$$W(\overline{G})>\frac{1}{2}\left(n^3-(2t+4)n^2+\left(3t^2+11t+19\right)n-6t^2-14t-8\right), \tag{37}$$

then G is Hamiltonian.

Proof. Since $W(\overline{G})>(1/2)(n^3-(2t+4)n^2+(3t^2+11t+19)n-6t^2-14t-8)$, by Lemma 4, we get $e(G)>\binom{n-t-1}{2}+t^2+2t+1$. By Lemma 11, we obtain that G is Hamiltonian or $G\subseteq L_n^t$ or N_n^t.

If $G\subseteq L_n^t$: note that $W(\overline{L_n^t})=n^2-tn-3n+t^2+t+2$. Then, if $G\subseteq L_n^t$, we have $W(\overline{G})\leq W(\overline{L_n^t})<(1/2)(n^3-(2t+4)n^2+(3t^2+11t+19)n-6t^2-14t-8)$, a contradiction.

If $G\subseteq N_n^t$: note that $W(\overline{N_n^t})=n^2-3tn-n+(5/2)t^2+(3/2)t$. Then, if $G\subseteq N_n^t$, we have $W(\overline{G})\leq W(\overline{N_n^t})<$

$(1/2)(n^3 - (2t+4)n^2 + (3t^2 + 11t + 19)n - 6t^2 - 14t - 8)$, a contradiction. □

Theorem 14. *Let $\delta(G) \geq t$ and $\overline{G}$ be a connected graph with $n(\geq 6t+5)$ vertices for some integers t satisfying the following condition:*

$$WW(\overline{G}) > \frac{1}{4}n^4 - \left(\frac{1}{2}t + 1\right)n^3 + \left(\frac{3}{4}t^2 + \frac{9}{4}t + \frac{3}{2}\right)n^2 - \left(\frac{3}{4}t^2 + \frac{3}{4}t + \frac{1}{4}\right)n - \left(\frac{3}{2}t^2 + \frac{7}{2}t + 2\right). \tag{38}$$

Therefore, G is Hamiltonian.

Proof. Since $WW(\overline{G}) > (1/4)n^4 - ((1/2)t+1)n^3 + ((3/4)t^2 + (9/4)t + (3/2))n^2 - ((3/4)t^2 + (3/4)t + (1/4))n - ((3/2)t^2 + (7/2)t + 2)$, by Lemma 5, we get $e(G) > \binom{n-t-1}{2} + t^2 + 2t + 1$. By Lemma 11, we obtain that G is Hamiltonian or $G \subseteq L_n^t$ or N_n^t.

If $G \subseteq L_n^t$: note that $WW(\overline{L_n^t}) = 3n^2 - 4tn - 9n + 4t^2 + 4t + 6$. Then, if $G \subseteq L_n^t$, we have $WW(\overline{G}) \leq WW(\overline{L_n^t}) < (1/4)n^4 - ((1/2)t+1)n^3 + ((3/4)t^2 + (9/4)t + (3/2))n^2 - ((3/4)t^2 + (3/4)t + (1/4))n - ((3/2)t^2 + (7/2)t + 2)$, a contradiction.

If $G \subseteq N_n^t$: note that $WW(\overline{N_n^t}) = 3n^2 - 10tn - 3n + 9t^2 + 5t$. Then, if $G \subseteq N_n^t$, we have $WW(\overline{G}) \leq WW(\overline{N_n^t}) < (1/4)n^4 - ((1/2)t+1)n^3 + ((3/4)t^2 + (9/4)t + (3/2))n^2 - ((3/4)t^2 + (3/4)t + (1/4))n - ((3/2)t^2 + (7/2)t + 2)$, a contradiction. □

Theorem 15. *Let $\overline{G}$ be a connected graph with $n(\geq 6t+5)$ vertices for some integer t. If $\delta(G) \geq t$ and $H(\overline{G}) < (((2t+2)n^2 - (3t^2 + 11t + 8)n + 6t^2 + 14t + 8)/(2n-2))$, then G is Hamiltonian.*

Proof. Since $H(\overline{G}) \leq (((2t+2)n^2 - (3t^2 + 11t + 8)n + 6t^2 + 14t + 8)/(2n-2))$, by Lemma 6, we get $e(G) > \binom{n-t-1}{2} + t^2 + 2t + 1$. By Lemma 11, we obtain that G is Hamiltonian unless $G \subseteq L_n^t$ or N_n^t.

If $G \subseteq L_n^t$: note that $H(\overline{L_n^t}) = (1/4)(n^2 - 3n + 2tn - 2t^2 - 2t + 2)$. Then, if $G \subseteq L_n^t$, we have $H(\overline{G}) \geq H(\overline{L_n^t}) > (((2t+2)n^2 - (3t^2 + 11t + 8)n + 6t^2 + 14t + 8)/(2n-2))$, a contradiction.

If $G \subseteq N_n^t$: note that $H(\overline{N_n^t}) = (1/4)(n^2 - n - 3t^2 + t)$. Then, if $G \subseteq N_n^t$, we have $H(\overline{G}) \geq H(\overline{N_n^t}) > (((2t+2)n^2 - (3t^2 + 11t + 8)n + 6t^2 + 14t + 8)/(2n-2))$, a contradiction. □

8. Hamilton-Connected of Graphs

Lemma 12 (see [20]). *Let G be a t-connected graph with n vertices, where $t \geq 2$. If $e(G) > ((n(n-1) - t(n-t-1))/2)$, then G is Hamilton-connected.*

By Lemmas 4, 5, 6, and 12 and by direct computations, we get Theorems 16, 17, and 18, respectively.

Theorem 16. *Let G be a t-connected graph with n vertices and $\overline{G}$ be a connected graph, where $t \geq 2$. If*

$$W(\overline{G}) > \frac{1}{2}n^3 - \frac{1}{2}(t+2)n^2 + \frac{1}{2}\left(t^2 + 3t + 1\right)n - t^2 - t, \tag{39}$$

then G is Hamilton-connected.

Theorem 17. *Let G be a t-connected graph with n vertices and $\overline{G}$ be a connected graph, where $t \geq 2$. If*

$$WW(\overline{G}) > \frac{1}{4}n^4 - \frac{1}{4}(t+2)n^3 + \frac{1}{4}\left(t^2 + 2t + 1\right)n^2 - \frac{1}{4}\left(t^2 - t\right)n - \frac{1}{2}t^2 - \frac{1}{2}t, \tag{40}$$

then G is Hamilton-connected.

Theorem 18. *Let G be a t-connected graph with n vertices and $\overline{G}$ be a connected graph, where $t \geq 2$. If*

$$H(\overline{G}) < \frac{(t+1)n^2 - \left(t^2 + 3t + 1\right)n + 2t^2 + 2t}{2(n-1)}, \tag{41}$$

then G is Hamilton-connected.

9. Traceable from Every Vertex of Graphs

Lemma 13 (see [20]). *Let G be a t-connected graph with n vertices, where $t \geq 2$. If $e(G) > ((n(n-1) - t(n-t))/2)$, then G is traceable from every vertex.*

By Lemmas 4, 5, 6, and 13 and by direct computation, we get Theorems 19, 20, and 21, respectively.

Theorem 19. *Let G be a t-connected graph with n vertices and $\overline{G}$ be a connected graph, where $t \geq 2$. If*

$$W(\overline{G}) > \frac{1}{2}n^3 - \left(\frac{1}{2}t + 1\right)n^2 + \frac{1}{2}\left(t^2 + 2t + 1\right)n - t^2, \tag{42}$$

then G is traceable from every vertex.

Theorem 20. *Let G be a t-connected graph with n vertices and $\overline{G}$ be a connected graph, where $t \geq 2$. If*

$$WW(\overline{G}) > \frac{1}{4}n^4 - \frac{1}{4}(t+2)n^3 + \frac{1}{4}\left(t^2 + t + 1\right)n^2 - \frac{1}{4}\left(t^2 - 2t\right)n - \frac{1}{2}t^2, \tag{43}$$

then G is traceable from every vertex.

Theorem 21. *Let G be a t-connected graph with n vertices and $\overline{G}$ be a connected graph, where $t \geq 2$. If*

$$H(\overline{G}) < \frac{(t+1)n^2 + \left(-t^2 - 2t - 1\right)n + 2t^2}{2n-2}, \tag{44}$$

then G is traceable from every vertex.

Data Availability

The data used to support the findings of this study are included within the article.

Conflicts of Interest

The authors declare that there are no conflicts of interest regarding the publication of this paper.

Acknowledgments

This work was jointly supported by the National Natural Science Foundation of China (grant no. 11871077), the Natural Science Foundation of Anhui Province (grant no. 1808085MA04), and the Natural Science Foundation of Department of Education of Anhui Province (grant no. KJ2017A362).

References

[1] H. Wiener, "Structural determination of paraffin boiling points," *Journal of the American Chemical Society*, vol. 69, no. 1, pp. 17–20, 1947.

[2] D. J. Klein, I. Lukovits, and I. Gutman, "On the definition of the hyper-wiener index for cycle-containing structures," *Journal of Chemical Information and Modeling*, vol. 35, no. 1, pp. 50–52, 1995.

[3] O. Ivanciuc, T.-S. Balaban, and A. T. Balaban, "Design of topological indices. Part 4. Reciprocal distance matrix, related local vertex invariants and topological indices," *Journal of Mathematical Chemistry*, vol. 12, no. 1, pp. 309–318, 1993.

[4] D. Plavšić, S. Nikolić, N. Trinajstić, and Z. Mihalić, "On the Harary index for the characterization of chemical graphs," *Journal of Mathematical Chemistry*, vol. 12, no. 1, pp. 235–250, 1993.

[5] Y. Gao, E. Zhu, Z. Shao, I. Gutman, and A. Klobučar, "Total domination and open packing in some chemical graphs," *Journal of Mathematical Chemistry*, vol. 56, no. 5, pp. 1481–1492, 2018.

[6] J.-B. Liu, X.-F. Pan, F.-T. Hu, and F.-F. Hu, "Asymptotic Laplacian-energy-like invariant of lattices," *Applied Mathematics and Computation*, vol. 253, pp. 205–214, 2015.

[7] J.-B. Liu and X.-F. Pan, "Minimizing Kirchhoff index among graphs with a given vertex bipartiteness," *Applied Mathematics and Computation*, vol. 291, pp. 84–88, 2016.

[8] J.-B. Liu, C. Wang, S. Wang, and B. Wei, "Zagreb indices and multiplicative zagreb indices of eulerian graphs," *Bulletin of the Malaysian Mathematical Sciences Society*, vol. 42, no. 1, pp. 67–78, 2019.

[9] J. B. Liu, J. Zhao, and Z. Zhu, "On the number of spanning trees and normalized Laplacian of linear octagonal-quadrilateral networks," *International Journal of Quantum Chemistry*, vol. 119, no. 17, Article ID e25971, 2019.

[10] Z. Shao, P. Wu, X. Zhang, D. Dimitrov, and J.-B. Liu, "On the maximum ABC index of graphs with prescribed size and without pendent vertices," *IEEE Access*, vol. 6, pp. 27604–27616, 2018.

[11] Z. Shao, P. Wu, Y. Gao, I. Gutman, and X. Zhang, "On the maximum ABC index of graphs without pendent vertices," *Applied Mathematics and Computation*, vol. 315, pp. 298–312, 2017.

[12] Z. Cui and B. Liu, "On Harary matrix, Harary index and Harary energy," *Match Communications in Mathematical and in Computer Chemistry*, vol. 68, pp. 815–823, 2012.

[13] G.-X. Cai, M.-L. Ye, G.-D. Yu, and L.-F. Ren, "Hyper-Wiener index and Hamiltonicity of graphs," *Ars Combinatoria*, vol. 139, pp. 175–184, 2018.

[14] H.-B. Hua and M. Wang, "On Harary index and traceable graphs," *Match Communications in Mathematical and in Computer Chemistry*, vol. 70, pp. 297–300, 2013.

[15] H.-B. Hua and B. Ning, "Wiener index, Harary index and Hamiltonicity of graphs," *Match Communications in Mathematical and in Computer Chemistry*, vol. 78, no. 1, pp. 153–162, 2016.

[16] R. Liu, X. Du, and H. Jia, "Wiener index on traceable and Hamiltonian graphs," *Bulletin of the Australian Mathematical Society*, vol. 94, no. 3, pp. 362–372, 2016.

[17] R.-F. Liu, X. Du, and H.-C. Jia, "Some observations on Harary index and traceable graphs," *Match Communications in Mathematical and in Computer Chemistry*, vol. 77, no. 1, pp. 195–208, 2017.

[18] R. Li, "Wiener index and some Hamiltonian properties of graphs," *International Journal of Mathematics and Soft Computing*, vol. 5, no. 1, pp. 11–16, 2015.

[19] R. Li, "Harary index and some Hamiltonian properties of graphs," *AKCE International Journal of Graphs and Combinatorics*, vol. 12, no. 1, pp. 64–69, 2015.

[20] G.-D. Yu, L.-F. Ren, and X.-X. Li, "Wiener index, hyper-wiener index, harary index and hamiltonicity properties of graphs," *Applied Mathematics-A Journal of Chinese Universities*, vol. 34, no. 2, pp. 162–172, 2019.

[21] T. Zeng, "Harary index and Hamiltonian property of graphs," *Match Communications in Mathematical and in Computer Chemistry*, vol. 70, pp. 645–649, 2013.

[22] B. Li and B. Ning, "Spectral analogues of Moon-Moser's theorem on Hamilton paths in bipartite graphs," *Linear Algebra and Its Applications*, vol. 515, pp. 180–195, 2017.

[23] B.-L. Li and B. Ning, "Spectral analogues of Erdos and Moon-Moser's theorems on Hamilton cycles," *Linear Multilinear Algebra*, vol. 64, no. 11, pp. 1152–1169, 2016.

[24] G.-D. Yu, Y. Fang, and Y.-Z. Fan, "Spectral radius and hamiltonicity of graphs," *Discussiones Mathematicae Graph Theory*, vol. 39, pp. 951–974, 2019.

Hindawi
Journal of Chemistry
Volume 2019, Article ID 4291943, 11 pages
https://doi.org/10.1155/2019/4291943

Research Article

Topology-Based Analysis of OTIS (Swapped) Networks O_{K_n} and O_{P_n}

Hai-Xia Li,[1] Sarfaraz Ahmad,[2] and Iftikhar Ahmad[2,3]

[1]*Department of General Education, Anhui Xinhua University, Hefei 230088, China*
[2]*Department of Mathematics, COMSATS University of Islamabad, Lahore Campus, Lahore 54000, Pakistan*
[3]*Department of Mathematics, Riphah International University, Lahore Campus, Lahore 54000, Pakistan*

Correspondence should be addressed to Iftikhar Ahmad; iffi6301@gmail.com

Received 2 September 2019; Accepted 10 October 2019; Published 7 November 2019

Guest Editor: Shaohui Wang

In the fields of chemical graph theory, topological index is a type of a molecular descriptor that is calculated based on the graph of a chemical compound. In this paper, M-polynomial O_{K_n} and O_{P_n} networks are computed. The M-polynomial is rich in information about degree-based topological indices. By applying the basic rules of calculus on M-polynomials, the first and second Zagreb indices, modified second Zagreb index, general Randić index, inverse Randić index, symmetric division index, harmonic index, inverse sum index, and augmented Zagreb index are recovered.

1. Introduction

Cheminformatics is a new branch of science which relates chemistry, mathematics, and computer sciences. Quantitative structure-activity relationship (QSAR) and quantitative structure-property relationship (QSPR) are the main components of cheminformatics which are helpful to study physicochemical properties of chemical compounds [1–3].

A topological index is a numeric quantity associated with the graph of chemical compound, which characterizes its topology and is invariant under graph automorphism [4–6]. There are numerous applications of graph theory in the field of structural chemistry. The first well-known use of a topological index in chemistry was by Wiener in the study of paraffin boiling points [7–9]. After that, in order to explain physicochemical properties, various topological indices have been introduced and studied [10, 11].

A computer network is a digital telecommunications network which allows nodes to share resources. In computer networks, computing devices exchange data with each other using connections (data links) between nodes. These data links are established over cable media such as wires or optic cables, or wireless media such as WiFi. Optical transpose interconnection system (OTIS) networks were initially contrived to give productive network to new optoelectronic computer models that profit by both optical and electronic advancements [12]. In OTIS networks, processors are orchestrated into groups. Electronic inter-connects are used between processors within the same cluster, while optical links are used for intercluster communication. Various algorithms have been produced for directing, determination/arranging, certain numerical calculations, Fourier transformation [13], matrix multiplication [14], image processing [15], and so on [16, 17]. The structure of an interconnection system can be scientifically modeled by a graph. The vertices of this graph are the processor nodes and the edges are the connections between the processors. The topology of a graph decides the manner by which vertices are associated by edges. From the topology of a system, certain properties can be decided. The diameter of a graph is the maximum distance between any two vertices of the graph.

Definition 1 (OTIS (swapped) network $O_{K_{n+2}}$). The OTIS (swapped) network is derived from the graph Ω, which is a graph with vertex set $V(O_\Omega) = <g, p> \mid g, p \in V(\Omega)$ and edge set $E(O_\Omega) = <g, p_1>, <g, p_2> g \in V(\Omega), (p_1, p_2) \in E(\Omega) \cup (<g, p>, <g, p, g>) \mid g, p \in V(\Omega)$ and $g \neq p$.

The graph of OTIS (swapped) network $O_{K_{n+2}}$ given in Figure 1 has $(n^3/2) + 3n^2 + (11n/2) + 3$ edges and $(n+2)^2$ vertices.

Definition 2 (OTIS (swapped) network O_{P_n}). Let P_n be path of n vertices and OP_n be OTIS (swapped) network with basis

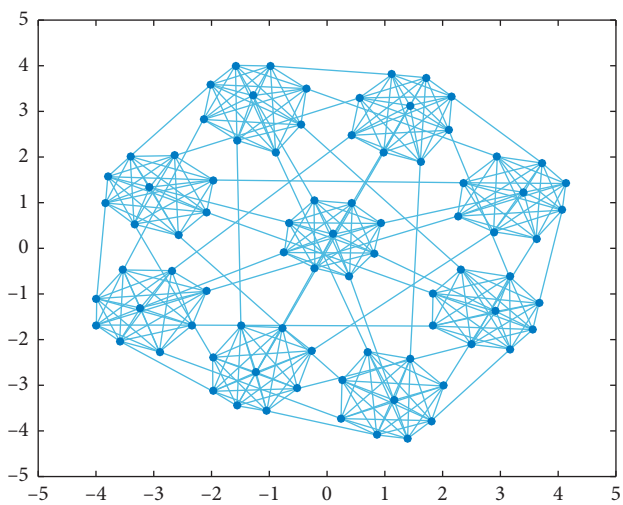

Figure 1: O_{K_7}.

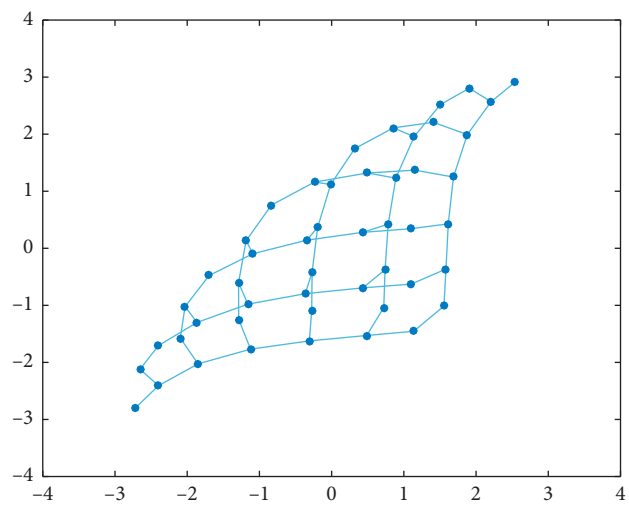

Figure 2: OP_7.

network P_n. An OTIS (swapped) network with the basis network P_6 is shown in Figure 2.

The OTIS (swapped) network graph O_{p_n} given in Figure 2 has $(3/2)(n^2 - n)$ edges and n^2 vertices.

In this paper, we aim to compute degree-dependent topological indices of OTIS (swapped) networks O_{K_n} and O_{P_n}. In Section 2, we give definitions and literature review about TIs. In Sections 3 and 4, we present the methodology and application of our results in chemistry, respectively. Section 5 contains our main results, and Section 6 concludes our paper.

2. Topological Indices (TIs)

TIs are numbers which depend on the molecular graph and are helpful in deciding the properties of the concerned molecular compound [18–20]. We can consider TI as a function which assigns a real number to each molecular graph, and this real number is used as a descriptor of the concerned molecule. From the TIs, a variety of physical and chemical properties like heat of evaporation, heat of formation, boiling point, chromatographic retention, surface tension, and vapor pressure of understudy molecular compound can be identified. A TI gives us the mathematical language to study a molecular graph. There are three types of TIs:

(1) Degree-based TIs

(2) Distance-based TIs

(3) Spectrum-based TIs

The first type of TI depends upon the degree of vertices, second one depends upon the distance of vertices and the third type of TI depends upon the spectrum of graph.

2.1. Zagreb Indices. To compute total π-electron energy, the following TI is defined:

$$M_1(G) = \sum_{v \in V(G)} d_v^2. \tag{1}$$

But soon it was observed that this index increases with increases in branching of the skeleton of carbon atoms. After 10 years, Balaban et al. wrote a review [21], in which he declared M1 and M2 are among the degree-based TIs and named them as Zagreb group indices. The name Zagreb group indices was soon changed to Zagreb indices (ZIs), and nowadays, M_1 and M_2 are abbreviated as first Zagreb index and second Zagreb index.

In 1975, Gutman et al. gave a remarkable identity [22]. Hence, these two indices are among the oldest degree-based descriptors, and their properties are extensively investigated. The mathematical formulae of these indices are

$$\begin{aligned} M_1(G) &= \sum_{uv \in E(G)} d_u + d_v, \\ M_2(G) &= \sum_{uv \in E(G)} d_u d_v. \end{aligned} \tag{2}$$

For detailed survey about these indices, we refer [23–26]. Doslic et al. [27] gave the idea of augmented ZI, whose mathematical formula is

$$\mathrm{AZI}(G) = \sum_{uv \in E(G)} \left(\frac{d_u d_v}{d_u + d_v - 2} \right)^3. \tag{3}$$

2.2. Randić or Connectivity Index. Historically, ZIs are the very first degree-based TIs, but these indices were used for completely different purposes; therefore, the first genuine degree-based TI is the Randić index (RI) which was given in 1975 by Randić [28] as

$$R_{-1/2}(G) = \sum_{uv \in E(G)} \frac{1}{\sqrt{d_u d_v}}. \tag{4}$$

Firstly, Randić named it as a branching index, which was soon named as connectivity index, and nowadays, it is called as RI. The RI is the most popular degree-based TI and has been extensively studied by both mathematicians and chemists. Randić himself wrote two reviews [29, 30], and

many papers and books on this topological invariant are present in the literature; few of them are [31–34]. Researchers recognized the importance of the Randić index in drug design. Bollbás and Erdos, famous mathematicians of that time investigated some hidden mathematical properties of RI [35]; after that, RI was worth studying, and a surge of publications began [36–39]. An unexpected mathematical quality of the Randić index was discovered recently, which tells us about the relation of this topological invariant with the normalized Laplacian matrix [38, 40, 41]. The GRI known as general RI [42] is defined as

$$R_\alpha(G) = \sum_{uv\in E(G)} (d_u d_v)^\alpha. \tag{5}$$

2.3. M-Polynomial. The mathematical formula of M-polynomial is

$$M(G; x, y) = \sum_{uv\in E(G)} \left(x^{d_u} y^{d_v}\right). \tag{6}$$

Detailed survey about the definitions of other TIs computed in this paper and relation of TIs with M-polynomial can be seen in [43, 44], where

$$\begin{aligned} D_x(f(x,y)) &= x\frac{\partial}{\partial x}(f(x,y)),\\ D_y(f(x,y)) &= y\frac{\partial}{\partial y}(f(x,y)),\\ S_x(f(x,y)) &= \int_0^x \frac{f(t,y)}{t}\,\mathrm{d}t,\\ S_y(f(x,y)) &= \int_0^y \frac{f(x,t)}{t}\,\mathrm{d}t,\\ J(f(x,y)) &= J(f(x,x)),\\ Q_\alpha(f(x,y)) &= x^\alpha(f(x,y)). \end{aligned} \tag{7}$$

3. Methodology

To compute the M-polynomial of a graph G, we need to compute the number of vertices and edges in it and divide the edge set into different classes with respect to the degrees of end vertices. From the M-polynomials, we can recover many degree-dependent indices by applying some differential and integral operators.

4. Applications in Chemistry

A topological description is used to depict the features of the studied compounds, and indices of graph-theoretical origin are used to investigate the correlations between structure and biological activity [45–48]. For example, the Randić index demonstrates great relationship with the physical property of alkanes. The geometric arithmetic index has a similar role as that of the Randić index. The sum-connectivity index is helpful in guessing the melting point of compounds. Zagreb indices are used to calculate π-electron energy.

5. Main Results

In this section, we compute M-polynomials of understudy networks and recover nine TIs from these polynomials.

5.1. Results for OP_n

Theorem 1. *Let OP_n be the swapped network; then,*

$$\begin{aligned} M(G; x, y) &= 2xy^3 + 3x^2y^2 + (6n-14)x^2y^3\\ &\quad + \left(\frac{3(n-2)(n-3)}{2}\right)x^3y^3. \end{aligned} \tag{8}$$

Proof. The OP_n network has the following four types of edges based on the degree of end vertices:

$$\begin{aligned} E_{\{1,3\}}(OP_n) &= \{uv \in E(OP_n) : d_u = 1, d_v = 3\},\\ E_{\{2,2\}}(OP_n) &= \{uv \in E(OP_n) : d_u = 2, d_v = 2\},\\ E_{\{2,3\}}(OP_n) &= \{uv \in E(OP_n) : d_u = 2, d_v = 3\},\\ E_{\{3,3\}}(OP_n) &= \{uv \in E(OP_n) : d_u = 3, d_v = 3\}, \end{aligned} \tag{9}$$

such that

$$\begin{aligned} \left|E_{\{1,3\}}(OP_n)\right| &= 2,\\ \left|E_{\{2,2\}}(OP_n)\right| &= 3,\\ \left|E_{\{2,3\}}(OP_n)\right| &= (6n-14),\\ \left|E_{\{3,3\}}(OP_n)\right| &= \left(\frac{3(n-2)(n-3)}{2}\right). \end{aligned} \tag{10}$$

Now, from the definition of M-polynomial, we have

$$\begin{aligned} M(G; x, y) &= \sum_{\delta\le i\le j\le\Delta} m_{ij}x^iy^j\\ &= \sum_{1\le 3} m_{13}x^1y^3 + \sum_{2\le 2} m_{22}x^2y^2 + \sum_{2\le 3} m_{23}x^2y^3\\ &\quad + \sum_{3\le 3} m_{33}x^3y^3\\ &= \left|E_{\{1,3\}}(OP_n)\right|x^1y^3 + \left|E_{\{2,2\}}(OP_n)\right|x^2y^2\\ &\quad + \left|E_{\{2,3\}}(OP_n)\right|x^2y^3\\ &\quad + \left|E_{\{3,3\}}(OP_n)\right|x^3y^3\\ &= 2xy^3 + 3x^2y^2 + (6n-14)x^2y^3\\ &\quad + \left(\frac{3(n-2)(n-3)}{2}\right)x^3y^3. \end{aligned} \tag{11}$$

□

Corollary 1. *Let OP_n be the swapped network; then,*

$$M_1(OP_n) = 9n^2 - 15n + 4. \tag{12}$$

Proof. Let

$$f(x,y) = M(G;x,y) = 2xy^3 + 3x^2y^2 + (6n-14)x^2y^3 + \left(\frac{3(n-2)(n-3)}{2}\right)x^3y^3. \tag{13}$$

Then,

$$\begin{aligned} D_x(f(x,y)) &= 2xy^3 + 6x^2y^2 + 2(6n-14)x^2y^3 + \left(\frac{9(n-2)(n-3)}{2}\right)x^3y^3, \\ D_y(f(x,y)) &= 6xy^3 + 6x^2y^2 + 3(6n-14)x^2y^3 + \left(\frac{9(n-2)(n-3)}{2}\right)x^3y^3. \end{aligned} \tag{14}$$

Now, we have

$$\begin{aligned} M_1(OP_n) &= D_xf + D_yf\big|_{x=y=1} \\ &= 9n^2 - 15n + 4. \end{aligned} \tag{15}$$

□

Corollary 2. *Let OP_n be the swapped network; then,*

$$M_2(OP_n) = \frac{27n^2}{2} - \frac{63n}{2} + 15. \tag{16}$$

Proof. Let

$$f(x,y) = M(G;x,y) = 2xy^3 + 3x^2y^2 + (6n-14)x^2y^3 + \left(\frac{3(n-2)(n-3)}{2}\right)x^3y^3. \tag{17}$$

Then,

$$\begin{aligned} D_y(f(x,y)) &= 6xy^3 + 6x^2y^2 + 3(6n-14)x^2y^3 + \left(\frac{9(n-2)(n-3)}{2}\right)x^3y^3, \\ D_xD_y(f(x,y)) &= 6xy^3 + 12x^2y^2 + 6(6n-14)x^2y^3 + \left(\frac{27(n-2)(n-3)}{2}\right)x^3y^3. \end{aligned} \tag{18}$$

Now, we have

$$\begin{aligned} M_2(OP_n) &= D_xD_yf\big|_{x=y=1} \\ &= \frac{27n^2}{2} - \frac{63n}{2} + 15. \end{aligned} \tag{19}$$

□

Corollary 3. *Let OP_n be the swapped network; then,*

$${}^mM_2(OP_n) = \frac{n^2}{6} + \frac{n}{6} + \frac{1}{12}. \tag{20}$$

Proof. Let

$$f(x,y) = M(G;x,y) = 2xy^3 + 3x^2y^2 + (6n-14)x^2y^3 + \left(\frac{3(n-2)(n-3)}{2}\right)x^3y^3. \tag{21}$$

Then,

$$\begin{aligned} S_y(f(x,y)) &= \left(\frac{2}{3}\right)xy^3 + \left(\frac{3}{2}\right)x^2y^2 + \left(\frac{(6n-14)}{3}\right)x^2y^3 + \left(\frac{(n-2)(n-3)}{2}\right)x^3y^3, \\ S_xS_y(f(x,y)) &= \left(\frac{2}{3}\right)xy^3 + \left(\frac{3}{4}\right)x^2y^2 + \left(\frac{(6n-14)}{6}\right)x^2y^3 + \left(\frac{(n-2)(n-3)}{6}\right)x^3y^3. \end{aligned} \tag{22}$$

Now, we have

$$\begin{aligned} {}^mM_2(OP_n) &= S_xS_yf\big|_{x=y=1} \\ &= \frac{n^2}{6} + \frac{n}{6} + \frac{1}{12}. \end{aligned} \tag{23}$$

□

Corollary 4. *Let OP_n be the swapped network; then,*

$$R_\alpha\left((OP_n) = 6^\alpha + 6^\alpha 2^\alpha + 3^\alpha 2^\alpha(6n-14) + \frac{9^\alpha 3^\alpha(n-2)(n-3)}{2^\alpha}\right). \tag{24}$$

Proof. Let

$$f(x,y) = M(G;x,y) = 2xy^3 + 3x^2y^2 + (6n-14)x^2y^3 + \left(\frac{3(n-2)(n-3)}{2}\right)x^3y^3. \tag{25}$$

Then,

$$D_y^\alpha(f(x,y)) = 6^\alpha xy^3 + 6^\alpha x^2y^2 + 3^\alpha(6n-14)x^2y^3 + \left(\frac{9^\alpha(n-2)(n-3)}{2^\alpha}\right)x^3y^3,$$

$$D_x^\alpha D_y^\alpha\left((f(x,y)) = 6^\alpha xy^3 + 6^\alpha 2^\alpha x^2y^2 + 3^\alpha 2^\alpha(6n-14)x^2y^3 + \left(\frac{9^\alpha 3^\alpha(n-2)(n-3)}{2^\alpha}\right)x^3y^3\right). \tag{26}$$

Now, we have

$$R_\alpha\left((OP_n)\right) == D_x^\alpha D_y^\alpha f|_{x=y=1} = 6^\alpha + 6^\alpha 2^\alpha + 3^\alpha 2^\alpha(6n-14) + \frac{9^\alpha 3^\alpha(n-2)(n-3)}{2^\alpha}. \tag{27}$$

□

Corollary 5. *Let OP_n be the swapped network; then,*

$$RR_\alpha\left((OP_n) = \frac{2^\alpha}{3^\alpha} + \frac{3^\alpha}{2^{2\alpha}} + \frac{6n-14}{3^\alpha 2^\alpha} + \frac{(n-2)(n-3)}{2^\alpha 3^\alpha}\right). \tag{28}$$

Proof. Let

$$f(x,y) = M(G;x,y) = 2xy^3 + 3x^2y^2 + (6n-14)x^2y^3 + \left(\frac{3(n-2)(n-3)}{2}\right)x^3y^3. \tag{29}$$

Then,

$$S_y^\alpha(f(x,y)) = \left(\frac{2^\alpha}{3^\alpha}\right)xy^3 + \left(\frac{3^\alpha}{2^\alpha}\right)x^2y^2 + \left(\frac{(6n-14)}{3^\alpha}\right)x^2y^3 + \left(\frac{(n-2)(n-3)}{2^\alpha}\right)x^3y^3,$$

$$S_x^\alpha S_y^\alpha\left((f(x,y)) = \left(\frac{2^\alpha}{3^\alpha}\right)xy^3 + \left(\frac{3^\alpha}{2^{2\alpha}}\right)x^2y^2 + \left(\frac{(6n-14)}{3^\alpha 2^\alpha}\right)x^2y^3 + \left(\frac{(n-2)(n-3)}{2^\alpha 3^\alpha}\right)x^3y^3\right). \tag{30}$$

Now, we have

$$RR_\alpha\left((OP_n) == S_x^\alpha S_y^\alpha f|_{x=y=1} = \frac{2^\alpha}{3^\alpha} + \frac{3^\alpha}{2^{2\alpha}} + \frac{6n-14}{3^\alpha 2^\alpha} + \frac{(n-2)(n-3)}{2^\alpha 3^\alpha}. \tag{31}$$

□

Corollary 6. *Let OP_n be the swapped network; then,*

$$\mathrm{SSD}(OP_n) = 3n^2 - 2n + \frac{1}{3}. \tag{32}$$

Proof. Let

$$f(x,y) = M(G;x,y) = 2xy^3 + 3x^2y^2 + (6n-14)x^2y^3 + \left(\frac{3(n-2)(n-3)}{2}\right)x^3y^3. \tag{33}$$

Then,

$$S_xD_y(f(x,y)) = 6xy^3 + 3x^2y^2 + \left(\frac{3(6n-14)}{2}\right)x^2y^3 + \left(\frac{3(n-2)(n-3)}{2}\right)x^3y^3,$$

$$D_xS_y(f(x,y)) = \left(\frac{2}{3}\right)xy^3 + 3x^2y^2 + \left(\frac{2(6n-14)}{3}\right)x^2y^3 + \left(\frac{3(n-2)(n-3)}{2}\right)x^3y^3. \tag{34}$$

Now, we have

$$\mathrm{SSD}(OP_n) = \left(D_xS_yf + S_xD_yf\right)\Big|_{x=y=1} = 3n^2 - 2n + \frac{1}{3}. \tag{35}$$

□

Corollary 7. *Let OP_n be the swapped network; then,*

$$H(OP_n) = 2\left(\frac{n^2}{4} - \frac{n}{20} - \frac{1}{20}\right). \tag{36}$$

Proof. Let

$$f(x,y) = M(G;x,y) = 2xy^3 + 3x^2y^2 + (6n-14)x^2y^3 + \left(\frac{3(n-2)(n-3)}{2}\right)x^3y^3. \tag{37}$$

Then,

$$J(f(x,y)) = 5x^4 + (6n-14)x^5 + \left(\frac{3(n-2)(n-3)}{2}\right)x^6,$$

$$2S_xJ(f(x,y)) = 2\left(\frac{5x^4}{4} + \frac{(6n-14)x^5}{5} + \frac{(n-2)(n-3)x^6}{4}\right). \tag{38}$$

Now, we have

$$H(OP_n) = 2S_x J f\big|_{x=1} = 2\left(\frac{n^2}{4} - \frac{n}{20} - \frac{1}{20}\right). \tag{39}$$

□

Corollary 8. *Let OP_n be the swapped network; then,*

$$I(OP_n) = \frac{9n^2}{4} - \frac{81n}{20} - \frac{129}{5}. \tag{40}$$

Proof. Let

$$f(x,y) = M(G;x,y) = 2xy^3 + 3x^2y^2 + (6n-14)x^2y^3 + \left(\frac{3(n-2)(n-3)}{2}\right)x^3y^3. \tag{41}$$

Then,

$$\begin{aligned}
D_y(f(x,y)) &= 6xy^3 + 6x^2y^2 + 3(6n-14)x^2y^3 + \left(\frac{9(n-2)(n-3)}{2}\right)x^3y^3,\\
D_xD_y(f(x,y)) &= 6xy^3 + 12x^2y^2 + 6(6n-14)x^2y^3 + \left(\frac{27(n-2)(n-3)}{2}\right)x^3y^3,\\
JD_xD_y(f(x,y)) &= 18x^4 + 6(6n-14)x^5 + \left(\frac{27(n-2)(n-3)}{2}\right)x^6,\\
S_xJD_xD_y(f(x,y)) &= \frac{18x^4}{4} + \left(\frac{6(6n-14)}{5}\right)x^5 + \left(\frac{27(n-2)(n-3)}{12}\right)x^6.
\end{aligned} \tag{42}$$

Now, we have

$$I(OP_n) = S_xJD_xD_yf\big|_{x=1} = \frac{9n^2}{4} - \frac{81n}{20} - \frac{129}{5}. \tag{43}$$

□

Corollary 9. *Let OP_n be the swapped network; then,*

$$A(OP_n) = \frac{729n^2}{64} - \frac{573n}{64} - \frac{413}{32}. \tag{44}$$

Proof. Let

$$f(x,y) = M(G;x,y) = 2xy^3 + 3x^2y^2 + (6n-14)x^2y^3 + \left(\frac{3(n-2)(n-3)}{2}\right)x^3y^3. \tag{45}$$

Then,

$$\begin{aligned}
D_y^3(f(x,y)) &= 54xy^3 + 24x^2y^2 + 27(6n-14)x^2y^3 + \left(\frac{81(n-2)(n-3)}{2}\right)x^3y^3,\\
D_x^3D_y^3(f(x,y)) &= 54xy^3 + 192x^2y^2 + 216(6n-14)x^2y^3 + \left(\frac{2187(n-2)(n-3)}{2}\right)x^3y^3,\\
JD_x^3D_y^3(f(x,y)) &= 246x^4 + 216(6n-14)x^5 + \left(\frac{2187(n-2)(n-3)}{2}\right)x^6,\\
Q_{-2}JD_x^3D_y^3(f(x,y)) &= 246x^2 + 216(6n-14)x^3 + \left(\frac{2187(n-2)(n-3)}{2}\right)x^4,\\
S_x^3Q_{-2}JD_x^3D_y^3(f(x,y)) &= \frac{123x^2}{4} + 8(6n-14)x^3 + \left(\frac{729(n-2)(n-3)}{64}\right)x^4.
\end{aligned} \tag{46}$$

Now, we have

$$A(OP_n) = S_x^3Q_{-2}JD_x^3D_y^3f\big|_{x=1} = \frac{729n^2}{64} - \frac{573n}{64} - \frac{413}{32}. \tag{47}$$

□

5.2. Results for (OR_k)

Theorem 2. *Let OR_k be the swapped network; then,*

$$M(G;x,y) = nkx^ky^{k+1} + \left(\frac{n^2(k+1) - n(1+2k)}{2}\right)x^{k+1}y^{k+1}. \tag{48}$$

Proof. The OR_k network has the following two types of edges based on the degree of end vertices:

$$\begin{aligned}
E_{\{k,k+1\}}(OR_k) &= \{uv \in E(OR_k) : d_u = k, d_v = k+1\},\\
E_{\{k+1,k+1\}}(OR_k) &= \{uv \in E(OR_k) : d_u = k+1, d_v = k+1\},
\end{aligned} \tag{49}$$

such that

$$\left|E_{\{k,k+1\}}(OR_k)\right| = nk,$$
$$\left|E_{\{k+1,k+1\}}(OR_k)\right| = \frac{n^2(k+1)-n(1+2k)}{2}. \tag{50}$$

Now, from the definition of M-polynomial, we have

$$\begin{aligned} M(G;x,y) &= \sum_{\delta\le i\le j\le\Delta} m_{ij}x^i y^j \\ &= \sum_{k\le k+1} m_{k(k+1)}x^k y^{k+1} + \sum_{k+1\le k+1} m_{(k+1)(k+1)}x^{k+1}y^{k+1} \\ &= \left|E_{\{k,k+1\}}(OR_k)\right|x^k y^{k+1} + \left|E_{\{k+1,k+1\}}(OR_k)\right|x^{k+1}y^{k+1} \\ &= nkx^k y^{k+1} + \left(\frac{n^2(k+1)-n(1+2k)}{2}\right)x^{k+1}y^{k+1}. \end{aligned} \tag{51}$$

□

Corollary 10. *Let (OR_k) be the swapped network; then,*

$$M_1(OR_k) = 2nk^2 + nk + n^2(k+1)^2 - n(k+1)(1+2k). \tag{52}$$

Proof. Let

$$f(x,y) = M(G;x,y) = nkx^k y^{k+1} + \left(\frac{n^2(k+1)-n(1+2k)}{2}\right)x^{k+1}y^{k+1}. \tag{53}$$

Then,

$$\begin{aligned} D_x(f(x,y)) &= nk^2x^k y^{k+1} + (k+1)\left(\frac{n^2(k+1)-n(1+2k)}{2}\right)x^{k+1}y^{k+1}, \\ D_y(f(x,y)) &= nk(k+1)x^k y^{k+1} + (k+1)\left(\frac{n^2(k+1)-n(1+2k)}{2}\right)x^{k+1}y^{k+1}. \end{aligned} \tag{54}$$

Now, we have

$$\begin{aligned} M_1(OR_k) &= D_x f + D_y f\big|_{x=y=1} \\ &= 2nk^2 + nk + n^2(k+1)^2 - n(k+1)(1+2k). \end{aligned} \tag{55}$$

□

Corollary 11. *Let (OR_k) be the swapped network; then,*

$$M_2(OR_k) = nk^3 + nk^2 + \frac{n^2(k+1)^3}{2} - \frac{n(k+1)^2(1+2k)}{2}. \tag{56}$$

Proof. Let

$$f(x,y) = M(G;x,y) = nkx^k y^{k+1} + \left(\frac{n^2(k+1)-n(1+2k)}{2}\right)x^{k+1}y^{k+1}. \tag{57}$$

Then,

$$\begin{aligned} D_y(f(x,y)) &= nk^2x^k y^{k+1} + nkx^k y^{k+1} + (k+1)\left(\frac{n^2(k+1)-n(1+2k)}{2}\right)x^{k+1}y^{k+1}, \\ D_xD_y(f(x,y)) &= nk^3x^k y^{k+1} + nk^2x^k y^{k+1} + (k+1)^2\left(\frac{n^2(k+1)-n(1+2k)}{2}\right)x^{k+1}y^{k+1}. \end{aligned} \tag{58}$$

Now, we have

$$\begin{aligned} M_2(OR_k) &= D_xD_y f\big|_{x=y=1} \\ &= nk^3 + nk^2 + \frac{n^2(k+1)^3}{2} - \frac{n(k+1)^2(1+2k)}{2}. \end{aligned} \tag{59}$$

□

Corollary 12. *Let (OR_k) be the swapped network; then,*

$${}^mM_2(OR_k) = \frac{nk}{(k^2+k)} + \frac{n^2}{(2k+2)} - \frac{n(1+2k)}{2(k+1)^2}. \tag{60}$$

Proof. Let

$$f(x,y) = M(G;x,y) = nkx^k y^{k+1} + \left(\frac{n^2(k+1)-n(1+2k)}{2}\right)x^{k+1}y^{k+1}. \tag{61}$$

Then,

$$\begin{aligned} S_y(f(x,y)) &= \left(\frac{nk}{(k+1)}\right)x^k y^{k+1} + \left(\frac{n^2(k+1)-n(1+2k)}{2(k+1)}\right)x^{k+1}y^{k+1}, \\ S_xS_y(f(x,y)) &= \left(\frac{nk}{(k^2+k)}\right)x^k y^{k+1} + \left(\frac{n^2(k+1)-n(1+2k)}{2(k+1)^2}\right)x^{k+1}y^{k+1}. \end{aligned} \tag{62}$$

Now, we have

$$\begin{aligned} {}^{m}M_2(OR_k) &= S_xS_yf\big|_{x=y=1} \\ &= \frac{nk}{(k^2+k)} + \frac{n^2}{(2k+2)} - \frac{n(1+2k)}{2(k+1)^2}. \end{aligned} \tag{63}$$

□

Corollary 13. *Let (OR_k) be the swapped network; then,*

$$R_\alpha\Big((OR_k) = nk^{3\alpha} + nk^{2\alpha} + (k+1)^{2\alpha}\left(\frac{n^2(k+1)-n(1+2k)}{2^\alpha}\right)x^{k+1}y^{k+1}\Big). \tag{64}$$

Proof. Let

$$f(x,y) = M(G;x,y) = nkx^ky^{k+1} + \left(\frac{n^2(k+1)-n(1+2k)}{2}\right)x^{k+1}y^{k+1}. \tag{65}$$

Then,

$$\begin{aligned} D_y^\alpha(f(x,y)) &= nk^{2\alpha}x^ky^{k+1} + nk^\alpha x^ky^{k+1} + (k+1)^\alpha\left(\frac{n^2(k+1)-n(1+2k)}{2}\right)x^{k+1}y^{k+1}, \\ D_x^\alpha D_y^\alpha\Big((f(x,y)) &= nk^{3\alpha}x^ky^{k+1} + nk^{2\alpha}x^ky^{k+1} + (k+1)^{2\alpha}\left(\frac{n^2(k+1)-n(1+2k)}{2}\right)x^{k+1}y^{k+1}\Big). \end{aligned} \tag{66}$$

Now, we have

$$\begin{aligned} R_\alpha\Big((OR_k) &== D_x^\alpha D_y^\alpha f\big|_{x=y=1} \\ &= nk^{3\alpha} + nk^{2\alpha} + (k+1)^{2\alpha}\left(\frac{n^2(k+1)-n(1+2k)}{2^\alpha}\right)x^{k+1}y^{k+1}. \end{aligned} \tag{67}$$

□

Corollary 14. *Let (OR_k) be the swapped network; then,*

$$RR_\alpha\Big((OR_k) = \frac{n}{(k+1)^\alpha} + \left(\frac{n^2(k+1)-n(1+2k)}{(k+1)^{2\alpha}2^\alpha}\right)\Big). \tag{68}$$

Proof. Let

$$f(x,y) = M(G;x,y) = nkx^ky^{k+1} + \left(\frac{n^2(k+1)-n(1+2k)}{2}\right)x^{k+1}y^{k+1}. \tag{69}$$

Then,

$$\begin{aligned} S_y^\alpha(f(x,y)) &= \left(\frac{nk^\alpha}{(k+1)^\alpha}\right)x^ky^{k+1} + \left(\frac{n^2(k+1)-n(1+2k)}{2^\alpha(k+1)^\alpha}\right)x^{k+1}y^{k+1}, \\ S_x^\alpha S_y^\alpha\Big((f(x,y)) &= \left(\frac{n}{(k+1)^\alpha}\right)x^ky^{k+1} + \left(\frac{n^2(k+1)-n(1+2k)}{2^\alpha(k+1)^{2\alpha}}\right)x^{k+1}y^{k+1}\Big). \end{aligned} \tag{70}$$

Now, we have

$$\begin{aligned} RR_\alpha\Big((OR_k) &== S_x^\alpha S_y^\alpha f\big|_{x=y=1} \\ &= \frac{n}{(k+1)^\alpha} + \left(\frac{n^2(k+1)-n(1+2k)}{(k+1)^{2\alpha}2^\alpha}\right). \end{aligned} \tag{71}$$

□

Corollary 15. *Let (OR_k) be the swapped network; then,*

$$\mathrm{SSD}(OR_k) = \frac{nk^2}{(k+1)} + nk + n + n^2(k+1) - n(1+2k). \tag{72}$$

Proof. Let

$$f(x,y) = M(G;x,y) = nkx^ky^{k+1} + \left(\frac{n^2(k+1)-n(1+2k)}{2}\right)x^{k+1}y^{k+1}. \tag{73}$$

Then,

$$\begin{aligned} S_xD_y(f(x,y)) &= nkx^ky^{k+1} + nx^ky^{k+1} + \left(\frac{n^2(k+1)-n(1+2k)}{2}\right)x^{k+1}y^{k+1}, \\ D_xS_y(f(x,y)) &= \left(\frac{nk^2}{(k+1)}\right)x^ky^{k+1} + \left(\frac{n^2(k+1)-n(1+2k)}{2}\right)x^{k+1}y^{k+1}. \end{aligned} \tag{74}$$

Now, we have

$$\begin{aligned} \mathrm{SSD}(OR_k) &= \left(D_xS_yf + S_xD_yf\right)\big|_{x=y=1} \\ &= \frac{nk^2}{(k+1)} + nk + n + n^2(k+1) - n(1+2k). \end{aligned} \tag{75}$$

□

Corollary 16. *Let (OR_k) be the swapped network; then,*

$$H(OR_k) = 2\left(\frac{nk}{2k+1} + \frac{n^2(k+1)}{4k+4} - \frac{n(1+2k)}{4k+4}\right). \quad (76)$$

Proof. Let

$$f(x,y) = M(G;x,y) = nkx^k y^{k+1} + \left(\frac{n^2(k+1) - n(1+2k)}{2}\right)x^{k+1}y^{k+1}. \quad (77)$$

Then,

$$J(f(x,y)) = nkx^{2k+1} + \left(\frac{n^2(k+1) - n(1+2k)}{2}\right)x^{2k+2},$$

$$2S_xJ(f(x,y)) = 2\left(\left(\frac{nk}{2k+1}\right)x^{2k+1} + \left(\frac{n^2(k+1)}{4k+4}\right)x^{2k+2} - \left(\frac{n(1+2k)}{4k+4}\right)x^{2k+2}\right). \quad (78)$$

Now, we have

$$H(OR_k) = 2S_xJf\big|_{x=1} = 2\left(\frac{nk}{2k+1} + \frac{n^2(k+1)}{4k+4} - \frac{n(1+2k)}{4k+4}\right). \quad (79)$$

□

Corollary 17. *Let (OR_k) be the swapped network; then,*

$$I(OR_k) = \frac{nk^3}{2k+1} + \frac{nk^2}{2k+1} + (k+1)^2\left(\frac{n^2(k+1) - n(1+2k)}{4k+4}\right). \quad (80)$$

Proof. Let

$$f(x,y) = M(G;x,y) = nkx^k y^{k+1} + \left(\frac{n^2(k+1) - n(1+2k)}{2}\right)x^{k+1}y^{k+1}. \quad (81)$$

Then,

$$\begin{aligned}
D_y(f(x,y)) &= nk(k+1)x^k y^{k+1} + (k+1)\left(\frac{n^2(k+1) - n(1+2k)}{2}\right)x^{k+1}y^{k+1},\\
D_xD_y(f(x,y)) &= nk^3x^k y^{k+1} + nk^2x^k y^{k+1} + (k+1)^2\left(\frac{n^2(k+1) - n(1+2k)}{2}\right)x^{k+1}y^{k+1},\\
JD_xD_y(f(x,y)) &= nk^3x^{2k+1} + nk^2x^{2k+1} + (k+1)^2\left(\frac{n^2(k+1) - n(1+2k)}{2}\right)x^{2k+2},\\
S_xJD_xD_y(f(x,y)) &= \left(\frac{nk^3}{2k+1}\right)x^{2k+1} + \left(\frac{nk^2}{2k+1}\right)x^{2k+1} + (k+1)^2\left(\frac{n^2(k+1) - n(1+2k)}{4k+4}\right)x^{2k+2}.
\end{aligned} \quad (82)$$

Now, we have

$$I(OR_k) = S_xJD_xD_yf\big|_{x=1} = \frac{nk^3}{2k+1} + \frac{nk^2}{2k+1} + (k+1)^2\left(\frac{n^2(k+1) - n(1+2k)}{4k+4}\right). \quad (83)$$

□

Corollary 18. *Let (OR_k) be the swapped network; then,*

$$A(OR_k) = \frac{nk^5(k+1)^2}{(2k-1)^3} + \frac{nk^4(k+1)^2}{(2k-1)^3} + (k+1)^6\left(\frac{n^2(k+1) - n(1+2k)}{8k^3}\right). \quad (84)$$

Proof. Let

$$f(x,y) = M(G;x,y) = nkx^k y^{k+1} + \left(\frac{n^2(k+1) - n(1+2k)}{2}\right)x^{k+1}y^{k+1}. \quad (85)$$

Then,

$$\begin{aligned}
D_y^3(f(x,y)) &= nk^2(k+1)^2x^ky^{k+1} + nk(k+1)^2x^ky^{k+1} \\
&\quad + (k+1)^3\left(\frac{n^2(k+1)-n(1+2k)}{2}\right)x^{k+1}y^{k+1}, \\
D_y^3D_y^3(f(x,y)) &= nk^5(k+1)^2x^ky^{k+1} + nk^4(k+1)^2x^ky^{k+1} \\
&\quad + (k+1)^6\left(\frac{n^2(k+1)-n(1+2k)}{2}\right)x^{k+1}y^{k+1}, \\
JD_y^3D_y^3(f(x,y)) &= nk^5(k+1)^2x^{2k+1} + nk^4(k+1)^2x^{2k+1} \\
&\quad + (k+1)^6\left(\frac{n^2(k+1)-n(1+2k)}{2}\right)x^{2k+2}, \\
Q_{-2}JD_y^3D_y^3(f(x,y)) &= nk^5(k+1)^2x^{2k-1} + nk^4(k+1)^2x^{2k-1} \\
&\quad + (k+1)^6\left(\frac{n^2(k+1)-n(1+2k)}{2}\right)x^{2k}, \\
S_x^3Q_{-2}JD_y^3D_y^3(f(x,y)) &= \left(\frac{nk^5(k+1)^2}{(2k-1)^3}\right)x^{2k-1} + \left(\frac{nk^4(k+1)^2}{(2k-1)^3}\right)x^{2k-1} \\
&\quad + (k+1)^6\left(\frac{n^2(k+1)-n(1+2k)}{8k^3}\right)x^{2k}.
\end{aligned} \tag{86}$$

Now, we have

$$\begin{aligned}
A(OR_k) &= S_x^3Q_{-2}JD_y^3D_y^3f\big|_{x=1} \\
&= \frac{nk^5(k+1)^2}{(2k-1)^3} + \frac{nk^4(k+1)^2}{(2k-1)^3} \\
&\quad + (k+1)^6\left(\frac{n^2(k+1)-n(1+2k)}{8k^3}\right).
\end{aligned} \tag{87}$$

□

6. Conclusion

In this paper, our focus is on swapped interconnection networks that allow systematic construction of large, scalable, modular, and robust parallel architectures, while maintaining many desirable attributes of the underlying basis network comprising its clusters. We have computed several TIs of underlined networks. Firstly, we computed M-polynomials of understudy networks, and then we recovered Zagreb indices, Randić indices, and some other indices [49–52].

Data Availability

The data used to support the findings of this study are included within the article.

Conflicts of Interest

The authors declare that they no conflicts of interest.

Authors' Contributions

All authors contributed equally to this study.

Acknowledgments

This study was partially supported by the Natural Science Foundation of Anhui Province (no. KJ2018A059).

References

[1] W. Gao, M. R. Farahani, and L. Shi, "Forgotten topological index of some drug structures," *Acta Medica Mediterranea*, vol. 32, no. 1, pp. 579–585, 2016.

[2] W. Gao, M. K. Siddiqui, M. Imran, M. K. Jamil, and M. R. Farahani, "Forgotten topological index of chemical structure in drugs," *Saudi Pharmaceutical Journal*, vol. 24, no. 3, pp. 258–264, 2016.

[3] W. Gao, W. Wang, and M. R. Farahani, "Topological indices study of molecular structure in anticancer drugs," *Journal of Chemistry*, vol. 2016, Article ID 3216327, 8 pages, 2016.

[4] M. Imran, A. Asghar, and A. Q. Baig, "On graph invariants of oxide network," *Engineering and Applied Science Letters*, vol. 1(2018), no. 1, pp. 23–28, 2018.

[5] G. Liu, Z. Jia, and W. Gao, "Ontology similarity computing based on stochastic primal dual coordinate technique," *Open Journal of Mathematical Sciences*, vol. 2(2018), no. 1, pp. 221–227, 2018.

[6] S. Noreen and A. Mahmood, "Zagreb polynomials and redefined Zagreb indices for the line graph of carbon nanocones," *Open Journal of Mathematical Analysis*, vol. 2(2018), no. 1, pp. 66–73, 2018.

[7] S. Hayat and M. Imran, "Computation of topological indices of certain networks," *Applied Mathematics and Computation*, vol. 240, pp. 213–228, 2014.

[8] S. Hayat and M. Imran, "Computation of certain topological indices of nanotubes covered by," *Journal of Computational and Theoretical Nanoscience*, vol. 12, no. 4, pp. 533–541, 2015.

[9] A. Q. Baig, M. Imran, and H. Ali, "On topological indices of poly oxide, poly silicate, DOX, and DSL networks," *Canadian Journal of Chemistry*, vol. 93, no. 7, pp. 730–739, 2015.

[10] Y. Bashir, A. Aslam, M. Kamran et al., "On forgotten topological indices of some dendrimers structure," *Molecules*, vol. 22, no. 6, p. 867, 2017.

[11] A. Aslam, J. L. Guirao, S. Ahmad, and W. Gao, "Topological indices of the line graph of subdivision graph of complete bipartite graphs," *Applied Mathematics & Information Sciences*, vol. 11, no. 6, pp. 1631–1636, 2017.

[12] G. C. Marsden, P. J. Marchand, P. Harvey, and S. C. Esener, "Optical transpose interconnection system architectures," *Optics Letters*, vol. 18, no. 13, pp. 1083–1085, 1993.

[13] A. Al-Ayyoub, A. Awwad, K. Day, and M. Ould-Khaoua, "Generalized methods for algorithm development on optical systems," *The Journal of Supercomputing*, vol. 38, no. 2, pp. 111–125, 2006.

[14] C. F. Wang and S. Sahni, "Matrix multiplication on the OTIS-mesh optoelectronic computer," *IEEE Transactions on Computers*, vol. 50, no. 7, pp. 635–646, 2001.

[15] C. F. Wang and S. Sahni, "Image processing on the OTIS-mesh optoelectronic computer," *IEEE Transactions on Parallel and Distributed Systems*, vol. 11, no. 2, pp. 97–109, 2000.

[16] C. F. Wang and S. Sahni, "Basic operations on the OTIS-mesh optoelectronic computer," *IEEE Transactions on Parallel and Distributed Systems*, vol. 9, no. 12, pp. 1226–1236, 1998.

[17] S. Rajasekaran and S. Sahni, "Randomized routing, selection, and sorting on the OTIS-mesh," *IEEE Transactions on Parallel and Distributed Systems*, vol. 9, no. 9, pp. 833–840, 1998.

[18] A. R. Virk, M. N. Jhangeer, and M. A. Rehman, "Reverse Zagreb and reverse hyper-zagreb indices for silicon carbide $Si_2C_3I[r,s]$ and $Si_2C_3II[r,s]$," *Engineering and Applied Science Letters*, vol. 1, no. 2, pp. 37–50, 2018.

[19] N. De, "Computing reformulated first Zagreb index of some chemical graphs as an application of generalized hierarchical product of graphs," *Open Journal of Mathematical Sciences*, vol. 2, no. 1, pp. 338–350, 2018.

[20] N. De, "Hyper Zagreb index of bridge and chain graphs," *Open Journal of Mathematical Sciences*, vol. 2, no. 1, pp. 1–17, 2018.

[21] A. T. Balaban, I. Motoc, D. Bonchev, and O. Mekenyan, "Topological indices for structureactivity correlations," in *Steric Effects in Drug Design*, pp. 21–55, Springer, Berlin, Germany, 1983.

[22] I. Gutman, B. Ruscic, N. Trinajstic, and C. F. Wilcox Jr., "Graph theory and molecular orbitals. XII. Acyclic polyenes," *The Journal of Chemical Physics*, vol. 62, no. 9, pp. 3399–3405, 1975.

[23] W. Gao, M. Asif, and W. Nazeer, "The study of honey comb derived network via topological indices," *Open Journal of Mathematical Analysis*, vol. 2, no. 2, pp. 10–26, 2018.

[24] H. Siddiqui and M. R. Farahani, "Forgotten polynomial and forgotten index of certain interconnection networks," *Open Journal of Mathematical Analysis*, vol. 1, no. 1, pp. 44–59, 2017.

[25] W. Gao, B. Muzaffar, and W. Nazeer, "K-Banhatti and K-hyper Banhatti indices of dominating David derived network," *Open Journal of Mathematical Analysis*, vol. 1, no. 1, pp. 13–24, 2017.

[26] W. Gao, A. Asghar, and W. Nazeer, "Computing degree-based topological indices of jahangir graph," *Engineering and Applied Science Letters*, vol. 1, no. 1, pp. 16–22, 2018.

[27] T. Doslic, B. Furtula, A. Graovac, I. Gutman, S. Moradi, and Z. Yarahmadi, "On vertex degree based molecular structure descriptors," *MATCH Communications in Mathematical and in Computer Chemistry*, vol. 66, no. 2, pp. 613–626, 2011.

[28] M. Randić, "Characterization of molecular branching," *Journal of the American Chemical Society*, vol. 97, no. 23, pp. 6609–6615, 1975.

[29] M. Randić, "On history of the Randić index and emerging hostility toward chemical graph theory," *MATCH Communications in Mathematical and in Computer Chemistry*, vol. 59, pp. 5–124, 2008.

[30] M. Randić, "The connectivity index 25 years after," *Journal of Molecular Graphics and Modelling*, vol. 20, no. 1, pp. 19–35, 2001.

[31] K. C. Das and I. Gutman, "Some properties of the second Zagreb index," *MATCH Communications in Mathematical and in Computer Chemistry*, vol. 52, no. 1, pp. 3–1, 2004.

[32] L. B. Kier and L. H. Hall, *Molecular Connectivity in Chemistry and Drug Research*, Academic Press, New York, NY, USA, 1976.

[33] L. B. Kier and L. H. Hall, *Molecular Connectivity in Structure-Activity Analysis*, Research Studies, Boston, MA, USA, 1986.

[34] X. Li and I. Gutman, *Mathematical Aspects of Randić-Type Molecular Structure Descriptors*, University of Kragujevac, Kragujevac, Serbia, 2006.

[35] B. Bollobás and P. Erdos, "Graphs of extremal weights," *Ars Combinatoria*, vol. 50, pp. 225–233, 1998.

[36] Y. Hu, X. Li, Y. Shi, T. Xu, and I. Gutman, "On molecular graphs with smallest and greatest zeroth-order general Randić index," *MATCH Communications in Mathematical and in Computer Chemistry*, vol. 54, no. 2, pp. 425–434, 2005.

[37] Y. Ma, S. Cao, Y. Shi, I. Gutman, M. Dehmer, and B. Furtula, "From the connectivity index to various Randić-type descriptors," *MATCH Communications in Mathematical and in Computer Chemistry*, vol. 80, no. 1, pp. 85–106, 2018.

[38] I. Gutman, B. Furtula, and S. B. Bozkurt, "On Randić energy," *Linear Algebra and its Applications*, vol. 442, pp. 50–57, 2014.

[39] X. Li and Y. Shi, "A survey on the Randić index," *MATCH Communications in Mathematical and in Computer Chemistry*, vol. 59, no. 1, pp. 127–156, 2008.

[40] M. Cavers, S. Fallat, and S. Kirkland, "On the normalized Laplacian energy and general Randić index R-1 of graphs," *Linear Algebra and its Applications*, vol. 433, no. 1, pp. 172–190, 2010.

[41] S. B. Bozkurt, A. D. Gungor, I. Gutman, and A. S. Cevik, "Randić matrix and Randić energy," *MATCH Communications in Mathematical and in Computer Chemistry*, vol. 64, pp. 239–250, 2010.

[42] L. Pogliani, "From molecular connectivity indices to semi-empirical connectivity terms: recent trends in graph theoretical descriptors," *Chemical Reviews*, vol. 100, no. 10, pp. 3827–3858, 2000.

[43] J. B. Liu, M. Younas, M. Habib, M. Yousaf, and W. Nazeer, "M-polynomials and degree-based topological indices of VC5C7[p, q] and HC5C7[p, q] nanotubes," *IEEE Access*, vol. 7, pp. 41125–41132, 2019.

[44] M. Riaz, W. Gao, and A. Q. Baig, "M-polynomials and degree-based topological indices of some families of convex polytopes," *Open Journal of Mathematical Sciences*, vol. 2, no. 1, pp. 18–28, 2018.

[45] M. S. Anjum and M. U. Safdar, "K Banhatti and K hyper-Banhatti indices of nanotubes," *Engineering and Applied Science Letters*, vol. 2, no. 1, pp. 19–37, 2019.

[46] Z. Shao, A. R. Virk, M. S. Javed, M. A. Rehman, and M. R. Farahani, "Degree based graph invariants for the molecular graph of Bismuth Tri-Iodide," *Engineering and Applied Science Letters*, vol. 2, no. 1, pp. 01–11, 2019.

[47] L. Yan, M. R. Farahani, and W. Gao, "Distance-based indices computation of symmetry molecular structures," *Open Journal of Mathematical Sciences*, vol. 2, no. 1, pp. 323–337, 2018.

[48] R. Kanabur and S. K. Hosamani, "Some numerical invariants associated with V-phenylenic nanotube and nanotori," *Engineering and Applied Science Letters*, vol. 1, no. 1, pp. 1–9, 2018.

[49] J. B. Liu, C. Wang, and S. Wang, "Zagreb indices and multiplicative Zagreb indices of eulerian graphs," *Bulletin of the Malaysian Mathematical Sciences Society*, vol. 42, pp. 67–78, 2019.

[50] J. B. Liu and X. F. Pan, "Asymptotic Laplacian-energy-like invariant of lattices," *Applied Mathematics and Computation*, vol. 253, pp. 205–214, 2015.

[51] J. B. Liu and X.-F. Pan, "Minimizing Kirchhoffindex among graphs with a given vertex bipartiteness," *Applied Mathematics and Computation*, vol. 291, pp. 84–88, 2016.

[52] J. B. Liu, J. Zhao, and Z. Zhu, "On the number of spanning trees and normalized Laplacian of linear octagonal-quadrilateral networks," *International Journal of Quantum Chemistry*, vol. 2019, Article ID e25971, , 2019.

Hindawi
Journal of Chemistry
Volume 2019, Article ID 7297253, 9 pages
https://doi.org/10.1155/2019/7297253

Research Article

M-Polynomial and Topological Indices of Benzene Ring Embedded in P-Type Surface Network

Hong Yang,[1] A. Q. Baig,[2] W. Khalid,[3] Mohammad Reza Farahani,[4] and Xiujun Zhang[1]

[1]*Key Laboratory of Pattern Recognition and Intelligent Information Processing, Institutions of Higher Education of Sichuan Province, Chengdu University, Chengdu 610106, China*
[2]*Department of Mathematics, COMSATS Institute of Information Technology, Attock Campus, Islamabad, Pakistan*
[3]*Punjab College of Commerce and Science, Attock Campus, Lahore, Pakistan*
[4]*Department of Applied Mathematics, Iran University of Science and Technology (IUST) Narmak, 16844 Tehran, Iran*

Correspondence should be addressed to Xiujun Zhang; woodszhang@cdu.edu.cn

Received 3 July 2019; Accepted 8 October 2019; Published 3 November 2019

Academic Editor: Robert Zaleśny

The representation of chemical compounds and chemical networks with the M-polynomials is a new idea, and it gives nice and good results of the topological indices. These results are used to correlate the chemical compounds and chemical networks with their chemical properties and bioactivities. In this article, particular attention will be put on the derivation of M-polynomial for the benzene ring embedded in the P-type surface network in 2D. Furthermore, the topological indices based on the degrees are also derived by using the general form of M-polynomial of the benzene ring embedded in the P-type surface network $BR(m, n)$. In the end, the graphical representation and comparison of the M-polynomial and the topological indices of the benzene ring embedded in the P-type surface network in 2D are described.

1. Introduction

The chemical compounds can be represented by using the mathematical tools of graph theory. The mathematical models that are based on the polynomials of the chemical compounds and crystal structures can be used in order to predict and forecast their chemical properties and bioactivities. Mathematical chemistry is rich in tools like functions and polynomials which predict the properties of molecular graphs and crystal structures. The topological descriptors are the numerical parameters of the chemical graph which characterize its topology and are usually graph invariants. They explain the structure of chemical compounds mathematically and are utilized in the study of quantitative structure property and activity relationships (QSPR/QSAR).

A topological index is a numerical value which describes and explains an important information about the chemical structure. A great variety of such indices are studied and used in theoretical chemistry, pharmaceutical research, drugs, and different areas of science. The properties like boiling point, strain energy, viscosity, fracture toughness, and heat of formation are connected to the chemical structure under study. This fact plays a major role in the field of chemical graph theory [1–22].

The computation of the general polynomial is formed whose derivatives or integrals or composition of both are evaluated at some particular point. Then, the simplified form yields the molecular descriptor. For instance, there are polynomials like forgotten polynomials, Zagreb polynomials, and Hosoya polynomials, but these polynomials give rise to one or two topological indices [23–26]. The Hosoya polynomial is a polynomial whose derivatives evaluated at 1 give Wiener and hyper Wiener index [27]. The Hosoya polynomial and Zagreb polynomials are considered to be of the general form in the determination of distance-based and degree-based indices, respectively. The M-polynomial is a new and recent polynomial. It will open up new results of chemical graphs and insights in the study of topological descriptors based on degrees. The main importance of this polynomial is that it can give exact forms of more than ten degree-based molecular

descriptors [28, 29]. Rapid development and advancements are being made in this new polynomial. Recently, Kwun et al. computed M-polynomial and topological indices of V-phenylenic nanotube and nanotori [30].

The M-polynomial of a graph G is formulated as [28]

$$M(G;x,y)=\sum_{\delta\le i\le j\le j} m_{ij}(G)x^i y^j, \tag{1}$$

where $m_{ij}(G)$ is the number of edges $uv\in E(G)$ such that $(d_u,d_v)=(i,j)$, $\delta=\min d_v \mid v\in V(G)$, and $\Delta=\max d_v \mid v\in V(G)$.

The path number was the first distance-based topological index defined by Wiener [31] in 1947. This index is now called as the Wiener index. It has many famous mathematical and chemical applications [31, 32]. Later on, Milan Randić proposed and formulated the Randić index of a graph $GR_{-(1/2)}(G)$.

$$R_{-(1/2)}(G)=\sum_{uv\in E(G)}\frac{1}{\sqrt{d_u d_v}}. \tag{2}$$

The general Randić index was proposed and defined independently by Bollobás et al. [33] and Amić et al. [34]. Due to its useful and important results in the field of mathematical chemistry, it has been widely used by both mathematicians and chemists. For a survey of these results, see references [35–38]. The general Randić index and inverse Randić index are formulated as

$$\begin{aligned} R_\alpha(G)&=\sum_{uv\in E(G)}(d_u d_v)^\alpha,\\ RR_\alpha(G)&=\sum_{uv\in E(G)}\frac{1}{(d_u d_v)^\alpha}. \end{aligned} \tag{3}$$

The first and second Zagreb indices are introduced by Gutman and Trinajstić [25, 39, 40]. Both first and second Zagreb indices and the second modified index are formulated as

$$\begin{aligned} M_1(G)&=\sum_{uv\in E(G)}(d_u+d_v),\\ M_2(G)&=\sum_{uv\in E(G)}(d_u d_v),\\ {}^mM_2(G)&=\sum_{uv\in E(G)}\frac{1}{d_u d_v}. \end{aligned} \tag{4}$$

Recently, the symmetric division deg index of a graph G is introduced [41]. It is the significant index which is used to determine the total surface area of polychlorobiphenyls [42] and is defined as

$$SDD(G)=\sum_{uv\in E(G)}\left(\frac{\min(d_u,d_v)}{\max(d_u,d_v)}+\frac{\max(d_u,d_v)}{\min(d_u,d_v)}\right). \tag{5}$$

The other version of the Randic index is the harmonic index [43] and is defined as

$$H(G)=\sum_{uv\in E(G)}\frac{2}{d_u+d_v}. \tag{6}$$

The inverse sum index is formulated as [44]

$$I(G)=\sum_{uv\in E(G)}\frac{d_u d_v}{d_u+d_v}. \tag{7}$$

The augmented Zagreb index gives best approximation of heat of formation of alkanes [45, 46]. It is formulated as [47]

$$A(G)=\sum_{uv\in E(G)}\left(\frac{d_u d_v}{d_u+d_v-2}\right)^3. \tag{8}$$

Let $M(G;x,y)=f(x,y)$, and then Table 1 relates above described topological indices with M-polynomial [28], where

$$\begin{aligned} Q_\alpha(f(x,y))&=x^\alpha f(x,y),\\ J(f(x,y))&=f(x,x),\\ S_x&=\int_0^x\frac{f(t,y)}{t}dt,\\ S_y&=\int_0^y\frac{f(x,t)}{t}dt,\\ D_x&=x\frac{\partial(f(x,y))}{\partial x},\\ D_y&=y\frac{\partial(f(x,y))}{\partial y}. \end{aligned} \tag{9}$$

2. Main Results and Discussion

OḰeeffe et al. have distributed around a quarter century a letter managing two 3D systems of benzene, and one of the structures was known as 6.82P (or additionally polybenzene) and has a place with the space gather Im3m, compared with the P-type surface [48]. Actually, this is insertion of the hexagon fix in the surface of negative ebb and flow P. The P-type surface is coordinated to the Cartesian arranges in the Euclidean space. The reader can discover more about this intermittent surface in [49, 50]. This structure was required to be combined as 3D carbon solids and no such combination was accounted before. This has aroused a lot of research enthusiasm of researchers to carbon nanoscience. As much as the graphenes were picked up a moment Nobel prize after C_{60}, fullerenes have also been studied in depth, see detail in [51, 52].

The molecular graph of the benzene ring embedded in the P-type surface network is depicted in Figure 1. The cardinality of vertices and edges of the given molecular graph are $24mn$ and $32mn-2m-2n$, respectively. The vertex set consists of two vertex partitions in the benzene ring embedded in the P-type surface network, as shown in Table 2. Furthermore, the edge set consists of three edge partitions. The first edge partition contains $4m+4n$ edges uv, where $\deg(u)=\deg(v)=2$. The second edge partition

Table 1: The relationship of topological indices with M-polynomial.

Topological descriptor	Derivation from $f(x,y)$
$R_\alpha(G)$, $\alpha \in \mathbb{R}$	$(D_x^\alpha D_y^\alpha)(f(x,y))\|_{x=y=1}$
$RR_\alpha(G)$, $\alpha \in \mathbb{R}$	$(S_x^\alpha S_y^\alpha)(f(x,y))\|_{x=y=1}$
$M_1(G)$	$(D_x + D_y)(f(x,y))\|_{x=y=1}$
$M_2(G)$	$(D_x D_y)(f(x,y))\|_{x=y=1}$
${}^mM_2(G)$	$(S_x S_y)(f(x,y))\|_{x=y=1}$
$H(G)$	$2S_x J(f(x,y))\|_{x=1}$
$SDD(G)$	$(D_x S_y + S_x D_y)(f(x,y))\|_{x=y=1}$
$I(G)$	$S_x J D_x D_y(f(x,y))\|_{x=1}$
$A(G)$	$S_x^3 Q_{-2} J D_x^3 D_y^3(f(x,y))\|_{x=1}$

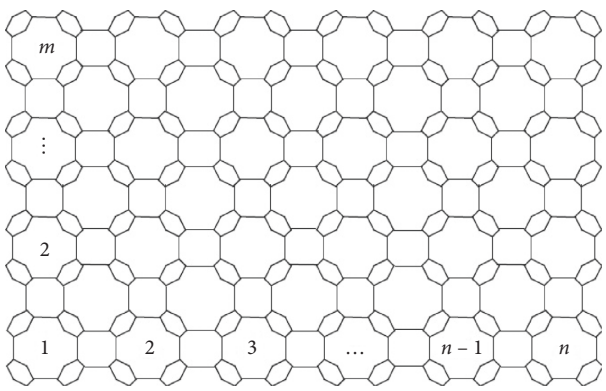

Figure 1: Chemical graph of the benzene ring embedded in a P-type surface network in 2D.

Table 2: Vertex partition of the benzene ring embedded in the P-type surface network based on degrees of each vertex.

d_v	2	3
Frequency	$8mn + 4m + 4n$	$16mn - 4m - 4n$

contains $16mn$ edges uv, where $\deg(u) = 2$ and $\deg(v) = 3$. The third edge partition contains $16mn - 2m - 2n$ edges uv, where $\deg(u) = \deg(v) = 3$. Table 3 shows the edge partition in the benzene ring embedded in the P-type surface network. We compute the M-polynomial of the benzene ring embedded in the P-type surface network. Also, we present the graphical representation of this graph in 2D and 3D by using Maple 13. In the end, we compute and simplify the topological indices by using the M-polynomial of the benzene ring embedded in the P-type surface network.

3. M-Polynomial of Benzene Ring Embedded in P-Type Network

Theorem 1. *Consider the graph of a benzene ring embedded in the P-type surface network $BR(m,n)$ with $m,n > 1$, and then the M-polynomial of this graph is given by*

$$M(\mathrm{BR}(m,n);x,y) = (4m+4n)x^2y^2 + (16mn)x^2y^3 + (16mn - 6m - 6n)x^3y^3. \tag{10}$$

Table 3: Edge partition of the benzene ring embedded in the P-type surface network based on degrees of end vertices of each edge.

(d_u, d_v)	$(2,2)$	$(2,3)$	$(3,3)$
Frequency	$4m + 4n$	$16mn$	$16mn - 6m - 6n$

Proof. Let the graph of a benzene ring embedded in the P-type surface network with m and n being the number of unit cells in the columns and rows, respectively. It consists of two vertices and three edge partitions. From Figure 1, it is easy to observe that

$$\begin{aligned} |V(\mathrm{BR}(m,n))| &= 24mn, \\ |E(\mathrm{BR}(m,n))| &= 32mn - 2m - 2n. \end{aligned} \tag{11}$$

From Table 2, it can be seen that there are two partitions of the vertex set of the benzene ring embedded in the P-type surface network.

$$\begin{aligned} V_1(\mathrm{BR}(m,n)) &= \{u \in V(\mathrm{BR}(m,n)) \mid d_u = 2\}, \\ V_2(\mathrm{BR}(m,n)) &= \{u \in V(\mathrm{BR}(m,n)) \mid d_u = 3\}, \end{aligned} \tag{12}$$

such that

$$\begin{aligned} |V_1(\mathrm{BR}(m,n))| &= 8mn + 4m + 4n, \\ |V_2(\mathrm{BR}(m,n))| &= 16mn - 4m - 4n. \end{aligned} \tag{13}$$

From Table 3, it can be seen that there are three partitions of the edge set of the benzene ring embedded in the P-type surface network.

$$\begin{aligned} E_1(\mathrm{BR}(m,n)) &= \{uv \in E(G) \mid d_u = 2, d_v = 2\}, \\ E_2(\mathrm{BR}(m,n)) &= \{uv \in E(G) \mid d_u = 2, d_v = 3\}, \\ E_3(\mathrm{BR}(m,n)) &= \{uv \in E(G) \mid d_u = 3, d_v = 3\}, \end{aligned} \tag{14}$$

such that

$$\begin{aligned} |E_1(\mathrm{BR}(m,n))| &= 4m + 4n, \\ |E_2(\mathrm{BR}(m,n))| &= 16mn, \\ |E_3(\mathrm{BR}(m,n))| &= 16mn - 6m - 6n. \end{aligned} \tag{15}$$

Now, applying the definition of M-polynomial to the graph of the benzene ring embedded in the P-type network, we have

$$\begin{aligned} M(\mathrm{BR}(m,n);x,y) &= \sum_{i \le j} m_{ij} x^i y^j \\ &= \sum_{i \le j} m_{ij} x^i y^j \\ &= \sum_{uv \in E_1(G)} m_{22} x^2 y^2 + \sum_{uv \in E_2(G)} m_{23} x^2 y^3 \\ &\quad + \sum_{uv \in E_3(G)} m_{33} x^3 y^3 \\ &= |E_1(G)| x^2 y^2 + |E_2(G)| x^2 y^3 \\ &\quad + |E_3(G)| x^3 y^3, \\ M(\mathrm{BR}(m,n);x,y) &= (4m+4n)x^2y^2 + (16mn)x^2y^3 \\ &\quad + (16mn - 6m - 6n)x^3y^3. \end{aligned} \tag{16}$$

The 3D graphical representation of M-polynomial of the benzene ring embedded in the P-type surface network $BR(m,n)$ is depicted in Figure 2. This is plotted by using Maple 13. The graph shows different behavior by fixing the values of m and n and changing the parameters x and y. If the 2D graphical representation of M-polynomial of $BR(m,n)$ can be formed by considering the parameter x to be the positive value, then the graph increases by increasing the values of x, and the graph lies in the first and third quadrant. The same behavior occurs for positive values of y, as depicted in Figures 3(a) and 3(b). If the parameter x is taken to be the negative value, then the graph increases by increasing the values of x, and the graph lies in the second and fourth quadrant. The same behavior occurs for negative values of y.

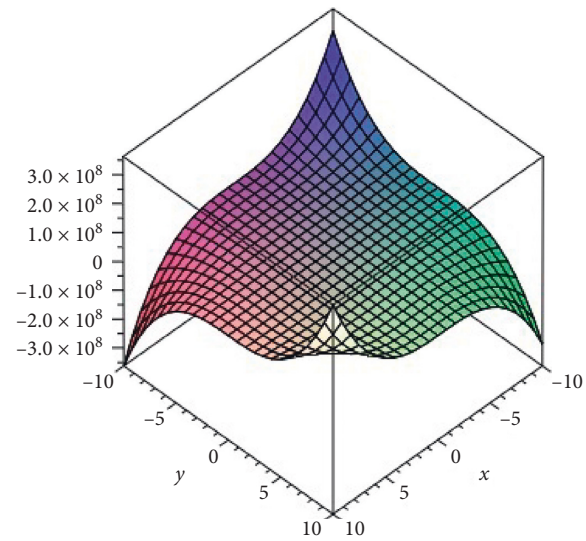

Figure 2: The 3D plot of M-polynomial of the benzene ring embedded in the P-type surface network.

4. Topological Indices Derived from M-Polynomial of BR (m,n)

The following proposition computes the degree-based topological indices that are derived from the M-polynomial of the molecular graph of the benzene ring embedded in the P-type surface network.

Proposition 1. *Consider the graph G be a benzene ring embedded in the P-type surface network with $m,n>1$; then, we have the following degree-based topological indices:*

(1) $M_1(G) = 176mn - 20m - 20n$

(2) $M_2(G) = 240mn - 38m - 38n$

(3) ${}^{m}M_2(G) = (40mn + 3m + 3n)/9$

(4) $SDD(G) = (200mn - 12m - 12n)/3$

(5) $H(G) = 176mn/15$

(6) $I(G) = (24mn - 25m - 25n)/5$

(7) $A(G) = (9928mn - 1163m - 1163n)/32$

(8) $RR_\alpha(G) = (16mn)((2^\alpha + 3^\alpha)/2^\alpha 3^{2\alpha}) + (m+n)((4(3^{2\alpha}) - 6(2^{2\alpha}))/6^{2\alpha})$

(9) $R_\alpha(G) = (16mn)(3^{2\alpha} + 6^\alpha) + (m+n)(4(2^{2\alpha}) - 6(3^{2\alpha}))$

Proof. Consider the molecular graph of G be a benzene ring embedded in the P-type surface network with $m,n>1$; its M-polynomial is simplified in the first theorem. Now, consider the following:

$$\begin{aligned} M(G;x,y) &= f(x,y), \\ f(x,y) &= (4m+4n)x^2y^2 + (16mn)x^2y^3 \\ &\quad + (16mn - 6m - 6n)x^3y^3. \end{aligned} \tag{17}$$

In order to prove the above nine results, we use the following formulas:

$$\begin{aligned} Q_\alpha(f(x,y)) &= x^\alpha f(x,y), \\ J(f(x,y)) &= f(x,x), \\ S_x &= \int_0^x \frac{f(t,y)}{t}\,dt, \\ S_y &= \int_0^y \frac{f(x,t)}{t}\,dt, \\ D_x &= x\frac{\partial(f(x,y))}{\partial x}, \\ D_y &= y\frac{\partial(f(x,y))}{\partial y}. \end{aligned} \tag{18}$$

Now, we have the following computations:

$$D_x(f(x,y)) = 2(4m+4n)x^2y^2 + 2(16mn)x^2y^3 + 3(16mn - 6m - 6n)x^3y^3, \tag{19}$$

$$D_y(f(x,y)) = 2(4m+4n)x^2y^2 + 3(16mn)x^2y^3 + 3(16mn - 6m - 6n)x^3y^3, \tag{20}$$

$$D_xD_y(f(x,y)) = 4(4m+4n)x^2y^2 + 6(16mn)x^2y^3 + 9(16mn - 6m - 6n)x^3y^3, \tag{21}$$

$$S_x(f(x,y)) = \frac{(4m+4n)}{2}x^2y^2 + \frac{(16mn)}{2}x^2y^3 + \frac{(16mn - 6m - 6n)}{3}x^3y^3, \tag{22}$$

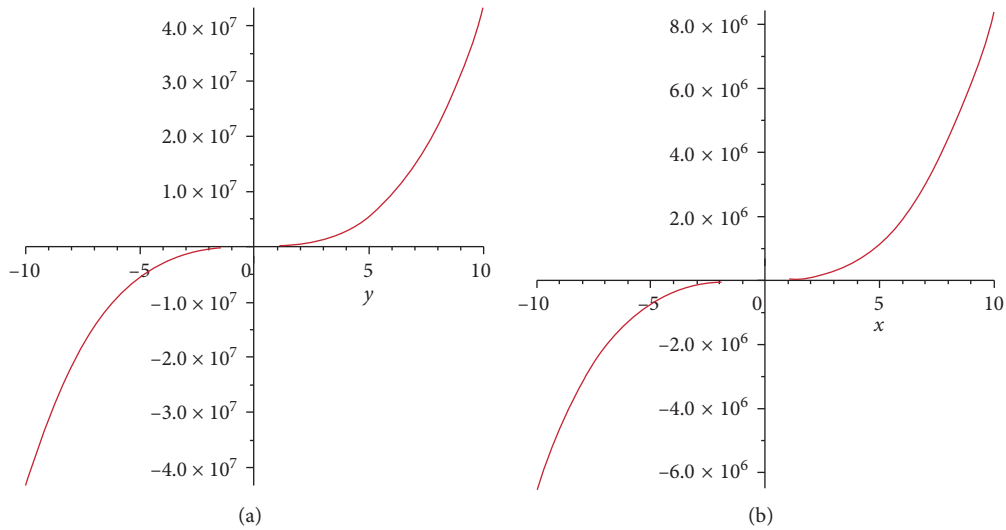

Figure 3: (a) The 2D plot of M-polynomial of the benzene ring embedded in the P-type surface network by fixing the parameter x. (b) The 2D plot of M-polynomial of the benzene ring embedded in the P-type surface network by fixing the parameter y.

$$S_xS_y(f(x,y)) = \frac{(4m+4n)}{4}x^2y^2 + \frac{(16mn)}{6}x^2y^3 + \frac{(16mn-6m-6n)}{9}x^3y^3, \tag{23}$$

$$S_xD_y(f(x,y)) = (4m+4n)x^2y^2 + \frac{3(16mn)}{2}x^2y^3 + (16mn-6m-6n)x^3y^3, \tag{24}$$

$$D_xS_y(f(x,y)) = (4m+4n)x^2y^2 + \frac{2(16mn)}{3}x^2y^3 + (16mn-6m-6n)x^3y^3, \tag{25}$$

$$D_x^{\alpha}D_y^{\alpha}(f(x,y)) = 2^{2\alpha}(4m+4n)x^2y^2 + 6^{\alpha}(16mn)x^2y^3 + 3^{2\alpha}(16mn-6m-6n)x^3y^3, \tag{26}$$

$$S_x^{\alpha}S_y^{\alpha}(f(x,y)) = \frac{(4m+4n)}{2^{2\alpha}}x^2y^2 + \frac{(16mn)}{6^{\alpha}}x^2y^3 + \frac{(16mn-6m-6n)}{3^{2\alpha}}x^3y^3, \tag{27}$$

$$S_xJ(f(x,y)) = \frac{(4m+4n)}{4}x^4 + \frac{(16mn)}{5}x^5 + \frac{(16mn-6m-6n)}{6}x^6, \tag{28}$$

$$S_xJD_xD_y(f(x,y)) = (4m+4n)x^4 + \frac{6(16mn)}{5}x^5 + \frac{3(16mn-6m-6n)}{2}x^6, \tag{29}$$

$$S_x^3Q_{-2}JD_x^3D_y^3(f(x,y)) = 8(4m+4n)x^2 + 8(16mn)x^3 + \frac{729(16mn-6m-6n)}{64}x^4. \tag{30}$$

Now, by using all the aforementioned values from equations (19)–(30) in Table 1, the topological indices defined in Table 1 are obtained.

(1) $M_1(G) = 176mn - 20m - 20n$

(2) $M_2(G) = 240mn - 38m - 38n$

(3) ${}^mM_2(G) = (40mn + 3m + 3n)/9$

(4) $SDD(G) = (200mn - 12m - 12n)/3$

(5) $H(G) = 176mn/15$

(6) $I(G) = (24mn - 25m - 25n)/5$

(7) $A(G) = (9928mn - 1163m - 1163n)/32$

(8) $RR_{\alpha}(G) = (16mn)((2^{\alpha} + 3^{\alpha})/2^{\alpha}3^{2\alpha}) + (m+n)((4(3^{2\alpha}) - 6(2^{2\alpha}))/6^{2\alpha})$

(9) $R_{\alpha}(G) = (16mn)(3^{2\alpha} + 6^{\alpha}) + (m+n)(4(2^{2\alpha}) - 6(3^{2\alpha}))$

The symmetric division, harmonic, inverse sum, and augmented Zagreb indices are plotted by using Maple 13. The graphical representation depicts different behavior of indices by changing the parameters m and n. The blue, green, red, and black colors show the symmetric division, harmonic, inverse sum, and augmented Zagreb indices, respectively, as depicted in Figure 4(a). Figure 4(b) illustrates

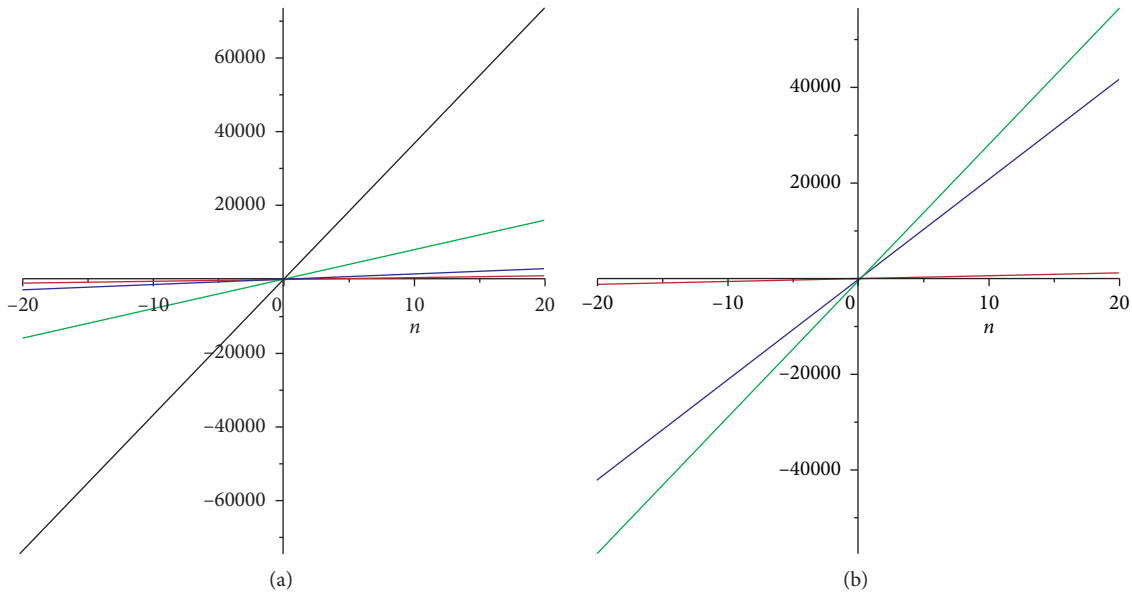

Figure 4: (a) Plot of symmetric division, harmonic, inverse sum, and augmented Zagreb index for fix n parameter. (b) Plot of first Zagreb, second Zagreb, and modified Zagreb index for fix m parameter.

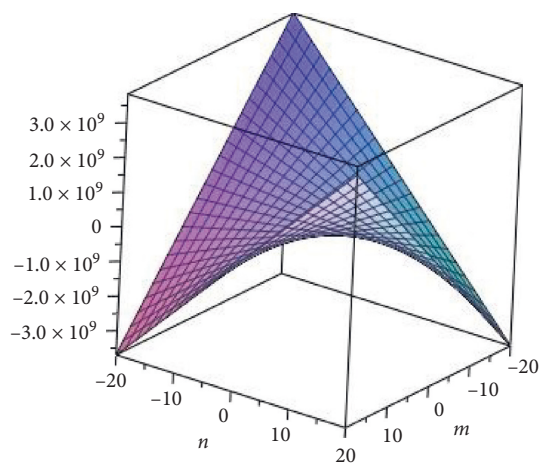

Figure 5: The 3D plot of Randić index for $\mathrm{BR}(m,n)$.

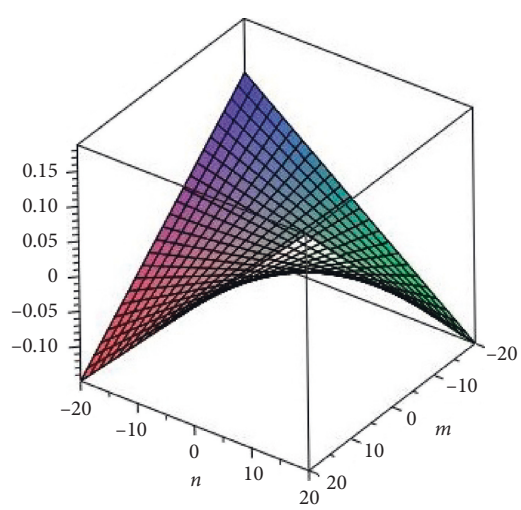

Figure 6: The 3D plot of the inverse Randić index for $\mathrm{BR}(m,n)$.

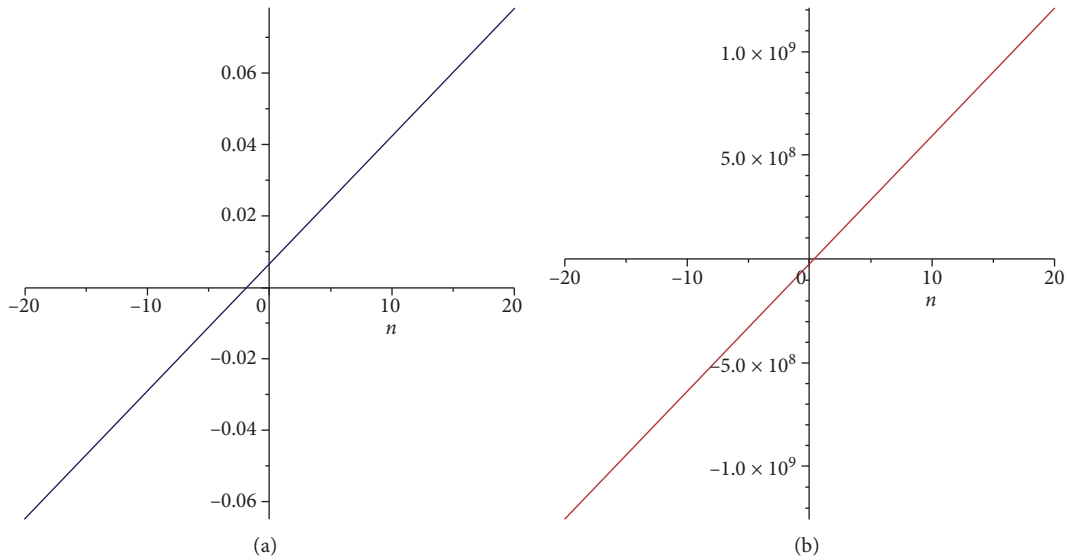

Figure 7: (a) The 2D plot of the Randić index for $BR(m, n)$. (b) The 2D plot of the inverse Randić index for $BR(m, n)$.

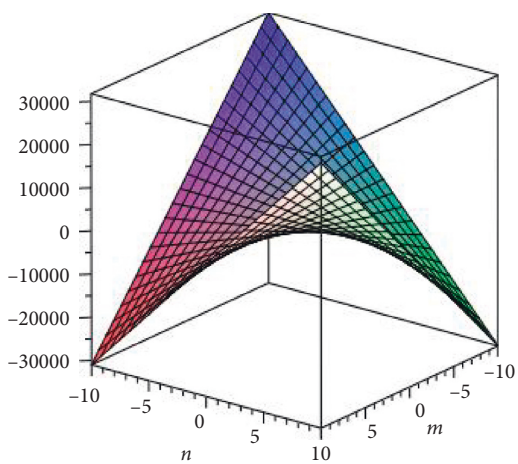

Figure 8: The 3D plot of the augmented Zagreb index for $BR(m, n)$.

the first Zagreb index in blue color, second Zagreb index in green color, and modified Zagreb index in red color.

The 3D plot of the Randić index and inverse Randić index is illustrated in Figures 5 and 6, respectively. It is clearly seen from the graphs that by increasing the values of the parameters m and n, the graph of 5 increases faster than the graph of 6. It can be concluded that the Randić index increases faster than the inverse Randić index.

The 2D plot of the inverse Randić index is depicted in Figure 7(a). This is achieved by using Maple 13 and fixing the value of the parameter m or n. In both cases, if values of the parameter increases then the graph increases gradually and shows different behavior. The 2D plot of the Randić index is depicted in Figure 7(b). By increasing the values of the parameters, the graph increases and depicts different behavior.

Figure 8 illustrates the 3D plot of the augmented Zagreb index for the molecular graph $BR(m, n)$. By increasing the values of the given parameters, the value of indices increases. The value indices of $BR(m, n)$ increase by changing the values of parameters m and n. The indices derived here are the functions that depend on the values of parameters, where m and n are the independent parameters and the index is the dependent parameter. □

5. Conclusions

We have computed the general form of M-polynomial for the molecular graph of the benzene ring embedded in the P-type surface network $BR(m, n)$ for the first time. The graphical representation of M-polynomial of $BR(m, n)$ and some of its indices have plotted for different values of the given parameters. Furthermore, we have derived and simplified the exact results for degree-based topological indices of $BR(m, n)$ from the M-polynomial of $BR(m, n)$.

In future, we will sketch and design some new chemical graphs/networks and compute their M-polynomial and examine their underlying topological properties.

Data Availability

The data used to support the findings of this study are available from the corresponding author upon request.

Conflicts of Interest

The authors declare that there are no conflicts of interest regarding the publication of this paper.

Acknowledgments

This work was supported by the Key Project of Sichuan Provincial Department of Education (grant nos. 17ZA0079 and 18ZA0118); Soft Scientific Research Foundation of Sichuan Provincial Science and Technology Department (grant no. 2018ZR0265); and COMSATS Attock and

National University of Sciences and Technology, Islamabad, Pakistan.

References

[1] A. Q. Baig, M. Imran, and H. Ali, "On topological indices of poly oxide, poly silicate, DOX, and DSL networks," *Canadian Journal of Chemistry*, vol. 93, no. 7, pp. 730–739, 2015.

[2] A. Q. Baig, M. Imran, W. Khalid, and M. Naeem, "Molecular description of carbon graphite and crystal cubic carbon structures," *Canadian Journal of Chemistry*, vol. 95, no. 6, pp. 674–686, 2017.

[3] H. Deng, J. Yang, and F. Xia, "A general modeling of some vertex-degree based topological indices in benzenoid systems and phenylenes," *Computers and Mathematics with Applications*, vol. 61, no. 10, pp. 3017–3023, 2011.

[4] W. Gao, M. R. Farahani, and L. Shi, "Forgotten topological index of some drug structures," *Acta Medica Mediterranea*, vol. 32, pp. 579–585, 2016.

[5] W. Gao and M. R. Farahani, "Degree-based indices computation for special chemical molecular structures using edge dividing method," *Applied Mathematics and Nonlinear Sciences*, vol. 1, no. 1, pp. 94–117, 2015.

[6] I. Gutman and O. E. Polansky, *Mathematical Concepts in Organic Chemistry*, Springer-Verlag New York, New York, NY, USA, 1986.

[7] W. Gao, M. K. Siddiqui, M. Imran, M. K. Jamil, and M. R. Farahani, "Forgotten topological index of chemical structure in drugs," *Saudi Pharmaceutical Journal*, vol. 24, no. 3, pp. 258–264, 2016.

[8] X. Zhang, H. Jiang, J.-B. Liu, and Z. Shao, "The cartesian product and join graphs on edge-version atom-bond connectivity and geometric arithmetic indices," *Molecules*, vol. 23, no. 7, p. 1731, 2018.

[9] X. Zhang, X. Wu, S. Akhter, M. Jamil, J.-B. Liu, and M. Farahani, "Edge-version atom-bond connectivity and geometric arithmetic indices of generalized bridge molecular graphs," *Symmetry*, vol. 10, no. 12, p. 751, 2018.

[10] J.-B. Liu and X.-F. Pan, "Minimizing Kirchhoff index among graphs with a given vertex bipartiteness," *Applied Mathematics and Computation*, vol. 291, pp. 84–88, 2016.

[11] J.-B. Liu, X.-F. Pan, F.-T. Hu, and F.-F. Hu, "Asymptotic Laplacian-energy-like invariant of lattices," *Applied Mathematics and Computation*, vol. 253, pp. 205–214, 2015.

[12] J.-B. Liu, X.-F. Pan, L. Yu, and D. Li, "Complete characterization of bicyclic graphs with minimal Kirchhoff index," *Discrete Applied Mathematics*, vol. 200, pp. 95–107, 2016.

[13] Y. W. Zhu, Y. Zhang, J. B. Yuan, and X. M. Wang, "FTP: an approximate fast privacy-preserving equality test protocol for authentication in Internet of things," *Security and Communication Networks*, vol. 2018, Article ID 6909703, 9 pages, 2018.

[14] Y. Zhu, X. Li, J. Wang, Y. Liu, and Z. Qu, "Practical secure naïve Bayesian classification over encrypted big data in cloud," *International Journal of Foundations of Computer Science*, vol. 28, no. 6, pp. 683–703, 2017.

[15] X. Li, Y. Zhu, J. Wang, and J. Zhang, "Efficient and secure multi-dimensional geometric range query over encrypted data in cloud," *Journal of Parallel and Distributed Computing*, vol. 131, pp. 44–54, 2019.

[16] Y. Gao, E. Zhu, Z. Shao, I. Gutman, and A. Klobučar, "Total domination and open packing in some chemical graphs," *Journal of Mathematical Chemistry*, vol. 56, no. 5, pp. 1481–1492, 2018.

[17] Z. Shao, P. Wu, X. Zhang, D. Dimitrov, and J.-B. Liu, "On the maximum ABC index of graphs with prescribed size and without pendent vertices," *IEEE Access*, vol. 6, pp. 27604–27616, 2018.

[18] Z. Shao, P. Wu, Y. Gao, I. Gutman, and X. Zhang, "On the maximum ABC index of graphs without pendent vertices," *Applied Mathematics and Computation*, vol. 315, pp. 298–312, 2017.

[19] M. R. Farahani, W. Gao, A. Q. Baig, and W. Khalid, "Molecular description of copper(II) oxide," *Macedonian Journal of Chemistry and Chemical Engineering*, vol. 36, no. 1, pp. 93–99, 2017.

[20] S. Hayat, M. A. Malik, and M. Imran, "Computing topological indices of honeycomb derived networks," *Romanian Journal of Information Science and Technology*, vol. 18, pp. 144–165, 2015.

[21] G. Rücker and C. Rücker, "On topological indices, boiling points, and cycloalkanes," *Journal of Chemical Information and Computer Sciences*, vol. 39, no. 5, pp. 788–802, 1999.

[22] D. Vukičević and A. Graovac, "Valence connectivities versus Randić, Zagreb, and modified Zagreb index: a linear algorithm to check discriminative properties of indices in acyclic molecular graphs," *Croatica Chemica Acta*, vol. 77, pp. 501–508, 2004.

[23] K. C. Das and I. Gutman, "Some properties of the second Zagreb index," *Match-Communications in Mathematical and in Computer Chemistry*, vol. 52, pp. 103–112, 2004.

[24] M. Eliasi and B. Taeri, "Hosoya polynomial of zigzag polyhex nanotorus," *Journal of the Serbian Chemical Society*, vol. 73, pp. 313–319, 2008.

[25] I. Gutman and K. C. Das, "The first Zagreb index 30 years after," *Match-Communications in Mathematical and in Computer Chemistry*, vol. 50, pp. 83–92, 2004.

[26] H. Hosoya, "On some counting polynomials in chemistry," *Discrete Applied Mathematics*, vol. 19, no. 1–3, pp. 239–257, 1988.

[27] M. R. Farahani, "Hosoya polynomial, wiener and hyper wiener indices of some regular graphs," *Informatics Engineering, an International Journal (IEIJ)*, vol. 1, no. 1, pp. 9–13, 2013.

[28] E. Deutsch and S. Klavzar, "M-Polynomial and degree-based topological indices," *Iranian Journal of Mathematical Chemistry*, vol. 6, pp. 93–102, 2015.

[29] M. Munir, W. Nazeer, S. Rafique, and S. Kang, "M-polynomial and related topological indices of nanostar dendrimers," *Symmetry*, vol. 8, no. 9, p. 97, 2016.

[30] Y. C. Kwun, M. Munir, W. Nazeer, S. Rafique, and S. Min Kang, "M-Polynomials and topological indices of V-phenylenic nanotubes and nanotori," *Scientific Reports*, vol. 7, no. 1, 2017.

[31] H. Wiener, "Structural determination of paraffin boiling points," *Journal of the American Chemical Society*, vol. 69, no. 1, pp. 17–20, 1947.

[32] A. A. Dobrynin, R. Entringer, and I. Gutman, "Wiener index of trees: theory and applications," *Acta Applicandae Mathematicae*, vol. 66, no. 3, pp. 211–249, 2001.

[33] B. Bollobás and P. Erdös, "Graphs of extremal weights," *Ars Combinatoria*, vol. 50, pp. 225–233, 1998.

[34] D. Amić, D. Bešlo, B. Lučić, S. Nikolić, and N. Trinajstić, "The vertex-connectivity index revisited," *Journal of Chemical Information and Computer Sciences*, vol. 38, no. 5, pp. 819–822, 1998.

[35] G. Caporossi, I. Gutman, P. Hansen, and L. Pavlović, "Graphs with maximum connectivity index," *Computational Biology and Chemistry*, vol. 27, no. 1, pp. 85–90, 2003.

[36] Y. Hu, X. Li, Y. Shi, T. Xu, and I. Gutman, "On molecular graphs with smallest and greatest zeroth-order general Randić index," *Match-Communications in Mathematical and in Computer Chemistry*, vol. 54, pp. 425–434, 2005.

[37] I. Gutman, M. Randić, and X. Li, "Mathematical aspects of Randić type molecular structure descriptors," *Mathematical Chemistry Monographs No. 1*, University of Kragujevac, Kragujevac, Serbia, 2006.

[38] M. Randić, "On history of the Randić index and emerging hostility toward chemical graph theory," *Match-Communications in Mathematical and in Computer Chemistry*, vol. 59, pp. 5–124, 2008.

[39] I. Gutman and N. Trinajstić, "Graph theory and molecular orbitals. Total φ-electron energy of alternant hydrocarbons," *Chemical Physics Letters*, vol. 17, no. 4, pp. 535–538, 1972.

[40] N. Trinajstic, S. Nikolic, A. Milicevic, and I. Gutman, "On Zagreb indices," *Kemija u Industriji*, vol. 59, pp. 577–589, 2010.

[41] C. K. Gupta, V. Lokesha, B. S. Shetty, and P. S. Ranjini, "On the symmetric division deg index of graph," *Southeast Asian Bulletin of Mathmatics*, vol. 41, no. 1, pp. 1–23, 2016.

[42] V. Lokesha and T. Deepika, "Symmetric division deg index of tricyclic and tetracyclic graphs," *International Journal of Scientific & Engineering Research*, vol. 7, no. 5, pp. 53–55, 2016.

[43] L. Zhong, "The harmonic index for graphs," *Applied Mathematics Letters*, vol. 25, no. 3, pp. 561–566, 2012.

[44] K. Pattabiraman, "Inverse sum indeg index of graphs," *AKCE International Journal of Graphs and Combinatorics*, vol. 15, no. 2, pp. 155–167, 2018.

[45] E. Estrada, L. Torres, L. Rodríguez, and I. Gutman, "An atom-bond connectivity index: modelling the enthalpy of formation of alkanes," *Indian Journal of Chemistry*, vol. 37A, no. 10, pp. 849–855, 1998.

[46] B. Furtula, A. Graovac, and D. Vukičević, "Augmented Zagreb index," *Journal of Mathematical Chemistry*, vol. 48, no. 2, pp. 370–380, 2010.

[47] Y. Huang, B. Liu, and L. Gan, "Augmented Zagreb index of connected graphs," *Match-Communications in Mathematical and in Computer Chemistry*, vol. 67, pp. 483–494, 2012.

[48] M. ÓKeeffe, G. B. Adams, and O. F. Sankey, "Predicted new low energy forms of carbon," *Physical Review Letters*, vol. 68, pp. 232–328, 1992.

[49] M. V. Diudea, *Nanostructures, Novel Architecture*, NOVA, New York, NY, USA, 2005.

[50] M. V. Diudea and C. L. Nagy, *Periodic Nanostructures*, Springer, Dordrecht, Netherlands, 2007.

[51] K. Y. Amsharov and M. Jansen, "A C_{78} fullerene precursor: toward the direct synthesis of higher fullerenes," *Journal of Organic Chemistry*, vol. 73, no. 7, pp. 293–934, 2008.

[52] Y. Shi, "Note on two generalizations of the Randić index," *Applied Mathematics and Computation*, vol. 265, pp. 1019–1025, 2015.

Hindawi
Journal of Chemistry
Volume 2019, Article ID 6031568, 8 pages
https://doi.org/10.1155/2019/6031568

Research Article

Minimum Detour Index of Tricyclic Graphs

Wei Fang,[1,2] **Zheng-Qun Cai**,[3] **and Xiao-Xin Li**[4]

[1]*School of Mathematical Sciences, Anhui University, Hefei 230601, China*
[2]*College of Information & Network Engineering, Anhui Science and Technology University, Fengyang 233100, China*
[3]*School of Foreign Studies, Anhui Jianzhu University, Hefei 230601, China*
[4]*School of Big Data and Artificial Intelligence, Chizhou University, Chizhou 247000, China*

Correspondence should be addressed to Zheng-Qun Cai; caizhengqun1983@163.com

Received 7 July 2019; Accepted 5 September 2019; Published 13 October 2019

Guest Editor: Shaohui Wang

The detour index of a connected graph is defined as the sum of the detour distances (lengths of longest paths) between unordered pairs of vertices of the graph. The detour index is used in various quantitative structure-property relationship and quantitative structure-activity relationship studies. In this paper, we characterize the minimum detour index among all tricyclic graphs, which attain the bounds.

1. Introduction

Let G be a simple and connected graph with $|V(G)| = n$ and $|E(G)| = m$ and $N_G(u)$ be the neighbor vertex set of vertex u, then $d_G(u) = |N_G(u)|$ is called the degree of u. If $m = n - 1 + c$, then G is called a c-cyclic graph. If $c = 0, 1, 2$, and 3, then G is a tree, unicyclic graph, bicyclic graph, and tricyclic graph, respectively. Denote by $\mathscr{T}_n$ the set of all tricyclic graphs of order n.

Let $\widehat{\mathscr{T}} = \left\{\widehat{\mathscr{T}}^i \mid 1 \le i \le 15\right\}$, where graphs $\widehat{\mathscr{T}}^i$ for $i = 1, 2, \ldots, 15$ are defined in Figure 1. By [1, 2], we know that for any $\mathscr{T}^i \in \mathscr{T}_n$, $\mathscr{T}^i$ can be obtained from $\widehat{\mathscr{T}}^i$ $(1 \le i \le 15)$ by attaching trees to some of its vertices. We call $\widehat{\mathscr{T}}^i$ the base of $\mathscr{T}^i$.

A block of the graph G is a maximal 2-connected subgraph of G. A cactus is a connected graph in which no edge lies in more than one cycle, such that each block of a cactus is either an edge or a cycle. A vertex shared by two or more cycles is called a cut vertex. In this paper, denote $\mathscr{C}_n^l$ be the set of all cacti of order n and l cycles, where $l \ge 1$. The length of the cycles may be different and the length of each cycle is at least 3.

The concept of "topological index" was first proposed by Haruo Hosoya for characterizing the topological nature of a graph. Such graph invariants are usually related to the distance function $d(-,-)$.

The detour distance [3, 4] (also known under the name elongation) between vertices u and v in G is the length of a longest path between them, denoted by $l(u, v \mid G)$. Note that $l(u, u \mid G) = 0$ for any $u \in V(G)$; see [5] for a discussion. The detour index of the graph G is defined as [4–9]

$$\omega(G) = \frac{1}{2} \sum_{u,v \in V(G)} l(u, v \mid G). \tag{1}$$

For a connected graph G with $u \in V(G)$, let $L(u \mid G) = \sum_{v \in V(G)} l(u, v \mid G)$, then

$$\omega(G) = \frac{1}{2} \sum_{u \in V(G)} L(u \mid G). \tag{2}$$

If we use the notion of the detour matrix [4], which is an $n \times n$ matrix whose (i, j)-element is $l(v_i, v_j \mid G)$ with $V(G) = \{v_1, v_2, \ldots, v_n\}$, then the detour index is equal to the half-sum of the (off diagonal) elements of the detour matrix. The detour index has been applied to chemistry, especially in quantitative structure-activity relationship (QSAR) studies; see [7, 10] for more details. A new branch cheminformatics is a combination of mathematics and chemistry. This branch studies QSAR/QSPR study, physicochemical properties and topological indices such as Zagreb Indices [11], Kirchhoff index [12], Hosoya index [13] and so on to predict

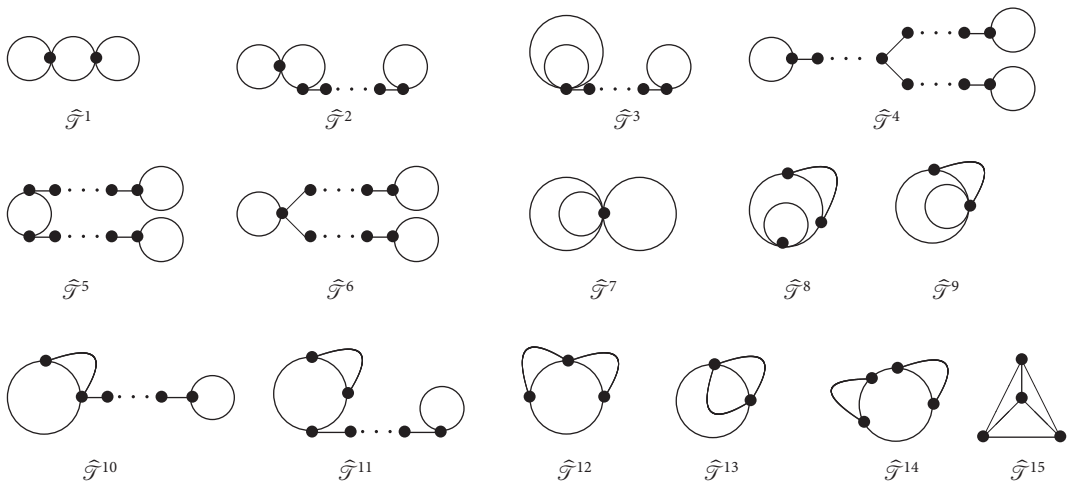

Figure 1: The fifteen types of bases for tricyclic graphs.

physicochemical properties and biological activities of the chemical compounds theoretically.

In this paper, we consider the minimum detour index among all tricyclic graphs.

2. Preliminaries

In this section, we will introduce some useful lemmas and graph transformations.

2.1. Edge-Lifting Transformation [14, 15]. Let G_1 and G_2 be two graphs with $n_1 \geq 2$ and $n_2 \geq 2$ vertices, respectively. If G is the graph obtained from G_1 and G_2 by adding an edge between a vertex u_0 of G_1 and a vertex v_0 of G_2, G' is the graph obtained by identifying u_0 of G_1 to v_0 of G_2 and adding a pendant edge to $u_0\,(v_0)$, then G' is called the edge-lifting transformation of G (see Figure 2).

Lemma 1 (see [16]). *Let G be defined as in Figure 2, and G' is obtained from G by the edge-lifting transformation (see Figure 2). Then, $\omega(G) > \omega(G')$.*

Denote $\mathcal{T}_n^{(1)} = \{\mathcal{T}^1, \mathcal{T}^7, \mathcal{T}^8, \mathcal{T}^9, \mathcal{T}^{12}, \mathcal{T}^{13}, \mathcal{T}^{14}, \mathcal{T}^{15}\}$ (see Figure 1).

By Lemma 1, we can verify that if $\mathcal{T} \in \mathcal{T}_n$ attains the minimum detour index of all graphs in $\mathcal{T}_n$, then the following two conditions hold:

(i) The base $\widehat{\mathcal{T}}$ of $\mathcal{T}$ is one of $\widehat{\mathcal{T}}_n^{(1)}$

(ii) The graph $\mathcal{T}$ is obtained from $\widehat{\mathcal{T}}$ by attaching some pendant edges

Remark 1. In order to determine the tricyclic graphs which attain the minimum detour index of all graphs in $\mathcal{T}_n$, we just need to discuss the tricyclic graphs in $\mathcal{T}$, where $\widehat{\mathcal{T}} \in \mathcal{T}_n^{(1)}$.

2.2. Cycle-Edge Transformation. Let $\mathcal{C} \in \mathcal{C}_n^l$ be a cactus as shown in Figure 3, where $C_r = v_1 v_2 \ldots v_r v_1$ is the biggest cycle of $\mathcal{C}$, $r \geq 4$. Denote the vertex set $W_{v_i} = N_{G_i}(v_i) = N_G(v_i) \cap V(G_i)$, $1 \leq i \leq r$. $\mathcal{C}'$ is the graph obtained from $\mathcal{C}$ by deleting the edges $v_2 v_3$ and v_2 to W_{v_2}, meanwhile adding the edges $v_1 v_3$ and v_1 to W_{v_2}.

We say that $\mathcal{C}'$ is obtained from $\mathcal{C}$ by the cycle-edge transformation (see Figure 3).

Lemma 2 (see [16]). *Let $\mathcal{C} \in \mathcal{C}_n^l$ be a cactus as shown in Figure 3 with $r \geq 4$, and $\mathcal{C}'$ be the cycle-edge transformation of $\mathcal{C}$ (see Figure 3). Then, $\omega(\mathcal{C}) > \omega(\mathcal{C}')$.*

2.3. Cycle-Lifting Transformation. Let $\mathcal{C}_1 \in \mathcal{C}_n^l$ be a cactus as shown in Figure 4. Denote $W_{v_i} = N_{G_i}(v_i) = N_G(v_i) \cap V(G_i)$ for $1 \leq i \leq 3$. Let $\mathcal{C}_1'$ be the graph obtained from $\mathcal{C}_1$ by deleting the edges $v_2 v_x$ for $v_x \in W_{v_2}$ and adding the edges $v_1 v_x$ for $v_x \in W_{v_2}$.

We say that $\mathcal{C}_1'$ is the cycle-lifting transformation of $\mathcal{C}_1$ (see Figure 4).

Lemma 3 (see [16]). *Let $\mathcal{C}_1'$ be the cycle-lifting transformation of $\mathcal{C}_1$ (see Figure 4). Then, $\omega(\mathcal{C}_1) > \omega(\mathcal{C}_1')$.*

2.4. Operation I. We define Operation I as follows. Let G and G' be a simple and connected graph as shown in Figure 5. $v_1 v_2 \ldots v_p$ be the path in a cycle. Denote $W_{v_i} = \{w \mid w v_i \in E(G) \text{ and } d(w) = 1, 1 \leq i \leq p, p \geq 3\}$, and G' be the graph obtained from G by deleting the edges $v_2 v_3$, $v_2 w$ for $w \in W_{v_2}$ and adding the edges $v_1 v_3, v_1 w$ for $w \in W_{v_2}$ (see Figure 5).

Lemma 4. *Let G and G' be the graph shown in Figure 5. Then, $\omega(G) > \omega(G')$.*

Proof. Let $V(G) = V(G') = \{v_1, v_2, v_3, \ldots, v_n\}$, and $W_{v_i} = \{w \mid w v_i \in E(G) \text{ and } d(w) = 1, 1 \leq i \leq p\}$. For the vertices $v_i, v_j \in V(G - v_2)$, obviously

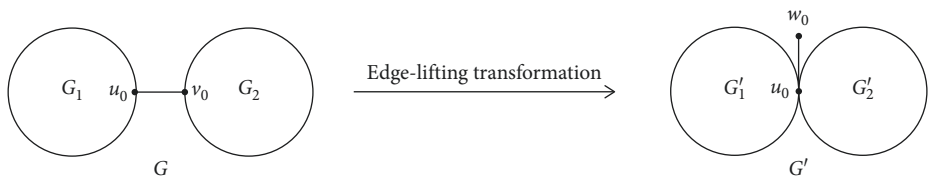

Figure 2: The edge-lifting transformation.

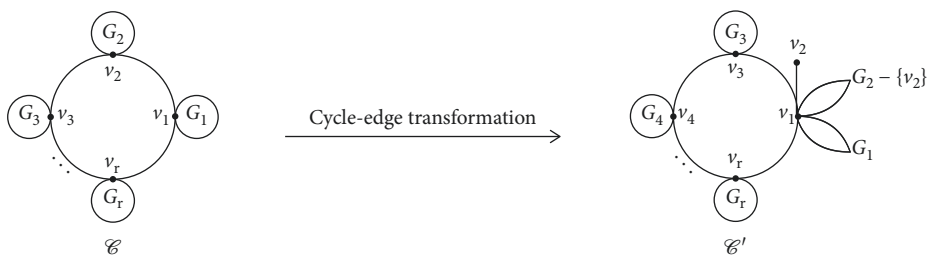

Figure 3: The cycle-edge transformation.

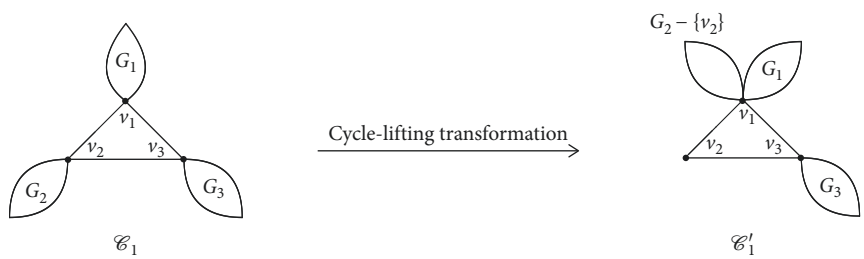

Figure 4: The cycle-lifting transformation.

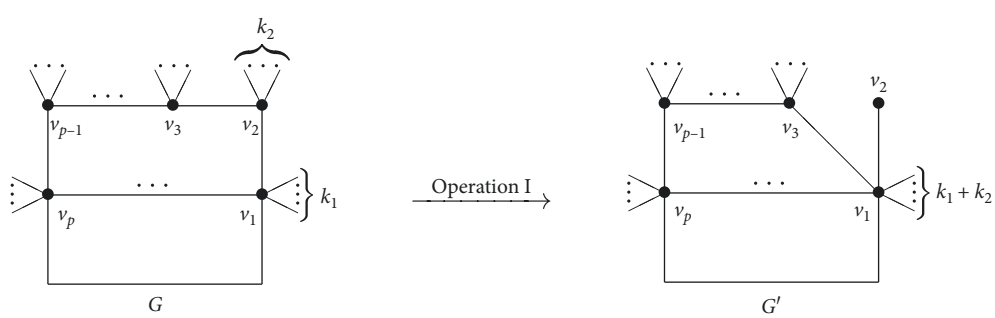

Figure 5: Operation I on graph G.

$$l(v_i, v_j \mid G) \geq l(v_i, v_j \mid G'), \tag{3}$$

$$l(v_1, v_2 \mid G) > l(v_1, v_2 \mid G') = 1. \tag{4}$$

Let P_i be the set of the longest path between v_2 and v_i in G and Q_i be the set of the longest path between v_1 and v_i in G, where $3 \leq i \leq n$.

Case 1. $v_1v_2 \in E(P_i)$ and $v_2v_3 \in E(P_i)$, where $3 \leq i \leq n$.

Obviously, for $3 \leq i \leq n$, $l(v_2, v_i \mid G) = l(v_2, v_i \mid G') - 1$. On the other hand, if $v_1v_2 \in E(P_i)$ and $v_2v_3 \in E(P_i)$, then $v_1v_2, v_2v_3 \in \mathscr{L}_i$, where $\mathscr{L}_i$ be the any one longest path between v_1 and v_i in G. Therefore, $l(v_1, v_i \mid G) = l(v_1, v_i \mid G') + 1$, and

$$\begin{aligned} &l(v_2, v_i \mid G) + l(v_1, v_i \mid G) \\ &\quad = l(v_2, v_i \mid G') + l(v_1, v_i \mid G'), \quad 3 \leq i \leq n. \end{aligned} \tag{5}$$

Case 2. $v_1v_2 \notin E(P_i)$ and $v_2v_3 \in E(P_i)$. Obviously, for $3 \leq i \leq n$, we have

$$\begin{aligned} l(v_2, v_i \mid G) &= l(v_3, v_i \mid G) + 1 \\ &> l(v_1, v_i \mid G) + 1 \\ &\geq l(v_1, v_i \mid G') + 1 \\ &= l(v_2, v_i \mid G'). \end{aligned} \tag{6}$$

Case 3. $v_1v_2 \in E(P_i)$ and $v_2v_3 \notin E(P_i)$. Obviously, for $3 \leq i \leq n$, we have

$$l(v_2, v_i \mid G) = l(v_2, v_i \mid G'). \tag{7}$$

Case 4. $v_1v_2 \notin E(P_i)$ and $v_2v_3 \notin E(P_i)$. Obviously, $v_i \in W_{v_2} \subset V(G)$, and

$$l(v_2, v_i \mid G) = l(v_1, v_i \mid G') = 1, \tag{8}$$

$$l(v_1, v_i \mid G) > l(v_2, v_i \mid G') = 2. \tag{9}$$

By (5)–(9), we have

$$\begin{aligned} &l(v_2, v_i \mid G) + l(v_1, v_i \mid G) \\ &\quad \geq l(v_2, v_i \mid G') + l(v_1, v_i \mid G'), \quad 3 \leq i \leq n. \end{aligned} \tag{10}$$

By (3), (4), and (10), we have $\omega(G) > \omega(G')$. □

2.5. Operation II. We define Operation II as follows. Let G and G' be a simple and connected graph as shown in Figure 6. Denote $v_1v_2v_3v_1$ be a cycle with length 3, $W_{v_i} = \{w \mid wv_i \in E(G) \text{ and } d(w) = 1, i = 1, 2\}$, and G' be the graph obtained from G by deleting the edges v_2w for $w \in W_{v_2}$ and adding the edges v_1w for $w \in W_{v_2}$ (see Figure 6).

Lemma 5. *Let G and G' be the graph shown in Figure 6. Then, $\omega(G) > \omega(G')$, and the equality holds if and only if $G \cong G'$.*

Proof. Let $V(G) = V(G') = \{v_1, v_2, v_3, \ldots, v_n\}$. For the vertices $v_i, v_j \in V(G) - W_{v_2}$, $v_x, v_y \in W_{v_2}$, we have

$$l(v_i, v_j \mid G) = l(v_i, v_j \mid G'), \tag{11}$$

$$l(v_x, v_y \mid G) = l(v_x, v_y \mid G') = 2. \tag{12}$$

For the vertices $v_i \in V(G) - W_{v_2} - \{v_1, v_2\}$, $w \in W_{v_2}$, we have

$$\begin{aligned} &l(w, v_i \mid G) \\ &\quad = \max\{3 + l(v_1, v_i \mid G), 3 + l(v_3, v_i \mid G)\} \\ &\quad \geq \max\{1 + l(v_1, v_i \mid G), 3 + l(v_3, v_i \mid G)\} \\ &\quad = \max\{1 + l(v_1, v_i \mid G'), 3 + l(v_3, v_i \mid G')\} \\ &\quad = l(w, v_i \mid G'), \end{aligned} \tag{13}$$

especially, if $G \ncong G'$, then

$$l(w, v_3 \mid G) > l(w, v_3 \mid G'), \tag{14}$$

$$\begin{aligned} l(w, v_1 \mid G) &= l(v_1, v_2 \mid G) + 1 \\ &= l(v_1, v_2 \mid G') + 1 \\ &= l(w, v_2 \mid G'), \end{aligned} \tag{15}$$

$$l(w, v_2 \mid G) = l(w, v_1 \mid G') = 1. \tag{16}$$

By (11)–(16), we have $\omega(G) \geq \omega(G')$, and the equality holds if and only if $G \cong G'$. □

Denote $\mathcal{T}_n^{(2)} = \{\mathcal{T}^{16}, \mathcal{T}^{17}, \mathcal{T}^{18}, \mathcal{T}^{19}, \mathcal{T}^{20}, \mathcal{T}^{21}\}$; see Figure 7.

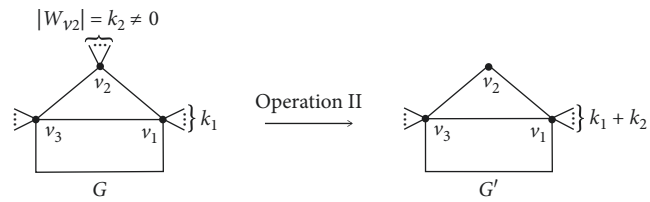

Figure 6: Operation II on graph G.

By Lemma 2–5, we can verify that if $\mathcal{T} \in \mathcal{T}_n$ attains the minimum detour index of all graphs in $\mathcal{T}_n$, then $\mathcal{T} \in \mathcal{T}_n^{(2)}$.

Remark 2. In order to determine the tricyclic graphs which attain the minimum detour index of all graphs in $\mathcal{T}_n$, we just need to discuss the tricyclic graphs in $\mathcal{T}$, where $\widehat{\mathcal{T}} \in \mathcal{T}_n^{(2)} = \{\mathcal{T}^{16}, \mathcal{T}^{17}, \mathcal{T}^{18}, \mathcal{T}^{19}, \mathcal{T}^{20}, \mathcal{T}^{21}\}$; see Figure 7.

2.6. Operation III. We define Operation III as follows. Let $G \in \mathcal{T}^{17} \cup \mathcal{T}^{18} \cup \mathcal{T}^{20} \cup \mathcal{T}^{21}$ as shown in Figure 7. Denote $W_{v_i} = \{w \mid wv_i \in E(G) \text{ and } d(w) = 1\}$ and G' be the graph obtained from G by deleting the edges v_3w for $w \in W_{v_3}$ and adding the edges v_1w for $w \in W_{v_3}$ (see Figures 8–11).

Lemma 6. *Let G_i and $G_i'(1 \leq i \leq 4)$ be the graph in Figures 8–11. Then, $\omega(G) \geq \omega(G')$, and the equality holds if and only if $G \cong G'$.*

Proof. Let $V(G_1) = V(G_1') = \{v_1, v_2, v_3, \ldots, v_n\}$. For the vertices $v_i, v_j \in V(G) - W_{v_3} - \{v_1, v_3\}$; $v_x, v_y \in W_{v_3}$, we have

$$l(v_i, v_j \mid G_1) = l(v_i, v_j \mid G_1'), \tag{17}$$

$$l(v_x, v_y \mid G_1) = l(v_x, v_y \mid G_1') = 2, \tag{18}$$

$$l(v_1, v_i \mid G_1) = l(v_1, v_i \mid G_1'), \tag{19}$$

$$l(v_3, v_x \mid G_1) = l(v_1, v_x \mid G_1'), \tag{20}$$

$$l(v_3, v_i \mid G_1) \geq l(v_1, v_i \mid G_1'), \tag{21}$$

$$\begin{aligned} l(v_x, v_i \mid G_1) &= l(v_3, v_i \mid G_1) + 1 \\ &= l(v_3, v_i \mid G_1') + 1 \\ &\geq l(v_1, v_i \mid G_1') + 1 \\ &= l(v_x, v_i \mid G_1'), \end{aligned} \tag{22}$$

$$l(v_x, v_5 \mid G_1) = 5 > 3 = l(v_x, v_5 \mid G_1'). \tag{23}$$

By (17)–(23), we have $\omega(G_1) > \omega(G_1')$.

Similarly, we have $\omega(G_i) \geq \omega(G_i')$, and the equality holds if and only if $G_i \cong G_i'$ $(i = 2, 3, 4)$. □

2.7. Operation IV. We define Operation IV as follows. Let $G \in \mathcal{T}^{19}$ as shown in Figure 12. Denote $W_{v_i} = \{w \mid wv_i \in E(G) \text{ and } d(w) = 1\}$, and G' be the graph obtained from G

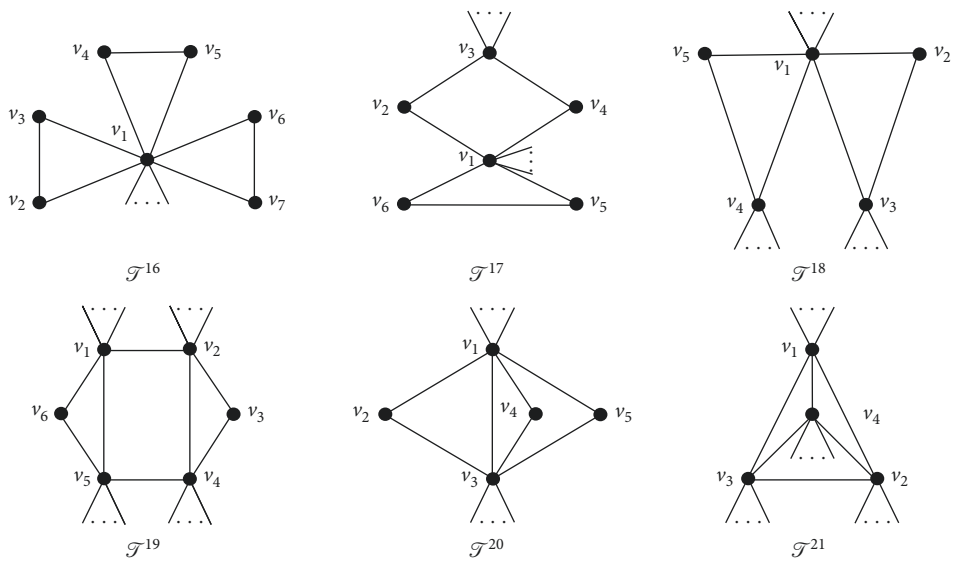

Figure 7: Graph $\mathcal{T}_n^{(2)}$.

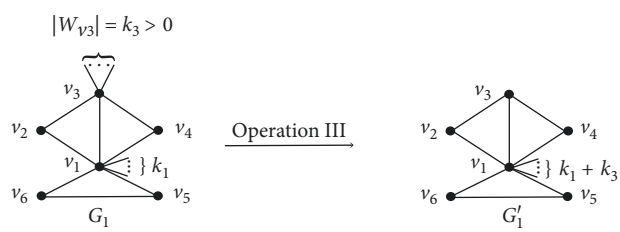

Figure 8: Operation III on graph $G_1 \in \mathcal{T}^{17}$.

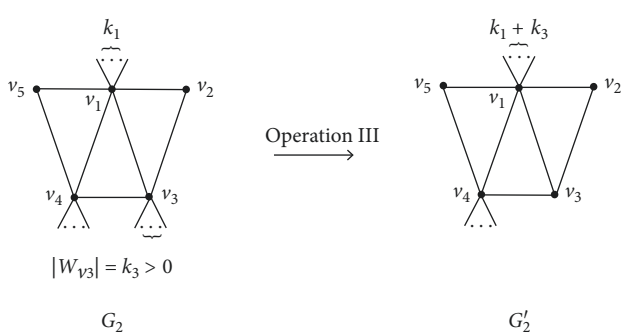

Figure 9: Operation III on graph $G_2 \in \mathcal{T}^{18}$.

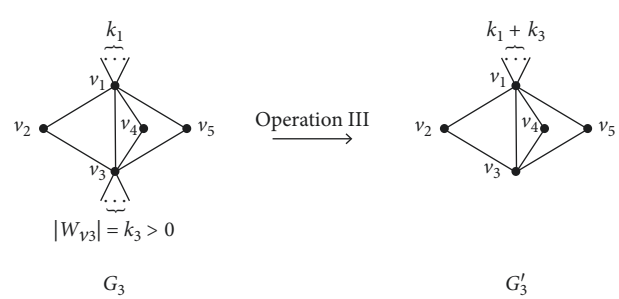

Figure 10: Operation III on graph $G_3 \in \mathcal{T}^{20}$.

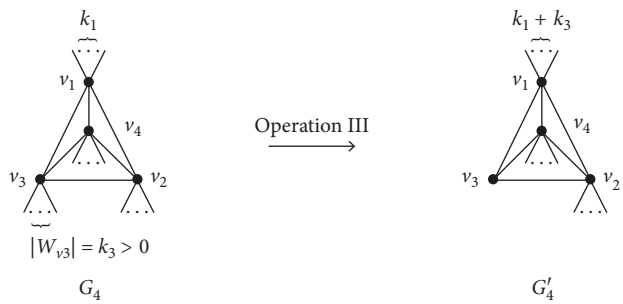

Figure 11: Operation III on graph $G_4 \in \mathcal{T}^{21}$.

by deleting the edges $v_i w$ for $w \in W_{v_i}, i = 2, 4, 5$ and adding the edges $v_1 w$ for $w \in W_{v_i}, i = 2, 4, 5$ (see Figure 12).

Lemma 7. *Let G and G' be the graph shown in Figure 12. Then, $\omega(G) \geq \omega(G')$ with equality holding if and only if $G \cong G'$.*

Proof. Let $V_1 = \{v_i \mid 1 \leq i \leq 6\}$, $V_2 = V(G) - V_1$, we have

$$\begin{aligned}\omega(G) = &\sum_{v_x, v_y \in V_1} l(v_x, v_y \mid G) \\ &+ \sum_{v_x \in V_1, v_y \in V_2} l(v_x, v_y \mid G) \\ &+ \sum_{v_x, v_y \in V_2} l(v_x, v_y \mid G),\end{aligned} \tag{24}$$

$$\begin{aligned}\omega(G') = &\sum_{v_x, v_y \in V_1} l(v_x, v_y \mid G') \\ &+ \sum_{v_x \in V_1, v_y \in V_2} l(v_x, v_y \mid G') \\ &+ \sum_{v_x, v_y \in V_2} l(v_x, v_y \mid G').\end{aligned} \tag{25}$$

Obviously,

$$\begin{aligned}\sum_{v_x, v_y \in V_1} l(v_x, v_y \mid G) &= \sum_{v_x, v_y \in V_1} l(v_x, v_y \mid G'), \\ \sum_{v_x \in V_1, v_y \in V_2} l(v_x, v_y \mid G) &= + \sum_{v_x \in V_1, v_y \in V_2} l(v_x, v_y \mid G'),\end{aligned} \tag{26}$$

$$\begin{aligned}l(v_x, v_y \mid G) = l(v_x, v_y \mid G') = 2, \quad v_x, v_y \in W_{v_i}, \\ l(v_x, v_y \mid G) > 2 = l(v_x, v_y \mid G'), \\ v_x \in W_{v_i},\ v_y \in W_{v_j},\ i \neq j.\end{aligned} \tag{27}$$

Therefore,

$$\begin{aligned}&\omega(G) - \omega(G') \\ &= \sum_{v_x, v_y \in V_2} l(v_x, v_y \mid G) - \sum_{v_x, v_y \in V_2} l(v_x, v_y \mid G') \\ &\geq 0,\end{aligned} \tag{28}$$

and the equality holds if and only if $G \cong G'$. □

Denote $\mathcal{T}_n^{(3)} = \{\mathcal{T}^{16} \cup \mathcal{T}^{22} \cup \mathcal{T}^{23} \cup \mathcal{T}^{24} \cup \mathcal{T}^{25} \cup \mathcal{T}^{26}\}$ (see Figure 13).

By Lemma 6-7, we can verify that if $\mathcal{T} \in \mathcal{T}_n$ attains the minimum detour index of all graphs in $\mathcal{T}_n$, then $\widehat{\mathcal{T}} \in \mathcal{T}_n^{(3)}$.

Remark 3. In order to determine the tricyclic graphs which attain the minimum detour index of all graphs in $\mathcal{T}_n$, we just need to discuss the tricyclic graphs in $\mathcal{T}$, where $\widehat{\mathcal{T}} \in \mathcal{T}_n^{(3)} = \{\mathcal{T}^{16}, \mathcal{T}^{22}, \mathcal{T}^{23}, \mathcal{T}^{24}, \mathcal{T}^{25}, \mathcal{T}^{26}\}$ (see Figure 13).

3. Results and Discussion

From the discussions of Section 2, we can verify that if $\mathcal{T} \in \mathcal{T}_n$ attains the minimum detour index of all graphs in $\mathcal{T}_n$, then $\omega(\mathcal{T}) = \min\{\omega(G)\}$, where $\widehat{G} \in \mathcal{T}_n^{(3)} = \{\mathcal{T}^{16}, \mathcal{T}^{22}, \mathcal{T}^{23}, \mathcal{T}^{24}, \mathcal{T}^{25}, \mathcal{T}^{26}\}$.

Theorem 1. *Let $\mathcal{T}_n^{(3)}$ be defined as in Figure 13.*

(1) *When $n = 4$ or $n \geq 8$, $\mathcal{T}^{26}$ is the unique graph which attains the minimum detour index of all graphs in $\mathcal{T}_n$ and $\omega(\mathcal{T}^{26}) = n^2 + 4n - 14$.*

(2) *When $n = 5$ or $n = 6$, $\mathcal{T}^{25}$ is the unique graph which attains the minimum detour index of all graphs in $\mathcal{T}_n$ and $\omega(\mathcal{T}^{25}) = n^2 + 5n - 21$.*

(3) *When $n = 7$, $\mathcal{T}^{25}$ and $\mathcal{T}^{26}$ are the graphs which attain the minimum detour index of all graphs in $\mathcal{T}_n$ and $\omega(\mathcal{T}^{25}) = \omega(\mathcal{T}^{26}) = 63$.*

Proof. It can be checked directly that

$$\begin{aligned}&L(v_1 \mid \mathcal{T}^{16}) = n + 5; \\ &L(v_i \mid \mathcal{T}^{16}) = 3n - 1, \text{ where } 2 \leq i \leq 7; \\ &L(w \mid \mathcal{T}^{16}) = 2n + 3, \text{ where } w \in W_{v_1}.\end{aligned} \tag{29}$$

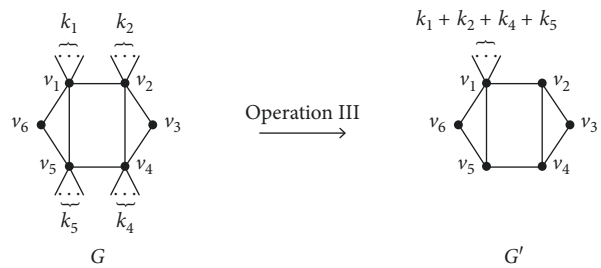

Figure 12: Operation IV on graph $G \in \mathcal{T}^{19}$.

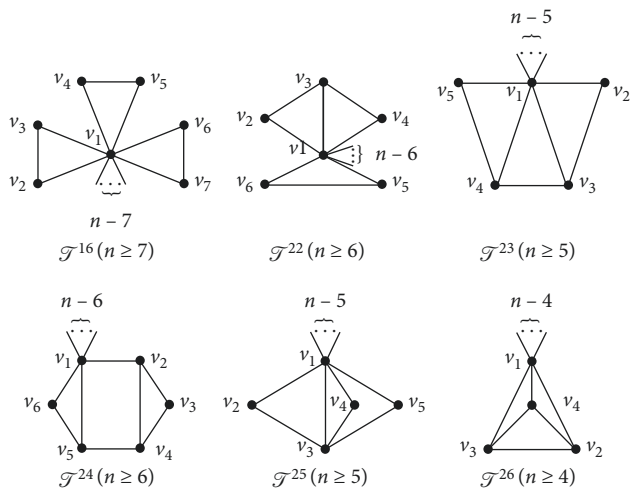

Figure 13: Graph $\mathcal{T}_n^{(3)}$.

Therefore,

$$\begin{aligned}\omega\left(\mathcal{T}^{16}\right) &= \frac{1}{2}\sum_{u\in V\left(\mathcal{T}^{16}\right)} L\left(u \mid \mathcal{T}^{16}\right)\\ &= \frac{1}{2}\left[(n+5)+6(3n-1)+(2n+3)(n-7)\right]\\ &= n^2+4n-11, \quad n\geq 7.\end{aligned} \tag{30}$$

Similarly, we have

$$\begin{aligned}\omega\left(\mathcal{T}^{22}\right) &= n^2+5n-15\\ &= n^2+4n+(n-15), \quad n\geq 6,\\ \omega\left(\mathcal{T}^{23}\right) &= n^2+8n-27\\ &= n^2+4n+(4n-27), \quad n\geq 5,\\ \omega\left(\mathcal{T}^{24}\right) &= n^2+15n-57\\ &= n^2+4n+(11n-57), \quad n\geq 6,\\ \omega\left(\mathcal{T}^{25}\right) &= n^2+5n-21\\ &= n^2+4n+(n-21), \quad n\geq 5,\\ \omega\left(\mathcal{T}^{26}\right) &= n^2+4n-14, \quad n\geq 4.\end{aligned} \tag{31}$$

(1) When $n = 4$ or $n \geq 8$, obviously, $\mathcal{T}^{26}$ is the unique graph which attains the minimum detour index of all graphs in $\mathcal{T}_n$ and $\omega(\mathcal{T}^{26}) = n^2 + 4n - 14$.

(2) When $n = 5$ or $n = 6$, obviously, $\mathcal{T}^{25}$ is the unique graph which attains the minimum detour index of all graphs in $\mathcal{T}_n$ and $\omega(\mathcal{T}^{25}) = n^2 + 5n - 21$.

(3) When $n = 7$, obviously, $\mathcal{T}^{25}$ and $\mathcal{T}^{26}$ are the graphs which attain the minimum detour index of all graphs in $\mathcal{T}_n$ and $\omega(\mathcal{T}^{25}) = \omega(\mathcal{T}^{26}) = 63$. □

4. Conclusions

Mathematical chemistry is an area of research in chemistry in which mathematical tools are used to solve problems of chemistry. Chemical graph theory is an important area of research in mathematical chemistry which deals with topology of molecular structures such as the mathematical study of isomerism and the development of topological descriptors or indices. In this paper, we first introduce some useful graph transformations, and then we determine the minimum detour index of all tricyclic graphs. In addition, all the corresponding extremal graphs are characterized.

Data Availability

The data used to support the findings of this study are available from the corresponding author upon request.

Conflicts of Interest

The authors declare no conflicts of interest regarding the content and implications of this manuscript.

Acknowledgments

This work was supported by the open project of Anhui University (no. KF2019A01), the Natural Science Research Foundation of the Department of Education of Anhui Province (no. KJ2019A0817), and the Project of Teaching Team of Chizhou University (no. 2016XJXTD02).

References

[1] W. Fang, H. Yu, Y. Gao, G. Jing, and Z. Li, "Maximum Balaban index and sum-Balaban index of tricyclic graphs," *MATCH Communications in Mathematical and in Computer Chemistry*, vol. 79, pp. 717–742, 2018.

[2] D. Wang, S. Tan, and L. Zhu, "On the lower and upper bounds for different indices of tricyclic graphs," *Journal of Applied Mathematics and Computing*, vol. 51, no. 1-2, pp. 1–11, 2016.

[3] F. Buckley and F. Harary, *Distance in Graphs*, Addison-Wesley, Reading, MA, USA, 1990.

[4] O. Ivanciuc and A. T. Balaban, "Design of topological indices—part 8: path matrices and derived molecular graph invariants," *MATCH Communications in Mathematical and in Computer Chemistry*, vol. 30, pp. 141–152, 1994.

[5] G. Rücker and C. Rücker, "Symmetry-aided computation of the detour matrix and the detour index," *Journal of Chemical Information and Computer Sciences*, vol. 38, no. 4, pp. 710–714, 1998.

[6] I. Lukovits, "The detour index," *Croatica Chemica Acta*, vol. 69, pp. 873–882, 1996.

[7] J.-B. Liu, M. Younas, M. Habib, M. Yousaf, and W. Nazeer, "M-Polynomials and degree-based topological indices of $VC_5C_7[p,q]$ and $HC_5C_7[p,q]$ nanotubes," *IEEE Access*, vol. 7, pp. 41125–41132, 2019.

[8] X. Qi and B. Zhou, "Minimum detour index of unicyclic graphs with given maximum degree," *Ars Combinatoria*, vol. 102, pp. 193–200, 2011.

[9] X. Qi, "Detour index of bicyclic graphs," *Utilitas Mathematica*, vol. 90, pp. 101–113, 2013.

[10] N. Trinajstić, S. Nikolić, B. Lŭcić, D. Amić, and Z. Mihalić, "The detour matrix in chemistry," *Journal of Chemical Information and Computer Sciences*, vol. 37, no. 4, pp. 631–638, 1997.

[11] J.-B. Liu, C. Wang, and S. Wang, "Zagreb indices and multiplicative zagreb indices of eulerian graphs," *Bulletin of the Malaysian Mathematical Sciences Society*, vol. 42, pp. 67–78, 2019.

[12] J.-B. Liu and X. F. Pan, "Minimizing Kirchhoffindex among graphs with a given vertex bipartiteness," *Applied Mathematics and Computation*, vol. 291, pp. 84–88, 2016.

[13] J.-B. Liu, J. Zhao, J. Min, and J. Cao, "On the Hosoya index of graphs formed by a fractal graph," *Fractals: Complex Geometry, Patterns, and Scaling in Nature and Society*, 2019.

[14] H. Deng, "On the Balaban index of trees," *MATCH Communications in Mathematical and in Computer Chemistry*, vol. 66, pp. 253–260, 2011.

[15] H. Deng, "On the sum-Balaban index," *MATCH Communications in Mathematical and in Computer Chemistry*, vol. 66, pp. 273–284, 2011.

[16] W. Fang, H. Yu, Y. Gao, G. Jing, Z. Li, and X. Li, "Minimum Detour index of cactus graphs," *Ars Combinatoria*, vol. 144, pp. 293–307, 2019.

Hindawi
Journal of Chemistry
Volume 2019, Article ID 8035204, 12 pages
https://doi.org/10.1155/2019/8035204

Research Article

Fast Model Predictive Control Based on Adaptive Alternating Direction Method of Multipliers

Yu Li,[1] **Qiming Zou**,[2] **Xiaoru Ji**,[1] **Chanyuan Zhang**,[1] **and Ke Lu**[1,3]

[1]*School of Management Science and Engineering, Anhui University of Technology, Ma'anshan, China*
[2]*School of Computer Science and Technology, Harbin Institute of Technology, Harbin, China*
[3]*School of Automation, Southeast University, Nanjing, China*

Correspondence should be addressed to Qiming Zou; qimingzou@aliyun.com and Ke Lu; luke.airoot@gmail.com

Received 29 July 2019; Accepted 6 September 2019; Published 30 September 2019

Guest Editor: Jia-Bao Liu

Model Predictive Control (MPC) can effectively handle control problem with disturbances, multicontrol variables, and complex constraints and is widely used in various control systems. In MPC, the control input at each time step is obtained by solving an online optimization problem, which will cause a time delay in real time on embedded computers with limited computational resources. In this paper, we utilize adaptive Alternating Direction Method of Multipliers (a-ADMM) to accelerate the solution of MPC. This method adaptively adjusts penalty parameter to balance the value of primal residual and dual residual. The performance of this approach is profiled via the control of a quadcopter with 12 states and 4 controls and prediction horizon ranging from 10 to 40. The simulation results demonstrate that the MPC based on a-ADMM has a significant improvement in real-time and convergence performance and thus is more suitable for solving large-scale optimal control problems.

1. Introduction

Model Predictive Control (MPC) [1, 2], a.k.a. receding horizon control, is a classical optimization-based control strategy for multivariable constrained systems. Since its appearance in the 1970s, MPC has been widely applied in a variety of areas, such as the transportation system [3, 4], grid system [5], and water distribution system [6]. MPC only utilizes the first element of the control input sequence obtained by solving an optimization problem. On the one hand, although receding horizon way makes MPC robust to model bias and external noises, MPC requires solving the optimization problem in each control cycle, which may cause a large time delay. On the other hand, low-complexity optimization algorithms have been motivated by the fact that several of these recent applications exploit microcontroller that has limited computing power [7–9].

For linear systems with a quadratic cost function and multiple linear constraints, MPC can be easily transformed into a standard quadratic programming (QP) form [10]. Therefore, off-the-shelf QP solvers can be used in this case. Most of them can be categorized into one of the two main classes, i.e., active-set and interior-point methods. Interior-point methods have become common choice for implementation because of its good convergence performance [11, 12]. However, it tends to demand significant online computation effort to compute the input. Recently, some modified methods have been proposed to reduce the computational complexity [13]. For example, Domahidi et al. decreased the computational burden by introducing a low-rank matrix forward substitution scheme and extended the interior-point methods to applications on low-cost embedded hardware. Compared to interior-point methods, active-set methods need on average substantially more iterations, but each iteration is computationally much cheaper and can be ward- or hot-start. For example, a parametric active-set algorithm for quadratic programming (qpOASES) is another commonly used QP solver which is applicable when numerous related QPs are solved sequentially, by exploiting the geometric property of state space [14].

Unfortunately, since qpOASES is an active-set-based method, it is limited to small- to medium-scale QP problem and sensitive to the external disturbance [14].

Aforementioned methods are centralized optimization algorithms, which are not appropriate for real-time large-scale applications on low-cost embedded computers. On the contrary, due to its success in solving large-scale optimization problems and pretty low computational complexity, distributed optimization algorithms have drawn increasing attention [15]. As a distributed optimization algorithm, Alternating Direction Method of Multipliers (ADMM) is a strong algorithm for solving convex optimization problems [16, 17]. ADMM was first introduced in the mid-1970s for the numerical solution of partial differential equations [18, 19] and particularly useful for solving optimization problems that are too large to be handled by generic optimization solvers. Because of its fast processing speed and good convergence performance, the method has been used in a large number of areas, such as compressed sensing [20], neural network [21], and image processing [22]. More details can be found in [17]. This wide range of applications has triggered a great interest in developing a better and more comprehensive understanding of the theoretical properties of ADMM.

ADMM has been proved to be an excellent fit for QP problems, since it can achieve linear convergence with strong convexity assumptions [23]. However, a drawback of ADMM is that the number of iterations required to converge is highly dependent on the step-size parameters. Unfortunately, analytic results for the optimal choice of penalty parameter are not available except for very special problems [24, 25]. In the special case of a strictly convex quadratic problem, criteria for choosing an optimal constant penalty have been recently proposed in [24, 26]. Although the optimal penalty parameter can significantly improve practical convergence, these methods make strong assumptions about the objective and constraint matrix. By introducing relaxation parameter, a method called relaxed ADMM uses past iterations to compute the current one. Instead of the fixed penalty parameter, Aybat and Iyengar [27] suggested using a penalty parameter sequence. Another different approach to the above methods is to accelerate ADMM by adaptively modifying the penalty parameter. As one of the adaptive ADMM methods, residual balancing (RB) [28] tunes penalty parameter to keep both residuals of similar magnitude. We borrow the idea from this method to further improve the convergence of ADMM combined with MPC.

In this paper, we utilize a-ADMM to efficiently solve the MPC problem, and the performance is verified by multiple simulation experiments. To be more specific, we transform the standard MPC problem into a distributed formulation and then take advantage of a-ADMM to solve this problem. We verified the method on an Unmanned Aerial Vehicle (UAV) control problem, and this mechanical control system includes 12 states and 4 control inputs [29]. We tested our method on different settings, i.e., the prediction horizon N ranges from 10 to 40. For each setting, MPC requires the solution of a QP with $(12+4)\times N$ variables and $(12+4)\times 2\times N$ inequality constraints. In this complex UAV control problem, a-ADMM algorithm achieves an absolute improvement of real-time response ability over conventional interior-point method and convergence performance over other ADMM variations.

The paper is organized as follows. Section 2 briefly introduces MPC, ADMM, and some ADMM variations. Section 3 describes the main procedures of the transformation from MPC to the distributed optimization problem and the application of a-ADMM in this specific problem. In Section 4, we compared the method with some baselines in the UAV control task. Finally, the conclusion is drawn and our future work is declared in Section 5. Appendix A describes how to formulate the QP problem of MPC in some details.

2. Backgrounds

2.1. Model Predictive Control. MPC is an optimal control approach which can handle multiple constraints on states and control inputs. Using a receding horizon control framework, MPC is robust to the model bias and external noises, which makes MPC fit well for highly complex multivariable industry processes.

In this paper, the following discrete-time linear time-invariant system is considered:

$$\mathcal{X}_{t+1} = A\mathcal{X}_t + B\mathcal{U}_t, \tag{1}$$

where $\mathcal{X}_t \in \mathbb{R}^n$ and $\mathcal{U}_t \in \mathbb{R}^m$ denote the state and control input, respectively, at time step t. $A \in \mathbb{R}^{n\times n}$ and $B \in \mathbb{R}^{n\times m}$ are the system and control matrices, respectively. For the regulation problem, at each time step t, MPC solves the finite horizon optimal control problem:

$$\min_{\mathcal{U}} \ \mathcal{X}_N^T P \mathcal{X}_N + \sum_{t=1}^{N-1} \left[\mathcal{X}_t^T Q \mathcal{X}_t + \mathcal{U}_t^T R \mathcal{U}_t\right], \tag{2a}$$

$$\text{s.t.} \quad \mathcal{X}_{t+k+1|t} = A\mathcal{X}_{t+k|t} + B\mathcal{U}_{t+k|t}, \quad k = 0, \ldots, N-1, \tag{2b}$$

$$\mathcal{X}_{\min} \le \mathcal{X}_{t+k|t} \le \mathcal{X}_{\max}, \quad k = 1, \ldots, N, \tag{2c}$$

$$\mathcal{U}_{\min} \le \mathcal{U}_{t+k|t} \le \mathcal{U}_{\max}, \quad k = 1, \ldots, N, \tag{2d}$$

$$\mathcal{X}_0 = \mathcal{X}_t, \tag{2e}$$

where N is the prediction horizon. $\mathcal{X}_{t+k|t}$ denotes the predicted state vector at time $t+k$, obtained by applying the input sequence $u_t, \ldots, u_{t+k-1}$. $\mathcal{X}_{\max} \in \mathbb{R}^n$ and $\mathcal{X}_{\min} \in \mathbb{R}^n$ define constraints on state variable $\mathcal{X}$, $\mathcal{U}_{\max} \in \mathbb{R}^m$ and $\mathcal{U}_{\min} \in \mathbb{R}^m$ define constraints on input variable $\mathcal{U}$. $P \in \mathbb{R}^{n\times n}$ and $Q \in \mathbb{R}^{n\times n}$ are stage and terminal matrices which penalize the state deviation at the end of the prediction horizon N and over the entire horizon, respectively. $R \in \mathbb{R}^{m\times m}$ is the cost matrix for the control inputs. Typically, $P \succeq 0$, $Q \succeq 0$, and $R \succ 0$.

In MPC, control inputs are obtained by solving open-loop optimal control problem (2a)–(2e) [10]. To be more specific, at each time step t, the optimization problem (2a)–(2e) is solved by taking the current state $\mathcal{X}_t$ as initial

state of the problem and generates a sequence of optimal control input. However, according to receding horizon framework of MPC, only the first element of the control input sequence is applied to the plant. The remaining solutions are culled, and optimal control problem with new initial state $\mathcal{X}_{t+1}$ will be solved again at the next time step $t+1$.

2.2. Alternating Direction Method of Multipliers. ADMM is a strong algorithm which can efficiently solve convex optimization problems, and it can decompose the global problem into several smaller and easy-to-solve local subproblems [30]. Because of its fast processing speed and good convergence performance, ADMM has received tremendous interest and approval for solving numerous problems in machine learning, statistics, and signal processing [17, 31–33].

ADMM can efficiently solve the optimization problems of the following standard form:

$$\min_{\mathcal{U}} \quad f(\mathcal{U}), \tag{3a}$$

$$\text{s.t.} \quad \mathcal{U} \in C, \tag{3b}$$

where f and C are convex. This problem can be rewritten in another form as

$$\min_{\mathcal{U},\mathcal{Z}} \quad f(\mathcal{U}) + g(\mathcal{Z}), \tag{4a}$$

$$\text{s.t.} \quad \mathcal{U} - \mathcal{Z} = 0, \tag{4b}$$

where g is the indicator function of C, $\mathcal{U}$ is primal variable, and $\mathcal{Z}$ is separate variable. The augmented Lagrangian is defined as

$$L_\rho(\mathcal{U},\mathcal{Z},c) = f(\mathcal{U}) + g(\mathcal{Z}) + \left(\frac{\rho}{2}\right)\left\|\mathcal{U} - \mathcal{Z} + c\right\|_2^2, \quad \rho > 0, \tag{5}$$

where ρ is the step size (or penalty parameter) and c is the scaled dual variable. The general augmented Lagrange multiplier method is to minimize L_ρ, w.r.t. $\mathcal{U}$ and $\mathcal{Z}$ at the same time. This is in difficulty and does not exploit the fact that the objective function is separable. To remedy this issue, ADMM decomposes the global problem (4) into two subproblems and minimizes $\mathcal{U}$ and $\mathcal{Z}$, respectively, with the following three steps:

$$\mathcal{U}^{k+1} := \arg\min\left(f(\mathcal{U}) + \frac{\rho}{2}\left\|\mathcal{U} - \mathcal{Z}^k + c^k\right\|_2^2\right), \tag{6a}$$

$$\mathcal{Z}^{k+1} := \arg\min\left(g(\mathcal{Z}) + \frac{\rho}{2}\left\|\mathcal{U}^{k+1} - \mathcal{Z} + c^k\right\|_2^2\right), \tag{6b}$$

$$c^{k+1} := c^k + \mathcal{U}^{k+1} - \mathcal{Z}^{k+1}. \tag{6c}$$

Under rather mild conditions, ADMM converges for any constant penalty parameter [34]. The convergence of ADMM is based on the primal and dual residuals:

$$\begin{aligned} r^k &= \mathcal{U}^k - \mathcal{Z}^k, \\ s^k &= -\rho\left(\mathcal{Z}^k - \mathcal{Z}^{k-1}\right). \end{aligned} \tag{7}$$

It has been observed that the algorithm approaches to the optimal solution when the primal and dual residuals approach to zero. Generally, the iterative process is terminated if

$$\left\|r^k\right\|_2 \le \sqrt{p}\varepsilon^{\text{abs}} + \varepsilon^{\text{rel}} \max\left\{\left\|\mathcal{U}^k\right\|_2, \left\|\mathcal{Z}^k\right\|_2\right\}, \tag{8a}$$

$$\left\|s^k\right\|_2 \le \sqrt{n}\varepsilon^{\text{abs}} + \varepsilon^{\text{rel}}\left\|(c\rho)^k\right\|_2, \tag{8b}$$

where $\varepsilon^{\text{abs}} > 0$ is absolute tolerance and $\varepsilon^{\text{rel}} > 0$ is relative tolerance. However, ρ has an immediate effect on the convergence element of the algorithm, and inappropriate tuning of this algorithm parameter may render the method moderative.

One way of accelerating the convergence properties of the algorithm is to utilize previous iterates when computing the following ones. This practical method is called relaxed Alternating Direction Method of Multipliers (r-ADMM) [35] that replaces $\mathcal{U}_{k+1}$ with $\alpha^k\mathcal{U}_{k+1} - (1-\alpha^k)\mathcal{Z}^k$ in the $\mathcal{Z}-$ and $c-$ updates (6a)–(6c), yielding

$$\mathcal{U}^{k+1} := \arg\min\left(f(\mathcal{U}) + \frac{\rho}{2}\left\|\mathcal{U} - \mathcal{Z}^k + c^k\right\|_2^2\right), \tag{9a}$$

$$\tilde{\mathcal{U}}^{k+1} := \alpha^k\mathcal{U}^{k+1} - \left(1-\alpha^k\right)\mathcal{Z}^k, \tag{9b}$$

$$\mathcal{Z}^{k+1} := \arg\min\left(g(\mathcal{Z}) + \frac{\rho}{2}\left\|\mathcal{U}^{k+1} - \mathcal{Z} + c^k\right\|_2^2\right), \tag{9c}$$

$$c^{k+1} := c^k + \mathcal{U}^{k+1} - \mathcal{Z}^{k+1}. \tag{9d}$$

The parameter $\alpha^k \in (0,2)$ is called the relaxation parameter. Note that letting $\alpha^k = 1$ for all k recovers the original ADMM iterations. Empirical studies have illustrated that overrelaxation, i.e., letting $\alpha^k > 1$, is often beneficial and the guideline $\alpha^k \in [1.5, 1.8]$ has been proposed [36].

Another approach for improving the convergence properties of the algorithm is to utilize different penalty parameters for each iteration. Adaptive Alternating Direction Method of Multipliers (a-ADMM) [28] is based on the following observation: increasing ρ^k strengthens the penalty term and leads to smaller primal residuals but larger dual ones; on the contrary, decreasing ρ^k results in smaller dual residuals and larger primal residuals. As both residuals must be small at convergence, it requires adjusting ρ to keep both primal residuals and dual residuals of the same magnitude. A simple and effective scheme for this purpose is as follows:

$$\rho^{k+1} := \begin{cases} \tau^{\text{incr}}\rho^k, & \text{if } \left\|r^k\right\|_2 > \mu\left\|s^k\right\|_2, \\ \dfrac{\rho^k}{\tau^{\text{decr}}}, & \text{if } \left\|s^k\right\|_2 > \mu\left\|r^k\right\|_2, \\ \rho^k, & \text{otherwise}, \end{cases} \tag{10}$$

where $\mu > 1$, $\tau^{\text{incr}} > 1$, and $\tau^{\text{decr}} > 1$. Using different penalty parameter ρ^k for each iteration k, a-ADMM can converge quickly and be insensitive to the initial penalty parameter. However, without a careful choice of μ, τ^{incr}, and τ^{decr}, this algorithm may fail to converge [28].

3. Fast MPC Based on Adaptive ADMM

3.1. Adaptive ADMM MPC. We focus on improving MPC by solving its QP problem with a-ADMM. In this work, the standard MPC problem is transformed into an equivalent QP problem which could be easily decomposed into several smaller local subproblems. And a-ADMM could be finally adopted to efficiently solve the resulting problem.

MPC problem ((2a)–(2e)) can be expressed as a QP problem when the system dynamic and constraints are linear and the cost function is quadratic [10]. Specifically, by substituting $\mathcal{X}_{t+k|t} = A^k \mathcal{X}_t + \sum_{j=0}^{k-1} A^j B \mathcal{U}_{t+k-1-j}$ into the cost function, the optimization problem equations (2a)–(2e) can be formulated as

$$\min_{\mathcal{U}} \quad \mathcal{U}^T H \mathcal{U} + \mathcal{X}_t^T C^T \mathcal{U} + \mathcal{X}_t^T Y \mathcal{X}_t, \tag{11a}$$

$$\text{s.t.} \quad G\mathcal{U} \le W + S\mathcal{X}_t, \tag{11b}$$

where $\mathcal{U} = [\mathcal{U}_t^T, \mathcal{U}_{t+1}^T, \ldots, \mathcal{U}_{t+N-1}^T]^T$ is the optimization vector and H, C, Y, G, W, and S are constant matrices that can be easily obtained offline. Note that H has to be positive definite for the convexity of this problem. The detailed process of this transformation is shown in Appendix A.

As the problem is determined by the current state $\mathcal{X}_t$, the implementation of MPC requires the online solution of problem ((11a) and (11b)) at each time step. Although off-the-shelf QP solvers, e.g., active-set methods [37] and interior-point methods [11], are available, it may demand significant computation effort in order to compute the input $\mathcal{U}_t$ online.

Fortunately, the QP problem (11a) and (11b) can be further transformed into ADMM standard form by introducing a split vector $\mathcal{Z}$ named slack vector (see [17]):

$$\min_{\mathcal{U},\mathcal{Z}} \quad f(\mathcal{U}) + g(\mathcal{Z}), \tag{12a}$$

$$\text{s.t.} \quad \mathcal{U} - \mathcal{Z} = 0, \tag{12b}$$

where $f(\mathcal{U}) = \mathcal{U}^T H \mathcal{U} + \mathcal{X}_t^T C^T \mathcal{U} + \mathcal{X}_t^T Y \mathcal{X}_t$ is the initial objective function with qualified domain and $g(\mathcal{Z}) = I(\mathcal{Z})$ is defined as the indicator function:

$$I(\mathcal{Z}) := \begin{cases} 0, & \text{if } G\mathcal{Z} \le W + S\mathcal{X}_t, \\ +\infty, & \text{otherwise.} \end{cases} \tag{13}$$

The augmented Lagrangian is defined as

$$L_\rho(\mathcal{U}, \mathcal{Z}, c) = f(\mathcal{U}) + g(\mathcal{Z}) + \left(\frac{\rho}{2}\right) \left\| \mathcal{U} - \mathcal{Z} + c \right\|_2^2, \quad \rho > 0, \tag{14}$$

where ρ is the penalty parameter and c is the dual parameter. We propose to solve problem (11a) and (11b) with a-ADMM as follows:

$$\mathcal{U}^{k+1} := \arg\min \left(\mathcal{U}^T H \mathcal{U} + \mathcal{X}_t^T C^T \mathcal{U} + \frac{\rho}{2} \left\| \mathcal{U} - \mathcal{Z}^k + \mathcal{C}^k \right\|_2^2 \right), \tag{15a}$$

$$\mathcal{Z}^{k+1} := \arg\min \left(I(\mathcal{Z}) + \frac{\rho}{2} \left\| \mathcal{U}^{k+1} - \mathcal{Z} + \mathcal{C}^k \right\|_2^2 \right), \tag{15b}$$

$$\mathcal{C}^{k+1} := \mathcal{C}^k + \mathcal{U}^{k+1} - \mathcal{Z}^{k+1}, \tag{15c}$$

where the penalty parameter ρ is a piecewise linear function as equation (10). As the optimizer $\mathcal{U}$ is only needed, the term involving Y is usually removed from problem (11a) and (11b). Since both residuals must be small at convergence, ρ is tuned to keep both residuals of similar magnitude.

3.2. Convergence Analysis of Adaptive ADMM-MPC. He et al. [28] proved that convergence is guaranteed for a-ADMM when either of the two following conditions is satisfied:

Condition 1 (bounded increasing):

$$\sum_{k=1}^{\infty} \left(\eta^k\right)^2 < \infty, \tag{16}$$

where $\eta^k = \sqrt{\max\{(\rho^k/\rho^k - 1), 1\} - 1}$.

Condition 2 (bounded decreasing):

$$\sum_{k=1}^{\infty} \left(\theta^k\right)^2 < \infty, \tag{17}$$

where $\theta^k = \sqrt{\max\{(\rho^k - 1/\rho^k), 1\} - 1}$.

Condition 1 (Condition 2) suggests that the increasement (decreasement) of adaptive penalty parameter is bounded.

Based on the above analysis, the framework of a-ADMM algorithm is portrayed in Algorithm 1.

4. Simulation Experiment

We evaluated our approach on an UAV control task. The dynamic model of UAV used in this experiment is from [29] and can be expressed as follows:

$$m\ddot{x} = -u \sin\theta - \beta\dot{x}, \tag{18a}$$

$$m\ddot{y} = u \cos\theta \sin\phi - \beta\dot{y}, \tag{18b}$$

$$m\ddot{z} = u \cos\theta \cos\phi - mg - \beta\dot{z}, \tag{18c}$$

$$\ddot{\theta} = \tilde{t}_\theta, \tag{18d}$$

$$\ddot{\phi} = \tilde{t}_\phi, \tag{18e}$$

$$\ddot{\psi} = \tilde{t}_\psi, \tag{18f}$$

where x, y, and z denote the position of the UAV and θ, ϕ, and ψ denote the rotation angle of the UAV around the Cartesian coordinate axis. The damping coefficient β takes into account the actual friction effect. This dynamic model has 12 states $\mathcal{X} \in \mathbb{R}^{12}$ and 4 control inputs $\mathcal{U} \in \mathbb{R}^4$. For the purpose of designing a appropriate MPC controller for UAV, the nonlinear dynamic model ((18a)–(18f)) is linearized at the equilibrium point (see [29]):

$$\begin{cases} \mathcal{X}_{t+1} = A\mathcal{X}_t + B\mathcal{U}_t, \\ \mathcal{Y}_t = C\mathcal{X}_t, \end{cases} \tag{19}$$

where $\mathcal{X}_t = [\theta, \phi, \psi, x, y, z, \dot{\theta}, \dot{\phi}, \dot{\psi}, \dot{x}, \dot{y}, \dot{z}]' \in \mathbb{R}^{12}$ is the state vector, $\mathcal{U}_t = [u, \tilde{t}_\theta, \tilde{t}_\phi, \tilde{t}_\psi] \in \mathbb{R}^4$ is the input vector, and $\mathcal{Y}_t \in \mathbb{R}^{12}$ is the output vector. Assuming that the UAV system is completely measurable, and the observation matrix C is a 12×12 identity matrix. The coefficient matrices A and B are as follows:

$$A = \begin{bmatrix} 1 & 0 & 0 & 0 & 0 & 0 & 0.1 & 0 & 0 & 0 & 0 & 0 \\ 0 & 1 & 0 & 0 & 0 & 0 & 0 & 0.1 & 0 & 0 & 0 & 0 \\ 0 & 0 & 1 & 0 & 0 & 0 & 0 & 0 & 0.1 & 0 & 0 & 0 \\ 0.0488 & 0 & 0 & 1 & 0 & 0 & 0.0016 & 0 & 0 & 0.0992 & 0 & 0 \\ 0 & -0.0488 & 0 & 0 & 1 & 0 & 0 & -0.0016 & 0 & 0 & 0.0992 & 0 \\ 0 & 0 & 0 & 0 & 0 & 1 & 0 & 0 & 0 & 0 & 0 & 0.0992 \\ 0 & 0 & 0 & 0 & 0 & 0 & 1 & 0 & 0 & 0 & 0 & 0 \\ 0 & 0 & 0 & 0 & 0 & 0 & 0 & 1 & 0 & 0 & 0 & 0 \\ 0 & 0 & 0 & 0 & 0 & 0 & 0 & 0 & 1 & 0 & 0 & 0 \\ 0.9734 & 0 & 0 & 0 & 0 & 0 & 0.0488 & 0 & 0 & 0.9846 & 0 & 0 \\ 0 & -0.9734 & 0 & 0 & 0 & 0 & 0 & -0.0488 & 0 & 0 & 0.9846 & 0 \\ 0 & 0 & 0 & 0 & 0 & 0 & 0 & 0 & 0 & 0 & 0 & 0.9846 \end{bmatrix},$$
$$B = \begin{bmatrix} 0 & -0.0726 & 0 & 0.0726 \\ -0.0726 & 0 & 0.0726 & 0 \\ -0.0152 & 0.0152 & -0.0152 & 0.0152 \\ 0 & -0.0006 & -0.0000 & 0.0006 \\ 0.0006 & 0 & -0.0006 & 0 \\ 0.0106 & 0.0106 & 0.0106 & 0.0106 \\ 0 & -1.4512 & 0 & 1.4512 \\ -1.4512 & 0 & 1.4512 & 0 \\ -0.3049 & 0.3049 & -0.3049 & 0.3049 \\ 0 & -0.0236 & 0 & 0.0236 \\ 0.0236 & 0 & -0.0236 & 0 \\ 0.2107 & 0.2107 & 0.2107 & 0.2107 \end{bmatrix}. \tag{20}$$

The baseline methods we compared in our experiments are as follows.

4.1. Interior-Point Method (IPM). IPM is the mostly used QP solver modeling the problem constraints as parametrized penalty functions which also referred to as barrier functions. At each iteration, an unconstrained optimization problem is solved for varying barrier function until the optimum is achieved.

4.2. qpOASES: a Parametric Active-Set Algorithm for Quadratic Programming. qpOASES is a very used QP solver which is applicable when numerous related QPs are solved sequentially, by exploiting the geometric property of state space [14].

4.3. Alternating Direction Method of Multipliers (ADMM). ADMM is a strong algorithm for solving convex optimization problems [16, 17] which decomposes the global

a-ADMM algorithm
Initialization: optimization variables $\mathcal{U}^0$, $\mathcal{Z}^0$, $\mathcal{C}^0$
While not converge by stopping criteria ((8a) and (8b)) and k¡maxiter **do**
  $\mathcal{U}^{k+1} := \arg\min(\mathcal{U}^T H \mathcal{U} + \mathcal{X}_t^T C^T \mathcal{U} + \rho/2\|\mathcal{U} - \mathcal{Z}^k + \mathcal{C}^k\|_2^2)$
  $\mathcal{Z}^{k+1} := \arg\min(I(\mathcal{Z}) + \rho/2\|\mathcal{U}^{k+1} - \mathcal{Z} + \mathcal{C}^k\|_2^2)$
  $\mathcal{C}^{k+1} := \mathcal{C}^k + \mathcal{U}^{k+1} - \mathcal{Z}^{k+1}$
  if $\|r^k\|_2 > \|s^k\|_2$
    $\rho^{k+1} = \tau^{\text{incr}}\rho^k$
  else if $\|s^k\|_2 > \|r^k\|_2$
    $\rho^{k+1} = \rho^k/\tau^{\text{decr}}$
  else $\rho^{k+1} = \rho^k$
  end if
  $k = k + 1$
end while
Output: optimal control input $\mathcal{U}^*$

Algorithm 1: a-ADMM algorithm framework.

problem into several smaller and easy-to-solve local subproblems [30].

4.4. Relaxed Alternating Direction Method of Multipliers (r-ADMM). r-ADMM is one of the variants of ADMM which introduces relaxation parameter α to relax the update of the optimal solution. Empirical studies have illustrated that overrelaxation is beneficial to the convergence [36].

We first fixed the prediction horizon $N = 10$ to find the optimal setting of ADMM and r-ADMM: the penalty parameter ρ and the relaxation parameter α. Figure 1 gives the results of different values of parameters. As can be seen, the average number of iterations depends significantly on the penalty parameter ρ and the relaxation parameter α. Based on this result, we simply set $\rho = 0.7$ and $\alpha = 1.5$ in the following experiments.

Similarly, we used the same control task to find the optimal setting of a-ADMM. According to the theory of a-ADMM, the relaxation parameter α is fixed and can be set $\alpha = 1.5$ based on previous results. However, different from ADMM, the penalty parameter ρ of a-ADMM is a piecewise linear function as equation (10) influenced by three other parameters, i.e., μ, τ^{incr}, and τ^{decr}. Figure 2 gives the results of different values of μ, τ^{incr}, and τ^{decr} on the UAV control task when the prediction horizon $N = 10$. Based on the lowest average iterations of each setting, we set $\mu = 10$, $\tau^{\text{incr}} = 2$, and $\tau^{\text{decr}} = 10$ in the following experiments, and the optimization variables $\mathcal{U}^0$, $\mathcal{Z}^0$, and $\mathcal{C}^0$ are all initialized to a zero vector, so that the initial strategy of optimization variables does not affect the performance comparison of these algorithms (IPM, qpOASES, ADMM, r-ADMM, and a-ADMM). The parameters of these algorithms are listed in Table 1.

The feedback loop controls the quadcopter to land on a platform located at coordinate position $(0, 0, 0)$. As shown in Figure 3, the closed-loop performance (including the feasibility and stability) of ADMM and a-ADMM is exactly the same. The reason is that, with the same absolute tolerance ε^{abs} and relative tolerance ε^{rel}, ADMM and a-ADMM converge to the same optimal solution leading to the same closed-loop performance.

Figure 4 gives our real-time performance of each method on the UAV control task. This figure shows the cumulative running time of our method and other baselines with the prediction horizon N ranging from 10 to 40. From the simulation results, it can be seen that, combined with MPC, ADMM and its variants significantly outperform custom QP solver, IPM, and qpOASES. With the increment of the task complexity, the running time of IPM and qpOASES increases obviously, while that of ADMM, r-ADMM, and a-ADMM basically remains unchanged.

As shown in Figure 4, there is not much difference in the cumulative running time of several variants of the ADMM algorithm. In this part, we aim to further investigate the difference in the cumulative number of iterations between them. Figure 5 portrays the cumulative iteration number of each method when the prediction horizon N ranging from 10 to 40. Apparently, although ADMM and its variations have the similar real-time performance, a-ADMM significantly outperforms all other baselines in terms of convergence performance under all the task settings. qpOASES proposes to move on a straight line in the state space when transitioning from the "old" QP problem to the "new" one. The reason why the cumulative iteration number of qpOASES stays stable after several time steps is mainly because the state of quadcopter has converged to the objective region, and the adjacent QP problem is quite similar.

5. Conclusions

In this paper, we utilize a-ADMM to accelerate the solution of MPC. We firstly transform the standard MPC problem into a distributed formulation and then take advantage of a-ADMM to solve this problem. We verified this method on an UAV control problem and compared a-ADMM with IPM, ADMM, and r-ADMM under different control settings, i.e., the prediction horizon N ranging from 10 to 40. The experimental results have shown that a-ADMM can greatly improve the effectiveness of MPC. As a future and

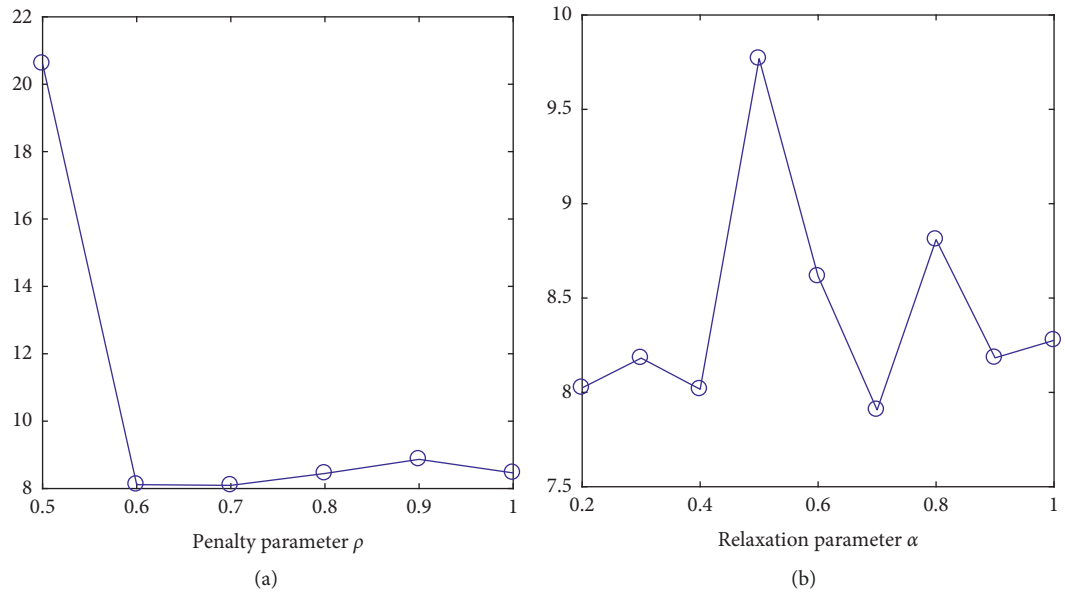

Figure 1: Effect of penalty parameter ρ of ADMM (a) and relaxation parameter α of r-ADMM (b) in terms of average number of iterations taken to converge. For each setting, algorithms are performed 50 times on the UAV control task ($N = 10$) with random initial states.

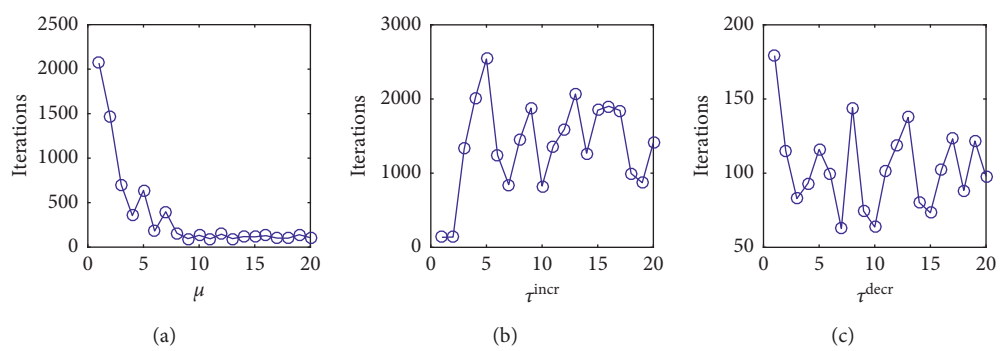

Figure 2: Effect of μ (a), τ^{incr}, (b) and τ^{decr} (c) in terms of average number of iterations taken to converge. For each setting, a-ADMM is performed 50 times on the UAV control task ($N = 10$) with random initial states.

Table 1: List of algorithmic parameters.

Parameters	IPM	qpOASES	ADMM	r-ADMM	a-ADMM
ρ	—	—	0.7	0.7	Adaptive
$\mathscr{U}^0$	0	0	0	0	0
$\mathscr{Z}^0$	0	0	0	0	0
$\mathscr{C}^0$	0	0	0	0	0
α	—	—	1	1.5	1
ε^{abs}	—	—	$1e-2$	$1e-2$	$1e-2$
ε^{rel}	—	—	$1e-4$	$1e-4$	$1e-4$
μ	—	—	—	—	10
τ^{incr}	—	—	—	—	2
τ^{decr}	—	—	—	—	10
Maxiter	1000	1000	1000	1000	1000

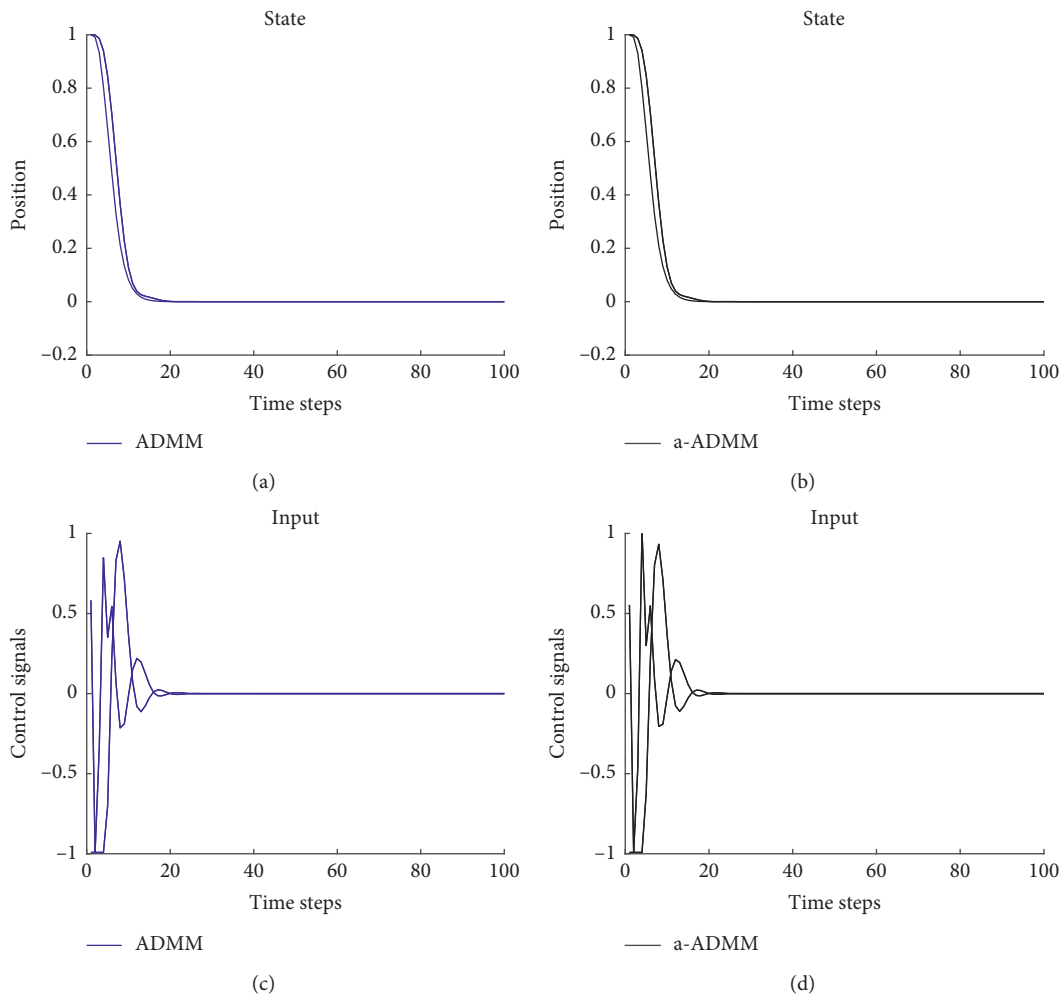

Figure 3: Closed-loop performance (running time on y-axis) versus number of time steps (time steps on x-axis) of ADMM and a-ADMM on UAV control task with $N = 10$.

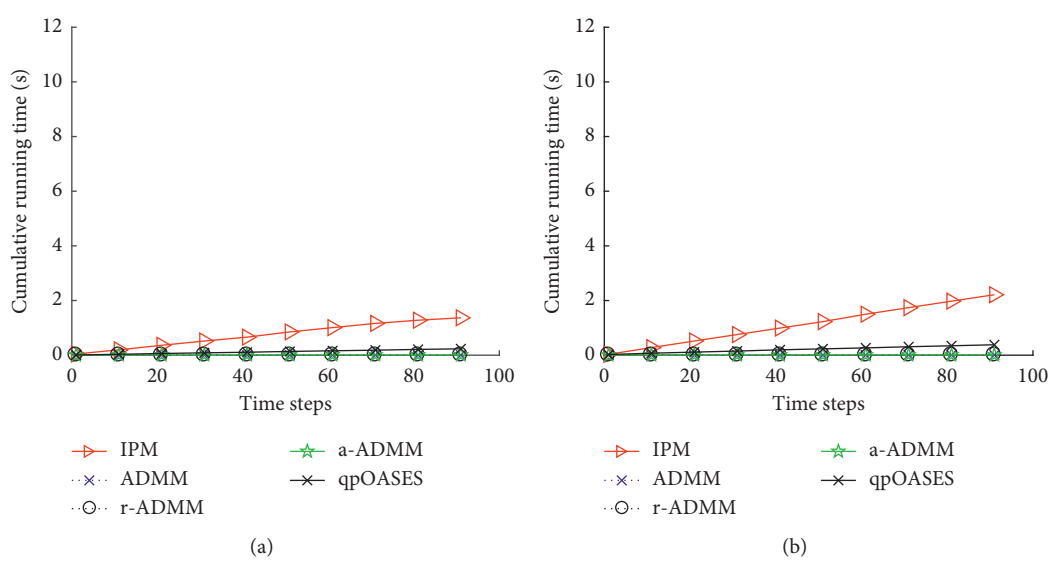

Figure 4: Continued.

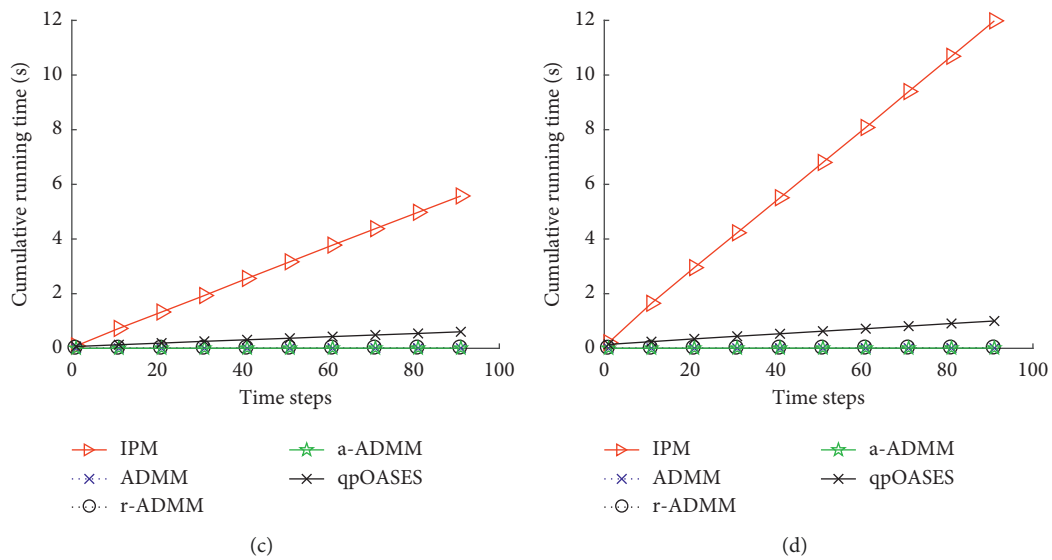

Figure 4: Real-time performance (running time on y-axis) versus number of time steps (time steps on x-axis) of IPM, qpOASES, ADMM, r-ADMM, and a-ADMM on UAV control task with N ranging from 10 to 40: (a) $N = 10$, (b) $N = 20$, (c) $N = 30$, and (d) $N = 40$.

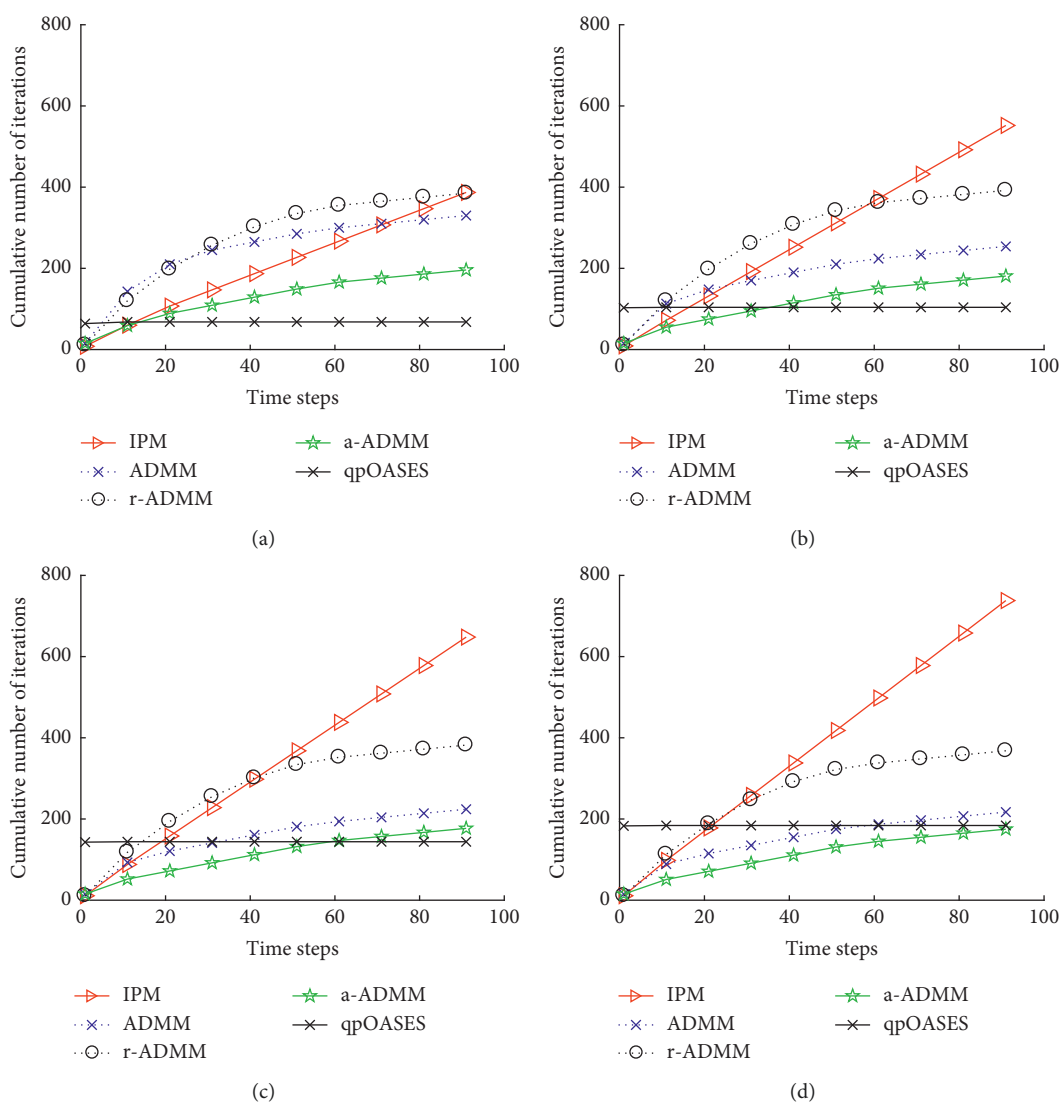

Figure 5: Convergence performance (cumulative number of iterations on y-axis) versus number of time steps (time steps on x-axis) of IPM, qpOASES, ADMM, r-ADMM, and a-ADMM on UAV control task with N ranging from 10 to 40: (a) $N = 10$, (b) $N = 20$, (c) $N = 30$, and (d) $N = 40$.

noteworthy research direction, one might provide better scheme for adaptively adjusting penalty parameter considering more complex constraints.

Appendix

A. Equivalent Representation of $\mathcal{X}_{t+k}$

The linear MPC problem can be expressed as QP problem by substituting $X_{t+k} = A^k\mathcal{X}_t + \sum_{j=0}^{k-1} A^j B\mathcal{U}_{t+k-1-j}$ into cost function. Firstly, we verified that $\mathcal{X}_{t+k}$ has an equivalent representation based on the following transformation:

$$\begin{aligned}
\mathcal{X}_{t+1} &= A\mathcal{X}_t + B\mathcal{U}_t,\\
\mathcal{X}_{t+2} &= A\mathcal{X}_{t+1} + B\mathcal{U}_{t+1}\\
&= A\left(A\mathcal{X}_t + B\mathcal{U}_t\right) + B\mathcal{U}_{t+1}\\
&= A^2\mathcal{X}_t + AB\mathcal{U}_t + B\mathcal{U}_{t+1},\\
\mathcal{X}_{t+3} &= A\mathcal{X}_{t+2} + B\mathcal{U}_{t+2}\\
&= A\left(A^2\mathcal{X}_t + AB\mathcal{U}_t + B\mathcal{U}_{t+1}\right) + B\mathcal{U}_{t+2}\\
&= A^3\mathcal{X}_t + A^2B\mathcal{U}_t + AB\mathcal{U}_{t+1} + B\mathcal{U}_{t+2}\\
&\cdots\\
&\cdots\\
\mathcal{X}_{t+k} &= A^k\mathcal{X}_t + \sum_{j=0}^{k-1} A^j B\mathcal{U}_{t+k-1-j}.
\end{aligned} \tag{A.1}$$

The conclusion can be deduced, $\mathcal{X}_{t+k} = A^k\mathcal{X}_t + \sum_{j=0}^{k-1} A^j B\mathcal{U}_{t+k-1-j}$. Having disposed of this preliminary step, we begin to prove the equivalent form of the objective function in Appendix B.

B. The Transformation of the Objective Function

Secondly, we transform the objective function into its equivalent form. As previously mentioned, the objective function can be casted into $\mathcal{U}^T H\mathcal{U} + 2\mathcal{X}_t^T C^T\mathcal{U} + \mathcal{X}_t^T Y\mathcal{X}_t$ by substituting $\mathcal{X}_{t+k} = A^k\mathcal{X}_t + \sum_{j=0}^{k-1} A^j B\mathcal{U}_{t+k-1-j}$, and the formula is derived as follows:

$$\begin{aligned}
\mathcal{X}_{t+k} &= A^k\mathcal{X}_t + \sum_{j=0}^{k-1} A^i B\mathcal{U}_{t+k-1-i}, \quad k = 1, 2, \ldots, N\\
&= A^k\mathcal{X}_t + A^{k-1}B\mathcal{U}_t + A^{k-2}B\mathcal{U}_{t+1} + \cdots + AB\mathcal{U}_{t+N-2}\\
&\quad + B\mathcal{U}_{t+N-1},
\end{aligned} \tag{A.2}$$

Set $T_k = [A^{k-1}B, A^{k-2}B, \ldots, B]$ and $\mathcal{U} = [\mathcal{U}_t, \mathcal{U}_{t+1}, \ldots, \mathcal{U}_{t+N-1}]$, and $A^{k-1}B\mathcal{U}_t + A^{k-2}B\mathcal{U}_{t+1} + \cdots + AB\mathcal{U}_{t+N-2} + B\mathcal{U}_{t+N-1}$ can be expressed as $T_k\mathcal{U}$ consequently,

$$\begin{aligned}
\mathcal{X}_{t+k} &= A^k\mathcal{X}_t + T_k\mathcal{U},\\
\mathcal{X}_{t+k}^T &= \mathcal{X}_t^T\left(A^k\right)^T + \mathcal{U}^T T_k^T,\\
\mathcal{X}_{t+k}^T Q\mathcal{X}_{t+k} &= \left(\mathcal{X}_t^T\left(A^k\right)^T + \mathcal{U}^T T_k^T\right)Q\left(A^k\mathcal{X}_t + T_k\mathcal{U}\right)\\
&= \left(\mathcal{X}_t^T\left(A^k\right)^T Q + \mathcal{U}^T T_k^T Q\right)\left(A^k\mathcal{X}_t + T_k\mathcal{U}\right)\\
&= \mathcal{X}_t^T\left(A^k\right)^T QA^k\mathcal{X}_t + \mathcal{X}_t^T\left(A^k\right)^T QT_k\mathcal{U} + \mathcal{U}^T T_k^T QA^k\mathcal{X}_t + \mathcal{U}^T T_k^T QT_k\mathcal{U}\\
&= \mathcal{X}_t^T\left(A^k\right)^T QA^k\mathcal{X}_t + 2\mathcal{X}_t^T\left(A^k\right)^T QT_k\mathcal{U} + \mathcal{U}^T T_k^T QT_k\mathcal{U}\\
&= \mathcal{X}_t^T y\mathcal{X}_t + 2\mathcal{X}_t^T c\mathcal{U} + U^T h\mathcal{U},
\end{aligned} \tag{A.3}$$

where

$$\begin{cases}
y = \left(A^k\right)^T QA^k,\\
c = \left(A^k\right)^T QT_k,\\
h = T_k^T QT_k,
\end{cases} \tag{A.4}$$

In a similar way, $\mathcal{X}_N^T P\mathcal{X}_N$ can be rewritten and finally obtained as

$$J\left(\mathcal{U}, \mathcal{X}_t\right) = \mathcal{U}^T H\mathcal{U} + 2\mathcal{X}_t^T C^T\mathcal{U} + \mathcal{X}_t^T Y\mathcal{X}_t, \tag{A.5}$$

where

$$\begin{aligned}
Y &= \sum_{k=0}^{N-1}\left(A^k\right)^T QA^k + \left(A^N\right)^T PA^N,\\
C &= \sum_{k=0}^{N-1}\left(A^k\right)^T QT_k + \left(A^N\right)^T PT^N,\\
H &= \sum_{k=0}^{N-1} T_k^T QT_k + T_N^T PT_N + M,\\
\mathbf{M} &= \begin{pmatrix} R & & \\ & \ddots & \\ & & R \end{pmatrix}.
\end{aligned} \tag{A.6}$$

C. The Transformation of Constraints

The last part is about the transformation of constraints, and the formula is derived as follows:

$$\begin{aligned} \mathcal{X}_{\min} \le \mathcal{X}_{t+k|t} \le \mathcal{X}_{\max}, \quad k = 0, \ldots, N-1, \\ \mathcal{U}_{\min} \le \mathcal{U}_{t+k|t} \le \mathcal{U}_{\max}, \quad k = 0, \ldots, N-1. \end{aligned} \tag{A.7}$$

By substituting $\mathcal{X}_{t+k} = A^k \mathcal{X}_t + \sum_{j=0}^{k-1} A^j B \mathcal{U}_{t+k-1-j}$, the constraints are equivalent to $G\mathcal{U} \le W + S\mathcal{X}_t$ through the following process:

$$\begin{cases} T_k = \left[A^{k-1}B, A^{k-2}B, \ldots, B\right], \\ \mathcal{X}_{t+k} = A^k \mathcal{X}_t + T_k \mathcal{U} \\ \mathcal{U}_k = \left[\mathcal{U}_t, \mathcal{U}_{t+1}, \ldots, \mathcal{U}_{t+N-1}\right], \end{cases} \tag{A.8}$$

$$\mathcal{X}_{\min} \le \mathcal{X}_{t+k} \le \mathcal{X}_{\max}. \tag{A.9}$$

By substituting formula (A.8) into formula (A.9), we obtain

$$\mathcal{X}_{\min} \le A^k \mathcal{X}_t + T_k \mathcal{U} \le \mathcal{X}_{\max}. \tag{A.10}$$

The solution of $\mathcal{U}$ is obtained as follows:

$$T_k^{-1}\left(\mathcal{X}_{\min} - A^k \mathcal{X}_t\right) \le \mathcal{U} \le T_k^{-1}\left(\mathcal{X}_{\max} - A^k \mathcal{X}_t\right). \tag{A.11}$$

That is,

$$\begin{cases} \mathcal{U}_k \le T_k^{-1} \mathcal{X}_{\max} - T_k^{-1} A^k \mathcal{X}_t, \\ -\mathcal{U}_k \le -T_k^{-1} \mathcal{X}_{\min} + T_k^{-1} A^k \mathcal{X}_t. \end{cases} \tag{A.12}$$

Formula (A.12) is equivalent to

$$G\mathcal{U} \le W + S\mathcal{X}_t, \tag{A.13}$$

where

$$\begin{cases} G = [1, -1]^T, \\ W = T_k^{-1} \otimes \left[\mathcal{X}_{\max}, \mathcal{X}_{\min}\right]^T, \\ E = \left[T_k^{-1} A^k, T_k^{-1} A^k\right]^T. \end{cases} \tag{A.14}$$

Data Availability

We use simulation data, and our model and related hyperparameter are provided in our paper.

Conflicts of Interest

The authors declare that they have no conflicts of interest.

Acknowledgments

This work was jointly supported by the National Natural Science Foundation of China (11871077), the Natural Science Foundation of Anhui Province (1808085MA04), and the Natural Science Foundation of Department of Education of Anhui Province (KJ2017A362).

References

[1] A. Bemporad, M. Morari, V. Dua, and E. N. Pistikopoulos, "The explicit linear quadratic regulator for constrained systems," *Automatica*, vol. 38, no. 1, pp. 3–20, 2002.

[2] Y.-G. Xi, D.-W. Li, and S. Lin, "Model predictive control—status and challenges," *Acta Automatica Sinica*, vol. 39, no. 3, pp. 222–236, 2013.

[3] M. Burger, M. van den Berg, A. Hegyi, B. De Schutter, and J. Hellendoorn, "Considerations for model-based traffic control," *Transportation Research Part C: Emerging Technologies*, vol. 35, pp. 1–19, 2013.

[4] K. Lu, P. P. Du, J. D. Cao, Q. Zou, T. He, and W. Huang, "A novel traffic signal split approach based on explicit model predictive control," *Mathematics and Computers in Simulation*, vol. 155, pp. 105–114, 2019.

[5] K. Samir, C. Patricio, R. Vargas, U. Ammann, and J. Rodriguez, "Model predictive control–a simple and powerful method to control power converters," *IEEE Transactions on Industrial Electronics*, vol. 56, no. 6, pp. 1826–1838, 2009.

[6] L. Zhang, M. Pan, and S. Quan, "Model predictive control of water management in PEMFC," *Journal of Power Sources*, vol. 180, no. 1, pp. 322–329, 2008.

[7] G. Valencia-Palomo, J. A. Rossiter, and F. R. López-Estrada, "Improving the feed-forward compensator in predictive control for setpoint tracking," *ISA Transactions*, vol. 53, no. 3, pp. 755–766, 2014.

[8] G. Valencia-Palomo and J. A. Rossiter, "Efficient suboptimal parametric solutions to predictive control for PLC applications," *Control Engineering Practice*, vol. 19, no. 7, pp. 732–743, 2011.

[9] B. Huyck, J. De Brabanter, B. De Moor, J. F. Van Impe, and F. Logist, "Online model predictive control of industrial processes using low level control hardware: a pilot-scale distillation column case study," *Control Engineering Practice*, vol. 28, pp. 34–48, 2014.

[10] A. Bemporad, "Model predictive control design: new trends and tools," in *Proceedings of the 45th IEEE Conference on Decision and Control*, pp. 6678–6683, San Diego, CA, USA, December 2006.

[11] A. Domahidi, A. U. Zgraggen, M. N. Zeilinger, M. Morari, and C. N. Jones, "Efficient interior point methods for multistage problems arising in receding horizon control," in *Proceedings of the 2012 IEEE 51st IEEE Conference on Decision and Control (CDC)*, pp. 668–674, Maui, HI, USA, December 2012.

[12] B. Stellato, G. Banjac, P. Goulart, A. Bemporad, and S. Boyd, "OSQP: an operator splitting solver for quadratic programs," in *Proceedings of the UKACC 12th International Conference on Control*, p. 339, Sheffield, UK, September 2018.

[13] F. A. Potra and S. J. Wright, "Interior-point methods," *Journal of Computational and Applied Mathematics*, vol. 124, no. 1-2, pp. 281–302, 2000.

[14] H. J. Ferreau, C. Kirches, A. Potschka, H. G. Bock, and M. Diehl, "qpOASES: a parametric active-set algorithm for quadratic programming," *Mathematical Programming Computation*, vol. 6, no. 4, pp. 327–363, 2014.

[15] P. D. Christofides, R. Scattolini, D. Muñoz de la Peña, and J. Liu, "Distributed model predictive control: a tutorial review and future research directions," *Computers & Chemical Engineering*, vol. 51, pp. 21–41, 2013.

[16] V. Sindhwani, R. Roelofs, and M. Kalakrishnan, "Sequential operator splitting for constrained nonlinear optimal control," in *Proceedings of the American Control Conference 2017*, pp. 4864–4871, Seattle, WA, USA, May 2017.

[17] S. Boyd, N. Parikh, E. Chu, B. Peleato, and J. Eckstein, "Distributed optimization and statistical learning via the alternating direction method of multipliers," *Foundations and Trends in Machine Learning*, vol. 3, no. 1, pp. 1–122, 2011.

[18] J. M. Bioucas-Dias and M. A. T. Figueiredo, "Alternating direction algorithms for constrained sparse regression: application to hyperspectral unmixing," in *Proceedings of the 2nd Workshop on Hyperspectral Image and Signal Processing: Evolution in Remote Sensing*, pp. 1–4, Reykjavik, Iceland, June 2010.

[19] M. A. T. Figueiredo and J. M. Bioucas-Dias, "Restoration of poissonian images using alternating direction optimization," *IEEE Transactions on Image Processing*, vol. 19, no. 12, pp. 3133–3145, 2010.

[20] C. Zhao, R. Wang, and G. Wen, "Better and faster, when ADMM meets CNN: compressive-sensed image reconstruction," in *Advances in Multimedia Information Processing—PCM 2017*, Springer, Cham, Switzerland, 2017.

[21] A. Samaneh, F. Jiashi, J. Stefanie, and D. Trevor, "Auxiliary image regularization for deep cnns with noisy labels," 2015, http://arxiv.org/abs/1511.07069.

[22] J. H. R. Chang, C. L. Li, B. Poczos, B. V. K. Vijaya Kumar, and A. C. Sankaranarayanan, "One network to solve them all—solving linear inverse problems using deep projection models," in *Proceedings of the 2017 IEEE International Conference on Computer Vision*, Venice, Italy, October 2017.

[23] D. Boley, "Local linear convergence of the alternating direction method of multipliers on quadratic or linear programs," *SIAM Journal on Optimization*, vol. 23, no. 4, pp. 2183–2207, 2013.

[24] A. U. Raghunathan and S. D. Cairano, "Alternating direction method of multipliers for strictly convex quadratic programs: optimal parameter selection," in *Proceedings of the American Control Conference*, pp. 4324–4329, Washington, DC, USA, June 2014.

[25] A. U. Raghunathan and S. D. Cairano, "Optimal step-size selection in alternating direction method of multipliers for convex quadratic programs and model predictive control," in *Proceedings of the Symposium on Mathematical Theory of Networks and Systems*, pp. 807–814, Beer Sheva, Israel, June 2014.

[26] E. Ghadimi, A. Teixeira, I. Shames, and M. Johansson, "Optimal parameter selection for the alternating direction method of multipliers (ADMM): quadratic problems," *IEEE Transactions on Automatic Control*, vol. 60, no. 3, pp. 644–658, 2015.

[27] N. S. Aybat and G. Iyengar, "An alternating direction method with increasing penalty for stable principal component pursuit," *Computational Optimization and Applications*, vol. 61, no. 3, pp. 635–668, 2015.

[28] B. S. He, H. Yang, and S. L. Wang, "Alternating direction method with self-adaptive penalty parameters for monotone variational inequalities," *Journal of Optimization Theory and Applications*, vol. 106, no. 2, pp. 337–356, 2000.

[29] A. Bemporad, C. A. Pascucci, and C. Rocchi, "Hierarchical and hybrid model predictive control of quadcopter air vehicles," *IFAC Proceedings Volumes*, vol. 42, no. 17, pp. 14–19, 2009.

[30] P. Giselsson and S. Boyd, "Linear convergence and metric selection for douglas-rachford splitting and ADMM," *IEEE Transactions on Automatic Control*, vol. 62, no. 2, pp. 532–544, 2017.

[31] N. Liu and J. Wang, "Energy sharing for interconnected microgrids with a battery storage system and renewable energy sources based on the alternating direction method of multipliers," *Applied Sciences*, vol. 8, no. 4, p. 590, 2018.

[32] L. Wang, Y. Chen, F. Lin, Y. Chen, F. Yu, and Z. Cai, "Impulse noise denoising using total variation with overlapping group sparsity and Lp-pseudo-norm shrinkage," *Applied Sciences*, vol. 8, no. 11, p. 2317, 2018.

[33] C. Manss and D. Shutin, "Global-entropy driven exploration with distributed models under sparsity constraints," *Applied Sciences*, vol. 8, no. 10, p. 1722, 2018.

[34] G. Euhanna, T. André, S. Iman, and J. Mikael, "Optimal parameter selection for the alternating direction method of multipliers (ADMM): quadratic problems," *IEEE Transactions on Automatic Control*, vol. 60, no. 3, pp. 644–658, 2015.

[35] J. Eckstein and D. P. Bertsekas, "On the Douglas-Rachford splitting method and the proximal point algorithm for maximal monotone operators," *Mathematical Programming*, vol. 55, no. 1–3, pp. 293–318, 1992.

[36] J. Eckstein and M. C. Ferris, "Operator-splitting methods for monotone affine variational inequalities, with a parallel application to optimal control," *INFORMS Journal on Computing*, vol. 10, no. 2, pp. 218–235, 1998.

[37] K. Scheinberg, "An efficient implementation of an active set method for SVMs," *Journal of Machine Learning Research*, vol. 7, pp. 2237–2257, 2006.

Hindawi
Journal of Chemistry
Volume 2019, Article ID 8517548, 6 pages
https://doi.org/10.1155/2019/8517548

Research Article

Theoretical Researches about $\mathfrak{u}$-Maximal Subgroups and Its Applications in Charactering $\mathrm{Int}_{\mathfrak{u}}(G)$

Li Zhang[1] and Zheng-Qun Cai[2]

[1]*School of Mathematics and Physics, Anhui Jianzhu University, Hefei 230601, China*
[2]*School of Foreign Studies, Anhui Jianzhu University, Hefei 230601, China*

Correspondence should be addressed to Zheng-Qun Cai; caizhengqun1983@163.com

Received 11 July 2019; Accepted 23 August 2019; Published 16 September 2019

Guest Editor: Shaohui Wang

Let G be a finite group and $\mathfrak{u}$ be the class of all finite supersoluble groups. A supersoluble subgroup U of G is called $\mathfrak{u}$-maximal in G if for any supersoluble subgroup V of G containing U, $V = U$. Moreover, $\mathrm{Int}_{\mathfrak{u}}(G)$ is the intersection of all $\mathfrak{u}$-maximal subgroups of G. This paper obtains some new criteria on $\mathrm{Int}_{\mathfrak{u}}(G)$, by assuming that some subgroups of G are either Φ-I-supplemented or Φ-I-embedded in G. Here, a subgroup H of G is called Φ-I-supplemented in G if there exists a subnormal subgroup T of G such that $G = HT$ and $(H \cap T)H_G/H_G \leq \Phi(H/H_G)\mathrm{Int}_{\mathfrak{u}}(G)$ and Φ-I-embedded in G if there exists a S-quasinormal subgroup T of G such that HT is S-quasinormal in G and $(H \cap T)H_G/H_G \leq \Phi(H/H_G)\mathrm{Int}_{\mathfrak{u}}(G)$.

1. Introduction

As we know, the model of chemical substances, such as crystal, is a graph, whose change process can be represented by symmetric groups or others. Therefore, group theory plays an important role in chemistry and physics ([1, 2]). However, this paper focuses on a question in group theory, which will promote its development and, consequently, contribute chemistry and physics in many ways.

Throughout this paper, all groups are finite. G always denotes a group, p denotes a prime, and $\pi(G)$ is the set of all prime divisors of $|G|$. All unexplained notation and terminology are standard, as in [3, 4, 5].

Recall that a class $\mathfrak{F}$ of groups is called a formation if $\mathfrak{F}$ is closed under taking homomorphic images and subdirect products. A formation $\mathfrak{F}$ is said to be (1) saturated, if $G \in \mathfrak{F}$ whenever $G/\Phi(G) \in \mathfrak{F}$ and (2) hereditary, if $H \in \mathfrak{F}$ whenever $H \leq G \in \mathfrak{F}$. Following ([3], Chap. III, Definition 3.1), a subgroup U of G is called $\mathfrak{F}$-maximal in G provided that (1) $U \in \mathfrak{F}$ and (2) if $U \leq V \leq G$ and $V \in \mathfrak{F}$, then $U = V$. Moreover, $\mathrm{Int}_{\mathfrak{F}}(G)$ [6] denotes the intersection of all $\mathfrak{F}$-maximal subgroups of G. As we know, the $\mathfrak{F}$-hypercentre $Z_{\mathfrak{F}}(G)$ of G is the largest normal subgroup of G such that each G-chief factor H/K below $Z_{\mathfrak{F}}(G)$ satisfies $H/K \rtimes G/C_G(H/K) \in \mathfrak{F}$. Clearly, $Z_{\mathfrak{F}}(G) \leq \mathrm{Int}_{\mathfrak{F}}(G)$ for any group G (see ([6], Theorem C)).

Let $\mathfrak{F}$ be a hereditary saturated formation and N be a normal subgroup of G contained in $Z_{\mathfrak{F}}(G)$. Then, the following holds (1) $AN \in \mathfrak{F}$ for any subgroup A of G with $A \in \mathfrak{F}$ and (2) $T \in \mathfrak{F}$ for any subgroup T of G with $T/N \in \mathfrak{F}$. It is well known that the extensive applications of $\mathfrak{F}$-hypercentral subgroups are based on the above properties, and there are two main topics about $\mathfrak{F}$-hypercentre: (1) the influence of $\mathfrak{F}$-hypercentral subgroups on the structure of finite groups; (2) the criteria of $\mathfrak{F}$-hypercentral subgroups.

However, in [6], Theorem C shows that the above two properties still hold when $N \leq \mathrm{Int}_{\mathfrak{F}}(G)$, instead of the stronger condition $N \leq Z_{\mathfrak{F}}(G)$. Therefore, it would be rather natural and of great significance to study $\mathrm{Int}_{\mathfrak{F}}(G)$. In fact, some recent results in this topic can be found in, for example, [6, 7, 8–12]. Particularly, in [6, 10], the authors have shown that $Z_{\mathfrak{u}}(G) < \mathrm{Int}_{\mathfrak{u}}(G)$ in general, given the condition under which $Z_{\mathfrak{u}}(G) = \mathrm{Int}_{\mathfrak{u}}(G)$ holds for every group G.

In connection with the topic of $Z_{\mathfrak{u}}(G)$, a question naturally arises as follows:

Question 1. Can we give a condition under which a normal subgroup of G is contained in $\mathrm{Int}_{\mathfrak{u}}(G)$?

In [9], Chen et al. gave some conditions under which a normal subgroup of G contained in $\mathrm{Int}_{\mathfrak{u}}(G)$. In this paper, we still pay attention to Question 1. Furthermore, we explore new criteria by the help of the following notion.

Definition 1. Let H be a subgroup of a group G. Then, H is called

(1) Φ-I-supplemented in G if there exists a subnormal subgroup T of G such that $G = HT$ and $(H \cap T)H_G/H_G \leq \Phi(H/H_G)\mathrm{Int}_{\mathfrak{u}}(G/H_G)$

(2) Φ-I-embedded in G if there exists a S-quasinormal subgroup T of G such that HT is S-quasinormal in G and $(H \cap T)H_G/H_G \leq \Phi(H/H_G)\mathrm{Int}_{\mathfrak{u}}(G/H_G)$

Our main results are the following:

Theorem 1. *Let E be a normal subgroup of G. For every prime $p \in \pi(E)$ and every noncyclic Sylow p-subgroup P of E, assume that all maximal subgroups of P are either Φ-I-supplemented or Φ-I-embedded in G. Then $E \leq Int_{\mathfrak{u}}(G)$.*

Theorem 2. *Let E be a normal subgroup of G. For every prime $p \in \pi(E)$ and every noncyclic Sylow P-subgroup P of E, assume that all cyclic subgroups of P with order P and 4 (when P is a nonabelian 2-group) are either Φ-I-supplemented or Φ-I-embedded in G. Then, $E \leq Int_{\mathfrak{u}}(G)$.*

2. Preliminaries

Lemma 1 (see [13], Chapter 1 or [4], Chapter 1, Lemmas 5.34 and 5.35]). *Assume that H is a subgroup of G, $E \leq G$, and $N \trianglelefteq G$.*

(1) If H is S-quasinormal in G, then $H \cap E$ is S-quasinormal in E

(2) If H is S-quasinormal in G, then HN/N is S-quasinormal in G/N

(3) Assume that H is a p-group, then H is S-quasinormal in G if and only if $O^p(G) \leq N_G(H)$

(4) The set of S-quasinormal subgroups of G is a sublattice of the subnormal subgroup lattice of G

(5) If H is S-quasinormal in G, then H^G/H_G is nilpotent

(6) If H is a π-group and H is subnormal in G, then $H \leq O_\pi(G)$

Lemma 2 ([6], Theorem C). *Let $\mathfrak{F}$ be a nonempty hereditary saturated formation. Assume that H, E, and N are subgroups of G with $N \trianglelefteq G$.*

(1) $\mathrm{Int}_{\mathfrak{F}}(H)N/N \leq \mathrm{Int}_{\mathfrak{F}}(HN/N)$

(2) $\mathrm{Int}_{\mathfrak{F}}(H) \cap E \leq \mathrm{Int}_{\mathfrak{F}}(H \cap E)$

(3) If $H/H \cap \mathrm{Int}_{\mathfrak{F}}(G) \in \mathfrak{F}$, then $H \in \mathfrak{F}$

(4) If $N \leq \mathrm{Int}_{\mathfrak{F}}(G)$, then $\mathrm{Int}_{\mathfrak{F}}(G/N) = \mathrm{Int}_{\mathfrak{F}}(G)/N$

(5) $Z_{\mathfrak{F}}(G) \leq \mathrm{Int}_{\mathfrak{F}}(G)$

Lemma 3. *Assume that H is a Φ-I-supplemented (resp., Φ-I-embedded) subgroup of G.*

(1) If N is a normal subgroup of G satisfying either $N \leq H$ or $(|H|, |N|) = 1$, then HN/N is Φ-I-supplemented (resp., Φ-I-embedded) in G/N

(2) If K is a subgroup of G containing H, then H is Φ-I-supplemented (resp., Φ-I-embedded) in K

Proof. As the proof for Φ-I-embedded subgroups is similar, we just assume that H is Φ-I-supplemented in G. Then, G has a subnormal subgroup T such that $G = HT$ and $(H \cap T)H_G/H_G \leq \Phi(H/H_G)\mathrm{Int}_{\mathfrak{u}}(G/H_G)$.

(1) Clearly, TN/N is a subnormal subgroup of G such that $G/N = HN/N \cdot TN/N$. Consider $HN \cap TN$. If $N \leq H$, then $H \cap TN = (H \cap T)N$ by the modular law. Assume that $(|H|, |N|) = 1$. Then $(|HN \cap T : H \cap T|, |HN \cap T : N \cap T|) = (|N \cap HT|, |H \cap NT|) = 1$, which implies that $HN \cap T = (H \cap T)(N \cap T)$. Thus, $HN \cap TN = (H \cap T)N$ in both cases. Note that $H_G N/N \leq (HN/N)_{G/N} = (HN)_G/N$, and there exists the isomorphism:

$$\begin{aligned} \frac{(HN \cap TN)(HN)_G}{(HN)_G} &= \frac{(H \cap T)(HN)_G}{(HN)_G} \\ &\cong \frac{(H \cap T)H_G/H_G \cdot (HN)_G/H_G}{(HN)_G/H_G}. \end{aligned} \tag{1}$$

So from ([3], Chap. A, Theorem 9.2(e)) and Lemma 2(1), it follows that $(HN \cap TN)(HN)_G/(HN)_G \leq \Phi(HN/(HN)_G)\mathrm{Int}_{\mathfrak{u}}(G/(HN)_G)$. By the definition, HN/N is Φ-I-supplemented in G/N.

(2) Assume that $T_0 = T \cap K$. Clearly, T_0 is subnormal in G and $HT_0 = HT \cap K = K$. Note that $H_G \leq H_K$ and the isomorphism

$$\frac{(H \cap T)H_K}{H_K} \cong \frac{(H \cap T)H_G/H_G \cdot H_K/H_G}{H_K/H_G}. \tag{2}$$

Therefore, by ([3], Chap. A, Theorem 9.2(e)) and Lemma 2(2), $(H \cap T)H_K/H_K \leq \Phi(H/H_K)\mathrm{Int}_{\mathfrak{u}}(K/H_K)$. So H is Φ-I-supplemented in K. □

Lemma 4 ([9], Lemmas 2.3 and 2.8).

(1) Let p be a prime divisor of $|G|$ with $(|G|, p-1) = 1$. Then, $\mathrm{Int}_{\mathfrak{u}}(G) \leq \mathrm{Int}_{\mathfrak{N}^p}(G)$, where $\mathfrak{N}^p$ denotes the class of all p-nilpotent groups.

(2) Assume that $\mathfrak{F}$ is a nonempty hereditary saturated formation. Let N_1, N_2 be normal subgroups of G, $I_1/N_1 = \mathrm{Int}_{\mathfrak{F}}(G/N_1)$ and $I_2/N_2 = \mathrm{Int}_{\mathfrak{F}}(G/N_2)$. Then, $I_1 \cap I_2/(N_1 \cap N_2) = \mathrm{Int}_{\mathfrak{F}}(G/(N_1 \cap N_2))$.

Lemma 5.

(1) If T is a subnormal subgroup of G such that $|G : T|$ is a power of p, then $O^p(G) \leq T$([13], Lemma 1.1.11).

(2) Assume that N is a minimal normal subgroup of G. Then, $N \leq O^p(G)$ or $|N| = p$.

Proof. If $N \nleq O^p(G)$, then $N \cap O^p(G) = 1$. Note that $NO^p(G)/O^p(G)$ is a minimal normal subgroup of the p-group $G/O^p(G)$. So the G-isomorphism $N \cong NO^p(G)/O^p(G)$ shows that $|N| = p$. □

Lemma 6 ([3], Chap. A, Lemma 8.4). *Let N be a nilpotent normal subgroup of G and M a maximal subgroup of G satisfying $N \nleq M$. Then, $N \cap M$ is a normal subgroup of G.*

Lemma 7 ([5], Chap. VI, Theorem 4.7). *Let P be a Sylow p-subgroup of G and N a normal subgroup of G. If $P \cap N \leq \Phi(P)$, then N is p-nilpotent.*

3. Proofs of Main Theorems

The following two propositions are main steps in the proof of Theorems 1 and 2, which also have independent meanings (see Corollaries 1 and 2).

Proposition 1. *Let P be a Sylow p-subgroup of G, where p is a prime divisor of $|G|$ with $(|G|, p-1) = 1$. Assume that all maximal subgroups of P are either Φ-I-supplemented or Φ-I-embedded in G. Then, G is p-nilpotent.*

Proof. Suppose that the assertion is false and let G be a counterexample for which $|G|$ is minimal. We proceed via the following steps:

(1) G has the unique minimal normal subgroup.

Let N be a minimal normal subgroup of G. Assume that M/N is an arbitrary maximal subgroup of PN/N, which is a Sylow p-subgroup of G/N. Then $M = M \cap PN = (M \cap P)N$. Denote $P_1 = M \cap P$. Since $|P : P_1| = |PN : M| = p$, P_1 is a maximal subgroup of P. By the hypothesis, G has a subnormal (resp., S-quasinormal) subgroup T such that P_1 is Φ-I-supplemented (resp., Φ-I-embedded) in G. Note that $P_1 \cap N = P \cap N$ is a Sylow p-subgroup of N, so $|P_1N \cap T : P_1 \cap T| = |N \cap P_1T : P_1 \cap N|$ is a p'-number. However, $|P_1N \cap T : N \cap T| = |P_1 \cap TN : P_1 \cap N|$ is a p-number. So we have $P_1N \cap T = (P_1 \cap T)(N \cap T)$ and then $M/N \cap TN/N = (P_1N \cap TN)/N = (P_1 \cap T)N/N$. Similarly as Lemma 3, it is easy to show that TN/N is a subnormal (resp., S-quasinormal) subgroup of G/N such that M/N is Φ-I-supplemented (resp., Φ-I-embedded) in G/N. Therefore, G/N satisfies the hypothesis. So the choice of G implies that G/N is p-nilpotent. Consequently, N is the unique minimal normal subgroup of G.

(2) $O_{p'}(G) = 1$ and $\mathrm{Int}_{\mathfrak{u}}(G) = 1$.

If $O_{p'}(G) \neq 1$, then the uniqueness of N implies that $N \leq O_{p'}(G)$. In the case, $G/O_{p'}(G)$ is p-nilpotent and so is G, a contradiction. Keep Lemmas 2(3) and 5(1) in mind. It is easy to obtain that $\mathrm{Int}_{\mathfrak{u}}(G) = 1$.

(3) $O_p(G) = 1$.

If $O_p(G) > 1$, then $N \leq O_p(G)$ and $|N| > p$. Clearly, $N \nleq \Phi(G)$. Then, there exists a maximal subgroup M of G such that $N \nleq M$. Together with the uniqueness of N, $G = N \rtimes M$. Note that $O_p(G) \cap M \trianglelefteq G$ by Lemma 6, so $O_p(G) \cap M = 1$ and, consequently, $O_p(G) = N(O_p(G) \cap M) = N$. Here, $P = N \rtimes (P \cap M)$ and then $|P : P \cap M| = |N| > p$. Thus, P has a maximal subgroup P_1 such that $P \cap M < P_1 < P$. Clearly, $(P_1)_G = 1$ and by the hypothesis, P_1 is either Φ-I-supplemented or Φ-I-embedded in G.

First assume that P_1 is Φ-I-supplemented in G. Combining with (2), there exists a subnormal subgroup T of G such that $G = P_1T$ and $P_1 \cap T \leq \Phi(P_1)$. According to Lemma 5, we have $N \leq O^p(G) \leq T$, which deduces that $P_1 \cap N \leq P_1 \cap T \leq \Phi(P_1)$. In this case, $P_1 = P_1 \cap N(P \cap M) = (P_1 \cap N)(P \cap M) = P \cap M$, a contradiction.

Now suppose that P_1 is Φ-I-embedded in G, that is, there exists a S-quasinormal subgroup T of G such that P_1T is S-quasinormal in G and $P_1 \cap T \leq \Phi(P_1)$. If $T = 1$, then P_1 is S-quasinormal in G. From Lemma 1(3) and the choice of P_1, we deduce that $P_1 \trianglelefteq G$, a contradiction. So $T > 1$. We further assume that $T_G = 1$. By Lemma 1(5), T^G is nilpotent. Combining with (2), T^G is a p-group. Hence $T \leq T^G = N$, which implies that $P_1T \leq P_1N = P$, that is, P_1T is a S-quasinormal p-subgroup of G. From Lemma 1(4)(6), it follows that $P_1T \leq O_p(G) = N$, which shows that $P_1 \leq N$ and consequently $N = P$. In this case, by Lemma 1(3), T is normal in G. Hence, the minimality of N implies that $T = N$. Consequently, $P_1 = P_1 \cap T \leq \Phi(P_1)$, which shows that $P_1 = 1$, a contradiction. Therefore, $T_G > 1$ and the uniqueness of N implies $N \leq T_G \leq T$. Consequently, $P_1 \cap N \leq P_1 \cap T \leq \Phi(P_1)$. Similarly as the above, it is impossible. So we should assume that $O_p(G) = 1$.

(4) Final contradiction.

Assume that $N = G$, that is, G is a simple group. For any maximal subgroup P_1 of P, if T is a subnormal (resp., S-quasinormal) subgroup of G such that P_1 is Φ-I-supplemented (resp., Φ-I-embedded) in G, then $T = G$. As a result, $P_1 = P_1 \cap T \leq \Phi(P_1)$, that is, $P_1 = 1$, a contradiction. Therefore, $N < G$. If $P \leq N$, then N satisfies the hypothesis by Lemma 3(2). So the choice of G and the relationship $N < G$ deduce that N is p-nilpotent, which contradicts (2) and (3). In general, we conclude $1 < P \cap N < P$. Let P_1 be a maximal subgroup of P containing $P \cap N$. Then $(P_1)_G = 1$ and P_1 is either Φ-I-supplemented or Φ-I-embedded in G.

First assume that P_1 is Φ-I-supplemented in G. So there exists a subnormal subgroup T of G such that $G = P_1T$ and $P_1 \cap T \leq \Phi(P_1)$. According to Lemma 6, we have that $N \leq O^p(G) \leq T$. Hence,

$P_1 \cap N \leq P_1 \cap T \leq \Phi(P_1)$. Note that $P_1 \cap N = P \cap N$ and $\Phi(P_1) \leq \Phi(P)$. So $P \cap N \leq \Phi(P)$. However, it deduces that N is p-nilpotent by Lemma 7, a contradiction.

If P_1 is Φ-I-embedded in G, then G has a S-quasinormal subgroup T such that P_1T is S-quasinormal in G and $P_1 \cap T \leq \Phi(P_1)$. Note that $T = 1$ implies that P_1 is S-quasinormal in G, which contradicts (3) and Lemma 1(4)(6). Moreover, if $T_G = 1$, then by Lemma 1(5) and the uniqueness of N, $N \leq T^G$ and N is nilpotent, which contradicts (1) and (3). Therefore, $T_G > 1$ and consequently $N \leq T_G \leq T$. In this case, we finally conclude that $P \cap N = P_1 \cap N \leq P_1 \cap T \leq \Phi(P_1) \leq \Phi(P)$. By Lemma 7, we also have that N is p-nilpotent, a contradiction. This contradiction completes the proof. □

Proposition 2. *Let P be a Sylow p-subgroup of G, where p is a prime divisor of $|G|$ with $(|G|, p-1) = 1$. Assume that all cyclic subgroups of P of order p and order 4 (when P is a nonabelian 2-group) are either Φ-I-supplemented or Φ-I-embedded in G. Then, G is p-nilpotent.*

Proof. Suppose that the assertion is false and let G be a counterexample of minimal order.

Let M be a proper subgroup of G and M_p a Sylow p-subgroup of M. Then, $M_p \leq P^g$ for some $g \in G$. Now consider M^g, which has a Sylow p-subgroup $M_p^g \leq P$. By Lemma 3(2), M^g satisfies the hypothesis for G. So M^g is p-nilpotent by the minimality of G. Consequently, M is p-nilpotent, and G is a minimal non-p-nilpotent group. By [14], Theorem 3.4.11, the following hold (i) $G = P \rtimes Q$, where $P = G^{\mathfrak{N}}$ and Q is a Sylow q-subgroup of G with $q \neq p$; (ii) $P/\Phi(P)$ is a noncyclic G-chief factor; (iii) the exponent of P is p or 4 (when P is a nonabelian 2-subgroup). Take $x \in P/\Phi(P)$, and denote $H = \langle x \rangle$. Then, H has order p or 4, $H_G \leq \Phi(P)$, and $\Phi(H/H_G) = 1$. Moreover, H is either Φ-I-supplemented or Φ-I-embedded in G by the hypothesis.

First assume that H is Φ-I-embedded in G. Let T be a S-quasinormal subgroup of G such that HT is S-quasinormal in G and $(H \cap T)H_G/H_G \leq \mathrm{Int}_{\mathfrak{u}}(G/H_G)$. Note that $P/\Phi(P)$ is a G-chief factor, so we separate the proof into three cases: (1) $P \cap T_G = P$; (2)$P \cap T^G \leq \Phi(P)$; (3) $P \cap T_G \leq \Phi(P)$ and $P \cap T^G = P$. If the first case holds, then $P \leq T$ and consequently $H/H_G = (H \cap T)H_G/H_G \leq \mathrm{Int}_{\mathfrak{u}}(G/H_G)$. From Lemmas 2(1) and 4(1), we further deduce that $1 < H\Phi(P)/\Phi(P) \leq \mathrm{Int}_{\mathfrak{u}}(G/\Phi(P)) \leq \mathrm{Int}_{\mathfrak{N}^p}(G/\Phi(P))$, where $\mathfrak{N}^p$ denotes the class of all p-nilpotent groups. So $P\Phi(P)/\Phi(P) \leq \mathrm{Int}_{\mathfrak{N}^p}(G/\Phi(P))$ by (ii). Together with Lemma 2(3), we finally have that $G/\Phi(P)$ is p-nilpotent, and so is G, a contradiction. In case (2), we have $P \cap T \leq \Phi(P)$. Then $H\Phi(P)/\Phi(P) = H(P \cap T)\Phi(P)/\Phi(P) = P/\Phi(P) \cap HT\Phi(P)/\Phi(P)$ is S-quasinormal in G by Lemma 1(2)(4). Note that $P/\Phi(P)$ is abelian. So $H\Phi(P)/\Phi(P) \trianglelefteq G/\Phi(P)$ according to Lemma 1(3). Consequently, $P/\Phi(P) = H\Phi(P)/\Phi(P)$ by (ii), a contradiction. Lastly, suppose that case (3) holds, that is, $P \cap T_G \leq \Phi(P)$ and $P \leq T^G$. If $T^G = G$, then G/T_G is p-nilpotent by Lemma 1(5). By (i), we have that $G/(P \cap T_G)$ is p-nilpotent, and furthermore, $G/\Phi(P)$ is p-nilpotent, which deduces that G is p-nilpotent, a contradiction. So we have $P \leq T^G < G$ and T^G is p-nilpotent as G is a minimal non-p-nilpotent group. Note that $O_{p'}(G) = 1$, so $T \leq T^G = P$. By Lemma 1(2), we obtain that $T\Phi(P)/\Phi(P)$ is a S-quasinormal subgroup of $G/\Phi(P)$ contained in $P/\Phi(P)$. Consequently, we deduce that $T\Phi(P)/\Phi(P) \trianglelefteq G/\Phi(P)$ from Lemma 1(3). Therefore, $T\Phi(P) = \Phi(P)$ or $T\Phi(P) = P$, that is, $T \leq \Phi(P)$ or $T = P$. However, from the proof of cases (1) and (2), we know that it is impossible.

Then assume that H is Φ-I-supplemented in G, and T is a subnormal subgroup of G such that $G = HT$ and $(H \cap T)H_G/H_G \leq \mathrm{Int}_{\mathfrak{u}}(G/H_G)$. Clearly, $P \leq O^p(G) \leq T$ by Lemma 5(1). So we have $H/H_G = (H \cap T)H_G/H_G \leq \mathrm{Int}_{\mathfrak{u}}(G/H_G)$. Similarly as the first case above, we know that it is impossible. Thus, the assertion holds.

Now we true to prove Theorems 1 and 2. □

Proof of Theorem 1. Suppose that the result is false and let (G, E) be a counterexample for which $|G| + |E|$ is minimal. We proceed via the following steps.

(1) E is a p-group.

Assume that $|\pi(E)| > 1$, p is the smallest prime divisor of $|E|$ and E_p is a Sylow p-subgroup of E. If E_p is cyclic, then E is p-nilpotent (see [15], Theorem 10.1.9). Now assume that E_p is noncyclic. From the hypothesis and Lemma 3(2), it follows that E satisfies the hypothesis of Proposition 1. So we have that E is still p-nilpotent. Let $E_{p'}$ be the normal p'-Hall subgroup of E. Then $E_{p'}$ is a normal subgroup of G and $(G, E_{p'})$ satisfies the hypothesis. Hence $E_{p'} \leq \mathrm{Int}_{\mathfrak{u}}(G)$ by the choice of (G, E).

Suppose that E_p is cyclic. Then, $E/E_{p'} \leq Z_{\mathfrak{u}}(G/E_{p'})$ for the G-isomorphism $E/E_{p'} \cong E_p$. By Lemma 2(5), $E/E_{p'} \leq \mathrm{Int}_{\mathfrak{u}}(G/E_{p'})$. Now assume that E_p is noncyclic. By Lemma 3(1), we can easily obtain that $(G/E_{p'}, E/E_{p'})$ satisfies the hypothesis. Analogously, the choice of (G, E) implies that $E/E_{p'} \leq \mathrm{Int}_{\mathfrak{u}}(G/E_{p'})$. Therefore, in any case, $E/E_{p'} \leq \mathrm{Int}_{\mathfrak{u}}(G/E_{p'})$. Furthermore, $E \leq \mathrm{Int}_{\mathfrak{u}}(G)$ by Lemma 2(4), a contradiction. Thus, $|\pi(E)| = 1$, that is, E is a p-group.

(2) $G/E \in \mathfrak{u}$.

Since $E \nleq Int_{\mathfrak{u}}(G)$, there exists a $\mathfrak{u}$-maximal subgroup X of G such that $E \nleq X$. By Lemma 3(2), (EX, E) satisfies the hypothesis for (G, E). If $EX < G$, then the choice of (G, E) implies that $E \leq \mathrm{Int}_{\mathfrak{u}}(EX)$. Note that EX/E is supersoluble for the isomorphism $EX/E \cong X/E \cap X$. So $EX \in \mathfrak{u}$ by Lemma 2(3). Furthermore, the choice of X implies $EX = X$, that is, $E \leq X$. This contradiction shows that $G = EX$ and, consequently, G/E is supersoluble as $G/E \cong X/E \cap X$.

(3) G has the unique Sylow p-subgroup.

Let q be the largest prime dividing $|G|$ and G_q a Sylow q-subgroup of G. Assume that $q > p$. Note that G/E is supersoluble. So $G_qE/E \trianglelefteq G/E$ and

$G_qE \trianglelefteq G$. Consider (G_qE, E), which satisfies the hypothesis by Lemma 3(2). Note that p is the smallest prime divisor of $|G_qE|$ and E is the Sylow p-subgroup of G_qE. So by Proposition 1, G_qE is p-nilpotent. Therefore, $G_q \trianglelefteq G_qE$ and, consequently, $G_q \trianglelefteq G$. Now consider $(G/G_q, G_qE/G_q)$, which satisfies the hypothesis by Lemma 3(1). So the choice of (G, E) implies that $G_qE/E \leq \mathrm{Int}_{\mathfrak{u}}(G/E)$. Moreover, the isomorphism $(G/G_q)/(G_qE/G_q) \cong (G/E)/(G_qE/E)$ deduces that $(G/G_q)/(G_qE/G_q)$ is supersoluble. Together with Lemma 2(3), we finally obtain G/G_q is supersoluble. Furthermore, G is supersoluble by the isomorphism $G \cong G/(E \cap G_q)$. This contradiction shows $q = p$. So (3) holds.

(4) Final contradiction.

Let N be a minimal normal subgroup of G contained in E. Consider $(G/N, E/N)$, which satisfies the hypothesis by Lemma 3(1). So the choice of (G, E) implies that $E/N \leq \mathrm{Int}_{\mathfrak{u}}(G/N)$. Note that $(G/N)/(E/N)$ is supersoluble by the isomorphism $(G/N)/(E/N) \cong G/E$. Combining with Lemma 2(3), G/N is supersoluble. Therefore, $N \nleq \Phi(G)$ and N is the unique minimal normal subgroup of G contained in E.

Note that $E \cap \Phi(G)$ is a normal subgroup of G contained in E. So the uniqueness of N implies that $E \cap \Phi(G) = 1$. Consequently, E is the direct product of the minimal normal subgroups of G contained in E (see [14], Chap. 1, Lemma 1.8.17). Furthermore, $E = N$ by the uniqueness of N.

Note that $E \cap Z(G_p)$ is a nontrivial normal subgroup of G. So $E \cap Z(G_p) = E$, that is, $E \leq Z(G_p)$. Take P_1 be an arbitrary maximal subgroup of E. Clearly, $(P_1)_G = 1$, $\Phi(P_1) = 1$ and by the hypothesis, P_1 is either Φ-I-supplemented or Φ-I-embedded in G.

Assume that P_1 is Φ-I-supplemented in G. Let T be a subnormal subgroup of G such that $G = P_1T$ and $P_1 \cap T \leq \mathrm{Int}_{\mathfrak{u}}(G)$. Then, $1 < E \cap T \trianglelefteq G$ and, consequently, $E \cap T = E$ by the minimality of E. In this case, $P_1 = P_1 \cap T \leq \mathrm{Int}_{\mathfrak{u}}(G)$, which implies $E \leq \mathrm{Int}_{\mathfrak{u}}(G)$ by the minimality of E again, a contradiction.

Now suppose that P_1 is Φ-I-embedded in G and T is a S-quasinormal subgroup of G such that P_1T is S-quasinormal in G and $P_1 \cap T \leq \mathrm{Int}_{\mathfrak{u}}(G)$. It is easy to show that the above holds if T is replaced by $T \cap E$. So, without loss of generality, assume that $T \leq E$. Since T is S-quasinormal in G, we have $T \trianglelefteq G$ by Lemma 1(3) and the relationship $E \leq Z(G_p)$. Therefore, $T = 1$ or $T = E$. If $T = 1$, then P_1 is S-quasinormal in G and, similarly as above, $P_1 \trianglelefteq G$, which contradicts the minimality of E. But if $T = E$, then $P_1 = P_1 \cap T \leq \mathrm{Int}_{\mathfrak{u}}(G)$, which also deduces a contradiction as above. So the proof is completed. □

Proof of Theorem 2. Suppose that the result is false and let (G, E) be a counterexample for which $|G| + |E|$ is minimal. Then, G is not supersolvable. Similarly as steps (1) and (2) in the proof of Theorem 1, assume that $G^{\mathfrak{u}} \leq E$ and E is a p-group.

Let M be any proper subgroup of G. Consider $(M, E \cap M)$, which satisfies the hypothesis for (G, E) by Lemma 3(2). So the minimality of (G, E) deduces that $E \cap M \leq \mathrm{Int}_{\mathfrak{u}}(M)$. Note that $M/E \cap M$ is supersolvable by the isomorphism $M/E \cap M \cong ME/E \leq G/E$. So M is supersolvable by Lemma 2(3). Consequently, G is a minimal nonsupersolvable group and from ([14], Theorem 3.4.2), we deduce that (i) $E = G^{\mathfrak{u}}$ is a p-subgroup of G; (ii) $E/\Phi(E)$ is a noncyclic G-chief factor; (iii) the exponent of E is p or 4 (when E is a non-abelian 2-group). Similarly, as step (3) of the proof of Theorem 1, the Sylow p-subgroup G_p of G is normal in G. Note that $E/\Phi(E) \cap Z(G_p/\Phi(E))$ is a nontrivial normal subgroup of $G/\Phi(E)$, so $E/\Phi(E) \leq Z(G_p/\Phi(E))$.

Take $x \in E/\Phi(E)$, and denote $H = \langle x \rangle$. Then, H has order p or 4, $H_G \leq \Phi(E)$, and $\Phi(H/H_G) = 1$. By the hypothesis, H is either Φ-I-supplemented or Φ-I-embedded in G.

Assume that H is Φ-I-embedded in G. Let T be a S-quasinormal subgroup of G such that HT is S-quasinormal in G and $(H \cap T)H_G/H_G \leq \mathrm{Int}_{\mathfrak{u}}(G/H_G)$. Clearly, $T \cap E$ is another S-quasinormal subgroup of G such that H is Φ-I-embedded in G. So without loss of generality, assume that $T \leq E$. Then, $T\Phi(E)/\Phi(E)$ is a S-quasinormal subgroup of $G/\Phi(E)$ contained in $E/\Phi(E)$. Together with Lemma 1(3) and the relationship $E/\Phi(E) \leq Z(G_p/\Phi(E))$, we have $T\Phi(E)/\Phi(E) \trianglelefteq G/\Phi(E)$. Thus, $T \leq \Phi(E)$ or $T = E$. If $T \leq \Phi(E)$, then $H\Phi(E)/\Phi(E) = HT\Phi(E)/\Phi(E)$ is S-quasinormal in G and then $H\Phi(E)/\Phi(E) \trianglelefteq G/\Phi(E)$. The choice of H shows that $E/\Phi(E) = H\Phi(E)/\Phi(E)$, which contradicts (ii). Assume that $T = E$. Then, $H/H_G = (H \cap T)H_G/H_G \leq \mathrm{Int}_{\mathfrak{u}}(G/H_G)$ and by Lemma 2(2), $H\Phi(E)/\Phi(E) \leq \mathrm{Int}_{\mathfrak{u}}(G/\Phi(E))$. Together with (ii), we have $E/\Phi(E) \leq \mathrm{Int}_{\mathfrak{u}}(G/H_G)$. Recall that G/E is supersoluble. Therefore, $G/\Phi(E)$ is supersoluble by the isomorphism $(G/\Phi(E))/(E/\Phi(E)) \cong G/E$ and Lemma 2(3). Furthermore, we have G is supersoluble, a contradiction.

Now assume that H is Φ-I-supplemented in G and T is a subnormal subgroup of G such that $G = HT$ and $(H \cap T)H_G/H_G \leq \mathrm{Int}_{\mathfrak{u}}(G/H_G)$. It is easy to show that $(E \cap T)\Phi(E) \trianglelefteq G$. So $E \cap T \leq \Phi(E)$ or $E \leq T$. Similarly as the above, $E \leq T$ is impossible. However, $E \cap T \leq \Phi(E)$ implies that $E = E \cap HT = H(E \cap T) = H$, which contradicts (ii). Then, we complete the proof. □

4. Some Applications

The following result follows directly from Lemma 2(3) and Theorems 1 and 2.

Corollary 1. *Let E be a normal subgroup of G such that G/E is supersoluble. Then, G is supersoluble if and only if for every prime $p \in \pi(E)$ and every noncyclic Sylow p-subgroup P of E, one of the following holds*

(1) *All maximal subgroups of P are either Φ-I-supplemented or Φ-I-embedded in G*

(2) *All cyclic subgroups of P with order p and* 4 (*when P is a non-abelian 2-group*) *are either* Φ-*I-supplemented or* Φ-*I-embedded in G*

Recall also that a subgroup H of G is called as follows: c-normal in G [16] if G has a normal subgroup T such that $G = HT$ and $H \cap T \leq H_G$; $\mathfrak{u}_c$-normal in G [17] if G has a subnormal subgroup T such that $G = HT$ and $(H \cap T)H_G/H_G \leq Z_{\mathfrak{u}}(G/H_G)$; $S\Phi$-supplemented in G [18] if G has a subnormal subgroup T such that $G = HT$ and $H \cap T \leq \Phi(H)$. Obviously, c-normal subgroups, $\mathfrak{u}_c$-normal subgroups, and $S\Phi$-supplemented subgroups of G are all Φ-I-supplemented in G. Hence, we have the following.

Corollary 2. *G is supersoluble, if one of the following holds*

(a) Every maximal subgroup of every Sylow subgroup of G is $\mathfrak{u}_c$*-normal in G ([17], Corollary 1.3)*

(b) All cyclic subgroups of G with prime order or order 4 are $\mathfrak{u}_c$*-normal in G ([17], Corollary 1.5)*

(c) Every maximal subgroup of every Sylow subgroup of G is c-normal in G ([16], Theorem 4.1)

(d) All cyclic subgroups of G with prime order or order 4 are c-normal in G ([16], Theorem 4.2)

From Proposition 2, we obtain the following.

Corollary 3 ([19], Lemma 3.1). *Let p be the smallest prime dividing* $|G|$ *and P a Sylow p-subgroup of G. If all subgroups of P with order p or order 4 are c-normal in G, then G is p-nilpotent.*

Corollary 4 ([18], Theorem 3.1). *Let P be a Sylow p-subgroup of G, where p is a prime dividing* $|G|$ *such that* $(|G|, p-1) = 1$. *If every maximal subgroup of P is* $S\Phi$*-supplemented in G, then G is p-nilpotent.*

Moreover, Theorem 3 in [20] and Theorems 3.3 and 3.4 in [21] follow directly from Theorem 1.

Data Availability

The data used to support the findings of this study are available from the corresponding author upon request.

Conflicts of Interest

The authors declare no conflicts of interest regarding the content and implications of this manuscript.

Acknowledgments

This work was supported by the Start-up Scientific Research Foundation of Anhui Jianzhu University (2017QD20) and the Key Research Projects of Natural Science in Anhui Province (KJ2019A0784).

References

[1] D. M. Bishop, *Group Theory and Chemistry*, Clarendon Press, Oxford, UK, 1973.

[2] The University of California Davis, *Group Theory and its Application to Chemistry*, University of California Davis, Davis, CA, USA, 2010.

[3] K. Doerk and T. Hawkes, *Finite Soluble Groups*, Walter de Gruyter, Berlin, Geramany, 1992.

[4] W. Guo, *Structure Theory for Canonical Classes of Finite Groups*, Springer, Dordrecht, Netherlands, 2015.

[5] B. Huppert, *Endliche Gruppen I*, Springer-Verlag, Berlin, Germany, 1967.

[6] A. N. Skiba, "On the $\mathfrak{F}$-hypercentre and the intersection of all $\mathfrak{F}$-maximal subgroups of a finite group," *Journal of Pure and Applied Algebra*, vol. 216, pp. 789–799, 2012.

[7] R. Bear, "Group elements of prime power index," *Transactions of the American Mathematical Society*, vol. 75, no. 1, pp. 20–47, 1953.

[8] J. C. Beidleman and H. Heineken, "A note on intersections of maximal F-subgroups," *Journal of Algebra*, vol. 333, no. 1, pp. 120–127, 2011.

[9] X. Chen, W. Guo, and A. N. Skiba, "On generalized $\mathfrak{U}$-hypercentral subgroups of a finite group," *Journal of Algebra*, vol. 442, pp. 190–201, 2015.

[10] W. Guo and A. N. Skiba, "On the intersection of the $\mathfrak{F}$-maximal subgroups and the generalized $\mathfrak{F}$-hypercentre of a finite group," *Journal of Algebra*, vol. 366, pp. 112–125, 2012.

[11] A. V. Sidorov, "On properties of the $\mathfrak{F}$-hypercentre of finite groups," *Problems in Algebra*, vol. 10, pp. 141–143, 1996.

[12] A. N. Skiba, "On the intersection of all maximal $\mathfrak{F}$-subgroups of a finite group," *Journal of Algebra*, vol. 343, no. 1, pp. 173–182, 2011.

[13] A. Ballester-Bolinches, R. Esteban-Romero, and M. Asaad, *Products of Finite Groups*, Walter de Gruyter, Berlin, Germany, 2010.

[14] W. Guo, *The Theory of Classes of Groups*, Science Press-Kluwer Academic Publishers, Beijing, Germany, 2000.

[15] D. J. S. Robinson, *A Course in the Theory of Groups*, Springer-Verlag, Berlin, Germany, 1982.

[16] Y. Wang, "C-normality of groups and its properties," *Journal of Algebra*, vol. 180, no. 3, pp. 945–965, 1996.

[17] A. Y. Alsheik Ahmad, J. J. Jaraden, and A. N. Skiba, "On $\mathfrak{U}_c$-normal subgroups of finite groups," *Algebra Colloquium*, vol. 14, no. 1, pp. 25–36, 2007.

[18] X. Li and T. Zhao, "$S\Phi$-supplemented subgroups of finite groups," *Ukrainian Mathematical Journal*, vol. 64, no. 1, pp. 102–109, 2012.

[19] M. Asaad and M. E. Mohamed, "On c-normality of finite groups," *Journal of the Australian Mathematical Society*, vol. 78, no. 3, pp. 297–304, 2005.

[20] J. Buckley, "Finite groups whose minimal subgroups are normal," *Mathematische Zeitschrift*, vol. 15, no. 1, pp. 15–17, 1970.

[21] D. Li and X. Guo, "The influence of c-normality of subgroups on the structure of finite groups," *Journal of Pure and Applied Algebra*, vol. 150, no. 1, pp. 53–60, 2000.